AGEM²

Kolumban Hutter
Yongqi Wang

Fluid and Thermodynamics

Volume 1: Basic Fluid Mechanics

Springer

Advances in Geophysical and Environmental Mechanics and Mathematics

Kolumban Hutter · Yongqi Wang

Fluid and Thermodynamics

Volume 1: Basic Fluid Mechanics

Kolumban Hutter
c/o Versuchsanstalt für Wasserbau,
    Hydrologie und Glaziologie
ETH Zürich
Zürich
Switzerland

Yongqi Wang
Department of Mechanical Engineering
Technische Universität Darmstadt
Darmstadt, Hessen
Germany

Printed on acid-free paper

Preface

Fluid and thermodynamics (FTD) are generally taught at technical universities as separate subjects and this separation can be justified simply by reasons of the assigned time; the elements of each subject can be introduced within a semester of ~ 15 weeks. Most likely, these outer educational boundaries may even have well furthered this separation. Intellectually, the two subjects, however, belong together, especially since for all but ideal fluids the second law of thermodynamics imposes constraint conditions on the parameters of the governing equations (generally partial differential equations) that are then used in the fluid dynamic part of the joint effort to construct solutions to physically motivated initial boundary value problems that teach us important facts of the behavior of the motion of the fluid under certain circumstances.

One of the authors (K.H.) found this combination of fluid and thermodynamics as an assigned one-semester course, when he started in 1987 in the Department of Mechanics at Technische Universität Darmstadt (at that time 'Technische Hochschule') as successor of the late Prof. Dr. rer.nat. Ernst Becker (1929–1984). With K.H's emphasized interest in continuum mechanics and thermodynamics, this dual understanding of the mathematical description of fluid matter was ideal and the assignment to teach it was a welcome challenge, which was declared as a 'credo' to the working environment in both teaching and research in his group.

The course notes of FTD taught to upper-class electrical engineers for 18 years were quickly worked out into the book 'Fluid und Thermodynamik – eine Einführung' and published by Springer Verlag, Berlin etc., (ISBN 3-540-59235-0, second edition). All the chapters of this book—some slightly extended—have been translated (by K.H.) into the English language and are interwoven in this treatise with chapters, which, as a whole, should provide a fairly detailed understanding of FTD.

All subjects of this treatise of FTD have been taught in one or another form as lectures in courses to students at Technische Universität Darmstadt, Swiss Federal Institute of Technology in Zürich (ETHZ), and in guest lectures in advanced courses at other universities and research institutions worldwide. The audience in

these courses consisted of students, doctoral candidates and postdoctoral assistants of engineering (civil, mechanical, chemical, mechanics), natural sciences (meteorologists, oceanographers, geophysicists), mathematics and physics. Some of the topics included are as follows:

- Fluid mechanics,
- Continuum mechanics and thermodynamics,
- Mechanics of environmentally related systems (glacier, ice-sheet mechanics, physical oceanography, lake physics, soil motion, avalanches, debris, and mud flows),
- Vorticity and angular momentum,
- Turbulence modeling (of zeroth, first and second order),
- Regular and singular perturbations,
- Continuum mechanics and thermodynamics of mixtures,
- Continuum mechanics and thermodynamics of COSSERAT continua and COSSERAT mixtures,
- Theoretical glaciology,
- Shallow creeping flows of landslides, glaciers, and ice sheets,

and others. It is hoped that we were successful in designing a coherent picture of the intended text FTD.

Writing the book chapters also profited from books that were written earlier by us and co-authors [1–6].

Fluid and Thermodynamics
Volume 1: Basic Fluid Mechanics

This volume consists of 10 chapters and begins in an introductory **Chap. 1** with some historical facts, definition of the subject field and lists the most important properties of liquids.

This descriptive account is then followed in **Chap. 2** by the simple mathematical description of the fundamental hydrostatic equation and its use in analyses of equilibrium of fluid systems and stability of floating bodies, the derivation of the ARCHIMEDEan principle and determination of the pressure distribution in the atmosphere.

Chapter 3 deals with hydrodynamics of ideal incompressible (density preserving) fluids. Streamlines, trajectories, and streaklines are defined. A careful derivation of the balances of mass and linear momentum is given and it is shown how the BERNOULLI equation is derived from the balance law of momentum and how it is used in applications. In one-dimensional smooth flow problems the momentum and BERNOULLI equations are equivalent. For discontinuous processes with jumps this is not so. Nevertheless the BERNOULLI equation is a very useful equation in

many engineering applications. This chapter ends with the balance law of moment of momentum and its application for EULER's turbine equation.

The conservation law of angular momentum, presented in **Chap. 4**, provides the occasion to define circulation and vorticity and the vorticity theorems, among them those of HELMHOLTZ and ERTEL. The goal of this chapter is to build a fundamental understanding of vorticity.

In **Chap. 5** a collection of simple flow problems in ideal fluids is presented. It is shown how vector analytical methods are used to demonstrate the differential geometric properties of vortex-free flow fields and to evaluate the motion-induced force on a body in a potential field. The concept of virtual mass is defined and two-dimensional fluid potential flow is outlined.

This almanac of flows of ideal fluids is complemented in **Chap. 6** by the presentation of the solution techniques of two-dimensional potential flow by complex-valued function theoretical methods using conformal mappings. Potential flows around two-dimensional air foils, laminar free jets, and the SCHWARZ–CHRYSTOFFEL transformations are employed to construct the mathematical descriptions of such flows through a slit or several slits, around air wings, free jets, and in ducts bounding an ideal fluid.

The mathematical physical study of viscous flows starts in **Chap. 7** with the derivation of the general stress–strain rate relation of viscous fluids, in particular NAVIER–STOKES fluids and more generally, non-NEWTONian fluids. Application of these equations to viscometric flows, liquid films, POISEUILLE flow, and the slide bearing theory due to REYNOLDS and SOMMERFELD demonstrate their use in an engineering context. Creeping flow for a pseudo-plastic fluid with free surface then shows the application in the glaciological-geological context.

Chapter 8 continues with the study of two-dimensional and three-dimensional simple flow of the NAVIER–STOKES equations. HAGEN–POISEUILLE flow and the EKMAN theory of the wall-near wall-parallel flow on a rotating frame (Earth) and its generalization are presented as solutions of the NAVIER–STOKES equations in the half-space above an oscillating wall and that of a stationary axisymmetric laminar jet. This then leads to the presentation of PRANDTL's boundary layer theory with flows around wedges and the BLASIUS boundary layer and others.

In **Chap. 9** two- and three-dimensional boundary layer flows in the vicinity of a stagnation point are studied as are flows around wedges and along wedge sidewalls. The flow, induced in the half plane above a rotating plane, is also determined. The technique of the boundary layer approach is commenced with the BLASIUS flow, but more importantly, the boundary layer solution technique for the NAVIER–STOKES equations is explained by use of the method of matched asymptotic expansions. Moreover, the global laws of the steady boundary layer theory are explained with the aid of the HOLSTEIN–BOHLEN procedure. The chapter ends with a brief study of non-stationary boundary layers, in which an impulsive start from rest, flow in the vicinity of a pulsating body, oscillation induced drift current, and non-stationary plate boundary layers are studied.

In **Chap. 10** pipe flow is studied for laminar (HAGEN–POISEUILLE) as well as for turbulent flows; this situation culminates via a dimensional analysis to the well-known

Moody diagram. The volume ends in this chapter with the plane boundary layer flow along a wall due to Prandtl and von Kármán with the famous logarithmic velocity profile. This last problem is later reanalyzed as the controversies between a power and logarithmic velocity profile near walls is still ongoing research today.

Fluid and Thermodynamics
Volume 2: Advanced Fluid Mechanics and Thermodynamic Fundamentals

This volume consists of 10 chapters and commences in **Chap. 11** with the determination of the creeping motion around spheres at rest in a Newtonian fluid. This is a classical problem of singular perturbations in the form of matched asymptotic expansions. For creeping flow the acceleration terms in Newton's law can be ignored to approximately calculate flow around the sphere by this so-called Stokes approximation. It turns out that far away from the sphere the acceleration terms become larger than those in the Stokes solution, so that the latter solution violates the boundary conditions at infinity. This lowest order correction of the flow around the sphere is due to Oseen (1910). In a systematic perturbation expansion the outer— Oseen—series and the inner—Stokes—series with the small Reynolds number as perturbation parameter must be matched together to determine all boundary and transition conditions of inner and outer expansions. This procedure is rather tricky, i.e., not easy to understand for beginners. This theory, originally due Kaplun and to Lagerström has been extended, and the drag coefficient for the sphere, which also can be measured is expressible in terms of a series expansion of powers of the Reynolds number. However, for Reynolds numbers larger than unity, convergence to measured values is poor. About 20–30 years ago a new mathematical approach was designed—the so-called Homotopy Analysis Method; it is based on an entirely different expansion technique, and results for the drag coefficient lie much closer to the experimental values than values obtained with the 'classical' matched asymptotic expansion, as shown in Fig. 11.11. Incidentally the laminar flow of a viscous fluid around a cylinder can analogously be treated, but is not contained in this treatise.

Chapter 12 is devoted to the approximate determination of the velocity field in a shallow layer of ice or granular soil, treated as a non-Newtonian material flowing under the action of its own weight and assuming its velocity to be so small that Stokes flow can be assumed. Two limiting cases can be analyzed: (i) In the first, the flowing material on a steep slope (which is the case for creeping landslides or snow on mountain topographies with inclination angles that are large). (ii) In the second case the inclination angles are small. Situation (ii) is apt to ice flow in large ice sheets such as Greenland and Antarctica, important in climate scenarios in a warming atmosphere. We derive perturbation schemes in terms of a shallowness parameter in the two situations and discuss applications under real-world conditions.

In shallow rapid gravity driven free surface flows the acceleration terms in NEWTON's law are no longer negligible. **Chapter 13** is devoted to such granular flows in an attempt to introduce the reader to the challenging theory of the dynamical behavior of fluidized cohesionless granular materials in avalanches of snow, debris and mud, etc. The theoretical description of moving layers of granular assemblies begins with the one-dimensional depth integrated MOHR–COULOMB plastic layer flows down inclines—the so-called SAVAGE–HUTTER theory—but then continues with the general formulation of the model equations referred to topography following curvilinear coordinates with all its peculiarities in the theory and the use of shock-capturing numerical integration techniques.

Chapter 14 on uniqueness and stability provides a first flavor into the subject of laminar-turbulent transition. Two different theoretical concepts are in use and both assume that the laminar–turbulent transition is a question of loss of stability of the laminar motion. With the use of the energy method one tries to find upper bound conditions for the laminar flow to be stable. More successful for pinpointing the laminar-turbulent transition has been the method of linear instability analysis, in which a lowest bound is searched for, at which the onset of deviations from the laminar flow is taking place.

In **Chap. 15**, a detailed introduction to the modeling of turbulence is given. Filter operations are introduced to separate the physical balance laws into evolution equations for the averaged fields on the one hand, and into fluctuating or pulsating fields on the other hand. This procedure generates averages of products of fluctuating quantities, for which closure relations must be formulated. Depending upon the complexity of these closure relations, so-called zeroth, first, and higher order turbulence models are obtained: simple algebraic gradient-type relations for the flux terms, one or two equation models, e.g., k-ε, k-ω, in which evolution equations for the averaged correlation products are formulated, etc. This is done for density preserving fluids as well as so-called BOUSSINESQ fluids and convection fluids on a rotating frame (Earth), which are important models to describe atmospheric and oceanic flows.

Chapter 16 goes back one step by scrutinizing the early zeroth order closure relations as proposed by PRANDTL, VON KÁRMÁN and collaborators. The basis is BOSSINESQ's (1872) ansatz for the shear stress in plane parallel flow, τ_{12}, which is expressed to be proportional to the corresponding averaged shear rate $\partial \bar{v}_1 / \partial x_2$ with coefficient of proportionality $\rho \varepsilon$, where ρ is the density and ε a kinematic turbulent viscosity or turbulent diffusivity $[\mathrm{m}^2 \ \mathrm{s}^{-1}]$. In turbulence theory the flux terms of momentum, heat, and suspended mass are all parameterized as gradient-type relations with turbulent diffusivities treated as constants. PRANDTL realized from data collected in his institute that ε was not a constant but depended on his mixing length squared and the magnitude of the shear rate (PRANDTL 1925). This proposal was later improved (PRANDTL 1942) to amend the unsatisfactory agreement at positions where shear rates disappeared. The 1942-law is still local, which means that the REYNOLDS stress tensor at a spatial point depends on spatial velocity derivatives at the *same* position. PRANDTL in a second proposal of his 1942-paper suggested that the turbulent diffusivity should depend on the velocity *difference* at the points where

the velocity of the turbulent path assumes maximum and minimum values. This proposal introduces some non-locality, yielded better agreement with data, but PRANDTL left the gradient-type dependence in order to stay in conformity with BOUSSINESQ. It does neither become apparent nor clear that PRANDTL or the modelers at that time would have realized that non-local effects would be the cause for better agreement of the theoretical formulations with data. The proposal of complete non-local behavior of the REYNOLDS stress parameterization came in 1991 by P. EGOLF and subsequent research articles during $\sim$20 years, in which also the local strain rate (= local velocity gradient) is replaced by a difference quotient. We motivate and explain the proposed Difference Quotient Turbulence Model (DQTM) and demonstrate that for standard two-dimensional configurations analyzed in this chapter its performance is superior to other zeroth order models.

The next two chapters are devoted to thermodynamics; first, fundamentals are attacked and, second a field formulation is presented and explored.

Class experience has taught us that thermodynamic fundamentals (**Chap. 17**) are difficult to understand for novel readers. Utmost caution is therefore exercised to precisely introduce terminology such as 'states', 'processes', 'extensive', 'intensive', and 'molar state variables' as well as concepts like 'adiabatic', and 'diathermal walls', 'empirical' and 'absolute temperature', 'equations of state', and 'reversible' and 'irreversible processes'. The core of this chapter is, however, the presentation of the First and Second Law of Thermodynamics. The *first law* balances the energies. It states that the time rate of change of the kinetic plus internal energies are balanced by the mechanical power of the stresses and the body forces plus the thermal analogies, which are the flux of heat through the boundary plus the specific radiation also referred to as energy supply. This conservation law then leads to the definitions of the caloric equations of state and the definitions of specific heats. The Second Law of Thermodynamics is likely the most difficult to understand and it is introduced here as a balance law for the entropy and states that all physical processes are irreversible. We motivate this law by going from easy and simple systems to more complex systems by generalization and culminate in this tour with the Second Law as the statement that entropy production rate cannot be negative. Examples illustrate the implications in simple physical systems and show where the two variants of entropy principles may lead to different answers.

Chapter 18 extends and applies the above concepts to continuous material systems. The Second Law is written in global form as a balance law of entropy with flux, supply and production quantities, which can be written in local form as a differential statement. The particular form of the Second Law then depends upon which postulates the individual terms in the entropy balance are subjected to. When the entropy flux equals heat flux divided by absolute temperature and the entropy production rate density is requested to be non-negative, the entropy balance law appears as the CLAUSIUS–DUHEM inequality and its exploitation follows the axiomatic procedure of open systems thermodynamics as introduced by COLEMAN and NOLL. When the entropy flux is left arbitrary but is of the same function class as the other constitutive relations and the entropy supply rate density is identically zero, then the entropy inequality appears in the form of MÜLLER. In both cases the Second

Law is expressed by the requirement that the entropy production rate density must be non-negative, but details of the exploitation of the Second Law in the two cases are subtly different from one another. For standard media such as elastic and/or viscous fluids the results are the same. However, for complex media they may well differ from one another. Examples will illustrate the procedures and results.

Chapter 19 on gas dynamics illustrates a technically important example of a fluid field theory, where the information deduced by the Second Law of Thermodynamics delivers important properties, expressed by the thermal and caloric equations of state of, say, ideal and real gases. We briefly touch problems of acoustics, steady isentropic flow processes and their stream filament theory. The description of the propagation of small perturbations in a gas serves in its one-dimensional form ideally as a model for the propagation of sound, for e.g. in a flute or organ pipe, and it can be used to explain the DOPPLER shift occurring when the sound source is moving relative to the receiver. Moreover, with the stream filament theory the sub- and supersonic flow through a nozzle can be explained. In the final section the three-dimensional theory of shocks is derived as the set of jump conditions on surfaces for the balance laws of mass, momentum, energy, and entropy. Their exploitation is illustrated for steady surfaces for simple fluids under adiabatic flow conditions. These problems are classics; gas dynamics, indeed forms an important advanced technical field that was developed in the twentieth century as a subject of aerodynamics and astronautics and important specialties of mechanical engineering.

Chapter 20 is devoted to the subjects 'Dimensional analysis, similitude and physical experimentation at laboratory scale', topics often not systematically taught at higher technical education. However, no insider would deny their usefulness. Books treating these subjects separately and in sufficient detail have appeared since the mid-twentieth century. We give an account of dimensional analysis, define dimensional homogeneity of functions of mathematical physics, the properties of which culminate in BUCKINGHAM's theorem (which is proved in an appendix to the chapter); its use is illustrated by a diversity of problems from general fluid dynamics, gas dynamics, and thermal sciences, e.g., propagation of a shock from a point source, rising gas bubbles, RAYLEIGH–BÉNARD instability, etc. The theory of physical models develops rules, how to down- or up-scale physical processes from the size of a prototype to the size of the model. The theory shows that in general such scaling transformations are practically never exactly possible, so that scale effects enter in these cases, which distort the model results in comparison to those in the prototype. In hydraulic applications, this leads to the so-called FROUDE and REYNOLDS models, in which either the FROUDE or REYNOLDS number, respectively, remains a mapping invariant but not the other. Application on sediment transport in rivers, heat transfer in forced convection, etc., illustrate the difficulties. The chapter ends with the characterization of dimensional homogeneity of the equations describing physical processes by their governing differential equations. The NAVIER–STOKES–FOURIER–FICK fluid equations serve as illustration.

The intention of this treatise is, apart from presenting its addressed subjects, a clear, detailed, and somewhat rigorous mathematical presentation of FTD on the basis of limited knowledge as a prerequisite. Calculus or analysis of functions of a

single or several variables, linear algebra and the basics of ordinary and partial differential equations are assumed to be known, as is the theory of complex functions. The latter is not universally taught in engineering curricula of universities; we believe that readers not equipped with the theory of complex functions can easily familiarize themselves with its basics in a few weeks' reading effort.

A second goal of this treatise is to frame the individual subjects in their historical content by providing biographical sketches of the inventors of the particular concepts. The science of fluid and thermodynamics began in the Western world more than 2000 years ago, e.g., by ARCHIMEDES in Syracuse. First careful observations on turbulence were described by LEONARDO DA VINCI and on the motion of falling bodies by GALILEO GALILEI. Mathematical description of the motion of physical bodies was begun by ISAAC NEWTON, and DESCARTES. EULER and father JOHANN and son DANIEL BERNOULLI introduced, among others, the continuous methods for ideal, i.e., reversible materials. Most of this research took place in the seventeenth and eighteenth centuries and was perfected in the upcoming nineteenth and twentieth centuries. The recognition of the energy balance equation and the entropy imbalance statement as physical laws are achievements of the nineteenth and first part of the twentieth century and are associated with scientists like SADI CARNOT, JULIUS MAYER, HERMANN HELMHOLTZ, RUDOLF CLAUSIUS, PIERRE MAURICE, MARIE DUHEM, WILLIAM THOMSON (LORD KELVIN), WILLIARD GIBBS, and MAX PLANK, to name a few.

The solutions of the (initial) boundary value problems which ensue from the emerging equations have been solved by a large number of follow-up scientists from the mid-nineteenth century to present, of whom a few stand out distinguishingly: OSBORNE REYNOLDS, LORD RAYLEIGH, LUDWIG PRANDTL, THEODORE VON KÁRMÁN, G.I. TAYLOR, HERMANN SCHLICHTING, and many others. The history, which evolved from the work of all these scientists, is fascinating. By listing short biographical sketches of those scientists who contributed to the development of fluid and thermodynamics, we hope to guide the reader to a coherent historical development of the fascinating subject of fluid and thermodynamics.

We regard this dual approach as a justified procedure, especially since the twenty-first century university students do no longer sufficiently appreciate the fact, on which shoulders of giants and predecessors we stand.

The books have been jointly drafted by us from notes that accumulated during years. As mentioned before, the Chaps. 1–3, 5, 7, 10, 17–20 are translated (and partly revised) from 'Fluid- und Thermodynamik – eine Einführung'. Many of the other chapters were composed in handwriting and TEXed by K.H. and substantially improved and polished by Y.W. We share equal responsibility for the content and the errors that still remain. Figures, which are taken from others, are reproduced and mostly redrawn, but mentioned in the acknowledgment and/or figure captions. Nevertheless a substantial number of figures have been designed by us. However, we received help for their electronic production: Mr. ANDREAS ROHRER, from the Laboratory of Hydraulics, Hydrology and Glaciology at ETH Zurich (VAW), drew figures for Chaps. 8 and 9 and the student assistants Mr. WALDEMAR SURNI and Mr. JAN BATTRAM from the Institute of Fluid Dynamics at Technische Universität Darmstadt aided in the production of figures of several other chapters. Mr. ANDREAS

SCHLUMPF from VAW and Ms. ALEXANDRA PAUNICA and Prof. LOANA LUCA drew figures for Chap. 6 and several other chapters.

It is custom of most publishers to ask referees to review book manuscripts shortly before submission for printing by experts of the subjects treated in the forthcoming book. It is, however, also almost consequential that reviewers for a two-volume treatise of more than 1200 pages can hardly be found, simply because of the excessive labor that goes with such an assignment. Nevertheless this burden was taken up by two emeriti, Dr.-Ing. PETER HAUPT, Professor of Mechanics at the University of Kassel, Germany and Dr. rer. nat, Dr. h.c. HANS DIETER ALBER, Professor of Mathematics, Technical University, Darmstadt, Germany. We thoroughly thank these colleagues for their extensive help. Their criticisms and recommendations are gratefully incorporated in the final version of the manuscript.

K.H. wishes to express his sincere thanks to ETH Zurich and in particular to Prof. Dr. R. BOES for the allowance to share a desk as an emeritus professor from Darmstadt at the Laboratory of Hydraulics, Hydrology and Glaciology at ETH Zurich and he equally thanks Profs. Dr. MARTIN FUNK and Dr. WILLI H. HAGER, members of this laboratory, for their support. Y.W. would like to express his thanks to Prof. Dr. MARTIN OBERLACK for the free and constructive collaboration in his fluid dynamic working unit at Technische Universität Darmstadt.

This treatise was planned as a three-volume project, and, indeed, two chapters of a possible volume III have already been written. We still hold up this intention, but the advanced age of one of us does not guarantee that we will be successful in this endeavor. We shall see …

Finally, we thank Springer Verlag, and in particular Dr. Annett Buettner, for the interest in our FTD treatise and AGEM^2, in general.

Zürich   Kolumban Hutter
Darmstadt   Yongqi Wang
February 2016

References

1. Hutter, K., Jöhnk, K.: Continuum Methods of Physical Modeling—Continuum Mechanics, Dimensional Analysis, Turbulence, p. 635. Springer, Berlin (2004)
2. Hutter, K., Wang, Y., Chubarenko, I.: Physics of Lakes—Vol. I Foundation of the Mathematical and Physical Background, p. 434. Springer, Berlin (2011a)
3. Hutter, K., Wang, Y., Chubarenko, I.: Physics of Lakes—Vol. II Lakes as Oscillators, p. 646. Springer, Berlin (2011b)
4. Hutter, K., Wang, Y., Chubarenko, I.: Physics of Lakes—Vol. III Methods of Understanding Lakes as Components of the Geophysical Environment, p. 605. Springer, Berlin (2014)
5. Pudasaini, S.P., Hutter, K.: Avalanche Dynamics—Dynamics of Rapid Flows of Dense Granular Avalanches, p. 602. Springer, Berlin (2007)
6. Schneider, L., Hutter, K.: Solid-Fluid Mixtures of Frictional Materials in Geophysical and Geotechnical Context, p. 247. Springer, Berlin (2009)

Contents

Chapter 1
Introduction

Abstract This chapter provides a first impression of what the general aims and scopes of fluid and thermodynamics are as special topics of engineering and natural sciences. In a first section short historical notes and definitions of the subject fields are given: What scientific fields are represented by 'Mechanics' and 'Thermodynamics'? What terminology is used in both specialties to set the important vocabulary within NEWTONian mechanics and in thermodynamics as representative axioms to arrive at balances of mass, momenta, energy and entropy? Concepts like 'body', 'motion', 'force', 'power', 'work', 'temperature' and 'heat' need precise definitions to define NEWTONian mechanics and the First Law of Thermodynamics. These laws form principal statements of universality; however, to formulate any mathematically closed theory, statements of material behavior are requested. In a second subsection, properties of liquids are briefly discussed. This is done with focus on simple shear experiments to shed light on behaviors of solids and fluids. Elastic and viscous behavior are described as are the special responses of elastic, viscous and more complicated behavior of pure water and salty water as functions of density, pressure, temperature and salinity, known as thermal equations of state.

Keywords Newtonian mechanics · Irreversible thermodynamics · Definition of solids, fluids and gases · Material response · Elastic, viscous behavior · Thermal equation of states

List of Symbols

Roman Symbols

D	Strain rate tensor
G	Effective shear modulus
T	Temperature
t^R	Deviator of the viscous Cauchy stress

Greek Symbols

α	Second grade viscosity
γ	Shear angle
$\dot{\gamma}$	Shear strain rate
$\nu = \eta/\rho$	Kinematic viscosity
ρ	Mass density
η	Dynamic viscosity
τ	Shear stress
τ_f	Yield shear stress

1.1   Historical Notes and Definition of the Subject Field

Fluid- and thermodynamics are **field theories**, of which the principal goals are to mathematically describe the classical physical processes in continuous media. In so doing the intentions usually are the determination of the temporal evolution of the density, and the motion and temperature distributions in each **material point** of a body. Thermodynamics is an extension of mechanics insofar as the latter deals only with the determination of the density and the motion of material particles; thermodynamics, by contrast, is necessary if one is also interested in the heating of a body.

Mechanics is concerned with the formulation and definition of entities such as **body, motion, force, power, work**; it deals with the fundamental laws connecting these entities. It has its historic and scientific background in NEWTON's (1642–1727) [8] principles and its predecessors and thus dates back to the 17th century. The systematic application of the fundamental mechanical principles to continuous media with finite extent has, however, been created in the 18th century and is largely due to the Swiss mathematician LEONHARD EULER (1707–1783) [4, 5] from Basel who spent his whole professional life at the Academies in St. Petersburg and Berlin. Similarly, the first systematic treatise on fluid dynamics is DANIEL BERNOULLI's (1700–1782) *Hydrodynamica* published in 1738 [3]; it is rooted in the superb mathematical school of the 18th century in Basel.

Mechanics can be divided into several subfields according to different characterizations: **Kinematics** is the science of the geometry of the motion of a body; in its description no use is generally made of the forces that act on a body; one is rather concerned with the conditions which allow a body to move and how the trace of such a motion can be described. Alternatively, **statics** is the science of the geometry of the forces and as such is not related to the motion of a body. It deals with the characterization and identification of the forces which may act on a body; it is the science of the mechanical equilibrium, i.e., those mechanical processes which do not change in the course of time. **Kinetics** or **dynamics**, finally, establish a connection between the forces (which may already be reduced by the methods of statics to their most convenient form) acting on the body or between bodies and their motions (which equally may, with methods of kinematics, have been put into their most adequate form). The

methods of kinematics allow selections of the dynamically possible motions from all those which are kinematically in principle admissible.

Since bodies comprising of different materials behave differently when being subject to the same given forces, it is also customary to divide mechanics according to the characterization of the objects in question. **Rigid bodies** are size and shape preserving, **elastic, viscous** and **plastic bodies** are deformable and **liquids** or **fluids**, such as water, are characterized as bodies, which respond to any shearing deformation, no matter how small, but are relatively size preserving, whereas **gases**, such as air, entail the tendency to fill the largest possible available space.

Thermodynamics is the science of heat in which notions like **heat, temperature, energy** and **entropy** are clarified. As an independent scientific field it is younger than mechanics and was given birth in the first half of the 19th century in technical efforts to quantify thermal machines as regards their degree of efficiency. The French engineer NICOLAS IÉONARD SADI CARNOT (1796–1832) was likely the first to formulate in his memoir of 1824 in general form the problem of generation of usable mechanical work from heat. In so doing, he spoke out, not directly, but at least implicitly the principle of the equivalence of heat and mechanical power.

The transferability of mechanical power, also called working, into heat and vice versa, was explicitly spoken out by the German physician JULIUS ROBERT MAYER (1814–1878) in a paper published in 1842. He may be regarded as the founder of the **First Law of Thermodynamics**. The theoretical achievements of thermodynamics were finally given their intermediate complete form by RUDOLF JULIUS EMANUEL CLAUSIUS (1822–1888) with his formulation of the **Second Law of Thermodynamics**, who in 1865, created the term entropy. Independently, and almost simultaneously (1851), the Scottish natural philosopher WILLIAM, THOMSON (LORD KELVIN, 1824–1907) arrived at a different formulation of the second law. To him, we also owe the concept of absolute temperature, now called Kelvin-temperature. It is a measure of hotness of a body point, motivated by the second law, which is independent of the special properties of the empirical temperature scale of special thermometers. Incidentally, since the sixties of the 20th century thermodynamics has experienced a vivid revival, in particular with regard to its mechanical formulation and physical foundation.

In the context of continuum physics, mechanics and thermodynamics cannot strictly be separated; it is rather so that with the first law of thermodynamics a statement of interconnection between mechanical and thermal energies is made. The second law of thermodynamics, however, is concerned with transformations of thermal mechanical and other energies into one another; it expresses the fact, based on uncountable many observations, that the transformation from mechanical into thermal energies is preferred to the reverse transformation from thermal to mechanical energies. This directional preference is expression of the principle of irreversibility of thermodynamic processes, a **principle of universality**.

According to the classical understanding, however, thermodynamics cannot deal with arbitrarily rapid and arbitrarily spatially varying processes. Only those processes can be described which are sufficiently close to thermodynamic equilibrium. Modern thermodynamics is concerned in parts with such extensions, but they will not be dealt with in this book.

1.2 Properties of Liquids

As already noted, fluids as opposed to solids, are distinguished by the fact that they respond to shearing loads and give way, no matter how small the shearing may be; this means that a fluid deforms indefinitely if shear stresses are applied to it and that it can only persist in equilibrium if no shear stresses are acting. Contrary to this, shear stresses in a solid body cause only finite deformations, so that states of equilibrium with non-trivial shear stresses are possible.

To explain this in greater detail we imagine the following (gedanken)-experiment, see **Fig. 1.1**. Let a material, of which the deformation properties are to be determined, be positioned between two mutually displaceable plates, their motion being parallel to each other. For $t < 0$ we imagine the set-up to be at rest. This configuration of the material at rest is made visible by drawing vertical stripes across the side boundaries.
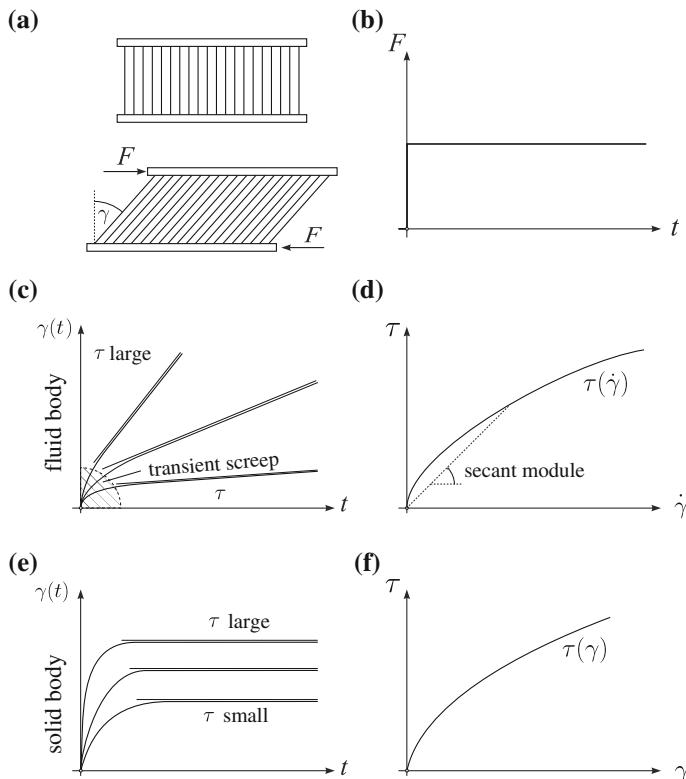
Fig. 1.1 Simple shear test. (**a**) *Shear deformation of a material held between two parallel plates subject to a tangential force; γ is the shear angle.* (**b**) *Temporal distribution of the force F applied at a plate of the creep test.* (**c**) *Creep curves for a fluid subject to different shear tractions.* (**d**) *Creep curves for a particular fluid, relating the shear stress τ to the asymptotic value of $\dot{\gamma}$.* (**e**) *Creep curves of a solid body, and* (**f**) *corresponding stress-strain relation $\tau(\gamma)$*

At $t = 0$ the two plates are loaded with a force F of constant magnitude as shown. As a consequence of this loading, a relative displacement of the two plates will occur and the material will deform; the vertical stripes will become increasingly inclined as time goes on. The qualitative behavior of such **creep curves** $\gamma(t)$ is shown in Fig. 1.1c for a few different values of the external load, which here is represented by the shear traction $\tau = F/A$, where F is the force acting on the plates, and A is the contact area of one of the plates with the material.

One can identify in the sketched creep curves a regime of decelerated shear angle (hatched domain in Fig. 1.1c), which obviously is due to the sudden application of the force F and is of transient character. This so-called **primary** or **transient creep** is in Fig. 1.1c slowly transformed into a **stationary** or **steady state** or **secondary creep**, which for each shear stress τ is characterized by a constant value of $\dot{\gamma}$.[1] We assume that $\dot{\gamma} > 0$ for all τ, so that according to the above definition the response is that of a fluid. In this case one can, as illustrated in Fig. 1.1d, assign to each τ of the creep experiments the corresponding asymptotic value of $\dot{\gamma}$. In this way one arrives at the law $\dot{\gamma} = f_f(\tau)$ or $\tau = \tau_f(\dot{\gamma})$, where $\dot{\gamma}$ in these relations is supposed to represent exclusively the value of the shear rate for large times, Fig. 1.1d.

If on the contrary, all creep curves approach for large time a horizontal asymptote, Fig. 1.1e, then the material under consideration is a solid body; in this case the constitutive relation has the form $\gamma = f_s(\tau)$, in which γ is the shear angle in the creep curve measured for large time t, Fig. 1.1f,

$$\gamma = \frac{\tau}{G(\tau)} \quad \text{for a solid body}, \qquad \dot{\gamma} = \frac{\tau}{\eta(\tau)} \quad \text{for a fluid.} \tag{1.1}$$

The coefficient G is called **effective shear modulus** and η is the **dynamic shear viscosity**; both are parameters, which may depend on the shear stress τ (and perhaps other quantities, e.g., temperature) and may in the panels d and f of Fig. 1.1 be interpreted as secant moduli. The formulas (1.1), therefore, describe nonlinear behavior.

With the laws (1.1) the essential properties of fluids and solids are described. Let us now add a few peculiarities of these laws:

- The deformation behavior of many solid bodies can be described by a linear relation between γ and τ. The shear modulus is in this case a pure material constant. If this constant shear modulus G is complemented by a second elastic constant, e.g., YOUNG's modulus E,[2] which can be determined by an analogous tension-

---

[1]In material science creep experiments are often further continued beyond this secondary creep regime. Creep curves then often show at large stresses a further accelerated regime that merges at large strains into another steady regime, now called tertiary creep.

[2]THOMAS YOUNG (1773–1829), physician, physicist and Egyptologist. He described the modulus of elasticity, E, in 1807 and further described it in his *A Course of Lectures on Natural Philosophy and the Mechanical Arts* (1807) [11]. However, the first use of the concept of YOUNG's modulus in experiments was by GIORDANO RICATTI in 1782—predating YOUNG by 25 years [10]. Furthermore the idea can be traced to a paper by EULER published in 1727, some 80 years before THOMAS YOUNG's 1807-paper. Excerpt from http://en.wikipedia.org/wiki/Thomas_Young_(scientist).

compression test, then a complete set of material parameters for the so-called
linearly isotropic Hookean material is known. HOOKE's law,[3] incidentally, is
for many technically relevant materials a useful idealization e.g., for concrete,
steel aluminum and soil or rock.

- If for a fluid, the relation between $\dot{\gamma}$ and τ is linear, then the material is called
a **Newtonian fluid** or a **linearly viscous** liquid. As for a solid body, a complete
characterization of a NEWTONian fluid is also given by two parameters, called vis-
cosities. For volume preserving fluids, which in this book will almost exclusively
be in focus, this second, so-called bulk viscosity will not arise, so that the shear
viscosity suffices for the characterization of the viscous behavior. Alternatively,
it is often customary when dealing with the theory of viscous fluids to set the
bulk viscosity equal to zero, even though the fluid may be compressible. This sup-
position is the so-called STOKES hypothesis. It has a statistical background, and
indeed one proves in the kinetic theory of gases that for a monatomic gas the bulk
viscosity must vanish. The dimension of η is $[\text{ML}^{-1}\text{T}^{-1}]$.
Besides the dynamic viscosity also the **kinematic viscosity** is in use. It is defined
as

$$\nu = \eta/\rho \tag{1.2}$$
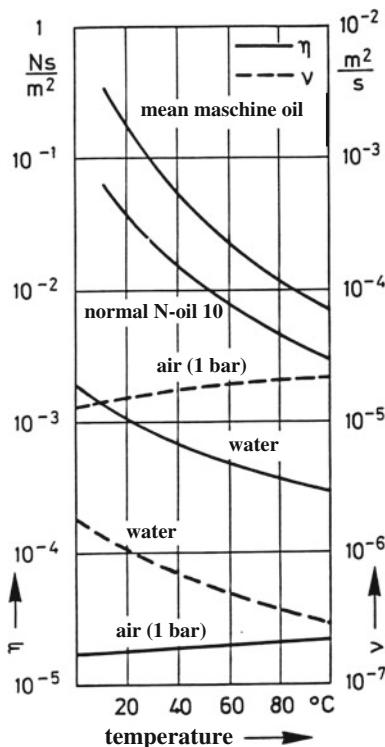
and has the dimension $[\text{L}^2\text{T}^{-1}]$.

- The mechanical behavior of many technically relevant fluids can adequately be
described by the idealized material law of a NEWTONian fluid; this is in particular
the case for water, air and some oils. However, the viscosity is in most cases not a
'material constant', but generally depends also on the temperature, pressure and,
if salts or impurities are contaminating the fluid, on the mass concentrations of
these tracers. The dependencies of the viscosity on the pressure and on the impu-
rities can in most cases be ignored in comparison to that of the temperature. For
computational purposes the viscosity is often set constant. **Figure 1.2** displays the
temperature dependences of some NEWTONian fluids; it indicates that the viscosity
of the liquids shown in the figure decreases with increasing temperature, whereas
it increases for air. These behaviors are typical for liquids and gases, respectively.
Figure 1.3 illustrates, how the dynamic shear and bulk viscosities vary for a pres-
sure of 10^5 Pa with temperature and Fig. 1.3b shows, again for pure water, how the
shear viscosity changes with the pressure. Finally, **Fig. 1.4** shows how η changes
with the temperature and salinity.

- There are many fluids, in particular products of the chemical industry such as
oils, polymeric melts, paints, but also geological materials such as lava in volcanic
eruptions, the fluid in the asthenosphere, or glacier ice, which behave under simple
shear like non-NEWTONian fluids according to the law $\dot{\gamma} = f_f(\tau)$, or yet more

---

[3]ROBERT HOOKE (1635–1702) was a contemporary of ISAAC NEWTON and was from 1662 onward
the curator of experiments of the Royal Society of London. His most important work is *Micrographia*
[6], which laid the foundation of microscopy. His *Lectiones Cutleriana* (1679) [7] contain the law
ut tensio sic vis', which is now HOOKE's Law of Elasticity. Based on http://de.wikipedia.org/wiki/
Robert_Hooke#Rezeption_und_Nachwirkung.

Fig. 1.2 Viscosities. *Viscosity plots (solid curves) η and kinematic viscosity ν (dashed) as functions of the temperature for different materials.* From ERNST BECKER (1929–1984), Technische Strömungslehre, Teubner, Stuttgart, 4th Edition (1977)

complicated flow laws. Some of these laws are sketched in **Fig. 1.5**. The creep law of the so-called **dilatant** and **pseudoplastic** fluids of Fig. 1.5a, b can often with good accuracy be represented by

$$\dot{\gamma} = A\tau^n, \tag{1.3}$$

in which A is (at least) temperature dependent and n is a constant. For dilatant fluids $0 < n < 1$ and for pseudoplastic fluids $n > 1$. The **Newton**ian fluid with $n = 1$ is equally covered by formula (1.3). In the literature this non-linear law bears several names: NORTON-HOFF law[4] in metallurgy, REINER-RIWLIN law[5]

---

[4]FREDERICK HARWOOD NORTON (1896–1963) was an American material scientist, who primarily worked on creep resistance of steels. His book [9] written while NORTON was working at the Massachusetts Institute of Technology summarizes his studies on the creep of steel at elevated temperature differently from linear viscous fluids.

NICOLAS J. HOFF (1906–1973) was a Hungarian-Swiss-American applied mechanician who was equally involved in the study of creep flow of solids at elevated temperature.

[5]MARKUS REINER (1886–1976) was a German-Israeli engineer and applied mathematician, specialized in rheology. Miss R. RIWLIN is REINERS junior collaborator for the well known REINER-RIWLIN fluid

$$t^R = 2\eta D + \alpha D^2, \quad \eta, \alpha = \text{constant}.$$
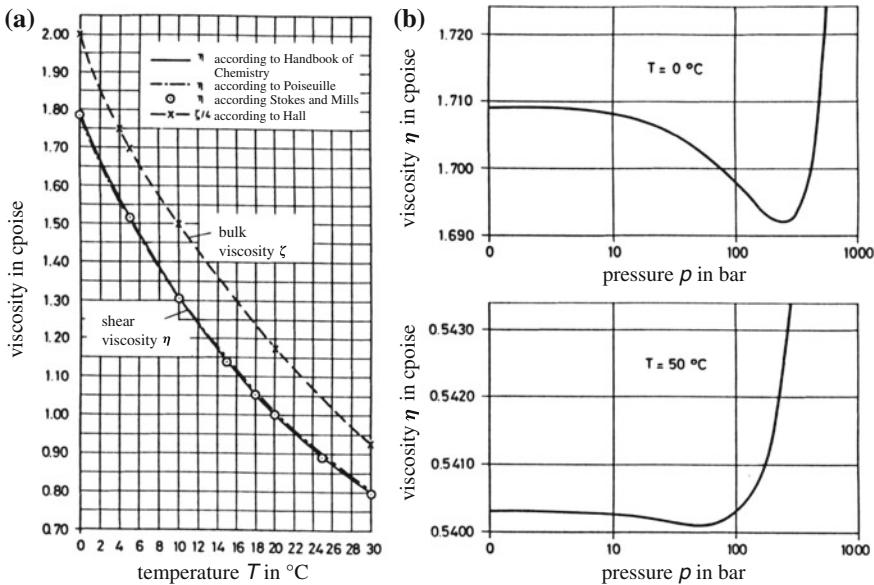
Fig. 1.3 Dynamic viscosities. (**a**) *Dynamic shear and bulk viscosities of pure water as functions of the temperature for a pressure of* 10^5 *Pa.* (**b**) *Dynamic shear viscosity as function of the pressure and temperature (1 cpoise* $= 10^{-2}$ *poise)*. From K. HUTTER and J. TRÖSCH: Über die hydrodynamischen und thermodynamischen Grundlagen der Seezirkulation. Mitt. Versuchsanstalt für Wasserbau, Hydrologie und Glaziologie an der ETH Zürich (1975)

in non-linear viscous fluid mechanics, GLEN's flow law[6] in glaciology, OSWALD DE WAELE law in rheology, etc. The other two flow laws which are sketched in Fig. 1.5c, d possess the property that the material behaves under simple shearing like a rigid body or a HOOKE an material, if the shear stress τ_f is below the yield stress; above it the response is essentially that of a (non)-NEWTONian fluid (which of the two cases prevails cannot be decided with Fig. 1.5). This is called BINGHAM fluid behavior.[7] For $|\tau| > \tau_f$ the material response is viscous with viscosity η and for an ideally plastic body it flows without any limit. Mathematically both laws can be expressed as

---

(Footnote 5 continued)

In the above, t^R is the stress deviator and D the strain rate tensor. Miss RIWLIN died soon after the completion of the paper in a car accident (1936), see Fig. 7.2 with a short biography on REINER. In continuum mechanics the above fluid carries the name REINER-RIVLIN fluid, (probably erroneously, attributed to RONALD SAMUEL RIVLIN (1915–2005), a nephew of Miss RIWLIN and equally an illustrious figure in rheology.

[6]JOHN GLEN (1927–) is a British ice physicist. He is reader in the Department of Physics of Birmingham University, England and is serving as Editor of the J. Glaciology for more than 60 years.

[7]EUGENE COOK BINGHAM (1878–1945) was a British material scientist studying the behavior of non-linear viscous fluids and plastic creep [1]. He coined together with MARKUS REINER the term '*Rheology*'.
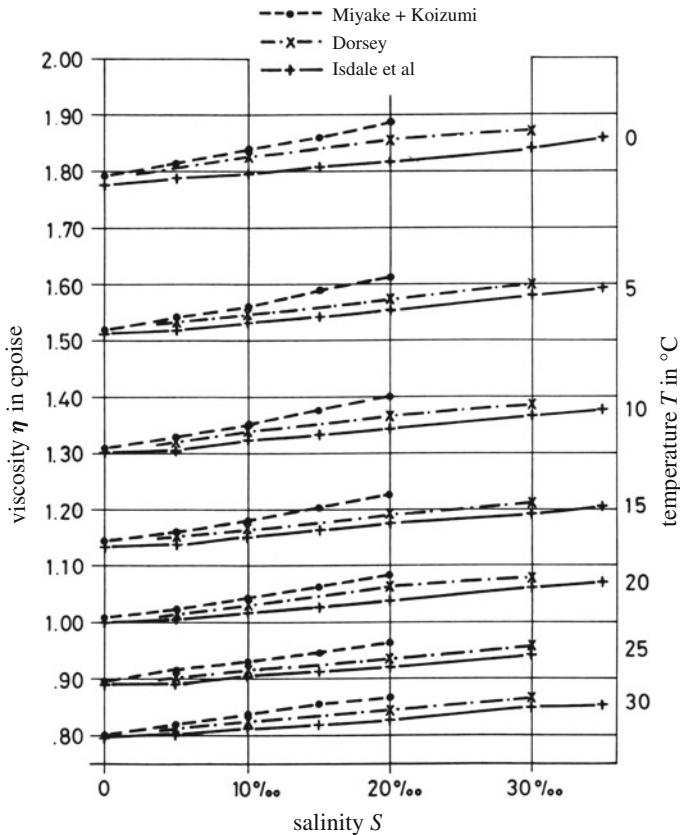
Fig. 1.4 Shear viscosity for salt water. *Dynamic shear viscosity of marine water plotted against salinity and parameterized for temperature.* From K. HUTTER and J. TRÖSCH: Über die hydrodynamischen und thermodynamischen Grundlagen der Seezirkulation, Mitt. Versuchsanstalt für Wasserbau, Hydrologie und Glaziologie an der ETH Zürich (1975)

$$\dot{\gamma} = \begin{cases} 0, & \text{if } \tau < \tau_f, \\ \dfrac{\tau - \tau_f}{\eta}, & \text{if } \tau \geqslant \tau_f, \end{cases} \qquad (1.4)$$

in which for a plastic body $\eta = 0$ and only values $\tau = \tau_f$ are possible. Toothpaste behaves in good approximation as a BINGHAM fluid. On the other hand, many metals under large stresses can approximately be treated as ideally plastic materials. If the regime beyond the yield stress is non-linear, the material is referred to as **generalized** BINGHAM **type**.[8]

---

[8] A fundamental book, in which complex constitutive behavior for continuous media is dealt with is [2].

(a)

(b)

(c)

(d)
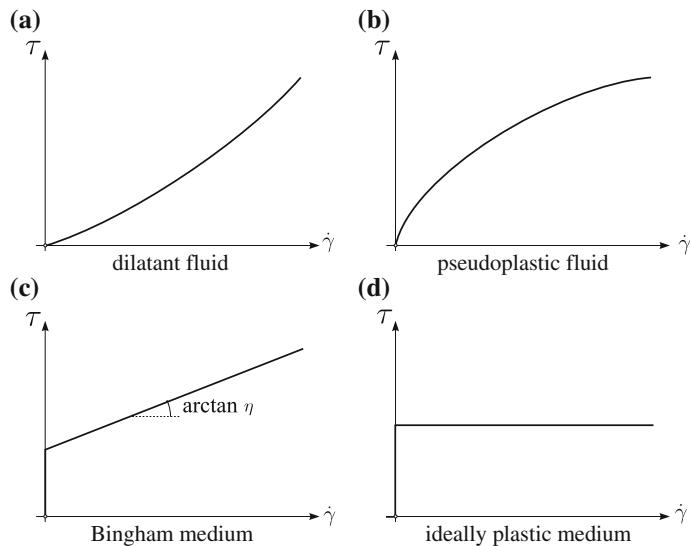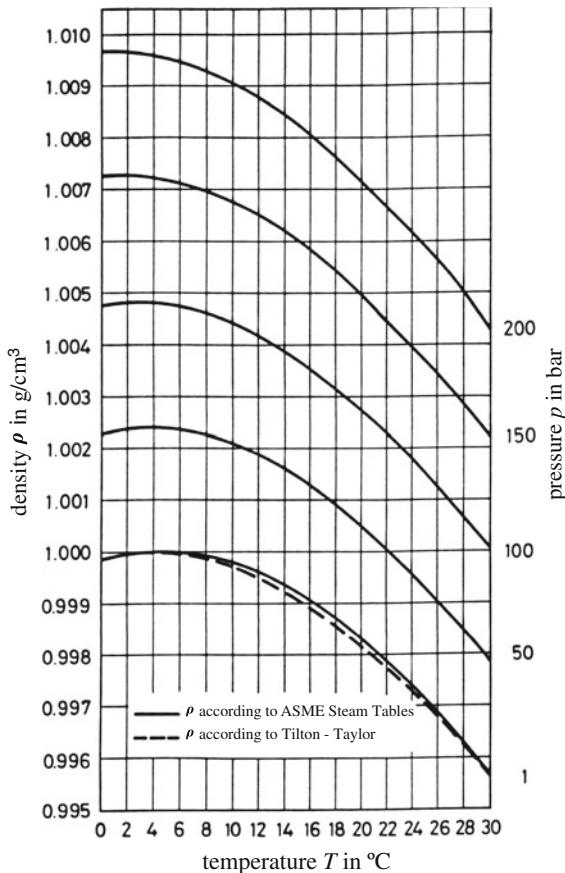
Fig. 1.5 Shear viscosity plotted against $\dot{\gamma}$. *Functional relations between shear stress τ and shear rate $\dot{\gamma}$ for various non-*NEWTON*ian liquids.* (**a**) *dilatant or structurally viscous liquids* (**b**) *pseudoplastic shear thinning liquids,* (**c**) BINGHAM *medium* (**d**) *ideally plastic body*

We already noted earlier that liquids are characterized by the fact that they are relatively size preserving, whilst gases have the tendency to fill the largest possible space available. Often, liquids can be assumed to be **completely volume** or **density preserving**. In these cases the density is temporally and spatially constant; consequently, of the field variables: density, motion and temperature, the first no longer forms an unknown field. The deformations are restricted in these cases to **isochoric (volume preserving) transformations**. The density or volume preserving body is to be distinguished from the **incompressible** body of which the density function is independent of the pressure, whilst other dependences, e.g., on temperature or salinity are all permissible. It follows from this, in particular, that in incompressible continua the density is an unknown field and motions are, in general not isochoric.

In engineering practice the term density preserving' and 'incompressible' are often taken as synonymous with the understanding that the denotation 'incompressible' is identified with 'density preserving' or 'volume preserving'. Pure water is neither density preserving nor incompressible. In **Fig. 1.6** at fixed pressure it, however, enjoys the distinct property that in the temperature range $T \in [0, 30)$ °C the density function does not monotonically vary with temperature. At normal pressure water is heaviest at 4 °C (exactly at 3.8 °C). This non-monotonic behavior is preserved, also at very high pressures. However, different sources report distinct results. Added salt also exerts its influence on the density of water; whereby the salt composition is strictly also of

Fig. 1.6 Density of pure water. *Density of pure water as a function of the temperature and pressure.* From K. HUTTER and J. TRÖSCH: Über die hydrodynamischen und thermodynamischen Grundlagen der Seezirkulation, Mitt. Versuchsanstalt für Wasserbau, Hydrologie und Glaziologie an der ETH Zürich (1975)
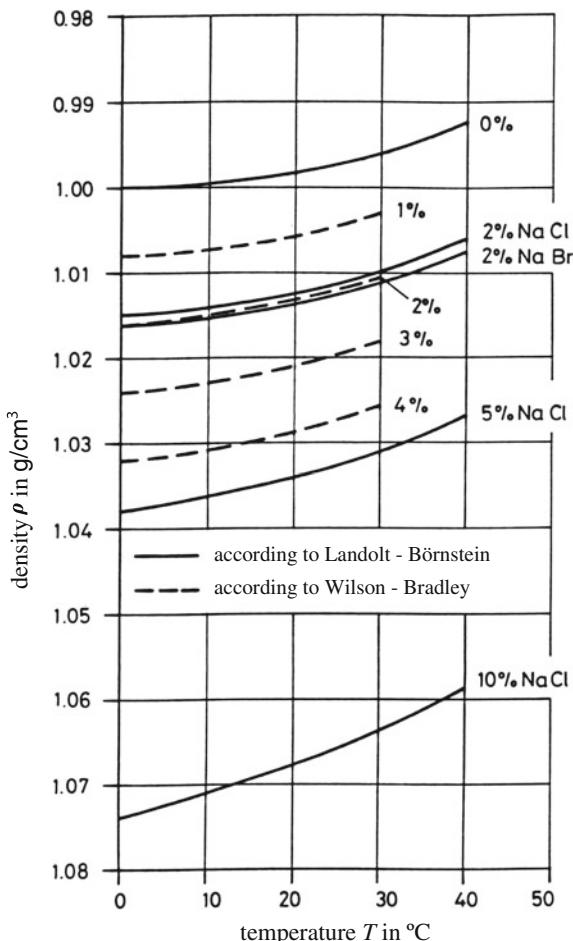
significance, see **Fig. 1.7**. For many technical applications, water can be treated as density preserving. Figure 1.6 allows estimating, under which prerequisites such an assumption is justified. If, however, buoyancy forces due to temperature differences are acting, then only a weaker assumption of incompressibility is justified. This is the case for the atmosphere, the ocean and lakes.

Gases are compressible; it is therefore important in gas dynamic flow problems to account for the temperature and pressure dependences of the density. This **thermal equation of state** is for gases always non-linear, a fact that makes construction of solutions for such problems generally much more difficult than analogous problems of fluid mechanics.

Now, it is, however so that in many gas-dynamic flows the variability of the density can be ignored, since the density differences in the flow field remain small. This is the case in particular, when the flow velocities of the gas remain small in comparison to the **speed of sound** of the gas. This statement, however, must be dealt with care, because these conditions are necessary but not sufficient in order that the assumption

Fig. 1.7 Density of salt water. *Density of water-salt solutions as functions of the temperature and parameterized for different salt concentrations.* From K. HUTTER and J. TRÖSCH: Über die hydrodynamischen und thermodynamischen Grundlagen der Seezirkulation, Mitt. Versuchsanstalt für Wasserbau, Hydrologie und Glaziologie an der ETH Zürich (1975)

of density preserving is justified. For instance, the influence of pressure differences by buoyancy forces must equally be negligible. As an example, air heated by solar irradiation rises due to the temperature dependence of the density function despite the fact that no wind may blow.

References

1. Bingham, E.C.: Fluidity and Plasticity. McGraw Hill, New York (1922)
2. Bird, R.B., Stewart, W.E., Lightfoot, E.N.: Transport Phenomena, 2nd edn. (2006). Wiley, New York (1960). ISBN: 13-978-047011 5398
3. Carmody, T., Kobus, H.: Translation of Hydrodynamica (Daniel Bernoulli) and Hydraulica (Johann Bernoulli). Dover Publications, New York (1964)

4. Euler, L.: Mémoire de l' Academie des Sciences de Berlin, **5**, 185–217 (1750). L. Euleri Opera Omnia, ser. Sec, **5**, 81–108 (1752)
5. Euler, L.: Mémoire de l' Academie des Sciences de Berlin, **11**, 274–315 (1755). Opera Omnia, ser. Sec., **12**, 54–91
6. Hooke, R.: Micrographia or Some Physiological Descriptions of Minute bodies Made by Magnifying Glasses with Observations and Inquiries Thereupon. London (1665). Dover Publications, New York (1961)
7. Hooke, R.: Lectiones Cutleriana, or a Collection of Lectures. John Martyn Printer to the Royal Society (1679)
8. Newton, I.: Philosphiae Naturalis Principia Mathematica. London (1687) 1st edn. (1703) 2nd edn. (1726) 3rd edn
9. Norton, F.H.: The Creep of Steel at High Temperatures. McGraw-Hill Book Company, New York [etc.] (1929)
10. Truesdell, C.A.: The Rational Mechanics of Flexible or Elastic Bodies, 1638–1788: Introduction to Leonhardi Euleri Opera Omnia, Vol. X and XI, Seriei Secundae. Orell Füssli (1960)
11. Young, T.: A Course of Lectures on Natural Philosophy and the Mechanical Arts. Taylor and Walton, London (1807)

Chapter 2
Hydrostatics

Abstract Fluid pressure is introduced based on the formulation of the equilibrium equations (force and moment balances). This gives rise to the introduction of body and surface specific forces and the definition of normal shear tractions on surfaces. Liquids in equilibrium are based on the assumption that shear tractions vanish, which, through the equilibrium conditions, yield a unique definition of the concept of 'hydrostatic pressure'. This leads, naturally, to the fundamental equation of hydrostatics, which subsequently is applied to various examples of density preserving liquids: among these are communicating vessels, PASCAL's paradoxon, manometers, hydraulic heavers, buoyancy and stability of floating bodies. Two sections extend this to hydrostatics in accelerated reference systems and pressure distribution in a still atmosphere.

List of Symbols

Roman Symbols

A, A_x, A_y, A_z	Surfaces with arbitrary spatial orientation, perpendicular to the x-axis, …, ...
$\mathrm{d}A, \mathrm{d}A_x, \ldots$	Surface elements on general plane,—on plane perpendicular to the x-direction
A, a	Area
$\boldsymbol{A}$	Buoyancy force
$\boldsymbol{a}$	Vector in $\mathcal{R}^3$ (mostly an acceleration)
$\frac{\mathrm{d}\boldsymbol{a}}{\mathrm{d}t}$	Time rate of change of $\boldsymbol{a}$ as referred to an inertial frame
$\frac{\delta\boldsymbol{a}}{\delta t}$	Time rate of change of $\boldsymbol{a}$ relative to a non-inertial frame
$\boldsymbol{b} = \frac{\mathrm{d}^2\boldsymbol{x}}{\mathrm{d}t^2}$	Acceleration vector, absolute acceleration
$\boldsymbol{b}_r = \frac{\delta^2\boldsymbol{r}}{\delta t^2}$	Relative acceleration vector
$\boldsymbol{b}_c$	CORIOLIS acceleration: $\boldsymbol{b}_c = 2\boldsymbol{\omega} \times \frac{\delta\boldsymbol{r}}{\delta t}$

$\boldsymbol{b}_f$	'Guiding' acceleration: $\boldsymbol{b}_f = \frac{\mathrm{d}^2\boldsymbol{r}_0}{\mathrm{d}t^2} + \boldsymbol{\omega} \times (\boldsymbol{\omega} \times \boldsymbol{r}) + \frac{\delta\boldsymbol{\omega}}{\delta t} \times \boldsymbol{r}$
C_{xy}	Deviator moment of inertia
$D = \rho_K/\rho_f$	Density ratio of a body suspended in a fluid with density ρ_f
$\mathcal{D}$	Symbol for a domain
$\boldsymbol{e}_x, \boldsymbol{e}_y, \boldsymbol{e}_z$	Cartesian basis; unit vectors in the x-, y-, z-directions
F	Force
$\boldsymbol{G}, \boldsymbol{g}$	Gravity force, specific gravity
h, h_1, h_2	Height, depth variables
$h_M = I_S/V_{\mathbb{E}}$	Metacentric height
δh	Difference of heights
I_S	Moment of inertia of the area enclosed by the water line of a ship
I_x, I_y	Moments of inertia
K_O	Total surface force on the body surface ∂V
K_V	Total volume force for the volume V
$\boldsymbol{k}$	Body force per unit mass: $\boldsymbol{k} = (k_x, k_y, k_z)$
M	Mass of a body
ΔM	Mass increment
M_V	Total moment of $\rho\boldsymbol{k}$ for the volume V
$\mathcal{M}$	Metacenter
N^2	Square of the buoyancy frequency: $N^2 = -\frac{\frac{\mathrm{d}\rho}{\mathrm{d}\zeta}(0)g}{\rho(0)}$
n	Polytrope exponent
$\boldsymbol{n}$	Unit normal vector
p	Pressure
$p(\rho)$	Barotropic pressure
R	Gas constant
r	Radius
S	Center of mass of a body
$S_{\mathbb{E}}$	Center of mass of the displaced fluid center
T	Temperature
$\boldsymbol{t}$	CAUCHY Stress tensor
$\boldsymbol{tn}$	Traction on a surface element with unit normal vector $\boldsymbol{n}$
$V, V_{\mathbb{E}}$	Volume of the body, volume of the displacement fluid
$\boldsymbol{v}_a, \boldsymbol{v}_f, \boldsymbol{v}_r$	Absolute velocity, fixed body velocity, relative velocity
$\boldsymbol{x}$	Position vector
(x_C, y_C)	Position of the center of the two-dimensional area of domain $\mathcal{D}$

Greek Symbols

α	Free surface inclination of the fluid in a container with constant acceleration
Δ	LAPLACE operator, $\Delta = \nabla^2$
ΔM	Mass increment
ΔV	Volume increment
ε	Relative density difference: $\varepsilon = (\rho_2 - \rho_1)/\rho_2$
ζ_S	z-coordinate of the center of gravity of an element V of air

$\eta = a/A$	Ratio of two areas
$\delta\phi$	Infinitesimal rotation angle of a ship
ρ_F, ρ_f, ρ_G	Density of a fluid,—gas
ψ	Body force potential
λ	Slope of the water line of a floating body
$\sigma\boldsymbol{n}$	Normal stress of the surface traction $\boldsymbol{tn}$
τ	Shear traction, shear stress
$\boldsymbol{\omega}$	Angular velocity of a non-inertial frame relative to another (inertial) frame
$\boldsymbol{\omega} \times (\boldsymbol{\omega} \times \boldsymbol{r})$	Centripetal acceleration
$\dot{\boldsymbol{\omega}} \times \boldsymbol{r}$	EULER acceleration

2.1 Some Basic Concepts

Hydrostatics is the science of the **mechanical equilibria** of fluids and gases; when applied exclusively to gases it is also called **aerostatics**. In this chapter our intention is to describe its fundamental rules from a common viewpoint. Before turning to that, however, let us note a few typical features of proper fluids and proper gases. Because of their relatively large density (as compared to gases) proper fluids are nearly density preserving. Both gases and liquids have the tendency to fill the space, which is at their disposal. However, whereas gases do this without any restriction, liquids climb in a capillary and are capable to form droplets, if the spatial dimensions of the liquid masses are sufficiently small, **Fig. 2.1**a, b. These properties of liquids can be traced back to **surface tension**, which, at last, is due to the interactions of the liquid molecules in the immediate vicinity of the boundary of the liquid. Figure 2.1c displays the distribution of the attractive or repelling interaction force, to which two molecules at distance d are exposed; d_0 corresponds approximately to the diameter of the molecules. For gases, the mean diameter of two molecules is usually several mean molecule diameters (approximately $10d_0$ or more); the molecules are separated such that only very weak mutual cohesive interaction forces are effective. Only occasionally two gas molecules approach each other so closely that they repel each other. In these cases the interaction force is very large and of short duration. This justifies a simplified interacting force model, in which the interaction force for gases is restricted to ideal impacts. This also explains, why their densities are smaller than for liquids, and why no surface tension exists in gases.

In solid and fluid bodies the molecules are so densely packed together as is permitted by the repulsive forces. In solid bodies the bonds between the single molecules at a fixed position are permanent, and the molecules oscillate about their equilibrium positions (point $\mathcal{P}$ in Fig. 2.1c). At melting the density of almost all substances falls by a few percents (exception: water), and it is somewhat paradoxical that such a small reduction of the molecular distance gives rise to such large changes of the mobility of the material. One assumes that the molecules combine to clusters and that these clusters move relative to one another, whereby the arrangement of the molecules continuously changes.

(a)

(b)

(c)

interaction force

repulsion

$\mathcal{P}$ attraction

d_0 d

(d)

modulus of the molecule
force directed into
the body

K
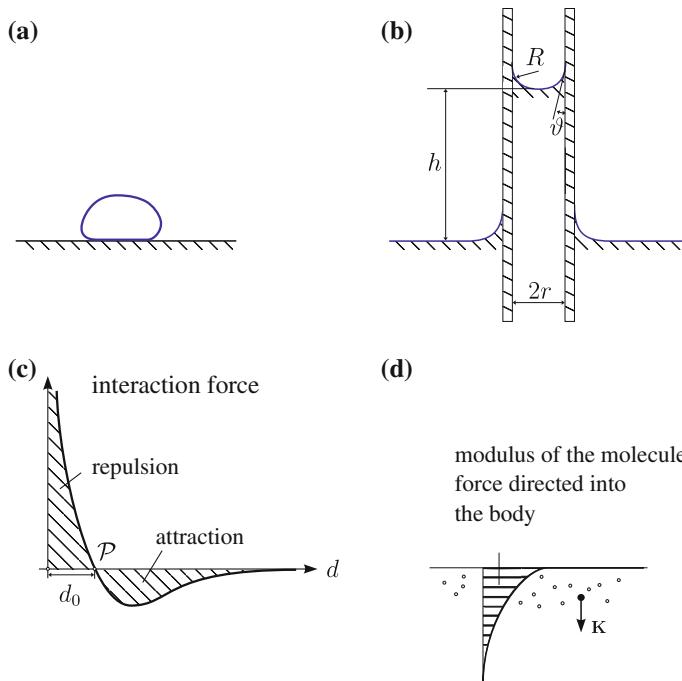
Fig. 2.1 Explaining surface stresses. (**a**) *Small droplet of a fluid of which the shape dependence is due to the surface stresses.* (**b**) *Because of the surface tension a liquid rises in a capillary tube to a height given by the weight of the fluid in the capillary tube and the surface tension acting at the meniscus.* (**c**) *Interaction force between two molecules plotted against the distance of the molecules.* (**d**) *Distribution of the force acting on a molecule as a function of the distance from the bounding surface*

The molecular origin of the surface stresses (tension) lies in the fact that the intermolecular interaction force at larger molecular distances corresponds effectively to an attractive force. In a molecule close to the bounding free surface the interacting force with the neighbouring molecules is reduced to a force directed *into* the fluid, Fig. 2.1d. In other words, a free surface of a liquid has the tendency to diminish its size.

Finally, we remark that, in spite of the above applied molecular structure of liquids and gases, these bodies will be viewed as **continua**, in which each geometric point is occupied by mass and thus can be identified as a material point. If we adopt this viewpoint in the ensuing developments, it is meaningful to define specific quantities of physical variables. In this spirit we call ρ **mass density** or simply **density** for brevity, and regard it as the limit

$$\rho = \lim_{\Delta V \to 0} \frac{\Delta M}{\Delta V}$$

of the mass ΔM of a fluid element volume ΔV, when the latter becomes vanishingly small. The existence of such limits follows from the continuity assumption and will subsequently tacitly be assumed to hold. Finally, we also will often use the term **fluid particle**. By this we shall not mean the above mentioned molecules, but small elements equipped with fluid mass, which are considered to be marked by some means.

2.2 Fluid Pressure

In order to describe the mechanical equilibrium (**Fig. 2.2**) an arbitrary material volume V with boundary ∂V is cut out of a body. 'Material' means that the boundary ∂V is occupied at all times by the same fluid particles; this means in particular, that no fluid particles cross the boundary ∂V. According to the fundamental laws of mechanics this isolated volume is in mechanical equilibrium, if the body forces (which are acting at the volume element) and the surface forces (acting on the surface elements) reduce to the null force and a null moment (cutting principle). If one denotes by k the **specific body force** (per unit mass) and by t_n the **surface force** (force per unit surface area), also called **traction**, then the mechanical **forces** applied to the body

$$K_V = \int_V \rho k \, dV, \qquad K_O = \int_{\partial V} t_n \, dA \qquad (2.1)$$

and the mechanical **moments** relative to the origin of the coordinate system

$$M_V = \int_V x \times \rho k \, dV, \qquad M_O = \int_{\partial V} x \times t_n \, dA \qquad (2.2)$$

Fig. 2.2 Material volume. *Material volume V with boundary ∂V, the specific body force ρk dV and the surface force t_n dA. O is the origin of the Cartesian coordinates x, y, z*
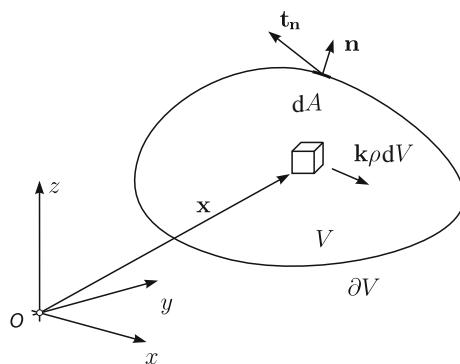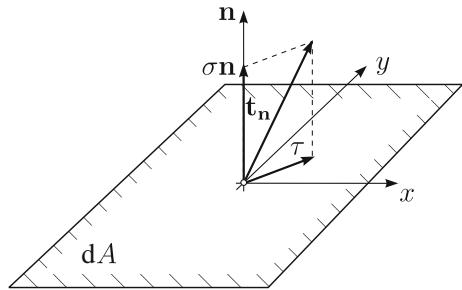
Fig. 2.3 Stress vector.
Surface element d*A with*
associated stress vector t_n,
its component normal to the
element, σn and the shear
stress component τ
tangential to the surface

are the total volume and surface forces and the total volume and surface moments with respect to the origin of the coordinates, respectively. x is the **position vector** from the coordinate origin to the volume element dV and $\times$ denotes the vector product in three dimensions. K_V and M_V are therefore the volume forces and volume moments, integrated over the volume of their infinitesimal counterparts, and K_O and M_O are the corresponding surface forces and surface moments. Equilibrium prevails, if

$$K_V + K_O = 0, \qquad M_V + M_O = 0. \tag{2.3}$$

These equations express the force and moment conditions of the mechanical equilibrium.[1]

In the above considerations the stress vector t_n has tacitly been assumed as the cutting force per unit surface. This definition implies that the stress in the interior of a body depends on the position $\mathcal{P}$ as well as on the exterior unit normal vector n of the surface element on which the stress vector is acting. Consequently, for two surface elements with unit normal vectors n_1 and n_2 in the same point $\mathcal{P}$, one must expect two stress vectors t_{n_1} and t_{n_2}, which are generally distinct. The state of stress in the interior of a body is therefore not described by a spatially dependent vector, but rather by a **tensor**, i.e., by a quantity, which depends upon the position $\mathcal{P}$ and the orientation n.
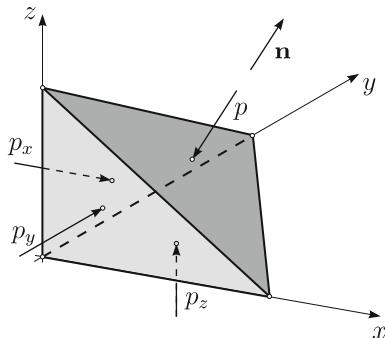
The stress vector or the specific surface force t_n can vectorially be decomposed for each surface element dA into a contribution perpendicular to the surface element, σn, and a contribution τ, parallel to the surface element, **Fig. 2.3**,

$$t_n = \sigma n + \tau. \tag{2.4}$$

The first contribution on the right-hand side of (2.4), σn is called the **normal stress**; σ can be positive or negative and is then called **tensile stress** or **pressure**. The second

---

[1]It is assumed that the reader is familiar with the concepts of the mechanics of rigid bodies as commonly taught in elementary mechanics courses at universities in compendia treating 'statics, dynamics and strength of materials'.

Fig. 2.4 Pressure forces. *Infinitesimal tetrahedron with three side surfaces normal to the coordinate axes, onto which the pressures p_x, p_y, p_z act. Perpendicular to the inclined surface with exterior unit normal vector $\boldsymbol{n}$, the pressure p applies*

quantity is called **shear stress** or **shear traction**.[2] Within the surface element it can have an arbitrary orientation. In Chap. 1, a fluid (gas or liquid) was defined as a material, which under the action of shear stresses is continuously deformed. This statement can now be made more precise by the statement that in a liquid at rest or in a gas at rest, no shear stresses can be withheld.: i.e., $\boldsymbol{\tau} = \boldsymbol{0}$. Furthermore, and excluding side effects such as surface tension, the normal stress is always negative, hence a pressure. This statement may even serve as a definition of a fluid. According to this definition a material is a fluid, if in equilibrium

$$\boldsymbol{t_n} = -p\boldsymbol{n} \tag{2.5}$$

holds. The scalar p is called **hydrostatic pressure**, **fluid pressure** or simply **pressure**.

According to the concepts introduced here to for, it is possible that the pressure may depend on the position as well as on the orientation of the surface element at which it applies: $p = p(\boldsymbol{x}, \boldsymbol{n})$. However, the following statement holds: *The hydrostatic pressure p only depends on the position, but not on the orientation of the surface element at which it applies*: $p = p(\boldsymbol{x})$.

To prove this statement, consider the fluid element of **Fig. 2.4**, which has the form of a tetrahedron with three edges parallel to the coordinate axes. If its inclined side surface is denoted by dA, its external unit normal vector by $\boldsymbol{n} = (n_x, n_y, n_z)$ and the remaining side surfaces by dA_x, dA_y, dA_z, then simple geometric considerations show that

$$\mathrm{d}A_x = n_x\,\mathrm{d}A, \quad \mathrm{d}A_y = n_y\,\mathrm{d}A, \quad \mathrm{d}A_z = n_z\,\mathrm{d}A. \tag{2.6}$$

If, moreover, p, p_x, p_y, p_z are the pressures acting on the four bounding surface elements of the infinitesimal tetrahedron, then the resulting cutting forces

$$p\,\mathrm{d}A, \quad p_x n_x\,\mathrm{d}A, \quad p_y n_y\,\mathrm{d}A, \quad p_z n_z\,\mathrm{d}A \tag{2.7}$$

---

[2]*Traction* is equivalent to *vector*. At a surface element the traction is decomposed into normal traction and shear traction.

Table 2.1 Units for pressure

Denotation	
Pascal	$1\,\text{Pa} = 1\,\text{N}\,\text{m}^{-2} = 1\,\text{kg}\,\text{m}^{-1}\text{s}^{-2}$
Bar	$1\,\text{bar} = 10^5\,\text{Pa}$
Technical atmosphere	$1\,\text{at} = 1\,\text{kp}\,\text{cm}^{-2} = 0.981\,\text{bar}$
Physical atmosphere	$1\,\text{atm} = 760\,\text{Torr} = 760\,\text{mmHg} = 1.013\,\text{bar}$
Torr	$1\,\text{Torr} = 133.3\,\text{mbar} = 13.3\,\text{kPa}$

are of second order small, because they are proportional to the areal increment $\mathrm{d}A$. Body forces such as the weight of the tetrahedral element are of third order small and can be ignored in comparison to the pressure contributions. An example for this omission is the pressure difference between the element $\mathrm{d}A$ and a parallel element through the point $\mathcal{P}$. The three components of the force balance for the element yields

$$p_x n_x \, \mathrm{d}A - p n_x \, \mathrm{d}A = 0, \ldots, \tag{2.8}$$

in which dots indicate cyclic replacements of the indices x, y, z and the omitted statements represent the equilibrium conditions in the y- and z-directions. Therefore, (2.8) implies

$$p_x = p_y = p_z = p. \tag{2.9}$$
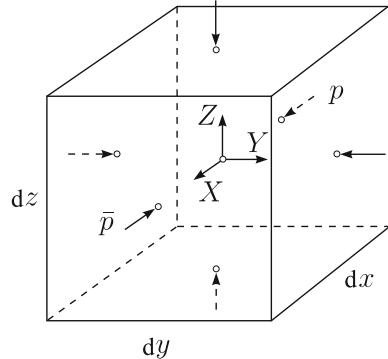
The hydrostatic pressure is therefore independent of the orientation of the surface element and a scalar valued function of space. The stress state in a fluid or gas at rest is therefore known once the pressure $p(\boldsymbol{x})$ is known in dependence of the space variable.

The physical dimension for the pressure is force per unit area, viz., $[p] = [FL^{-2}]$; in the International System of Units it is measured in Pascal [Pa], whereby $1\,\text{Pa} = 1\,\text{N}\,\text{m}^{-2}$. Other, less common and older units are collected in **Table 2.1**.

2.3 Fundamental Equation of Hydrostatics

The basis for the derivation of the fundamental equation of hydrostatics has already been laid down in the last subsection, the force and moment conditions (2.3) were written down for the forces applied on the body with volume V and boundary ∂V. Since according to the cutting principle the force and moment condition can be applied to any volume V with boundary ∂V, we consider in **Fig. 2.5** a fluid element with the shape of a cube with side lengths $\mathrm{d}x, \mathrm{d}y, \mathrm{d}z$. In this volume element also forces which are of third order small are now taken into account. Such a force is the specific body force $\boldsymbol{k} = (k_x, k_y, k_z)$. To third order accuracy $\boldsymbol{k}$ may be assumed to

Fig. 2.5 Pressure and body force. *Elementary cube with side lengths* dx, dy, dz, *loaded by the body forces* $X = \rho k_x$, $Y = \rho k_y$, $Z = \rho k_z$ *and the pressure* $p(\boldsymbol{x})$

apply at the center of gravity of the elementary cube; it consists in most cases just of the specific gravity force and gives rise to the components

$$(\rho k_x, \rho k_y, \rho k_z)\, dx dy dz. \tag{2.10}$$

Moreover, the differences of the wetting forces at opposite side areas must now be accounted for. For example, at the sides perpendicular to the x-axis one has the cutting forces

$$p\, dy dz, \qquad \bar{p}\, dy dz = \left(p + \frac{\partial p}{\partial x} dx \right) dy dz. \tag{2.11}$$

Force equilibrium in the x-, y-, z-directions yields

$$\rho k_x\, dx dy dz - \left(p + \frac{\partial p}{\partial x} dx \right) dy dz + p\, dy dz = 0,$$

$$\rho k_y\, dx dy dz - \left(p + \frac{\partial p}{\partial y} dy \right) dy dz + p\, dz dx = 0, \tag{2.12}$$

$$\rho k_z\, dx dy dz - \left(p + \frac{\partial p}{\partial z} dz \right) dx dy + p\, dx dy = 0,$$

from which one easily deduces

$$\frac{\partial p}{\partial x} = \rho k_x, \qquad \frac{\partial p}{\partial y} = \rho k_y, \qquad \frac{\partial p}{\partial z} = \rho k_z, \tag{2.13}$$

equations, which connect the fluid pressure with the specific body force. Equations (2.13) can be summarized by the vector equation

$$\operatorname{grad} p = \rho \boldsymbol{k}, \tag{2.14}$$

an equation which is known as the **fundamental hydrostatic equation**. According to this equation the largest pressure rise points into the direction of the specific body force. Before proceeding with the general theory, let us add a few comments, related to the derivation of (2.14).

- By using the partial derivative in the derivation of (2.11) it was tacitly assumed that the pressure field is differentiable. Indeed, the expression for $\bar{p}$ in $(2.11)_2$ is a truncated Taylor series expansion of order 1 in the x-direction.
- The equilibrium condition for the forces must also be complemented by the equilibrium condition for the moments, and this can be done relative to the center of the cube. The moment of the specific body force, which does not exactly attack at the center, is of fourth order small and can be ignored. The same is true for the moments of the surface forces. The reader may become convinced about this by considering the pressure forces with points of attack, which do not lie in the centers of the surface rectangles. The only terms, which then arise in the momentum condition, are of fourth order small. It follows that the moment condition is automatically satisfied with the satisfaction of the fundamental hydrostatic equation.

Finally, we remark that the fundamental hydrodynamic equations can equally be derived with the above employed procedure. This will be done in the next chapter; here, we only note that owing to the **principle of d'Alembert** one simply needs to complement the specific body force by D'ALEMBERT's **inertial force**.[3] The latter can be written in the form $-\rho\boldsymbol{b}$, where $\boldsymbol{b}$ is the acceleration vector. Thus, Eq. (2.14) assumes the more general form

$$\operatorname{grad} p = \rho(\boldsymbol{k} - \boldsymbol{b}) \tag{2.15}$$

and holds in this form for moving accelerating fluids, provided the state of stress can also be reduced to a pure pressure.

The fundamental hydrostatic equations (2.14) can elegantly be derived, if the Gauss law is used in Eqs. (2.1) and (2.2). Indeed, with

$$\boldsymbol{K}_O = \int_{\partial V} \boldsymbol{t_n} \, \mathrm{d}A = -\int_{\partial V} p\boldsymbol{n} \, \mathrm{d}A = -\int_V \operatorname{grad} p \, \mathrm{d}V,$$

$$\boldsymbol{M}_O = \int_{\partial V} \boldsymbol{x} \times \boldsymbol{t_n} \, \mathrm{d}A = -\int_{\partial V} \boldsymbol{x} \times p\boldsymbol{n} \, \mathrm{d}A = -\int_V \boldsymbol{x} \times \operatorname{grad} p \, \mathrm{d}V, \tag{2.16}$$

---

[3] JEAN LE ROND D'ALEMBERT (1717–1783), mathematician, physicist and philosopher. In mechanics he is best known for his principle, according to which mass times acceleration can be replaced by the inertial force as stated above.

Eq. (2.3) take the forms

$$\int\limits_{V} (\rho \boldsymbol{k} - \operatorname{grad} p)\, \mathrm{d}V = \boldsymbol{0} \,,$$

$$\int\limits_{V} \big(\boldsymbol{x} \times (\rho \boldsymbol{k} - \operatorname{grad} p)\big)\, \mathrm{d}V = \boldsymbol{0} \tag{2.17}$$

and are satisfied for an arbitrary, in particular an infinitely small volume, provided the integrand functions in (2.17) vanish. This requirement implies (2.14). On the other hand, the fundamental hydrostatic equation (2.14) implies that equations (2.17) are automatically satisfied. The derivation also implies that satisfaction of $(2.17)_1$ automatically leads to satisfaction of $(2.17)_2$: 'Equilibrium of the forces guarantees equilibrium of the moments'.

Forming the curl of both sides of (2.14) yields

$$\operatorname{curl} (\rho \boldsymbol{k}) = 0. \tag{2.18}$$

Thus, the liquid or gas is only at rest if the body force $\rho \boldsymbol{k}$ is **irrotational** or free of vorticity. If one introduces with

$$-\operatorname{grad} \Psi = \rho \boldsymbol{k}$$

the potential of the body force, Ψ, Eq. (2.14) takes the form

$$\operatorname{grad} (p + \Psi) = 0. \tag{2.19}$$

This equation expresses the fact that the sum $p + \Psi$ must have a constant value, c,

$$p + \Psi = c. \tag{2.20}$$

Equipotential surfaces for Ψ are the same surfaces as those of constant pressure.
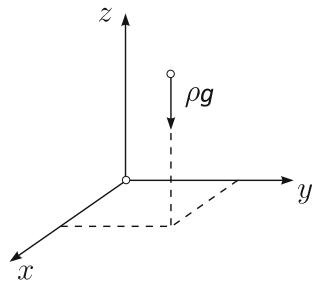
For the gravity field we have $\boldsymbol{k} = -g\boldsymbol{e}_z$, where g is the gravity constant and $\boldsymbol{e}_z$ the unit vector against gravity, see **Fig. 2.6**. Equation (2.14) then yields

$$\frac{\partial p}{\partial x} = \frac{\partial p}{\partial y} = 0, \quad \frac{\partial p}{\partial z} = -\rho g, \tag{2.21}$$

so that the pressure is only a function of z : $p = p(z)$. The third equation of (2.21) is thus only integrable, if the density ρ is equally at most a function of z : $\rho = \rho(z)$, so that

$$p(z) = p_0 - \int\limits_{z_0}^{z} (\rho g)(\bar{z})\, \mathrm{d}\bar{z}, \tag{2.22}$$

Fig. 2.6 Gravity field for a constant ***g*** *Gravity field with body force* $-\rho\boldsymbol{g}$ *in the negative z-direction. The coordinate system is Cartesian and* ***g*** *is constant*

which simplifies for a density preserving fluid to

$$p(z) = p_0 - \rho g(z - z_0). \tag{2.23}$$

Surfaces of constant pressure are the planes $z = $ const.

In general, one needs for a fluid for unique determination of the pressure not only a functional equation but also a relation between density, pressure and temperature, $p = p(\rho, T)$; this is the **thermal equation of state**. If the variation of the temperature is small and can be ignored, then $p = p(\rho)$. These are material equations and identify different sorts of fluids. Two special cases are

- the *density preserving fluid* with $\rho = $ const.,
- the *barotropic* or *elastic fluid* with $p = p(\rho)$.

Here, the first can be regarded as a special case of the second. For these two cases some basic problems of hydrostatics will now be analyzed.

2.4   Pressure Distribution in a Density Preserving Heavy Fluid

According to Eq. (2.23), the fluid pressure in a density preserving fluid at equilibrium is a linear function of the vertical coordinate. If, for instance a vessel of arbitrary shape, **Fig. 2.7**, is filled with a density preserving fluid and inserted in a gas (air), which can be regarded as incompressible, then a wall element at depth z is subject to two pressures. From the inside the force $p(z)\,\mathrm{d}A$ is acting, whilst $p_0\,\mathrm{d}A$ is acting from the outside, where p_0 is the atmospheric pressure, which may in many situations be assumed to be constant, because the density of the gas and therefore also the pressure variation in the vertical direction are negligibly small. The resulting force onto the wall element has the direction of the exterior unit vector and the modulus

$$\mathrm{d}P = (p - p_0)\,\mathrm{d}A = \rho gz\,\mathrm{d}A. \tag{2.24}$$

Fig. 2.7 Force onto a wall of a container. *Arbitrary vessel with surface element* dA *and exterior unit normal vector* ***n*** *of the wall of the vessel. The pressure inside is given by* p, *that outside is given by* p_0
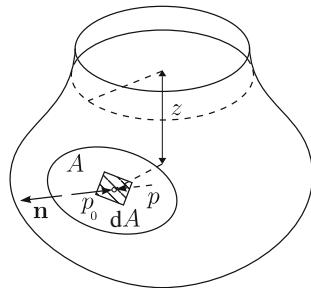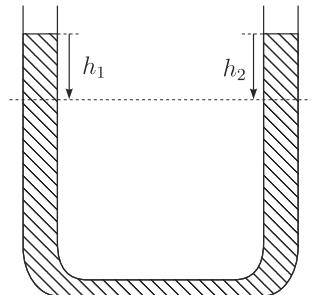
Fig. 2.8 Communicating vessel. *In a communicating vessel the free surfaces of its arms are at the same height*

The resultant of the elementary pressure forces acting on a given partial area A is obtained by reducing all these forces to a single force and possibly a moment in an arbitrary point.

In a communicating vessel, **Fig. 2.8**, the pressures at depth h_1 in the left arm and h_2 in the right arm can be computed with the aid of (2.23); because the two reference points are at the same height, their pressures are the same so,

$$\rho g h_1 = \rho g h_2 \quad \Rightarrow \quad h_1 = h_2. \tag{2.25}$$

In other words: a density preserving fluid in two communicating vessels is only in equilibrium, if both free surfaces are at the same level. Incidentally, this argument can easily be extended to a whole series of communicating vessels.

Equation (2.24) also explains the so-called **Pascal paradox**.[4] To explain it, consider **Fig. 2.10**, in which three vessels, symmetric to their mid plumb line and with the same basal surface but different volumes are shown. The resultant force of the fluid pressure exerted on the basal surface is in the three cases the same, namely a single force acting on the symmetry axis, $p = \rho g h A$, directed downward. For vessels with *freely movable* base, the force $F = P$ would have to be applied to hold the bottom surface at rest, irrespective of the total weight of the fluid contained in the vessel. If on the other hand, each arrangement is weighted, the three arrangements obviously

---

[4]BLAISE PASCAL (1623–1662), French mathematician and physicist. He is known for his paradox and the 'Pascal triangle'. For his short biography see **Fig. 2.9**

have different weights. The reasons are the on-loading (Fig. 2.10d) and de-loading (Fig. 2.10e, f) effects of the fluid pressure on the respective walls.

Fig. 2.9 BLAISE PASCAL (19. June 1623–19. Aug. 1662)

BLAISE PASCAL was a French mathematician, physicist, literary man and Christian philosopher. His earliest work was in the natural and applied sciences where he made important contributions to the study of fluids and clarified the concepts of pressure and vacuum by generalizing work of EVANGELISTA TORRICELLI (1608–1647). In 1642, still as a teenager he started pioneering work on calculating machines called Pascalins and finished several of these. He is known in hydrostatics for his paradox, see Fig. 2.10, and in mathematics via his 'Traité du triangle arithmétique' (1653) for the PASCAL Triangle, a tabular presentation for the binomial coefficients

$$
\begin{array}{ccccccccccc}
 & & & & & 1 & & & & & \\
 & & & & 1 & & 1 & & & & \\
 & & & 1 & & 2 & & 1 & & & \\
 & & 1 & & 3 & & 3 & & 1 & & \\
 & 1 & & 4 & & 6 & & 4 & & 1 & \\
1 & & 5 & & 10 & & 10 & & 5 & & 1 \\
\end{array}
$$

The text is based on http://www.wikipedia.org

In **hydraulic presses** the hydrostatic pressure is used to lift large weights with small forces. **Figure. 2.11** explains the principle of such a press machine. The forces F_1 and F_2, which are applied to the platforms A_1 and A_2, respectively, generate immediately below the platforms the pressures $p_1 = F_1/A_1$ and $p_2 = F_2/A_2$. The oil in the communicating vessel with density ρ is in equilibrium, provided

$$
\frac{F_1}{A_1} = \frac{F_2}{A_2} + \rho g h, \tag{2.26}
$$

where h is the level difference between the platforms. In the practice of hydraulic presses we have $\rho g h \ll F_2/A_2$, so that with sufficient accuracy we have
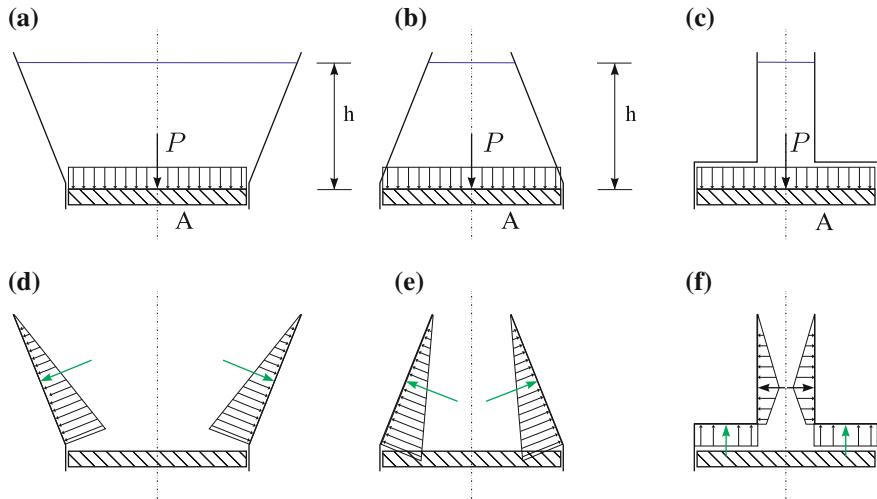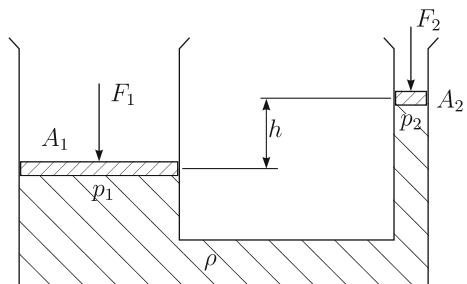
Fig. 2.10 Pascal paradox. *Three vessels, symmetric to their mid plumb line and with identical basal surfaces A but different volumes. In panels* (**a**), (**b**) *and* (**c**) *the pressures are shown which are exerted on the basal surface, all equal, whilst panels* (**d**), (**e**) *and* (**f**) *show the pressure distributions on the walls*

Fig. 2.11 Hydraulic press. *A load F_1 put on a large platform A_1 can be lifted with a small force F_2 on a small platform A_2*
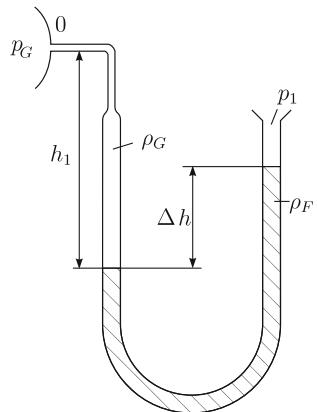
$$\frac{F_1}{A_1} \cong \frac{F_2}{A_2} \quad \text{or} \quad \frac{A_1}{A_2} \cong \frac{F_1}{F_2} \quad \text{or} \quad F_1 \cong \frac{A_1}{A_2} F_2. \tag{2.27}$$

With $A_1 \gg A_2$ the hydraulic press allows to lift a large force F_1 with the application of a small force F_2. We mention, the above calculation assumes a quasi-static lift operation, in which accelerations can be ignored; needless to say that F_1 and F_2 contain the weights of the platforms.

U-tubes or **U-shaped manometers** are essentially also communicating vessels. The arrangement of **Fig. 2.12** allows determination of the gas pressure at the connecting point of the manometer with the gas vessel by measuring the level difference Δh of the free surfaces in the two arms of the manometer with density ρ_F. Indeed,

Fig. 2.12 U-tube
manometer. *The pressure p_G*
in the gas-container can be
determined by measuring the
displacement Δh of the
manometer fluid with density
ρ_F and the external
pressure p_1

if one measures in the two arms the pressure at the lower of the menisci, once from
the gas container and once from the right arm, one obtains, see Fig. 2.12,

$$p_G + \rho_G g h_1 \quad \text{and} \quad p_1 + \rho_F g \Delta h. \qquad (2.28)$$

The two expressions must be equal, so that

$$p_G = p_1 + \rho_F g \Delta h \left(1 - \frac{\rho_G h_1}{\rho_F \Delta h} \right). \qquad (2.29)$$

Since $\rho_G / \rho_F \ll 1$, this yields approximately

$$p_G - p_1 = \rho_F g \Delta h. \qquad (2.30)$$

The pressure difference between the interior of the gas container and its exterior (the
atmosphere) is approximately equal to the weight of the displaced manometer fluid.

To *measure small pressure differences* the type of manometer sketched in **Fig. 2.13**
can be used. It is a communicating vessel that is filled with two immiscible fluids
of different densities. For the determination of the pressure, it is necessary that the
meniscus, i.e., interface of the two fluids is positioned in the thin tube-like part of
the U-tube, and that it does not leave this part during the experiment. Let us assume
that the two cylindrical containers possess the same cross section A and that the
connecting tube has a cross sectional area given by a. Moreover, it is assumed that
the two fluids with pressures p_1 and p_2 and position of the meniscus at $\mathcal{M}_0$ are in
equilibrium (panel (a) in Fig. 2.13). For this arrangement we then have

$$p_1 + \rho_1 g h_1 = p_2 + \rho_2 g h_2. \qquad (2.31)$$

With appropriate valves it can be achieved that always the same position $\mathcal{M}_0$
defines this equilibrium. If then the pressure p_2 is increased by Δp, the position $\mathcal{M}_0$
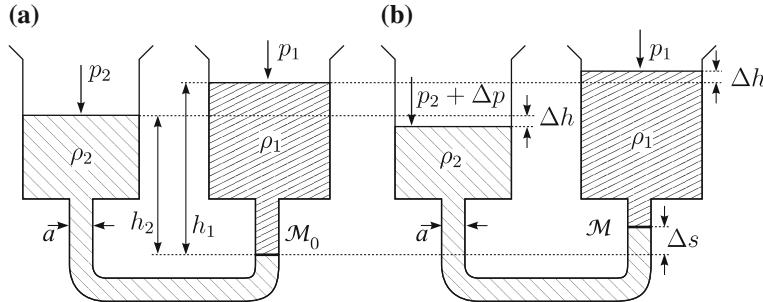
Fig. 2.13 U-tube manometer for the measurement of small pressure differences. *The manometer is filled with fluids of different density $\rho_1 < \rho_2$. In panel (**a**) it is shown when the two fluids are in equilibrium. Panel (**b**) shows the displaced configuration when Δp is applied in the left container*

of the meniscus will be displaced by the amount Δs into position $\mathcal{M}$. Because of the supposed density preserving of the two fluids, the free surfaces in the two cylinders will also be shifted by the amount Δh. Mass balance also requests that

$$A\Delta h = a\Delta s. \tag{2.32}$$

Finally, the pressure at the new position of the meniscus $\mathcal{M}$ can be computed for the left and right arms and must be equal to one another. This yields

$$p_1 + \rho_1 g(h_1 + \Delta h - \Delta s) = p_2 + \Delta p + \rho_2 g(h_2 - \Delta h - \Delta s). \tag{2.33}$$

With the aid of (2.31) this equation reduces to

$$\rho_1 g(\Delta h - \Delta s) = \Delta p - \rho_2 g(\Delta h + \Delta s), \tag{2.34}$$

which, owing to (2.32), can be transformed into
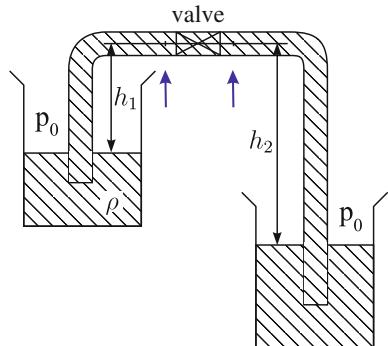
$$\Delta s = \frac{\Delta p}{\rho_2 g}\left(\frac{\rho_2 - \rho_1}{\rho_2} + \frac{\rho_2 + \rho_1}{\rho_2}\frac{a}{A}\right)^{-1} = \left(\frac{\Delta p}{\rho_2 g}\right)\underbrace{\frac{1}{\epsilon(1-\eta) + 2\eta}}_{[(1)]} \tag{2.35}$$

with

$$\epsilon := \frac{\rho_2 - \rho_1}{\rho_2} \quad \text{and} \quad \eta = \frac{a}{A}.$$

It is seen that Δs is independent of the absolute pressures p_1 and p_2. The quantities ϵ and η are generally small, implying that the factor $[(1)]$ in (2.35) is large relative to '1'. Consequently, even small pressure differences Δp may generate large displacements Δs. If one chooses $\eta \ll \epsilon$, then the displacement Δs is essentially determined by

Fig. 2.14 Hydraulic heaver.
The fluid in the hydraulic
heaver can be at rest in the
displayed position if the
valve is closed; else, a
volume flow sets in from the
upper to the lower container

the relative density difference. If on the other hand, $\epsilon \ll \eta$, then the relative density difference does not influence Δs but rather the ratio of the areas, η.

In a **hydraulic heaver** two containers, filled with a density preserving fluid and free surface at different levels, may be connected with a U-tube as shown in **Fig. 2.14**. It is assumed that initially the U-tube is equally filled with the fluid and that the valve is closed. With the notations of Fig. 2.14 the pressures left and right of the valve are given by, see (2.23),

$$p_1 = p_0 - \rho\, g h_1, \qquad p_2 = p_0 - \rho\, g h_2, \tag{2.36}$$

so that the pressure difference is given by

$$p_1 - p_2 = \rho g(h_2 - h_1) > 0. \tag{2.37}$$

This says, there is a pressure difference (gradient) from the container with higher free surface to that with lower free surface, which is reduced after opening the valve by fluid flow into the container with the lower free surface.

For the determination of the *fluid pressure onto plane* (not necessarily vertical) *walls*, it is advantageous to use a coordinate system with origin, which is the intersecting point between the plane free water surface and the direction of steepest descent, see **Fig. 2.15**. If the vertical coordinate through this point is denoted by z, then the resulting pressure force, applied on a partial surface A can be written as

$$F = \int_A (p - p_0)\, \mathrm{d}A = \rho\, g \sin\alpha \int_A y\, \mathrm{d}A = \rho\, g \sin\alpha\, y_C A, \tag{2.38}$$

in which

$$y_C = \frac{1}{A} \int_A y\, \mathrm{d}A \tag{2.39}$$

(a) **(b)**
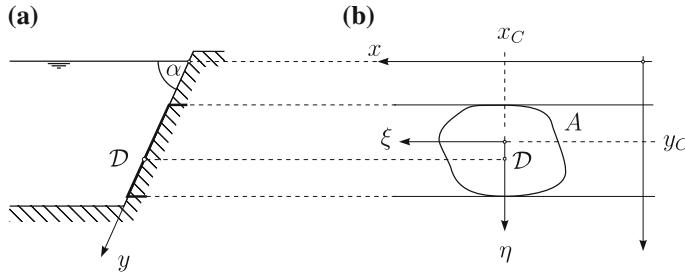
Fig. 2.15 Fluid pressure onto a plane wall inclined by the angle α. (**a**) *View of a container with plane wall, onto which the resulting pressure force, applied onto domain $\mathcal{D}$ (shown as heavy line) is to be determined.* (**b**) *Normal view onto the inclined wall with domain $\mathcal{D}$ of area A, for which the resulting force is to be determined. The x-coordinate lies in the water line, whereas the y-coordinate is in the direction of steepest descent. The origin of the (ξ, η) coordinates is in the center of the area A*

denotes the y-coordinate of the center of the area A. The total pressure force acting on area A equals the product of the area with its resultant pressure force acting on the center of A. In order to find the **center of pressure** $\mathcal{D}$ with the coordinates $(x_{\mathcal{D}}, y_{\mathcal{D}})$ one computes the balance of the static moment of the total force F and equates this to the sum of the static moments of the infinitesimal pressure forces $\mathrm{d}p = p\,\mathrm{d}A$ with respect to the coordinate axes; this argument leads to the two equations

$$x_{\mathcal{D}} F = \int_A x(\rho g \sin \alpha\, y)\,\mathrm{d}A = \rho g \sin \alpha \int_A xy\,\mathrm{d}A,$$
$$y_{\mathcal{D}} F = \int_A y(\rho g \sin \alpha\, y)\,\mathrm{d}A = \rho g \sin \alpha \int_A y^2\,\mathrm{d}A. \tag{2.40}$$
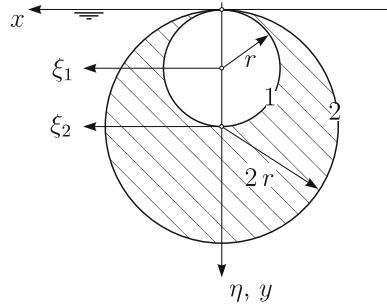
The two integrals on the far right,

$$I_x = \int_A y^2\,\mathrm{d}A, \qquad C_{xy} = -\int_A xy\,\mathrm{d}A, \tag{2.41}$$

only depend on the form and size of the area A, and are called **moments of inertia** of the area with respect to the coordinates x and y. With these denotations and with (2.38) one obtains

$$x_{\mathcal{D}} = \frac{C_{xy}}{y_C A}, \qquad y_{\mathcal{D}} = \frac{I_x}{y_C A}. \tag{2.42}$$

Fig. 2.16 Center of pressure. *Computation of the center of pressure for a moon-like plate*

If one, finally, introduces the moments of inertia with respect to the coordinates through the center of the area A, I_ξ and $C_{\xi\eta}$, and uses the so-called STEINER formulas

$$I_x = I_\xi + y_C^2 A, \qquad C_{xy} = C_{\xi\eta} - y_C x_C A, \qquad (2.43)$$

one obtains

$$x_\mathcal{D} = x_C - \frac{C_{\xi\eta}}{y_C A}, \qquad y_\mathcal{D} = y_C + \frac{I_\xi}{y_C A}. \qquad (2.44)$$

Because I_ξ is always positive the center of pressure $y_\mathcal{D}$ always lies below the center of the area, y_C. Moreover, if A is symmetric with respect to the η-axis, then $C_{\xi\eta} = 0$ and, consequently, $x_\mathcal{D} = x_C$.

Let A be a rectangle with side lengths a and b of which the η-axis agrees with the symmetry axis of the rectangle. Then, $F = \rho g a b y_s$ and $I_\xi = ab^3/12$, so that

$$x_\mathcal{D} = x_C, \qquad y_\mathcal{D} = y_C + \frac{b^2}{12 y_C}. \qquad (2.45)$$

Finally, let us compute the center of pressure for the shaded area of **Fig. 2.16**, formed by two circles, of which the highest points touch the free surface, and lying in a vertical plane. The example illustrates how one can avoid the complicated computations of the moment of inertia I_ξ by employing the moment of inertia for the centers of the circles and the shifting rules of STEINER. It is clear that the center of pressure must lie on the symmetry line (the η- and y-axes). In these coordinates $C_{\xi\eta} = 0$. If one composes the moon-like area by circles and determines pressure centers of the circles individually, then simple computations suffice. Let the subscripts 1 and 2 stand for the small and large circles, respectively. With reference to Fig. 2.16 the resultant pressure forces onto the individual circular disks are (see formulas (2.40))

$$F_1 = \rho g r^3 \pi, \qquad F_2 = 8 \rho g r^3 \pi. \qquad (2.46)$$

With the moments of inertia relative to the centers of the circles given by[5]

$$I_{\xi_1} = \frac{1}{4}\pi r^4, \qquad I_{\xi_2} = 4\pi r^4, \tag{2.47}$$

one obtains with the aid of $(2.44)_2$

$$y_{D_1} = r + \frac{\pi r^4}{4}\frac{1}{\pi r^3} = \frac{5}{4}r, \qquad y_{D_2} = \frac{5}{2}r. \tag{2.48}$$

To obtain the pressure center of the composed disk (large circle minus small circle) one now expresses the following statement:

| Static moment of the difference pressure force $F_2 - F_1 = 7\rho g r^3 \pi$ with respect to the x-axis | = | Difference of the static moments of the pressure forces onto the individual disks with respect to the x-axis |

or

$$\left\{(7\rho g r^3 \pi)y_D\right\} = \left\{-(\rho g r^3 \pi)\frac{5}{4}r + (8\rho g r^3 \pi)\frac{5}{2}r\right\},$$
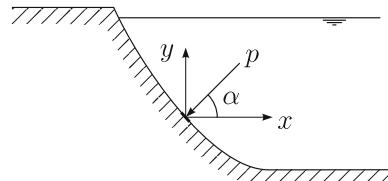
which implies

$$y_D = \frac{75}{28}r = 2.68r. \tag{2.49}$$

Incidentally, the center of mass of the moon-like disk is at $y_C = \frac{7}{3}r = 2.33r$ and thus, as expected, above the pressure center.

Evaluation of the resulting pressure force on curved walls is similarly conducted. In such computations the pressure, which is perpendicular to the areal increment dA must be decomposed into components parallel to the Cartesian coordinates and only

Fig. 2.17 Fluid pressure acting on curved surface

---

[5]Note I_{ξ_1} for a circle is half of the polar moment of inertia, which is given by $I_0 = \int_A r^2 r dr d\phi = 2\pi \int_A r^3 dr = \frac{1}{2}\pi r^4$.
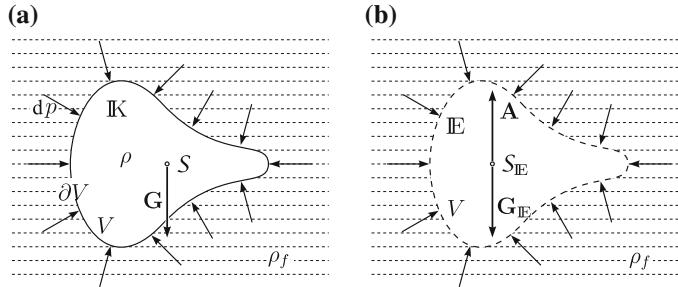
Fig. 2.18 ARCHIMEDES' principle. (**a**) *A rigid body* $\mathbb{K}$ *with volume V and boundary* ∂V, *completely immersed in a density preserving fluid loaded by the pressures p and gravity force* **G** *with point of attack* $\mathcal{S}$. (**b**) *Replacement of the original body by the body* $\mathbb{E}$ *with center of gravity* $\mathcal{S}_{\mathbb{E}}$, *consisting of the fluid and loaded by the external pressures and the gravity force* $\boldsymbol{G}_{\mathbb{E}}$. *The resultant force of the pressures applied at the surface can be summarized as the buoyancy force* **A** *which equilibrates the weight* $\boldsymbol{G}_{\mathbb{E}}$. *So,* $|A| = |G|$ *and* **A** *and* $\boldsymbol{G}_{\mathbb{E}}$ *are in opposite directions*

afterward the resultants of the components are computed. With reference to **Fig. 2.17** this yields

$$F_x = \int_A p(y) \cos \alpha \, \mathrm{d}A, \qquad F_y = \int_A p(y) \sin \alpha \, \mathrm{d}A. \qquad (2.50)$$

Often these integrations can be avoided, e.g. by applying the ARCHIMEDEan principle (see below).

2.5 Hydrostatic Buoyancy of Floating Bodies

Consider an arbitrary, rigid body $\mathbb{K}$ completely immersed in an incompressible fluid of density ρ_f, **Fig. 2.18**a, and floating. Among the external forces acting on this body are (i) the gravity forces, applied in each volume element, but which can be summed to the resultant weight and whose point of attack is the gravity center $\mathcal{S}$ and (ii) the elementary pressures acting on the body surface. Using the methods introduced in the last subsection these pressures can be composed to a single force. This computation will be performed below; however, here we wish to first demonstrate the result using a trick, which is attributed to ARCHMEDES.[6]

---

[6]ARCHMEDES (∼287 B.C.–212 B.C.) ancient Greek mathematician, physicist and engineer, founder of hydrostatic and geometric statics. For his short biography see **Fig. 2.19**.
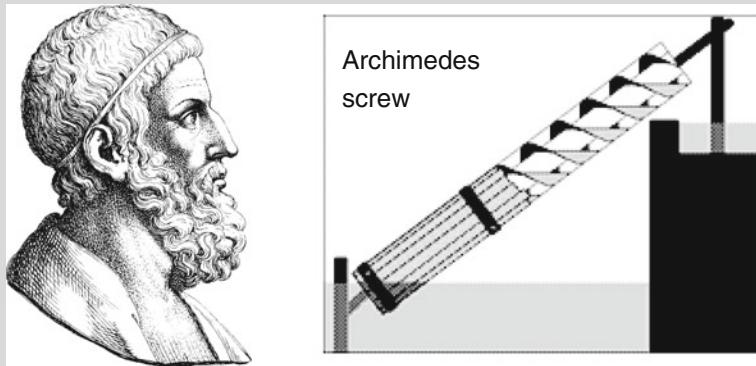
Fig. 2.19 ARCHIMEDES (∼287 BC–∼212 BC)
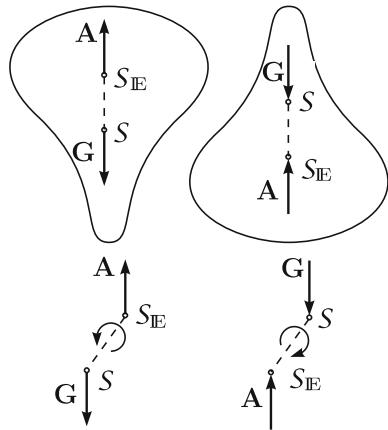
Detail of an antique engraved portrait of ARCHIMEDES and his screw

Famous ancient Greek mathematician and inventor, ARCHIMEDES lived ca. 290–280 BC in Syracuse (Sicily). The truth of this statement is seriously questioned in the modern historical literature [1]. The most commonly related story about ARCHIMEDES tells how he invented a method for measuring the volume of an object with an irregular shape. According to VITRUVIUS, a new crown in the shape of a laurel wreath had been made for King HIERON II, and ARCHIMEDES was asked to determine whether it was of solid gold, or whether silver had been added by a dishonest goldsmith. ARCHIMEDES had to solve the problem without damaging the crown, so he could not melt it down in order to measure its density as a cube, which would have been the simplest solution. While taking a bath, he noticed that the level of the water rose as he got in. He realized that this effect could be used to determine the volume of the crown, and therefore its density after weighing it. The density of the crown would be lower if cheaper and less dense metals had been added. He then went to the streets naked, so excited by his discovery that he had forgotten to dress, exclamating 'Eureka!' 'I have found it!'. The story about the golden crown does not appear in the known works of ARCHIMEDES and its truth is seriously questioned in the modern literature [1], but in his treatise *On Floating Bodies* he gives the principle known in hydrostatics as ARCHIMEDES' *Principle*. This states that a body immersed in a fluid experiences a buoyant force equal to the weight of the displaced fluid.

A large part of ARCHIMEDES' work in engineering arose from fulfilling the needs of his home city of Syracuse. The Greek writer ATHENAEUS of Naucratis described how King HIERON II commissioned ARCHIMEDES to design a huge ship, the *Syracusia*, which could be used for luxury travel, carrying supplies, and as a naval warship. The *Syracusia* is said to have been the largest ship built in classical antiquity. According to ATHENAEUS, it was capable of carrying 600 people and included garden decorations, a gymnasium and a temple dedicated to the goddess Aphrodite among its facilities. Since a ship of this size would leak a considerable amount of water through the hull, the ARCHIMEDES screw was purportedly developed in order to remove the bilge water. It was turned by hand, and could also be used to transfer water from a low-lying body of water into irrigation canals. The ARCHIMEDES screw described in Roman times by VITRUVIUS may have been an improvement on a screw pump that was used to irrigate the Hanging Gardens of Babylon.

The text is based on http://www.wikipedia.org and http://www.brown.edu

Fig. 2.20 Equilibrium
positions. *Defining stable
and unstable equilibrium
configurations: If $\mathcal{S}_{\mathbb{E}}$ lies
above $\mathcal{S}$ (panel at the left)
the equilibrium configuration
is stable, else it is called
unstable (panel at the right)*

Because the body is floating in the fluid one may cut it out in imagination and replace it by any other body, hence e.g. the fluid itself, Fig. 2.18b. This replaced body $\mathbb{E}$ has the same volume V and the same weight $\boldsymbol{G}_{\mathbb{E}} = \rho_f g V \boldsymbol{e}_z$ in a center of gravity which may differ from the center of gravity $\mathcal{S}$ of $\mathbb{K}$. Since the fluid replacement body is at rest, the pressure distributions, which are the same for $\mathbb{K}$ and $\mathbb{E}$ can be reduced to a single force pointing upward, the so-called **buoyancy force A** with the modulus
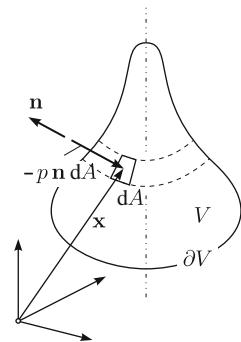
$$A = \rho_f g V. \tag{2.51}$$

This argument shows that the pressures acting on the body $\mathbb{K}$ can be reduced to a force with vertical line of action. Moreover, it is now clear that a rigid body immersed in a density preserving fluid and floating in there, can only be in equilibrium if (i) $\boldsymbol{G} = -\boldsymbol{A}$ and (ii) if the centers of gravity $\mathcal{S}$ of $\mathbb{K}$ and $\mathcal{S}_{\mathbb{E}}$ of $\mathbb{E}$ lie on a vertical line. Such an **equilibrium configuration** is **stable**, if $\mathcal{S}_{\mathbb{E}}$ lies above $\mathcal{S}$ and it is unstable, when $\mathcal{S}_{\mathbb{E}}$ lies below $\mathcal{S}$, see **Fig. 2.20**. Indeed, a small deviation from the equilibrium configuration (by a small rotation) causes a moment, driving the body back into the equilibrium in the first case, but further away from it in the second case. Incidentally, it is quite obvious that for $\mathcal{S}_{\mathbb{E}} = \mathcal{S}$ every orientation of the body is an equilibrium configuration; in this case the equilibrium configurations are called **indifferent**.

The ARCHIMEDEan buoyancy force formula (2.51) can quite easily be derived, if the Gauss law is used. With reference to **Fig. 2.21**, we may write

$$\boldsymbol{A} = -\int_{\partial V} p\boldsymbol{n} \, \mathrm{d}A \overset{(\text{Gauss})}{=} -\int_V \operatorname{grad} p \, \mathrm{d}V$$

$$= -\int_V \operatorname{grad}(p_0 - \rho_f g z) \, \mathrm{d}V = \rho_f g \boldsymbol{e}_z \int_V \mathrm{d}V = \rho_f g V \boldsymbol{e}_z, \tag{2.52}$$

Fig. 2.21 Explaining the derivation of the ARCHIMEDEan buoyancy force formula

in which e_z is a unit vector in the z-direction. The point of attack of the buoyancy force can correspondingly be derived from the moment condition, formulated with respect to the origin of the coordinate system. Accordingly, this can be expressed as

Static moment of the buoyancy force with respect to the origin of the coordinate system	$=$	Sum of all static moments of the infinitesimal pressures at the body surface with respect to the origin of the coordinate system.

If one denotes by $\boldsymbol{x}_A$ the position vector of the point of attack of $\boldsymbol{A}$, the above statement reads
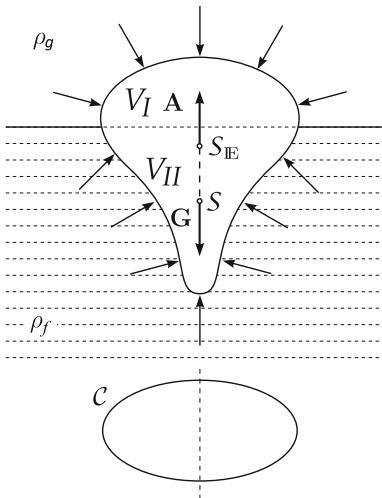
$$\boldsymbol{x}_A \times \rho_f g V \boldsymbol{e}_z = -\int_{\partial V} \boldsymbol{x} \times p\boldsymbol{n}\, \mathrm{d}A \stackrel{\text{(Gauss)}}{=} -\int_V \boldsymbol{x} \times \operatorname{grad} p\, \mathrm{d}V$$

$$= -\int_V \boldsymbol{x} \times \operatorname{grad}(p_0 - \rho_f g z)\, \mathrm{d}V$$

$$= \int_V \boldsymbol{x} \times \rho_f g \boldsymbol{e}_z\, \mathrm{d}V = \rho_f g \left[\int_V \boldsymbol{x}\, \mathrm{d}V\right] \times \boldsymbol{e}_z,$$

which, after division by $\rho_f g V$, may also be written as

$$\left(\boldsymbol{x}_A - \underbrace{\frac{1}{V}\int_V \boldsymbol{x}\, \mathrm{d}V}_{\boldsymbol{x}_{\mathbb{E}}}\right) \times \boldsymbol{e}_z = (\boldsymbol{x}_A - \boldsymbol{x}_{\mathbb{E}}) \times \boldsymbol{e}_z = \boldsymbol{0}. \qquad (2.53)$$

The second term on the left can be interpreted as the center of gravity, $\boldsymbol{x}_{\mathbb{E}}$, of the replaced fluid as has been identified in (2.53). Because the coordinate system can be arbitrarily selected with respect to the orientation of gravity, it is concluded that (2.53) holds for all $\boldsymbol{e}_z$, so that $\boldsymbol{x}_A = \boldsymbol{x}_{\mathbb{E}}$ by necessity. The point of attack of the

Fig. 2.22 Equilibrium
position of a rigid body,
partly immersed into a fluid.
*The water line $\mathcal{C}$ is defined as
the intersection between the
body and the water surface.
The center of gravity $\mathcal{S}_\mathbb{E}$ can
be computed from the density
ρ_f of the displaced fluid*

resultant buoyancy force is therefore the center of gravity of the replaced fluid body. This corroborates the result, obtained previously in a different way.

For a body, which floats at the surface as shown in **Fig. 2.22**, curve $\mathcal{C}$, along which the body intersects the water surface, is referred to as **water line**. On the body surface above this water line the pressure is that of the air which is generally assumed to be constant. The buoyancy force can be calculated as for a fully submerged body. In this process one must, however, account for the fact that the replaced fluid is composed of two different media. It consists below the water line of a fluid with density ρ_f, above it of a gas with density ρ_g. Often the mass of the gas can be ignored ($\rho_g = 0$); in this case the buoyancy force is again given by (2.51), but V is the volume of the submerged part of the body. It agrees in this approximation with the volume of the displaced fluid.

The first equilibrium condition, namely $\boldsymbol{A} = -\boldsymbol{G}$ determines the depth of immersion; the second, according to which $\mathcal{S}$ and $\mathcal{S}_\mathbb{E}$ must both lie on a vertical line is no longer as easy to determine as with the completely submersed body, because the column of the displaced fluid is now variable and dependent upon the depth of immersion and orientation of the body. For the same reason, the stability analysis of an equilibrium position is also more complicated, as one can see from the photo of **Fig. 2.23**, in which equilibria of various cylindrical corks with different aspect ratios (side length to beam length), floating on still water are shown. Depending on the aspect ratio the stable equilibrium position may have horizontal, inclined or vertical cylinder axis.

In the subsequent paragraphs the **stability of the equilibrium position** of partly submerged bodies is analyzed, if these bodies are long in the direction perpendicular to the drawing plane and possess in their equilibrium position a symmetry plane as shown in the left panel of **Fig. 2.24**a. If this body is rotated by a small angle $\delta\phi$ about the intersection of the symmetry plane and the water surface, then the displaced
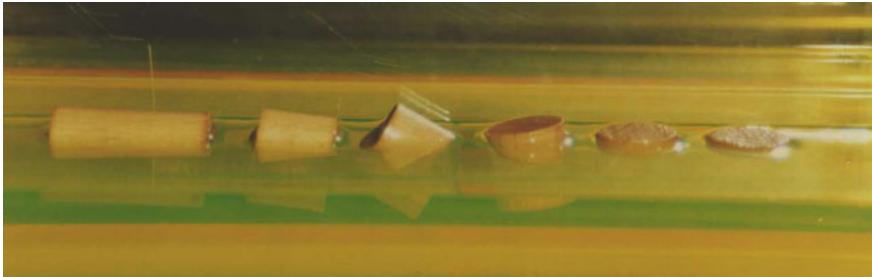
Fig. 2.23 Equilibrium positions of cylindrical corks with different aspect ratios. *A circular disk with large diameter relative to its thickness ($d \gg h$) floats stably with vertical cylinder axis. If the height is larger than the diameter of the disk ($h \gg d$) the stable equilibrium position has horizontal cylinder axis. If $h \cong d$ the stable equilibrium has inclined cylinder axis. For details see main text*
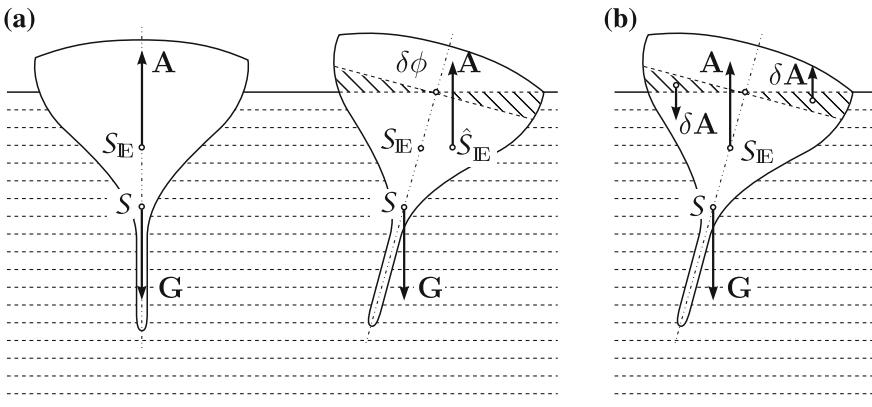
Fig. 2.24 Explaining the stability of equilibrium positions. (**a**) *Floating body, shown in its equilibrium position and a position that is rotated out of the equilibrium by an angle $\delta\phi$ with gravity force $\boldsymbol{G}$ and point of attack $\mathcal{S}$ and the centers $\mathcal{S}_{\mathbb{E}}$ and $\hat{\mathcal{S}}_{\mathbb{E}}$, respectively of the buoyancy force of the replaced body in vertical and rotated positions. (**b**) Same as in (**a**) but with buoyancy force now split into the buoyancy acting in $\mathcal{S}_{\mathbb{E}}$ and the additional incremental buoyancy forces $\delta\boldsymbol{A}$ and $-\delta\boldsymbol{A}$ due to the rotation of the body out of the equilibrium*
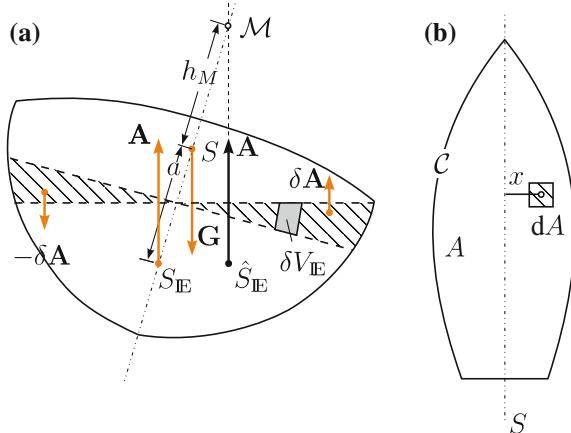
fluid experiences an increase of the buoyancy force on that side at which the body is inclined toward the water; it experiences an equal reduction of the buoyancy on the other side. As a consequence the center of gravity moves from the position $\mathcal{S}_{\mathbb{E}}$ to a position $\hat{\mathcal{S}}_{\mathbb{E}}$, see Fig. 2.24a.

If the center of gravity $\mathcal{S}$ of the body lies below $\mathcal{S}_{\mathbb{E}}$ as it is the case for yachts, then the body weight $\boldsymbol{G}$ and the displaced buoyancy force $\boldsymbol{A}$ build an erecting couple, rotating the body back to its normal floating position, which is thus stable. This can also be seen as follows, Fig. 2.24b: The buoyancy of the slightly rotated body can be composed of the force $\boldsymbol{A}$ in $\mathcal{S}_{\mathbb{E}}$ plus an infinitesimal couple ($\delta\boldsymbol{A}$, $-\delta\boldsymbol{A}$), applied at the centers of the 'triangular' shaded positions of the immersed and emerged volume

Fig. 2.25 Evaluation of the metacentric height.
(**a**) *Floating body rotated out of its equilibrium subjected to the buoyancy force A in $\mathcal{S}_{\mathbb{E}}$, and displaced A in $\hat{\mathcal{S}}_{\mathbb{E}}$. The point of intersection of the line of action of the displaced buoyancy force and the symmetry plane of the boat defines the metacenter $\mathcal{M}$.*
(**b**) *Explaining the evaluation of the areal moment of inertia for the area defined by $\mathcal{C}$*

increments. These displacements correspond to an additional buoyancy δA to the right of the body symmetry line, and a reduced buoyancy $-\delta A$ to the left of it. In this way one obtains two couples (G, A) and $(\delta A, -\delta A)$ of which in Fig. 2.24 both are working against an increase of $\delta\phi$. For most boats (e.g. dinghy, jolly-boat) the center of gravity $\mathcal{S}$ of the body lies above $\mathcal{S}_{\mathbb{E}}$. If, in this case (G, A) is again the couple formed with the buoyancy in $\mathcal{S}_{\mathbb{E}}$ and $(\delta A, -\delta A)$, that describing the effect of the displaced fluid, then only this second couple has the tendency to reduce the angle $\delta\phi$ and erect the boat. The stability now depends on the fact which of the two couples has the larger modulus. If one counts 'erecting' moments positive and if one denotes by a the distance between $\mathcal{S}$ and $\mathcal{S}_{\mathbb{E}}$, then the moment of the pair (G, A) and an infinitesimal rotation $\delta\phi$ is given by

$$\delta M_1 = Aa\delta\phi = -\rho_f g a V_{\mathbb{E}} \delta\phi, \tag{2.54}$$

where $V_{\mathbb{E}}$ is the volume of the displaced fluid. With the aid of **Fig. 2.25** the contribution of the infinitesimal replaced fluid can be represented by differential volume elements $\delta V_{\mathbb{E}} = x\delta\phi\, dA$, of which the buoyancy is given by $\rho_f g x \delta\phi\, dA$ and gives rise to the 'erecting' moment

$$\delta M_2 = \int\limits_A \rho_f g x^2 \mathrm{d}\phi\, \mathrm{d}A = \rho_f g \delta\phi \int\limits_A x^2 \, \mathrm{d}A, \tag{2.55}$$

in which A is the area of the water surface that is enclosed by the water line $\mathcal{C}$, and the integral on the far right is the areal moment of inertia of the area enclosed by $\mathcal{C}$ with respect to the symmetry line $\mathcal{S}$. If one defines

$$I_S = \int\limits_A x^2 \, \mathrm{d}A,$$

one obtains, by adding (2.54) and (2.55)

$$\delta M = \delta M_1 + \delta M_2 = \rho_f g(I_s - a V_{\mathbb{E}})\delta\phi. \tag{2.56}$$

The condition that $\delta M > 0$ and that, therefore, the boat returns to the normal equilibrium position, is

$$I_s - a V_{\mathbb{E}} \geqslant 0 \quad \text{or} \quad h_M = \frac{I_s}{V_{\mathbb{E}}} - a \geqslant 0. \tag{2.57}$$

The quantity h_M is a length; it is called the **metacentric height** and the intersection of the symmetry line with the vertical through $\hat{\mathcal{S}}_{\mathbb{E}}$ is called the **metacenter** $\mathcal{M}$. With the definition of h_M, (2.56) takes the form

$$\delta M = \left(\rho_f g V_{\mathbb{E}}\right) h_M \delta\phi = G h_M \delta\phi. \tag{2.58}$$

The stability condition (2.57) can thus also be so interpreted that one considers the couple, consisting of G and the buoyancy force A in $\mathcal{S}_{\mathbb{E}}$ and directly writes for the 'erecting' moment $\delta M = G h_M \delta\phi$. The metacentric height is therefore the distance between $\mathcal{S}$ of $\mathbb{K}$ and $\mathcal{M}$ (which is the intersection point between the line of action of the displaced buoyancy force and the symmetry line of the boat). Incidentally the higher the metacenter lies above $\mathcal{S}$, the larger is the 'erecting' moment. Practically one preferably does not make the metacenter too large in order to reduce the frequency of the oscillation of the ship in heavy sea.

As an example consider the **floating behavior of a beam**[7] of quadratic cross section with side length a and density ρ_K. Assume its length ℓ to be large in comparison to a, $\ell \gg a$, so that no stable equilibrium configuration exists with lengthwise inclination as for a cork in Fig. 2.23. The emerging mathematical problem is then plane. If the ratio of the densities of the beam, ρ_K and the fluid ρ_f is denoted by $D = \rho_K/\rho_f$, the volume of the displaced fluid is given by

$$V_{\mathbb{E}} = Da^2. \tag{2.59}$$

Apart from the trivially symmetric, and for the other values of $D \in [0, 1]$ non-symmetric, represented equilibrium positions in panel (a) of **Fig. 2.26** (top), all those equilibrium positions, which are sketched in panels (b) and (c), are possible. Concentrating for the moment on the water line in panel (b) (solid, bold), rising from the lower left to the upper right with parameterization

$$y = \lambda x + aD \tag{2.60}$$

---

[7]The computations for this example are a bit involved. In a first reading a reader may wish to simply concentrate on the physical implications of the computations.

(a)

$$0 < \lambda < 1 \qquad\qquad \lambda = 0 \qquad \lambda = 1$$

(b)

(c)
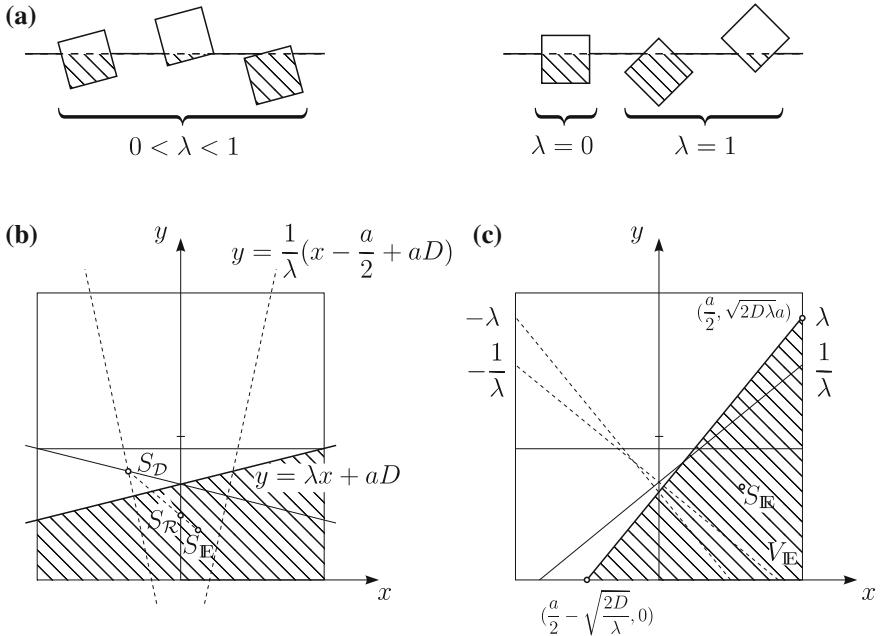
Fig. 2.26 Floating configurations of a beam with quadratic cross sections. (**a**) *Possible equilibrium positions at different values of the inclination of the water line.* (**b**) *Four different physically equivalent equilibrium positions (solid and dashed). For one case the wetted area is shown dashed.* (**c**) *Four possible additional equilibrium positions, if the wetted area is a triangle*

and yet still unknown positive slope λ, this water line intersects the vertical sides of the square, if

$$\lambda \leqslant \begin{cases} 2D, & \text{for } 0 \leqslant D \leqslant 0.5, \\ 2(1-D), & \text{for } 0.5 \leqslant D \leqslant 1. \end{cases} \tag{2.61}$$
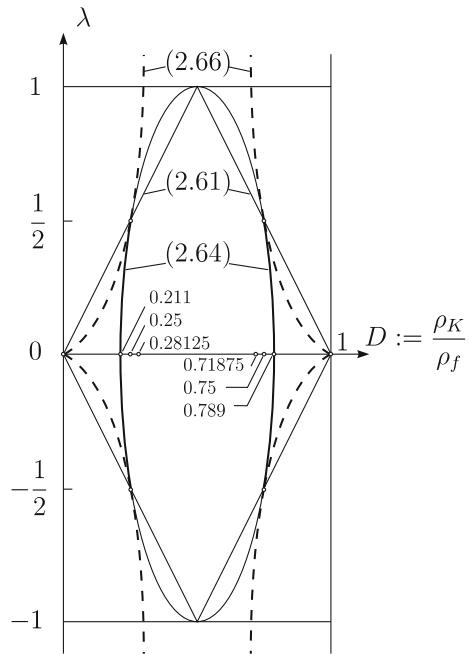
The coordinates of the center of gravity $\mathcal{S}_{\mathbb{E}}$ of the trapezoidal cross section of the displaced fluid can most easily be computed from those of the rectangle $\mathcal{S}_R$, and the triangle $\mathcal{S}_D$, both of which are indicated in Fig. 2.26b. Applying the static moments with respect to the vertical and horizontal axes shows that

$$\left(x_{\mathcal{S}_{\mathbb{E}}}, y_{\mathcal{S}_{\mathbb{E}}}\right) = \left(\frac{\lambda a}{12D}, \frac{\lambda^2 a}{24D} + \frac{aD}{2}\right). \tag{2.62}$$

To fix a value for the water-line slope λ we employ the condition that $\mathcal{S}_{\mathbb{E}}$ lies vertically below $\mathcal{S}$. To this end we write with

$$y = -\frac{1}{\lambda}\left(x - \frac{\lambda a}{12D}\right) + \frac{\lambda^2 a}{24D} + \frac{aD}{2} \tag{2.63}$$

Fig. 2.27 Water line slopes
for beams with quadratic
cross section. *Slope λ of the
water line as a function of the
density ratio $D = \rho_K / \rho_f$.
The solid, respectively
dashed, segments of ellipses
are defined in equation
(2.64) and (2.66). Equation
(2.61) constrains the domain
of validity of the two curved
segments*

that straight line, which is perpendicular to the water line (2.60), and is identically
satisfied for $x = x_{S_{\mathbb{E}}}$, $y = y_{S_{\mathbb{E}}}$ as given in (2.62). We now also request that the point $\mathcal{S}$
lies on the line (2.63), i.e., (2.63) is identically satisfied for $(x, y) = (0, a/2)$, which
leads to the equation

$$\left(\frac{D - \frac{1}{2}}{1/\sqrt{12}}\right)^2 + \lambda^2 = 1. \tag{2.64}$$

In a Cartesian coordinate system with D- and λ-axes it represents an ellipse with
center $(\frac{1}{2}, 0)$ and semi axes $a = 0.2887$ and $b = 1$. Note also that, if λ is an admissible
water line, so is $-\lambda$; this corresponds to a mirroring of the beam at the vertical
symmetry line. If, moreover, the inequalities (2.61) are taken into account then only
the bold segments in **Fig. 2.27** are admissible equilibrium configurations.

To each pair of equilibrium configurations (D, λ) and $(D, -\lambda)$ one also may
construct a further pair, namely $(0, 1/\lambda)$, $(0, -1/\lambda)$ for the two dashed water lines,
which so far were not discussed; they possess reciprocal slopes. These equilibria
follow simply from geometric evidence of symmetry and do not require further
proof.

At last the equilibrium configuration of Fig. 2.26c must be scrutinized with regard
to its stability. The reader may show in an analogous way as above that the possible
equilibrium positions for $\lambda > 0$ are in this case given by

$$(\lambda - 1)\left[3\sqrt{\lambda} - 2\sqrt{2D}(\lambda + 1)\right] = 0, \qquad 0 \leqslant D \leqslant 0.5,$$
$$(\lambda - 1)\left[3\sqrt{\lambda} - 2\sqrt{2(1 - D)}(\lambda + 1)\right] = 0, \; 0.5 \leqslant D \leqslant 1. \tag{2.65}$$

They correspond to the trivial equilibrium with $\lambda = 1$ and to those having three and five wetted subsurface edges, respectively, Fig. 2.26a. From the formal invariance of (2.65) under the replacement $D \to (1 - D)$ it follows that to each equilibrium configuration with three wetted edges there corresponds a configuration with five wetted edges and equal slope λ of the water line. Because (2.65) is also formally invariant under the replacement $\lambda \to 1/\lambda$, there are additional equilibrium configurations $(D, 1/\lambda)$, corresponding to those with (D, λ) with reciprocal slope. If one puts the expressions with brackets in (2.65) equal to zero, the following quadratic equations

$$\lambda^2 - 2\beta\lambda + 1 = 0, \; \beta = \tfrac{9}{16D} - 1, \qquad D \leqslant 0.5,$$
$$\lambda^2 - 2\hat{\beta}\lambda + 1 = 0, \; \hat{\beta} = \tfrac{9}{16(1-D)} - 1, \; D > 0.5, \tag{2.66}$$

with positive discriminant and thus real λ are obtained, provided

$$0 \leqslant D \leqslant 0.28125, \quad \text{respectively,} \quad 0.71875 \leqslant D \leqslant 1. \tag{2.67}$$

The segments of the curves (2.66) are shown in Fig. 2.27 as dashed lines. They are drawn for $\lambda > 0$ and are mirrored at the horizontal D-coordinate for $\lambda < 0$. These curves smoothly continue the elliptic arches at $\lambda = \pm\frac{1}{2}$, and the admissible equilibria lie above and below, respectively, the straight lines, given by (2.61).

So far all possible equilibrium configurations have been given for a floating long beam with quadratic cross section. There remains to identify, which of these are, respectively, stable, indifferent and unstable.

In order to determine the stability, for instance, of the trivial position $\lambda = 0$, we compute the position of the metacenter. For reasons of symmetry we have $x_{\mathcal{M}} = 0$ and (2.57), $y_{\mathcal{M}} = I_s / V_{\mathbb{E}} - a$, or

$$\mathcal{M}(\lambda) = \left(0, \; \frac{a}{12D} + \frac{\lambda^2}{24D} + \frac{aD}{2}\right). \tag{2.68}$$
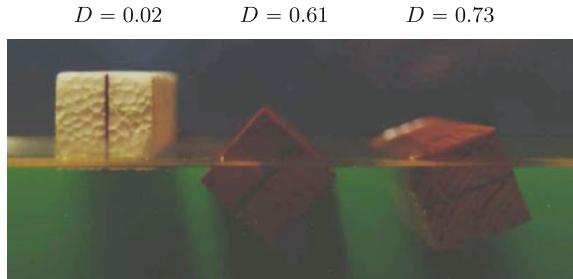
We may now request that for $\lambda \to 0$ the metacenter lies above the center of gravity of the body. This condition yields

$$\lim_{\lambda \to 0}\left(\frac{a}{12D} + \frac{\lambda^2}{24D} + \frac{aD}{2}\right) > \frac{a}{2}, \tag{2.69}$$

from which the stability condition

$$D < \frac{1}{2} - \frac{1}{2\sqrt{3}} \cong 0.211 \tag{2.70}$$

Fig. 2.28 Equilibrium
configurations of a beam
with quadratic cross section.
*The three values of the
density ratio $D = \rho/\rho_K$
correspond to the equilibria
$\lambda = 0, \lambda = 1$ and $0 < \lambda < 1$*

$D = 0.02 \qquad D = 0.61 \qquad D = 0.73$
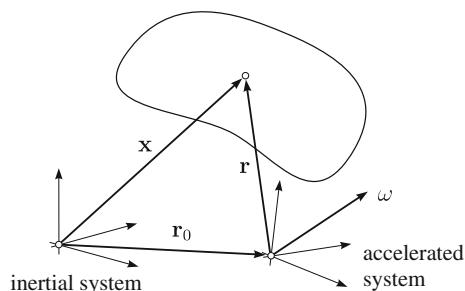
follows. With increasing value of the density ratio above the value $D = 0.211$ list of
the beam to the right or left occurs; it enhances this rotated position with increasing
D, until the position with $\lambda = \pm 1$, $\diamondsuit$, becomes stable for $D \in [0.28125, 0.1875]$. If
D is further increased beyond the value $D = 0.71875$, the beam will again tilt from
its preferred stable position $\diamondsuit$ with $\lambda = \pm 1$ (which is unstable for $0.789 \leq D \leq 1$)
into the stable position $\square$ for $\lambda = 0$; its proof is straightforward if not easy and is
left to the reader.

The photo in **Fig. 2.28** and the figure legend corroborate this analysis.

2.6 Hydrostatics in an Accelerated Reference System

According to the considerations in Sect. 2.3 the fundamental hydrostatic equation
establishes equilibrium between the pressure gradient and the specific body force,
see Eq. (2.14). If the fluid is referred to a non-inertial reference system, then basically
a dynamical system is in our hands, for which, using D'ALEMBERT's principle, the
extended dynamical equation (2.15) is applicable with an acceleration vector $\boldsymbol{b}$,
referred to the absolute inertial system (at rest), see **Fig. 2.29**. If the state of the
motion of the accelerated reference system, whose origin in the absolute system is
given by the vector $\boldsymbol{r}_0$ and if its velocity vector is $\dot{\boldsymbol{r}}_0$ and the angular velocity is $\boldsymbol{\omega}$,
then according to the laws of kinematics of the relative motion, the temporal change

Fig. 2.29 Accelerated
reference system. *Body
referred to an inertial system
and an accelerated system
moving relative to the first
system with velocity $\dot{\boldsymbol{r}}_0$ and
angular velocity $\boldsymbol{\omega}$*

x

r

ω

$\mathbf{r}_0$

accelerated
system

inertial system

of a vector $\boldsymbol{a}$ (relative to the inertial system and denoted by $\mathrm{d}\boldsymbol{a}/\mathrm{d}t$) equals its relative temporal change (relative to the accelerated system and denoted by $\delta\boldsymbol{a}/\delta t$) plus the contribution due to the rotation of the accelerated system, viz.,

$$\frac{\mathrm{d}\boldsymbol{a}}{\mathrm{d}t} = \frac{\delta\boldsymbol{a}}{\delta t} + \boldsymbol{\omega} \times \boldsymbol{a}. \tag{2.71}$$

This formula is immediately understood, if a vector $\boldsymbol{a}$ is considered which is rigidly connected to the accelerated system and for which $\delta\boldsymbol{a}/\delta t = \boldsymbol{0}$, so that $\mathrm{d}\boldsymbol{a}/\mathrm{d}t = \boldsymbol{\omega} \times \boldsymbol{a}$. Application of the rule (2.71) to the position vector

$$\boldsymbol{x} = \boldsymbol{r}_0 + \boldsymbol{r} \tag{2.72}$$

yields the relation

$$\underbrace{\frac{\mathrm{d}\boldsymbol{x}}{\mathrm{d}t}}_{\boldsymbol{v}_a} = \underbrace{\frac{\mathrm{d}\boldsymbol{r}_0}{\mathrm{d}t} + \boldsymbol{\omega} \times \boldsymbol{r}}_{\boldsymbol{v}_f} + \underbrace{\frac{\delta\boldsymbol{r}}{\delta t}}_{\boldsymbol{v}_r} = \boldsymbol{v}_f + \boldsymbol{v}_r \tag{2.73}$$

between the **absolute velocity** $\boldsymbol{v}_a$, the **fixed body velocity** $\boldsymbol{v}_f$[8] and the **relative velocity** $\boldsymbol{v}_r$; here, $\boldsymbol{v}_f$ is called '**fixed body velocity**', because its definition corresponds to that virtual velocity which obtains, if the body were fixed to the moving frame. Applying the rule (2.71) to (2.73), finally yields

$$\begin{aligned}
\frac{\mathrm{d}^2\boldsymbol{x}}{\mathrm{d}t^2} &= \left(\frac{\delta}{\delta t} + \boldsymbol{\omega}\times\right)\left(\frac{\mathrm{d}\boldsymbol{r}_0}{\mathrm{d}t} + \boldsymbol{\omega} \times \boldsymbol{r} + \frac{\delta\boldsymbol{r}}{\delta t}\right) \\
&= \frac{\mathrm{d}^2\boldsymbol{r}_0}{\mathrm{d}t^2} + \frac{\delta\boldsymbol{\omega}}{\delta t} \times \boldsymbol{r} + \boldsymbol{\omega} \times \frac{\delta\boldsymbol{r}}{\delta t} + \boldsymbol{\omega} \times (\boldsymbol{\omega} \times \boldsymbol{r}) + \frac{\delta^2\boldsymbol{r}}{\delta t^2} + \boldsymbol{\omega} \times \frac{\delta\boldsymbol{r}}{\delta t} \\
&= \underbrace{\frac{\delta^2\boldsymbol{r}}{\delta t^2}}_{\boldsymbol{b}_r} + \underbrace{2\boldsymbol{\omega} \times \frac{\delta\boldsymbol{r}}{\delta t}}_{\boldsymbol{b}_c} + \underbrace{\frac{\mathrm{d}^2\boldsymbol{r}_0}{\mathrm{d}t^2} + \boldsymbol{\omega} \times (\boldsymbol{\omega} \times \boldsymbol{r}) + \frac{\delta\boldsymbol{\omega}}{\delta t} \times \boldsymbol{r}}_{\boldsymbol{b}_f}
\end{aligned}$$

or

$$\boldsymbol{b} = \boldsymbol{b}_r + \ddot{\boldsymbol{r}}_0 + 2\boldsymbol{\omega} \times \dot{\boldsymbol{r}} + \boldsymbol{\omega} \times (\boldsymbol{\omega} \times \boldsymbol{r}) + \dot{\boldsymbol{\omega}} \times \boldsymbol{r}. \tag{2.74}$$

Here,

$$\boldsymbol{b} = \frac{\mathrm{d}^2\boldsymbol{x}}{\mathrm{d}t^2} \text{ is the } \textbf{absolute acceleration},$$

$$\boldsymbol{b}_r = \frac{\delta\boldsymbol{r}}{\delta t^2} \text{ is the } \textbf{relative acceleration},$$

---

[8]In the English literature $\boldsymbol{v}_f$ is not separately defined; it is that rigid body velocity, which agrees in each body point with the velocity of the same geometric point that performs the motion of the accelerated reference frame.

$$b_c = 2\boldsymbol{\omega} \times \frac{\delta \boldsymbol{r}}{\delta t} = 2\boldsymbol{\omega} \times \dot{\boldsymbol{r}} \text{ is the CORIOLIS \textbf{acceleration}},$$

$$\boldsymbol{b}_f = \frac{\mathrm{d}^2 \boldsymbol{r}_0}{\mathrm{d}t^2} + \boldsymbol{\omega} \times (\boldsymbol{\omega} \times \boldsymbol{r}) + \frac{\delta \boldsymbol{\omega}}{\delta t} \times \boldsymbol{r} \text{ is the '\textbf{guiding}' \textbf{acceleration}}.$$

Incidentally, except for $\ddot{\boldsymbol{r}}_0$ dots represent in (2.74), differentiations with respect to time relative to the accelerated frame of reference, and

$$\boldsymbol{\omega} \times (\boldsymbol{\omega} \times \boldsymbol{r}) \qquad \text{is called \textbf{centripetal acceleration}},$$
$$\dot{\boldsymbol{\omega}} \times \boldsymbol{r} \qquad \text{is called EULER \textbf{acceleration}}.$$

If the fluid particle is at rest in the accelerated frame, then $\boldsymbol{b}_r = \boldsymbol{0}$ and $\dot{\boldsymbol{r}} = \boldsymbol{0}$; so, Eq. (2.74) is simplified to

$$\boldsymbol{b} = \ddot{\boldsymbol{r}}_0 + \boldsymbol{\omega} \times (\boldsymbol{\omega} \times \boldsymbol{r}) + \dot{\boldsymbol{\omega}} \times \boldsymbol{r}$$

and (2.15) takes the form

$$\mathrm{grad}\; p = \rho\,[\boldsymbol{k} - \ddot{\boldsymbol{r}}_0 - \boldsymbol{\omega} \times (\boldsymbol{\omega} \times \boldsymbol{r}) - \dot{\boldsymbol{\omega}} \times \boldsymbol{r}]. \tag{2.75}$$

This is the **hydrostatic equation relative to an accelerated frame of reference** whose motion is given by $\boldsymbol{r}_0(t)$ and $\boldsymbol{\omega}(t)$.
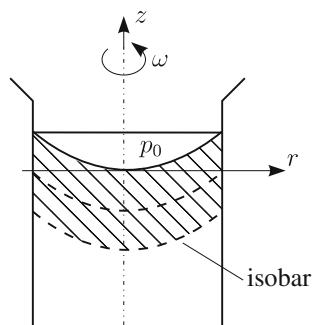
For a **first special case** of a permanently rotating system we have $\ddot{\boldsymbol{r}}_0 = \boldsymbol{0}$, $\dot{\boldsymbol{\omega}} = \boldsymbol{0}$, $\boldsymbol{\omega} = \omega \boldsymbol{e}_z$. The acceleration in (2.74) is then given by, see **Fig. 2.30**,

$$\boldsymbol{b} = \omega \boldsymbol{e}_z \times [\omega \boldsymbol{e}_z \times (r\boldsymbol{e}_r + z\boldsymbol{e}_z)] = -\omega^2 r \boldsymbol{e}_r, \tag{2.76}$$

in which $\boldsymbol{e}_r$ and $\boldsymbol{e}_z$ are unit vectors in the radial and axial directions. The fundamental hydrostatic equation (2.75) reduces to

$$\mathrm{grad}\; p = -\rho g \boldsymbol{e}_z + \rho r \omega^2 \boldsymbol{e}_r \tag{2.77}$$

Fig. 2.30 Hydrostatics in a rotating system. *The free surface and the isobaric surfaces in a rotating system are circular paraboloids*

and for a density preserving fluid integrates to

$$p - p_0 = -\rho g z + \frac{\rho \omega^2}{2} r^2, \tag{2.78}$$

in which p_0 is the constant of integration, i.e., the pressure at $r = z = 0$. According to (2.77) the pressure gradient has a positive radial component with modulus $\rho r \omega^2$, which can be identified with the centrifugal force; moreover, it has also a vertical component due to gravity and of size ρg and acting downward. If p_0 is chosen to be the atmospheric pressure at the free surface, then $p = p_0$ and

$$z = \frac{\omega^2}{2g} r^2. \tag{2.79}$$

According to this equation the free surface is a circular paraboloid. The surfaces of constant pressure, the **isobaric surfaces**

$$z = \frac{\omega^2}{2g} r^2 - \frac{p_1 - p_0}{\rho g}, \qquad p_1 = \text{const.} \tag{2.80}$$

are surfaces, congruent to (2.79), but vertically displaced by $(p_1 - p_0)/(\rho g)$.

In the above computations the fluid has been assumed to be density preserving, but the hydrostatic equation (2.75) is not restricted to this case. To clarify, which density distributions $\rho(r, z)$ of a non-density preserving fluid are possible, we form on both sides of (2.77) the 'curl' and obtain this way

$$\text{curl grad } p = \mathbf{0} \quad \longrightarrow \quad \frac{\partial \rho}{\partial r} = -\frac{\omega^2}{g} r \frac{\partial \rho}{\partial z}. \tag{2.81}$$
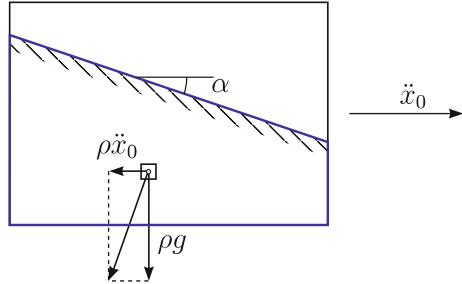
This result implies that in a permanently rotating but only axially stratified fluid, a relative state of equilibrium is not possible. Because of the axial stratification the fluid builds also a radial density variation. If one considers for this a fluid with thermal equation of state of the form $\rho = \rho(T)$, then (2.81) can be expressed as the integrability condition for the temperature:

$$\frac{\partial T}{\partial r} = -\frac{\omega^2}{g} r \frac{\partial T}{\partial z}. \tag{2.82}$$

If the fluid is at rest in the rotating coordinate system, then the temperature must also obey the steady state heat equation in cylindrical coordinates

$$\Delta T = \frac{1}{r} \frac{\partial}{\partial r} \left(r \frac{\partial T}{\partial r} \right) + \frac{\partial^2 T}{\partial z^2} = 0, \tag{2.83}$$

Fig. 2.31 Hydrostatics in the translatorically accelerated system. *For constant acceleration* $\ddot{x}_0 = $ const. *the free surface is inclined by the amount* $\tan \alpha \ddot{x}_0/g$

an equation, which shall be taken here for granted without proof. The only simultaneous solutions of (2.82) and (2.83), as can be shown, are uniform temperatures, $T = $ const.: there cannot be a stratification. If, however, the centripetal accelerations are ignored in (2.82), then $\partial T/\partial r = 0$, and (2.83) implies therefore $T = A + \Delta z$. In a permanently, slowly rotating incompressible fluid, which is thermally stratified in the z-direction, equilibria are possible provided the axial temperature is linear.

Finally, we remark that the ARCHIMEDEan principle also remains valid for hydrostatic conditions of permanently rotating density preserving fluids. Indeed, if one replaces the body with volume V, immersed in the fluid and at rest, by the displaced fluid, this fluid is trivially at rest. The pressure forces, applied to the boundary of the volume V are, thus, in equilibrium with the weight $\rho g V$ and the radial centrifugal force $\rho V \omega^2 r_{\mathbb{E}}$, where $r_{\mathbb{E}}$ denotes the radial distance of the center of gravity of the displaced fluid from the rotation axis.

We leave it to the reader to show that this argument can also be applied to the even more general equation (2.75). Further, he/she may convince him/herself how such arguments explain the functioning of a centrifugal pump.

As a **second special case** of the fundamental hydrostatic equation (2.75) let us evaluate the position of the free surface of the water in a translatorically accelerated container, **Fig. 2.31**. Equation (2.75) reduces in this case to

$$\operatorname{grad} p = -\rho(g\boldsymbol{e}_z + \ddot{\boldsymbol{r}}_0), \tag{2.84}$$

which for constant ρ and constant acceleration $\ddot{\boldsymbol{r}}_0 = (\ddot{x}_0, \ddot{y}_0, \ddot{z}_0)$ can be integrated to

$$p - p_0 = -\rho(\ddot{x}_0 x + \ddot{y}_0 y + \ddot{z}_0 z) - \rho g z, \tag{2.85}$$

in which p_0 denotes the constant pressure on the free surface. The geometry of the free surface is therefore given by

$$z = -\frac{1}{g + \ddot{z}_0}\left(\ddot{x}_0 x + \ddot{y}_0 y\right),$$

or if $\ddot{y}_0 = \ddot{z}_0 = 0$

$$z = -x \tan \alpha, \qquad \tan \alpha = \frac{\ddot{x}_0}{g}. \tag{2.86}$$

For a co-moving observer the fluid is at rest; he experiences as body force a downward acting gravity force against ρg and a horizontal volume force of size $\rho \ddot{x}_0$ acting against the acceleration $\ddot{x}_0$.

2.7 Pressure Distribution in the Still Atmosphere

Let us return to the fundamental hydrostatic equation (2.14) and determine the pressure distribution in the atmosphere subject to the gravity field. Assume that the Earth has spherical symmetry with radius r_0 and that the gravity force changes with distance from the Earth's center according to NEWTON's gravity law

$$g(r) = g_0 \frac{r_0^2}{r^2}, \tag{2.87}$$

where g_0 denotes the acceleration due to gravity on the free surface. The pressure gradient has for spherical symmetry only a radial component, so that the hydrostatic equation takes the form

$$\frac{dp}{dr} = -g_0 \rho \frac{r_0^2}{r^2} \tag{2.88}$$

and becomes integrable, if this equation is complemented by an additional equation, in which pressure and density are related to one another. If this relation is given by the **equation of state for ideal gases**

$$p = \rho R T, \tag{2.89}$$

in which R is the **specific gas constant** and T the **absolute temperature**, then with the assumption of a constant temperature, i.e., an **isothermal atmosphere**, the pressure would be determined by

$$p = p_0 \exp \left(\frac{g_0 r_0^2}{RT} \left(\frac{1}{r} - \frac{1}{r_0} \right) \right), \tag{2.90}$$

in which p_0, r_0, g_0 are corresponding values at the Earth's surface. With the aid of (2.89) the variable ρ can equally be evaluated.

In lieu of an isothermal atmosphere one assumes as a rule a **polytrope atmosphere**, which is given by

$$\rho = \rho_0 \left(\frac{p}{p_0} \right)^n \tag{2.91}$$

with **polytrope exponent** $n > 0$. Eliminating between (2.91) and (2.89) the pressure, one obtains for the temperature the formula

$$T = \frac{p_0}{R\rho_0^{1/n}} \rho^{(1-n)/n}.$$

(2.92)

From this formula one concludes for $0 < n < 1$ that the temperature rises with increasing density and remains bounded for all densities $\rho \geqslant 0$. By contrast, for $n > 1$, the exponent of ρ in (2.92) is negative so that the temperature falls with increasing density; for $\rho \to 0$ we then have $T \to \infty$. For $n = 1$ the polytropic atmosphere is as well isothermal. In the lower atmosphere, the so-called **troposphere**—these are the lowest 8–12 km—the exponent $n = 0.8$ is an adequate approximation to a realistic density distribution.

Substitution of (2.91) into (2.88) yields the separable differential equation

$$\frac{\mathrm{d}p}{p^n} = -\frac{g_0\rho_0}{p_0^n}\frac{r_0^2}{r^2}\mathrm{d}r$$

(2.93)

for the pressure as a function of the distance from the center of the Earth. (2.93) requires separate integration for $n = 1$ and $n \neq 1$. The result is

$$\frac{p}{p_0} = \begin{cases} \exp\left(-\dfrac{\rho_0 g_0 r_0^2}{p_0}\left(\dfrac{1}{r_0} - \dfrac{1}{r}\right)\right), & n = 1, \\ \left\{1 - (1-n)\dfrac{\rho_0 g_0 r_0^2}{p_0}\left(\dfrac{1}{r_0} - \dfrac{1}{r}\right)\right\}^{1/(1-n)}, & n \neq 1. \end{cases}$$

(2.94)

The solution for $n = 1$ has been given already in (2.90). Ordinarily one is interested in values of r, which deviate only slightly from r_0; so, when using TAYLOR series expansion we have

$$\frac{1}{r_0} - \frac{1}{r} = \frac{1}{r_0}\left(1 - \frac{r_0}{r}\right) = \frac{1}{r_0}\left(1 - \frac{r_0}{r_0 + z}\right)$$

$$= \frac{1}{r_0}\left(1 - \frac{1}{1 + \dfrac{z}{r_0}}\right) = \frac{1}{r_0}\left(\frac{z}{r_0} + \mathcal{O}\left(\left(\frac{z}{r_0}\right)^2\right)\right).$$

(2.95)

If this expression is substituted into (2.94)$_2$ for $n \neq 1$, one obtains

$$\frac{p}{p_0} \cong \left(1 - (1-n)\frac{z}{H}\right)^{1/(1-n)}, \quad H = \frac{p_0}{\rho_0 g_0}.$$

(2.96)

H denotes an upper bound for the thickness of the troposphere for which (2.96) delivers reliable values for the pressure. With

$$\rho_0 = 1.293 \text{ kg m}^{-3}, \quad p_0 = 1.013 \cdot 10^5 \text{ kg s}^{-2}\text{m}^{-2}, \quad g_0 = 9.81 \text{ m s}^{-2}$$

one obtains $H \cong 8 \times 10^3$ m, which roughly is indeed the thickness of the troposphere or somewhat smaller. If relation (2.96) is being expanded in a TAYLOR series for small values of z/H, then the linear approximation

$$\frac{p}{p_0} \cong 1 - \frac{z}{H} = 1 - \frac{\rho_0 g_0}{p_0} z, \quad \frac{z}{H} \ll 1 \tag{2.97}$$

is obtained, valid for the lower troposphere. This linear dependence in the z-coordinate corresponds to that of a density preserving fluid.

If, alternatively, the argument of the exponential function in (2.90) is linearized in z/H, one obtains the **barometric height formula**

$$\frac{p}{p_0} = \exp\left(-\frac{\rho_0 g_0}{p_0} z\right) = \exp\left(-\frac{z}{H}\right), \quad n = 1, \tag{2.98}$$

which, after further TAYLOR series expansion for $z/H \ll 1$ yields again (2.97).

To close this exposition on the hydrostatic equation, let us ask, under which conditions an atmospheric layer of air at rest remains stable. To this end, we consider a small element of air, isolated from the ambient air, and assume that its density variations can be ignored across its vertical extent. This element of air is comparable to a balloon, which floats at its height, i.e., its weight and buoyancy forces are equilibrated. For the ensuing analysis we assume linear density distribution of the atmosphere with height. If such an element is vertically displaced by the distance ζ, its buoyancy changes, because it is now positioned in an environment of different density. If one assumes that this density varies negligibly in the extent of the particle motion, then, locally, the buoyancy can be evaluated with the aid of the ARCHIMEDEan principle; one obtains $\rho(\zeta_s)gV$ where ζ_s is the z-coordinate of the center of gravity of the element of air with volume V. The element is, thus, subjected to the upward pointing vertical force

$$[\rho(\zeta_s) - \rho(0)]gV \cong \frac{d\rho}{d\zeta}(0)gV\zeta_s, \tag{2.99}$$

in which TAYLOR series expansion has been used to obtain the expression on the far right: $\rho(\zeta_s) = \rho(0) + (d\rho/d\zeta)\zeta_s + \cdots$. If one regards the particle of air (or the balloon) as a rigid body or as a mass point, then

$$\rho(0)\dot{\zeta}_s V \tag{2.100}$$

is its momentum. NEWTON's second law, thus leads to the equation of motion

$$\rho_0 \ddot{\zeta}_s V = \frac{\mathrm{d}\rho}{\mathrm{d}\zeta}(0)g\zeta_s V \quad \Longrightarrow \quad \ddot{\zeta}_s - \frac{\frac{\mathrm{d}\rho}{\mathrm{d}\zeta}(0)g}{\rho(0)}\zeta_s = \ddot{\zeta}_s + N^2\zeta_s = 0. \qquad (2.101)$$

The factor

$$N^2 = -\frac{\frac{\mathrm{d}\rho}{\mathrm{d}\zeta}(0)g}{\rho(0)}$$

has the dimension of a squared frequency. N is called **buoyancy frequency** or
BRUNT- VÄISÄLÄ **frequency** and is a measure for the stability of the air particle
in its layer. Indeed, Eq. (2.101) describes for $N^2 > 0$ a harmonic motion

$$\zeta_s = A\sin(Nt) + B\cos(Nt), \qquad N^2 > 0 \qquad (2.102)$$

with constants of integration A and B. If the particle is displaced out of its equilibrium
position, it will harmonically oscillate about its equilibrium position. This oscillation
will in reality be damped, an effect, which has been ignored in the above analysis.
Thus, the air particle will in reality return to its original equilibrium position. We say
in this case that *the air is stably stratified*. If, on the contrary, $N^2 < 0$, the density of
the air grows with height. The solution of (2.101) is then

$$\zeta_s = A\exp(|N|t) + B\exp(-|N|t), \quad N^2 < 0 \qquad (2.103)$$

and possesses exponential character. An initial perturbation will move the particle
with growing time farther and farther away from its initial position. The fluid particle
can no longer return to its initial position. For $N^2 < 0$ *the mass of the air is therefore
unstably stratified*.

The reader may show that the air in a homogeneous layer is in an indifferent state
of equilibrium.

Reference

1. Fachlexikon: Forscher und Erfinder. 3. Auflage. Harri Deutsch Verlag, Thun-Frankfurt (1992)

Chapter 3
Hydrodynamics of Ideal Liquids

Abstract This chapter starts with kinematic concepts such as 'motion', 'velocity', 'EULERian and LAGRANGEan descriptions', and then proceeds to describe 'streamlines', 'trajectories' and 'streak lines', illuminating these with illustrative examples. Next, the balance laws of mass and linear momentum are discussed both in global and local form and specialized to EULERian fluids. The BERNOULLI equation, defined as the path-integration of the scalar product of the momentum equation with the velocity field is given extensive space; it is discussed both when referred to non-inertial and inertial frames and when the integration is conducted along any path or along streamlines. Ample space is devoted to applications of the BERNOULLI equation to typical examples, e.g., venturi pipes, PRANDTL pipes, TORRICELLI flow out of a vessel, including clepsydra clocks. Global formulations of the momentum equation are equally touched and applied to the problem of BORDA's exit flows, impact of a jet on a wall, mixing processes of non-uniform velocities in plane conduits, hydraulic jumps and flow of a density preserving fluid through a periodic grid of wings. Aerodynamics is given a first glimpse by studying plane flow around infinitely long wings, specifically by deriving the KUTTA-JOUKOWSKI condition of smooth flow off the wing's trailing edge, which fixes the circulation around the wing. The chapter closes with a presentation of the balance of moment of momentum and its application to the SEGNER water wheel and EULER's turbine equation.

Keywords Kinematics · Streamlines · Trajectories · Streaklines · Balances of mass and linear momentum · BERNOULLI equation · Plane wing theory · Balance of moment of momentum

List of Symbols

Roman Symbols

A	Cross sectional area of a flow filament
$\boldsymbol{a}$	Acceleration vector
$\boldsymbol{b} = \dot{\boldsymbol{v}}$	Acceleration vector
$C = \mathrm{d}Q/\mathrm{d}h$	Kinematic wave speed
c_Q, c_L	Lift coefficient
D	Diffusivity

E	Entrainment rate
$E_{\text{kin}}, E_{\text{pot}}$	Kinetic, potential energy
$\{e_x, e_y, e_z\}$	Cartesian basis in the present configuration
$g, (g)$	Gravity constant, (vector)
h	Height or depth of a fluid layer in a channel
I_V	Momentum of a body V
K_V	Volume force of a body with volume V
$K_{\partial V}$	Surface force on a body with surface ∂V
K_Q	KUTTA-JOUKOWSKI flow-induced force on a wing: $K_Q = \rho v_\infty \times \Gamma$
K_w	Drag force on a wing
K	Resultant force acting on a body by the surrounding fluid
L	Power of working (of a pump)
L, ℓ	Length of a pipe
$L_{\mathcal{O}}$	Angular momentum of a point mass relative to $\mathcal{O}$
M	Mass flow
$\dot{m} = \rho Q$	Mass flux through a pipe cross section
$M_{\mathcal{O}}$	Moment of the body and surface forces relative to point $\mathcal{O}$
$N = M\omega$	Power of working of the moment of a shaft rotating with angular velocity w
n	Unit vector at a surface element perpendicular to the element
p, p_B, p_C	Pressure, reference pressures
$p^* = p + \rho g z$	Piezometric pressure
$P(p)$	Pressure function
Q	Volume source, volume flow
R	(Universal) gas constant
R	Reactive force on a pipe
$\mathbb{R}$	REYNOLDS number
s	Arc length, coordinate along a smooth curved line
S_1, S_2	Flow induced forces at cross sections 1 and 2 of a pipe
T	Temperature, period of oscillation
t	Time, distance of neighboring wings in a periodic grid of wings
t	CAUCHY stress tensor
$t_{(n)} = tn$	Traction vector on a smooth surface with unit normal vector n
(t)	Matrix of t
$t_{xx}, t_{xy}, \ldots, t_{zz}$	Components of t referred to a basis $\{e_x, e_x, e_z\}$
t^T	Transpose of t
U	Specific body force potential
U, V	Velocity components of the center of a body
$v = (u, v, w)$	Velocity vector, components of v in the present configuration
$\dot{v}$	Acceleration vector

W	Work done on a fluid
W_p	Work done on a fluid by the pressure
$\boldsymbol{x}, \boldsymbol{X}$	Position of a material point in the present and reference configuration
$\boldsymbol{x} = \boldsymbol{\chi}(\boldsymbol{X}, t)$	Motion function of a particle $\boldsymbol{X}$

Greek Symbols

$\alpha = \frac{A_e}{A_i} = 0.5$	Contraction coefficient of the exit cross sectional area of the BORDA exit mouth
$\alpha = 0.61$	Contraction coefficient of the exit cross sectional area of a sharp exit cross section
$\Gamma = \oint_{\mathfrak{C}} \boldsymbol{v} \cdot \mathrm{d}\boldsymbol{x}$	Circulation of a flow field around a closed curve $\mathfrak{C}$
ε	Ratio of the local area to the cross sectional area of a pipe
ζ_{Carnot}	Dimensionless pressure or energy loss coefficient
η	Degree of efficiency of a turbine
ξ, η, ζ	Cartesian coordinates attached to a body
$\Phi(\boldsymbol{X}, t)$	Field quantity referred to the reference configuration
$\varphi(\boldsymbol{x}, t)$	Field quantity referred to the present configuration
ϕ	Field quantity
$\dot{\phi}$	Total derivative of ϕ
ρ	(Mass) density
$\boldsymbol{\chi}(\boldsymbol{X}, t)$	Motion function from the reference to the present configuration

Miscellaneous Symbols

grad $\boldsymbol{v}$, div $\boldsymbol{v}$, curl $\boldsymbol{v}$	Gradient, divergence, rotation of the differentiable field $\boldsymbol{v}$
$\frac{\mathrm{d}}{\mathrm{d}t}$	Total time derivative holding the particle fixed
$\frac{\partial}{\partial t}, \frac{\mathrm{d}}{\mathrm{d}t}$	Partial time derivative, local time derivative holding the present position fixed
$\boldsymbol{a} \times \boldsymbol{b}$	Cross product of the vectors $\boldsymbol{a}$ and $\boldsymbol{b}$. $(\boldsymbol{a} \times \boldsymbol{b})_i = \varepsilon_{i,j,k} a_j b_k$
$\hat{=}$	Sign for an isomorphism

After having dealt with in the last chapter with hydro*statics*, the science of the mechanical equilibrium of fluids, we shall in this chapter focus attention on the important aspects of hydro*dynamics*. To this end, after a brief introduction into the basic notions of kinematics, we shall address the central dynamical principles, which are the balance laws of mass, linear and angular momenta, as well as the balance law of mechanical energy, which led to one of the most important equations of hydrodynamics. This is the so-called **Bernoulli equation**, derived and presented by DANIEL BERNOULLI (1700–1782) [3] in his famous memoir '*Hydrodynamica*', published in 1738. This equation forms one of the most significant auxiliary tools of today's design elements in the engineering sciences.

The topics dealt with in this chapter are the fundamental physical laws of ideal and (mostly) density preserving liquids of continuous bodies as they cover about a third

of a basic course in fluid or hydrodynamics. The basic principles can also be learnt in a course on elementary continuum mechanics, e.g., [4, 8, 19], but formulas are put here into forms that are particularly apt for hydrodynamic applications. The subjects are equally taught in many books and treatises of hydrodynamics and hydraulics of the past hundred years: mention might be made of [1, 5, 11, 12, 15, 17, 18, 20, 21, 25–27], to name just a few. Of more than just historical profit is also to look into older books on hydrodynamics, e.g., [10, 22] or even [3] and others.

3.1   Basic Kinematic Concepts
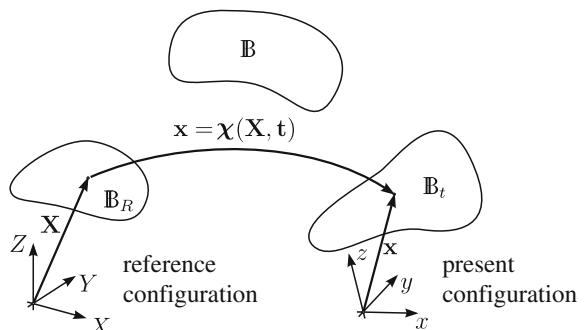
3.1.1   Motion, Velocity

Basic in the treatment of hydrodynamic problems is the notion of a **material point** or **material particle**. By this we mean a point in three-dimensional space to which mass is attached. Thus, to every point a positive mass **density** is assigned which is to be interpreted as mass per unit volume. The particles are identified by their position vectors of their places, which in three-dimensional space can uniquely be described either by Cartesian, cylindrical or any other arbitrary coordinates. Generally, that is, when the particle is in motion, its position changes with time. Thus, one will interpret x as a function of time t and the initial position X (taken at $t = t_0$, usually at $t = 0$), viz.,

$$x = \chi(X, t), \tag{3.1}$$

and must for obvious reasons assume this relation to be bijective, i.e., one-to-one and onto, as well as in general differentiable. In particular, because of $X = \chi(X, 0)$ one may identify the particle with the position vector X at $t = 0$; we say that X is the 'identifier' or 'name' of the particle. A set of material particles, mostly infinitely large and continuously distributed, constitutes a **material domain** or **material region** or a **body** $\mathbb{B}$, see **Fig. 3.1**. At $t \neq 0$ this set can be identified with a spatial region that is 'filled' with material points and is called the **configuration of the body**

Fig. 3.1 Configuration of a body. *Body* $\mathbb{B}$, *its reference configuration* $\mathbb{B}_R$ *and present configuration* $\mathbb{B}_t$. *Both configurations are referred to their bases X, Y, Z and x, y, z, respectively. The motion of a material point is defined by the map* $x = \chi(X, t)$

at time t or the **present** or **current configuration** $\mathbb{B}_t$. *One* configuration of $\mathbb{B}$ is distinguished, namely that at time $t = 0$; it corresponds to the body at its initial position but may be any configuration, perhaps one, which the body will never assume during its motion; it is called the **reference configuration** $\mathbb{B}_R$. If relation (3.1) is known for all particles of a body, then it obviously maps the reference configuration $\mathbb{B}_R$ onto the present configuration $\mathbb{B}_t$. If the entirety of these mappings is unique, then to each present configuration there corresponds its pre-image, the reference configuration X and vice versa. To guarantee a deterministic relation between the reference and present configurations, this uniqueness is important, since only with such a deterministic property the **motion** of a body can be meaningfully determined as a temporal sequence of configurations.

In fluid dynamics the motion of a fluid particle is usually described by a relation for the velocity as a function of space and time. The **velocity** $\boldsymbol{v}(\boldsymbol{x}, t)$ is defined as the time rate of change of the motion function $\chi(X, t)$ at fixed particle

$$\boldsymbol{v}(\boldsymbol{x}, t) = \left.\frac{\mathrm{d}\chi(X, t)}{\mathrm{d}t}\right|_{X=\text{fixed}} = \frac{\partial\chi(X, t)}{\partial t}, \tag{3.2}$$

or if $\{\boldsymbol{e}_x, \boldsymbol{e}_y, \boldsymbol{e}_z\}$ is a Cartesian basis for the three-dimensional velocity space,

$$\boldsymbol{v}(\boldsymbol{x}, t) = u(\boldsymbol{x}, t)\boldsymbol{e}_x + v(\boldsymbol{x}, t)\boldsymbol{e}_y + w(\boldsymbol{x}, t)\boldsymbol{e}_z. \tag{3.3}$$

Similarly, the **acceleration** of a particle is defined as the time rate of change per unit time of the velocity function; it is therefore given by

$$\boldsymbol{b}(\boldsymbol{x}, t) = \left.\frac{\mathrm{d}\boldsymbol{v}}{\mathrm{d}t}\right|_{X=\text{fixed}} = \dot{\boldsymbol{v}}(\boldsymbol{x}, t). \tag{3.4}$$

In the above formulae the velocity $\boldsymbol{v}(\boldsymbol{x}, t)$ and acceleration $\boldsymbol{b}(\boldsymbol{x}, t)$ are the velocity and acceleration of the particle X, which at time t is at the position $\boldsymbol{x}$, but the expressions e.g. on the right-hand side of (3.2) are functions of X and t. Obviously, to obtain on the left-hand side a function of $\boldsymbol{x}$ and t one must substitute for X the expression $X = \chi^{-1}(\boldsymbol{x}, t)$, in which $\chi^{-1}(\cdot)$ is the inverse function of $\chi(\cdot)$. This shows explicitly that the motion $\chi(X, t)$ must be an invertible function of X, if formulae such as (3.2)–(3.4) are meaningful expressions. Moreover, the fact that in the same formulae temporal change of a quantity is calculated, whilst the *particle is held fixed* has been set in evidence by adding a subscript '$X =$ fixed'; similarly, we have used the 'Roman d' as the symbol denoting differentiation. Henceforth we shall dispense with the index and shall interpret the 'Roman d' as a differentiation symbol for a temporal derivative holding the material particle fixed. This derivative, which as in (3.4), is also denoted by a superimposed dot, is called **material** or **substantive derivative**.

Once again, in formulae (3.2) and (3.4) the velocity and acceleration fields are represented as functions of the spatial coordinate $\boldsymbol{x}$ of the present configuration as well as time t. Generally, a field quantity ϕ (e.g. velocity, acceleration, specific

energy or pressure, etc.) can be represented either as a function of these variables, viz., $\phi = \varphi(\boldsymbol{x}, t)$, or else as a function of the material coordinate X in the reference configuration and time t, so that $\phi = \Phi(X, t)$. The **spatial representation**

$$\phi = \varphi(\boldsymbol{x}(t), t) = \varphi(x(t), y(t), z(t), t) \tag{3.5}$$

is also called **Eulerian representation**.[1] It constitutes the natural description of hydrodynamics, since fluids and gases are mostly bounded by rigid walls, on which the spatial coordinate $\boldsymbol{x}$ of a material particle is generally temporally constant, whilst the fluid particles can move along them. The **material description**

$$\phi = \Phi(X, t) = \Phi(X, Y, Z, t), \tag{3.6}$$

also called the **Lagrangean description**, however, is the natural setting for solid bodies, since they are commonly bounded by material walls, which may deform in the course of time. The material or substantive derivative of a physical quantity ϕ may, with the aid of (3.6), be written as

$$\dot{\phi} = \frac{\mathrm{d}\phi}{\mathrm{d}t} = \frac{\partial \Phi(X, t)}{\partial t}. \tag{3.7}$$

Hence, in the material description the material time derivative of a function $\Phi(X, t)$ is obtained by forming the partial derivative of this function with respect to time. By contrast, in the Eulerian description, (3.5) implies instead

$$\dot{\phi} = \frac{\mathrm{d}\phi}{\mathrm{d}t} = \frac{\partial \varphi}{\partial t} + \frac{\partial \varphi}{\partial x}u + \frac{\partial \varphi}{\partial y}v + \frac{\partial \varphi}{\partial z}w$$
$$= \underbrace{\frac{\partial \varphi}{\partial t}}_{\text{local derivative.}} + \underbrace{(\mathrm{grad}\,\varphi)\,\boldsymbol{v}}_{\text{convective derivative}}, \tag{3.8}$$

in which the expression in the first line is valid when a Cartesian coordinate representation is used, whereas the expression in the second line gives the coordinate invariant representation. The material derivative of a physical quantity ϕ can be interpreted as that change of ϕ per unit time which is experienced by an observer traveling with the fluid particle. In its spatial representation it is composed, according to (3.8), of two contributions. The first, $\partial \phi/\partial t$, is the so-called **local derivative**, which represents

---

[1] The Eulerian description is also the preferential description in the mechanics of rigid bodies. For instance,

$$\boldsymbol{v}(\boldsymbol{x}, t) = \boldsymbol{v}_s(t) + \boldsymbol{\omega}(t) \times (\boldsymbol{x} - \boldsymbol{x}_s(t)),$$

where $\boldsymbol{v}_s(t)$ and $\boldsymbol{\omega}(t)$ are the velocity and angular velocity at the reference point $\boldsymbol{x}_s(t)$.

the change of ϕ when $\boldsymbol{x}$ is held fixed, the second $(\text{grad }\phi)\boldsymbol{v}$ denotes the **convective**[2] or less frequently **advective** derivative and represents the change of ϕ caused by the transport due to the velocity and vanishes for all spatially uniform fields ϕ.

In the above derivations no prerequisites were made regarding the character of the field ϕ. If $\varphi = \rho(\boldsymbol{x}, t)$ is a scalar, then Eq. (3.8) reads

$$\dot{\rho} = \frac{\partial \rho}{\partial t} + (\text{grad }\rho) \cdot \boldsymbol{v}, \tag{3.9}$$

in which in Cartesian coordinates, grad ρ is given by

$$\text{grad }\rho = \left(\frac{\partial \rho}{\partial x}, \frac{\partial \rho}{\partial y}, \frac{\partial \rho}{\partial z} \right). \tag{3.10}$$

If, however, $\varphi = \boldsymbol{v}$ is a vector field, then (3.8) takes the form

$$\dot{\boldsymbol{v}} = \frac{\partial \boldsymbol{v}}{\partial t} + (\text{grad }\boldsymbol{v})\boldsymbol{v} = \frac{\partial \boldsymbol{v}}{\partial t} + \text{grad}\left(\frac{|\boldsymbol{v}|^2}{2} \right) - \boldsymbol{v} \times \text{curl }\boldsymbol{v}, \tag{3.11}$$

in which the validity of the expression on the far right can be corroborated by evaluation in Cartesian components, and where the Cartesian representation of grad $\boldsymbol{v}$ is given by

$$\text{grad }\boldsymbol{v} = \begin{pmatrix} \dfrac{\partial u}{\partial x} & \dfrac{\partial u}{\partial y} & \dfrac{\partial u}{\partial z} \\[2mm] \dfrac{\partial v}{\partial x} & \dfrac{\partial v}{\partial y} & \dfrac{\partial v}{\partial z} \\[2mm] \dfrac{\partial w}{\partial x} & \dfrac{\partial w}{\partial y} & \dfrac{\partial w}{\partial z} \end{pmatrix}, \tag{3.12}$$

and $|\boldsymbol{v}|$ is the modulus of the velocity. Hence, the gradient of a scalar is a vector and that of a vector a **tensor of rank 2**. Finally, we mention that in some older and applied literature (particularly in engineering) the gradient of a vector field is defined by the transpose to (3.12), so that in this case the convective acceleration (3.11)$_1$ would have to be differently written. We shall use convention (3.12), which is popular in the mathematical literature.

The above considerations can be summarized by the following concise formula:

$$\dot{\phi} = \frac{\partial \Phi}{\partial t} = \underbrace{\frac{\partial \varphi}{\partial t}}_{\text{local derivative}} + \underbrace{(\text{grad }\varphi)\boldsymbol{v}}_{\text{convective or advective derivative}}. \tag{3.13}$$

$$\underbrace{\phantom{\frac{\partial \Phi}{\partial t} = \frac{\partial \varphi}{\partial t} + (\text{grad }\varphi)\boldsymbol{v}}}_{\text{material or substantive derivative}}$$

---

[2]When using "convective" acceleration one usually tacitly assumes that a term $(\partial \phi/\partial z)w$ is present; by contrast, "advective" acceleration means that $(\partial \phi/\partial x)u + (\partial \phi/\partial y)v$ are dominant. However, this interpretation is not unanimously used, but very popular in geophysics.

These explanations should have made clear that for the description of a physical field, one must distinguish between its value and its functional dependence on the independent variables. We shall here always work with the spatial or EULERian description and may then without loss of uniqueness of interpretation choose for the value of a field and its functional representation the same symbol and thus write

$$\phi = \phi\,(\boldsymbol{x}, t). \tag{3.14}$$

In so doing we, however, assume that the independent variables are known in advance. In critical cases, it is always advantageous to differentiate between a function and its value.

With this convention of notation one must in the spatial description strictly differentiate between $\dot{\phi} = \mathrm{d}\phi/\mathrm{d}t$ and $\partial\phi/\partial t$. A physical quantity, for which $\dot{\phi}$ vanishes at all times, whence for which the value of ϕ for a fixed particle is constant, is often called a **conservative quantity**, in other words, ϕ is **materially constant**. Alternatively, processes for which the value of ϕ is constant for an observer fixed in space, i.e., $\partial\phi/\partial t = 0$ are **steady** or **stationary**, in short

$$\begin{aligned}
\frac{\mathrm{d}\phi}{\mathrm{d}t} &= 0 \Longleftrightarrow \phi \text{ is materially constant,} \\
\frac{\partial\phi}{\partial t} &= 0 \Longleftrightarrow \phi \text{ is stationary.}
\end{aligned} \tag{3.15}$$

3.1.2 Streamlines, Trajectories, Streaklines

The motion of a fluid in a region is known as soon as the velocity field $\boldsymbol{v}(\boldsymbol{x}, t)$ is known in all spatial points of the region at all times $t > 0$. The velocity assigns to each point in space a direction (see **Fig. 3.2**), and since the velocity field $\boldsymbol{v}(\boldsymbol{x}, t)$ is usually time dependent, this direction field does also change with time. For a visual interpretation of the state of motion of a fluid field, one uses distinct sets of curves which can be derived from a given velocity field. These sets of curves are the so-called **streamlines, trajectories** and **streaklines**, which all deliver different pictures of the flow field.
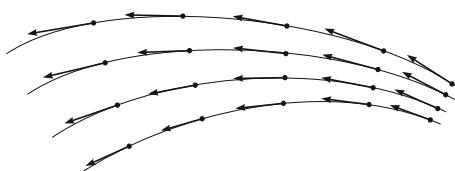
Fig. 3.2 Graph of streamlines. *If one imagines that at $t = \tau$ the velocity vectors are plotted in each spatial point, then by drawing the curves, which are everywhere tangential to the velocity vectors, one generates the streamlines*

- A **streamline** at $t = \tau$ is a line of which the tangents in each point agree with the direction of the velocity vectors. They are, therefore, the integral curves of the orientation field at time $t = \tau$, given by the field $\boldsymbol{v}(\boldsymbol{x}, \tau)$. If $\mathrm{d}\boldsymbol{x} = (\mathrm{d}x, \mathrm{d}y, \mathrm{d}z)$ is a vectorial line element of the streamline at time $t = \tau$, then this element is parallel to the orientation field of the velocity vector $\boldsymbol{v} = (u, v, w)$, if

$$\mathrm{d}\boldsymbol{x} = \mathrm{d}\sigma\, \boldsymbol{v}\,(\boldsymbol{x}(\sigma), \tau)\,, \tag{3.16}$$

or

$$\frac{\mathrm{d}\boldsymbol{x}}{\mathrm{d}\sigma} = \boldsymbol{v}\,(\boldsymbol{x}(\sigma), \tau)\,, \tag{3.17a}$$

in which the factor of proportionality $\mathrm{d}\sigma$ can be regarded as an increment of the curve parameter σ. In Cartesian component form the parallelism of $\mathrm{d}\boldsymbol{x}$ and $\boldsymbol{v}$ can also be expressed by the chain of equalities

$$\mathrm{d}x : \mathrm{d}y : \mathrm{d}z = u : v : w$$

from which, upon introducing the curve parameter σ the three equations

$$\frac{\mathrm{d}x}{\mathrm{d}\sigma} = u(x, y, z, \tau), \quad \frac{\mathrm{d}y}{\mathrm{d}\sigma} = v(x, y, z, \tau), \quad \frac{\mathrm{d}z}{\mathrm{d}\sigma} = w(x, y, z, \tau) \tag{3.17b}$$

emerge, which correspond to the component representations of (3.17a). Integration of these ordinary differential equations, subject to the initial conditions

$$\sigma = 0: \quad \boldsymbol{x} = \boldsymbol{x}_0 = (x_0, y_0, z_0) \tag{3.17c}$$

delivers that streamline, which goes through the point $\boldsymbol{x} = \boldsymbol{x}_0$.
Incidentally, it is possible to assign to σ the meaning of the arc length of the streamline; this is the case, if (3.17a) is written as

$$\frac{\mathrm{d}\boldsymbol{x}}{\mathrm{d}s} = \frac{\boldsymbol{v}(\boldsymbol{x}, \tau)}{|\boldsymbol{v}(\boldsymbol{x}, \tau)|}, \quad s = 0: \ \boldsymbol{x} = \boldsymbol{x}_0. \tag{3.18}$$

Such a normalization is not compelling for the integration and neither is it usually advantageous.
- The **trajectories** are different from the streamlines. These are those lines, which are traversed by the particles in the course of their actual motion. Here, the time is no longer held fixed; this implies that for the determination of the trajectory neither (3.17a–3.17c) nor (3.18) must be solved, but the initial value problem

$$\frac{\mathrm{d}\boldsymbol{x}}{\mathrm{d}t} = \boldsymbol{v}\,(\boldsymbol{x}(t), t)\,, \quad t = \tau: \ \boldsymbol{x} = \boldsymbol{x}_0, \tag{3.19}$$

which, as in (3.17a–3.17c), could equally be written down in component form. As opposed to (3.18), the curve parameter in (3.19) is the time, which on the right-hand side also occurs as an independent parameter, a fact that is not so for σ in (3.17a–3.17c).

A system of ordinary differential equations, in which the parameter with respect to which the equation is integrated does not arise as an argument in the function on the right-hand side, is called **autonomous**; else it is called **non-autonomous**. For our purposes, the difference is not of importance, since by adding the equation $\sigma = t$, it can easily be shown that Eq. (3.19) can be transformed into a new autonomous system that is enlarged by one equation. Indeed, with $\sigma = t$, we have $d/dt = d/d\sigma$ and $dt/d\sigma = 1$, so that (3.19) may also be written as

$$\frac{dt}{d\sigma} = 1, \quad \frac{dx}{d\sigma} = v(x, t),$$
$$\sigma = \tau : \quad t = \tau, \quad x = x_0. \tag{3.20}$$
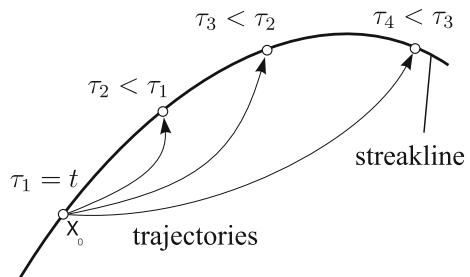
For each τ and each x_0 the initial value problem (3.19) or (3.20) yields that trajectory, which at time $t = \tau$ goes through the point $x = x_0$; it can mathematically be written in the form

$$x = x(t; x_0, \tau). \tag{3.21}$$

If one fixes τ, but varies x_0, then (3.21) represent the totality of all trajectories, which at time $t = \tau$ had the positions x_0.

- Equation (3.21) is the ideal function to define the third kinematic quantity, the so-called **streakline**, see **Fig. 3.3**. It connects at the fixed time t the positions of those particles, which at any earlier times $\tau < t$ passed the fixed position x_0, Fig. 3.3. Consequently one obtains the equation of the streakline at time t through x_0 from all trajectories which passed at any time $\tau < t$ through x_0; technically, one must in Eq. (3.21) hold t and x_0 fixed, whilst τ varies and takes the role of the curve parameter.

Fig. 3.3 Streaklines. *The streakline at time t through a point x_0 is obtained by connecting all positions of those particles, which at any earlier time τ passed the position x_0*

Experimentally, streamlines, trajectories and streaklines can be observed by adequately marking the fluid particles. This can, for instance, be done by adding to the fluid small particular impurities, which move in good approximation with the same speed as the fluid particles. If the fluid receives e.g., at the fixed spatial point x_0 for a very short time a point-like color or smoky tracer, then this small impurity mass moves nearly diffusion-free with the particle and traces its trajectory. By relatively long light exposure, or even better, by stroboscopic photography, the trajectory of the fluid particle carrying the tracer particle can be made visible, see **Fig. 3.4**. If, on the other hand, a colored tracer is continuously added at the fixed spatial point x_0, as e.g. the smoke from the tip of a cigarette, see **Fig. 3.5**, then with every photographic snapshot one obtains a streakline belonging to x_0. Sometimes, the flow of the fluid is made visible by adding to it aluminum powder, or confettis, if the flow at a free fluid surface is to be made visible. Taking photographs of the flow region with short light exposure will generate on the plate short strikes, which mark the orientation field of the velocities at the time of exposure; these small vectorial elements can usually easily be connected by eye or with a French curve; these curves then mimic the streamlines, see **Fig. 3.6**. All these methods assume plane motion; for three-dimensional flows the visualization of the flow field is much more difficult to determine, usually with advanced experimental techniques. Such techniques are e.g. known as **particle tracking velocimetry** (PTV) and **particle image velocimetry** (PIV) methods, in which the transparent fluid is enlightened by a laser sheet and the

Fig. 3.4 Trajectories. *Photography of the trajectory of a boomerang in the evening twilight.* (*From* F. Hess, The aerodynamics of boomerangs. *Scientific American* 1968)
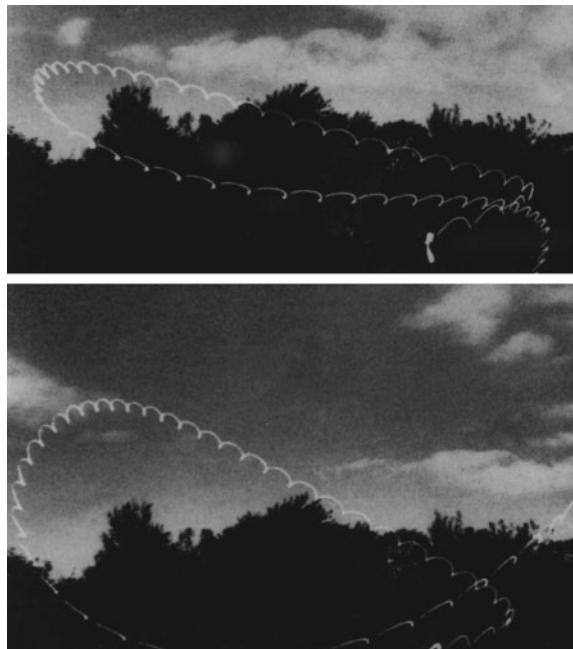
Fig. 3.5 Streaklines of a
cigarette smoke

flow within the laser sheet is rapidly photographed with digital cameras perpendic-
ular to the sheet. Electronically identifiable spots in consecutive photographic shots
allow then determination of the displacement field of the spots within the image field
of the photographs from which the velocity field can be deduced.

In a spatial point, streamlines and trajectories are for a particular time tangential
to one another, however, in general, they are not the same curves; for the tangents
of the trajectories are determined by those velocity vectors, which a fluid particle
possesses in its true motion, i.e., consecutively at later and later times. By contrast,
the streamlines are tangential to the velocity field at a fixed moment $t = \tau$. In a
steady flow the streamlines do not deform with time since the velocity field $\boldsymbol{v}$ only
depends on the space coordinate; in this case they are the same as the trajectories.
Such congruence also prevails for some unsteady flows, as e.g. in all rectilinear
parallel flows.

The streamlines which pass through a spatially fixed simply connected area A form
a **streamline tube**, **Fig. 3.7**. In unsteady flows this tube deforms together with the
deformation of the streamlines; in steady flows, however, it preserves the position
and form, and since it can in this case be regarded as a bundle of trajectories, it
contains always the same fluid particles. Since, moreover, at their walls, the velocity
is tangential to these walls, they could in the steady flow case be imagined to be
replaced by a real, solid pipe, without any implied changes of the flow. In the interior,
if effects of friction are ignored, a streamline tube with infinitesimal cross section
dA, is a **streamline filament**.
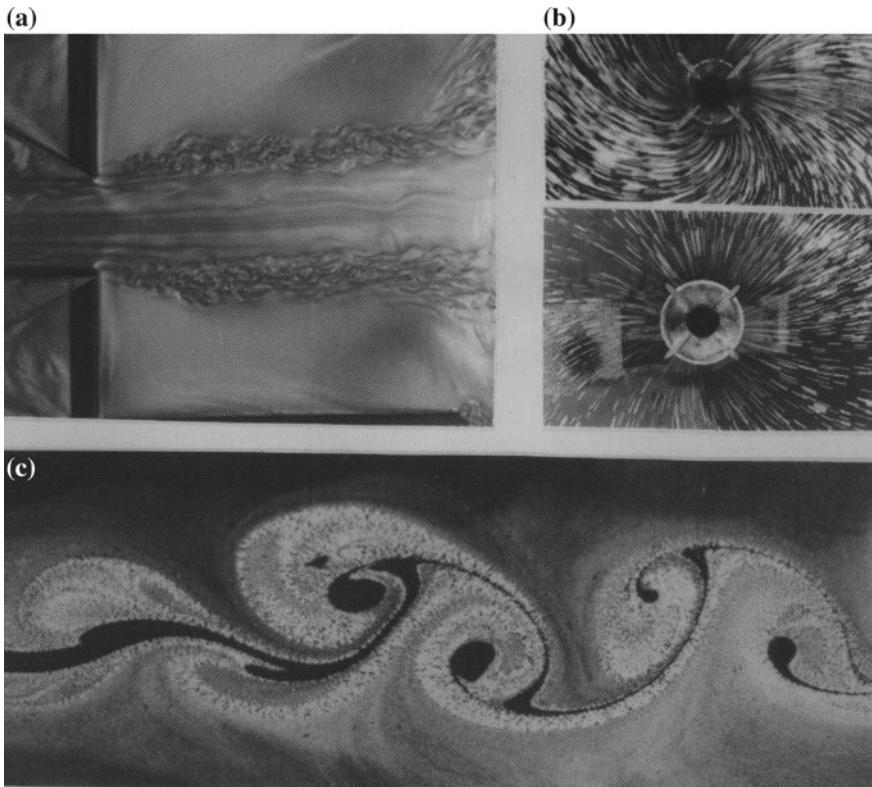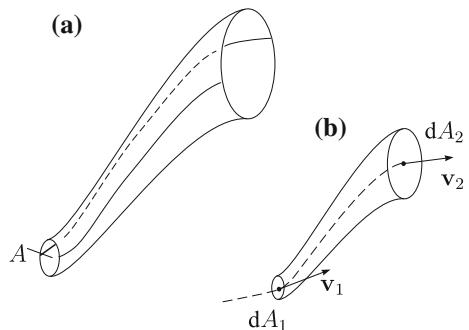
Fig. 3.6 Streamlines. **a** *Sudden widening of a channel at strong flow from left. The strong shearing that arises at the transition from the jet interior to the quiescent neighboring fluid is made visible with aluminum powder. Photo* W.H. HAGER, VAW. **b** *Free surface motion in a flow into a vertical pipe. The flow is made visible with confettis, VAW Photo 23476/23478,* **c** *von* KÁRMÁN-*vortex street in the wake of the flow past a cylinder. Photo* R. PRIEN

Fig. 3.7 Definition of a flow filament and a flow tube. **a** *All streamlines starting from a simple closed curve make up a flow tube with spatially varying cross section A.* **b** *If the cross section is infinitesimal, then the volume swept out by these streamlines is a flow filament*

Finally, let us explain the difference between streamlines and trajectories by the following example: A two-dimensional fluid source with strength Q moves with constant speed U in the negative x-direction in an otherwise infinite plane bath of fluid at rest, **Fig. 3.8**. If the point of the source would be at rest, then conservation of mass would imply on a circle with distance r from the source $2\pi r v_r = Q$, from which the radial velocity is obtained as

$$v_r = \frac{Q}{2\pi r}, \tag{3.22}$$

or in Cartesian components,

$$u = \frac{Q}{2\pi r} \cos \vartheta = \frac{Q\xi}{2\pi(\xi^2 + \eta^2)},$$
$$v = \frac{Q}{2\pi r} \sin \vartheta = \frac{Q\eta}{2\pi(\xi^2 + \eta^2)}, \tag{3.23}$$

in which ξ and η are the Cartesian components with origin at the point of the source. Since the flow is steady, the streamlines, trajectories and streaklines are the same, namely the radial lines through the point of the source.

If the point source moves with constant velocity U to the left, then in the coordinates (ξ, η), which are fixed with the source, a constant parallel flow with magnitude U in the positive ξ-direction is added to the flow (3.23), so that the velocity is now given by

$$u_\xi = U + \frac{Q\xi}{2\pi(\xi^2 + \eta^2)}, \qquad v_\eta = \frac{Q\eta}{2\pi(\xi^2 + \eta^2)}. \tag{3.24}$$
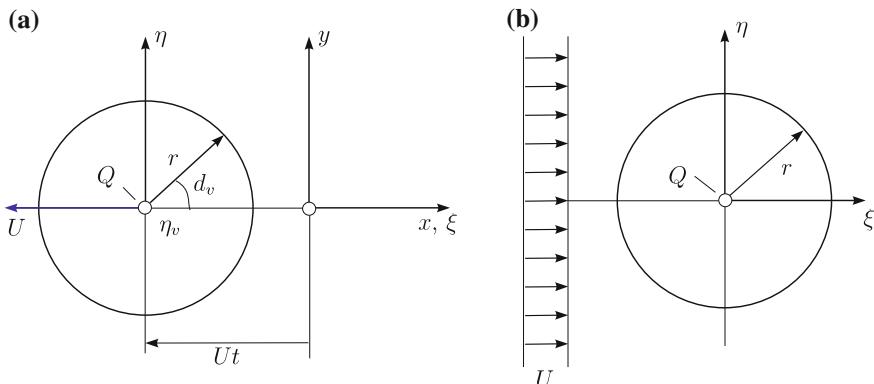
Fig. 3.8 Plane flow from a point source. **a** *A point source with strength Q is imagined to move with constant speed to the left in an otherwise quiescent bath.* **b** *Same situation as seen by an observer moving with the source. The source point is now subject to a parallel flow from the left*

For an observer, who moves with the source point, this flow is steady and the streamlines, and relative trajectories can be computed from

$$\frac{Q}{2\pi} \arctan\left(\frac{\eta}{\xi}\right) + U\eta = \psi, \tag{3.25}$$

as can relatively easily be seen. Indeed, the stream function ψ and the velocity components u_ξ, v_η are related by

$$u_\xi = \frac{\partial \psi}{\partial \xi}, \qquad v_\eta = -\frac{\partial \psi}{\partial \eta}.$$
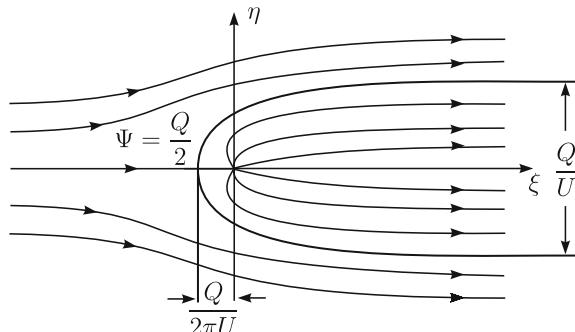
With u_ξ, v_η given by (3.24), it can be verified that (3.25) generates (3.24). Here, ψ assumes on each streamline a constant value. **Figure 3.9** shows the graph of them: The region is divided into two sub-regions, one containing the source and forming a 'body', open to the right with blunt nose, the other comprising its exterior region. None of these sub-regions exchanges mass with the other, because their common boundary, shown in Fig. 3.9 somewhat thicker than the other streamlines, is streamline for both. The **stagnation point** of this flow, i.e., the point at which the velocity is zero, is, according to (3.24) positioned on the ξ-axis at a distance $\xi_S = -Q/(2\pi U)$ from the origin ahead of the point source. In this point the flow bifurcates the streamline on the ξ-axis; that approaching the stagnation point from the left is 'split' at the stagnation point to form the boundary contour of the mentioned blunt half-body. As one can easily deduce, one obtains for $\xi \to \infty$ the limit value $u \to U$, so that the mass balance $Q = bU$ yields the semi-width of the half-body as $\xi \to \infty$.

The coordinate system (x, y) of the spatially fixed observer and the source-fixed coordinate system (ξ, η) are, according to Fig. 3.8a, connected by the so-called **Galilei transformation**.

$$\xi = x + Ut, \qquad \eta = y. \tag{3.26}$$

Fig. 3.9 Steady parallel plane flow plus flow from a stationary source. *Streamlines or trajectories as seen by an observer at rest*

An observer fixed with the laboratory frame (x, y) sees a velocity field that is in the x-direction reduced by the value U, namely

$$
\begin{aligned}
u_x &= \frac{Q\xi}{2\pi(\xi^2 + \eta^2)} = \frac{Q(x + Ut)}{2\pi[(x + Ut)^2 + y^2]}, \\
v_y &= \frac{Q\eta}{2\pi(\xi^2 + \eta^2)} = \frac{Qy}{2\pi[(x + Ut)^2 + y^2]}.
\end{aligned}
\tag{3.27}
$$

Thus, in the spatially fixed coordinates (x, y) the velocities are time dependent, the motion is unsteady and the streamlines and trajectories are different from one another.

The streamlines can be computed according to (3.18) from the proportions

$$
\mathrm{d}y : \mathrm{d}x = v_y(x, y, \tau) : u_x(x, y, \tau),
$$

or with (3.27) from

$$
\frac{\mathrm{d}y}{\mathrm{d}x} = \frac{y}{x + U\tau},
\tag{3.28}
$$

which, by the method of separation of variables, can be integrated, yielding

$$
y = c(x + U\tau),
\tag{3.29}
$$

in which c denotes a constant of integration. Hence, the streamlines are, as for the spatially fixed source, the radial straight lines through the source point, **Fig. 3.10**a.
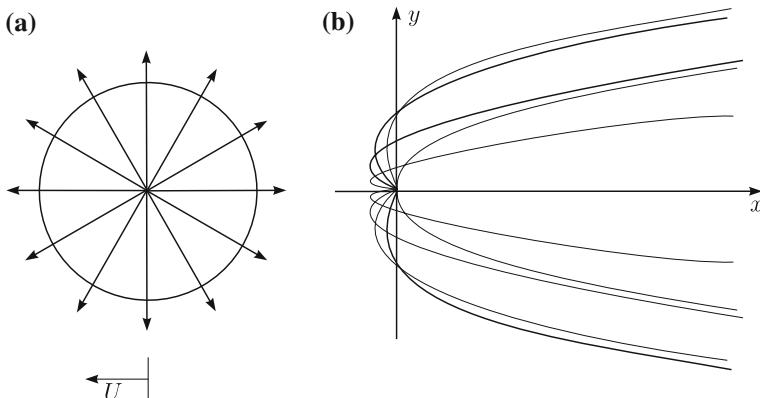
Fig. 3.10 Moving source. **a** *Flow from a source moving with constant speed to the left in a still bath.* **b** *Trajectories obtained by integrating equations (3.30)*

According to (3.19), the trajectories are obtained by integrating the system

$$\begin{aligned}
\frac{dx}{dt} &= u_x = \frac{Q(x + Ut)}{2\pi[(x + Ut)^2 + y^2]}, \\
\frac{dy}{dt} &= u_y = \frac{Qy}{2\pi[(x + Ut)^2 + y^2]}
\end{aligned} \tag{3.30}$$

of ordinary differential equations subject to the initial conditions $x = x_0$, $y = y_0$ at $t = 0$. This integration is best performed numerically. Figure 3.10b shows the trajectories through the initial points

$$x_0 = k \cos\left(\frac{j\pi}{n}\right), \quad y_0 = k \sin\left(\frac{j\pi}{n}\right), \quad (j = 1, \ldots, 2n).$$
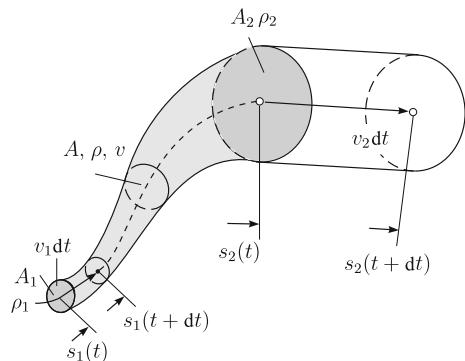
For $2n$ initial points which, at time $t = 0$ are regularly and concentrically distributed around a circle (x_0, y_0).

3.2 Mass Balance, Continuity

In the last section fundamental kinematic properties of fluids in motion were studied. In this and the following sections we shall now address dynamical properties. Here, we shall discuss the **law of mass conservation**. It says: *The mass of a body bounded by material points is temporally constant*, or expressed for a spatially fixed volume: *The growth of the mass in a spatially fixed volume equals the difference between the flow of mass into and out of the volume through its boundary.*

The mathematical formulation of this physically obvious statement will first be made clear by considering a flow filament. This will give us the possibility to get to know the conservation law of mass in the first of the above formulations. Hence, we consider a material volume, which at time t agrees with a segment of a flow filament

Fig. 3.11 Flow filament. *Illustrating the derivation of the balance of mass* (3.33)

between the cross sections $A_1 = A(s_1(t), t)$ and $A_2 = A(s_2(t), t)$, see **Fig. 3.11**. The mass which is stored in this flow filament is given by

$$\int_{s_1(t)}^{s_2(t)} \rho(s, t) A(s, t) \, \mathrm{d}s$$

and its time rate of change must, because of mass conservation, vanish:

$$\frac{\mathrm{d}}{\mathrm{d}t} \int_{s_1(t)}^{s_2(t)} \rho(s, t) A(s, t) \, \mathrm{d}s = 0. \tag{3.31}$$

Fig. 3.12 GOTTFRIED WILHELM LEIBNIZ (1. July 1646–12. Nov. 1716) *Left* Portrait by CHRISTOPH BERNHARD FRANCKE, ~1700; Herzog Anton Ulrich-Museum, Braunschweig and signature. *Right* Leibniz Four-Species calculating machine—Original ~1690. *Source* Museum Herrenhausen Palace. *Photo* HAJOTTHU

GOTTFRIED WILHELM LEIBNIZ was a German philosopher, mathematician, diplomat and historian. He invented, among many other things, the infinitesimal calculus and documented this in 1684 in the *acta eruditorum*. NEWTON published his independently developed infinitesimal calculus in 1687, but had developed its fundamentals already in 1666. This led to a bitter priority fight between the two that continued over several generations of continental and British mathematicians. LEIBNIZ created the symbols $(\mathrm{d}f/\mathrm{d}x)$ and $(\int f \mathrm{d}x)$ for the differential and integral of a function f. This notation became preferable to NEWTON's fluxions.

Many significant inventions go back to LEIBNIZ, e.g., his mechanical calculator, an arithmetic calculating machine, of which there are five versions. Its concept was a historical milestone. It is, however, doubtful, whether a properly working version of this machine did exist at LEIBNIZ' time. A correctly working counter plea from LEIBNIZ' construction maps was first realized in 1990 by JOACHIM LEHMANN in Dresden. A replica by Prof. ERWIN STEIN was also shown at several LEIBNIZ Exhibitions 'Leibniz – Philosopher, Mathematician, Physicist and Engineer …' in German and English, worldwide, now permanently established at the University Hannover, Germany.

The text is based on http://www.wikipedia.org

Mathematically, the left-hand side of this expression is the derivative of an integral with respect to the parameter t, whereby the integrand function as well as its upper and lower limit functions depend on this parameter. For the differentiation of such integrals the **Leibniz rule**[3] must hold, namely for any differentiable function $F = \rho A$

$$\frac{d}{dt} \int_{s_1(t)}^{s_2(t)} F(s, t)\, ds$$

$$= \int_{s_1(t)}^{s_2(t)} \frac{\partial F}{\partial t}(s, t)\, ds + F(s_2(t), t)\, \frac{ds_2}{dt} - F(s_1(t), t)\, \frac{ds_1}{dt}, \qquad (3.32)$$

or, since $ds/dt = v$ denotes the algebraic velocity of the fluid particles,

$$\int_{s_1(t)}^{s_2(t)} \frac{\partial(\rho A)}{\partial t}(s, t)\, ds + \rho_2 A_2 v_2 - \rho_1 A_1 v_1 = 0. \qquad (3.33)$$

This equation represents the mass balance statement for a flow filament and holds true for an arbitrary segment of a fluid filament between two cross sections at time t for a steady or unsteady flow of a compressible or density preserving fluid. Under conditions of steady state, (3.33) simplifies to

$$\rho_1 A_1 v_1 = \rho_2 A_2 v_2. \qquad (3.34)$$

The quantity $\rho A v$ is called **mass flow**; it is often denoted by $\dot{m}$. Equation (3.34), expresses the fact that for steady flows the mass flow through a flow filament is temporally constant, so that in this case the relation

$$\rho A v = \dot{m} = \text{const.} \qquad (3.35)$$

must hold. An additional special case of Eq. (3.33) is obtained for a density preserving fluid, for which $\rho_1 = \rho_2 = \text{const.}$, so that in this case (3.33) takes the form

$$\int_{s_1(t)}^{s_2(t)} \frac{\partial A}{\partial t}(s, t)\, ds + A_2 v_2 - A_1 v_1 = 0, \qquad (3.36)$$

which simplifies for steady flows to

$$A_2 v_2 = A_1 v_1 \qquad (3.37)$$

---

[3]For a short biography of LEIBNIZ see **Fig. 3.12**.

and may also be written as

$$Av = Q = \text{const.} \tag{3.38}$$

Q is called the volume flow through the flow filament, which is temporally constant for a density or volume preserving fluid. Since the mass does not arise in the balance statements (3.36) and (3.38), these relations are also called **continuity equations**.

Incidentally, (3.36) also shows that for density preserving fluids the simple forms of the continuity equation, (3.36) to (3.38) are also valid for unsteady flows, if the flow filament does not change spatially with time, i.e., if $\partial A/\partial t = 0$. This case prevails for a rigid pipe, which is subject to unsteady flow of a density preserving fluid, but not necessarily for a flexible garden hose. This example should also make clear that the formulae, derived for the balance law of mass for a flow filament can also be employed for **flow tubes**, provided the densities and velocities do not vary too much across the flow-tube-cross sections. Here, we mean by the flow-tube-cross section that area, which is perpendicular to a selected flow line in the middle of the tube.

For the derivation of the equation of mass balance in its general differential form, consider the spatially constant cubic element of **Fig. 3.13**a. The time rate of change of its mass by density change per unit time is given by

$$\frac{\partial \rho}{\partial t}\, \mathrm{d}x\mathrm{d}y\mathrm{d}z. \tag{3.39}$$
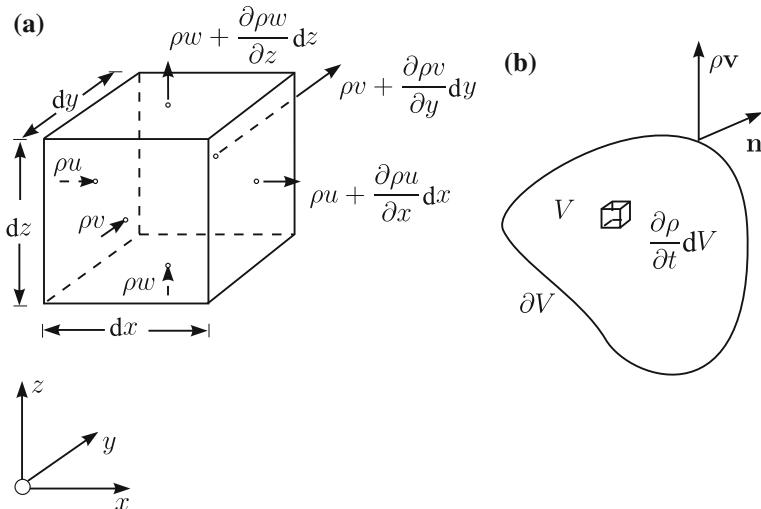
Fig. 3.13 Mass balance. **a** *Mass fluxes through the surfaces of an infinitesimal cube.* **b** *Steady, i.e., spatially fixed volume V with boundary ∂V*

Through the surface element perpendicular to the x-axis that is bounding the cube to the left with area $\mathrm{d}y\mathrm{d}z$ the mass flow $\rho u \mathrm{d}u \mathrm{d}z$ enters the cube; analogously, the mass flow that leaves the infinitesimal cube at the right edge is given by $[\rho u + (\partial(\rho u)/\partial x)\mathrm{d}x]\mathrm{d}y\mathrm{d}z$. Together one thus obtains, if mass growth is counted as positive,

$$\left\{ \rho u - \left[\rho u + \frac{\partial(\rho u)}{\partial x}dx \right] \right\} \mathrm{d}y\mathrm{d}z = -\frac{\partial(\rho u)}{\partial x}\mathrm{d}x\mathrm{d}y\mathrm{d}z. \tag{3.40}$$

To this one must add the contributions of the mass flow through those surface elements which are perpendicular to the y- and z-axes; they are easily seen to be given by

$$-\frac{\partial(\rho v)}{\partial y}\mathrm{d}x\mathrm{d}y\mathrm{d}z \quad \text{and} \quad -\frac{\partial(\rho w)}{\partial z}\mathrm{d}x\mathrm{d}y\mathrm{d}z. \tag{3.41}$$

In the above, u, v and w are the components of the velocity vector $\boldsymbol{v}$. In total, the mass flow entering the cube volume per unit time is given by

$$-\left(\frac{\partial(\rho u)}{\partial x} + \frac{\partial(\rho v)}{\partial y} + \frac{\partial(\rho w)}{\partial z} \right) \mathrm{d}x\mathrm{d}y\mathrm{d}z. \tag{3.42}$$

This must be equal to the growth of mass (3.39), so that

$$\frac{\partial\rho}{\partial t}\mathrm{d}x\mathrm{d}y\mathrm{d}z = -\left(\frac{\partial(\rho u)}{\partial x} + \frac{\partial(\rho v)}{\partial y} + \frac{\partial(\rho w)}{\partial z} \right) \mathrm{d}x\mathrm{d}y\mathrm{d}z, \tag{3.43}$$

from which one easily obtains the general local form of the conservation law of mass

$$\frac{\partial\rho}{\partial t} + \operatorname{div}(\rho\boldsymbol{v}) = 0. \tag{3.44}$$

This equation can also be differently written, if product differentiation is used in its second term on the left-hand side, e.g., $\operatorname{div}(\rho\boldsymbol{v}) = (\operatorname{grad}\rho)\cdot\boldsymbol{v} + \rho\operatorname{div}\boldsymbol{v}$, yielding

$$\frac{\partial\rho}{\partial t} + (\operatorname{grad}\rho)\cdot\boldsymbol{v} + \rho\operatorname{div}\boldsymbol{v} = 0,$$

or, in view of (3.8)

$$\frac{\mathrm{d}\rho}{\mathrm{d}t} + \rho\operatorname{div}\boldsymbol{v} = 0. \tag{3.45}$$

Equations (3.44) and (3.45) are two equivalent forms of the mass balance equation. For a density preserving material one has $\dot{\rho} = 0$, and (3.45) is thus reduced to the equation

$$\operatorname{div}\boldsymbol{v} = 0 \quad \text{(density preserving)}, \tag{3.46}$$

an equation which is known as **continuity equation**. In a density preserving or volume preserving fluid the velocity field is **solenoidal**, that is divergence free. Equation (3.46) also expresses volume preserving; indeed, one may put $\rho = 1$ in the derivation of (3.44) from (3.39) and then express with (3.44) volume preserving, which in this case reduces to

$$\text{div } \boldsymbol{v} = 0 \qquad \text{(volume preserving)}. \qquad (3.47)$$

Thus, density and volume preserving in one-constituent continua are the same thing.

Alternatively, for steady state conditions, for which $\partial \rho / \partial t = 0$, (3.44) simplifies to

$$\text{div } (\rho \boldsymbol{v}) = 0 \qquad \text{(stationarity)}. \qquad (3.48)$$

The quantity $\rho \boldsymbol{v}$ is called the **specific mass flux**, which, according to (3.48) must be solenoidal. For density preserving fluids the statement (3.48) reduces to (3.46), as one might have expected.

The local form of the balance law of mass can also be derived in the following mathematically elegant form. To this end we consider the spatially fixed volume V of Fig. 3.13b. The mass growth rate in V is given by

$$\int_V \frac{\partial \rho}{\partial t} \, dV, \qquad (3.49)$$

and this must be equal to the mass flow through the surface,

$$-\int_{\partial V} (\rho \boldsymbol{v}) \cdot \boldsymbol{n} \, dA. \qquad (3.50)$$

Here, $\boldsymbol{n}$ denotes the exterior unit vector, which explains the negative sign since (3.50) is a mass loss. Thus, one has

$$\int_V \frac{\partial \rho}{\partial t} \, dV = -\int_{\partial V} (\rho \boldsymbol{v}) \cdot \boldsymbol{n} \, dA. \qquad (3.51)$$

If in the surface integral term one applies the divergence theorem,[4]

$$\int_{\partial V} (\rho \boldsymbol{v}) \cdot \boldsymbol{n} \, dA = \int_V \text{div } (\rho \boldsymbol{v}) \, dV, \qquad (3.52)$$

[4]See Appendix 5.A, where the divergence theorem or GAUSS law is derived.

for which differentiability of the density and velocity fields must be assumed as well as simple connectivity of V, then Eq. (3.51) can be written as

$$\int_V \left\{ \frac{\partial \rho}{\partial t} + \text{div}\,(\rho \boldsymbol{v}) \right\} \mathrm{d}V = 0. \tag{3.53}$$

This equation holds for any spatially fixed volume V that is completely filled by the fluid; in particular this volume can be infinitesimally small for which the integrand function must vanish. One, thus has recovered Eq. (3.44).

We wish, before closing this sub-section, present two applications of the conservation law of mass and continuity, respectively. In the *first problem* we consider a fluid discharged into a quiescent ambient fluid of the same density through a very long slit, see **Fig. 3.14**a. We presume steady conditions and also assume plane flow. This ideally prevails, if the slit is infinitely long and the mass flux through it is constant along the slit. The fluid leaving the slit is spreading in the still fluid as a **jet** with symmetric bell shaped profile of the horizontal velocity along the x-axis which is positioned in the middle of the slit. With increasing distance from the slit the width of the jet grows about linearly. We define the boundary of the jet as that distance from the jet axis where the longitudinal velocity has dropped to a non-measurable value. However, at the boundary of the jet a non-vanishing transverse velocity component toward the jet axis exists and, as will be shown later when we discuss the BERNOULLI equation, is toward the jet axis and this contributes to a mass growth along the jet axis. If the two-dimensional steady mass balance equation (3.48),

$$\frac{\partial(\rho u)}{\partial x} + \frac{\partial(\rho v)}{\partial y} = 0,$$
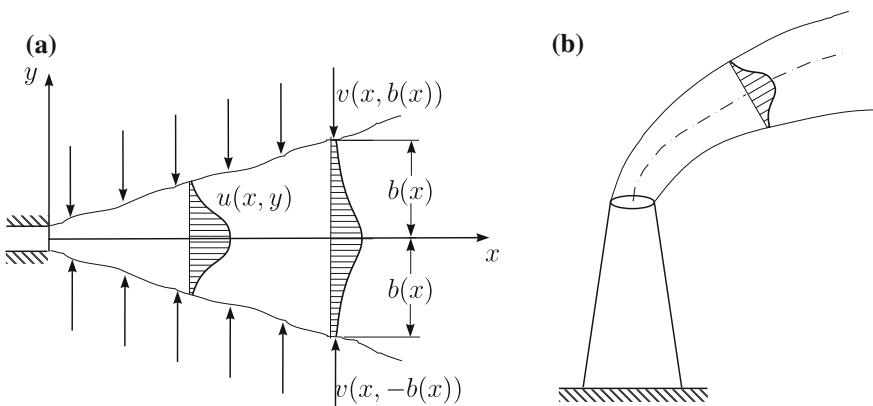
Fig. 3.14 Turbulent jet. **a** *Plane stationary jet with horizontal velocity profile $u(x, y)$ along the axis and transverse velocity $v(x, b(x))$ at the jet boundary.* **b** *Diffusion of chimney smoke*

is integrated across the width of the jet, one obtains

$$\int_{-b(x)}^{b(x)} \frac{\partial(\rho u)}{\partial x}\,dy + \rho v\big|_b - \rho v\big|_{-b} = 0. \tag{3.54}$$

Now, because of symmetry one has $v(x, b(x)) = -v(x, -b(x))$ and with the use of the LEIBNIZ rule (3.32), applied to the integral term, one concludes

$$\int_{-b(x)}^{b(x)} \frac{\partial(\rho u)}{\partial x}\,dy \equiv \frac{d}{dx}\int_{-b(x)}^{b(x)} \rho u\,dy - 2u\,(x, b(x))\,\frac{db}{dx}, \tag{3.55}$$

in which the boundary terms add up together because of symmetry. Equation (3.54), thus can also be written as

$$\frac{d}{dx}\int_{-b\,(x)}^{b(x)} \rho u\,dy = -2\rho\left[v\,(x, b\,(x)) - u\,(x, b(x))\,\frac{db}{dx}\right]. \tag{3.56}$$

If one denotes with

$$M = \int_{-b(x)}^{b(x)} \rho u\,dy \quad \text{and} \quad E = -2\rho\left[v\,(x, b(x)) - u\,(x, b(x))\,\frac{db}{dx}\right], \tag{3.57}$$

the **mass flow** M, integrated over the jet cross section, and the mass that is entrained into the jet across and perpendicular to the jet boundary—the so-called **entrainment rate** E—then Eq. (3.56) can also be written as
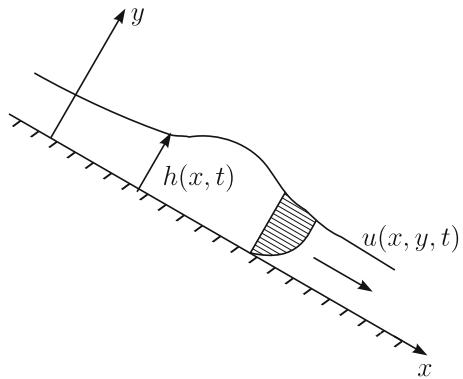
$$\frac{dM}{dx} = E. \tag{3.58}$$

The growth of the mass per unit length along the jet is, therefore, equal to the rate of entrained fluid from the quiescent environment across the jet boundary. Such balance statements which are integrated over the jet cross section are used in many practical applications, for instance also in diffusion problems of chimney smoke, see Fig. 3.14b.

As a *second example* we consider the flow of a density preserving fluid with free surface along an inclined plane, see **Fig. 3.15**. This flow can serve as a model for the flow of water in a very wide river. If one integrates the continuity equation

$$\frac{\partial u}{\partial x} + \frac{\partial v}{\partial y} = 0 \tag{3.59}$$

Fig. 3.15 Channel flow.
*Plane channel flow with free
surface, illustrating the
derivation of the kinematic
wave equation*

in a similar fashion as in the last example from $y = 0$ to $y = h(x, t)$, where $h(x, t)$
denotes the layer thickness, then one obtains

$$\int_0^{h(x,t)} \frac{\partial u}{\partial x} \mathrm{d}y + v\,(x, h(x, t), t) - v(x, 0, t) = 0, \tag{3.60}$$

in which the velocity component $v(x, 0, t)$ vanishes, since the flow is tangential to the
base. Moreover, if one interchanges in the first term differentiation and integration,
while using the LEIBNIZ rule,

$$\int_0^{h(x,t)} \frac{\partial u}{\partial x} \mathrm{d}y = \frac{\partial}{\partial x} \int_0^{h(x,t)} u\,\mathrm{d}y - u\,(x, h(x, t), t) \frac{\partial h}{\partial x}, \tag{3.61}$$

then Eq. (3.60) takes the form

$$\frac{\partial}{\partial x} \int_0^{h(x,t)} u(x, y, t)\,\mathrm{d}y - \left(u(x, h, t)\frac{\partial h}{\partial x} - v(x, h, t) \right) = 0, \tag{3.62}$$

which still can be simplified. To this end, consider the free surface, which obeys the
equation

$$F(x, y, t) \equiv h(x, t) - y = 0. \tag{3.63}$$

Because this surface is a material surface for all time, equation (3.63) must also hold
in differentiated form, $\mathrm{d}F/\mathrm{d}t = 0$ or $F(x, y, t) = 0$

$$\frac{\mathrm{d}F}{\mathrm{d}t} = \frac{\partial h}{\partial t} + \frac{\partial h}{\partial x}\frac{\partial x}{\partial t} - \frac{\partial y}{\partial t} = \frac{\partial h}{\partial t} + \left(u(x, h, t)\frac{\partial h}{\partial x} - v(x, h, t) \right) = 0, \quad (3.64)$$

in which $u(x, h)$ as well as $v(x, h)$ are the components of the velocity of the fluid particles sitting on the surface. With (3.64), Eq. (3.62) becomes

$$\frac{\partial h}{\partial t} + \frac{\partial}{\partial x} \int\limits_0^{h(x,t)} u(x, y, t)\, \mathrm{d}y = 0. \tag{3.65}$$

Relations (3.64) and (3.65) are called **kinematic surface equations**, since they are derived from kinematic relations only. Equation (3.65), however, does not suffice to develop with it an equation of motion for the free surface, $h(x, t)$. If, however, other considerations deliver a relation between the volume flow

$$Q = \int\limits_0^{h(x,t)} u(x, y)\, \mathrm{d}y, \tag{3.66}$$

and the layer thickness h, for instance

$$Q = \hat{Q}(h), \tag{3.67}$$

then, because of the so-called **kinematic wave equation**

$$\frac{\partial h}{\partial t} + \hat{C}(h)\frac{\partial h}{\partial x} = 0, \quad \text{with} \quad \hat{C} := \frac{\mathrm{d}\hat{Q}}{\mathrm{d}h} > 0. \tag{3.68}$$

This equation is for any non-constant function $\hat{C}(h)$ a non-linear evolution equation for the thickness of the fluid film. Incidentally, one may corroborate by substitution of

$$h(x, t) = F[x - \hat{C}(h)t] \tag{3.69}$$

into Eq. (3.68) that (3.69) is an implicit solution of Eq. (3.68) for every differentiable $F(\cdot)$, where

$$h(x, 0) = F(x) \tag{3.70}$$

gives F a meaning in terms of the initial profile. If $\hat{C}(h) = C = \text{const.}$, then (3.69) represents a wave, for which the wave form, given at $t = 0$ by $F(x)$ is maintained without distortion and which moves with speed C in the direction of the positive x-axis, see **Fig. 3.16**a. If $\hat{C}(h)$ is a function monotonically growing with h, then $h_1 > h_2$ implies $\hat{C}(h_1) > \hat{C}(h_2)$, so points on the surface with $h = h_1$ will travel faster than points with $h = h_2$. A wave form which is bell shaped at $t = 0$ will steepen with increasing time, and the wave front will at some time ahead overtop, see Fig. 3.16b. If this is to be avoided, there is nothing else left than to generalize the
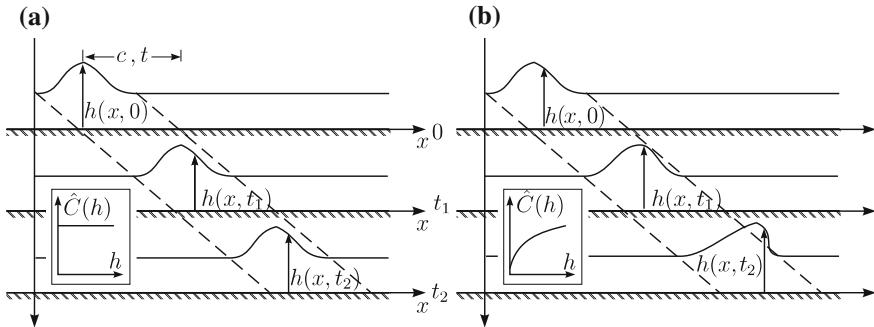
Fig. 3.16 Propagation of surface waves. **a** *Perseverance of the wave form for $\hat{C}$* = constant. **b** *Steepening of the wave profile for monotonically increasing $\hat{C}(h)$*

ansatz (3.67) for the volume flow Q. For instance, if we set

$$Q = \hat{Q}\left(h, \frac{\partial h}{\partial x}\right),\tag{3.71}$$

and, thus, request that Q depends on both h and $\partial h/\partial x$, it can be easily shown that Eq. (3.68) must be replaced by

$$\frac{\partial h}{\partial t} + \hat{C}\left(h, \frac{\partial h}{\partial x}\right)\frac{\partial h}{\partial x} - \hat{D}\left(h, \frac{\partial h}{\partial x}\right)\frac{\partial^2 h}{\partial x^2} = 0,\tag{3.72}$$

in which

$$\hat{C} = \frac{\partial \hat{Q}}{\partial h} > 0 \quad \text{and} \quad \hat{D} = -\frac{\partial \hat{Q}}{\partial(\partial h/\partial x)} \quad (> 0).\tag{3.73}$$

It is seen that, apart from the local and convective terms in (3.72) a **diffusive term** (involving the second space derivative) has entered Eq. (3.72), which can be shown to counteract the mentioned steepening of the wave, if the diffusivity $\hat{D}$ is positive.

It is now clear, how relations (3.67) and (3.71) would have to be postulated in order to still generalize the wave equation for h. Here, we will restrict ourselves to these few remarks.

3.3 Balance of Linear Momentum

In the hydrostatic theory of Chap. 2, on using the equilibrium equations, we established a relation between the pressure and the specific volume force, gravity; no other forces were involved. In a fluid in motion, apart from the pressure there also arise in

general shear stresses (see Chap. 1), in particular when these motions deviate from a rigid body motion. These shear stresses can under certain conditions be ignored in comparison to the pressure. If this is so, one speaks of a **frictionless** or **inviscid flow**.[5] Alternatively, one may envisage a fluid which is not capable of sustaining shear stresses at all; in this case one speaks of a **frictionless** or **inviscid fluid**. The shear stresses which arise in a flow field are due to the friction in the interior of a body and are thus a property of the material, not the flow. In this chapter we restrict considerations to inviscid fluids; flows of viscous fluids will be the topic of Chap. 7.
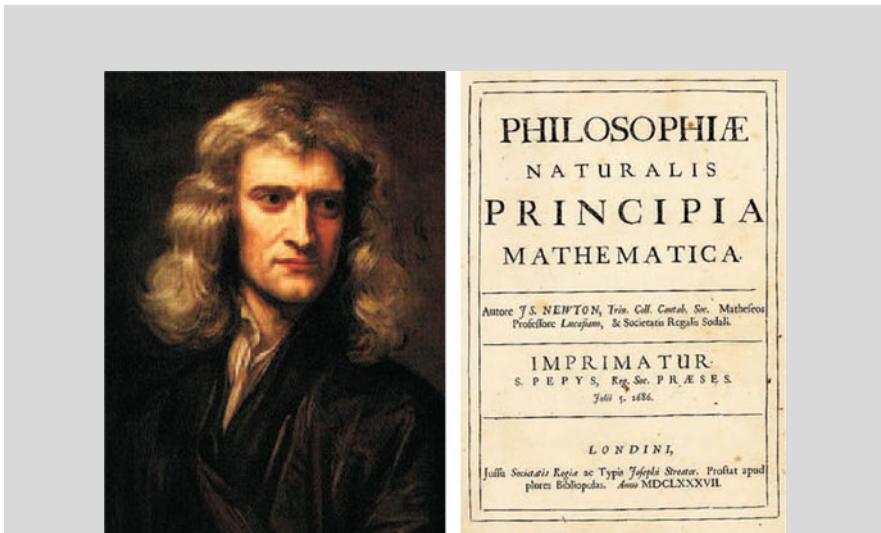
Fig. 3.17 Godfrey KNELLER's 1689 portrait of Isaac NEWTON (aged 46) (http://www.library.usyd.edu.au/) and NEWTON's *Principia*, the most important book on natural philosophy published in the early modern period

Sir ISAAC NEWTON (4. Jan. 1643–31. March 1727) was an English physicist, mathematician, astronomer, natural philosopher, alchemist, and theologian who is considered as one of the most influential people in human history. His 1687 publication of the *Philosophiae Naturalis Principia Mathematica* (usually called the *Principia*) is among the most influential books in the history of science, laying the groundwork for most of classical mechanics. In this work, NEWTON described universal gravitation and the three laws of motion which dominated the scientific view of the physical universe for the next three centuries. NEWTON showed that the motions of objects on Earth and of celestial bodies are governed by the same set of natural laws by demonstrating the consistency between KEPLER's laws of planetary motion and his theory of gravitation, thus removing the last doubts about heliocentrism and advancing the scientific revolution.

---

[5]This term is actually ill-defined. A flow cannot be inviscid; it is the fluid, which might be inviscid.

NEWTON also built the first practical reflecting telescope and developed a theory of colour based on the observation that a prism decomposes white light into the many colours that form the visible spectrum. He also formulated an empirical law of cooling and viscous friction and studied the speed of sound.

In mathematics, NEWTON shares the credit with Gottfried LEIBNIZ for the development of the differential and integral calculus, but LEIBNIZ published his work first. For years there was friction between the two countries over priority. Moreover, the science of fluxions (NEWTON's terminology) and differential calculus (LEIBNIZ's terminology) differed in notation. Today the latter is favoured. He also demonstrated the generalised binomial theorem, developed NEWTON's method for approximating the roots of a function, and contributed to the study of power series.

LAGRANGE once said that NEWTON was the greatest genius who ever lived, and once added that NEWTON was also 'the most fortunate, for we cannot find more than once a system of the world to establish'. NEWTON himself had been rather more modest of his own achievements, famously writing in a letter to Robert HOOKE in February 1676: 'If I have seen further it is by standing on the shoulders of Giants.'

The text is based on http://www.wikipedia.org

Foundation of the balance law of momentum is NEWTON's **fundamental law**,[6] often called his second law, which is the statement

$$\boxed{\begin{array}{l}\text{Time rate of change} \\ \text{of momentum of a body}\end{array}} \quad = \quad \boxed{\begin{array}{l}\text{Sum of all forces acting} \\ \text{on the body}\end{array}} \quad . \quad (3.74)$$

This is NEWTON's fundamental law how it is spoken out today. A more popular version which is known to virtually every high school student is

$$\boxed{\text{Mass times acceleration}} \quad = \quad \boxed{\begin{array}{l}\text{Sum of the forces} \\ \text{acting on the body}\end{array}} \quad , \quad (3.75)$$

but this is less general,[7] and (3.74) implies (3.75) but not vice versa.
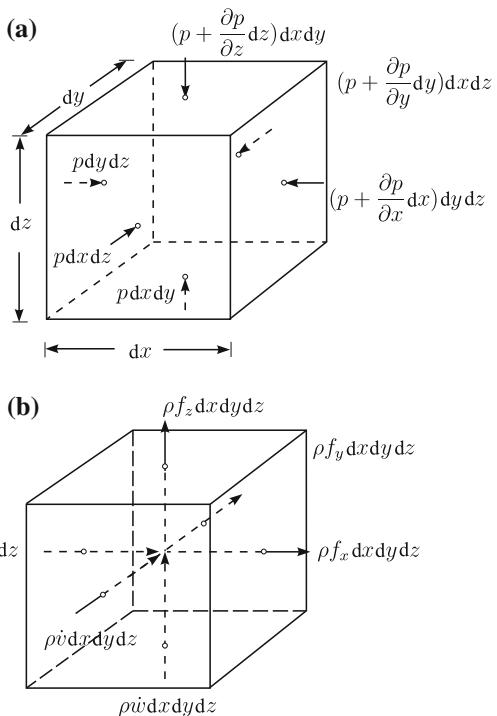
A possibility to quantify the above statement (3.74) consists in applying it to an infinitesimal material volume element. The infinitesimal cube of **Fig. 3.18** is loaded in its center of gravity by the specific body force ρf_z. In an inviscid fluid the surface forces are restricted to the pressure forces. On the two surface elements perpendicular to the x-axis these forces are given by

$$p\,\mathrm{d}y\mathrm{d}z \quad \text{and} \quad \left(p + \frac{\partial p}{\partial x}\mathrm{d}x\right)\mathrm{d}y\mathrm{d}z;$$

---

[6]For a short biography of NEWTON see **Fig. 3.17**.

[7]The difference of the two formulations is shown when NEWTON's fundamental law is written down for the motion of a rocket with exhaustion of burning fuel.

Fig. 3.18 Illustrating the
derivation of the EULER
equations. **a** *Infinitesimal
cube with pressure forces
acting on the surface
elements.* **b** *Same as in* (a),
*but now showing the volume
forces and the time rates of
changes of the momenta*

these forces are parallel to the x-axis and point into the cube. Similar pressure forces
also act on the other four surface elements as sketched in Fig. 3.18a. If $\boldsymbol{v} = (u, v, w)$
denotes the velocity vector with which the cubic element moves, then its momentum
change ($=$ mass $\times$ acceleration) is given by $\rho(\mathrm{d}u/\mathrm{d}t)\mathrm{d}t\mathrm{d}x\mathrm{d}y\mathrm{d}z$.[8] Application in

---

[8]The derivation of this formula for an infinitesimal cube is best obtained, if one applies the formula

$$\frac{\mathrm{d}}{\mathrm{d}t}\int_V \rho\boldsymbol{v}\,\mathrm{d}V = \int_V \frac{\partial(\rho\boldsymbol{v})}{\partial t}\,\mathrm{d}V + \int_{\partial V}\rho\boldsymbol{v}(\boldsymbol{v}\cdot\boldsymbol{n})\,\mathrm{d}A$$

to an infinitesimal cube fixed in space. If we apply this formula to the x-momentum and the cube
of Fig. 3.18, we obtain

$$\left\{\frac{\partial(\rho u)}{\partial t} + \frac{\partial}{\partial x}\left(\rho u^2\right) + \frac{\partial}{\partial y}(\rho uv) + \frac{\partial}{\partial z}(\rho uw)\right\}\mathrm{d}x\mathrm{d}y\mathrm{d}z$$

$$= \left[u\underbrace{\left\{\frac{\partial\rho}{\partial t} + \frac{\partial\rho u}{\partial x} + \frac{\partial\rho v}{\partial y} + \frac{\partial\rho w}{\partial z}\right\}}_{\text{balance of mass}=0} + \rho\underbrace{\left\{\frac{\partial u}{\partial t} + u\frac{\partial u}{\partial x} + v\frac{\partial u}{\partial y} + w\frac{\partial u}{\partial z}\right\}}_{\mathrm{d}u/\mathrm{d}t}\right]\mathrm{d}x\mathrm{d}y\mathrm{d}z$$

$$= \rho\frac{\mathrm{d}u}{\mathrm{d}t}\mathrm{d}x\mathrm{d}y\mathrm{d}z.$$

the x-direction of NEWTON's fundamental law in the form (3.75) thus leads to the statement

$$\rho \frac{\mathrm{d}u}{\mathrm{d}t}\,\mathrm{d}x\mathrm{d}y\mathrm{d}z = p\,\mathrm{d}y\mathrm{d}z - \left(p + \frac{\partial p}{\partial x}\mathrm{d}x\right)\mathrm{d}y\mathrm{d}z + \rho f_x\,\mathrm{d}x\mathrm{d}y\mathrm{d}z. \qquad (3.76)$$

Analogous statements can also be derived for NEWTON's law in the y- and z-directions, of which the derivation is left to the reader. If both sides of these equations are divided by the cubic volume $\mathrm{d}x\mathrm{d}y\mathrm{d}z$, then one obtains

$$\begin{aligned}
\rho \frac{\mathrm{d}u}{\mathrm{d}t} &= -\frac{\partial p}{\partial x} + \rho f_x, \\
\rho \frac{\mathrm{d}v}{\mathrm{d}t} &= -\frac{\partial p}{\partial y} + \rho f_y, \\
\rho \frac{\mathrm{d}w}{\mathrm{d}t} &= -\frac{\partial p}{\partial z} + \rho f_z,
\end{aligned} \qquad (3.77)$$

or in symbolic vector notation

$$\rho \frac{\mathrm{d}\boldsymbol{v}}{\mathrm{d}t} = -\mathrm{grad}\,p + \rho\boldsymbol{f}. \qquad (3.78)$$

These equations have first been derived for an ideal fluid continuum by LEONHARD EULER (1707–1783).[9] For this reason, they are called the **Euler equations**.

  In the above derivation no assumption regarding the prerequisites of the system, relative to which the fluid is moving has been made; the only assumption was that the element was material. In an **inertial system**, the acceleration is given by

$$\frac{\mathrm{d}\boldsymbol{v}}{\mathrm{d}t} = \frac{\partial \boldsymbol{v}}{\partial t} + (\mathrm{grad}\,\boldsymbol{v})\boldsymbol{v} = \frac{\partial \boldsymbol{v}}{\partial t} + \mathrm{grad}\left(\frac{|\boldsymbol{v}|^2}{2}\right) - \boldsymbol{v} \times \mathrm{curl}\,\boldsymbol{v}, \qquad (3.79)$$

and in a system which rotates with constant angular velocity ω, see **Fig. 3.20**, it takes the form

$$\begin{aligned}
\frac{\mathrm{d}\boldsymbol{v}}{\mathrm{d}t} &= \frac{\partial \boldsymbol{v}}{\partial t} + (\mathrm{grad}\,\boldsymbol{v})\boldsymbol{v} + \boldsymbol{\omega} \times (\boldsymbol{\omega} \times \boldsymbol{x}) + 2\boldsymbol{\omega} \times \boldsymbol{v} \\
&= \frac{\partial \boldsymbol{v}}{\partial t} + \mathrm{grad}\left(\frac{|\boldsymbol{v}|^2}{2}\right) - \boldsymbol{v} \times \mathrm{curl}\,\boldsymbol{v} - \mathrm{grad}\left(\frac{\omega^2 \hat{r}^2}{2}\right) + 2\boldsymbol{\omega} \times \boldsymbol{v}, \quad (3.80)
\end{aligned}$$

---

[9]For a short biographical sketch of EULER see **Fig. 3.19**.
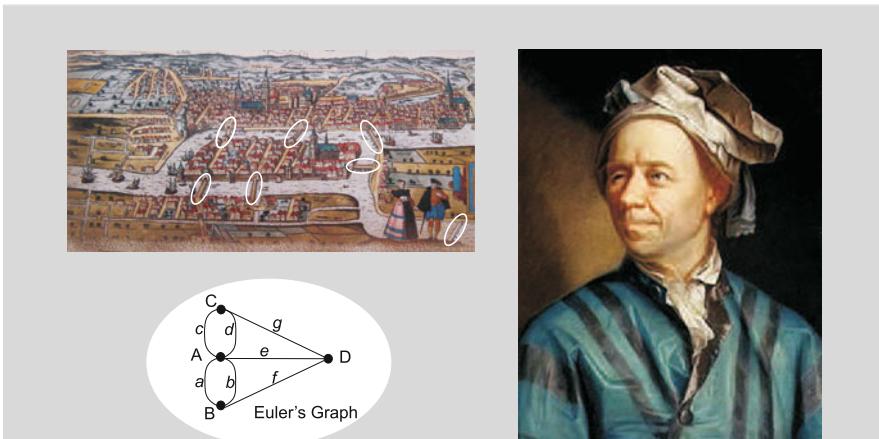
Fig. 3.19 *Right* Leonhard EULER. Portrait by Emanuel HANDMANN 1753 (http://en.wikipedia.org/). *Left* The Graph Theory originates with Leonard EULER's 1736 paper 'The Seven Bridges of Königsberg'. Map of Königsberg in EULER's time showing the actual layout of the seven bridges, highlighted by *ovals*
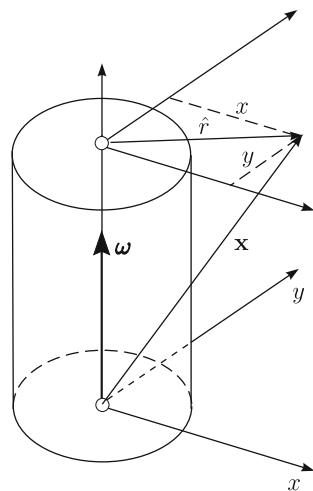
LEONHARD EULER (15. April 1707–18. Sept. 1783) was a pioneering Swiss mathematician and physicist who spent most of his life in Russia and Germany. EULER's early formal education started in Basel. At the age of thirteen he enrolled at the University of Basel, and in 1723, received his Master of Philosophy with a dissertation that compared the philosophies of DESCARTES and NEWTON. In May 1727 EULER arrived in St. Petersburg, took a position in the mathematics department of the Russian Academy of Sciences, just established by PETER the Great, and settled into life in St. Petersburg. EULER swiftly rose through the ranks in the academy and was made professor of physics in 1731 and head of the mathematics department. Concerned about the continuing turmoil in Russia, EULER left St. Petersburg in 1741 to take a post at the Berlin Academy. He lived for 25 years in Berlin, where he wrote over 380 articles. In 1766, exposed to conditions of negligence by the emperor FRIEDRICH the Great, EULER accepted an invitation of CATHERINE the Great to return to the St. Petersburg Academy where he spent the rest of his life.

EULER made important discoveries in fields as diverse as infinitesimal calculus and graph theory. He also introduced much of the modern mathematical terminology and notation, particularly for mathematical analysis. He is also renowned for his work in mechanics. For instance, he complemented NEWTON's Second Law by the Balance of Angular Momentum, the second pillar of classical continuum physics. EULER worked in almost all areas of mathematics: geometry, infinitesimal calculus, trigonometry, algebra, and number theory, as well as continuum physics, lunar theory and other areas of physics. He has been exceptionally productive; if printed, his works, many of which are of fundamental interest, would occupy between 60 and 80 quarto volumes.

Some of EULER's greatest successes were in solving real-world problems analytically, and in describing numerous applications of the BERNOULLI numbers, VENN diagrams, EULER numbers, the constants e and π, continued fractions and integrals. He demonstrated equivalence of LEIBNIZ's differential calculus and NEWTON's Method of Fluxions, and developed tools that made it easier to apply calculus to physical problems. In the context of this book his work is apparent through the EULER equations, the equations of motion of inviscid fluids.

The text is based on http://www.wikipedia.org

Fig. 3.20 Explaining the derivation of the centripetal acceleration. *In a reference system which rotates about the z-axis the centripetal acceleration can be expressed in a point according to formula (3.82); it involves ω and $\hat{r}$, the angular velocity and the distance of the point in question from the axis*

where, in the second expression (3.80) the relation

$$\boldsymbol{\omega} \times (\boldsymbol{\omega} \times \boldsymbol{x}) = -\text{grad}\left(\frac{\omega^2 \hat{r}^2}{2}\right) \tag{3.81}$$

has been used, in which $\hat{r}$ is the distance of a point from the axis of rotation.

Incidentally, relation (3.81) can easily be proved; to this end we only must write down the component forms $\boldsymbol{\omega} = (0, 0, \omega)$ and $\boldsymbol{x} = (x, y, z)$, see Fig. 3.20, and then obtain, after performing the vector product (3.81) twice,

$$\begin{aligned} \boldsymbol{\omega} \times (\boldsymbol{\omega} \times \boldsymbol{x}) &= -(\omega^2 x, \omega^2 y, 0) \\ &= -\text{grad}\left(\frac{\omega^2(x^2 + y^2)}{2}\right) = -\text{grad}\left(\frac{\omega^2 \hat{r}^2}{2}\right). \end{aligned} \tag{3.82}$$

Before presenting the first transformations and applications of the EULER equations we wish to derive these once more in a different, and likely more appropriate and mathematically more elegant way. As opposed to the first derivation by an infinitesimal element, this derivation is a **global formulation of the momentum balance equation** or NEWTON's law. By this we mean the application of the law of balance of momentum to a finite material volume V with boundary ∂V, see **Fig. 3.21**a. The application of the statement (3.74) to these new conditions reads as follows: *The time rate of change of the momentum of the material volume V equals the sum of the volume and surface forces acting on the body*, explicitly as a formula

$$\frac{\mathrm{d}\boldsymbol{I}_V}{\mathrm{d}t} = \boldsymbol{K}_V + \boldsymbol{K}_{\partial V}, \tag{3.83}$$
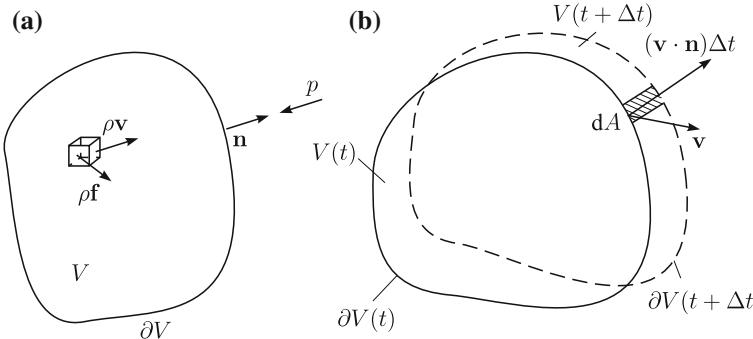
Fig. 3.21 Global formulation of the momentum balance. **a** *Material volume V with boundary ∂V. Volume element with specific volume force and specific momentum, surface element* d*A with exterior unit normal vector **n** and pressure p.* **b** *Volume V with boundary ∂V at two different times t and t + Δt with momentum flux through the surface element* d*A*

in which I_V is the momentum of the body with volume V and K_V and $K_{\partial V}$ denote the volume and surface forces, respectively. With the obvious representations

$$I_V = \int_{V(t)} \rho v \, \mathrm{d}V, \quad K_V = \int_{V(t)} \rho f \, \mathrm{d}V, \quad K_{\partial V} = - \int_{\partial V(t)} p n \, \mathrm{d}A, \qquad (3.84)$$

in which n is the exterior unit normal vector on ∂V, (3.83) takes the form

$$\frac{\mathrm{d}}{\mathrm{d}t} \int_V \rho v \, \mathrm{d}V = - \int_{\partial V} p n \, \mathrm{d}A + \int_V \rho f \, \mathrm{d}V. \qquad (3.85)$$

This equation is the global form of the balance law of linear momentum, however, only for the special situation that the surface forces comprise of normal tractions, i.e., pressures. For the evaluation of the time rate of change of the momentum, $\mathrm{d}I_V/\mathrm{d}t$, consider Fig. 3.21b, which shows the material volume at time t (solid curve) and $t + \Delta t$ (dashed curve), respectively; their momenta can be denoted as $I_V(t + \Delta t)$ and $I_V(t)$, respectively and may be parameterized as follows:

$$I_{V(t+\Delta t)} = \int_{V(t+\Delta t)} \left(\rho v + \frac{\partial \rho v}{\partial t} \Delta t \right) \mathrm{d}V$$

$$= \int_{V(t)} \left(\rho v + \frac{\partial \rho v}{\partial t} \Delta t \right) \mathrm{d}V + \Delta t \oint_{\partial V(t)} \rho v (v \cdot n) \, \mathrm{d}A,$$

$$I_V(t) = \int_{V(t)} \rho v \, \mathrm{d}V,$$

from which

$$\dot{\boldsymbol{I}}_{V(t)} = \lim_{\Delta t \to 0} \frac{1}{\Delta t} \{\boldsymbol{I}_V(t + \Delta t) - \boldsymbol{I}_V(t)\}$$

$$= \int_{V(t)} \frac{\partial(\rho \boldsymbol{v})}{\partial t} dV + \oint_{\partial V(t)} \rho \boldsymbol{v}(\boldsymbol{v} \cdot \boldsymbol{n}) dA \qquad (3.86)$$

ensues.[10] The time rate of change of the momentum of the material body $V(t)$ is, thus composed of an integral of the local change of the momentum plus a momentum flux across the surface $\partial V(t)$. The global form of the balance of momentum (3.85) can, therefore also be written in the form

$$\int_{V(t)} \frac{\partial(\rho \boldsymbol{v})}{\partial t} dV + \oint_{\partial V(t)} \rho \boldsymbol{v}(\boldsymbol{v} \cdot \boldsymbol{n}) dA = - \oint_{\partial V(t)} p \boldsymbol{n} dA + \int_{V(t)} \rho \boldsymbol{f} dV. \qquad (3.87)$$

This form will later be used for the evaluation of the force exerted on a body that is held submerged in a fluid which flows around it and, thus, via the tractions along its boundary, exerts a force on it.

For the derivation of the EULER equations from (3.87), we apply in the surface integrals the GAUSS law as follows[11]

---

[10]Equation (3.86) can also be viewed as a special case of the so-called **Reynolds transport theorem**, according to which for a continuously differentiable scalar, vectorial and tensorial field $\boldsymbol{a}$ the following expression

$$\frac{d}{dt} \int_{V(t)} \boldsymbol{a} \, dV = \int_{V(t)} \frac{\partial \boldsymbol{a}}{\partial t} dV + \oint_{\partial V(t)} \boldsymbol{a}(\boldsymbol{v} \cdot \boldsymbol{n}) dA$$

holds true. In (3.86), $\boldsymbol{a} = \rho \boldsymbol{v}$.

[11]The tensor product $\boldsymbol{v} \otimes \boldsymbol{v}$ of the vector variable $\boldsymbol{v}$ is that rank-2 tensor which in component representation has the form

$$\boldsymbol{v} \otimes \boldsymbol{v} \mathrel{\hat{=}} \begin{pmatrix} v_1 v_1 & v_1 v_2 & v_1 v_3 \\ v_2 v_1 & v_2 v_2 & v_2 v_3 \\ v_3 v_1 & v_3 v_2 & v_3 v_3 \end{pmatrix}.$$

Its divergence is given by the column vector

$$\text{div}\,(\boldsymbol{v} \otimes \boldsymbol{v}) = \begin{pmatrix} \dfrac{\partial v_1 v_1}{\partial x} + \dfrac{\partial v_1 v_2}{\partial y} + \dfrac{\partial v_1 v_3}{\partial z} \\[2ex] \dfrac{\partial v_2 v_1}{\partial x} + \dfrac{\partial v_2 v_2}{\partial y} + \dfrac{\partial v_2 v_3}{\partial z} \\[2ex] \dfrac{\partial v_3 v_1}{\partial x} + \dfrac{\partial v_3 v_2}{\partial y} + \dfrac{\partial v_3 v_3}{\partial z} \end{pmatrix}.$$

With these definitions the result (3.88) can easily be understood when written in component form. For a detailed explanation of the symbol "$\hat{=}$" see the footnote in connection with (3.275).

$$\oint_{\partial V(t)} \rho \boldsymbol{v}(\boldsymbol{v} \cdot \boldsymbol{n}) \, \mathrm{d}A = \int_{V(t)} \mathrm{div}\,(\rho \boldsymbol{v} \otimes \boldsymbol{v}) \, \mathrm{d}V,$$

$$-\oint_{\partial V(t)} p\boldsymbol{n} \, \mathrm{d}A \quad = -\int_{V(t)} \mathrm{grad}\, p \, \mathrm{d}V, \tag{3.88}$$

so that (3.87) takes the form

$$\int_{V(t)} \left(\frac{\partial(\rho \boldsymbol{v})}{\partial t} + \mathrm{div}\,(\rho \boldsymbol{v} \otimes \boldsymbol{v}) + \mathrm{grad}\, p - \rho \boldsymbol{f} \right) \mathrm{d}V = 0, \tag{3.89}$$

a relation which must hold for any material volume $V(t)$; in particular if a material volume element $\mathrm{d}V$ is used we conclude that the term in parentheses in (3.89) must vanish by itself, which implies that

$$\frac{\partial(\rho \boldsymbol{v})}{\partial t} + \mathrm{div}\,(\rho \boldsymbol{v} \otimes \boldsymbol{v}) = -\mathrm{grad}\, p + \rho \boldsymbol{f} \tag{3.90}$$

holds. Using product differentiation, the left-hand side of this equation can be brought into the form

$$\left(\frac{\partial \rho}{\partial t} + \mathrm{div}\,(\rho \boldsymbol{v}) \right) \boldsymbol{v} + \rho \left(\frac{\partial \boldsymbol{v}}{\partial t} + (\mathrm{grad}\, \boldsymbol{v})\boldsymbol{v} \right). \tag{3.91}$$

The first term in brackets vanishes, because mass balance must also be satisfied, see Eq. (3.44), so that (3.91) becomes

$$\rho \left(\frac{\partial \boldsymbol{v}}{\partial t} + (\mathrm{grad}\, \boldsymbol{v})\boldsymbol{v} \right) = -\mathrm{grad}\, p + \rho \boldsymbol{f}, \tag{3.92}$$

an equation, which agrees with the EULER equations (3.78).

3.4 Bernoulli's Equation

The equation, whose derivation is usually attributed to father JOHANN (1667–1748) and son DANIEL BERNOULLI (1700–1782),[12] actually goes back to LEONHARD EULER, is most likely the most famous equation of the entire hydrodynamic literature. With today's mathematical physical tools, it can be directly derived from the linear momentum equation; *the* BERNOULLI *equation is essentially nothing else than the balance of mechanical energy of an ideal fluid following the motion along a given or thought trajectory.*

---

[12]For a short biography of DANIEL BERNOULLI see **Fig. 3.22**.
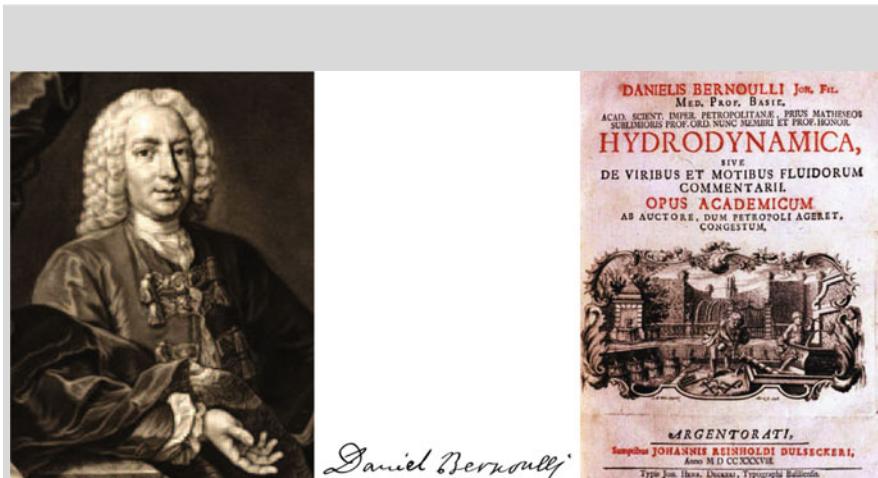
Fig. 3.22 DANIEL BERNOULLI (8. Feb. 1700–17. March 1782)

DANIEL BERNOULLI is a Swiss mathematician, physicist and physician of the famous family BERNOULLI. He was the son of the mathematician JOHANN BERNOULLI (1667–1748); NIKLAUS II BERNOULLI (1695–1726) was his brother and JAKOB I. BERNOULLI (1655–1705) his uncle. He was a pupil of GOTTFRIED WILHELM LEIBNIZ (1646–1716) and cooperated with LEONHARD EULER (1707–1783). He studied medicine in Basel and Heidelberg and was in 1720 promoted to Dr. med. in Basel. Until 1725 he travelled and established his name as a mathematician with papers on the RICATTI equation. In 1725 he and his brother received positions at the Russian Academy of Sciences in St. Petersburg. He returned back to Basel in 1733 and stayed there for the rest of his life. He had chairs of anatomy & botany, anatomy & physiology and since 1750 of physics.

The relations of DANIEL with his father were somewhat stressed. When both of them shared together the first prize in a scientific competition at the Academy in Paris, DANIEL was disowned by his father as the latter could not stand the shame to be compared with his son. DANIEL won this prize 10 times.

Daniel published in 1738 his principal work *Hydrodynamica*, which contains as one particular result what is now known as BERNOULLI's equation. The research results published in there were also published by his father JOHANN in a memoir with the title *Hydraulica*, as a plagiarism though, since he predated it by 7 years. Somewhat ironically, historians of mathematics found out that LEONHARD EULER had derived the BERNOULLI equation even before DANIEL BERNOULLI.

An English translation of 'Hydrodynamica' and 'Hydraulica' is given in [3].

The text is based on http://www.wikipedia.org

To introduce the reader into the essential ideas, we consider the plane flow filament of a density preserving fluid shown in **Fig. 3.23**a and cut out from it an infinitesimal spatially fixed element. Panel *b* in Fig. 3.23 displays the forces that act on this element and panel *c* shows the momentum fluxes at the left and right cross sections due to the flow through this filament. The time rate of change of the momentum, within this flow-filament increment is given by

$$\rho \, \mathrm{d}A \, \mathrm{d}s \, \frac{\partial u}{\partial t} \tag{3.93}$$

and must be balanced, i.e., be equal to the force and momentum flux components in the direction tangential to the filament and counted positive when they are in the same direction as the flow, explicitly,

$$
\begin{aligned}
p\mathrm{d}A - &\left(p + \frac{\partial p}{\partial s}\mathrm{d}s\right)\mathrm{d}A - \rho g \sin\alpha \mathrm{d}A \, \mathrm{d}s + (\rho u \mathrm{d}A)u \\
&- \left(\rho u + \frac{\partial(\rho u)}{\partial s}\mathrm{d}s\right)\mathrm{d}A \, u \\
&= -\frac{\partial p}{\partial s}\mathrm{d}s \, \mathrm{d}A - \rho g \sin\alpha \, \mathrm{d}A \, \mathrm{d}s - \rho\frac{\partial u}{\partial s}\mathrm{d}s \, \mathrm{d}A \, u.
\end{aligned}
\tag{3.94}
$$

(a)

(b)

(c)
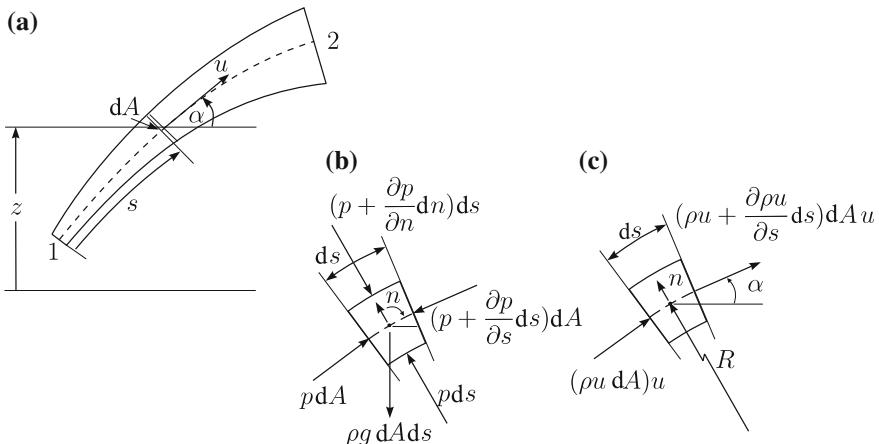
Fig. 3.23 Deriving the Bernoulli equation for a plane flow filament. **a** *Geometry of the flow filament and the two limiting integration sections 1 and 2 on the axis of the filament.* **b** *Forces acting on the flow filament.* **c** *Momentum flow through the cross sections of the element*

If we equate the two expressions (3.93) and (3.94) and divide the resulting equation by ds dA we obtain

$$\rho\left(\frac{\partial u}{\partial t} + \frac{\partial u}{\partial s}u\right) = -\frac{\partial p}{\partial s} - \rho g \sin\alpha = -\frac{\partial p}{\partial s} - \rho g\frac{dz}{ds}.$$

Owing to the assumption of density preserving, this momentum balance in the direction of the streamline can also be written as

$$\frac{\partial(\rho u)}{\partial t} + \frac{\partial}{\partial s}\left(\frac{\rho u^2}{2} + p + \rho gz\right) = 0$$

or after integration between $s = s_1$ and $s = s_2$ for fixed t

$$\int_{s_1}^{s_2}\frac{\partial(\rho u)}{\partial t}ds + \frac{\rho u_2{}^2}{2} + p_2 + \rho gz_2 = \frac{\rho u_1{}^2}{2} + p_1 + \rho gz_1. \qquad (3.95)$$

This is the **Bernoulli equation**, valid for unsteady flow of a density preserving inviscid fluid.

Complementary to the above we shall now also derive the momentum balance perpendicular to the flow filament. If one denotes the radius of curvature of the streamline in the center of the mass element by R, then the acceleration in the direction of R and positive away from the center of curvature is given by u^2/R. The momentum balance in the direction normal to the streamline filament and written for the element of Fig. 3.23 is therefore given by

$$\rho\frac{u^2}{R}dA\,ds = p\,ds - \left(p + \frac{\partial p}{\partial n}dn\right)ds - \rho g\cos\alpha\,dA\,ds, \qquad (3.96)$$

or, since d$A = 1 \cdot dn$

$$\rho\frac{u^2}{R} = -\frac{\partial p}{\partial n} - \rho g\cos\alpha. \qquad (3.97)$$

This formula can be used to evaluate the pressure gradient $\partial p/\partial n$ perpendicular to the element as soon as the algebraic speed u is known.

After this introductory example we now wish to derive the BERNOULLI equation with utmost rigor from the EULER equations. We refer the latter to a coordinate system that is rotating with constant angular velocity. With (3.78) and (3.80) these equations take the form

$$\frac{\partial \boldsymbol{v}}{\partial t} + \text{grad}\left(\frac{|\boldsymbol{v}|^2}{2} - \frac{\omega^2\hat{r}^2}{2}\right) + 2\boldsymbol{\omega}\times\boldsymbol{v} - \boldsymbol{v}\times\text{curl}\,\boldsymbol{v} = -\frac{\text{grad}\,p}{\rho} + \boldsymbol{f}. \qquad (3.98)$$

If both sides of this equation are scalarly multiplied with the vectorial line increment
dx and the resulting equation is then integrated at fixed time t along a smooth curve
which is everywhere tangential to dx from an initial point 1 to an end point 2, then
(3.98) becomes

$$\int\limits_1^2 \left(\frac{\partial v}{\partial t} + \operatorname{grad}\left(\frac{|v|^2}{2} - \frac{\omega^2 \hat{r}^2}{2} \right) + 2\omega \times v - v \times \operatorname{curl} v \right) \cdot \mathrm{d}x$$

$$= -\int\limits_1^2 \frac{\operatorname{grad} p \cdot \mathrm{d}x}{\rho} + \int\limits_1^2 f \cdot \mathrm{d}x, \tag{3.99}$$

or, if the specific body force f is derived from the potential,

$$f = -\operatorname{grad} U, \tag{3.100}$$

and the pressure increment along the path of integration is abbreviated by

$$\mathrm{d}p = \operatorname{grad} p \cdot \mathrm{d}x, \tag{3.101}$$

then

$$\int\limits_1^2 \frac{\partial v}{\partial t} \cdot \mathrm{d}x + \int\limits_1^2 \operatorname{grad}\left(\frac{|v|^2}{2} - \frac{\omega^2 \hat{r}^2}{2} + U \right) \cdot \mathrm{d}x + \int\limits_{p_1}^{p_2} \frac{\mathrm{d}p}{\rho}$$

$$= \int\limits_1^2 (v \times \operatorname{curl} v) \cdot \mathrm{d}x - \int\limits_1^2 (2\omega \times v) \cdot \mathrm{d}x. \tag{3.102}$$

The integrand in the second term can be written as a total differential in the form

$$d \left(\frac{|v|^2}{2} - \frac{\omega^2 \hat{r}^2}{2} + U \right). \tag{3.103}$$

So, a direct integration is possible, so that Eq. (3.102) takes the alternative form

$$\int\limits_1^2 \frac{\partial v}{\partial t} \cdot \mathrm{d}x + \left[\frac{|v|^2 - \omega^2 \hat{r}^2}{2} + U \right]_2 - \left[\frac{|v|^2 - \omega^2 \hat{r}^2}{2} + U \right]_1 + \int\limits_{p_1}^{p_2} \frac{\mathrm{d}p}{\rho}$$

$$= \int\limits_1^2 (v \times \operatorname{curl} v) \cdot \mathrm{d}x - \int\limits_1^2 (2\omega \times v) \cdot \mathrm{d}x. \tag{3.104}$$

In general, i.e., for arbitrarily smooth paths of integration the two integrals on the right hand sides of this equation cannot be simplified, however, if the path, along which one integrates is a **streamline** (dx is parallel to v, for which the triple products in (3.104) vanish), then the two terms on the right-hand sides vanish. We wish to limit attention to integrations along streamlines, and obtain in this case for *unsteady flows of compressible or volume preserving fluids the* BERNOULLI *equation* in the form

$$\int_1^2 \frac{\partial v}{\partial t} \cdot dx + \left[\frac{|v|^2 - \omega^2 \hat{r}^2}{2} + U \right]_2 - \left[\frac{|v|^2 - \omega^2 \hat{r}^2}{2} + U \right]_1 + \int_{p_1}^{p_2} \frac{dp}{\rho} = 0, \quad (3.105)$$

which is valid in this form for a frame of reference that is rotating with constant angular velocity ω. All forms of the BERNOULLI equation which arise in applications are special cases of this equation.

A **barotropic fluid** or (gas) is a fluid of which the *thermal equation of state* is given by

$$p = p(\rho) \qquad \text{or} \qquad \rho = \rho(p). \quad (3.106)$$

The pressure of such a fluid is therefore exclusively a function of the density or vice versa. For such fluids the integrated pressure

$$P(p) = \int_{p_0}^{p} \frac{d\bar{p}}{\rho(\bar{p})} \quad (3.107)$$

called **pressure function**, in which p_0 is an arbitrary constant, can be defined. With its aid, the integral term in (3.105) involving the pressure can explicitly be integrated to yield

$$\int_{p_1}^{p_2} \frac{dp}{\rho(p)} = P(p_2) - P(p_1) = P_2 - P_1. \quad (3.108)$$

Therefore, the **Bernoulli equation for a barotropic fluid** takes the simple form

$$\int_1^2 \frac{\partial v}{\partial t} \cdot dx + \left(P_2 + \frac{v_2^2}{2} - \frac{\omega^2 \hat{r}_2^2}{2} + U_2 \right) - \left(P_1 + \frac{v_1^2}{2} - \frac{\omega^2 \hat{r}_1^2}{2} + U_1 \right) = 0, \quad (3.109)$$

in which we have written v^2 for $|\boldsymbol{v}|^2$, as we shall henceforth often do. This equation can for **steady state processes** be further simplified to

$$P + \frac{v^2}{2} - \frac{\omega^2 \hat{r}^2}{2} + U = C = \text{const.} \tag{3.110}$$

along streamlines, steady processes.

The constant C in this equation takes, from streamline to streamline, a different value, since the integration is performed along streamlines. If the flow is free of vorticity, curl $\boldsymbol{v} = \boldsymbol{0}$, and if in addition the frame of reference is an inertial frame ($\boldsymbol{\omega} = \boldsymbol{0}$), then the two terms on the right-hand side of Eq. (3.104) both vanish, irrespectively along which kind of smooth curve the integration point 1 and point 2 is performed. In this case, the quantity

$$P + \frac{v^2}{2} + U = C \tag{3.111}$$

is a constant throughout the space occupied by the fluid in vortex free motion.

Additional special forms of the BERNOULLI equation are obtained, if one restricts considerations to special forms of the thermal equation of state or the specific body force. If the fluid is density preserving, the pressure function (for $p_0 = 0$) takes the form

$$P = \frac{p}{\rho}, \tag{3.112}$$

and if the specific body force is restricted to the gravity force, we have

$$U = gz, \tag{3.113}$$

in which the z-axis is directed upward. In this case, the BERNOULLI equation takes for unsteady flows the form

$$\int_1^2 \frac{\partial \boldsymbol{v}}{\partial t} \cdot \mathrm{d}\boldsymbol{x} + \left(\frac{p_2}{\rho} + \frac{v_2^2 - \omega^2 \hat{r}_2^2}{2} + gz_2 \right) - \left(\frac{p_1}{\rho} + \frac{v_1^2 - \omega^2 \hat{r}_1^2}{2} + gz_1 \right) = 0, \tag{3.114}$$

and can easily be specialized for steady flows or/and an inertial frame of reference. For steady flows and a rest frame, Eq. (3.114) becomes

$$\frac{p}{\rho} + gz + \frac{v^2}{2} = \text{const.}, \tag{3.115}$$

which may well be the most popular or best known form of the BERNOULLI equation. Incidentally, one often lumps the dynamic pressure p and the pressure due to gravity $\rho g z$ together according to

$$p^* = p + \rho g z, \tag{3.116}$$

and calls p^* the **piezometric pressure**. With it, the BERNOULLI equation for steady flows can be written in a particularly simple form,

$$p^* + \frac{\rho v^2}{2} = \text{const.} \tag{3.117}$$
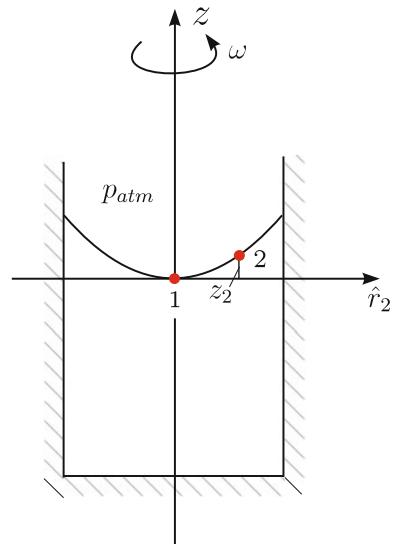
For a density preserving fluid at rest in a permanently rotating system, Eq. (3.114) implies

$$\frac{p}{\rho} - \frac{\omega^2 \hat{r}^2}{2} + g z = \text{const.} \tag{3.118}$$

If this equation is applied on two points of the free surface of a fluid, kept in a rotating cylinder, see **Fig. 3.24**, one obtains

$$\frac{p_2}{\rho} - \frac{\omega^2 \hat{r}_2^2}{2} + g z_2 = \frac{p_1}{\rho}, \tag{3.119}$$

Fig. 3.24 BERNOULLI equation. *Application of the* BERNOULLI *equation to a fluid with free surface that is at rest in the rotating system*

a relation, which for $p_1 = p_2 = p_{atm}$ reduces to

$$z_2 = \frac{\omega^2 \hat{r}_2^2}{2g}.$$
(3.120)

The free surface of a rotating ideal fluid has—as shown earlier already—the shape
of an axisymmetric paraboloid.

3.5 Simple Applications of the Bernoulli Equation

Example 3.1
Consider a density preserving fluid in the constant gravity field, which rests on an
infinite horizontal plane, **Fig. 3.25**. If one writes the BERNOULLI equation (3.115) for
the points 0 and 1 of the figure, one obtains (on omitting the index 1)

$$\frac{p}{\rho} + gz = \left(\frac{p}{\rho}\right)_0 = \text{const},$$

or

$$p = p_0 - \rho gz.$$
(3.121)
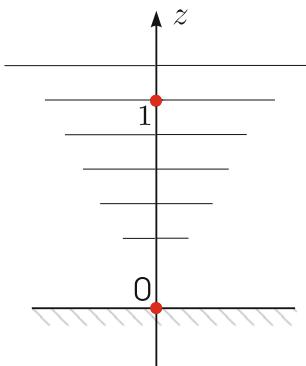
In a density preserving fluid subject to a constant gravity field the pressure decreases
linearly with increasing height.

Example 3.2
Let the half space of Fig. 3.25 be filled with an ideal gas of which the thermal equation
of state is given by

$$p = RT\rho,$$
(3.122)

Fig. 3.25 BERNOULLI
equation. *Application to a
fluid at rest*

in which T is the absolute temperature and R the gas constant. If the gas has in the entire half space the same temperature, then $T = $ const.; under such isothermal conditions the pressure function assumes the form

$$P = \int_{p_0}^{p} \frac{d\bar{p}}{\rho} = R\,T \int_{p_0}^{p} \frac{d\bar{p}}{\bar{p}} = R\,T \, \ln\left(\frac{p}{p_0}\right), \tag{3.123}$$

so that the BERNOULLI equation (3.115) for the gas at rest ($\boldsymbol{v} = \boldsymbol{0}$), subject to gravity takes the form

$$R\,T \, \ln\left(\frac{p}{p_0}\right) + gz = \text{const} = 0, \tag{3.124}$$

which can also be written as

$$p = p_0 \, \exp\left(-\frac{gz}{RT}\right). \tag{3.125}$$

This is the so-called **barometric pressure formula**. For small values of z, or more precisely, for $|gz/(RT)| \ll 1$, the exponential function can be developed into a TAYLOR series expansion, so that with its first two terms the pressure becomes

$$p \simeq p_0 - \frac{p_0}{RT}gz = p_0 - \rho_0 gz, \tag{3.126}$$

again (3.121), where ρ is to be replaced by ρ_0, the pressure at $z = 0$.

Example 3.3
A **Venturi tube** or **Venturi pipe** is a segment of a pipe, whose cross sectional diameter is linearly reduced from an area of value A_1 to the value A_2 and then increases again to the value A_1, see **Fig. 3.26**. The Venturi tube is used to measure, under steady state pipe flow conditions, the mean axial velocity in the pipe or the volume flux. Prerequisite is that the pressures can be measured at the cross sections 1 and 2. If we write for the wall near streamline in the two cross sections the BERNOULLI equation of a volume preserving fluid, we obtain

$$\frac{p_1}{\rho} + \frac{v_1^2}{2} + gz_1 = \frac{p_2}{\rho} + \frac{v_2^2}{2} + gz_2, \tag{3.127}$$

or with the **piezometric pressure** $p^* = p + \rho gz$,

$$\frac{p_1^*}{\rho} + \frac{v_1^2}{2} = \frac{p_2^*}{\rho} + \frac{v_2^2}{2}. \tag{3.128}$$

Adding to this the continuity relation

$$A_1 v_1 = A_2 v_2, \tag{3.129}$$

one may eliminate between the last two equations the velocity v_1 and then obtains for the velocity v_2 and the through flux Q, respectively
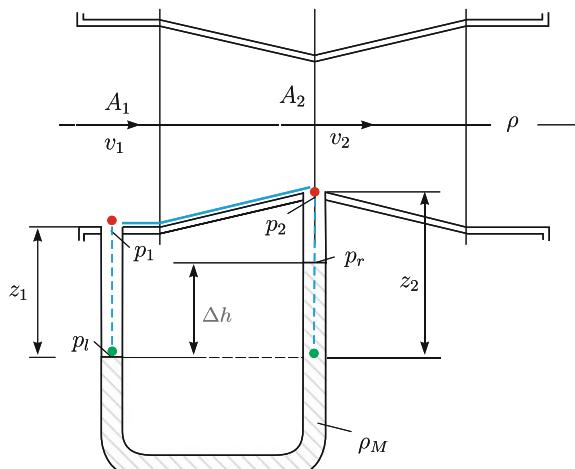
$$v_2 = \sqrt{\frac{\left(\frac{2}{\rho}\right)(p_1^* - p_2^*)}{1 - \left(\frac{A_2}{A_1}\right)^2}}, \qquad Q = A_2 v_2. \tag{3.130}$$

With the exception of the geometric quantities A_1, A_2 and the density ρ the steady flux through the pipe is given by the piezometric pressure difference $p_1^* - p_2^*$ via the square root formula (3.130).

Example 3.4

In the last example it remained unanswered, how the pressure difference $p_1^* - p_2^*$ is measured. The instrument, by which this can be done, is the **manometer**; its working principle is also shown in Fig. 3.26. The Venturi tube has along its lowest wall points two circular holes, one before or at cross section 1, the other at cross section 2; the two holes are connected by a hose (generally plastic and/or glass) forming a 'communicating' pipe. This manometer is filled with a fluid with density ρ_M, and one may measure the difference Δh in height of the menisci in the two left and right legs. The upper parts of the manometer up to the drill holes in the Venturi are filled with the (lighter) fluid of the pipe flow. If we now formulate the BERNOULLI equation for the points at the drill holes (but within the connecting tubes to the manometer

Fig. 3.26 Venturi pipe segment. *Explaining the steady flow formula (3.130)*

fluid, separately in the left and right leg one obtains the two equations

$$p_l = p_1 + \rho g z_1, \quad p_r = p_2 + \rho g (z_2 - \triangle h). \tag{3.131}$$

Alternatively, the BERNOULLI equation, formulated between the two menisci of the manometer fluid yields

$$p_l = p_r + \rho_M g \triangle h. \tag{3.132}$$

Consequently, the manometer does not show the true pressure difference $p_1 - p_2$ but the piezometric pressure difference

$$p_l - p_r = (p_1 + \rho g z_1) - (p_2 + \rho g z_2) + \rho g \triangle h = p_1^* - p_2^* + \rho g \triangle h. \tag{3.133}$$

In view of Eq. (3.132), we thus have

$$p_1^* - p_2^* = \rho_M g \left(1 - \frac{\rho}{\rho_M}\right) \triangle h, \tag{3.134}$$

in which the second term within the bracket can often be ignored (e.g. when the pipe fluid is air and the manometer liquid is mercury).

Example 3.5
On the surface of a body at rest, which is completely submerged in a fluid which moves, there is at least one point on the surface at which the fluid velocity vanishes. This point is called the **stagnation point**. The streamline in the fluid connected to this point is called **stagnation streamline**; at the stagnation point this streamline separates into two, following the upper and lower body contour, see **Fig. 3.27**a. In the **Prandtl flow tube** this fact is exploited by submerging a small streamlined body into the flowing fluid. With this body the flow tube of Fig. 3.27b that is filled with a manometer fluid of density ρ_M is connected. If this PRANDTL flow tube is small as compared to the size of the region that is filled by the fluid and if the flow tube is submerged in the fluid such that its long axis is parallel to the local flow, then the flow will build a stagnation point at the point 1, whilst at point 2 unperturbed external flow will approximately prevail, of which the velocity and pressure will be denoted by V_∞ and p_∞, respectively, see Fig. 3.27b. If one writes the BERNOULLI equation for points 1 and 2 in the surrounding fluid, one obtains

$$p_S^* = p_\infty^* + \frac{\rho}{2} v_\infty^2, \tag{3.135}$$

where $p_S = p_1$ denotes the stagnation pressure and the asterisks refer to piezometric pressures. Analogously, one obtains from the BERNOULLI equation, written for the menisci of the manometer fluid in the two legs

$$p_S^* - p_\infty^* = \rho_M g \triangle h. \tag{3.136}$$

(a)

stagnation
streamline

stagnation point

(b)

v_∞

v_∞

Δh

ρ_M
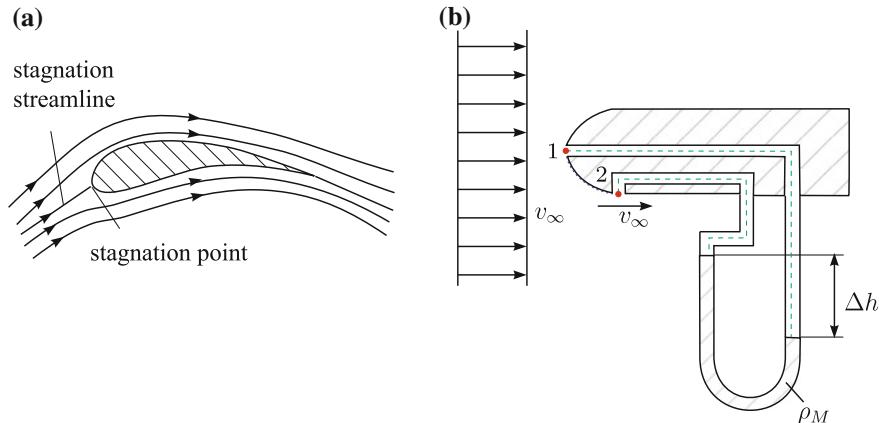
Fig. 3.27 PRANDTL stagnation tube. **a** *Flow in the vicinity of a stagnation point.* **b** *Sketch of the principle of a* PRANDTL *tube*

The two last expressions imply
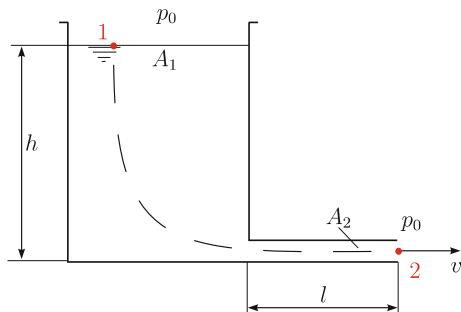
$$v_\infty = \sqrt{2\frac{\rho_M}{\rho}g\Delta h}. \tag{3.137}$$

The velocity in the immediate vicinity of the PRANDTL flow tube is therefore known, if one knows the densities of the fluid and manometer fluid and if one measures Δh.

Example 3.6
Consider now a container filled with a density preserving fluid which is emptied through a piece of a tube of length l that is connected with the container through a bottom outlet at the wall, see **Fig. 3.28**. Let the cross sections of the container and the tube have areas A_1 and A_2, respectively, and assume that A_1 is large as compared to A_2, so that the fluid velocity in the container can be ignored in comparison to the

Fig. 3.28 Discharge from a container. *The time evolution of the velocity at the end cross section of the tube is governed by the container height h and the tube length l*

p_0

A_1

h

A_2 p_0

v

l

velocity in the tube. The flow in this emptying process of the container is unsteady, so that the BERNOULLI equation, written along the dashed streamline in Fig. 3.28 between point 1 on the free surface and point 2 at the exit cross section of the tube, must be used in the form (3.114) (in which the terms due to the rotation of the frame of reference must be dropped). Since the velocities within the container are negligibly small, we have along the drawn streamline

$$\int_{1}^{2} \frac{\partial \boldsymbol{v}}{\partial t} \cdot \mathrm{d}\boldsymbol{x} \cong \frac{\mathrm{d}v}{\mathrm{d}t} l, \tag{3.138}$$

so that Eq. (3.114) with $\omega = 0$ takes the form

$$\frac{\mathrm{d}v}{\mathrm{d}t} l + \left(\frac{v^2}{2} + \frac{p_0}{\rho} \right) - \left(\frac{p_0}{\rho} + gh \right) = 0, \tag{3.139}$$

which can also be written as

$$\frac{\mathrm{d}v}{\mathrm{d}t} + \frac{v^2}{2\,l} - \frac{gh}{l} = 0. \tag{3.140}$$

It constitutes an ordinary differential equation of the first order for v. We shall present its solution subject to the initial condition $v(0) = 0$, a start from rest. To this end, let us introduce with

$$\varphi(\tau) = \frac{v}{\sqrt{2gh}} \quad \text{and} \quad \tau = t \frac{\sqrt{2gh}}{2l}, \tag{3.141}$$

a dimensionless velocity and a dimensionless time; introducing them into (3.140) transforms this equation into

$$\frac{\mathrm{d}\varphi}{\mathrm{d}\tau} + \varphi^2 = 1 \quad \text{or} \quad \frac{\mathrm{d}\varphi}{1 - \varphi^2} = \mathrm{d}\tau, \tag{3.142}$$

which, subject to the initial condition $\phi(0) = 0$ can be integrated, with the solution[13]
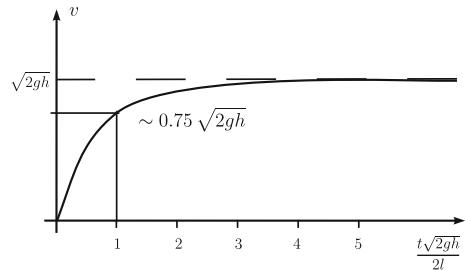
$$\tau = \text{Areatanh } \varphi \quad \text{or} \quad \varphi = \tanh \tau. \tag{3.143}$$

If one goes back again to the original variables, then (3.143) transforms into

$$v = \sqrt{2gh} \ \tanh \left(\frac{\sqrt{2gh}}{2l} t \right), \tag{3.144}$$

---

[13] Atanh or Areatanh is the inverse function of tanh, sometimes also written as $\tanh^{-1}$.

Fig. 3.29 Exit flow from a
container. *Time evolution of
the exit velocity after sudden
opening of a valve*

which is graphically displayed in **Fig. 3.29**. For $t \to \infty$ this formula reduces to

$$v = \sqrt{2gh}, \tag{3.145}$$

the so-called **Torricelli formula**, named after EVANGELISTA TORRICELLI, for his
short biography see **Fig. 3.30**. Incidentally, it can also be derived by means of the
BERNOULLI equation under assumptions of steady motion; indeed, if in Eq. (3.139)
we ignore the term involving $d(\cdot)/dt$, which is due to the unsteadiness, we directly
obtain (3.145). Formula (3.144), therefore, gives us a hint, how long it takes after
opening a valve and initiating a flow until a steady state flow is reached. Since the
free surface in the container moves slowly downward (if no adequate inflow counter-
balances this) such steady state conditions are seldom exactly satisfied.

TORRICELLI formula (3.145) does not depend on quantities pertinent to the fluid
material, only the gravity and the height; this is why the exit velocity out of the nozzle
of the vessel is the same for e.g. water and mercury.

With the aid of TORRICELLI's formula one may calculate the time Δt it takes to
empty a container from an initial height h_i to a final height h_f. To this end one only
needs to write down the continuity equation for the system. During a time increment
dt the exit flow through the tube cross section 2 is given by $A_2 v dt$. During the
same time increment the free surface in the container is lowered by $-dh$, which
corresponds to a volume $-A_1 dh$. If we equate these expressions, we obtain

$$\frac{dh}{dt} = -\frac{A_2}{A_1} v = -\frac{A_2}{A_1}\sqrt{2gh}, \tag{3.146}$$

or

$$dt = -\frac{1}{\sqrt{2g}}\frac{A_1}{A_2}\frac{dh}{\sqrt{h}}, \tag{3.147}$$

which can be integrated as follows

$$\Delta t = \int_0^{\Delta t} dt = -\frac{1}{\sqrt{2g}}\frac{A_1}{A_2}\int_{h_a}^{h_f}\frac{dh}{\sqrt{h}} = \sqrt{\frac{2}{g}}\frac{A_1}{A_2}\left(\sqrt{h_a} - \sqrt{h_f}\right). \tag{3.148}$$

Fig. 3.30 EVANGELISTA TORRICELLI (15. Oct. 1608–25. Oct. 1647)

EVANGELISTA TORRICELLI was an Italian physicist and mathematician and has worked briefly under GALILEO GALILEI. He applied in the year 1640 the Galilean laws of gravity to the flow of a liquid out of a vessel through a thin tube. If the vessel has constant cross section, then formula (3.145) applies, which is called TORRICELLI's formula. TORRICELLI also worked on pressure distributions in vessels, which is the reason why the old pressure unit 'Torr' is called after him. In 1642, after the death of GALILEO GALILEI, TORRICELLO became his successor as grand-ducal mathematician and chair of mathematics at the University of Pisa.

Besides his work on the water outflow from punctured vessels TORRICELLI also became known through his invention of the mercury *barometer*; he also studied *projectiles* and how they move through air, and he gave a scientific description of the cause of *wind* in the Earth's atmosphere. In mathematics he became famous for his discovery of the TORRICELLI trumpet, whose surface area is infinite, whereas its volume is finite. This created a philosophical dispute on the nature of infinity e.g. involving the philosopher THOMAS HOBBES (1588–1679). TORRICELLI also was a pioneer in the area of infinite series and the method of *indivisibles*.

The text is based on http://www.wikipedia.org

A complete emptying for which $h_f = 0$, therefore lasts the time

$$\triangle t = \sqrt{\frac{2h_a}{g}} \frac{A_1}{A_2}. \tag{3.149}$$

In the above example the cross sectional area A_1 of the vessel has been assumed to be constant, i.e., h-independent. If it varies with h, Eq. (3.146) may be used to construct a fluid mechanical clock; however, according to formula (3.148) equal time steps Δt correspond to nonlinear height steps $dh/\sqrt{h}$. To construct a clock for

which equal time steps would correspond to equal space steps of the free surface, requires A_1 to vary as $A_1 = c\sqrt{2gh}$, c[s] is a constant. For this choice (3.146) implies

$$\frac{\mathrm{d}h}{\mathrm{d}t} = -\frac{A_2}{c} \longrightarrow h = -\frac{A_2}{c}t + h_a, \tag{3.150}$$

where h_a is the initial height. If the vessel is axisymmetric, $A_1 = r^2\pi = c\sqrt{2gh}$, in which r is the vessel radius at height h, this yields

$$H = \frac{\pi^2}{2g\,c^2}r^4 = \text{const} \times r^4. \tag{3.151}$$

This solution has been a significant achievement of water clock makers through several thousand years. More specifically, ancient clock makers were aware of the fact that the rate of flow of water out of a punctured vessel is not uniform, but its first clear statement is by EVANGELISTA TORRICELLI, and the likely first printed solution, equivalent to (3.151) was in the year 1686 in a posthumous book by the French physicist EDMÉ MARIOTTE; for details, see [16].

Such clocks are called *clepsydrae*, which were the chronometers of the Egyptians, Greeks and Romans and the word derives from ancient greek and is composed of 'steal' ($\kappa\lambda\epsilon\pi\tau\epsilon\,\tilde{\iota}\nu$) and 'water' ($\upsilon\delta\omega\rho$). 'Ancient water clocks consisted of an earthenware bowl with one or more holes in the bottom from which water escapes ($\sim$ was stolen). The oldest extant clepsydra, which today is in the Science Museum in London, comes from Karak in Upper Egypt and was made about 1400 BC', from [16], see **Fig. 3.31**a. 'Early design of clepsydrae could only approximate the ideal shape as expressed by (3.151). The clepsydra of Karak was likely such an approximation. Its shape is compared with the quartic curve in panel b) of Fig. 3.31. The two curves are very close to each other, however, even though the geometric differences are quite
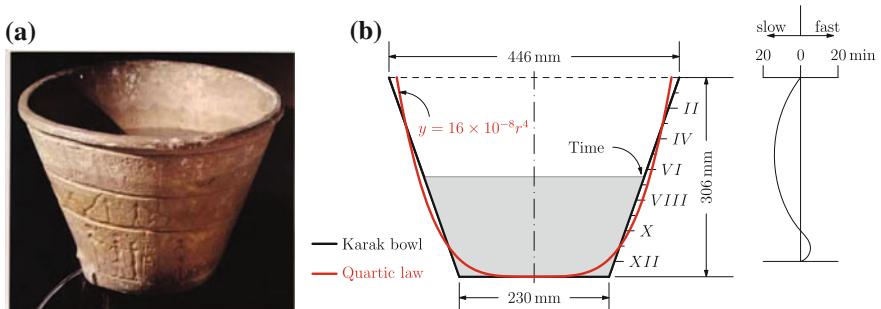
Fig. 3.31 a Oldest known clepsydra is the Karak bowl from ∼1400 B.C. **b** Karak bowl approximation and exact quartic law geometry for linear decreases of water level. The curve on the *right* shows how much the water level drop is faster and slower, respectively. Courtesy McNown [13] © La Houille Blanche

small, they still account for considerable timing errors, which may have delayed the development of Egyptian Astronomy', [13].

It is interesting that the young ISAAC NEWTON at age 12 built several water clocks at his home in Woolstrhorp. Sadly, they do not survive, [see, however, [14]]. He presented two different versions of water clocks.

Moreover, according to [16], the Egyptians had some awareness that the shape of the vessel would influence the downfall speed of the free water surface, but it was TORRICELLI who first made a clear statement. The first printed solution of the problem was 1686 in a posthumous book by the French physicist EDME MARIOTTE.
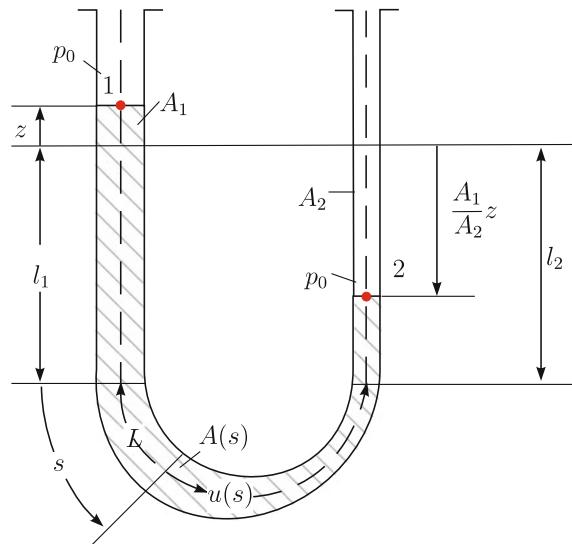
Example 3.7

As a further application of the BERNOULLI equation to an unsteady problem, let us look at an oscillation of a water column in a U-shaped tube with variable cross section, see **Fig. 3.32**. We assume that the two vertical legs have constant cross section whereas the connecting curved part continuously adjusts the cross section to those of the two legs. We further assume that during motion the menisci will never leave the domains of the vertical legs. Figure 3.32 shows the system when the water level in the left tube is displaced by the amount z from the rest position. Because of continuity (note the fluid is density preserving) the water level in the right tube is then correspondingly displaced downward by the amount $(A_1/A_2)z$. Again because of continuity, we then have

$$A_1\dot{z} = -A(s)u(s) = -A_2u_2, \qquad (3.152)$$

in which the negative sign accounts for the fact that $\dot{z}$ and $u(s)$ are counted positive in opposite directions. To apply the BERNOULLI equation (3.114) (in which $\omega = 0$)

Fig. 3.32 Communicating pipes. *Oscillations of a fluid in a U-shaped tube*

to the points 1 and 2 on the free surfaces of the menisci, we first compute the integral

$$
\int_1^2 \frac{\partial u}{\partial t} \, ds = -\ddot{z}(z + l_1) - \int_0^L \frac{A_1}{A(s)} \ddot{z} \, ds - \frac{A_1}{A_2} \ddot{z} \left(l_2 - \frac{A_1}{A_2} z \right)
$$

$$
= -\ddot{z} \left\{ z + l_1 + \int_0^L \frac{A_1}{A(s)} \, ds + \frac{A_1}{A_2} l_2 - \frac{A_1^2}{A_2^2} z \right\}
$$

$$
= -\ddot{z} \mathcal{L}(z), \tag{3.153}
$$

in which $\mathcal{L}(z)$ denotes a generalized length. With it, the BERNOULLI equation takes the form

$$
-\ddot{z}\mathcal{L}(z) + \left[\frac{p_0}{\rho} + \left(\frac{A_1}{A_2} \right)^2 \frac{\dot{z}^2}{2} - \frac{A_1}{A_2} gz \right] - \left[\frac{p_0}{\rho} + \frac{\dot{z}^2}{2} + gz \right] = 0, \tag{3.154}
$$

or after rearrangements,

$$
\ddot{z}\mathcal{L}(z) + \frac{1}{2} \left[1 - \left(\frac{A_1}{A_2} \right)^2 \right] \dot{z}^2 + g \left(1 + \frac{A_1}{A_2} \right) z = 0. \tag{3.155}
$$

This is a nonlinear ordinary differential equation describing the oscillation of the free surface in the left leg. The nonlinearity arises in the generalized length as well as in the kinetic energy. Linearization for small displacements and velocities from the position at rest leads to the differential equation of a harmonic oscillator

$$
\ddot{z} + \frac{g \left(1 + \dfrac{A_1}{A_2} \right)}{\mathcal{L}(0)} z = 0. \tag{3.156}
$$
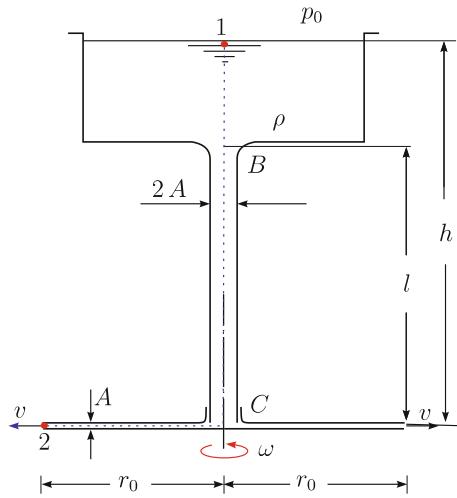
With the circular frequency ω and period T given by

$$
\omega^2 = \frac{g \left(1 + \dfrac{A_1}{A_2} \right)}{\mathcal{L}(0)}, \qquad T = \frac{2\pi}{\omega}. \tag{3.157}
$$

Example 3.8
This example illustrates the application of the **Bernoulli equation** when it is referred to a **rotating frame of reference**. To this end, let us consider the fluid container of **Fig. 3.33**. This container is connected with a vertical pipe to a horizontal tube with two arms that can rotate about the central vertical axis of the pipe. We assume the two tubes to rotate with constant angular velocity ω. At their end cross sections with a distance r_0 from the axis of rotation, fluid from the container leaves the system

Fig. 3.33 Rotating exit flow
from a container. BERNOULLI
equation relative to a
rotating frame: Exit flow
from a rotating tube

with the speed v. The cross sectional areas of the tubes and the connecting pipe are A
and $2A$, respectively. The constant angular velocity must be maintained by a motor.
We also suppose that the cross sectional area of the container is large in comparison
to the exit cross sectional area A: this implies that the velocity of the free surface of
the container and any point within the container can be ignored. Thus, the level h of
the free surface remains constant. Consequently, steady conditions prevail, and the
BERNOULLI equation, written for points 1 and 2, takes the form

$$\frac{p_1}{\rho} + \frac{v_1^2 - \omega^2 \hat{r}_1^2}{2} + gz_1 = \frac{p_2}{\rho} + \frac{v_2^2 - \omega^2 \hat{r}_2^2}{2} + gz_2. \qquad (3.158)$$

For the two points 1 and 2 in Fig. 3.33 we have

$$\begin{aligned} p_1 &= p_0, & v_1 &= 0, & \hat{r}_1 &= 0, & z_1 &= h, \\ p_2 &= p_0, & v_2 &= v, & \hat{r}_2 &= r_0, & z_2 &= 0. \end{aligned} \qquad (3.159)$$

Substitution of these relations in Eq. (3.158) leads to an equation for $v_2 = v$ with the
result

$$v = v_{\text{stat}} = \sqrt{2gh \left(1 + \frac{\omega^2 r_0^2}{2gh}\right)}. \qquad (3.160)$$

If one is also interested in the pressures at the points B and C, then these can equally
be determined with the aid of the BERNOULLI equation (3.158). If one identifies in
this equation point 1 with C and point 2 with the exit cross section, then we have

$$
\begin{aligned}
p_1 &= p_C, & v_1 &= v_C, & \hat{r}_1 &= 0, & z_1 &= 0, \\
p_2 &= p_0, & v_2 &= v, & \hat{r}_2 &= r_0, & z_2 &= 0.
\end{aligned}
\tag{3.161}
$$

With these identifications we conclude from (3.158)

$$
p_C = p_0 + \frac{1}{2}\rho\left(v^2 - v_C^2\right) - \frac{1}{2}\rho\omega^2 r_0^2.
\tag{3.162}
$$

This pressure, however, can only be computed, if also v_C is known. If we identify point C with the end point of the vertical pipe, we have, owing to continuity,

$$
vA = \frac{1}{2}v_C 2A = v_C A \qquad \Longrightarrow \qquad v = v_C,
\tag{3.163}
$$

so that

$$
p_C = p_0 - \frac{1}{2}\rho\omega^2 r_0^2
\tag{3.164}
$$

is obtained. Analogously, one may also proceed for the computation of the pressure in point B; to this end we write the BERNOULLI equation for points B and C in the vertical pipe, and then show that

$$
p_B = p_C - \rho g l = p_0 - \frac{1}{2}\rho\omega^2 r_0^2 - \rho g l,
\tag{3.165}
$$

as the reader may corroborate.

Let us now alter the question slightly and assume that the end cross sections of the two tubes are closed by valves, but suddenly opened at $t = 0$ by some mechanism, and let us ask what the time evolution is for the exit velocity $v(t)$ in these end cross sections. In this case, the BERNOULLI equation between points 1 and 2 of Fig. 3.33 is applied in the form (3.114); we must evaluate the integral

$$
\int_1^2 \frac{\partial \boldsymbol{v}}{\partial t} \cdot \mathrm{d}\boldsymbol{x} = \int_1^2 \frac{\partial v}{\partial t}\,\mathrm{d}s = \frac{\mathrm{d}v}{\mathrm{d}t}(l + r_0),
\tag{3.166}
$$

in which the integration is along the streamline from point 1 to 2. Within the container the velocity is assumed to be negligibly small and no contribution is accounted for in the vertical pipe, and in the rotating tube it is equal to v (because the cross sectional areas have been accordingly chosen); this justifies the expression in the far right of (3.166). With it and with the identification (3.159) Eq. (3.114) now takes the form

$$
(l + r_0)\frac{\mathrm{d}v}{\mathrm{d}t} + \frac{v^2}{2} = gh + \frac{\omega^2 r_0^2}{2},
\tag{3.167}
$$

or with the definition (3.160) of the steady state exit velocity v_{stat},

$$2(l_0 + r_0)\frac{\mathrm{d}v}{\mathrm{d}t} + v^2 = v_{\text{stat}}^2. \tag{3.168}$$

The solution of the non-linear differential equation, subject to the initial condition $v(0) = 0$, is

$$v(t) = v_{\text{stat}} \tanh\left(\frac{v_{\text{stat}}\, t}{2\,(l + r_0)}\right), \tag{3.169}$$

as can easily be verified (see the derivation of (3.144)). Equation (3.169) also shows that for $t \to \infty$ the velocity $v(t)$ approaches the asymptotic value v_{stat}.

Example 3.9
In this example we shall derive an important, often employed formula for the power of working of a fluid machine under steady working conditions. The derivation will make it clear that the BERNOULLI equation (in the form ignoring the frictional effects as derived here) agrees with the balance of mechanical energy. As a preparation to the evaluation of the power of working of a fluid machine, let us formulate the energy balance for a fluid mass that is contained in a flow tube. *The change of the total energy (i.e. the change of the kinetic and potential energy) of the fluid mass in the time increment* $\mathrm{d}t$ *is equal to the work done by the fluid mass during this time increment.* **Figure 3.34** shows in its left panel the flow tube and the isolated material volume at time t, in the right panel that at time $t + \mathrm{d}t$. If ρ_1, p_1, v_1, A_1 and ρ_2, p_2, v_2, A_2 are, respectively the densities, pressures, velocities and cross sectional areas in the cross sections bounding the flow tube, then, because of leaving the space between the cross sections 1 and 1' the fluid mass loses energy of the amount
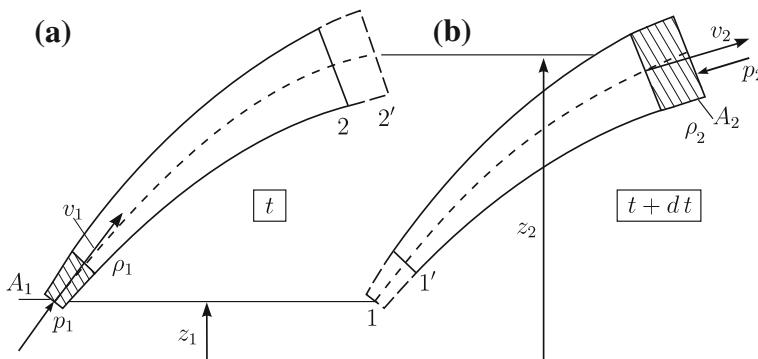
Fig. 3.34 Energy balance. *Energy balance for a fluid mass in a flow tube.* **a** *Fluid mass in the flow tube at time* t. **b** *Fluid mass in the flow tube at time* $t + \mathrm{d}t$.

$$d(E_{\text{kin}} + E_{\text{pot}})_1 = -\left(\rho_1 A_1 v_1 dt \frac{v_1^2}{2} + \rho_1 g A_1 v_1 dt \, z_1\right). \qquad (3.170)$$

Correspondingly, it gains the similar amount

$$d(E_{\text{kin}} + E_{\text{pot}})_2 = \left(\rho_2 A_2 v_2 dt \frac{v_2^2}{2} + \rho_2 g A_2 v_2 dt \, z_2\right), \qquad (3.171)$$

because it acquires now space between the cross sections 2 and 2'. The work that is done during this time on the fluid is composed of the work done by the pressures when the bounding cross sections move from 1 to 1' and from 2 to 2', respectively

$$dW_1 = p_1 A_1 v_1 dt - p_2 A_2 v_2 dt, \qquad (3.172)$$

as well as the pressures within the flow tube

$$dW_2 = \int_1^2 pAv \, dt = \int_1^2 p \, dV, \qquad (3.173)$$

which is caused by the volume changes when the fluid mass is displaced; dv, thus denotes the volume increment. If in the balance of mechanical energy

$$d(E_{\text{kin}} + E_{\text{pot}}) = dW_1 + dW_2, \qquad (3.174)$$

the expressions obtained above are substituted and if the identifications

$$\begin{aligned} \rho_1 v_1 A_1 dt = \rho_2 v_2 A_2 dt = dm, \\ A_1 v_1 dt = dV_1, \quad A_2 v_2 dt = dV_2 \end{aligned} \qquad (3.175)$$

are used, one obtains

$$\left[\left(\frac{v_2^2}{2} + gz_2\right) - \left(\frac{v_1^2}{2} + gz_1\right)\right] dm = p_1 dV_1 - p_2 dV_2 + \int_1^2 p \, dV, \qquad (3.176)$$

or after division by dm and with the obvious definition $dV/dm = (1/\rho) = \nu$

$$\left(\frac{v_2^2}{2} + gz_2\right) - \left(\frac{v_1^2}{2} + gz_1\right) = p_1 \nu_1 - p_2 \nu_2 + \int_1^2 p d\nu. \qquad (3.177)$$

The right-hand side can also be differently written, if the change of integration variables, explained in **Fig. 3.35**, is used,
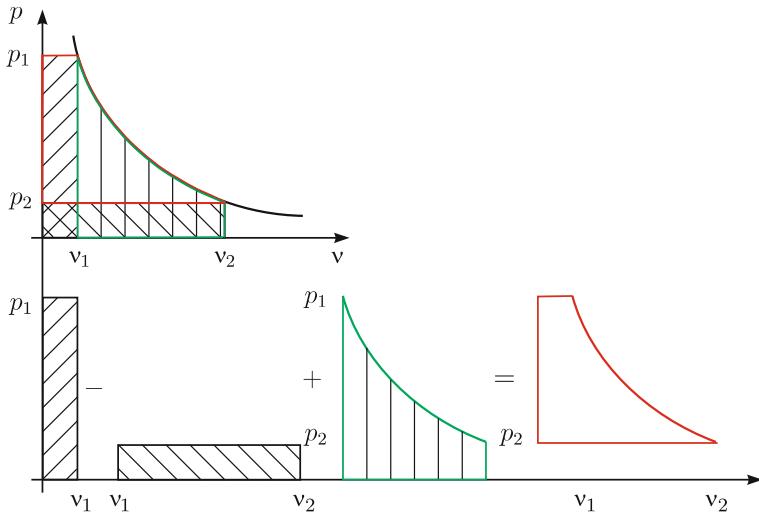
Fig. 3.35 Explaining the evaluation of the working done by the pressure. *The integration in the (p, v) diagram, treating p as the integration variable $\int_{p2}^{p} v \mathrm{d}p$ (upper graph) can also be performed by integrating over the specific volume (lower graph), and is obtained by adding/subtracting the three indicated surfaces*

$$\int\limits_{2}^{1} v \mathrm{d}p = -\int\limits_{0}^{2} \frac{\mathrm{d}p}{\rho} + \int\limits_{0}^{1} \frac{\mathrm{d}p}{\rho}, \tag{3.178}$$

so that relation (3.177) can also be written as

$$\frac{v_2^2}{2} + \int\limits_{0}^{2} \frac{\mathrm{d}p}{\rho} + gz_2 = \frac{v_1^2}{2} + \int\limits_{0}^{1} \frac{\mathrm{d}p}{\rho} + gz_1, \tag{3.179}$$
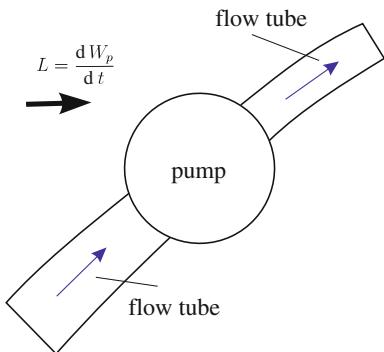
which agrees with the BERNOULLI equation for steady flows of compressible fluids. This brings us now back to the problem we initially intended to attack.

To facilitate the ensuing developments we imagine that our machine is a pump of which the inlet and outlet pipes are flow tubes, see **Fig. 3.36**. The change of the total energy in the time increment $\mathrm{d}t$ of the fluid mass bounded by the flow tubes and the pump must then be equal to the working done on the fluid mass by the pressures plus the power of the pump $L\mathrm{d}t = \mathrm{d}W_P$; thus, the equation

$$\mathrm{d}(E_{\mathrm{kin}} + E_{\mathrm{pot}}) = \mathrm{d}W_1 + \mathrm{d}W_2 + \mathrm{d}W_P \tag{3.180}$$

must hold. If one substitutes here relations (3.170)–(3.173) and also uses (3.178), then one obtains

Fig. 3.36 Explaining the power of working for a fluid machine

$$\left[\left(\frac{v_2^2}{2} + gz_2\right) - \left(\frac{v_1^2}{2} + gz_1\right)\right] = -\int_1^2 \frac{\mathrm{d}p}{\rho} + \frac{\mathrm{d}W_P}{\mathrm{d}m}, \qquad (3.181)$$

which, with the definition of the power

$$L = \frac{\mathrm{d}W_P}{\mathrm{d}t} = \frac{\mathrm{d}W_P}{\mathrm{d}m}\frac{\mathrm{d}m}{\mathrm{d}t} = \frac{\mathrm{d}W_P}{\mathrm{d}m}\dot{m}, \qquad (3.182)$$

goes over into

$$L = \dot{m}\left[\left(\frac{v_2^2}{2} + gz_2\right) - \left(\frac{v_1^2}{2} + gz_1\right) + \int_1^2 \frac{\mathrm{d}p}{\rho}\right]. \qquad (3.183)$$

The quantity $\dot{m}$ is the mass flux transported by the pump, and L is the power of working of the pump, i.e., the work done per unit time by the pump on the fluid.

For density preserving fluids ($\rho_1 = \rho_2 = \rho$) the mass flux $\dot{m}$ can be replaced by the volume flux Q, according to

$$\dot{m} = \rho Q; \qquad (3.184)$$

instead of (3.181) we then obtain

$$L = Q\left[\left(\frac{\rho v_2^2}{2} + p_2 + \rho gz_2\right) - \left(\frac{\rho v_1^2}{2} + p_1 + \rho gz_1\right)\right]. \qquad (3.185)$$

Often in these formulae the gravity potential can be ignored. If the flow machine is a turbine and not a pump, the formulae (3.183) and (3.185) remain valid, if L is replaced by $-L$. This means that the fluid provides the working $+L$ to the turbine.

With this we wish to close the series of applications of the BERNOULLI equation.

3.6   Global Formulation of the Momentum Equation

We have been dealing with the balance law of momentum, i.e., with NEWTON's fundamental law already in Sect. 3.3. Let us repeat it here once more and as applied to a material volume: The time rate of change of the momentum of the fluid mass kept in the volume V is equal to the applied external volume and surface forces, explicitly

$$\frac{\mathrm{d}\boldsymbol{I}_V}{\mathrm{d}t} = \boldsymbol{K}_V + \boldsymbol{K}_{\partial V}, \tag{3.186}$$

or with the quantities $\boldsymbol{I}_V$, $\boldsymbol{K}_V$ and $\boldsymbol{K}_{\partial V}$, defined in (3.84)

$$\frac{\mathrm{d}}{\mathrm{d}t} \int_{V(t)} \rho \boldsymbol{v} \mathrm{d}V = - \int_{\partial V(t)} p\boldsymbol{n}\mathrm{d}A + \int_{V(t)} \rho \boldsymbol{f} \mathrm{d}V, \tag{3.187}$$

in which $\boldsymbol{n}$ is the unit vector external to V. On the left-hand side of (3.187) we recognize the time rate of change of the specific momentum integrated over the volume V; regarding the terms on the right-hand side the surface integral term is the resultant force of all pressure tractions exerted on the surface ∂V of V (shear tractions do not arise in ideal fluids) and the second integral on the right-hand side is the sum of all volume forces acting within the volume V. An alternative form of the term on the left-hand side of (3.187) was also given in Sect. 3.3, see Eq. (3.87); accordingly, the balance law of momentum can also be written in the form

$$\int_{V(t)} \frac{\partial(\rho \boldsymbol{v})}{\partial t} \mathrm{d}V + \int_{\partial V(t)} \rho \boldsymbol{v}(\boldsymbol{v}\cdot\boldsymbol{n})\, \mathrm{d}A = - \int_{\partial V(t)} p\,\boldsymbol{n}\, \mathrm{d}A + \int_{V(t)} \rho \boldsymbol{f} \mathrm{d}V. \tag{3.188}$$

This equation is the starting point of the following considerations for the evaluation of the force exerted on the fluid-submerged body by the fluid circumflowing it. We restrict the analysis to **steady conditions** for which $\partial(\rho \boldsymbol{v})/\partial t = \boldsymbol{0}$ and assume the specific force $\rho \boldsymbol{f}$ is given by the potential

$$\rho \boldsymbol{f} = -\mathrm{grad}\, U. \tag{3.189}$$

The integral of the volume forces can then be transformed to a surface integral (we use the GAUSS law)

$$\int_{V(t)} \rho \boldsymbol{f} \mathrm{d}V = - \int_{V(t)} \mathrm{grad}\, U \mathrm{d}V = - \int_{\partial V} U\boldsymbol{n}\mathrm{d}A, \tag{3.190}$$

so that (3.188) for steady flows assumes the form

$$\int_{\partial V} (\rho \boldsymbol{v}(\boldsymbol{v}\cdot\boldsymbol{n}) + (p + U)\boldsymbol{n})\, \mathrm{d}A = 0\,, \qquad \text{(I)}. \tag{3.191}$$

To this equation we shall later refer as (I).

For further transformations of this equation, consider the material volume displayed in **Fig. 3.37**. It contains a body which is circumflown by the fluid with volume V_2 and surface A_2. Thus, the surface ∂V of the material volume V (excluding the submerged body) is therefore not simply connected as it consists of the exterior 'hull' A_1 and the body surface A_2 (with an exterior unit normal vector that is pointing into the volume V_2). If we imagine the volume cut along a line that is shown as dashed line in Fig. 3.37, then the surface of the cut volume is enlarged by the doubly-cut surface; the volume with this bounding surface is now simply connected. We shall now apply Eq. (3.191) to the material surface so extended.

The contributions along the cut surfaces eliminate one another, since at corresponding opposing points the exterior unit normal are in opposite directions. Thus, one obtains
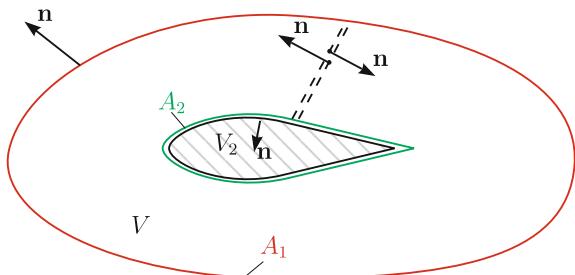
$$\int_{A_1} (\rho \boldsymbol{v}(\boldsymbol{v}\cdot\boldsymbol{n}) + (p + U)\boldsymbol{n})\, \mathrm{d}A = -\int_{A_2} p\boldsymbol{n}\, \mathrm{d}A - \int_{A_2} U\boldsymbol{n}\, \mathrm{d}A. \tag{3.192}$$

Here, the contribution of the momentum flux on the right-hand side has been omitted (because it vanishes) since it is *assumed* that the fluid adheres to the body (no formation of cavitation), the boundary velocity is therefore tangential, for which $\boldsymbol{v} \cdot \boldsymbol{n} = 0$. Note also that the force, exerted on the body by the fluid, is given by

$$\boldsymbol{K} = \int_{A_2} p\boldsymbol{n}\, \mathrm{d}A. \tag{3.193}$$

Moreover, the second integral on the right-hand side of (3.192) can be transformed into a volume integral, if we imagine the fluid to be continued into the body V_2;

Fig. 3.37 Computation of the resultant force exerted by a fluid on a submerged body, here shown in two-dimensions

applying again the GAUSS law for V_2, we obtain

$$\int_{A_2} U\boldsymbol{n}\,\mathrm{d}A = -\int_{V_2} \mathrm{grad}\,U\,\mathrm{d}V = \int_{V_2} \rho\boldsymbol{f}\,\mathrm{d}V. \qquad (3.194)$$

The negative sign in the middle term can be understood, if it is recognized that $\boldsymbol{n}$ for the volume V_2 is an interior unit vector, but the GAUSS law holds for surface integrals, formulated with exterior unit vectors. If we substitute (3.193) and (3.194) into (3.192) we obtain

$$\boldsymbol{K} = -\int_{V_2} \rho\boldsymbol{f}\,\mathrm{d}V - \int_{A_1} (\rho\boldsymbol{v}(\boldsymbol{v}\cdot\boldsymbol{n}) + (p+U)\boldsymbol{n})\,\mathrm{d}A\,, \quad \text{(II)}. \qquad (3.195)$$

This formula will be referred to as (II). Evidently, the force exerted on a body that is circumflown by a fluid comprises two contributions; the first is due to the specific volume force and corresponds to the Archimedean buoyancy force of the displaced mass, the second contains a contribution of the piezometric pressure $p^* = p + U$, as well as the direct contribution of the flow. If the contribution of the specific body force is small, the Archimedean buoyancy force and the contribution of the potential can be dropped. In this case (3.195) simplifies to

$$\boldsymbol{K} = -\int_{A_1} (\rho\boldsymbol{v}(\boldsymbol{v}\cdot\boldsymbol{n}) + p\boldsymbol{n})\,\mathrm{d}A\,, \qquad \text{(III)}. \qquad (3.196)$$
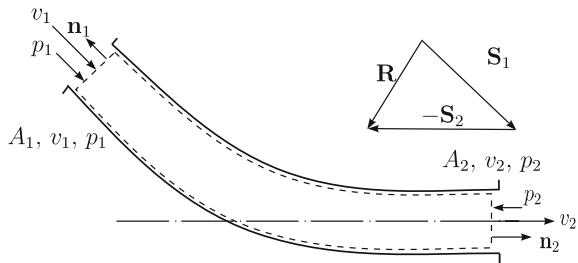
This formula will be referred to (III). The formulae (I)–(III) hold for compressible as well as density preserving fluids. Incidentally, in deriving these formulae we have not employed any assumptions about the outer surface A_1 other than it is material and completely submerged in the fluid domain. One may in applications of the formulae (3.195) and (3.196) choose the surface A_1 such that the arising integrals are easy to compute. The formulae (I)–(III) form the basis for the applications treated in Sects. 3.7 and 3.8.

3.7 Applications of the Balance Law of Momentum in Integrated Form

3.7.1 Reaction Forces Due to Fluid Flow Through Pipes

Consider the curved piece of the pipe of **Fig. 3.38**. We wish to evaluate the force, which under steady state conditions is exerted by the flowing fluid on the pipe element. Since in this example we are not concerned with a body that is circumflown by a fluid,

Fig. 3.38 Curved pipe segment. *Evaluation of the flow induced force acting on the pipe segment*

but rather a fluid that is bounded by the pipe, we wish to apply the global balance law in the form (3.191), i.e., formula (I). The surface ∂V is made up in Fig. 3.38 of the material volume outlined by the dashed line and is composed of the mantle area and the cross sectional areas A_1 and A_2. If one sets $U = 0$ and thus ignores the effect of the gravity force, then there follows from (3.191) by dividing the integrals into the contributions of the mantle and the cross sectional areas

$$\underbrace{\int_M p\boldsymbol{n} \, \mathrm{d}A}_{\boldsymbol{R}} + (\rho v_2^2 + p_2)A_2\boldsymbol{n_2} + (\rho v_1^2 + p_1)A_1\boldsymbol{n_1} = \boldsymbol{0}. \qquad (3.197)$$

The first integral over the mantle surface represents the resultant force $\boldsymbol{R}$ exerted by the fluid on the pipe wall, so the last equation implies

$$\boldsymbol{R} = (\rho v_1^2 + p_1)A_1(-\boldsymbol{n_1}) - (\rho v_2^2 + p_2)A_2\boldsymbol{n_2} = \boldsymbol{S}_1 - \boldsymbol{S}_2. \qquad (3.198)$$

Accordingly, the mantle force is given as the difference of the two forces $\boldsymbol{S}_1$ and $\boldsymbol{S}_2$, which are the pressure plus momentum fluxes integrated over the respective cross sections. When pipe orientations change considerably these forces are very large, and, of course, the structural engineer must account for them.

3.7.2 Borda Exit Orifice

Consider, **Fig. 3.39**, a fluid container of which the exit opening with area A_i is moved by a pipe far into the interior of the container. The pressure p_i is larger than the external pressure p_e; so, an exit cross section A_i is so small and the container so large that one can ignore the velocity inside the container in comparison to the velocity in the outflow jet. Analogously, the pressure inside the container may (with the exception of the vicinity of the end of the pipe) be assumed to be constant and different from the exterior pressure p_e. Experience, or simply observation of the experiment teaches us that the end cross section A_e of the exit jet far from the orifice is smaller than the pipe cross section A_i, $A_e < A_i$. We define the **contraction coefficient** α by
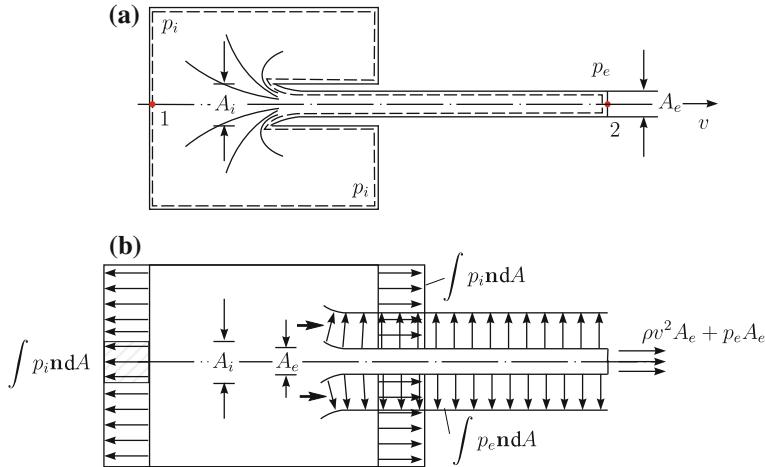
Fig. 3.39 BORDA exit mouth. *Explaining the calculation of the jet contraction.* **a** *Delineation of the fluid volume along the dashed boundary.* **b** *Along the vertical walls, the pressure is* p_i, *along the free jet it is* p_e

$$\alpha = \frac{A_e}{A_i} < 1, \tag{3.199}$$

and wish to evaluate this contraction coefficient for the BORDA exit orifice.[14]

To this end, we consider the fluid volume as outlined in Fig. 3.39a by the dashed line. Along this line the tractions exerted by the surroundings consist of pressures only. Along the free jet this pressure is constant and equal to p_e and its orientation is everywhere perpendicular to the surface, at which it applies. In the interior of the container this pressure is equal to p_i, except at the tube ends, where large velocities arise. Let us now apply the global momentum balance in the horizontal direction; to this end we start from its steady form (I) in (3.191). Accordingly, along the entire container wall we have $v \cdot n = 0$; moreover, the total force exerted on the vertical container walls, and counted positive if it points to the left is given by $p_i A_i$ (the horizontal walls and mantle of the pipe do not contribute to the horizontal wall force). Along the mantle surface of the jet, one also has $v \cdot n = 0$, since the fluid velocity is tangential to this surface. Moreover, the integral $\int p_e n da$ can be expressed as a force pointing to the right and having the value $p_e(A_i - A_e)$. Finally, the integral (3.191) evaluated over the cross sectional area is given by $\rho v^2 A_e + p_e A$. If all these contributions are added together, one obtains

$$-p_i A_i + p_e(A_i - A_e) + (\rho v^2 A_e + p_e A_e) = 0,$$

[14]For a short biography of BORDA see **Fig. 3.40**.

Fig. 3.40 JEAN-CHARLES DE BORDA (4. May 1733–20. Feb. 1799)

JEAN-CHARLES DE BORDA was a French mathematician, mariner, and military engineer. He is known much more for his engineering work related to construction of ships, water turbines, measurements of the longitude, chronometers, instrument construction and even inventing a voting system, known as BORDA count, rather than the exit flow property and efficiency of a special orifice or fluid mouth piece. He was a member of the French academy and his name is stated on the Eiffel tower among 71 others.

The text is based on http://www.wikipedia.org

or

$$\rho v^2 A_e - (p_i - p_e) A_i = 0. \tag{3.200}$$

This is one equation that serves for the evaluation of v and A_e. A further equation can be obtained by establishing the BERNOULLI equation along a line in the middle of the jet stream from point 1 to point 2. This equation is
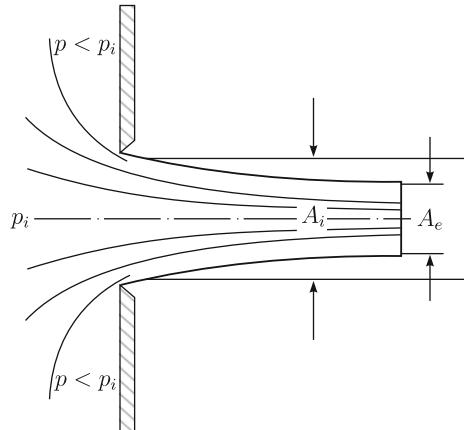
$$p_i = p_e + \frac{\rho}{2} v^2. \tag{3.201}$$

From both equations $(p_i - p_e)$ can be eliminated, which yields

$$\alpha = \frac{A_e}{A_i} = 0.5. \tag{3.202}$$

Fig. 3.41 Exit cross section.
The contraction of a jet flowing out of an orifice depends on the geometric form of the orifice

For the BORDA exit orifice, the asymptotic jet cross section is thus exactly half as large as the exit cross section.

A jet is always reduced in area if the opening from which it exits is not ideally rounded. At optimal rounding of the exit cross section one has $\alpha = 1$; for the sharp exit cross section of **Fig. 3.41** one can show that under laminar flow conditions

$$\alpha = \frac{\pi}{2 + \pi} \cong 0.61. \tag{3.203}$$

The computation was given by GUSTAV KIRCHHOFF (1824–1887) as early as 1860. For a short biography of KIRCHHOFF see **Fig. 3.42**.

It may be instructive to deepen this discussion somewhat and to search for the causes of the difference of the above result with the BORDA exit mouth. For the exit with sharp and pointed walls, see Fig. 3.41, the velocity component at the tip that is parallel to the wall does not vanish. One therefore concludes from the BERNOULLI equation for a streamline following the vertical wall that the pressure along the wall is not constant; it varies and is not even known a priori. Consequently, the contribution of the pressure in the expression (3.200) is no longer given by $p_i A_i$, but is somewhat larger, $-\lambda p_i A_i$, $\lambda > 1$; balance of momentum is, therefore, given here by

$$\rho v^2 A_e - (p_i \lambda - p_e) A_i = 0. \tag{3.204}$$

Alternatively, the BERNOULLI equation (3.201) then yields for the contraction coefficient

$$\alpha = \frac{A_e}{A_i} = \frac{1}{2} + \frac{\lambda - 1}{2(1 - p_e/p_i)} > \frac{1}{2}. \tag{3.205}$$
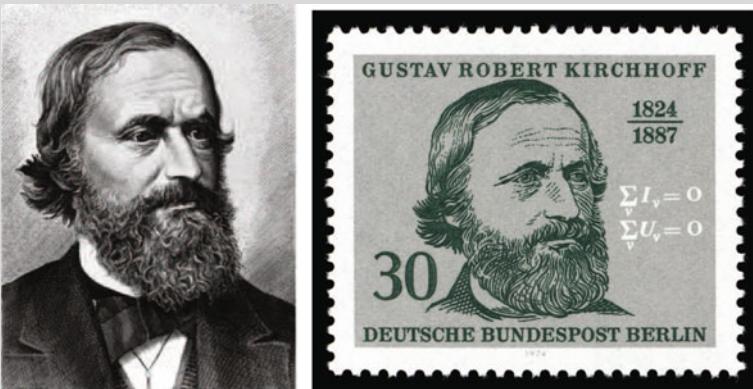
Fig. 3.42 GUSTAV ROBERT KIRCHHOFF (12. March 1824–17. Oct. 1887)

GUSTAV ROBERT KIRCHHOFF was a German physicist, educated at the university in Königsberg (Kaliningrad, Russia), worked in Breslau (Wroclaw, Poland), Heidelberg, Germany and then assumed the chair of theoretical physics at the Berlin University, where he was from 1875 to 1886. He is best known for his rules of electric current circuits (Kirchhoff rules). In engineering he is known for the KIRCHHOFF-LOVE plate theory (corresponding to the BERNOULLI-NAVIER beam theory). In continuum mechanics the first and second PIOLA-KIRCHHOFF stress tensors play an important role for the formulation of solid body constitutive modeling.

In February 1974, the German Postal Service printed the postal stamp shown above to commemorate KIRCHHOFF's 150th anniversary.

The text is based on http://www.wikipedia.org
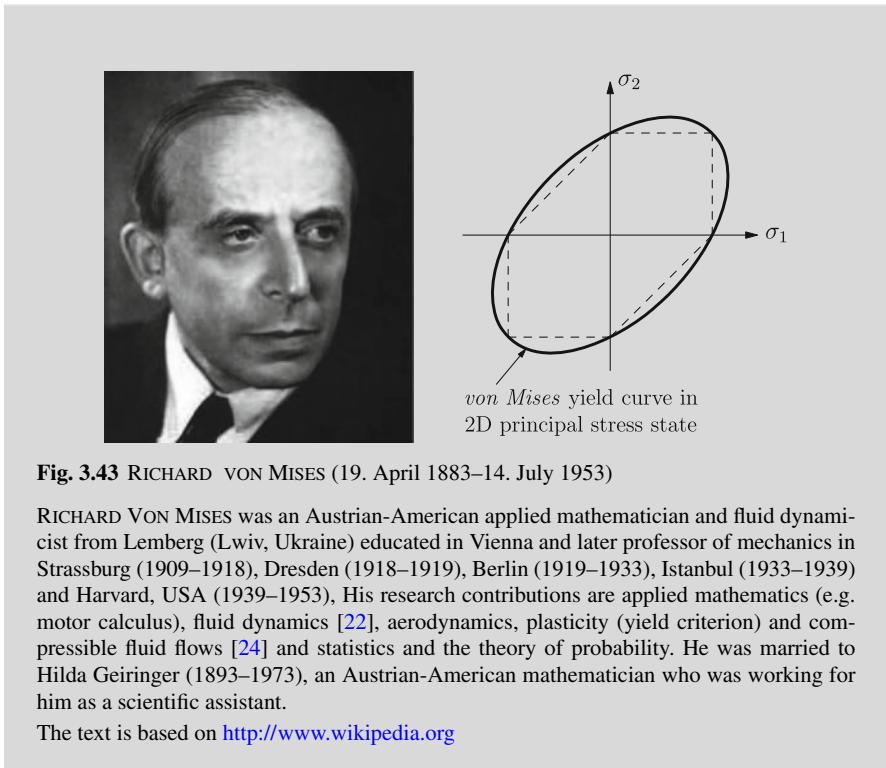
The value $\alpha = 0.61$ holds for a long slit and can be evaluated with methods of complex valued function theory. For a sharp circular exit numerical computations with the respective theory yield $\alpha = 0.58$, thus a value only slightly different from the value $\alpha = 0.61$. With known value of α, one obtains for the volume flux[15]

$$Q = A_e v = \alpha A_i v = \alpha A_i \sqrt{\frac{2(p_i - p_e)}{\rho}}. \tag{3.206}$$

This result is valid for inviscid fluids and must for real fluids be corrected, since these fluids adhere to walls; as a consequence, the volume flux is decreased when compared with the value (3.206). One writes

$$Q = \varphi \alpha A_i \sqrt{\frac{2(p_i - p_e)}{\rho}} \quad \text{with} \quad \varphi < 1, \tag{3.207}$$

---

[15]More on contraction coefficients is given by VON MISES [23] and Hunt [7]. For a short biography of VON MISES see **Fig. 3.43**.

von Mises yield curve in
2D principal stress state

Fig. 3.43 RICHARD VON MISES (19. April 1883–14. July 1953)

RICHARD VON MISES was an Austrian-American applied mathematician and fluid dynamicist from Lemberg (Lwiv, Ukraine) educated in Vienna and later professor of mechanics in Strassburg (1909–1918), Dresden (1918–1919), Berlin (1919–1933), Istanbul (1933–1939) and Harvard, USA (1939–1953), His research contributions are applied mathematics (e.g. motor calculus), fluid dynamics [22], aerodynamics, plasticity (yield criterion) and compressible fluid flows [24] and statistics and the theory of probability. He was married to Hilda Geiringer (1893–1973), an Austrian-American mathematician who was working for him as a scientific assistant.

The text is based on http://www.wikipedia.org

where $\varphi < 1$ only deviates slightly from the value 1. The product $\mu = \varphi \alpha$ is called **orifice coefficient**. It is usually determined experimentally.

3.7.3 Impact of a Free Jet on a Wall

We now consider the free jet of **Fig. 3.44** that impinges on a flat wall with an angle β, as shown in the figure; the fluid comprising the jet is density preserving and the velocity is constant throughout the jet. We are interested in the force exerted by the jet on the wall in the direction perpendicular to the wall and how the jet splits, i.e., what portions of the jet move up and down the wall, respectively. To this end, we consider the volume enclosed by the dashed line in Fig. 3.44. The velocities of the jet and the two leaving wall jets all have the same value, if we ignore the influence of gravity; one can easily see this, if one writes the BERNOULLI equation for two points of the free surface streamlines (points 1, 2 and 1′, 3, respectively in Fig. 3.44). Indeed, the free surface is everywhere exposed to the same atmospheric pressure; from mass balance it follows that the thicknesses of the two wall jets are given by ϵh and $(1 - \epsilon)h$, where ϵ is to be determined. As for the momentum equation, one does not need to account for the atmospheric pressure, because it is acting along the entire boundary with the same value and, thus, drops out of this balance anyhow.

Fig. 3.44 Free jet impinging a wall. *Explaining the evaluation of the force exerted by the jet on the wall*

If one now writes down the balance of momentum in the form (I), (3.191), one obtains, with the notation of Fig. 3.44,

$$- (\rho v h)v \, \cos \beta + K_x = 0, \tag{3.208}$$

and for the y-direction

$$- (\rho v h)v \, \sin \beta + \rho v \varepsilon h v - \rho v (1 - \varepsilon) h v = 0. \tag{3.209}$$

In these relations a thickness of 1 has been assumed for the jet, and frictional forces along the walls have been ignored. Therefore, one obtains
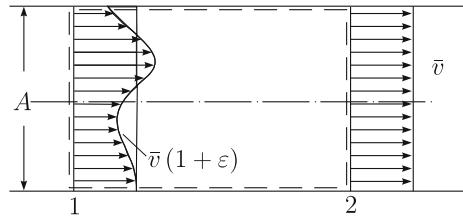
$$K_x = \rho v^2 h \, \cos \beta, \qquad \epsilon = \tfrac{1}{2}(1 + \sin \beta). \tag{3.210}$$

For $\beta = 0°$, one obtains $\epsilon = \tfrac{1}{2}$; then boundary jets are of equal size, a result one would expect simply for reasons of symmetry, and the reactive force at the wall is a maximum. For $\beta = 90°$ we have $\epsilon = 1$ and $K_x = 0$, the jet progresses unchanged along the wall.

3.7.4 Mixing Processes

Consider a steady flow through a pipe or along a plate, **Fig. 3.45**. Let us suppose that, owing to an upstream disturbance, a non-uniform velocity profile exists in cross section 1. Downstream of this cross section the velocity profile will become more and more uniform, until in cross section 2 it will again be completely uniform. This uniformization of the velocity field is associated with a pressure rise between the cross sections 1 and 2, which we now wish to calculate.

Fig. 3.45 Flattening
velocity profiles.
Uniformization of the
velocity profile is
accompanied with a pressure
rise

If we denote the average velocity in a cross section by $\bar{v}$ and the non-uniform velocity by

$$v(x, y) = \bar{v}\,(1 + \varepsilon(x, y)),\qquad(3.211)$$

then equality of the volume flow through cross sections 1 and 2 implies

$$\int_{A_1} \bar{v}(1 + \varepsilon)\mathrm{d}A = \int_{A_2} \bar{v}\mathrm{d}A,\qquad(3.212)$$

from which

$$\int_{A_1} \varepsilon\mathrm{d}A = 0\qquad(3.213)$$

may be deduced. For the formulation of the momentum balance we choose the volume that is outlined in Fig. 3.45 by the dashed line. If the equation is written down for the x-axis, then only the contributions of the pressures and momentum fluxes in the cross sections 1 and 2 are to be accounted for; in particular one has (see Eq. (3.191))

$$-\int_{A_1} \rho\bar{v}^2(1 + \varepsilon)^2\mathrm{d}A - p_1 A_1 + \rho\bar{v}^2 A_2 + p_2 A_2 = 0,\qquad(3.214)$$

or since there is no change in cross section to be accounted for, $A_1 = A_2$, we have
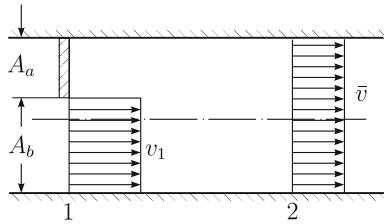
$$p_2 = p_1 + \rho\bar{v}^2\,\overline{\varepsilon^2}.\qquad(3.215)$$

In this formula the result (3.213) is incorporated, and $\overline{\epsilon^2}$ is defined as

$$\overline{\varepsilon^2} = \frac{1}{A}\int_A \varepsilon^2\mathrm{d}A.\qquad(3.216)$$

Owing to the uniformization of the velocity profile, the pressure rises from p_1 to $p_2 > p_1$.

Fig. 3.46 CARNOT's abrupt
energy loss. *According to
Eq. (3.220) the pressure due
to a sudden cross section
widening increases*

As an example let us consider a steady flow in a pipe, which experiences in cross
section 1 a sudden reduction of the cross sectional area, e.g. by partly closing a valve,
see **Fig. 3.46**. If one denotes the closed and open parts of the cross sections by A_a
and A_b, respectively, then continuity implies

$$\bar{v} = v_1 \frac{A_b}{A_a + A_b}. \tag{3.217}$$

In addition we have

$$\begin{aligned} v_a &= \bar{v}(1 + \varepsilon_a) = 0 \quad \Rightarrow \varepsilon_a = -1, \\ v_b &= \bar{v}(1 + \varepsilon_b) = v_1 \Rightarrow \varepsilon_b = \frac{v_1}{\bar{v}} - 1 = \frac{A_a}{A_b}. \end{aligned} \tag{3.218}$$

With these relations one obtains from (3.216)

$$\overline{\varepsilon^2} = \frac{\varepsilon_a{}^2 A_a + \varepsilon_b{}^2 A_b}{A_a + A_b} = \frac{A_a + \dfrac{A_a{}^2}{A_b}}{A_a + A_b} = \frac{A_a}{A_b}. \tag{3.219}$$

So, the pressure, p_2 in cross section 2 with uniform velocity profile follows from
(3.215) and is given by

$$p_2 = p_1 + \rho \bar{v}^2 \frac{A_a}{A_b} = p_1 + \rho \bar{v}(v_1 - \bar{v}), \tag{3.220}$$
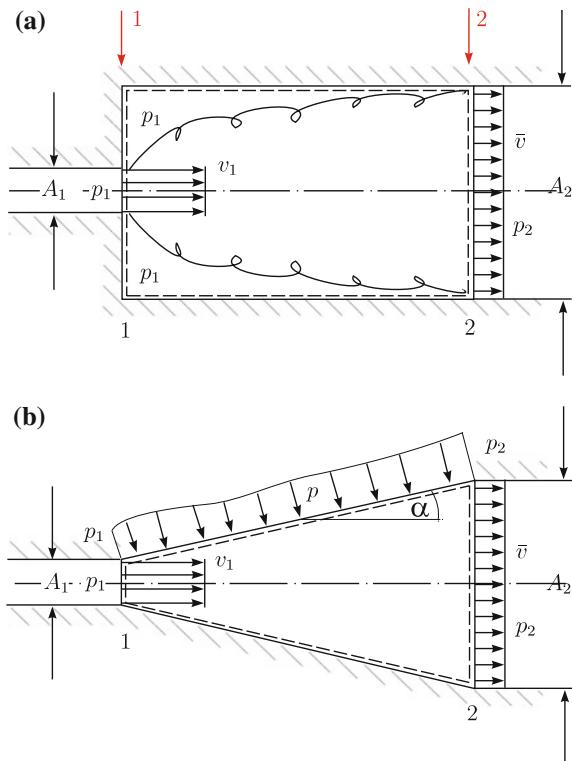
where also (3.217) has been used. The pressure rise, which arises at a discontinuous
extension of a pipe, is therefore given by

$$\triangle p = \rho \bar{v}(v_1 - \bar{v}). \tag{3.221}$$

Mathematically, this problem is entirely equivalent to 'CARNOT's shock loss', after
N.L.S. CARNOT (1796–1832),[16] see **Fig. 3.47**a. This problem concerns a cylindrical
pipe that is suddenly widened from cross section A_1 to cross section A_2. The fluid

---

[16]NICOLAS LÉONARD SADI CARNOT (1796–1832) was a French military engineer and physicist.
His work mainly deals with thermodynamics. We shall present his vita in Vol. 2, Chaps. 17 and 18.

Fig. 3.47 CARNOT's abrupt
energy loss, diffusion. **a** *A
sudden widening of the cross
section leads to an abrupt
CARNOT loss of energy and
the indicated dead water
zones.* **b** *When the cross
sectional widening is
continuous and slow no dead
water zones are formed and
the associated pressure
difference is smaller and
given by Eq.* (3.228)

enters with velocity v_1 (and pressure p_1) as a jet the larger pipe segment in which, after the widening of the jet cross section, a uniform velocity profile $\bar{v}$ is established. The pressure rise is here also given by equation (3.119), where in this case $\bar{v}$ can be calculated in terms of v_1 from the continuity equation $v_1 A_1 = \bar{v} A_2$.

In the above sudden widening of the cross section the fact is important that the jet fluid mixes with the neighboring fluid, this as a result of the stresses which one establishes. These shear stresses can be traced back to the internal friction of the real fluid between the cross sections 1 and 2, which we shall calculate below. Such shear stresses also arise at the walls of the wider pipe and, strictly, ought to be taken into account in the energy balance. It can, however, be shown that the influence of these shear stresses in the force balance is of minor significance; this is also the reason, why we have neglected the shear stresses in the above analysis.

The energy loss due to this inner friction can nevertheless be determined. If we write with

$$p_1 + \rho \frac{v_1^2}{2} = C_1 \quad \text{and} \quad p_2 + \rho \frac{v_2^2}{2} = C_2 \tag{3.222}$$

the total pressures in the cross sections 1 and 2, then we may not set C_1 equal to C_2, because owing to the energy loss, the BERNOULLI equation is not valid. However, the difference $C_1 - C_2$ yields exactly the mechanical energy loss between the cross sections 1 and 2 which is given by

$$\triangle E = C_1 - C_2 = p_1 - p_2 + \frac{\rho}{2}(v_1{}^2 - v_2^2). \tag{3.223}$$

For discontinuous pipe widening, since $v_2 = \bar{v}$ in this case, it can be written as

$$\triangle E_{\text{Carnot}} = -\rho\bar{v}\,(v_1 - \bar{v}) + \frac{\rho}{2}(v_1^2 - \bar{v}^2) = \frac{\rho}{2}(v_1 - \bar{v})^2. \tag{3.224}$$

Alternatively, one may write (3.223) also as

$$p_1 + \rho\frac{v_1^2}{2} = p_2 + \rho\frac{v_2^2}{2} + \triangle E, \tag{3.225}$$

and has obtained in this way a BERNOULLI type equation for flows with internal friction, where the latter is accounted for by the term $\triangle E$.

Since the pressure and the specific kinetic energy (per unit volume) have the same physical dimension, the denotation for the loss $\triangle E$ is not unique. One speaks either of an energy loss or a pressure loss. It is also customary to write $\triangle E$ as

$$\triangle E = \zeta\frac{\rho}{2}v_{\text{char}}^2, \tag{3.226}$$

in which v_{char} is a velocity that is adjusted to the problem at hand. In this way a **dimensionless pressure** or **energy loss coefficient** can be defined. If one chooses $v_{\text{char}} = v_1$, then one may write the CARNOT pressure loss as

$$\zeta_{\text{Carnot}} = \frac{\triangle E_{\text{Carnot}}}{\frac{\rho}{2}v_1^2} = \left(1 - \frac{\bar{v}}{v_1}\right)^2 = \left(1 - \frac{A_1}{A_2}\right)^2. \tag{3.227}$$

For a **continuous widening of the cross section**, as e.g. for the **diffusor** of Fig. 3.47b a 'dead water zone' does not form,[17] and the flow does not separate from the wall, because the streamlines follow the continuous changes of the cross sections. The BERNOULLI equation remains valid. In this case, this means one may now set in (3.222) $C_1 = C_2$ and then obtains

$$\triangle p_{\text{Bernoulli}} = \frac{\rho}{2}\left(v_1^2 - \bar{v}^2\right). \tag{3.228}$$

It is educational to still continue with this example. It is, namely so that the momentum balance is the general statement, not the BERNOULLI equation, and maintains in this

---

[17] Of course, the opening angle α in Fig. 3.47 must be sufficiently small to guarantee such conditions.

case its validity. If we apply it in the form [(3.191), (I)] to the volume, indicated by the dashed lines in Fig. 3.47b, then apart from the pressures and momentum fluxes of the cross sections 1 and 2 in the x-direction, also the wall pressures along the conical cross sectional widening contribute to this balance in the x-direction. Indeed, the momentum balance in the horizontal direction takes the form

$$- \left(p_1 + \rho v_1^2 \right) A_1 - \int_M p \, \sin \alpha \, \mathrm{d}A + \left(p_2 + \rho \bar{v}^2 \right) A_2 = 0. \tag{3.229}$$

Here, the integral term represents the resultant force in the x-direction exerted by the fluid on the mantle surface, which one can evaluate with the BERNOULLI pressure difference (3.228): explicitly,

$$K = \int_M p \, \sin \alpha \, \mathrm{d}A = \frac{\rho}{2} v_1^2 (A_2 - A_1) - \frac{\rho}{2} v_1^2 A_1 + \frac{\rho}{2} \bar{v}^2 A_2 + p_1 (A_2 - A_1)$$

$$= \frac{\rho}{2} v_1^2 \frac{(A_2 - A_1)^2}{A_2} + p_1 (A_2 - A_1). \tag{3.230}$$

For the CARNOT discontinuous cross sectional widening this force is contained in the contribution of the cross section 1.

3.7.5 Hydraulic Jump

Consider a steady flow of water in a channel with constant rectangular cross section in which the water flows with free surface from left to right, Fig. 3.48. Far upstream we assume the flow has been heavily accelerated, for instance by guiding the flow through a channel segment with large slope. The upstream flow is supposed to be **supercritical** with large velocity and small water depth. In the channel segment shown in Fig. 3.48 the water flow is suddenly decelerated as the state of flow changes discontinuously into a substantially slower flow with large water depth and so-called **subcritical** state. Such a discontinuous transition arising in channel flows is called a **hydraulic jump**. It arises for instance, if the water in a channel flows through a segment with large slope that quickly merges into a region with small slope.

Far upstream and far downstream of the hydraulic jump steady flow conditions prevail with constant water depths over long distances. This means that hydrostatic pressure conditions prevail in these regions. In addition, we assume as a simplification that velocity profiles are constant over depth. The sum of the pressure and momentum flux, integrated over the cross sections 1 and 2 are, thus, given by

$$S_i = \rho v_i^2 h_i + \frac{1}{2} \rho g h_i^2 \qquad (i = I, II). \tag{3.231}$$
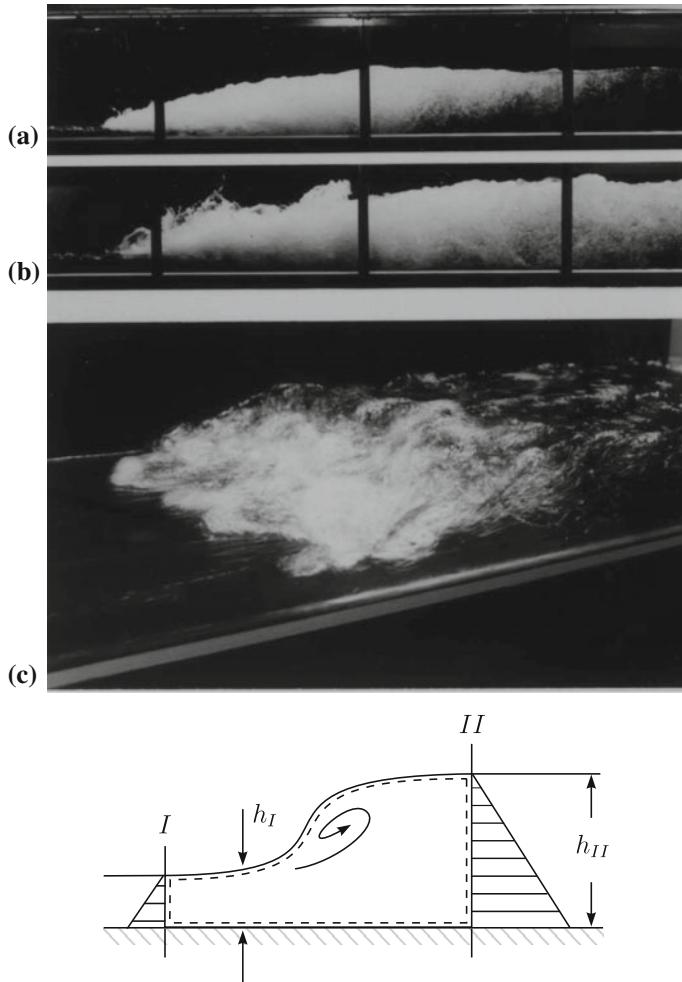
Fig. 3.48 Free surface channel flow. *Steady state flow in an open channel. In a transition from supercritical to subcritical flow, a so-called hydraulic jump is formed. On the left, a sketch, explaining the principle; above, photography of hydraulic jump with* FROUDE *number* $Fr = v/\sqrt{gh} \approx 4$. **a** *Calm water surface.* **b** *Violent water surface.* **c** *Perspective view.* (*Photo* courtesy Prof. Dr. W.H. HAGER, VAW).

Even though in a hydraulic jump the high turbulent activity is generating a large energy loss and even though also shear tractions at the bottom and the walls arise, these do not have to be considered in the momentum balance that follows. This balance, formulated for the dashed volume in Fig. 3.48, takes the form

$$S_I = \rho v_I^2 h_I + \frac{1}{2}\rho g h_I^2 = \rho v_{II}^2 h_{II} + \frac{1}{2}\rho g h_{II}^2 = S_{II}. \qquad (3.232)$$

An additional relation follows from the continuity equation

$$v_I h_I = v_{II} h_{II}.$$ (3.233)

If one eliminates from these relations the velocity v_{II}, one obtains the quadratic equation

$$h_{II}^2 + h_{II} h_I - \frac{2v_I^2}{g} h_I = 0$$ (3.234)

for h_{II} with the single positive solution

$$h_{II} = -\frac{h_I}{2} + \sqrt{\frac{h_I^2}{4} + \frac{2v_I^2 h_I}{g}}.$$ (3.235)

Thus, we have been able to evaluate the water depth and depth averaged velocity below the hydraulic jump, if the corresponding quantities are given above the hydraulic jump.

No hydraulic jump arises when $h_I = h_{II}$; this condition is given, provided that

$$h_{cr}^2 = \frac{v_{cr}^2 h_{cr}}{g} \quad \text{or} \quad h_{cr}^3 = \frac{Q^2}{g}$$ (3.236)

holds, in which $Q = vh$ is the volume flux that is assumed to be known. Conditions (3.236) are called critical, and correspondingly, h_{cr} is the**critical water depth**; it represents for h_I and h_{II} a limiting value as h_I is always smaller, and h_{II} always larger than the critical water depth. Moreover, it is easily shown with the aid of (3.234) that h_{II} grows with decreasing h_I.

Let us also evaluate the energy that is destroyed in a hydraulic jump. If one writes the BERNOULLI equation for the free surface streamline at the cross sections I and II (it is clear that within the strong turbulent regime of the hydraulic jump this is doubtful), then we obtain

$$\rho \frac{v_I^2}{2} + \rho g h_I = C_1, \qquad \rho \frac{v_{II}^2}{2} + \rho g h_{II} = C_2.$$ (3.237)

However, one cannot set $C_1 = C_2$, as this would assume no energy loss through the hydraulic jump, and it would contradict equation (3.235). The difference $C_1 - C_2$ yields exactly this difference,

$$\triangle E_{\text{jump}} = C_1 - C_2 = \frac{\rho}{2} \left(v_I^2 - v_{II}^2 \right) + \rho g (h_I - h_{II}).$$ (3.238)

If one uses here also the relations

$$v_I^2 \;=\; \frac{g}{2}\frac{h_{II}\,(h_I + h_{II})}{h_I}\,, \qquad v_{II}^2 \;=\; \frac{g}{2}\frac{h_I\,(h_I + h_{II})}{h_{II}}, \qquad (3.239)$$

which can be obtained from Eqs. (3.232) and (3.233), then the energy loss in the hydraulic jump takes the form

$$\triangle E_{\text{jump}} \;=\; \rho g \frac{(h_{II} - h_I)^3}{4h_I h_{II}} \;=\; \rho g \triangle H, \qquad (3.240)$$

which was first evidenced in this form by J.A.CH. BRESSE in 1862. For a short biography of BRESSE see **Fig. 3.49**.

Fig. 3.49 JACQUES ANTOINE CHARLES BRESSE (9. Oct. 1822–22. May 1883)

JACQUES ANTOINE CHARLES BRESSE was a French applied mathematician and hydraulician. He was Professor at the Ecole Nationale Supérieure des Ponts-et-Chaussées in Paris. His contribution is chiefly to gradually varied flows in open channel hydraulics.

BRESSE was a teacher for over 50 years, which he preferred to administration. His main achievements were in engineering statics. He published 'Cours Mécanique Appliquée' [2] in two volumes, the second of which covered hydraulics. It is characterized by depth in thoughts and simplicity of approach. The hydraulics part covers the hydraulic jump, based on the balance of linear momentum and steady channel flow in a concise and direct approach.

The text is based on http://www.wikipedia.org and [6]

According to this, the above calculations show a close analogy between the hydraulic jump and the sudden cross section expansion in a pipe according to CARNOT. There also exists a further analogy between a hydraulic jump and a gas dynamic shock. According to this analogy the subcritical channel flow corresponds to subsonic flow in gas-dynamics, whilst the supercritical flow corresponds to the supersonic condition.

3.8   Plane Flow Around Infinitely Long Wings

In Sect. 3.6 the force was computed which is exerted on a submerged body by the flow of an ideal fluid around it. When the gravity force is ignored, this force is given by Eq. (3.196), or

$$K = - \int_{A_1} (\rho v(v \cdot n) + pn)\, \mathrm{d}A, \tag{3.241}$$

in which A_1 is any simply closed area that completely surrounds the body within the fluid. We shall now apply this formula to the problem of steady flow around a wing. We shall restrict considerations to plane flows.
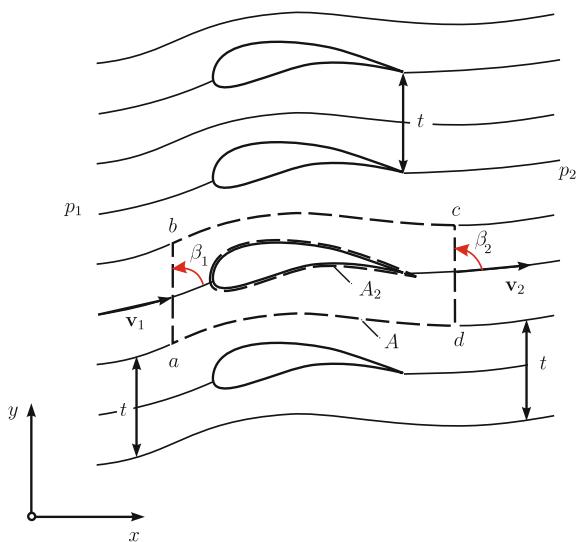
3.8.1   Flow Through a Periodic Grid of Wings

Let us begin with the simplest example of steady plane flow through a periodic grid of wings, **Fig. 3.50**. Because of the periodicity of the grid, all flow quantities are periodic in the y-direction with the period t, the distance between the wings. The flow field far upstream, ahead of the grid is a parallel flow with a constant velocity vector v, which is inclined to the vertical direction by the angle β_1. The pressure ahead of the grid is equally constant and given by p_1. Therefore, the BERNOULLI constant has for all streamlines the same value $C = p_1 + \frac{1}{2}\rho v_1^2$. By the grid the flow is turned, so that far behind the grid, that is far downstream, again a parallel flow prevails, but now with different velocity vector v_2, different angle β_2 and with pressure p_2,which also differs in general from p_1. The BERNOULLI constant, however, agrees with that ahead of the grid.

To evaluate the force which is exerted by the fluid on the wing, we consider the volume bounded by the dashed closed line in Fig. 3.50. It is made up by the two segments of streamlines ad and bc (which are congruent as they have the same relative position between two wings) and by the two lines ab and dc, respectively, which are parallel to the y-axis and sufficiently before and behind the grid that parallel flow prevails at those x-positions. Mass balance, applied to this control volume says that the volume flow through the area dc (since the element $abcd$ is a flow tube) is given by

$$u_1 t = v_1 \, \sin \beta_1 \, t = v_2 \, \sin \beta_2 \, t = u_2 t \qquad \Longrightarrow \qquad u_1 = u_2 = u. \quad (3.242)$$

The horizontal velocity component remains preserved, see **Fig. 3.51**a. (The x- and y-axes are perpendicular and parallel, respectively, to the direction of the grid array).

For the application of formula (3.241) along the surface $abcd$ we note first that $\boldsymbol{v} \cdot \boldsymbol{n}$ vanishes along the streamlines ad and bc. Moreover then, the pressures in congruent points of these streamlines are the same, but the unit exterior normal vectors are pointing in opposite directions, so that the integrals $\int p\boldsymbol{n} dA$ along ad and bc cancel each other. For the evaluation of (3.241), we, therefore, have to consider only the contributions of the pressures and momentum fluxes along ab and dc. Thus, we may write
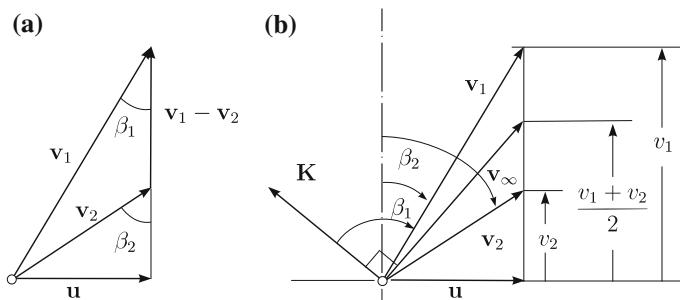
Fig. 3.51 Calculation of the flow induced force for a wing in a periodic grid. **a** *The velocity component perpendicular to the wing is preserved.* **b** *The flow fluid at infinity, $\boldsymbol{v}_\infty$ and the flow induced force $\boldsymbol{K}$ are perpendicular to one another*

$$\int\limits_a^b \rho v(v \cdot n) dA = -\rho v_1 ut, \quad \int\limits_b^c \rho v(v \cdot n) dA = \rho v_2 ut,$$

$$\int\limits_a^b p n \, dA = -p_1 t e_x, \quad \int\limits_d^c p n \, dA = p_2 t e_x. \tag{3.243}$$

Here, we have accounted for the fact that the horizontal component of the velocity vector is preserved; e_x is the unit vector in the x-direction. If we substitute (3.243) into (3.241), we obtain

$$K = \rho(v_1 - v_2)ut + (p_1 - p_2)t e_x$$
$$= \underbrace{\rho(v_1 - v_2)ut e_y}_{y-\text{component}} + \underbrace{(p_1 - p_2)t e_x}_{x-\text{component}} \tag{3.244}$$

To determine the x-component of this force, respectively, to evaluate the pressure p_2, let us write down the BERNOULLI equation between two points of a streamline, one far upstream, the other far downstream; this yields

$$p_1 + \rho\frac{v_1^2}{2} = p_2 + \rho\frac{v_2^2}{2}, \tag{3.245}$$

in which v_1 and v_2 are the y-components of the velocities v_1 and v_2, as the contributions of the x-components cancel each other. Thus, one obtains from (3.245)

$$p_1 - p_2 = \frac{\rho}{2}\left(v_2^2 - v_1^2\right) = \frac{\rho}{2}(v_1 + v_2)(v_2 - v_1), \tag{3.246}$$

and may therefore write

$$K_x = -\rho\frac{v_1 + v_2}{2}(v_1 - v_2)t, \qquad K_y = \rho u(v_1 - v_2)t. \tag{3.247}$$

If we define with

$$\Gamma \ \ = = (v_1 - v_2)t,$$
$$v_\infty = \tfrac{1}{2}(v_1 + v_2) = u e_x + \tfrac{1}{2}(v_1 + v_2)e_y, \tag{3.248}$$

the **circulation** Γ (per unit depth around the wing and the arithmetic mean of the asymptotic velocities, then the force components (3.247) can also be written as

$$K_x = -\rho v_\infty \Gamma, \qquad K_y = \rho u_\infty \Gamma. \tag{3.249}$$

The flow induced force acting on a wing with thickness 1 is, thus, given by the density of the fluid, ρ, the asymptotic velocity, v_∞, and the circulation of the flow around the wing.

The following comments complement the foregoing calculations in a useful way:

- The reader can easily corroborate the property $\boldsymbol{K} \cdot \boldsymbol{v}_\infty = 0$; in other words, the flow induced force that is exerted on a wing is perpendicular to $\boldsymbol{v}_\infty$ and forms with $\boldsymbol{v}_\infty$ a positively oriented pair, see Fig. 3.51b.
- We have called above the quantity Γ in (3.248) the circulation. Generally, the **circulation** of a velocity field along a **simply closed smooth curve** is defined as

$$\Gamma = \oint_{\mathcal{L}} \boldsymbol{v} \cdot \mathrm{d}\boldsymbol{x}, \tag{3.250}$$

in which $\mathrm{d}\boldsymbol{x}$ denotes the vectorial line element along the curve $\mathcal{L}$ of which the direction also defines the orientation around which the closed curved integral is traversed. It is customary to choose $\mathrm{d}\boldsymbol{x}$ such that the closed curve is traversed in the clockwise direction, **Fig. 3.52**.

Let us now calculate the circulation for the control volume swept out by the dashed line of Fig. 3.50 along $abcda$. The contributions along the streamlines da and bc drop out because the velocities along these streamlines are the same, but the directions of $\mathrm{d}\boldsymbol{x}$ during integration are opposite to one another. Thus, there only remain the contributions along the vertical y-axes along the segments cd and ab
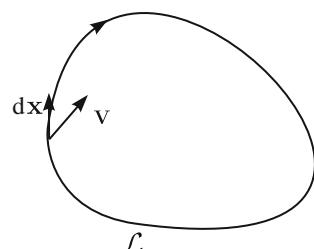
$$\Gamma = (v_1 - v_2)\, t, \tag{3.251}$$

which is identical to formula (3.248).

- From vector calculus one knows that for any vector field $\boldsymbol{v}$, which is differentiable in a simply connected region, bounded by a smooth curve $\mathcal{L}$, the STOKES theorem must hold, namely

$$\oint_{\mathcal{L}} \boldsymbol{v} \cdot \mathrm{d}\boldsymbol{x} = \int_{A} (\mathrm{curl}\, \boldsymbol{v}) \cdot \boldsymbol{n}\, \mathrm{d}A. \tag{3.252}$$

Fig. 3.52 Evaluation of the circulation. *In the calculation of the integral (3.250) the orientation is clockwise*
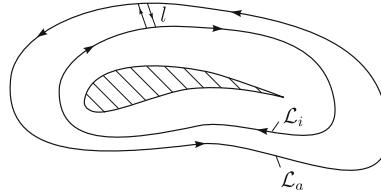
Fig. 3.53 Circulation. *In an irrotational flow, the value of the circulation along closed lines, which by deformation may be made congruent to each other without crossing boundaries, remains unchanged*

If curl $\boldsymbol{v}$ vanishes, the field is irrotational, and the circulation along each closed curve that bounds a simply connected region vanishes as well.

- The flow field of an ideal fluid is always vortex free or irrotational, if it has developed from a state of rest; so curl $\boldsymbol{v} = \boldsymbol{0}$ holds. One can prove this by taking the curl of the momentum equation; this yields $\mathrm{d}(\mathrm{curl}\,\boldsymbol{v})/\mathrm{d}t = \boldsymbol{0}$, or after integration curl $\boldsymbol{v} = \mathrm{fct}(\boldsymbol{x})$. This function is the zero function for a motion starting from rest. We therefore have in such cases curl $\boldsymbol{v} = \boldsymbol{0}$.

Now, the region encircling a wing of the grid is not simply connected. It can, however, be made simply connected by cutting it along l as shown in **Fig. 3.53**. In the cut region the STOKES theorem is valid and can be applied to the closed path shown in the figure. With curl $\boldsymbol{v} = \boldsymbol{0}$ we then have

$$\oint_{\mathcal{L}_i} \boldsymbol{v} \cdot \mathrm{d}\boldsymbol{x} + \int_{l} \boldsymbol{v} \cdot \mathrm{d}\boldsymbol{x} - \oint_{\mathcal{L}_a} \boldsymbol{v} \cdot \mathrm{d}\boldsymbol{x} - \int_{l} \boldsymbol{v} \cdot \mathrm{d}\boldsymbol{x} = 0, \qquad (3.253)$$

or

$$\oint_{\mathcal{L}_i} \boldsymbol{v} \cdot \mathrm{d}\boldsymbol{x} = \oint_{\mathcal{L}_a} \boldsymbol{v} \cdot \mathrm{d}\boldsymbol{x} = \Gamma. \qquad (3.254)$$

Therefore, the circulation is independent of the curve along which the integration is performed: one may justly speak of *the* circulation of the flow around the wing.

- If we define with

$$\boldsymbol{\Gamma} = -\Gamma \boldsymbol{e}_z, \qquad (3.255)$$

a vector perpendicular to the (x, y)-plane, of which the value is given by the circulation and which points into the positive z-direction if the circulation around the body in the (x, y)-plane is counterclockwise, then formulae (3.249) can be elegantly expressed by the vectorial equation

$$\boldsymbol{K} = \rho \boldsymbol{v}_\infty \times \boldsymbol{\Gamma}. \qquad (3.256)$$

This is a formula which has originally not been derived for the periodic grid of wings, but for a single wing and will be similarly derived in the next section. The formula bears a double name after KUTTA and JOUKOWSKI, who both found it independently. For the short biographies of KUTTA, RUNGE and JOUKOWSKI, see **Figs. 3.54**, **3.55** and **3.56**, respectively.

3.8.2 *Flow Around a Single Wing*

Formally, plane flow around a single wing can be deduced from the results which were derived for the periodic grid of wings by holding a particular wing fixed and performing the limit $t \rightarrow \infty$, in which the other wings move to infinity. Under such conditions it is evident that with growing t the deviation of the flow from its

KUTTA-JOUKOWSKI formula (theorem)

$$\boldsymbol{K}_Q = \rho \boldsymbol{v}_\infty \times \boldsymbol{\Gamma}$$

in an inviscid fluid
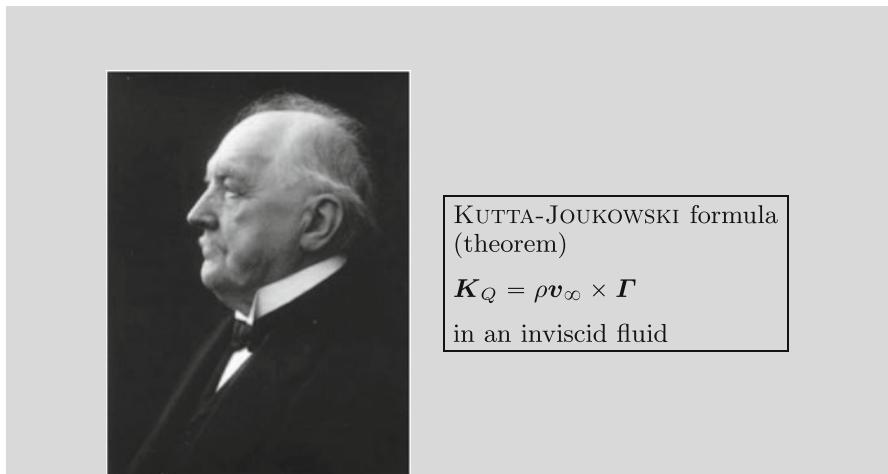
Fig. 3.54 MARTIN WILHELM KUTTA (3. Nov. 1867–25. Oct.1944)

MARTIN WILHELM KUTTA was born in Pitschen, Upper Silesia (today Byczyna, Poland). He attended the University of Breslau from 1885 to 1890, and continued his studies in Munich until 1894, when he became assistant of WALTHER FRANZ ANTON VON DYCK (1856–1934). From 1898, he spent half a year at the University of Cambridge, and between 1899 and 1909 he worked again as an assistant of VON DYCK in Munich. From 1909 to 1910 he was adjunct professor at the Friedrich Schiller University in Jena. He was professor at the RWTH Aachen from 1910 to 1912. WILHELM KUTTA became professor at the University of Stuttgart in 1912, where he stayed until his retirement in 1935.

In 1901, he co-developed the RUNGE-KUTTA method, used to solve ordinary differential equations numerically. He is also remembered for the JOUKOWSKI-KUTTA aerofoil, the KUTTA-JOUKOWSKI theorem and the KUTTA condition in aerodynamics. KUTTA died in Fürstenfeldbruck, Germany in 1944.

The text is based on http://www.wikipedia.org

Fig. 3.55 Carl David Tolmé Runge (30. Aug. 1856–3. Jan.1927)

Carl David Tolmé Runge studied literature, philosophy and mathematics at the Universities Munich and Berlin where he was influenced by Kronecker, Weierstrass and Kummer. He was professor of mathematics at the Technical High School Hannover from 1886–1904 and then moved to the University of Göttingen where he occupied the first chair of *applied* mathematics. He is known in fluid mechanics primarily through the Runge-Kutta method for the integration of ordinary differential equations in initial boundary value problems.

(Much following the 'Law of academic marriage, that the talent of a professor in the 19th–20th century is inherited to the son-in law': Richard Courant was married to Runge's daughter Nerina, (Nina), and Jürgen Moser was married to Richard Courant's daughter Gertrude, as was Ludwig Prandtl married to August Föppl's daughter Gertrud).

The text is based on http://www.wikipedia.org
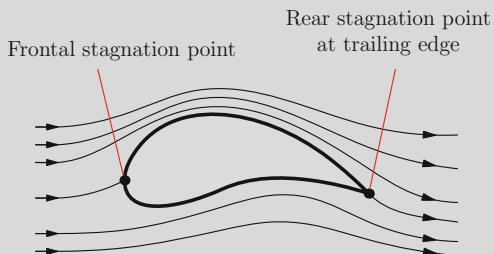
uniformity becomes less and less, such that v_1 and v_2 and consequently also p_1 and p_2 in the limit as $t \to \infty$ agree with one another and can be identified with v_∞ and p_∞, respectively. This limit process is, according to (3.251), however, only meaningful if the circulation takes a finite value different from zero,

$$\Gamma = \lim_{t \to \infty} (v_1 - v_2)t = \text{finite}, \tag{3.257}$$

implying the **Kutta-Joukowski formula**

$$\boldsymbol{K}_Q = \rho \boldsymbol{v}_\infty \times \boldsymbol{\Gamma}, \qquad K_Q = \rho u_\infty \Gamma. \tag{3.258}$$

Frontal stagnation point

Rear stagnation point
at trailing edge

The KUTTA-JOUKOWSKI condition at the
rear stagnation point of an airfoil requires
the circulation around the airfoil to be such
that the flow off the two-dimensional wing
is smooth

Fig. 3.56 NIKOLAI YERGOROWICH JOUKOWSKI (17. Jan. 1847–17. March 1921)

NIKOLAY JERGOROWITSCH SCHUKOWSKI (or NIKOLAI YERGEROWITSCH ZHUKOWSKY or
NIKOLAI YERGOROWICH JOUKOWSKI) [all three spellings can be found] was a Russian
mathematician aero and hydro-dynamicist. He is regarded as the founder of the Russian aero
and hydrodynamics. He was the first scientist to explain mathematically the origin of the
aerodynamic lift through his circulation hypothesis. Moreover, he used conformal mapping
to create the KUTTA-JOUKOWSKI aerofoils. He also postulated the so-called JOUKOWSKI
condition determining the circulation around plane wings such that the flow from the trailing
edge of a wing had to be smooth.

The text is based on http://www.wikipedia.org

Consequently, the force, caused by the flow around the wing is perpendicular to the
velocity far up or far downstream. The force K_Q is called the **hydrodynamic lift**, but
would better be called the **hydrodynamic normal force**; this is so, because this force
may be directed upward or downward, depending upon the sign of the circulation.
Thus, the circulation represents the decisive quantity determining the hydrodynamic
lift. Qualitatively, its effect can be explained with the BERNOULLI equation as follows:
Due to the circulation, the flow at the upper part of the wing is enlarged relative to
the velocity of approach, see **Fig. 3.57** (left), and the pressure relative to the pressure
p_∞ is decreased. Along the lower part of the wing this is reversed, i.e., the velocity is
reduced relative to the upstream velocity and the pressure on the profile is enlarged.
If these pressures are integrated around the profile contour, a force K_1 will result,
which is directed upward.

One may easily show that Γ must be proportional to both, u_∞ and the length of the
wing, L. To see this, we consider the dimension of the wing to be kept, but enlarge the
value of u_∞. The definition (3.252) of the circulation then immediately shows that Γ
increases with the growth of the velocity. If, on the other hand, we similarly enlarge
or decrease the size of the wing, but keep the velocity u_∞ fixed, then one has along
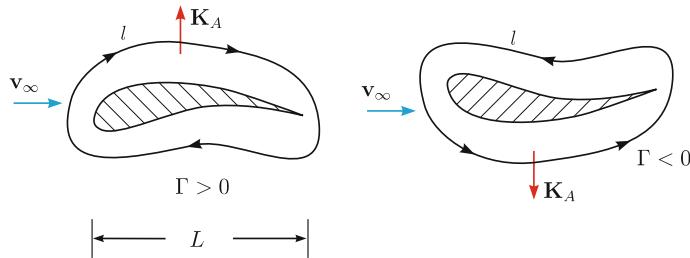
Fig. 3.57 KUTTA-JOUKOWSKI formula. *Depending upon the sign of the circulation the hydrodynamic lift force points upward or downward*

an affinely changed curve $\mathcal{L}$ around the wing the same (tangential) velocities; the length of the closed curve, along which the integration must be performed to evaluate the circulation, however, has changed according to the stretching or squeezing ratio. Thus, the circulation must also be proportional to a typical dimension of the wing, e.g. its length; we may therefore also write

$$K_L = c_L \frac{\rho u_\infty^2}{2} L, \qquad (3.259)$$

in which c_L is known as the **lift coefficient**: $\frac{1}{2}\rho u_\infty^2$ is the stagnation pressure of the upstream flow, and the product $\frac{1}{2}\rho u_\infty^2 L$ is a force per unit depth of the wing. Hence the lift coefficient is a dimensionless number which depends on the shape of the wing profile as well as its orientation relative to the direction of the upstream flow.

In the explanation given above it has been assumed that the circulation around the wing profile has a given fixed value. Now, the mathematical theory of the hydrodynamics of ideal fluids shows, that there are theoretically an infinite number of plane flows around a profile which differ by the value of the circulation; i.e., *for every value of the circulation*, Γ, *there exists a possible flow of an ideal fluid around a wing profile.* In other words, with the theory of ideal fluids the circulation cannot be determined. In **Fig. 3.58** two possible flows around a profile are sketched with different values of the circulation. In one case (panel a) the trailing edge is circumflown, in the second (panel b) the flow detaches smoothly from the rear end of the profile. Experience has shown that, if the angle of attack, α, of the wing is not too large, indeed, a smooth flow at the rear profile tip will be established. This is shown in the picture of Fig. 3.58. The reason for this behavior cannot be understood as long as the fluid is regarded as frictionless. If one conjectures, however, and follows the **Kutta-Joukowski hypothesis**, that the velocity at the pointed trailing edge remains bounded away from infinity, as it is so for the smooth flow from the edge, then one has a criterion, according to which the circulation can mathematically be determined.

In this way, as we shall see, the theory yields for a flat plate or a circular segment, see **Fig. 3.59**, inclined at an angle α relative to the flow at infinity

(a)

$\Gamma_1 < \Gamma_2$

Γ_1

u_∞

α

(b)

$\Gamma_2 > \Gamma_1$

Γ_2

u_∞

α

(c)

Flow should not break
at the back end
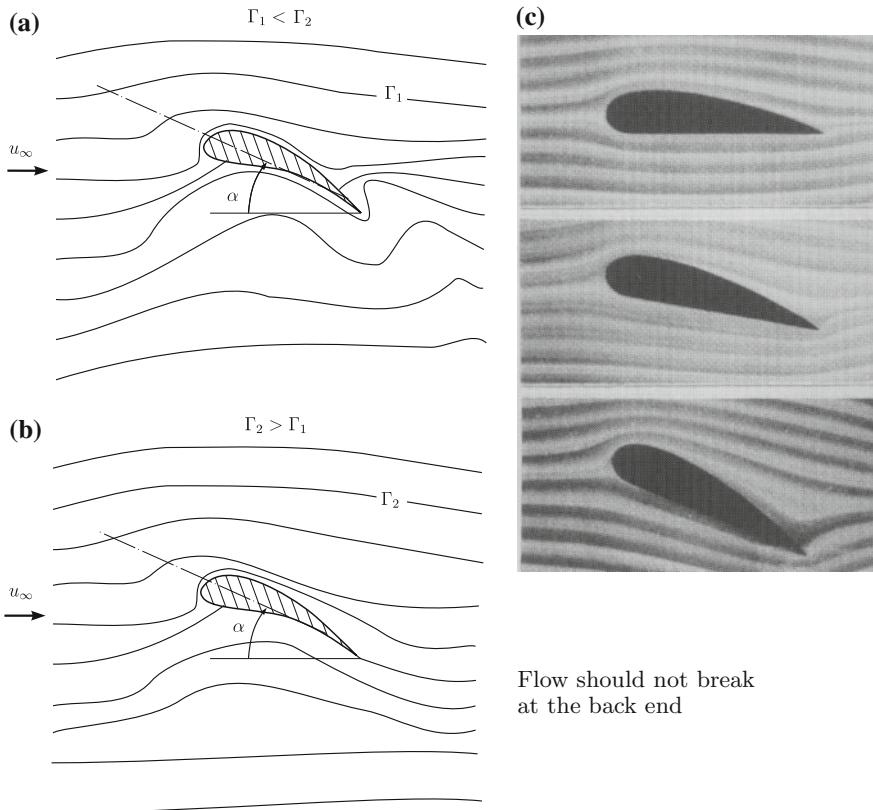
Fig. 3.58 KUTTA-JOUKOWSKI condition. **a, b** *In an inviscid fluid, flows with arbitrary circulation are possible. The* KUTTA-JOUKOWSKI *condition chooses the circulation such that the wing at the pointed trailing edge is smoothly flown by.* **c** *Photographs of the streamlines around a wing with different angles of attack*

(a)

u_∞

α

(b)

$\vartheta/4$

u_∞

α

ϑ
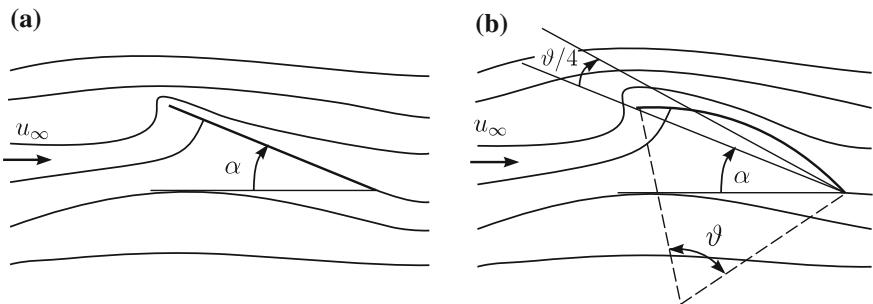
Fig. 3.59 Flow past infinitely thin wings. **a** *Plate with non-vanishing angle of attack.* **b** *Inclined circular segment*

$$c_L = 2\pi \sin \alpha \sim 2\pi\alpha \,, \qquad\qquad\qquad\qquad \text{(plate)},$$

$$c_L = 2\pi \sin\left(\alpha + \frac{\vartheta}{4}\right) \sim 2\pi\left(\alpha + \frac{\vartheta}{4}\right)\,, \qquad \text{(circular segment)}. \qquad (3.260)$$

For small angles α the coefficient of lift, thus, grows to first order linearly with the angle.

We have determined above the value of the circulation by use of the KUTTA-JOUKOWSKI criterion, but we have not answered the question, how such a circulation is built in the initial period of the of motion from rest to, say, lift-off. In fact, effects of internal friction are responsible for it, which can explain the **existence** of a non-vanishing circulation. At the very first instant of the motion the fluid demonstrates the tendency to move around the sharp trailing edge. This would, however, require very large—theoretically infinitely large—velocity at the tip of the edge. Instead, a counter clockwise rotating eddy or vortex will be formed, which moves from the tip of the trailing edge downstream that is followed by a surface across which the velocity suffers a jump; this is a so-called **vortex sheet**. In order that the total angular momentum in the fluid is preserved, a circulation flow builds up in the clockwise direction around the wing. This circulation grows until the jump of the tangential velocity in the streamlines immediately above and below the wing profile within the vortex sheet vanishes. This process is the physical basis of the KUTTA-JOUKOWSKI condition.
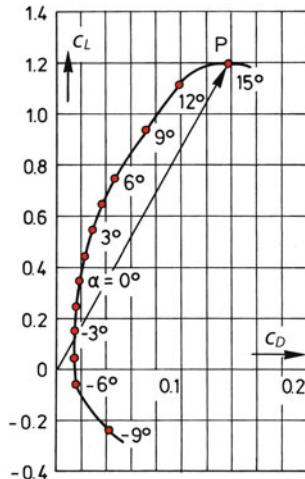
Infinitely long wings, which are analyzed with the theory of ideal fluids do yield a flow drag that obviously exists for real fluids. For wings with finite length LUDWIG PRANDTL (1875–1953)[18] in Göttingen and before him LANCHASTER (1868–1946) in England developed a theory for finite wings, which allows estimation of a drag coefficient. In general, one is, however, faced to conduct experiments; accordingly, one determines for a given profile and various different angles of attack the drag coefficient c_D, with the aid of which the drag force K per unit width can be determined,

$$K_D = c_D \frac{\rho u_\infty^2}{2} L. \qquad (3.261)$$

There are various different (graphical) representations for c_L and c_D. For instance, one may plot them against the angle of attack for various different REYNOLDS numbers, $\mathbb{R} = u_\infty L/\nu$, where ν is the kinematic viscosity. It is then recognized that for large REYNOLDS numbers the lift coefficient c_L is practically independent of $\mathbb{R}$, whilst c_D shows some dependence. It is, however, customary to combine the two coefficients to a two-dimensional vector (c_D, c_L) in a Cartesian coordinate system. One obtains this way a graph that is known as **polar diagram**, see **Fig. 3.60**. In this diagram the arrow from the origin O to an arbitrary point P is parallel and proportional to the force due to the flow and comprising of drag and lift. The polar diagram of Fig. 3.60 also shows parameter values of α along the curve. One can see, the lift

---

[18]A short vita of PRANDTL is given in Vol. 2, Chap. 17.

Fig. 3.60 Polar diagram. *In a viscous fluid the lift coefficient c_L and the drag coefficient c_D for a wing profile are experimentally determined. The angle α of attack is shown parametrically*

assumes its maximum at $\alpha \approx 15°$ and the drag grows quickly in this neighborhood. Both these behaviors cannot be explained with an inviscid fluid model. For angles of attack so large, the flow at the upper side of the profile becomes unstable and forms a downstream vorticity field. If the body at the trailing edge is not pointed but blunt (as e.g. for a sphere, a cylinder or a plate oriented other than parallel to the upstream velocity, i.e. perpendicular) the flow becomes already unstable at rather small REYNOLDS numbers and leaves a relatively large vorticity 'laden' region behind the body. The drag existence of such bodies must obviously be much larger.

3.9 Balance of Moment of Momentum

The **balance of angular momentum** used here in the form of balance of moment of momentum is an additional fundamental law, which complements the fundamental law of NEWTON and is a compulsory additional law whenever a body is of finite extent. Balance of momentum, formulated for any body is the statement

$$\frac{d\boldsymbol{I}}{dt} = \boldsymbol{K}. \tag{3.262}$$

Accordingly, the time rate of change of the momentum equals the resultant external force acting on the body. In (3.262) the momentum is a vector, whose line of attack passes through the center of mass of the body; analogously also the force $\boldsymbol{K}$ must be thought to pass through this line of attack.

For a system of N mass points we have

$$I = \sum_{\alpha=1}^{N} m_\alpha \dot{x}_\alpha , \qquad\qquad K = \sum_{\alpha=1}^{N} K_\alpha, \qquad\qquad (3.263)$$

where m_α, $\dot{x}_\alpha$ and K_α are the mass, velocity and the force of the mass point α with the position vector x_α and the center of mass is given by

$$x = \sum_\alpha m_\alpha x_\alpha \Big/ \sum_\beta m_\beta. \qquad\qquad (3.264)$$

If one forms for a mass point α the moment of the momentum with respect to the origin of the coordinate system, O, then one obtains the moment of momentum, also called **angular momentum**, which can be written as

$$L_O^\alpha = x_\alpha \times (m_\alpha \dot{x}_\alpha). \qquad\qquad (3.265)$$

The angular momentum of a system of mass points is defined as the sum of the individual angular momenta and is, thus, given by

$$L_O = \sum_\alpha x_\alpha \times m_\alpha \dot{x}_\alpha. \qquad\qquad (3.266)$$

If one forms the time derivative of the angular momentum so defined, one obtains for a **system of mass points**

$$\dot{L}_O = \left(\sum_\alpha x_\alpha \times m_\alpha \dot{x}_\alpha \right)^{\cdot} = \sum_\alpha x_\alpha \times (m_\alpha \ddot{x}_\alpha). \qquad\qquad (3.267)$$
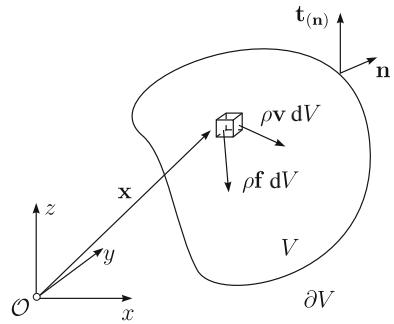
In view of the balance of linear momentum, this can also be written as

$$\dot{L}_O = \sum_\alpha x_\alpha \times K_\alpha = \sum_\alpha M_O^\alpha, \qquad\qquad (3.268)$$

in which M_O^α is the moment of the force K_α, that acts on the mass point α with respect to the origin of the coordinate system. The time rate of change of the angular momentum with respect to the point $\mathcal{O}$ is, thus, equal to the moment with respect to the same point of all the forces that act on the system of mass points.

For a system of mass points the law of angular momentum (3.268) is therefore a consequence of the law of (linear) momentum. However, for general bodies, this is not so. Hence one must consider the law of angular momentum or the law of moment of momentum as an independent physical postulate, which complements the law of linear momentum. This postulate is exactly of the form (3.268), and so, we may think

Fig. 3.61 Explaining the definition of the angular momentum. *The angular momentum of a body with volume V and boundary ∂V with respect to a point $\mathcal{O}$* equals its moment of momentum

it to be *motivation* for the postulation of the law angular momentum in its general form

$$\dot{\boldsymbol{L}}_{\mathcal{O}} = \boldsymbol{M}_{\mathcal{O}}, \tag{3.269}$$

in words: With respect to the point $\mathcal{O}$ the time rate of change of the angular momentum equals the moment of all volume forces and volume couples as well as of all surface forces and surface couples.

For a continuous body, we define the angular momentum with respect to $\mathcal{O}$ as the integral of the moments of momenta of all mass elements, see **Fig. 3.61**,

$$\boldsymbol{L}_{\mathcal{O}} = \int_V \boldsymbol{x} \times \rho \boldsymbol{v} \, \mathrm{d}V, \tag{3.270}$$

and, correspondingly, the moment with respect to $\mathcal{O}$ as the sum of the moments due to the volume and surface forces,

$$\boldsymbol{M}_{\mathcal{O}} = \int_V \boldsymbol{x} \times \rho \boldsymbol{f} \, \mathrm{d}V + \int_{\partial V} \boldsymbol{x} \times \boldsymbol{t}_{(\boldsymbol{n})} \, \mathrm{d}A. \tag{3.271}$$

In this formula it is assumed that no external body couples arise.

With (3.270) and (3.271) the balance law of angular momentum (3.269) is, therefore,

$$\dot{\boldsymbol{L}}_{\mathcal{O}} = \frac{\mathrm{d}}{\mathrm{d}t} \int_V \boldsymbol{x} \times \rho \boldsymbol{v} \, \mathrm{d}V = \int_{\partial V} \boldsymbol{x} \times \boldsymbol{t}_{(\boldsymbol{n})} \mathrm{d}A + \int_V \boldsymbol{x} \times \rho \boldsymbol{f} \, \mathrm{d}V = \boldsymbol{M}_{\mathcal{O}}. \tag{3.272}$$

To exploit this equation further, we must specifically address the first term on its right-hand side. The specific surface forces, or better surface tractions, $\boldsymbol{t}_{(\boldsymbol{n})}$ can be decomposed into the so-called **normal stresses** (better: **normal tractions**) acting perpendicular to the surface on which they apply and the **shear stresses** (better:
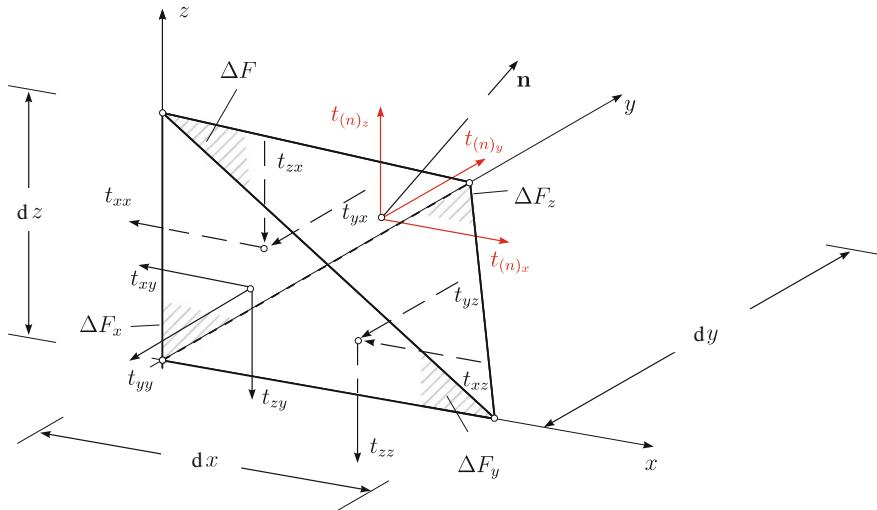
Fig. 3.62 CAUCHY stress tensor. *To find the interpretation of the* CAUCHY *stress tensor we consider an infinitesimal material tetrahedron with three triangular boundary surfaces perpendicular to the coordinate lines and an inclined element with exterior unit normal vector **n**. On each surface element we have normal and shear stresses*

shear tractions) which are parallel to the surface element. To see this more clearly, let us cut an infinitesimal volume element out of the body that has the shape of a tetrahedron with surface elements, of which three are perpendicular to the coordinate axes x, y, z, whilst the fourth is bounding these and has unit exterior normal $\boldsymbol{n}$, see **Fig. 3.62**. If we introduce, as indicated in Fig. 3.62 within the surface elements ΔF_x, ΔF_y, ΔF_z, which are perpendicular to the x, y and z-axes, respectively, the normal stresses t_{xx}, t_{yy}, t_{zz} and the shear stresses t_{xy}, t_{yz}, t_{zx} and if we formulate the equilibrium conditions for this element, then one may show, since $\Delta F_j = n_j \Delta F$, $j = x, y, z$, that the following component representations must hold[19]:

$$
\begin{aligned}
t_{(n)_x} &= t_{xx}n_x + t_{xy}n_y + t_{xz}n_z, \\
t_{(n)_y} &= t_{yx}n_x + t_{yy}n_y + t_{yz}n_z, \\
t_{(n)_z} &= t_{zx}n_x + t_{zy}n_y + t_{zz}n_z,
\end{aligned}
\tag{3.273}
$$

---

[19]In the above **normal stresses** are positive when they are tensions and negative when they are pressures. For the **shear stresses** we used the following convention. The first index refers to the direction of the coordinate axis into which the vector of shear traction points. The second index refers to the direction of the unit normal vector of the areal element on which the shear traction acts. A shear traction vector is positive, if it points together with the unit normal vector into a positive or negative direction of the coordinates. Finally, Eq. (3.274) are the result of momentum balance; however, since one restricts attention to quantities that are small of order h^2, (where h is a typical length of a tetrahedron edge), the balance of momentum reduces in this case to a force balance of surface forces.

$$\frac{\mathrm{d}}{\mathrm{d}t}\int_{V}\rho\boldsymbol{v}\mathrm{d}v = \int_{\partial V}\boldsymbol{tn}\mathrm{d}a + \int_{V}\rho\boldsymbol{f}\mathrm{d}v$$

$$\longrightarrow \qquad \rho\frac{\mathrm{d}\boldsymbol{v}}{\mathrm{d}t} = \mathrm{div}\,\boldsymbol{t} + \rho\boldsymbol{f}$$

The CAUCHY stress tensor arises in CAUCHY's work on elasticity when writing the momentum balance relation as shown above in the EULERian description (see e.g. (3.85)), in which $\boldsymbol{t} = -p\boldsymbol{1}$ is restricted to a pressure tensor

Fig. 3.63 BARON AUGUSTIN-LOUIS CAUCHY (21. Aug. 1789–23 May 1857)

BARON AUGUSTIN-LOUIS CAUCHY was a French mathematician who was an early pioneer of analysis. He started the project of formulating and proving the theorems of infinitesimal calculus in a rigorous manner. He also gave several important theorems in complex analysis and initiated the study of permutation groups in abstract algebra. Among approximately eight hundred research articles and five complete textbooks, there are works on symmetric functions, symmetry groups and the theory of higher-order algebraic equations, the proof of FERMAT's polygonal number theorem and papers on celestial mechanics. He invented the name for the determinant, systematized its study, gave definitions of limit, continuity, and convergence and founded complex analysis by discovering the CAUCHY-RIEMANN equations. He presented a mathematical treatment of optics, hypothesized that ether had the mechanical properties of an elastic medium, and published classical papers on wave propagation in liquids and isotropic and anisotropic elastic media. Between 1830 and 1839 CAUCHY published three versions of treatises in elasticity. He was a man of strong convictions, and a devout Catholic.

The text is partly based on http://www.wikipedia.org

which can also be written symbolically as

$$\boldsymbol{t}_{(n)} = \boldsymbol{tn}, \tag{3.274}$$

in which $\boldsymbol{t}$ is called CAUCHY stress tensor; it has the following nine Cartesian components[20]:

$$\boldsymbol{t} \,\hat{=}\, \begin{pmatrix} t_{xx} & t_{xy} & t_{xz} \\ t_{yx} & t_{yy} & t_{yz} \\ t_{zx} & t_{zy} & t_{zz} \end{pmatrix}. \tag{3.275}$$

---

[20]On the left-hand side $\boldsymbol{t}$ represents the CAUCHY stress tensor; on the right-hand side stands its matrix referred to Cartesian coordinates. The symbol $\hat{=}$ is not an equality sign, because second rank tensors are not equal to matrices, but they are equivalent to tensors and the symbol $\hat{=}$ states that the left and right hand-sides express the same 'mathematical substance'. One also says that $\boldsymbol{t}$ and its matrix are isomorphic to one another. For a short biographical sketch see **Fig. 3.63**.

As a first application of the balance of angular momentum (3.272), consider the infinitesimal volume element of **Fig. 3.64**; let dh be a symbol representing dx, dy and dz and approaching the limit $dh \to 0$ at the same order as dx, dy and dz. In the ensuing analysis we shall apply the balance of angular momentum such that only terms which are small of order $\mathcal{O}(h^2)$ are accounted for, whilst terms which are smaller are dropped. Under such prerequisites one may ignore the angular momentum of the cubic element relative to its center of mass, since it is of order $\mathcal{O}(h^4)$ small. Similarly, the differences of the stresses between two parallel and opposite surface elements are negligible because they are of order $\mathcal{O}(h^3)$ small, and their moments with respect to the center of mass are of $\mathcal{O}(h^4)$ small. A possible volume force is of $\mathcal{O}(h^3)$ and its moment with respect to the center of the cube is of $\mathcal{O}(h^4)$, which is equally negligible. The balance of angular momentum applied to the infinitesimal cube, thus, reduces to a balance of moments of the surface forces. With reference to Fig. 3.64 this balance, formulated for an axis parallel to the z-axis through the center of the cube reads
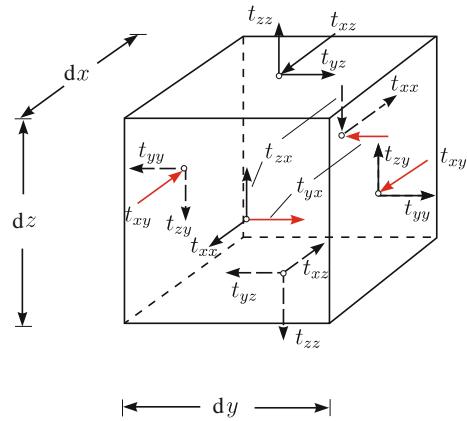
$$(t_{yx}dydz)dx - (t_{xy}dxdz)dy = 0,$$

or if this relation is complemented by analogous statements of moments parallel to the x- and y-axes,

$$t_{xy} = t_{yx}, \quad t_{yz} = t_{zy}, \quad t_{zx} = t_{xz}. \tag{3.276}$$

These relations say that the CAUCHY stress tensor is symmetric; consequently, only six of nine components of the CAUCHY stress tensor are independent of one another. This result alone is demonstration of the fact that the balance law of angular

Fig. 3.64 Symmetry of the CAUCHY stress tensor. *Infinitesimal cube with surface elements perpendicular to the coordinate lines. Also shown are the normal and shear stresses on each surface element*

momentum is an independent statement; for this result could not have been derived from the balance law of linear momentum.

Let us return to the global formulation of the balance law of angular momentum (3.272); we wish to write this equation in a slightly different form. With REYNOLDS' transport theorem, to which we drew attention in the footnote to Eq. (3.86), $\dot{\boldsymbol{L}}_{\mathcal{O}}$ can also be written as

$$
\begin{aligned}
\dot{\boldsymbol{L}}_{\mathcal{O}} &= \int_{V} \frac{\partial}{\partial t}(\boldsymbol{x} \times \rho \boldsymbol{v}) \mathrm{d}V + \int_{\partial V} (\boldsymbol{x} \times \rho \boldsymbol{v})(\boldsymbol{v} \cdot \boldsymbol{n}) \mathrm{d}A \\
&= \int_{V} \left(\frac{\partial}{\partial t}(\boldsymbol{x} \times \rho \boldsymbol{v}) + \operatorname{div}(\boldsymbol{x} \times \rho \boldsymbol{v} \otimes \boldsymbol{v}) \right) \mathrm{d}V = \boldsymbol{M}_{\mathcal{O}}. \quad (3.277)
\end{aligned}
$$

Here, we have in the second term on the right-hand side of the first line transformed the surface integral into a volume integral by employing the GAUSS law. In this somewhat complicated application of the GAUSS law it may be advantageous to express the various terms in component form as follows:

$$
(\boldsymbol{x} \times \rho \boldsymbol{v}) \cdot (\boldsymbol{v} \cdot \boldsymbol{n}) \quad \longrightarrow \quad (\epsilon_{ijk} x_j \rho v_k)(v_l n_l) = \underbrace{(\epsilon_{ijk} x_j \rho v_k v_l)}_{a_{il}} n_l,
$$

so,

$$
\int_{\partial V} (\boldsymbol{x} \times \rho \boldsymbol{v})(\boldsymbol{v} \cdot \boldsymbol{n}) \mathrm{d}A = \int_{\partial V} a_{il} n_l \mathrm{d}A = \int_{V} a_{il,l} \mathrm{d}V.
$$

Going back to symbolic notation, we immediately have (3.277).
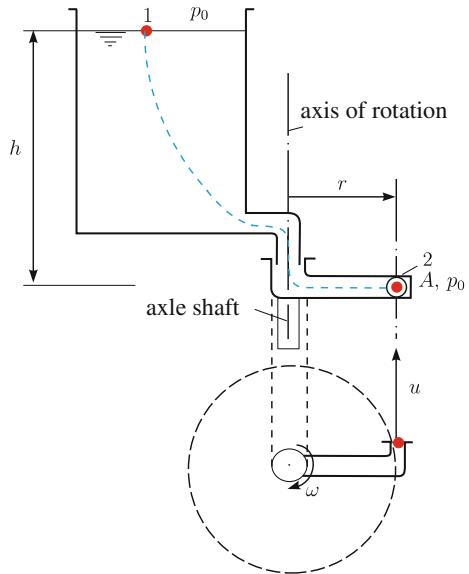
For steady state conditions, (3.277) reduces to

$$
\int_{\partial V} (\boldsymbol{x} \times \rho \boldsymbol{v})(\boldsymbol{v} \cdot \boldsymbol{n}) \mathrm{d}A = \boldsymbol{M}_{\mathcal{O}}, \quad (3.278)
$$

a form that is particularly convenient for applications. Alternatively, on using (3.277) as well as the balance laws of mass and linear momentum, one could derive from (3.272) the symmetry of the CAUCHY stress tensor (and no more).

In ideal fluids, no shear forces can arise. Hence, these terms vanish in the balance of angular momentum, for which the latter would make a non-trivial statement. It follows: *For an ideal fluid the balance of angular momentum is trivially satisfied.*

Fig. 3.65 SEGNER's water
wheel. SEGNER'*s water
wheel, the simplest example
of a turbine. Above view from
the side. Below plan view of
the rotating arm*

3.10   Applications of the Balance of Angular Momentum

3.10.1   Segner's Water Wheel

SEGNER's[21] water wheel, see **Fig. 3.65**, is the simplest realization of a turbine. From
a container water flows through a pipe of which the end piece rotates about a vertical
axis. The exit flow through this last piece is horizontal and azimuthal. We assume
that the cross section of the container is so large that the change of the free water
level can be ignored and that also the water velocity within the container is negligibly
small.

If u denotes the *absolute* and v the *relative velocity* in the horizontal exit orifice,
we have

$$v = u + \omega r, \qquad (3.279)$$

and the system loses water at a rate $Q = vA$. The momentum flux, which the system
loses in the azimuthal direction, is given by $\rho Q u$; it yields a change of angular
momentum with respect to the axis of rotation having the amount

$$\dot{\boldsymbol{L}} = \rho Q u r \boldsymbol{e}_z = \rho A u v r \boldsymbol{e}_z,$$

---

[21]JOHANN ANDREAS SEGNER (1704–1777), Professor at the University Göttingen. For a historical
biography see [9].

where r denotes the distance of the center of the exit orifice to the axis of rotation and where e_z is the unit vector in this axis of rotation. The balance law of angular momentum, formulated for the axis of rotation, thus yields the moment

$$M = \rho A u v r e_z,\tag{3.280}$$

associated with this change of angular momentum that can be taken up by a user.

To calculate the absolute velocity at the exit orifice, we apply the BERNOULLI equation along a streamline between point 1 (on the water surface) and point 2 (at the orifice). For steady conditions of a rotating system it holds true in the form (3.110) and leads to the relation

$$\frac{p_0}{\rho} + gh = \frac{p_0}{\rho} + \frac{v^2}{2} - \frac{\omega^2 r^2}{2},\tag{3.281}$$

in which p_0 denotes the atmospheric pressure. With the definition of the dimensionless quantity

$$\xi = \frac{\omega r}{\sqrt{2gh}},\tag{3.282}$$

(3.279) and (3.281) can be used to write the absolute velocity u as

$$u = v - \omega r = \sqrt{2gh}\left(\sqrt{1 + \xi^2} - \xi\right).\tag{3.283}$$

If this is substituted into (3.280), the modulus of the moment can be written as

$$\frac{M}{M_0} = \sqrt{1 + \xi^2}\left(\sqrt{1 + \xi^2} - \xi\right),\tag{3.284}$$

in which $M_0 = 2\rho gh A r$ is a reference moment, which depends on the dimensions of the SEGNER water wheel and the density ρ. Its value equals that of M_0, if $\omega = 0$ ($\xi = 0$) and may be identified with the moment at starting. For very large rotation speed, whence $\omega \to \infty$ ($\xi \to \infty$), one obtains from (3.284)

$$\begin{aligned}
\lim_{\xi \to \infty} \frac{M}{M_0} &= \lim_{\xi \to \infty} \xi^2 \sqrt{1 + \frac{1}{\xi^2}}\left[\sqrt{1 + \frac{1}{\xi^2}} - 1\right]\\
&= \lim_{\xi \to \infty} \xi^2 \left(1 + \frac{1}{2\xi^2} + \cdots\right)\left(1 + \frac{1}{2\xi^2} + \cdots - 1\right)\\
&= \lim_{\xi \to \infty} \frac{1}{2}\left(1 + \frac{1}{2\xi^2} + \cdots\right)(1 + \cdots) = \frac{1}{2}.
\end{aligned}\tag{3.285}$$
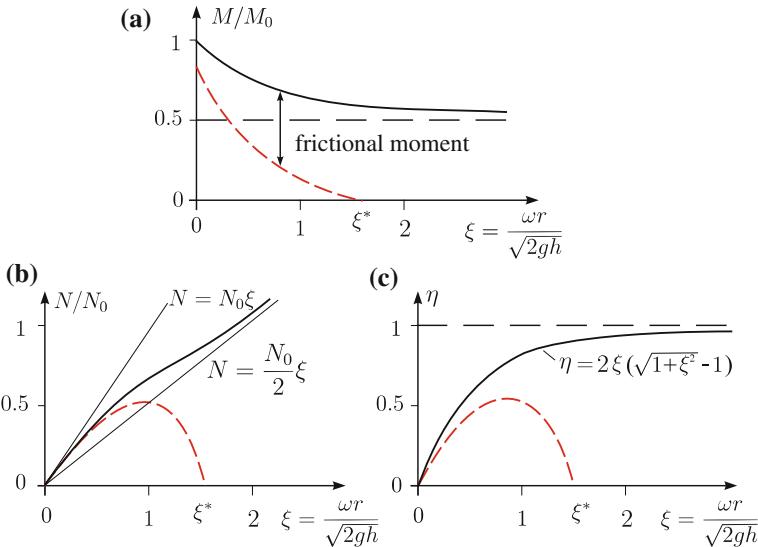
Fig. 3.66 Characteristics of SEGNER's water wheel. **a** *Dimensionless moment as a function of the dimensionless angular speed.* **b** *Dimensionless power of working as a function of the dimensionless angular speed* **c** *Degree of efficiency as a function of the dimensionless angular speed. Solid curves are valid for the inviscid fluid, dashed curves hold for a viscous fluid.* ξ^* *is the dimensionless angular speed for which no usable power of working is generated by the system*

For infinitely large angular rotation rates the moment $M = \frac{1}{2}M_0$ is finite and half as large as the moment at inception. This means physically that the wheel would increase its rotation rate without limit, if one would not take and use the moment at some angular speed. In reality this is always so, also at running idle, at which frictional moments bound the maximum possible angular speed, say at $\xi = \xi^*$. **Figure 3.66**a displays with the solid curve relation (3.284) and with the dashed curve, a curve that is reduced by the frictional moments for the actually usable moments.

The power of working is defined by $N = M\omega$ and can be evaluated with the aid of (3.282) and (3.284); it is given by

$$
\begin{aligned}
N &= N_0\xi\sqrt{1+\xi^2}\left(\sqrt{1+\xi^2}-\xi\right), \\
N_0 &= \rho A(2gh)^{3/2}.
\end{aligned}
\tag{3.286}
$$

It is easy to compute the limiting behavior

$$
\begin{aligned}
N &\simeq N_0\xi + O(\xi^2), & \xi &\to 0, \\
N &\sim \frac{N_0\xi}{2} + O\left(\frac{1}{\xi^2}\right), & \xi &\to \infty.
\end{aligned}
\tag{3.287}
$$

The power of working thus grows linearly with the angular speed. Of course, because of the frictional moments which are always present, this is not possible. Indeed, for $\xi = \xi^*$ the available power of working must vanish. The graphs for (3.286) and its amended version (dashed) are displayed in Fig. 3.66b.

Finally, we wish to illustrate the degree of efficiency, η, of the SEGNER water wheel. It is defined as the ratio of the available power of working N to the maximum possible power of working $\tilde{N}$; the latter is given by the potential energy

$$\tilde{N} = \rho Q g h = N_0 \frac{1}{2}\sqrt{1 + \xi^2}, \tag{3.288}$$

which the system loses per unit time. Thus we have

$$\eta = \frac{N}{\tilde{N}} = 2\xi \left[\sqrt{1 + \xi^2} - \xi\right]. \tag{3.289}$$

This degree of efficiency is always smaller than 1, since only a part of the available potential energy can be transferred to usable power of working. The ideal value of the degree of efficiency reachable by (3.289) approaches the value 1 when $\xi \to \infty$. In reality, however, no usable power of working is available at $\xi = \xi^*$, since all power is used up by internal friction of the system. Figure 3.66c shows the efficiency curves again for both cases.

3.10.2   Euler's Turbine Equation

EULER's turbine is essentially a radial turbine, in which to a cylindrical case water is centrally supplied, which at the outer radial boundary is again leaving the case. Within the case, concentrically with its axis, a freely rotating wheel with a large number of guiding wings is positioned. The flow from the center to the outer boundary sets the wheel in rotation and thus transmits a moment to the shaft of the rotating wheel, **Fig. 3.67**a.

For the evaluation of this moment we wish to apply the balance law of angular momentum in the form (3.277)$_1$ to a control volume which is bounded by the entrance and exit surfaces of the ring of the wings, A_1 and A_2, with the radii r_e and r_a, respectively, as well as the bottom and top lids of the turbine case. The balance law of angular momentum then reads

$$\boldsymbol{M} = \int\!\!\int_{A_1 \cup A_2} (\boldsymbol{x} \times \rho\boldsymbol{v})\,(\boldsymbol{v}\cdot\boldsymbol{n})\mathrm{d}A. \tag{3.290}$$
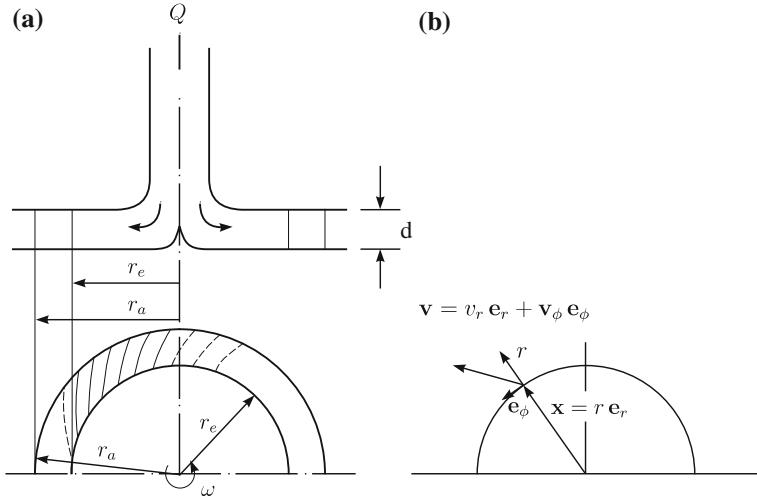
Fig. 3.67 Illustrating EULER's turbine equation. **a** *Cut through a turbine (schematic). The inflow is axially from above. The turning wheel has inner and outer radii r_e and r_a, respectively and rotates with angular speed ω.* **b** *Direction of the velocity vector v at the outer tips of the shovels and its division into radial and azimuthal components*

With reference to Fig. 3.67b the velocities in the entrance and the exit cross sections can be written as

$$v = v_r e_r + v_\varphi e_\varphi, \tag{3.291}$$

so that with

$$n_e = -e_r , \qquad n_a = e_r , \qquad x = r e_r. \tag{3.292}$$

The scalar product $v \cdot n$ and the vector product $x \times \rho v$ are given by

$$\begin{aligned} (v \cdot n)_e &= -v_r^e , & (v \cdot n)_a &= v_r^a , \\ (x \times \rho v)_e &= \rho v_\varphi^e r_e e_z, & (x \times \rho v)_a &= \rho v_\varphi^a r_a e_z. \end{aligned} \tag{3.293}$$

If we set in addition

$$2\pi d\, r_e v_r^e = 2\pi d\, r_a v_r^a = Q, \tag{3.294}$$

then (3.290) can be written as

$$M = \rho Q \,(r_a v_\varphi^a - r_e v_\varphi^e) e_z, \tag{3.295}$$

in which Q denotes the volume flow.

Equation (3.290) is called **Euler's turbine equation**. It holds both for turbines and pumps. For turbines, Eq. (3.295) defines the power of working M_ω, which is available for further use; for pumps this power of working must be brought by a motor, in order to transport the volume of flow Q. It is possible to judiciously select the orientations of the shovels such that v_φ^a differs from v_φ^e so as to optimize the efficiency.

References

1. Becker, E.: Technische Strömungslehre. Teubner, Stuttgart (1985)
2. Bresse, C.: Cours de Mécanique Appliquiée, 3rd edn, vol. 2. Hydraulique. Mallet-Bachelier, Paris (1879)
3. Carmody, T., Kobus, H.: Translation of *Hydrodynamica* (Daniel Bernoulli) and *Hydraulica* (Johann Bernoulli), 456 pp. Dover Publ. Inc., New York (1968)
4. Chadwick, P.: Continuum Mechanics: Concise Theory and Problems. Dover Publications Inc., Mineola, New York (2012)
5. Gersten, K.: Einführung in die Strömungsmechanik, 6. Vieweg, Aufl (1991)
6. Hager, W.H.: Hydraulicians in Europe, 1800–2000. IAHR Monograph (2003)
7. Hunt, B.W.: Numerical solution of an integral equation for flow from a circular orifice. J. Fluid Mech. **31** (1968)
8. Hutter, K., Joehnk, K.: Continuum Methods of Physical Modeling. Springer, Berlin, etc. (2004)
9. Kleinert, A.: Johann Andreas (von) Segner (1704–1777). Martin-Luther Universität, Halle-Wittenberg, FB Mathematik und Informatik, Reports on Didactics and History of Mathematics, vol. 19, pp. 15–20 (2002)
10. Kozeny, J.: Hydraulik. Ihre Grundlagen und praktische Anwendung. Springer, Wien (1953)
11. Kuhlmann, H.: Strömungsmechanik. Pearson (2007)
12. Kundu, P.K., Kohen, I.M., Dowling, D.R.: Fluid Mechanics, 5th edn. Elservier (2012)
13. McNown, J.S.: When time flowed—The Story of the Clepsydra. La Houille Blanche **5** (1976)
14. Mills, A.A.: Newton's water clocks and the fluid mechanics of clepsydrae. Notes and Records of the Royal Society of London, vol. 37, pp. 35–61 (1982–1983). Errata, vol. 38 (1983)
15. Panton, R.L.: Incompressible Flow. Wiley (1984)
16. Rickey, V.F.: The Clepsydra. http://fredrickey.info/hm/CalcNotes/clepsydra.pdf
17. Schade, H., Kunz, E.: Strömungslehre. de Gruyter, 3. Aufl. (2007)
18. Siegloch, W.: Technische Fluidmechanik. VDI (1996)
19. Spencer, A.J.M.: Continuum Mechanics. Courier Corporation, Mineola, New York (2004)
20. Spurk, J.H., Aksel, N.: Fluid Mechanics, 2nd edN. Springer, Berlin etc. (2008). [Also in German: Strömungslehre, Einführung in die Theorie der Strömungen, 3.Aufl. Springer, Berlin etc. (2007)]
21. Tritton, D.J.: Physical Fluid Mechanics. Clarendon Press (1988)
22. von Mises, R.: Elemente der Technischen Hydromechanik. Teil I. Teubner Verlag, Leipzig und Berlin (1914)
23. von Mises, R.: Berchnung von Ausfluß- und Überganszahlen. Zeitschrift Verein Deutscher Ingenieure, Band, vol. 61 (1917)
24. von Mises, R.: Mathematical Theory of Compressible Fluid Flow. Dover, Completed by H. Geiringer and G. S. S. Ludford (2004). ISBN: 13-978-0486439419 (1958)
25. White, F.M.: Fluid Mechanics, 7th edn. McGraw-Hill (2011)
26. Wilcox, D.C.: Basic Fluid Mechanics. DCW Industries (1998)
27. Zierep, J., Bühler, K.: Strömungsmechank. Springer, Berlin, etc. (1991)

Chapter 4
Conservation of Angular Momentum—Vorticity

Abstract This chapter is devoted to concepts that can be deduced from mathematical statements centered around angular momentum of a classical (spin-free) fluid continuum in three-dimensional EUCLIDian space. Circulation is defined as the integral along a closed simple three-dimensional curve of the scalar product of a smooth velocity field with a vectorial line increment. It leads directly into KELVIN's circulation theorem, which states that the circulation of an ideal barotropic fluid subject to conservative forces along a material curve is preserved. Its generalization in a non-inertial system to non-barotropic, viscous fluids shows how the growth rate of the circulation around a material curve is contributed among frame rotation, non-barotropicity and dissipative stress contributions. The definitions of 'vortex lines', 'vortex tubes' and 'vortex surfaces' then provide the occasion to prove among other things that vortex tubes in ideal fluids must either be closed within the interior of the domain of the fluid or else end at boundaries. The HELMHOLTZ vorticity theorem, derived from the momentum equation for an ideal, density preserving barotropic fluid by straightforward mathematical transformations states that the material time rate of change of the vorticity per unit mass in three-dimensional space is given by vortex stretching and vortex tilting. This result also holds for such a fluid in a non-inertial frame and leads naturally to the TAYLOR- PROUDMAN theorem that 'steady slow flow of a density preserving fluid takes place in a plane perpendicular to the axis of rotation'. Potential vorticity theorems, originally derived by ERTEL, are special conservation laws of fluid dynamics in rotating systems for a scalar quantity formed with the vorticity weighted by a flow related quantity. There are several forms of this conservation law, particularly relevant in metrology and oceanography.

Keywords Circulation · KELVIN's theorem · HELMHOLTZ' vorticity theorem · Potential vorticity theorem

List of Symbols

Roman Symbols

$\mathcal{A}, \mathcal{A}_\mathfrak{C}$	Area, area spanned by loop $\mathfrak{C}$
$\boldsymbol{B} = \boldsymbol{F}\boldsymbol{F}^T$	Left CAUCHY- GREEN deformation tensor
$\boldsymbol{C} = \boldsymbol{F}^T\boldsymbol{F}$	Right CAUCHY- GREEN deformation tensor
$\boldsymbol{D}$	Strain rate tensor, Stretching tensor: $\boldsymbol{D} = \text{sym grad } \boldsymbol{v}$
d	Differential increment
$\boldsymbol{F}$	Deformation gradient
$f = 2\Omega \sin\phi$	First CORIOLIS parameter
$f = 2\Omega \cos\phi$	Second CORIOLIS parameter
$\boldsymbol{f}$	Specific body force per unit mass
$\boldsymbol{g}$	Gravity vector
$\{\boldsymbol{i}, \boldsymbol{j}, \boldsymbol{k}\}$	Standard unit Cartesian basis in the (x, y, z) directions
I_A, II_A, III_A	Invariants of the second order tensor $\boldsymbol{A}$
$\boldsymbol{L}_\mathcal{O}$	Angular momentum of a body with respect to point $\mathcal{O}$
$\boldsymbol{L} = \text{grad } \boldsymbol{v}$	Velocity gradient tensor (rank 2)
$\boldsymbol{\ell}$	Specific body couple
$\boldsymbol{m}$	Couple stress tensor (rank 3)
$\boldsymbol{n}$	Unit normal vector on a body surface
$O, \mathcal{O}$	Origin of coordinates
p	Pressure
P	Pressure function: $\mathrm{d}P = \mathrm{d}p/\rho$
$\boldsymbol{R}$	Rotation tensor: $\boldsymbol{R} = \boldsymbol{F}\boldsymbol{U}^{-1} = \boldsymbol{V}^{-1}\boldsymbol{F}$
r	Radial coordinate
s	Specific spin
$\boldsymbol{T}_v$	Viscous CAUCHY stress tensor
$\boldsymbol{t}_{(\boldsymbol{n})}$	CAUCHY stress traction at the surface with unit normal vector $\boldsymbol{n}$
U	Body force potential ($\boldsymbol{f} = -\text{grad } U$)
$\boldsymbol{U} = \sqrt{\boldsymbol{C}}$	Right stretch tensor
V	Volume of a material body
∂V	Surface area of V
$\boldsymbol{V} = \sqrt{\boldsymbol{B}}$	Left stretch tensor
$\boldsymbol{v}$	Velocity vector
$\boldsymbol{v}_{\text{abs}}$	Absolute velocity
$\boldsymbol{v}_{\text{rel}}$	Relative velocity
v_r, v_ϕ	Radial, azimuthal velocity components in polar coordinates
$\boldsymbol{w} = \text{curl } \boldsymbol{v}$	Vorticity vector
$\boldsymbol{W}$	Vorticity tensor: $\boldsymbol{W} = \text{skw grad } \boldsymbol{v}$
$\boldsymbol{x}, \boldsymbol{y}$	Position vectors in the present configuration
$\boldsymbol{X}, \boldsymbol{Y}$	Position vectors in the reference configuration

Greek Symbols

Γ	Circulation around a closed double point free circuit $\mathfrak{C}$
$\dot{\gamma}$	Shear rate

$\zeta = (\text{curl } \boldsymbol{v})_z$ z-component of the vorticity field curl $\boldsymbol{v}$

$\boldsymbol{\Theta}$ Rank-2 symmetric tensor of inertia

π_λ Potential vorticity associated with λ

$\langle \pi \rangle_{\text{bt}}$ Barotropic potential vorticity

$\langle \pi \rangle_{\text{bt}}^{\text{rigid}}$ Barotropic potential vorticity in the rigid lid approximation

π_{bc} Baroclinic potential vorticity

ρ Mass density

ϕ Geographical latitude

ψ Differential vector field

$\Omega, \boldsymbol{\Omega}$ Algebraic, vectorial velocity of the Earth

$\boldsymbol{\omega}$ Angular velocity, vorticity per unit mass $\boldsymbol{\omega} = \boldsymbol{w}/\rho$

In Chap. 3, Sect. 3.9, formula (3.272) the balance law of angular momentum was stated in global form as follows:

$$\dot{\boldsymbol{L}}_{\mathcal{O}} \equiv \frac{\mathrm{d}}{\mathrm{d}t} \int_V \underbrace{\boldsymbol{x} \times \rho \boldsymbol{v}}_{(1)} \, \mathrm{d}V = \int_{\partial V} \underbrace{\boldsymbol{x} \times \boldsymbol{t}_{(\boldsymbol{n})}}_{(2)} \, \mathrm{d}A + \int_V \underbrace{\boldsymbol{x} \times \rho \boldsymbol{f}}_{(3)} \, \mathrm{d}V \equiv \boldsymbol{M}_{\mathcal{O}}. \quad (4.1)$$

In this formula the underbraced terms are

(1) the moment of the momentum of a unit volume element $\mathrm{d}V$ at position $\boldsymbol{x}$ with respect to the origin of the coordinates;
(2) the moment of the surface traction on a surface increment with respect to the origin of the coordinates;
(3) the moment of the specific body force at position $\boldsymbol{x}$ with respect to the origin of the coordinates.

In all three cases the angular momentum quantity is the moment of the corresponding momentum quantity, and so, the conservation law of *angular momentum* is, strictly in this case the conservation law of *moment of momentum*.[1] Using the CAUCHY stress representation (3.274) $\boldsymbol{t}_{(\boldsymbol{n})} = \boldsymbol{t}\boldsymbol{n}$ and applying (4.1) to a tetrahedral infinitesimal element, it was then shown that the CAUCHY stress tensor is symmetric. Conversely, the balance law of angular momentum is easily shown to be satisfied as an identity in this case. This well-known result is taken as motivation for the attitude to ignore consideration of angular momentum balance by simply requesting the CAUCHY stress

---

[1]If angular momentum is more than just moment of momentum, then the respective terms are

$$(1) = \boldsymbol{x} \times \rho \boldsymbol{v} + \rho \boldsymbol{s}, \qquad \boldsymbol{s} = \boldsymbol{\Theta}\boldsymbol{\omega},$$
$$(2) = \boldsymbol{x} \times \boldsymbol{t}_{(\boldsymbol{n})} + \boldsymbol{m}_{(\boldsymbol{n})}, \qquad \boldsymbol{m}_{(\boldsymbol{n})} = \boldsymbol{m}\,\boldsymbol{n},$$
$$(3) = \boldsymbol{x} \times \rho \boldsymbol{f} + \rho \boldsymbol{\ell}.$$

Here, $\boldsymbol{s}$ is called the specific spin, which is linearly related to the angular velocity $\boldsymbol{\omega}$ with the symmetric tensor of inertia $\boldsymbol{\Theta}$; $\boldsymbol{m}$ is the couple stress tensor, a skew-symmetric tensor of rank-3 and $\boldsymbol{\ell}$ is the specific body couple. A continuum theory, of which some of these variables are not zero, is called a **polar theory** and the materials are called **Cosserat materials**, according to the COSSERAT brothers, who presented such complex materials in 1909 [2]. Special versions of such materials are called **micropolar** and **micromorphic** materials, respectively.

tensor to be symmetric. Such a procedure is justified if all balance equations are pointwise satisfied. However, since physically linear momentum is associated with the *translational* motion and angular momentum with the rotary motion, the rotational behavior of a body can often better be identified, if the law of balance of angular momentum is explicitly employed.

In Chap. 3, Sect. 3.10, the global form of the balance law of angular momentum was applied to SEGNER's water wheel and to EULER's turbine equation. These are two standard examples of engineering science, where direct application of the balance law of angular momentum has led to significant practical applications. Fluid processes in the atmosphere, ocean and lakes, and in more sophisticated engineering problems than those above, exhibit rotary motions of all scales, from large gyres down to smallest swirls and eddies.

Fluid mechanics possesses a number of intricate propositions related to the idea of conservation of rotary motion to the water itself, but equally also to 'water structures', like gyres, water currents and large streams. In this chapter, our intention is to analyze the phenomenon 'rotation', 'circulation', 'vorticity' by a somewhat deeper approach and to use these general features for a deeper physical understanding of basic fluid motion (**Fig. 4.1**).

Fig. 4.1 Various vortical motions visible due to phytoplankton bloom in the Baltic Sea on 02.08.1999 (satellite image from http:// visibleearth.nasa.gov/)

4.1 Circulation

Our focus will be mostly ideal (inviscid) fluids, but not exclusively. We begin with

Definition 4.1 Let $\mathfrak{C}$ be a closed, smooth, simple, i.e., double-point free material line in $\mathbb{R}^3$. The circulation of a flow field along $\mathfrak{C}$ is then defined as the line integral

$$\Gamma := \oint_{\mathfrak{C}} \boldsymbol{v}(\boldsymbol{x}, t) \cdot \mathrm{d}\boldsymbol{x}, \tag{4.2}$$

where $\boldsymbol{v}(\boldsymbol{x}, t)$ is the velocity field, defined in a region encompassing $\mathfrak{C}$, $\mathrm{d}\boldsymbol{x}$ is the line increment tangential to the line, and the time is held fixed. Its dimension is $[\mathrm{m}^2\mathrm{s}^{-1}]$. ∎

We emphasize that the closed curve $\mathfrak{C}$ may be three-dimensional. A direct implication of this definition is obtained, if the material time derivative of the circulation is evaluated. Indeed,
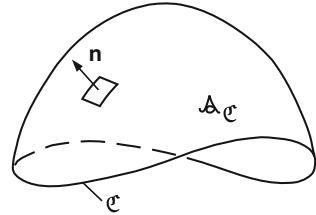
$$
\begin{aligned}
\dot{\Gamma} &= \frac{\mathrm{d}}{\mathrm{d}t} \oint_{\mathfrak{C}} \boldsymbol{v} \cdot \mathrm{d}\boldsymbol{x} = \oint_{\mathfrak{C}} (\dot{\boldsymbol{v}} \cdot \mathrm{d}\boldsymbol{x} + \boldsymbol{v} \cdot (\mathrm{d}\boldsymbol{x})^{\cdot}) \\
&= \oint_{\mathfrak{C}} (\dot{\boldsymbol{v}} \cdot \mathrm{d}\boldsymbol{x} + \boldsymbol{v} \cdot (\boldsymbol{L}\mathrm{d}\boldsymbol{x})) = \oint_{\mathfrak{C}} (\dot{\boldsymbol{v}} + \boldsymbol{L}^T \boldsymbol{v}) \cdot \mathrm{d}\boldsymbol{x} \\
&= \oint_{\mathfrak{C}} \left(\dot{\boldsymbol{v}} + \operatorname{grad}\left(\frac{v^2}{2}\right) \right) \cdot \mathrm{d}\boldsymbol{x}.
\end{aligned} \tag{4.3}
$$

In this chain of transformations we have used the fact that $\boldsymbol{L} = \operatorname{grad} \boldsymbol{v}$ and $\boldsymbol{L}^T \boldsymbol{v} = \operatorname{grad}(v^2/2)$, $v^2 = \boldsymbol{v} \cdot \boldsymbol{v}$. In the next step of transformation we recall STOKES' integral theorem; according to it, one has (see Appendix 5.B to Chap. 5)

$$\oint_{\mathfrak{C}} \boldsymbol{\psi} \cdot \mathrm{d}\boldsymbol{x} = \iint_{\mathcal{A}_{\mathfrak{C}}} \operatorname{curl} \boldsymbol{\psi} \cdot \mathrm{d}\boldsymbol{A}, \tag{4.4}$$

in which $\boldsymbol{\psi}$ is any differentiable vector field in three dimensions and $\mathcal{A}_{\mathfrak{C}}$ is any smooth surface spanned by the closed curve $\mathfrak{C}$, see **Fig. 4.2** with vectorial surface element $\mathrm{d}\boldsymbol{A} = \boldsymbol{n}\mathrm{d}a$. If we apply STOKES' theorem to the vector field $\boldsymbol{\psi} = \operatorname{grad}(v^2/2)$, we obtain

Fig. 4.2 Simple closed curve $\mathfrak{C}$, spanning an area $\mathcal{A}_\mathfrak{C}$ *Note, there are an infinity of smooth surfaces spanned by $\mathfrak{C}$ in $\mathbb{R}^3$*

$$\oint_\mathfrak{C} \operatorname{grad}\left(\frac{v^2}{2}\right) \cdot \mathrm{d}x = \iint_{\mathcal{A}_\mathfrak{C}} \underbrace{\operatorname{curl} \operatorname{grad}\left(\frac{v^2}{2}\right)}_{\mathbf{0}} \cdot \mathrm{d}A = 0. \tag{4.5}$$

This vanishes, because the curl of any gradient field is identically zero. Applying (4.5) to (4.3), we obtain
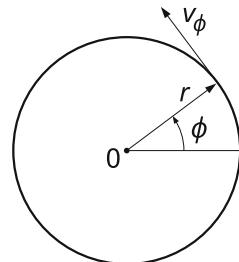
$$\dot{\Gamma} = \oint_\mathfrak{C} \dot{v} \cdot \mathrm{d}x. \tag{4.6}$$

This result holds for any differentiable vector field $v(x, t)$, not just the velocity field, along any closed simple smooth material curve $\mathfrak{C}$ that can be shrunk to zero without leaving the region where $\dot{v}$ is continuously differentiable. The material does not need to be an ideal fluid, not even a fluid. The result is formally interesting, because the total time derivative 'outside' the integral simply carries over to the integrand function in (4.6).

As an example consider a potential vortex, **Fig. 4.3**, for which the water particles move in concentric circles around a center O with radial and azimuthal velocities

$$v_r = 0, \qquad v_\phi = \frac{c}{r}, \tag{4.7}$$

Fig. 4.3 Azimuthal velocity v_ϕ in circles around a center with velocity strength given by (4.7)

respectively, where c is a constant. Then,

$$\Gamma = \int_0^{2\pi} \frac{c}{r} r \mathrm{d}\phi = 2\pi c \quad \rightarrow \quad c = \frac{\Gamma}{2\pi}.$$ (4.8)

Note that the value of Γ is independent of the radius of the circle, which is selected to evaluate Γ. So, the circulation is here defined by (4.7). Note as well that the curl of the velocity field (4.7) vanishes in the entire current field except the origin.

Let us now specialize (4.6) for an EULER fluid, i.e. an inviscid fluid of which the momentum equation takes the form

$$\dot{\boldsymbol{v}} = -\frac{1}{\rho}\mathrm{grad}\ p + \boldsymbol{f}.$$ (4.9)

If we substitute this into (4.6), then we have

$$\dot{\Gamma} = -\oint_{\mathfrak{C}} \frac{1}{\rho} \underbrace{\mathrm{grad}\ p \cdot \mathrm{d}\boldsymbol{x}}_{\mathrm{d}p} + \oint_{\mathfrak{C}} \boldsymbol{f} \cdot \mathrm{d}\boldsymbol{x}.$$ (4.10)

In the first integrand we have indicated that $\mathrm{grad}\ p \cdot \mathrm{d}\boldsymbol{x} = \mathrm{d}\ p$ is simply the incremental change of p along $\mathfrak{C}$. In a *barotropic* ideal fluid p is a unique function of the density $p = p(\rho)$; thus $\mathrm{d}p/\rho$ can be viewed as the differential $\mathrm{d}P$ of a new function $P(\rho)$, the so-called *pressure function*; so,

$$\oint_{\mathfrak{C}} \frac{\mathrm{grad}\ p \cdot \mathrm{d}\boldsymbol{x}}{\rho} = \oint_{\mathfrak{C}} \frac{\mathrm{d}p}{\rho} = \oint_{\mathfrak{C}} \mathrm{d}P = 0,$$ (4.11)

of which the integral vanishes, because $\mathfrak{C}$ is closed, so that the initial and end points of the integration are the same. Moreover, if we also assume that the body force possesses a unique *potential*, i.e., $\boldsymbol{f} = -\mathrm{grad}\ U$, then with the same arguments we have

$$\oint_{\mathfrak{C}} \boldsymbol{f} \cdot \mathrm{d}\boldsymbol{x} = -\oint_{\mathfrak{C}} \mathrm{grad}\ U \cdot \mathrm{d}\boldsymbol{x} = -\oint_{\mathfrak{C}} \mathrm{d}U = 0.$$ (4.12)

With (4.11) and (4.12) the right-hand side of (4.10) vanishes. This result is summarised as

Theorem 4.1 (Kelvin's circulation theorem, after Lord KELVIN, 1824–1907)
In any flow-field of an ideal, barotropic fluid with conservative body forces, the circulation, calculated for any material, closed, smooth curve $\mathfrak{C}$ is temporally constant, symbolically,

$$\frac{d\Gamma}{dt} = \frac{d}{dt} \oint_{\mathfrak{c}} \mathbf{v} \cdot d\boldsymbol{x} = \oint_{\mathfrak{c}} \dot{\boldsymbol{v}} \cdot d\boldsymbol{x} = 0 \iff \begin{Bmatrix} \textit{ideal, barotropic fluid} \\ \textit{with conservative} \\ \textit{body forces} \end{Bmatrix} \quad (4.13)$$

∎

This theorem and its derivation allow us to state a number of intricate corollaries. To formulate these, we need the following definition:

Definition 4.2 A differentiable vector field ψ in a region of $\mathbb{R}^n$, $n \leqslant 3$, is called **irrotational** or **vortex-free**, if throughout this region

$$\text{curl } \psi = \nabla \times \psi = 0. \tag{4.14}$$

If the vector field ψ is the fluid velocity, then $\boldsymbol{w} = \text{curl } \boldsymbol{v}$ is called the **vorticity** of the flow field.   ∎

With this definition, the corollaries of KELVIN's theorem now read as follows:

(1) Consider an irrotational acceleration field, curl $\dot{\boldsymbol{v}} = \mathbf{0}$, in an ideal, barotropic fluid subject to a conservative body force. Then according to (4.11), (4.12), the conditions of KELVIN's circulation theorem are satisfied. Therefore, Γ is constant along material lines, but may vary from trajectory to trajectory.

(2) In a barotropic ideal fluid subject to a conservative body force the circulation is a conserved quantity, $\dot{\Gamma} = 0$. Hence according to the above item, $\dot{\Gamma} = 0$ implies curl $\dot{\boldsymbol{v}} = \mathbf{0}$. So, if curl $\boldsymbol{v} = \mathbf{0}$ in the entire flow-field at the initial time, then curl $\boldsymbol{v} = \mathbf{0}$ at any later time. In words: *An irrotational flow field in a barotropic ideal fluid at an initial time remains irrotational for all time* as long as the velocity field remains differentiable, i.e., no discontinuities are formed.
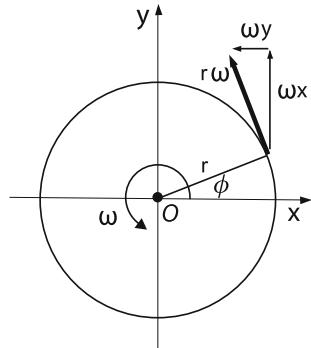
We may interpret vorticity as the *tendency to form vortices*. In atmospheric and oceanographic applications the dominant large scale flows are the water currents generated by wind, waves, density gradients, i.e., triggering mechanisms which, typically, generate horizontal water motions. The dominant component of the vorticity vector is then

$$\zeta := (\text{curl } \boldsymbol{v})_z = \hat{\boldsymbol{k}} \cdot \text{curl } \boldsymbol{v} = \frac{\partial v}{\partial x} - \frac{\partial u}{\partial y}, \tag{4.15}$$

where $\hat{\boldsymbol{k}}$ is the unit vector in the z-direction. This is also the vorticity in plane, two-dimensional flow. (u, v) are the horizontal velocity components of the velocity field $\boldsymbol{v}$; ζ is counted positive for counter-clockwise rotation when viewed from above. This is the same sense as the Earth's rotation in the northern hemisphere. The assumption that the flow is basically two-dimensional remains generally true, if the water flow in a lake or ocean or the air flow in the atmosphere extends over distances greater than a few kilometers.

For a rigid rotation around the origin O of the Oxy coordinate system, the velocity vector is tangential to circles, with linear speed $v_\phi = r\omega$ (positive for counter-clockwise rotation), where ω is the angular velocity of this rigid-body motion around

Fig. 4.4 Rigid rotation about the center O with angular velocity ω, the Cartesian components being given by
$u = -v_\phi \sin \phi = -\omega\, y$,
$v = v_\phi \cos \phi = \omega\, x$

the origin O. With reference to **Fig. 4.4** the velocity components are easily seen to be $(u, v) = \omega(-y, x)$, so that $\zeta = 2\,\omega$, according to (4.15). The angular momentum of a parcel with density ρ at a distance r from O with respect to O is in this case given by $\rho r^2 \omega$. Note also that the circulation around the origin of a circular path with radius r is given by $\Gamma = \Gamma(r) = 2\pi\omega r^2$ and depends on the radius of the circle. It is *not* a property of the vortex as a whole.

A direct application of this last example is the *planetary vorticity*, experienced by every body on Earth. Everything on Earth rotates with the Earth. The *absolute velocity*, i.e., the velocity of an object on Earth measured from an inertial frame, not participating in the rotation of the Earth, is composed of the *relative velocity* (measured by an observer on Earth) and the *planetary velocity*, which is a rotation around the NS-axis with angular velocity $\boldsymbol{\Omega}$. This planetary velocity for any particle on the Earth's surface is a rigid rotation with $v_\phi = (r \cos \phi)\Omega$ and vorticity vector $\boldsymbol{\omega}_{\text{plane}} = 2\,\Omega\,\hat{\boldsymbol{k}}$, with $\hat{\boldsymbol{k}}$ in the direction of the rotation axis. At the geographical latitude ϕ, this vector has a component tangential to the Earth surface, pointing towards north, $\tilde{f}$, and a component pointing towards the zenith, f, viz.,

$$\boldsymbol{\omega}_{\text{plane}} = \tilde{f}\hat{\boldsymbol{e}}_y + f\hat{\boldsymbol{e}}_z,$$
$$\tilde{f} := 2\Omega \cos \phi, \quad f := 2\Omega \sin \phi, \tag{4.16}$$

in which $\hat{\boldsymbol{e}}_y$ and $\hat{\boldsymbol{e}}_z$ are unit vectors tangential to the meridian and pointing towards North and directed towards the zenith, respectively. Moreover, f and $\tilde{f}$ are called the first and second CORIOLIS parameters.

Absolute vorticity is the sum of the relative and planetary vorticity,

$$\text{curl } \boldsymbol{v}_{\text{abs}} = \text{curl } \boldsymbol{v}_{\text{rel}} + 2\boldsymbol{\Omega}$$
$$= \left(\frac{\partial w}{\partial y} - \frac{\partial v}{\partial z}\right) \hat{\boldsymbol{e}}_x + \left(\frac{\partial u}{\partial z} - \frac{\partial w}{\partial x} + \tilde{f}\right) \hat{\boldsymbol{e}}_y + \left(\frac{\partial v}{\partial x} - \frac{\partial u}{\partial y} + f\right) \hat{\boldsymbol{e}}_z, \tag{4.17}$$
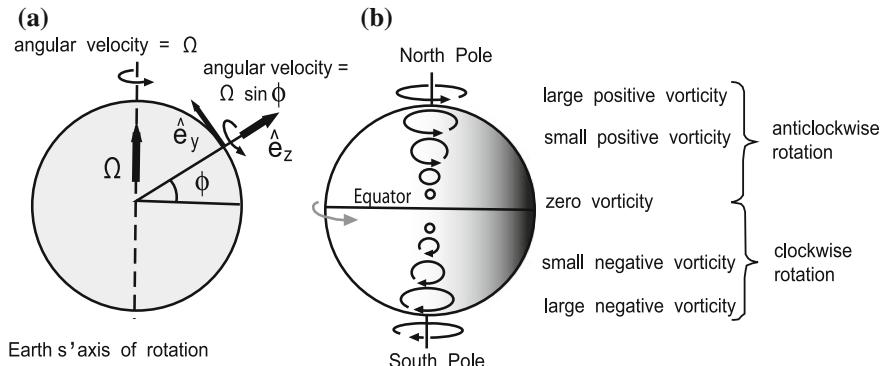
Fig. 4.5 a Diagram showing the derivation of the expression of the planetary vorticity of a fluid parcel on the surface of the Earth at latitude ϕ. **b** Schematic diagram illustrating the variations of the $\hat{e}_z$-component of the planetary vorticity with latitude; the circular arrows represent the value of f in the direction $\hat{e}_z$ (viewed from above) at different latitudes, redrawn from [1]

in which the expression on the second line is written in the basis $\{\hat{e}_x, \hat{e}_y, \hat{e}_z\}$ (see **Fig. 4.5**). For plane motion, or conditions for which the shallow water approximation is justified, the above relation reduces to

$$\zeta_{\text{abs}} = \zeta_{\text{rel}} + f, \qquad \zeta_{\text{rel}} = \frac{\partial v}{\partial x} - \frac{\partial u}{\partial y}. \tag{4.18}$$

Relative vorticity ζ_{rel}, is usually much smaller than f, and it is greatest at the edges of fast currents.

Most of the above statements concern inviscid, barotropic fluids. An important question is, however, how the circulation changes with time, when the fluid is non-barotropic and viscous. In this case the expression (4.6) is still valid, but the acceleration via the balance of linear momentum and written in a non-inertial frame now takes the form[2]

$$\dot{v} = -\frac{1}{\rho}\,\text{grad}\,p + \frac{1}{\rho}\,\text{div}\,\boldsymbol{T}_v + \boldsymbol{f} - 2\boldsymbol{\Omega} \times \boldsymbol{v}, \tag{4.19}$$

where $\boldsymbol{T}_v$ is the dissipative viscous stress. Thus, (4.6) may be written as

$$\dot{\Gamma} = -\int_{\mathfrak{C}} \frac{1}{\rho}\text{grad}\,p \cdot d\boldsymbol{x} + \int_{\mathfrak{C}} \frac{1}{\rho}\,(\text{div}\,\boldsymbol{T}_v)\cdot d\boldsymbol{x} + \underbrace{\int_{\mathfrak{C}} \boldsymbol{f}\cdot d\boldsymbol{x}}_{\overset{(4.12)}{=}0} - \int_{\mathfrak{C}} 2(\boldsymbol{\Omega} \times \boldsymbol{v})\cdot d\boldsymbol{x} \tag{4.20}$$

---

[2]Strictly, the contribution $\boldsymbol{\Omega} \times (\boldsymbol{\Omega} \times \boldsymbol{x})$ should be included on the right-hand side of (4.19). Instead, we regard the pressure to be reduced by $P_\Omega = -\frac{1}{2}\Omega^2\,\boldsymbol{r}_\perp^2 \cdot \boldsymbol{r}_\perp^2$, where $\boldsymbol{r}_\perp = \boldsymbol{r} - (\boldsymbol{r}\cdot\hat{\boldsymbol{k}})\boldsymbol{r}$.

for a conservative body force. The pressure term in (4.20) can be transformed using STOKES' theorem (4.4) as follows:

$$\int_{\mathfrak{C}} \frac{\text{grad } p}{\rho} \cdot d\boldsymbol{x} = \int_{\mathcal{A}_{\mathfrak{C}}} \text{curl} \left(\frac{\text{grad } p}{\rho} \right) \cdot d\boldsymbol{a} = -\int_{\mathcal{A}_{\mathfrak{C}}} \frac{\text{grad } \rho \times \text{grad } p}{\rho^2} \cdot d\boldsymbol{a}. \quad (4.21)$$

Therefore,

$$\dot{\Gamma} = -\int_{\mathfrak{C}} 2\boldsymbol{\Omega} \times \boldsymbol{v} \cdot d\boldsymbol{x} + \int_{\mathcal{A}_{\mathfrak{C}}} \frac{\text{grad } \rho \times \text{grad } p}{\rho^2} \cdot d\boldsymbol{a} + \int_{\mathfrak{C}} \frac{1}{\rho} (\text{div } \boldsymbol{T}_v) \cdot d\boldsymbol{x}. \quad (4.22)$$

Evidently, there are three mechanisms which are responsible for the time rate of change of the relative circulation, (1) the circulation due to the CORIOLIS force per unit mass, (2) that due to the pressure per unit mass and (3) the circulation due to the viscous stresses per unit mass. The first term vanishes, if the frame of reference is inertial ($\boldsymbol{\Omega} = \boldsymbol{0}$), the second term is zero if $\rho = \rho(p)$ since then grad ρ is parallel to grad p and the third term vanishes in an inviscid fluid.

4.2 Simple Vorticity Theorems

The ensuing analysis is facilitated, if we first define simple concepts connected with vorticity. The concepts are analogous to those when flow tubes and flow filaments are introduced.

Definition 4.3 A vortex line is an integral curve of the orientation field of the vorticity vector field $\boldsymbol{w} = \text{curl } \boldsymbol{v}$, i.e., it is the solution of the ordinary differential equation

$$\left. \begin{array}{l} \dfrac{d\boldsymbol{x}}{d\sigma} = \boldsymbol{w}(\boldsymbol{x}, t), \\ \sigma = 0, \quad \boldsymbol{x} = \boldsymbol{x}_0, \end{array} \right\} \quad (4.23)$$

where σ parameterizes the vortex line through the point $\boldsymbol{x} = \boldsymbol{x}_0$, and the time t is held fixed. ∎

This definition allows us to form additional concepts. To this end, let $\mathfrak{C}$ be a simple double-point free, closed material curve $\mathfrak{C}$ in a flow field with non-vanishing circulation ($\Gamma \neq 0$). Consider now all those vortex lines which have their origin $\boldsymbol{x}_0$ on the (closed) curve $\mathfrak{C}$. The area spanned by $\mathfrak{C}$ is called the cross section of the tube. We are led then to the

(a)   **(b)**   **(c)**
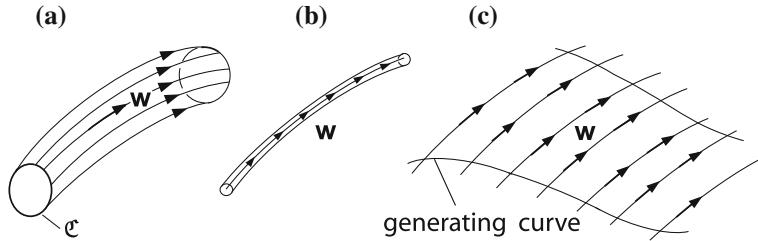
Fig. 4.6 a A simple closed double-point free curve having with each vortex line one point in common defines a **vortex tube**. **b** A vortex tube with infinitesional cross section is called a **vortex filament**. **c** All vortex lines having one point in common with a generating curve form a **vortex surface**, or a **vortex sheet**

Definition 4.4 (*see* **Fig. 4.6**)

(1) All vortex lines through a closed double point free curve $\mathfrak{C}$ form a **vortex tube**.
(2) A vortex tube with infinitesimal cross section is called a **vortex filament**.
(3) All vortex lines having one point common with a generating (open or closed) curve form a **vortex surface**.   ∎

Let us now prove a number of simple lemmas. All these lemmas concern configurations on the mantle surface of vortex tubes. We summarize them in the following.

Theorem 4.2

 (i)   *The circulation of a flow field evaluated for a simply connected closed curve $\mathfrak{C}_1$ that lies on the mantle surface of a vortex tube is zero, see* **Fig. 4.7**a.
 (ii) *For every closed curve that lies completely on the mantle surface of a vortex tube and encircles it, the circulation has the same value, i.e., the vortex tube is characterized by the value of its circulation, Fig. 4.7b.*
(iii) *Vortex tubes in ideal barotropic fluids cannot end in the interior of a fluid. They must therefore be closed, i.e., torus-like, or they must end at boundaries of flow fields.*
(iv) *Vortex tubes in an ideal barotropic fluid are material tubes.*   ∎

Proof: For statement (*i*), we evaluate the circulation around any closed double-point free curve $\mathfrak{C}_i$, that lies on the mantle surface of a vortex tube and can be shrunk to a single point on this surface, as follows, see Fig. 4.7a,

$$\Gamma_{\mathfrak{C}_1} = \oint_{\mathfrak{C}_1} \boldsymbol{v} \cdot \mathrm{d}\boldsymbol{x} = \iint_{\mathcal{A}} \underbrace{\boldsymbol{w} \cdot \boldsymbol{n}}_{0}\, \mathrm{d}a = 0. \tag{4.24}$$
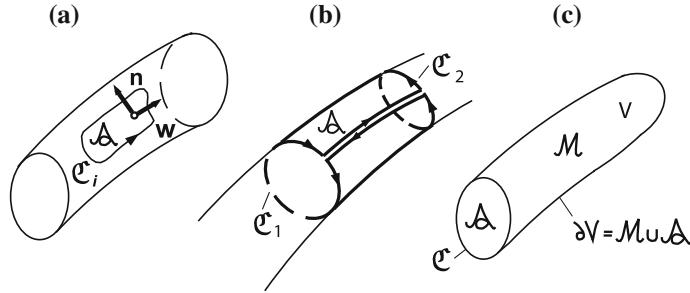
Fig. 4.7 **a** Circulation loop $\mathfrak{C}_1$ completely situated on the mantle surface of a vortex tube, enclosing a simply connected region. **b** Two circulation loops encircling a vortex tube, complemented by a 'cut' along a boundary vortex line. The cut path is a circulation loop on the mantle surface of the vortex tube encircling a simply connected region; this explains that $\Gamma_{\mathfrak{C}_1} = \Gamma_{\mathfrak{C}_2}$. **c** A vortex tube assumed to end within the fluid. It has volume V and surface $\partial V = \mathcal{M} \cup \mathcal{A}$ where $\mathcal{M}$ is the mantle surface and $\mathcal{A}$ the tube cross section spanned by the loop $\mathfrak{C}$

In this chain of equalities we have employed the STOKES theorem and then have used the fact that, on the mantle surface of a vortex tube, $\boldsymbol{w} = \operatorname{curl} \boldsymbol{v}$ and $\boldsymbol{n}$ are perpendicular to one another.

To prove statement (ii), consider Fig. 4.7b showing two closed curves, $\mathfrak{C}_1$ and $\mathfrak{C}_2$ enclosing the same vortex tube. If these curves are, in imagination, connected with two neighboring vortex lines, then a closed line, completely on the mantle surface of the vortex tube, is formed, of which the circulation as indicated in the graph must vanish owing to statement (i). Since the path along the two neighboring vortex lines is traversed in opposite directions, these contributions cancel out so that

$$\Gamma_{\mathfrak{C}_1} - \Gamma_{\mathfrak{C}_2} = 0 \quad \Rightarrow \quad \Gamma_{\mathfrak{C}_1} = \Gamma_{\mathfrak{C}_2}. \tag{4.25}$$

Since the choice of $\mathfrak{C}_1$ and $\mathfrak{C}_2$ is arbitrary, it follows that a vortex tube is characterized by the value of its circulation.

To prove item (iii) of the theorem, let us assume that the tube ends as shown in Fig. 4.7c. Then, the portion of the vortex tube from a selected cross section to its end has finite volume V, and one may consider the divergence of the vorticity field, $\operatorname{div} \boldsymbol{w} = \operatorname{div} \operatorname{curl} \boldsymbol{v} = 0$, which vanishes identically for any differentiable field $\boldsymbol{v}$. Then, we may deduce the following chain of identities

$$0 = \int_V \operatorname{div} \boldsymbol{w} \, dV \overset{(1)}{=} \int_{\partial V = \mathcal{M} \cup \mathcal{A}} \boldsymbol{w} \cdot \boldsymbol{n} \, dA \overset{(2)}{=} \int_{\mathcal{A}} \boldsymbol{w} \cdot \boldsymbol{n} \, dA \overset{(3)}{=} \oint_{\mathfrak{C}} \boldsymbol{v} \cdot d\boldsymbol{x} = \Gamma_{\mathfrak{C}}. \tag{4.26}$$

Here, $\mathcal{M}$ is the mantle surface and $\mathcal{A}$ the cross section as shown in Fig. 4.7c. The volume integral of $\operatorname{div} \boldsymbol{w}$ vanishes, since the integrand function vanishes. Step '$\overset{(1)}{=}$' follows as a consequence of the divergence theorem. The integral over the mantle surface,

$$\int_{\mathcal{M}} \boldsymbol{w} \cdot \boldsymbol{n} \, \mathrm{d}A = 0,$$

vanishes since $\boldsymbol{w}$ and $\boldsymbol{n}$ are perpendicular to one another on the mantle surface of a vortex tube. This explains step '$\stackrel{(2)}{=}$'. At '$\stackrel{(3)}{=}$' STOKES' theorem is used for the cross sectional area spanned by $\mathfrak{C}$. However, this integral is not allowed to vanish, since it is the circulation of the vortex tube.

It follows, the assumption that the vortex tube ends within a barotropic ideal fluid is faulty. Vortex tubes are either closed, torus-like objects as best manifested in smoke rings, see **Fig. 4.8**, or they end at boundary walls.

Panel (a) in Fig. 4.8 is a photograph of a rapid exit flow of water into a horizontal pipe from a large tank with free surface taken in the Laboratory of Hydraulics, Hydrology and Glaciology at ETH, Zurich. At $t = 0$ valves in the BORDA-type exit pipe and at the left end of the tank (not seen in the picture) are opened such that after a transient period steady conditions are established with constant level of the free surface. Vorticity is generally concentrating via a single or several vortex tubes, which sometimes are connecting the free and basal surfaces, but more often the free surface and the far end in the pipe; this latter situation is displayed in panel (a). In both cases the vortex tubes begin and end at boundaries. *Waterspouts, landspouts* or at large scales *tornados* are violently rotating columns of air that are in contact with both, the surface of the Earth and a cumulonimbus cloud, or, in rare cases the base of a cumulus cloud, panel (b). Because the velocity field in such a storm is primarily horizontal, its vorticity is basically vertical. Most tornados have wind speeds less than $175 \, \mathrm{km \, h^{-1}}$, tube widths of $75 \, \mathrm{m}$, and they travel several kilometers before dissipating. However, much larger tornados have occasionally also been observed. From outer space their cloud structure (photographed from a satellite) looks like a gigantic vortex, much like that shown in panel (c), which shows the flow state of a turbine intake in a water reservoir. Common, every-day examples are exit-flow vortices in bathtubs. What one sees from the outside is reminiscent of the picture in panel (c), but structurally it is analogous to the situation in panel (a). Panel (d) shows a vortex ring, which experienced smokers can easily generate. Classroom demonstrations use a wooden box with one circular hole at one side wall. The box is initially filled with smoky air. Hitting the vertical wall opposite to the wall with the hole will induce a shock at the edge of the hole which creates the vortex ring which is leaving the box.

To prove statement (iv) that vortex tubes are material tubes, we consider a circulation loop on the mantle of a vortex tube as shown Fig. 4.7a. For this loop, $\Gamma_{\mathfrak{C}_i} = 0$. Since in a barotropic ideal fluid KELVIN's theorem also holds, we also have $\dot{\Gamma}_{\mathfrak{C}_i} = 0$. These two facts together prove the statement. They say that the value of $\Gamma_{\mathfrak{C}_i}$ is carried with the material as the time proceeds, expressing exactly the fact that vortex tubes are material tubes, if the fluid is barotropic and ideal.   ∎
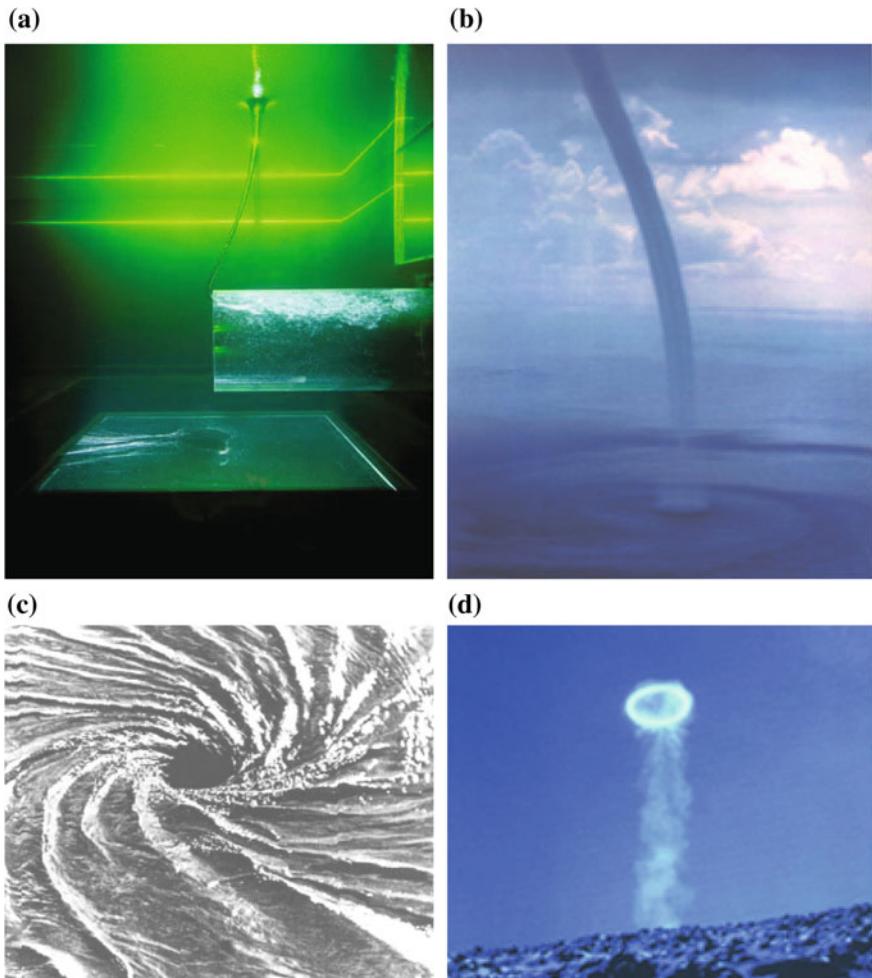
Fig. 4.8 Photographs of four well known vortex phenomena. **a** *Vortex connecting the free surface and the far end of a* BORDA-*type mouth in a hydraulic laboratory experiment with large steady through flow,* ©*Dr.* G. MÖLLER, *reproduced with permission (for detail see main text)* [12]; **b** *waterspout, or tornado over water (from* http://www.srh.noaa.gov/); **c** *Vortex at a turbine intake at Arapuni in New Zealand (from E.N. da C. Audrade. New Scientist (1963)); **d** in October 1969 an explosion of gas created this vortex ring on the snow-capped volcano Mount Actna in Sicily (copyright by Haroun Tazieff) (such rings are often created with cigarette smokes)*

One additional implication is that all differentiable flows of ideal and barotropic fluids [these are the conditions that KELVIN's theorem holds] which start from rest, are irrotational, since they are trivially irrotational, when they are at rest. This makes also clear that this cannot hold in a flow involving shock discontinuities, since across the shock differentiability is violated.

Finally, let us describe the distinctive properties of so-called **Bernoulli surfaces** $\mathcal{S}_B$. Such surfaces are generated by a selected vortex line and all the streamlines through this vortex line, see **Fig. 4.9**. The surface swept out by all the streamlines defines the BERNOULLI surface belonging to the selected vortex line. If one regards the selected vortex line as a material line, this line will, with time, be carried away on $\mathcal{S}_B$. In other words, stream and vortex lines lie in this case on the same surface $\mathcal{S}_B$. Two arbitrary points 1 and 2 on this surface can be connected by a curve on $\mathcal{S}_B$. So, if $\boldsymbol{v}$ and $\boldsymbol{\omega}$ are the velocity and vectorial vorticity, respectively at a surface point on $\mathcal{S}_B$, then $\boldsymbol{v} \times \boldsymbol{\omega}$ is perpendicular to $\mathcal{S}_B$ and $(\boldsymbol{v} \times \boldsymbol{\omega}) \cdot \mathrm{d}\boldsymbol{x}$ vanishes, if $\mathrm{d}\boldsymbol{x}$ is the vectorial line increment along a curve on $\mathcal{S}_B$. For a barotropic inviscid fluid in steady motion the momentum equation takes the form

$$\mathrm{grad} \left(\frac{v^2}{2} + P - U \right) = \boldsymbol{v} \times \boldsymbol{\omega},$$

which, when integrated along any path on $\mathcal{S}_B$ from point 1 to point 2, yields

$$\int_1^2 \mathrm{grad} \left(\frac{v^2}{2} + P - U \right) \cdot \mathrm{d}\boldsymbol{x} = \int_1^2 \underbrace{(\boldsymbol{v} \times \boldsymbol{\omega})}_{=0} \cdot \mathrm{d}\boldsymbol{x} = 0,$$
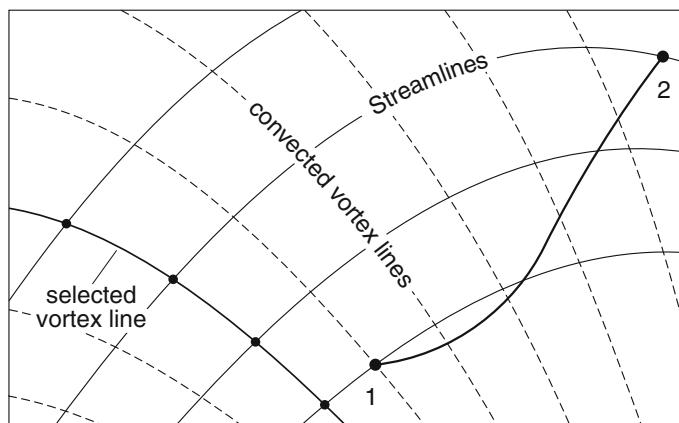
Fig. 4.9 BERNOULLI surface $\mathcal{S}_B$. *These surfaces are constructed by selecting a particular fixed vortex line (heavy solid in the figure) and considering all streamlines through this vortex line (light solid), this generating the BERNOULLI surface $\mathcal{S}_B$ belonging to this vortex line. As a material line this vortex line is convected on $\mathcal{S}_B$ (dashed). On any path from point 1 to point 2 on $\mathcal{S}_B$ the quantity $v^2/2 + P - U$ is constant*

or

$$\left(\frac{v^2}{2} + P - U\right) = \text{constant}.$$

BERNOULLI surfaces are, thus, those surfaces in a barotropic fluid for which ($\frac{v^2}{2} + P - U$) remains invariant.

4.3 Helmholtz Vorticity Theorem

A very important result that can directly be deduced from a transformation of the momentum equation of an ideal fluid is the vorticity theorem due to HERMANN HELMHOLTZ (1821–1894)[3]. To derive it, we consider the EULER equations (valid for an ideal fluid),

$$\frac{\partial \boldsymbol{v}}{\partial t} - \boldsymbol{v} \times \boldsymbol{w} + \text{grad}\left(\frac{v^2}{2}\right) = -\frac{1}{\rho}\,\text{grad}\,p + \boldsymbol{f}$$

and apply to it the curl-operator; this yields

$$\frac{\partial \boldsymbol{w}}{\partial t} - \text{curl}\,(\boldsymbol{v} \times \boldsymbol{w}) = -\text{curl}\left(\frac{1}{\rho}\,\text{grad}\,p\right) + \text{curl}\,\boldsymbol{f}, \qquad (4.27)$$

in which $\boldsymbol{w} = \text{curl}\,\boldsymbol{v}$, as before. This equation is often called the **vorticity equation**. We also used the fact that $\text{curl}\,(\text{grad}\,(\cdot)) = \boldsymbol{0}$. Recalling the vector identities

$$\begin{aligned}
\text{curl}\,(\boldsymbol{a} \times \boldsymbol{b}) &= (\text{grad}\,\boldsymbol{a})\boldsymbol{b} - (\text{grad}\,\boldsymbol{b})\boldsymbol{a} - \boldsymbol{a}\,\text{div}\,\boldsymbol{b} - \boldsymbol{b}\,\text{div}\,\boldsymbol{a}, \\
\text{curl}\,(\lambda\boldsymbol{b}) &= (\text{grad}\,\lambda) \times \boldsymbol{b} - \lambda\,\text{curl}\,\boldsymbol{b},
\end{aligned} \qquad (4.28)$$

(these can best be proved by using Cartesian index notation), using the first in $\boldsymbol{v} \times \boldsymbol{w}$ and the second in grad p/ρ, viz.,

$$\begin{aligned}
\text{curl}\,(\boldsymbol{v} \times \boldsymbol{w}) &= (\text{grad}\,\boldsymbol{v})\boldsymbol{w} - (\text{grad}\,\boldsymbol{w})\boldsymbol{v} - \boldsymbol{w}\,\text{div}\,\boldsymbol{v}, \\
\text{curl}\left(\frac{1}{\rho}\text{grad}\,p\right) &= \text{grad}\left(\frac{1}{\rho}\right) \times \text{grad}\,p - \frac{1}{\rho^2}\text{grad}\,\rho \times \text{grad}\,p
\end{aligned} \qquad (4.29)$$

---

[3]For a short biographical sketch of HELMHOLTZ see **Fig. 4.10**.

Fig. 4.10 HERMANN LUDWIG FERDINAND VON HELMHOLTZ (31. Aug. 1821–8. Sept. 1894)

HERMANN LUDWIG FERDINAND VON HELMHOLTZ was a German physician and physicist who made significant contributions to many areas of modern science. In physiology and psychology, he is known for his mathematical description of the eye, theories of vision, ideas on the visual perception of space, color vision research, and on the sensation of tone, perception of sound, and empiricism. In physics, he is known for his theories on the conservation of energy, work in electrodynamics, chemical thermodynamics, and on a mechanical foundation of thermodynamics. In analysis, he is known for the theorem that a differentiable vector field can be split into irrotational and solenoidal parts, a theorem of significance in mathematical physics. As a philosopher, HELMHOLTZ is known for his philosophy of science, ideas on the relation between the laws of perception and the laws of nature, the science of aesthetics, and ideas on the civilizing power of science. A large German association of research institutions, the HELMHOLTZ Gesellschaft (Association), is named after him.

The text is partly based on http://www.wikipedia.org

(here we used the fact that div $\boldsymbol{w} = 0$ and curl grad $p = \boldsymbol{0}$), then (4.27) may, alternatively, be written as

$$\underbrace{\frac{\partial \boldsymbol{w}}{\partial t} + (\text{grad } \boldsymbol{w})\,\boldsymbol{v}}_{\frac{\mathrm{d}\boldsymbol{w}}{\mathrm{d}t}} + \underbrace{\boldsymbol{w}\,\text{div}\,\boldsymbol{v}}_{-\frac{\boldsymbol{w}}{\rho}\frac{\mathrm{d}\rho}{\mathrm{d}t}}$$
$$= (\text{grad }\boldsymbol{v})\boldsymbol{w} + \frac{1}{\rho^2}(\text{grad }\rho) \times (\text{grad }p) + \text{curl }\boldsymbol{f}. \tag{4.30}$$

Note that the first two terms on the left-hand side of this equation are equal to $\mathrm{d}\,\boldsymbol{w}/\mathrm{d}t$ and the last term can be transformed with the aid of the mass balance to $-\boldsymbol{w}\frac{1}{\rho}\frac{\mathrm{d}\rho}{\mathrm{d}t}$. All

three terms together are also expressible as $\rho \frac{\mathrm{d}}{\mathrm{d}t}(\boldsymbol{w}/\rho)$. Thus, Eq. (4.30) also takes the alternative form

$$\frac{\mathrm{d}}{\mathrm{d}t}\left(\frac{\boldsymbol{w}}{\rho}\right) = (\mathrm{grad}\,\boldsymbol{v})\frac{\boldsymbol{w}}{\rho} + \frac{1}{\rho^3}\mathrm{grad}\,\rho \times \mathrm{grad}\,p + \frac{1}{\rho}\mathrm{curl}\,\boldsymbol{f}. \qquad (4.31)$$

This is the first form of the HELMHOLTZ equation. It is often simply referred to as the **vorticity equation** and holds in this form for an ideal, *inviscid* fluid. For a barotropic fluid, $p = p(\rho)$ and $\mathrm{grad}\,p = (\mathrm{d}p/\mathrm{d}\rho)\mathrm{grad}\,\rho$, and the term with the cross product on the right-hand side of (4.31) vanishes since $\mathrm{grad}\,\rho$ is parallel to $\mathrm{grad}\,p$. Moreover, if the specific volume force is conservative, $\boldsymbol{f} = -\mathrm{grad}\,U$, then the HELMHOLTZ theorem may be summarized as follows:

Theorem 4.3 Helmholtz' vorticity theorem
Consider an ideal, barotropic, compressible or density preserving fluid exposed to a conservative force field. Let $\boldsymbol{v}(\boldsymbol{x}, t)$ be its differentiable velocity field, $\boldsymbol{w}(\boldsymbol{x}, t)$ its vorticity field and $\rho(\boldsymbol{x}, t)$ the density field. Then,

$$\frac{d}{dt}\left(\frac{\boldsymbol{w}}{\rho}\right) = (\mathrm{grad}\,\boldsymbol{v})\frac{\boldsymbol{w}}{\rho}, \qquad (4.32)$$

*or, if we introduce the **vorticity per unit mass** ω by $\boldsymbol{w} = \rho\,\omega$,*

$$\frac{d}{dt}(\boldsymbol{\omega}) = (\mathrm{grad}\,\boldsymbol{v})\boldsymbol{\omega}. \qquad (4.33)$$

$\blacksquare$

The proof is immediate from (4.31). This theorem can easily be explored with results that have important theoretical implications.

As a first application, consider **plane flow** in the (x, y)-plane. Then,

$$\mathrm{grad}\,\boldsymbol{v} = \begin{pmatrix} \dfrac{\partial u}{\partial x} & \dfrac{\partial u}{\partial y} & 0 \\[2mm] \dfrac{\partial v}{\partial x} & \dfrac{\partial v}{\partial y} & 0 \\[2mm] 0 & 0 & 0 \end{pmatrix} \quad \text{and} \quad \boldsymbol{w} = \begin{pmatrix} 0 \\[1mm] 0 \\[1mm] \dfrac{\partial v}{\partial x} - \dfrac{\partial u}{\partial y} \end{pmatrix}, \qquad (4.34)$$

so that $(\mathrm{grad}\,\boldsymbol{v})\boldsymbol{w} = \boldsymbol{0}$. In this case, (4.33) reduces to

$$\frac{\mathrm{d}\boldsymbol{\omega}}{\mathrm{d}t} = \boldsymbol{0} \qquad \Rightarrow \qquad \boldsymbol{\omega} = \mathrm{const} \;\; \text{on particle trajectories,} \qquad (4.35)$$

or since for plane flow $\boldsymbol{\omega} = (\zeta/\rho)\hat{\boldsymbol{k}}$,

$$\frac{\mathrm{d}}{\mathrm{d}t}\left(\frac{\zeta}{\rho}\right) = 0 \qquad \Rightarrow \qquad \frac{\zeta}{\rho} = \mathrm{const} \;\; \text{on particle trajectories.} \qquad (4.36)$$

In plane flow, the vorticity per unit mass is a conserved quantity, a vector perpendicular to the plane of motion that is carried along with the fluid particle.

The behavior is quite different in **three-dimensional flow**. In this case, the right-hand side of (4.31) or (4.33) does not necessarily vanish. More specifically, (4.33) can easily be integrated, the result being

$$\boldsymbol{\omega}(t) = \boldsymbol{F}(t)\boldsymbol{\omega}(\tau) = \boldsymbol{F}(t)\boldsymbol{\omega}_0, \tag{4.37}$$

where t is the present time, whilst τ is the initial time for which $\boldsymbol{F} = \boldsymbol{1}$, and $\boldsymbol{F}$ is the deformation gradient

$$\boldsymbol{F} = \frac{\partial \boldsymbol{\chi}(X, t)}{\partial X}. \tag{4.38}$$

To corroborate the result (4.37), we take

$$\begin{aligned}
\dot{\boldsymbol{\omega}} = \dot{\boldsymbol{F}}\boldsymbol{\omega}(\tau) = \frac{\partial \dot{\boldsymbol{x}}}{\partial X}\boldsymbol{\omega}(\tau) = \frac{\partial \boldsymbol{v}}{\partial \boldsymbol{x}}\frac{\partial \boldsymbol{\chi}}{\partial X}\boldsymbol{\omega}(\tau) \\
= (\operatorname{grad}\boldsymbol{v})\boldsymbol{F}(t)\boldsymbol{\omega}(\tau) = (\operatorname{grad}\boldsymbol{v})\boldsymbol{\omega}(t),
\end{aligned}$$

which is (4.33), as expected.

To interpret the result (4.37) recall that for a continuous motion $\boldsymbol{x} = \boldsymbol{\chi}(X, t)$ the material line increment $\mathrm{d}\boldsymbol{x}$ at time t is related to the corresponding vectorial line increment at the initial time, $\mathrm{d}X$, according to

$$\mathrm{d}\boldsymbol{x} = \boldsymbol{F}\mathrm{d}X. \tag{4.39}$$

This agrees formally with (4.37) and implies: *The vorticity vectors per unit mass, $\boldsymbol{\omega}$, change with time exactly as vectorial material line elements do*. For constant density, i.e., density preserving fluids, this can also be expressed as follows: *When vortex filaments are stretched the specific vorticity increases, when they are squeezed it decreases*.

A further property can directly be obtained from (4.33) or (4.37) by decomposing the deformation into strain (rate) and rotation (rate). Recall that the velocity gradient,

$$\begin{aligned}
\operatorname{grad}\boldsymbol{v} &= \boldsymbol{D} + \boldsymbol{W}, \\
\boldsymbol{D} &:= \operatorname{sym}(\operatorname{grad}\boldsymbol{v}), \quad \boldsymbol{W} = \operatorname{skw}(\operatorname{grad}\boldsymbol{v})
\end{aligned} \tag{4.40}$$

can be additively decomposed into its symmetric and skew-symmetric parts, and that the symmetric part, $\boldsymbol{D}$, called *strain rate tensor* or *stretching tensor*, describes the rate of strain at a point, whilst $\boldsymbol{W}$ is the *vorticity tensor* that describes the local rotation and is related to the vorticity vector $\boldsymbol{\omega}$ according to

$$\boldsymbol{W}\boldsymbol{a} = \boldsymbol{w} \times \boldsymbol{a} \quad \text{for all} \quad \boldsymbol{a} \neq \boldsymbol{0}. \tag{4.41}$$

With the decomposition (4.40), (4.33) reads

$$\dot{\boldsymbol{\omega}} = \boldsymbol{D}\boldsymbol{\omega} + \boldsymbol{W}\boldsymbol{\omega}. \tag{4.42}$$

According to this formula, vortex lines change per unit time by the amount $\boldsymbol{D}\boldsymbol{\omega}$ through stretching and by the amount $\boldsymbol{W}\boldsymbol{\omega}$ through rotation.

The same conclusion, now integrated in time, can also be drawn from (4.37). To this end, the theorem of polar decomposition of $\boldsymbol{F}$ is used.

The theorem reads as follows:

Polar Decomposition Theorem. *Every second rank tensor $\boldsymbol{F}$ with* $\det \boldsymbol{F} \neq \boldsymbol{0}$ *permits two polar decompositions*, namely,

$$\boldsymbol{F} = \boldsymbol{R}\boldsymbol{U} = \boldsymbol{V}\boldsymbol{R}, \tag{4.43}$$

with the following properties:

- *$\boldsymbol{V}$ and $\boldsymbol{U}$ are symmetric,*

$$\boldsymbol{V} = \boldsymbol{V}^T, \quad \boldsymbol{U} = \boldsymbol{U}^T. \tag{4.44}$$

- *$\boldsymbol{V}$ and $\boldsymbol{U}$ are positive definite,*

$$\boldsymbol{x} \cdot \boldsymbol{V}\boldsymbol{x} \geq 0, \quad \boldsymbol{x} \cdot \boldsymbol{U}\boldsymbol{x} \geq 0, \quad \forall \boldsymbol{x} \in \mathcal{R}^3 \tag{4.45}$$

  and they have the same eigenvalues.
  This part of the deformation gradient corresponds to a pure strain; $\boldsymbol{U}$ and $\boldsymbol{V}$ are called the right and left stretch tensors respectively.[4] The denotation right and left implies that $\boldsymbol{U}$ stands to the right and $\boldsymbol{V}$ stands to the left of $\boldsymbol{R}$, no more!
- *$\boldsymbol{R}$ is proper orthogonal,*

$$\boldsymbol{R}\boldsymbol{R}^T = \boldsymbol{R}^T\boldsymbol{R} = \boldsymbol{I}, \quad \det \boldsymbol{R} = +1. \tag{4.46}$$

- *The polar decomposition is unique.[5]* ∎

The above described polar decomposition enables us to interpret the deformation (**Fig. 4.11**) by stating that rotation follows stretch or stretch follows rotation.

We shall not prove this polar decomposition theorem here. For this purpose the reader may e.g. consult [17] or [9]. Here, we simply provide an instructive recipe to construct $\boldsymbol{U}$, $\boldsymbol{V}$ and $\boldsymbol{R}$ from a given $\boldsymbol{F}$. This construction follows essentially the steps of the proof of the theorem.

Step 1: For a prescribed deformation gradient $\boldsymbol{F}$ one forms the right, $\boldsymbol{C}$, and left, $\boldsymbol{B}$, CAUCHY- GREEN deformation tensors as follows:

$$\boldsymbol{C} = \boldsymbol{F}^T\boldsymbol{F}, \quad \boldsymbol{B} = \boldsymbol{F}\boldsymbol{F}^T. \tag{4.47}$$

---

[4]Note, we use 'stretch' to denote deformation associated with 'strain' and 'stretching' to express 'strain rate'.

[5]The polar decomposition is unique for a tensor $\boldsymbol{F}$ which is non-singular. For details see TRUESDELL & NOLL (1965) [17], Sect. 23, or any book on continuum mechanics, e.g. HUTTER & JÖHNK (2004) [9].
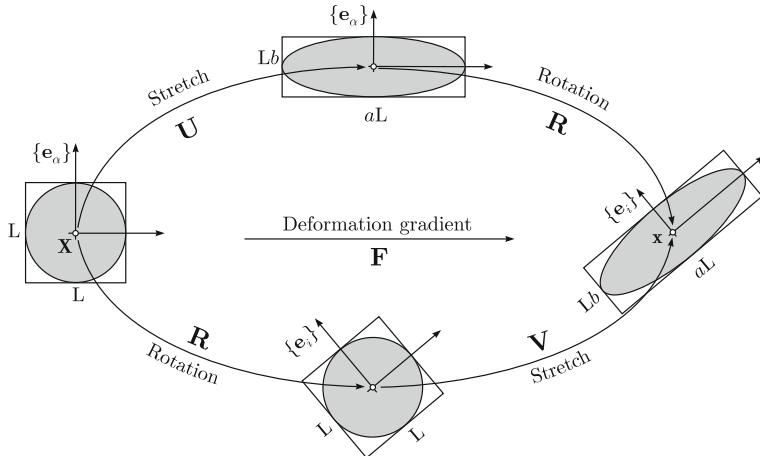
Fig. 4.11 Polar decomposition of the deformation gradient, interpreted as the compositional process of stretch followed by rotation or vice versa

These are both obtained by 'matrix multiplication' of the respective 3×3 schemes of $\boldsymbol{F}$ and $\boldsymbol{F}^T$, respectively. It is easy to see that $\boldsymbol{C}$ and $\boldsymbol{B}$ are both symmetric: $\boldsymbol{C} = \boldsymbol{C}^T, \boldsymbol{B} = \boldsymbol{B}^T$.

Step 2: The proof of the polar decomposition theorem shows that U and V are obtained as square roots of $\boldsymbol{C}$ and $\boldsymbol{B}$, respectively, viz.,

$$U = \sqrt{\boldsymbol{C}}, \quad V = \sqrt{\boldsymbol{B}}. \tag{4.48}$$

Since $\boldsymbol{C}$ and $\boldsymbol{B}$ are symmetric positive definite 3×3 matrices, their square roots are evaluated by spectral decompositions, which are expressible as

$$\boldsymbol{C} = \sum_\alpha \lambda_\alpha^{(C)} \boldsymbol{e}_\alpha \otimes \boldsymbol{e}_\alpha, \quad \boldsymbol{B} = \sum_i \lambda_i^{(B)} \boldsymbol{e}_i \otimes \boldsymbol{e}_i. \tag{4.49}$$

Here, $\lambda_\alpha^{(C)}$ and $\lambda_i^{(B)}$ are eigenvalues of $\boldsymbol{C}$ and $\boldsymbol{B}$, respectively, and $\boldsymbol{e}_\alpha$, $\boldsymbol{e}_i$ are the associated eigenvectors. These are computed by solving the eigenvalue equations

$$\left(\boldsymbol{C} - \lambda_\alpha^{(C)} \boldsymbol{I}\right) \boldsymbol{e}_\alpha = \boldsymbol{0}, \quad \left(\boldsymbol{B} - \lambda_i^{(B)} \boldsymbol{I}\right) \boldsymbol{e}_i = \boldsymbol{0}, \tag{4.50}$$

whose characteristic equations are of the form

$$\lambda^3 - I_A \lambda^2 + II_A \lambda - III_A = 0, \tag{4.51}$$

$$I_A := \mathrm{tr} A, \quad II_A := \tfrac{1}{2}\left(I_A^2 - I_{A^2}\right), \quad III_A := \det A, \tag{4.52}$$

in which λ stands for $\lambda_\alpha^{(C)}$ and $\lambda_i^{(B)}$, and A stands for U and V, respectively. It can be proved that the eigenvalues $\lambda_\alpha^{(C)}$ and $\lambda_i^{(B)}$ *have the same values*, but the associated eigenvectors are related by

$$e_i = Re_\alpha. \tag{4.53}$$

Equations (4.51), (4.52) allow determination of the three eigenvalues $\left(\lambda_\alpha^{(C)}\right)_j = \left(\lambda_i^{(B)}\right)_j$, $j = 1, 2, 3$ and then, Eq. (4.50) yields the eigenvectors $\{e_\alpha^j\}$ and $\{e_i^j\}$ [It suffices just to solve one of these equations, as we shall see].

For the computations of U and V one then applies the spectral theorem, which says that

$$U = \sqrt{C} = \sum_\alpha \sqrt{\lambda_\alpha^{(C)}} e_\alpha \otimes e_\alpha, \quad V = \sqrt{B} = \sum_i \sqrt{\lambda_i^{(B)}} e_i \otimes e_i, \tag{4.54}$$

U and V are called right and left **stretch tensors**.

Step 3: For the determination of the **rotation matrix** R we start from the polar decomposition (4.43) and write this as $R = FU^{-1} = V^{-1}F$. In a first attempt the polar decompositions

$$U^{-1} = \sum_\alpha \sqrt{\frac{1}{\lambda_\alpha^{(C)}}} e_\alpha \otimes e_\alpha, \quad V^{-1} = \sum_i \sqrt{\frac{1}{\lambda_i^{(B)}}} e_i \otimes e_i \tag{4.55}$$

are constructed, which is possible, since U and V are positive definite. With these, R can be computed by using
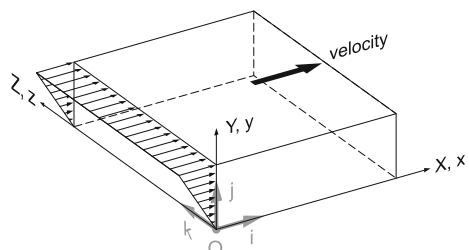
$$R = FU^{-1} = V^{-1}F. \tag{4.56}$$

Example: Simple Shearing

Consider Cartesian coordinates, $\{X, Y, Z\}$ in the reference system and $\{x, y, z\}$ in the present configuration with identical bases $[i, j, k]$, see **Fig. 4.12**. Simple shearing is then defined by

$$x = X + Y\dot{\gamma}t, \quad y = Y, \quad z = Z, \tag{4.57}$$

Fig. 4.12 Simple shearing. *A viscous fluid is held between two parallel plates. The top plate moves with constant velocity in the x-direction; the bottom plate is at rest. The shear rate $\dot{\gamma}$ characterizes this motion*

in which $\dot{\gamma}$ is the constant shear rate and t is time. With

$$
\begin{aligned}
\frac{\partial x}{\partial X} &= 1, & \frac{\partial x}{\partial Y} &= \dot{\gamma}t, & \frac{\partial x}{\partial Z} &= 0, \\
\frac{\partial y}{\partial X} &= 0, & \frac{\partial y}{\partial Y} &= 1, & \frac{\partial y}{\partial Z} &= 0, \\
\frac{\partial z}{\partial X} &= 0, & \frac{\partial z}{\partial Y} &= 0, & \frac{\partial z}{\partial Z} &= 1
\end{aligned}
\tag{4.58}
$$

the deformation gradient F and its transpose are given by

$$
F = \begin{pmatrix} 1 & \dot{\gamma}t & 0 \\ 0 & 1 & 0 \\ 0 & 0 & 1 \end{pmatrix}, \quad
F^T = \begin{pmatrix} 1 & 0 & 0 \\ \dot{\gamma}t & 1 & 0 \\ 0 & 0 & 1 \end{pmatrix},
\tag{4.59}
$$

from which, via trivial matrix multiplication the right and left CAUCHY- GREEN deformation tensors follow as

$$
C = F^T F = \begin{pmatrix} 1 & \dot{\gamma}t & 0 \\ \dot{\gamma}t & 1 + (\dot{\gamma}t)^2 & 0 \\ 0 & 0 & 1 \end{pmatrix},
$$

$$
B = F F^T = \begin{pmatrix} 1 + (\dot{\gamma}t)^2 & \dot{\gamma}t & 0 \\ \dot{\gamma}t & 1 & 0 \\ 0 & 0 & 1 \end{pmatrix}.
\tag{4.60}
$$

Via time differentiation of (4.57) the velocity field is deducible as

$$
v = \begin{pmatrix} u \\ v \\ w \end{pmatrix} = \begin{pmatrix} \dot{\gamma}Y \\ 0 \\ 0 \end{pmatrix} = \begin{pmatrix} \dot{\gamma}y \\ 0 \\ 0 \end{pmatrix},
\tag{4.61}
$$

from which the spatial velocity gradient, grad v, follows as

$$
\text{grad } v = L = \begin{pmatrix} 0 & \dot{\gamma} & 0 \\ 0 & 0 & 0 \\ 0 & 0 & 0 \end{pmatrix}.
\tag{4.62}
$$

Strain rate (stretching) and vorticity tensors are obtained as symmetric and skew-symmetric parts of L,

$$
D = \tfrac{1}{2}(L + L^T) = \begin{pmatrix} 0 & \dot{\gamma}/2 & 0 \\ \dot{\gamma}/2 & 0 & 0 \\ 0 & 0 & 0 \end{pmatrix},
\tag{4.63a}
$$

$$W = \tfrac{1}{2}\left(L - L^T\right) = \begin{pmatrix} 0 & \dot{\gamma}/2 & 0 \\ -\dot{\gamma}/2 & 0 & 0 \\ 0 & 0 & 0 \end{pmatrix}, \qquad (4.63b)$$

whereas the vorticity vector $\boldsymbol{\omega}$, dual to W is given by $\dot{\gamma}k = \boldsymbol{\omega}$. The rate of motion, expressed by $L = D + W$ is composed of *stretching*, D, and *tilting*, W.

The integrated motion change is expressed by $F = RU = VR$ in (4.43). To evaluate U, V and R, the spectral decompositions of C and B, as indicated in (4.50) must be evaluated. This requires the solution of the eigenvalue problems for C and B, which can be written as

$$\begin{pmatrix} 1 - \lambda & \dot{\gamma}t & 0 \\ \dot{\gamma}t & 1 - \lambda + (\dot{\gamma}t)^2 & 0 \\ 0 & 0 & 1 - \lambda \end{pmatrix} \begin{pmatrix} e_{\alpha_1} \\ e_{\alpha_2} \\ e_{\alpha_3} \end{pmatrix} = \begin{pmatrix} 0 \\ 0 \\ 0 \end{pmatrix}, \quad \text{for } C, \ \lambda := \lambda_\alpha^{(C)},$$

$$(4.64)$$

$$\begin{pmatrix} 1 - \lambda + (\dot{\gamma}t)^2 & \dot{\gamma}t & 0 \\ \dot{\gamma}t & 1 - \lambda & 0 \\ 0 & 0 & 1 - \lambda \end{pmatrix} \begin{pmatrix} e_{i_1} \\ e_{i_2} \\ e_{i_3} \end{pmatrix} = \begin{pmatrix} 0 \\ 0 \\ 0 \end{pmatrix}, \quad \text{for } B, \ \lambda := \lambda_i^{(B)},$$

where e_{α_k} and e_{i_ℓ}, $k, \ell = 1, 2, 3$, are the associated eigenvectors and the indices $(\cdot)_\alpha$ and $(\cdot)_i$ are labels to identify the reference and present configurations, respectively. Both equations (4.64) lead to the same characteristic equation

$$(1 - \lambda)[(1 - \lambda)^2 - \lambda(\dot{\gamma}t)^2] = 0 \qquad (4.65)$$

with the three independent solutions

$$\lambda_{\alpha,i}^{(1)} = 1, \quad \lambda_{\alpha,i}^{(2,3)} = \left(1 + \frac{(\dot{\gamma}t)^2}{2}\right) \pm \sqrt{\left(1 + \frac{(\dot{\gamma}t)^2}{2}\right)^2 - 1}, \qquad (4.66)$$

in which the subscripts $(\cdot)_{\alpha,i}$ are reminders that (4.66) are eigenvalues for C as well as B, respectively. Back-substitution of the eigenvalues (4.66) into (4.64) allows determination of the eigenvectors (of unit length). The results of the routine computations are as follows:
for the eigenvectors of C:

- for $\lambda = 1$:

$$e_\alpha^{(1)} = \begin{pmatrix} 0 \\ 0 \\ 1 \end{pmatrix}, \qquad (4.67)$$

- for λ as given in $(4.66)_2$:

$$
e_\alpha^{(2,3)} = \begin{pmatrix} -\dfrac{\dot{\gamma}t}{\delta^{1/2}} \\[2ex] \dfrac{-(\dot{\gamma}t)^2/2 \mp \beta^{1/2}}{\delta^{1/2}} \\[2ex] 0 \end{pmatrix},
\tag{4.68}
$$

for the eigenvectors of $\boldsymbol{B}$:

- for $\lambda = 1$:

$$
e_i^{(1)} = \begin{pmatrix} 0 \\ 0 \\ 1 \end{pmatrix},
\tag{4.69}
$$

- for λ as given in $(4.66)_2$:

$$
e_i^{(2,3)} = \begin{pmatrix} \dfrac{\dot{\gamma}t}{\delta^{1/2}} \\[2ex] -\dfrac{-(\dot{\gamma}t)^2/2 \pm \beta^{1/2}}{\delta^{1/2}} \\[2ex] 0 \end{pmatrix},
\tag{4.70}
$$

in which

$$
\beta = \left(1 + \frac{(\dot{\gamma}t)^2}{2}\right)^2 - 1, \quad \delta = \left(-\frac{(\dot{\gamma}t)^2}{2} \mp \beta^{1/2}\right)^2 + (\dot{\gamma}t)^2.
\tag{4.71}
$$

With equations (4.66) for the eigenvalues and (4.67)–(4.71) for the eigenvectors exact solutions for the spectral representations of $\boldsymbol{C}$, $\boldsymbol{B}$, (4.50); $\boldsymbol{U}$, $\boldsymbol{V}$, (4.54); $\boldsymbol{U}^{-1}$, $\boldsymbol{V}^{-1}$, (4.55) are known for any arbitrary time $t > 0$. For the interpretation of the formulae (4.49), (4.54), (4.55) the exterior products $\boldsymbol{e}_\alpha \otimes \boldsymbol{e}_\alpha$ and $\boldsymbol{e}_i \otimes \boldsymbol{e}_i$ must be expressed by the components of $\boldsymbol{e}_\alpha$ and $(\boldsymbol{e}_i)$, respectively, in the Cartesian basis $(\boldsymbol{i}, \boldsymbol{j}, \boldsymbol{k})$. So, if $\boldsymbol{e} = (e_{\alpha_1}, e_{\alpha_2}, e_{\alpha_3})$, then

$$
\boldsymbol{e}_\alpha \otimes \boldsymbol{e}_\alpha = \begin{pmatrix} e_{\alpha_1}e_{\alpha_1} & e_{\alpha_1}e_{\alpha_2} & e_{\alpha_1}e_{\alpha_3} \\ e_{\alpha_2}e_{\alpha_1} & e_{\alpha_2}e_{\alpha_2} & e_{\alpha_2}e_{\alpha_3} \\ e_{\alpha_3}e_{\alpha_1} & e_{\alpha_3}e_{\alpha_2} & e_{\alpha_3}e_{\alpha_3} \end{pmatrix} = \sum_{i=1}^{3}\sum_{j=1}^{3} e_{\alpha_i}e_{\alpha_j}\boldsymbol{i} \otimes \boldsymbol{j},
\tag{4.72}
$$

and similarly for $\boldsymbol{e}_i \otimes \boldsymbol{e}_i$.

According to the polar decomposition theorem the (non-singular) deformation gradient F can be decomposed as follows (note, this is a product decomposition):

$$F = RU = VR. \tag{4.73}$$

Here, U and V are called right and left stretch tensors and R is an orthogonal transformation, $RR^T = 1$; moreover, $U^2 = F^T F$ and $V^2 = FF^T$. It is shown in kinematics of continuous motions that U and V describe the strain that has accumulated since the onset of the motion, whilst R describes the accumulated rotation. So, according to (4.37) and (4.73)

$$\boldsymbol{\omega} = RU\boldsymbol{\omega}_0 = VR\boldsymbol{\omega}_0. \tag{4.74}$$

In the first representation the total change of a vortex filament is represented as a stretch followed by a rotation; in the second this order is reversed, (see Fig. 4.11). In short one says: Vortex filaments in three-dimensional motions are deformed by **stretching** and **tilting**.

The HELMHOLTZ vorticity theorem can also be applied to ideal fluids referred to a permanently rotating frame of reference with constant angular velocity $\boldsymbol{\Omega}$. In this case the EULER equations of a barotropic fluid subject to a conservative body force take the form[6]

$$\frac{\partial \boldsymbol{v}}{\partial t} - \boldsymbol{v} \times \boldsymbol{w} = -\text{grad}\left(P(\rho) + \frac{v^2}{2} + U - \frac{|\boldsymbol{\Omega}|^2 \hat{r}^2}{2}\right) - 2\boldsymbol{\Omega} \times \boldsymbol{v}. \tag{4.75}$$

Here P is the pressure function of the barotropic fluid, U is the potential of the specific body force, $\Omega \hat{r}^2/2$ is the potential due to the rotation of the frame of reference due to $(\boldsymbol{\Omega} \times (\boldsymbol{\Omega} \times \boldsymbol{x}))$, see Eqs. (3.80), (3.98), and the last term on the right-hand side is the CORIOLIS force. For $\boldsymbol{\Omega} = $ constant equation (4.75) can also be rewritten as

$$\frac{\partial \boldsymbol{v}}{\partial t} - \boldsymbol{v} \times (\boldsymbol{w} + 2\boldsymbol{\Omega}) = -\text{grad}\left(P(\rho) + \frac{v^2}{2} + U - \frac{\Omega^2 \hat{r}^2}{2}\right), \tag{4.76}$$

and if we take its curl, the term on the right-hand side vanishes and the left-hand side becomes

$$\frac{\partial(\boldsymbol{w} + 2\boldsymbol{\Omega})}{\partial t} - \text{curl}\,(\boldsymbol{v} \times (\boldsymbol{w} + 2\boldsymbol{\Omega})) = \boldsymbol{0}, \tag{4.77}$$

in which we have added $\partial(2\boldsymbol{\Omega})/\partial t \equiv \boldsymbol{0}$.

The remainder of the computations now parallels that from (4.27) to (4.31) and will not be repeated here. The result is

---

[6]Note, $\hat{r}$ is the radial distance of the point in question from the axis of rotation.

Theorem 4.4 Helmholtz' vorticity theorem in a permanently rotating frame
*Consider an ideal, barotropic, compressible or density preserving fluid. Let $v(x, t)$
be its differentiable velocity field, $w(x, t)$ its vorticity field, $\boldsymbol{\Omega}$ the angular velocity
of the frame and $\rho(x, t)$ the density field. Then,*

$$\frac{\mathrm{d}}{\mathrm{d}t} \left(\frac{w + 2\boldsymbol{\Omega}}{\rho} \right) = (\mathrm{grad}\, v) \left(\frac{w + 2\boldsymbol{\Omega}}{\rho} \right). \tag{4.78}$$

The sum $w + 2\boldsymbol{\Omega}$ is called the **absolute vorticity**.   ∎

The solution of equation (4.78) is, of course, again given by

$$\left(\frac{w + 2\boldsymbol{\Omega}}{\rho} \right)(x, t) = F(x, t) \left(\frac{w + 2\boldsymbol{\Omega}}{\rho} \right)_0 \tag{4.79}$$

and interpretations of vortex stretching and vortex tilting are the same as before, now
applied to the absolute vorticity.

Let us now apply (4.78) to *plane flow* or flows for which the shallow water assump-
tion is justified. Then $\tilde{f} = 0$, $\omega_{\mathrm{abs}} = (\zeta + f)\hat{k}$ and the right-hand side of (4.78)
vanishes since $(\mathrm{grad}\, v)$ and $(w + 2\boldsymbol{\Omega})/\rho$ are orthogonal to one another. So,

$$\frac{\mathrm{d}}{\mathrm{d}t} \left(\frac{\zeta + f}{\rho} \right) = \frac{1}{\rho} \frac{\mathrm{d}\zeta_{\mathrm{abs}}}{\mathrm{d}t} - \frac{1}{\rho^2} \frac{\mathrm{d}\rho}{\mathrm{d}t} \zeta_{\mathrm{abs}} \overset{!}{=} 0, \tag{4.80}$$

which, on using the mass balance equation $\dot{\rho} = -\rho(\frac{\partial u}{\partial x} + \frac{\partial v}{\partial y})$ takes the form

$$\frac{\mathrm{d}\zeta_{\mathrm{abs}}}{\mathrm{d}t} + \zeta_{\mathrm{abs}} \left(\frac{\partial u}{\partial x} + \frac{\partial v}{\partial y} \right) = 0,$$

or

$$\frac{\mathrm{d}(\zeta + f)}{\mathrm{d}t} + (\zeta + f) \left(\frac{\partial u}{\partial x} + \frac{\partial v}{\partial y} \right) = 0. \tag{4.81}$$

This equation can also be derived by different methods. The derivation from (4.78),
however, shows particularly clearly that (4.81) does neither contain any vortex
stretching nor vortex tilting since the right-hand side of (4.78) vanishes for the deriva-
tion of (4.81). It is also clear where the second term on the left-hand side comes form:
It is due to density variations.

A further consequence of Theorem 4.4 is

Theorem 4.5 Taylor-Proudman theorem[7]
*A steady slow-flow of a density preserving fluid in a rotating system is (essentially)
plane. The flow takes place in a plane perpendicular to the axis of rotation.*   ∎

---

[7]For a biography of PROUDMAN see **Fig. 4.13**.

For the **proof** we note that $\boldsymbol{\Omega}$ is constant; so, of the left-hand side of (4.78) only the quadratic term (grad $\boldsymbol{w}$)$\boldsymbol{v}/\rho$ survives, which is of higher order small. The right-hand side reduces in first order to (grad $\boldsymbol{v}$)($2\boldsymbol{\Omega}/\rho$); so,

$$(\text{grad } \boldsymbol{v})\boldsymbol{\Omega} + \mathcal{O}(2) = \boldsymbol{0}, \tag{4.82}$$

where $\mathcal{O}(2)$ are terms of second order small. If we choose a Cartesian coordinate system such that its z-axis is in the direction of $\boldsymbol{\Omega}$, then this equation can be interpreted as $\partial \boldsymbol{v}/\partial z \cong 0$, i.e., the velocity field remains unchanged in the direction of $\boldsymbol{\Omega}$. Changes or variations in the velocity field only occur in planes perpendicular to $\boldsymbol{\Omega}$. The velocity field is essentially plane and perpendicular to $\boldsymbol{\Omega}$. ∎

Fig. 4.13 JOSEPH PROUDMAN (30. Dec. 1888–26. June 1975)

JOSEPH PROUDMAN was a distinguished British mathematician and oceanographer of international repute. His theoretical studies into the oceanic tides not only 'solved practically all the remaining tidal problems which are soluble within the framework of classical hydrodynamics and analytical mathematics' but laid the basis of a tidal prediction service (developed with A.T. DOODSON) of great international importance. This tidal research began under the influence of HORACE LAMB, at that time in Manchester. PROUDMAN carried out his professional career almost exclusively at Liverpool, where he was the first professor of applied mathematics since 1916 and of physical oceanography from 1933 to his retirement in 1954. In theoretical oceanography he is known for the TAYLOR- PROUDMAN theorem.

The text is based on http://www.wikipedia.org

4.4 Potential Vorticity Theorem

Another theorem that is important in rotating fluids and has found applications in meteorology and oceanography is the vorticity theorem due to ERTEL (1904–1971).[8] It is known as the **Theorem of conservation of potential vorticity**.[9] To derive it, we start from (4.78), HELMHOLTZ' vorticity theorem for a barotropic ideal fluid referred to a rotating frame. Moreover, we assume that a differentiable scalar function $\lambda(\boldsymbol{x}, t)$ is given for which the evolution equation

$$\frac{\mathrm{d}\lambda(\boldsymbol{x}, t)}{\mathrm{d}t} = \psi_\lambda(\boldsymbol{x}, t) \tag{4.83}$$

holds, where $\psi_\lambda(\boldsymbol{x}, t)$ is a prescribed differentiable function. We now take (4.78) and multiply both sides scalarly with grad λ. This yields

$$\frac{\mathrm{d}}{\mathrm{d}t}\left(\frac{\boldsymbol{w} + 2\boldsymbol{\Omega}}{\rho}\right) \cdot (\mathrm{grad}\,\lambda) = (\mathrm{grad}\,\boldsymbol{v})\left(\frac{\boldsymbol{w} + 2\boldsymbol{\Omega}}{\rho}\right) \cdot (\mathrm{grad}\,\lambda). \tag{4.84}$$

Alternatively, we may prove the vector identity

$$\begin{aligned}\left(\frac{\boldsymbol{w} + 2\boldsymbol{\Omega}}{\rho}\right) \cdot \frac{\mathrm{d}}{\mathrm{d}t}(\mathrm{grad}\,\lambda) = &\left(\frac{\boldsymbol{w} + 2\boldsymbol{\Omega}}{\rho}\right) \cdot \mathrm{grad}\left(\frac{\mathrm{d}\lambda}{\mathrm{d}t}\right) \\ &- (\mathrm{grad}\,\lambda) \cdot \left(\mathrm{grad}\,\boldsymbol{v}\left(\frac{\boldsymbol{w} + 2\boldsymbol{\Omega}}{\rho}\right)\right).\end{aligned} \tag{4.85}$$

(It may most easily be proved using Cartesian index notation.) When Eqs. (4.84) and (4.85) are added together, the two terms on the left-hand side can be combined to yield

$$\frac{\mathrm{d}}{\mathrm{d}t}\left(\frac{1}{\rho}(\boldsymbol{w} + 2\boldsymbol{\Omega}) \cdot \mathrm{grad}\,\lambda\right), \tag{4.86}$$

whilst the right-hand side becomes

$$\frac{1}{\rho}(\boldsymbol{w} + 2\boldsymbol{\Omega})\mathrm{grad}\left(\frac{\mathrm{d}\lambda}{\mathrm{d}t}\right) = \left(\frac{\boldsymbol{w} + 2\boldsymbol{\Omega}}{\rho}\right) \cdot \mathrm{grad}\,\psi_\lambda, \tag{4.87}$$

where (4.83) has been used. We now introduce

---

[8]For a short biographical sketch of ERTEL see **Fig. 4.14**.

[9]ERTEL, HANS (1904–1971) published his potential vorticity theorem in 1942 [4] with follow-up papers in the same year [5–7], but his work remained, relatively unknown until TRUESDELL (1951) [16] proved that ERTEL's vorticity theorems hold in average for any medium suffering no tangential acceleration on any boundary and summarized the work in a survey in the 'Handbuch der Physik' (TRUESDELL & TOUPIN (1960) [18]). HIDE (1983) [8] published a magnetic analogue of his potential vorticity theorem and KATZ (1983) [11] and TREDER (1970) [15] applied it to relativity. A selection of papers is given by SCHRÖDER & TREDER [14].

Fig. 4.14 HANS ERTEL (24. March 1904–2. July 1971)

HANS ERTEL was a German natural scientist and a pioneer in geophysics, meteorology and hydrodynamics. He developed into a capable theoretical physicist early on and was able to publish research results or theoretical approaches in this subject already as a young man. ERTEL's famous potential vorticity theorem of 1941–43 belongs today to the basic work of modern geo- and astrophysics. The main areas of emphasis in his research were physical hydrography (more than 60 works), theoretical hydrodynamics, special hydrodynamics of the northern German seas and coasts, hydraulic nomography, hydrographic cartography, the history of European weather and theoretical fluid mechanics. As a member of the *Deutsche Akademie der Wisschaften zu Berlin, East Germany*, (DAW, German Academy of Sciences, Berlin), ERTEL founded and led the Institute for Physical Hydrography of this academy. In 1949, he was elected to be a full member of the DAW and was its vice president from 1951 to 1961. The research on geo-ecology, which began under his leadership, is considered to be pioneering work today.

The text is partly based on http://verplant.org/history-geophysics/.

Definition 4.5 Let $w = \mathrm{curl}\, v$ be the vorticity field of the velocity field of an ideal barotropic fluid and $\lambda(x, t)$ a differentiable scalar field. Let, moreover, $\boldsymbol{\Omega}$ be the constant angular velocity of the frame of reference. Then

$$\pi_\lambda := \frac{1}{\rho}(w + 2\boldsymbol{\Omega}) \cdot \mathrm{grad}\, \lambda \tag{4.88}$$

is called the **potential vorticity associated with** λ.   ∎

Equating (4.86) and (4.87) yields the following.

Theorem 4.6 Potential vorticity theorem, Ertel's vorticity theorem. *Let v be the velocity field of an ideal, barotropic compressible or density preserving fluid and $w + 2\boldsymbol{\Omega}$ its absolute vorticity. Let, moreover, $\lambda(\boldsymbol{x}, t)$ and $\psi_\lambda(\boldsymbol{x}, t)$ be two differentiable scalar fields which satisfy the evolution equation (4.83). Let, furthermore, the potential vorticity π_λ associated with λ be defined as in Definition 4.5. Then, this potential vorticity obeys the evolution equation*

$$\frac{d\pi_\lambda}{dt} = \left(\frac{w + 2\boldsymbol{\Omega}}{\rho} \right) \cdot \operatorname{grad} \psi_\lambda. \tag{4.89}$$

∎

Note, there is not only one single potential vorticity equation, but there are many; each λ and ψ_λ, satisfying (4.83), give rise to its own potential vorticity equation.

If ψ_λ is not a function of $\boldsymbol{x}$, $\psi = \psi(t)$, with $\operatorname{grad} \psi_\lambda = 0$, then (4.89) implies the following

Theorem 4.7 Potential vorticity corollary *Assume that the conditions of Theorem 4.6 are fulfilled, but that, specially, ψ_λ is at most a function of the time. Then, the potential vorticity is conserved along particle trajectories, in formulae:*

$$\frac{d\lambda}{dt} = \psi_\lambda(t) \quad \Rightarrow \quad \frac{d\pi_\lambda}{dt} = 0. \tag{4.90}$$

∎

Obviously, for $\psi_\lambda = 0$ the same conclusion holds.

Let us give a number of examples:

(1) Consider flow of an ideal fluid parallel to the (x, y)-plane which itself is rotating with angular velocity $\boldsymbol{\Omega} = \Omega \hat{\boldsymbol{e}}_z$. Select

$$\lambda = z, \quad \operatorname{grad} \lambda = \hat{\boldsymbol{e}}_z, \quad \psi_\lambda = 0, \quad \operatorname{grad} \psi_\lambda = 0. \tag{4.91}$$

Then, according to (4.88)
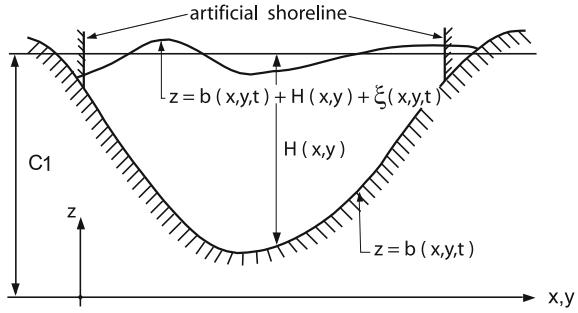
$$\pi_{\lambda=z} = \frac{\zeta + 2\Omega}{\rho}. \tag{4.92}$$

This potential vorticity agrees with the absolute vorticity per unit mass. With (4.91) and (4.92), the conservation law of potential vorticity is the same as the HELMHOLTZ vorticity theorem. Indeed, forming $d\pi_{\lambda=z}/dt = 0$ yields

$$\frac{d}{dt}(\zeta + 2\Omega) - \frac{\dot{\rho}}{\rho}(\zeta + 2\Omega) = 0 \tag{4.93}$$

or when using the mass balance equation $\dot{\rho}/\rho = -(\partial u/\partial x + \partial v/\partial y)$,

Fig. 4.15 Vertical cut through a lake or ocean, indicating the free and bottom surfaces. Note, ξ is the surface elevation

$$\frac{\mathrm{d}}{\mathrm{d}t}(\zeta + 2\Omega) + (\zeta + 2\Omega)\left(\frac{\partial u}{\partial x} + \frac{\partial v}{\partial y}\right) = 0, \tag{4.94}$$

which is the same as (4.81), if we set $2\,\Omega = f$.

(2) Consider now a barotropic, density-preserving fluid in the shallow water approximation for which $\tilde{f} = 0$. Let

$$z = b(x, y, t) \quad \text{and} \quad z = b(x, y, t) + H(x, y) + \xi(x, y, t) \tag{4.95}$$

be equations for the basal and free surfaces, respectively, see **Fig. 4.15**, and choose λ and ψ_λ as in (4.91) of example (1). Then, dropping the constant density in (4.92), the potential vorticity equation (4.90)$_2$ takes the form

$$\frac{\mathrm{d}}{\mathrm{d}t}(\zeta + f) = 0. \tag{4.96}$$

It is known that in a barotropic fluid the horizontal velocity components (u, v) are independent of z. This implies that also $\zeta + f$ is independent of z. So, we wish to average (integrate) equation (4.96) over depth,

$$\int_b^{b+H+\xi} \frac{\mathrm{d}}{\mathrm{d}t}(\zeta + f)\mathrm{d}z = 0, \tag{4.97}$$

where ξ is the free surface deflection. Interchanging integration and differentiation and using LEIBNIZ' rule, transforms (4.97) into

$$\frac{\mathrm{d}}{\mathrm{d}t}\int_b^{b+H+\xi} (\zeta + f)\mathrm{d}z - (\zeta + f)|_{b+H+\xi}\left(\frac{\mathrm{d}b}{\mathrm{d}t} + \frac{\mathrm{d}(H + \xi)}{\mathrm{d}t}\right) + (\zeta + f)_b\frac{\mathrm{d}b}{\mathrm{d}t} = 0. \tag{4.98}$$

With the z-independence of $(\zeta + f)$, Eq. (4.98) simplifies to

$$\frac{d}{dt}((\zeta + f)(b + H + \xi)) - (\zeta + f)\frac{d}{dt}(H + \xi) = 0 \qquad (4.99)$$

or, after a simple transformation, and if b does not depend on time,

$$\frac{d}{dt}\left(\frac{\zeta + f}{H + \xi}\right) = \frac{d}{dt}\langle\pi\rangle_{bt} = 0. \qquad (4.100)$$

The function

$$\langle\pi\rangle_{bt} := \frac{\zeta + f}{H + \xi} \qquad (4.101)$$

is called the barotropic (depth averaged) potential vorticity. It is constant along horizontal projections of the particle trajectories. Note that in the derivation of (4.100) from (4.99) a division by $(H + \xi)$ is used; this implies that $(H + \xi)$ should never become zero and requires that vertical shore lines are introduced such that $H_{\text{shore}} > \max_{\text{along shore}} (|\xi|)$, as indicated in Fig. 4.15. In lakes $H \gg |\xi|$, over most part of the lake domain (except in shallow shore regions). Ignoring the latter, one may make use of the rigid lid assumption and drop in (4.101) ξ in comparison to H. In that case the barotropic potential vorticity is

$$\langle\pi\rangle_{bt}^{\text{rigid lid}} = \frac{\zeta + f}{H}. \qquad (4.102)$$

There is a second, alternative way of deriving (4.101), using a different potential vorticity, which equally leads to (4.100), (4.101). To see this, write (4.95) as

$$\begin{aligned} F_b &:= b(x, y, t) - z \equiv 0, \\ F_s &:= H(x, y) + b(x, y, t) + \xi(x, y, t) - z \equiv 0 \end{aligned} \qquad (4.103)$$

and observe that $H(x, y) + z = c_1 = \text{const}$. Then choose

$$\lambda_\varepsilon := \frac{H + z}{F_s - F_b + \varepsilon} = \frac{H + z}{H + \xi + \varepsilon} = \frac{c_1}{\varepsilon}, \qquad (4.104)$$

where $\varepsilon > 0$ is a small positive constant, which is needed to make λ_ε bounded in the entire lake domain. (We formally keep ε in all formulae and take the limit $\varepsilon \to 0$ in the final formulae.) With (4.104) we may define for a density preserving fluid ($\rho = \text{const}$)

$$\pi_H^\varepsilon = (\boldsymbol{w} + 2\boldsymbol{\Omega}) \cdot \text{grad}\,\lambda_\varepsilon = (\boldsymbol{w} + 2\boldsymbol{\Omega}) \cdot \text{grad}\left(\frac{H + z}{H + \xi + \varepsilon}\right)$$

and obtain with $\psi_{\lambda_\varepsilon} = 0$, the result $d\pi_{bt}/dt = 0$. In the shallow water approximation this reduces to

$$\pi_{bt}^{\varepsilon} = \frac{(\zeta + f)}{H + \xi + \varepsilon} \quad \underset{\varepsilon \to 0}{\longrightarrow} \quad \frac{\zeta + f}{H + \xi} \quad \underset{\xi \to 0}{\longrightarrow} \quad \frac{\zeta + f}{H}, \tag{4.105}$$

which is the same as (4.102). In (4.105) we have regularized the problem by choosing an adequate value for ε, whilst in (4.102) vertical shore lines were used to regularize the formula.

As an example, consider a column of homogeneous water in a current encompassing the entire depth of a real basin. Assume that the column is spinning (see **Fig. 4.16**) about its own axis, in the anti-clockwise direction on the Northern hemisphere, i.e. it has positive relative vorticity. What will happen if the rotating column moves into a region of greater depth? It will become longer and thinner, the water will spin faster, i.e., its relative vorticity will increase (i. e., become more positive). Looked at this from the point of view of angular momentum, the angular momentum of each particle of the water is $mr^2\omega$. When the column stretches, the average radius r decreases and so, for angular momentum to be conserved, the speed of rotation ω must increase. Because of the effect of changes of the length H of the water column, the property that is actually conserved is therefore not $(f + \zeta)$, the absolute vorticity, but $(f + \zeta)/H$, the potential vorticity.

(3) This is an example for a flow state under baroclinic conditions. Let

$$\lambda = \rho, \quad \frac{d\lambda}{dt} = \frac{d\rho}{dt} = -\rho \operatorname{div} \boldsymbol{v} = \psi_{\lambda},$$
$$\operatorname{grad} \psi_{\lambda} = \operatorname{grad}\left(\frac{d\rho}{dt}\right) = -\operatorname{grad}(\rho \operatorname{div} \boldsymbol{v}). \tag{4.106}$$

The **baroclinic potential vorticity** may then be defined as

$$\pi_{bc} = \pi_{\lambda = \rho} = \left(\frac{\boldsymbol{w} + 2\boldsymbol{\Omega}}{\rho}\right) \cdot \operatorname{grad} \rho, \tag{4.107}$$
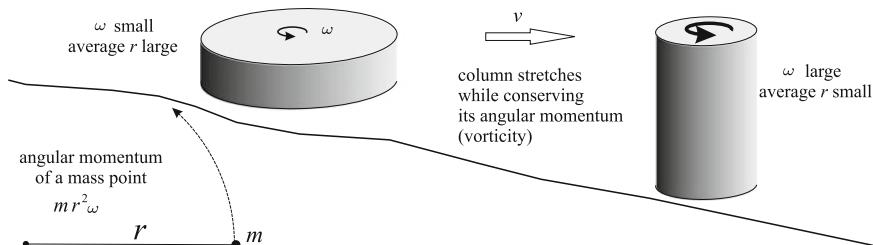
Fig. 4.16 Production of relative vorticity by the changes in the height of a fluid column. As the vertical fluid column moves from left to right, vertical stretching reduces the moment of inertia of the column, causing it to spin faster. The angular momentum of a particle of mass m moving with angular velocity ω in a circle of radius r is given by $mr^2\omega$ (after [1], with changes)

and the balance law of potential vorticity, (4.89) becomes

$$\frac{\mathrm{d}}{\mathrm{d}t}\left[\left(\frac{\boldsymbol{w}+2\boldsymbol{\Omega}}{\rho}\right)\cdot\operatorname{grad}\rho\right]=\left(\frac{\boldsymbol{w}+2\boldsymbol{\Omega}}{\rho}\right)\cdot\operatorname{grad}\left(\frac{\mathrm{d}\rho}{\mathrm{d}t}\right). \qquad (4.108)$$

So, in this case λ is strictly not conserved along particle trajectories, and neither is the baroclinic potential vorticity.

In the ocean or a lake under summer stratification, the density can be decomposed as

$$\rho(x,y,z,t)=\rho_0(z)+\rho'(x,y,z,t). \qquad (4.109)$$

In the metalimnion, i.e., the vicinity of the thermocline[10] we have $\rho_0 \gg \rho'$. Moreover, $\operatorname{grad}(\mathrm{d}\rho/\mathrm{d}t)=\operatorname{grad}(\mathrm{d}\rho'/\mathrm{d}t)$ can be expected to be very small. So, approximately in the shallow water approximation, for which $\tilde{f}=0$, the baroclinic potential vorticity reduces to

$$\pi_{bc}^{\mathrm{app}}\approx\frac{\zeta+f}{\rho_0}\frac{\mathrm{d}\rho_0}{\mathrm{d}z}\approx f\frac{1}{\rho_0}\frac{\mathrm{d}\rho_0}{\mathrm{d}z}, \qquad (4.110)$$

where the further approximation on the far right follows from the inequality $|\zeta|\ll f$. So, the potential vorticity π_{bc}^{app} is approximately conserved.

Formula $(4.110)_2$ is useful, because it allows the potential vorticity of various layers of a lake—epilimnion, metalimnion and hypolimnion—to be determined directly from hydrographic data without knowledge of the velocity field.

References

1. Bearman, G. (ed.): Ocean circulation. The Open University, p. 238. Butterworth-Heinemann, Oxford, Boston (1998)
2. Cosserat, E., Cosserat, F.: Théorie des corps déformables. Herrmann & Fils, Paris (1909)
3. Dietrich, G., Kalle, K., Krauss, W., Siedler, G.: General Oceanography, 2nd edn., Translated by Susanne and Hans Ulrich Roll. Wiley, New York (1980)
4. Ertel, H.: Ein neuer hydrodynamischer Erhaltungssatz. Die Naturwissenschaften. Jg. Heft 36 **30** 543–544 (1942)
5. Ertel, H.: Ein neuer hydrodynamischer Wirbelsatz. *Meteorologische Zeitschrift*, **59**. Jg. Heft **9**, 277–281 (1942)
6. Ertel, H.: Über hydrodynamische Wirbelsätze. Physik. Z. (Leipzig). Jg. Heft **59** 526–529 (1942)
7. Ertel, H.: Über das Verhältnis des neuen hydrodynamischen Wirbelsatzes zum Zirkulationssatz von V. Bjerknes. Meteorologische Zeitschrift. Jg. Heft 12 **59**, 161–168 (1942)
8. Hide, R.: The magnetic analogue of Ertel's potential vorticity theorem. Ann. Geophys. **1**(1), 59–60 (1983)

---

[10]The thermocline in a lake is that depth, where the vertical temperature gradient is largest.

9. Hutter, K., Jöhnk, K.: Continuum Methods of Physical Modeling, p. 635. Springer, Berlin (2004)
10. Hutter, K., Wang, Y., Chubarenko, I.: Physics of Lakes: Foundation of the Mathematical and Physical Background, vol. 1, p. XXViii+434. Springer, Berlin (2010)
11. Katz, J.: Relativistic potential vorticity. Proc. R. Soc. London A **391**, 415–418 (1984)
12. Möller, G.: Vortex-induced air entrainment rate at intakes. Mitteilung No. 220, Boes R.M. (ed.) Laboratory of Hydraulics, Hydrology and Glaciology, ETH Zurich (2013)
13. Pedlosky, J.: Geophysical Fluid Dynamics. Springer, Berlin (1982)
14. Schröder, W., Treder, H.-J.: Theoretical concepts and observational implications in meteorology and geophysics (Selected papers from the IAGA symposium to commemorate the 50th anniversary of Ertel's potential vorticity). Interdivisional commission on history of the International Association of Geomagnetism and Aeronomy. ISSN: 179-5658
15. Treder, H.-J.: Zur allgemeinen relativistischen und kovarianten Integralformen der Ertelschen Wirbeltheoreme. Gerlands Beitr. Geophys. **79**, 1 (1970)
16. Truesdell, C.A.: On Ertel's vorticity theorem. Zeitschrift für Angew. Math. & Phys. (ZAMP) **2**, 109–114 (1951)
17. Truesdell, C.A., Noll, W.: The non-linear field theories of mechanics In: Flügge S. (ed.) Encyclopedia of Physics, vol. III/3, p. 602. Berlin (1965)
18. Truesdell, C.A. and Toupin, R.C.: The Classical Field Theories of Mechanics Flügge, S. (ed.) Bd. III/1, Springer, Berlin (1960)
19. Zatsepin, A.G., Gritsenko, V.A., Kremenetsky, V.V., Poyarkov, S.G., Stroganov, OYu.: Laboratory and numerical investigation of process of propagation of density currents along bottom slope. Oceanology **45**(1), 5–15 (2005)

Chapter 5
An Almanac of Simple Flow Problems of Ideal Fluids

Abstract A primer on vector analysis lays the mathematical foundation used later in the chapter. GAUSS', Stokes' laws and the GREEN identities provide the mathematical prerequisites to determine a vector field from its sources and vortices. These concepts are then applied to potential flows due to a concentrated isotropic source, a doublet, parallel flows around a sphere and flows far away from compact three-dimensional source distributions. It is proved that (1) harmonic velocity fields of potential fields in a three-dimensional simply connected region subject to NEUMANN boundary condition delivers a unique velocity field; (2) that KELVIN's energy theorem holds, according to which the rotational motion in a simply connected region has the smaller kinetic energy than any other motion with the same NEUMANN boundary condition, and (3) the potential obeys the maximum-minimum principle, i.e. its maximum and minimum values are assumed on the boundary of the simply connected domain. Moreover, for steady potential flows around stationary three-dimensional rigid bodies, the force exerted by the fluid on the body vanishes. By contrast, the motion induced force on a body in general time dependent potential flow is given by the virtual added mass. These results change in plane potential flow around a two dimensional finite rigid region because the exterior of such a finite region is not simply connected, as already seen in Chap. 3. The interior two-dimensional problem, or the flow within the whole plane is a potential flow in a simply connected region. It is best treated with complex variable theory. Except for a few first examples, this technique is reserved to Chap. 6.

Keywords GAUSS, STOKES laws · GREEN's identities · Vortex free flow fields · Potential fields · Motion induced force on a body in potential flow · Plane flow configurations

List of Symbols

Roman Symbols

A, $\mathcal{A}$	Symbols for area
$A(\cdot) = 0$	Equation describing $\mathcal{A}$ or A
a	Radius of a sphere

$\dot{a}$	Growth rate of a
$\mathrm{d}\mathcal{A}, \mathrm{d}A, \mathrm{d}a$	Differential of areas
$b_k = -\dot{U}_\infty$	Inertial acceleration of a sphere by a parallel flow U
C, c	Constants of integration
d	Differential
$\mathrm{d}\boldsymbol{s}$	Vectorial length increment of a vortex filament
$\{\boldsymbol{e}_i\}$	Cartesian basis of unit vectors ($i = 1, 2, 3$)
$\iota = \sqrt{-1}$	Imaginary unit
J	JACOBIan determinant
$\{\boldsymbol{i}, \boldsymbol{j}, \boldsymbol{k}\}$	Standard orthonormal basis of a Cartesian coordinate system
$\boldsymbol{K}$	Force exerted on a body by a moving surrounding fluid
$\boldsymbol{M} = \int_V \boldsymbol{x} q \mathrm{d}v$	Dipole moment, doublet in V
$M' = \frac{2}{3}\pi a^3 \rho$	Virtual mass of a sphere
$m'_{ij} = m'_{ji}$	Tensor of virtual mass on an arbitrary body
$\boldsymbol{n}$	Unit normal vector on a smooth surface
$O, \mathcal{O}$	Origin of coordinates, oder symbol
P	Symbol for a point
p, p_∞	Pressure, – at infinity
$Q = \int_V q \mathrm{d}v$	Total source within V
Q_1, Q_2	Volume flux between the streamlines ψ_1 and ψ_2
q	Specific scalar valued source of a quantity per unit volume
R, r	Radial coordinates
$\mathcal{R}^n$	n-th dimensional real space
$\mathcal{R}$	Rotation matrix
$\boldsymbol{R}, \boldsymbol{r}$	Position vectors
$s, \mathrm{d}\boldsymbol{s}$	Arc length, vectorial length increment
T	Specific kinetic energy
$\boldsymbol{t}, t_{ij}, t_{xy}$	CAUCHY stress tensor (rank-2), components of $\boldsymbol{t}$
U, U_∞	Constant or time dependent x-velocity component of a body, of the fluid at ∞
u, v, w	Velocity components in the (x, y, z)-directions
$\boldsymbol{v}$	Velocity vector
V, V'	Volume, virtual volume of a sphere
$\boldsymbol{w} = \mathrm{curl}\, \boldsymbol{v}$	Vorticity vector of the velocity field $\boldsymbol{v}$
X, X, Y, Z	Position vector in the reference configuration, components of –
$\boldsymbol{x}, x, y, z$	Position vector in the present configuration, components of $\boldsymbol{x}$

Greek Symbols

Γ	Vorticity strength of a vortex filament per unit area, circulation
Δ	LAPLACE operator ($\Delta = \nabla^2$), symbol for length difference, symbol for increment

$\boldsymbol{\delta}, \delta_{ij}$	DIRAC matrix, $= 1$ if $i = j$, $= 0$ if $i \neq j$
δf	Symbol for increment of f
ε	Symbol for a small quantity
ε_{ijk}	ε tensor, LEVI- CIVITÁ tensor (rank-3)
ζ	z-component of the vorticity vector $\boldsymbol{w}$
$\boldsymbol{\xi} = (\xi, \eta, \zeta)$	Position vector
θ	Azimuthal coordinate, azimuth angle
ρ	Mass density per unit volume
ϕ, φ	Symbol for an unspecified function, velocity potential
ψ	Symbol for an unspecified function, stream function (2dim.)
$\psi(x, y, z) = \text{const.}, \chi(x, y, z) = \text{const.}$	Stream surfaces
$\Omega, d\Omega$	Solid angle, differential of solid angle
$\Omega = -U_\infty(t)x$	Potential of the inertial force of a translatorically moving non-inertial frame

Miscellaneous Symbols

grad $\boldsymbol{v}$, div $\boldsymbol{v}$, curl $\boldsymbol{v}$	Gradient, divergence rotation operators on $\boldsymbol{v}$
∇	Nabla operator
$\nabla \boldsymbol{v}, \nabla \cdot \boldsymbol{v}, \nabla \times \boldsymbol{v} = \text{curl } \boldsymbol{v}$	Gradient, divergence and curl of $\boldsymbol{v}$
$\boldsymbol{a} \cdot \boldsymbol{b}$	Inner product of $\boldsymbol{a}$ and $\boldsymbol{b}$
$\boldsymbol{a} \times \boldsymbol{b}$	Cross product of $\boldsymbol{a}$ and $\boldsymbol{b}$
$\boldsymbol{a} \otimes \boldsymbol{b}$	Dyadic (exterior) product of $\boldsymbol{a}$ and $\boldsymbol{b}$
$a \,\hat{=}\, b$	a and b are isomorphic to one another
$\phi, \phi = \phi + \iota\psi$	Complex potential of the real potential ϕ and the stream function in two dimensions

In this chapter a collection of simple flow problems of ideal fluids will be given. The intention is to build up knowledge of flow behavior in simple configurations of geometry and forces from which, by combination and extension, further solutions can be constructed. A second goal is to learn how such solutions are obtained by mathematical handling of the governing equations via the solution of boundary value problems. This automatically entails that a certain amount of mathematical technicalities must be employed. We, thus commence with well-known theorems of vector analysis, like GAUSS'[1] and STOKES'[2] Laws and GREEN's identities.[3] The latter will be applied to the POISSON equation. Then, we continue with the decomposition of an arbitrary but differentiable vector field into its vortex and source-free components, respectively; potential or harmonic fields are free of sources and vortices; they describe a large class of flows in two and three dimensions, which, as a whole, give rise to an interesting and useful collection of solutions for flow configurations of ideal fluids.

---

[1] For a short biography of GAUSS see Fig. 5.1.

[2] For a brief biography of George Gabriel Stokes see Chap. 7, Fig. 7.4, p. 358.

[3] For a short biography of GREEN see **Fig. 5.2**.

Fig. 5.1 Johann Carl Friedrich Gauss (30. April 1777–23. Feb. 1855)

Johann Carl Friedrich Gauss was a German mathematician and scientist who contributed significantly to number theory, statistics, analysis, differential geometry, geodesy, geophysics, electrostatics, astronomy and optics. Gauss was a child prodigy and he made his first ground-breaking mathematical discoveries while still a teenager. He completed *Disquisitiones Arithmeticae*, his magnum opus, in 1798 at the age of 21. He discovered a construction of the heptadecagon and invented modular arithmetic, greatly simplifying manipulations in number theory. Gauss proved the fundamental theorem of algebra which states that every non-constant single-variable polynomial over the complex numbers has at least one root. In 1831 Gauss developed a fruitful collaboration with the physicist Wilhelm Weber, leading to new knowledge in magnetism (including finding a representation for the unit of magnetism in terms of mass, length and time) and the discovery of Kirchhoff's circuit laws in electricity. He developed a method of measuring the horizontal intensity of the magnetic field which has been in use well into the second half of the 20th century and worked out the mathematical theory for separating the inner and outer sources of the Earth's magnetic field.

The text is partly based on http://www.wikipedia.org.

The portrait is published in *Astronomische Nachrichten* (1828)

Many of the detailed problems outlined and solved in this chapter can also be found in other books devoted to fluid mechanics. Mention might be made of [1, 2, 7].

Fig. 5.2 GEORGE GREEN (14. July 1793–31. May 1841)

GEORGE GREEN was a British mathematical physicist who wrote an Essay on the Application of Mathematical Analysis to the Theories of Electricity and Magnetism and fluid dynamics (Green 1828) [4, 5]. The essay introduced several important concepts, among them a theorem similar to the modern Green's theorem, the idea of potential functions as currently used in physics, and the concept of what are now called Green's functions. GREEN was the first person to create a mathematical theory of electricity and magnetism and applied it to fluids. His theory formed the foundation for the work of other scientists such as JAMES CLERK MAXWELL, WILLIAM THOMSON, and others. His work on potential theory ran parallel to that of CARL FRIEDRICH GAUSS.

Green's life story is remarkable in that he was almost entirely self-taught. He received only about one year of formal schooling as a child, between the ages of 8 and 9.

The text is based on http://www.wikipedia.org;
Portrait from: http://www.findagrave.com

5.1 General Concepts

5.1.1 A Primer on Vector Analysis

(a) The gradient:
Let $\mathcal{A} : A(x, y, z, t) = 0$ be a smooth, possibly moving surface in $\mathcal{R}^3$ and $\mathbf{n}(x, y, z, t)$ its oriented unit normal vector field. Moreover, let $\phi(x, y, z, t)$ and $\mathbf{v}(x, y, z, t)$ be a scalar and a vector field, defined in $\mathcal{R}^3 \cup \mathcal{R}^+$. For these we agree

on the definitions

$$\frac{d\phi}{dn} = (\text{grad } \phi) \cdot \boldsymbol{n}, \quad \frac{d\boldsymbol{v}}{dn} = (\text{grad } \boldsymbol{v})\boldsymbol{n} \tag{5.1}$$

and call $d\phi/dn$ and $d\boldsymbol{v}/dn$ the derivatives of ϕ and $\boldsymbol{v}$, respectively, perpendicular to $\mathcal{A}$. It seems clear how these concepts are applied to scalars and vectors in $\mathcal{R}^2$, where the surface becomes a line and $\boldsymbol{n}$ is the unit vector normal to this line. Generally, if $\boldsymbol{n}$ is any direction in $\mathcal{R}^3$ we may identify it with the orthonormal basis vectors $\{\boldsymbol{i}, \boldsymbol{j}, \boldsymbol{k}\}$ of a Cartesian coordinate system. Equation $(5.1)_1$ then yields

$$\begin{aligned}
\frac{d\phi}{di} &= [\text{grad } \phi] \cdot \boldsymbol{i} = \frac{\partial \phi}{\partial x}, \\
\frac{d\phi}{dj} &= [\text{grad } \phi] \cdot \boldsymbol{j} = \frac{\partial \phi}{\partial y}, \\
\frac{d\phi}{dk} &= [\text{grad } \phi] \cdot \boldsymbol{k} = \frac{\partial \phi}{\partial z},
\end{aligned} \tag{5.2}$$

so that

$$\text{grad } \phi = \frac{\partial \phi}{\partial x}\boldsymbol{i} + \frac{\partial \phi}{\partial y}\boldsymbol{j} + \frac{\partial \phi}{\partial z}\boldsymbol{k}. \tag{5.3}$$

Analogously, the gradient of a vector field $\boldsymbol{v} = v_1\boldsymbol{i} + v_2\boldsymbol{j} + v_3\boldsymbol{k}$ is defined by $(5.1)_2$ as

$$\frac{d\boldsymbol{v}}{dn} = [\text{grad } \boldsymbol{v}]\boldsymbol{n}. \tag{5.4}$$

With the choices $\boldsymbol{n} = \boldsymbol{i}, \boldsymbol{n} = \boldsymbol{j}, \boldsymbol{n} = \boldsymbol{k}$ one obtains the change of $\boldsymbol{v}$ along the straight lines parallel to the x-, y- and z-axes, respectively,

$$\begin{aligned}
\frac{d\boldsymbol{v}}{di} &= [\text{grad } \boldsymbol{v}]\boldsymbol{i} = \frac{\partial v_1}{\partial x}\boldsymbol{i} + \frac{\partial v_2}{\partial x}\boldsymbol{j} + \frac{\partial v_3}{\partial x}\boldsymbol{k}, \\
\frac{d\boldsymbol{v}}{dj} &= [\text{grad } \boldsymbol{v}]\boldsymbol{j} = \frac{\partial v_1}{\partial y}\boldsymbol{i} + \frac{\partial v_2}{\partial y}\boldsymbol{j} + \frac{\partial v_3}{\partial y}\boldsymbol{k}, \\
\frac{d\boldsymbol{v}}{dk} &= [\text{grad } \boldsymbol{v}]\boldsymbol{k} = \frac{\partial v_1}{\partial z}\boldsymbol{i} + \frac{\partial v_2}{\partial z}\boldsymbol{j} + \frac{\partial v_3}{\partial z}\boldsymbol{k},
\end{aligned} \tag{5.5}$$

or in matrix notation

$$\text{grad } \boldsymbol{v} = \begin{pmatrix} \dfrac{\partial v_1}{\partial x} & \dfrac{\partial v_1}{\partial y} & \dfrac{\partial v_1}{\partial z} \\[2mm] \dfrac{\partial v_2}{\partial x} & \dfrac{\partial v_2}{\partial y} & \dfrac{\partial v_2}{\partial z} \\[2mm] \dfrac{\partial v_3}{\partial x} & \dfrac{\partial v_3}{\partial y} & \dfrac{\partial v_3}{\partial z} \end{pmatrix}, \tag{5.6}$$

in which the components of the vectors $\mathrm{d}\boldsymbol{v}/\mathrm{d}i$, $\mathrm{d}\boldsymbol{v}/\mathrm{d}j$, $\mathrm{d}\boldsymbol{v}/\mathrm{d}k$ are collected as columns of the 3×3 matrix (5.6). In this representation the expression $[\mathrm{grad}\ \boldsymbol{v}]\boldsymbol{n}$ is to be understood as multiplication of the matrix $[\mathrm{grad}\ \boldsymbol{v}]$ with the column vector $\boldsymbol{n}$.

(b) The Gauss law(s):

We suggest the plural in this title even though the mathematical literature uses it primarily in the singular in its divergent form. There are, however, a multitude of versions. The basic statement is as follows: For any differentiable scalar field $\phi(\boldsymbol{x}, t)$ in a volume V with boundary $\mathcal{A}$ the basic lemma is

$$\iint_{\mathcal{A}} \phi n_i \, \mathrm{d}a = \iiint_{V} \frac{\partial \phi}{\partial x_i} \, \mathrm{d}v, \quad i = 1, 2, 3. \tag{5.7}$$

The integral of $\phi\boldsymbol{n}$ over the body boundary $\mathcal{A}$ equals the volume integral of the gradient of ϕ over the body volume V bounded by $\mathcal{A}$. The result (5.7) could be called the *gradient version* of GAUSS' *law*. A proof of (5.7) is given in Appendix 5.A to this chapter.[4] The reader may accept (5.7) in a first reading and may then continue to the many corollaries of the above statement.

The function ϕ in (5.7) is a scalar. The Cartesian components of a vector field $\boldsymbol{v}$ can also be interpreted as scalar quantities. Applying (5.7) to such a field yields

$$\iint_{\mathcal{A}} v_i n_j \, \mathrm{d}a = \iiint_{V} \frac{\partial v_i}{\partial x_j} \, \mathrm{d}v \quad \text{(for fixed } i, j = 1, 2, 3). \tag{5.8}$$

If i is set equal to j and summation is applied over doubly repeated indices, then (5.8) becomes

$$\iint_{\mathcal{A}} v_i n_i \, \mathrm{d}a = \iiint_{V} \frac{\partial v_i}{\partial x_i} \, \mathrm{d}v \quad \Longleftrightarrow \quad \iint_{\mathcal{A}} \boldsymbol{v} \cdot \boldsymbol{n} \, \mathrm{d}a = \iiint_{V} \mathrm{div}\ \boldsymbol{v} \, \mathrm{d}v. \tag{5.9}$$

This is called the *divergence theorem* and is almost exclusively identified as the *Gauss law*.

Similarly, for the cross product of $\boldsymbol{v}$ and $\boldsymbol{n}$ (5.7) implies

$$\iint_{\mathcal{A}} \boldsymbol{v} \times \boldsymbol{n} \, \mathrm{d}a = \iiint_{V} \mathrm{curl}\ \boldsymbol{v} \, \mathrm{d}v \quad \Longleftrightarrow \quad \iint_{\mathcal{A}} \varepsilon_{ijk} v_j n_k \, \mathrm{d}a = \iiint_{V} \varepsilon_{ijk} \frac{\partial v_j}{\partial x_k} \, \mathrm{d}v. \tag{5.10}$$

---

[4]Proofs of the GAUSS law or the divergence theorem and the STOKES theorem treated below are given in many books on engineering mathematics or in basic analysis courses of functions of several variables. We list just a few as alternatives to the proofs demonstrated in the appendices to this chapter [6, 10–12].

For a second rank tensor t with Cartesian components t_{ij} one may form $t_{ij}n_k$ to deduce the statement

$$\iint_{\mathcal{A}} t_{ij}n_k \, \mathrm{d}a = \iiint_V \frac{\partial t_{ij}}{\partial x_k} \, \mathrm{d}v. \tag{5.11}$$

More significant are those versions of (5.11), in which the index k is identified with the indices i or j and the summation rule is applied:

$$\iint_{\mathcal{A}} t_{ij}n_j \, \mathrm{d}a = \iiint_V \frac{\partial t_{ij}}{\partial x_j} \, \mathrm{d}v \iff \iint_{\mathcal{A}} t n \, \mathrm{d}a = \iiint_V \mathrm{div}_R t \, \mathrm{d}v,$$

$$\iint_{\mathcal{A}} n_i t_{ij} \, \mathrm{d}a = \iiint_V \frac{\partial t_{ij}}{\partial x_i} \, \mathrm{d}v \iff \iint_{\mathcal{A}} n t \, \mathrm{d}a = \iiint_V \mathrm{div}_L t \, \mathrm{d}v. \tag{5.12}$$

This result shows that a rank-2 tensor possesses a right and left divergence. It is easy to show that for

$$t = \begin{pmatrix} t_{11} \ t_{12} \ t_{13} \\ t_{21} \ t_{22} \ t_{33} \\ t_{31} \ t_{32} \ t_{33} \end{pmatrix} \tag{5.13}$$

these divergences are given by

$$\mathrm{div}_R t = \begin{pmatrix} \dfrac{\partial t_{11}}{\partial x} + \dfrac{\partial t_{12}}{\partial y} + \dfrac{\partial t_{13}}{\partial z} \\ \dfrac{\partial t_{21}}{\partial x} + \dfrac{\partial t_{22}}{\partial y} + \dfrac{\partial t_{23}}{\partial z} \\ \dfrac{\partial t_{31}}{\partial x} + \dfrac{\partial t_{32}}{\partial y} + \dfrac{\partial t_{33}}{\partial z} \end{pmatrix}, \quad \mathrm{div}_L t = \begin{pmatrix} \dfrac{\partial t_{11}}{\partial x} + \dfrac{\partial t_{21}}{\partial y} + \dfrac{\partial t_{31}}{\partial z} \\ \dfrac{\partial t_{12}}{\partial x} + \dfrac{\partial t_{22}}{\partial y} + \dfrac{\partial t_{32}}{\partial z} \\ \dfrac{\partial t_{13}}{\partial x} + \dfrac{\partial t_{23}}{\partial y} + \dfrac{\partial t_{33}}{\partial z} \end{pmatrix}. \tag{5.14}$$

In the mathematical literature div is chiefly interpreted as div_R, whereas in the engineering literature div is often used as div_L. In this book we use $\mathrm{div} = \mathrm{div}_R$.

It is now clear how any desired version of the GAUSS law can be constructed with combinations of products of components of tensor quantities.

(c) The Stokes law(s):
The rotation, curl , of a vector field describes the vectorial vortex strength of the field v. In Cartesian coordinates it is computed according to

$$\mathrm{curl}\, v = \left(\frac{\partial v_3}{\partial y} - \frac{\partial v_2}{\partial z} \right) i + \left(\frac{\partial v_1}{\partial z} - \frac{\partial v_3}{\partial x} \right) j + \left(\frac{\partial v_2}{\partial x} - \frac{\partial v_1}{\partial y} \right) k. \tag{5.15}$$

It can formally be evaluated as a determinant as follows

$$\operatorname{curl} \boldsymbol{v} = \begin{vmatrix} \boldsymbol{i} & \boldsymbol{j} & \boldsymbol{k} \\ \dfrac{\partial}{\partial x} & \dfrac{\partial}{\partial y} & \dfrac{\partial}{\partial z} \\ v_1 & v_2 & v_3 \end{vmatrix}. \tag{5.16}$$

To introduce STOKES' theorem, let $\boldsymbol{v}$ be a differentiable vector field over $\mathcal{R}^3$. Let, moreover, $\mathcal{C}$ be a closed double point free smooth curve in $\mathcal{R}^3$. Then, $\oint_{\mathcal{C}} \boldsymbol{v} \cdot \mathrm{d}\boldsymbol{x}$ is called the circulation of $\boldsymbol{v}$ around $\mathcal{C}$.[5] The STOKES law allows to relate the surface integral over $\mathcal{A}$ of the curl of the vector field $\boldsymbol{v}$ to its circulation

$$\oint_{\mathcal{C}} \boldsymbol{v} \cdot \mathrm{d}\boldsymbol{x} = \iint_{\mathcal{A}} (\operatorname{curl} \boldsymbol{v}) \cdot \boldsymbol{n} \, \mathrm{d}a. \tag{5.17}$$

This is STOKES law, but there are again several variants to it. It is proved in Appendix 5.B to this chapter. Alternative forms are obtained by choosing $\boldsymbol{v} = \varphi \left(\boldsymbol{e}_x, \boldsymbol{e}_y, \boldsymbol{e}_z \right)$:

$$\begin{aligned} \oint_{\mathcal{C}} (\varphi \boldsymbol{e}_x) \cdot \mathrm{d}\boldsymbol{x} &= \oint_{\mathcal{C}} \varphi \mathrm{d}x = \iint_{\mathcal{A}} \operatorname{curl} (\varphi \boldsymbol{e}_x) \cdot \boldsymbol{n} \, \mathrm{d}a = \iint_{\mathcal{A}} \left(\frac{\partial \varphi}{\partial z} n_y - \frac{\partial \varphi}{\partial y} n_z \right) \mathrm{d}a, \\ \oint_{\mathcal{C}} (\varphi \boldsymbol{e}_y) \cdot \mathrm{d}\boldsymbol{x} &= \oint_{\mathcal{C}} \varphi \mathrm{d}y = \iint_{\mathcal{A}} \operatorname{curl} (\varphi \boldsymbol{e}_y) \cdot \boldsymbol{n} \, \mathrm{d}a = \iint_{\mathcal{A}} \left(\frac{\partial \varphi}{\partial x} n_z - \frac{\partial \varphi}{\partial z} n_x \right) \mathrm{d}a, \quad (5.18) \\ \oint_{\mathcal{C}} (\varphi \boldsymbol{e}_z) \cdot \mathrm{d}\boldsymbol{x} &= \oint_{\mathcal{C}} \varphi \mathrm{d}z = \iint_{\mathcal{A}} \operatorname{curl} (\varphi \boldsymbol{e}_z) \cdot \boldsymbol{n} \, \mathrm{d}a = \iint_{\mathcal{A}} \left(\frac{\partial \varphi}{\partial y} n_x - \frac{\partial \varphi}{\partial x} n_y \right) \mathrm{d}a, \end{aligned}$$

which can be collected as the vector relation

$$\oint_{\mathcal{C}} \varphi \mathrm{d}\boldsymbol{x} = - \iint_{\mathcal{A}} (\operatorname{grad} \varphi) \times \boldsymbol{n} \, \mathrm{d}a. \tag{5.19}$$

If one substitutes in this last relation v_i for φ, one obtains

$$\oint_{\mathcal{C}} v_i \mathrm{d}\boldsymbol{x} = - \iint_{\mathcal{A}} (\operatorname{grad} v_i) \times \boldsymbol{n} \, \mathrm{d}a. \tag{5.20}$$

---

[5]Note that $\mathcal{C}$ need not lie in a plane; it may be three dimensional. Note, moreover, that the area $\mathcal{A}$ spanned over $\mathcal{C}$ may equally be a surface in $\mathcal{R}^3$; it need not be flat, and it is not unique.

This last formula leads to a further useful formula as follows

$$\sum_i \boldsymbol{e}_i \times \oint_{\mathfrak{e}} v_i \mathrm{d}\boldsymbol{x} = \oint_{\mathfrak{e}} \boldsymbol{v} \times \mathrm{d}\boldsymbol{x}$$

$$= -\iint_{\mathcal{A}} \underbrace{\sum_i \boldsymbol{e}_i \times (\mathrm{grad}\, v_i \times \boldsymbol{n})}_{-\mathrm{curl}\, \boldsymbol{v}}\, \mathrm{d}a = \iint_{\mathcal{A}} (\mathrm{curl}\, \boldsymbol{v}) \times \boldsymbol{n}\, \mathrm{d}a. \qquad (5.21)$$

A wealth of further formulae can also be derived, as is easily seen from the construction of the above formulae.

(d) Green's identities:
GREEN's identities follow from GAUSS' law by choosing in (5.9) instead of $\boldsymbol{v}$ the quantity $\phi\boldsymbol{v}$, where both ϕ and $\boldsymbol{v}$ are differentiable. This process yields

$$\iiint_V \mathrm{div}\,(\phi\boldsymbol{v})\, \mathrm{d}v = \iiint_V (\phi\, \mathrm{div}\, \boldsymbol{v} + \boldsymbol{v} \cdot \mathrm{grad}\, \phi)\, \mathrm{d}v = \iint_{\mathcal{A}} \phi\boldsymbol{v} \cdot \boldsymbol{n}\, \mathrm{d}a. \quad (5.22)$$

If we specialize here $\boldsymbol{v}$ as a gradient field, $\boldsymbol{v} = \mathrm{grad}\, \psi$, this leads directly to the **First Green Identity**

$$\iiint_V (\mathrm{grad}\, \phi \cdot \mathrm{grad}\, \psi)\, \mathrm{d}v = -\iiint_V \phi \Delta \psi\, \mathrm{d}v + \iint_{\mathcal{A}} \phi \frac{\partial \psi}{\partial n}\, \mathrm{d}a. \qquad (5.23)$$

Writing down (5.23) again with the roles of ϕ and ψ exchanged and subtracting the two expressions leads directly to the **Second** GREEN **Identity**

$$\iiint_V (\phi \Delta \psi - \psi \Delta \phi)\, \mathrm{d}a = \iint_{\mathcal{A}} \left(\phi \frac{\partial \psi}{\partial n} - \psi \frac{\partial \phi}{\partial n} \right)\, \mathrm{d}a. \qquad (5.24)$$
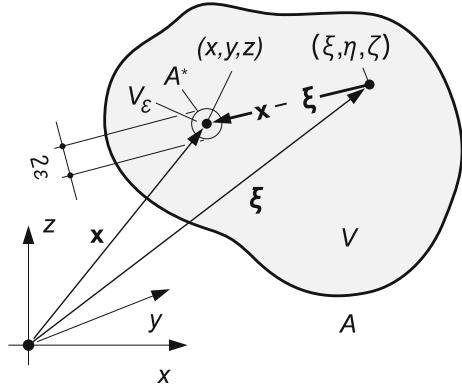
(e) Application:
The Second GREEN Identity can effectively be used to construct certain particular solutions to the POISSON equation[6]

$$\Delta \phi = f(\boldsymbol{x}), \quad \text{in } V \subset \mathcal{R}^3, \qquad (5.25)$$

subject to certain boundary conditions. They will become apparent when a solution is constructed. Let us select in (5.24)

---

[6]For a short biography of POISSON see Fig. 8.6.

Fig. 5.3 Explaining the application of the Second GREEN Identity (5.24), when ψ is given by (5.26). *Because the function $1/r$ is singular as $r \to 0$ we cut out a sphere of radius ε and center at $\boldsymbol{x}$ and apply (5.24) for $V\backslash V_\varepsilon$ and $A \cup A^*$*

$$\psi = \frac{1}{r}, \quad r = \sqrt{(x-\xi)^2 + (y-\eta)^2 + (z-\zeta)^2}, \tag{5.26}$$

where r is the distance between the two points $\boldsymbol{x} = (x, y, z)$, $\boldsymbol{\xi} = (\xi, \eta, \zeta)$ of which both lie in V, see **Fig. 5.3**. We treat (x, y, z) as the point at which ϕ is evaluated and (ξ, η, ζ) as the independent variables over which the integrals in (5.24) are to be evaluated. The function ψ in (5.26)$_1$ has a singularity at $\boldsymbol{x} = \boldsymbol{\xi}$, i.e., as $r \to 0$. For all other values of $\boldsymbol{x} \neq \boldsymbol{\xi}$, $\psi = 1/r$ satisfies the LAPLACE equation, $\Delta_{\boldsymbol{x}}\psi = 0$ (or $\Delta_{\boldsymbol{\xi}}\psi = 0$). We, thus, cut out a small sphere with radius ε and center at $\boldsymbol{x}$. For the volume $(V\backslash V_\varepsilon)$ the prerequisites of the Second GREEN Identity are then satisfied since $\Delta\psi = 0$ in $V\backslash V_\varepsilon$. Equations (5.24)–(5.26), therefore, imply

$$-\iiint\limits_{V\backslash V_\varepsilon} \frac{f}{r}\, dv = \iint\limits_{A\cup A^*} \left\{ \phi\frac{\partial(1/r)}{\partial n} - \frac{1}{r}\frac{\partial\phi}{\partial n} \right\} da. \tag{5.27}$$

Let us estimate the integrals over A^* on the right-hand side of this equation:

$$(i) \ \lim_{\varepsilon\to 0} \iint\limits_{A^*} \phi\frac{\partial}{\partial n}\left(\frac{1}{r}\right) da \overset{(1)}{=} -\lim_{\varepsilon\to 0}\left\{ \phi^* \iint\limits_{A^*} \frac{\partial}{\partial r}\left(\frac{1}{r}\right) da + \mathcal{O}(\varepsilon^3) \right\}$$

$$\overset{(2)}{=} \lim_{\varepsilon\to 0}\left\{ \phi(\boldsymbol{x}) \iint\limits_{A^*} \frac{1}{r^2}r^2 d\Omega \right\} \overset{(3)}{=} 4\pi\phi(\boldsymbol{x}), \tag{5.28}$$

$$(ii) \ \lim_{\varepsilon\to 0} \iint\limits_{A^*} \frac{1}{r}\frac{\partial\phi}{\partial n} \underbrace{da}_{r^2 d\Omega} = \frac{\mathcal{O}(\varepsilon^2)}{\mathcal{O}(\varepsilon)} = \mathcal{O}(\varepsilon) \to 0, \quad \text{as } \varepsilon \to 0.$$

In this chain of identities step "$\stackrel{(1)}{=}$" employs the mean value theorem where ϕ^* is the mean value of ϕ on the surface A^* for which the limit value is $\phi(\boldsymbol{x})$. Moreover, $\mathrm{d}a$ is $r^2\mathrm{d}\Omega$, where $\mathrm{d}\Omega$ is the solid angle on the unit sphere, which explains step "$\stackrel{(2)}{=}$". The value of the integral $\iint_{A^*} \mathrm{d}\Omega = 4\pi$, explaining step "$\stackrel{(3)}{=}$". In the second term on the right-hand side of (5.27), $\partial\phi/\partial n$ is bounded in the vicinity of the point $\boldsymbol{x}$.

Substituting (5.28) into (5.27) yields the final result

$$\phi(\boldsymbol{x}) = -\frac{1}{4\pi} \iiint_V \frac{f}{r}\,\mathrm{d}v - \frac{1}{4\pi} \iint_A \left\{\phi\frac{\partial}{\partial n}\left(\frac{1}{r}\right) - \frac{1}{r}\frac{\partial\phi}{\partial n}\right\} \mathrm{d}a. \qquad (5.29)$$

By explicit differentiation it can be shown that the first term on the right-hand side of (5.29) is a particular solution of the equation $\Delta\phi = f$,

$$\phi(\boldsymbol{x}) = -\frac{1}{4\pi} \iiint_V \frac{f(\xi, \eta, \zeta)\,\mathrm{d}\xi\mathrm{d}\eta\mathrm{d}\zeta}{\sqrt{(x - \xi)^2 + (y - \eta)^2 + (z - \zeta)^2}}. \qquad (5.30)$$

The representation (5.29) shows how $\phi(\boldsymbol{x})$ depends upon the boundary values of ϕ and $\partial\phi/\partial n$.

5.1.2   Determination of a Vector Field from Its Sources and Vortices

In this section, we wish to answer the following question.

Question: *Consider a body volume V with boundary ∂V. Let*[7]

 (i) *a scalar field $q(\boldsymbol{x})$,*
(ii) *a vector field $\boldsymbol{w}(\boldsymbol{x})$ with div $\boldsymbol{w}(\boldsymbol{x}) = 0$*

be given. Construct in V a vector field $\boldsymbol{v}$ such that

$$\operatorname{div} \boldsymbol{v} = q, \qquad \operatorname{curl} \boldsymbol{v} = \boldsymbol{w}, \qquad \text{in } V \qquad (5.31)$$

and such that $\boldsymbol{v}$ satisfies on ∂V certain boundary conditions, which later will be identified.   □

The function $q(\boldsymbol{x})$ is the source field and $\boldsymbol{w}$ is the vortex field.

---

[7]The functions $q(\boldsymbol{x}, t)$, $\boldsymbol{w}(\boldsymbol{x}, t)$ and $\boldsymbol{v}(\boldsymbol{x}, t)$ may also depend on time t, but this dependence shall not be made explicit in the analysis which follows.

We approach this problem by decomposing the field $\boldsymbol{v}$ additively as

$$\boldsymbol{v} = \boldsymbol{v}_1 + \boldsymbol{v}_2 + \boldsymbol{v}_3, \tag{5.32}$$

in which the three different fields are subject to the following constraints:

$$(i) \quad \left\{ \begin{array}{l} \text{div } \boldsymbol{v}_1 = q \\ \text{curl } \boldsymbol{v}_1 = \boldsymbol{0} \end{array} \right\} \text{ define a vortex-free velocity field,} \tag{5.33}$$

$$(ii) \quad \left\{ \begin{array}{l} \text{div } \boldsymbol{v}_2 = 0 \\ \text{curl } \boldsymbol{v}_2 = \boldsymbol{w} \end{array} \right\} \text{ define a source-free velocity field,} \tag{5.34}$$

$$(iii) \quad \left\{ \begin{array}{l} \text{div } \boldsymbol{v}_3 = 0 \\ \text{curl } \boldsymbol{v}_3 = \boldsymbol{0} \end{array} \right\} \text{ define a harmonic velocity field.} \tag{5.35}$$

It is the goal to satisfy with $\boldsymbol{v}_1$ and $\boldsymbol{v}_2$ the source and vorticity conditions, and to match with $\boldsymbol{v}_3$ certain boundary conditions.

(a) Vortex-free irrotational fields $\boldsymbol{v}_1$:
Because curl $\boldsymbol{v}_1 = \boldsymbol{0}$, it is tempting to derive $\boldsymbol{v}_1$ from a scalar field φ such that

$$\boldsymbol{v}_1 = \text{grad } \varphi.$$

With this choice, a differentiable $\boldsymbol{v}_1$ is automatically irrotational. Satisfaction of $(5.33)_1$ implies then

$$\text{div } \boldsymbol{v}_1 = \text{div grad } \varphi = \Delta\varphi = q(\boldsymbol{x}). \tag{5.36}$$
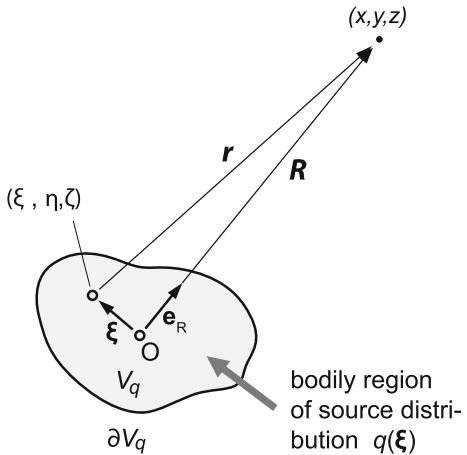
The potential φ must satisfy the POISSON equation. It says that all solutions for the velocity potential φ, which satisfy the POISSON equation, lead to an irrotational velocity field. A particular integral of (5.36) possesses the form (5.30), or explicitly

$$\varphi(\boldsymbol{x}) = -\frac{1}{4\pi} \iiint\limits_V \frac{q(\boldsymbol{\xi})}{|\boldsymbol{x} - \boldsymbol{\xi}|} \, dv(\boldsymbol{\xi}). \tag{5.37}$$

Simple differentiation of this expression determines the velocity field belonging to it, viz.,

$$\boldsymbol{v}_1 = -\frac{1}{4\pi} \text{grad} \iiint\limits_V \frac{q(\boldsymbol{\xi})}{r} \, dv = -\frac{1}{4\pi} \iiint\limits_V \text{grad}_x \left(\frac{q(\boldsymbol{\xi})}{r(\boldsymbol{x}, \boldsymbol{\xi})} \right) dv$$

$$= \frac{1}{4\pi} \iiint\limits_V \frac{q(\boldsymbol{\xi})}{r^3} \boldsymbol{r} \, dv = \frac{1}{4\pi} \iiint\limits_V \frac{q(\boldsymbol{\xi})}{|\boldsymbol{x} - \boldsymbol{\xi}|^3} (\boldsymbol{x} - \boldsymbol{\xi}) \, dv. \tag{5.38}$$

Fig. 5.4 Explaining the multipole representation of the flow (at point x) far away from a bodily region V_q, where the source distribution q is given. The origin of the coordinates lies within V_q

In the second expression of the first line, the subscript $(\cdot)_x$ of grad_x indicates that differentiation must be executed with respect to the variable x (and not ξ). As a further property, (5.38) also implies

$$\iiint_V \operatorname{div} \boldsymbol{v}_1 \, \mathrm{d}v = \iiint_V q(\boldsymbol{\xi}) \, \mathrm{d}v = \iint_{\mathcal{A}} \boldsymbol{v}_1 \cdot \boldsymbol{n} \, \mathrm{d}a. \tag{5.39}$$

The integral on the far right of this equation expresses the flow through the boundary of V normal to $\mathcal{A}$. It equals the total sum of the specific sources within V or: The sum of all sources in V equals the sum of volume flow through the boundary $\mathcal{A}$ of V.

Let us look at a number of simple *applications*.

(1) Asymptotic behavior of an irrotational velocity field $\boldsymbol{v}_1$ far away from a body carrying a source distribution q within a finite volume V_q. Our interest is in the general form of the fields φ or $\boldsymbol{v}_1$ at a large distance from V_q. Let us select the origin of the Cartesian coordinate system at a point inside of V_q; the point ξ, identifying the prescribed source lies within V_q, and point x is far away from V_q, see **Fig. 5.4**, which shows the definitions of the vectors $\boldsymbol{r}$, $\boldsymbol{R}$ and ξ. With reference to this figure we then have

$$\begin{aligned}
\boldsymbol{r} &= (\boldsymbol{R} - \boldsymbol{\xi}), \quad \boldsymbol{R} = (x, y, z), \quad \boldsymbol{\xi} = (\xi, \eta, \zeta), \\
\boldsymbol{r} &= (x - \xi, y - \eta, z - \zeta), \\
\frac{1}{r} &= \left\{ (x - \xi)^2 + (y - \eta)^2 + (z - \zeta)^2 \right\}^{-1/2}.
\end{aligned} \tag{5.40}$$

Moreover, because $|\xi| \ll |R|$, the function $1/r$ can be expanded into a TAYLOR series at $\xi = 0$, of which the first two members are given by

$$\frac{1}{r} = \frac{1}{R} - \xi \cdot \mathrm{grad}_x \frac{1}{R} + \dots = \frac{1}{R} + \frac{\xi \cdot e_R}{R^2} + \dots . \tag{5.41}$$

If this result is substituted into (5.37), one obtains

$$\varphi(x) \sim -\frac{1}{4\pi R} \underbrace{\left(\iiint_V q \, dv \right)}_{Q \, = \, \text{total source}} - \frac{1}{4\pi R^2} \underbrace{\left(\iiint_V \xi q(\xi) dv \right)}_{M \, = \, \left\{ \begin{array}{l} \text{dipole moment of the} \\ \text{distribution of } q(\xi) \end{array} \right\}} \cdot e_R, \tag{5.42}$$

so that

$$\varphi(x) \sim -\frac{Q}{4\pi R} - \frac{M \cdot e_R}{4\pi R^2},$$

$$\tag{5.43}$$

$$v_1(x) \sim \frac{Q}{4\pi R^2} e_R - \frac{1}{4\pi} \mathrm{grad}_x \frac{M \cdot e_R}{R^2} + \dots .$$

These expressions are the first two members of a multipole expansion of φ and v_1, respectively. We further note that when $Q = 0$, M is independent of the origin of the coordinate axes. M is then simply called the dipole moment of the distribution of the sources. To demonstrate this property we impose the rigid body transformation $\xi = \xi_T + \mathcal{R}\xi_R$, where ξ_T is a constant translation, which shifts the origin O to O', $\mathcal{R}$ is a constant rotation matrix, which rotates the Cartesian frame in O' relative to that in O. Using the definition of M in (5.42) and substituting for ξ the above rigid body translation, we find

$$M_O = \xi_T Q + \mathcal{R} \iiint_{V_q} \xi_R q \, dv = \xi_T Q + \mathcal{R} M_{O'}. \tag{5.44}$$

If $Q = 0$, then $M_O = \mathcal{R} M_{O'}$, which reduces to $M_O = M_{O'}$, if $\mathcal{R} = I$, else $M_O = \mathcal{R} M_{O'}$. This says that the value of M is independent of the choice of the origin and formula (5.44) shows how the components of the dipole moment transform under rotation of the coordinate system.

For an *isotropic singular point source*, i.e. an isotropic DIRAC[8] pulse with $q = 0$ for $|\xi| \neq 0$, but $q = \infty$ for $|\xi| = 0$, such that $\iiint_{V_q} q \, dv = Q$ and $M = 0$, formulae (5.43) reduce to

---

[8]For a short biography of DIRAC see **Fig. 5.5**.

Some properties of the δ-function:

- $\delta(x) = \begin{cases} 0, & x \neq 0, \quad |x| \in (0, \infty] \\ \infty, & x = 0, \end{cases}$

- $\displaystyle\int_{-\infty}^{\infty} \delta(x)\,\mathrm{d}x = 1,$

- $\delta(x) = \displaystyle\lim_{a \to 0}\left\{\frac{1}{\sqrt{\pi a}}\exp\left[\left(-\frac{x}{a}\right)^2\right]\right\}$

Fig. 5.5 Paul Adrein Maurice Dirac (8. Aug. 1902–20. Oct. 1984)

Paul Adrein Maurice Dirac was a famous quantum physicist, who won together with Scrödinger the 1933 Nobel Prize in Physics. He introduced the generalized function (distribution) $\delta(x) = 0$, for $x \neq 0$, but $\delta(0) = \infty$, such that $\int_{-\infty}^{\infty}\delta(x)\,\mathrm{d}x = 1$.

Dirac's working field was quantum physics. He gained international recognition in particular through his development of relativistic quantum mechanics. He earned his doctoral degree in 1926 in mathematical physics at the Cambridge University, England, was there fellow of the Saint John's College and received in 1932, at the age of 30 years, the Lucasian chair of mathematics, the chair once occupied by Isaac Newton.

The text is based on http://www.wikipedia.org

$$\varphi = -\frac{Q}{4\pi R} \quad \text{and} \quad \boldsymbol{v}_1 = \frac{Q}{4\pi R^2}\boldsymbol{e}_R. \tag{5.45}$$

This velocity field can naturally be obtained from a volume (or mass) balance equating the total mass production in a sphere of radius R to the flow of volume (mass) through the spherical surface with radius R; this yields $Q = 4\pi R^2 v_1(R)$, which agrees with $(5.45)_2$.
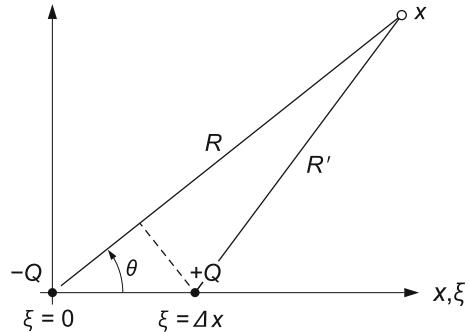
(2) Doublets are source-sink arrangements of point sources (one negative, one positive) which lead to a dipole induced flow, see **Fig. 5.6**. The velocity potential is in this case given by

$$\varphi = \frac{Q}{4\pi}\left\{\frac{1}{R} - \frac{1}{R'}\right\} \tag{5.46}$$

and is nothing else than a superposition of two singular point sources. When $|\Delta x| \ll \{R, R'\}$, we have approximately $R' = R - \Delta x \cos\theta$, or

$$\frac{1}{R'} = \frac{1}{R\left(1 - \frac{\Delta x}{R}\cos\theta\right)} = \frac{1}{R} + \frac{\Delta x}{R^2}\cos\theta. \tag{5.47}$$

Fig. 5.6 Two point sources ($-Q$ at $\xi = 0$ and $+Q$ at $\xi = \Delta x$) generate in the limit as $\Delta x \to 0$ a dipole flow field, also called a doublet field

Substituting (5.47) into (5.46) yields

$$
\begin{aligned}
\varphi &= -\frac{Q\Delta x}{4\pi R^2}\cos\theta = -\frac{\boldsymbol{M}\cdot\boldsymbol{e}_R}{4\pi R^2} &&(\boldsymbol{M} = Q\Delta x\boldsymbol{e}_x), \\
v_r &= \frac{Q\Delta x}{4\pi R^3}\cos\theta, \quad v_\theta = \frac{Q\Delta x}{4\pi R^3}\sin\theta &&(|\boldsymbol{M}| = Q\Delta x),
\end{aligned}
\tag{5.48}
$$

in which v_r and v_θ are the radial and meridional velocity components.

(3) Flows around a sphere: The above flow induced by a doublet has an immediate application in the construction of an irrotational flow around a sphere. To this end we choose in (5.48) the dipole as

$$
\boldsymbol{M} = -2\pi U_\infty a^3 \boldsymbol{e}_x,
\tag{5.49}
$$

in which U_∞ is a reference velocity (later identified as the constant upstream velocity of a steady parallel flow) and a is a reference length (later identified as the radius of the sphere). With the choice (5.49) the potential (5.48) takes the form

$$
\varphi_1 = \frac{1}{2}\frac{U_\infty a^3}{R^3}x, \qquad R^2 = x^2 + y^2 + z^2,
\tag{5.50}
$$

in which $\boldsymbol{e}_x \cdot \boldsymbol{e}_R = \cos\theta = x/R$ was substituted. We now add to the potential φ_1 the potential

$$
\varphi_2 = U_\infty x
\tag{5.51}
$$

of a three-dimensional flow parallel to the x-axis. Both, φ_1 and φ_2 are harmonic (except φ_1 at $R = 0$). Consequently, $\varphi_1 + \varphi_2$ is equally a solution of $\Delta\phi = 0$ which is given by the expressions

$$\varphi = \varphi_1 + \varphi_2 = U_\infty \left(x + \frac{a^3 x}{2R^3} \right),$$

$$u = \frac{\partial \varphi}{\partial x} = U_\infty \left(1 + \frac{a^3}{2R^3} - \frac{3}{2} \frac{a^3 x^2}{R^5} \right),$$

$$v = \frac{\partial \varphi}{\partial y} = -\frac{3}{2} U_\infty \frac{a^3}{R^5} xy,$$ (5.52)

$$w = \frac{\partial \varphi}{\partial z} = -\frac{3}{2} U_\infty \frac{a^3}{R^5} xz.$$

On the surface of the sphere, $R = a$, this implies

$$u(a) = \frac{3}{2} U_\infty \left(1 - \frac{x^2}{a^2} \right), \quad v(a) = -\frac{3}{2} U_\infty \frac{xy}{a^2}, \quad w(a) = -\frac{3}{2} U_\infty \frac{xz}{a^2}. \quad (5.53)$$

Now, since $u(a)x + v(a)y + w(a)z = 0$, where (x, y, z) is a vector normal to the surface of the sphere, we have $v(a) \cdot n = 0$; so, the velocity field is tangential to the sphere, and as $R \to \infty$, i.e., far away from the sphere, the formulae (5.52) imply $v(R \to \infty) = U_\infty e_x$, which is a flow parallel to the x-axis. The constructed velocity field represents an irrotational flow of a fluid with constant density around a sphere of radius a, as shown in **Fig. 5.7**. In the interior of the sphere a bounded dipole flow is generated by (5.52). This part of the solution is fictitious, because no fluid exists in the interior of the sphere, but the flow has rotational symmetry about the x-axis, as can easily be inferred from (5.52).
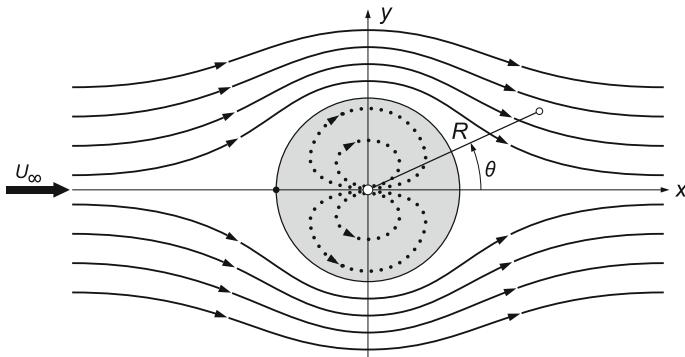
Fig. 5.7   Uniform parallel flow around a sphere. *The constant parallel velocity U_∞ at $x = -\infty$ flows symmetrically around the stagnant sphere with symmetries about the x-and y-axes. Within the sphere a fictitious bounded dipole flow is generated. The figure shows a cut in any meridional plane*

In a meridional plane, applying polar coordinates (R, θ), (5.52) implies, since $x = R\cos\theta$, $y = R\sin\theta$, $z = 0$,

$$u = U_\infty\left(1 + \frac{a^3}{R^3}\left(\frac{1}{2} - \frac{3}{2}\cos^2\theta\right)\right), \quad v = -\frac{3}{2}U_\infty\frac{a^3}{R^3}\sin\theta\cos\theta, \quad w = 0, \quad (5.54)$$

and at $R = a$,

$$u = \frac{3}{2}U_\infty\sin^2\theta, \quad v = -\frac{3}{2}U_\infty\sin\theta\cos\theta, \quad |v| = \frac{3}{2}U_\infty\sin\theta. \quad (5.55)$$

Especially interesting is the pressure distribution. For the case that $U_\infty = $ const. and that no volume force is acting, the BERNOULLI equation yields
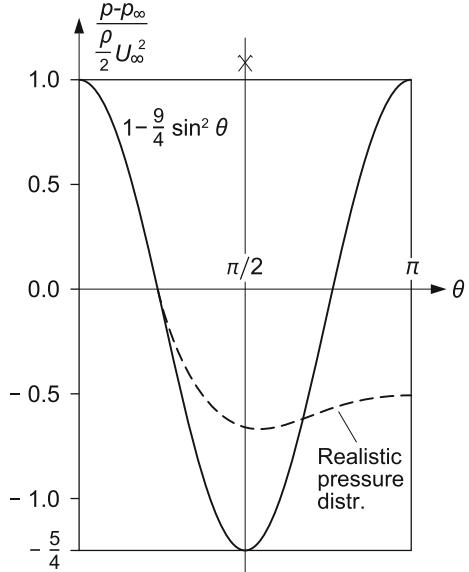
$$p_\infty + \frac{\rho}{2}U_\infty^2 = p + \frac{\rho}{2}\left(u^2 + v^2\right),$$

and on the surface of the sphere,

$$p = p_\infty + \frac{\rho}{2}U_\infty^2\left(1 - \frac{9}{4}\sin^2\theta\right). \quad (5.56)$$

This function is plotted in **Fig. 5.8**. The pressure $(p - p_\infty)/(\rho U_\infty^2/2)$ is periodic with period π, and so the pressure distribution on the upstream side equals that on

Fig. 5.8 Pressure distribution on the surface of a sphere at rest in a meridional plane due to a parallel irrotational flow *The solid curve is the plot for the solution (5.56). The dashed curve gives the realistic observed pressure distribution*

the downstream side, irrespective how the meridional plane is rotated about the x-axis. It follows that no resultant force due to the fluid pressure is exerted on the sphere. This result is contrary to experiences of laboratory measurements, which have shown that the pressure distribution on the upstream side differs from that on the downstream side of the sphere, as principally sketched in Fig. 5.8.

(b) Source-free, solenoidal vector fields v_2:
Such fields identically satisfy the equation div $v_2 = 0$. It is, thus tempting to introduce the vector potential a such that

$$v_2 = \text{curl}\, a. \tag{5.57}$$

Velocity fields v_2, determined in this form, are automatically solenoidal, since div (curl a) = 0 for any twice differentiable a. We now take

$$\text{curl}\, v_2 = \text{curl}\, (\text{curl}\, a) \stackrel{(1)}{=} \text{grad}\, (\text{div}\, a) - \Delta a, \tag{5.58}$$

where we have defined $\Delta a = (\Delta a_x, \Delta a_y, \Delta a_z)^T$. The identity $\stackrel{(1)}{=}$ is best verified by evaluating left- and right-hand sides in Cartesian component form. We now arbitrarily select div $a = 0$. This selection restricts the class of vector fields a to those which are solenoidal and selection must in general be corroborated by a-posteriori computation of div a. With (5.34), Eq. (5.58) is simplified to the vectorial POISSON equation

$$\Delta a = -w, \quad \Delta a_x = -w_x, \quad \dots, \quad \dots, \tag{5.59}$$

where $w = \text{curl}\, v_2$. A particular integral of this equation is (compare (5.30))

$$a_x = \frac{1}{4\pi} \iiint_V \frac{w_x(\xi, \eta, \zeta)\, d\xi d\eta d\zeta}{\sqrt{(x-\xi)^2 + (y-\eta)^2 + (z-\zeta)^2}}, \quad \dots, \quad \dots. \tag{5.60}$$

$$a = \frac{1}{4\pi} \iiint_V \frac{w(\xi, \eta, \zeta)}{r(x, \xi)}\, dv. \tag{5.61}$$

Integration is over that volume for which $w \neq 0$. At last, it must be verified, whether (5.60), (5.61) satisfy the constraint condition div $a = 0$. Explicitly,

$$\text{div}\, a = \frac{1}{4\pi} \iiint_V \text{div}_x \left(\frac{w}{r}\right) dv_\xi = \frac{1}{4\pi} \iiint_V w \cdot \text{grad}_x \left(\frac{1}{r}\right) dv_\xi$$

$$= -\frac{1}{4\pi} \iiint_V w \cdot \text{grad}_\xi \left(\frac{1}{r}\right) dv_\xi \stackrel{\text{div}_\xi w=0}{=} -\frac{1}{4\pi} \iiint_V \text{div}_\xi \left(\frac{w}{r}\right) dv_\xi$$

$$= -\frac{1}{4\pi} \iint_A \frac{w \cdot n}{r}\, dA = 0, \quad (\text{since } w = 0 \text{ on } A). \tag{5.62}$$

V extends over the region where $\boldsymbol{w} \neq \boldsymbol{0}$ and $\boldsymbol{w} = \boldsymbol{0}$ at the boundary A ($\boldsymbol{w} \cdot \boldsymbol{n} = 0$ would suffice). With the vector potential $\boldsymbol{a}$, given by (5.61), the velocity $\boldsymbol{v}_2$ is given by

$$\boldsymbol{v}_2 = \operatorname{curl} \boldsymbol{a} = \frac{1}{4\pi} \operatorname{curl} \iiint_V \frac{\boldsymbol{w}}{r} \, dv = \frac{1}{4\pi} \iiint_V \operatorname{curl}_x \left(\frac{\boldsymbol{w}}{r} \right) dv$$

$$= \frac{1}{4\pi} \iiint_V \frac{\boldsymbol{w} \times \boldsymbol{r}}{r^3} \, dv, \tag{5.63}$$

where

$$\operatorname{curl}_x \left(\frac{\boldsymbol{w}}{r} \right) = -\boldsymbol{w} \times \operatorname{grad}_x \left(\frac{1}{r} \right) \quad \text{and} \quad \operatorname{grad}_x \left(\frac{1}{r} \right) = -\frac{\boldsymbol{r}}{r^3}$$

have been used.

A special form of (5.63) is obtained, if it is applied to a thin vortex filament. In such a case we have $\boldsymbol{w} \, dv = |\boldsymbol{w}| ds \, da = \Gamma ds$, where $\Gamma := |\boldsymbol{w}| \, da$. Equation (5.63) now obtains

$$\boldsymbol{v}_2 = \frac{\Gamma}{4\pi} \oint \frac{ds \times \boldsymbol{r}}{r^3} \quad \text{(for a vortex filament with } \Gamma = |\boldsymbol{w}| \, da\text{).} \tag{5.64}$$

The integral path $\oint$ must be a closed loop $\mathcal{C}$, because a vortex filament, which lies completely in V, must be a closed loop, see Chap. 4 and **Figs. 5.9** and **5.10**. Evaluating $\boldsymbol{v}_2$ with the first expression (5.63), we get
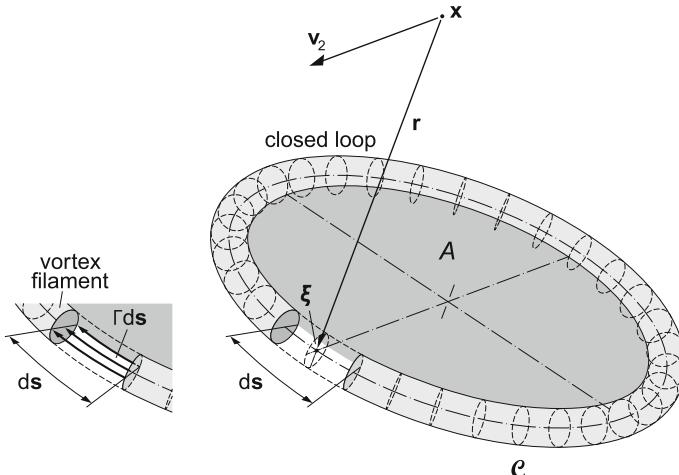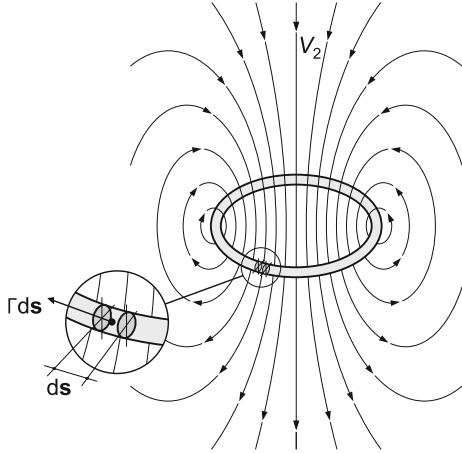
Fig. 5.9 Isolated closed loop of a vortex filament with vorticity strength Γds. Indicated is also the velocity vector $\boldsymbol{v}_2$ induced by Γds. Notice the right-hand dumb rule for $\boldsymbol{v}_2 \propto ds \times \boldsymbol{r}$

Fig. 5.10 Characteristic distribution of the velocity field induced by a closed vortex filament due to strength Γ (principal sketch)

$$v_2 = \frac{1}{4\pi}\mathrm{curl}\iiint_V \frac{w}{r}\,dv \overset{\text{vortex filament}}{=} \frac{\Gamma}{4\pi}\mathrm{curl}\oint_{\mathcal{C}} \frac{ds}{r}$$

$$\overset{(1)}{=} -\frac{\Gamma}{4\pi}\mathrm{curl}\iint_A \mathrm{grad}_\xi\left(\frac{1}{r}\right)\times n\,da$$

$$= -\frac{\Gamma}{4\pi}\iint_A \mathrm{curl}_x\left(\mathrm{grad}_\xi\left(\frac{1}{r}\right)\times n\right)da. \tag{5.65}$$

Here, STOKES' law has been used at "$\overset{(1)}{=}$" (see (5.17)) and A is the area spanned by the (double point free) loop $\mathcal{C}$ with unit normal vector n. Next, we use the vector identity

$$\mathrm{curl}_x(a\times b) \equiv (\mathrm{grad}_x a)b - (\mathrm{grad}_x b)a + a\,\mathrm{div}_x b - b\,\mathrm{div}_x a$$

and apply it to $a = \mathrm{grad}_\xi(1/r)$ and $b = n$; note that n does not depend on x (but only on ξ). This means that the two middle terms on the right-hand side of the last equation vanish, so that

$$\mathrm{curl}_x\left(\mathrm{grad}_\xi\left(\frac{1}{r}\right)\times n\right) = \mathrm{grad}_x\underbrace{\left\{\left[\mathrm{grad}_\xi\left(\frac{1}{r}\right)\right]\cdot n\right\}}_{\partial(1/r)/\partial n} \underbrace{-n\,\mathrm{div}_x\left(\mathrm{grad}_\xi\left(\frac{1}{r}\right)\right)}_{\substack{+n\,\mathrm{div}_x\mathrm{grad}_x(1/r) \\ \Delta(1/r)=0}}$$

$$= \mathrm{grad}_x\frac{\partial}{\partial n}\left(\frac{1}{r}\right). \tag{5.66}$$

Thus, an alternative form of writing (5.64) is

$$v_2 = -\frac{\Gamma}{4\pi} \mathrm{grad}_x \iint\limits_A \frac{\partial(1/r)}{\partial n}\,\mathrm{d}a, \tag{5.67}$$

in which A is the area spanned by the closed loop of the vortex filament. If we use

$$\frac{\partial}{\partial n}\left(\frac{1}{r}\right) = -\frac{1}{r^3}\left(\mathrm{grad}_\xi r\right)\cdot\boldsymbol{n} = \frac{1}{r^2}\boldsymbol{e}_r\cdot\boldsymbol{n},$$

$$\frac{\partial}{\partial n}\left(\frac{1}{r}\right)\mathrm{d}a = \frac{\boldsymbol{e}_r\cdot\boldsymbol{n}}{r^2}\,\mathrm{d}a = \mathrm{d}\Omega. \tag{5.68}$$

Yet, another way of writing (5.67) is, therefore,

$$v_2 = -\frac{\Gamma}{4\pi} \mathrm{grad}_x \iint\limits_A \mathrm{d}\Omega = -\frac{\Gamma}{4\pi} \mathrm{grad}_x \Omega. \tag{5.69}$$

The differential $\mathrm{d}\Omega$ is the increment, under which the area element of the area spanned by the closed vorticity filament is seen from the point x. Similarly, Ω is the solid angle under which the closed vortex filament is seen by an observer at x, see **Fig. 5.11**.
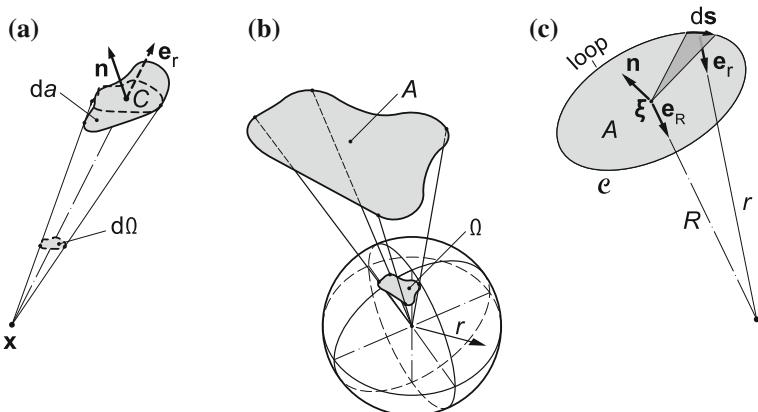
Fig. 5.11 Explaining the solid angle Ω and its increment $\mathrm{d}\Omega$. **a** *From point x an aerial increment of the area A, spanned by a closed vortex filament, appears as the shaded area with unit normal vector $\boldsymbol{n}$. The projection of this surface element onto a sphere through the point C perpendicular to $\boldsymbol{e}_r$ has the dashed periphery. The spherical projection of this (dashed) element defines the corresponding incremental solid angle $\mathrm{d}\Omega$. **b** Performing this for all $\mathrm{d}a$ of an area A yields the corresponding solid angle Ω. **c** Explaining the evaluation of the solid angle for the case that the point x is very far from the closed vortex filament*

The above analysis makes clear that the solenoidal velocity field v_2 of a closed vortex filament depends upon the area of the loop (and, of course, also the strength Γ). However, it is tempting to evaluate the asymptotic velocity field for the case that the point x is very far away from the loop. This situation then corresponds to that of panel c in Fig. 5.11, in which $|x - \xi|$ on a filament element can be approximated by $|(x - \xi)|_{\text{center}} = R$. The contribution of the shaded triangular element to the solid angle element,

$$d\Omega = \frac{1}{2} \frac{|ds \times (\xi - x)|}{r^2},$$

can be approximately written as

$$d\Omega \approx \frac{1}{2R^2} (ds \times (\xi - x)) \cdot e_r,$$

from which we deduce

$$\Omega = \frac{1}{2R^2} \oint (ds \times (\xi - x)_{\text{center}}) \cdot e_r$$

or

$$\Gamma\Omega = \frac{1}{2R^2} \left(\oint \Gamma ds \times (\xi - x)_{\text{center}} \right) \cdot e_r. \tag{5.70}$$

This last equation suggests the generalization to a region V_ω with continuously distributed vorticity,

$$\Gamma\Omega = \frac{1}{2R^2} \left(\iiint_{V_\omega} w \times \xi \, dv \right) \cdot e_r. \tag{5.71}$$

If we define the dipole moment of a closed vortex filament or a bounded vortex region by

$$M := \underbrace{\frac{1}{2} \iiint_{V_\omega} w \times \xi \, dV_\xi}_{\text{for a region}} = \underbrace{\frac{\Gamma}{2} \oint ds \times \xi}_{\text{loop of filament}}, \tag{5.72}$$

then (5.69) takes the form

$$v_2 = -\frac{1}{4\pi} \text{grad}_x \left(\frac{M \cdot e_R}{R^2} \right) + \mathcal{O}(R^{-4}). \tag{5.73}$$

From a bounded vortex region or a closed loop of a vortex filament only the dipole moment contributes to the velocity field far away from the vorticity source.

Fig. 5.12 PIERRE-SIMON LAPLACE (23. March 1749–5. March 1827)

PIERRE-SIMON LAPLACE was a French mathematician, physicist and astronomer, who worked on the theory of probability and differential equations. Among his mentors JEAN-BAPTISTE LE ROND D'ALEMBERT was particularly influential. His principal work was on Celestial Mechanics, which comprises 5 books, where he proved the stability of the Solar System, postulated the existence of Black Holes and worked on the Three Body Problem. The second strong activity of LAPLACE was in the Theory of Probability, which was set in a context of absolute determinism, that caused violent discussions and opposition and is still a debate despite the development of quantum mechanics later on.

Text is based on http://www.wikipedia.org

(c) Harmonic vector fields v_3:
Harmonic vector fields are irrotational *and* solenoidal. In a regular region they satisfy curl $v_3 = 0$, if they are derivable from a potential ϕ according to $v_3 = \operatorname{grad} \phi$ so that

$$\operatorname{div} \operatorname{grad} \phi = \Delta \phi = 0, \quad \text{in } V \subset \mathcal{R}^3. \tag{5.74}$$

Thus, harmonic fields are solutions of the LAPLACE[9] equation. Determination of ϕ from (5.74) requires prescription of boundary conditions along ∂V. We shall select these boundary conditions such that the flow of $v = v_1 + v_2 + v_3$ across the boundary is prescribed. $v \cdot n =$ known; this then yields for $v_3 \cdot n$

$$v_3 \cdot n = v \cdot n - (v_1 + v_2) \cdot n,$$

---

[9]For a short biography of LAPLACE see **Fig. 5.12**.

Fig. 5.13 Franz Ernst Neumann (11. Sept. 1798–23. May 1895)

Franz Ernst Neumann was a German physicist and is considered to be the founder of theoretical physics in Germany of the 19th century. He studied in Berlin (theology) and Jena (physics and mathematics) and wrote a doctoral dissertation on domains in crystallography under Christian Samuel Weiss (1780–1856). 1826 he moved to Königsberg (Kaliningrad) where he habilitated. 1829 he was called to full professor of mineralogy in the physics department of the Albertus University in Königsberg. Here he founded together with Carl-Gustav Jacobi (1804–1851) in 1834 the 'Königsberg Seminars in Mathematical Physics' which became a dominant periodical event in the academic life in Germany where he taught until 1877, but continued to stay active afterwards until his death at the age of 97 years.

The text is based on http://www.wikipedia.org; Portrait by Carl Steffeck (1886)

which also can be treated as known, if v_1 and v_2 are already determined. So, the boundary value problem that must be solved is

$$
\begin{aligned}
\Delta \phi &= 0, && \text{in } V \subset \mathcal{R}^3, \\
\frac{\partial \phi}{\partial n} &= v_3 \cdot n, && \text{on } \partial V.
\end{aligned}
\tag{5.75}
$$

This is a so-called Neumann[10] problem for the harmonic function ϕ.

––––––––––––––––––––

[10]For short biographies of Franz Ernst Neumann and Carl Gottfried Neumann see **Figs. 5.13** and **5.14**.
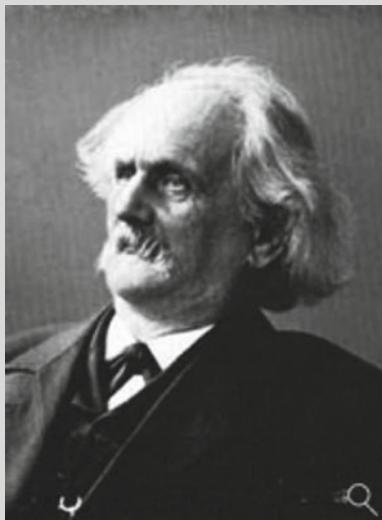
Fig. 5.14 CARL GOTTFRIED NEUMANN (7. May 1832–27. March 1925)

CARL GOTTFRIED NEUMANN, the son of the mathematical physicist and mineralogist FRANZ-ERNST-NEUMANN (1798–1895), was a mathematician, who studied in Königsberg (Kaliningrad) and habilitated in Halle. He was professor in Halle, Basel, Tübingen and for 42 years in Leipzig. Together with ALFRED CLEBSCH (1833–1872), he founded the Scientific Journal *Mathematische Annalen*. His interests were applications of mathematics to physics with significant results in potential theory, mechanics and electrodynamics. In pure mathematics his works on conformal mappings, ABEL functions and trigonometric series are of importance. He has had a lasting influence in mathematical sciences of the 19th century through his books e.g. [8, 9], and he is known through the flux boundary condition in boundary value problems.

The text is based on:

http://www.orden-pourlemerite.de/mitglieder/carl-gottfried-neumann

Remarks.

- The flow through ∂V must satisfy the following side condition:

$$\iint_{\partial V} \boldsymbol{v} \cdot \boldsymbol{n} \, \mathrm{d}a = \iiint_V q \, \mathrm{d}v, \quad \text{or}$$

$$\underbrace{\iint_{\partial V} \boldsymbol{v}_1 \cdot \boldsymbol{n} \, \mathrm{d}a}_{=\iiint_V q \, \mathrm{d}v} + \underbrace{\iint_{\partial V} \boldsymbol{v}_2 \cdot \boldsymbol{n} \, \mathrm{d}a}_{=0, \text{ since div } \boldsymbol{v}_2 = 0} + \iint_{\partial V} \boldsymbol{v}_3 \cdot \boldsymbol{n} \, \mathrm{d}a = \iiint_V q \, \mathrm{d}v,$$

implying that

$$\iint\limits_{\partial V} \boldsymbol{v}_3 \cdot \boldsymbol{n} \, \mathrm{d}a = \iint\limits_{\partial V} \frac{\partial \phi}{\partial n} \, \mathrm{d}a = 0.$$

This says that the surface integral $\iint (\partial \phi / \partial n) \, \mathrm{d}a$ must vanish, even though $\partial \phi / \partial n$ does not need to vanish locally. The solution to this problem has already been given in (5.29) as solution of the POISSON equation. Thus, setting $f = 0$, there,

$$4\pi \phi(\boldsymbol{x}) + \iint\limits_{\partial V} \phi \frac{\partial}{\partial n} \left(\frac{1}{r} \right) \mathrm{d}a = \iint\limits_{\partial V} \frac{\partial \phi}{\partial n} \left(\frac{1}{r} \right) \mathrm{d}a \qquad (5.76)$$

is obtained. This last equation is an *integral equation* for ϕ. With (see **Fig. 5.15**a)

$$\frac{\partial}{\partial n} \left(\frac{1}{r} \right) \mathrm{d}a = -\frac{1}{r^2} \frac{\partial r}{\partial n} \, \mathrm{d}a = -\frac{\mathrm{d}a}{r^2} \cos \theta = -\mathrm{d}\Omega, \qquad (5.77)$$

the second term on the left-hand side of (5.76) can differently be written such that (5.76) now takes the form

$$4\pi \phi(\boldsymbol{x}) - \iint\limits_{\partial V} \phi(\boldsymbol{\xi}) \mathrm{d}\Omega_\xi = \iint\limits_{\partial V} \frac{\partial \phi(\boldsymbol{\xi})}{\partial n} \frac{1}{r} \, \mathrm{d}v_\xi, \qquad (5.78)$$

in which $\boldsymbol{x}$ and $\boldsymbol{\xi}$ identify points in V and on ∂V, respectively; $\mathrm{d}\Omega$ is the surface solid angle under which the surface element $\mathrm{d}a$ on ∂V is seen from an observer at $\boldsymbol{x}$ in V. If the observer at $\boldsymbol{x}$ approaches the surface point $\boldsymbol{\xi}$, then,
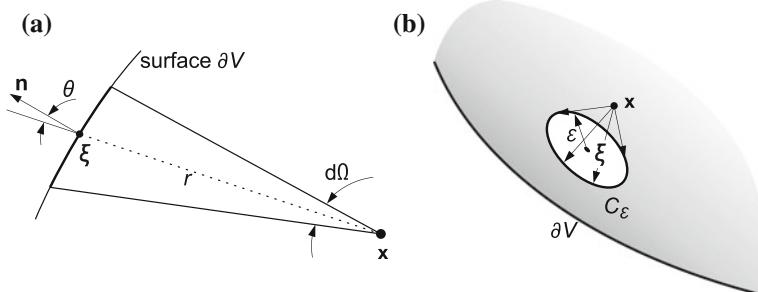
Fig. 5.15 a *Explaining how the area of a surface element ∂V is expressed in terms of the solid angle (5.77).* **b** *Evaluation of the solid angle between the observer position $\boldsymbol{x}$ as the surface point, $\boldsymbol{\xi}$, centered in a small surface circle C_ε, is approached*

$$\iint\limits_{\partial V} \phi_\xi \, d\Omega = \iint\limits_{C_\varepsilon} \phi_\xi \, d\Omega + \iint\limits_{\partial V \setminus C_\varepsilon} \phi_\xi \, d\Omega,$$

in which C_ε is a small circle with radius ε at the position $\boldsymbol{\xi} \leftarrow \boldsymbol{x}$. In this limit position the solid angle seen from $\boldsymbol{x}$ is only a semi-sphere, so that, see Fig. 5.15b,

$$\iint\limits_{C_\varepsilon} \phi_\xi \, d\Omega = \phi_\xi \int\limits_{C_\varepsilon} d\Omega = \phi_\xi \frac{4\pi}{2} = 2\pi\phi_\xi. \tag{5.79}$$

Therefore, (5.78) assumes the form

$$2\pi\phi(\boldsymbol{x}) - \lim_{C_\varepsilon \to 0} \iint\limits_{\partial V \setminus C_\varepsilon} \phi_\xi \, d\Omega_\xi = \iint\limits_{\partial V} \frac{\partial \phi}{\partial n} \left(\frac{1}{r}\right) d\Omega_\xi. \tag{5.80}$$

This is the integral equation, which one must solve for a harmonic NEUMANN problem.

- If one has to solve a DIRICHLET[11] problem

$$\begin{aligned} \Delta\phi &= 0, & \text{in } V \subset \mathcal{R}^3, \\ \phi &= \phi_0, & \text{on } \partial V, \end{aligned} \tag{5.81}$$

formula (5.78) directly yields

$$4\pi\phi(\boldsymbol{x}) = \iint\limits_{\partial V} \phi_0(\boldsymbol{\xi}) \, d\Omega_\xi + \iint\limits_{\partial V} \frac{\partial \phi}{\partial n} \left(\frac{1}{r}\right) da. \tag{5.82}$$

Here, the first integral on the right-hand side is known and the second integral is unknown.

- As an example, consider the velocity field in the entire domain $\mathcal{R}^3$. If q and $\boldsymbol{w}$ have compact support[12] in a finite domain of $\mathcal{R}^3$, then $q = 0$ and $\boldsymbol{w} = \boldsymbol{0}$ for some $x^2 + y^2 + z^2 > L^2$. We are now seeking a solution for $\boldsymbol{v}$ such that

$$\begin{aligned} \left.\begin{array}{c} \text{div } \boldsymbol{v} = q \\ \text{curl } \boldsymbol{v} = \boldsymbol{w} \end{array}\right\} & \quad \text{in a bounded domain } V \subset \mathcal{R}^3, \\ \boldsymbol{v} \to \boldsymbol{v}_\infty & \quad \text{for } x^2 + y^2 + z^2 \to \infty. \end{aligned} \tag{5.83}$$

The solution of this problem is given by

$$\boldsymbol{v} = \boldsymbol{v}_1 + \boldsymbol{v}_2 + \boldsymbol{v}_\infty,$$

---

[11] For a short biography of DIRICHLET see **Fig. 8.2**.

[12] Compact support of a function f defined in $\mathcal{R}^3$ means that $f \neq 0$ in $V \subset \mathcal{R}^3$ and $f = 0$ in $\mathcal{R}^3 / V$.

where $\boldsymbol{v}_1$ is irrotational and given by (5.38), $\boldsymbol{v}_2$ is solenoidal and explicitly given by the vector potential (5.70) or (5.71) and $\boldsymbol{v}_\infty$ is a constant field. $\boldsymbol{v}_1$ and $\boldsymbol{v}_2$ decay to zero as $x^2 + y^2 + z^2 \rightarrow \infty$ and, certainly, $\boldsymbol{v}_\infty$ is harmonic. This solution is also unique. Indeed, if $\boldsymbol{u}$ is the difference of two solutions, then this solution satisfies $\boldsymbol{u} = \operatorname{grad} \phi$ and $\Delta\phi = 0$ and $\operatorname{grad} \phi \rightarrow 0$ as $\boldsymbol{x} \rightarrow \infty$. Consider now an arbitrary sphere with radius R. We then can easily write down the following chain of inferences:

$$
0 = \iiint_{\text{sphere}} \Delta\phi \, \mathrm{d}v = \iint_{\partial\,(\text{sphere})} \frac{\partial\phi}{\partial R} \, \mathrm{d}a
$$

$$
= R^2 \iint_{\partial\,(\text{unit sphere})} \frac{\partial\phi}{\partial R} \, \mathrm{d}\Omega = R^2 \frac{\partial}{\partial R} \iint_{\partial\,(\text{unit sphere})} \phi \, \mathrm{d}\Omega.
$$

Hence, by integration

$$
\iint_{\partial\,(\text{unit sphere})} \phi \, \mathrm{d}\Omega = \text{const.}, \ \text{irrespective of } R \ \implies \ \phi = \text{const.} \rightarrow \operatorname{grad}\phi = 0.
$$

Since $\operatorname{grad} \phi = 0$ we also have $\boldsymbol{u} = \boldsymbol{0}$; there is only a single solution.　　　$\square$

5.2　Vortex-Free Flow Fields

5.2.1　Mathematical Preliminaries
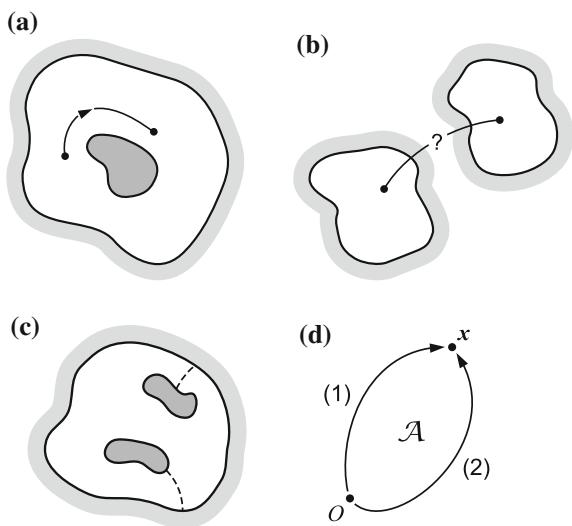
We begin by stating a few conceptions or definitions:

- A *connected open region* is a domain in which every point of the region can be reached by any other point of the region via a continuous path without leaving the region.
- A closed path is called *reducible*, if it can continuously be reduced to a point without leaving the region in this process.
- A region is called *simply connected*, if every closed path is reducible.
- A region is called *n-fold connected*, if $(n-1)$ cuts can make it simply connected.

The region of panel a of **Fig. 5.16** is connected, that of panel b is not. The region of panel a is doubly connected in $\mathcal{R}^2$, but simply connected in $\mathcal{R}^3$ (if it is also bounded in the third direction perpendicular to the sheet of paper). In $\mathcal{R}^3$ every closed path is reducible,[13] but this is not so in $\mathcal{R}^2$. Panel c in Fig. 5.16 shows a region, which is simply connected in $\mathcal{R}^3$, but doubly connected in $\mathcal{R}^2$. By the indicated cuts (dashed in the figure), the region can be made simply connected.

---

[13] if the regions that are excluded from $\mathcal{R}^3$ are bounded.

Fig. 5.16 Explaining connectivity of regions in $\mathcal{R}^2$ and $\mathcal{R}^3$. **a** *This annulus is a connected region. It is doubly connected in $\mathcal{R}^2$ but simply connected in $\mathcal{R}^3$.* **b** *This is not a connected region.* **c** *This region is simply connected in $\mathcal{R}^3$.* **d** *This panel explains, how the velocity field of an irrotational flow can be derived from the power of work integral. In simply connected regions this work integral is independent of the path*

Lemma 5.1 *Irrotational flows (*curl $v = 0$*) in simply connected regions possess a unique potential; it can be defined by*

$$\phi(x, y, z, t) = \int\limits_{0}^{x} v(x, y, z, t) \cdot \mathrm{d}x. \tag{5.84}$$

∎

Proof With reference to Fig. 5.16d, we may write

$$\int\limits_{(1)} v \cdot \mathrm{d}x - \int\limits_{(2)} v \cdot \mathrm{d}x = \oint\limits_{(1-2)} v \cdot \mathrm{d}x \overset{\text{Stokes law}}{=} \iint\limits_{\mathcal{A}} (\mathrm{curl}\, v) \cdot n\, \mathrm{d}a = 0.$$

In this expression, $\int\limits_{(1)}$ signifies integration along a path "1" from the origin O to the point x; similarly for $\int\limits_{(2)}$, which means integration along path "(2)" from O to the same point x. Thus, $\int\limits_{(1)} - \int\limits_{(2)}$ denotes the closed integral $\int\limits_{1-2}$ from O to x to O, to which STOKES' integral theorem may be applied. $\mathcal{A}$ is then any smooth surface area spanned by the closed loop "$1 - 2$". The last equation implies, since curl $v = 0$ by prerequisite,

$$\int\limits_{(1)} v \cdot \mathrm{d}x = \int\limits_{(2)} v \cdot \mathrm{d}x, \tag{5.85}$$

which states that the integral $\int \boldsymbol{v} \cdot \mathrm{d}\boldsymbol{x}$ is independent of the path of integration and can only depend on the initial and end points of the potential. Differentiation of (5.84) yields

$$\frac{\partial \phi}{\partial \boldsymbol{x}} = \operatorname{grad} \phi = \boldsymbol{v}(\boldsymbol{x}, t). \tag{5.86}$$

Remarks.

- In multiply connected regions the velocity potentials ϕ are no longer unique. An example is the potential vortex $v_\theta = c/r$, in which c is a constant, r is the radial distance and v_θ the azimuthal velocity. The velocity field is irrotational (curl $\boldsymbol{v} = \boldsymbol{0}$) except at $r = 0$ and possesses the potential $\phi = c\theta$. In this case ϕ experiences a jump by the value $2\pi c$, whenever the positive x-axis is crossed (from below). If the plane is cut along the positive x-axis uniqueness is re-established.
- The laws of STOKES, GAUSS and GREEN are in the stated forms (5.17), (5.7), (5.23), (5.24) valid, provided the regions, to which they are referred, are simply connected. On occasions in practice, this might have to be imposed by cuts. For instance, if we apply the first GREEN identity, (5.23) with $\psi = \phi$, $\Delta\phi = 0$, viz.,

$$\iiint\limits_{V} (\operatorname{grad} \phi)^2 \, \mathrm{d}v = \iint\limits_{\mathcal{A}} \phi \frac{\partial \phi}{\partial n} \, \mathrm{d}a$$

to the circular annulus region of the potential vortex, the surface integral vanishes (since $\partial\phi/\partial n = 0$ along the circular boundaries), whilst the volume integral on the left-hand side is non-negative, since $(\operatorname{grad} \phi)^2 \geqslant 0$; thus, $\phi \equiv$ constant.
- In a doubly connected region the circulation along any two closed, irreducible paths has identical values. Indeed, if a cut is introduced between the two closed irreducible paths "1" and "2", **Fig. 5.17**, and the circulation is evaluated along this extended closed path, then owing to STOKES' integral theorem and the potential
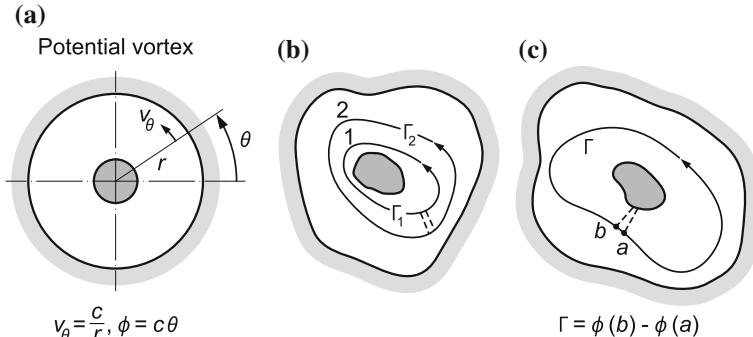
Fig. 5.17 Irrotational flows in doubly connected regions in $\mathcal{R}^2$. **a** *Potential vortex with azimuthal velocity $v_\theta = c/r$, $c =$ const. and velocity potential $\phi = c\theta$. The velocity potential is multi-valued, $\phi = c(2n\pi + \theta)$* **b** *In doubly connected regions the circulation along any two closed irreducible paths is the same constant for all such paths.* **c** *The value of Γ equals $\phi(b) - \phi(a)$, see the figure*

character of the flow (curl $\boldsymbol{v} = \boldsymbol{0}$), the value of this circulation vanishes, see Fig. 5.17b, the part along the cut is traversed twice and in opposite directions, so that its contribution to the circulation integral vanishes. This, thus, implies

$$\Gamma = \underbrace{\int_{(1)} \boldsymbol{v} \cdot \mathrm{d}\boldsymbol{x}}_{=\Gamma_1} - \underbrace{\int_{(2)} \boldsymbol{v} \cdot \mathrm{d}\boldsymbol{x}}_{=\Gamma_2} = 0 \quad \Longrightarrow \quad \Gamma_1 = \Gamma_2 \tag{5.87}$$

for any two closed irreducible paths. The value of the circulation for any such path is equal to the jump of the potential at the cut, which one must introduce to obtain a unique representation of the potential, Fig. 5.17b,

$$\Gamma = \int_a^b \boldsymbol{v} \cdot \mathrm{d}\boldsymbol{x} = \int_a^b (\mathrm{grad}\,\phi) \cdot \mathrm{d}\boldsymbol{x} = \int_a^b \mathrm{d}\phi = \phi(b) - \phi(a).$$

For the potential vortex flow in $\mathcal{R}^2$ (above), $\phi = c\theta$, this yields $\Gamma = 2\pi c$.

5.2.2 Potential Fields

We assume irrotational flows of density preserving fluids ($\rho = $ const.) in simply connected domains subject to NEUMANN boundary conditions. Such flows are solutions of the boundary value problem

$$\begin{aligned} \Delta\phi &= 0, & \text{in } V, \\ \frac{\partial\phi}{\partial\boldsymbol{n}} &= v_n, & \text{on } \partial V. \end{aligned} \tag{5.88}$$

The LAPLACE equation, $\Delta\phi = 0$, is a consequence of the fact that curl $\boldsymbol{v} = \boldsymbol{0}$ is identically satisfied with $\boldsymbol{v} = \mathrm{grad}\,\phi$ and the incompressibility condition, div $\boldsymbol{v} = 0$, then yields $\Delta\phi = 0$; moreover, the NEUMANN condition $(5.88)_2$ expresses that the volume flow through the boundary ∂V is prescribed by $v_n = \boldsymbol{v}_n \cdot \boldsymbol{n}$ for $\boldsymbol{x} \in \partial V$.

Potential flows satisfying (5.88) enjoy a number of distinct properties, which we shall prove in the ensuing analysis.

(a) Uniqueness:

Proposition 5.1 *Potential flows in a simply-connected domain, driven by the* NEUMANN *boundary condition are unique.* ∎

Proof Let ϕ_1 and ϕ_2 be smooth solutions of (5.88). Then, the difference solution $\phi_d = \phi_1 - \phi_2$ must satisfy the boundary value problem

$$\Delta\phi_d = 0, \quad \text{in } V,$$

$$\frac{\partial\phi_d}{\partial\boldsymbol{n}} = \boldsymbol{0}, \quad \text{on } \partial V.$$

(5.89)

Use of the first GREEN Identity (5.23) with $\phi = \psi = \phi_d$ then yields

$$\iiint\limits_V (\operatorname{grad}\phi_d)^2 \, dv = \iint\limits_A \phi_d \frac{\partial\phi_d}{\partial n} \, da = 0,$$

(5.90)

an equation, which only allows the solution $\operatorname{grad}\phi_d = 0$, since $(\operatorname{grad}\phi_d)^2 \geq 0$, whose integral must vanish. Therefore, $\operatorname{grad}\phi_1 = \operatorname{grad}\phi_2$. $\qquad\square$

(b) Expression for the kinetic energy:
A nice application of the First GREEN Identity in potential flows of density preserving fluids is the formula

$$T = \frac{\rho}{2} \iint\limits_{\partial V} \phi\frac{\partial\phi}{\partial n} \, da;$$

(5.91)

$\blacksquare$

The kinetic energy T in V is expressible as the surface integral of $\phi\,(\partial\phi/\partial n)$ over ∂V.

Proof By definition

$$T \overset{(1)}{=} \iiint\limits_V \frac{\rho}{2}\boldsymbol{v}^2 \, dv \overset{(2)}{=} \frac{\rho}{2} \iiint\limits_V (\operatorname{grad}\phi)^2 \, dv \overset{(3)}{=} \frac{\rho}{2} \iint\limits_{\partial V} \phi\frac{\partial\phi}{\partial n} \, da.$$

(5.92)
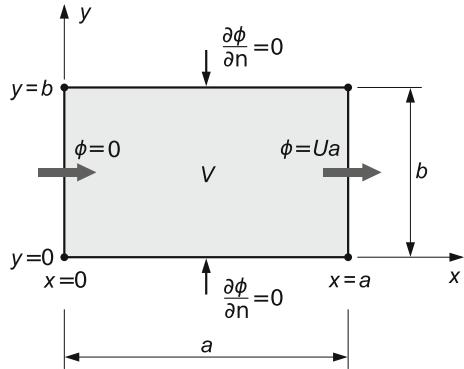
In step "$\overset{(1)}{=}$" we simply apply the definition of T; in step "$\overset{(2)}{=}$" we use the fact that in a potential flow the velocity field is a gradient field and in step "$\overset{(3)}{=}$" we use (5.90)$_1$. $\qquad\square$

This is easily verified for x-parallel potential flows, for which $\phi = Ux$, $\boldsymbol{v} = U\boldsymbol{e}_x$. With these expressions and the rectangle of **Fig. 5.18** one readily finds

$$T = \frac{\rho}{2} \iiint\limits_V \boldsymbol{v}^2 \, dv = \frac{\rho}{2}U^2 a\,b,$$
$$T = \frac{\rho}{2} \iint\limits_{\partial V} \phi\frac{\partial\phi}{\partial n} \, da = \frac{\rho}{2}(Ua)(Ub),$$

(5.93)

respectively.

Fig. 5.18 Rectangular
domain subject to the
potential flow $\phi = U\,x$
parallel to the x-axis for the
evaluation of the kinetic
energy according to
Eq. (5.93)

(c) KELVIN's energy theorem:

Proposition 5.2 (Lord KELVIN, 1849) *The irrotational motion of an incompressible fluid in a simply connected region V has the smaller kinetic energy than any other motion with the same normal velocity at its boundary ∂V.* ∎

Proof Let $\boldsymbol{v} = \operatorname{grad}\phi + \boldsymbol{v}'$, for which curl $\boldsymbol{v}' \neq \boldsymbol{0}$, $\Delta\phi = 0$ in V and $v_n = \operatorname{grad}\phi \cdot \boldsymbol{n}$. Now, on ∂V the boundary condition must be satisfied for the total velocity field. Therefore, we have

$$\boldsymbol{v} \cdot \boldsymbol{n} = v_n = \operatorname{grad}\phi \cdot \boldsymbol{n} + \boldsymbol{v}' \cdot \boldsymbol{n} = \underbrace{v_n}_{=0} + \boldsymbol{v}' \cdot \boldsymbol{n} = 0,$$

implying that $\boldsymbol{v}' \cdot \boldsymbol{n} = 0$ is the boundary condition for $\boldsymbol{v}'$. Thus, the kinetic energy of the total flow can be written as

$$
\begin{aligned}
T &= \frac{\rho}{2} \iiint\limits_V (\operatorname{grad}\phi + \boldsymbol{v}')^2 \, dv \\
&= \frac{\rho}{2} \iiint\limits_V (\operatorname{grad}\phi)^2 \, dv + \rho \iiint\limits_V \underbrace{\boldsymbol{v}' \cdot \operatorname{grad}\phi}_{\operatorname{div}(\phi\boldsymbol{v}')} \, dv + \frac{\rho}{2} \iiint\limits_V (\boldsymbol{v}')^2 \, dv \\
&= \frac{\rho}{2} \iiint\limits_V (\operatorname{grad}\phi)^2 \, dv + \rho \iint\limits_{\partial V} \underbrace{(\boldsymbol{v}' \cdot \boldsymbol{n})}_{=0} \phi \, da + \frac{\rho}{2} \iiint\limits_V (\boldsymbol{v}')^2 \, dv \\
&= \frac{\rho}{2} \iiint\limits_V (\operatorname{grad}\phi)^2 \, dv + \frac{\rho}{2} \iiint\limits_V (\boldsymbol{v}')^2 \, dv.
\end{aligned}
\tag{5.94}
$$

The kinetic energy of the flow with vorticity is larger by the kinetic energy of the deviation of the flow from that of the irrotational flow field. The minimum is reached for $\boldsymbol{v}' = \boldsymbol{0}$. □

(d) Maximum-minimum property:

Proposition 5.3 *The potential ϕ, as solution of (5.88), assumes its maximum and minimum on the boundary ∂V of V.*   ∎

Proof Let us start from (5.29), which was derived as a possible integral solution of the POISSON equation. With $f = 0$ this expression reduces to

$$4\pi\phi(\boldsymbol{x}) = -\iint\limits_{\partial V} \left\{ \phi\frac{\partial}{\partial n}\left(\frac{1}{r}\right) - \left(\frac{1}{r}\right)\frac{\partial\phi}{\partial n} \right\} \mathrm{d}a, \qquad (5.95)$$

valid for the LAPLACE equation. Applying this formula to a spherical surface A with radius R and center at $\boldsymbol{x}$, we have $\partial(1/r)/\partial n = -(1/R^2)$ and obtain

$$4\pi\phi(\boldsymbol{x}) = \frac{1}{R^2}\iint\limits_{A} \phi\,\mathrm{d}a + \frac{1}{R}\underbrace{\iint\limits_{A} \mathrm{grad}\,\phi \cdot \boldsymbol{n}\,\mathrm{d}a}_{\text{apply Gauss' law}}$$

$$= \frac{1}{R^2}\iint\limits_{A} \phi\,\mathrm{d}a + \frac{1}{R}\iiint\limits_{V} \underbrace{\mathrm{div}\,\mathrm{grad}\,\phi}_{\Delta\phi=0}\,\mathrm{d}v.$$

Thus,
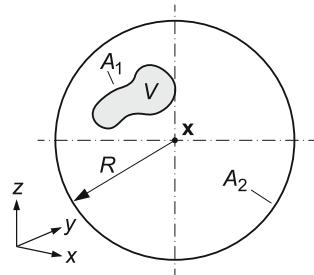
$$\phi(\boldsymbol{x}) = \frac{1}{4\pi R^2}\iint\limits_{A} \phi\,\mathrm{d}a. \qquad (5.96)$$

In other words: *The value of the potential at the center of the sphere is the mean value of its values on the spherical surface.* This is the mean value theorem of the potential theory. It implies that ϕ *must assume its maximum and its minimum on the boundary* ∂V. If it were not so, then the maximum $\max(\phi)$ must lie in the interior of V. A sphere with arbitrarily small radius and center at the position, where ϕ assumes its maximum, must on its surface necessarily have $\phi < \max\limits_{\text{on }\partial V}(\phi)$, in contradiction to the mean value theorem. The same procedure, used for $-\phi$ (instead of $+\phi$), also leads to the statement that ϕ must assume its minimum on the boundary ∂V.   □

We close this subsection with two remarks.

- *Every derivative of a potential function is again a potential function*. Provided no singularities are created by this differentiation in V, the following conclusion holds:
- *The maximum of the modulus of the velocity vector of a potential flow in V is assumed on the boundary ∂V of V.* If this maximum would occur within V, a local coordinate system could be so positioned that the x-axis would point in the direction of grad ϕ. Application of the above proof to $\partial\phi/\partial x$ then directly yields the statement.

Fig. 5.19   A region of a fluid
in $\mathcal{R}^n$, $n = 2, 3$. *The motion
of the fluid is generated by
the rigid body V with
boundary A_1. The fluid is
bounded by A_2, a sphere
with radius $R \to \infty$*

(e) Flow, generated by finite bodies in simply-connected regions of $\mathcal{R}^n$, $n = 2, 3$:
Basic assumption is here that the flow is exclusively generated by the motion of the
boundary A_1 of the body, see **Fig. 5.19**. Assume the domain of the flow to be three-
dimensional. Let us start again with formula (5.29) in which $f = 0$, and apply it to a
domain V, which is bounded by the moving body with surface A_1 and a large sphere
with radius R and surface A_2, whose center is located at the point $\boldsymbol{x}$, see Fig. 5.19.
This then yields

$$
4\pi\phi(\boldsymbol{x}) = -\iint\limits_{A_1} \left\{ \phi \frac{\partial}{\partial n}\left(\frac{1}{r}\right) - \left(\frac{1}{r}\right)\frac{\partial \phi}{\partial n} \right\} da
$$

$$
- \iint\limits_{A_2} \left\{ \phi \frac{\partial}{\partial n}\left(\frac{1}{r}\right) - \left(\frac{1}{r}\right)\frac{\partial \phi}{\partial n} \right\} da
$$

$$
= -\iint\limits_{A_1} \left\{ \phi \frac{\partial}{\partial n}\left(\frac{1}{r}\right) - \left(\frac{1}{r}\right)\frac{\partial \phi}{\partial n} \right\} da
$$

$$
+ \frac{1}{R^2}\iint\limits_{A_2} \phi \, da + \frac{1}{R}\iint\limits_{A_1} \frac{\partial \phi}{\partial n} \, da, \tag{5.97}
$$

where the transformation in the second integral on the right-hand side has already
been introduced in connection with the derivation of (5.96). Now, owing to the
divergence theorem, we have for the situation of Fig. 5.19

$$
\iiint\limits_V \underbrace{\Delta\phi}_{0} \, dv = \iiint\limits_V \text{div}\,(\text{grad}\,\boldsymbol{v})\, dv = \iint\limits_{A_2} \frac{\partial \phi}{\partial n}\, da + \iint\limits_{A_1} \frac{\partial \phi}{\partial n}\, da = 0,
$$

or

$$
\iint\limits_{A_2} \frac{\partial \phi}{\partial n}\, da = -\iint\limits_{A_1} \frac{\partial \phi}{\partial n}\, da =: Q \quad \text{(a finite constant)}. \tag{5.98}
$$

Employing (5.35) in (5.97) leads to

$$4\pi\phi(\boldsymbol{x}) = \underbrace{\frac{1}{R^2} \iint_{A_2} \phi \, \mathrm{d}a + \frac{Q}{R}}_{I = -\frac{Q}{R} + C} - \iint_{A_1} \left\{ \phi \frac{\partial}{\partial n} \left(\frac{1}{r} \right) - \left(\frac{1}{r} \right) \frac{\partial \phi}{\partial n} \right\} \mathrm{d}a. \quad (5.99)$$

The underbraced result in this formula can be obtained, if one defines

$$I = \frac{1}{R^2} \iint_{A_2} \phi \, \mathrm{d}a$$

$$= \frac{1}{R^2} \iint_{A_2} \phi \, (x + r \sin\theta \cos\varphi, \, y + r \sin\theta \sin\varphi, \, z + r \cos\theta) \, R^2 \sin\theta \mathrm{d}\theta \mathrm{d}\varphi$$

$$= \iint_{A_2} \hat{\phi}(R, \theta, \varphi, x, y, z) \underbrace{\sin\theta \mathrm{d}\theta \mathrm{d}\varphi}_{\mathrm{d}\Omega}.$$

It follows[14]

$$\frac{\mathrm{d}I}{\mathrm{d}R} = \iint_{A_2} \frac{\partial \hat{\phi}}{\partial R} \sin\theta \, \mathrm{d}\theta \mathrm{d}\varphi = \frac{1}{R^2} \iint_{A_2} \frac{\partial \hat{\phi}}{\partial n} \, \mathrm{d}a = \frac{Q}{R^2},$$

and by integration

$$I = -\frac{Q}{R} + C. \quad (5.101)$$

The constant C does not depend upon the position of the point $\boldsymbol{x}$, since $\partial I/\partial \boldsymbol{x} = (1/R^2) \iint_{A_2} (\partial \phi/\partial \boldsymbol{x}) \mathrm{d}a$. If one assume that grad $\phi \to 0$ as $R \to \infty$, one has $\partial I/\partial \boldsymbol{x} = \mathbf{0}$ for $R \to \infty$, so that C is independent of $\boldsymbol{x}$. C as a constant can be set to zero; this corresponds to a certain normalization of ϕ (which does not affect the velocity). Thus, (5.99) simplifies to

$$4\pi\phi(\boldsymbol{x}) = -\iint_{A_1} \left\{ \phi \frac{\partial}{\partial n} \left(\frac{1}{r} \right) - \left(\frac{1}{r} \right) \frac{\partial \phi}{\partial n} \right\} \mathrm{d}a. \quad (5.102)$$

---

[14]If we let $\boldsymbol{x} \to \infty$, we have $r \to R$ and (5.102) implies

$$(a) \quad \phi = \mathcal{O}(1/R), \text{ if } \iint_{A_1} \frac{\partial \phi}{\partial n} \, \mathrm{d}a \neq 0,$$

$$(b) \quad \phi = \mathcal{O}(1/R^2), \text{ if } \iint_{A_1} \frac{\partial \phi}{\partial n} \, \mathrm{d}a = 0.$$

$$(5.100)$$

(f) Steady potential flow around a stationary three-dimensional rigid body:
Assume that a finite body is fixed in 3-dimensional space filled with a density pre-
serving fluid in irrotational flow. The velocity field is then composed of $v = v_\infty + v'$,
where $v' = \operatorname{grad} \phi$; it must satisfy the boundary value problem

$$\begin{aligned} \Delta\phi &= 0, & \text{in } V, \\ \tfrac{\partial\phi}{\partial n} &= -v_\infty \cdot n, & \text{on } \partial V. \end{aligned} \qquad (5.103)$$

Because v_∞ is a parallel field, it satisfies the condition $\iint_A v_\infty \cdot n \, da = 0$; so,
according to (14), $\phi \to \mathcal{O}(1/R^2)$ as $R \to \infty$. These conditions imply

Proposition 5.4 *The force exerted on a body at rest by a three-dimensional steady
irrotational, incompressible flow field vanishes.*   ∎

Proof Ignoring the gravity force, the flow-induced force exerted on a fixed body is
given by

$$K = -\iint_{A_1} (\rho v(v \cdot n) + pn) \, da. \qquad (5.104)$$

A_1 is an arbitrary surface surrounding the body which in infinite space can be removed
to infinity, where the following asymptotic relations hold

$$\phi \sim \frac{1}{R^2}, \quad v' \sim \frac{1}{R^3}, \quad p \sim p_\infty + \mathcal{O}(R^{-3}).$$

Consequently,

$$K = -\iint_{A_1} \left\{ \underbrace{\rho v_\infty(v_\infty \cdot n) + p_\infty n}_{(1)} + \underbrace{\mathcal{O}(R^{-3})}_{(2)} \right\} da. \qquad (5.105)$$

Integral "(1)" vanishes for all closed surfaces; integral "(2)" is asymptotically of
$\mathcal{O}(1/R)$ and, therefore, also vanishes as $R \to \infty$.   □

This result is so important that we state it explicitly:

$$K = 0 \quad \text{in an irrotational steady flow in } \mathcal{R}^3. \qquad (5.106)$$

Remarks.

- In plane flow over $\mathcal{R}^2$ the corresponding flow induced force does not vanish. The
  reason for this is that the presence of the body makes the domain of the fluid flow
  a doubly-connected region. As can be shown, the velocity v' circulating around
  the body decays as $1/R$ as $R \to \infty$, so that the asymptotic term "(2)" in formula
  (5.105) generally integrates to a finite number.

- In three-dimensional space a non-zero force on a circumflown fixed body can only occur, if the velocity potential possesses singularities (e.g. vortex sheets) or if the flow is unsteady.

(g) Force on a sphere with variable radius in an unsteady flow field:
Let $U(t)$ be a parallel time-dependent potential flow field, against which a sphere with radius $a(t)$ moves with velocity $U_\infty(t)$, see **Fig. 5.20**. $U(t)$, $U_\infty(t)$ and $a(t)$ may all vary with time. In a coordinate system moving with the center of the sphere the upstream velocity is $U(t) + U_\infty(t)$. Moreover, in this non-inertial frame a 'virtual' body force is exerted on the sphere with potential

$$\Omega = -\dot{U}_\infty(t)x = -\dot{U}_\infty r \cos\theta. \tag{5.107}$$
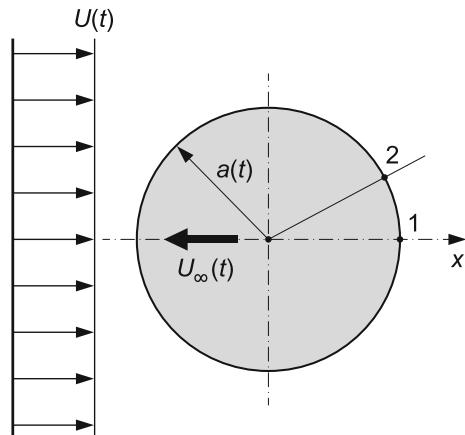
The velocity potential in the moving system is given by

$$\phi = (U + U_\infty)\left(r + \frac{a^3}{2r^2}\right)\cos\theta - \frac{\dot{a}a^2}{r}. \tag{5.108}$$

The first term on the right-hand side is the parallel-flow potential, see $(5.52)_1$, the second term corresponds to the radial velocity due to the variation of the radius of the sphere (flow due to a radial source, see $(5.45)_1$). The radial and azimuthal velocity components in a meridional plane are

$$
\begin{aligned}
v_r &= (U + U_\infty)\left(1 - \frac{a^3}{r^3}\right)\cos\theta + \frac{\dot{a}a^2}{r^2}, \\
v_\theta &= -(U + U_\infty)\left(1 + \frac{a^3}{2r^3}\right)\sin\theta.
\end{aligned}
\tag{5.109}
$$

Fig. 5.20 A sphere of time dependent radius $a(t)$ moving with variable velocity $U_\infty(t)$ against a parallel flow field $U(t)$. Both $U(t)$ and $U_\infty(t)$ are uni-directional

On the surface of the sphere this yields

$$v_r = \dot{a}, \quad v_\theta = -\tfrac{3}{2}(U + U_\infty) \sin \theta. \tag{5.110}$$

Moreover, the partial time derivative of ϕ is given by

$$\frac{\partial \phi}{\partial t} = (\dot{U} + \dot{U}_\infty)\left(r + \frac{a^3}{2r^2}\right) \cos \theta + \frac{3}{2}(U + U_\infty)\frac{\dot{a}a^2}{r^2} \cos \theta - \frac{(\dot{a}a^2)^{\cdot}}{r},$$
$$\frac{\partial \phi}{\partial t}\Big|_{r=a} = [(U + U_\infty)a]^{\cdot}\frac{3}{2}\cos \theta - \frac{(\dot{a}a^2)^{\cdot}}{a}, \tag{5.111}$$

and the BERNOULLI equation can be written in the form (see Sect. 3.4),

$$\frac{\partial \phi}{\partial t} + \frac{p}{\rho} + \frac{v^2}{2} + \Omega = F(t),$$
$$\Longrightarrow \frac{p}{\rho} = -\frac{\partial \phi}{\partial t} - \Omega - \frac{v^2}{2} + F(t), \quad \text{on } r = a. \tag{5.112}$$

Substituting (5.107), (5.110) and (5.111) into this equation yields

$$\frac{p}{\rho} = -\frac{3}{2}[(U + U_\infty)a]^{\cdot} \cos \theta + \dot{U}_\infty a \cos \theta - \frac{9}{8}(U + U_\infty)^2 \sin^2 \theta$$
$$-\frac{\dot{a}^2}{2} + F(t) + \frac{(\dot{a}a^2)^2}{a}. \tag{5.113}$$

The pressure distribution can be used to evaluate the total force exerted by the fluid on the sphere. In this computation the purely time-dependent terms do not contribute, their integration adds up to zero. Similarly, the component perpendicular to the x-direction equally drops out. There remains then the force in the x-direction

$$K_x = -2\pi a^2 \int_0^\pi p(\theta) \sin \theta \cos \theta \, d\theta$$

$$= \rho \left\{3\pi a^2[(U + U_\infty)a]^{\cdot} - 2\pi a^3 \dot{U}_\infty\right\} \underbrace{\int_0^\pi \cos^2 \theta \sin \theta \, d\theta}_{2/3}$$

$$= \frac{3}{2}\frac{4\pi}{3}a^3 \rho \left\{(\dot{U} + \dot{U}_\infty) + \frac{\dot{a}}{a}(U + U_\infty)\right\} - \frac{4\pi}{3}a^3 \rho \dot{U}_\infty. \tag{5.114}$$

With the definitions

$$V = \frac{4\pi}{3}a^3 \qquad \text{(volume of the sphere)},$$
$$V' = \frac{1}{2}\frac{4\pi}{3}a^3 \qquad \text{('virtual' volume of the sphere)},$$

(5.114) can also be expressed as

$$K_x = \rho(V + V')\dot{U} + \rho V'\dot{U}_\infty + \rho(V + V')(U + U_\infty)\frac{\dot{a}}{a}. \qquad (5.115)$$

This formula expresses the fact that the force exerted on a sphere in an unsteady flow field is

(i) due to the acceleration of the flow field, $\dot{U}(t)$,
(ii) due to the accelerating motion by the sphere itself, $\dot{U}_\infty(t)$,
(iii) due to the spatial expansion of the sphere itself, $\dot{a}(t)$.

Special cases are obtained, if any of these effects is absent:

(1) If $\dot{a} = 0$, $\dot{U} = b$ and $\dot{U}_\infty = -b_k$, then

$$K_x = \rho(V + V')b - \rho V'b_k. \qquad (5.116)$$

If the sphere has density ρ_k and (5.116) is the force exerted upon it, then $K_x = b_k V$, so that

$$b_k = \frac{\rho(V + V')}{\rho_k V + \rho V'}b. \qquad (5.117)$$

In this case the acceleration of the sphere is determined by the acceleration of the parallel flow.

(2) When $U = 0$ and $\dot{U}_\infty = b_k$, then

$$K_x = \rho V'b_k + \rho(V + V')(U + U_\infty)\frac{\dot{a}}{a}. \qquad (5.118)$$

In this case, for driving $\dot{a}$, K_x can only be evaluated, if also b_k is measured. If that motion is chosen such that $K_x = 0$, we obtain

$$b_k = -\frac{V' + V}{V'}(U + U_\infty)\frac{\dot{a}}{a}. \qquad (5.119)$$

This body acceleration is needed to eliminate the force due to the expansion rate $\dot{a}$ of the sphere.

5.3 Motion-Induced Force on a Body in Potential Flow. The Virtual Mass Concept

A force on a body subject to an inviscid fluid under three-dimensional motion is only generated, if the body is kept in unsteady flow. This problem will be studied in this section, first for a rigid sphere and then for a rigid body of general shape.

5.3.1 Force on a Sphere

Let us assume that the sphere is subject to motion by the velocity $-U_\infty(t)$ in an otherwise incompressible fluid at rest. In the reference system fixed with the translational motion of the sphere, the sphere is subject to the velocity $U_\infty(t)$ from $x = -\infty$. Since this reference system is not inertial, the sphere experiences the inertial force

$$\boldsymbol{f} = +\dot{U}_\infty \boldsymbol{e}_x, \tag{5.120}$$

corresponding to the force potential

$$\Phi = -\dot{U}_\infty x. \tag{5.121}$$

The BERNOULLI equation, written for two arbitrary points, 1, 2, see **Fig. 5.21**, in this non-inertial frame has the form

$$\int_1^2 \frac{\partial \boldsymbol{v}}{\partial t} \cdot d\boldsymbol{x} + \frac{v_2^2 - v_1^2}{2} + \frac{p_2 - p_1}{\rho} - \dot{U}_\infty(x_2 - x_1) = 0. \tag{5.122}$$

If the two points are chosen as in Fig. 5.21, then point 1 is a stagnation point with $\boldsymbol{v}_1 = \boldsymbol{0}$. For the variable point 2 on the surface of the sphere, the velocity has already been computed, see (5.110),

$$u_\theta = -\frac{3}{2}U_\infty \sin\theta \quad \text{(in point 2)}. \tag{5.123}$$
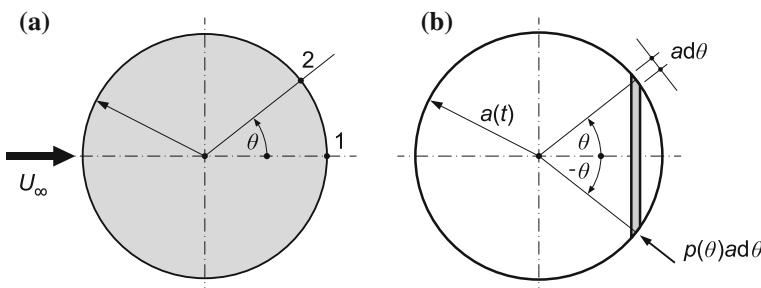
Fig. 5.21 Sphere with time-dependent radius $a(t)$ subject to a constant parallel field U_∞ of an ideal density preserving fluid. **a** *Variables as defined in a meridional plane* **b** *explaining the evaluation of the pressure resultant force on the sphere*

With these selections we have

$$\bullet \quad \int_1^2 \frac{\partial \boldsymbol{v}}{\partial t} \cdot \mathrm{d}\boldsymbol{x} = -\frac{3}{2}\dot{U}_\infty \int_0^\theta \sin\theta^* a\, \mathrm{d}\theta^* = -\frac{3}{2}\dot{U}_\infty a(1 - \cos\theta),$$

$$\bullet \quad -\dot{U}_\infty(x_2 - x_1) = \dot{U}_\infty a(1 - \cos\theta),$$

$$\bullet \quad \frac{v_2^2 - v_1^2}{2} = \frac{9}{8}U_\infty^2 \sin^2\theta,$$

so that the BERNOULLI equation yields the following expression for the pressure

$$\frac{p(\theta) - p_1}{\rho} = \frac{1}{2}\dot{U}_\infty a(1 - \cos\theta) - \frac{9}{8}U_\infty^2 \sin^2\theta, \qquad (5.124)$$

with the aid of which the resulting force on the sphere can be computed. Because $p(\theta)$ in (5.124) is an even function of the angle θ, the components of p perpendicular to the x-direction cancel each other, so that at most a resultant force in the x-direction will be generated; this force differential on a ring element is given by, see Fig. 5.21b,

$$\mathrm{d}K_x = -p(\theta)\cos\theta\, a\, \mathrm{d}\theta\, (2a\pi \sin\theta),$$

so that

$$K_x = -\int_0^\pi 2\pi a^2 p(\theta) \sin\theta \cos\theta\, \mathrm{d}\theta.$$

If the expression for the pressure, (5.124), is substituted in this formula, the term p_1 gives zero contribution, as do all other terms, except the term $-\frac{1}{2}\dot{U}_\infty a \cos\theta$. So, K_x follows from the expression

$$K_x = 2\pi a^2 \frac{\rho\dot{U}_\infty a}{2} \int_0^\pi \cos^2\theta \sin\theta\, \mathrm{d}\theta$$

$$= \pi a^3 \rho\dot{U}_\infty \underbrace{\int_0^\pi \frac{1}{3}\frac{\mathrm{d}}{\mathrm{d}\theta}\left(-\cos^3\theta\right) \mathrm{d}\theta}_{2/3} = \frac{2\pi a^3}{3}\rho\dot{U}_\infty. \qquad (5.125)$$

It is customary to define

$$M' = \frac{1}{2}\frac{4\pi}{3}a^3\rho \qquad (5.126)$$

as the *virtual mass for the sphere*; it is $\frac{1}{2} \times$ (the mass displaced by the sphere). An alternative way of writing K_x is, therefore

$$K_x = M' \dot{U}_\infty. \tag{5.127}$$

Because of axi-symmetry of the body shape and the motion, any other force component perpendicular to the x-axis automatically vanishes as has already been shown.

5.3.2 Force on a Body of Arbitrary Geometry

It will again be assumed that the body moves translatorically with velocity $-U(t)$ through a density preserving ideal fluid at rest. In the frame fixed to the body, this body is subject to the inertial force $f = -\dot{U} e_x$ with the potential $\Phi = -\dot{U} x$. Let us decompose the velocity field in the body-fixed non-inertial frame, v, into the velocity of approach U, and the velocity, q, in the laboratory frame,

$$v = U + q. \tag{5.128}$$

The BERNOULLI equation is given by

$$\int\limits_1^2 \frac{\partial v}{\partial t} \cdot \mathrm{d}x + \frac{v_2^2 - v_1^2}{2} + \frac{p_2 - p_1}{\rho} - \dot{U} \cdot (x_2 - x_1) = 0,$$

or with (5.128)

$$\int\limits_1^2 \frac{\partial q}{\partial t} \cdot \mathrm{d}x + \underbrace{\dot{U} \cdot (x_2 - x_1)} + U \cdot (q_2 - q_1) + \frac{q_2^2 - q_1^2}{2}$$

$$+ \frac{p_2 - p_1}{\rho} - \underbrace{\dot{U} \cdot (x_2 - x_1)} = 0, \tag{5.129}$$

in which the underbraced terms drop out. If we choose for point 1 an arbitrary fixed point and for point 2 a variable point and solve (5.129) for p/ρ, we obtain

$$\frac{p}{\rho} = -\int\limits_1 \frac{\partial q}{\partial t} \cdot \mathrm{d}x - \left(\frac{q^2}{2} + U \cdot q \right) + f_1(t).$$

In $f_1(t)$ all terms evaluated at point 1 are subsumed; they are, since x_1 is fixed, only functions of t. Moreover, the variable point is not especially indicated. If we also set

$$q = \text{grad } \phi \quad \longrightarrow \quad \int_1 \frac{\partial q}{\partial t} \cdot dx = \int_1 \frac{\partial \text{grad } \phi}{\partial t} \cdot dx = \frac{\partial \phi}{\partial t},$$

the above expression for p/ρ takes the form

$$\frac{p}{\rho} = -\frac{\partial \phi}{\partial t} - \left(\frac{q^2}{2} + U \cdot q\right) + f_1(t).$$

The flow-induced force on the body can now be written as

$$K = \iint_A pn \, da = -\rho \iint_A \left(\frac{\partial \phi}{\partial t} + \left(\frac{q^2}{2} + U \cdot q\right)\right) n \, da + 0$$

$$= -\rho \frac{d}{dt} \iint_A \phi n \, da - \rho \underbrace{\iint_{A \cup A^*} \left(\frac{q^2}{2} + U \cdot q\right) n \, da}_{I=0}. \qquad (5.130)$$

In these formulae n is the unit normal vector on the surface A pointing *into* the body. The second integral I will be shown below to vanish. Thus,
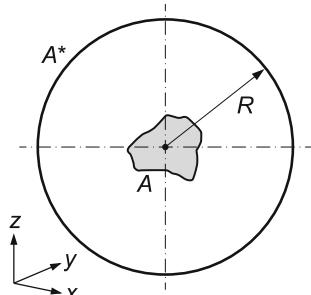
$$K = -\rho \frac{d}{dt} \iint_A \phi n \, da \quad (n \text{ is interior normal vector}). \qquad (5.131)$$

Proof that $I = 0$: For this proof we apply the facts (proven earlier) that far away from the body, q is asymptotically $\mathcal{O}(1/R^3)$ as $R \to \infty$, and the integral over the spherical surface A^* approaches zero, $I \to 0$ as $R \to \infty$. To prove these statements, note that owing to the identity

$$(U \cdot q)n \equiv U \times (n \times q) + (U \cdot n)q,$$

(which is best verified in Cartesian indical notation) the integral I can be written as, see **Fig. 5.22**,

Fig. 5.22 Explaining the evaluation of the force exerted by an ideal fluid of parallel flow on a body in three-dimensional space. The surface of the body is A and the flow is asymptotically estimated as $R \to \infty$

$$I = \iint\limits_{A \cup A^*} \left\{ U \times (n \times q) + (U \cdot n)q + \frac{q^2}{2}n \right\} da$$

$$= \iint\limits_{A \cup A^*} \left\{ U \times (n \times q) - (q \cdot n)q + \frac{q^2}{2}n \right\} da. \qquad (5.132)$$

The last step follows, because on A relation $v \cdot n = 0$ implies that $U \cdot n = -q \cdot n$. On A^* this transformation is irrelevant; for both versions the integrals vanish as $R \to \infty$. Now, we have the following integral representations:

- $$\iint\limits_{A \cup A^*} U \times (n \times q)\, da$$

$$= U \times \iint\limits_{A} n \times q\, da \stackrel{(5.10),\text{Gauss}}{=} -U \times \iiint\limits_{V} \underbrace{\mathrm{curl}\, q}_{=0}\, dv = 0,$$

- $$\iint\limits_{A \cup A^*} \left(\frac{q^2}{2}\mathbf{1} - q \otimes q \right) n\, da \stackrel{\text{Gauss}}{=} \iiint\limits_{V} \mathrm{div}\left(\frac{q^2}{2}\mathbf{1} - q \otimes q \right) dv$$

$$\stackrel{(*)}{=} \iiint\limits_{V} \left\{ \underbrace{\left(\mathrm{grad}^T q - \mathrm{grad}\, q \right) q}_{=0,\ \text{since}\ \mathrm{curl}\, q = 0} - q \cdot \underbrace{\mathrm{div}\, q}_{=\Delta\phi=0} \right\} dv = 0.$$

These results demonstrate that (5.132) vanishes, so $I = 0$. The step "$\stackrel{(*)}{=}$" is best verified by evaluation in Cartesian tensor notation.

Let us, finally, verify the result (5.131) for the sphere. The velocity field can in this case be composed by the potential of the parallel flow and the potential ϕ of the dipole flow, see (5.52)$_1$,

$$\phi = \frac{U_\infty(t)a^3 x}{2R^3}.$$

On the surface of the sphere, we have $\phi(a) = U_\infty(t)\frac{x}{2}$. The force, K_x, can, thus be written as

$$K_x = -\rho\frac{d}{dt}\iint\limits_{A} U_\infty \frac{x}{2} n_x\, da$$

$$= -\rho\dot{U}_\infty \int\limits_0^\pi \frac{a\cos\theta}{2}(-\cos\theta)2\pi a^2 \sin\theta\, d\theta$$

$$= \rho\pi a^3 \dot{U}_\infty \underbrace{\int\limits_0^\pi \cos^2\theta \sin\theta\, d\theta}_{2/3} = \frac{1}{2}\frac{4\pi}{3}a^3\rho\dot{U}_\infty,$$

which identically agrees with (5.127). □

Let us at last return to (5.131) to derive the *generalized concept of virtual mass*. On the surface of the body the potential ϕ must be in conformity with the boundary condition

$$\boldsymbol{v} \cdot \boldsymbol{n} = 0 = \boldsymbol{U} \cdot \boldsymbol{n} + \boldsymbol{q} \cdot \boldsymbol{n} = \boldsymbol{U} \cdot \boldsymbol{n} + \operatorname{grad} \phi \cdot \boldsymbol{n} \quad \text{on } A,$$

or

$$\frac{\partial \phi}{\partial n} = -\boldsymbol{U} \cdot \boldsymbol{n} = -U_1 n_1 - U_2 n_2 - U_3 n_3 \quad \text{on } A. \tag{5.133}$$

Additionally, ϕ must also satisfy the potential equation $\Delta \phi = 0$. Because of the linearity of the problem and in view of the boundary condition (5.133) it is tempting to assume ϕ in the form

$$\phi = U_1 \varphi_1 + U_2 \varphi_2 + U_3 \varphi_3, \tag{5.134}$$

so that each potential φ_α, $\alpha = 1, 2, 3$, satisfies the boundary value problem

$$\begin{aligned} \Delta \varphi_\alpha &= 0, &&\text{in } V, \\ &&&\qquad\qquad \alpha = 1, 2, 3. \\ \frac{\partial \varphi_\alpha}{\partial n} &= -n_\alpha, &&\text{on } A, \end{aligned} \tag{5.135}$$

The form of these equations shows that φ_α, $\alpha = 1, 2, 3$ are solely determined by the shape of the body. The force is now given by, see (5.131),

$$\begin{aligned} \boldsymbol{K} &= -\rho \frac{\mathrm{d}}{\mathrm{d}t} \iint_A \sum_{\alpha=1}^{3} U_\alpha \varphi_\alpha \, \mathrm{d}a = - \sum_{\alpha=1}^{3} \left(\rho \iint_A \varphi_\alpha \boldsymbol{n} \, \mathrm{d}a \right) \dot{U}_\alpha, \\ K_i &= \sum_{\alpha=1}^{3} \left(-\rho \iint_A \varphi_\alpha n_i \, \mathrm{d}a \right) \dot{U}_\alpha = \sum_{j=1}^{3} m'_{ij} \dot{U}_j, \end{aligned} \tag{5.136}$$

in which

$$m'_{ij} = -\rho \iint_A \varphi_j n_i \, \mathrm{d}a \tag{5.137}$$

is the *tensor of the virtual mass*. Because at the boundary A, $\partial \varphi_i / \partial n = -n_i$ must hold, a second and more convenient form of m'_{ij} is given by

$$m'_{ij} = \rho \iint_A \frac{\partial \varphi_i}{\partial n} \varphi_j \, \mathrm{d}a. \tag{5.138}$$

Consequently, we may write (5.136) as

$$K = m'\dot{U} \quad \Longleftrightarrow \quad K_i = m'_{ij}\dot{U}_j. \tag{5.139}$$

Remarks.

- The tensor m' is symmetric. Indeed,

$$m'_{ij} - m'_{ji} = \rho \iint_A \left\{ \varphi_j \frac{\partial \varphi_i}{\partial n} - \varphi_i \frac{\partial \varphi_j}{\partial n} \right\} \mathrm{d}a$$

$$= \rho \iint_{A \cup A^*} \left\{ \varphi_j \frac{\partial \varphi_i}{\partial n} - \varphi_i \frac{\partial \varphi_j}{\partial n} \right\} \mathrm{d}a. \tag{5.140}$$

The integral over the large sphere A^* vanishes because $\varphi \sim 1/R^3$ as $R \to \infty$. With the expression (5.140) the Second GREEN's Identity can be applied, so that

$$m'_{ij} - m'_{ji} = \rho \iiint_V \left(\Delta\varphi_j \varphi_i - \Delta\varphi_i \varphi_j \right) \mathrm{d}v = 0,$$

which vanishes, since $\Delta\varphi_i = 0$ for $i = 1, 2, 3$, proving the symmetry of m'_{ij}.
- The virtual mass concept can be usefully applied, if the kinetic energy of the fluid in the laboratory frame is evaluated. Indeed,

$$T = \frac{\rho}{2} \iiint_V q^2 \, \mathrm{d}v = \frac{\rho}{2} \iiint_V (\operatorname{grad} \phi)^2 \, \mathrm{d}v$$

$$\overset{\text{Green}}{=} \frac{\rho}{2} \iint_{A \cup A^*} \phi \frac{\partial \phi}{\partial n} \, \mathrm{d}a \overset{(*)}{=} \frac{\rho}{2} \iint_A \phi \frac{\partial \phi}{\partial n} \, \mathrm{d}a.$$

Here, the step "$\overset{(*)}{=}$" holds because $q \sim 1/R^3$ as $R \to \infty$, so that the integral over A^* vanishes as $R \to \infty$. So,

$$T = \frac{\rho}{2} \iint_A (U_i \varphi_i) \left(U_j \frac{\partial \varphi_j}{\partial n} \right) \mathrm{d}a$$

$$= \frac{1}{2} U_i U_j \, \rho \underbrace{\iint_A \varphi_i \frac{\partial \varphi_j}{\partial n} \, \mathrm{d}a}_{m'_{ij}} = \frac{1}{2} m'_{ij} U_i U_j, \tag{5.141}$$

in which summation over the indices ij is understood. Formula (5.141) also implies

$$m'_{ij} = \frac{\partial^2 T}{\partial U_i \partial U_j}. \tag{5.142}$$

- For the sphere the tensor of the virtual mass is isotropic, $m'_{ij} = m'\delta_{ij}$ with $m'_{11} = m'_{22} = m'_{33} = m' = (2/3)\pi a^3 \rho$.
- (5.141) also allows evaluation of the time rate of change of the kinetic energy:

$$\dot{T} = \tfrac{1}{2}m'_{ij}U_i\dot{U}_j + \tfrac{1}{2}m'_{ij}U_j\dot{U}_i$$
$$= m'_{ij}U_i\dot{U}_j = \left(m'_{ij}\dot{U}_j\right)U_i = \boldsymbol{K}\cdot\boldsymbol{U}. \qquad (5.143)$$

This formula states that the kinetic energy equals the power of working of the force acting on the body.

- The force can also be obtained from the LAGRANGEan equations[15]

$$\left(\frac{\partial T}{\partial \dot{q}_k}\right)^{\cdot} - \frac{\partial T}{\partial q_k} = K_k, \qquad (5.144)$$

in which q_k and $\dot{q}_k$ are the generalized degrees of freedom and associated velocities, respectively. With $\dot{q}_k = U_k$. and the recognition that T is not a function of q_k but only of $\dot{q}_k$, the LAGRANGEan equation yields $K_i = m'_{ij}\dot{U}_j$.

Fig. 5.23 JOSPH-LOUIS LAGRANGE (25. Jan. 1736–10. April 1813)
JOSEPH-LOUIS LAGRANGE (born in Turin Piedmont as GUISEPPE LODOVICO (LUIGI) LAGRANGIA) was an Italian-born mathematician and astronomer who lived his early life in Turin (1736–1766), then in Berlin, Prussia, where he was working at the Academy (1766–1787), and finally moved to Paris, France, where he became a member of the French Academy

---

[15] For a short biography of LAGRANGE see **Fig. 5.23**.

(1787–1813) and where he died. LAGRANGE, who had French ancestors on his father's side is alternatively considered a French and an Italian scientist. He survived the French revolution and became the first professor of analysis at the École Polytechnique upon its opening in 1794. NAPOLEON named him Count of the Empire in 1808. He is buried in the Panthéon.

LAGRANGE was born into an Italian family of wealth but before he was grown up, his father had lost most of his property in speculation, and young LAGRANGE had to rely on his own abilities for his position. He was educated at the college of Turin but had not shown any sign of mathematical distinction before he was 17 years old, when by chance he came across a paper by EDMUND HALLEY. Alone and unaided, he then threw himself into mathematical studies and became a mathematics lecturer in the artillery school at the age of 18.

LAGRANGE is known as one of the founders of calculus of variations. Starting 1754 he worked on the problem of extremizing functionals in a similar way to finding extrema of functions. He presented his δ-algorithm to EULER, leading to the EULER-LAGRANGE equations of variational calculus in 1756; when he reported his results, EULER was deeply impressed. LAGRANGE published his method in two memoirs of the Turin Society Taurinensia in 1762 and 1773. LAGRANGE also published in 1764 work on the libration of the Moon and gave an explanation as to why the same face was always turned to the Earth.

In 1756 EULER, with the support of MAUPERTUIS, had made an attempt to bring LAGRANGE to the Academy in Berlin, but when King FREDERICK of Prussia invited him in 1765 he responded that *It seems to me that Berlin would not be at all suitable for me while Mr.* EULER *is there*. 1766 EULER had returned to Saint Petersburg and LAGRANGE accepted. The next 20 years he published extensively in the Berlin and Turin transactions, most significantly his Mécanique Analytique.

In 1786 FREDERICK died and LAGRANGE accepted an offer by LOUIS XVI to move to Paris. He became a member of the French Academy of Sciences. There, he went through a phase of melancholy of his life, partly due to the turmoil of the French revolution, however, his life was never endangered; he was also supported by NPOLEON. In 1794 LAGRANGE was appointed professor of the École Polytechnique. In 1810 he commenced a thorough revision of his Mécanique Analytique, but could not completely revise it before his death in 1813.

Text based on http://www.wikipedia.org
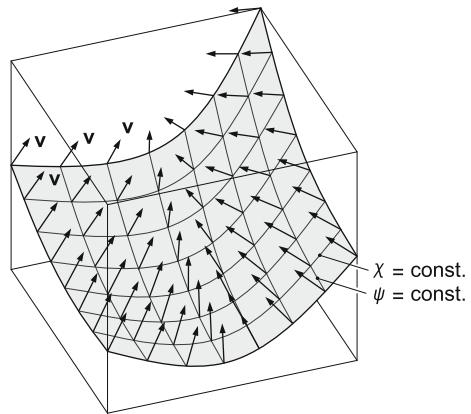
5.4   Plane Flow Configuration

5.4.1   Stream Function

In plane flow configurations the introduction of a stream function is a convenient and appropriate way of the mathematical description of the flow. To acquire a somewhat general understanding, let us first define the *stream function of a three-dimensional flow field*. To this end, consider two sets of stream surfaces, see **Fig. 5.24**,

$$\psi(x, y, z) = \text{const.}, \quad \chi(x, y, z) = \text{const.}. \tag{5.145}$$

These surfaces are declared to possess the property that each streamline lies in an
intersection point of the ψ- and χ-surfaces, and is perpendicular to the surface (5.145).
So, the velocity field is perpendicular to grad ψ- and grad χ-fields, which can be
expressed by the equation

$$\lambda\boldsymbol{v} = \text{grad}\,\psi \times \text{grad}\,\chi, \tag{5.146}$$

for some non-vanishing real λ. For a density preserving fluid (div $\boldsymbol{v} = 0$), (5.146)
implies

$$\text{div}\,(\lambda\boldsymbol{v}) = \boldsymbol{v} \cdot \text{grad}\,\lambda = \text{div}\,(\text{grad}\,\psi \times \text{grad}\,\chi) = 0. \tag{5.147}$$

The vanishing of the expression on the far right is easily seen, if the expression
is written in Cartesian index notation. It follows that $\boldsymbol{v} \cdot \text{grad}\,\lambda = 0$ or that $\boldsymbol{v} \perp$
grad λ. The value of λ changes only in the direction perpendicular to the streamlines.
Otherwise stated, the value of λ is constant for a streamline, or λ only depends on
the values of ψ and χ,

$$\lambda = \lambda(\phi, \chi). \tag{5.148}$$

Since this is so, *the ψ-and χ-surfaces can be so introduced that $\lambda = 1$*. To see this,
fix the stream surface $\chi = $ const. (i.e. choose a value for "const.") and choose a
ψ'-surface, $\psi' = f(\chi, \psi)$ adequately

$$\text{grad}\,\psi' \times \text{grad}\,\chi = (f_\chi \text{grad}\,\chi + f_\psi \text{grad}\,\psi) \times \text{grad}\,\chi$$
$$= \frac{\partial f}{\partial \psi}\text{grad}\,\psi \times \text{grad}\,\chi = \frac{\partial f}{\partial \psi}\lambda\boldsymbol{v}.$$

Obviously, if one chooses f such that $\partial f/\partial\psi = 1/\lambda(\psi, \chi)$, one obtains

$$\boldsymbol{v} = \operatorname{grad} \psi' \times \operatorname{grad} \chi. \tag{5.149}$$

Let us now state a number of inferences (we write ψ for ψ'):

- For plane flow one set of stream surfaces (the χ-functions) is parallel to the xy-plane, $z = \text{const.}$, and so, $\operatorname{grad} \chi = \boldsymbol{e}_z$. For this case (5.149) takes the form

$$\boldsymbol{v} = \operatorname{grad} \psi \times \boldsymbol{e}_z = \frac{\partial\psi}{\partial y}\boldsymbol{e}_x - \frac{\partial\psi}{\partial x}\boldsymbol{e}_y. \tag{5.150}$$

A possible dependence of ψ on z is irrelevant, because the flow in all planes is parallel to the xy-plane. Equation (5.150) suggests that

$$u(x, y) = \frac{\partial\psi}{\partial y}, \quad v(x, y) = -\frac{\partial\psi}{\partial x}. \tag{5.151}$$

With these assignments we also have

$$\psi(x, y) = \int\limits_{(0,0)}^{(x,y)} (u\mathrm{d}y - v\mathrm{d}x) = \int\limits_{(0,0)}^{(x,y)} \mathfrak{w} \cdot \mathrm{d}\boldsymbol{x}, \quad \mathfrak{w} = (-v, u)^T. \tag{5.152}$$

In simply connected domains the stream function, defined by (5.150)–(5.152) is unique. Indeed, if one forms the circulation integral along any closed loop $\mathcal{C}$, the value zero is obtained:
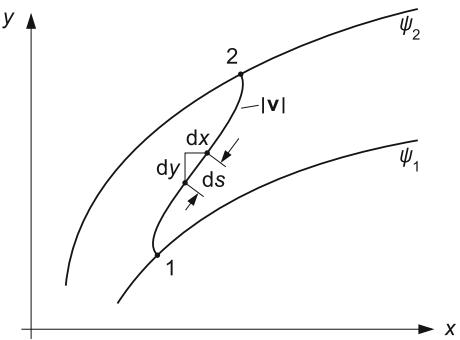
$$\oint\limits_{\mathcal{C}} \mathfrak{w} \cdot \mathrm{d}\boldsymbol{x} \overset{\text{Stokes}}{=} \iint\limits_{\mathcal{A}} \operatorname{curl} \mathfrak{w} \, \mathrm{d}a$$

$$= \iint\limits_{\mathcal{A}} \left(\frac{\partial u}{\partial x} + \frac{\partial v}{\partial y}\right) \mathrm{d}a = \iint\limits_{\mathcal{A}} \underset{=0}{\underbrace{\operatorname{div} \boldsymbol{v}}} \, \mathrm{d}a = 0.$$

- In steady flow, the stream function has a transparent interpretation, see **Fig. 5.25**. Equation (5.152) implies

$$\psi_2 - \psi_1 = \int\limits_{x_1,y_1}^{x_2,y_2} \mathfrak{w} \cdot \mathrm{d}\boldsymbol{x} = \int\limits_{x_1,y_1}^{x_2,y_2} \underset{|v|\mathrm{d}s}{\underbrace{\{u\mathrm{d}y - v\mathrm{d}x\}}} = Q_{1,2}, \tag{5.153}$$

where $Q_{1,2}$ *is the volume flux between the streamlines* ψ_1 *and* ψ_2.

Fig. 5.25 Two streamlines and a path of integration of the flow from point 1 on ψ_1 to point 2 on ψ_2. The flux of the potential fluid across this path from 1 to 2 is given by $Q_{12} = \psi_2 - \psi_1$, see (5.153)

Properties of the stream function: We shall itemize important properties of the stream function:

- The vorticity vector $\boldsymbol{w} = \text{curl } \boldsymbol{v}$ has in plane flow (of the xy-parallel planes) only a z-component

$$w_z = \frac{\partial v}{\partial x} - \frac{\partial u}{\partial y} = -\frac{\partial^2 \psi}{\partial x^2} - \frac{\partial^2 \psi}{\partial y^2} = -\Delta\psi. \tag{5.154}$$

- For plane flow of barotropic fluids with constant density the HELMHOLTZ vorticity theorem (see Chap. 4, (4.35) or (4.36)) applies, namely

$$\frac{\mathrm{d}w_z}{\mathrm{d}t} = 0 \quad \Longrightarrow \quad \frac{\partial w_z}{\partial t} + \frac{\partial w_z}{\partial x}u + \frac{\partial w_z}{\partial y}v = 0, \tag{5.155}$$

or with (5.154)

$$\frac{\partial \Delta\psi}{\partial t} + \frac{\partial \Delta\psi}{\partial x}\frac{\partial \psi}{\partial y} - \frac{\partial \psi}{\partial x}\frac{\partial \Delta\psi}{\partial y} = \frac{\Delta\psi}{\partial t} + J(\Delta\psi, \psi) = 0, \tag{5.156}$$

in which

$$J(a, b) = \frac{\partial a}{\partial x}\frac{\partial b}{\partial y} - \frac{\partial b}{\partial x}\frac{\partial a}{\partial y} = \frac{\partial(a, b)}{\partial(x, y)}$$

is the so-called JACOBIan *determinant*.[16] In steady, barotropic fluids the stream function obeys the equation

$$J(\Delta\psi, \psi) = \frac{\partial(\Delta\psi, \psi)}{\partial(x, y)} = 0. \tag{5.157}$$

---

[16]For a short biography of JACOBI see **Fig. 5.26**.

- If the flow is irrotational, then

$$\Delta\psi = 0, \tag{5.158}$$
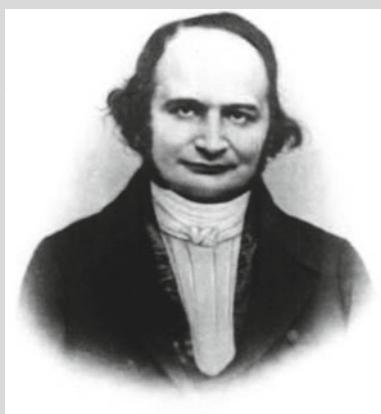
Fig. 5.26 CARL GUSTAV JACOB JACOBI (10. Dec. 1804–18. Feb. 1851)

CARL GUSTAV JACOB JACOBI was a German mathematician with exceptional talent. He grew up in Berlin within a Jewish family of bankers and reached university maturity at the age of 13 years. When entering the gymnasium (high school) he was instantly promoted to the highest class, but stayed there for 4 years, because the Berlin University did not accept students at an age below 16 years. He invested the time to study advanced mathematical literature, see e.g. [3]. In 1824 he graduated in Latin, Greek and mathematics and in 1825 he passed his doctoral exam and 1825/26 he passed his habilitation. From 1826–1843 he was first associate and since 1829 full professor in Königsberg (Kaliningrad), where he reformed together with FRANZ-ERNST NEUMANN by creating the 'mathematical physical seminar' the university education in the mathematical physical sciences. In 1843 he gave up his lecturing for reasons of health (he suffered from diabetes). His support was continued by the Prussian State, because of moral support from P.G.L. DIRICHLET and A. VON HUMBOLDT. He then went to Italy for recovery and soon returned; his financial support was continued, likely because of his membership to the Prussian Academy of Sciences since 1829. However, 1849 he lost all his support, because he had supported the 1848 revolution. He died in 1851 of smallpox.

JACOBI is known in mathematics and theoretical physics and engineering because of his fundamental work on Elliptic Functions, the HAMILTON-JACOBI theory in the theory of analytical dynamics of rigid bodies, continued fraction, JACOBI determinants, the invention of the symbol of partial differentiation, ∂. In celestial mechanics he introduced the sidereal coordinate system.

The text is based on http://www.wikipedia.org
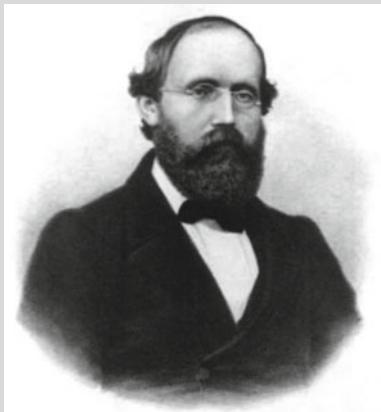
Fig. 5.27 GEORG FRIEDRICH BERNHARD RIEMANN (17. Sept. 1826–20. July 1866)

BERNHARD RIEMANN was a German mathematician, who, despite his short life, created significant results in analysis, differential geometry, mathematical physics and analytic number theory. His education started with Latin, Greek and Hebrew, but he eventually switched to mathematics and took lectures 1847–49 from P.G. DIRICHLET, J. STEINER and C.G.J. JACOBI in Berlin. In the period 1849–1851 he was in Göttingen writing his doctoral dissertation on function theory under C.F. GAUSS and continuing three years later with his habilitation in 1854 on the foundation of geometry. In 1857 he received an associate professorship in mathematics in Göttingen, but had to give it up because of exhaustion. He travelled to Italy and died there due to tuberculosis. His works are on RIEMANNian geometry, algebraic geometry and complex manifold theory. Text based on http://www.wikipedia.org

and (5.157) is trivially satisfied. However, for such flows v is also given by $v = \text{grad }\phi$. In this case we may, therefore, write

$$u = \frac{\partial \phi}{\partial x} = \frac{\partial \psi}{\partial y}, \quad v = \frac{\partial \phi}{\partial y} = -\frac{\partial \psi}{\partial x}. \tag{5.159}$$

These relations between ϕ and ψ are the well-known CAUCHY-RIEMANN[17] differential equations of complex variable theory, in which ϕ and ψ are the real and imaginary parts of a complex valued function.

- A holomorphic (or analytic or regular) complex function will be written as

$$\boldsymbol{\phi}(z) = \phi(x, y) + \iota\psi(x, y); \,, \tag{5.160}$$

where z is the complex argument $z = x + \iota y$, and $\iota = \sqrt{-1}$ is the imaginary unit. $\boldsymbol{\phi}$ is called the complex velocitypotential, whose real part is the two-dimensional

---

[17]For a short biography of RIEMANN see **Fig. 5.27**.
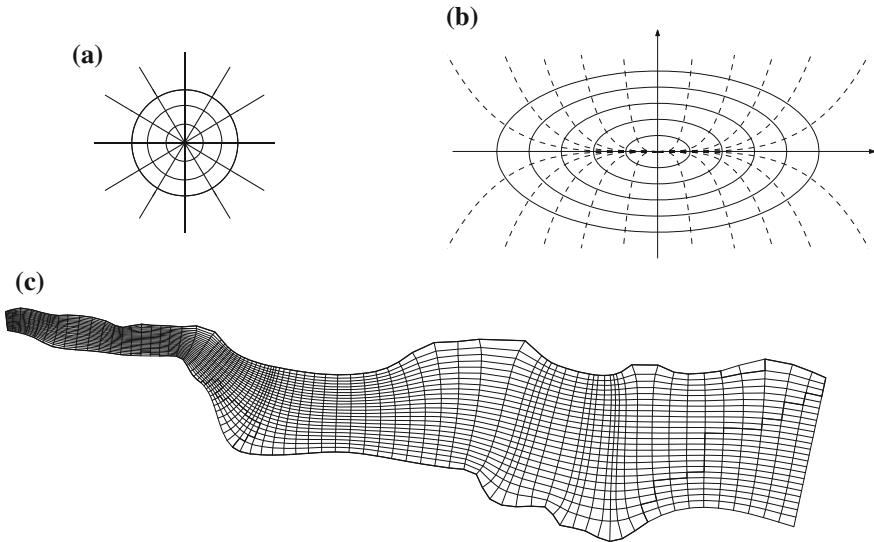
Fig. 5.28 Orthogonal curvilinear coordinate net, constructed with equi-potential lines, $\phi = $ const., and streamlines $\psi = $ const. **a** *Equipotential lines and streamlines of point source flow and potential vortex flow.* **b** *Analogous to* **a** *but e.g. a potential flow from a line source.* **c** *Orthogonal net of curvilinear coordinates in a region adjusted to Lake Constance, constructed by solving the* LAPLACE *equations*

'ordinary' velocity potential and whose imaginary part is the two-dimensional stream function. These properties will be used over and over below.

- The equi-potential lines, $\phi = $ const. and the streamlines $\psi = $ const. form an orthogonal net of lines (**Fig. 5.28**), which cover the two-dimensional flow domain. This is a direct consequence of the complex variable theory. However, the proof also follows a direct approach:

  (i) $\boldsymbol{v} = \text{grad}\,\phi$; therefore $\boldsymbol{v}$ is perpendicular to the lines $\phi = $ const.
  (ii) $\boldsymbol{v} = (\partial\psi/\partial y, -\partial\psi/\partial x)^T$; therefore, grad $\psi \cdot \boldsymbol{v} = 0$ and $\boldsymbol{v}$ is parallel to the lines $\psi = $ const..

The two statements prove the orthogonality of the lines $\phi = $ const. and $\psi = $ const..

This property of holomorphic functions is often used to numerically construct curvilinear orthogonal coordinates in two-dimensional domains, see Fig. 5.28.

5.4.2 *Simple Plane Flows of Ideal Fluids*

We present in this section a number of idealized flows of inviscid, density-preserving fluids. Potential and stream functions as well as the complex potentials will be stated; from all of these the components of the velocity fields can be derived in the respective coordinates.
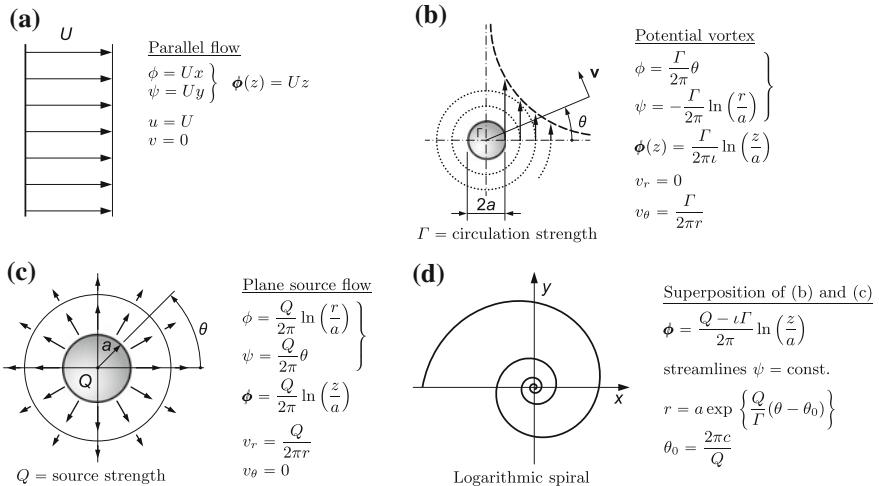
Fig. 5.29 Sketches of four different simple potential flows together with their potentials, stream functions, complex potentials and velocity components in two dimensions. **a** *Constant parallel flow*, **b** *Potential vortex*, **c** *Plane source flow from a single point source*, **d** *Superposition of potential vortex and plane source flows*

(a) Steady parallel flows with constant velocity in the x-direction are described by (see **Fig. 5.29**a:)

$$\left.\begin{array}{l} \phi = Ux, \\ \psi = Uy, \end{array}\right\} \quad \phi(z) = Uz, \tag{5.161}$$

in which $z = x + \iota y$. We may directly verify that

$$u = \frac{\partial \phi}{\partial x} = \frac{\partial \psi}{\partial y} = U,$$

$$v = \frac{\partial \phi}{\partial y} = -\frac{\partial \psi}{\partial x} = 0. \tag{5.162}$$

(b) Potential vortex around a rigid circular kernel of radius a:
Here, one has for the velocity

$$\mathbf{v} = \frac{\Gamma}{2\pi r}\mathbf{e}_\theta. \tag{5.163}$$

Γ is the circulation around the circular streamlines. The stream function and the potential are given by

$$\left.\begin{array}{l} \psi = -\frac{\Gamma}{2\pi}\ln\left(\frac{r}{a}\right), \\ \phi = \frac{\Gamma}{2\pi}\theta, \end{array}\right\} \quad \phi(z) = \frac{\Gamma}{2\pi\iota}\ln\left(\frac{z}{a}\right). \tag{5.164}$$

The stream function has a logarithmic singularity at $r = 0$, the potential is cyclic. The radial and azimuthal velocities can be determined via

$$v = \frac{\partial \phi}{\partial r} e_r + \frac{1}{r} \frac{\partial \phi}{\partial \theta} e_\theta = \frac{1}{r} \frac{\partial \psi}{\partial \theta} e_r - \frac{\partial \psi}{\partial r} e_\theta, \tag{5.165}$$

from which (5.163) can be verified. The complex potential is given by

$$\phi(z) = \phi + \iota \psi = \frac{\Gamma}{2\pi} \left(\theta - \iota \ln \left(\frac{r}{a} \right) \right) = \frac{\Gamma}{2\pi \iota} \left(\ln \left(\frac{r}{a} \right) + \iota \theta \right)$$

$$= \frac{\Gamma}{2\pi \iota} \ln \left(\frac{r e^{\iota \theta}}{a} \right) = \frac{\Gamma}{2\pi \iota} \ln \left(\frac{z}{a} \right). \tag{5.166}$$

Here we have used $z = x + \iota y = r e^{\iota \theta}$. For a summary see Fig. 5.29b.

(c) Plane flow from an isotropic point source:
Let the volume source be given by Q. Then, a simple argument of conservation of mass (or volume for constant density) across concentric circles shows that the velocity is radial and given by

$$v = \frac{Q}{2\pi r} e_r. \tag{5.167}$$

Therefore,

$$\left. \begin{array}{l} \phi = \dfrac{Q}{2\pi} \ln \left(\dfrac{r}{a} \right), \\ \psi = \dfrac{Q}{2\pi} \theta, \end{array} \right\} \qquad \phi = \frac{Q}{2\pi} \ln \left(\frac{z}{a} \right). \tag{5.168}$$

Note the complementarities of (5.168) and (5.166). For a summary see Fig. 5.29c.

(d) Superposition:
Different potential flows can be superposed owing to the linearity of the describing differential equation. Let v_1 and v_2 be the velocities of the potential flows

$$\begin{array}{l} v_1 = \operatorname{grad} \phi_1 = \operatorname{grad} \psi_1 \times e_z, \\ v_2 = \operatorname{grad} \phi_2 = \operatorname{grad} \psi_2 \times e_z. \end{array} \tag{5.169}$$

Then,

$$v = v_1 + v_2 = \operatorname{grad} (\phi_1 + \phi_2) = \operatorname{grad} (\psi_1 + \psi_2) \times e_z \tag{5.170}$$

is again a velocity field of a flow with potential $(\phi_1 + \phi_2)$ and stream function $(\psi_1 + \psi_2)$.

Superposition of isotropic source and potential vortex flows yields

$$\left.\begin{aligned}\phi &= \frac{Q}{2\pi}\ln\left(\frac{r}{a}\right) + \frac{\Gamma}{2\pi}\theta,\\ \psi &= \frac{Q}{2\pi}\theta - \frac{\Gamma}{2\pi}\ln\left(\frac{r}{a}\right),\end{aligned}\right\} \qquad \varPhi = \frac{Q - \iota\Gamma}{2\pi}\ln\left(\frac{z}{a}\right), \qquad (5.171)$$

as can easily be seen if (5.166) and (5.168) are added together. The streamlines are obtained, if one sets $\psi = $ const., i.e.,

$$\frac{Q}{2\pi}\theta - \frac{\Gamma}{2\pi}\ln\left(\frac{r}{a}\right) = c \implies \ln\left(\frac{r}{a}\right) = \frac{Q}{\Gamma}(\theta - \theta_0), \quad \theta_0 = \frac{2\pi c}{Q}.$$

This can also be written as

$$\frac{r}{a} = \exp\left\{\frac{Q}{\Gamma}(\theta - \theta_0)\right\}, \qquad (5.172)$$

of which the graph is a *logarithmic spiral*, see Fig. 5.29d.

(e) Two-dimensional stagnation point flow:
This flow is described by the stream function

$$\psi = \frac{U}{\ell}xy. \qquad (5.173)$$

U is a characteristic velocity and ℓ a characteristic length. The streamlines are the lines $xy = $ const., and the y-axis can be considered as a solid wall. With $\Delta\psi = 0$, the fluid motion is a potential flow with

$$\begin{aligned}u &= \frac{\partial\phi}{\partial x} = \frac{\partial\psi}{\partial y} = \frac{U}{\ell}x,\\ v &= \frac{\partial\phi}{\partial y} = -\frac{\partial\psi}{\partial x} = -\frac{U}{\ell}y.\end{aligned} \qquad (5.174)$$

Integrating these CAUCHY-RIEMANN differential equations yields

$$\phi = \frac{U}{2\ell}\left(x^2 - y^2\right), \quad \psi = \frac{U}{\ell}xy \qquad (5.175)$$

and, therefore,

$$\varPhi(z) = \frac{U}{2\ell}\left[(x^2 - y^2) + 2\iota xy\right] = \frac{U}{2\ell}(x + \iota y)^2 = \frac{U}{2\ell}z^2. \qquad (5.176)$$

This solution is an acceptable approximation of the flow in the vicinity of the stagnation point of a circular cylinder under parallel flow, see **Fig. 5.30**, whose complex potential is (see subsection (h))
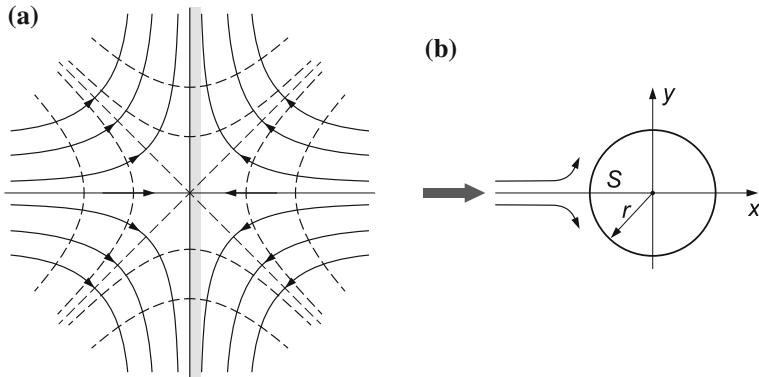
Fig. 5.30 Plane stagnation flow. **a** *Stream and equipotential lines and* **b** *close-up of the velocity of the stagnation point region, which can be approximated by the plane stagnation point flows*

$$\phi_0(z) = U_\infty \left(z + \frac{a^2}{z} \right). \tag{5.177}$$

Expanding this function into TAYLOR series about the stagnation point, thus, setting $z = -a + \zeta$, $|\zeta| \ll 1$, one obtains

$$\phi_0 = U_\infty \left\{ -a + \zeta + a^2 \left[-\frac{1}{a} - \frac{1}{a^2}\zeta + \frac{1}{a^3}\zeta^2 + \dots \right] \right\}$$

$$\approx -2aU_\infty + \frac{U_\infty}{a}\zeta^2 + \dots . \tag{5.178}$$

This agrees formally with (5.176), if one chooses $U/\ell = 2U_\infty/a$ and neglects the difference of the constant, $-2aU_\infty$. For convex two-dimensional cylindrical bodies a must be identified with the local radius of curvature of the cylinder at the stagnation point.

(f) Plane doublet:
Plane dipole flow can be constructed by superposing two source flows with equal strengths but opposite signs. With reference to **Fig. 5.31**a the complex potential is given by

$$\phi(z) = -\frac{Q}{2\pi} \{\ln(z - \Delta x) - \ln(z)\}$$

$$= \frac{Q}{2\pi} \ln \left(1 - \frac{\Delta x}{z} \right) \approx -\frac{Q}{2\pi} \frac{\Delta x}{z} + \mathcal{O}\left((\Delta x)^2\right). \tag{5.179}$$

The limit process $\Delta x \to 0$, such that $Q\Delta x = M \neq 0$ remains bounded, but $Q(\Delta x)^2 \to 0$, then delivers the complex potential of the two-dimensional dipole flow with dipole moment M,
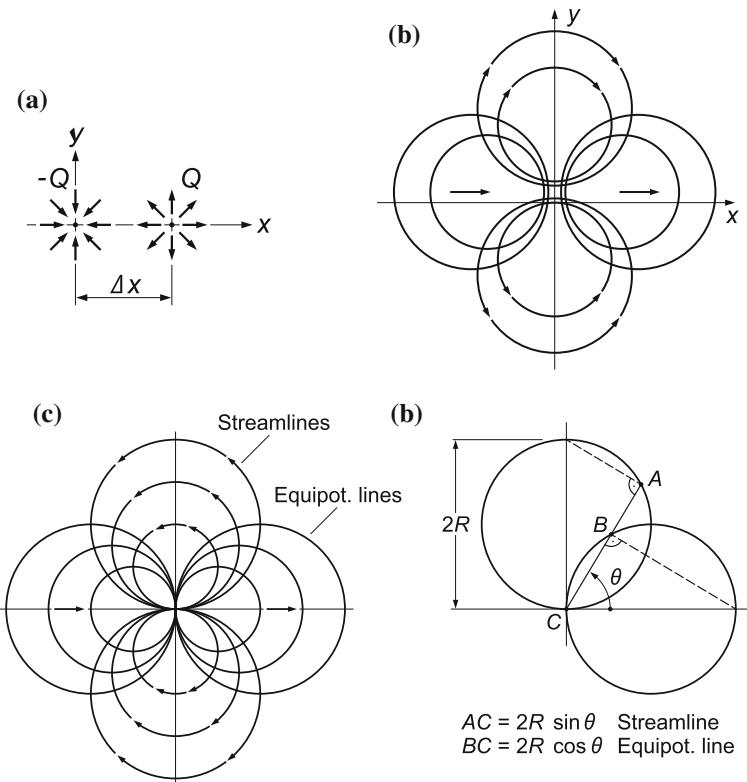
Fig. 5.31 Stream and potential lines due to a source doublet (panel **a** and **c** and a doublet of potential vortices. **a** *Arrangement of sources of equal but opposite strengths at* $(x, y) = [(0, 0)(\Delta x, 0)]$, **b** *Stream and equi-potential lines for a potential vortex doublet with strength* $\pm\Gamma$ *at* $(x, y) = [(0, 0)(0\Delta y)]$, **c** *Stream and equi-potential lines for a doublet of source flows in the limit when* $\Delta x \to 0$ *and* **d** *their construction*

$$\phi = -\frac{M}{2\pi z},\tag{5.180}$$

so that

$$\phi = -\frac{M}{2\pi r}\cos\theta, \quad \psi = \frac{M}{2\pi r}\sin\theta.\tag{5.181}$$

As illustrated in Fig. 5.31c, the stream and equi-potential lines are orthogonal circles through the coordinate origin, which are easily shown to obey the equations

$$\begin{aligned} x^2 + (y \pm R)^2 = R^2 &\quad \text{(streamlines)},\\ (x \pm R)^2 + y^2 = R^2 &\quad \text{(equi-potential lines)}. \end{aligned}\tag{5.182}$$

Here, R is the radius and parameter of the two sets of circles.

The flow distribution due to two potential vortices with equal but opposite strengths Γ at the points $(x, y) = (0, 0)$ and $(x, y) = (0, +\iota \Delta y)$ does equally represent the flow due to a plane doublet. When using the point vortex potential (5.166) employed for this composition, one obtains

$$\phi(z) = \phi + \iota \psi = -\frac{\Gamma}{2\pi \iota} \left\{ \ln \left(\frac{z}{a} \right) - \ln \left(\frac{z - \iota \Delta y}{a} \right) \right\} = \frac{\Gamma}{2\pi \iota} \ln \left(\frac{z - \iota \Delta y}{z} \right)$$

$$= \frac{\Gamma}{2\pi \iota} \ln \left(1 - \frac{\iota \Delta y}{z} \right) \approx -\frac{\Gamma \Delta y}{2\pi z} + \mathcal{O}(\Gamma (\Delta y)^2)$$

$$= -\frac{M}{2\pi z} \qquad (M = \lim_{\Delta y \to 0} \Gamma \Delta y = \text{bounded}). \qquad (5.183)$$

This is the same result as (5.180) and (5.181).

(g) Flow around a semi-infinite blunt body:
When superimposing the potentials of the parallel flow, $\phi(z) = Uz$, and of the plane source flow, $\phi(z) = Q/(2\pi) \ln(z/a)$, the complex potential

$$\phi(z) = Uz + \frac{Q}{2\pi} \ln \left(\frac{z}{a} \right) \qquad (5.184)$$

is obtained, from which, by separation of real and imaginary parts

$$\phi = Ux + \frac{Q}{2\pi} \ln \left(\frac{r}{a} \right), \quad \psi = \frac{Q}{2\pi} \theta + Uy \qquad (5.185)$$

can be deduced. The corresponding Cartesian velocities are given by
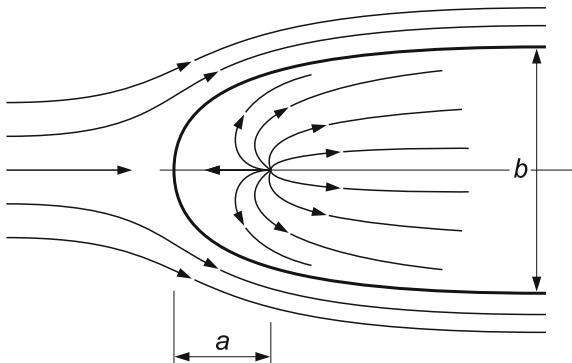
$$u = U + \frac{Qx}{2\pi r^2} = U + \frac{Q}{2\pi r} \cos \theta,$$
$$v = \frac{Q}{2\pi} \frac{ay}{r^2} = \frac{Q}{2\pi} \frac{a}{r} \sin \theta. \qquad (5.186)$$

The stagnation point lies at $x = -a$, $r = a$, where $u = 0$. Thus, from (5.186) $a = Q/(2\pi U)$. It belongs to the point $(x, y) = (-a, 0)$ of the bifurcating streamline. The width b at $x \to \infty$ can be computed by the mass balance statement, see **Fig. 5.32**,

$$Ub = Q \quad \implies \quad b = \frac{Q}{U} = 2\pi a. \qquad (5.187)$$

The contour of the semi-infinite body and the streamlines are displayed in Fig. 5.32. There are also streamlines inside the contour through which no flow takes place. These are generated by the source Q and the parallel-flow velocity.

Fig. 5.32 streamlines of the superposition of a parallel flow with upstream velocity U in the x-direction plus a source flow with strength Q at $(x, y) = (0, 0)$. The bifurcating streamline generates a contour of a semi-infinite virtual body with geometry defined by U and Q. The stagnation point is at $(x, y) = (-a, 0)$ and the width of the body is $b = 2\pi a$

Remark

- If one adds on the x-axis a second point sink of strength Q downstream of the source at $x = 0$, the total mass addition is zero. As a consequence, the bifurcating streamline will be closed so that the flow around a closed finite body is obtained.
- If a continuous source-sink distribution with vanishing total mass (or volume) is arranged along or close to the x-axis, this method leads to a flow around a body of which the geometry is determined by this source-sink distribution. This method can be used within an inverse method to determine the potential flow around bodies of rather general shape.

(h) Flow around a circular cylinder:
The flow is assumed to be perpendicular to the cylinder axis. This motion is a combination of the parallel flow and the dipole flow potentials. Thus,

$$\phi(z) = \phi + \iota\psi = Uz - \frac{M}{2\pi z} = U\left(z - \frac{M}{2\pi U}\frac{1}{z}\right). \tag{5.188}$$

If we now set $M/(2\pi U) = -a^2$, this complex potential transforms to

$$\phi(z) = \phi + \iota\psi = U\left(z + \frac{a^2}{z}\right) = U\left(re^{\iota\theta} + \frac{a^2}{r}e^{-\iota\theta}\right). \tag{5.189}$$

The stream and equi-potential lines are, therefore, given by

$$\phi = U\left(r + \frac{a^2}{r}\right)\cos\theta, \quad \psi = U\left(r - \frac{a^2}{r}\right)\sin\theta \tag{5.190}$$

with constant values for ϕ and ψ, respectively. Of significance is thebifurcating streamline, given by $\psi = 0$, or

$$\sin\theta = 0 \text{ and } r = a \quad \longrightarrow \quad \theta = 0, \pi \text{ and } r = a \text{ (circle)}. \tag{5.191}$$

The flow is symmetric to the x-axis and the radial and azimuthal velocities are obtained by differentiations of (5.190),

$$
\begin{aligned}
v_r &= \frac{\partial \phi}{\partial r} = U \left(1 - \frac{a^2}{r^2} \right) \cos \theta, \\
v_\theta &= \frac{1}{r} \frac{\partial \phi}{\partial \theta} = -U \left(1 + \frac{a^2}{r^2} \right) \sin \theta.
\end{aligned}
\tag{5.192}
$$

It is easy to verify that on the cylinder surface, for $r = a$, one has

$$
v_r = 0, \quad v_\theta = -2U \sin \theta.
\tag{5.193}
$$

Applying the BERNOULLI equation on a streamline between $x = \pm\infty$ (point 1) and a point on the periphery of the cylinder with azimuth angle θ (point 2) one obtains

$$
\underbrace{p + \frac{\rho}{2}(2U)^2 \sin^2 \theta}_{\text{point 2}} = \underbrace{p_\infty + \frac{\rho}{2}U^2}_{\text{point 1}} .
$$
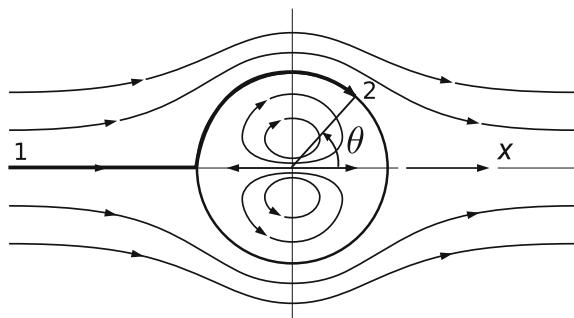
We find for the pressure coefficient

$$
c_p := \frac{p - p_\infty}{(\rho/2)U^2} = 1 - 4 \sin^2 \theta.
\tag{5.194}
$$

Because of the symmetry of the pressure distribution with respect to $\theta = \pi/2$ no flow-induced resultant force is introduced on the circular cylinder. The flow is characteristically very similar to that shown in Fig. 5.7 but now strictly two-dimensional. This is the reason why we show in **Fig. 5.33** the streamlines in a plane perpendicular to the cylinder axis.

This flow around the cylinder can be generalized by adding to it a plane potential vortex flow (5.166). The superposed complex potential and its real and imaginary parts are given by

Fig. 5.33 Uniform flow around a circular cylinder. *The constant parallel motion with upstream velocity U flows around the circular cylinder symmetrically with respect to the x-axis. Within the sphere a fictitious bounded plane dipole flow is generated. The figure shows a plane perpendicular to the cylinder axis*

$$\phi(z) = U\left(z + \frac{a^2}{z}\right) + \frac{\Gamma}{2\pi\iota}\ln\left(\frac{z}{a}\right),$$

$$\phi = U\left(r + \frac{a^2}{r}\right)\cos\theta + \frac{\Gamma}{2\pi}\theta, \tag{5.195}$$

$$\psi = U\left(r - \frac{a^2}{r}\right)\sin\theta - \frac{\Gamma}{2\pi}\ln\left(\frac{r}{a}\right).$$

The bifurcating streamline still coincides with the circle $r = a$, however, the flow is no longer symmetric with respect to the x-axis upstream and downstream of the cylinder. The velocity field is still around the cylinder with radius a, and their components are given by

$$v_r = \frac{\partial\phi}{\partial r} = U\left(1 - \frac{a^2}{r^2}\right)\cos\theta,$$

$$v_\theta = \frac{1}{r}\frac{\partial\phi}{\partial\theta} = -U\left(1 + \frac{a^2}{r^2}\right)\sin\theta + \frac{\Gamma}{2\pi r}, \tag{5.196}$$

with

$$v_r(a) = 0, \qquad\qquad v_r(\pm\infty) = U\cos\theta,$$

$$v_\theta(a) = -2U\sin\theta + \frac{\Gamma}{2\pi a}, \ v_\theta(\pm\infty) = -U\sin\theta. \tag{5.197}$$

It follows that the flow is tangential to the circle $r = a$, and infinitely far away from the cylinder, parallel to the x-axis. The stagnation points lie, where $v_\theta(a) = 0$, according to $(5.197)_2$ at

$$\sin\theta_{\text{stag}} = \frac{\Gamma}{4\pi U a}. \tag{5.198}$$

This formula shows that the stagnation point can only arise, if $|\sin\theta_{\text{stag}}| < 1$ or $|\Gamma| < 4\pi U a$. For $\Gamma < 0$ and $|\Gamma| < 4\pi U a$ the streamlines are qualitatively sketched in **Fig. 5.34**a. When $|\Gamma| > 4\pi U a$ a stagnation point does not arise on the cylinder surface; rather, a free stagnation point develops as a finite fluid mass circumflows the cylinder.

When $\Gamma \neq 0$, there exists a resultant flow-induced force on the cylinder, but it is only perpendicular to the global flow direction and has no x-component. The vanishing of this force in the x-direction follows from symmetry of the pressure, according to the BERNOULLI equation,

$$p_\infty + \frac{\rho}{2}U^2 = p + \frac{\rho}{2}\left(2U\sin\theta - \frac{\Gamma}{2\pi a}\right)^2$$

$$\implies \ p = p_\infty + \frac{\rho}{2}U^2\left\{1 - 4\sin^2\theta + \frac{2\Gamma}{\pi a U}\sin\theta - \frac{\Gamma^2}{4\pi^2 a^2 U^2}\right\} \tag{5.199}$$
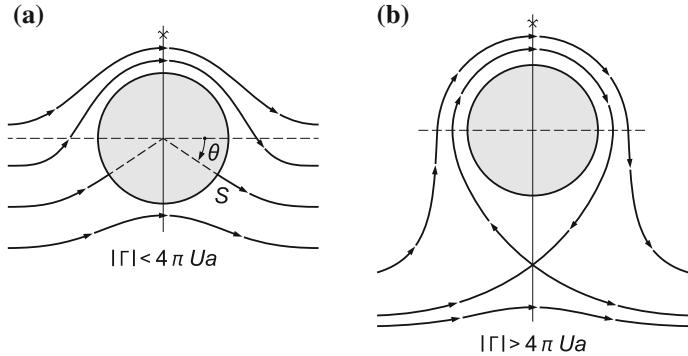
Fig. 5.34 Steady two-dimensional potential flow with non-vanishing circulation around a circular cylinder. **a** *streamlines when two stagnation points develop on the cylinder surface and* **b** *when a free stagnation point is formed*

with respect to the axis through the cylinder center perpendicular to the x-axis. The component of the force, K_y, in this direction then obtains as

$$dK_y = -p(\theta) a \sin\theta \, d\theta,$$

$$K_y = -a \int_0^{2\pi} p(\theta) \sin\theta \, d\theta = -a\rho \frac{U^2}{2} \frac{2\Gamma}{\pi a U} \underbrace{\int_0^{2\pi} \sin^2\theta \, d\theta}_{\pi}. \qquad (5.200)$$

Thus,

$$K_x = 0, \quad K_y = -\rho U \Gamma \quad \longrightarrow \quad \boldsymbol{K} = -\rho U \Gamma \boldsymbol{e}_y. \qquad (5.201)$$

This is the KUTTA-JOUKOWSKI *formula* for the force exerted by the parallel flow on the circular cylinder.

Remark In Subsect. 5.3.2 the force on a three-dimensional body due to potential flow was computed, both for steady and dynamic situations and the results

$$\boldsymbol{K}_{3D}^{\text{steady}} = \boldsymbol{0}, \qquad \boldsymbol{K}_{3D}^{\text{unsteady}} = m\dot{\boldsymbol{U}} \qquad (5.202)$$

were obtained. The quantity $\boldsymbol{m}$ is the tensor of added mass, see (5.138). Here, in two-dimensional flow situations, it can be shown that for $\Gamma = 0$, ϕ decays sufficiently fast far away from the cylinder that

$$\boldsymbol{K}_{2D}^{\text{steady}} = -\rho U \Gamma \boldsymbol{e}_y, \quad \left(\boldsymbol{K}_{2D}^{\text{unsteady}}\right)_{\Gamma=0} = m\dot{\boldsymbol{U}}, \qquad (5.203)$$

in which for the circular cylinder $\boldsymbol{m} = \rho \pi a^2 \boldsymbol{1}$.

Appendix 5.A: Proof of the Gradient Version of GAUSS' Law

In the subsequent analysis the notions of a *convex body* and a *semi-convex body* are used. In $\mathcal{R}^2$ a closed area is called semi-convex, if a straight line has at most two points of intersection with its boundaries, it is called semi-convex, if a straight line has at most two points of intersection with its boundaries or a section of it traces part of its boundary. In non-convex, plane, regions neither of these conditions is satisfied. In a finite body $\mathcal{K}$ in $\mathcal{R}^3$ convexity of $\mathcal{K}$ means that the intersection of a plane surface with $\mathcal{K}$ is a compact set of points, [i.e., the set does not consist of disjoint subsets]. On the other hand, $\mathcal{K}$ is semi-convex, when the above condition holds and a region of such a plane agrees with part of the boundary of $\mathcal{K}$. If none of these conditions prevails, the body is called non-convex.

Consider now a convex body $\mathcal{K}$ with boundary $\partial\mathcal{K}$, see **Fig. 5.35**. Our intention is the evaluation of $\int_{\mathcal{K}}(\partial\phi/\partial x)\,\mathrm{d}v$, where ϕ is a scalar smooth function over $\mathcal{K}$. With reference to **Fig. 5.36** and with $\mathrm{d}V = \mathrm{d}x\mathrm{d}y\mathrm{d}z$, integration yields

$$\int_{\mathcal{K}} \frac{\partial\phi}{\partial x}\mathrm{d}x\mathrm{d}y\mathrm{d}z = \int_{\mathcal{R}} [\phi_u(y, z) - \phi_\ell(y, z)]\,\mathrm{d}y\mathrm{d}z, \tag{5.204}$$

$$\phi_u(y, z) = \phi(f_u(y, z), y, z), \quad \phi_\ell(y, z) = \phi(f_\ell(y, z), y, z), \tag{5.205}$$
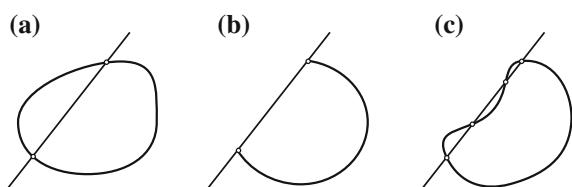
in which $x = f_u(y, z)$ and $x = f_\ell(y, z)$ denote the upper and lower portions of the surface $\partial\mathcal{K}$, and $\mathcal{R}$ is the projection of $\mathcal{K}$ into the yz-plane. Owing to the convexity of $\mathcal{K}$ the variation of y and z within the projection $\mathcal{R}$ of $\mathcal{K}$ measures via the functions f_u and f_ℓ the complete surface $\partial\mathcal{K}$ exactly once.

We now restrict our focus on the upper side of the body. A surface element on this area can be computed as follows: We select three points P_1, P_2, P_3, given by the position vectors $\boldsymbol{r}(y, z)$, $\boldsymbol{r}(y + \mathrm{d}y, z)$, $\boldsymbol{r}(y, z + \mathrm{d}z)$. For small values of $\mathrm{d}y$, $\mathrm{d}z$ the areal increment, spanned by the vectors $\overrightarrow{P_1 P_2}$ and $\overrightarrow{P_1 P_3}$, is given by

$$\mathrm{d}\mathcal{A}_u = \left| \frac{\partial\boldsymbol{r}}{\partial y} \times \frac{\partial\boldsymbol{r}}{\partial z} \right| \mathrm{d}y\mathrm{d}z. \tag{5.206}$$

The oriented vectorial surface element is then given by $\boldsymbol{n}\mathrm{d}\mathcal{A}_u = \mathrm{d}\boldsymbol{A}_u$. The unit normal vector $\boldsymbol{n}$ of the surface element is given by

Fig. 5.35 Illustrating the definition of convex **(a)**, semi-convex **(b)** and non-convex **(c)** areas in $\mathcal{R}^2$
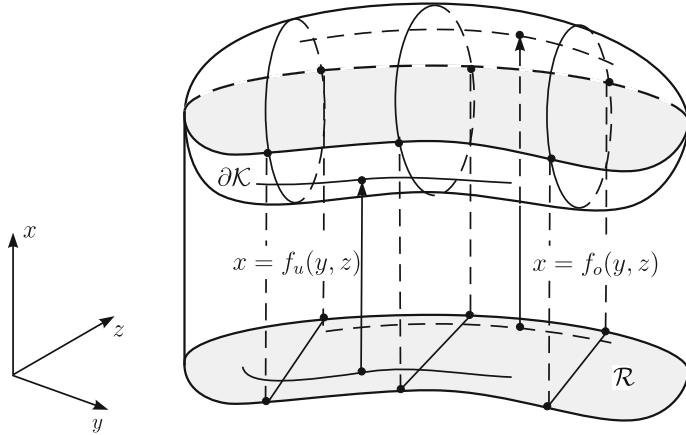
Fig. 5.36 Explaining the derivation of the gradient version of Gauss' law in $\mathcal{R}^3$. *For a convex body the integral $\int_{\mathcal{K}}(\partial\phi/\partial x)\,\mathrm{d}v$ is evaluated by integrating first in the z-direction and subsequently in the directions x and y. $\mathcal{R}$ is the projection of the three-dimensional body into the xy-plane. Moreover, $x = f_u(y, z)$ and $x = f_\ell(y, z)$ describe the upper and lower surfaces of $\partial\mathcal{K}$*

$$n = \pm \frac{(\partial r/\partial y) \times (\partial r/\partial z)}{|(\partial r/\partial y) \times (\partial r/\partial z)|},$$

so that the oriented vectorial surface element takes the form

$$\mathrm{d}A_u = \left(\frac{\partial r}{\partial y} \times \frac{\partial r}{\partial z}\right)\mathrm{d}y\mathrm{d}z,$$

or with the vector $r = f_u i + y j + z k$,

$$\mathrm{d}A_u = \left(1i - \frac{\partial f_u}{\partial y}j - \frac{\partial f_u}{\partial z}k\right)\mathrm{d}y\mathrm{d}z. \tag{5.207}$$

In this formula the orientation of n has been so taken that $\mathrm{d}A_u$ is a vector pointing out of $\mathcal{K}$.

In an analogous fashion the surface element on the lower part of $\partial\mathcal{K}$ can be computed; it yields

$$\mathrm{d}A_\ell = -\left(1i - \frac{\partial f_\ell}{\partial y}j - \frac{\partial f_\ell}{\partial z}k\right)\mathrm{d}y\mathrm{d}z. \tag{5.208}$$

Combining the last two formulae, thus, yields

$$\mathrm{d}A = \pm\left(1i - \frac{\partial f_{u,\ell}}{\partial y}j - \frac{\partial f_{u,\ell}}{\partial z}k\right)\mathrm{d}y\mathrm{d}z, \tag{5.209}$$

and it is obvious that $\mathrm{d}y\mathrm{d}z = \mathrm{d}A \cdot i$

Returning to formula (5.205) we, thus, obtain for a convex body

$$\int_{\mathcal{K}} \frac{\partial \phi}{\partial x}\,\mathrm{d}v = \int_{\mathcal{R}} (\phi_u(y,z) - \phi_\ell(y,z))\,\mathrm{d}y\mathrm{d}z = \int_{\partial\mathcal{K}} \phi \boldsymbol{i} \cdot \mathrm{d}\boldsymbol{A} = \int_{\partial K} \phi \boldsymbol{i} \cdot \boldsymbol{n}\,\mathrm{d}A. \quad (5.210)$$

Thus, the volume integral of $\partial\phi/\partial x$ has been expressed by the surface integral on the far right of (5.210).

If $\mathcal{K}$ is semi-convex, one may orient the coordinate system such that the plane part of $\partial\mathcal{K}$ is parallel to the xy-plane, see **Fig. 5.37**. If $\partial\mathcal{K}$ is divided into a convex part $\mathcal{A}$ and a non-convex part $\mathcal{B}$. The same arguments as before then yield again (5.210), in which the integration over $\partial\mathcal{K} = \mathcal{A} \cup \mathcal{B}$ can be split into integrals over $\mathcal{A}$ and $\mathcal{B}$, but for part $\mathcal{B}$ one has $\boldsymbol{i} \cdot \boldsymbol{n} = 0$. Formally, the result (5.210) remains valid.

This result can easily be extended to non-convex bodies. To this end one divides the body by plane cuts into a number of convex bodies [see **Fig. 5.38**, where a single plane cut has generated two semi-convex bodies]. For each of the two semi-convex bodies the result (5.210) applies. It is obvious that the contributions of the integral

Fig. 5.37 Semi-convex body. *The Cartesian coordinate system is oriented such that the flat boundary part B is parallel to the xy-plane*
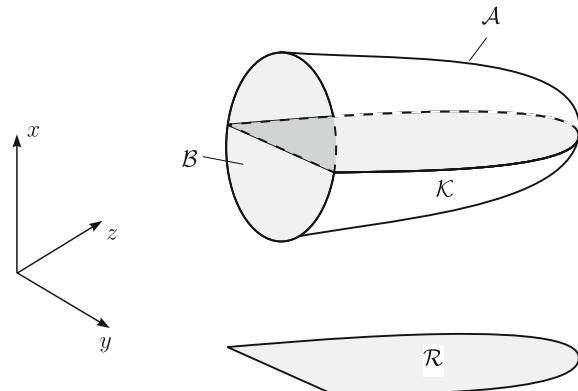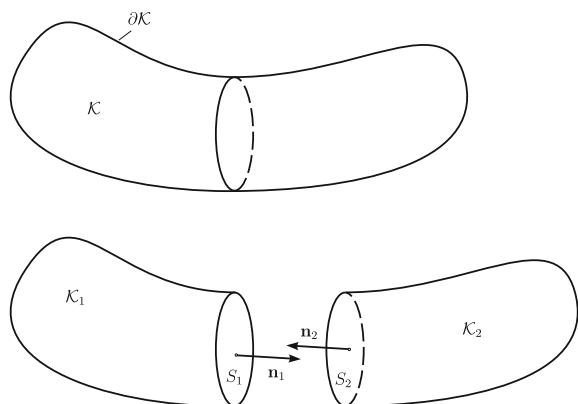
Fig. 5.38 Non-convex body. *Such bodies are split into a number of semi-convex bodies by plane cuts. The unit normal vectors on these planes of thus separated body parts are in opposite directions so that their contributions drop out in the integration of* (5.211)

over the cut surface yields the same absolute value, since at corresponding points on S_1 and S_2 the function values of ϕ are the same but the unit normal vectors point in opposite directions, $\boldsymbol{n}_1 = -\boldsymbol{n}_2$, so that

$$\int_{S_1} \phi \boldsymbol{n}_1 \, dA + \int_{S_2} \phi \boldsymbol{n}_2 \, dA = 0.$$

This result holds for all semi-convex parts of a non-convex body. We, thus, conclude: Independent of the shape of a body the following identity holds

$$\int_{\mathcal{K}} \frac{\partial \phi}{\partial x} \, dv = \int_{\partial \mathcal{K}} \phi \, (\boldsymbol{i} \cdot \boldsymbol{n}) \, dA. \tag{5.211}$$

This is the gradient version of GAUSS' law.

Appendix 5.B: Proof of Stokes' Law

Let $\boldsymbol{f}$ be a differentiable force field in $\mathcal{R}^3$. Then, $\boldsymbol{f} \cdot d\boldsymbol{x}$ is the infinitesimal work done by $\boldsymbol{f}$, if the point of attack of $\boldsymbol{f}$ is displaced by the vectorial displacement increment $d\boldsymbol{x}$. **Figure 5.39**a shows a right angle triangle with side length $2d\boldsymbol{x}$ and $2dy$ parallel to the x- and y-axes of three-dimensional Cartesian coordinates and surface area $dA_z = 2dxdy$. If the point of attack of the force is displaced along the edges of the triangle the values of the components of the force $\boldsymbol{f}$ at the midpoints
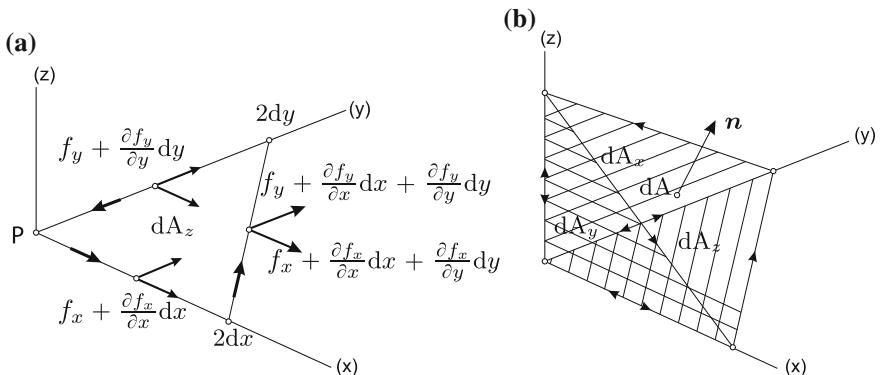
Fig. 5.39 Explaining the derivation of Stokes' theorem. **a** *Infinitesimal triangle in the* (xy)-*plane with sides* $2dx$ *and* $2dy$ *along the x- and y-axes. Components of the mid-points of the triangle, explaining the evaluation of the work done by* $\boldsymbol{f}$ *around the triangle.* **b** *The work done by* $\boldsymbol{f}$ *along the infinitesimal triangle with unit normal* $\boldsymbol{n}$ *can be evaluated by adding the work of* $\boldsymbol{f}$ *along the triangles in the xy-, yz- and xz-planes*

of the triangular edges are as indicated in the figure. The work done by a shift of $\boldsymbol{f}$ clockwise around the triangle is then to lowest order given by the expression

$$
\begin{aligned}
\mathrm{d}W_z &= \left(f_x + \frac{\partial f_x}{\partial x}\mathrm{d}x \right)(2\mathrm{d}x) + \left(f_x + \frac{\partial f_x}{\partial x}\mathrm{d}x + \frac{\partial f_x}{\partial y}\mathrm{d}y \right)(-2\mathrm{d}x) \\
&\quad + \left(f_y + \frac{\partial f_y}{\partial x}\mathrm{d}x + \frac{\partial f_y}{\partial y}\mathrm{d}y \right)(2\mathrm{d}y) + \left(f_y + \frac{\partial f_y}{\partial y}\mathrm{d}y \right)(-2\mathrm{d}y) \\
&= \frac{\partial f_x}{\partial y}\mathrm{d}y(-2\mathrm{d}x) + \frac{\partial f_y}{\partial x}\mathrm{d}x(2\mathrm{d}y) \\
&= \left(\frac{\partial f_y}{\partial x} - \frac{\partial f_x}{\partial y} \right)(2\mathrm{d}x\mathrm{d}y) = (\mathrm{curl}\,\boldsymbol{f})_z\,\mathrm{d}A_z.
\end{aligned}
\tag{5.212}
$$
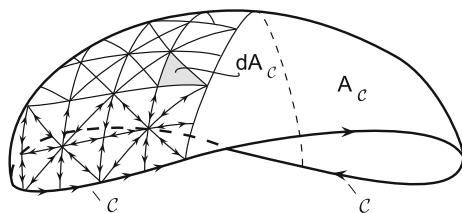
If we now generalize this two-dimensional situation to the infinitesimal triangle $\mathrm{d}A$ of the infinitesimal tetrahedron of Fig. 5.39b, with the orientation of the shift of $\boldsymbol{f}$ around the edges of the inclined triangle indicated by the exterior unit vector $\boldsymbol{n}$, then it is easily seen that this work can be composed as the sum of work done by the force field along the three triangles parallel to the xy-, yz- and zx-planes. In this process the work done along the coordinate-parallel axes cancels out because these lines are traversed twice in opposite directions. Thus,

$$
\begin{aligned}
\mathrm{d}W &= \mathrm{d}W_x + \mathrm{d}W_y + \mathrm{d}W_z \\
&= (\mathrm{curl}\,\boldsymbol{f})_x\mathrm{d}A_x + (\mathrm{curl}\,\boldsymbol{f})_y\mathrm{d}A_y + (\mathrm{curl}\,\boldsymbol{f})_z\mathrm{d}A_z \\
&= \mathrm{curl}\,\boldsymbol{f} \cdot \boldsymbol{n}\,\mathrm{d}A.
\end{aligned}
\tag{5.213}
$$

Here, the three contributions on the right-hand side have simply been written down by cyclic permuting the result (5.212). Moreover, the obvious geometric property $\mathrm{d}A_j = n_j\mathrm{d}A$ has also been used.

Consider, next a double-point free curve $\mathcal{C}$ in a region of $\mathcal{R}^3$, in which the continuous force field $\boldsymbol{f}$ is defined and span this loop by a smooth surface $A_{\mathcal{C}}$, which does not have the domain of definition of $\boldsymbol{f}$. (Note this surface is not uniquely specified.) This surface is filled with connected triangles as shown in **Fig. 5.40**. It is easily seen that the work done by the force field $\boldsymbol{f}$ around the closed loop can be calculated by evaluating the work done around all the infinitesimal triangles in the same orientation as that around $\mathcal{C}$. Since for interior infinitesimal triangles the edges are traced

Fig. 5.40 Surface $A_{\mathcal{C}}$ spanned by a smooth double point free closed curve $\mathcal{C}$. *The work done by a differentiable force field $\boldsymbol{f}$ around $\mathcal{C}$ is composed of the summation of the work around all infinitesimal triangles $\mathrm{d}A_{\mathcal{C}}$*

twice but in opposite directions in this process, the work along these infinitely many triangular sides vanishes. Alternatively, the work done along an infinitesimal triangle is given by $dW = (\mathrm{curl}\, \boldsymbol{f} \cdot \boldsymbol{n})dA$. Consequently, the total work performed by $\boldsymbol{f}$ on the surface is given by

$$W = \iint\limits_{A_e} (\mathrm{curl}\, \boldsymbol{f}) \cdot \boldsymbol{n}\, dA = \oint\limits_{\mathcal{C}} \boldsymbol{f} \cdot d\boldsymbol{x}. \qquad (5.214)$$

This is STOKES' theorem, here derived for a force field, however, it applies to any vector field e.g. the velocity field. In that case, the integral on the right-hand side of (5.214) is called the circulation of the velocity field around the loop $\mathcal{C}$.

References

1. Batchelor, G. K. (1967). *An introduction to Fluid Mechanics*. Cambridge, UK: Cambridge University Press.
2. Duncan, W. J., Thom, A. S., & Young, A. D. (1970). *Mechanics of Fluids*. London: Hodder Arnold.
3. Fröbe, S. und Wassermann, A.: *Die Bedeutendsten Mathematiker*, p 112. Marix Verlag, Wiesbaden (2007)
4. Green, G.: An essay on the application of mathematical analysis to the theories of electricity and magnetism. Nottingham (1828). [Printed for the Author by T. Wheelhouse, Nottingham. (Quarto, vii + 72 pages.)]
5. Green, G.: Mathematical Investigations concerning the Laws of the Equilibrium of Fluids analogous to the Electric Fluid, with other similar Researches. Cambridge Philosophical Society, 12 Nov 1832, printed in the Transactions 1833. Quatro, 64 pages.) Vol. III, Part I Communicated by Sir Edward French Bromhead, Bart., M.A., F.R.S.L. and E
6. Kreyszig, E. (2006). *Advanced Engineering Mathematics* (9th ed.). Hoboken, NJ, USA: Wiley.
7. Kundu, P. K., Cohen, I. M., & Dowling, D. R. (2016). *Fluid Mechanics* (6th ed.). Oxford: Academic Press.
8. Neumann, C.G.: *Vorlesungen über Riemann's Theorie der Abelschen Integrale* (1865)
9. Neumann, C.G.: *Hydrodynamische Untersuchungen: nebst einem Anhang über die Probleme der Eelektrostatik und die magnetische Induktion*. Teubner Leipzig (1883)
10. Popula, L.: *Mathematik für Ingenieure und Naturwissenschaftler*. Band 3 (3. Auflage) Vieweg, Braunschweig, Wiesbaden (1999)
11. Popula, L.: *Mathematik für Ingenieure und Naturwissenschaftler*. Bände 3 (9. Auflage) Vieweg, Braunschweig, Wiesbaden (2000)
12. Sokolnikoff, I. S., & Redheffer, R. M. (1966). *Mathematics of Physics and modern Engineering, XI+721 p* (2nd ed.). New York: McGraw-Hill.

Chapter 6
Function-Theoretical Methods Applied to Plane Potential Flows

Abstract Plane two-dimensional potential flows can be treated by methods of complex variable theory. A complex valued function of a complex variable consists of a real and imaginary part, which represent, respectively, the real velocity potential and stream function of a velocity field, which satisfy the CAUCHY-RIEMANN differential equations. Such a function may be viewed as a conformal (angle preserving) map from the $z = x + \iota y$ plane to the $\zeta = \xi + \iota \eta$ plane. More generally, if $\phi(z)$ represents a potential flow in the z-plane around a given body and $z = h(\zeta)$ is a conformal map from the z- to the ζ-plane, then $\phi(h(\zeta)) = \tilde{\phi}(\zeta)$ describes the potential flow in the ζ-plane around the image of the given body. Of immense constructive use is the following obvious extension of RIEMANN's theorem that 'every simply connected domain can conformally be mapped onto any other simply connected domain. The above facts are illustrated by means of a large number of examples: (generalized) stagnation point flows in and around wedges; source, circulation and dipole flows; flows with circulation around cylinders and plates; flows around circular segments and JOUKOWSKI and VON KÁRMÁN-TREFFTS profiles, etc. The circle theorem of MILNE-THOMSON achieves the reflection or mirror picture of a source at the periphery of the circle. This property can be used to construct potential jet flows through an orifice (as first solved by KIRCHHOFF in 1860), or a periodic arrangement of such slits. The chapter ends with an introduction into the theory of SCHWARZ-CHRISTOFFEL transformations and the demonstration of its usefulness in a number of hydraulically significant applications as potential flows through elliptical and polygonal pipes, as well as flows over a topographic step or from a bottom channel into a half space, etc.

Keywords Complex variable methods · CAUCHY-RIEMANN equations · RIEMANN's theorem · Potential flows around JOUKOWSKI and VON KÁRMÁN-TREFFTS profiles · SCHWARZ-CHRISTOFFEL transformations and their use in potential flows

List of Symbols

Roman Symbols

A, B, C	Constants of integration
a	Radius of a circle, semi-width of a laminar jet

b	Half-slit opening
c_A, c_L, c_ℓ	Lift coefficient
$f'(z)$	Derivative of $f(z)$ with respect to z
g	Gravity constant
h	Height, depth of a fluid layer
ι	Imaginary unit
$\boldsymbol{K}$	Force exerted by a potential flow on a 2-dimensional body
p	Pressure
Δp	Pressure difference
Q	Source (strength) of the velocity field $\boldsymbol{u} = (u, v)$ along $\mathfrak{C}$: $Q = \oint_{\mathfrak{C}} \boldsymbol{u} \cdot \boldsymbol{n} \mathrm{d}s$
R	Radius of a circle
r	Radial coordinate
s	Arc length
t	Periodicity of a periodic arrangement of slits
U	Constant velocity in the x-direction of an almost parallel flow
u, v	Velocity components in the x- and y-directions
$w = u - \iota v$	Complex velocity w as obtained by $w = \mathrm{d}\phi/\mathrm{d}z$
x, y	Cartesian coordinates
$z = x + \iota y$	Complex variable
$\lvert z \rvert$	Modulus of the complex valued z
$\bar{z}$	Conjugate complex of z

Greek Symbols

α	Polar angle of a complex number
Γ	Circulation of the velocity field $\boldsymbol{u} = (u, v)$ along the loop $\mathfrak{C}$: $\Gamma = \oint_{\mathfrak{C}} \boldsymbol{u} \cdot \mathrm{d}\boldsymbol{x}$
θ	Azimuthal angle, – coordinate, polar angle
ϕ	Potential function
ψ	Stream function
$\pmb{\phi} = \phi + \iota\psi$	Complex function, complex potential
$\bar{\phi}$	Complex conjugate of ϕ
$\zeta = g(z)$	Complex function
$z = h(\zeta)$	Inverse function of $g(z)$
ρ	Density
$\xi + \iota\eta$	Complex variable with real, ξ, and imaginary, η, parts

Miscellaneous Symbols

$\arcsin(\phi)$	Inverse function of $\sin(\phi)$
$\arccos(\phi)$	Inverse function of $\cos(\phi)$
$\mathrm{areasinh}(\phi)$	Inverse function of $\sinh(\phi)$
$\mathrm{areacosh}(\phi)$	Inverse function of $\cosh(\phi)$

6.1 General Principles

Function-theoretical methods can in fluid mechanics be applied to ideal fluids for which a velocity potential can be defined. They are restricted to two-dimensional flows ofdensity preserving inviscid fluids. Their use is based on two theorems of complex-variable theory, which we shall state in this section, but not prove them. The reader may consult any book[1] on complex variable theory.[2]

6.1.1 Some Notation and Mathematical Properties of Complex Functions

In the ensuing analysis $z = x + \iota y$ or $\zeta = \xi + \iota\eta$ will denote complex variables z or ζ with real parts x, ξ and imaginary parts y, η, respectively; $\iota = \sqrt{-1}$ is the imaginary unit. For complex variables we shall employ alternatively the 'Cartesian' or 'polar' representation, e.g.,

$$z = x + \iota y = r\,\exp(\iota\theta), \quad \text{where } r = \sqrt{x^2 + y^2}, \quad \theta = \arctan\left(\frac{y}{x}\right). \quad (6.1)$$

Recall that they can be transformed into one another by Eulers formula

$$\exp(\iota\theta) = \cos\theta + \iota\sin\theta. \quad (6.2)$$

Formulae (6.1) and (6.2) obviously imply

$$x = r\cos\theta, \quad y = r\sin\theta. \quad (6.3)$$

Note that the selection $(\theta + 2k\pi), k = 0, \pm 1, \pm 2, ...$ delivers the same position (x, y) in formula (6.3). For this reason the argument of a non-zero complex number $x + \iota y$ is the multivalued function

$$\arg z = \theta + 2k\pi, \quad k = 0, \pm 1, \pm 2, ..., \quad (6.4)$$

where θ is such that

$$\cos\theta = \frac{x}{\sqrt{x^2 + y^2}}, \quad \sin\theta = \frac{y}{\sqrt{x^2 + y^2}}. \quad (6.5)$$

---

[1] Such books are e.g. AHLFORS [3], CARATHEODORY [10], DRISCOLL and TREFETHEN [13], HENRICI [16–18], KNOPP [20], OLVER [23], SHAW [24], ZILL and SHANAHAN [27].

[2] The complex notation of the two-dimensional velocity field of an ideal, density-preserving fluid has already been introduced in Chap. 5, see Sect. 5.4: 'Plane Flow Configuration'. Apart from this, the reader is expected to know some basics of Complex Variable Theory.

The element of arg$z$, determined by the condition $\theta \in [0, 2\pi)$ and $k = 0$ is called the principal value of z and is denoted by arg$z$. Any element of arg$z$ is referred to as argument of z.

A complex valued function $z \mapsto \phi(z)$ of the complex variable z can be written in the form

$$\phi(z) = \phi(x + \iota y) = \phi(x, y) + \iota \psi(x, y). \tag{6.6}$$

Its real part $(x, y) \mapsto \phi(x, y)$, and its imaginary part $(x, y) \mapsto \psi(x, y)$, are real valued functions of the two real variables x and y. ϕ is called continuous, if both the real and imaginary parts are continuous. ϕ is called complex differentiable at the point z_0 if the limit

$$\lim_{z \to z_0} \frac{\phi(z) - \phi(z_0)}{z - z_0} = a \tag{6.7}$$

exists. The complex value a is called the complex derivative of ϕ at z_0 and is denoted by $\frac{d\phi}{dz}(z_0)$. The limit in (6.7) means that

$$\lim_{z_n \to z_0} \frac{\phi(z_n) - \phi(z_0)}{z_n - z_0} = a \tag{6.8}$$

holds for every sequence z_n of complex numbers, which tends to z_0. The sequence $z_n = x_n + \iota y_n$ can approach the complex number $z_0 = x_0 + \iota y_0$ in any way. In particular, we can choose for z_n the sequence $z_n = x_n + \iota y_0$ or the sequence $z_n = x_0 + \iota y_n$ with real sequences x_n and y_n satisfying $\lim_{n \to \infty} x_n = x_0$ and $\lim_{n \to \infty} y_n = y_0$. The first sequence approaches z_0 along the real axis, the second sequence approaches z_0 along the imaginary axis. From (6.6) and (6.8) we obtain for these sequences and for the partial derivatives $\partial\phi/\partial x$, $\partial\phi/\partial y$, $\partial\psi/\partial x$, $\partial\psi/\partial y$ of the real and imaginary parts that

$$\begin{aligned}
&\frac{\partial\phi}{\partial x}(x_0, y_0) + \iota \frac{\partial\psi}{\partial x}(x_0, y_0) \\
&= \lim_{n \to \infty} \left(\frac{\phi(x_n, y_0) - \phi(x_0, y_0)}{x_n - x_0} + \iota \frac{\psi(x_n, y_0) - \psi(x_0, y_0)}{x_n - x_0} \right) \\
&= \lim_{n \to \infty} \frac{\phi(x_n + \iota y_0) - \phi(x_0 + \iota y_0)}{x_n - x_0} = a \\
&= \lim_{n \to \infty} \frac{\phi(x_0 + \iota y_n) - \phi(x_0 + \iota y_0)}{\iota y_n - \iota y_0} \\
&= \lim_{n \to \infty} \left(\frac{\phi(x_0, y_n) - \phi(x_0, y_0)}{\iota(y_n - y_0)} + \iota \frac{\psi(x_0, y_n) - \psi(x_0, y_0)}{\iota(y_n - y_0)} \right) \\
&= -\iota \frac{\partial\phi}{\partial y}(x_0, y_0) + \frac{\partial\psi}{\partial y}(x_0, y_0). \tag{6.9}
\end{aligned}$$

If we compare the left and right hand sides of (6.9), we see that if ϕ is complex differentiable at the point $z_0 = x_0 + \iota y_0$, then the real and imaginary parts must satisfy the CAUCHY-RIEMANN differential equations

$$\frac{\partial \phi}{\partial x}(x_0, y_0) = \frac{\partial \psi}{\partial y}(x_0, y_0), \qquad \frac{\partial \phi}{\partial y}(x_0, y_0) = -\frac{\partial \psi}{\partial x}(x_0, y_0) \qquad (6.10)$$

at the point (x_0, y_0). Conversely, if ϕ and ψ are differentiable at (x_0, y_0) in the sense of functions of two real variables and if (6.10) holds, then ϕ is complex differentiable at $z_0 = x_0 + \iota y_0$.

If $\mathcal{D}$ is an open subset of the complex plane and if ϕ is complex differentiable at every point of $\mathcal{D}$, then ϕ is called regular, analytic or holomorphic. A holomorphic function on $\mathcal{D}$ is automatically infinitely often complex differentiable in $\mathcal{D}$, hence also the real and imaginary parts are infinitely often differentiable. Further differentiation of (6.10) leads to the Laplace equation

$$\frac{\partial^2 \phi}{\partial x^2} + \frac{\partial^2 \phi}{\partial y^2} = 0, \qquad \frac{\partial^2 \psi}{\partial x^2} + \frac{\partial^2 \psi}{\partial y^2} = 0, \qquad (6.11)$$

satisfied by the real and imaginary parts of a holomorphic function. The real and imaginary parts are therefore potential or harmonic functions. We call a complex function a complex potential function or a harmonic function, if the real and imaginary parts are both potential functions. Holomorphic functions are therefore complex potential functions.

If $(x, y) \mapsto \phi(x, y)$ is a given real valued function satisfying the Laplace equation

$$\frac{\partial^2 \phi}{\partial x^2}(x, y) + \frac{\partial^2 \phi}{\partial y^2}(x, y) = 0 \qquad (6.12)$$

for all (x, y) such that $z = x + \iota y$ belongs to the open, connected subset $\mathcal{D}$ of the complex plane, then the vector field

$$(x, y) \quad \mapsto \quad \left(-\frac{\partial \phi}{\partial y}(x, y), \frac{\partial \phi}{\partial x}(x, y) \right)$$

satisfies the integrability condition

$$\frac{\partial}{\partial y} \left(-\frac{\partial \phi}{\partial y} \right) = -\frac{\partial^2 \phi}{\partial y^2} = \frac{\partial^2 \phi}{\partial x^2} = \frac{\partial}{\partial x} \left(\frac{\partial \phi}{\partial x} \right),$$

hence this vector field is a gradient field, which means that it has a real valued potential ψ. This potential satisfies

$$\frac{\partial \psi}{\partial x}(x, y) = -\frac{\partial \phi}{\partial y}(x, y), \qquad \frac{\partial \psi}{\partial y}(x, y) = \frac{\partial \phi}{\partial x}(x, y). \qquad (6.13)$$

(a)

(b)
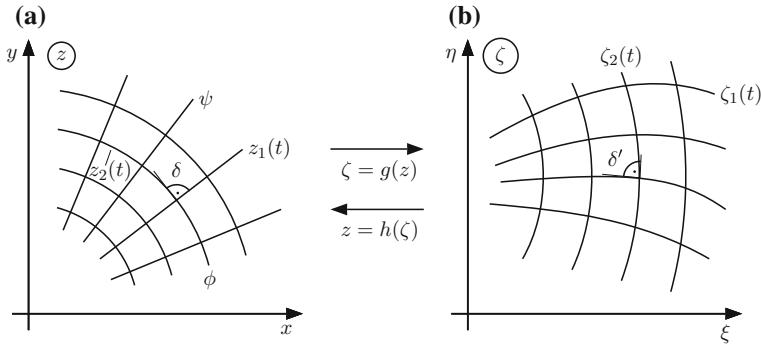
Fig. 6.1 Conformal mapping. *An orthogonal net in the z-plane, representing constant values of $\phi(z)$ and $\psi(z)$, respectively, is mapped onto an orthogonal net in the ζ-plane and vice versa*

These are the CAUCHY-RIEMANN differential equations for the complex function $\boldsymbol{\phi}$ defined by

$$\boldsymbol{\phi}(z) = \boldsymbol{\phi}(x + \iota y) = \phi(x, y) + \iota\psi(x, y).$$

Consequently, $\boldsymbol{\phi}$ is a holomorphic function on $\mathcal{D}$. It thus follows that to every real valued harmonic function ϕ an imaginary part ψ can be constructed such that $\boldsymbol{\phi} = \phi + \iota\psi$ is a holomorphic function. Likewise to every given harmonic function ψ a real part ϕ can be constructed such that $\boldsymbol{\phi} = \phi + \iota\psi$ is holomorphic.

Theorem 6.1 *Every holomorphic function*

$$\zeta = g(z) \quad \Longleftrightarrow \quad z = h(\zeta) \tag{6.14}$$

defines a conformal (angle conserving) mapping of regions of the z-plane into regions of the ζ-plane and vice versa, see **Fig. 6.1**. ∎

The preservation of the angle (congruity) can be demonstrated as follows; let $z_1(t)$ and $z_2(t)$ be two lines in the z-plane, in which t is the curve parameter. Therefore,

$$\dot{z}_1(t) = r_1 \exp(\iota\theta_1) = |\dot{z}_1| \exp(\iota\theta_1) \quad \longrightarrow \quad \theta_1 = \frac{1}{\iota} \ln\left(\frac{\dot{z}_1(t)}{|\dot{z}_1(t)|}\right),$$

$$\dot{z}_2(t) = r_2 \exp(\iota\theta_2) = |\dot{z}_2| \exp(\iota\theta_2) \quad \longrightarrow \quad \theta_2 = \frac{1}{\iota} \ln\left(\frac{\dot{z}_2(t)}{|\dot{z}_2(t)|}\right). \tag{6.15}$$

These two formulae for θ_1 and θ_2 yield

$$\iota(\theta_1 - \theta_2) = \iota\delta = \ln\left\{\frac{\dot{z}_1}{|\dot{z}_1|}\frac{|\dot{z}_2|}{\dot{z}_2}\right\} = \ln\left\{\frac{h'_1\dot{\zeta}_1}{|h'_1\dot{\zeta}_1|}\frac{|h'_2\dot{\zeta}_2|}{h'_2\dot{\zeta}_2}\right\}$$

$$= \ln\left\{\frac{\dot{\zeta}_1}{|\dot{\zeta}_1|}\frac{|\dot{\zeta}_2|}{\dot{\zeta}_2}\right\} = \iota\delta' \longrightarrow \delta = \delta', \tag{6.16}$$

where $h'_i = h'(\zeta_i(t))$, $i = 1, 2$. Here, δ and δ' are the angles between the two lines in the z-plane and ζ-plane, respectively. Therefore, an orthogonal net in the z-plane is mapped onto an orthogonal net in the ζ-plane.

In applications of fluid dynamics one interprets the inviscid flow in the z-plane with the complex potential $\boldsymbol{\phi}(z) = \phi(z) + \iota\psi(z)$. A quadratic net of stream- and equipotential lines (ϕ and ψ = const.) is then transferred to a quadratic net in the ζ-plane and defines there a new potential flow via

$$\boldsymbol{\phi}(z) = \boldsymbol{\phi}(h(\zeta)) = \tilde{\boldsymbol{\phi}}(\zeta). \tag{6.17}$$

One employs e.g. the conformal mapping between the z- and ζ-planes also to construct from the flow around geometrically simple bodies in one plane the corresponding potential flow around a second body with complicated outer contour. Basis for such a procedure is the following

Theorem 6.2 (due to RIEMANN) *Every simply connected domain, whose complement in the complex plane contains at least one point, can conformally be mapped onto a ball, see* **Fig. 6.2**. ∎

Thus, RIEMANNs theorem delivers the flow of an ideal density preserving fluid around an arbitrary body. In addition, the following properties hold.

(i) The complex potential $\boldsymbol{\phi}(z)$ is (with the exception of singular points: source, vortex center, dipole, ...) itself a holomorphic function of z. Via this function the quadratic coordinate net in the ϕ-plane is mapped onto the streamlines and equipotential lines in the z-plane. This is sketched in **Fig. 6.3**.
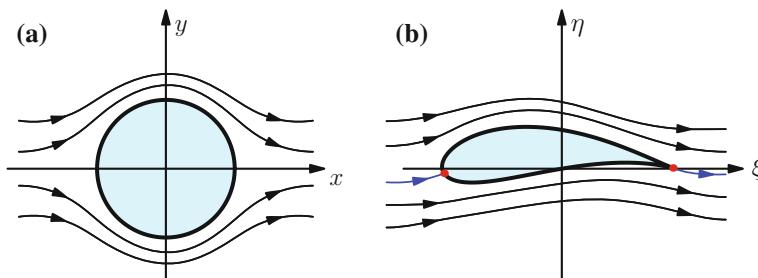
Fig. 6.2 Steady plane potential flow of a density preserving fluid around a circular body (**a**) can conformally be transformed to a plane potential flow around any body (**b**)
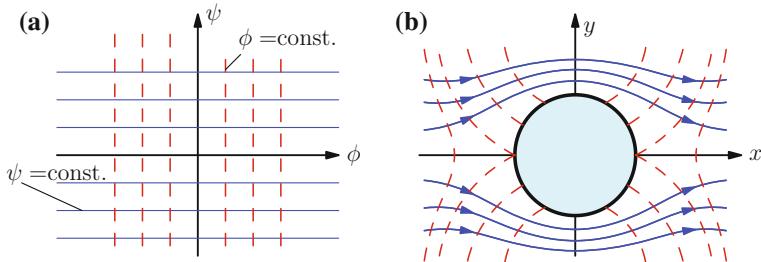
Fig. 6.3 Coordinate lines, $\phi = $ const., $\psi = $ const., in the ϕ-plane **a** are transformed to equipotential and streamlines **b** in the z-plane
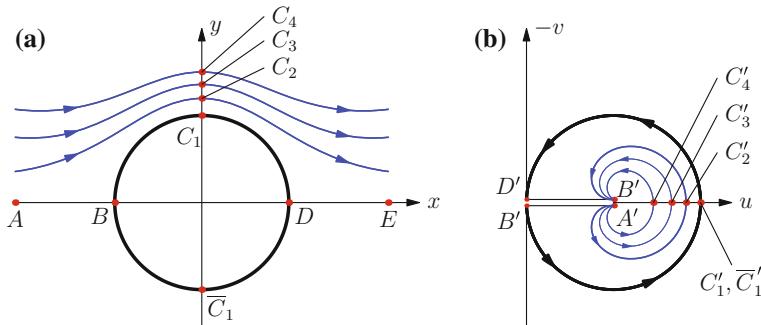
Fig. 6.4 x-parallel potential flow around a circular body. *Panel **a** shows the streamlines in the upper half plane, $y > 0$; Panel **b** shows the complex velocities $w(z)$ in the plane with the axes u and $-v$*

(ii) The derivative of $\phi(z)$,

$$w(z) := \frac{\mathrm{d}\phi(z)}{\mathrm{d}z} \tag{6.18}$$

is (with the exception of singular points) equally a holomorphic function of z. The function $w(z)$ is called the *complex velocity* and is given by

$$w(z) := \frac{\partial \phi}{\partial x} + \iota \frac{\partial \psi}{\partial x} \overset{*}{=} \frac{\partial \psi}{\partial y} - \iota \frac{\partial \phi}{\partial y} = u - \iota v, \tag{6.19}$$

where the step '$\overset{*}{=}$' follows from the CAUCHY-RIEMANN equations (6.8). The w-plane, thus, corresponds to the hodograph plane, mirrored at the real axis (see (6.19)). Clearly, the graph in the w-plane is conformally mapped into a graph in the z-plane. One may transfer the net of equipotential and streamlines of the z-plane into corresponding lines in the w-plane. The streamlines in this plane, however, are not intimately related to realistic streamlines. An example is displayed in **Fig. 6.4**.

The symmetric plane flow around a circular cylinder is mathematically described by the complex potential (see Chap. 5 formulae (5.189), (5.190))

$$\boldsymbol{\phi} = \phi + \iota\psi = U\left(z + \frac{a^2}{z}\right) = U\left(r\,\exp(\iota\theta) + \frac{a^2}{r}\,\exp(-\iota\theta)\right),$$

(6.20)

$$\phi = U\left(r + \frac{a^2}{r}\right)\cos\theta, \qquad \psi = U\left(r - \frac{a^2}{r}\right)\sin\theta,$$

whose stream (ψ) and potential (ϕ) lines are shown in Fig. 6.3b. The streamlines in the upper half plane are repeated in Fig. 6.4a and are there denoted by $C_1, ..., C_4$. The symmetry x-axis, reaching from A at $(-\infty, 0)$ to B at $(-a, 0)$, is split at B in the upper circular branch BC_1D and the lower branch $B\overline{C}_1D$; both then follow the symmetry x-axis from D to E at $(\infty, 0)$. The complex velocity is given by

$$w = \frac{\mathrm{d}\boldsymbol{\phi}}{\mathrm{d}z} = U\left(1 - \frac{a^2}{z^2}\right) = u - \iota v,$$

$$u = U\left\{1 - \frac{a^2r^2\left(\cos^2\theta - \sin^2\theta\right)}{r^4\left(\cos^2\theta + \sin^2\theta\right)^2}\right\} = U\left\{1 - \frac{a^2}{r^2}\cos(2\theta)\right\}, \qquad (6.21)$$

$$v = -2U\frac{a^2r^2\cos\theta\sin\theta}{r^4\left(\cos^2\theta + \sin^2\theta\right)^2} = -U\frac{a^2}{r^2}\sin(2\theta).$$

Note that these formulae imply that $u \to U$, if $z \to \infty$, and that $u_B = 0$, $u_{C_1} = 2U$, $u_D = 0$. Moreover, at any point in the exterior of the circle with radius a in the upper half plane, u is strictly positive with $0 < u < 2U$ and v is positive for $\frac{\pi}{2} < \theta < \pi$ but negative for $0 < \theta < \frac{\pi}{2}$.

If we now plot the velocity in the complex velocity plane $(u, -v)$, then it is clear that the points ABC_1DE in the (x, y)-plane with the semi-circle BC_1D are being mapped onto the full circle $B'C_1'D'$, see Fig. 6.4b, whilst the semi-infinite segments AB and DE are mapped to the finite segments $A'B'$ and $D'E'$ along the branch cut between AB (and DE). The velocities along the streamlines $C_1', ..., C_4'$ in Fig. 6.4b are constructed point by point by assigning the values of ψ along C_j, $(j = 1, 2, ...)$ in (6.20)$_3$ and then selecting values for $\theta \in [0, \pi]$. This then yields values for r from (6.20) and subsequently allows computation of u and v from (6.21)$_{2,3}$. These lines are equally sketched in Fig. 6.4.

It is now clear that the streamlines in the lower half-plane $y \leqslant 0$ must be determined by selecting the angle $\theta \in [0, -\pi]$. This covers the entire $(u, -v)$-plane and affords the introduction of the branch cut as indicated for this second RIEMANN sheet.

In a conformal mapping between the z- and ζ-planes the complex velocity transforms as follows:

$$\phi(z) = \phi(h(\zeta)) = \tilde{\phi}(\zeta), \qquad z = h(\zeta),$$

$$\tilde{w}(\zeta) = \frac{d\tilde{\phi}(\zeta)}{d\zeta} = \frac{d\phi(h(\zeta))}{dh}\frac{dh}{d\zeta} = \frac{d\phi(z)}{dz}\frac{dz}{dh}\frac{dh}{d\zeta} = \frac{d\phi(z)}{dz}\frac{dz}{d\zeta}, \tag{6.22}$$

$$\text{or } \tilde{w}(\zeta) = w(z)\frac{dz}{d\zeta} \quad \longrightarrow \quad \tilde{w}(\zeta)d\zeta = w(z)dz, \tag{6.23}$$

which implies that

$$\int_{\tilde{C}} \tilde{w}(\zeta)d\zeta = \int_{C} w(z)dz.$$
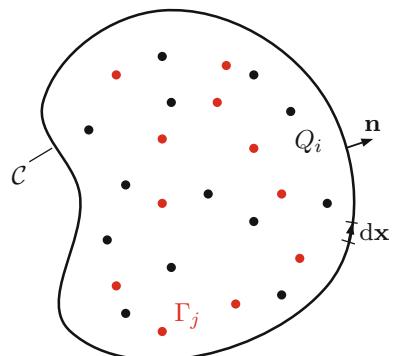
This property is important, as it implies theconservation of sources and circulation.

(iii) The *conservation law of sources and circulation* in a region within a closed simple double point free curve $\mathcal{C}$, which contains (point) sources Q_i and vortices with (point) circulations Γ_j of total strengths $Q = \sum_i Q_i$ and $\Gamma = \sum_j \Gamma_j$, can be proved by performing $\oint_{\mathcal{C}} w\, dz$, see **Fig. 6.5**,

$$\oint_{\mathcal{C}} w\, dz = \oint_{\mathcal{C}} (u - \iota v)(dx + \iota dy)$$

$$= \oint_{\mathcal{C}} (u dx + v dy) + \iota \oint_{\mathcal{C}} (u dy - v dx)$$

$$= \underbrace{\oint_{\mathcal{C}} \boldsymbol{u} \cdot d\boldsymbol{x}}_{\Gamma} + \iota \underbrace{\oint_{\mathcal{C}} (\boldsymbol{u} \cdot \boldsymbol{n}) ds}_{Q} = \Gamma + \iota Q, \tag{6.24}$$

in which the definitions of the total source and the total circulation in the region enclosed by the curve $\mathcal{C}$ have been used.

Fig. 6.5 Explaining the conservation law of sources and circulations in a two-dimensional region enclosed by a closed curve $\mathcal{C}$ under conformal mapping

An analogous computation in the ζ-plane leads to the result

$$\oint_{\tilde{\mathcal{C}}} \tilde{w} \, d\zeta = \tilde{\Gamma} + \iota \tilde{Q}. \tag{6.25}$$

If $\tilde{\mathcal{C}}$ is the image of $\mathcal{C}$ in the ζ-plane, all points in the z-plane within $\mathcal{C}$ will be mapped in the ζ-plane to points within the $\tilde{\mathcal{C}}$ curve, in particular also the source and circulation points $\tilde{Q}_i$, $\tilde{\Gamma}_j$. This implies that in total

$$\Gamma = \tilde{\Gamma}, \qquad Q = \tilde{Q}, \tag{6.26}$$

provided that $\int_{\tilde{\mathcal{C}}} \tilde{w}(\zeta) d\zeta = \int_{\mathcal{C}} w(z) dz$. The total source and the total circulation within a region enclosed by a simple closed curve remains conserved under conformal mapping.

6.1.2 Examples

(α) **Stagnation point flow**:
Let us start in the z-plane with the simple parallel-flow potential

$$\phi(z) = Uz \quad \longrightarrow \quad \begin{cases} \phi = Ux, \\ \psi = Uy, \end{cases} \tag{6.27}$$

and the conformal mapping

$$\frac{z}{\ell} = \left(\frac{\zeta}{\ell}\right)^2, \quad \text{where } \ell \text{ is a characteristic length.} \tag{6.28}$$

This transformation assigns to every z-value two ζ-values. If a branch cut from the coordinate origin to infinity is introduced, then this implies that ζ-values are restricted to a specially selected half plane; depending, where the branch cut is introduced, different half planes are selected. **Figure 6.6** illustrates this for branch cuts along the positive and negative real axes, respectively. Thus, one obtains

$$\tilde{\phi}(\zeta) = U \frac{\zeta^2}{\ell} \quad \longrightarrow \quad \begin{cases} \tilde{\phi} = \dfrac{U}{\ell} \left(\xi^2 - \eta^2\right), \\ \tilde{\psi} = \dfrac{U}{\ell} 2\xi\eta. \end{cases} \tag{6.29}$$

The equipotential lines are hyperbolas, whose asymptotes are the 45 and 135° lines, whilst those for the streamlines are the ξ- and η-axes. In Fig. 6.6, corresponding lines $y = $ const. and $\psi = $ const. appear in corresponding colors.
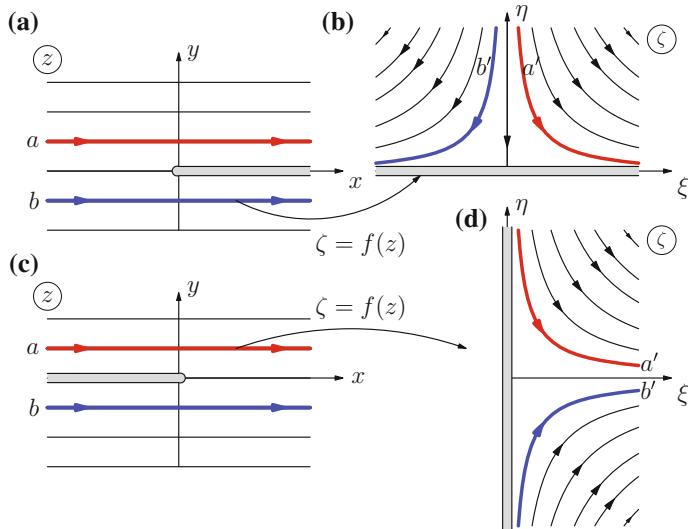
Fig. 6.6 Stagnation point flow onto a plane surface. *Panel **a** shows the streamlines of a constant parallel flow within the z-plane of the potential flow* (6.27), *corresponding to the stagnation point flow in panel **b** due to the conformal mapping* (6.28) *if the branch cut for the inverse mapping of* (6.28) *is made along the positive x-axis. Equally colored streamlines belong together. Panels **c** and **d** show the same mapping, if the branch cut is made along the negative x-axis*

(β) **Generalized stagnation point flow**:

Having been successful with the quadratic law (6.28) for the 'classical' stagnation point flow it is tempting to try with the generalization

$$\frac{z}{\ell} = \left(\frac{\zeta}{\ell}\right)^{2\pi/\alpha}, \quad 0 \leqslant \alpha \leqslant 2\pi,$$

$$\longrightarrow \quad z = \ell \left(\frac{r}{\ell}\right)^{2\pi/\alpha} \exp\left(\frac{2\pi\iota\theta}{\alpha}\right). \tag{6.30}$$
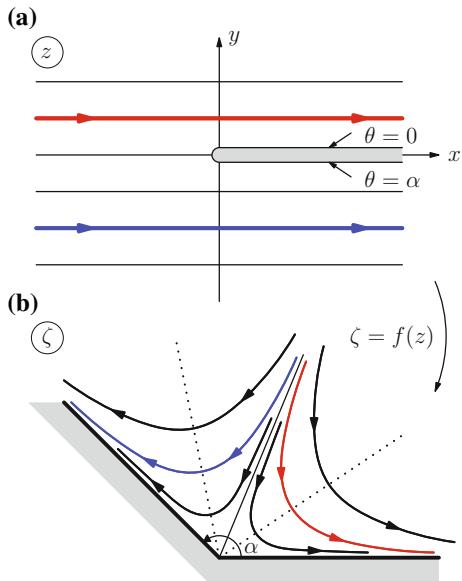
Figure 6.7 shows in panel **a** the streamlines of the parallel flow potential (6.27). If the branch cut in the z-plane is performed along the positive x-axis, then the entire z-plane is mapped by (6.30) onto the angular region $0 < \theta < \alpha$ in panel **b**. The streamlines of the parallel flow are then conformally mapped by (6.30) to the displayed stagnation point flow, whose complex potential is given by

$$\tilde{\phi}(\zeta) = U\ell \left(\frac{\zeta}{\ell}\right)^{2\pi/\alpha}, \tag{6.31}$$

Fig. 6.7 Generalized
stagnation point flow into a
wedge with opening angle α.
*Streamlines are shown as in
Fig.* 6.6. *Corresponding
streamlines in parallel flow*
(**a**) *and in the wedge regimes
with opening angle α* (**b**) *are
shown. The complex
potential and velocity are as
given in* (6.31) *and* (6.32)

with complex velocity

$$\tilde{w}(\zeta) = \frac{2\pi U}{\alpha} \left(\frac{\zeta}{\ell}\right)^{\frac{2\pi}{\alpha}-1}, \qquad |\tilde{w}(\zeta)| = \frac{2\pi U}{\alpha} \left(\frac{|\zeta|}{\ell}\right)^{\frac{2\pi}{\alpha}-1}. \qquad (6.32)$$
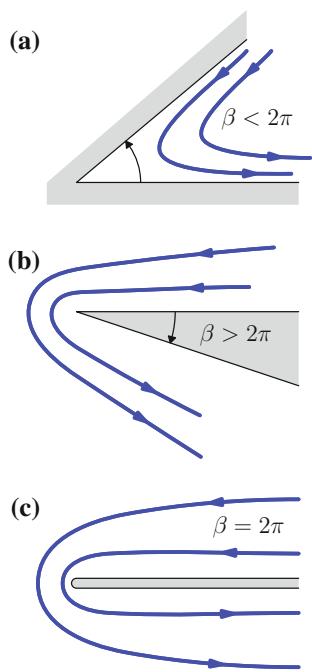
Accordingly, for $0 < \alpha < 2\pi$, one has $w = 0$ for $\zeta = 0$. The tip of the wedge of the
angular region is thus the stagnation point. Moreover, the modulus of the velocity
depends only on the distance from the origin.

Remarks:

- Solution (6.31) with (6.32) as shown in Fig. 6.7 holds true and is meaningful for
  $0 \leqslant \alpha \leqslant 2\pi$, **Fig. 6.8**.
- For $\alpha = 2\beta$ the potential flow in a wedge with $\beta < \pi$ is obtained. If $\beta > \pi$ the
  flow is that of a potential flow around a corner with complex velocity, Fig. 6.8b,

$$\tilde{w} = \frac{\pi U}{\beta} \left(\frac{\zeta}{\ell}\right)^{(\pi-\beta)/\beta}. \qquad (6.33)$$

Fig. 6.8 Streamlines of generalized stagnation point flow. **a** $\beta < \pi$, **b** $\beta > \pi$, **c** $\beta = 2\pi$

(a)

$\beta < 2\pi$

(b)

$\beta > 2\pi$

(c)

$\beta = 2\pi$

If (*i*) $\beta < \pi$, then $\tilde{w}(0) = 0$;
            the flow is stagnation point flow,
  (*ii*) $\beta > \pi$, then $\tilde{w}(0) \to \infty$;
            the velocity at the tip of the wedge is infinitely large;
            the flow is around the tip of the wedge,
 (*iii*) $\beta = 2\pi$, then $\tilde{w}(0) \to \infty$;
            this flow corresponds to a flow around a sharp edge of a plate,

$$\tilde{w}(\zeta) = \frac{U}{2} \left(\frac{\zeta}{\ell} \right)^{-1/2}. \qquad (6.34)$$

- In reality, infinitely long side boundaries cannot be realized; real flows of (nearly) density preserving fluids can, however, be closely identified with these solutions near edges and side boundaries.

  As an application of such flows consider surface water waves in sufficiently (ideally infinitely) deep water. For moderately large amplitudes the wave crowns are pointed as shown in **Fig. 6.9**. For even larger amplitudes these peaks are covered by crowns of foam. The vicinity of the wedges can, in the co-moving frame of reference, be interpreted as a potential flow in a wedge of opening angle β. Figure 6.9b shows that the BERNOULLI equation takes the form
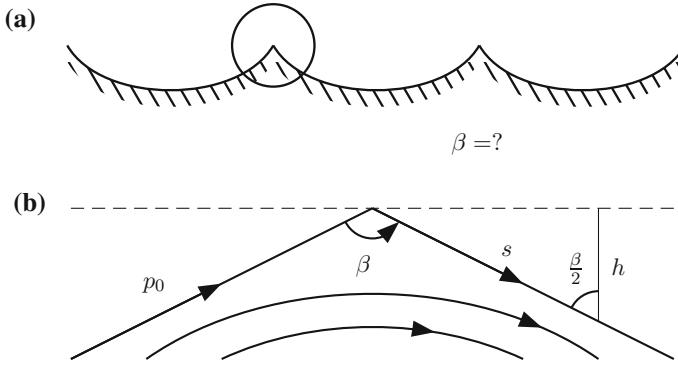
Fig. 6.9 Moderately large surface waves in an infinitely deep two-dimensional fluid half space.
a *Pointed steady wave crowns observed in a co-moving coordinate system.* **b** *Vicinity of a single wave crown. What is the size of the angle β?*

$$\frac{\rho}{2}v^2 + p - \rho g h = p_0,$$

or at the free surface, where $p = p_0$,

$$v^2 = 2gh.$$

Alternatively, with (6.33) the complex velocity is given by

$$w = \frac{\pi U}{\beta}\left(\frac{\varsigma}{\ell}\right)^{(\pi-\beta)/\beta},$$

or, after combining the last two expressions the relation

$$2g\,s\,\cos\left(\frac{\beta}{2}\right) = \frac{\pi^2 U^2}{\beta^2}\left(\frac{s}{\ell}\right)^{2(\pi-\beta)/\beta}$$

is obtained. By comparing the exponents of s and the coefficients on both sides of the equation, one obtains

$$2\,\frac{\pi-\beta}{\beta} = 1 \quad\longrightarrow\quad \beta = \tfrac{2}{3}\pi = 120° \text{ (!)},$$

$$2g\cos(60°) = \frac{\pi^2 U^2}{\frac{4}{9}\pi^2\ell} \quad\longrightarrow\quad U = \frac{2}{3}\sqrt{g\ell}.$$

(6.35)

This result for β is a concrete expression, which is corroborated by observations. The information $(6.35)_2$ on U is not so useful, since ℓ is not known. To find a concrete result, the theory of water waves must be consulted. In $(6.35)_2$ at least the dimension of the result is correct.

(γ) **Source, Circulation, Dipole Flows**:

These potential flows can equally be obtained from the uniform parallel flow potential $\phi(z) = Uz$ by corresponding adequate conformal mappings.

(i) Flow from a point source: Here, the conformal mapping and the complex potentials are given by

$$\frac{z}{\ell} = \frac{1}{2\pi} \ln\left(\frac{\zeta}{\ell}\right),$$

$$\phi = Uz, \quad \tilde{\phi}(\zeta) = \frac{U\ell}{2\pi} \ln\left(\frac{\zeta}{\ell}\right), \tag{6.36}$$

see also Fig. 5.29a, c in Chap. 5.

(ii) Vortex flow: Conformal mapping and complex potential are here given by

$$\frac{z}{\ell} = \frac{1}{2\pi} \ln\left(\frac{\zeta}{\ell}\right),$$

$$\phi(z) = -\iota Uz, \quad \tilde{\phi}(\zeta) = -\frac{\iota U\ell}{2\pi} \ln\left(\frac{\zeta}{\ell}\right). \tag{6.37}$$

These are displayed in Fig. 5.28a, b in Chap. 5.

(iii) Dipole flow: Conformal mapping and complex potential are given by

$$\frac{z}{\ell} = -\frac{\ell}{2\pi} \frac{1}{\zeta},$$

$$\phi(z) = Uz, \quad \tilde{\phi}(\zeta) = -\frac{U\ell^2}{2\pi} \frac{1}{\zeta}; \tag{6.38}$$

they are displayed in Fig. 5.30c in Chap. 5. This conformal mapping generates in the ζ-plane a dipole with moment $M = U\ell^2$. The straight horizontal streamlines in the z-plane transform, because of the circle-preservation of the mapping into circles through the origin of the ζ-plane.
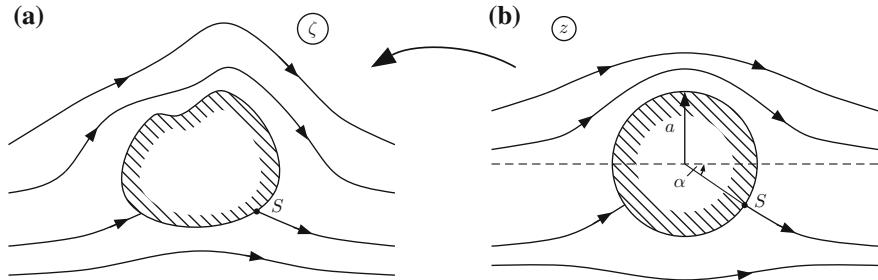
Fig. 6.10 Two-dimensional potential flow around an arbitrary two-dimensional body, conformally mapped to a potential flow around a circle. **a** *ζ-plane with arbitrary body*, **b** *z-plane with circle of radius a*

6.1.3 Steady Flow Around an Arbitrary Cylinder at Rest

Consider an arbitrary cylinder at rest, which is subjected to a steady two-dimensional potential flow from the left, **Fig. 6.10**. RIEMANNs theorem states that this flow can be conformally transformed to a corresponding flow around a circle. The complex potential of the flow around the circle has been given in Eq. (5.195) of Chap. 5, which is repeated,

$$\phi(z) = U\left(z + \frac{a^2}{z}\right) + \frac{\Gamma}{2\pi\iota}\ln\left(\frac{z}{a}\right), \quad \Gamma = -4\pi\,Ua\sin\alpha. \tag{6.39}$$

Here, U is the parallel velocity in the x-direction at infinity, Γ is the circulation around the circle with radius a and α is the angle, identifying the stagnation point as shown in Fig. 6.10. Hence,

$$\phi(z) = U\left(z + \frac{a^2}{z}\right) + 2\iota Ua\sin\alpha\ln\left(\frac{z}{a}\right). \tag{6.40}$$
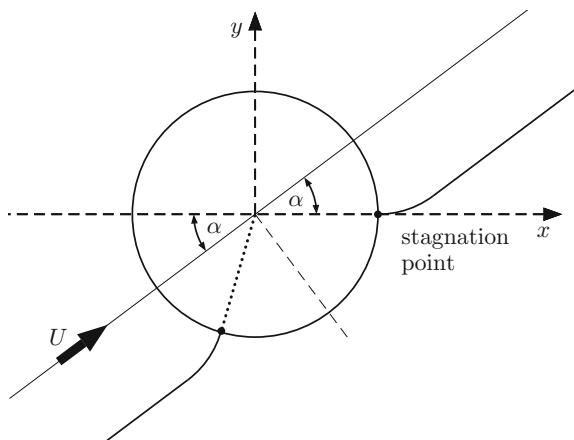
For the subsequent application it is advantageous to rotate the coordinate system such that the stagnation point in the lee lies on the x-axis. This affords a counter clockwise rotation by the angle $-\alpha$, or

$$z = \tilde{z}\,\exp(-\iota\alpha). \tag{6.41}$$

Replacing in (6.40) z by $\tilde{z}$ yields the potential of the flow around the sphere rotated by the angle $-\alpha$ as shown in **Fig. 6.11**. Substituting then (6.41) into (6.40) and dropping the tilde in the resulting expression yields

$$\phi(z) = U\left(z\,\exp(-\iota\alpha) + \frac{a^2}{z}\,\exp(\iota\alpha)\right) + 2\iota Ua\sin\alpha\ln\left(\frac{z}{a}\right), \tag{6.42}$$

Fig. 6.11 Rotated coordinate system by the angle $-\alpha$ for potential flow (6.42) around the circle with one stagnation point on the x-axis

in which the constant, $-2Ua\alpha \sin\alpha$, has been omitted, because fluid-dynamically only ϕ' is important.

For the evaluation of the flow around an arbitrary cylinder the conformal mapping $z = f(\zeta)$ must be found, which transforms the contour of the circle into the contour of the two-dimensional body. The following conditions must be satisfied to achieve this:

- The exterior region of the cylindrical body must be mapped onto the exterior of the circle.
- For $z \to \infty$ the mapping must satisfy $dz/d\zeta = 1$. This condition is based on (6.23) and guarantees that the approaching velocity U remains preserved.
- The stagnation point in the ζ-plane is mapped into a point on the periphery of the circle. This point determines the angle α.

The radius of the circle is determined by the circulation, Γ, which remains conserved according to (6.26). Of special interest is the force exerted by a steady potential flow on the two-dimensional body at rest. This force is given by the BLASIUS[3] formula [6, 7]. To determine it, let us start from

$$\boldsymbol{K} = - \oint_{\mathcal{C}} (\rho \boldsymbol{v}(\boldsymbol{v} \cdot \boldsymbol{n}) + p\boldsymbol{n})\, da, \tag{6.43}$$

where $\mathcal{C}$ is any double point free closed curve around the cylinder, see Chap. 3, formula (3.196). In a parallel flow BERNOULLIs equation takes the form

$$p + \frac{\rho}{2}|\boldsymbol{v}|^2 = C \quad = \text{const. in the entire fluid space}$$

$$\longrightarrow \quad p = C - \frac{\rho}{2}|\boldsymbol{v}|^2.$$

[3]HEINRICH BLASUS (1883–1970) was PRANDTL's first doctoral student. For a historical description of his work and life see HAGER [15]. A short biography is given in Chap. 9, Fig. 9.19.

Substituting this expression for p into (6.43) yields

$$\boldsymbol{K} = -\frac{\rho}{2} \oint_C \left(2\boldsymbol{v}(\boldsymbol{v} \cdot \boldsymbol{n}) - |\boldsymbol{v}|^2 \boldsymbol{n}\right) \mathrm{d}s,$$

(note the contribution of the constant C vanishes) or in Cartesian component form

$$K_x = -\rho \oint_C \left(u(u\mathrm{d}y - v\mathrm{d}x) - \tfrac{1}{2}(u^2 + v^2)\mathrm{d}y\right),$$

(6.44)

$$K_y = -\rho \oint_C \left(v(u\mathrm{d}y - v\mathrm{d}x) + \tfrac{1}{2}(u^2 + v^2)\mathrm{d}x\right),$$

in which $\boldsymbol{n}\mathrm{d}s = (\mathrm{d}y, -\mathrm{d}x)$ was used. The formulae (6.44) can be combined to a two-dimensional force vector

$$K_x - \iota K_y = \rho \oint_C \left\{uv(\mathrm{d}x + \iota\mathrm{d}y) + \tfrac{1}{2}(v^2 - u^2)(\mathrm{d}y - \iota\mathrm{d}x)\right\}$$

$$= \iota\frac{\rho}{2} \oint_C w^2(z)\mathrm{d}z,$$

(6.45)

in which w is the complex velocity. Formula (6.45) can easily be verified by the reader by direct substitution of $w = u - \iota v$, $z = x + \iota y$. (6.45) is known as BLASIUS' formula. With its use the KUTTA-JOUKOWSKI theorem can be derived: Let an arbitrary cylinder be given, which, at infinity, is subjected to the constant velocity U in the x-direction. Because the complex velocity is a holomorphic function, its mathematical expression can, for sufficiently large $|z|$, be represented by the LAURENT expansion

$$w(z) = U + \frac{A_1}{z} + \frac{A_2}{z^2} + \cdots,$$

(6.46)
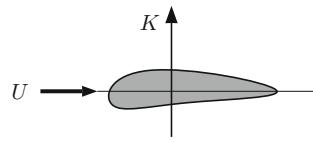
and its integration along a closed curve yields

$$\oint_C w(z)\mathrm{d}z \overset{*}{=} 2\pi\iota \sum (\text{residues}) \overset{**}{=} 2\pi\iota \sum (A_1)_i \overset{***}{=} \Gamma + \iota Q.$$

(6.47)

In this chain of expressions, A_1 is the residue and in step '$\overset{*}{=}$' the residue theorem of complex variable theory is applied, which states that the value of the integral $\oint_C w(z)\mathrm{d}z$ is computed by evaluating the residues of w at the singular points of w within C.[4] Step '$\overset{**}{=}$' follows from (6.24). For $Q = 0$, the residue is given by $A_1 = \Gamma/(2\pi\iota)$. Thus,

---

[4]For the reader not familiar with this theorem, some elements of complex variable theory are stated in the Appendix to this Chapter.

Fig. 6.12 In a steady
potential flow with constant
approaching velocity U the
force $\boldsymbol{K}$, exerted on the body
at rest, is perpendicular to
the approaching velocity U

$$\oint_{\mathcal{C}} w^2 dz = \oint_{\mathcal{C}} \left\{ U + \frac{A_1}{z} + \cdots \right\}^2 dz = \oint_{\mathcal{C}} \left\{ U^2 + 2U \frac{A_1}{z} + \cdots \right\} dz$$

$$= (2\pi\iota)(2U A_1) = (2\pi\iota) \left(2U \frac{\Gamma}{2\pi\iota} \right) = 2U \Gamma. \tag{6.48}$$

For these closed integrals to be meaningful, the curve $\mathcal{C}$ must lie in the circular
domain, where the LAURENT series converges. Comparing (6.48) with (6.45) implies

$$K_x - \iota K_y = \iota \frac{\rho}{2} 2U \Gamma = \iota \rho U \Gamma \quad \longrightarrow \quad \begin{cases} K_x = 0, \\ K_y = -\rho U \Gamma. \end{cases} \tag{6.49}$$

This is the BLASIUS formula, [8]. Essential in this result is the fact that the boundary
condition at the body surface requires tangency of the velocity field to the boundary
$\mathcal{C}$, $\boldsymbol{u} \cdot \boldsymbol{n} = 0$. This implies that $\oint_{\mathcal{C}} \boldsymbol{u} \cdot \boldsymbol{n} ds = 0$ on any simple closed curve $\mathcal{C}'$ encircling
the body. Consequently, the flow is source free, $Q = 0$ in the entire flow domain,
see (6.156).

Because U points into the x-direction, (6.49) states that the steady force exerted
by the potential flow on the two-dimensional body with contour $\mathcal{C}$ is perpendicular to
the approaching velocity U, **Fig. 6.12**. It is because of its aerodynamic significance
that it is called 'lift force'; better would be 'transverse force', because it is transverse
to U but not necessarily a lifting force.

6.1.4 The Kutta-Joukowski Mapping

This conformal mapping is defined by

$$\zeta = z + \frac{a^2}{z} = r \left(\exp(\iota\theta) + \frac{a^2}{r^2} \exp(-\iota\theta) \right). \tag{6.50}$$

It maps points of the circle $z = a \exp(\iota\theta)$ onto $\zeta = 2a \cos\theta$, i.e., onto the real section
$-2a \leqslant \xi \leqslant 2a$. Points of the circle $z = R \exp(\iota\theta)$ are mapped into
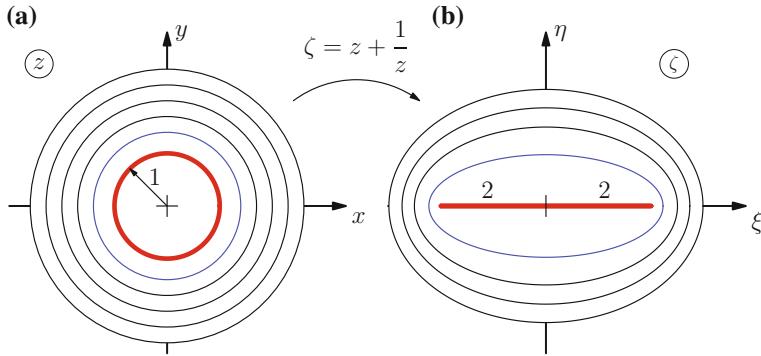
Fig. 6.13 KUTTA-JOUKOWSKI mapping (6.50). *Circles exterior and interior to the circle $r = 1$ in the z-plane are mapped onto ellipses (6.52) of the ζ-plane with branch cut between $x = -2$ and $x = 2$. The figure is drawn for $a = 1$*

$$\zeta = R \exp(\iota\theta) + \frac{a^2}{R} \exp(-\iota\theta),$$

$$\xi + \iota\eta = \left(R + \frac{a^2}{R}\right)\cos\theta + \iota\left(R - \frac{a^2}{R}\right)\sin\theta. \tag{6.51}$$

Separating from these equations real and imaginary parts and eliminating θ leads to the equation

$$\frac{\xi^2}{\left(R + \dfrac{a^2}{R}\right)^2} + \frac{\eta^2}{\left(R - \dfrac{a^2}{R}\right)^2} = 1, \tag{6.52}$$

tracing an ellipse. The eccentricity of the focal points, e, is

$$e^2 = \left(R + \frac{a^2}{R}\right)^2 - \left(R - \frac{a^2}{R}\right)^2 = 4a^2 \quad \longrightarrow \quad e = 2a.$$

This says that the focal points lie at the end points of the doubly-covered distance $-2a \leqslant \xi \leqslant 2a$. The circles with $R > 0$ are mapped onto real ellipses, **Fig. 6.13**; in other words, the exterior of the circle $z = a \exp(\iota\theta)$ is mapped on the ζ-plane with branch cut along $-2a \leqslant \xi \leqslant 2a$. The same holds true for the circles with $R < a$, which are mapped onto the second RIEMANN sheet through the branch cut.

OLVER [23] has looked at the JOUKOWSKI mapping $\zeta = \frac{1}{2}(z + \frac{1}{z})$ and drawn the images of circles, when their center is not at $z = 0$. **Figure 6.14** displays the effect on circles not centered at the origin and having various different shapes as indicated in Fig. 6.14. For circles passing through the singular point $z = 1$, the images are no longer smooth, but exhibit a cusp at $\zeta = 1$. It is evident from some of the shapes that these profiles played a role in early air craft designs.

| Center: $.2 + i$ | Center: $1 + i$ | Center: $-2 + 3i$ |
| Radius: $.8$ | Radius: 1 | Radius: $3\sqrt{2} \approx 4.2426$ |

| Center: $.2 + i$ | Center: $.1 + .3i$ | Center: $-.2 + .1i$ |
| Radius: 1.2806 | Radius: $.9487$ | Radius: 1.2042 |
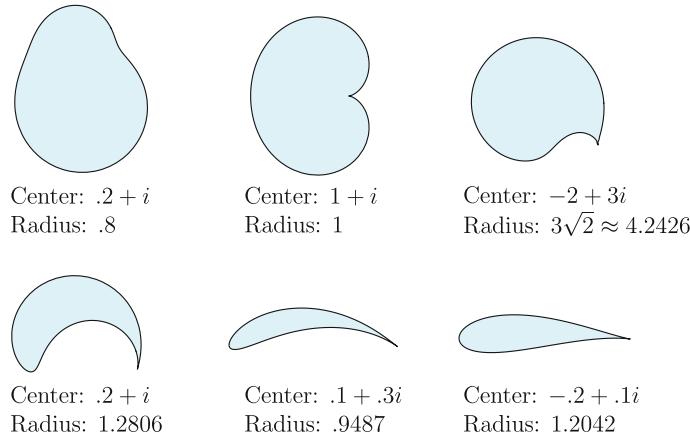
Fig. 6.14 Images obtained from circles via the JOUKOWSKImap $\zeta = \frac{1}{2}(z + \frac{1}{z})$ for non-centered circles with different radii. *The figure shows a subset of graphs from Fig. 22 of* PETER J. OLVER [23] © *by* OLVER, *reproduced with changes*

6.2   Applications

6.2.1   *Flow Over a Plane Plate*

Flow over a plane plate with angle of attack α and plate length $4a$ is investigated. The circulation Γ is so determined that the trailing edge is not circumflown but smoothly passed by, leaving the streamline parallel to the plate (this is the so-called KUTTA-JOUKOWSKI condition), see **Fig. 6.15**. According to formula (5.198) in Chap. 5 the circulation is given by

$$\Gamma = -4\pi \, Ua \sin\alpha = -\pi \, U\ell \sin\alpha. \tag{6.53}$$
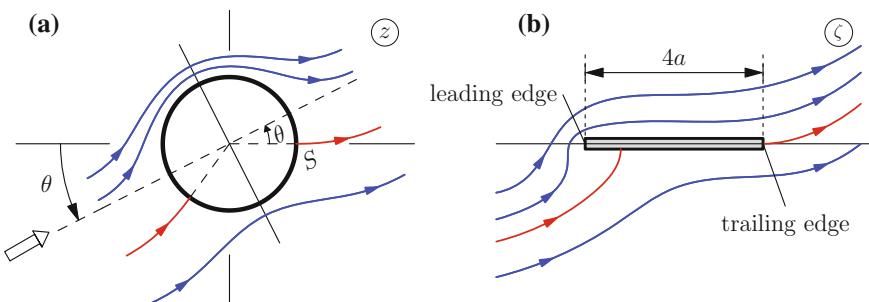
Fig. 6.15 Potential flow over a plane plate. *The circulation Γ is so selected that the flow off the trailing edge is tangential to the plate*. **a** *Flow around the circle in the z-plane*, **b** *flow over the plate*

According to $(6.49)_2$, this yields the *lift force*

$$K_y = -\rho U \, \Gamma = \rho \pi \, U^2 \ell \sin \alpha, \tag{6.54}$$

and for the *lift coefficient*

$$c_A = \frac{K_y}{\frac{\rho}{2} U^2 \ell} = 2\pi \sin \alpha. \tag{6.55}$$

The potential $\phi(z)$ in the z-plane is given by (6.42) and the velocity $w(z)$ follows by differentiation

$$w(z) = U \left(\exp(-\iota\alpha) - \frac{a^2}{z^2} \exp(\iota\alpha) \right) + 2\iota \, U \sin \alpha \left(\frac{a}{z} \right)$$

and with $z = a \, \exp(\iota\theta)$

$$\begin{aligned}
w(a \, \exp(\iota\theta)) &= U \, (\exp(-\iota\alpha) - \exp(\iota(\alpha - 2\theta))) + 2\iota U \sin \alpha \, \exp(-\iota\theta) \\
&= U \, \exp(-\iota\theta) \, (\exp(-\iota(\alpha - \theta)) - \exp(\iota(\alpha - \theta)) + 2\iota \sin \alpha) \\
&= 2\iota \, U \, \exp(-\iota\theta) \, (\sin(\theta - \alpha) + \sin \alpha) \, . \tag{6.56}
\end{aligned}$$

This expression allows determination of the plate circumflow in the ζ-plane. Indeed, with (6.23), or

$$\tilde{w}(\zeta) = \frac{w(z)}{d\zeta/dz}$$

and

$$\frac{d\zeta}{dz} \overset{(6.50)}{=} \left(1 - \frac{a^2}{z^2} \right) \overset{z=a\,\exp(\iota\theta)}{=} (1 - \exp(-2\iota\theta)) = \exp(-\iota\theta) \, 2\iota \sin \theta,$$
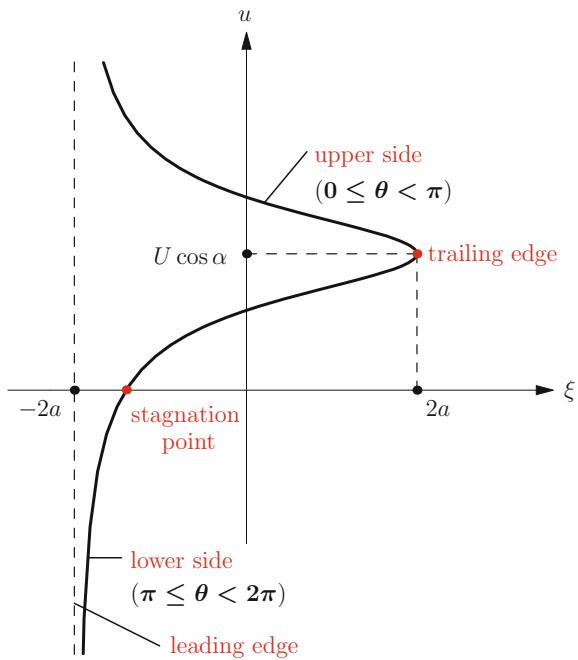
the complex velocity along (around) the plate takes the form

$$\begin{aligned}
\tilde{w}(\zeta)|_{\text{plate}} &= U \, \frac{\sin(\theta - \alpha) + \sin \alpha}{\sin \theta} \\
&= \frac{U}{\sin \theta} \, (\sin \theta \cos \alpha - \cos \theta \sin \alpha + \sin \alpha) \, .
\end{aligned}$$

This is real valued, i.e., $\tilde{w}_{\text{plate}} = (u, 0)$ as one would expect and can also be written as

$$u = U \cos \alpha \left(1 + \tan \alpha \frac{1 - \cos \theta}{\sin \theta} \right) = U \cos \alpha \left(1 + \tan \alpha \tan \left(\frac{\theta}{2} \right) \right). \tag{6.57}$$

Fig. 6.16 Horizontal velocity component along the plate, (6.57), plotted against $\xi = 2a \cos \theta$. *Upper and lower surfaces of the plate are indicated as are the stagnation point and the front and trailing edges*

This velocity profile is plotted in **Fig. 6.16** against $\xi = 2a \cos \theta$ (i.e., θ functions as curve parameter). ξ varies from $-2a$ to $2a$.

The behavior of the flow around the front edge can be estimated by introducing the angle σ according to $\theta = \pi - \sigma$. This implies

$$\xi = 2a \cos \theta = -2a \cos \sigma \approx -2a \left(1 - \frac{1}{2}\sigma^2 + \cdots \right)$$
$$= -2a + a\sigma^2 + \cdots .$$

The distance from the front edge, s, is therefore,

$$s = \xi + 2a \approx a\sigma^2.$$

Alternatively,

$$\tan\left(\frac{\theta}{2}\right) = \tan\left(\frac{\pi}{2} - \frac{\sigma}{2}\right) = \cotan\left(\frac{\sigma}{2}\right) \approx \frac{2}{\sigma} + \cdots = 2\sqrt{\frac{a}{s}}.$$

Therefore, according to (6.57),

$$u = U \cos \alpha + (U \sin \alpha) 2\sqrt{\frac{a}{s}} = 2U \sin \alpha \sqrt{\frac{a}{s}} + O(1), \quad s \to 0. \quad (6.58)$$
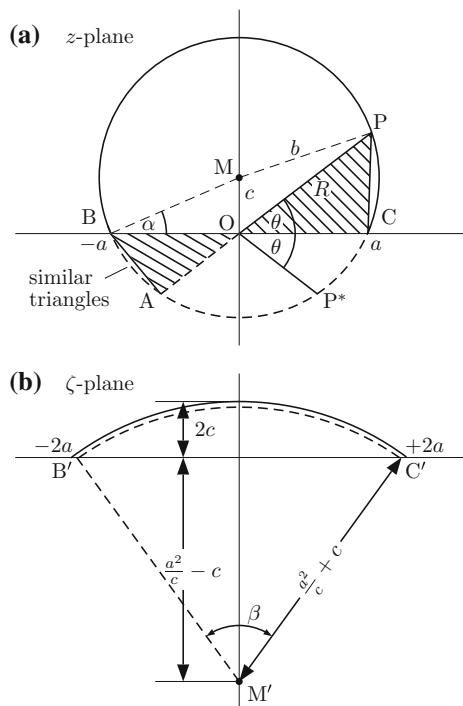
This result has essentially already been obtained in (6.34).

We wish to close the analysis of this example by stating D'ALEMBERT's para-doxon. According to the KUTTA-JOUKOWSKI theorem and BLASIUS' formula (6.49) the potential flow-induced force exerted on the plate is perpendicular to the direction of the upcoming velocity U and not perpendicular to the plate, as one might expect, as this force results from the pressure exerted on the plate, which is everywhere per-pendicular to the plate surface. The reason is that the infinitely large velocity at the front edge (square root singularity!) generates an infinitely large negative pressure ($p \to -\infty$), which in total exerts a finite suction force close to the front edge.

6.2.2 Potential Flow Over a Circular Segment

Such flows can also be determined by the KUTTA-JOUKOWSKI mapping (6.50). To demonstrate this, consider **Fig. 6.17**a. It shows in the z-plane a circle with center M on the y-axis, cutting the x-axis at the points $x = \pm a$. The straight segments AOP

Fig. 6.17 Mapping $\zeta = z + a^2/z$ of KUTTA-JOUKOWSKI. *A circle with center at M on the y-axis, cutting the x-axis at x = ±a is mapped on a doubly covered circular segment. For the proof, see main text*

and the segment BOC define two similar shaded triangles with angle θ at O. Denote the radius of the circle by b and the segment OM on the y-axis by c. The following properties of the conformal mapping $\zeta = z + a^2/z$ can be verified, respectively deduced:

- The similarity of the shaded triangles implies

$$\frac{\overline{OP}}{\overline{OC}} = \frac{\overline{OB}}{\overline{OA}} \implies \overline{OP} \cdot \overline{OA} = \overline{OC} \cdot \overline{OB} = a^2.$$

- If the position of P is identified with z, then the position of point P^* corresponds to the point a^2/z. Indeed, if the point P is expressed as $z = (R\cos\theta, R\sin\theta)$, then

$$(\overline{OP^*}\cos\theta, -\overline{OP^*}\sin\theta) = (\overline{OA}\cos\theta, -\overline{OA}\sin\theta)$$
$$= \frac{a^2}{\overline{OP}}(\cos\theta, -\sin\theta) \stackrel{*}{=} \frac{a^2}{\overline{OP}(\cos\theta, \sin\theta)} = \frac{a^2}{z}.$$

Here the step "$\stackrel{*}{=}$" follows because

$$\frac{a^2}{\overline{OP}}(\cos\theta, -\sin\theta) = \frac{a^2}{\overline{OP}}\exp(-\iota\theta) = \frac{a^2}{\overline{OP}\exp(\iota\theta)} = \frac{a^2}{\overline{OP}(\cos\theta, \sin\theta)}.$$

- If the construction with the shaded triangles in the z-plane is smoothly changed by moving the straight line $\overline{AOP}$ around point O, the point P will traverse the solid segment, and point A will concurrently traverse the dashed segment of the circle in the z-plane. However this rotation (of the straight line $\overline{AP}$) can be continued such that P traverses the dashed circular segment, whilst A traverses the solid segment. This says that both sides of the circle in the z-plane are mapped onto the same curved segment $\overline{B'C'}$ in the ζ-plane.
- This curve is a circle: If P is identified with z and $z = R\exp(\iota\theta)$, then

$$\zeta = R\exp(\iota\theta) + \frac{a^2}{R}\exp(-\iota\theta) = \xi + \iota\eta,$$
$$\xi = \left(R + \frac{a^2}{R}\right)\cos\theta, \qquad \eta = \left(R - \frac{a^2}{R}\right)\sin\theta. \tag{6.59}$$

Elimination of R from these expressions yields

$$\xi^2 \sin^2\theta - \eta^2\cos^2\theta = 4a^2\sin^2\theta\cos^2\theta. \tag{6.60}$$

In this equation $\sin \theta$ and $\cos \theta$ can be expressed in terms of ξ and η. With the aid of Fig. 6.17a application of the PYTHAGORAS theorem for the triangle MOC yields

$$a^2 = b^2 - c^2, \qquad R^2 - a^2 = R^2 + c^2 - b^2$$

and the law of sines for the triangle OPM states that

$$b^2 = R^2 + c^2 - 2\,Rc\sin\theta$$
$$\longrightarrow \quad 2\,Rc\sin\theta = R^2 + c^2 - b^2 = R^2 - a^2$$
$$\longrightarrow \quad 2c\sin\theta = \left(R - \frac{a^2}{R}\right) \overset{(6.59)}{=} \frac{\eta}{\sin\theta}. \tag{6.61}$$

Thus,

$$\sin^2\theta = \frac{\eta}{2c}, \qquad \cos^2\theta = 1 - \frac{\eta}{2c}. \tag{6.62}$$

If this is substituted into (6.60) and the emerging equation is slightly transformed, then

$$\xi^2 + \left\{\eta + \left(\frac{a^2}{c} - c\right)\right\}^2 = \left(\frac{a^2}{c} + c\right)^2 \tag{6.63}$$

is obtained, an equation of a circle with

$$\text{center at } (0, -(\tfrac{a^2}{c} - c)) \text{ and radius } = (\tfrac{a^2}{c} + c). \tag{6.64}$$

In a smooth flow along the circular segment the points $z = \pm a$ must be stagnation points in the z-plane. The point $z = +a$ corresponds to the KUTTA-JOUKOWSKI condition; $z = -a$ then automatically agrees for reasons of symmetry with the second stagnation point. Therefore, the circulation is given by

$$\Gamma = -4\pi\,Ub\sin\alpha = -4\pi\,Uc, \quad \text{since } b\sin\alpha = c \text{ (see Fig. 6.17)}, \tag{6.65}$$

and the 'lift force' and 'lift coefficient' take the forms

$$K_y = 4\pi\,\rho\,U^2 c, \qquad c_\ell = \frac{K_y}{\frac{\rho}{2}\,U^2\,4a} = 2\pi\,\frac{c}{a}. \tag{6.66}$$

Introducing the centric angle β at M', **Fig. 6.18**, of the circular segment and the trigonometric expressions

$$2a = r\sin\frac{\beta}{2} = 2r\sin\frac{\beta}{4}\cos\frac{\beta}{4}, \qquad 2c = r\left(1 - \cos\frac{\beta}{2}\right) = 2r\sin^2\frac{\beta}{4}$$
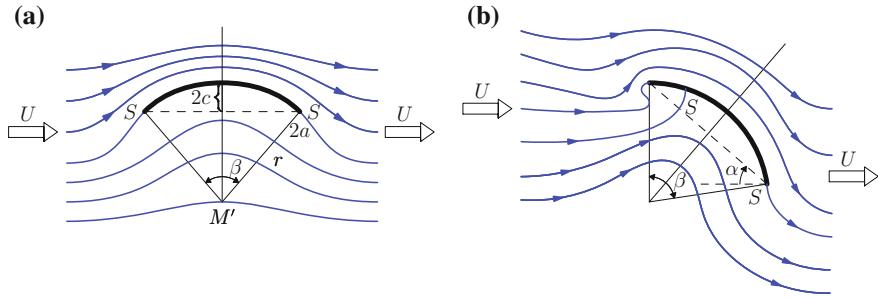
Fig. 6.18 KUTTA-JOUKOWSKI mapping applied to a circular wing. **a** *Smooth potential flow around a circular segment with definitions of geometric quantities* β, r, a, c *and* M'. *The flow is symmetric to the symmetry line.* **b** *Potential flow around a circular segment with angle of attack* α *and opening angle* β

and substituting these into $(6.66)_2$, finally, yields

$$c_\ell = 2\pi \, \tan \frac{\beta}{4}. \tag{6.67}$$

For a curved segment with angle of attack α relative to the direction of the approaching velocity U, the influences of the angle of attack and the curvature, α and β can be additively superposed, to obtain the 'lift' coefficient

$$c_\ell \approx 2\pi \sin \alpha + 2\pi \tan \frac{\beta}{4} \approx 2\pi \left(\alpha + \frac{\beta}{4} \right), \tag{6.68}$$
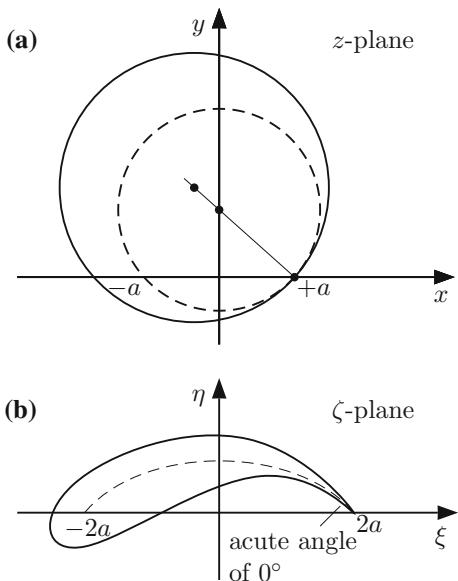
provided α and β are both small.

6.2.3 Realistic Air-Wings with Finite Thickness

KUTTA-JOUKOWSKI profiles are generated as images of the two circles shown in **Fig. 6.19**a. The dashed circle in the z-plane is mapped by the KUTTA-JOUKOWSKI transformation to the dashed circular segment, whereas the solid circle is mapped to the air-wing type profile with blunt frontal edge and the pointed trailing edge with zero opening angle in Fig. 6.19b. These properties are stated here, but not proved. Further examples of KUTTA-JOUKOWSKI profiles have already been shown in Fig. 6.14.

The disadvantage of the trailing edge of the KUTTA-JOUKOWSKI profiles is removed by the VON KÁRMÁN-TREFFTZ conformal mapping. To motivate it, write the KUTTA-JOUKOWSKI mapping in the two forms

Fig. 6.19 KUTTA-
JOUKOWSKI profiles. **a** *The
dashed circle with center on
the y-axis, cutting the x-axis
at the points z = ±a. The
larger solid circle generates
under the*
KUTTA-JOUKOWSKI mapping
the KUTTA-JOUKOWSKI
profile.
b *The* KUTTA-JOUKOWSKI
*mapping leads to the dashed
circular segment in the
ζ-plane and the solid*
KUTTA-JOUKOWSKI *contour.
The trailing edge at x = 2a
has zero thickness and equal
tangents from the upper and
lower profile part*

$$\zeta - 2a = z + \frac{a^2}{z} - 2a = \frac{1}{z}(z - a)^2,$$

$$\zeta + 2a = z + \frac{a^2}{z} + 2a = \frac{1}{z}(z + a)^2,$$

which allows the alternative expression for the KUTTA-JOUKOWSKI mapping:

$$\frac{\zeta - \mathbf{2}a}{\zeta + \mathbf{2}a} = \left(\frac{z - a}{z + a}\right)^{\mathbf{2}}. \tag{6.69}$$

Note the emphasized elements '**2**' in this expression. This motivated THEODORE
VON KÁRMÁN and ERICH TREFFTZ[5] to generalize the KUTTA-JOUKOWSKI mapping
as follows:

$$\frac{\zeta - \left(2 - \frac{\beta}{\pi}\right)a}{\zeta + \left(2 - \frac{\beta}{\pi}\right)a} = \left(\frac{z - a}{z + a}\right)^{\left(2 - \frac{\beta}{\pi}\right)}. \tag{6.70}$$

---

[5]For a biography of THEODORE VON KÁRMÁN (1881–1963) see Fig. 9.15. For a short biography of
ERICH TREFFTZ see **Fig. 6.20**.

Fig. 6.20 ERICH IMMANUEL TREFFTZ (21. Feb. 1888–21. Jan. 1937)

ERICH IMMANUEL TREFFTZ was a German mechanician, mathematician and university teacher. He started his university education in 1906 for two years in mechanical engineering at the 'Technische Hochschule' (TH) in Aachen, switched then to mathematics, from 1908 in Göttingen, where he worked under DAVID HILBERT, PAUL KOEBE and LUDWIG PRANDTL. He spent in 1909/10, at the recommendation of CARL RUNGE, some months at Columbia University and subsequently continued his studies at Strasbourg University with RICHARD VON MISES. Between 1912 and 1913 he was assistant at TH Aachen and completed his doctoral dissertation 'Über die Kontraktion kreisförmiger Flüssigkeitsstrahlen' (on the contraction of circular fluid jets). In World War I he was wounded and called in 1917 to the Aerodynamic Institute in Aachen, where he habilitated and was called as professor of mathematics at TH Aachen. 1922, TREFFTZ was called as professor of the mechanics institute of TH Dresden, where he primarily worked on aerodynamics, hydrodynamics, theory of elasticity and vibrations. In 1933 he became Editor of the 'Zeitschrift für Angewande Mathematik und Mechanik' (ZAMM) of the 'Gesellschaft für angewandte Mathematik und Mechanik' (GAMM) until his sudden death in 1937.

The text is based on http://www.wikipedia.org

This transformation reduces to the KUTTA-JOUKOWSKI mapping when $\beta = 0$. The following properties of (6.70) can straightforwardly be deduced:

- For $|z| \to \infty$ and $|\zeta| \to \infty$ (6.70) can be approximated by TAYLOR series expansions to

$$\frac{1 - \left(2 - \dfrac{\beta}{\pi}\right)\dfrac{a}{\zeta}}{1 + \left(2 - \dfrac{\beta}{\pi}\right)\dfrac{a}{\zeta}} = \left(\frac{1 - \dfrac{a}{z}}{1 + \dfrac{a}{z}}\right)^{\left(2 - \frac{\beta}{\pi}\right)} = \left(1 - 2\frac{a}{z}\right)^{\left(2 - \frac{\beta}{\pi}\right)}$$

$$\longrightarrow \quad \left\{1 - 2\left(2 - \frac{\beta}{\pi}\right)\frac{a}{\zeta}\right\} = \left\{1 - 2\left(2 - \frac{\beta}{\pi}\right)\frac{a}{z}\right\},$$

$$\longrightarrow \quad \zeta = z, \quad \text{as} \quad z \to \infty.$$

- Hence, $d\zeta/dz = 1$ as $z \to \infty$. This means that close to $z \to \infty$ the VON KÁRMÁN-TREFFTZ mapping is the identity mapping: The flow remains parallel steady flow with velocity U at infinity.
- With

$$\tilde{z} = z - a, \qquad \tilde{\zeta} = \zeta - \left(2 - \frac{\beta}{\pi}\right)a \tag{6.71}$$

one obtains from (6.70) in the neighborhood of $\tilde{z} = 0$ approximately

$$\tilde{\zeta} \stackrel{\text{prop}}{=} \tilde{z}^{\left(2 - \frac{\beta}{\pi}\right)}. \tag{6.72}$$

- With these properties the two arrows (see **Fig. 6.21**)

$$\tilde{z}_1 = R\,\exp(\iota\gamma), \qquad \tilde{z}_2 = R\,\exp\left(\iota(\gamma - \pi)\right) \tag{6.73}$$

are mapped to

$$\tilde{\zeta}_1 = R^{\left(2 - \frac{\beta}{\pi}\right)}\exp\left(\iota\left(2 - \frac{\beta}{\pi}\right)\gamma\right),$$

$$\tilde{\zeta}_2 = R^{\left(2 - \frac{\beta}{\pi}\right)}\exp\left(\iota\left(2 - \frac{\beta}{\pi}\right)\gamma\right)\exp(\iota\beta). \tag{6.74}$$
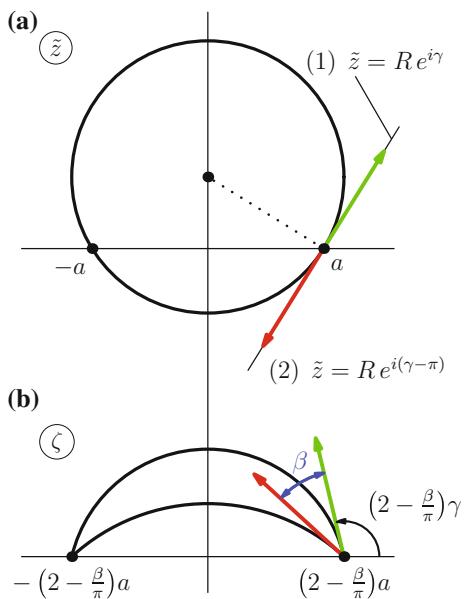
These are two vectors, enclosing the angle β (see Fig. 6.21). It can also readily be shown that the circle in Fig. 6.21a is mapped in Fig. 6.21b onto the twi-angle (sickle)[6] with finite edge angle β.

The VON KÁRMÁN-TREFFTZ profile is obtained, if one adds to the first circle (dashed in **Fig.** 6.22a) a second solid circle that is tangent to the first at $(a, 0)$. Its image is then shown in Fig. 6.22b and has a trailing edge angle β.

---
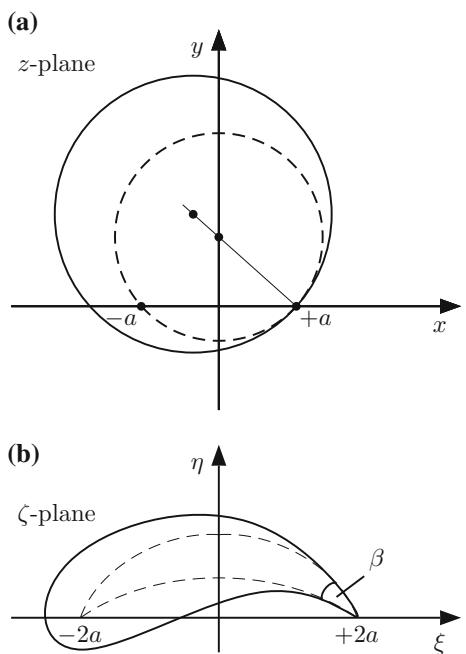
[6] 'Twi-angle' in analogy to 'Tri-angle', in German 'Zweieck' and 'Dreieck'.

Fig. 6.21 VON
KÁRMÁN-TREFFTZ conformal
mapping (6.70). **a** *The circle
with center on the y-axis and
intersections with the x-axis
at x = ±a. The tangent to
the circle at x = a defines
the two arrows in* (6.73).
b *Corresponding ζ-plane
with the twi-angle with
non-zero edge angle β*

(a)

$(1) \ \tilde{z} = R\,e^{i\gamma}$

$-a$

a

$(2) \ \tilde{z} = R\,e^{i(\gamma-\pi)}$

(b)

β

$\left(2 - \frac{\beta}{\pi}\right)\gamma$

$-\left(2 - \frac{\beta}{\pi}\right)a$

$\left(2 - \frac{\beta}{\pi}\right)a$

Fig. 6.22 VON
KÁRMÁN-TREFFTZ
transformation (6.70) and
construction of the VON
KÁRMÁN-TREFFTZ profile.
For details see main text

(a)

z-plane

y

$-a$

$+a$

x

(b)

η

ζ-plane

β

$-2a$

$+2a$

ξ

6.3 The Circle Theorem of Milne-Thomson

Let[7] $\phi(z)$ be the complex potential of a plane potential flow with point singularities (sources, vortices, dipoles). For physical reasons all these irregularities lie outside of a given circle with radius $|z| = a$. MILNE-THOMSONs statement is as follows [22]:

Theorem 6.3 *The potential flow around a given circle, generated by the singularities of the potential, is given by the complex potential*

$$\phi^*(z) = \phi(z) + \tilde{\phi}\left(\frac{a^2}{z}\right), \tag{6.75}$$

where

$$\tilde{\phi}(z) = \overline{\phi(\overline{z})}, \tag{6.76}$$

in which the overbar $\overline{a}$ denotes the complex conjugate of a. ∎

To prove this theorem, let us start from a TAYLOR series expansion of $\phi(z)$ about the non-singular point z_0. One then obtains

$$\phi(z) = a_0 + a_1(z - z_0) + a_2(z - z_0)^2 + \cdots,$$
$$\phi(\overline{z}) = a_0 + a_1(\overline{z} - z_0) + a_2(\overline{z} - z_0)^2 + \cdots,$$
$$\overline{\phi(\overline{z})} = \overline{a_0} + \overline{a_1}(z - \overline{z_0}) + \overline{a_2}(z - \overline{z_0})^2 + \cdots.$$

On the circle $|z| = a$ one has $a^2/z = \overline{z}$. For this reason we have on this circle

$$\tilde{\phi}\left(\frac{a^2}{z}\right) = \tilde{\phi}(\overline{z}) \overset{(6.76)}{=} \overline{\phi(\overline{\overline{z}})} = \overline{\phi(z)} \tag{6.77}$$

$$= \overline{a_0} + \overline{a_1}(\overline{z} - \overline{z_0}) + \overline{a_2}(\overline{z} - \overline{z_0})^2 + \cdots \tag{6.78}$$

or

$$\phi^*(z) = \phi(z) + \overline{\phi(z)} = 2\text{Re}\left(\phi(z)\right). \tag{6.79}$$

This result implies that $\text{Im}\left(\phi^*(z)\right) = 0$ on the circle $|z| = a$. In other words, the circle $|z| = a$ is streamline for $\phi^*(z)$, qed.

Examples

(α) *Constant parallel potential flow $\phi(z) = Uz$:*

This potential has a dipole singularity at infinity and one obtains for $\phi^*(z)$

---

[7]For a short biography of MILNE-THOMSON see **Fig. 6.23**.

$$\phi^*(z) = Uz + U\frac{a^2}{z} = U\left(z + \frac{a^2}{z}\right), \tag{6.80}$$

which is the well known velocity potential of parallel flow around a circle with radius a and approaching velocity U at infinity, see formula (5.189) in Chap. 5.

(β) *Reflection of a point source at a circle*:

Consider a potential flow induced by a point source Q at $x = x_0$, see **Fig. 6.24**a. The potential is then given by

$$\phi(z) = \frac{Q}{2\pi} \ln\left(\frac{z - x_0}{a}\right) \quad \text{and} \quad \phi\left(\frac{a^2}{\bar{z}}\right) = \frac{Q}{2\pi} \ln\left(\frac{\frac{a^2}{\bar{z}} - x_0}{a}\right). \tag{6.81}$$

Since $\ln \bar{z} = \overline{\ln(z)}$ one deduces from $(6.81)_2$
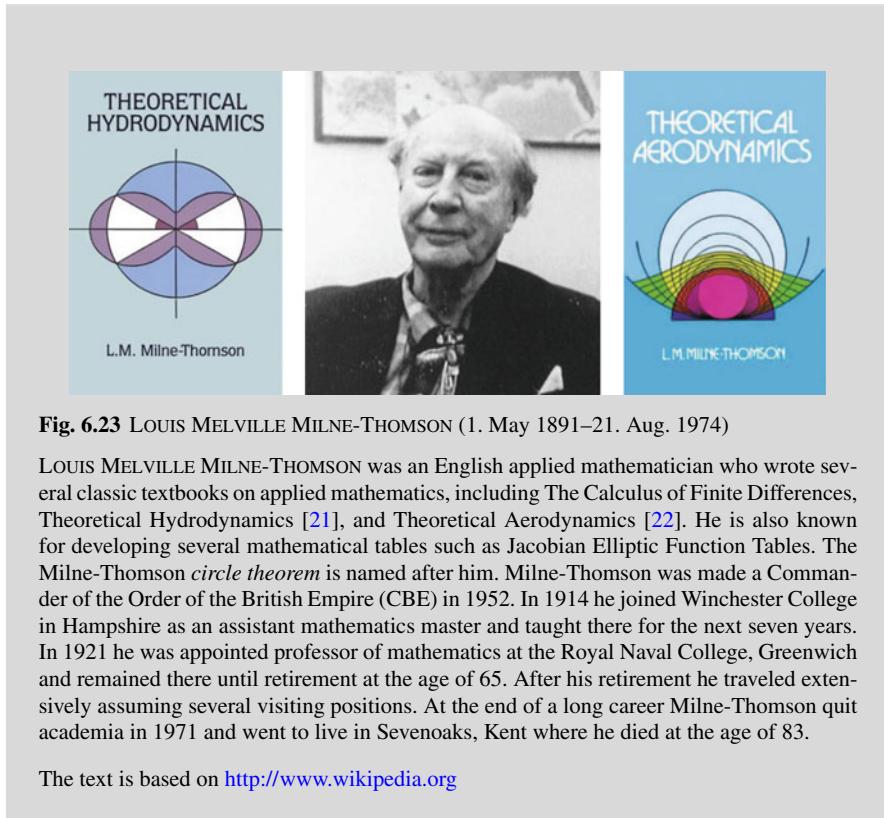
Fig. 6.23 Louis Melville Milne-Thomson (1. May 1891–21. Aug. 1974)

Louis Melville Milne-Thomson was an English applied mathematician who wrote several classic textbooks on applied mathematics, including The Calculus of Finite Differences, Theoretical Hydrodynamics [21], and Theoretical Aerodynamics [22]. He is also known for developing several mathematical tables such as Jacobian Elliptic Function Tables. The Milne-Thomson *circle theorem* is named after him. Milne-Thomson was made a Commander of the Order of the British Empire (CBE) in 1952. In 1914 he joined Winchester College in Hampshire as an assistant mathematics master and taught there for the next seven years. In 1921 he was appointed professor of mathematics at the Royal Naval College, Greenwich and remained there until retirement at the age of 65. After his retirement he traveled extensively assuming several visiting positions. At the end of a long career Milne-Thomson quit academia in 1971 and went to live in Sevenoaks, Kent where he died at the age of 83.

The text is based on http://www.wikipedia.org
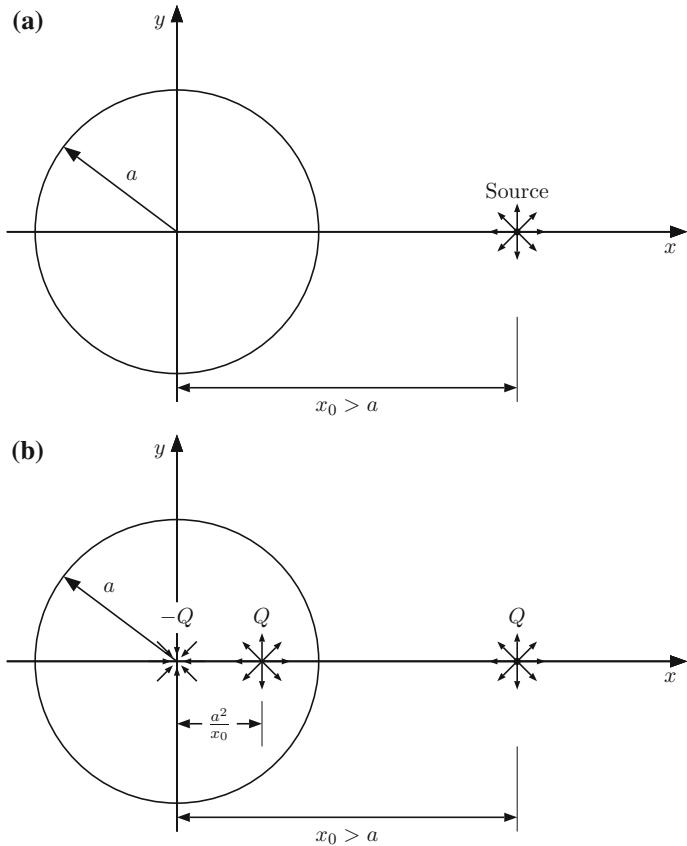
Fig. 6.24 Mirroring of a source term at a circle. **a** *Circle with radius a and the center at the origin* $z = 0$. *The point source is on the real axis at* x_0. **b** *Same as panel* (**a**) *but the sources at* $x = 0$ *and* $x = a^2/x_0$ *are also shown*

$$\overline{\phi\left(\frac{a^2}{\overline{z}}\right)} = \frac{Q}{2\pi} \ln\left(\frac{\frac{a^2}{z} - x_0}{a}\right) = \frac{Q}{2\pi} \ln\left(\frac{a^2 - x_0 z}{az}\right)$$

$$= \frac{Q}{2\pi} \ln\left(\frac{1 - \frac{x_0 z}{a^2}}{\frac{z}{a}}\right) = -\frac{Q}{2\pi} \ln\left(\frac{z}{a}\right) + \frac{Q}{2\pi} \ln\left(\left(z - \frac{a^2}{x_0}\right)\left(-\frac{x_0}{a^2}\right)\right)$$

$$= -\frac{Q}{2\pi} \ln\left(\frac{z}{a}\right) + \frac{Q}{2\pi} \ln\left(\frac{z - \frac{a^2}{x_0}}{a}\right) + \underbrace{\frac{Q}{2\pi}\left(\ln\left(-\frac{x_0}{a}\right)\right)}_{\text{const.}}.$$

Except for a non-relevant constant, this yields the potential

$$\phi^*(z) = \frac{Q}{2\pi} \left\{ \ln\left(\frac{z - x_0}{a}\right) + \ln\left(\frac{z - \frac{a^2}{x_0}}{a}\right) - \ln\left(\frac{z}{a}\right) \right\}, \tag{6.82}$$

in which the above constant has been dropped. All three contributions are source terms according to Fig. 6.24b.

It is possible to symmetrize the source and sink arrangement as sketched in **Fig. 6.25**a. The complex potential is then given by
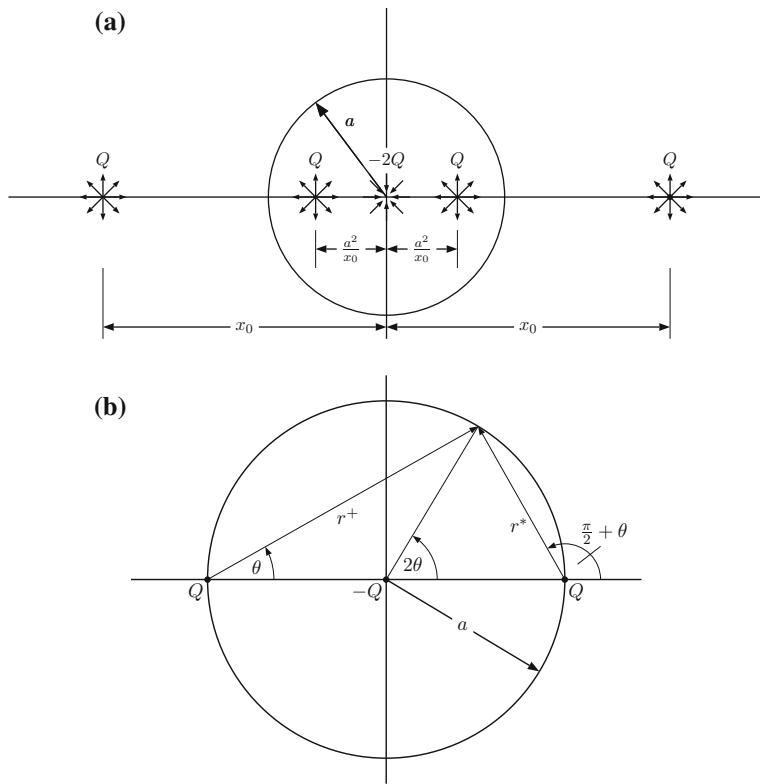
Fig. 6.25 Symmetrized distribution of source terms corresponding to Fig. 6.24. **a** *Source-sink distribution and* **b** *limit distribution when the two sources lie on the periphery of the circle and a sink at the coordinate origin*

$$\phi^*(z) = \frac{Q}{2\pi}\left\{\ln\left(\frac{z-x_0}{a}\right) + \ln\left(\frac{z-\frac{a^2}{x_0}}{a}\right) - \ln\left(\frac{z}{a}\right)\right.$$

$$\left. + \ln\left(\frac{z+x_0}{a}\right) + \ln\left(\frac{z+\frac{a^2}{x_0}}{a}\right) - \ln\left(\frac{z}{a}\right)\right\}$$

$$= \frac{Q}{2\pi}\ln\left\{\frac{z^2-x_0^2}{a^2}\cdot\frac{z^2-\left(\frac{a^2}{x_0}\right)^2}{a^2}\cdot\frac{a^2}{z^2}\right\}. \tag{6.83}$$

In the limit when non-centric sources move on the x-axis to the periphery of the circle with radius a, see Fig. 6.25a, and Q is replaced by $Q/2$, (6.83) is easily seen in this case to reduce to

$$\phi^*(z) = \frac{Q}{2\pi}\ln\left\{\left(\frac{z-a}{a}\right)\left(\frac{z+a}{a}\right)\left(\frac{a}{z}\right)\right\}. \tag{6.84}$$

If one sets here for $|z| = a$ the equivalents

$$(z-a) = r^*\exp\left(\iota\left(\theta+\frac{\pi}{2}\right)\right), \quad (z+a) = r^+\exp(\iota\theta), \quad z = r\,\exp(2\iota\theta),$$

one obtains

$$\psi^* = \mathrm{Im}\left(\phi^*(z)\right) = \frac{Q}{2\pi}\left(\theta+\theta+\frac{\pi}{2}-2\theta\right) = \frac{Q}{4} = \mathrm{const.},$$

or, the circle $|z| = a$ is streamline.

6.4   Laminar Free Jets

Plane laminar free jets can also be studied with function theoretical methods. In what follows, we shall analyse two-dimensional potential flow out of a slit orifice and a regular array of such apertures.

6.4.1   Flow Through a Slit Orifice in a Vertical Wall

The situation is sketched in **Fig. 6.26**. Plane flow of a density preserving ideal fluid from a vessel with pressure $p + \Delta\,p$ through a slit of width $2b$ is considered. Gravity is ignored; so, the jet in the space exterior to the vessel is basically symmetric and horizontal and has width $2a$. The outside pressure is constant and has value p. Of
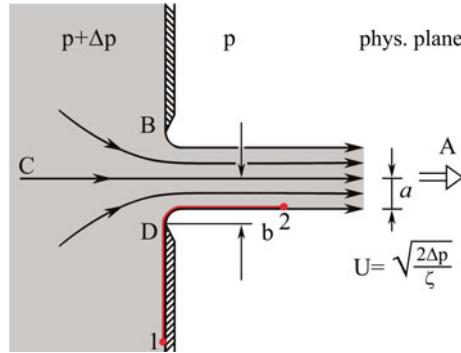
Fig. 6.26 Laminar jet of a two-dimensional density-preserving fluid through a slit orifice from a large vessel. *The pressure in the vessel is $p + \Delta p$, where p is the constant external pressure. C and A label the side walls far from the orifice to the left and the jet cross section to the right. B and D identify the points at the upper and lower edge of the slit aperture. The slit height is $2b$ and the jet width far to the right is $2a < 2b$. Points 1 and 2 mark two points of the streamline (red) at the wall (where $w = 0$) and the lower free boundary of the jet. Gravity is ignored so that C–A is a symmetry line of the flow*
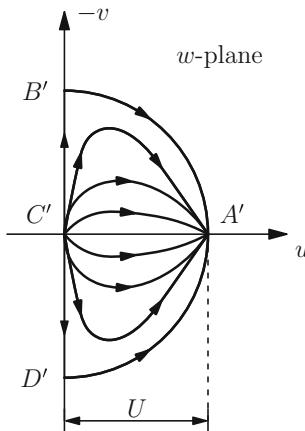
Fig. 6.27 Hodograph (w)-plane for the potential flow displayed in Fig. 6.26. *The points A', B', C', D' correspond to the points A, B, C, D in Fig. 6.26. The quarter circles $D'A'$ and $A'B'$ are the w-images of the velocity of the free boundaries of the jet. The point C' represents a source of strength $2Ua$, which is counterbalanced by a sink at A' of the same strength. The oriented streamlines inside the semi-circle depict the velocity distribution along streamlines from any position in the vessel back-wall to the cross section far downstream. These streamlines are only qualitatively drawn*

interest are the points A, B, C, D as indicated in the figure; A and C are at $(\pm\infty, 0)$ and B and D bound the orifice at $(0, \pm b)$.

Consider the w-(or hodograph) plane, **Fig. 6.27**. In this plane the velocities of the free boundaries of the jet are mapped onto the quarter circles $D'A'$ and $A'B'$. To see
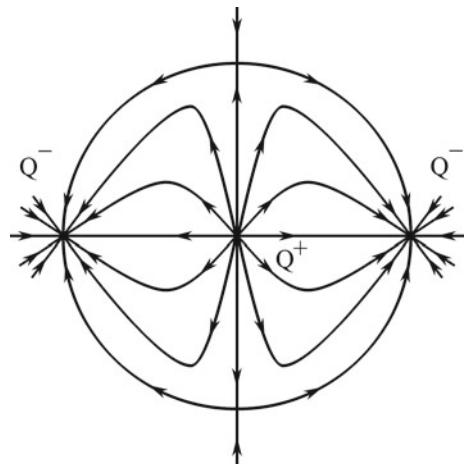
this, let us apply the BERNOULLI equation along the streamline from point 1 at the wall to point 2 on the free lower streamline (Fig. 6.26). This yields

$$\frac{p + \Delta p}{\rho} = \frac{p}{\rho} + \frac{U^2}{2} \quad \longrightarrow \quad U = \sqrt{\frac{2\Delta p}{\rho}} = \text{constant.} \qquad (6.85)$$

Thus, along the free boundary streamline the modulus of the velocity is constant and, therefore, mapped in the hodograph plane to the two quarter circles $D'A'$ and $A'B'$ (Fig. 6.27). The streamlines in the 'physical' plane are mapped into streamlines of the fictitious flow in the complex w-(hodograph) plane. This flow in the complex hodograph plane is often easy to construct, because its singularities (sources, sinks) are known and because the jet free boundary velocities are fictitious streamlines. In Fig. 6.27 this fictitious flow is sketched. Depending upon, which streamline in Fig. 6.26 from the distant vessel wall is chosen (C' in Fig. 6.27 represents a state of rest, whose pre-image in Fig. 6.26 is the zero velocity at all points along the wall) the corresponding fictitious w-streamline in Fig. 6.27 connects C' with A' (A' is the image of all x-velocities U in the jet cross section A). The total flux is obviously given by $Q = 2Ua$. Since this source 'sits' at C' and, correspondingly, the sink of the same strength at A', which are central and periphery points of the circle, this circle can only be a streamline of the fictitious w-flow if the source-sink arrangement is symmetrized as shown in **Fig. 6.28**. At the center of this circle 'sits' a source of strength

$$Q^+ = 2 \cdot 2Ua = 4Ua. \qquad (6.86)$$

Fig. 6.28 Symmetrized hodograph as constructed from Fig. 6.27 with the indicated source-sink distribution. *The corresponding potential, motivated by (6.84), is given by (6.88). Streamlines are qualitative only*

Similarly, at the points $w = (\pm U, 0)$ sit sinks

$$Q^- = 4 \, U a \qquad (6.87)$$

of equal strength. The complex potential of this flow has been shown to be given by (6.84) (in which $a = U$); hence

$$\tilde{\phi}(w) = \frac{Q}{2\pi} \left\{ \ln\left(\frac{w}{U}\right) - \ln\left(\frac{w-U}{U}\right) - \ln\left(\frac{w+U}{U}\right) \right\}. \qquad (6.88)$$

It is our next intention to determine the shape of the jet boundary in the z-plane. To this end, the conformal mapping $z = z(w)$ is needed. In particular, the pre-image of the semi-circle $|w| = U$, $\mathrm{Re}(w) \geqslant 0$ in the z-plane is in focus. One has

$$w = \frac{\mathrm{d}\phi}{\mathrm{d}z} = \frac{\mathrm{d}\tilde{\phi}}{\mathrm{d}w} \frac{\mathrm{d}w}{\mathrm{d}z} \quad \longrightarrow \quad \frac{\mathrm{d}z}{\mathrm{d}w} = \frac{1}{w} \frac{\mathrm{d}\tilde{\phi}}{\mathrm{d}w}. \qquad (6.89)$$

Substitution of $\mathrm{d}\tilde{\phi}/\mathrm{d}w$ from (6.88) yields

$$\frac{\mathrm{d}z}{\mathrm{d}w} = \frac{1}{w} \frac{\mathrm{d}\tilde{\phi}}{\mathrm{d}w} = \frac{Q}{2\pi} \left\{ \frac{1}{w^2} - \frac{1}{w(w-U)} - \frac{1}{w(w+U)} \right\}. \qquad (6.90)$$

Applying partial fraction, i.e.,

$$\frac{1}{w(w-U)} = -\frac{1}{Uw} - \frac{1}{U(U-w)}, \qquad \frac{1}{w(w+U)} = \frac{1}{Uw} - \frac{1}{U(U+w)},$$

(6.90) can also be written as

$$\begin{aligned}
\frac{\mathrm{d}z}{\mathrm{d}w} &= \frac{Q}{2\pi} \left\{ \frac{1}{w^2} + \frac{1}{U(U-w)} + \frac{1}{U(U+w)} \right\} \\
&= \frac{Q}{2\pi U^2} \left\{ \left(\frac{U}{w}\right)^2 + \frac{1}{1-w/U} + \frac{1}{1+w/U} \right\},
\end{aligned}$$

or with $\omega := w/U$,

$$\frac{\mathrm{d}z}{\mathrm{d}\omega} = \frac{Q}{2\pi U} \left\{ \frac{1}{\omega^2} + \frac{1}{1-\omega} + \frac{1}{1+\omega} \right\}.$$

Integration of this equation is straightforward and yields

$$z(\omega) = \frac{Q}{2\pi U} \left\{ -\frac{1}{\omega} + \ln(1+\omega) - \ln(1-\omega) \right\} + k,$$

or

$$z(w) = \frac{Q}{2\pi U} \left\{ -\frac{U}{w} + \ln\left(1 + \frac{w}{U}\right) - \ln\left(1 - \frac{w}{U}\right) \right\} + k. \qquad (6.91)$$

The streamline of the upper jet boundary is given by $w = U\exp(\iota\theta)$ for $0 \leqslant \theta \leqslant \pi/2$. Substitution of this representation into (6.91) yields

$$
\begin{aligned}
z(\theta) &= \frac{Q}{2\pi U}\left\{-\exp(-\iota\theta) + \ln\left(1 + \exp(\iota\theta)\right) - \ln\left(1 - \exp(\iota\theta)\right)\right\} + k \\
&= \frac{Q}{2\pi U}\left\{-\exp(-\iota\theta) + \ln\left(\frac{1 + \exp(\iota\theta)}{1 - \exp(\iota\theta)}\right)\right\} + k \\
&= \frac{Q}{2\pi U}\left\{-\exp(-\iota\theta) + \iota\frac{\pi}{2} + \ln\left(\frac{\sin\theta}{1 - \cos\theta}\right)\right\} + k \\
&= \frac{Q}{2\pi U}\left\{-\exp(-\iota\theta) + \ln\left(\frac{\sin\theta}{1 - \cos\theta}\right)\right\} + k^*, \quad 0 \leqslant \theta \leqslant \pi/2 \quad (6.92)
\end{aligned}
$$

with a new constant k^*. This constant is determined by evaluating (6.92) for $\theta = \pi/2$. This corresponds to point B in Fig. 6.26 and $z = \iota b$. So,

$$\iota b = \frac{Q}{2\pi U}(\iota) + k^* \overset{(6.86)}{=} \iota\frac{2a}{\pi} + k^* \quad\longrightarrow\quad k^* = \iota\left(b - \frac{2a}{\pi}\right). \qquad (6.93)$$

The upper jet boundary at the far right is described by $\theta \to 0^+$. For this value the real part of $\lim_{z\to 0^+}(z(\theta))$ is infinitely large (owing to the logarithmic term in (6.92)). Thus, $Im\left(\lim_{z\to 0^+} z(\theta)\right) = \iota a$, so that (6.92) now implies

$$\iota a = k^* \quad\overset{(6.93)}{\longrightarrow}\quad \frac{a}{b} = \frac{\pi}{2+\pi} = 0.6110,$$
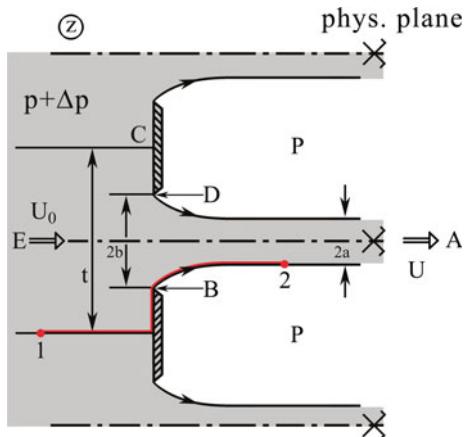
a result already obtained by KIRCHHOFF in 1860. The contraction of the plane jet through an orifice with sharp edges is 0.611, which, incidentally differs from the loss of BORDA-CARNOT, which is 0.5.

6.4.2 Potential Flow Through a Periodic Arrangement of Slits

The above function-theoretical approach can also be applied to the flow of an ideal incompressible fluid through a periodic arrangement of slits of width $2b$ and slit distance t. Two elements of this infinite arrangement and geometric notation are shown in **Fig. 6.29**. Given quantities are t, b, Δp and unknowns are $2a =$ asymptotic jet width, $U =$ asymptotic jet velocity at the far right and $U_0 =$ average velocity flux in the vessel, related to U by mass (volume) balance according to

$$U_0 t = 2Ua.$$

Fig. 6.29 Infinite
two-dimensional
arrangement of slits from a
vessel into free space. *Two
elements are shown, which
are thought to be infinitely
complemented. Geometry
and notation of typical
quantities are indicated. The
pressure in the vessel is
p + Δp where p is the
pressure in the exterior
space. Gravity is ignored so
that the jet is straight and
symmetric*

Gravity will be ignored. Application of the BERNOULLI equation between two points
on the symmetry axis of a jet, one point to the far left in the vessel, the other point to
the far right, where the jet has reached the asymptotic width $2a$ (see Fig. 6.29, red),
yields

$$\frac{p + \Delta p}{\rho} + \frac{U_0^2}{2} = \frac{p}{\rho} + \frac{U^2}{2} \quad \longrightarrow \quad U^2 - U_0^2 = \frac{2\,\Delta p}{\rho}. \tag{6.94}$$

In the hodograph plane the image points of E and A, E' and A' in **Fig. 6.30**, are
locations of concentrated source and sink. Both points lie on the real axis of the
hodograph plane. Since C in Fig. 6.29 is a stagnation point, its image point must
be at the origin of the hodograph plane. The free boundaries of the jet are again
quarter circles $B'A'$ and $A'D'$ (in Fig. 6.30), which can be proved by formulating the
BERNOULLI equation between points 1 and 2 along the (red) streamline in Fig. 6.29.
The hodograph must therefore, look as displayed in Fig. 6.30.

The strength of the source at E' per slit is

$$Q = U_0 t. \tag{6.95}$$

This can be mirrored at the circle with radius U_0. It follows that the sink in A' is,
consequently, given by

$$-2Q = -2U_0 t. \tag{6.96}$$

The complete symmetrized source and sink distribution is given by the arrange-
ment as shown in **Fig. 6.31**. This arrangement then guarantees according to MILNE-
THOMSON's theorem that the speed of the velocity at the free jet is constant with
value U; [i.e., the circle in the hodograph plane is streamline of the virtual velocity].

In particular, at A' one has a sink of strength $2Q$ and at E' a source with strength
Q. This source must be complemented by a source, external to the circle at U^2/U_0 to
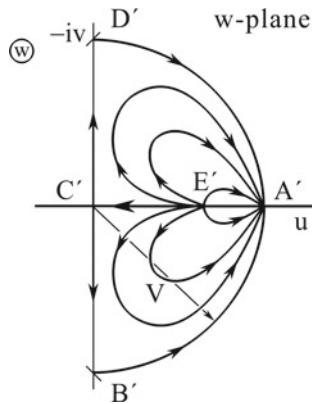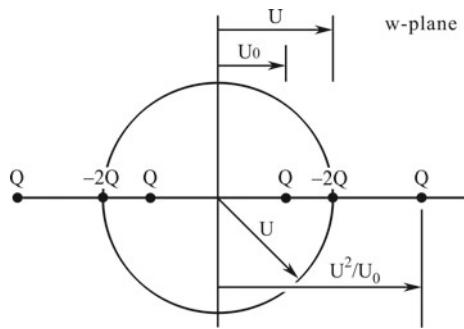
Fig. 6.30 Hodograph plane corresponding to one unit of the infinite slit-plate arrangement. *The point C' marks the stagnation point with vanishing velocity, E' and A' are the mapped velocity points of E and A with horizontal velocities U_0 and U, respectively. The velocities along the free jet boundaries are given by the two quarter circles $B'A'$ and $A'D'$. The figure also displays the characteristic symmetric streamlines in the hodograph plane*

Fig. 6.31 Hodograph plane with source-sink distribution for a periodic arrangement of slits as displayed in Fig. 6.29

satisfy the circular mirroring property. The set of this arrangement is finally mirrored at the imaginary axis of the w-plane.

The complex potential for the source-sink arrangement of Fig. 6.31 is given by

$$
\begin{aligned}
\hat{\phi}(w) &= \frac{U_0 t}{2\pi}\left\{ \ln\left(\frac{w - U_0}{U}\right) + \ln\left(\frac{w - U^2/U_0}{U}\right) - 2\ln\left(\frac{w - U}{U}\right) \right. \\
&\qquad\left. + \ln\left(\frac{w + U_0}{U}\right) + \ln\left(\frac{w + U^2/U_0}{U}\right) - 2\ln\left(\frac{w + U}{U}\right) \right\} \\
&= \frac{U_0 t}{2\pi}\left\{ \ln\left(\frac{w^2 - U_0^2}{U^2}\right) + \ln\left(\frac{w^2 - (U^2/U_0^2)^2}{U^2}\right) - 2\ln\left(\frac{w^2 - U^2}{U^2}\right) \right\}.
\end{aligned}
$$

$$(6.97)$$

Next, one applies (6.89), which is integrated from C' to D', and hence from $w = 0$ to $w = -\iota U$, corresponding to $z = \iota(t/2)$ and $z = b$. This leads to

$$\iota(t/2 - b) = \int_0^{-\iota U} \frac{1}{w} \frac{\mathrm{d}\tilde{\phi}}{\mathrm{d}w} \mathrm{d}w. \tag{6.98}$$

Equations (6.94), (6.97) and (6.98) allow computation of U and U_0, if Δp, t and b are prescribed. The semi-width of the jet follows thereafter from the mass (volume) balance

$$U_0 t = 2 a U \quad \text{or} \quad a = \frac{U_0}{2 U} t. \tag{6.99}$$

The construction of such solutions is given by MILNE-THOMSON [22].

Remarks

1. In the limit as $t \to \infty$, $b \to \infty$ the above periodic slit example contains the KIRCHHOFF plate problem, provided the plate width $t - 2b = \ell$ remains constant. In this case $U \to U_0$, and if in the limit process U is to remain finite, (6.94) shows that $\Delta p \to 0$. As suggested by Fig. 6.31 the singular source points move with $U \to U_0$ to the circle with radius U and combine with the sink $-2Q$. Alternatively, the sources, exterior to the circle, move to $\pm\infty$. It can be shown that the singularities in the hodograph become in this limit quadrupoles in the points $w = \pm U$, see **Fig. 6.32**.
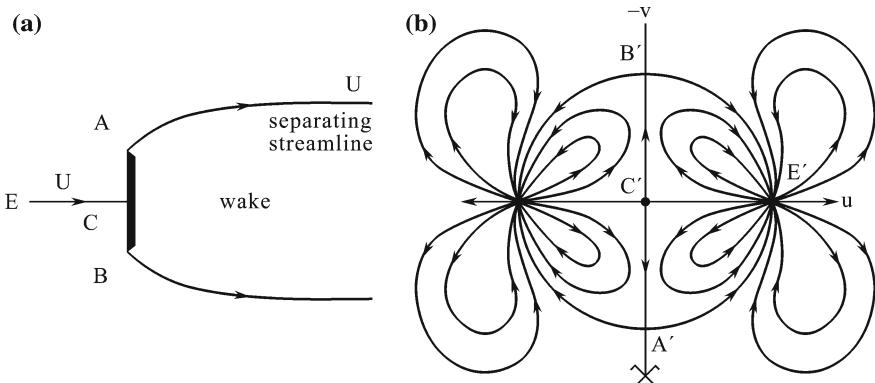
Fig. 6.32 Potential flow onto a plate. **a** *The constant velocity U at $x = \infty$ is normal to the plate. The streamline separating the outer flow from the wake has constant speed.* **b** *Hodograph plane: C' with vanishing velocity corresponds to the stagnation point C in panel (**a**). The separation streamline is mapped on the quarter circles $A'E'$ and $B'E'$*

(a)   **(b)**
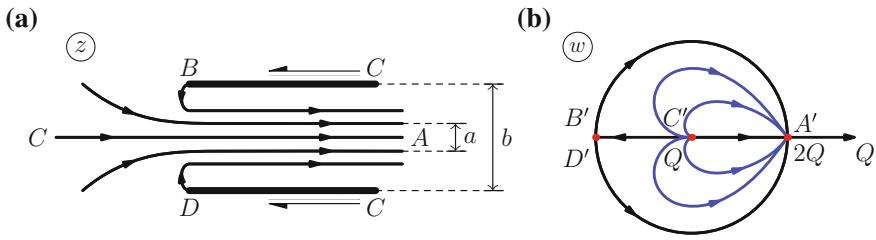
Fig. 6.33 BORDA exit mouth. **a** *Zoom of the flow through the exit opening (full figure see Chap.* 3, *Fig.* 3.39) *with special points indicated as* A, B, C, D *and opening width* b *and jet width* a. **b** *Hodograph plane with points* A', B', C', D' *as conformal map points of* A, B, C, D. *sources* (Q) *and sink* $(-2Q)$ *are also indicated*

2. In the so-called BORDA exit flow from a vessel (see **Fig. 6.33**a) shows a zoom of the flow through the exit opening. This problem has already been looked at in Chap. 3, Sect. 3.7.2 (pp. 120–124), and the contraction coefficient $\alpha = a/b$ has been determined there to be $\alpha = 0.5$. The indicated points are shown in panel (a) of Fig. 6.33. The points C have zero velocity and are in the hodograph plane (Fig. 6.33b mapped to the origin C'. Point A is a sink point mapped to A' on the real axis of the w-plane. C' is a source and its point mirrored on the circle, lies in Fig. 6.33 on the real axis at $\pm\infty$. The singularities $+Q$ lie at the center of the hodograph plane and on the real axis at $\pm\infty$ and the sink strength $2Q$ lies at A'. This distribution of singularities in the w-plane determines the potential flow with MILNE-THOMSON's method, see [22]. The solution for the contraction coefficient has been determined with other methods in Chap. 3 as already mentioned with the result $\alpha = a/b = 0.5$.

6.5 Schwarz-Christoffel Transformation

A[8] problem that arises frequently in fluid flow applications is that of constructing the flow of an ideal, incompressible fluid inside a polygonal domain or bounded by straight line segments. **Figure 6.36** displays a number of such situations: Two-dimensional (2D) horizontal flow over abrupt or smooth steps, Fig. 6.36a, b, c; 2D channel flow induced by a point discharge, Fig. 6.36d; parallel flow onto a rigid plate, Fig. 6.36e; 2D channel flow in the vicinity of a cross sectional change, Fig. 6.36f; laminar pipe flow through rectangular and polygonal cross sections, Fig. 6.36g, h, i. Such problems can be solved by finding in each case a one-to-one complex mapping of the half plane $y \geqslant 0$ onto a polygonal region that is a conformal mapping in the

---

[8]For short biographies of SCHWARZ and CHRISTOFFEL see **Fig. 6.34** and **Fig. 6.35**, respectively.

domain $y > 0$. The existence of such a mapping is guaranteed by the RIEMANN mapping theorem; however, whereas this theorem asserts the existence of a mapping under well described conditions, it does not provide a construction of it. A class of such transformations has independently been found by K.H.A. SCHWARZ and E.B. CHRISTOFFEL in the 19th century; they are known today as §CHWARZ-CHRISTOFFEL transformations, which provide an explicit formula for the derivative of a conformal mapping from the upper half plane onto a bounded or unbounded polygonal region, Fig. 6.36.

Fig. 6.34 KARL HERMANN AMANDUS SCHWARZ (25. Jan. 1843–30. Nov. 1921)

KARL HERMANN AMANDUS SCHWARZ was a German mathematician, known for his work in complex analysis. He originally studied chemistry in Berlin but ERNST EDUARD KUMMER (1810–1893) and KARL WEIERSTRASS (1815–1897) persuaded him to change to mathematics. Between 1867 and 1869 he worked in Halle, then in Zürich. From 1875 he worked at Göttingen University, dealing with the subjects of complex analysis, differential geometry and the calculus of variations. His works include *Bestimmung einer speziellen Minimalfläche* (determination of a special minimal surface), which was crowned by the Berlin Academy in 1867 and printed in 1871, and *Gesammelte mathematische Abhandlungen* (collected mathematical treatises, 1890). In 1892 he became a member of the Berlin Academy of Science and a professor at the University of Berlin, where his students included LIPÓT FEJÉR, PAUL KOEBE and ERNST
ZERMELO. He died in Berlin. In complex variable theory he is known for the SCHWARZ-CHRISTOFFEL transformation.

The text is based on http://www.wikipedia.org

Fig. 6.35 Elwin Bruno Christoffel (10. Nov. 1829–15. March 1900)

Elwin Bruno Christoffel attended the Jesuit Gymnasium and Friedrich-Wilhelms Gymnasium in Cologne and studied at the University of Berlin with Peter Gustav Lejeune Dirichlet, among others, where he received a doctorate in 1856 for a thesis on the motion of electricity in homogeneous bodies. In 1859, he became a Privatdozent at the University of Berlin. In 1862 he was appointed to a chair at the Polytechnic School in Zurich left vacant by Dedekind. After moving to the Gewerbeakademie in Berlin (now part of the Technical University of Berlin) in 1869, Christoffel became a professor at the University of Strasbourg in 1872, where he remained until retiring in 1894. Christoffel worked on conformal maps, potential theory, invariant theory, tensor analysis, mathematical physics, geodesy, and shock waves. The Christoffel symbol, Riemann-Christoffel tensor, Christoffel-Darboux formula, and Schwarz-Christoffel mapping are named after him.

The text is based on http://www.wikipedia.org

6.5.1   Build-up of the General Schwarz-Christoffel Transformation

Schwarz-Christoffel transformations are a special type of conformal maps from one complex plane into another. These transforms are explained in many books, in which complex analysis in a single complex variable is treated. Among such books mention might be made of [2, 5, 11, 14, 27]. In the text below, we shall follow in large parts the structure of [27].
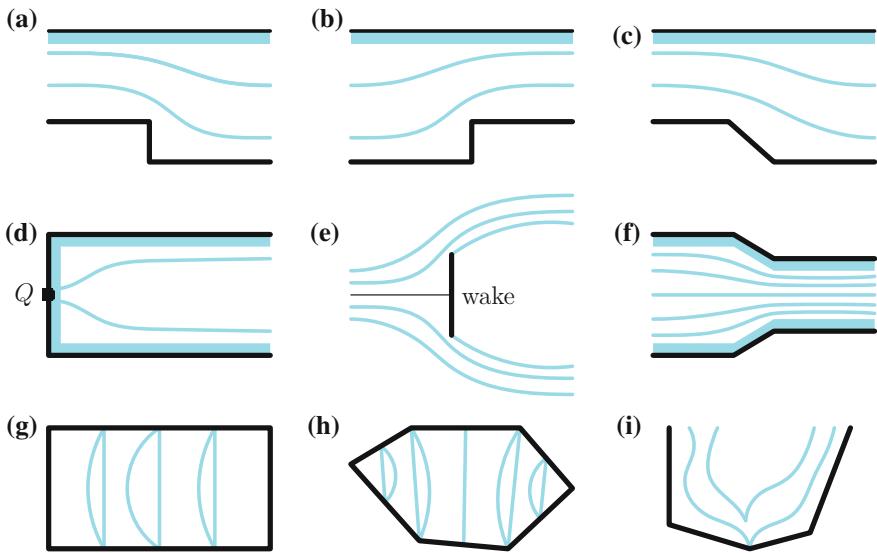
Fig. 6.36 Two-dimensional flow configurations of an incompressible fluid. **a, b, c** *Flow over an abrupt or continuous step in a channel with top free surface or rigid lid.* **d** *2D channel flow from a concentrated source at the channel end.* **e** *2D flow onto a rigid immobile plate.* **f** *2D channel flow through a narrowing width.* **g, h** *Pipe flow through a rectangular and polygonal cross section.* **i** *Flow in a 2D polygonal region*

(a) Building stones of the Schwarz-Christoffel transformation.
Consider the following complex function:

$$w = f(z) = (z - x_1)^{\alpha/\pi} \tag{6.100}$$

from the z- to the w-plane, where x_1 and α are real numbers and $0 < \alpha < 2\pi$. The mapping (6.100) is a composition of the translation $T(z) = z - x_1$ followed by the power function $F(z) = z^{\alpha/\pi}$. When written in polar form, $z - x_1 = r \exp(\iota \theta)$, $r > 0$, we have

$$f(z) = F(T(z)) = (r \exp(\iota \theta))^{\alpha/\pi} = r^{\alpha/\pi} \exp(\iota(\alpha\theta/\pi)). \tag{6.101}$$

The effect of $f(z)$, $r > 0$, $\theta \in (-\pi, \pi)$ is to stretch or contract the modulus of z and to rotate z through α/π radians about the origin to increase ($\alpha > 0$) the argument of z to $\alpha\theta/\pi$ of w. Under the composition $w = F(T(z)) = (z - x_1)^{\alpha/\pi}$ a ray attached to the point x_1 and being inclined by the angle θ in the z-plane is mapped in the w-plane to a ray attached to the origin $w = 0$ and inclined by the angle $\alpha\theta/\pi$ (see **Fig. 6.37**). In this interpretation the arguments of $f(z)$ in equations (6.100) and (6.101) are chosen as principal values (compare the text after (6.3)).

(a) A ray emanating from x_1 **(b)** Image of the ray in (a)
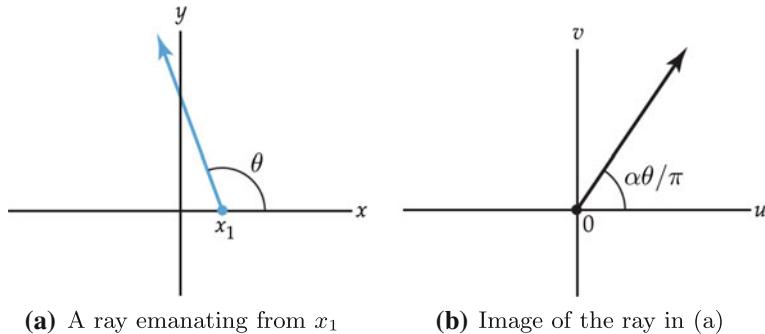
Fig. 6.37 The mapping $w(z) = (z - x_1)^{\alpha/\pi}$. **a** *A ray attached in the z-plane to x_1 and inclined by the angle θ is mapped by $w(z)$ in* **(b)** *to a ray attached to the origin $w = 0$ and inclined by the angle $\alpha\,\theta/\pi$, [27]. © Jones and Bartlett publishers, reproduced with changes*

The map (6.100) on the half-plane $y \geqslant 0$ enjoys the following properties:

- The set consisting of x_1 and the rays with $\arg(z - x_1) = \theta, 0 \leqslant \theta \leqslant \pi$ is mapped onto the point $w = 0$ and the rays with $\arg(w) = \alpha\,\theta/\pi, 0 \leqslant \alpha\,\theta/\pi \leqslant \alpha$.
- Thus, the image of the half plane $y \geqslant 0$ is the point $w = 0$ together with the wedge $0 \leqslant \arg(w) \leqslant \alpha$, **Fig. 6.38**.
- The derivative of the function f in (6.100),

$$ f'(z) = \frac{\alpha}{\pi} \, (z - x_1)^{(\alpha/\pi)-1} \,, \tag{6.102} $$

does not vanish when $y > 0$; therefore, $w = f(z)$ is a conformal mapping at any point z with $y > 0$.

(a) The half-plane $y \geqslant 0$ **(b)** The image of the the half-plane

Fig. 6.38 The mapping $w(z) = (z - x_1)^{\alpha/\pi}$. *The upper half-plane plus the point x_1 (shaded)* **(a)** *is conformally mapped to the wedge (shaded) in the w-plane with opening angle α* **(b)**, *[27]. © Jones and Bartlett publishers, reproduced with changes*

Subsequently, when dealing with SCHWARZ-CHRISTOFFEL transformations, we shall often work with $f'(z)$ rather than with $f(z)$.

Consider now a new function, which is analytic in $y > 0$ and whose derivative is given by

$$f'(z) = A\,(z - x_1)^{(\alpha_1/\pi)-1}\,(z - x_2)^{(\alpha_2/\pi)-1}\,, \tag{6.103}$$

where $x_1, x_2, \alpha_1, \alpha_2$ are real numbers, $x_1 < x_2$ and A is a complex constant. Moreover, the arguments of both functions on the right-hand side of (6.103) are taken as principal values.[9]

To determine the image of $f(z)$, whose derivative is given by (6.103), let us choose in this formula for z the real value t. In this restriction we have

$$w'(t) = A\,(t - x_1)^{(\alpha_1/\pi)-1}\,(t - x_2)^{(\alpha_2/\pi)-1}\,; \tag{6.104}$$

t may vary from $(-\infty$ to $x_1)$, from $(x_1$ to $x_2)$ and from $(x_2$ to $\infty)$. Looking at the argument of $w'(z)$, we get

$$\arg(w'(t)) = \arg(A) + \left(\frac{\alpha_1}{\pi} - 1\right)\arg(t - x_1) + \left(\frac{\alpha_2}{\pi} - 1\right)\arg(t - x_2). \tag{6.105}$$

From this representation one easily deduces

- If $t \in (-\infty, x_1)$, then $\arg(t - x_1) = \arg(t - x_2) = \pi$; so,

$$\arg(w'(z))|_{t\in(-\infty,x_1)} = \arg(A) + \alpha_1 + \alpha_2 - 2\,\pi. \tag{6.106}$$

---

[9]At this point it may be helpful to recall computational rules of the complex function (6.103) z^α, where the principal value of the complex power is understood. For real α and complex z, $z \neq 0$, one defines the *complex power function* as

$$z^\alpha \equiv |z|^\alpha \exp\{\iota\alpha(\theta + 2\pi k)\}\,, \quad k = 0, \pm 1, \pm 2, \dots\,.$$

For $\theta = \arg z$ and $k = 0$ one gets the *principal value* of the complex power function, also denoted by z^α,
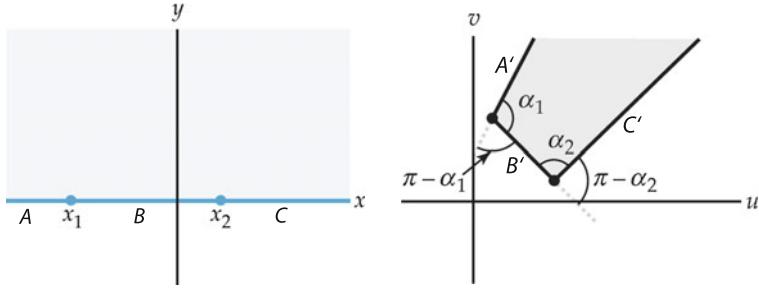
$$z^\alpha = |z|^\alpha \exp(\iota\alpha\arg z)\,.$$

Note that

$$\begin{aligned} \arg(z^\alpha) &\neq \alpha\arg z \quad \text{(choose e.g. } \alpha = 2,\ z = -1),\\ \arg\left(z_1^{\alpha_1} z_2^{\alpha_2}\right) &\neq \alpha_1\arg z_1 + \alpha_2\arg z_2. \end{aligned}$$

Moreover, if z_1^α and z_2^α are the principal values of the corresponding complex powers, the product $z_1^\alpha z_2^\alpha$ may not be the principal value of $(z_1 z_2)^\alpha$. For instance,

$$(-4)^{1/2}(-9)^{1/2} = 2e^{-\iota\pi/2} \cdot 3e^{\iota\pi/2} = 6e^{\iota\pi} = -6, \quad \text{but} \quad ((-4) \cdot (-9))^{1/2} = 6.$$

(a) The upper half-plane $y \geqslant 0$ **(b)** The image of the region in (a)

Fig. 6.39 SCHWARZ-CHRISTOFFEL map defined by $f'(z)$ given in (6.103). *The three segments* A($-\infty, x_1$), B(x_1, x_2) *and* C(x_2, ∞) *(a) are conformally mapped onto* A′, B′ *and* C′ *in the w-plane (b). The interior angles between the segments are* α_1 *and* α_2 *with external angles* $\pi - \alpha_1$ *and* $\pi - \alpha_2$. *The points* x_1 *and* x_2 *are mapped to* w_1 *and* w_2, *respectively. Internal angles are counted positive when they point in the counterclockwise direction from the i-th to the (i + 1)-st segment,* [27]. © *Jones and Bartlett publishers, reproduced with changes*

- If $t \in (x_1, x_2)$, then $\arg(t - x_1) = 0$, $\arg(t - x_2) = \pi$; so,

$$\arg(w'(z))|_{t \in (x_1, x_2)} = \arg(A) + \alpha_2 - \pi. \tag{6.107}$$

- If $t \in (x_2, \infty)$, then $\arg(t - x_1) = \arg(t - x_2) = 0$; so,

$$\arg(w'(z))|_{t \in (x_2, \infty)} = \arg(A). \tag{6.108}$$

From these statements we conclude:

The intervals $(-\infty, x_1)$, (x_1, x_2) and (x_2, ∞) are each mapped on their own line segment $w = f(z)$, and changes in the argument are $\pi - \alpha_1$ from segment A′ to segment B′ and $\pi - \alpha_2$ from segment B′ to segment C′, **Fig. 6.39**. This figure shows the images w_1, w_2 of x_1, x_2 and the interior angles α_1, α_2 and corresponding exterior angles $\pi - \alpha_1$, $\pi - \alpha_2$, respectively. The exterior angles between successive sides of the polygonal boundary are given by the change in the argument of w' from one interval to the next. If $\alpha_1 + \alpha_2 > \pi$, then the polygonal region is unbounded, if $\alpha_1 + \alpha_2 < \pi$, the triangle is bounded and the third vertex in Fig. 6.39b is $\pi - \alpha_1 - \alpha_2$. Moreover, for convex polygons (here triangles) the sum of the external wedge angles adds up to 2π.

(b) The general Schwarz-Christoffel mapping.

It is now becoming pretty clear how the general SCHWARZ-CHRISTOFFEL transformation has to be constructed. Let $f(z)$ be a function, which is holomorphic (analytic) in the domain $y > 0$ and possesses the derivative

$$f'(z) = A (z - x_1)^{(\alpha_1/\pi)-1} (z - x_2)^{(\alpha_2/\pi)-1} \cdots (z - x_n)^{(\alpha_n/\pi)-1}, \tag{6.109}$$

where $x_1 < x_2 < \cdots < x_n, 0 < \alpha_i < 2\pi$ for $1 \leqslant i \leqslant n$ and A is a complex constant. As before, the arguments of all product functions on the right-hand side of (6.109) are restricted to principal values by definition. Then, the upper half-plane $y \geqslant 0$ is mapped by $w = f(z)$ onto an unbounded polygonal region with interior angles $\alpha_1, \alpha_2, ..., \alpha_n$. The function given by the SCHWARZ-CHRISTOFFEL formula (6.109) is a conformal mapping in the domain $y > 0$. More explicitly stated, it is a conformal mapping from the upper half-plane onto a polygonal region. When extended to the region $y \geqslant 0$ it is still well defined, but it is only conformal in the domain $y > 0$. The points $x_1, x_2, \ldots, x_n$ may be singular points of (6.109).

In practical problems of the construction of $f'(z)$ by (6.109) one generally has some freedom in selecting the points x_k. Their adequate selection may simplify computations. As (6.109) provides only an explicit formula for $f'(z)$, the function $f(z)$ must be determined by integration,

$$f(z) = A\,g(z) + B,$$

(6.110)

$$g(z) = \int^z (\tilde{z} - x_1)^{(\alpha_1/\pi)-1}(\tilde{z} - x_2)^{(\alpha_2/\pi)-1} \cdots (\tilde{z} - x_n)^{(\alpha_n/\pi)-1}\mathrm{d}\tilde{z},$$

in which the lower limit is generally free to be selected. In this formula $f(z)$ has been written as the composition of two mappings, (i) the linear mapping $Aw + B$, which allows us to rotate, stretch (or contract), and translate the polygonal region produced by (ii) $w = g(z)$.

The SCHWARZ-CHRISTOFFEL transformation can also be used in combination with one or more other conformal mappings. This property is based on the following proposition:

Proposition 6.1 *If $w = f(z)$ is an analytic function of the complex variable $z = x + \iota y$ and $\zeta = g(w)$ is an analytic function of the complex variable $w = u + \iota v$, then the composition $\zeta = h(z) = g(f(z))$ is an analytic function of z.* ∎

For a proof the reader may consult the literature e.g. [9]. For the composite function of two conformal maps to be conformal the derivatives of the individual functions $f(x)$ and $g(w)$ must not vanish:

$$f'(z) \neq 0, \qquad g'(w) \neq 0.$$

The basis of such multifold compositions of conformal mappings is RIEMANNs mapping theorem, which guarantees the existence of a conformal map from any simply connected domain to the unit disk. The construction of such transformations for particular geometric configurations is not an easy task by itself. An extensive catalogue can be found in [19] and numerical schemes for constructing conformal maps are surveyed in [12].
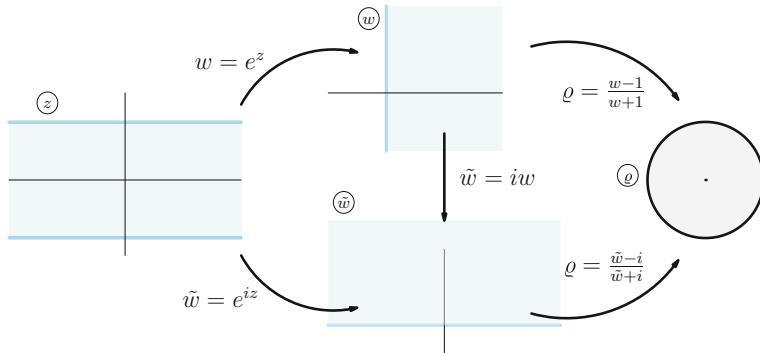
Fig. 6.40 Composite conformal transformation from a strip to the interior of the unit circle. *There may be several paths to go from the strip to the unit circle*

As an example [23] the reader may show that the function

- $w = \exp(z)$ maps the horizontal strip $S := \{-\frac{\pi}{2} < \mathrm{Im}(z) < \frac{\pi}{2}\}$ conformally onto the right half-plane $R := \{\mathrm{Re}(w) > 0\}$;
- $\zeta = h(w) = \iota\, w$ rotates the right half-plane R conformally to the upper half-plane $U = h(R)$ (or rotates the entire complex plane by $\pi/2$).
- $\zeta = (w-1)/(w+1)$ maps the right half-plane R conformally to the unit disk $D = \{|\zeta| < 1\}$, see **Fig. 6.40**.

It follows that

$$\zeta = \frac{\exp(z) - 1}{\exp(z) + 1} \qquad (6.111)$$

is a one-to one conformal map from the strip S to the unit disk $D = \{|z| < 1\}$. Moreover, the inverse $h^{-1}(z) = -\iota\, z$ maps U to $R = h^{-1}(U)$. Therefore, to map the upper half-plane to the unit disk, we compose these two maps and then get

$$\zeta = g(h^{-1}(z)) = \frac{-\iota\, z - 1}{-\iota\, z + 1} = \frac{\iota\, z + 1}{\iota\, z - 1} \quad \text{from } U \text{ to } D. \qquad (6.112)$$

Figure 6.40 summarizes these transformations.

6.5.2 *Examples of Schwarz-Christoffel Transformations*

In the ensuing paragraphs we shall present examples, which make use of the SCHWARZ-CHRISTOFFEL transformation in the presentation of mappings from the upper half space onto regions of more complex structure.

(a) Half-plane $y \geqslant 0$ **(b)** Semi-infinite strip
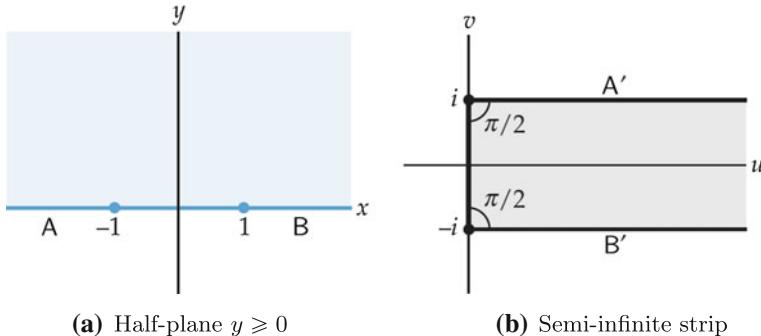
Fig. 6.41 Conformal map from the upper half-plane onto a semi-infinite strip $u > 0$, $-1 < v < 1$, $x > 0$. $f(z)$ is given by (6.114). © *Jones and Bartlett publishers, reproduced with changes, see* [27]

(a) Semi-infinite strip.
We refer to [27] and **Fig. 6.41**. The polygonal region defined by $u \geqslant 0$, $-1 \leqslant v \leqslant 1$ has vertices at $w = \pm \iota$ with internal angles $\alpha_1 = \alpha_2 = \pi/2$. Thus, formula (6.103) applies with $x_1 = -1$, $x_2 = 1$, yielding

$$f'(z) = A(z+1)^{-1/2}(z-1)^{-1/2} = \frac{A}{(z^2-1)^{1/2}}. \tag{6.113}$$

In (6.113), for $(z^2 - 1)^{1/2}$ the principal value is understood, because for both $(z+1)^{1/2}$ and $(z-1)^{1/2}$ the principal values are used. We can further write

$$(z^2 - 1)^{1/2} = \left((-1)(1 - z^2) \right)^{1/2} = (-1)^{1/2}(1 - z^2)^{1/2} = \iota(1 - z^2)^{1/2},$$

since the principal value of $(-1)^{1/2}$ is $+\iota$. Therefore

$$f'(z) = \frac{A}{\iota} \frac{1}{(1 - z^2)^{1/2}} = -A \iota \frac{1}{(1 - z^2)^{1/2}}$$

$$\longrightarrow f(z) = -A \iota \underbrace{\int_0^z \frac{d\tilde{z}}{(1 - \tilde{z}^2)^{1/2}}}_{\arcsin(z)} + B = -A \iota \arcsin(z) + B.$$

Choosing $f(-1) = -\iota$ and $f(1) = \iota$ fixes the constants A and B, according to

$$\left. \begin{array}{l} +A \iota \dfrac{\pi}{2} + B = -\iota \\[2mm] -A \iota \dfrac{\pi}{2} + B = +\iota \end{array} \right\} \quad \longrightarrow \quad A = -\dfrac{2}{\pi}, \quad B = 0.$$

(a) Half-plane $y \geqslant 0$ **(b)** Polygonal region
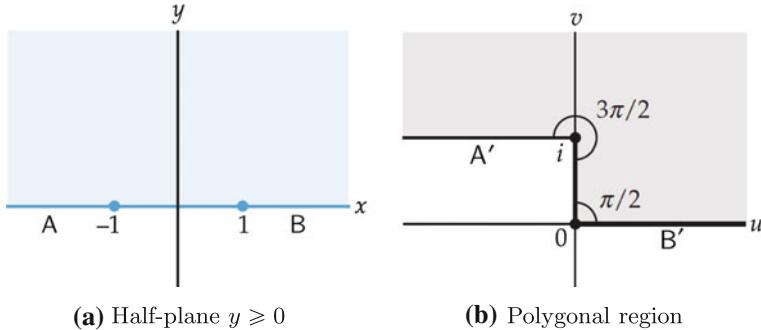
Fig. 6.42 Conformal map from the upper half-plane (**a**) onto the 'down-stepped' upper half plane (**b**) © *Jones and Bartlett publishers, reproduced with changes, see* [27]

So,

$$f(z) = \iota \frac{2}{\pi} \arcsin(z). \tag{6.114}$$

(b) Construction of a conformal map from the upper half-plane onto a 'down-stepped' upper half-plane.

According to the SCHWARZ-CHRISTOFFEL formulae (6.103) and (6.110) and **Fig. 6.42** this polygonal region has internal angles $\alpha_1 = 3\pi/2$ and $\alpha_2 = \pi/2$; moreover, we wish to have the points $x_1 = -1$ and $x_2 = 1$ being mapped to $w_1 = \iota$ and $w_2 = 0$. Thus,

$$f'(z) = A(z+1)^{1/2}(z-1)^{-1/2} = A\frac{z+1}{\sqrt{z^2-1}}$$

$$= A\left\{ \frac{z}{(z^2-1)^{1/2}} + \frac{1}{(z^2-1)^{1/2}} \right\}$$

$$\longrightarrow f(z) = A\left\{ \underbrace{\int_1^z \frac{\tilde{z}\,d\tilde{z}}{\sqrt{\tilde{z}^2-1}}}_{\sqrt{z^2-1}} + \underbrace{\int_1^z \frac{d\tilde{z}}{\sqrt{\tilde{z}^2-1}}}_{\text{areacosh}(z)} \right\} + B$$

$$= A\left\{ \sqrt{z^2-1} + \text{areacosh}(z) \right\} + B.$$
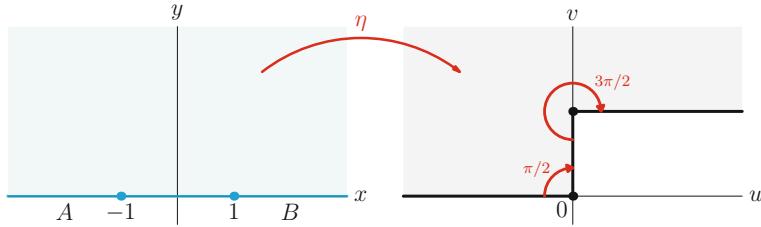
Fig. 6.43 Conformal map from the upper half-plane onto the 'up-stepped' upper half-plane

The[10] lower limit '1' in the integral of this formula is chosen for convenience since
the curly bracket will be singular when $z = 1$. Other choices will lead to different
values for B. The constants A and B will be fixed by the conditions that $f(-1) = \iota$
and $f(0) = 0$. This yields

$$\left.\begin{array}{l} A\,\text{areacosh}(-1) + B = A\,\pi\iota + B = \iota \\ A\,\text{areacosh}(+1) + B = \qquad\quad B = 0 \end{array}\right\} \quad \longrightarrow \quad A = \frac{1}{\pi}, \quad B = 0,$$

so that

$$f(z) = \frac{1}{\pi}\left\{\sqrt{z^2 - 1} + \text{areacosh}(z)\right\}. \tag{6.115}$$

The line segments A and B are mapped onto A′ and B′, respectively.

**(c) Construction of a conformal map from the upper half-plane to a half-plane
with 'rising step boundary', see Fig. 6.43.**
With the internal angles $\alpha_1 = \pi/2, \alpha_2 = 3\pi/2$ and $x_1 = -1, x_2 = 1$ formula (6.103)
takes the form

$$f'(z) = A(z+1)^{-1/2}(z-1)^{1/2} = A\,\frac{z-1}{\sqrt{z^2-1}}$$

$$= A\left\{\frac{z}{(z^2-1)^{1/2}} - \frac{1}{(z^2-1)^{1/2}}\right\}$$

$$\longrightarrow f(z) = A\left\{\sqrt{z^2-1} - \text{areacosh}(z)\right\} + B.$$

---

[10] Notations for inverse hyperbolic functions are not unique; on the American continent one generally
writes $\cosh^{-1}(x)$, $\sinh^{-1}(x)$, etc., whilst in Europe the corresponding denotations [since the late
20th century] are $\text{arccosh}(x)$, $\text{arcsinh}(x)$ etc., even though $\text{areacosh}(x)$, $\text{areasinh}(x)$ etc., have been
in use already much earlier. Yet alternative denotations are $\text{Ch}(x)$, $\text{Sh}(x)$ and $\text{Ach}(x)$, $\text{Ash}(x)$
for their inverses. We shall avoid $\cosh^{-1}$, $\sinh^{-1}$, in order not to confuse these with $1/\cosh(x)$,
$1/\sinh(x)$.

(a) Half-plane $y \geqslant 0$ **(b)** Equilateral triangle
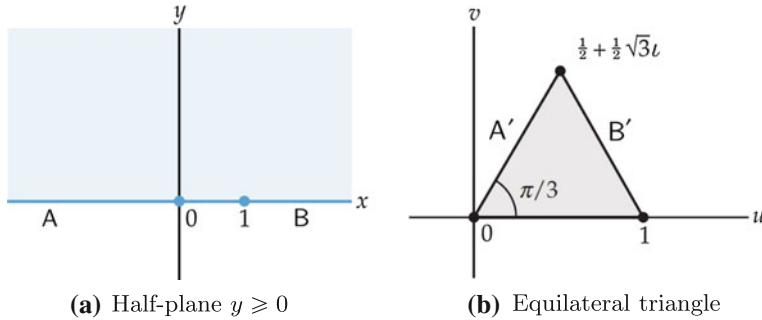
Fig. 6.44 Conformal map from the upper half-plane **(a)** onto the interior of an equilateral triangle **(b)** © *Jones and Bartlett publishers, reproduced with changes, see* [27]

The constants A and B are determined by requesting that $f(-1) = 0$ and $f(1) = \iota$. This yields

$$\left. \begin{array}{l} -A\,\mathrm{areacosh}(-1) + B = -A\,\pi\iota + B = 0 \\ -A\,\mathrm{areacosh}(+1) + B = \qquad\qquad B = \iota \end{array} \right\} \quad \longrightarrow \quad A = \frac{1}{\pi}, \quad B = \iota,$$

so that

$$f(z) = \frac{1}{\pi} \left\{ \sqrt{z^2 - 1} - \mathrm{areacosh}(z) \right\} + \iota. \tag{6.116}$$

(d) Equilateral triangle.
Next we construct the SCHWARZ-CHRISTOFFEL transformation for the conformal mapping of the upper half-plane onto the polygonal region bounded by the equilateral triangle with the vertices $w_1 = 0$, $w_2 = 1$ and $w_3 = \frac{1}{2}(1 + \sqrt{3}\,\iota)$, **Fig. 6.44**.
   A conformal mapping of the SCHWARZ-CHRISTOFFEL type is obtained for this triangle by restricting the number n in the counting index of (6.109) to $n = 2$. With the internal angles of the triangle being $\alpha_1 = \alpha_2 = \alpha_3 = \pi/3$ and by choosing $x_1 = 0$, $x_2 = 1$, (6.109) takes the form

$$f'(z) = A\,z^{-2/3}(z-1)^{-2/3}, \tag{6.117}$$

from which we conclude

$$f(z) = A \int_0^z \frac{d\tilde{z}}{\tilde{z}^{2/3}\,(\tilde{z}-1)^{2/3}} + B,$$

where A and B are again complex constants. The requirement $f(0) = 0$ implies $B = 0$. Then, from $f(1) = 1$ one gets

(a)

(b)
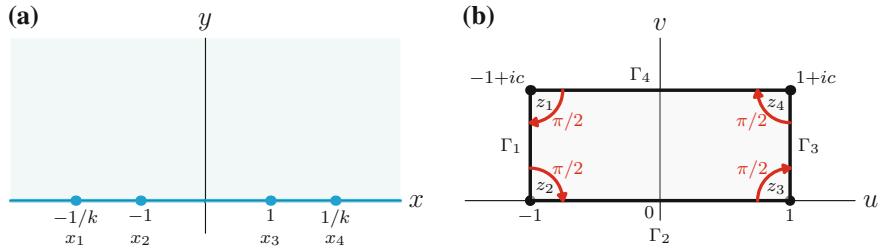
Fig. 6.45 Conformal mapping from a rectangle to the upper half-plane *This maps the 4 corner points* (**b**) *symmetrically to the points shown in* (**a**). *The 4 interior angles are all equal to* $\alpha_j = \pi/2$, $j = 1, 2, 3, 4$

$$f(1) = A \underbrace{\int_0^1 \frac{d\tilde{z}}{\tilde{z}^{2/3}(\tilde{z}-1)^{2/3}}}_{=:\Gamma} = 1 \quad \longrightarrow \quad A = \frac{1}{\Gamma}.$$

Therefore,

$$f(z) = \frac{1}{\Gamma} \int_0^z \frac{d\tilde{z}}{\tilde{z}^{2/3}(\tilde{z}-1)^{2/3}}. \tag{6.118}$$

This result cannot be expressed in terms of elementary functions, it must be evaluated numerically.

(e) Rectangle.
Find a conformal transformation that maps the interior of the rectangle $\{|x| < 1, 0 < y < c, c > 0\}$ onto the half-plane $\text{Im}(\zeta) > 0$, **Fig. 6.45**. This rectangle has the vertices at $z = \pm 1$ and $z = \pm 1 + \iota c$, [11].

The formula (6.110) is applicable with $n = 4$, but only three of the four points $x_1, ..., x_4$ are freely assignable. Instead we explore alternatively the symmetry and then write/choose

$$\begin{array}{llll} \zeta_1 = -1 + \iota c, & \zeta_2 = -1, & \zeta_3 = +1, & \zeta_4 = 1 + \iota c, \\ x_1 = -1/k, & x_2 = -1, & x_3 = +1, & x_4 = 1/k, \end{array} \tag{6.119}$$

where $k > 0$ is a real constant to be determined. The symmetry of the position of the rectangle in the ζ-plane suggests to map the origin of the z-plane to the origin of the ζ-plane so that in formula (6.110) we must select $B = 0$ and $z_0 = 0$. Since the interior angles are all $\alpha_i = \pi/2$, $i = 1, ..., 4$, we, thus have

$$\zeta = f(z) = A' \int_0^z \frac{d\tilde{z}}{\sqrt{(\tilde{z} - 1)(\tilde{z} + 1)(\tilde{z} - 1/k)(\tilde{z} + 1/k)}}$$

$$= A' \int_0^z \frac{d\tilde{z}}{\sqrt{(\tilde{z}^2 - 1)(\tilde{z}^2 - 1/k^2)}}$$

$$= A \int_0^z \frac{d\tilde{z}}{\sqrt{(1 - \tilde{z}^2)(1 - k^2\tilde{z}^2)}}, \quad A = k A',$$

$$= A E(k, z), \tag{6.120}$$

in which A is a new constant to be determined, and the appropriate branch of the multi-valued integrand must be chosen so that for $\text{Im}(z) > 0$

$$0 < \arg(z - x_i) < \pi, \quad i = 1, ..., 4. \tag{6.121}$$

The conformal transformation from the upper half z-plane to the rectangle of Fig. 6.45b is therefore expressible in terms of the *standard elliptic integral $E(k, z)$ of the first kind* [1], subject to the branch consistent with (6.121) and to the determination of A and k.

These constants are evaluated by requiring that the vertices of the rectangle in Fig. 6.45 take the desired positions in the ζ-plane. We wish to map the point x_3 (in the z-plane) to the point $\xi = 1$ in the ζ-plane: $f(1) = 1$. When integrating along the x-axis, (6.120) yields

$$A E(k, 1) = 1 \quad \longrightarrow \quad A K(k) = 1, \tag{6.122}$$

in which $K(k) := E(k, 1)$ is the *complete elliptic integral of the first kind* [1].

As second condition the requirement $f(1/k) = 1 + \iota c$, paired with an integration of (6.120) along the x-axis from $x = 0$ to $x = 1/k$, yields

$$1 + \iota c = A \int_0^{1/k} (\cdots) dx = A \underbrace{\int_0^1 (\cdots) dx}_{f(1)} + A \underbrace{\int_1^{1/k} (\cdots) dx}_{:=K_1(k)}$$

$$= f(1) + A K_1(k). \tag{6.123}$$

Along the segment $1 < x < 1/k$, $\sqrt{1 - k^2x^2}$ is real and $\sqrt{1 - x^2}$ is pure imaginary. Consequently, $K_1(k)$ (the second term on the right-hand side) is imaginary, implying that

$$c = A K_1(k). \tag{6.124}$$

Relations (6.122) and (6.123) determine the real constants A and $K(k)$. This fixes the transformation $\zeta = f(z)$ that maps the half-plane $\text{Im}(z) > 0$ onto the interior of the rectangle. The inverse transformation of (6.120) is given by

$$z = \text{sn}\left(\frac{\zeta}{A}, k\right),$$

where $\text{sn}(t, k)$ is the JACOBI an elliptic function, see E.T. WHITTAKER (1873–1956) and G.N. WATSON (1886–1965) [26] 'Modern Analysis', Chap. 22 or M. ABRAMOWITZ and I. STEGUN [1].

(f) Half-plane with a horizontal line deleted.
The SCHWARZ-CHRISTOFFEL transformation can also be used to construct a conformal mapping from the upper half-plane onto a half-plane with the horizontal half-line $\{v = \pi, -\infty < u \leqslant 0\}$ deleted, as shown in **Fig. 6.46**c. This example is given in G. ZILL and P.D. SHANAHAN's book [27], which we follow here. The situation in Fig. 6.46c can be regarded as the limit geometry of the configuration in Fig. 6.46b with polygonal lower boundary, when the boundary point u_0 approaches the far left

(a) Half-plane $y \geqslant 0$ **(b)** Polygonal region

(c) Limit of polygonal regions
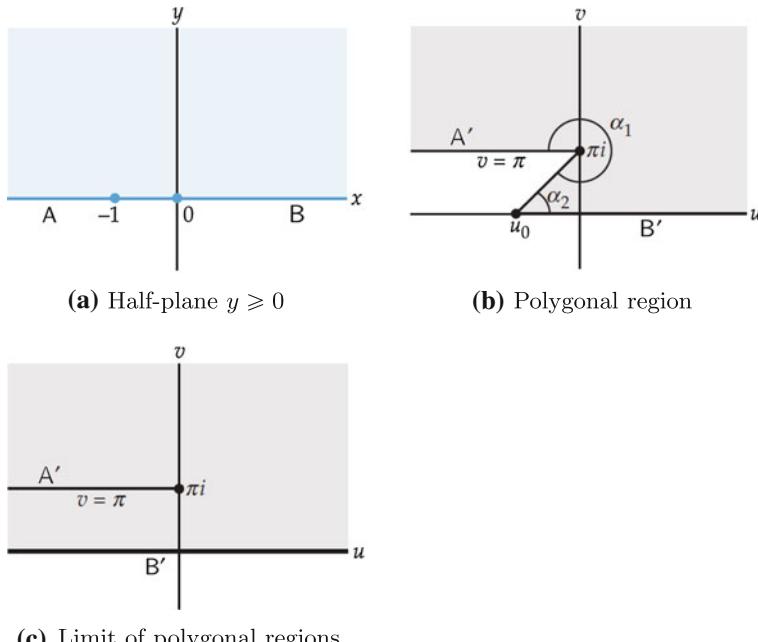
Fig. 6.46 Conformal map from the upper half plane, (**a**), to the half-plane with the line $\{v = \pi, -\infty < u \leqslant 0\}$ deleted, (**c**) *Panel* **a** *shows the half-plane* $y \geqslant 0$, *panel* **b** *shows the half plane with backward 'down-step', whilst panel* **c** *shows the limit configuration of panel (b), if the point* u_0 *has been shifted to the left.* $u_0 \rightarrow -\infty$, [27]. ©*Jones and Bartlett publishers, reproduced with changes*

on the u-axis: $u_0 \to -\infty$. The domain, consisting of the upper half-plane minus the line $\{v = \pi, -\infty < u < \infty\}$ will be denoted as D.

Application of the SCHWARZ-CHRISTOFFEL transformation (6.109) to this example with the vertices of the polygonal region at $w_1 = \iota\pi$ and $w_2 = u_0$, respectively, and the corresponding interior angles $\alpha_1 \to 2\pi$ and $\alpha_2 \to 0$. Thus, the derivative of $\tilde{f}$ in (6.109) is given by

$$\tilde{f}' = A(z+1)^{(\alpha_1/\pi)-1} z^{(\alpha_2/\pi)-1} \longrightarrow A(z+1)\frac{1}{z} = A\left(1 + \frac{1}{z}\right). \qquad (6.125)$$

Thus, the desired conformal mapping $\tilde{f}$, obtained by integration of (6.125) is given by

$$\tilde{f}(z) = A(z + \ln(z)) + B, \qquad (6.126)$$

in which A and B are complex constants.

"In order to determine the appropriate values of the constants A and B, consider the function $g(z) = z + \ln(z)$ on the upper half-plane $y \geqslant 0$. The function g has a point of discontinuity at $z = 0$, thus, it is advisable to separately consider the boundary half-lines $\{y = 0, -\infty < x < 0\}$ and $\{y = 0, 0 < x < \infty\}$ of the half-plane $y \geqslant 0$, called subsequently the left and right half-lines, respectively. If $z = x + 0^+\iota$ is on the left half-line, then $\arg(z) = \pi$ and so, $g(z) = x + \ln(|x|\exp(\iota\pi)) = x + \ln|x| + \iota\pi$. Moreover, the function $x + \ln|x|$ takes for $x < 0$ all values from $-\infty$ to -1. On the other hand, if $z = x + 0^+\iota$ is on the right half-line, then $\arg(z) = 0$ and so, $g(z) = x + \ln|x|$ takes on values from $-\infty$ to ∞. Therefore, the image of the positive x-axis is the whole u-axis (in the w-plane). It follows that the image of the half-plane $y \geqslant 0$ under $g(z) = z + \ln(z)$ is the region defined by $v \geqslant 0$, with the horizontal half-line $\{v = \pi, -\infty < u \leqslant -1\}$ deleted. To include the 'missing' interval $-1 \leqslant u \leqslant 0$, $\tilde{f}$ in (6.126) must be shifted by a translation of unity: $f = \tilde{f} + 1$", [27],

$$f(z) = z + \ln(z) + 1. \qquad (6.127)$$

(g) Inviscid density preserving flow around and past objects.
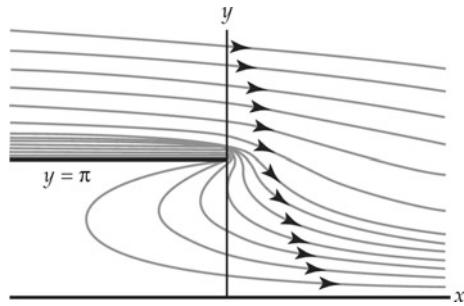
(i) Flow from an underwater cantilever plate:
Consider horizontal 2D parallel flow of water as an ideal fluid above a cantilever plate in a half-space as shown in panel (c) of Fig. 6.46. If we replace in (6.127) the symbol z by the symbol w, then one obtains the conformal mapping

$$z = \tilde{\phi}_1(w) = w + \ln(w) + 1 \qquad (6.128)$$

from the upper half-plane $v > 0$ onto the domain $\mathcal{D}$ of Fig. 6.46c. If we envisage $\tilde{\phi} = Uz$ as the complex velocity potential (with $U = 1$) of the parallel flow in the upper w-half-plane, then the streamlines are given by the horizontal lines $v = c$, where c is a constant. In $\mathcal{D}$ of the upper (x, y)-half-plane the corresponding streamlines are given by $w(t) = t + \iota c$, $-\infty < t < \infty$, or according to (6.128),

$$z(t) = x(t) + \iota\, y(z) = w(t) + \ln |t + \iota\, c| + \iota. \tag{6.129}$$

For any given c this is the parameter representation of the streamlines, if t varies
from $-\infty$ to $+\infty$, viz.,

$$x(t) = t + \tfrac{1}{2} \ln \left(t^2 + c^2\right) + 1, \quad y(t) = c + \arg(t + \iota\, c). \tag{6.130}$$

ZILL and SHANAHAN [27] plotted the streamlines as shown in **Fig. 6.47** using *Mathematica*. This flow obviously corresponds to the parallel constant flow above the
cantilever plate to the left, whereas below this plate the fluid is at rest at the far left.

ZILL and SHANAHAN [27] emphasize the fact that the stream function ψ, on which
the streamlines of Fig. 6.47 are based, is a harmonic function—as it must be for all
conformal mappings—but this function need not be unique, i.e. other potentials may
exist, which are conformal mappings of the upper half plane, $v > 0$ onto $\mathcal{D}$. The
authors demonstrate this by the following example.

(ii) Parallel exit flow of water from a bottom duct into a still fluid half-space:
The decisive step is the recognition that also

$$z = \tilde{\tilde{\phi}}_2(w) = w + \exp(w) + 1 \tag{6.131}$$

is a one-to-one conformal mapping of the upper half-plane $v > 0$ onto the domain
$\mathcal{D}$ shown in Fig. 6.46c. The reader may prove this by him/herself. The streamlines
for this flow are parameterized by writing $z = t + \iota c, \forall t \in (-\infty, +\infty)$
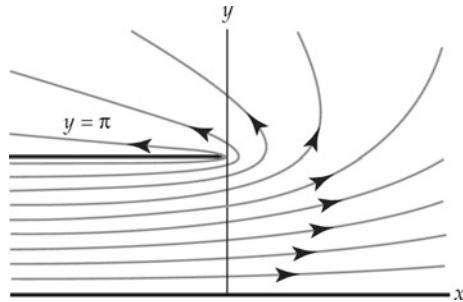
$$z(t) = \tilde{\tilde{\phi}}_2(t + \iota\, c) = t + \iota\, c + \exp(t + \iota\, c) + 1,$$

or

$$x(t) = t + \exp(t)\cos(c) + 1, \quad y(t) = c + \exp(t)\sin(c), \quad -\infty < t < \infty. \tag{6.132}$$

Some streamlines to this example are shown in **Fig. 6.48**. They corroborate the
anticipated title of this flow.

(iii) Plane parallel potential flow of a fluid down or up a finite step:
In the formulae (6.115) and (6.116) one-to-one conformal maps were presented,
which map the upper half-plane onto down-stepped or up-stepped upper half planes
as displayed in Figs. 6.42 and 6.43:

$$z = \tilde{\phi}_3(w) = \frac{1}{\pi}\left\{\sqrt{w^2-1} + \text{areacosh}(w)\right\},$$

$$z = \tilde{\phi}_4(w) = \frac{1}{\pi}\left\{\sqrt{w^2-1} - \text{areacosh}(w)\right\} + \iota. \tag{6.133}$$

$\tilde{\phi}_3$ is the complex potential to the 'parallel' flow in the 'down-stepped' upper-half-
plane, and streamlines for this flow are given by selecting $w = t + \iota c$ in $(6.133)_1$
and varying $t \in (-\infty, \infty)$ for parametrized values of c. This yields

$$z(t) = \frac{1}{\pi}\left\{\sqrt{(t+\iota c)^2-1} + \text{areacosh}(t+\iota c)\right\}. \tag{6.134}$$

Similarly, for the 'upstepped' case, given by $(6.133)_2$

$$z(t) = \frac{1}{\pi}\left\{\sqrt{(t+\iota c)^2-1} - \text{areacosh}(t+\iota c)\right\} + \iota. \tag{6.135}$$

Both sets of streamlines are displayed in **Fig. 6.49**.

With this example we stop here, but would like to mention that the technique of
conformal mapping is a very efficient and popular method of two-dimensional analy-
sis to solve boundary value problems of potential theory in many branches of the
applied sciences. The cited literature provides a guide to find a wealth of further ex-
amples. A particularly didactic text is [27], and with applications in two-dimensional
fluid mechanics JOSEPH H. SPURK's and NURI AKSEL's 'Fluid Mechanics' Chap. 10
[25].

(a) Flow down a step   **(b)** Flow up a step
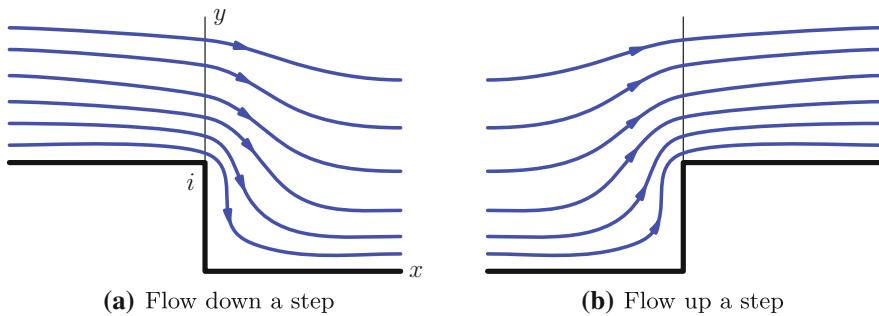
Fig. 6.49 Streamlines for 'parallel' potential flow down (**a**) and up (**b**) a step

Appendix 6.A Some Facts on Complex Functions

6.A.1 Cauchy's Theorem

Suppose that a function f is analytic in a simply connected domain $\mathcal{D}$ and f' is continuous in $\mathcal{D}$. Then, for every simple closed contour $\mathcal{C}$ in $\mathcal{D}$ we have

$$\oint_{\mathcal{C}} f(z)\mathrm{d}z = 0. \tag{6.136}$$

Proof The proof of this theorem follows from an immediate application of GREEN's theorem. To this end, let $P(x, y)$ and $Q(x, y)$ be real valued functions, which, along with their first order partial derivatives, are continuous on a domain that contains $\mathcal{C}$ and $\mathcal{R}$, then

$$\oint_{\mathcal{C}} (P\mathrm{d}x + Q\mathrm{d}y) = \iint_{\mathcal{R}} \left(\frac{\partial Q}{\partial x} + \frac{\partial P}{\partial y}\right)\mathrm{d}A. \tag{6.137}$$

Now, let $f(z) = u + \iota v$ and build
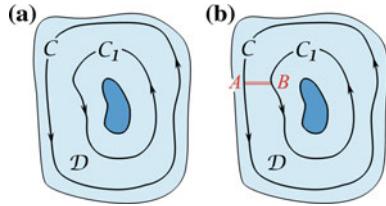
$$\oint_{\mathcal{C}} f(z)\mathrm{d}z = \oint_{\mathcal{C}} [u(x, y)\mathrm{d}x - v(x, y)\mathrm{d}y] + \iota \oint_{\mathcal{C}} [v(x, y)\mathrm{d}x + u(x, y)\mathrm{d}y]$$
$$= \iint_{\mathcal{R}} \left(-\frac{\partial v}{\partial x} - \frac{\partial u}{\partial y}\right)\mathrm{d}A + \iota \iint_{\mathcal{R}} \left(\frac{\partial u}{\partial x} - \frac{\partial v}{\partial y}\right)\mathrm{d}A, \tag{6.138}$$

in which it is quite clear how P and Q need to be identified with u and v to obtain the second line of (6.138). Employing next the CAUCHY-RIEMANN equations

$$\frac{\partial u}{\partial x} = \frac{\partial v}{\partial y}, \quad \text{and} \quad \frac{\partial u}{\partial y} = -\frac{\partial v}{\partial x}$$

in (6.138) completes the proof.   ∎

Fig. 6.50 a Two simple
closed curves $\mathcal{C}$ and $\mathcal{C}_1$ in a
doubly connected domain $\mathcal{D}$.
b By the cut AB the domain
consisting of $\mathcal{C}$ and $\mathcal{C}_1$ plus
the interior of $\mathcal{C}$ and the
exterior of $\mathcal{C}_1$ is simply
connected

An immediate consequence of CAUCHY's theorem states that in a doubly con-
nected domain as shown in **Fig. 6.50**a the curve $\mathcal{C}$, along which the CAUCHY integral
is performed, can be deformed to a second simply connected closed curve [here $\mathcal{C}_1$]
with the result that the integral

$$\oint_{\mathcal{C}} f(z)\mathrm{d}z - \oint_{\mathcal{C}_1} f(z)\mathrm{d}z = 0 \tag{6.139}$$

has still the value zero, Fig. 6.50a.

Proof Assume that f is analytic on each simple contour and at each point interior to
$\mathcal{C}$ and exterior to $\mathcal{C}_1$. By introducing the cross cut AB (Fig. 6.50b) a simply connected
region is generated and CAUCHY's integral takes the form

$$\oint_{\mathcal{C}} f(z)\mathrm{d}z + \int_{AB} f(z)\mathrm{d}z - \oint_{\mathcal{C}_1} f(z)\mathrm{d}z - \int_{AB} f(z)\mathrm{d}z = 0,$$

implying

$$\oint_{\mathcal{C}} f(z)\mathrm{d}z = \oint_{\mathcal{C}_1} f(z)\mathrm{d}z. \tag{6.140}$$

∎

An obvious generalization of this situation is the CAUCHY theorem for multiply
connected domains, as shown in **Fig. 6.51**. Suppose that $\mathcal{C}$, $\mathcal{C}_1$, $\mathcal{C}_2$, ..., $\mathcal{C}_n$ are simple
closed curves, all with positive orientation and such that $\mathcal{C}_1$, ..., $\mathcal{C}_n$ are interior to $\mathcal{C}$,
but the region's interior to each $\mathcal{C}_k$, $k = 1, ..., n$ have no points in common. If f is
analytic on each contour and at each point in $\mathcal{C}$ but exterior to all $\mathcal{C}_k$, $k = 1, ..., n$,
then

$$\oint_{\mathcal{C}} f(z)\mathrm{d}z = \sum_{k=1}^{n} \oint_{\mathcal{C}_k} f(z)\mathrm{d}z \quad k = 1, ..., n. \tag{6.141}$$

The proof is a simple extension to the proof of (6.139) and is left to the reader.

Fig. 6.51 a Contour
integration in a multiply
connected domain $\mathcal{D}$.
b Domain $\mathcal{D}$ made simply
connected with cuts
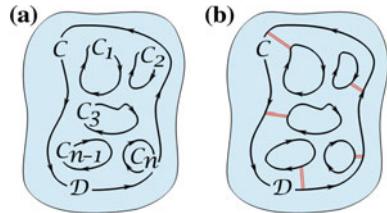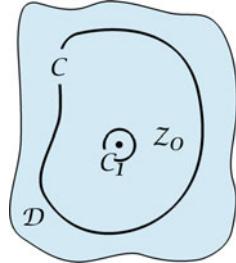
Fig. 6.52 Sketch for proof
of Cauchy's integral formula

6.A.2 Cauchy's Integral Formula

Suppose that f is analytic in a simply connected domain $\mathcal{D}$ and $\mathcal{C}$ any simple closed
contour lying entirely within $\mathcal{D}$. Then for any point z_0 within $\mathcal{C}$,

$$f(z) = \frac{1}{2\pi\iota} \oint_{\mathcal{C}} \frac{f(z)}{z - z_0} dz. \tag{6.142}$$

Proof With the above prerequisite, let $\mathcal{C}_1$ be a circle centered at z_0 with radius
sufficiently small, so that $\mathcal{C}_1$ lies in the interior of $\mathcal{C}$, see **Fig. 6.52**. Thus, we have

$$\oint_{\mathcal{C}} \frac{f(z)}{z - z_0} dz = \oint_{\mathcal{C}_1} \frac{f(z)}{z - z_0} dz = \oint_{\mathcal{C}_1} \frac{f(z_0) - f(z_0) + f(z)}{z - z_0} dz$$

$$= f(z_0) \underbrace{\oint_{\mathcal{C}_1} \frac{1}{z - z_0} dz}_{(1) = 2\pi\iota} + \underbrace{\oint_{\mathcal{C}_1} \frac{f(z) - f(z_0)}{z - z_0} dz}_{(2) = 0}$$

$$= 2\pi\iota f(z_0). \tag{6.143}$$

Here,

(1) $= \oint_{\mathcal{C}_1} \frac{dz}{z - z_0} = \oint_{\mathcal{C}_1} \frac{\iota\varepsilon \exp(\iota s)}{\varepsilon \exp(\iota s)} ds = \iota \oint_{\mathcal{C}_1} ds = 2\pi\iota,$
   where $(z - z_0) = \varepsilon \exp(\iota s)$.
(2) Since f is continuous at z_0, we know that for any arbitrarily small $\varepsilon > 0$ there
   exists a $\delta(\varepsilon) > 0$, such that $|f(z) - f(z_0)| < \varepsilon$, whenever $|z - z_0| < \delta$. Thus,

if $|z - z_0| = \alpha\delta$, $0 < \alpha < 1$ (for instance $\alpha = \frac{1}{2}$), then

$$\left| \oint_{\mathcal{C}_1} \frac{f(z) - f(z_0)}{z - z_0} dz \right| \leqslant \frac{\varepsilon}{\alpha\delta} 2\pi\alpha\delta = 2\pi\varepsilon \overset{\varepsilon \to 0}{\longrightarrow} 0.$$

It follows: (2) = 0.

Thus, from (6.143) we get

$$f(z_0) = \frac{1}{2\pi\iota} \oint_{\mathcal{C}} \frac{f(z)}{z - z_0} dz. \tag{6.144}$$

If f is analytic at all points within and on a simple closed contour $\mathcal{C}$, and z_0 is a point in the interior to $\mathcal{C}$, then the representation (6.144) applies. ∎

A second CAUCHY formula reads as follows: Suppose that f is analytic in a simply connected domain $\mathcal{D}$, and $\mathcal{C}$ is any simple closed contour lying entirely within $\mathcal{D}$. Then for any point z_0 within $\mathcal{C}$,

$$f^{(n)}(z_0) = \frac{n!}{2\pi\iota} \oint_{\mathcal{C}} \frac{f(z)}{(z - z_0)^{n+1}} dz, \tag{6.145}$$

specifically,

$$f(z_0) = \frac{1}{2\pi\iota} \oint_{\mathcal{C}} \frac{f(z)}{(z - z_0)} dz,$$
$$f'(z_0) = \frac{1}{2\pi\iota} \oint_{\mathcal{C}} \frac{f(z)}{(z - z_0)^2} dz,$$
$$f''(z_0) = \frac{2}{2\pi\iota} \oint_{\mathcal{C}} \frac{f(z)}{(z - z_0)^3} dz.$$
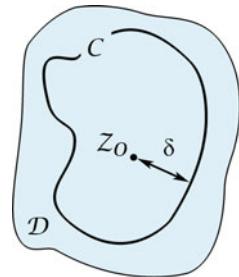
A sketch of the proof for $n = 1$ follows below; that for arbitrary $n = 2, 3, ...$ can be completed by induction.

Proof for $n = 1$: We begin with the definition of the derivative and write

$$f'(z_0) = \lim_{\Delta z \to 0} \frac{f(z_0 + \Delta z) - f(z_0)}{\Delta z}$$
$$\overset{(1)}{=} \lim_{\Delta z \to 0} \frac{1}{2\pi\iota\Delta z} \left\{ \oint_{\mathcal{C}} \frac{f(z)dz}{z - (z_0 + \Delta z)} - \oint_{\mathcal{C}} \frac{f(z)dz}{z - z_0} \right\}$$
$$= \lim_{\Delta z \to 0} \frac{1}{2\pi\iota} \left\{ \oint_{\mathcal{C}} \frac{f(z_0)dz}{(z - (z_0 + \Delta z))(z - z_0)} \right\}. \tag{6.146}$$

In '$\overset{(1)}{=}$' the two function values in the numerator of the first line have been expressed by CAUCHY's integral (6.144). Because f is analytic on $\mathcal{C}$, a finite maximum M exists

Fig. 6.53 A simple closed
contour $\mathcal{C}$ with a point z_0 in
the interior to $\mathcal{C}$. δ be the
shortest distance of z_0
between inside $\mathcal{C}$ and point z
on $\mathcal{C}$

on $\mathcal{C}$ such that $|f(z)| \leqslant M$ for all points on $\mathcal{C}$. Next, let δ be the shortest distance
of z_0 between inside $\mathcal{C}$ and point z on $\mathcal{C}$, see **Fig. 6.53**. Thus, for all points on $\mathcal{C}$ we
have

$$|z - z_0| \geqslant \delta \quad \text{and therefore} \quad \frac{1}{|(z - z_0)|^2} < \frac{1}{\delta^2}.$$

Furthermore, if we choose $|\Delta z| < \alpha\delta, 0 < \alpha < 1$, then

$$|z - z_0 - \Delta z| \geqslant ||z - z_0| - |\Delta z|| \geqslant \delta - |\Delta z| \geqslant (1 - \alpha)\delta.$$

Now, we evaluate the expression

$$\left| \oint_{\mathcal{C}} \frac{f(z)\mathrm{d}z}{(z - z_0)^2} - \oint_{\mathcal{C}} \frac{f(z)\mathrm{d}z}{(z - z_0 - \Delta z)(z - z_0)} \right|$$
$$= \left| \oint_{\mathcal{C}} \frac{-\Delta z\, f(z)\mathrm{d}z}{(z - z_0 - \Delta z)(z - z_0)^2} \right| \leqslant \frac{L\,M}{(1 - \alpha)\,\delta^3} |\Delta z| \overset{\Delta z \to 0}{\longrightarrow} 0, \quad (6.147)$$

in which L is the length of $\mathcal{C}$, and $L\,M$ is an upper bound of $\oint_{\mathcal{C}} f(z)\mathrm{d}z$. Therefore,
we have shown that

$$f'(z_0) = \lim_{\Delta z \to 0} = \frac{f(z_0 + \Delta z) - f(z)}{\Delta z} = \frac{1}{2\pi\iota} \oint_{\mathcal{C}} \frac{f(z)\mathrm{d}z}{(z - z_0)^2},$$
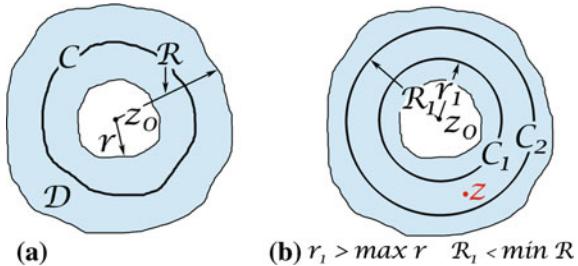
which agrees with (6.145)$_3$ for $n = 1$.   ∎

6.A.3 Laurent Series

LAURENT series are a generalization of power series and for these the so-called
LAURENT's theorem holds true.

Laurent's Theorem: If f is analytic within the annular domain $\mathcal{D}$ defined by $r <$
$|z - z_0| < R$, then f has the series representation

Fig. 6.54 a Contour for the
proof of LAURENT's theorem
b Two circles forming an
annulus containing the
contour $\mathcal{C}$

(a)

(b) $r_1 > max\ r \quad R_1 < min\ R$

$$f(z) = \sum_{k=-\infty}^{k=\infty} a_k(z - z_0)^k, \tag{6.148}$$

valid for $r < |z - z_0| < R$. The coefficients are given by

$$a_k = \frac{1}{2\pi\iota} \oint_{\mathcal{C}} \frac{f(s)\,ds}{(s - z_0)^{k+1}}\,ds, \quad k = 0, \pm 1, \pm 2, ..., \tag{6.149}$$

where $\mathcal{C}$ is a simple closed curve that lies entirely within $\mathcal{D}$ and has z_0 in its interior.

Proof With reference to **Fig. 6.54**, let $\mathcal{C}_1$ and $\mathcal{C}_2$ be concentric circles with center z_0 and radii r_1 and R_2, where $r < r_1 < R_2 < R$. Let, moreover, z be a fixed point in $\mathcal{D}$ that also satisfies the inequality $r_1 < |z - z_0| < R_2$. Then, obviously

$$f(z) = \frac{1}{2\pi\iota} \oint_{\mathcal{C}_2} \frac{f(s)}{s - z}\,ds - \frac{1}{2\pi\iota} \oint_{\mathcal{C}_1} \frac{f(s)}{s - z}\,ds, \tag{6.150}$$

in which

$$\frac{1}{2\pi\iota} \oint_{\mathcal{C}_2} \frac{f(s)}{s - z}\,ds = \sum_{k=0}^{\infty} a_k(z - z_0)^k, \tag{6.151}$$

where

$$a_k = \frac{1}{2\pi\iota} \oint_{\mathcal{C}_2} \frac{f(s)}{(s - z_0)^{k+1}}\,ds, \quad k = 0, 1, 2, ...$$

Now, we proceed as follows:

$$-\frac{1}{2\pi\iota} \oint_{\mathcal{C}_1} \frac{f(s)\,ds}{(s - z)} = \frac{1}{2\pi\iota} \oint_{\mathcal{C}_1} \frac{f(s)\,ds}{(z - z_0) - (s - z_0)}$$

$$= \frac{1}{2\pi\iota} \oint_{\mathcal{C}_1} \frac{f(s)}{(z - z_0)} \left\{ \frac{1}{1 - \frac{s - z_0}{z - z_0}} \right\} ds$$

$$= \frac{1}{2\pi\iota} \oint_{\mathcal{C}_1} \frac{f(s)}{(z-z_0)} \left\{ 1 + \left(\frac{s-z_0}{z-z_0}\right) + \left(\frac{s-z_0}{z-z_0}\right)^2 + \dots \right.$$

$$\left. + \left(\frac{s-z_0}{z-z_0}\right)^{n-1} + \frac{(s-z_0)^n}{(z-s)(z-z_0)^{n-1}} \right\} ds$$

$$= \sum_{k=1}^{n} \frac{a_{-k}}{(z-z_0)^k} + R_n(z),$$

where

$$a_{-k} = \frac{1}{2\pi\iota} \oint_{\mathcal{C}_1} \frac{f(s)}{(s-z)^{-k+1}} ds, \quad k = 1, 2, \dots, (n-1),$$

$$(6.152)$$

$$R_n(z) = \frac{1}{2\pi\iota(z-z_0)^n} \oint_{\mathcal{C}} \frac{f(s)(s-z_0)^n}{z-s} ds.$$

Now, let d be the distance from z to z_0, $|z - z_0| = d$, and let M be the maximum value of $|f(z)|$ on the contour $\mathcal{C}_1$. Then, with $|s - z_0| = r_1$, we obtain

$$|z - s| = |z - z_0 - (s - z_0)| \geqslant |z - z_0| - |s - z_0| = d - r_1.$$

Therefore,

$$|R_n(z)| = \left| \frac{1}{2\pi\iota(z-z_0)^n} \oint_{\mathcal{C}_1} \frac{f(s)(s-z_0)^n}{z-s} ds \right|$$

$$\leqslant \frac{1}{2\pi\, d^n} \frac{M r_1^n}{d-r_1} 2\pi\, r_1 = \frac{M\, r_1}{d-r_0} \left(\frac{r_1}{d}\right)^n.$$

Because $r_1 < d$, we obtain $\lim_{n\to\infty} |R_n(z)| \to 0$ as $n \to \infty$ and, consequently,
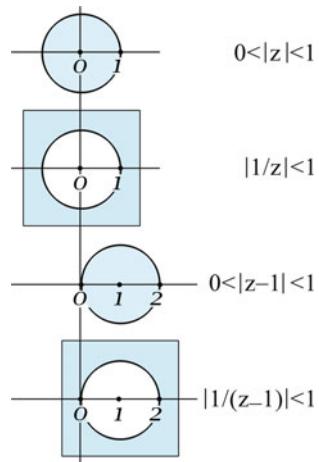
$$-\frac{1}{2\pi\iota} \oint_{\mathcal{C}_1} \frac{f(s)}{s-z} ds = \sum_{k=1}^{\infty} \frac{a_{-k}}{(z-z_0)^k},$$

in which the coefficients a_{-k} are given in (6.152). Combining all results (6.150)–(6.152) yields

$$f(z) = \sum_{k=-\infty}^{k=\infty} a_k (z-z_0)^k, \qquad (6.153)$$

$$a_k = \oint_{\mathcal{C}} \frac{f(z)}{(z-z_0)^{k+1}} dz, \quad k = 0, \pm 1, \pm 2, \dots,$$

where the contours have been replaced by any simple contour $\mathcal{C}$ in $\mathcal{D}$. ∎

Fig. 6.55 The function
$f(z)/(z-1)$ can (among
others) be expressed as the
LAURENT series valid in the
stated angular domains

$0<|z|<1$

$|1/z|<1$

$0<|z-1|<1$

$|1/(z-1)|<1$

For LAURENT series the following denotation is customary: The terms with neg-
ative k are called the *principal part* and those with positive k are called the *analytic
part*. As an example

$$f(z) = \frac{\sin z}{z^5} = \frac{1}{z^5}\left(z - \frac{z^3}{3!} + \frac{z^5}{5!} - \frac{z^7}{7!} + \cdots\right)$$

$$= \underbrace{\frac{1}{z^4} - \frac{1}{3! \, z^2} + \frac{1}{5!}}_{\text{principal part}} \underbrace{- \frac{z^2}{7!} + \frac{z^4}{9!} + \cdots}_{\text{analytic part}}.$$

Problem: Show that the function $f(z)/(z-1)$ can (among others) be expressed as
the following LAURENT series valid in the stated angular domains, which are also
shown graphically in **Fig. 6.55**,

- $f(z) = -\dfrac{1}{z} - 1 - z - z^2 - z^3 - \cdots, \quad 0 < |z| < 1.$
- $f(z) = \dfrac{1}{z^2} + \dfrac{1}{z^3} + \dfrac{1}{z^4} + \dfrac{1}{z^5} + \cdots, \quad |1/z| < 1.$
- $f(z) = -\dfrac{1}{z-1} - 1 + (z-1) - (z-1)^2 - (z-1)^3 \cdots, \quad 0 < |z-1| < 1.$
- $f(z) = \dfrac{1}{(z-1)^2} - \dfrac{1}{(z-1)^3} + \dfrac{1}{(z-1)^4} - \cdots, \quad \left|\dfrac{1}{z-1}\right| < 1.$

6.A.4 Zeros and Singularities

Going back to the representation (6.153) of LAURENT series, the following classification of isolated singular points is customary:

1. If the principal part of the LAURENT series vanishes, i. e., if all the coefficients $a_{-k}, k \geqslant 1$, vanish, then $z = z_0$ is called a *removable singularity*

   Ex: $\dfrac{\sin z}{z} = 1 - \dfrac{z^2}{3!} + \dfrac{z^4}{5!} - \dfrac{z^5}{6!} + ...,\quad |z| < \infty. \ \text{ for } z = 0, \ \dfrac{\sin z}{z} = 1.$

2. If the principal part contains a finite number of nonzero terms, then $z = z_0$ is called a *pole*. If $a_{-n} \neq 0$ for $n \geqslant 1$, then $z = z_0$ is called a *pole of order n*. For a pole of order '1', then the principal value contains exactly one term with coefficient $a_{-1} \neq 0$. For this case the pole is called *simple*.
   Ex: $f(z) = 1/[(z-1)^2(z-3)]$ possesses the LAURENT series

   $$f(z) = -\underbrace{\frac{1}{2(z-1)^2} - \frac{1}{4(z-1)}}_{\text{principal part}} - \frac{1}{8} - \frac{z-1}{16}...\quad \text{valid for } 0 \leqslant |z-1| < 2.$$

   Since $a_{-2} \neq 0$, we conclude that $z = 1$ is a pole of order 2.
   Ex: The function

   $$\frac{\sin z}{z^2} = \frac{1}{z} - \frac{z}{3!} + \frac{z^3}{5!}...\quad \text{for } 0 < |z| < \infty$$

   has a pole of order 1, because $a_{-1} = 1 \neq 0$.
3. If the principal part contains infinitely many nonzero terms, then $z = z_0$ is called an *essential singularity*.
   Ex: The function

   $$\exp\left(\frac{1}{z}\right) = 1 + \left(\frac{1}{z}\right) + \frac{1}{2!}\left(\frac{1}{z}\right)^2 + \frac{1}{3!}\left(\frac{1}{z}\right)^3 + ...$$

   possesses only the principal part and no analytic part.

A number z_0 is called a *zero* of the function f, if $f(z_0) = 0$. One says that an analytic function f has a *zero of order n* at $z = z_0$ if

$$f(z_0) = f'(z_0) = f''(z_0) = ... = f^{(n-1)}(z_0) = 0 \quad \text{but } f^{(n)}(z_0) \neq 0. \quad (6.154)$$

Ex:

1. An almost obvious fact, which the reader is asked to prove, is the following statement: A function f that is analytic in some disk $|z - z_0| < R$ has a zero of order n at $z = z_0$, if and only if f can be written as

$$f(z) = (z - z_0)^n \phi(z),$$

in which ϕ is analytic at $z = z_0$ and $\phi(z_0) \neq 0$.

2. The function $f(z) = z \sin^2 z$ has a zero of order 2 at $z = 0$ and can be written as

$$f(z) = z^2 \phi(z), \quad \phi(z) = 1 - \frac{z^4}{3!} - \frac{z^8}{5!} + \ldots .$$

3. If the function $f(z) = g(z)/h(z)$ and $g(z)$ and $h(z)$ are analytic at $z = z_0$ and h has a zero of order n at $z = z_0$ and $g(z_0) \neq 0$, then the function $f(z)$ has a pole of order n at $z = z_0$. In this case

$$f(z) = \frac{g(z)}{\phi(z)(z - z_0)^n}. \qquad (6.155)$$

6.A.5 Residues and Residue Theorem

Given a complex function f, having an isolated singularity at $z = z_0$, then f has the LAURENT series representation

$$f(z) = \sum_{k=-1}^{k=\infty} a_k (z - z_0)^k = \ldots + \frac{a_{-2}}{(z - z_0)^2} + \frac{a_{-1}}{(z - z_0)} + a_0 + a_1(z - z_0) + \ldots .$$

Definition The coefficient a_{-1} of $1/(z - z_0)$ in the LAURENT series given above is called the *Residue* of the function f at the isolated singularity z_0, in short notation,

$$a_{-1} = \text{Res}(f(z), z_0). \qquad (6.156)$$

A LAURENT series with a finite number of terms in its principal part, $a_{-k}, k = 1, 2, \ldots, n$, $a_{-k} = 0, k > n$, and $a_{-n} \neq 0$ has an isolated at $z = z_0$.

If f has a pole of order n at $z = z_0$, then

$$\text{Res}(f(z), z_0) = \frac{1}{(n-1)!} \lim_{z \to z_0} \frac{d^{n-1}}{dz^{n-1}} \left((z - z_0)^n f(z) \right) . \qquad (6.157)$$

Ex:

1. For a simple pole, i.e., a pole of order 1, this formula yields

$$\text{Res}(f(z), z_0) = \lim_{z \to z_0} \left((z - z_0) f(z) \right) .$$

If $f(z) = g(z)/h(z)$ and g and h are analytic and $g(z_0) \neq 0$, then $\text{Res}(f(z), z_0) = g(z_0)/h'(z_0)$. This is easy to see, since

$$h'(z) = \lim_{z \to z_0} \frac{h(z) - h(z_0)}{z - z_0} = \lim_{z \to z_0} \frac{h(z)}{z - z_0}.$$

So,

$$\mathrm{Res}(f(z), z_0) = \lim_{z \to z_0} (z - z_0) \frac{g(z)}{h(z)} = \lim_{z \to z_0} \left(\frac{g(z)}{\frac{h(z)}{z - z_0}} \right) = \frac{g(z_0)}{h'(z_0)}.$$

2. The function $f(z) = 1/[(z+1)^2(z+3)]$ has a simple pole at $z = -3$ and a pole of order 2 at $z = -1$. One may easily confirm, using (6.157)

- $\mathrm{Res}(f(z), -3) = \lim_{z \to -3} (z + 3) f(z) = \lim_{z \to -3} \frac{1}{(z+1)^2} = \frac{1}{4}$,
- $\mathrm{Res}(f(z), -1) = \frac{1}{1!} \lim_{z \to -1} \frac{\mathrm{d}}{\mathrm{d}z} \left((z+1)^2 f(z) \right)$

$$= \lim_{z \to -1} \left(-\frac{1}{(z+3)^2} \right) = -\frac{1}{4}.$$

Cauchy's Residue Thoerem: Let $\mathcal{D}$ be a simply connected domain and $\mathcal{C}$ a simple closed contour lying entirely within $\mathcal{D}$. If the function f is analytic on and within $\mathcal{D}$, except at a finite number of isolated singular points $z_1, z_2, ..., z_n$ within $\mathcal{C}$, then

$$\oint_{\mathcal{C}} f(z)\mathrm{d}z = 2\pi \iota \sum_{k=1}^{n} \mathrm{Res}(f(z), z_k). \tag{6.158}$$

Proof Suppose $\mathcal{C}_1, \mathcal{C}_2, ..., \mathcal{C}_n$ are circles centered at $z_1, z_2, ..., z_n$, respectively. Assume, moreover, that each circle $\mathcal{C}_k$ has a radius r_k small enough so that $\mathcal{C}_1, \mathcal{C}_2, ..., \mathcal{C}_n$ are mutually disjoint and are interior to the simple closed curve $\mathcal{C}$. Then, it can easily be proved by using CAUCHY's integral theorem that

$$\oint_{\mathcal{C}} f(z)\mathrm{d}z = \sum_{k=1}^{n} \oint_{\mathcal{C}_k} f(z)\mathrm{d}z. \tag{6.159}$$

Important in this result is that the cut plane as shown in **Fig. 6.56** is simply connected. Now, in (6.152),
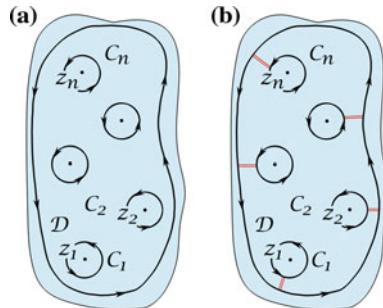
$$a_{-1}^{(\ell)} = \frac{1}{2\pi \iota} \oint_{\mathcal{C}_\ell} f(z)\mathrm{d}z,$$

in which ℓ denoted the ℓ-th circle of Fig. 6.56. Therefore,

$$\oint_{\mathcal{C}} f(z)\mathrm{d}z = 2\pi \iota \sum_{\ell=1}^{n} \mathrm{Res}(f(z), z_\ell). \tag{6.160}$$

∎

Fig. 6.56 **a** n singular poles within contour $\mathcal{C}$ for a complex function f. Each pole can be encircled by mutually non-intersection circles, which lie completely in $\mathcal{D}$. **b** By introducing cuts (in red) CAUCHYs theorem can be applied to the extended contour in order to obtain (6.158)

In words: The closed integral of the function f, which is analytic in $\mathcal{D}$ except at n isolated poles inside $\mathcal{C}$ is obtained by summing all the residues of the n poles multiplied with $2\pi\iota$. In (6.160), $\mathcal{C}$ must lie within the circular domain, where the LAURENT series converges.

References

1. Abramowitz, M., Stegun, I.: Handbook of Mathematical Functions with Formulas, Graphs, and Mathematical Tables. Dover Publications, New York (1964). ISBN: 978-0-486-61272-0
2. Agarwal, R. P., Perera, K., & Pinelas, S. (2010). *An Introduction to Complex Analysis*. New York: Springer.
3. Ahlfors, L.: Complex Analysis, 3rd edn. McGraw-Hill (1979)
4. Anderson, J.: Fundamentals of Aerodynamics. McGraw Hill, Toronto (1991). ISBN: 0-07-001679-8
5. Back, J., & Newman, D. J. (2010). *Complex Analysis*. Berlin: Springer.
6. Blasius, H.: Grenzschichten in Flüssigkeiten mit kleiner Reibung. Ph.D. dissertation, University of Göttingen (1907)
7. Blasius, H.: Grenzschichten in Flüssigkeiten mit kleiner Reibung. Zeitschr. Math. Phys. **56**, 1–37; **60**, 397–398 (1908)
8. Blasius, H. (1910). Funktionstheoretische Methoden in der Hydrodynamik. *Zeitsch. Math. Phys.*, *58*, 90–110.
9. Caratheodory, C.: Conformal Representation. Cambridge University Press (1932)
10. Caratheodory, C.: Theory of Functions of a Complex Variable (2 volumes), 2nd edn. Chelsea, New York (1977). ISBN: 0-8218-3780-X
11. Carrier, G.F., Krook, M., Pearson, C.E.: Functions of a Complex Variable - Theory and Technique. SIAM, Society of Industrial and Applied Mathematics (2005)
12. Delillo, T. K. (1994). The accuracy of numerical conformal mapping methods: a survey of examples and results. *SIAM J. Numer. Anal.*, *31*, 788–812.
13. Driscoll, T.A., Threfethen, L.N.: Schwarz-Christoffel Mapping. Cambridge University Press (2002). ISBN:0-521-80726-3
14. Gong, S., Gong, Y.: Concise Complex Analysis. World Scientific Publ. Comp. Co. Pte. Ltd. (2007)
15. Hager, W. H. (2003). Blasius: a life in research and education. *Exp. Fluids*, *34*, 566–571.
16. Henrici, P.: Applied and Computational Complex Analysis. Power Series-Integration-Conformal Mapping-Location of Zeros, vol. 1. Wiley (1974). ISNB: 0-471-37244-7
17. Henrici, P.: Applied and Computational Complex Analysis. Special Functioins-Integral Transfiorms-Asymptotics-Continued Fractions, vol. 2. Wiley (1977). ISNB: 0-471-01525-3

18. Henrici, P.: Applied and Computational Complex Analysis. Discrete Fourier Analysis-Cauchy Integrals Construction of Conformal Maps-Univalent Functions, vol. 3. Wiley (1974). ISNB: 0-471-08703-3
19. Ivanov, V. I., & Trubetskov, M. K. (1995). *Handbook of Conformal Mapping with Computer Aided Visualization*. Boca Raton, Fl: CRC Press.
20. Knopp, K.: Theory of Functions, Pats I and II (Translation from the German). Dover Publications on Mathematics (1996)
21. Milne-Thomson, L.M.: Theoretical Hydrodynamics, 5th edn. Dover Publications (1968). ISNB:0-486-68970-0
22. Milne-Thomson, L.M.: Theoretical Aerodynamics, 4th edn. Dover Publications (1973). ISNB: 0-486-61980-X
23. Olver, P.J.: Conformal Analysis and Conformal Mapping (2013). http://www.math.umn.edu/~olver/ln_/cml.pdf
24. Shaw, W.T.: Complex Analysis with Mathematica. Cambridge University Press (2006). ISBN: 9780521836265
25. Spurk, J.H., Aksel, N.: Fluid Mechanics. Springer, Berlin (2008)
26. Whittaker, E. T., & Watson, G. N. (1952). *Modern Analysis*. New York: Cambridge University Press.
27. Zill, D., Shanahan, P.: A First Course in Complex Analysis with Applications. Jones and Bartlett Learning (2009)

Chapter 7
Viscous Fluids

Abstract The equations of motion for viscous fluids are obtained from the mass and momentum equations by parametrization of the viscous stress tensor as an isotropic function of the strain rate tensor D with scalar coefficients, which are themselves functions of the invariants of the latter (and possibly additional scalar field quantities such as e.g., the temperature and salinity). NEWTONian fluid materials emerge by linearization of this parametrization in D. They are materially described by a shear viscosity and for compressible liquids (gases) an additional bulk viscosity. The emerging equations appear as NAVIER- STOKES equations. For water, experimentally supported expressions for these parameters are given in Chap. 1. The simplest nonlinear forms of the viscosity functions generate the material descriptions of dilatant and pseudoplastic liquids, which appear in rheology as power law fluids for which plane wall shear flows are studied. Applications address viscometry, hover craft and viscous HAGEN-POISEUILLE flows, the REYNOLDS-SOMMERFELD slide bearing model, shallow three-dimensional free surface flows applied to the flows in large ice sheets such as Greenland and Antarctica, significant for estimations of sea level rise due to anthropogenic production of greenhouse gases.

Keywords NEWTONian · NAVIER-STOKES fluids · Viscometric flows · Slide bearing theory · Shallow free surface flows · REINER-RIWLIN fluids · Dilatant, pseudoplastic fluids

List of Symbols

Roman Symbols

$A(\rho, T)$	Rate factor
a	Gap width of a slide bearing
$a_\perp$	Accumulation/ablation rate function
$a_\perp^{b,h}$	Accumulation/ablation rate function at the base, – at the free surface, deposition/entrainment rate function
$b(x, y, t) = z$	Position of the basal surface of a pressure drag flow
c_p, c_v	Specific heat at constant pressure, – at constant volume
$\mathcal{C}, C$	Drag coefficient

$\boldsymbol{D}$	Strain rate tensor, stretching tensor: $\boldsymbol{D} = \frac{1}{2}(\boldsymbol{L} + \boldsymbol{L}^T)$
$\mathcal{D}$	Depth integrated horizontal diffusivity
e	Eccentricity
$\boldsymbol{E}$	Distortion tensor: $\boldsymbol{E} = \boldsymbol{D} - \frac{1}{3}(\text{tr}(\boldsymbol{D}))\boldsymbol{1}$
$F(II_{\boldsymbol{t}^R})$	Fluidity, creep response function
F_N	Total normal force, carried by an oil pressure cushion
F_w	Tangential frictional force in an oil pressure cushion
$\boldsymbol{f}$	Specific body force
h	Gap width of a COUETTE viscometer, height of a fluid layer
$h(x, y, t) = z$	Position of the free surface in a pressure-drag flow
$H(x, y, t)$	Thickness function of a free surface pressure-drag flow
$I_{\boldsymbol{D}}, II_{\boldsymbol{D}}, III_{\boldsymbol{D}}$	Invariants of the second order tensor $\boldsymbol{D}$
$J_1, ..., J_5$	BOLTZMANN constant
K	Force exerted on a body at rest by a fluid
L	Power of working in an oil pressure cushion
l	Semi-length of an oil pressure cushion
$\boldsymbol{L} = \text{grad }\boldsymbol{v}$	Velocity gradient
M	Moment, applied at the outer cylinder of a COUETTE viscometer, applied torque in a slide bearing
m	Exponent in a power law fluid
$N_h a_\perp^h, N_b a_\perp^b$	Vertical accumulation/ablation rate functions at the free surface/at the base
$\boldsymbol{n}$	Unit vector perpendicular to a surface
p	Pressure
Q	Volume flow through a slit or a channel, activation energy
Q_{geoth}	Geothermal heat flow
$\boldsymbol{q}$	Heat flux vector
r, r'	Inner and outer radius of a slide bearing shaft
r_0	Inner radius of a COUETTE viscometer
S_0	SOMMERFELD number
$s(x)$	Integrated accumulation rate function (p. 416)
T	Absolute or KELVIN temperature
$\boldsymbol{t}$	CAUCHY stress tensor
$t_{xx}, t_{xy}, ..., t_{zz}$	Cartesian components of $\boldsymbol{t}$
$\boldsymbol{t}^R$	Frictional CAUCHY stress tensor
$\text{tr}\,\boldsymbol{D}$	Trace operator of $\boldsymbol{D}$
$u(y)$	Longitudinal velocity component in a 2D channel
u_w	Wall velocity
u, v, w	Velocity components of $\boldsymbol{v} = (u, v, w)$
$\boldsymbol{u}_\parallel, u_\perp$	Tangential, normal velocity components
$\boldsymbol{u}_H$	Horizontal velocity vector
$\boldsymbol{V}_H$	Horizontal flux vector
$\boldsymbol{v}$	Velocity vector
x, y, z	Cartesian coordinates

Greek Symbols

α	Exponent in a power law fluid (p. 375), Opening angle of a cone-plate viscometer, inclination angle of an inclined plane film flow in plane POISEUILLE flow
α, β	Coefficients in the FROBENIUS expansion of $h(\xi)$ (p. 417)
γ	Shear angle
$\dot{\gamma}$	Shear rate
Δ	LAPLACE operator, $\Delta = \nabla^2 = $ div grad
ε	Internal energy, – Dimensionless eccentricity in slide bearings
η	Dynamic viscosity
$\nu = \eta/\rho$	Kinematic viscosity
κ, λ	Coefficients in the REINER-RIWLIN fluid
μ	Effective solid drag coefficient, shear viscosity
$\boldsymbol{\tau}, \tau(y)$	Shear stress
$\zeta = \lambda + \frac{2}{3}\mu$	Bulk viscosity
ϕ	Polar angle
$\Phi(x, y, z, t) = 0$	Kinematic equation for a surface
σ_y	Normal stress in the y-direction
ω	Angular velocity

Miscellaneous Symbols

$d/dt = (\cdot)^{\cdot}$	Total (material) time derivative
$\partial/\partial t$	Partial (local) time derivative
$\text{tr}\,\boldsymbol{A}$	Trace of the rank-2 tensor $\boldsymbol{A}$
∇_H	Horizontal 2D nabla operator
$[\![\phi]\!]$	Jump of the variable ϕ across a surface
$\Theta(T) = \exp\left(-\frac{Q}{kT}\right)$	ARRHENIUS law

In the previous chapters the interior friction of the fluid was omitted. In Chap. 1 the most important facts and observations, which can be traced back to friction, were in fact explained with the aid of creep experiments, however, a detailed description of the viscous stresses was not presented. This is understandable, because it was in Chaps. 2 and 3 nowhere necessary to know or understand the mechanism of the interior friction. In this and in subsequent chapters it is our intention to address these questions which can only quantitatively be attacked if internal frictional effects are taken into account. In the next section the general fundamental equations of viscous fluids will be derived; then, laminar **wall bounded shear flows** or wall bounded **layer flows** will be studied and eventually applied to a number of technically and environmentally relevant problems. Flows through pipes and ducts will be dealt with in a separate chapter.

7.1   Fundamental Dynamical Equations of Viscous Fluids

Let us recall the creep experiment, which was discussed in Chap. 1: **Figure 7.1** displays in a general sketch a shear test, in which a fluid, positioned between two parallel rigid plates, is sheared by a translating motion of the upper plate. If the plate moves with constant velocity u_w, then a velocity profile will be established, which will in the y-direction very nearly be linear, viz.,

$$u(y) = \frac{u_w}{h} y, \tag{7.1}$$

where h is the distance of the two plates. If one imagines that at time $t = 0$ a vertical material line is marked, this line will, with growing time, be inclined. The shear velocity $\dot{\gamma}$ is the time rate of change of this shear angle and is given by $\mathrm{d}u/\mathrm{d}y$,

$$\dot{\gamma} = \frac{\mathrm{d}u}{\mathrm{d}y}. \tag{7.2}$$

Viscous fluids can be distinguished among each other by the amount of resistance which they exert against this shearing. If τ is the shear traction applied to the plates, the relation
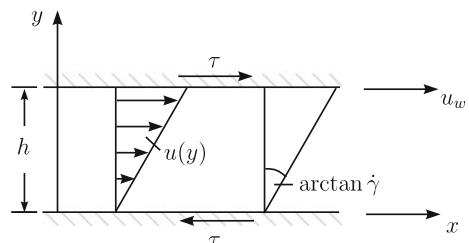
$$\dot{\gamma} = \frac{\tau}{\eta(|\tau|)} \tag{7.3}$$

can be postulated, in which η is the **effective dynamic (shear) viscosity** and appears here as a function of the modulus of the shear traction.

The above proposed relation between shear stress and shear velocity was motivated with the aid of a relatively simple, controllable experiment; it now needs to be generalized for a general state of motion for the fluid. To this end, recall the momentum balance law, which was stated in Eq. (3.85) in the **global** form

$$\frac{\mathrm{d}}{\mathrm{d}t} \int_V \rho \boldsymbol{v} \, \mathrm{d}V = \int_{\partial V} \boldsymbol{tn} \, \mathrm{d}A + \int_V \rho \boldsymbol{f} \, \mathrm{d}V, \tag{7.4}$$

Fig. 7.1 Simple shear experiment *In a movement of the upper wall relative to the lower wall a velocity field is established, which is linear in the y-coordinate*

to which the **local** equation

$$\left\{ \begin{array}{c} \dfrac{\partial(\rho\boldsymbol{v})}{\partial t} + \mathrm{div}\,(\rho\boldsymbol{v}\otimes\boldsymbol{v}) \\[2mm] \rho\dfrac{\mathrm{d}\boldsymbol{v}}{\mathrm{d}t} \end{array} \right\} = \mathrm{div}\,\boldsymbol{t} + \rho\boldsymbol{f} \qquad (7.5)$$

corresponds (see e.g. Eqs. (3.90) and (3.92)).[1] In the above Eq. (7.4) we employ the general expression $\int_{\partial V} \boldsymbol{t}\boldsymbol{n}\,\mathrm{d}A$. Equation (7.4) states that the time rate of change of the momentum of the material body occupying the volume V is balanced by the sum of the surface forces and body forces. This is nothing else than NEWTON's second law. In the local form of the balance law of momentum, $(7.5)_1$ expresses that 'the time rate of change of momentum equals the sum of the forces applied to the body', whilst $(7.5)_2$ says that 'mass times acceleration equals the sum of the forces applied to the body'. The former is the more general version of the two and this is how ISAAC NEWTON formulated it. Moreover in the local form of the balance law of momentum the surface forces appear as the divergence of the CAUCHY stress tensor $\boldsymbol{t}$. It is often convenient to split the CAUCHY stress tensor into an isotropic pressure tensor $-p\boldsymbol{1}$ plus a **frictional tensor** $\boldsymbol{t}^R$—more generally an **extra stress tensor**, also representative of more than just frictional effects—so that

$$\boldsymbol{t} = -p\boldsymbol{1} + \boldsymbol{t}^R. \qquad (7.6)$$

In Cartesian coordinates, i.e., referred to a fixed orthogonal coordinate system, $\boldsymbol{t}$ possesses the representation

$$\begin{pmatrix} t_{xx} & t_{xy} & t_{xz} \\ t_{yx} & t_{yy} & t_{yz} \\ t_{zx} & t_{zy} & t_{zz} \end{pmatrix} = \begin{pmatrix} -p & 0 & 0 \\ 0 & -p & 0 \\ 0 & 0 & -p \end{pmatrix} + \begin{pmatrix} t^R_{xx} & t^R_{xy} & t^R_{xz} \\ t^R_{yx} & t^R_{yy} & t^R_{yz} \\ t^R_{zx} & t^R_{zy} & t^R_{zz} \end{pmatrix} \qquad (7.7)$$

with

$$\begin{aligned} t^R_{xy} = t_{xy}, \quad t^R_{xz} = t_{xz}, \quad t^R_{yx} = t_{yx}, \\ t^R_{yz} = t_{yz}, \quad t^R_{zx} = t_{zx}, \quad t^R_{zy} = t_{zy}. \end{aligned}$$

It was shown also in Sect. 3.6, when applying the balance law of moment of momentum to a continuous body, that $\boldsymbol{t}$ and, therefore, also $\boldsymbol{t}^R$ are symmetric rank-2 tensors. Of the nine components in (7.7), therefore, only six are independent. If the decomposition of the stress tensor (7.6) is substituted into (7.5) and the identity $\mathrm{div}\,(p\boldsymbol{1}) = \mathrm{grad}\,p$ is used, then one obtains

---

[1]In that equation the surface term was only written for an isotropic (hydrostatic) stress state.

$$
\left\{
\begin{array}{c}
\dfrac{\partial(\rho\boldsymbol{v})}{\partial t} + \mathrm{div}\,(\rho\boldsymbol{v}\otimes\boldsymbol{v}) \\[2mm]
\rho\dfrac{d\boldsymbol{v}}{dt} \\[2mm]
\rho\left(\dfrac{\partial\boldsymbol{v}}{\partial t} + (\mathrm{grad}\,\boldsymbol{v})\boldsymbol{v}\right) \\[2mm]
\rho\left(\dfrac{\partial\boldsymbol{v}}{\partial t} + \mathrm{grad}\,\dfrac{|\boldsymbol{v}|^2}{2} - \boldsymbol{v}\times\mathrm{curl}\,\boldsymbol{v}\right)
\end{array}
\right\}
= -\mathrm{grad}\ p + \mathrm{div}\,\boldsymbol{t}^R + \rho\boldsymbol{f}. \qquad (7.8)
$$

In these expressions four different forms of the time rate of change of momentum have been introduced. The first is the local balance law in its so-called **conservation form** as it directly evolves from (7.4). The remaining three show the momentum change on the left-hand side of the equation as 'mass times acceleration' and have been obtained by use of the additional product differentiations from the first (see (3.90), (3.91)) and use of the mass balance; they, thus, imply higher smoothness properties than (7.8)$_1$. Incidentally, the three acceleration expressions in (7.8)$_{2,3,4}$ have already been given in (3.11). In Cartesian coordinates the momentum equations take the forms:

1. When they are in *conservative form*

$$
\begin{aligned}
\frac{\partial(\rho u)}{\partial t} &+ \frac{\partial}{\partial x}\left(\rho u^2\right) + \frac{\partial}{\partial y}\left(\rho uv\right) + \frac{\partial}{\partial z}\left(\rho uw\right) \\[2mm]
&= -\frac{\partial p}{\partial x} + \frac{\partial t_{xx}^R}{\partial x} + \frac{\partial t_{xy}^R}{\partial y} + \frac{\partial t_{xz}^R}{\partial z} + \rho f_x, \\[2mm]
\frac{\partial(\rho v)}{\partial t} &+ \frac{\partial}{\partial x}\left(\rho uv\right) + \frac{\partial}{\partial y}\left(\rho v^2\right) + \frac{\partial}{\partial z}\left(\rho vw\right) \\[2mm]
&= -\frac{\partial p}{\partial y} + \frac{\partial t_{yx}^R}{\partial x} + \frac{\partial t_{yy}^R}{\partial y} + \frac{\partial t_{yz}^R}{\partial z} + \rho f_y, \\[2mm]
\frac{\partial(\rho w)}{\partial t} &+ \frac{\partial}{\partial x}\left(\rho uw\right) + \frac{\partial}{\partial y}\left(\rho vw\right) + \frac{\partial}{\partial z}\left(\rho w^2\right) \\[2mm]
&= -\frac{\partial p}{\partial z} + \frac{\partial t_{zx}^R}{\partial x} + \frac{\partial t_{zy}^R}{\partial y} + \frac{\partial t_{zz}^R}{\partial z} + \rho f_z.
\end{aligned}
\qquad (7.9)
$$

2. When they are *not in conservative form*

$$
\begin{aligned}
\rho\left\{\frac{\partial u}{\partial t} + \frac{\partial u}{\partial x}u + \frac{\partial u}{\partial y}v + \frac{\partial u}{\partial z}w\right\} &= -\frac{\partial p}{\partial x} + \frac{\partial t_{xx}^R}{\partial x} + \frac{\partial t_{xy}^R}{\partial y} + \frac{\partial t_{xz}^R}{\partial z} + \rho f_x, \\[2mm]
\rho\left\{\frac{\partial v}{\partial t} + \frac{\partial v}{\partial x}u + \frac{\partial v}{\partial y}v + \frac{\partial v}{\partial z}w\right\} &= -\frac{\partial p}{\partial y} + \frac{\partial t_{yx}^R}{\partial x} + \frac{\partial t_{yy}^R}{\partial y} + \frac{\partial t_{yz}^R}{\partial z} + \rho f_y, \ (7.10) \\[2mm]
\rho\left\{\frac{\partial w}{\partial t} + \frac{\partial w}{\partial x}u + \frac{\partial w}{\partial y}v + \frac{\partial w}{\partial z}w\right\} &= -\frac{\partial p}{\partial z} + \frac{\partial t_{zx}^R}{\partial x} + \frac{\partial t_{zy}^R}{\partial y} + \frac{\partial t_{zz}^R}{\partial z} + \rho f_z.
\end{aligned}
$$

The EULER equations of an ideal fluid differ from Eqs. (7.8), (7.9) and (7.10) only by the fact that the extra stress t^R is missing. In a concrete problem these equations must be complemented by the balance law of mass, given in (3.44).

The local balance laws of mass and momentum comprise a set of four equations for the unknown field quantities ρ, v, p and t^R. Ignoring possible thermal effects, hence neglecting the role of the temperature, it is necessary to establish additional relations for seven of the total of eleven field quantities ρ, v, p, t^R in order that a system of equations is obtained, which is at least principally integrable. The procedure of selection of these **material** or **constitutive relations** is different for compressible and density preserving fluids:

- For **compressible fluids** the density ρ and velocity field v are regarded as the basic field quantities to be determined; so, functional relations are sought for the pressure p as well as the viscous stress t^R, e.g.,

$$p = \hat{p}(\rho), \qquad t^R = \hat{t}^R(v, \text{grad } v, \rho). \tag{7.11}$$

  The first of these relations was already presented when barotropic fluids were discussed.

- For **density preserving fluids** the density is a constant, known quantity, so that only ten of the above eleven fields are unknown. Here, the pressure p and the velocity field v are regarded as the independent fields, and in lieu of (7.11) a single material equation must be formulated for the viscous frictional stress only,

$$t^R = \hat{t}^R(v, \text{grad } v). \tag{7.12}$$

Let us now present the material equation for the stress tensor. Being motivated by the introductory shearing test of Chap. 1, it is reasonable to suppose that t^R can neither depend on the velocity v nor on the skew-symmetric part of grad v. A strict proof of this is of principal nature and is given in books on continuum mechanics, e.g. [17]. Therefore, t^R can only depend on the symmetric part of the velocity gradient, $L := \text{grad } v$. The standard variable in this regard is

$$D = \tfrac{1}{2}(L + L^T), \tag{7.13}$$

where L^T is the transpose of L. Thus $t^R = t^R(D, \rho)$ for the compressible case and $t^R = t^R(D)$ for the density preserving material. The rank-2 tensor D is called **strain-rate tensor**, **rate of strain tensor** or **stretching tensor**. It then follows from considerations of algebra that the most general representation for a symmetric rank-2 tensor t^R in terms of a scalar ρ and another symmetric rank-2 tensor, D, is of the form[2]

$$t^R = \lambda(\text{tr } D)\mathbf{1} + 2\eta D + \kappa D^2, \tag{7.14}$$

---

[2] Any rank-2 function, continuously differentiable in a domain centered at the origin where $D = 0$, can be expressed as a power series of D, which through the CALEY-HAMILTON theorem, can be replaced by a second order polynomial in D. This is demonstrated in books on Linear Algebra.

in which λ, η, κ are scalar coefficients which themselves are functions of ρ and scalar invariants of $\boldsymbol{D}$, which are independent of the coordinates to which $\boldsymbol{D}$ is referred. These are related to the eigenvalues of $\boldsymbol{D}$ and are here the three quantities

$$I_{\boldsymbol{D}} = \text{tr}\,\boldsymbol{D}, \qquad II_{\boldsymbol{D}} = \tfrac{1}{2}\text{tr}\,\boldsymbol{D}^2, \qquad III_{\boldsymbol{D}} = \det\boldsymbol{D}. \tag{7.15}$$

Therefore,

$$\begin{aligned}
\lambda &= \hat{\lambda}(I_{\boldsymbol{D}}, II_{\boldsymbol{D}}, III_{\boldsymbol{D}}, \rho), \\
\eta &= \hat{\eta}(I_{\boldsymbol{D}}, II_{\boldsymbol{D}}, III_{\boldsymbol{D}}, \rho), \\
\kappa &= \hat{\kappa}(I_{\boldsymbol{D}}, II_{\boldsymbol{D}}, III_{\boldsymbol{D}}, \rho).
\end{aligned} \tag{7.16}$$

When temperature variations are significant a dependence on T and grad T may be added to the right-hand side of (7.16). In the above relations tr $\boldsymbol{A}$ is the trace of the 3×3 scheme $\boldsymbol{A}$, the sum of the diagonal elements. We emphasize that we did not above derive the representations (7.14)–(7.16), but only gave a motivation for them and shall accept them in this form. In the context of rheology they were derived in this full general form by MARKUS REINER (1886–1976) and R. RIWLIN[3]; consequently, a fluid obeying the constitutive relation (7.14), (7.16) is called a REINER-RIWLIN fluid.

In Cartesian coordinates the velocity gradient is given by

$$\boldsymbol{L} = \begin{pmatrix} \dfrac{\partial u}{\partial x} & \dfrac{\partial u}{\partial y} & \dfrac{\partial u}{\partial z} \\[2mm] \dfrac{\partial v}{\partial x} & \dfrac{\partial v}{\partial y} & \dfrac{\partial v}{\partial z} \\[2mm] \dfrac{\partial w}{\partial x} & \dfrac{\partial w}{\partial y} & \dfrac{\partial w}{\partial z} \end{pmatrix}, \tag{7.17}$$

so that the strain rate or stretching tensor takes the form

$$\boldsymbol{D} = \begin{pmatrix} \dfrac{\partial u}{\partial x} & \dfrac{1}{2}\left(\dfrac{\partial u}{\partial y} + \dfrac{\partial v}{\partial x}\right) & \dfrac{1}{2}\left(\dfrac{\partial u}{\partial z} + \dfrac{\partial w}{\partial x}\right) \\[3mm] & \dfrac{\partial v}{\partial y} & \dfrac{1}{2}\left(\dfrac{\partial v}{\partial z} + \dfrac{\partial w}{\partial y}\right) \\[3mm] \text{(sym.)} & & \dfrac{\partial w}{\partial z} \end{pmatrix}, \tag{7.18}$$

from which we read off

$$\text{tr}\,\boldsymbol{D} = \frac{\partial u}{\partial x} + \frac{\partial v}{\partial y} + \frac{\partial w}{\partial z} = \text{div}\,\boldsymbol{v}. \tag{7.19}$$

The other quantities of (7.14) can now in principle be computed from (7.18).

---

[3] For a biography of M. REINER and circumstances why the REINER-RIVILIN fluid should be named REINER-RIWLIN fluid see **Fig. 7.2**.

Fig. 7.2 MARKUS REINER (5. Jan. 1886–25. April 1976)

MARKUS REINER, born in Czernowitz, then within the Austro-Hungarian Empire, now Rumania received a degree in civil engineering from the 'Technische Hochschule' in Vienna and worked before World War 1 (WW1) in Berlin and Essen and again in Czernowitz. After WW1, as a convinced Zionist he emigrated to Palestine 'doing hard manual work' [27] and then was employed by the British Mandate Government until 1948. After the founding of the state of Israel, he became professor at the Technion in Haifa, where at the Ceremony of his 90th birthday the 'Markus Reiner Chair of Rheology', located within the Department of Engineering was founded.

In the late 1920's M. REINER and Prof. E.C. BINGHAM (1878–1945) founded the journal and society of 'Rheology', eventually to become the American Soc. Rheology, but REINER could not participate in its first conference in 1929. It was at this time and occasion that the name 'Rheology' was officially accepted for the 'Science of the Deformation of Flow of Matter'. According to SCOTT-BLAIR [27], REINER also pointed out that, if one waits long enough, most systems will be found to flow. The Prophetess *Deborah* said: 'the mountains flowed before the Lord': so, REINER defined the Deborah number 'to relate the relaxation time of a system to the experimental time.'

Before 1929, REINER had worked on a number of projects now considered as rheology. As said in [27] 'he developed 'the REINER-RIWLIN-Equation'—his colleague Miss R. RIWLIN was killed in a road accident. Her nephew, Ronald S. Rivlin (now spelled with a 'V') is a well-known [British]-American rheologist'. This information was a surprise for one of us (K.H). Evidently, R. RIWLIN and *not* R. RIVLIN is the research partner of the REINER-RIWLIN fluid. Some other achievements are given in [26].

The text is based on [27]

Now, all only strain rate dependent stress parameterizations request for their description a constitutive equation of the complexity (7.14). A few simple ones will now be discussed.

7.1.1   Newtonian Fluids

These are the simplest ones of all REINER-RIWLIN fluids, which account for internal friction. They are defined by the fact that t^R depends *linearly* on D. In aian fluid, therefore, the term involving D^2 cannot arise, and so κ must vanish, and λ and η cannot depend on D (and thus involve only the density ρ (and the temperature)). Therefore, a NEWTONian fluid has the stress-stretching relation

$$t^R = \lambda(\text{div } v)\mathbf{1} + 2\eta D, \qquad \{\lambda, \eta\} = \{\hat{\lambda}, \hat{\eta}\}(\rho, T). \tag{7.20}$$

The two coefficient functions have the dimension of dynamic viscosities. Referred to Cartesian coordinates, the law (7.20) takes the form

$$
\begin{aligned}
t_{xx}^R &= \lambda \text{div } v + 2\eta \frac{\partial u}{\partial x}, & t_{xy}^R &= \eta\left(\frac{\partial u}{\partial y} + \frac{\partial v}{\partial x}\right), \\
t_{yy}^R &= \lambda \text{div } v + 2\eta \frac{\partial v}{\partial y}, & t_{yz}^R &= \eta\left(\frac{\partial v}{\partial z} + \frac{\partial w}{\partial y}\right), \\
t_{zz}^R &= \lambda \text{div } v + 2\eta \frac{\partial w}{\partial z}, & t_{zx}^R &= \eta\left(\frac{\partial w}{\partial x} + \frac{\partial u}{\partial z}\right).
\end{aligned}
\tag{7.21}
$$

The material equations (7.20) and (7.21) are the true domain of classical fluid dynamics; often people identify with 'fluid dynamics' the pursuit with materials, which belong to the class of (7.20) and (7.21). Such fluids are also called **Newtonian fluids** or **Navier-Stokes fluids**, because ISAAC NEWTON (1642–1727) anticipated in his principal work, *Principia* (1687) [22], the simple linear relation between stress and strain rate for simple shearing, and NAVIER (1785–1836)[4] as well as STOKES (1819–1903)[5] were the first to postulate the law (7.20) in three-dimensional form.

Simple shear flow is characterized by the fact that the flow field is plane and only varies in the direction perpendicular to the plane of flow. With reference to **Fig. 7.5**, one may thus write

$$u = u(z, t) \qquad v = v(z, t), \qquad w = 0, \tag{7.22}$$

and then finds from (7.21) that the only non-trivial frictional stress components are

$$t_{xz}^R = \eta\frac{\partial u}{\partial z}, \qquad t_{yz}^R = \eta\frac{\partial v}{\partial z}. \tag{7.23}$$

---

[4]For a short biography of NAVIER see **Fig. 7.3**.

[5]For a short biography of STOKES see **Fig. 7.4**.

Such flows are called free or wall bounded **layer flows**, and the simple shear experiment is a special case of these. The result (7.23) makes also clear that the coefficient η has the dimension of a dynamic viscosity.

Bernoulli-Navier Beams:

$$M = -EI\frac{\mathrm{d}^2 w}{\mathrm{d}x^2} \qquad \text{(Bending moment)}$$

$$\sigma = \frac{M}{I}z \qquad \text{(Normal stress)}$$

Fig. 7.3 CLAUDE-LOUIS NAVIER (born CLAUDE LOUIS MARIE HENRI NAVIER (10. Feb. 1785–21. Aug. 1836)

CLAUDE-LOUIS NAVIER was a French engineer and physicist who specialized in mechanics. After the death of his father in 1793, NAVIER's mother left his education in the hands of his uncle EMILAND GAUTHEY, an engineer with the Corps of Bridges and Roads (Corps des Ponts et Chaussées). In 1802, Navier enrolled at the École polytechnique, and in 1804 continued his studies at the École Nationale des Ponts et Chaussées, from which he graduated in 1806. He eventually succeeded his uncle as Inspecteur general at the Corps des Ponts et Chaussées. He directed the construction of bridges at Choisy, Asnières and Argenteuil in the Department of the Seine, and built a footbridge to the Île de la Cité in Paris. In 1824, NAVIER was admitted into the French Academy of Science. In 1830, he took up a professorship at the École Nationale des Ponts et Chaussées, and in the following year succeeded exiled AUGUSTIN LOUIS CAUCHY as professor of calculus and mechanics at the École polytechnique.

NAVIER formulated the general theory of elasticity in a mathematically usable form (1821), making it available to the field of construction with sufficient accuracy for the first time. In 1819 he succeeded in determining the zero line of mechanical stress, correcting GALILEO GALILEI's incorrect results, and in 1826 he established the elastic modulus as a property of materials independent of the second moment of area. In classical beam theory his name is associated with the BERNOULLI-NAVIER assumption of 'plane cross sections remain plane under deformation'. In 1826 he clearly differentiated between the modulus of elasticity, E as a material property and the areal moment of inertia, I, as a geometric property of the cross section of a beam. NAVIER is therefore often considered to be the founder of modern structural analysis.

His major contribution however remains the NAVIER-STOKES equations (1822), central to fluid mechanics, which he and GEORGE GABRIEL STOKES derived independently of each other.

The text is based on http://www.wikipedia.org
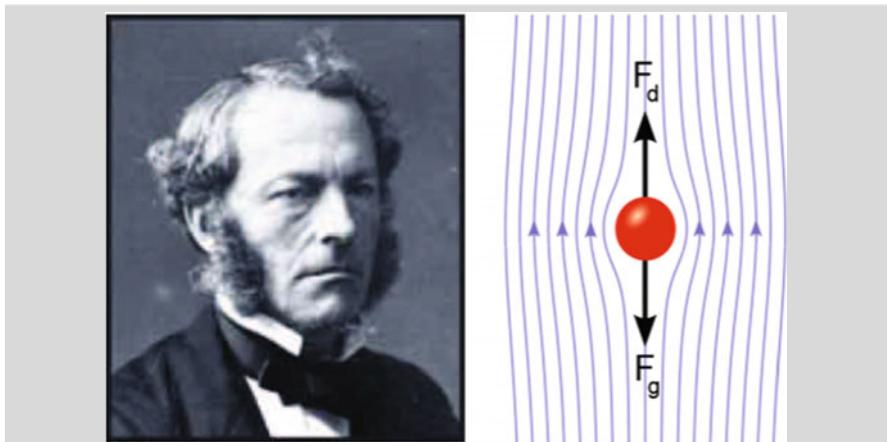
Fig. 7.4 George Gabriel Stokes (13. Aug. 1819–1. Feb. 1903). Right panel: Creeping flow past a sphere: streamlines and forces

Sir George Gabriel Stokes, first Baronet, FRS was a mathematician and physicist, who at Cambridge made important contributions to fluid mechanics, optics and mathematical physics. He matriculated 1837 at Pembroke College and later became one of its fellows. In 1849 he was appointed Lucasian professor of mathematical physics at Cambridge University, a post he held until his death. He was made baronet in 1889. He became a fellow of the Royal Society, London, in 1851 and was its president from 1885 to 1890 and had been its secretary since 1854.

His contributions to science are immense. A good summary can be found in the web page stated below. In this note we limit considerations to mentioning contributions to fluid mechanics. His first published papers—1842, 1843—were on the steady motion of incompressible fluids. These were followed in 1845 by a paper on the friction of fluids in motion and in 1850 by another on the effects of the internal friction of fluids on the motion of pendulums. He made several contributions to the theory of sound, including a discussion of the effect of wind on the intensity of sound and an explanation of how the intensity is influenced by the nature of the gas in which the sound is produced. These works put the science of fluid dynamics on a new footing and provided e.g. an explanation of the suspension of clouds in air and the subsidence of ripples and waves in water as well as flow of water in rivers and channels and the skin resistance of ships.

Stokes' work on fluid motion led to the fundamental equations of fluid dynamics of linearly viscous bodies (Navier-Stokes equations). Moreover, it yielded his calculating the terminal velocity of a sphere falling in a viscous medium, now known as Stokes' law. He derived in this paper an expression for the frictional drag force exerted on spherical objects with very small Reynolds numbers. This work is the basis of the falling sphere viscometer. Given a liquid of unknown viscosity contained in a cylinder at rest and determining experimentally the terminal fall velocity of known diameter and density allows evaluation of the liquid's viscosity, see above sketch. The same theory also explains why small water droplets (or ice crystals) can remain suspended in air (as clouds) until they grow to a crystal size and start falling.

Stokes held conservative religious values and beliefs and was e.g. vice president of the British and Foreign Bible Society.

The text is based on http://www.wikipedia.org

A further particular motion is **isotropic expansion** or **isotropic compression**, **Fig. 7.6**. It is described by a motion, in which all fluid particles move radially, either away from a center or toward it. The stretching tensor is therefore proportional to the unit tensor, $\boldsymbol{D} = \dot{\varepsilon}\boldsymbol{1}$. Because of (7.18) and (7.21), only normal stresses are activated in this case, and because of $\dot{\varepsilon} = \partial u/\partial x = \partial v/\partial y = \partial w/\partial z$ we also have div $\boldsymbol{v} = 3\dot{\varepsilon}$, so that (7.20) takes the form

$$\boldsymbol{t}^R = (3\lambda + 2\eta)\dot{\varepsilon}\boldsymbol{1}. \tag{7.24}$$

Now, it is easy to see, that an infinitesimal cube, which experiences in the three coordinate directions the rates of extension, $\dot{\varepsilon}$, is subjected to a volume strain rate $\dot{V}$ of magnitude $\dot{V} = 3\dot{\varepsilon}$. One may thus also write (7.24) as

$$\boldsymbol{t}^R = \left(\lambda + \tfrac{2}{3}\eta\right)\dot{V}\boldsymbol{1}. \tag{7.25}$$

Under isotropic expansion or compression of a NEWTONian fluid the only non-trivial viscous stresses are isotropic tension or compression stresses with a viscosity

$$\zeta = \lambda + \tfrac{2}{3}\eta. \tag{7.26}$$

Fig. 7.5 Plane bounded layer flow *In a shear flow the velocity field is everywhere parallel to a distinguished plane (here the (x, y)-plane), and varies in the direction perpendicular to it*
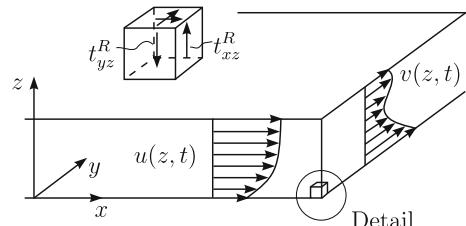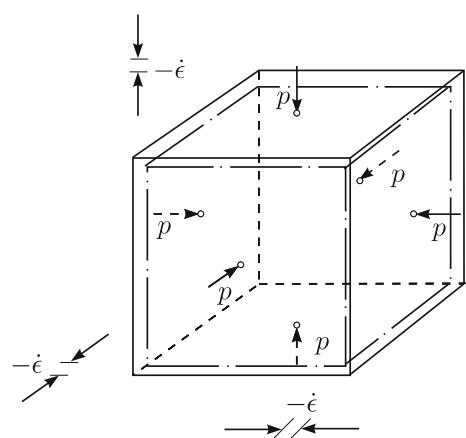
Fig. 7.6 Isotropic compression *A material cube, subjected to the same compression in all directions experiences a unique compression rate* $\dot{\varepsilon}$

The quantities η and ζ have the dimension of viscosities.

If one introduces the **distortion rate tensor**—often only denoted **distortion tensor** –

$$\boldsymbol{E} = \boldsymbol{D} - \tfrac{1}{3}(\operatorname{div}\boldsymbol{v})\boldsymbol{1}, \tag{7.27}$$

then (7.20) can also be written as

$$\boldsymbol{t}^R = \zeta(\operatorname{div}\boldsymbol{v})\boldsymbol{1} + 2\eta\boldsymbol{E}. \tag{7.28}$$

One can easily show that tr $\boldsymbol{E} = 0$, and conclude that the first term in (7.28) describes the influence of the **volume change**, whilst the second accounts for the **distortion rate** of the viscous stresses. In the form (7.28) the stress-strain rate law of a NEWTONian fluid takes a particularly perceptual form. The effects of the volume viscosity and shear viscosity are additively separated. One also recognizes from this separation, which experiments an experimentalist ought to perform, in order to determine numerical values for ζ and η. In the simple shear test sketched above and described in detail in Chap. 1, the shear viscosity can be determined. In an isotropic compression test we have $\boldsymbol{E} = \boldsymbol{0}$, and it is at least in principle possible to determine numerical values for the volume viscosity.

Now, shear viscosities of many fluids are relatively well known; quite contrary to volume viscosities. Reason for this is, first, that in density preserving fluids the latter do not arise since div $\boldsymbol{v} = 0$ and, therefore, cannot experimentally be determined and, second, that in nearly density preserving fluids the first term in (7.28) is of much less significance than the second and, thus, can be ignored; third, for (monatomic) gases the assumption $\zeta = 0$ can be proved to be (nearly) satisfied. Often one therefore puts

$$\zeta = 0, \tag{7.29}$$

an assumption which is due to GEORGE G. STOKES (1840) and since then known as **Stokes assumption**. Figure 1.2 in Chap. 1 displays the temperature dependence of the shear viscosity of some NEWTONian fluids. Figure 1.3a gives a plot for the shear and volume viscosity of pure water at normal pressure (10^5 Pa) and Fig. 1.3b shows the dependence of the shear viscosity with the pressure. Finally, Fig. 1.4 displays the shear viscosity of sea water with variations of the temperature and salinity.

The determination of numerical values of the shear viscosity ofdensity preserving Newtonian fluids was first undertaken by JEAN LÉONAR POISEUILLE (1797–1861) and almost simultaneously by GOTTHILF HEINRICH LUDWIG HAGENHAGEN (1797–1884) in fluid flow experiments through thin glass tubes, for biographies, see **Figs. 7.7** and **7.8** and a more detailed account in [28].[6] The first derivation of a steady flow of a NEWTONian viscous fluid through circular pipes based on the NAVIER-STOKES equations—the parabolic velocity profile—was given by

---

[6]See also http://www.deutsche-biographie.de/ppn11638039X.html.

JAKOB EDUARD Hagenbach-Hagenbach-Bischoff (1833–1910), a Swiss Physicist at the University in Basel, in 1860 [12].[7]

Fig. 7.7 JEAN LÉONARD POISEUILLE (22. April 1797 – 26. Dec. 1861)

JEAN LÉONARD POISEUILLE studied at École Polytechnique physics and mathematics and earned in 1828 his doctorate with a dissertation entitled 'Recherches sur la force du coeur aortique'. His interest was in the flow of liquids through pipes, such as blood flow in capillaries and veins. He experimentally derived and in 1840-1846 formulated and published his *flow law*—now known as HAGEN-POISEUILLE equation – which applies to laminar flow of viscous liquids through pipes. His research led directly to experimental methods of the determination of the viscosity of viscous fluids.

Poiseuille lived his professional life largely unnoticed and was not very successful in his research. He failed three times the election to the Académie des Sciences... . The present form of what we know as POISEUILLE equation was, in 1860, derived by EDUARD HAGENBACH (1833–1910, professor of physics in Basel). The quadratic velocity profile was first derived by GEORGE GABRIEL STOKES in his famous paper of 1845, who was not aware of POISEUILLE's or GOTTHILF HAGEN's experiments. Today we refer to the HAGEN-POISEUILLE equation for laminar pipe flow.

The text is based on http://www.wikipedia.org and [14]

---

[7]See however also [28] and http://www.deutsche-biographie.de/ppn11638039X.html.
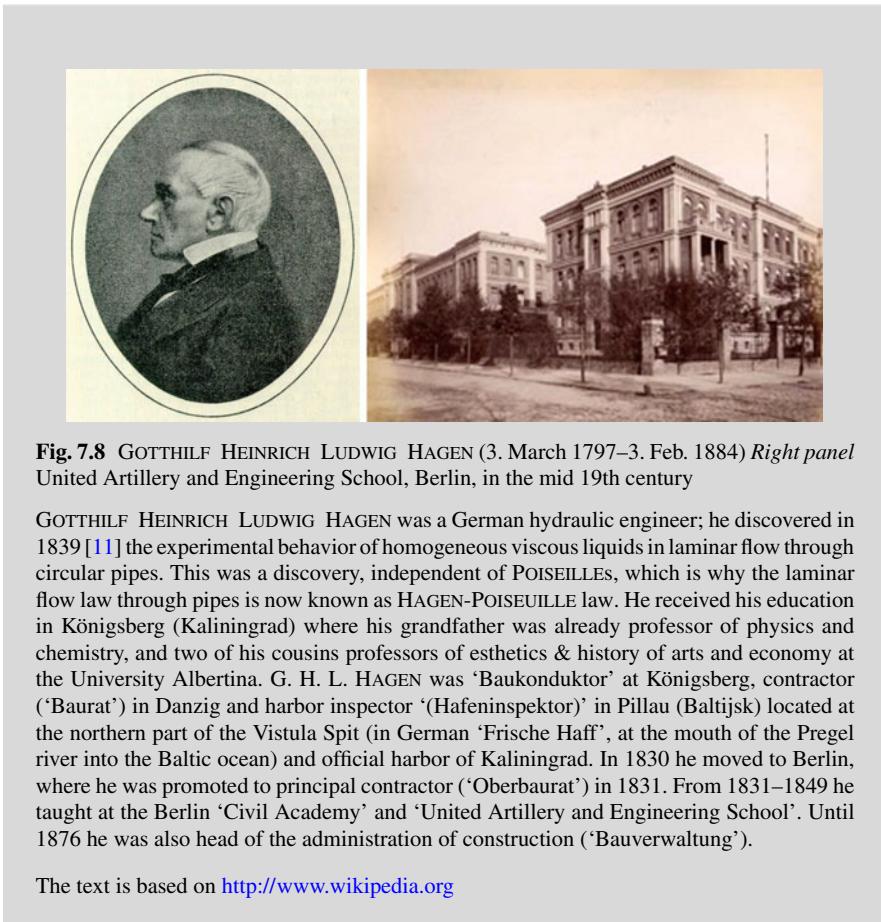
Fig. 7.8 Gotthilf Heinrich Ludwig Hagen (3. March 1797–3. Feb. 1884) *Right panel* United Artillery and Engineering School, Berlin, in the mid 19th century

Gotthilf Heinrich Ludwig Hagen was a German hydraulic engineer; he discovered in 1839 [11] the experimental behavior of homogeneous viscous liquids in laminar flow through circular pipes. This was a discovery, independent of Poiseilles, which is why the laminar flow law through pipes is now known as Hagen-Poiseuille law. He received his education in Königsberg (Kaliningrad) where his grandfather was already professor of physics and chemistry, and two of his cousins professors of esthetics & history of arts and economy at the University Albertina. G. H. L. Hagen was 'Baukonduktor' at Königsberg, contractor ('Baurat') in Danzig and harbor inspector '(Hafeninspektor)' in Pillau (Baltijsk) located at the northern part of the Vistula Spit (in German 'Frische Haff', at the mouth of the Pregel river into the Baltic ocean) and official harbor of Kaliningrad. In 1830 he moved to Berlin, where he was promoted to principal contractor ('Oberbaurat') in 1831. From 1831–1849 he taught at the Berlin 'Civil Academy' and 'United Artillery and Engineering School'. Until 1876 he was also head of the administration of construction ('Bauverwaltung').

The text is based on http://www.wikipedia.org

Numerical values of shear viscosities of a large number of substances are collected in tables of the chemical industry. For distinguished fluids, formulae have been developed which summarize the experimental results. Such formulae are commonly not dimensionally homogeneous; i.e. the values of various physical variables must be substituted in specific units. This requires care when applying these formulae. For **pure water** two such old and simple formulae are [5, 25]

$$
\begin{aligned}
\text{J.L. Poiseuille :} \quad & \eta = \frac{17.8}{1. + 0.0337T + 0.00022T^2} , \\
\text{N.E. Dorsey :} \quad & \frac{1}{\eta} + 120 = 2.1482\Big((T - 8.435) \\
& \qquad + \sqrt{8078.1 + (T - 8.435)^2}\Big).
\end{aligned}
\tag{7.30}
$$

Here, the temperature is to be substituted in degrees Celsius and the numerical value, which one obtains for η, is in millipoise (1 mpoise $= 10^{-3}$poise $= 10^{-4}$kgm^{-1}s^{-1}). The formulae are valid for a temperature interval $T \in [0, 50]\,°$C and do not contain a pressure dependence, but hold for pressures $p \in [10^5, 10^7]$ Pa. Further formulae for a larger temperature range, which also exhibit a pressure dependence are the ASME-Steam Tables [1].
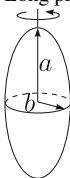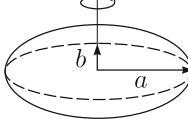
The values of the dynamic shear viscosity (as well as the volume viscosity, if it is of significance), are also determined by the content of *tracers in solution and in suspension*. The salinity of sea water has an influence on its viscosity, and in general, the composition of the salts in solution exerts an influence on the value of η. Figure 1.4, Chap. 1 provides an estimate about the order of magnitude of this effect. The figure displays results for sea water and a pure NaCl-solution. If one interprets the impurities in solution and suspension as dispersed inclusions with near-spherical geometry, then one may assume that also the mixture of the fluid and the tracer substances behave just like an isotropic fluid material with a shear viscosity, which is composed of the viscous properties of the bearer fluid and the geometry of the concentration and material properties of the inclusions. In the simplest case, if n denotes the volume fraction of the inclusions in the mixture, then for $n \ll 1$ one may write

$$\eta = \eta_0(1 + \phi_1 n + \phi_2 n^2 + \cdots), \tag{7.31}$$

where η_0 is the viscosity of the pure fluid and $\phi_1, \phi_2, \ldots$ parameterize the shape and material response of the suspended particles. Numerical values for ϕ_1 and ϕ_2 (where known) are listed in **Table 7.1**. Besides, it is emphasized that formula (7.31) only holds for small volume fractions and assumes that the particle shape does not assume a preferred orientation of the suspension, which would lead to an induced anisotropy of the mixture. Finally, we mention that the determination of the material properties of **solutions** and **suspensions** is a very interesting, challenging and difficult field of research of theoretical fluid mechanics, in particular theoretical rheology and material science of polymers, which was initiated for rigid spherical particles by ALBERT EINSTEIN (1879–1955).[8] If Eq. (7.27) is substituted into the balance law of linear momentum (7.8), then these equations can be written as

---

[8]Incidentally, this work has been ALBERT EINSTEIN's doctoral dissertation at the University of Zurich. His goal in this paper was the determination of the size of the sugar molecules in water solution by measuring the viscosities of the bearer fluid, η_0, and of the mixture of water plus sugar, η. If one then also knows the mass fractions of water and sugar, then one may with the simultaneous assumption of the spherical shape of the sugar molecules compute the volume fraction n of the sugar in the mixture from which an estimate for the diameter of the spheres ensues. This paper of EINSTEIN on hydrodynamics has been published *after* his pioneering publications on special relativity, BROWNian motion and photoelectric effect (for which he captured the 1921 Nobel prize) in the year 1905. The likely reason was that EINSTEIN's first version of his doctoral dissertation was not accepted for reasons of its brevity ($\sim$30 pages). EINSTEIN then prolonged it by a single additional sentence at the end. Whether the thesis was then accepted, because EINSTEIN had gained fame in the meantime, is unknown [6–8]. Interesting is also, that a computational error remained undiscovered; the amendment was published by EINSTEIN himself in 1911.

Table 7.1 Suspensions *Correction coefficients for the viscosity* (7.31)

Inclusions			ϕ_1	ϕ_2	Reference
Rigid spheres			2.5	7.6	EINSTEIN (1906, 1911) [9]
					BATCHELOR & GREEN (1972) [4]
Viscous spherical droplets with viscosity η'			$2.5\dfrac{\eta' + \frac{2}{3}\eta}{\eta' + \eta}$	–	TAYLOR (1932) [29]
Long prolate circular ellipses	$\epsilon = \dfrac{a - b}{a} = 0$		2.5		
	0.2		2.36		
	0.5		2.17	–	JEFFEREY (1923) [18]
	0.8		2.04		
	1.0		2.00		
Rigid circular ellipses	$\epsilon = \dfrac{a - b}{a} = 0$		2.5		
	0.2		2.43		
	0.5		2.31	–	JEFFEREY (1923) [18]
	0.8		2.17		
	1.0		2.06		

$$
\left.
\begin{cases}
\dfrac{\partial(\rho \boldsymbol{v})}{\partial t} + \mathrm{div}\,(\rho \boldsymbol{v} \otimes \boldsymbol{v}) \\[2mm]
\rho \dfrac{\mathrm{d}\boldsymbol{v}}{\mathrm{d}t} \\[2mm]
\rho\left(\dfrac{\partial \boldsymbol{v}}{\partial t} + (\mathrm{grad}\,\boldsymbol{v})\boldsymbol{v}\right) \\[2mm]
\rho\left(\dfrac{\partial \boldsymbol{v}}{\partial t} + \mathrm{grad}\,\dfrac{|\boldsymbol{v}|^2}{2} - \boldsymbol{v} \times \mathrm{curl}\,\boldsymbol{v}\right)
\end{cases}
\right\}
$$
$$
= -\mathrm{grad}\ p + \mathrm{grad}\,(\zeta \mathrm{div}\,\boldsymbol{v}) + 2\mathrm{div}\,(\eta \boldsymbol{E}) + \rho \boldsymbol{f}. \qquad (7.32)
$$

In this form, Eq. (7.32), complemented by the balance law of mass (3.45) are known as the **Navier-Stokes equations** of a compressible fluid. Often they are written down for the special situation that η and ζ are constants. If the fluid is density preserving,

then balance of mass reduces to div $\boldsymbol{v} = 0$ and $\boldsymbol{E} = \boldsymbol{D}$, so that the NAVIER-STOKES equations reduce to

$$\text{div } \boldsymbol{v} = 0, \qquad \rho \frac{\mathrm{d}\boldsymbol{v}}{\mathrm{d}t} = -\text{grad } p + 2\text{div }(\eta \boldsymbol{D}) + \rho \boldsymbol{f}. \tag{7.33}$$

Note that ζ does not arise. If, in addition the shear viscosity is constant, then, since

$$\text{div }(\eta \boldsymbol{D}) = \eta \text{div } \boldsymbol{D} = \frac{\eta}{2}\left(\text{div grad } \boldsymbol{v} + \text{grad div } \boldsymbol{v}\right) = \frac{\eta}{2}\Delta \boldsymbol{v}, \tag{7.34}$$

the final form of the NAVIER-STOKES equations of a density preserving fluid with constant η takes the form

$$\text{div } \boldsymbol{v} = 0, \qquad \frac{\mathrm{d}\boldsymbol{v}}{\mathrm{d}t} = -\frac{1}{\rho}\text{grad } p + \nu \Delta \boldsymbol{v} + \boldsymbol{f}. \tag{7.35}$$

In (7.34), (7.35) Δ denotes the LAPLACE operator here applied to the velocity field; $\Delta \boldsymbol{v}$ is the vector having the components $\Delta \boldsymbol{v} = (\Delta u, \Delta v, \Delta w)$. Simultaneously we defined with

$$\nu = \frac{\eta}{\rho}, \tag{7.36}$$

the so-called **kinematic viscosity** with dimension $[\nu] = [\text{m}^2\text{s}]$.

In Cartesian components equations $(7.35)_2$ take the forms

$$\begin{aligned}
\frac{\mathrm{d}u}{\mathrm{d}t} &= -\frac{1}{\rho}\frac{\partial p}{\partial x} + \nu \Delta u + f_x, \\
\frac{\mathrm{d}v}{\mathrm{d}t} &= -\frac{1}{\rho}\frac{\partial p}{\partial y} + \nu \Delta v + f_y, \\
\frac{\mathrm{d}w}{\mathrm{d}t} &= -\frac{1}{\rho}\frac{\partial p}{\partial z} + \nu \Delta w + f_x,
\end{aligned} \tag{7.37}$$

with

$$\Delta u = \frac{\partial^2 u}{\partial x^2} + \frac{\partial^2 u}{\partial y^2} + \frac{\partial^2 u}{\partial z^2}, \quad \dots, \quad \dots .$$

Finally, with the vector identity

$$\Delta \boldsymbol{v} = -\text{curl }(\text{curl } \boldsymbol{v}) + \text{grad div } \boldsymbol{v}, \tag{7.38}$$

$(7.35)_2$ can also be written in the form

$$\frac{\partial \boldsymbol{v}}{\partial t} + \text{grad }\frac{|\boldsymbol{v}|^2}{2} - \boldsymbol{v} \times \text{curl } \boldsymbol{v} = -\frac{1}{\rho}\text{grad } p - \nu \text{curl }(\text{curl } \boldsymbol{v}) + \boldsymbol{f}. \tag{7.39}$$

Here, the NAVIER-STOKES equations appear in a form, which is particularly conve-
nient for theoretical considerations. A **potential flow**, for instance, is defined by the
condition curl $\boldsymbol{v} = \boldsymbol{0}$. In such flows one reads from Eq. (7.39): *Every potential flow
is solution of the incompressible (density preserving)* NAVIER-STOKES *equations*.
Indeed, the NAVIER-STOKES equations reduce in this case to the EULER equations,
which must also be fulfilled for a potential flow.

7.1.2   Dilatant and Pseudoplastic Density Preserving Fluids

Consider a material obeying the constitutive relations (7.14), (7.16); we define **dila-
tant** and **pseudoplastic**[9] density preserving fluids as viscous fluids with the following
special properties:

- The viscous stress tensor $\boldsymbol{t}^R$ is for all time **collinear** to the stretching (strain rate)
  tensor $\boldsymbol{D}$

$$\boldsymbol{t}^R = 2\eta\boldsymbol{D}. \tag{7.40}$$

  Differently expressed, this means that $\boldsymbol{t}^R$ and $\boldsymbol{D}$ as symmetric rank-2 tensors
  possess the same principal axes.
- The effective viscosity η, which, according to (7.16), may depend on the invariants

$$\operatorname{tr}\boldsymbol{D}(= 0), \qquad \tfrac{1}{2}\operatorname{tr}\boldsymbol{D}^2 \qquad \det\boldsymbol{D}$$

  of the tensor $\boldsymbol{D}$, in fact only depends on the second invariant (but not on the third)
  and possibly also on the temperature T (and the density ρ)

$$\eta = \hat{\eta}\left(T, \rho, \tfrac{1}{2}\operatorname{tr}\boldsymbol{D}^2\right). \tag{7.41}$$

Now, in (7.40) the stress tensor $\boldsymbol{t}^R$ is represented as a function of the stretch-
ing tensor $\boldsymbol{D}$. Naturally, the inverse representation is also possible, i.e., $\boldsymbol{D}$ can be
represented as a function of $\boldsymbol{t}^R$, provided this inversion is conceptually possible:

$$\boldsymbol{t}^R = 2\hat{\eta}(T, \rho, II_{\boldsymbol{D}})\boldsymbol{D}, \quad \boldsymbol{D} = \tfrac{1}{2}\hat{f}(T, \rho, II_{\boldsymbol{t}^R})\boldsymbol{t}^R, \tag{7.42}$$

in which

$$II_{\boldsymbol{D}} = \frac{1}{2}\operatorname{tr}\boldsymbol{D}^2, \qquad\qquad II_{\boldsymbol{t}^R} = \frac{1}{2}\operatorname{tr}(\boldsymbol{t}^R)^2.$$

---

[9]In the literature, pseudoplastic behavior is also known as **shear thinning** behavior, because the
effective viscosity decreases with increasing shear stress. This effect occurs because e.g. in poly-
mers the structure of the entangling of the molecules changes under deformation. For this reason
pseudoplastic materials are in German also called structurally viscous materials.

The function $\hat{f}(\cdot)$ is an inverse viscosity and is called **fluidity**. Now, one may be faced with the problem to determine the inverse representation $(7.42)_2$ if $(7.42)_1$ is known or vice versa. In the general case when $\hat{f}(\cdot)$ and $\hat{\eta}(\cdot)$ depend on T or ρ or both, this is not possible. However, if one assumes that either the effective viscosity or the fluidity can be product decomposed in the following form:

$$\hat{f}(\rho, T, II_{t^R}) = A(\rho, T)F(II_{t^R}), \tag{7.43}$$

then with the help of $(7.42)_2$ and (7.43) one can derive

$$II_D = \tfrac{1}{2}\text{tr}\,\boldsymbol{D}^2 = \tfrac{1}{2}\text{tr}\left(\tfrac{1}{4}A^2(\rho, T)F^2(II_{t^R})(\boldsymbol{t}^R)^2\right)$$
$$= A^2(\rho, T)\underbrace{\tfrac{1}{4}F^2(II_{t^R})II_{t^R}}_{\phi(II_{t^R})} = A^2(\rho, T)\phi(II_{t^R}), \tag{7.44}$$

from which one can define

$$II_{t^R} = \phi^{-1}\left(\frac{II_D}{A^2(\rho, T)}\right), \tag{7.45}$$

provided $\phi(\cdot)$ is invertible. Alternatively, by use of $(7.42)_1$ one may analogously derive the relation

$$II_{t^R} = 4\hat{\eta}^2(\rho, T, II_D)II_D, \tag{7.46}$$

so that (7.44) takes the form

$$II_D = \underbrace{A^2(\rho, T)\tfrac{1}{4}F^2(II_{t^R})4\hat{\eta}^2(\rho, T, II_{t^R})}_{=1} II_D,$$

which, interpreted as an identity, implies for $\hat{\eta}(\cdot)$ the representation

$$\hat{\eta}(\rho, T, II_D) = \frac{1}{A(\rho, T)F(II_{t^R})} = \frac{1}{A(\rho, T)F\left(\phi^{-1}\left(\dfrac{II_D}{A^2(\rho, T)}\right)\right)}. \tag{7.47}$$

This formula represents the intended inversion. It may be recognized that, even though the fluidity was expressed in product form, such a product form does not hold in general in the inverse relation. If (7.43) has no temperature and density dependence, one may set $A = 1$ and then obtains from (7.47)

$$\hat{\eta}(II_D) = \frac{1}{F\left(\phi^{-1}(II_D)\right)}, \tag{7.48}$$

from which the inversion is evident.

Similarly, to (7.43), one may also suppose a product decomposition for the viscosity,

$$\hat{\eta}(\rho, T, II_{\boldsymbol{D}}) = B(\rho, T)\mu(II_{\boldsymbol{D}}), \tag{7.49}$$

and then may derive in an analogous way that

$$\hat{f}(\rho, T, II_{t^R}) = \frac{1}{B(\rho, T)\left(\psi^{-1}\left(\dfrac{II_{t^R}}{B^2(\rho, T)}\right)\right)}, \tag{7.50}$$

where ψ^{-1} is the inverse function of ψ, which is given by

$$\psi(II_{\boldsymbol{D}}) = \mu^2(II_{\boldsymbol{D}})II_{\boldsymbol{D}}. \tag{7.51}$$

Analogously as above, when the effective viscosity is given in product form, then the fluidity may not have product form. This is only so, if the creep response functions $F(II_{t^R})$ or $\mu(II_{\boldsymbol{D}})$ are power laws. We leave this proof to the reader.

In a simple shear test, see Fig. 7.1, t^R and $\boldsymbol{D}$ are given by the single components τ and $\dot{\gamma}/2$, respectively

$$t^R = \begin{pmatrix} 0 & \tau & 0 \\ \tau & 0 & 0 \\ 0 & 0 & 0 \end{pmatrix}, \quad \boldsymbol{D} = \begin{pmatrix} 0 & \dot{\gamma}/2 & 0 \\ \dot{\gamma}/2 & 0 & 0 \\ 0 & 0 & 0 \end{pmatrix}, \tag{7.52}$$

so that

$$(t^R)^2 = \begin{pmatrix} \tau^2 & 0 & 0 \\ 0 & \tau^2 & 0 \\ 0 & 0 & 0 \end{pmatrix}, \quad II_{t^R} = \tau^2,$$

$$\tag{7.53}$$

$$\boldsymbol{D}^2 = \begin{pmatrix} \dot{\gamma}^2/4 & 0 & 0 \\ 0 & \dot{\gamma}^2/4 & 0 \\ 0 & 0 & 0 \end{pmatrix}, \quad II_{\boldsymbol{D}} = \dot{\gamma}^2/4.$$

Therefore, the laws (7.42) take the forms

$$\tau = 2\hat{\eta}(\rho, T, \dot{\gamma}^2/4)\frac{\dot{\gamma}}{2}, \qquad \dot{\gamma} = \hat{f}(\rho, T, \tau^2)\tau^2, \tag{7.54}$$

$$\tau = 2B(\rho, T)\mu(II_{\boldsymbol{D}})\frac{\dot{\gamma}}{2}, \qquad \frac{\dot{\gamma}}{2} = \frac{1}{2}A(\rho, T)F(II_{t^R})\tau^2,$$

and agree functionally with Eq. (7.3). Dilatant and pseudoplastic fluids are materials which belong to the class (7.54). They are exclusively determined by the characteristics of the creep curves, see **Fig. 7.9**, in which the shear stress τ is plotted against

shear rate $\dot{\gamma}$. Dilatant fluids show a convex creep curve; pseudoplastic fluids, however, exhibit concave creep curves. The slope of the secant from the origin $(\tau, \dot{\gamma}) = (0, 0)$ to a general point of the creep curve yields the numerical value of the **effective viscosity** at that point.

Of special significance is the behavior of the creep curve in the vicinity of small stress or small shearing. If the creep curve possesses a finite inclination, then $\eta_0 = \hat{\eta}(\rho, T, 0) < \infty$; the material exhibits at small stress or small stretching NEWTONian behavior, according to which

$$\tau = \eta_0 \dot{\gamma} \quad \text{or} \quad \dot{\gamma} = f_0 \tau.$$

If, however, this slope is infinitely large, then the fluid exhibits an infinitely large viscosity, $\eta_0 = \infty$ or fluidity zero, $f_0 = 0$. This case occurs very often in mathematical fits of data of pseudoplastic fluids. This is also the reason why the material law is often given in either one of the representations (7.54) or (7.42) to be able to work with regularized functions. These laws are then often also called **finite viscosity laws** as opposed to infinite viscosity laws.

A popular material law is the **power law**. Depending upon the field of science in which it is used it is attributed to different scientists. In rheology it is attributed to[10] THOMAS GRAHAM (1850), GOY (1910), WILHELM OSTWALD ARNAND DE WAELE (1925) or MARKUS REINER (1929); in metallurgy it is called
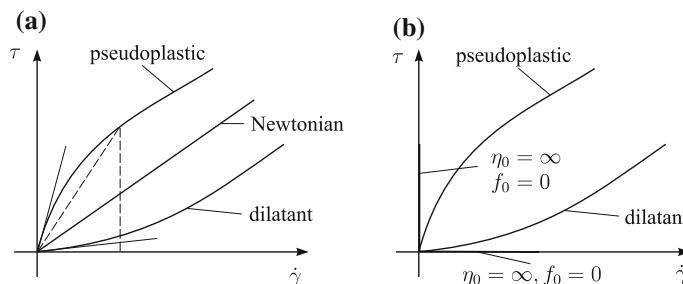
Fig. 7.9 Creep curves of various non- Newtonian fluids. **a** *The dilatant fluid behaves over-linearly, whilst a pseudoplastic fluid has an under-linear creep curve.* **b** *Behavior of a dilatant and pseudoplastic fluid in the vicinity of small stress and small stretching*

10

- THOMAS GRAHAM (1805–1869); British chemist from Glasgow, who worked on the diffusion of gases, and rheology of colloids.
- WILHELM OSTWALD (1853–1932) was a Baltic-German physical chemist who is known in rheology through his rheometer. In 1909 he won the Nobel prize in chemistry.
- ARNAND DE WAELE (1887–1966) was a British chemist noted for his contributions to rheology.
- JOHN GLEN (*1927) is a British ice physicist. His power law for the creep deformation of ice appeared in 1953 [10].

after FREDERICK HARWOOD NORTON (1896–1965) who proposed the law in 'Creep of steel at high temperature' [23] (1929), (1929) and in glaciology (cryology) it is named after John Glen (1953), who determined creep curves of polycrystalline ice for $T \in [190 - 273.13]\,^\circ\text{K}$. It possesses the form

$$f = f(T, \tau^2) = A(T)(\tau^2)^{(n-1)/2} = A(T)|\tau|^{(n-1)}, \qquad n > 1 \tag{7.55}$$

with positive monotonic function $A(T)$ and constant $n > 1$. Whereas its fluidity approaches zero as $\tau \to 0$, its viscosity

$$\eta(T, \dot{\gamma}^2/4) = \frac{1}{A(T)} \left(4\frac{\dot{\gamma}^2/4}{A^2(T)} \right)^{(1-n)/(2n)} \tag{7.56}$$

becomes infinitely large as $\dot{\gamma} \to 0$ or $\eta \to \infty$. By contrast, dilatant fluids are often described by the power law

$$\eta(T, \dot{\gamma}^2/4) = B(T) \left(\frac{\dot{\gamma}^2}{4} \right)^{(m-1)/2}, \quad m > 1$$

with positive $B(T)$ and constant $m > 1$. Whereas in this law the viscosity vanishes for vanishing stretching, $\eta(T, 0) = \eta_0 = 0$, it is the fluidity

$$f(T, \tau^2) = \frac{1}{B(T)} \left(\frac{1}{4} \frac{\tau^2}{B^2(T)} \right)^{(1-m)/(2m)},$$

which is now infinite at $\tau = 0$.

It is obviously not surprising that such singularities cause difficulties in numerical computations. To avoid these, the power law representations are replaced by formulations which lead to finite viscosities (or nonzero fluidities) at the origin of the $(\dot{\gamma}, \tau)$-plane,[11]

$$f(T, \tau^2) = A(T) \left(k + (\tau^2)^{(n-1)/2} \right), \qquad n \geq 1, \tag{7.57}$$

in which k is a constant.

For creep of polycrystalline materials one alternative suggestion to the above power law is

$$F(T, \tau) = A(T) \frac{\sinh^n(\tau/\tau_0)}{(\tau/\tau_0)}, \tag{7.58}$$

---

[11] Power law structure for the creep law is not the only condition for making the creep function an infinite viscosity law. Neither is a polynomial law with linear behavior close to small stresses or stretching the only way of regularizing the creep law. If one uses sinh laws then the $\sinh^{(n-1)/2}$-law exhibits finite viscosity behavior for $n = 1$ and infinite viscosity characteristics for $n \neq 1$. Incidentally, material scientists attribute the non-triviality of k to "diffusion creep".

where A is the rate factor, n is the exponent of the sinh-function and τ and τ_0 are octahedral shear stresses (square-root of the second invariant of the viscous stress tensor t^R) and τ_0 is a reference value of it. Such a sinh-power law with $n > 1$ is helpful when doubly-logarithmic stress-stretching curves deviate at large strain rates ($\dot{\gamma} \approx (10^{-1} - 10^1)s^{-1}$) or stresses from linearity. However, for $n > 1$ the law (7.58) has infinite viscosity at zero viscous stress. To regularize it, a NEWTONian term must be added, so that (7.58) is altered to

$$F(T, \tau) = A(T) \left\{ k + \frac{\sinh^n (\tau/\tau_0)}{(\tau/\tau_0)} \right\}. \tag{7.59}$$

Creep of isotropic polycrystalline ice has been modeled this way, see [15].

7.2 Plane Wall Bounded Shear Flows

Consider a density preserving fluid subject to steady state ($\partial(\cdot)/\partial t = 0$) and plane ($\partial(\cdot)/\partial z = 0$) flows, as shown in Fig. 7.1 as a **thin film** or **slot flow**. If the coordinate system is put into the plane of the flow with the x-axis in the wall at rest and the y-axis perpendicular to it, then the velocity field is given by

$$u = u(y), \qquad v = w = 0, \tag{7.60}$$

i.e., the single longitudinal velocity component $u(y)$. If one now restricts considerations to the NAVIER-STOKES Eqs. (7.37), a linear viscous fluid, one can easily demonstrate with the aid of (7.60) that all acceleration terms du/dt etc., vanish. If, moreover, also the specific body force vanishes ($f = 0$), it follows from Eqs. (7.37) that

$$\frac{\partial p}{\partial x} = \eta \frac{d^2 u}{dy^2}, \qquad \frac{\partial p}{\partial y} = 0, \qquad \frac{\partial p}{\partial z} = 0. \tag{7.61}$$

The last two equations state that the pressure is at most a function of x; consequently, the partial derivatives of the pressure in (7.61) can be replaced by the total derivatives, so that $(7.61)_1$ can be written as

$$\underbrace{\frac{dp}{dx}}_{\text{function of } x} = \underbrace{\eta \frac{d^2 u}{dy^2}}_{\text{function of } y}. \tag{7.62}$$

The left-hand side of this equation is only a function of x, whereas the right-hand side is a function of y only. Thus, the two functions can only be equal to one another if they are constant,

$$\frac{dp}{dx} = c, \qquad \eta \frac{d^2 u}{dy^2} = c, \qquad c = \text{constant}. \tag{7.63}$$

If one knows the pressure at two distinguished positions, which lie a distance l apart as shown in **Fig. 7.10**, then c is given by

$$c = \frac{p_2 - p_1}{l},$$ (7.64)

and Eq. $(7.63)_1$ can be integrated to

$$p = p_1 + \frac{p_2 - p_1}{l} x.$$ (7.65)

Similarly, integration of equation $(7.63)_2$ leads to

$$u(y) = \frac{p_2 - p_1}{2\eta l} y^2 + C_1 y + C_2$$ (7.66)

with constants of integration C_1 and C_2, which can be determined by satisfying the boundary conditions

$$u(0) = 0 \quad u(h) = u_w.$$

This yields
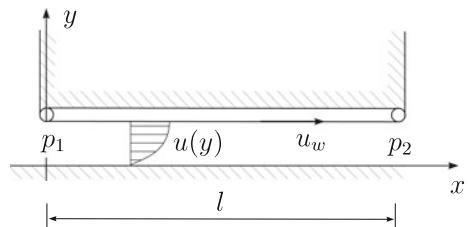
$$C_1 = \frac{u_w}{h} - \frac{p_2 - p_1}{2\eta l} h, \quad C_2 = 0,$$ (7.67)

and substitution of these into (7.66), finally yields

$$u(y) = \frac{p_2 - p_1}{2\eta l} h^2 \left(\left(\frac{y}{h}\right)^2 - \frac{y}{h} \right) + \frac{u_w}{h} y.$$ (7.68)

Thus, the velocity distribution in the slot is determined, if the pressure difference $p_2 - p_1$ and the conveyer velocity u_w are known. Because of the dependence of (7.68) on $p_2 - p_1$ and u_w, such plane wall bounded shear flows are known as **pressure-drag flows**. By substitution of Eq. (7.68) into the relation $\tau = \eta \mathrm{d}u/\mathrm{d}y$ the shear stress distribution $\tau(y)$ can be computed including the boundary values $\tau(0)$ and $\tau(h)$:

Fig. 7.10 Plane wall bounded shear flows (flows through a slot) *Possible realization of a pressure-drag flow with an ideal conveyer belt driving the motion*

$$\tau(y) = \eta \left\{ \frac{u_w}{h} + \frac{p_2 - p_1}{2\eta\, l} h \left(2\frac{y}{h} - 1 \right) \right\},$$

$$\tau(0) = \eta \left\{ \frac{u_w}{h} - \frac{p_2 - p_1}{2\eta\, l} h \right\}, \qquad (7.69)$$

$$\tau(h) = \eta \left\{ \frac{u_w}{h} + \frac{p_2 - p_1}{2\eta\, l} h \right\}.$$

They consist of two contributions, the shear stresses due to the motion of the wall as well as those due to the pressure gradient. If the latter vanishes, i.e., if $p_1 = p_2$, then the shear stress is constant across the slot; if $p_2 \neq p_1$ then the shear stress distribution across the slot is linear and the shear stresses at the lower wall at rest differ from those at the upper wall, which moves. For the ensuing discussion it is also advantageous to evaluate the **volume flow** Q:

$$Q = \int\limits_0^h u(y)\mathrm{d}y = h \int\limits_0^1 u(\zeta)\mathrm{d}\zeta = \frac{u_w h}{2} - \frac{p_2 - p_1}{12\eta\, l} h^3. \qquad (7.70)$$

A positive pressure gradient reduces the volume flow, a negative one enhances it. For the discussion of the various conditions of volume flow we refer to **Fig. 7.11**. First, we note that with vanishing pressure gradient the volume flow is in the same direction as the motion of the wall, $Q > 0$; the velocity profile is linear and the shear stress distribution is uniform. If the wall is at rest a positive volume flow can only arise, if $p_1 > p_2$. The fluid is in this case pressed by the higher pressure p_1 from left to right; the velocity distribution in the slot is symmetrically distributed, but the shear stress is skew-symmetric across the slot. Now, if additionally, the upper wall is moved and $p_1 > p_2$, the bulgy velocity profile is preserved with a maximum, which arises above the slot's center line and with shear stresses which are smaller in the upper part of the slot. If the maximum of the velocity profile reaches the upper wall, the shear stress vanishes there and is positive everywhere below it. On the other hand, if $p_2 > p_1$, the volume flow is only positive if the contribution due to the motion of the wall in Eq. (7.70) is larger than that due to the pressure difference. The curvature of the velocity profile is now negative and the shear stress distribution exhibits a positive gradient in the y-direction. For a given pressure difference $p_2 - p_1 > 0$ one can always reach a positive volume flow $Q > 0$ by simply adjusting u_w accordingly. In this case the arrangement of Fig. 7.10 works as a pump; it transports fluid from a lower pressure into a region of higher pressure. Such a pumping effect is e.g. applied in extrusions of plastics.

Let us generalize this steady slot flow of linearly viscous fluids to the case of a **dilatant** or **pseudoplastic fluid**. In so doing we equally start from the plane velocity distribution (7.60), but will employ the momentum balance equations from (7.10), which, on neglecting the specific volume force $\boldsymbol{f}$, reduce to the equations

$$\frac{\mathrm{d}p}{\mathrm{d}x} = \frac{\mathrm{d}\tau(y)}{\mathrm{d}y}, \qquad \frac{\partial p}{\partial y} = 0, \qquad \frac{\partial p}{\partial z} = 0. \qquad (7.71)$$

In this result we used the fact that for plane layer flows the viscous stress t^R possesses the representation $(7.52)_1$. Equation (7.71) demonstrate, as already mentioned earlier that

$$p = p_1 + \frac{p_2 - p_1}{l} x, \tag{7.72}$$

so that $(7.71)_1$ leads to the differential equation

$$\frac{d\tau(y)}{dy} = \frac{p_2 - p_1}{l} \tag{7.73}$$

for the shear stress distribution. In Eqs. (7.71)–(7.73) the material behavior is not yet included. If one now uses the constitutive relation $(7.54)_1$, but ignores a possible temperature dependence, one is led to

$$\frac{d}{dy}\left\{\eta\left[\left(\frac{1}{2}\frac{du}{dy}\right)^2\right]\frac{1}{2}\frac{du}{dy}\right\} = \frac{p_2 - p_1}{l}. \tag{7.74}$$

Subsequent computations can only be continued with an explicit constitutive relation for η, which we assume in the form

$$\eta = B\left(\frac{1}{2}\left|\frac{du}{dy}\right|\right)^{m-1}, \qquad B = \text{constant}, \tag{7.75}$$

so that (7.74) takes the form

$$\frac{d}{dy}\left\{\left|\frac{du}{dy}\right|^{m-1}\frac{du}{dy}\right\} = \alpha, \qquad \alpha = \frac{2^m(p_2 - p_1)}{Bl}, \tag{7.76}$$

which, upon a first integration, becomes

$$\left|\frac{du}{dy}\right|^{m-1}\frac{du}{dy} = \alpha y + C_1. \tag{7.77}$$

The continuation of this computation now depends on the sign of du/dy. We restrict considerations to the cases, in which $(du/dy(0))$ is positive (all situations in Fig. 7.11, except that in panel f). Then, one obtains for $du/dy > 0$, $0 \le y \le y_{\max}$ (where $y_{\max}$ is the position where the maximum velocity arises):
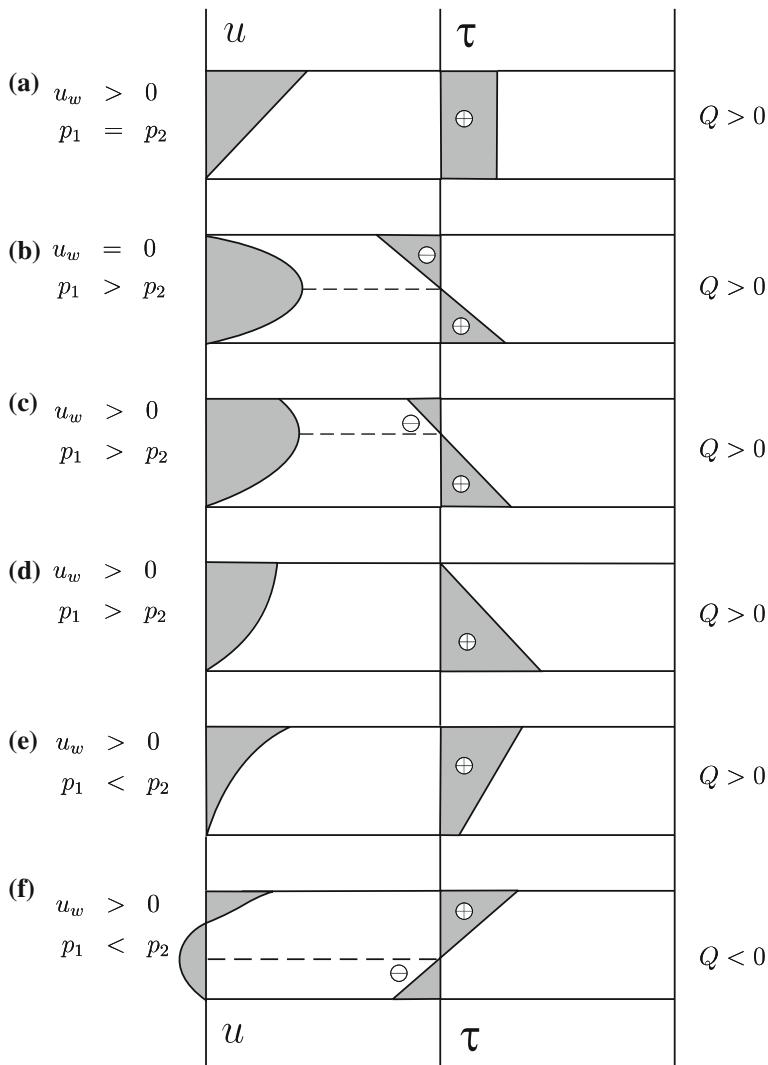
Fig. 7.11   Velocity and pressure distributions in pressure-drag flows **a** *Vanishing pressure difference.* **b** *No motion of the wall, only pressure difference.* **c** *Pressure difference and motion of the wall act in the same direction.* **d** *If wall velocity and pressure difference are properly selected, the shear stress at the moving wall can be made to vanish.* **e, f** *If the pressure gradient is negative, the curvature of the velocity profile is negative; if $Q > 0$, the pressure-drag mechanism works as a pump*

$$\frac{\mathrm{d}u}{\mathrm{d}y} = (\alpha y + C_1)^{1/m}$$

$$\longrightarrow \quad u = \frac{(\alpha y + C_1)^{(m+1)/m}}{\alpha \left(\frac{m+1}{m}\right)} + D_1 \tag{7.78}$$

$$\longrightarrow \quad u = \frac{(\alpha y + C_1)^{(m+1)/m} - C_1^{(m+1)/m}}{\alpha \left(\frac{m+1}{m}\right)},$$

where the expression in the last row of (7.78) follows from the satisfaction of the boundary condition $u(y = 0) = 0$. The location of the velocity maximum is obtained from $(7.78)_1$

$$y_{\max} = -\frac{C_1}{\alpha}. \tag{7.79}$$

- If $y_{\max} > h$, Fig. 7.11, then the unknown constant C_1, which corresponds to $(\mathrm{d}u/\mathrm{d}y)^m$ at the non-moving wall, one may evaluate C_1 from $(7.78)_3$ as follows

$$u_w \frac{m+1}{m}\alpha = (\alpha h + C_1)^{(m+1)/m} - C_1^{(m+1)/m}. \tag{7.80}$$

Its value must be determined numerically.
- If, on the other hand $y_{\max} = h$, then (7.79) implies $C_1 = -\alpha h$ and (7.80) allows evaluation of u_w as follows

$$u_w \frac{m+1}{m}\alpha = -(-\alpha h)^{(m+1)/m}. \tag{7.81}$$

Note that, since α is negative in this case, the solution for u_w from (7.81) is necessarily positive (as it must be).
- If, finally, $y_{\max} < h$, then the relations (7.78) alone do not suffice to determine the velocity profile. To the above regime one must then add a regime with $\mathrm{d}u/\mathrm{d}y < 0$.

For $\mathrm{d}u/\mathrm{d}y < 0$, $y_{\max} < y < h$, one obtains from Eq. (7.77)

$$\left(-\frac{\mathrm{d}u}{\mathrm{d}y}\right)^m = -(\alpha y + C_1)$$

$$\longrightarrow \quad \frac{\mathrm{d}u}{\mathrm{d}y} = -[-(\alpha y + C_1)]^{1/m},$$

$$\tag{7.82}$$

$$\longrightarrow \quad u = \frac{[-(\alpha y + C_1)]^{(m+1)/m}}{\alpha \left(\frac{m+1}{m}\right)} + D_2$$

$$u = u_w + \frac{[-(\alpha y + C_1)]^{(m+1)/m} - [-(\alpha h + C_1)]^{(m+1)/m}}{\alpha \left(\frac{m+1}{m}\right)},$$

in which the expression in the last line has been obtained by satisfying the boundary condition $u(h) = u_w$.

In the last step of the determination of the velocity profile one must smoothly connect the profiles $(7.77)_3$ and $(7.82)_4$ at the location $y = y_{max}$ of the velocity maximum. To this end one first sets $\alpha y_{max} + C_1 = 0$ (see (7.79)) and then obtains, by equating the two expressions for $u(y_{max})$

$$u_m \frac{m+1}{m}\alpha = (-(\alpha h + C_1))^{(m+1)/m} - C_1^{(m+1)/m}. \tag{7.83}$$

This is formally the same as (7.80). For given pressure difference, material constant α and slot width h, the constant C_1 can be computed. With this value for C_1, it then can be determined with Eq. (7.79), which of the three cases, $y_{max} > h$, or $y_{max} = h$ or $y_{max} < h$ prevails, which then determines also the velocity field $u(y)$ and the volume flux

$$Q = \int_0^h u(y)\mathrm{d}y.$$

Thus, after a number of intermediate computational steps

$$Q\frac{m+1}{m}\alpha = \begin{cases} \dfrac{m(\alpha h + C_1)^{(2m+1)/m}}{(2m+1)} - C_1^{(m+1)/m}h, & -\dfrac{C_1}{\alpha} > h, \\[4ex] -C_1^{(m+1)/m}h, & -\dfrac{C_1}{\alpha} = h, \\[4ex] \dfrac{1}{\alpha}C_1^{(2m+1)/m} - \dfrac{m}{(2m+1)\alpha} & \\ [-(\alpha h + C_1)]^{(2m+1)/m} & \\[2ex] +\dfrac{1}{\alpha}[-(\alpha h + C_1)]^{(2m+1)/m} & -\dfrac{C_1}{\alpha} < h. \\[2ex] +(m+1)/m\alpha u_w(h + \dfrac{C_1}{\alpha}), & \end{cases} \tag{7.84}$$

Let us close these somewhat complicated computations with a number of clearing remarks:

- If the pressure difference vanishes, $p_2 - p_1 = 0$, then $\alpha = 0$ and C_1 cannot be determined from (7.82), since this equation reduces to a trivial statement. However, in this case Eq. (7.77) helps, since $\mathrm{d}u/\mathrm{d}y$ remains now constant across the slot with a value u_w/h, so that

$$C_1 = \left(\frac{u_w}{h}\right)^m.$$
(7.85)

- For a NEWTONian fluid one has

$$m = 1, \quad B = 2\eta, \quad \alpha = \frac{p_2 - p_1}{\eta \, l}.$$
(7.86)

Substitution of this relation into (7.83) shows that

$$C_1 = \frac{u_w}{h} - \frac{p_2 - p_1}{2\eta l}h,$$
(7.87)

a relation, which agrees with (7.67); substitution into (7.78) and (7.84) then corroborates equations (7.68) and (7.70).

- A special case is plane flow between two parallel plates at rest. In this case, one has $u_w = 0$ and $y_{\max} = h/2$, or according to (7.79)

$$C_1 = -\frac{\alpha h}{2}$$
(7.88)

and, therefore,

$$u = \frac{(-\alpha\frac{h}{2})^{(m+1)/m}\left(\left(1 + \frac{y}{h/2}\right)^{(m+1)/m} - 1\right)}{\alpha\left(\frac{m+1}{m}\right)},$$
(7.89)

$$Q = \frac{2m}{(2m+1)\alpha^2}\left(-\alpha\frac{h}{2}\right)^{(2m+1)/m}.$$

If one substitutes here the values of (7.86) one recovers the velocity distribution and the volume flow of **plane Poiseuille flow**.

7.3   Applications

In this section, stationary flows of viscous fluids are the focus as they occur in a number of applications in engineering and the applied sciences. However, besides the technicalities of these problems, we are as much interested in the principles how the stated problems are led to their solutions.

7.3.1 Couette Viscometer

This instrument is standard for the measurement of the shear viscosity of density preserving fluids and consists of a system of two concentric cylinders of which the outer one moves whereas the inner cylinder is (in general) at rest. The gap between the cylinders is filled with a fluid. If the outer cylinder is rotated about the common concentric axis with constant circumferential speed u_w, then a stationary flow will be established in most parts of the annulus except close to the bottom and the lid of the cylinder and after transient processes have died out during the spin-up of the flow. The velocity vector then consists solely of the azimuthal component; see **Fig. 7.13**. In other words a wall bounded shear flow in layers perpendicular to the cylinder axis is formed. This configuration is called a **Couette flow** after MAURICE MARIC ALFRED COUETTE (1858–1943), a French rheologist. For his short biography see **Fig. 7.12**.

It appears to be obvious, and this will explicitly be corroborated below, that with small gap width h and compared to this large radius r_0 of the inner cylinder COUETTE flow will only marginally deviate from the plane slot flow of a NEWTONian fluid. Because of the periodicity in the azimuthal coordinate a pressure gradient $(p_2 - p_1)/l$ cannot be formed. The COUETTE flow is a pure drag flow. With $p_1 = p_2 = p_0$ the velocity in the gap grows linearly, see Eq. (7.68), from the inner radius to the outer radius $u = (u_w/h)y$, and the shear stresses are therefore constant and, according to (7.69) given by $\tau(y) = \eta\, u_w/h$. The moment acting on the inner cylinder can be computed via the shear stresses and takes the form

$$M = (2\pi\, r_0\tau)r_0 b = 2\pi\, r_0^2 b\eta\frac{u_w}{h}. \tag{7.90}$$

This axial torque must be in equilibrium with the exterior moment acting on the outer cylinder. If this latter moment is measured, then, together with the other data, the viscosity can be computed from (7.90),

$$\eta = \frac{Mh}{2\pi\, r_0^2 b u_w}. \tag{7.91}$$

In an experiment one measures M and u_w and may with these evaluate the angle of shearing $\dot\gamma = u_w/h$ and the dynamic viscosity η, thus determining experimentally the creep curve $\eta(\gamma)$.

The above analysis is based on the assumption of plane slot flow, which is only approximately correct, provided $h \ll r_0$. We now wish to test this assumption and will for this purpose start from the cylindrical geometry. If one thinks the fluid to be cut by a concentric cylinder of radius $r \in [r_0, r_0 + h]$, then on the inner boundary of this cylinder mantle the shear stresses $\tau(r)$ will act; the torque of these shear stresses about the cylinder axis will be given by

$$M(r) = 2\pi\, r^2 b\tau(r) \tag{7.92}$$
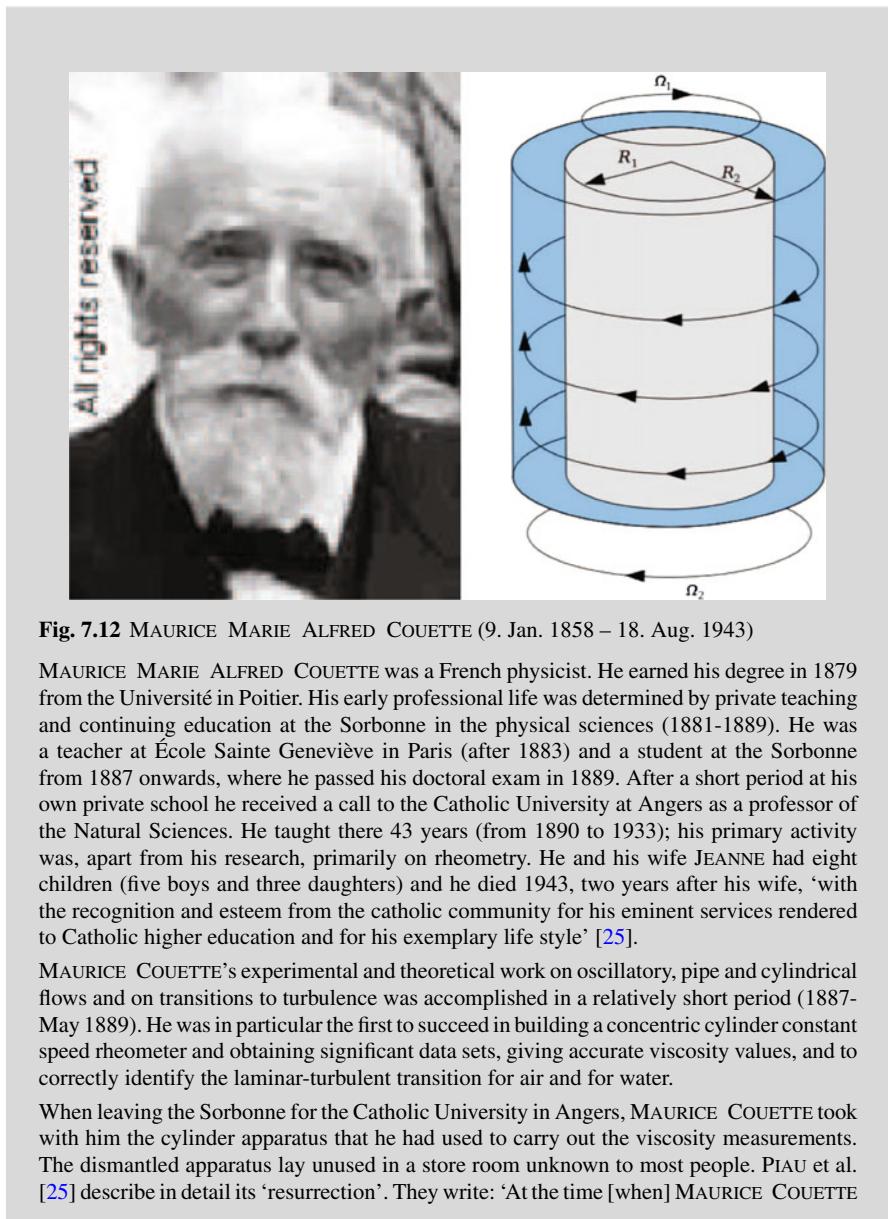
Fig. 7.12 MAURICE MARIE ALFRED COUETTE (9. Jan. 1858 – 18. Aug. 1943)

MAURICE MARIE ALFRED COUETTE was a French physicist. He earned his degree in 1879 from the Université in Poitier. His early professional life was determined by private teaching and continuing education at the Sorbonne in the physical sciences (1881-1889). He was a teacher at École Sainte Geneviève in Paris (after 1883) and a student at the Sorbonne from 1887 onwards, where he passed his doctoral exam in 1889. After a short period at his own private school he received a call to the Catholic University at Angers as a professor of the Natural Sciences. He taught there 43 years (from 1890 to 1933); his primary activity was, apart from his research, primarily on rheometry. He and his wife JEANNE had eight children (five boys and three daughters) and he died 1943, two years after his wife, 'with the recognition and esteem from the catholic community for his eminent services rendered to Catholic higher education and for his exemplary life style' [25].

MAURICE COUETTE's experimental and theoretical work on oscillatory, pipe and cylindrical flows and on transitions to turbulence was accomplished in a relatively short period (1887-May 1889). He was in particular the first to succeed in building a concentric cylinder constant speed rheometer and obtaining significant data sets, giving accurate viscosity values, and to correctly identify the laminar-turbulent transition for air and for water.

When leaving the Sorbonne for the Catholic University in Angers, MAURICE COUETTE took with him the cylinder apparatus that he had used to carry out the viscosity measurements. The dismantled apparatus lay unused in a store room unknown to most people. PIAU et al. [25] describe in detail its 'resurrection'. They write: 'At the time [when] MAURICE COUETTE

was beginning the construction of his apparatus and carrying out his first measurements, a young British researcher ARNULPH MALLOCK, who was the nephew of WILLIAM FROUDE, joined Lord RAYLEIGH's Laboratory'. His measurements, done in 1888 with a viscometer (of which the outer and inner cylinder could independently be rotated) were published in [21]. In the text of his thesis MAURICE COUETTE referred to these first British tests. He analyzed the problems of out-of-balance and end effects that had not been taken into account in the design of the apparatus' [25]. A more detailed report appeared in 1895 [21], based on measurements done between 1893 and 1895. A further analysis with MALLOCK's apparatus was also carried out by G.I. TAYLOR in 1932 [29] addressing the errors, ranging from the dimensions of the cylinders, the type of bottom, etc. These errors are all the more serious when the inner cylinder is the one that moves.

The text is based on [24] and http://www.wikipedia.org

and must, owing to conservation of moment of momentum be constant in steady motion, implying

$$M(r) = 2\pi \, r^2 b\tau(r) = 2\pi r_0^2 b\tau_0 \quad \rightarrow \quad \tau(r) = \tau_0 \left(\frac{r_0}{r}\right)^2. \qquad (7.93)$$

Contrary to plane shear flow, the shear stresses in COUETTE flow are not constant across the gap, but follow a quadratic hyperbola.

To relate the shear stresses with the shearing $\dot{\gamma}$, we consider **Fig. 7.14**; with its aid we easily deduce

$$\dot{\gamma} = \frac{\mathrm{d}u}{\mathrm{d}r} - \frac{u}{r}, \qquad (7.94)$$

so that, in view of $\tau(r) = \eta\dot{\gamma}$ we obtain

Fig. 7.13 COUETTE flow. *A density preserving viscous fluid in a cylindrical gap of height b and width h. The outer cylinder rotates with a velocity u_w, the inner cylinder is at rest. This arrangement leads to a steady velocity field, which is linearly distributed across the gap*
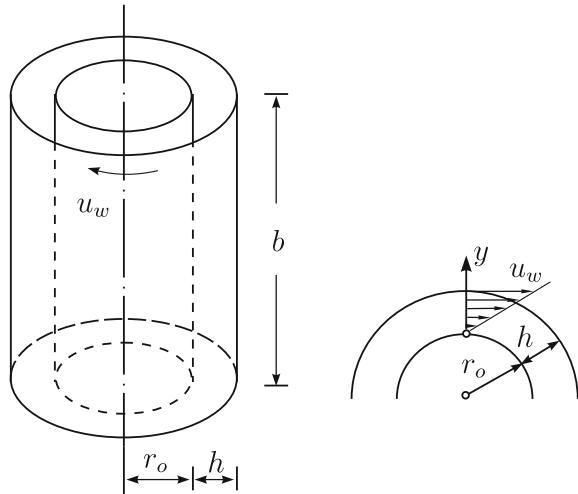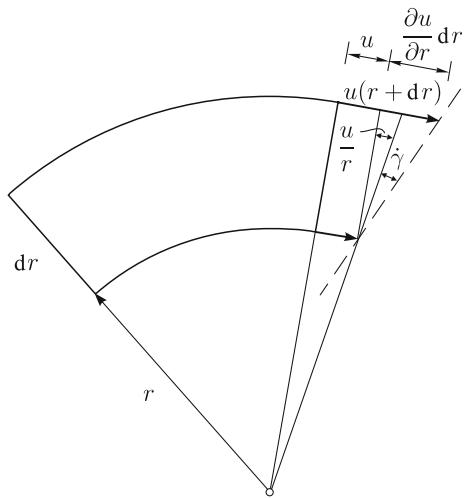
Fig. 7.14 Strain rate in cylindrical coordinates. *In configurations of flows in the azimuthal direction $\dot{\gamma}$ is composed of two contributions* (7.94)

$$\eta \left(\frac{du}{dr} - \frac{u}{r} \right) = \eta\, r \frac{d}{dr} \left(\frac{u}{r} \right) = \tau_0 \left(\frac{r_0}{r} \right)^2 . \tag{7.95}$$

For a NEWTONian fluid with constant shear viscosity η, this differential equation can be integrated and yields

$$u(r) = Cr - \frac{\tau_0 r_0^2}{2\eta\, r}, \tag{7.96}$$

with constant of integration C. The two free constants C and τ_0 are obtained from the boundary conditions

$$u(r_0) = 0 \quad \text{and} \quad u(r_0 + h) = u_w \tag{7.97}$$

yielding after straightforward computations

$$u(r) = u_w \frac{r - \frac{r_0^2}{r}}{r_0 + h - \frac{r_0^2}{r_0+h}}. \tag{7.98}$$

If one introduces the variable $y = r - r_0$ measuring the distance from the inner cylinder through the gap, then (7.98) can also be written as

$$u(r) = u_w \frac{(1 + \dfrac{y}{r_0}) - \dfrac{1}{1 + y/r_0}}{(1 + \dfrac{h}{r_0}) - \dfrac{1}{1 + h/r_0}} \simeq u_w \frac{(1 + \dfrac{y}{r_0}) - (1 - \dfrac{y}{r_0})}{(1 + \dfrac{h}{r_0}) - (1 - \dfrac{h}{r_0})} \simeq u_w \frac{y}{h}, \quad (7.99)$$

in which in several terms TAYLOR series expansion has been applied with truncation at first order since $y \ll r_0$ and $h \ll r_0$. Incidentally, the expression at the far right in (7.99) verifies the expression used earlier, namely that the assumption of a small gap width, $h \ll r_0$, reduces COUETTE flow essentially to *plane* shear flow.

7.3.2 Cone Plate Viscometer

In rheological applications a large number of different arrangements are at disposal for the determination of the effective viscosity of fluids. The cone plate viscometer, **Fig. 7.15**, consists of a (theoretically infinitely wide) cone, which stands with its tip perpendicularly on a flat non-moving plate and rotates steadily with angular velocity ω about its central axis. The space between cone and plate is filled with a viscous fluid. Under the prerequisite that the angle α between cone and plate is small ($\alpha \ll 1$), the flow in the gap at constant rotation of the cone can approximately be treated as a layered bounded plane shear flow.

At the distance r from the tip of the cone the velocity is then given by

$$u = \omega r \frac{y}{h(r)} \cong \frac{\omega y}{\alpha}, \quad (7.100)$$

in which $h(r)/r = \tan \alpha \approx \alpha$ has been used, an approximation, which satisfies the boundary conditions $u(0) = 0$ and $u(h) = \omega r$. Inspection of Fig. 7.15 shows that

$$\dot{\gamma} = \frac{\mathrm{d}u}{\mathrm{d}y} = \frac{\omega}{\alpha} = \text{const.}, \quad (7.101)$$
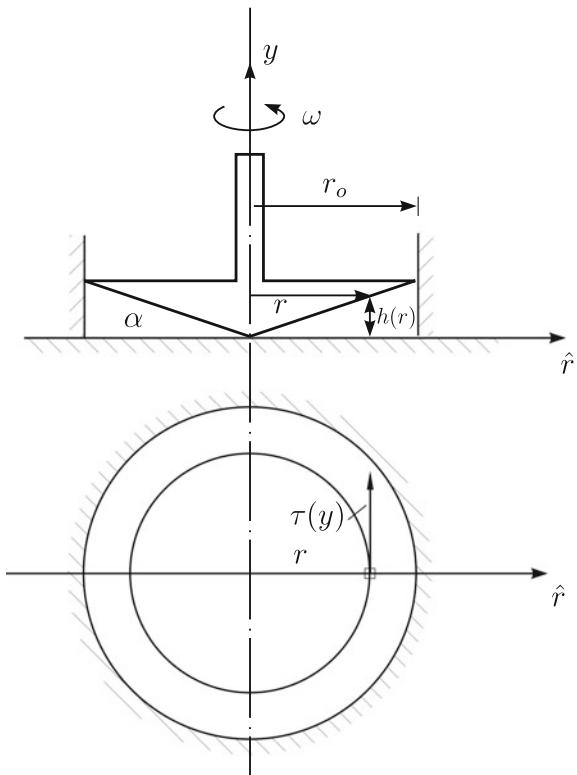
implying that the azimuthal shear stress in the fluid is given by

$$\tau = \eta \dot{\gamma} = \eta \frac{\omega}{\alpha}, \quad (7.102)$$

which is constant in every point of the fluid. In particular, these shear stresses apply in every point of the cone surface and can be summed to evaluate the torque with respect to the rotation axis,

$$M = \int_A \tau(r)\, r\, \mathrm{d}A = 2\pi \eta \frac{\omega}{\alpha} \int_0^{r_0} r^2 \mathrm{d}r = \frac{2\pi}{3} r_0^3 \eta \frac{\omega}{\alpha}, \quad (7.103)$$

Fig. 7.15 Cone and plate viscometer. *In the gap between a plate and a cone rotating about a vertical axis a viscous fluid is positioned and is kept in motion by the rotation of the cone; in the ideal case it moves along circles. The fluid in the annulus of radius r and width* dr *experiences a shearing, because its velocity vanishes at the plate owing to the no-slip condition. On the cone it assumes the velocity u = rω and varies linearly across the gap*

which can also be written as
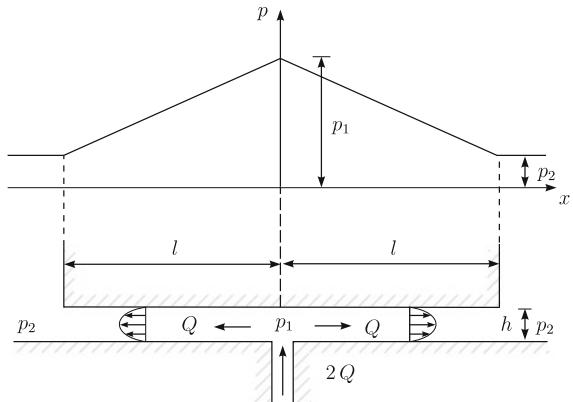
$$M = \frac{2\pi}{3} r_0^3 \tau \quad \longrightarrow \quad \tau = \frac{3M}{2\pi r_0^3}. \tag{7.104}$$

In a shear test, the moment M and the angular velocity ω are measured. With these and with (7.101), (7.103), and (7.104), $\dot{\gamma}$, τ and η can then be determined, so that the creep curves $\eta(\dot{\gamma})$ or $\eta(\tau)$ are equally fixed.

7.3.3 Hover Craft or Oil Pressure Cushion

Consider a plane floor and a homogeneous, rectangular block placed on the floor, both having smooth contact surfaces. Assume that between floor and block a small gap of width h is kept by steadily pressing a density preserving fluid (oil) through a vertical slit from below. The fluid in the slot between the basal surface of the block and the bottom surface is pressed out by the load of the block, but compensated and

Fig. 7.16 Hover craft. *A rectangular block is pressed with a force F_N against a plane. The gap between the two contacting surfaces is filled with a viscous fluid, which is pressed out of the gap, right and left, but continuously fed from below to maintain steady conditions. The pressure at the top of the slit is p_1; the outside pressure is p_2 and the total volume flow is $2Q$*

continuously and symmetrically fed from below, **Fig. 7.16**. In practice the oil that is pressed out and fed from below in fact circulates in a cycle, which is kept by a pump in stationary action. Here, to simplify the formulation we restrict ourselves to a plane situation. The volume flow $2Q$ is thought to be fed through a vertical slit from below; perpendicular to the plane of Fig. 7.16 the entire arrangement is (infinitely) long or closed by (ideal) frictionless walls. This width is constant and of size b. Moreover, it is assumed that the cross section of the vertical slit is small and that the height h of the gap between floor and bottom of the block is small in comparison to the depth b and half length l of the block, see Fig. 7.16, $h \ll l$, $h \ll b$.

Disregarding the immediate vicinity of the vertical slit and the outer boundaries of the gap, one may regard the flow in both half gaps as a plane layered flow with volume flux Q, which is driven by the pressure difference between the gap center and the outer space of the arrangement. The pressure loss from the interior to the exterior can be assumed to be linear, in which case the formulae of Sect. 7.2 apply. If the block is at rest, $u_w = 0$, Eq. (7.70) gives the pressure difference

$$p_1 - p_2 = \frac{12\eta \, l Q}{h^3 b}. \tag{7.105}$$

The total vertical force exerted by the block on the fluid in the gap is in equilibrium with the sum of the distributed pressure. Because of linearity, we obtain for this pressure force

$$F_N = \frac{p_1 - p_2}{2} 2bl = \frac{12\eta l^2}{h^3} Q. \tag{7.106}$$

The smaller the gap width h is, the larger will be the force F_N. The block, thus can be pressed against the floor, it will never touch it.

Of course, with growing load, it will increasingly become difficult to maintain a constant volume flow Q. To determine this dependence, let us compute the power

of working, L, of the pumps generating the volume flow $2Q$. The latter was already determined in Chap. 3, formula (3.185), and one obtains in the present case

$$L = 2Q(p_1 - p_2), \tag{7.107}$$

or, if Eqs. (7.105) and (7.106) are used

$$L = \frac{h^3}{6\eta l^3 b} F_N^2 = \frac{12\eta l}{bh^3}(2Q^2). \tag{7.108}$$

According to the first formula the power of working of the pumps, L, grows for fixed gap width h with the square of the normal force F_N. Alternatively, for given normal force F_N, the power of working is the smaller, the smaller the gap width, the larger the dimensions of the body, l and b, and the larger the viscosity η of the applied fluid are. However, if the power of working is measured relative to the volume flow, the second of the formulae (7.108) shows that with constant volume flow the power decreases with the third power of the gap width, h. One knows generally the force F_N and therefore needs relation $(7.108)_1$.

If the body is at rest, no resultant tangential shear force will act, since the shear stresses in the two halves of the gap are pointing in opposite directions. If one assumes instead that for some reason the body is moving with velocity u_w to the right, then, in view of Eq. $(7.69)_3$, the additional shear stresses

$$\tau = \eta \frac{u_w}{h} \tag{7.109}$$

apply at the lower bottom and point toward left, which can be summed to the tangential frictional force

$$F_w = \tau\, 2lb = 2lb\eta \frac{u_w}{h}. \tag{7.110}$$

With the aid of (7.106) and (7.110) an **effective drag coefficient** μ can be computed as the ratio of the tangential and normal forces,
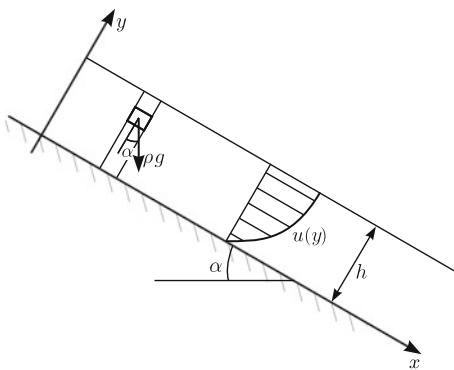
$$\mu = \frac{F_w}{F_N} = \frac{bh^2}{6Ql} u_w. \tag{7.111}$$

Interestingly, this drag coefficient does not depend upon the viscosity of the fluid. It is proportional to u_w and inversely proportional to Q and can be made arbitrarily small by increasing the volume flow and decreasing the value of the longitudinal velocity u_w.

This result of fluid friction stands in utmost contrast to the dry, so-called **Coulomb**[12] **friction**, for which the drag coefficient μ depends upon the surface roughness of the contacting surfaces and is explicitly independent of the velocity

[12]For a short biography of COULOMB see Fig. 13.8 in Vol. 2, Chap. 13.

Fig. 7.17 Plane film flow. *The stationary plane flow of a density preserving viscous fluid subject to its own weight performs a simple shear flow*

u_w. The drag force is then always proportional to the normal force. This is not so for fluid friction, for which small velocity u_w also yields small drag resistance. Such oil-pressure cushions or hover or air-craft devices are used in mechanical engineering to slowly move heavy machine tools. Incidentally, the same principle is also used in **pneumatic** or **air cushion vehicles** or hover craft, of which the motion, based on jet propulsion, does not depend on large friction.[13] Finally, we remark that the above applications were all restricted to plane flow. In engineering applications axisymmetric configurations are also important and can be treated in an analogous fashion, as can also other cases.

7.3.4 Flows of Liquid Films

All examples dealt with so far were concerned with flows for which the specific body force did not play a role and could safely be ignored. We shall now look at a situation, in which gravity plays a key role; this is always so, when the flow is induced by gravity. Let us consider the film flow displayed in **Fig. 7.17**, which is generated by the gravity force. If we again start from a plane steady layer flow, the velocity field is given by

$$u = u(y), \quad v = w = 0.$$

If, moreover, the stress components are independent of the x- and z-coordinates $(\partial(\cdot)/\partial x = \partial(\cdot)/\partial z = 0)$, which is reasonable for a fluid layer of constant depth h, then the momentum equations (7.10) in the STOKES approximation reduce to

$$\frac{\partial \tau}{\partial y} + \rho g \sin \alpha = 0, \qquad \frac{\partial \sigma_y}{\partial y} - \rho g \cos \alpha = 0, \tag{7.112}$$

---

[13]Interesting accounts on history, design and uses of hovercraft can be found in the internet.

in which $(f_x, f_y) = g(\sin \alpha, -\cos \alpha)$, and $t_{xy}^R = \tau$, $\sigma_y = -p + \tau_{yy}^R$ have been employed. The continuity equation of a density preserving material is trivially satisfied. To (7.112) a material equation for the stresses must be added, which we formulate as a non-NEWTONian fluid equation with dilatant or pseudoplastic behavior, viz.,

$$\frac{\mathrm{d}u}{\mathrm{d}y} = 2AF(\tau^2)\tau. \tag{7.113}$$

Finally, the boundary conditions

$$\sigma_y(y = h) = 0, \quad \tau(y = h) = 0, \quad u(y = 0) = 0 \tag{7.114}$$

must be satisfied. The first two of these express stress free conditions of the free surface, the third formulates no-slip at the basal surface. Equations (7.112), subject to the boundary conditions (7.114) can be integrated, which yields

$$\tau(y) = \rho g \sin \alpha(h - y), \quad \sigma_y(y) = -\rho g \cos \alpha(h - y), \quad 0 \le y \le h. \tag{7.115}$$

These formulae show that in a stationary plane film flow the stress distribution is independent of the material behavior. This material law is only visible in the velocity profile. Indeed, by integration of (7.113), the downslope velocity distribution takes the form
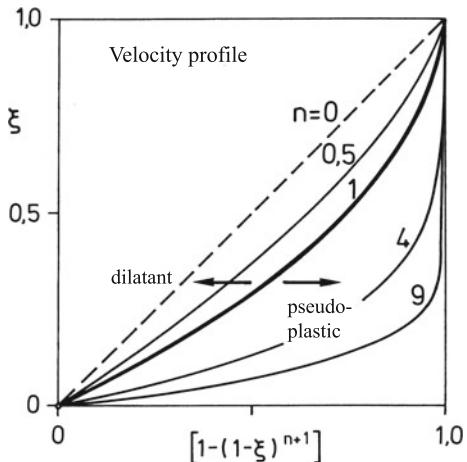
$$u(y) = 2A \int_0^y F(\tau^2(\bar{y}))\tau(\bar{y})\mathrm{d}\bar{y}, \tag{7.116}$$

which satisfies the no-slip condition. If one uses the power law $F(x) = x^{(n-1)/2}$ one easily deduces from (7.115) and (7.116)

$$
\begin{aligned}
u(y) &= 2A \int_0^y \tau^n(\bar{y})\mathrm{d}\bar{y} \\
&= 2A(\rho g \sin \alpha)^n \int_0^y (h - y)^n \mathrm{d}y \\
&= -\frac{2A(\rho g \sin \alpha)^n}{n + 1} \left[(h - y)^{n+1} - h^{n+1}\right], \\
&= -\frac{2A(\rho g \sin \alpha)^n h^{n+1}}{n + 1} \left[\left(1 - \frac{y}{h}\right)^{n+1} - 1\right],
\end{aligned}
\tag{7.117}
$$

see **Fig. 7.18**. One can easily verify that the velocity field has at $y = h$ a vanishing tangent, i.e., $u(y)$ approaches the free surface perpendicularly to the latter (except when $n = 0$). Moreover, it has for fixed y and $n > 0$ a slope which grows with

Fig. 7.18 Plane film flow. *Velocity profiles of dilatant and pseudoplastic fluids, in which the power law $\dot{\gamma} = \text{const.} \times \tau^n, n > 0$ holds*
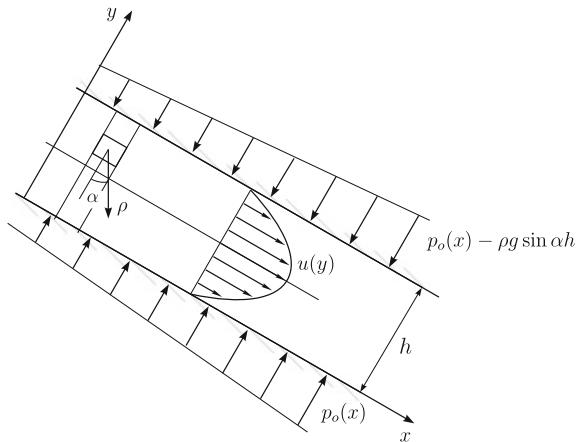
increasing y, and, as $n \to \infty$ it approaches **plug flow** for all $y \in (0, h]$ and a non-vanishing sliding velocity for $y = 0$. Dilatant and pseudoplastic velocity profiles are separated by the quadratic velocity profile of the NEWTONian fluid ($n = 1$)

$$u(y) = -\frac{\rho g \sin \alpha h^2}{2\eta} \left[\left(1 - \frac{y}{h}\right)^2 - 1 \right], \qquad (7.118)$$

where $A = (4\eta)^{-1}$ has been substituted. Pseudoplastic fluids have velocity profiles, which are bulgier than those of a NEWTONian fluid, whilst dilatant fluids are less belly. This may be used experimentally to determine numerical values for n.

Fig. 7.19 Plane POISEUILLE flow. *The weight of the fluid does not influence the velocity profile but the value of the maximum velocity*

7.3.5   Influence of the Weight of a Fluid in Plane Poiseuille Flow

Let us look at a plane layer flow between two parallel plates inclined by the angle α, see **Fig. 7.19**, and a distance $h = $ const. apart. This time, we wish to include in the momentum equation the gravity force as well as the longitudinal pressure gradient. With the assumption of steady state flow the momentum equations in the x- and y-directions read

$$
\begin{aligned}
-\frac{\partial p}{\partial x} + \frac{\partial \sigma'_x}{\partial x} + \frac{\partial \tau}{\partial y} + \rho g \sin \alpha = 0, \\
\frac{\partial \tau}{\partial x} - \frac{\partial p}{\partial y} + \frac{\partial \sigma'_y}{\partial y} - \rho g \cos \alpha = 0.
\end{aligned}
\tag{7.119}
$$

Here, the pressure and the viscous stresses are separately introduced, and the notation $t^R_{xx} = \sigma'_x, t^R_{yy} = \sigma'_y, t^R_{xy} = \tau$ has been used. Because of the assumption of plane layer flow, $u = u(y)$, $v = w = 0$, and the constitutive assumption $t^R = 2\eta(II_D)D$ for the viscous stresses the viscous normal stresses vanish, $\sigma'_x = \sigma'_y = 0$, whereas for τ one has the well-known relation

$$
\tau = \eta \frac{du}{dy}.
\tag{7.120}
$$

The shear stress is merely a function of y. Therefore, Eq. (7.119)$_2$ reduces to

$$
\frac{dp}{dy} = -\rho g \cos \alpha \quad \longrightarrow \quad p = -\rho g (\cos \alpha) y + p_0(x)
\tag{7.121}
$$

and can straightforwardly be integrated with p_0 as a 'function of integration'. It can be interpreted as the pressure that is exerted by the lower plate onto the fluid. From (7.119)$_1$ we therefore have

$$
\frac{d\tau}{dy} = -\left(\rho g \sin \alpha - \frac{dp_0}{dx} \right) =: -r,
\tag{7.122}
$$

or after a further integration

$$
\tau = -r(y - y_0),
\tag{7.123}
$$

in which the constant of integration, y_0, is still unknown. Incidentally, since τ can only depend on y, only a linear pressure distribution, $dp/dx = $ const. is compatible with the assumption of layer flow. Substitution of (7.123) into (7.120) yields the differential equation

$$
\frac{du}{dy} = -\frac{r}{\eta}(y - y_0),
\tag{7.124}
$$

or after a further integration

$$u(y) = -\frac{r}{\eta}\left(\frac{y^2}{2} - y_0 y\right) + u_0. \tag{7.125}$$

If we now use the boundary conditions $u(0) = u(h) = 0$ the constants of integration become

$$u_0 = 0, \qquad y_0 = \frac{h}{2}, \tag{7.126}$$

so that

$$u(y) = \frac{h^2}{2\eta}\left(\frac{\mathrm{d}p_0}{\mathrm{d}x} - \rho g \sin\alpha\right)\left(\left(\frac{y}{h}\right)^2 - \left(\frac{y}{h}\right)\right) \tag{7.127}$$

ensues. When comparing this with (7.68), the contribution to the longitudinal velocity of the longitudinal pressure gradient is lowered by the longitudinal contribution of the gravity force. The weight, thus, has qualitatively the same contribution as a negative pressure gradient. Its influence in a vertical shaft is greatest.

7.3.6 Slide Bearing Theory

Consider an axle shaft of radius r, which rotates with circumferential velocity u_w and sticks completely sealed in a bearing housing of radius $r' = r + a$. We assume a very small gap with width a between shaft and housing, $a \ll r$, so that with sufficient accuracy plane COUETTE flow can be assumed for the lubricating oil within the gap, see **Fig. 7.20**. If the shaft rotates concentrically to the housing, a current distribution is established, which is independent of the azimuth angle ϕ. In particular, the shear stress at the shaft mantle is constant along the circumference; this implies that the resulting force vanishes, and, consequently, the rotating shaft cannot carry a non-vanishing shearing force across the shaft.

Under general loads the shaft is therefore eccentrically positioned relative to the housing. If e denotes the distance of the centers of the shaft and housing, it follows from panel (b) of Fig. 7.20 that

$$r + h = r' + e \cos\phi, \tag{7.128}$$
$$h = a + e \cos\phi. \tag{7.129}$$

Hence, the gap width is a periodic even function in ϕ, depending on the eccentricity $\varepsilon = e/a$. We seek a relation between the torque M in the shaft and the shearing force K, which both depend on the circumferential speed u_w as well as on the characteristic lengths r, a and e: $M = M(u_w, r, e, a)$ and $K = K(u_w, r, e, a)$. For their determination recall the formulas for the volume flow, (7.70), and velocity,

(7.68), of NEWTONian fluids. Because of the rotational geometry here and the plane situation there, we need to employ the identification

$$\frac{p_2 - p_1}{l} = \frac{1}{r}\frac{\mathrm{d}p}{\mathrm{d}\phi},$$ (7.130)

in which $\mathrm{d}p/\mathrm{d}\phi$ is now not constant but a function of ϕ. Substituting (7.130) into (7.68) and (7.70) yields

$$u(y) = \frac{h^2}{2r\eta}\frac{\mathrm{d}p}{\mathrm{d}\phi}\left(\left(\frac{y}{h}\right)^2 - \frac{y}{h}\right) + \frac{u_w}{h}y,$$ (7.131)

$$Q = \frac{u_w h}{2} - \frac{1}{12\eta r}\frac{\mathrm{d}p}{\mathrm{d}\phi}h^3 =: \frac{u_w h_0}{2}.$$ (7.132)

Here, h_0 is a constant, not yet determined, which fixes the volume flow Q. Equation (7.132) determines

$$\frac{\mathrm{d}p}{\mathrm{d}\phi} = 6\eta r u_w \left(\frac{1}{h^2} - \frac{h_0}{h^3}\right),$$ (7.133)

from which we obtain the pressure

$$p(\phi) - p(0) = 6\eta \, r u_w \left\{ \int_0^\phi \frac{\mathrm{d}\xi}{h^2(\xi)} - \int_0^\phi \frac{h_0 \mathrm{d}\xi}{h^3(\xi)} \right\}$$
$$= 6\eta \, r u_w \left(J_2(\phi) - J_3(\phi)h_0 \right).$$ (7.134)
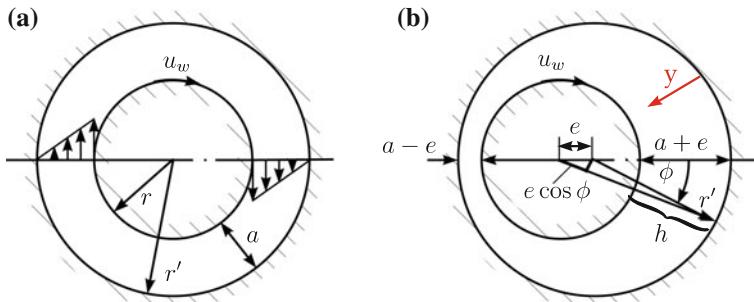
Fig. 7.20   Slide bearing **a** *A rotating shaft with circumferential velocity u_w and radius r at constant motion without load.* **b** *same as in* (**a**), *but in non-centric rotation with eccentricity e*

Table 7.2 Integrals

$$J_1 = \int_0^{2\pi} \frac{d\phi}{a + e\cos\phi} = 2\pi(a^2 - e^2)^{-1/2}$$

$$J_2 = -\frac{dJ_1}{da} = \int_0^{2\pi} \frac{d\phi}{(a + e\cos\phi)^2} = 2\pi a(a^2 - e^2)^{-3/2}$$

$$J_3 = -\frac{1}{2}\frac{dJ_2}{da} = \int_0^{2\pi} \frac{d\phi}{(a + e\cos\phi)^3} = 2\pi(a^2 + \tfrac{e^2}{2})(a^2 - e^2)^{-5/2}$$

$$J_4 = \frac{1}{e}(J_1 - aJ_2) = \int_0^{2\pi} \frac{\cos\phi\,d\phi}{(a + e\cos\phi)^2} = -2\pi e(a^2 - e^2)^{-3/2}$$

$$J_5 = \frac{1}{e}(J_2 - aJ_3) = \int_0^{2\pi} \frac{\cos\phi\,d\phi}{(a + e\cos\phi)^3} = -3\pi ea(a^2 - e^2)^{-5/2}$$

Note J_j without a written argument means evaluation for $\phi = 2\pi$. If we explicitly write $J_j(\phi)$ then $\phi \in [0, 2\pi)$

When (7.129) is used the functions J_2 and J_3 can be computed; they are given in Table 7.2. Because of the periodicity requirement $p(2\pi) = p(0)$ (7.134) implies[14]

$$J_2(2\pi) - J_3(2\pi)h_0 = 0 \quad \text{or} \quad h_0 = \frac{J_2(2\pi)}{J_3(2\pi)} = a\frac{a^2 - e^2}{a^2 + e^2/2}. \tag{7.135}$$

h_0 is that gap width for which the pressure gradient (7.133) vanishes. If this value is fixed, then (7.129) determines the angle ϕ_0 and therefore the position for which $dp/d\phi$ vanishes.

For the computation of the shear stresses we use the definition $\tau = \eta du/dy$ and apply (7.131); when evaluating τ at $y = h$ we obtain

$$\tau(h) = \eta\frac{u_w}{h} + \frac{h}{2r}\frac{dp}{d\phi} = \eta\frac{u_w}{h} + 3\eta u_w\frac{h - h_0}{h^2} = \eta u_w\frac{4h - 3h_0}{h^2}, \tag{7.136}$$
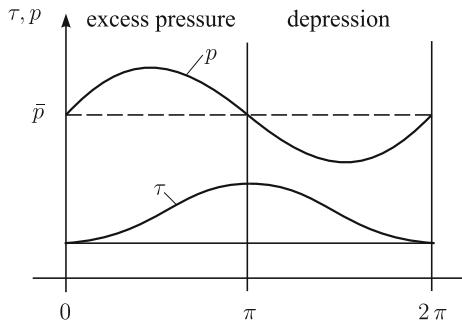
which, owing to (7.129) is an even function of $\phi : \tau(\phi) = \tau(-\phi)$. Thus, we deduce for the applied torque

$$M = \int_0^{2\pi} r\tau(\phi)r\,d\phi = \eta r^2 u_w\left\{4\int_0^{2\pi}\frac{d\phi}{h} - 3h_0\int_0^{2\pi}\frac{d\phi}{h^2}\right\}$$

$$= \eta r^2 u_w\left\{4J_1(2\pi) - 3\frac{J_2^2(2\pi)}{J_3(2\pi)}\right\}, \tag{7.137}$$

or with Table 7.2

---

[14]For the definitions of the integrals J_j, $j = 1, 2, ..., 5$ and their values see Table 7.2.

Fig. 7.21 Pressure and shear stress distribution at the periphery of the shaft. *The shear stress is a symmetric and the pressure difference a skew symmetric function of the angle ϕ from the symmetry axis*

$$M = \frac{2\pi\eta r^2 u_w a^2 + 2e^2}{\sqrt{a^2 - e^2}a^2 + e^2/2},$$ (7.138)

which, incidentally, is a function of u_w, r, e and a. For $e = 0$ one obtains the load-free concentric moment

$$M(e = 0) = \frac{2\pi\eta r^2}{a}u_w.$$ (7.139)

This torque can equally very easily be computed with the shear stress $\tau = \eta u_w/a$ that applies for the concentric position of the shaft with the housing.
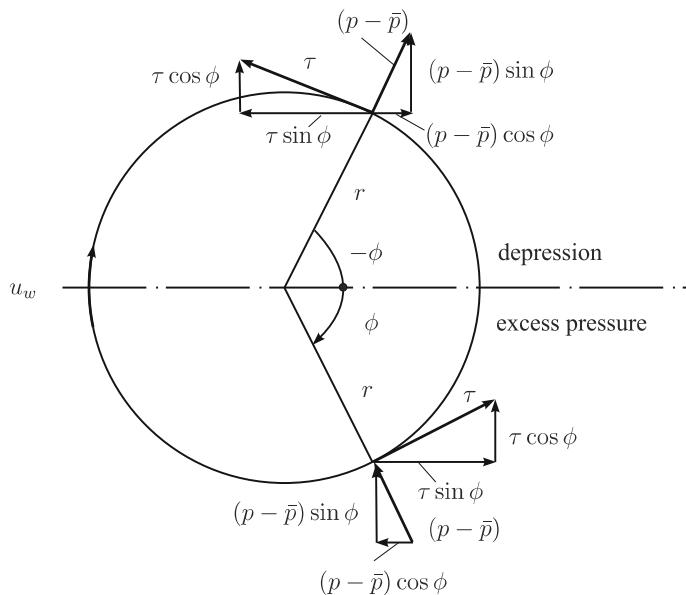
Fig. 7.22 Pressure and shear stress distribution along the periphery of the shaft

To evaluate the **shear force** of the shaft, we note that this force obtains from the totality of the shear stresses and normal pressures, which apply along the periphery of the shaft. Furthermore, we already stated above that τ is an even function of ϕ; similarly, one may become convinced that the deviation $(p - \bar{p})$, of the pressure from its mean value is an odd function of ϕ. Indeed, with (7.134) and (7.129) it follows that $\mathrm{d}\xi/h^j(\xi)$ as given in ξ for all $j = 1, 2, ..., 5$ so that $\int_0^\phi \mathrm{d}\xi/h^j(\xi)$ is odd, see **Fig. 7.21**. These properties are now used in the evaluation of the shear force K. **Figure 7.22** shows a cross section of the shaft at two surface elements on the periphery of the shaft which are symmetrically positioned from the symmetry line between the shaft and the housing at $\pm\phi$. The shear stresses, τ, and pressure differences, $p - \bar{p}$ are also shown as are their components parallel and perpendicular to the symmetry axis separating the regions of low and high pressures of the flow. Inspection of the figure shows that the horizontal components of the shear stresses and the pressure differences of the pairs of the peripheral elements cancel each other; the shearing force, therefore, cannot have a horizontal component; it is always oriented perpendicularly to the displacement of the shaft. Therefore it follows that

$$K = \int\limits_0^{2\pi} (p - \bar{p}) r \sin\phi \, \mathrm{d}\phi + \int\limits_0^{2\pi} \tau \, r \cos\phi \, \mathrm{d}\phi$$

or
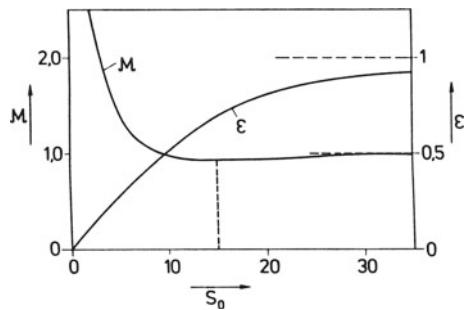
$$\frac{K}{r} = \int\limits_0^{2\pi} (p - \bar{p}) \sin\phi \, \mathrm{d}\phi + \int\limits_0^{2\pi} \tau \cos\phi \, \mathrm{d}\phi$$

$$= -(p - \bar{p})\big|_0^{2\pi} + \int\limits_0^{2\pi} \left\{ \frac{\mathrm{d}p}{\mathrm{d}\phi} + \tau \right\} \cos(\phi) \, \mathrm{d}\phi. \tag{7.140}$$

Here, the expression in the last line has been obtained using integration by parts in the first integral of the first line of (7.140). The integrated part vanishes because of the periodicity of $\cos\phi$. With the aid of (7.133) and (7.135) the remaining contributions can be eliminated:

$$\frac{\mathrm{d}p(h)}{\mathrm{d}\phi} = \mathcal{O}\left(\frac{\eta \, u_w}{h} \frac{r}{h} \right), \qquad \tau(h) = \mathcal{O}\left(\frac{\eta \, u_w}{h} \right), \tag{7.141}$$

or $\mathrm{d}p/\mathrm{d}\phi = \mathcal{O}(\tau(h) \cdot \frac{r}{h}) \gg \tau(h)$. Thus, it is permissible in the evaluation of K to ignore the contributions of the shear stresses. It then follows approximately

Fig. 7.23 Friction in
lubricated gears.
*Dimensionless torque $\mathcal{M}$
and eccentricity ε as
functions of the*
SOMMERFELD number

$$\frac{K}{r} \cong \int\limits_{0}^{2\pi} \frac{\mathrm{d}p}{\mathrm{d}\phi} \cos\phi \,\mathrm{d}\phi$$

$$= 6\eta r u_w \left(\int\limits_{0}^{2\pi} \frac{\cos\phi}{h^2(\phi)} \mathrm{d}\phi - h_0 \int\limits_{0}^{2\pi} \frac{\cos\phi}{h^3} \mathrm{d}\phi \right)$$

$$= 6\eta r u_w (J_4 - h_0 J_5) = \frac{6\eta r u_w}{a} \left(J_1 - \frac{J_2^2}{J_3} \right)$$

or

$$\frac{K}{r} = \frac{6\pi\eta\, u_w}{\sqrt{a^2 - e^2}} \frac{e}{a^2 + e^2/2}. \tag{7.142}$$

This formula can easily be put in dimensionless form as follows:

$$S_0 := \frac{K}{\eta\, u_w} \frac{a^2}{r^2} = \frac{6\pi\varepsilon}{\sqrt{1 - \varepsilon^2}\left(1 + \frac{1}{2}\varepsilon\right)}, \quad \text{where} \quad \varepsilon = \frac{e}{a}. \tag{7.143}$$

S_0 is called SOMMERFELD number[15], which is determined by the velocity u_m, the
viscosity of the lubricating oil η and the geometric quantities a and r and allows
through (7.143) evaluation of ε. If the latter is known, (7.138) and (7.143) allow
computation of the associated torque,

---

[15]ARNOLD SOMMERFELD (1868–1951), Professor of theoretical physics for decades at the University in Munich and OSBORN REYNOLDS (1842–1912), Physics Professor at Cambridge University UK, developed this theory of lubrication of gears. Theirs and other pioneers' work on the theory of hydrodynamic lubrication are collected in "Ostwalds Klassiker der exakten Wissenschaften, Vol. 218: Theorie der hydrodynamischen Schmierung" with fundamental contributions by N. PETROW, O. REYNOLDS, A. SOMMERFELD and A.G.M. MICHEL. The second treatise of this Volume of OSTWALD's classics has been edited by S. ZIMA and is published by Verlag Harri Deutsch (227 pp.) in the year 2000. ISBN 978-3-8171- 3218-8. For a brief biographical sketch of SOMMERFELD, see Vol. 2, Chap. 14, Fig. 14.5.

$$\mathcal{M} = \frac{M}{Ka} = \frac{1}{3\varepsilon} + \frac{2}{3}\varepsilon = \phi(S_0). \tag{7.144}$$

In this equation use has been made of the fact that according to (7.143) ε may be regarded as a function of S_0, which also makes $\mathcal{M}$ a function of S_0. Both relations are plotted in **Fig. 7.23**. The value of ε grows monotonically with S_0; it has the limit property that $S_0 \to \infty$ as $\varepsilon \to 1$. By contrast, $\mathcal{M} \to \infty$ as $\varepsilon \to 0$ or as $S_0 \to 0$, but $\mathcal{M}$ approaches its minimum value $\mathcal{M}_{\min} = 0.94$ at $S_0 = 15$ and slowly grows beyond this value and reaches $\mathcal{M}_\infty = 1$ as $S_0 \to \infty$. For small loads K and large velocities u_w, the eccentricity torque and even more so the scaled torque $\mathcal{M}$ depend strongly on S_0. For large loads, i.e., $S_0 > 15$, this dependence is weak.

7.4 Three-Dimensional Creeping Flow of a Pseudoplastic Fluid with Free Surface

In this section our intention is to consider a rather complex case of a pressure-drag flow which by and large can still be handled with simple analytical methods. Consider a very viscous fluid on a rigid (mainly horizontal) plate, which possesses a free surface and spreads owing to the action of gravity. Ignoring thermal effects we search for the evolution of the velocity field and the geometry of the free surface as functions of space and time.

An example of such a creep flow, which we may daily observe is the spreading of honey on the breakfast plate. Practical examples can be found in chemical and process engineering (spreading of polymers), in soil mechanics (creeping flow of
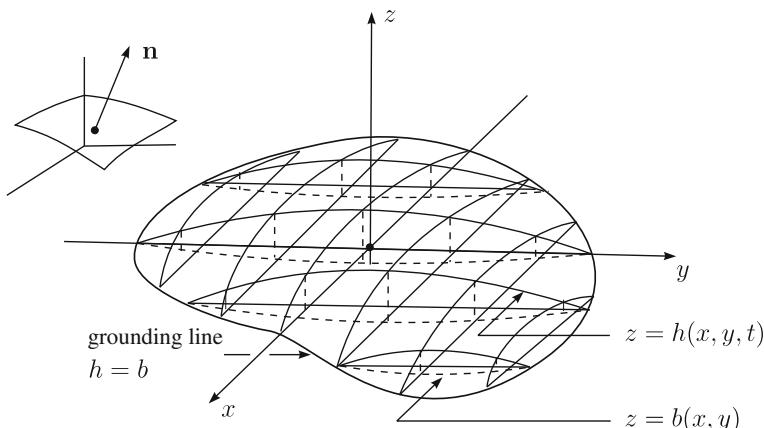
Fig. 7.24 Three dimensional pressure-drag flows with free surface. *The geometries of such deforming fluids are flat and slowly varying in the horizontal directions. The free surface $z = h(x, y, t)$ and the basal surface $z = b(x, y, t)$ bound the geometry of such fluids. Often, the basal surface is a time independent function $z = b(x, y)$ when deformations of the rock bed underneath are ignored. The exterior unit normal vector of the free surface is denoted by $\boldsymbol{n}$*

soil slopes) and geophysics (motion of ice sheets), etc. Sandy soils, which slowly deform under their own weight and thus may slowly change the landscape, can be modeled as visco-plastic fluids. Under the assumption that such soils sit on rocky, rigid ground, soil slopes can be viewed as pressure-drag flows of a pseudoplastic fluid with free surface. The motion of ice in ice sheets (Greenland, Antarctica) and glaciers subjected to varied climate conditions is another example of such flows: The motion of the ice, however, is in this case coupled with the energetic processes, because the constitutive equation for the viscous stress exhibits strong temperature dependence. We shall account for such a dependence of the viscous stress by making the phenomenological parameters such as viscosity or fluidity to depend on a scalar, or a number of scalars. The formulation of the pressure-drag approximation does not depend on the fact whether the constitutive relation for the viscous stress depends on such a scalar parameter, which may be described by separate evolution equations, e.g., the energy equation when thermal effects are of significance. In most of such cases thermodynamics, i.e., the first and second laws of thermodynamics, must be applied.

The deforming masses are long and broad and relatively flat, see **Fig. 7.24**. with the exception of the vicinity of the **margin**, where the free surface touches the basal surface (this is sometimes called **grounding line** and in glaciers **snout**), the horizontal variations of the geometry and therefore also the stresses and velocities are small. One may likely be able to ignore quantities $\partial(\cdot)/\partial x$ and $\partial(\cdot)/\partial y$ as compared to those involving $\partial(\cdot)/\partial z$ and thus can simplify the governing equations. Additionally, we suppose that the creeping motion of the masses in question is so slow that the acceleration terms (in the momentum equations, NEWTONs second law) can be ignored in comparison to the stress divergence and body force (gravity), a condition, which can be expressed in terms of a negligibly small FROUDE[16] number. This simplification is called the **Stokes assumption**. It reduces NEWTONs law to a force balance.

Let $\boldsymbol{t}$ be the CAUCHY stress tensor, which consists of the pressure and the viscous stress $\boldsymbol{t}^R$. In Cartesian coordinates with horizontal x- and y-axes and vertical z-axis (positive upward), the equilibrium conditions read

$$-\frac{\partial p}{\partial x} + \frac{\partial t_{xx}^R}{\partial x} + \frac{\partial t_{xy}^R}{\partial y} + \frac{\partial t_{xz}^R}{\partial z} = 0,$$

$$-\frac{\partial p}{\partial y} + \frac{\partial t_{yx}^R}{\partial x} + \frac{\partial t_{yy}^R}{\partial y} + \frac{\partial t_{zx}^R}{\partial z} = 0, \tag{7.145}$$

$$-\frac{\partial p}{\partial z} + \frac{\partial t_{zx}^R}{\partial x} + \frac{\partial t_{zy}^R}{\partial y} + \frac{\partial t_{zz}^R}{\partial z} = \rho g,$$

---

[16]For a short biography of FROUDE see **Fig. 7.25**.

Fig. 7.25 William Froude (28. Nov. 1810–4. May 1879)

William Froude was a British naval architect and hydro-dynamicist. Most of his work is on ship design. This led to the method of determining the minimum of the frictional force of a ship hull by model techniques, which is based upon what is now called Froude (number) similitude: i.e. invariance of the ratio of the kinetic energy to the gravitational potential energy. See, however, W.H. Hager [13] (personal communication), who argues that the denotation 'Froude number' should not be associated with Froude.
The text is based on http://www.wikipedia.org

in which ρg is the specific gravity force. These equations are complemented by the continuity equation

$$\frac{\partial u}{\partial x} + \frac{\partial v}{\partial y} + \frac{\partial w}{\partial z} = 0 \tag{7.146}$$

and the material equation (7.42) of the pseudoplastic fluid, namely

$$\boldsymbol{D} = \tfrac{1}{2} A F(II_{\boldsymbol{t}^R}) \boldsymbol{t}^R, \qquad A = A(T_\alpha), \quad \alpha = 1, 2, ..., \nu, \tag{7.147}$$

where A is a factor, which may depend on a number of parameters T_α[17] and is externally described. F is the fluidity, assumed to depend on the second viscous stress invariant. In Cartesian coordinates equations (7.147) take the forms

---

[17]E.g. T_1 the temperature; T_j, $j \geq 2$ for polycrystalline ice a parameter identifying impurities, such as dust, or a bubble parameter in a foamy material, etc.

$$\frac{\partial u}{\partial x} = \tfrac{1}{2} AF\, t^R_{xx}, \qquad \frac{\partial v}{\partial z} + \frac{\partial w}{\partial y} = AF\, t^R_{yz},$$

$$\frac{\partial v}{\partial y} = \tfrac{1}{2} AF\, t^R_{yy}, \qquad \frac{\partial w}{\partial x} + \frac{\partial u}{\partial z} = AF\, t^R_{xz}, \qquad (7.148)$$

$$\frac{\partial w}{\partial z} = \tfrac{1}{2} AF\, t^R_{zz}, \qquad \frac{\partial u}{\partial y} + \frac{\partial v}{\partial x} = AF\, t^R_{xy}.$$

Equations (7.145), (7.146), and (7.148) together form the field equations, which, together, and complemented by constitutive parameterizations for A and F determine the velocity components u, v, w, if also adequate boundary conditions are supplied.

On the basis of the assumption that the geometry of the creeping masses is flat and the variation of the topography in the horizontal direction is slow, one can assume that not only $\partial u/\partial x$ and $\partial v/\partial y$ are small in comparison to $\partial u/\partial z$ and $\partial v/\partial z$, but that $\partial w/\partial z$ is of comparable order of magnitude to $\partial u/\partial x$ and $\partial v/\partial y$ (owing to the continuity equation). Ignoring these, one may conclude from (7.148) that one can drop $t^R_{xx}, t^R_{yy}, t^R_{zz}$ and t^R_{xy} to first approximation

$$t^R_{xx} \sim 0, \quad t^R_{yy} \sim 0, \quad t^R_{zz} \sim 0, \quad t^R_{xy} \sim 0, \qquad (7.149)$$

and, second, that the right column of (7.148) reduces to the two equations

$$\frac{\partial u}{\partial z} = AF t^R_{xz} \qquad \frac{\partial v}{\partial z} = AF t^R_{yz}. \qquad (7.150)$$

The equilibrium conditions (7.145) now reduce to

$$-\frac{\partial p}{\partial x} + \frac{\partial t^R_{xz}}{\partial z} = 0, \quad -\frac{\partial p}{\partial y} + \frac{\partial t^R_{yz}}{\partial z} = 0, \quad -\frac{\partial p}{\partial z} - \rho g = 0, \qquad (7.151)$$

where in $(7.151)_3$ the fact was also used that t^R_{xz} and t^R_{yz} are slowly varying in the horizontal directions and thus can be ignored in comparison to $\partial p/\partial z$ and ρg. Note that $(7.151)_{1,2}$ have exactly the form of a pressure-drag flow and the vertical momentum (force) balance reduces to the hydrostatic pressure balance.

With the reductions (7.149) the viscous stress and its square are approximately given by

$$\boldsymbol{t}^R = \begin{pmatrix} 0 & 0 & t^R_{xz} \\ 0 & 0 & t^R_{yz} \\ t^R_{xz} & t^R_{yz} & 0 \end{pmatrix}, \quad (\boldsymbol{t}^R)^2 = \begin{pmatrix} (t^R_{xz})^2 & t^R_{xz} t^R_{yz} & 0 \\ t^R_{xz} t^R_{yz} & (t^R_{yz})^2 & 0 \\ 0 & 0 & (t^R_{xz})^2 + (t^R_{yz})^2 \end{pmatrix}, \quad (7.152)$$

so that the second invariant of $\boldsymbol{t}^R$ takes the simple approximate form

$$II_{\boldsymbol{t}^R} = \tfrac{1}{2} \left(\mathrm{tr}\, (\boldsymbol{t}^R)^2 \right) \approx (t^R_{xz})^2 + (t^R_{yz})^2. \qquad (7.153)$$

To integrate the above equations boundary conditions are needed; these are now presented, step by step along with the integration of the equations. For instance, the free surface has vanishing surface traction, if the atmospheric pressure and the wind stress at the surface are ignored. If

$$z = h(x, y, t) \tag{7.154}$$

describes the upper surface, then

$$\mathbf{n} = \frac{(-\partial h/\partial x, -\partial h/\partial y, 1)}{N} \sim (0, 0, 1), \tag{7.155}$$

$$N^2 = 1 + \left(\frac{\partial h}{\partial x}\right)^2 + \left(\frac{\partial h}{\partial y}\right)^2 \sim 1$$

defines the exterior unit normal vector, which, because of the assumption of slow variation of the geometry, $z = h(x, y, t)$ points in the positive z-direction. The condition of a stress free boundary, $\mathbf{tn} = \mathbf{0}$, implies in the assumed shallowness approximation

$$p = 0, \quad t_{xz}^R = 0, \quad t_{yz}^R = 0, \quad \text{at} \quad z = h(x, y, t). \tag{7.156}$$

Integration of (7.151), subject to these conditions at the free surface, thus implies

$$\left.\begin{array}{l} p(z) = \rho g(h - z) = \rho g H, \\[4pt] t_{xz}^R(z) = \rho g \dfrac{\partial h}{\partial x}(z - h) = -\rho g H \dfrac{\partial h}{\partial x}, \\[4pt] t_{yz}^R(z) = \rho g \dfrac{\partial h}{\partial y}(z - h) = -\rho g H \dfrac{\partial h}{\partial y}, \end{array}\right\} \quad b(x, y, t) < z < h(x, y, t), \tag{7.157}$$

in which $H(z) = (h - z)$ is the depth of the mass above the position z. This result is worth emphasizing. The pressure at the level z is equal to the weight of the column above this point. In this spirit one speaks of a **hydrostatic pressure distribution**. The shear stresses are alternatively proportional to this hydrostatic pressure with multiplying factors given by $\partial h/\partial x$ and $\partial h/\partial y$, which are small owing to the slow variation of the geometry. If one collects the stresses t_{xz}^R and t_{yz}^R to a vector $\boldsymbol{\tau} = (t_{xz}^R, t_{yz}^R)$, Eqs. (7.157)$_{2,3}$ can be written as

$$\boldsymbol{\tau} = -\rho g H \nabla_H h, \qquad \nabla_H h = \left(\frac{\partial h}{\partial x}, \frac{\partial h}{\partial y}\right), \tag{7.158}$$

where ∇_H is the two-dimensional Nabla operator. One important consequence of the above Eq. (7.158) is the fact that with a change of depth z (or H) the modulus of the shear stress will change, but not the direction. The reason for this behavior is that the orientation of $\boldsymbol{\tau}$ in the horizontal plane is given by $\nabla_H h(x, y, t)$ alone. A further property of (7.158) is that $\boldsymbol{\tau}$ points in the opposite direction of $\nabla_H h$, whose

direction is that of steepest ascent of the free surface at that location. So, τ points in the *direction of steepest descent*. Moreover, at a dome $\nabla_H h = 0$, so there are no shear stresses acting at a dome.

For the determination of the velocity distribution, recall Eqs. (7.150) and note that in view of (7.153) and (7.157)$_{2,3}$

$$\left.\begin{array}{l} \dfrac{\partial u}{\partial z} = -\rho g \dfrac{\partial h}{\partial x} A F(\tau^2) H(z), \\[2mm] \dfrac{\partial v}{\partial z} = -\rho g \dfrac{\partial h}{\partial x} A F(\tau^2) H(z), \end{array}\right\} \quad \tau^2 = -\rho^2 g^2 H^2(z) \left\{ \left(\dfrac{\partial h}{\partial x}\right)^2 + \left(\dfrac{\partial h}{\partial y}\right)^2 \right\}. \tag{7.159}$$

Provided the parameter A (the so-called rate factor) is known, the right-hand sides of (7.159) are known and integration in the z-direction is possible:

$$u(x, y, z, t) = u_b - \rho g \frac{\partial h}{\partial x} \int_0^z A(T_j(\bar{z})) F(\tau^2(\bar{z})) H(\bar{z}) \mathrm{d}\bar{z},$$

$$v(x, y, z, t) = v_b - \rho g \frac{\partial h}{\partial y} \int_0^z A(T_j(\bar{z})) F(\tau^2(\bar{z})) H(\bar{z}) \mathrm{d}\bar{z}, \tag{7.160}$$

where (u_b, v_b) are the horizontal velocity components at the basal surface. In (7.155) we have not identified the variables x, y, t, which may arise in u_b, v_b, b, $A(T_j)$, $j = 1, 2, \ldots$ and τ^2. If the basal surface is given by the equation

$$z = b(x, y, t), \tag{7.161}$$

and if the variable transformation

$$\zeta = \frac{h - z}{H_b}, \qquad H_b = h - b \tag{7.162}$$

is used, Eqs. (7.160) can be combined to the vector equation

$$\boldsymbol{u}_H(x, y, z, t) = \boldsymbol{u}_H^b$$

$$- \rho g H_b^2 \left(\int_{\zeta = H(z)/H_b}^1 A\left(T_j(\bar{\zeta})\right) F\left((\rho g H_b)^2 (\nabla_H h)^2 \bar{\zeta}^2\right) \bar{\zeta} \, \mathrm{d}\bar{\zeta} \right) \nabla_H h, \tag{7.163}$$

in which $\boldsymbol{u}_H = (u, v)$ and $\boldsymbol{u}_H^b = (u_b, v_b)$ are the horizontal velocities at depth z and the bottom surface, respectively. If at time t the geometry of the creeping mass is described and the parameters A and F are known functions of their variables, then

the horizontal velocity field in the entire shallow mass is determined, provided, of course, also the horizontal velocity field $\boldsymbol{u}_b$ at the base is known.

The vertical velocity component can be determined by use of the continuity equation from which we get

$$\frac{\partial w}{\partial z} = -\left(\frac{\partial u}{\partial x} + \frac{\partial v}{\partial y}\right) \quad \rightarrow \quad w(x, y, x, t) = w_b(x, y, t) - \int_b^z \left(\frac{\partial u}{\partial x} + \frac{\partial v}{\partial y}\right)(\bar{z})\mathrm{d}\bar{z},$$

$$(7.164)$$

in which w_b is the z-component of the basal velocity and the integrand function on the far right is the horizontal divergence of the velocity given in (7.163). With $(u, v) = \boldsymbol{u}$ and $w_b = \boldsymbol{u}_b \cdot \nabla_H h$, the vertical velocity can also be written as

$$w(x, y, z, t) = -\nabla_H \cdot \int_b^z \boldsymbol{u}(x, y, \bar{z}, t)\mathrm{d}\bar{z} = -\nabla_H \cdot \left(H_b \int_{(h-z)/H_b}^1 \boldsymbol{u}(x, y, \xi, t)\mathrm{d}\xi\right).$$

$$(7.165)$$

To find an adequate representation of the basal boundary condition, let us assume that the equation

$$\Phi(x, y, z, t) = 0$$

describes the geometry of the (possibly) moving basal surface. If it is assumed that this surface is material, so that no mass moves through it, its **kinematic equation** is given by

$$\frac{\partial \Phi}{\partial t} + (\mathrm{grad}\, \Phi) \cdot \boldsymbol{u} = 0, \tag{7.166}$$

or

$$\frac{\partial \Phi/\partial t}{\| \,\mathrm{grad}\, \Phi \,\|} + \boldsymbol{u} \cdot \boldsymbol{n} = 0 \quad \longrightarrow \quad u_\perp := \boldsymbol{u} \cdot \boldsymbol{n} = -\frac{\partial \Phi/\partial t}{\| \,\mathrm{grad}\, \Phi \,\|}, \tag{7.167}$$

where $\boldsymbol{u}$ is the three-dimensional material velocity on the surface. The normal speed is called **displacement speed** and is thus given by the function Φ. It vanishes, if the surface does not move. In the tangential direction the fluid velocity is given by

$$\boldsymbol{u}_\| := \boldsymbol{u} - (\boldsymbol{u} \cdot \boldsymbol{n})\boldsymbol{n}, \tag{7.168}$$

and the **no-slip condition** therefore states that

$$\boldsymbol{u}_\| = \boldsymbol{0} \quad \text{and} \quad u_\perp = -\frac{\partial \Phi/\partial t}{\| \,\mathrm{grad}\, \Phi \,\|}. \tag{7.169}$$

For a basal surface, which is at rest, we have $\partial \Phi / \partial t = 0$, and this simply states that all three components of the basal fluid velocity vanish. A moving surface with vanishing tangential slip is, however, characterized by

$$\boldsymbol{u}_{\parallel}^b := \boldsymbol{u}^b - (\boldsymbol{u}^b \cdot \boldsymbol{n})\boldsymbol{n} = \boldsymbol{0}, \qquad u_{\perp}^b = -\frac{\partial \Phi / \partial t}{\parallel \operatorname{grad} \Phi \parallel}. \tag{7.170}$$

It is not difficult to become convinced that for shallow geometries of the creeping fluid masses, these relations are approximated as

$$(u, v)^b = (0, 0), \qquad w = -\frac{\partial \Phi}{\partial t}. \tag{7.171}$$

Often, basal surfaces are lubricated and allow viscous sliding to take place. For material surfaces $u_{\perp}$ is then still given by $(7.169)_2$, but for $\boldsymbol{u}_{\parallel}^b$ a viscous sliding law is assumed, $\boldsymbol{u}_{\parallel}^b = \mathcal{C}\boldsymbol{\tau}_{\parallel}^b$, where $\mathcal{C}$ is a drag coefficient, which may depend on $\parallel \boldsymbol{\tau}_{\parallel}^b \parallel$ and possibly additional variables. For viscous sliding one thus has

$$\boldsymbol{u}_{\parallel}^b = \mathcal{C}\boldsymbol{\tau}_{\parallel}^b \quad \text{and} \quad u_{\perp}^b = -\frac{\partial \Phi / \partial t}{\parallel \operatorname{grad} \Phi \parallel}. \tag{7.172}$$

For slowly varying geometries in the sense that $|\partial \Phi / \partial x| \ll |\partial \Phi / \partial z|$ and $|\partial \Phi / \partial y| \ll |\partial \Phi / \partial z|$, this reduces to

$$(u, v)^b = \mathcal{C}(\tau_{xz}^b, \tau_{yz}^b) = -\mathcal{C}\rho g H_b \left(\frac{\partial h}{\partial x}, \frac{\partial h}{\partial y} \right), \quad w^b = -\frac{\partial \Phi}{\partial t}. \tag{7.173}$$

Choosing $\Phi = b(x, y, t) - z = 0$, where $b(x, y, t)$ describes the z-coordinate of the basal surface, we have
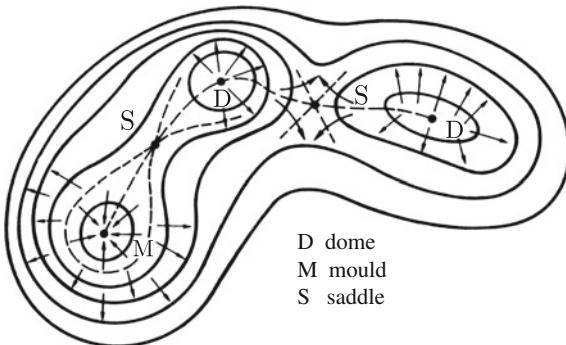
$$\frac{\partial \Phi}{\partial t} = \frac{\partial b}{\partial t}, \quad \parallel \operatorname{grad} \Phi \parallel = \left\{ 1 + \left(\frac{\partial b}{\partial x} \right)^2 + \left(\frac{\partial b}{\partial y} \right)^2 \right\}^{1/2} \overset{*}{\cong} 1 \tag{7.174}$$

for general and shallow (asterisk) geometries, respectively.

Equations (7.163)–(7.174) allow the following practical inferences, which may be corroborated by observations in laboratory experiments or in the field. Such tests allow delineation of the validity of the theory:

- In every (x, y)-position the horizontal velocity field $\boldsymbol{u}$ is proportional to the horizontal gradient $\nabla_H h$ of the topography of the free surface. Since the gradient $-\nabla_H h$ points into the direction of the steepest descent of the surface topography, the horizontal projections of the streamlines are the orthogonal trajectories of the level lines of the free surface.

Fig. 7.26 Three-dimensional pressure-drag flow with free surface topography. *The streamlines of the horizontal components of the velocity field are the orthogonal trajectories of the level lines. The flow is always away from a dome (D) and toward a trough (M, mould) and a saddle point defines a watershed*

D dome
M mould
S saddle

- Along any vertical line into the material the orientation of the horizontal projection of the velocity does not change. The graphs of the streamlines for $\boldsymbol{u}$ are in each depth (constant z) of the (x, y)-plane the same.
- A **dome**, **trough** or **saddle point** of the surface topography is located at positions of vanishing horizontal velocity components. This property again holds for all points in a vertical line (e.g. a bore hole in an ice sheet) through a dome, a trough or a saddle point, see **Fig. 7.26**. A flow is always away from a dome or toward a trough, and a saddle point marks the position of a 'watershed'. In other words, the lines of steepest ascent which connect the saddle point to the next neighboring dome separates the fluid on one side of the saddle from the fluid of the other side of the saddle. Furthermore, a trough must be filled with time, because mass flows always toward the local minimum, except, of course, if the location of the trough functions as a sink, which must be due to an artificial device.

The above results are simple deductions of Eqs. (7.163)–(7.174) and can be partly verified. In the laboratory the spreading of a mass of a very viscous fluid (oil, polymers, honey, ...) on a horizontal or slightly inclined plane can be photographed with photogrammetric techniques to measure the surface topography and its evolution. Level lines are the proper graphical means to visualize this. When the surface is also seeded by colored particles the evolution of the surface velocity can equally be measured by particle tracking velocimetry (PTV) or by particle image velocimetry (PIV) techniques, which subsequently allow determination of the streamlines. If conditions of pressure-drag flows prevail, then the streamlines and the orthogonal trajectories of the level lines are the same lines. If this agreement is satisfied, the temporal evolution of the margin of such viscous mass flows may be used to determine the creep response function $F(II_{t^R})$ as an alternative to the viscometer flow technique. This does not seem to have been done in the past.

Routine application of the three-dimensional pressure-drag flow theory is used in climatology, when the flow and the growth and retreat of large ice sheets (e.g., Greenland, Antarctica) are studied. Here, the appropriateness of the pressure-drag flow can be tested by satellite altimetry from which accurate topographic maps of today's Earth's ice sheets are known. The same photographic or altimetric technique
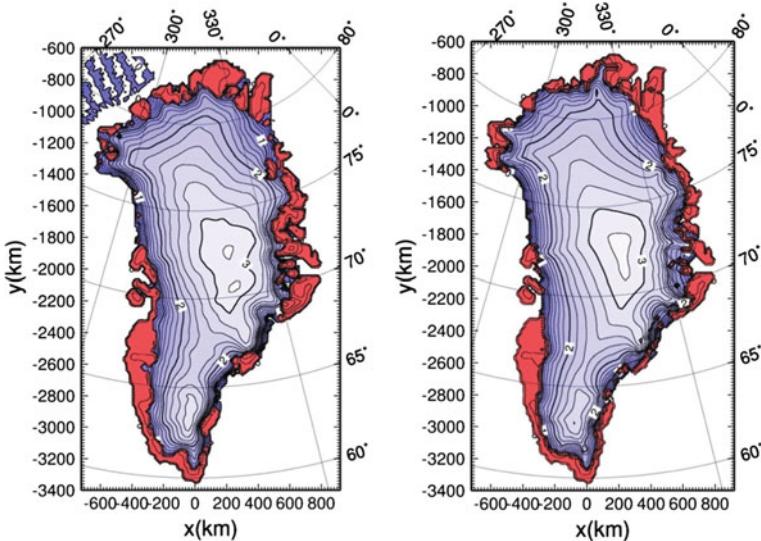
Fig. 7.27 Reproduction of today's geometry of the Greenland Ice Sheet. *As determined from measurements (left panel) and computed for steady state conditions (right panel).* • Start with today's geometry, temperature and accumulation formulations and an initial temperature of $-10\,°C$; • Perform computations subject to external boundary conditions for 10^5 years, using the shallow ice approximation. *For more details see main text.* ©*R. Greve, reproduced with permission*

by satellite also allows visualizing the surface traces of the streamlines of the ice motion. Field glaciologists have long conjectured the orthogonality of the level lines and the projections of the surface streamlines into the horizontal plane. **Figure 7.27**[18] shows the topography of the Greenland Ice Sheet, on the left for the mid 20th century (the graph is a compilation of data taken during the entire 100 years from roughly 1900 to 2000) and on the right as computed with the so called **shallow-ice approximation** (SIA),[19] which is nothing else than the pressure-drag theory, when the pseudoplastic creep law for ice is given by

$$F(II_{t^R}) = (II_{t^R})^{(n-1)/2}\,, \quad n = 3, \quad A = A_0\Theta(T), \tag{7.175}$$

---

[18]The computations for the right panel of Fig. 7.27 were performed by R. GREVE with the software SICOPOLIS, available through http://www.sicopolis.net.

[19]We propose here the denotation **Shallow Flow Approximation, SFA**, since it applies in many practical examples of geophysical and environmental fluid mechanics, e.g., in creeping flow of earth masses on mountain slopes, in certain lava flows, in deformations of salt domes, etc. The SFA is similar to the shallow water approximation (SWA), but it is not the same. We also wish to mention that there exist several variants of the SFA which differ from one another whether the flow is primarily horizontal or downhill, see the following chapter.

where the **power law** for F is called in glaciology **Glen's flow law**, whilst for cold ice (i.e., ice which does not reach the melting point) the rate factor A is a function of the absolute temperature, T. The numerical value of A_0 depends on the choice for n and $\Theta(T)$. A popular choice is the **Arrhenius law**

$$\Theta(T) = \exp\left(-\frac{Q}{kT}\right),$$

in which Q is the so-called **activation energy**, k is BOLTZMANN's constant and T the KELVIN temperature.

We see that the shallow ice approximation is a coupled field theory, in which the velocity (or the displacement) field is coupled with the temperature field. The latter is determined in the ice sheet by the heat equation of a density preserving fluid[20]

$$\left.\begin{array}{c} \rho\dfrac{\mathrm{d}\varepsilon}{\mathrm{d}t} \\[2ex] \rho\left\{\dfrac{\partial\varepsilon}{\partial t} + \dfrac{\partial\varepsilon}{\partial x}u + \dfrac{\partial\varepsilon}{\partial y}v + \dfrac{\partial\varepsilon}{\partial z}w\right\} \\[2ex] \dfrac{\partial(\rho\varepsilon)}{\partial t} + \dfrac{\partial(\rho\varepsilon)}{\partial x}u + \dfrac{\partial(\rho\varepsilon)}{\partial y}v + \dfrac{\partial(\rho\varepsilon)}{\partial z}w \end{array}\right\} = -\mathrm{div}\,\boldsymbol{q} + \mathrm{tr}\,(\boldsymbol{t}^R\boldsymbol{D}), \quad (7.176)$$

in which the left-hand sides are physically equivalent expressions for the time rate of change of the internal energy ε, and $\boldsymbol{q}$ is the heat flux vector. With the constitutive postulates

$$\varepsilon = \int_{T_0}^{T} c_p(\bar{T})\,\mathrm{d}\bar{T}, \qquad \boldsymbol{q} = -\kappa(T)\mathrm{grad}\,T. \qquad (7.177)$$

With (7.147), the heat equation takes the form

$$\rho c_p(T)\frac{\mathrm{d}T}{\mathrm{d}t} = \mathrm{div}\,(\kappa(T)\mathrm{grad}\,T) + A(T)F(II_{t^R})II_{t^R}, \qquad (7.178)$$

in which only one of the possible forms of the left-hand sides of (7.176) has been written down. The specific heat c_p, the heat conductivity $\kappa(T)$ and the rate factor $A(T)$ are prescribed functions of the temperature.

Equation (7.178) is second order in the spatial variable and thus requires prescription of boundary conditions: the surface temperature $T(z = h) = T_s(x, y, t)$ and a flux of heat through the basal surface prescribed by the geothermal heat flow. It turns out, however, that the transient thermal response of ice sheets strongly depends on the thermal coupling of the ice sheet with the solid ground, at least to a depth of about 5 km. Therefore, the heat equation in the ice sheet and in such a **lithospheric**

---

[20]This equation follows from the balance law of energy (first law of thermodynamics) and will be derived from first principles in Chap. 17 (Vol. 2), see equation (17.85).
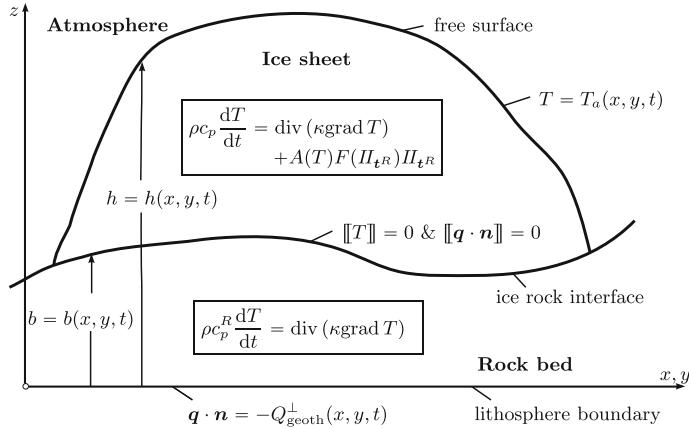
Fig. 7.28 Boundary value problem for heat flow in an ice sheet-rock bed system. *The differential equations for the temperature T in the ice sheet and a solid layer, app. 5 km thick beneath the ice sheet, are framed in boxes. At the free surface the surface temperature T_a is prescribed through the entire period for which the equations are solved (generally for $10^5 - 10^6$ years). At the ice-rock bed interface the temperature and the geothermal heat flow are continuous. At the lower boundary of the rock bed the geothermal heat flow is prescribed throughout the time of integration. For further details see main text*

layer must be solved interactively as sketched in **Fig. 7.28**. This entails formulation of boundary and transition conditions as follows

(i) at the free surface: $T(x, y, z = h, t) = T_a(x, y, t)$, at $z = h(x, y, t)$,

(ii) at the ice-rock interface: $[\![T]\!] = 0$, $[\![q \cdot n]\!] = a_\perp^b$, at $z = b(x, y, t)$,   (7.179)

(iii) $q \cdot n = -Q_{\text{geoth}}^\perp$, at $z = z_l(x, y)$.

Here, T_a is the atmospheric temperature at the free surface; it is a climatic input through space and time, for which robust parameterizations exist. $Q_{\text{geoth}}^\perp$ is the geothermal heat flow, which is often assumed to be constant, but may vary in space and time. Moreover, $[\![f]\!] = f^+ - f^-$ is the difference of f on the (+)-side and (-)-side of the ice-rock bed interface. So, $[\![T]\!] = 0$ and $[\![q \cdot n]\!] = a_\perp^b$ means that the temperature across the ice rock bed interface is continuous and the jump in heat flow equals the melting rate $a_\perp^b$, which is set to zero in Figs. 7.28 and 7.29 by assuming that no melting of ice occurs there.

The flat geometry assumption is not yet implemented in Eqs. (7.178) and (7.179), but this can easily be done by recognizing that

$$\bullet \quad \frac{\partial}{\partial x}\left(\kappa \frac{\partial t}{\partial x}\right) + \frac{\partial}{\partial y}\left(\kappa \frac{\partial t}{\partial y}\right) + \frac{\partial}{\partial z}\left(\kappa \frac{\partial t}{\partial z}\right) \approx \frac{\partial}{\partial z}\left(\kappa \frac{\partial t}{\partial z}\right),$$

- the convective changes of the temperature must be fully kept, since $(\partial T/\partial x)u$ and $(\partial T/\partial y)v$ are of the same order of magnitude as $(\partial T/\partial z)w$,
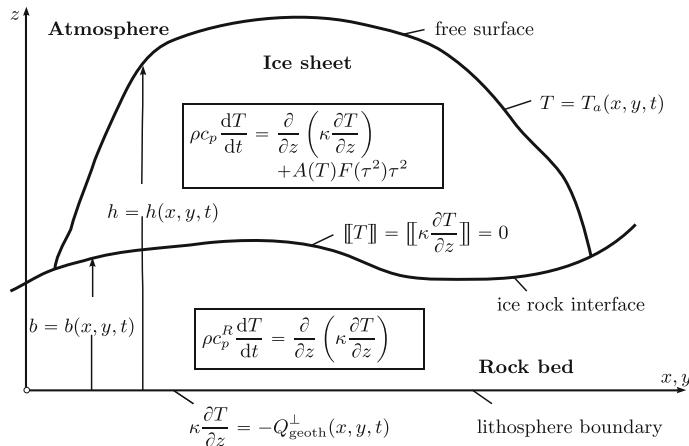
Fig. 7.29 Same as Fig. 7.28 but with simplifications of the SFA (or SIA) incorporated. τ^2 is defined in (7.159)

- $\boldsymbol{q} \cdot \boldsymbol{n} \sim -\kappa \dfrac{\partial T}{\partial z}$.

Figure 7.29 displays the approximate boundary value problem in this shallow flow approximation. The convective terms remain unchanged but diffusion in the horizontal direction is dropped and only diffusion in the vertical direction is kept. As such the partial differential equation for the temperature is of the advection-diffusion-reaction type. For the full equations displayed in Fig. 7.28 diffusion operates in all directions and the equation is fully **parabolic**. In the reduction to the shallow flow approximation diffusion in the (x, y)-directions is missing and the equation is **mixed hyperbolic-parabolic**. The thermo-mechanical coupling in the energy equation is in the last term on the right-hand side, which is the **stress power**, also called **strain-heating** term; it is a production term of heat which raises the temperature.

Finally, to be able to perform a forward integration in time, the velocity, temperature, geometry and initial conditions must be prescribed. These pertain to the

- initial geometry of the ice sheet, say $j \times 10^5$ years ago, $j \geq 1$,
- initial temperature distribution, often taken to be constant and at $-10\,°C$.

Via (7.160), (7.163), (7.164) one may compute the initial velocity distribution. This velocity field may then be substituted into the heat equation, from which the new temperature distribution can be determined, etc.

Up to now, all computed results are based on assumed knowledge of the geometry of the deforming viscous fluid masses. Along with the derived equations, these can, however, also be computed. To this end, let $\boldsymbol{u} = \boldsymbol{u}_H + w\boldsymbol{e}_z$ be the velocity vector decomposed into its horizontal, $\boldsymbol{u}_H$, and vertical, w, components, and consider

$$0 = \int_b^h \nabla \cdot \boldsymbol{u} \, dz = \int_b^h \nabla_H \cdot \boldsymbol{u}_H \, dz + w_h - w_b$$

$$= \nabla_H \cdot \int_b^h \boldsymbol{u}_H \, dz + [w_h - \boldsymbol{u}_H^h \nabla_H h] - [w_b - \boldsymbol{u}_H \nabla_H^b b] = 0, \quad (7.180)$$

in which the LEIBNIZ rule of differentiation of an integral has been used; $\boldsymbol{u}_H^h$ and $\boldsymbol{u}_H^b$ are the horizontal velocities at the free and bottom surfaces, respectively. Expressions for the bracketed terms in (7.180) need to be expressed alternatively. This is done with the **kinematic surface equations** for the free and basal surfaces. For a material surface, which for all time is covered by the same particles this equation is given by (7.166), where $\Phi(x, y, z, t) = 0$ represents the equation of the surface; $\boldsymbol{u}$ in this case is the three-dimensional velocity vector of the fluid particles. Ice sheets and glaciers grow by solid **precipitation** of snow and shrink by **melting** and **evaporation** of ice. For this case the kinematic surface equation is given by

$$\frac{\partial \Phi}{\partial t} + (\text{grad } \Phi) \cdot \boldsymbol{V}_h = 0, \quad \text{on the free surface} \quad z = h(x, y, t), \quad (7.181)$$

in which $\boldsymbol{V}_h$ is now the possibly non-material velocity of the surface points. If $\boldsymbol{V}_h$ is the material velocity on the side of the free surface of the fluid, (7.181) can also be written as

$$\frac{\partial \Phi/\partial t}{\| \text{grad } \Phi \|} + \boldsymbol{u}_h \cdot \boldsymbol{n} = -a_\perp, \quad \boldsymbol{n} = \frac{\text{grad } \Phi}{\| \text{grad } \Phi \|}, \quad a_\perp = (\boldsymbol{V}_h - \boldsymbol{u}_h) \cdot \boldsymbol{n}, \quad (7.182)$$

or with $\Phi(x, y, z, t) = z - h(x, y, t)$ for the free surface

$$\frac{\partial h}{\partial t} + \left[(\nabla_H h) \cdot \boldsymbol{u}_H^b - w_h \right] = N_h a_\perp^h, \quad N_h^2 = 1 + \left(\frac{\partial h}{\partial x} \right)^2 + \left(\frac{\partial h}{\partial y} \right)^2. \quad (7.183)$$

The quantity $a_\perp^h$ is a **surface flow density** (dimensionally a velocity), i.e., the time rate of change of the addition of volume of fluid mass per unit surface area, and it is positive for mass addition. In the glaciological application it is called **accumulation-ablation (rate) function**,[21] positive as snow-fall rate per unit surface area and negative as melting rate of ice. This function, $a_\perp(x, y, t)$, must be prescribed through the ice ages by climatologists.

Similarly, if $b(x, y, t) - z = 0$ is the kinematic equation for the basal surface at which melting of ice may occur, the analogue equation to (7.183) is

---

[21] More often, and inappropriately denoted as such, glaciologists and climatologists call it also "mass balance"; "mass balance" is, however, already occupied with a different meaning, see Chap. 3, Sect. 3.2.

$$\frac{\partial b}{\partial t} + \left[(\nabla_H b) \cdot \boldsymbol{u}_H^b - w_b\right] = -N_b a_\perp^b, \quad N_b^2 = 1 + \left(\frac{\partial b}{\partial x}\right)^2 + \left(\frac{\partial b}{\partial y}\right)^2. \quad (7.184)$$

The quantity $a_\perp^b > 0$ is the melting ($a_\perp^b < 0$ freezing) rate at the basal surface due to thermodynamic processes. Using (7.183) and (7.184) in (7.180) to eliminate the bracketed terms yields the evolution equation

$$\frac{\partial(h-b)}{\partial t} + \nabla_H \cdot \int_b^h \boldsymbol{u}_H(z)\mathrm{d}z = N_h a_\perp^h + N_b a_\perp^b. \quad (7.185)$$

It is easy to see from this equation that $a_\perp^h > 0$ corresponds to accumulation of snow, whilst $a_\perp^b > 0$ models melting of basal ice. This term must not be parameterized but is given by thermodynamic considerations.[22] If the temperature at the base of the ice sheet is everywhere below the melting temperature, then no phase changes occur there and, thus, $a_\perp^b = 0$. In any case, (7.185) is an evolution equation for h and b. Only if the basal surface is immobile, it becomes a single evolution for h; else a model for the motion of the basal surface must be added.

With the definition, see (7.160),

$$\Upsilon(\cdot, z) = A(T_j(z))f(\tau^2(z))H(z), \quad (7.186)$$

the horizontal flux, $\boldsymbol{V}_H$, is given by

$$\boldsymbol{V}_H := \int_b^h \boldsymbol{u}_H \mathrm{d}z = \boldsymbol{u}_H^b(h-b) - \rho g \nabla_H h \int_b^h \int_b^z \Upsilon(\cdot, \bar{z})\mathrm{d}\bar{z}\mathrm{d}z.$$

Using integration by parts[23] in the double integral, this may, alternatively, be written as

$$\boldsymbol{V}_H = \boldsymbol{u}_H^b H_b(z) - (\rho g \nabla_H h) \int_b^h H(z)\Upsilon(z)\mathrm{d}z$$

$$= \boldsymbol{u}_H^b H_b(\zeta) + (\rho g \nabla_H h)H_b^2 \int_0^1 \Upsilon(\zeta)\zeta^2 \mathrm{d}\zeta$$

$$= \boldsymbol{u}_H(\zeta) + (\rho g \nabla_H h)H_b^3 \int_0^1 A(T_j(\zeta))f(\tau^2(\zeta))\zeta^3 \mathrm{d}\zeta. \quad (7.187)$$

---

[22] At the present stage of knowledge, where thermodynamics of phase changes have not yet been presented, $a_\perp^b$ cannot be given in detail yet, see e.g. HUTTER (1984) [16].

[23] $\int_b^h 1 \int_b^z f(\bar{z})\mathrm{d}\bar{z}\mathrm{d}z = \left[z\int_b^z f(\bar{z})\mathrm{d}\bar{z}\right]_b^h - \int_b^h zf(z)\mathrm{d}z = \int_b^h \underbrace{(h-b)}_{H(z)} f(z)\mathrm{d}z.$

When substituted into (7.185) the depth integrated kinematic equation takes the form

$$
\frac{\partial H_b}{\partial t} + \nabla_H \cdot \left\{ \underbrace{\boldsymbol{u}_H^b H_b}_{\text{sliding}} - \underbrace{\rho g H_b^2 \nabla_H h \int_0^1 \Upsilon(\zeta)\zeta^2 \mathrm{d}\zeta}_{\text{deformational creep}} \right\} = \underbrace{N_h a_\perp^h}_{\substack{\text{accumulation} \\ -\text{ablation at surface}}} + \underbrace{N_b a_\perp^b}_{\text{basal melting}} ,
$$

(7.188)

in which the physical 'sources' are identified in the various terms. Sliding and deformational creep together build the total motion and contribute to the spreading of the fluid mass by advection and diffusion as we shall soon see. Addition of fluid mass from above is provided by the accumulation rate function and from below by possible surfacial phase change processes.

If the fluid adheres to the bed, then $\boldsymbol{u}_H^b = \boldsymbol{0}$. Alternatively, one may employ a viscous sliding law $\boldsymbol{u}_\parallel^b = -C(|\boldsymbol{t}_\parallel^b|, \cdot)\boldsymbol{t}_\parallel^b$ where the drag coefficient may depend on the modulus of the basal shear traction (and possibly other variables: normal pressure, temperature). With the shallowness assumption – the pressure-drag approximation – one has $\boldsymbol{u}_\parallel^b = -C(|\boldsymbol{\tau}_s|, \cdot)\boldsymbol{\tau}_b$, $\boldsymbol{\tau}_b = -\rho g H_b \nabla_H h$, so that in view of (7.187)

$$
\boldsymbol{u}_H^b = C(\rho g H_b \parallel \nabla_H h \parallel, \cdot)\rho g H_b \nabla_H h,
$$

$$
\boldsymbol{V}_H = \left\{ C(\rho g H_b \parallel \nabla_H h \parallel, \cdot)\rho g H_b + \rho g H_b^2 \int_0^1 \Upsilon(\zeta)\zeta^2 \mathrm{d}\zeta \right\} \nabla_H h \quad (7.189)
$$

$$
= \Psi(H_b, \parallel \nabla_H h \parallel, \cdot)\nabla_H h.
$$

Consequently, in the shallow flow limit, (7.185) can now be written as

$$
\frac{\partial H_b}{\partial t} + \nabla_H \cdot [\Psi(H_b, \parallel \nabla_H \parallel)\nabla_H h] = a_\perp^h + a_\perp^b, \tag{7.190}
$$

$$
\frac{\partial H_b}{\partial t} + \underbrace{[\nabla_H \Psi(H_b, \parallel \nabla_H \parallel)]}_{\mathcal{C}} \nabla_H h - \underbrace{\Psi(H_b, \parallel \nabla_H \parallel)}_{-\mathcal{D}} \nabla_H^2 h = a_\perp^h + a_\perp^b, \tag{7.191}
$$

$$
\frac{\partial H_b}{\partial t} + \underbrace{\mathcal{C}(H_b, \parallel \nabla_H h \parallel)\nabla_H h}_{\text{Advection}} - \underbrace{\mathcal{D}(H_b, \parallel \nabla_H h \parallel)\nabla_H^2 h}_{\text{Diffusion}} = \underbrace{a_\perp^h + a_\perp^b}_{\text{Reaction}}, \tag{7.192}
$$

in which for positive fluidity the diffusivity $\mathcal{D}$ is nonnegative but vanishes for $H_b = 0$, hence along the margin. Moreover, diffusion also vanishes at domes. $\mathcal{C}$ is the drag coefficient at the basal surface, which vanishes when the no-slip condition ($\mathcal{C} = 0$) applies but approaches infinity ($\mathcal{C} \to \infty$) for ideal, frictionless sliding.
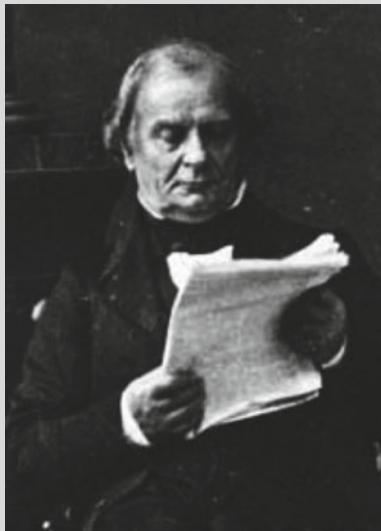
Fig. 7.30 Benoit Paul Émile Clapeyron (26. Feb. 1799 – 28. Jan. 1864)
Benoit Paul Émile Clapeyron was a French engineer and physicist, one of the founders of thermodynamics. Born in Paris, Clapeyron studied at the École polytechnique and the École des mines, before leaving for Saint Petersburg in 1820 to teach at the *École des Travaux Publics*. He returned to Paris only after the Revolution of July 1830, supervising the construction of the first railway line connecting Paris to Versailles and Saint-Germain. In 1834, he made his first contribution to the creation of modern thermodynamics by publishing a report entitled *Mémoire sur la puissance motrice de la chaleur (Memoir on the Motive Power of Heat)*, in which he developed the work of the physicist Nicolas Léonard Sadi Carnot, deceased two years before.

Carnot had developed a compelling analysis of a generalized heat engine, but he had employed the clumsy and already unfashionable caloric theory. Clapeyron, presented Carnot's work in a more accessible and analytic graphical form, showing the Carnot cycle as a closed curve on an indicator diagram, a chart of pressure against volume. In 1843, he developed the idea of a reversible process, already suggested by Carnot and made a definitive statement of *Carnot's principle*; this is now known as the second law of thermodynamics. These foundations enabled him to make substantive extensions of Clausius' work, including the formula, now known as the Clausius-Clapeyron relation, which characterizes the phase transition between two phases of matter. He further considered questions of phase transitions in what later became known as Stefan problems.

The text is based on http://www.wikipedia.org

Equation (7.192) is a non-linear partial differential equation for the surface topography and has the form of an **advection-diffusion-reaction equation**. It is, however, special insofar as, at the boundary of the integration domain, the diffusivity assumes zero values. Such equations are called **singular**. Such boundary singularities generally require formulation of regularity conditions, which makes solutions of initial boundary value problems difficult. In principle, however, for given temporal and spatial distributions of the reaction terms and given initial geometry

$$h = h_0(x, y), \qquad \text{for } t = 0 \tag{7.193}$$

and for given basal topography, e.g., $z - b(x, y, t) \equiv 0$, the evolution of the deforming viscous creeping fluid mass can be computed.

Such computations are intensively performed in today's climate research community, even under more general situations than described above, when the weight of the fluid (ice in ice sheets) deforms the ground on which it sits and thus induces a motion of the function $z = b(x, y, t)$. Moreover, the constitutive behavior of ice as a very viscous fluid has been an adequate postulate early on in glaciology, and thermodynamic considerations have also come into play, as the ice in ice sheets may reach at depth the melting point. So, one differentiates in large ice masses between cold and temperate ices, whose temperature is below the melting point and at pressure melting, respectively. The temperature in such temperate ice is given by the CLAUSIUS-CLAPEYRON[24] equation [i.e., $T_{\text{melt}} = -\mathcal{C}(p - p_0)$ the melting temperature is pressure dependent] and the balance law of internal energy is an equation determining the water fraction in an ice water mixture. Furthermore, impurities within the ice may affect its material response through the diffusive transport within the polycrystalline ice. All these complexities can be and are incorporated in the pressure-drag flow of large ice sheets.[25]

In a closing attempt of our analysis, which will disclose the limitations of the pressure drag approximation, let us look at the following simplified situation:

- Flat rigid bed with no basal melting: $b(x, y, t) \equiv 0$, $a_\perp^b(x, y, t) = 0$.
- Isothermal flow: $A(T_j) = A = \text{const.}$, i.e., constant rate factor.
- Power law creep response function: $f(\tau^2(z)) = (\rho g H(z)^{(n-1)} \|\nabla_H h\|)^{(n-1)}$.
- Slow variation of velocities and geometry (pressure-drag flow).

With these assumptions Eq. (7.188) turns out to have the form

$$\frac{\partial h}{\partial t} - \nabla_H \cdot \left\{ \left[C\rho g h^2 + \frac{A(\rho g h)^n}{n+2} h^2 \| \nabla_H h \|^{(n-1)} \right] \nabla_H h \right\} = a_\perp^h. \tag{7.194}$$

---

[24] For a short biography of CLAPEYRON see **Fig. 7.30**.

[25] One of the most important reasons of such computations is the estimation of how much ice of the Earth's ice sheets (Greenland and Antarctica and others, including glaciers) will melt under the anthropogenically caused increase of the Greenhouse gases in the Earth's atmosphere in the coming decades and centuries and how much this melting contributes to a possible Earth's surface temperature increase and sea level rise.

This equation describes the entire range of creep: For no-slip one may set $C = 0$, for 'sliding-only' on an ideal basal surface we may set $A = 0$. For finite values of A and C viscous sliding and deformational creep operate together. In the reduction to one spatial dimension the Nabla operator ∇_H is replaced by $\partial/\partial x$. Steady state solutions are then given by the equation

$$\frac{\partial}{\partial x}\left\{\frac{A(\rho g h)^n}{n+2}h^2\left|\frac{dh}{dx}\right|^{(n-1)}\frac{dh}{dx}\right\} = -a_\perp^h(x). \tag{7.195}$$

Such steady state solutions of (7.194) do only exist when $a_\perp^h(x, y)$ is an arbitrary non-trivial function of the spatial coordinates only. For such steady solutions the total mass added by the accumulation function $a_\perp^h(x, y)$ must vanish,

$$\int_{\mathcal{A}} a_\perp^h(x, y)\,dA \equiv 0, \tag{7.196}$$

where $\mathcal{A}$ is the total area of the fluid-bedrock interface. A first integration of (7.195) yields

$$\frac{A(\rho g)^n h^{n+2}}{n+2}\left|\frac{dh}{dx}\right|^{(n-1)}\frac{dh}{dx} = -\int_0^x a_\perp^h(\bar{x})\,d\bar{x} = -s(x), \tag{7.197}$$

where $x = 0$ is the location of the maximum height (hence a dome at which $dh/dx = 0$). Since $a_\perp^h > 0$ there, we also have $s(x) > 0$, at least for some $x_0 > 0$. Therefore, dh/dx is negative for $x \in (0, x_0]$, until for $x = x_G$ the grounding line is reached; it can be computed from

$$\int_0^{x_G} a_\perp^h\,dx = s(x_G) \equiv 0. \tag{7.198}$$

Now, since $dh/dx < 0$, (7.197) can be transformed to

$$h^{(n+2)/n}\frac{dh}{dx} = \left(\frac{n+2}{A(\rho g)^n}s(x)\right)^{1/n}, \quad \longrightarrow$$

$$\frac{n}{2(n+1)}\frac{d}{dx}\left(h^{2(n+1)/n}\right) = -\left(\frac{n+2}{A(\rho g)^n}s(x)\right)^{1/n}, \tag{7.199}$$

which is directly integrable and yields

$$h^{2(n+1)/n} = \frac{2(n+1)}{n}\int_x^{x_G}\left(\frac{n+2}{A(\rho g)^n}s(\bar{x})\right)^{1/n}d\bar{x}. \tag{7.200}$$

In this result the constant of integration has been determined such that $h(x_G) = 0$.

Note that the solution (7.200) does not in all points $x \in [0, x_G)$ satisfy the prerequisites of slow variation of $h(x)$; otherwise stated, the solution, expressed as (7.200) is not uniformly valid in $x \in [0, x_G)$. This can be made explicit by use of (7.200). Indeed, when introducing the transformation $\xi = x_G - x$, (7.200) becomes

$$
h^{2(n+1)/n}(\xi) = \frac{2(n+1)}{n} \int\limits_{0}^{\xi} \frac{n+2}{A(\rho g)^n} s(\bar{\xi}) \mathrm{d}\bar{\xi}, \qquad 0 \leq \xi \leq x_G. \tag{7.201}
$$

For differentiable $s(\xi)$ we may replace $s(\xi)$ by its TAYLOR series expansion

$$
s(\xi) = s_0 + s_1 \xi + s_2 \xi^2 + \cdots = -a_{\perp}^h|_{x=x_G} \xi + \mathcal{O}(\xi^2), \quad \xi \ll 1, \tag{7.202}
$$

in which $s(0) = 0$ and $s_1 = -a_{\perp}^h|_{x=x_G}$, see (7.198), have been used. With the representation (7.202), (7.201) takes the form

$$
h^{2(n+1)/n}(\xi) = \frac{2(n+1)}{n} \frac{(n+2)}{A(\rho g)^n} (-a_{\perp}^h)|_{x=x_G} \frac{\xi^2}{2} + \mathcal{O}(\xi^3). \tag{7.203}
$$

Substitution of the so-called FROBENIUS[26] expansion of h about $\xi = 0$,

$$
h(\xi) = \alpha \xi^{\beta} \left(1 + h_1 \xi + \mathcal{O}(\xi^2)\right) \tag{7.204}
$$

into (7.203) allows determination of the coefficients α and β

$$
\alpha = \left(-a_{\perp}^h|_{x=x_G}\right) \frac{(n+1)(n+2)}{A(\rho g)^n}, \qquad \beta = \frac{n}{n+1} < 1. \tag{7.205}
$$

Both are positive and $0 \leq \beta \leq 1$, if n varies from 0 to ∞. For shear-thinning fluids, $0 < n < 1$, β varies from 0 to $\frac{1}{2}$; for pseudoplastic fluids, $1 < n < \infty$, β varies from $\frac{1}{2}$ to 1. So, in this case h has a singularity at $x = x_G$ with slope $(\mathrm{d}h/\mathrm{d}x)(x = x_G) = \infty$. For a NEWTONian fluid this singularity is of square root type.[27]

Such singular behavior is a well-known disturbing fact of the general theoretical model, which we have glossed over so far. Let us scrutinize the causes and locations of these singularities of this shallow flow approximation. **Figure 7.32** illustrates where this approximation breaks down. It occurs as follows:

---

[26]For a short biography of FROBENIUS see **Fig. 7.31**.

[27]The reader should be aware of the fact that the result (7.204) holds, provided the no-slip boundary condition applies. When basal slip is included the singularity may depend on either sliding or differential creep or both. The behavior depends upon the form of the sliding law and the flow law of the fluid and how they compete.
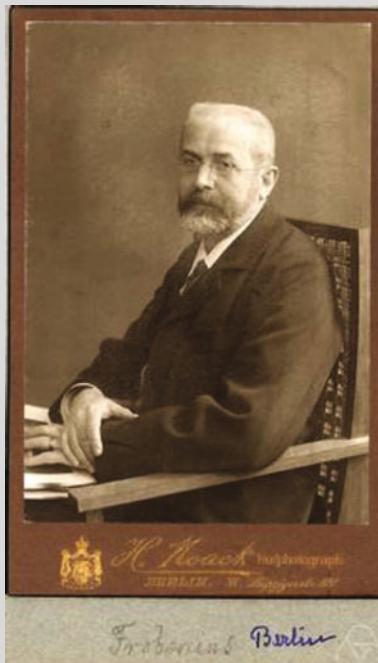
Fig. 7.31 FERDINAND GEORG FROBENIUS (26. Oct. 1849 – 3. Aug. 1917)

FERDINAND GEORG FROBENIUS, called Georg, was a German mathematician. He earned his Gymnasium education in Berlin-Charlottenburg, studied in 1867 first at the 'Georg-August-Universität' in Göttingen and then at the 'Friedrich-Wilhelms-Universität' Berlin. He received his doctoral degree from KARL WEIERSTRASS and EDUARD KUMMER; He then served as a Gymnasium teacher in Berlin, but was called in 1870, without ever having earned a Habilitation degree, as associate professor to the Berlin University and in 1871 to the 'Swiss Polytechnicum' (now ETH) in Zurich. In 1891, he returned as successor of LEOPOLD KRONECKER to Berlin. He was a member of the Prussian Academy of Sciences and of Leopoldina.

The text is based on http://www.wikipedia.org

1. In the neighborhood of the margin, the slope of the surface profile is very large—infinitely large at the margin—and it tapers off as one moves perpendicularly to the margin tangent into the fluid mass. Slopes become very quickly small.
2. At the position (x_D, y_D) of a dome, it is known that the horizontal velocity $\boldsymbol{u}_H$ vanishes. This is so, because at (x_D, y_D) the tangent plane to the free surface is horizontal, as $\nabla_H h = \mathbf{0}$, and so the horizontal velocity vanishes there as well (see (7.163) and (7.189)). It follows that the fundamental assumption of the shallow flow approximation, namely that the vertical fluid velocities are small when compared with the horizontal velocities, is violated.
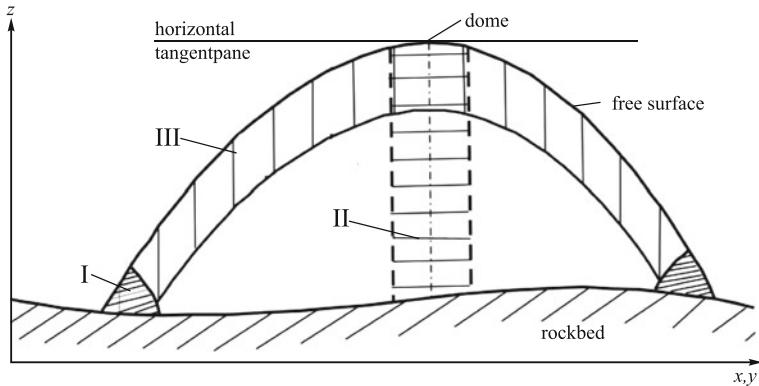
Fig. 7.32 Regions where the shallow flow approximation breaks down. (I) *Marginal domain in the vicinity where the creeping fluid touches the ground.* (II) *Column around the vertical line through a dome.* (III) *Boundary layer region near the free surface*

3. In a boundary layer, close to the free surface, this shallow flow approximation generates large (at the free surface infinitely large) viscous stresses t_{xx}^R, t_{yy}^R, t_{zz}^R, t_{xy}^R. True, these stress components do not arise in the mathematical formulae determining the flow, temperature and geometry of the moving finite ice masses, but they can be evaluated and the fact that they become infinitely large at the free surface is disturbing. Mathematically, they are given by (7.147) or

$$t_{ij}^R = \frac{D_{ij}}{\frac{1}{2} A F(II_{t^R})}. \tag{7.206}$$

D_{ij} can be calculated for all $i, j = 1, 2, 3$ using the velocity field (7.163) and (7.164); similarly, also $A(T)$ and II_{t^R} can be evaluated from the shallow flow approximation, in which $II_{t^R} = \tau^2$ (see (7.159)). At the free surface $\tau^2 = 0$, since $H(z) = h - z = 0$; it follows that $F_{\text{free surface}} = F(0)$. It was explained earlier that in an infinite viscosity law $F(0) = 0$, whereas in a finite viscosity law $F(0) \neq 0$. So, the stresses (7.206) are infinitely large when computed with the SFA with a constitutive model exhibiting the infinite viscosity property.

Measures ought to be taken to counteract the inadequacy of the shallow flow approximation in the three domains shown in Fig. 7.32. A first step to this end is to replace the infinite viscosity law by a finite viscosity law as e.g. expressed in (7.57). This requires the experimental determination of the parameter k in the creep law (7.57). This then equally renders the completion of evaluation of all stress terms without generating infinite values at the free surface and at the positions of domes. In actual ice sheet computations the problem of the non-uniformity of the solutions of the differential equations (7.192) for the evolution of the free surface of ice sheets is

only partly solved. Numerical specialists do not in general resolve the regions close to the margins, the free surface and the cylinder below a dome by grid refinement; these domains are regarded as passive layers/regions, of which the subgrid behavior does not propagate into the main domain of the flow. It is assumed that the considerable stiffening of the near surface layer is adequately softened by not too detailed grid resolution. Similarly, the marginal domain is neither resolved in detail. As a result, the slope of the free surface topography at the margin will remain bounded, but this will hopefully not unduly falsify the flow in the interior of the fluid mass. An alternative procedure is to introduce a sliding law with parameterization of the drag coefficient C as a function of the flow layer thickness, such that integration of equation (7.192) in the vicinity of the grounding line forces the surface slope to remain bounded.

Within the context of singular perturbation theory the problem of the non-uniform validity of the shallow flow approximation is solved by employing the *methods of matched asymptotic expansions*. This entails construction of the so-called inner and outer solutions of the governing equations. The solution of the SFA-equations is the lowest order outer approximation of such a perturbation expansion. The governing equations in the free surface boundary layer and the cylindrical region below the dome are constructed from adequate rescaling of the governing equations. The corresponding solutions are called the inner solutions (valid inside the boundary layers). The uniformly valid solution is obtained by matching inner and outer solutions. The local, inner solution for the free surface boundary layer has been constructed by JOHNSON and MCMEEKING [19], and that in the thin region below the free surface and close to the ice divide (2 dimensions) or a dome (3 dimensions) by WILSHINSKY and CHUGUNOV [30, 31]. The near margin solution is more difficult, because the equations of the inner problem are the full STOKES equations. In any case, the full implementation of the shallow flow problem by composing the outer and inner solutions has not yet been performed. The alternative procedure, which has been pursued, is to regularize the flow law (7.57) by adding a NEWTONian term. This brings the shallow flow approximation into a form that a regular perturbation expansion can be formally carried to second order. This has first been done by DAMBARU R. BARAL et al. (1999, 2001) [2, 3] and is further also analyzed by NINA KIRCHNER et al. (2011) [20]. The success of this method in ice sheet scenarios is promising, but bears its limitations, because convergence is generally slow. It has thus been suggested to abandon the SFA altogether and to solve the full STOKES equations instead. At least at the present time (2014), such STOKES solvers applied to ice sheet flow (Greenland, Antarctica) allow integration over only a few hundred years, but not through entire ice ages ($>10^5$ years), which is needed for climate reconstructions. This makes so-called second order shallow ice/flow approximations the much more attractive alternative, at least at the present time.

References

1. ASME-Steam Tables: Thermodynamics properties of steam. Am. Soc. Mech. Eng. New York (1940)
2. Baral, D.: Asymptotic theories of large scale motion, temperature and moisture distributions in land based polythermal ice shields and in floating ice shelves—A critical review and new developments, Ph.D. thesis, Darmstadt University of Technology, Darmstadt, Germany (1999)
3. Baral, D.R., Hutter, K., Greve, R.: Asymtotic theories of large scale motion, temperature and moisture distributions in land based polythermal ice sheets. A critical review and new developments. Appl. Mech. Rev. **54**(3), 215–256 (2001)
4. Batchelor, G.K., Green, J.T.: The hydrodynamic interaction of two small freely moving spheres in a linear flow field. J. Fluid Mech. **56**, 375 (1972)
5. Dorsey, N.E.: Properties of Ordinary Water Substance. Reinhold Publishing Corporation, New York (1940)
6. Einstein, A.: Über einen die Erzeugung und Verwandlung des Lichtes betreffenden heuristischen Gesichtspunkt. Annalen der Physik **322**(6), 132–148 (1905)
7. Einstein, A.: Über die von der molekularkinetischen Theorie der Wärme geforderte Bewegung von in ruhenden Flüssigkeiten suspendierten Teilchen. Annalen der Physik. **322**(8), 549–560 (1905)
8. Einstein, A.: Zur Elektrodynamik bewegter Körper. Annalen der Physik und Chemie **17**, 891–921 (1905)
9. Einstein, A.: Eine neue Bestimmung der Moleküldimensionen. Annalen der Physik und Chemie, Bd. **29**, 289 (1906), with correction in Bd. **34**, 591 (1911)
10. Glen, J.W.: The creep of polycrystalline ice. Proc. R. Soc. Lond. **A228**, 519–538 (1953)
11. Hagen, G.H.L.: Ueber die Bewegung des Wassers in engen cylindrischen Röhren. Annalen der Physik **46**, 423–442 (1839)
12. Hagenbach-Bischoff, J.E.: Über die Bestimmung der Zähigkeit einer Flüssigkeit durch Ausflu aus Röhren. Verhh. d. Naturforsch. Ges. in Basel **2** (1860)
13. Hager, W.H., Castro-Orgaz, O.: William Froude and the Froude number. ASCE Forum Paper. (submitted)
14. Hager, W.H.: Hydraulicians in Europe, 1800–2000. IHAR-monograph (2003)
15. Hutter, K.: Theoretical Glaciology. Reidel Dortrecht (1983)
16. Hutter, K.: Ice and snow mechanics, a challenge to theoretical and applied mechanics. In: Proceedings XVI-ICTAM Congress. Copenhagen, North Holland Publishing Company (1984)
17. Hutter, K., Jöhnk, K.: Continuum Methods of Physical Modeling. Springer, Berlin (2004)
18. Jeffrey. G.B.: The motion of elliptical particles immersed in a viscous fluid. Proc. R. Soc. Lond. **102A**, 161 (1923)
19. Johnson, R.E., McMeeking, R.M.: Near surface flow in glaciers obeying Glen's flow law. Q. J. Mech. Appl. Math. **37**, 273–291 (1984)
20. Kirchner, N., Hutter, K., Jakobsson, M., Gyllencreutz, R.: Capabilities and limitations of numerical ice sheet models: a discussion for Earth scientists and modelers. Quat. Sci. Rev. **30**(25–26), 3691–3704 (2011)
21. Mallock, A.: Experiments on fluid viscosity. Philos. Trans. R. Soc. Lond. **187**, 41–56 (1895)
22. Newton, I.: Principia. Original title: Philosophiae Naturalis Principia (Latin, 1687). Published in English (1728)
23. Norton, F.H.: The Creep of Steel at High Temperatures. McGraw-Hill, New York (1929)
24. Piau, J.M., Bremond, M., Couette, J.M., Piau, M.: Maurice Couette, one of the founders of rheology. Rheolog. Acta **33**, 357–368 (1994)
25. Poiseuille, J.L.: Rechercs experimentales sur le movement des liquids dans les tubes de trés petits diamétres. Compes Rendue, **11**, 961 (1840), **12** (1841)
26. Reiner, M.: Selected Papers on Rheology. Amsterdam (1975)
27. Scott Blair, G.W.: Markus Reiner 1886–1976: Obituary. J. Texture Stud. **7**, 151–152 (1976)
28. Sutera, S.P.: The history of Poiseuille's law. Annu. Rev. Fluid Mech. **25**, 1–19 (1993)

29. Taylor, G.I.: The viscosity of a fluid containing small drops of another fluid. Proc. R. Soc. Lond. **138A**, 41 (1932)
30. Wilshinsky, A., Chugunov, V.A.: Modeling ice mechanics by perturbation methods. J. Glaciol. **43**(144), 352–358 (1997)
31. Wilshinsky, A., Chugunov, V.A.: Modeling ice flow in various glacier zones. GAMM. J. Appl. Math. Mech. **65**(3), 479–493 (2001)

Chapter 8
Simple Two- and Three-Dimensional Flow Problems of the Navier-Stokes Equations

Abstract This chapter begins with studying steady state layer flows through cylindrical conduits (ellipse, triangle, rectangle) and use of the PRANDTL membrane analogy. This study of the NAVIER-STOKES fluids is important in geophysical fluid dynamics and is manifest in EKMAN's theory and its extensions, where non-inertial effects chiefly influence the details of the fluid flow, evidenced in the EKMAN spiral in atmospheric and oceanic boundary flows and in free geostrophic flows as their outer solutions. Extensions of the behavior exhibited by the assumption of constant (turbulent) viscosity are based on influences of depth dependence of the viscosity which influences the circulation pattern of such steady flows. Unsteady flows are analyzed for viscous flows along an oscillating wall and the growth of a viscous boundary layer as a response of an initial tangential velocity jump with time. The chapter closes with the study of an axial laminar jet and viscous flows in a converging two-dimensional channel.

List of Symbols

Roman Symbols

A, B, C	Constants (of integration)
c_μ	Constant in the definition $\nu = c_\mu k^2/\varepsilon$
D	EKMAN depth
$\mathfrak{D}$	Domain in $\mathcal{R}^2$ or $\mathcal{R}^3$
erf	Error function
erfc	Complementary error function
$\boldsymbol{f} = (f_x, f_y, f_z)$	Body force per unit mass, Cartesian components of –
$f, \tilde{f}$	First and second CORIOLIS parameter
$\boldsymbol{F}, F = |\boldsymbol{F}|$	Force vector acting on a body,
g	Gravity constant

h	Height, depth of a fluid layer
$\mathcal{H}$	HEAVISIDE function
$\iota = \sqrt{-1}$	Imaginary unit
I_n, K_n	Modified BESSEL functions of order n
J_n, Y_n	BESSEL functions of order n
k	Specific turbulent kinetic energy, wave number
ker, kei	Radial BESSEL functions of order n
$L, \bar{L}$	Stress power, mean stress power
p	Pressure
Q	Discharge, volume flow
r	Radial coordinated
R	Radius of a circle or sphere
$\mathbb{R}, \mathbb{R}_r$	REYNOLDS number
$T = 2\pi/\omega$	Period
t	Time
$\boldsymbol{t}, \boldsymbol{t}^E, \boldsymbol{t}^R$	CAUCHY stress tensor, extra –, frictional –
U	Constant velocity in the x-direction
u_s, v_s	x-velocity, y-velocity at the water surface
$\boldsymbol{v} = (u, v, w)$	Velocity, components of the 3D velocity field
$u^* = \sqrt{\tau_s/\rho}$	Shear velocity at the free surface
w	Deflection of a membrane
v_r, v_θ	Radial, azimuthal velocity components for axisymmetric flow
$\mathsf{w} = u + \iota v$	Complex velocity
W_s	Modulus of a surface current
x, y, z	Cartesian coordinates in three dimensional space
$z, \mathfrak{z}$	Vertical coordinate, dimensionless
z_0	Roughness length
$\bar{z}$	Conjugate complex of z

Greek Symbols

α	Deflection angle (in the EKMAN problem); Semi-opening angle
ϕ	Field variable
η	Dynamic viscosity $\eta = \rho\nu$
ν, ν_s	Kinematic viscosity, – on the free surface
θ	Azimuthal coordinate
ρ	Mass density
ε	Specific turbulent dissipation rate
$\lambda = 2\pi/k$	Wave length
$\boldsymbol{\tau}, \tau_{xz}, \tau_{yz}$	Shear stress, – components
ω	Frequency
$\boldsymbol{\Omega}$	Angular velocity of the Earth
∇	Nabla operator
∇_H	Two-dimensional (horizontal) Nabla operator

8.1 Introductory Review

The derivation of the NAVIER-STOKES (NS) equations as presented in this book is done routinely with a solid background of modern rational continuum mechanics. First steps toward a formulation of the dynamics of a uniform viscous fluid were done by ISAAC NEWTON in his Principia (1687) [36]. "It was many years later that the NAVIER-STOKES equations, as we know them, were deduced from various physical hypotheses, and various forms, by CLAUDE LOUIS MARIE HENRI NAVIER (1827) [35], SIMÉON DENIS POISSON (1831) [39], ADHÉMAR JEAN CLAUDE BARRÉ DE SAINT-VENANT (1843) [44] and GEORGE GABRIEL STOKES (1854) [48]. STOKES (1846) [49] himself reviewed the methods and hypotheses of these authors, and presented a short rational derivation of the equations" [14].

The intention in this chapter is the presentation of exact solutions of boundary value problems of the NS-equations. DRAZIN and RILEY (2006) [14] state "Much of the early history of the exact solutions [of the NS-equations] has been recorded by CLIFFORD A. TRUESDELL (1954) [53]; also many textbooks, such as GEORGE K. BATCHELOR (1967) [3], contain brief accounts of the most important exact solutions. More extensive accounts are to be found in treatises on the flow of a viscous fluid, such as HUGH LATIMER DRYDEN, FRANCIS DOMINIC MURNAGHAN and HARRY BATEMAN (1932) [15], HERRMANN SCHLICHTING (1979) [45], GERALD B. WHITHAM (1963) [59] and PACO ALEX LAGERSTROM (1996) [30]. R. BERKER (1963) [4] described the exact solutions in great detail …. WANG (1989, 1990, 1991) [54–56] has recently written review articles" [14]. To our knowledge DRAZIN and RILEY [14] presented the most recent summary of the state of the art in their monograph "The NAVIER-STOKES equations: a classification of flows and exact solutions", and their philosophy for the selection is that a solution is 'significant', either in a historical or novel sense, or, perhaps most importantly that it offers insight into the dynamical behavior of viscous fluids" [14]. Beyond these, our own emphasis will also be educational and, therefore, certainly far less complete than their work.

In the ensuing sections the NS-equations for density preserving fluids

$$\operatorname{div} \boldsymbol{v} = 0, \quad \frac{\mathrm{d}\boldsymbol{v}}{\mathrm{d}t} = -\frac{1}{\rho}\operatorname{grad} p + \nu\nabla^2\boldsymbol{v} + \boldsymbol{f} \tag{8.1}$$

will be employed in various coordinates, mainly in two-dimensional specializations. For easy access, they are written here in Cartesian coordinates

$$\begin{aligned}
&\frac{\partial u}{\partial x} + \frac{\partial v}{\partial y} + \frac{\partial w}{\partial z} = 0, \\
&\frac{\mathrm{d}u}{\mathrm{d}t} = -\frac{1}{\rho}\frac{\partial p}{\partial x} + \nu\left(\frac{\partial^2 u}{\partial x^2} + \frac{\partial^2 u}{\partial y^2} + \frac{\partial^2 u}{\partial z^2}\right) + f_x, \\
&\frac{\mathrm{d}v}{\mathrm{d}t} = -\frac{1}{\rho}\frac{\partial p}{\partial y} + \nu\left(\frac{\partial^2 v}{\partial x^2} + \frac{\partial^2 v}{\partial y^2} + \frac{\partial^2 v}{\partial z^2}\right) + f_y, \\
&\frac{\mathrm{d}w}{\mathrm{d}t} = -\frac{1}{\rho}\frac{\partial p}{\partial z} + \nu\left(\frac{\partial^2 w}{\partial x^2} + \frac{\partial^2 w}{\partial y^2} + \frac{\partial^2 w}{\partial z^2}\right) + f_z,
\end{aligned} \tag{8.2}$$

in which

$$\frac{d\phi}{dt} = \frac{\partial \phi}{\partial t} + u\frac{\partial \phi}{\partial x} + v\frac{\partial \phi}{\partial y} + w\frac{\partial \phi}{\partial z}. \tag{8.3}$$

$d\phi/dt$ is the material derivative, and $\boldsymbol{v} = (u, v, w)$, $\boldsymbol{f} = (f_x, f_y, f_z)$, whilst $\rho =$ constant.

8.2   Steady State Layer Flows

Such flows are characterized by the following assumptions:

$$
\begin{aligned}
&\text{(i)} \quad \frac{\partial \boldsymbol{v}}{\partial t} = 0, \quad \frac{\partial \boldsymbol{v}}{\partial x} = \boldsymbol{0}, \quad \frac{\partial p}{\partial x} \neq 0, \\
&\text{(ii)} \quad \boldsymbol{f} = (f_x, f_y, f_z) = \boldsymbol{0}, \\
&\text{(iii)} \quad u = u(y, z), \quad v = 0, \quad w = 0.
\end{aligned} \tag{8.4}
$$

Layer flows can also be defined in curvilinear coordinates, but they will be restricted here to Cartesian coordinates. Item (i) above expresses stationarity in time of the processes, in which the velocity $\boldsymbol{v}$ does not vary with x, but may be driven by a nontrivial pressure gradient in that direction. Item (ii) states that the processes are not driven by body forces and item (iii) states that the velocity is in the x-direction and varies only in the y- and z-directions.

With the prerequisite (iii) the mass balance equation $(8.2)_1$ is identically satisfied and the remaining Eq. $(8.2)_{2-4}$ take the forms

$$
\begin{aligned}
0 &= -\frac{1}{\rho}\frac{\partial p}{\partial x} + \nu\left(\frac{\partial^2 u}{\partial y^2} + \frac{\partial^2 u}{\partial z^2}\right), \\
0 &= -\frac{1}{\rho}\frac{\partial p}{\partial y}, \quad 0 = -\frac{1}{\rho}\frac{\partial p}{\partial z}.
\end{aligned} \tag{8.5}
$$

The last two of these equations yield $p = p(x)$ and the first implies $\partial^2 p/\partial x^2 = 0$, from which $\partial p/\partial x = C = $ constant follows. Therefore, there remains the single equation

$$\frac{\partial^2 u}{\partial y^2} + \frac{\partial^2 u}{\partial z^2} = \frac{1}{\eta}\frac{\partial p}{\partial x} \quad \Longleftrightarrow \quad \nabla^2 u = \frac{1}{\eta}\frac{\partial p}{\partial x}, \quad \text{in } \mathcal{D} \tag{8.6}$$

with the standard boundary condition

$$u = 0 \quad \text{on } \partial\mathcal{D}. \tag{8.7}$$

$\mathcal{D}$ is the region, in which (8.6) is to be solved, subject to (8.7) along $\partial\mathcal{D}$, see **Fig. 8.1**.
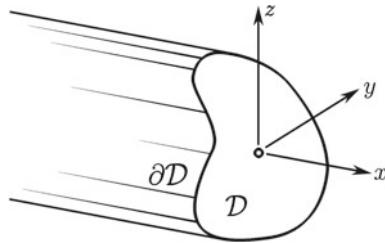
Fig. 8.1 Cylindrical conduit of arbitrary cross-section $\mathcal{D}$ and boundary $\partial\mathcal{D}$. *The coordinate x is in the axial direction, generally the direction of the dominant velocity component. The cross section is perpendicular to the x-direction within the (y, z) plane*

8.2.1 Hagen-Poiseuille Flow

(a) The boundary value problem for general cross-sections.
Consider a conduit of arbitrary but constant cross section, Fig. 8.1, filled with a viscous fluid and subjected to the pressure gradient dp/dx. Then, laminar flow in the pipe is described by (8.5), or[1]

$$\nabla^2 u = \underbrace{\frac{\partial^2 u}{\partial y^2} + \frac{\partial^2 u}{\partial z^2}}_{\text{Cartesian coord.}} = \frac{1}{\eta}\frac{dp}{dx}, \quad \text{in } \mathcal{D},$$

$$u = 0, \qquad\qquad\qquad \text{on } \partial\mathcal{D}. \tag{8.8}$$

This is a so-called DIRICHLET[2] boundary value problem for the POISSON equation, in which its right-hand side is a constant.

For laminar flow through a circular pipe the LAPLACE operator in polar coordinates is given by

$$\nabla^2 u = \frac{\partial^2 u}{\partial r^2} + \frac{1}{r}\frac{\partial u}{\partial r} + \frac{1}{r^2}\underbrace{\frac{\partial u}{\partial \theta}}_{=0} = \frac{\partial^2 u}{\partial r^2} + \frac{1}{r}\frac{\partial u}{\partial r} = \frac{1}{r}\frac{d}{dr}\left(r\frac{du}{dr}\right), \tag{8.9}$$

provided the velocity field has no azimuthal dependence ($\partial u/\partial\theta = 0$). With (8.9) Eq. (8.8)$_1$ possesses the solution

$$u = A\ln r + B + \frac{1}{4\eta}\frac{dp}{dx}r^2 \tag{8.10}$$

---

[1]For biographies on Hagen and Poiseulle see Figs. 7.8 und 7.7.
[2]After JOHANN PETER GUSTAV LEJEUNE DIRICHLET (1805–1859), see **Fig. 8.2**.
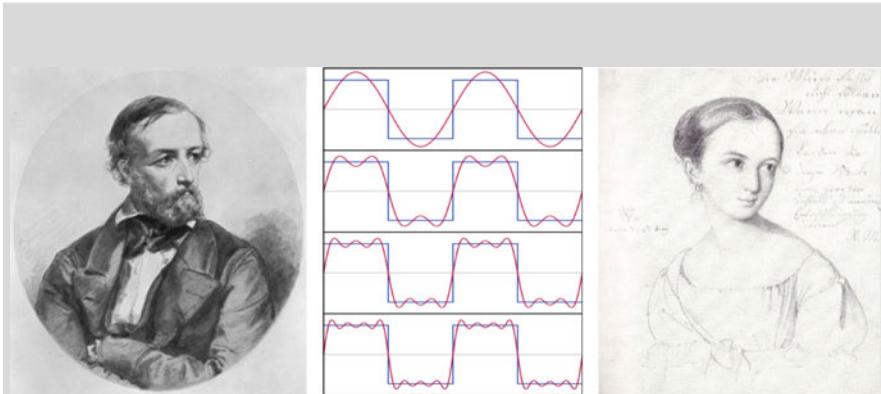
Fig. 8.2 JOHANN PETER GUSTAV LEJEUNE DIRICHLET (13. Feb. 1805–5. May 1859)

JOHANN PETER GUSTAV LEJEUNE DIRICHLET was a German mathematician, who made deep contributions to number theory, FOURIER series and other topics of mathematical analysis. He attended classes at the '*Collège de France*' and the '*Faculté des Sciences de Paris*'. His first original research (at the age of early 20) was a proof of FERMAT's last theorem in 1825 for the case $n = 5$ [for $n > 2$ there is no solution for $a^n + b^n = c^n$ for entire n]. This brought him instant fame. In 1827 he received a doctoral degree by honor from the University at Bonn (Germany) and passed his Habilitation degree on the recommendation of ALEXANDER VON HUMBOLDT. Subsequently, he taught in Breslau (now Wroclaw), but moved to the FRIEDRICH WILHELMS University in Berlin in 1828, where he became full Professor of Mathematics in 1839. In 1832 he was elected a member of the Prussian Academy of Sciences. In 1855, he followed KARL FRIEDRICH GAUSS as professor of upper mathematics at the University of Göttingen.

DIRICHLET was introduced by ALEXANDER VON HUMBOLDT to the Bankers Family ABRAHAM MENDELSOHN BARTHOLDY and married in 1832 ABRAHAM's daughter REBECKA MENDELSOHN, the sister of FELIX and FANNY MENDELSOHN. The above 1823-drawing of REBECKA is by the painter WILHELM HENSEL, who was married to FANNY MENDELSOHN. When DIRICHLET moved to Berlin, he was assigned by the ministry in 1831 to undertake a renewed habilitation qualification, and even though he wrote a Habilitationsschrift as needed, he postponed giving a mandatory lecture in Latin for another 20 years. As a consequence, he did not reach full rights in the faculty and depended on additional emoluments as a teacher at the Berlin Military School.

In mathematics DIRICHLET worked on number theory, analysis and mathematical physics. He found and proved e.g. the convergence conditions for FOURIER series decompositions. The middle panel above pictures the first four FOURIER approximations for a square wave.

The text is based on http://www.wikipedia.org

with the constants of integration A and B. Regularity of the solution at $r = 0$ requires $A = 0$, and $(8.8)_2$ yields for $r = R$

$$0 = B + \frac{1}{4\eta}\frac{\mathrm{d}p}{\mathrm{d}x}R^2 \quad\Longrightarrow\quad B = -\frac{1}{4\eta}\frac{\mathrm{d}p}{\mathrm{d}x}R^2,$$

so that

$$u(r) = \frac{1}{4\eta}\frac{\mathrm{d}p}{\mathrm{d}x}\left(r^2 - R^2\right). \tag{8.11}$$

It follows for a flow in the positive x-direction ($u > 0$) that the pressure gradient, $\mathrm{d}p/\mathrm{d}x$, must be negative; or the flow is against the pressure gradient. The volume (mass) flow is then given by

$$Q = \int_0^R 2\pi r u(r)\,\mathrm{d}r = \frac{\pi}{2\eta}\frac{\mathrm{d}p}{\mathrm{d}x}\int_0^R \left(r^3 - rR^2\right)\mathrm{d}r = -\frac{\pi}{8\eta}\frac{\mathrm{d}p}{\mathrm{d}x}R^4. \qquad (8.12)$$

The volume flow through the circular pipe grows with the fourth power of the pipe diameter; alternatively, it is linear in the pressure gradient.

Remarks

- For general non-circular cross sections the DIRICHLET boundary value problem (8.8) may be solved with the method of conformal mapping.
- Between the laminar HAGEN- POISEUILLE flow and the displacement of a thin membrane, orthogonally loaded by a constant transverse loading distribution, there exists a mathematical analogy. If w is the displacement function of the membrane and p the transverse loading distribution within $\mathcal{D}$, of the membrane spanned along $\partial\mathcal{D}$, then

$$\left.\begin{array}{ll} \nabla^2 w = -\dfrac{p}{S}, & \text{in } \mathcal{D}, \\[2mm] w = 0, & \text{on } \partial\mathcal{D} \end{array}\right\} \quad S = \text{constant prestress distribution} \qquad (8.13)$$

describes the transverse thin film deformation. This is the same DIRICHLET boundary value problem as (8.8). The analogy is known as PRANDTL's *soap film analogy*, **Fig. 8.3**. It is a useful helping kit to find a qualitative picture of the flow distribution through conduits with general, but constant cross-sections.

(b) Elliptical, rectangular and triangular cross-sections.

(α) For *elliptical cross sections* the boundary $\partial\mathcal{D}$ may be given by the equation

$$\frac{y^2}{a^2} + \frac{z^2}{b^2} - 1 = 0 \qquad (8.14)$$

and the trial function

$$u = C\left(\frac{y^2}{a^2} + \frac{z^2}{b^2} - 1\right) \qquad (8.15)$$

for the axial velocity distribution satisfies the condition $u = 0$ on the boundary. If (8.15) is substituted into the POISSON equation (8.8)$_1$, an equation for the determination of C emerges, namely

$$C = \frac{1}{2\eta}\frac{\mathrm{d}p}{\mathrm{d}x}\frac{a^2 b^2}{a^2 + b^2}. \qquad (8.16)$$
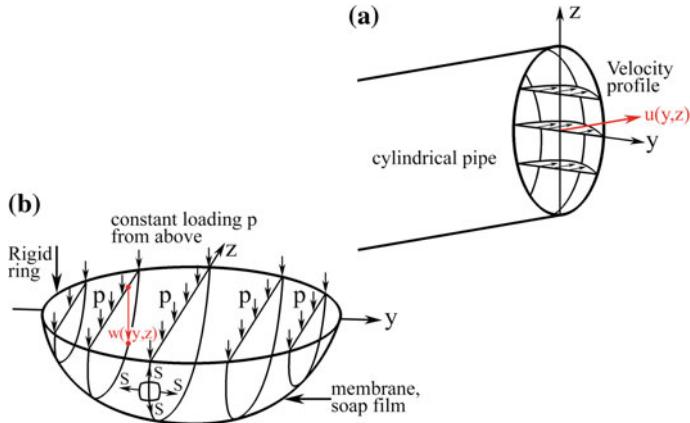
Fig. 8.3 Explaining PRANDTL's soap film analogy. **a** *Flow of a linear viscous fluid through a circular conduit, the velocity distribution is a rotational paraboloid.* **b** *Deflection of a thin membrane (soap film) spanned over a circular ring and loaded with a constant pressure p from above. The prestress S is isotropic and constant*

The axial laminar velocity distribution in the elliptical pipe is, thus, given by

$$u = \frac{1}{2\eta} \frac{dp}{dx} \frac{a^2 b^2}{a^2 + b^2} \left(\frac{y^2}{a^2} + \frac{z^2}{b^2} - 1 \right) \tag{8.17}$$

and the volume flow is given by

$$Q = 4 \int_0^a \int_0^z u(y, \tilde{z}) \, d\tilde{z} dy, \qquad z = b \sqrt{1 + \frac{y^2}{a^2}}$$

$$= \frac{2}{\eta} \frac{dp}{dx} \frac{a^2 b^2}{a^2 + b^2} \int_0^a dy \int_0^z \left(\frac{y^2}{a^2} + \frac{\tilde{z}^2}{b^2} - 1 \right) d\tilde{z}$$

$$= \frac{2}{\eta} \frac{dp}{dx} \frac{a^2 b^2}{a^2 + b^2} \int_0^a \left(\frac{y^2 z(y)}{a^2} + \frac{z^3(y)}{3b^2} - z(y) \right) dy$$

$$= \frac{2}{\eta} \frac{dp}{dx} \frac{a^2 b^2}{a^2 + b^2} \int_0^a \left\{ b \frac{y^2}{a^2} \left(1 + \frac{y^2}{a^2} \right)^{1/2} + \frac{b}{3} \left(1 + \frac{y^2}{a^2} \right)^{3/2} \right.$$

$$\left. - b \left(1 + \frac{y^2}{a^2} \right)^{1/2} \right\} dy$$

$$= \frac{2}{\eta} \frac{dp}{dx} \frac{a^2 b^2}{a^2 + b^2} \frac{2}{3} b \int\limits_0^a \left(2\frac{y^2}{a^2} - 1\right) \left(1 + \frac{y^2}{a^2}\right)^{1/2} dy$$

$$= \frac{2}{\eta} \frac{dp}{dx} \frac{a^2 b^2}{a^2 + b^2} \frac{2}{3} ab \underbrace{\int\limits_0^1 (2\xi^2 - 1) (1 + \xi^2)^{1/2} d\xi}_{\mathfrak{Q} = \mathfrak{Q}_1 - \mathfrak{Q}_2}$$

$$= \frac{4}{3\eta} \frac{dp}{dx} \frac{a^3 b^3}{a^2 + b^2} (\mathfrak{Q}_1 - \mathfrak{Q}_2), \tag{8.18}$$

where[3]

$$\mathfrak{Q}_1 = \int\limits_0^1 \xi \underbrace{\left(2\xi\sqrt{1 + \xi^2}\right)}_{\frac{d}{d\xi}\left(\frac{2}{3}(1+\xi^2)^{3/2}\right)} d\xi \overset{\text{int. by parts}}{=} \frac{2}{3}\xi \left(1 + \xi^2\right)^{3/2}\Big|_0^1 - \frac{2}{3} \int\limits_0^1 (1 + \xi)^{3/2} d\xi$$

$$= \frac{2}{3}\left\{(2)^{3/2} - \underbrace{\int\limits_0^1 \left(1 + \xi^2\right)^{3/2} d\xi}_{\frac{1}{4}\left\{(2)^{3/2}+\frac{3}{2}\left(\sqrt{2}+\ln(1+\sqrt{2})\right)\right\}}\right\}$$

$$= \frac{1}{4}\left(3\sqrt{2} - \ln(1 + \sqrt{2})\right), \tag{8.19}$$

$$\mathfrak{Q}_2 = \int\limits_0^1 (1 + \xi^2)^{1/2} d\xi = \frac{1}{2}\left\{\sqrt{2} + \ln(1 + \sqrt{2})\right\}. \tag{8.20}$$

Consequently,

$$\mathfrak{Q} = \mathfrak{Q}_1 - \mathfrak{Q}_2 = \frac{1}{4}\left(\sqrt{2} - 3\ln(1 + \sqrt{2})\right). \tag{8.21}$$

With the formulae (8.18) and (8.21) the steady volume flow through any elliptical cross section can now be evaluated.

---

[3]For evaluation of the integrals the following formulae are used:

$$\int \sqrt{x^2 + a^2} dx = \frac{1}{2}x\sqrt{x^2 + a^2} + \frac{1}{2}a^2 \ln\left(x + \sqrt{x^2 + a^2}\right),$$

$$\int \left(x^2 + a^2\right)^{3/2} dx = \frac{1}{4}x \left(x^2 + a^2\right)^{3/2} + \frac{3}{8}a^2 x\sqrt{x^2 + a^2} + \frac{3}{8}a^4 \ln\left(x + \sqrt{x^2 + a^2}\right).$$

(β) For *rectangular cross-sections* the solution to (8.8) is given in the appendix to this chapter. The results are

$$
\begin{aligned}
u(y, z) &= -\frac{1}{2} \frac{p' h^2}{\eta} \left\{ \frac{y}{h} - \left(\frac{y}{h} \right)^2 \right\} + \frac{4p'h^2}{\eta \, \pi^3} \sum_{n=0}^{\infty} \frac{N_n}{D_n}, \\
N_n &= \left\{ \sinh \left[\frac{(2n+1)\pi z}{h} \right] + \sinh \left[\frac{(2n+1)\pi(l-z)}{h} \right] \right\} \\
&\quad \times \sin \left[\frac{(2n+1)\pi y}{h} \right], \\
D_n &= (2n+1)^3 \sinh \left[\frac{(2n+1)\pi l}{h} \right]
\end{aligned}
\tag{8.22}
$$

where $p' = \mathrm{d}p/\mathrm{d}x$ and

$$
\begin{aligned}
Q &= \iint\limits_{\text{rectangle}} \rho \, u(y, z) \, \mathrm{d}y \mathrm{d}z \\
&= \frac{-p' h^3 \, l}{12 \, \nu} + \frac{16 p' h^4}{\pi^5 \nu} \sum_{n=0}^{\infty} \frac{\left\{ \cosh \left[\frac{(2n+1)\pi l}{h} \right] - 1 \right\}}{(2n+1)^5 \sinh \left[\frac{(2n+1)\pi l}{h} \right]}
\end{aligned}
\tag{8.23}
$$

for the axial velocity distribution within the cross-section and the mass flux along the channel. l and h are the width and height of the rectangle. The above solution has been constructed by BOUSSINESQ in 1868 [6]. According to DRAZIN and RILEY [14], ROWELL and FINLAYSON [43] also considered the channel of rectangular cross-section with one of the bounding walls moving in the flow direction.

(γ) For *triangular cross-sections*, see [14] and **Fig. 8.4**, it is no longer easy to find an exact solution. BOUSSINESQ (1868) [6] considered

$$
u(y, z) = \frac{1}{4\eta} \frac{\mathrm{d}p}{\mathrm{d}x}(y - h)(y - az)(y - bz),
\tag{8.24}
$$

which vanishes on the three sides of the triangle, Fig. 8.4. Substitution of (8.24) into (8.8) shows that $a = -b = \sqrt{3}$ is the only possibility that (8.24) is an exact solution. Thus, this triangle must be equilateral of side $2h/\sqrt{3}$ with

$$
\begin{aligned}
u(y, z) &= \frac{1}{4\eta} \frac{\mathrm{d}p}{\mathrm{d}x}(y - h)\left(y^2 - 3z^2\right), \\
Q &= -\frac{(\mathrm{d}p/\mathrm{d}x)h^4}{60\sqrt{3}\nu}.
\end{aligned}
\tag{8.25}
$$
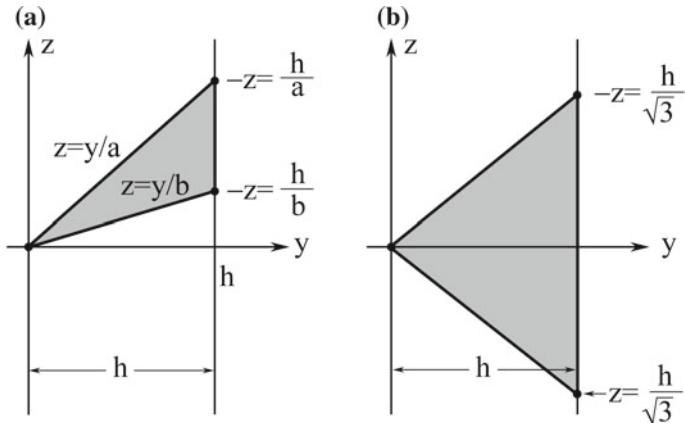
Fig. 8.4 Triangular cross sections. **a** *The velocity distribution (8.24) is such that u = 0 along the heavy solid boundary.* **b** *The velocity distribution (8.24) is only an exact solution of (8.8) for a triangle of equilateral side* $2h/\sqrt{3}$

P.G. DRAZIN and N. RILEY also mention PROUDMAN's[4] (1914)-solution [41] of the flow through the right-angled isosceles triangle.

These results transpire that the trial solutions of the form (8.24) can only form exact solutions of (8.8) in special cases. It is, however, possible to start from a trial function, which satisfies the boundary conditions exactly, e.g. for the triangle of **Fig. 8.5** by

$$u = \lambda z \left(\frac{c}{b}y - z\right)\left(\frac{c}{a-b}(a-y) - z\right) = \lambda\bar{u}, \tag{8.26}$$

involving the free parameter λ, to be so determined that the error is minimized (the ansatz (8.26) does not satisfy (8.8)). As measure of the error, it is tempting to use the residue
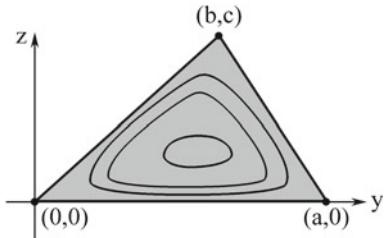
$$R(\lambda) := \int_\Delta \left\{\nabla^2 u(\lambda) - \frac{1}{\eta}\frac{dp}{dx}\right\}^2 da. \tag{8.27}$$

Minimizing condition is

$$\frac{dR}{d\lambda} = 2 \int_\Delta \left\{\nabla^2 u(\lambda) - \frac{1}{\eta}\frac{dp}{dx}\right\}\frac{d\nabla^2 u}{d\lambda}da = 0 \tag{8.28}$$

---

[4]For a biography of PROUDMAN see Fig. 4.13.

Fig. 8.5 Triangular cross section with longitudinal velocity distribution (8.26). *For b = a/2. the triangle is equilateral and the solution (8.26) is exact. In this case (8.26) transforms to (8.25) if a = 2h/√3 and c = h.*

and, owing to $\nabla^2 u(\lambda) = \lambda \nabla^2 \bar{u}$, $\mathrm{d}(\nabla^2 u)/\mathrm{d}\lambda = \nabla^2 \bar{u}$, takes the form

$$\lambda \int_\Delta \left(\nabla^2 \bar{u} \right)^2 \mathrm{d}a - \frac{1}{\eta} \frac{\mathrm{d}p}{\mathrm{d}x} \int_\Delta \nabla^2 \bar{u} \, \mathrm{d}a = 0, \tag{8.29}$$

determining λ as

$$\lambda = \frac{1}{\eta} \frac{\mathrm{d}p}{\mathrm{d}x} \frac{\displaystyle\int_\Delta \left(\nabla^2 \bar{u} \right) \mathrm{d}a}{\displaystyle\int_\Delta \left(\nabla^2 \bar{u} \right)^2 \mathrm{d}a} = \frac{1}{\eta} \frac{\mathrm{d}p}{\mathrm{d}x} \frac{b}{c} \frac{(b-a)}{(c^2 + b^2 - ab)}, \tag{8.30}$$

implying

$$u = \frac{1}{\eta} \frac{\mathrm{d}p}{\mathrm{d}x} \frac{b}{c} \frac{(b-a)}{(c^2 + b^2 - ab)} \, z \left(\frac{c}{b} y - z \right) \left(\frac{c}{a-b}(a-y) - z \right) \tag{8.31}$$

as approximate steady velocity distribution for any triangular conduit.

Problem 8.1 As an exercise, the reader may determine the approximate velocity distribution in the rectangle $-a < y \leqslant a$, $b \leqslant z < b$ by selecting

$$u = \lambda(y^2 - a^2)(z^2 - b^2). \tag{8.32}$$

◆

(c) Upper and lower bounds for the discharge Q for the laminar flow through general cross-sections.
The ensuing developments are motivated by WHEELER [58]. Consider once more the boundary value problem (8.8), but write POISSON's[5] differential equation as

$$[\eta/(\partial p/\partial x)]\nabla^2 u = 1. \tag{8.33}$$

---

[5]After SIMÉON DENIS POISSON (1781–1840), see **Fig. 8.6**.

Poisson bracket

$$\{f, g\} := \sum_{i=1}^{N} \left(\frac{\partial f}{\partial q_i} \frac{\partial g}{\partial p_i} - \frac{\partial f}{\partial p_i} \frac{\partial g}{\partial q_i} \right)$$

$$\text{for } f, g = f, g(p_i, q_i, t)$$

Fig. 8.6 Siméon Denis Poisson (21. June 1781–25. April 1840)

Siméon Denis Poisson was a French mathematician, geometer and physicist. He was born as the son of a soldier and later civil servant. Siméon Poisson, as a result of the wish of his father, should study medicine and was sent to his uncle in Fontaimbleau, a practical surgeon, but interrupted this education in 1796 and studied mathematics at the 'École centrale' in Fontaimbleau and later in 1798, owing to his superb performance at the 'École Polytechnique' in Paris, where he received supervision from Laplace and Lagrange. He finished his studies in 1800 and became professor in 1802 and, in 1806, successor of Jean Baptiste Joseph Fourier, who was sent by Napoléon to Grenoble.

Poisson studied waves, acoustics, elasticity and heat, as well as electric properties of solid bodies. This led to his contributions in electrostatics and potential theory. In 1818 he predicted the so-called Poisson-spot, which only forms, if light possesses wave property. He doubted his own prediction and engaged in a vital dispute with Augustin Jean Fresnel which ended once Fraicois Aragon had experimentally corroborated the spot.

Poisson was elected in 1812 a corresponding, and in 1830, a foreign Member of the Prussian Academy of Sciences. He became in 1818 a Fellow of the Royal Society and 1822 a Member of the American Academy of Arts and Sciences. In applied mathematics Poisson is known for the Poisson equation and in the theory of probability for the Poisson distribution. In Analytical Hamiltonian Mechanics the Poisson bracket is a convenient tool to simply express the Hamiltonian equations of motion, see above formula.

The text is based on http://www.wikipedia.org

With the abbreviation $\partial p / \partial x \equiv p'$ the volume flux may be written as

$$Q = \int_{\mathcal{D}} u \, \mathrm{d}a = \int_{\mathcal{D}} u \cdot 1 \, \mathrm{d}a = \frac{\eta}{p'} \int_{\mathcal{D}} u \nabla^2 u \, \mathrm{d}a. \tag{8.34}$$

Noting that

$$u \nabla^2 u = u \, \mathrm{div} \, \mathrm{grad} \, u = \mathrm{div} \, (u \, \mathrm{grad} \, u) - (\mathrm{grad} \, u)^2, \tag{8.35}$$

this may be put into the form

$$Q = \frac{\eta}{p'} \int_{\partial D} u(\operatorname{grad} u \cdot \boldsymbol{n}) \mathrm{d}s - \frac{\eta}{p'} \int_{D} (\operatorname{grad} u)^2 \, \mathrm{d}a, \tag{8.36}$$

in which the divergence theorem has also been used. On the boundary one has $u = 0$, so

$$Q = -\frac{\eta}{p'} \int_{D} (\operatorname{grad} u)^2 \, \mathrm{d}a. \tag{8.37}$$

This formula will now be used to derive upper and lower bounds for Q.

To determine the *lower bound*, let us choose a function $v(y, z)$ in D with $v = 0$ on ∂D. For this function one may write

$$-\frac{p'}{\eta} \int_{D} v \, \mathrm{d}a \overset{(8.33)}{=} -\int_{D} v \nabla^2 u \, \mathrm{d}a = -\int_{D} v (\operatorname{div} \operatorname{grad} u) \, \mathrm{d}a$$

$$= -\int_{D} \operatorname{div} (v \operatorname{grad} u) \, \mathrm{d}a + \int_{D} \operatorname{grad} v \cdot \operatorname{grad} u \, \mathrm{d}a$$

$$\overset{\text{Gauss}}{=} -\underbrace{\int_{\partial D} v (\operatorname{grad} u \cdot \boldsymbol{n}) \, \mathrm{d}s}_{v=0, \text{ on } \partial D} + \int_{D} \operatorname{grad} v \cdot \operatorname{grad} u \, \mathrm{d}a$$

$$= \int_{D} \operatorname{grad} v \cdot \operatorname{grad} u \, \mathrm{d}a. \tag{8.38}$$

Squaring both sides of this equation yields[6]

---

[6]To prove the SCHWARZ inequality, consider two vector fields $\boldsymbol{a}$ and $\boldsymbol{b}$ and take

$$\int_{D} (\boldsymbol{a} + \lambda \boldsymbol{b})^2 \, \mathrm{d}a \geqslant 0$$

$$\longrightarrow \int_{D} a^2 \mathrm{d}a + 2\lambda \int_{D} \boldsymbol{a} \cdot \boldsymbol{b} \, \mathrm{d}a + \lambda^2 \int_{D} b^2 \mathrm{d}a \geqslant 0.$$

With the choice

$$\lambda = -\frac{\displaystyle\int_{D} \boldsymbol{a} \cdot \boldsymbol{b} \, \mathrm{d}a}{\displaystyle\int_{D} b^2 \mathrm{d}a},$$

$$\frac{p'^2}{\eta^2}\left(\int_{\mathcal{D}} v\,\mathrm{d}a\right)^2 = \left(\int_{\mathcal{D}} \mathrm{grad}\,v\cdot\mathrm{grad}\,u\,\mathrm{d}a\right)^2$$

$$\overset{\text{Schwarz}}{\leqslant} \int_{\mathcal{D}}(\mathrm{grad}\,v)^2\,\mathrm{d}a\cdot\int_{\mathcal{D}}(\mathrm{grad}\,u)^2\,\mathrm{d}a$$

$$\overset{(8.37)}{=} -\frac{p'}{\eta}Q\int_{\mathcal{D}}(\mathrm{grad}\,v)^2\,\mathrm{d}a,$$

implying

$$-\frac{p'}{\eta}\frac{\left(\displaystyle\int_{\mathcal{D}} v\,\mathrm{d}a\right)^2}{\displaystyle\int_{\mathcal{D}}(\mathrm{grad}\,v)^2\,\mathrm{d}a} \leqslant Q. \tag{8.39}$$

For an *upper bound*, a vector field $\boldsymbol{w}$ in $\mathcal{D}$ is chosen, such that in $\mathcal{D}$ div $\boldsymbol{w} = p'/\eta$. With such a choice, one has $(\eta/p')\mathrm{div}\,\boldsymbol{w} = 1$ and, therefore,

$$\int_{\mathcal{D}} u\,\mathrm{d}a = \frac{\eta}{p'}\int_{\mathcal{D}}\mathrm{div}\,(u\,\boldsymbol{w})\,\mathrm{d}a - \frac{\eta}{p'}\int_{\mathcal{D}}\boldsymbol{w}\cdot\mathrm{grad}\,u\,\mathrm{d}a$$

$$\overset{\text{Gauss}}{=} \frac{\eta}{p'}\underbrace{\int_{\partial\mathcal{D}} u(\boldsymbol{w}\cdot\boldsymbol{n})\,\mathrm{d}s}_{u=0\,\text{on}\,\partial\mathcal{D}} - \frac{\eta}{p'}\int_{\mathcal{D}}\boldsymbol{w}\cdot\mathrm{grad}\,u\,\mathrm{d}a$$

$$= -\frac{\eta}{p'}\int_{\mathcal{D}}\boldsymbol{w}\cdot\mathrm{grad}\,u\,\mathrm{d}a. \tag{8.40}$$

(Footnote 6 continued)

this yields

$$\int_{\mathcal{D}} a^2\,\mathrm{d}a\cdot\int_{\mathcal{D}} b^2\,\mathrm{d}a - 2\left(\int_{\mathcal{D}} \boldsymbol{a}\cdot\boldsymbol{b}\,\mathrm{d}a\right)^2 + \left(\int_{\mathcal{D}} \boldsymbol{a}\cdot\boldsymbol{b}\,\mathrm{d}a\right)^2 \geqslant 0$$

$$\longrightarrow \int_{\mathcal{D}} a^2\,\mathrm{d}a\cdot\int_{\mathcal{D}} b^2\,\mathrm{d}a \geqslant \left(\int_{\mathcal{D}} \boldsymbol{a}\cdot\boldsymbol{b}\,\mathrm{d}a\right)^2, \text{ q.e.d.}$$

Now,

$$(\boldsymbol{w} - \operatorname{grad} u)^2 = \boldsymbol{w}^2 - 2\boldsymbol{w} \cdot \operatorname{grad} u + (\operatorname{grad} u)^2 \geqslant 0$$
$$\longrightarrow \quad \boldsymbol{w} \cdot \operatorname{grad} u \leqslant \tfrac{1}{2} \left(\boldsymbol{w}^2 + (\operatorname{grad} u)^2 \right)$$

and, therefore, in view of (8.40),

$$\underbrace{\int_{\mathcal{D}} u \, \mathrm{d}a}_{Q} \leqslant -\frac{\eta}{2p'} \int_{\mathcal{D}} \boldsymbol{w}^2 \mathrm{d}a \underbrace{- \frac{\eta}{2p'} \int_{\mathcal{D}} (\operatorname{grad} u)^2 \, \mathrm{d}a,}_{=Q/2, \ (8.37)}$$

or

$$Q \leqslant -\frac{\eta}{p'} \int_{\mathcal{D}} \boldsymbol{w}^2 \mathrm{d}a. \qquad (8.41)$$

Relations (8.39) and (8.41) can be combined to the statement

$$-\frac{\partial p/\partial x}{\eta} \frac{\left(\int_{\mathcal{D}} v \, \mathrm{d}a \right)^2}{\int_{\mathcal{D}} (\operatorname{grad} v)^2 \, \mathrm{d}a} \leqslant Q \leqslant -\frac{\eta}{\partial p/\partial x} \int_{\mathcal{D}} \boldsymbol{w}^2 \mathrm{d}a. \qquad (8.42)$$

Note that the estimates (8.31) for triangles and (8.32) for rectangles allow evaluation of lower bounds of Q.
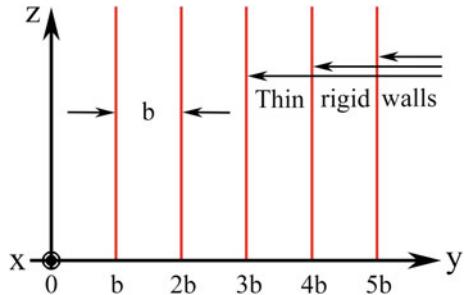
(d) Simple model for the action of a paint brush.[7]

Consider infinitely thin rigid sheets, a distance b apart from one another, standing perpendicular to the plane $z = 0$ and of infinite extent in the z- and x-directions, **Fig. 8.7**. Assume that these sheets move with constant speed U parallel to the x-direction. The spaces between the sheets are filled with a viscous fluid. The sheets are interpreted to function as rows of hairs of a paint brush when it is guided to paint a flat surface and the fluid between the sheets is identified with the paint. The model of this paint-brush consists of the flow of the paint between the moving sheets and the flow of paint onto the xy-plane.

In the coordinate system moving with the sheets the walls are at rest and the xy-plane ($z = 0$) moves with the velocity U. Because of the infinite extent of the sheets, no pressure gradient is formed in the x-direction ($\mathrm{d}p/\mathrm{d}x = 0$) so that the following boundary value problem must be solved:

---

[7]This example is taken from pencil notes of the late Prof. ERNST BECKER (1929–1984), lent to K. HUTTER by Prof. J. UNGER.

Fig. 8.7 Model for a paint brush. *The rigid sheets move with constant speed U in the x-direction (out of the drawing plane). The xy-plane is at rest*

$$
\begin{array}{ll}
\nabla^2 u = 0, & 0 < y < b, \quad 0 < z < \infty, \\
u = 0, & y = 0, \; y = b, \; y = 2b, \; \ldots, \\
u = U, & z = 0, \\
u = 0, & z \to \infty.
\end{array} \tag{8.43}
$$

Because this boundary value problem does not involve the viscosity η, its solution can neither depend on it. It is tempting to seek a separation of variables solution

$$
u(y, z) = f(y)g(z), \tag{8.44}
$$

which yields

$$
\frac{f''(y)}{f(y)} = -\frac{g''(z)}{g(z)} = \text{const.},
$$

in which primes denote univariate differentiation with respect to the indicated variables. Solutions are

$$
\left.
\begin{array}{l}
f(y) = \sin\left(\dfrac{n\pi y}{b}\right), \\[2mm]
g(z) = \exp\left(\dfrac{n\pi z}{b}\right), \; \exp\left(\dfrac{-n\pi z}{b}\right),
\end{array}
\right\} \quad n = 1, 2, \ldots, \infty. \tag{8.45}
$$

The function $f(y)$ satisfies the zero boundary condition at the sheets. Boundedness of the solution as $z \to \infty$ forbids the occurrence of the positive exponential $\exp(n\pi z/b)$. Consequently, the general solution takes the form

$$
u(y, z) = \sum_{n=1}^{\infty} A_n \sin\left(\frac{n\pi y}{b}\right) \exp\left(-\frac{n\pi z}{b}\right), \tag{8.46}
$$

and the boundary condition at $z = 0$ leads to

$$
U = \sum_{n=1}^{\infty} A_n \sin\left(\frac{n\pi z}{b}\right). \tag{8.47}
$$

The coefficients A_k are obtained from the FOURIER decomposition

$$U \int_0^b \sin\left(\frac{k\pi y}{b}\right) dy = \underbrace{\int_0^b A_n \sin\left(\frac{n\pi y}{b}\right) \sin\left(\frac{k\pi y}{b}\right)}_{\frac{b}{2}A_k} = \begin{cases} \frac{2b}{k\pi}U, & (k \text{ odd}) \\ 0, & (k \text{ even}) \end{cases}$$

$$\longrightarrow \quad A_k = \begin{cases} \dfrac{4\,U}{k\pi}, & k = 1, 3, 5, \dots, \\ 0, & k = 2, 4, 6, \dots. \end{cases} \tag{8.48}$$

and, thus, the solution is given by

$$u(y, z) = \frac{4\,U}{\pi} \sum_{n=1,3,5,\dots}^{\infty} \frac{1}{n} \exp\left(-\frac{n\pi z}{b}\right) \sin\left(\frac{n\pi y}{b}\right) \tag{8.49}$$

and yields for the volume flow between the sheets

$$Q = \int_0^b dy \int_0^\infty u(y,z)dz = \frac{4U}{\pi} \sum_{1,3,5,\dots}^{\infty} \int_0^b \sin\left(\frac{n\pi y}{b}\right) dy \int_0^\infty \exp\left(-\frac{n\pi z}{b}\right) dz$$

$$= \frac{8\,U\,b^2}{\pi^3} \sum_{1,3,5,\dots}^{\infty} \frac{1}{n^3} = 0.27\,Ub^2. \tag{8.50}$$

As expected, Q does not depend on η. Modeling Q by a layer of height h and width b gives

$$Q = hUb \quad \longrightarrow \quad h = 0.27\,b. \tag{8.51}$$

One can think of h as the layer thickness of paint leaving the brush in the painting operation.

8.2.2   Ekman Theory and Its Extensions

Let us now look at steady layer flow when the reference frame is not inertial but rotating as the Earth rotates. The water is assumed to be homogeneous. EKMAN[8] (1905) [16] was the first to look at this problem; he constructed the basic solution for wind induced currents—called *drift currents*—in an infinitely deep open sea. Later,

---

[8]For a biography of EKMAN see **Fig. 8.8**.

generalizations of his theory to account for steady and time dependent motion in finite deep oceans, horizontally infinite or bounded, were looked at.[9]

The EKMAN theory and some generalizations of it will be treated here in greater detail, because of its significance in meteorology, oceanography and physical limnology and because of its conceptual importance of these branches of geophysical fluid dynamics.

Fig. 8.8 VAGN WALFRID EKMAN (3. May 1874–9. March 1954)

VAGN WALFRID EKMAN was a Swedish oceanographer. He became committed to oceanography at the University of Uppsala on hearing VILHELM BJERKNES lectures on fluid dynamics. During the expedition of the *Fram*, FRIDTJOF NANSEN had observed that icebergs tend to drift not in the direction of the prevailing wind but at an angle of 20°–40° to the right. BJERKNES (1862–1955) invited EKMAN, still a student, to investigate the problem and, in 1905, EKMAN published his theory of the EKMAN spiral which explains the phenomenon in terms of the balance between frictional effects in the ocean and the CORIOLIS force, which arises from planetary rotation. On completing his doctorate in Uppsala in 1902, EKMAN joined the International Laboratory for Oceanographic Research, Oslo, where he worked for seven years, not only extending his theoretical work but also developing experimental techniques and instruments e.g. the EKMAN current meter and EKMAN water bottle (see **Fig. 8.9**). From 1910 to 1939 he continued his theoretical and experimental work at the University of Lund, where he was professor of mechanics and mathematical physics. He was elected a member of the Royal Swedish Academy of Sciences in 1935. A gifted amateur bass singer, pianist, and composer, he continued working right up to his death.

The text is based on http://www.wikipedia.org

---

[9]This subsection follows closely parts of a corresponding subsection in [28].
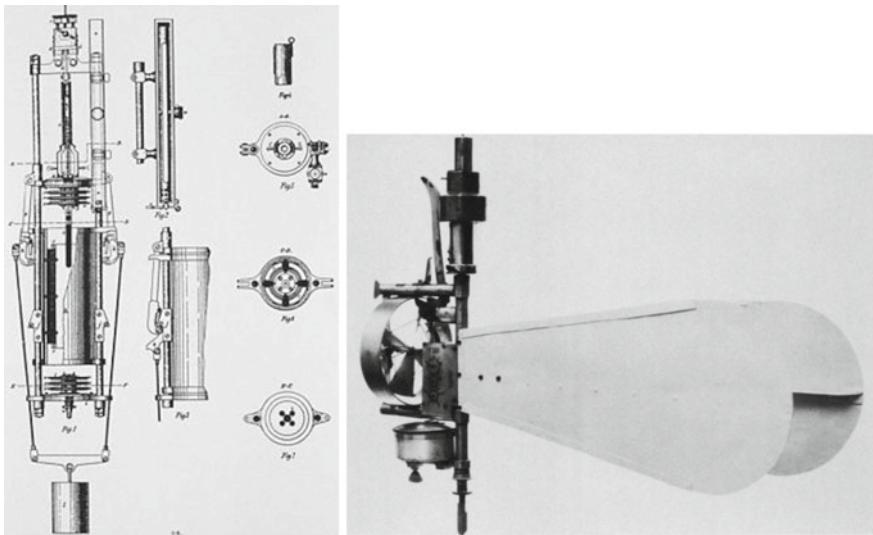
Fig. 8.9 The Ekman water bottle (*left*) and current meter (*right*). *The* Ekman water bottle *is a sea water temperature sample device. The cylinder is dropped at the desired depth; the trap door below is opened to let the water enter and then closed tightly. This can be repeated at different depths as each sample goes to a different chamber of the insulated bottle. It was used for greater depths during the research cruises of 1903 and 1904. The first instruments made, however, were too delicate; after being used for some time, the brass rods which press the lids towards both ends of the cylinder and close the water-bottle, became bent and therefore did not work sufficiently well. For this reason the instruments had to be frequently tested and repaired. As they are now made, they work very well and are very easily handled. The* Ekman *current meter is a mechanical flowmeter invented by* Vagn Walfrid Ekman *in 1903. It comprises a propeller with a mechanism to record the number of revolutions, a compass and a recorder with which to record the direction, and a vane that orients the instrument so the propeller faces the current. It is mounted on a free-swinging vertical axis suspended from a wire and has a weight attached below.* The text and figures are based on http://www.wikipedia.org

In an Earth-fixed coordinate system tangential at a point on the spherical Earth's surface, the acceleration terms on the left-hand side of Eq. (8.2) must be complemented by the Coriolis[10] acceleration $2\boldsymbol{\Omega} \times \boldsymbol{v}$, where $\boldsymbol{\Omega}$ is the angular velocity of the Earth and $\boldsymbol{v}$ is the water particle velocity, measured in the rotating coordinate system. This yields in a coordinate system x-east, y-north, z-zenith

$$\boldsymbol{\Omega} = \left(0, \tfrac{1}{2}\tilde{f}, \tfrac{1}{2}f\right), \quad f = 2\Omega \sin\phi, \quad \tilde{f} = 2\Omega \cos\phi,$$

in which f and $\tilde{f}$ are the first and second Coriolis parameters and ϕ is the latitude angle.

---

[10]For a biography of Coriolis see **Fig. 8.10**. As an addendum to the issue of the Coriolis force Amir D. Aczel's book [1] makes an exciting weekend reading.
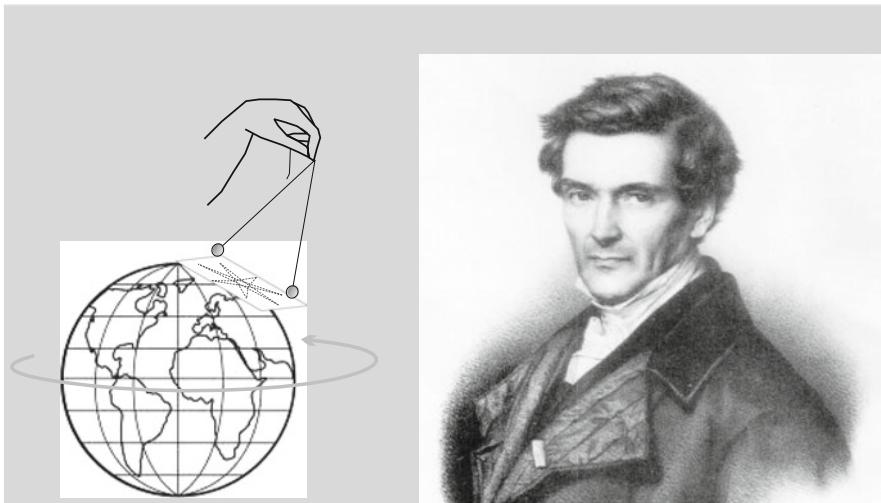
Fig. 8.10 GASPARD- GUSTAVE DE CORIOLIS (21. May 1792–19. Sept. 1843). A sketch of the FOUCAULT pendulum (*left*) is the most explicit demonstration of action of the CORIOLIS force

GASPARD-GUSTAVE DE CORIOLIS, a French mathematician, mechanical engineer and scientist, was born in Paris. In 1816 he became a tutor at the École Polytechnique, in 1829—a professor of mechanics at the École Centrale des Arts et Manufactures. Upon the death of NAVIER in 1836, CORIOLIS succeeded him in the chair of applied mechanics at the École des Ponts and Chaussées and to NAVIER's place in the Académie des Sciences. In 1838 he succeeded DULONG as *Directeur des études* (director of studies) in the École Polytechnique. He died in 1843 at the age of 51 in Paris.

CORIOLIS is best known for his work on the supplementary forces that are detected in a rotating frame of reference, and one of those forces nowadays bears his name. In 1835, he published the paper that made his name famous, *Sur les équations du mouvement relatif des systèmes de corps* (On the equations of relative motion of a system of bodies). He showed that the laws of motion could be used in a rotating frame of reference if an extra term called the CORIOLIS acceleration is added to the equations of motion. It deals with the transfer of energy in rotating systems like waterwheels. CORIOLIS discussed the supplementary forces that are detected in a rotating frame of reference, and one of them would eventually bear his name. The term 'CORIOLIS force' was, however, not used until the beginning of the 20th century. Today, the name CORIOLIS has become strongly associated with geophysical fluid dynamics.

CORIOLIS was the first to coin the term 'work' for the transfer of energy by a force acting through a distance. In 1829 he published a textbook, *Calcul de l'Effet des Machines* ('Calculation of the Effect of Machines'). In this period the correct expression for kinetic energy, $\frac{1}{2}v^2$, and its relation to mechanical work became established. CORIOLIS worked to extend the notion of kinetic energy and work to rotating systems. His first paper, *Sur le principe des forces vives dans les mouvements relatifs des machines* (On the principle of kinetic energy in the relative motion in machines), was read to the Académie des Sciences. In 1835 he published a mathematical memoir on collisions of spheres: *Théorie Mathématique des Effets du Jeu de Billard*, considered a classic on the subject.

The text is based on http://www.wikipedia.org

(a) Ekman spiral below the water surface.

Consider the currents produced in an ocean or lake of infinite extent, which are generated under the following restricting assumptions:

- The water is homogeneous, $\rho = $ constant;
- the horizontal pressure gradient vanishes

$$\nabla_H p = 0, \qquad \frac{\partial p}{\partial x} = \frac{\partial p}{\partial y} = 0;$$

- the vertical velocity is zero, $w = 0$;
- the horizontal components of the extra stress tensor t^E (or the so-called frictional stress tensor t^R) vanish

$$\sigma_{xx} = \sigma_{yy} = \tau_{xy} = 0;$$

- the vertical momentum balance reduces to the hydrostatic pressure equation;
- the vertical viscosity coefficient is constant, $\nu = $ constant;
- processes are steady: $\partial(\cdot)/\partial t = 0$.

With these assumptions, the horizontal momentum equations reduce to

$$\frac{1}{\rho}\frac{\partial \tau_{zx}}{\partial z} = -fv, \qquad \frac{1}{\rho}\frac{\partial \tau_{zy}}{\partial z} = fu, \tag{8.52}$$

and the closure relations for the shear stresses take the forms

$$\tau_{zx} = \rho\nu\frac{\partial u}{\partial z}, \qquad \tau_{zy} = \rho\nu\frac{\partial v}{\partial z}. \tag{8.53}$$

Substituting these relations into (8.52) and observing that ρ and ν are constant, yields

$$\frac{\partial^2 u}{\partial z^2} = -\frac{f}{\nu}v, \qquad \frac{\partial^2 v}{\partial z^2} = \frac{f}{\nu}u. \tag{8.54}$$

These two second order differential equations of the real valued variables u and v can be written as a single second order equation of the complex variable

$$\mathrm{w} = u + \iota v, \tag{8.55}$$

where $\iota = \sqrt{-1}$. Indeed, adding $\iota \times$ (8.54)$_2$ to (8.54)$_1$ yields

$$\frac{d^2\mathrm{w}}{dz^2} = \frac{\iota f}{\nu}\mathrm{w} = \frac{2\iota f}{2\nu}\mathrm{w} = \frac{(\iota + 1)^2 f}{2\nu}\mathrm{w}, \tag{8.56}$$

or

$$\frac{d^2\mathsf{w}}{dz^2} = \frac{(\iota + 1)^2\pi^2}{D^2}\mathsf{w}, \tag{8.57}$$

where

$$D := \pi\sqrt{\frac{2\nu}{f}} \tag{8.58}$$

has the dimension of a length and is called the *Ekman depth*. Solutions of (8.57) are only functions of z and have the form

$$\mathsf{w}(z) = A\,\exp\left\{\frac{(1+\iota)\pi}{D}z\right\} + B\,\exp\left\{-\frac{(1+\iota)\pi}{D}z\right\} \tag{8.59}$$

with two constants of integration, A and B.

(α) *Infinite depth* EKMAN *current*

These constants follow from the boundary conditions

$$\begin{aligned}
\tau_{zx} + \iota\tau_{zy} &= \rho\nu\frac{\partial\mathsf{w}}{\partial z} = -\iota\tau_s \quad \text{at } z = 0, \\
\mathsf{w} &= 0 \quad \text{at } z = h.
\end{aligned} \tag{8.60}$$

The first states that the constant wind shear stress τ_s acts in the y-direction and is uniformly distributed over the entire free surface, the latter states that the bottom surface is impenetrable. VAGN WALFRID EKMAN looked at an infinitely deep ocean, $h \to \infty$. For this case, (8.60)$_2$ implies $A = 0$, and (8.60)$_1$ yields

$$\mathsf{w}(z) = (1 + \iota)\frac{D\tau_s}{2\pi\nu\rho}\,\exp\left\{-\frac{(1+\iota)\pi}{D}z\right\}, \tag{8.61}$$

which may, alternatively, be written as

$$\mathsf{w}(z) = \frac{\sqrt{2}\pi\tau_s}{\rho fD}\,\exp\left\{-\pi\frac{z}{D}\right\}\exp\left\{\iota\left(\frac{\pi}{4} - \pi\frac{z}{D}\right)\right\}. \tag{8.62}$$

To derive this, we have used the identity $(1 + \iota) = \sqrt{2}\,\exp(\iota\pi/4)$. At the surface $z = 0$ this yields

$$\mathsf{w}(z = 0) = \mathsf{w}_s = \frac{\sqrt{2}\pi\tau_s}{\rho fD}\,\exp\left\{\frac{\iota\pi}{4}\right\}, \tag{8.63}$$

or using EULER's formula $e^{\iota\varphi} = (\cos\varphi + \iota\sin\varphi)$,

$$\mathbf{w}_s = (u + \iota v) = W_s \left(\cos\pi/4 + \iota\sin\pi/4\right), \tag{8.64}$$

$$W_s = \frac{\sqrt{2}\pi\tau_s}{\rho fD}. \tag{8.65}$$

Here, W_s is the strength of the surface current in terms of the wind shear stress. Since the wind has been assumed to blow in the positive y-direction, the current at the free surface is at 45° to the right of the wind (to the left on the Southern Hemisphere). Moreover, it follows from (8.62) that the horizontal current decreases exponentially with depth (as $\exp(-\pi z/D)$), and its deflection angle to the right of the wind is given by $\pi/2 - (\pi/4 - \pi z/D) = \pi/4 + \pi z/D$. This angle increases with depth. So, with increasing depth the current at a fixed xy-position rotates cum sole around the vertical line at that position. Its modulus (absolute value) is given by

$$|\mathbf{w}| = W_s \exp\left(-\pi\frac{z}{D}\right), \tag{8.66}$$

and its angle to the right of the wind is given by

$$\alpha(z) = \left(\pi\frac{z}{D} + \frac{\pi}{4}\right). \tag{8.67}$$

This current system is called the EKMAN spiral after EKMAN (1905) [16] who first described it. **Figure 8.11** displays in panel a this current system. At the EKMAN depth, $z = D$, the modulus of the current relative to the current at the surface takes the value

$$\frac{|\mathbf{w}|_{z=D}}{W_s} = e^{-\pi} \sim \frac{1}{23} = 0.043, \tag{8.68}$$

and its direction is opposite to the surface current. At the depth of twice the EKMAN depth, $z = 2D$, the direction of the current is the same as that on the water surface, and its modulus is

$$\frac{|\mathbf{w}|_{z=2D}}{W_s} = e^{-2\pi} \sim \frac{1}{535} = 0.0019. \tag{8.69}$$

If the velocities at increasing depth are projected onto the xy-plane (panel b) of Fig. 8.11) the tips of the current vectors trace a logarithmic spiral, which coils indefinitely around the origin of the xy-coordinate system. If the components of the horizontal current in the direction of the surface current and perpendicular to it are plotted against z, then the two curves in Fig. 8.11c are obtained.
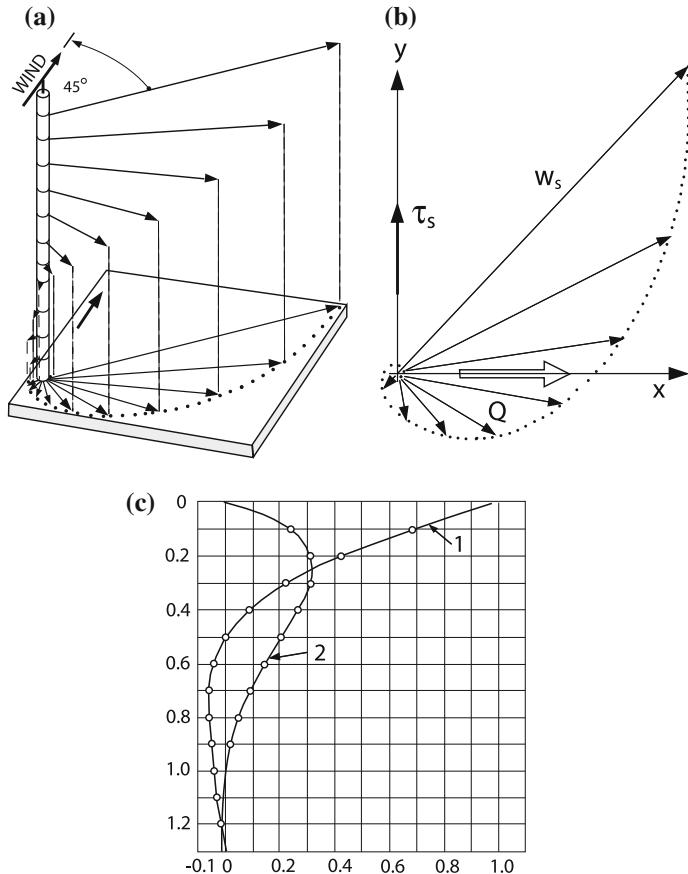
Fig. 8.11 EKMAN spiral. **a** *Plotted in perspective view;* **b** *shown in the projection into the hodograph plane, tracing a logarithmic spiral;* **c** *plotted as components in the direction of the surface current, (1), and perpendicular to it, (2). Shown as double arrow in (b) is also the vertically integrated total volume (mass) flux Q, which is 90° to the right of the wind shear stress, constructed from figures by Laska* [33] © *Laboratory of Hydraulics, Hydrology and Glaciology at ETH Zurich*

The vertically integrated volume flux may be written as

$$
Q = Q_x + \iota Q_y \quad = \int_{-\infty}^{0} \mathrm{w}\,\mathrm{d}z
$$

$$
= \frac{\sqrt{2}\pi\tau_s}{\rho f D} \int_{0}^{\infty} \exp\left\{-\frac{\pi}{D}z(1+\iota) + \iota\frac{\pi}{4}\right\} \mathrm{d}z
$$

$$
= \frac{\tau_s}{\rho f}. \tag{8.70}
$$

This is also called the total transport; it is directed perpendicular to the wind stress and to the right of it.

(β) *Finite depth* EKMAN *current*

Let us start by assuming a layer of a homogeneous fluid of infinite extent and constant finite depth h that is subjected to a steady uniform wind. In this case, the steady complex valued drift current can also be determined by (8.59), but it is now advantageous to write the general solution in the form

$$\mathsf{w}(z) = A \sinh\left\{\frac{(1 + \iota)\pi}{D}(z - h)\right\} + B \cosh\left\{\frac{(1 + \iota)\pi}{D}(z - h)\right\}, \quad (8.71)$$

which is simply another linear combination of the fundamental solution of (8.57). A and B are constants of integration to be determined by the boundary conditions

$$\rho\nu\frac{\partial\mathsf{w}}{\partial z}(0) = -\iota\tau_s \quad \text{(prescribed shear in the } y \text{ direction),}$$
$$\mathsf{w}(h) = 0 \qquad \text{(no slip).} \tag{8.72}$$

The second of these implies $B = 0$ and the first yields A such that

$$\mathsf{w}(z) = (1 + \iota)\frac{D\tau_s}{2\pi\rho\nu}\frac{\sinh\{(1 + \iota)a(1 - \mathfrak{z})\}}{\cosh\{(1 + \iota)a\}}, \tag{8.73}$$

where

$$a = \frac{\pi h}{D}, \qquad \mathfrak{z} = \frac{z}{h}. \tag{8.74}$$

Vertical structures of the current from (8.73) are illustrated in **Fig. 8.12** for various values of h/D. The spiral for $h/D = 1.25$ is very close to the EKMAN spiral for the infinitely deep ocean $h/D \to \infty$. The graph shows the important influence of bottom friction in a fluid layer whose depth is smaller than the EKMAN depth D. As h decreases, the deflection angle of the current from the wind direction decreases and the effect of the Earth's rotation becomes smaller. For very small values of a, TAYLOR series expansions transform (8.73) into

$$\mathsf{w}(z) = \frac{\iota h\tau_s}{\nu\rho}(1 - \mathfrak{z}), \qquad \left(\frac{\pi h}{D} \ll 1\right). \tag{8.75}$$

This says that the currents are in the direction of the wind, independent of the rotation of the Earth and they decay linearly with depth.

The thin dashed line in Fig. 8.12 connects the surface points of the spirals for particular values of h/D. As the curve is traced, the angle between the Oy-axis and the straight line connecting the origin O with one of its points defines the angle between the direction of the wind and the surface current for that value of h/D. This
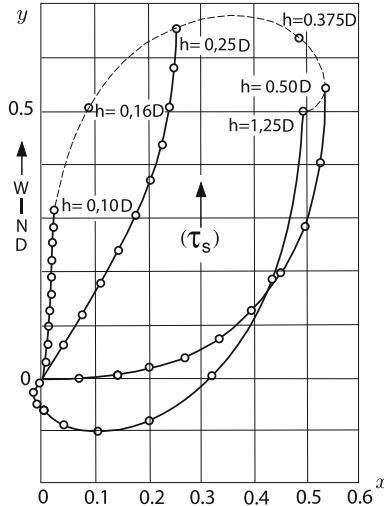
Fig. 8.12 Finite depth EKMAN spirals. *Vertical structure of the wind-induced current for the* EKMAN *problem in a basin of finite depth h for h/D = 0.1, 0.25, 0.5, 1.25 marked in steps of 0.1h from the surface down to the bottom. The thin dashed line connects the velocities at the free surface for h/D ∈ [0.1, 1.25]. For h/D > 0.5, the rotation of the current through the* EKMAN *layer is nearly 45°; for h/D < 0.5 this angle of deviation is smaller, for h/D < 0.1 practically 0°, adapted from* HEAPS *(1984)* [24]. © *Laboratory of Hydraulics, Hydrology and Glaciology at ETH Zurich*

Table 8.1 Deflection angle of the surface current velocity from the direction of the wind for the EKMAN problem in a finite depth basin

h/D	0.1	0.25	0.5	0.75	1.0	1.5
α	5°	21.5°	45°	45.5°	45°	45°

deflection angle can be shown to be given by

$$\alpha = \frac{\pi}{4} - \arctan\left\{\frac{\sin(2a)}{\sinh(2a)}\right\}, \tag{8.76}$$

and is given in **Table 8.1** for a selection of h/D-values. This table shows that for $h/D > 0.5$ the deflection angle is practically 45°; it only takes smaller values for $h/D < 0.5$.

   Finally, the total volume transport is given by

$$Q = \int_0^h \mathsf{w}(z)\mathrm{d}z = \frac{(1+\iota)D\tau_s}{2\pi\rho\nu h}\frac{1}{\cosh\{(1+\iota)a\}}\int_0^1 \sinh\{(1+\iota)a(1-\mathfrak{z})\}\mathrm{d}\mathfrak{z}$$

$$= \frac{\tau_s}{\rho f}\left\{1 - \frac{1}{\cosh\{a(1+\iota)\}}\right\}. \tag{8.77}$$

Clearly, as $h \to \infty$ ($a \to \infty$), we have $\alpha \to \pi/4$ and $Q_x \to \tau_s/(\rho f)$, $Q_y \to 0$, as expected.

The physical understanding of this finite depth EKMAN problem also profits from the following, alternative interpretation of the current structure. Under a steady current, friction at the fluid bed generates an EKMAN spiral also above the bottom surface. As the current decreases towards the bottom from the main stream flow, it rotates counter clockwise, in the opposite sense to the wind-driven near-surface EKMAN spiral.

(γ) *Non-constant Vertical Eddy Viscosity*

The assumption of a constant viscosity is not realistic for the vertical distribution of the horizontal wind-induced current in the free surface EKMAN layer. This layer is almost always subjected to turbulence, i.e. fluctuating horizontal velocities which give rise to turbulent shear stresses, in particular surface parallel shear stresses. These are measurable in terms of fluctuations of horizontal velocity components and the density. Alternatively, these stresses can also be expressed in terms of the strain rate tensor D of the *mean* motion[11] in the form $\tau = 2\rho\nu_t D$, where ν_t is the turbulent viscosity, often called *eddy viscosity*, to express its presence as a result of the meso-scale turbulent eddies. Measurements show that, in the ocean or in a lake, ν_t varies with depth with a near zero value at the free surface, growing with depth, reaching a maximum value at some depth, say at $0.2 \times H$, and beyond this level is rapidly decreasing. On the other hand, the simplifications which led to EKMAN's equation remain valid; the only change is a different postulate for the vertical distribution of the eddy viscosity.

EKMAN's problem of wind induced flow has been solved by MADSEN (1977) [34] by assuming that the eddy viscosity increases linearly with depth from a value of zero at the free surface, $z = 0$. The law of increase follows LUDWIG PRANDTL's theory of turbulent boundary layer (1933) [40], in which

$$\nu = \kappa u_* z, \qquad u_* := \sqrt{\tau_s/\rho}, \tag{8.78}$$

where $\kappa = 0.41$ is THEODORE VON KÁRMÁN's constant and u_* is the friction velocity. Substituting (8.78) into (8.53) and the resulting expression into (8.52) yields

$$\frac{\mathrm{d}}{\mathrm{d}z}\left(z\frac{\mathrm{d}w}{\mathrm{d}z}\right) = \frac{\iota f}{\kappa u_*}w, \qquad w = u + \iota v, \qquad z \in (0, \infty). \tag{8.79}$$

In an infinitely deep ocean this equation must be solved subject to the boundary conditions

$$\begin{aligned} -\rho\kappa u_* z\frac{\mathrm{d}w}{\mathrm{d}z} &= \tau_s = \tau_{sx} + \iota\tau_{sy}, & z &\to 0, \\ w &= \text{bounded}, & z &\to \infty. \end{aligned} \tag{8.80}$$

---

[11]We write here D rather than $\langle D \rangle$, which was used to denote the strain rate tensor of the mean velocity field. We do this for simplicity of notation.

The first relates the vertical shear stress to the wind shear stress at the surface; the second requires finiteness of the current at infinity. Note also that $(8.80)_1$ requires $d\mathsf{w}/dz$ to behave as $\sim z^{-1}$ when $z \to 0$ approaches the free surface to make a non-vanishing shear stress possible; this is equivalent to a logarithmic singularity of w as $z \to 0$.

Let

$$\xi = \frac{\iota f}{\kappa u_*} z \quad \to \quad \frac{d}{dz} = \frac{\iota f}{\kappa u_*} \frac{d}{d\xi}. \tag{8.81}$$

Then, Eqs. (8.79), (8.80) take the forms

$$\frac{d}{d\xi}\left(\xi\frac{d\mathsf{w}}{d\xi}\right) = \mathsf{w}, \qquad \xi \in (0, \infty),$$

$$-\rho\kappa u_*\xi\frac{d\mathsf{w}}{d\xi} = \tau_s, \qquad \xi \to 0, \tag{8.82}$$

$$\mathsf{w} = \text{bounded}, \qquad \xi \to \infty.$$

Equation $(8.82)_1$ can be put into the standard form of BESSEL's[12] differential equation of zeroth order. It possesses the general solution

$$\mathsf{w} = AI_0(2\sqrt{\xi}) + BK_0(2\sqrt{\xi}), \tag{8.83}$$

where A, B are arbitrary constants of integration and I_0, K_0 are the *modified* BESSEL functions of zeroth order (ABRAMOWITZ and STEGUN (1965) [2]). Since I_0 exhibits an exponential growth as $\xi \to \infty$, we must have $A = 0$. The second constant, B, then follows from $(8.82)_2$,

$$-\kappa u_*\xi\frac{d\mathsf{w}}{d\xi}\bigg|_{\xi\to 0} = \kappa u_*\sqrt{\xi}BK_1(2\sqrt{\xi}) = \frac{\tau_s}{\rho} \text{ as } \xi \to 0, \tag{8.84}$$

in which K_1 is the first order modified BESSEL function of the second kind. Substituting for K_1 its asymptotic expansion for small ξ (ABRAMOWITZ and STEGUN (1965) [2]), we obtain $B = 2\tau_s/(\rho\kappa u_*)$ or

$$\mathsf{w} = \frac{2}{\rho\kappa u_*}K_0\left(2\sqrt{\xi}\right)\tau_s. \tag{8.85}$$

---

[12]For a biography of FRIEDRICH WILHELM BESSEL see **Fig. 8.13**.

Fig. 8.13 FRIEDRICH WILHELM BESSEL (22. July 1784–17. March 1846)
Right panel Königsberg Observatory with its heliometer tower around 1830

FRIEDRICH WILHELM BESSEL was a primarily self taught astronomer. He improved by careful observation the astronomical constants, and by accounting for the instrument errors the preciseness of the astronomical data observations, discovered the parallax, founded the investigation of the comets and determined the dimensions of the Earth's body.

BESSEL, after prematurely leaving the gymnasium education due to insufficient performance in Latin, made an apprenticeship as a tradesman in Bremen. During this time, he was already attracted by astronomy reading *The Electrician* and performed his self-education that was successful because of his tenacious working habits. In 1806 he went to the observatory of J.H. SCHRÖTER to Lilienthal, where he stayed until 1810 and produced a number of scientific memoirs on the astronomy of comets. In 1810 he went to Königsberg, where he supervised the construction of the observatory, and, after the completion in 1813 became its director and simultaneously Professor of Astronomy at its University. These positions he held until his death.

Most of BESSEL's work is on careful astronomical observations. His early work on the observational data of J. BRADLEY—almost unknown at that time—appeared in 1818 as '*Fundamenta Astronomiae*'. From 1821–1833 he made accurate determinations of the positions of stars. He was the first to succeed in determining the annual parallax of the fixed star 61 Cygni, thus corroborating the Copernican heliocentric theory. In his investigation of problems connected with planetary perturbations, he encountered an ordinary differential equation, whose solution functions are now known as BESSEL functions.

Text based on http://www.wikipedia.org and
– Anonymous: Fachlexikon Forscher und Erfinder. Nikol Verlagsgesellschaft mbH & Co.KG, Hamburg
– Funk & Wagnalls' Standard Reference Encyclopedia

For uniform wind-shear stress in the y-direction of the form $\tau_s = \iota\tau_{s,y}$ and with $\tau_{s,y} = \rho u_*^2$ and $\bar{\xi} = -\iota\xi = fz/(\kappa u_*)$, (8.85) can be shown (MADSEN (1977) [34]) to be expressible as

$$\mathsf{w} = \iota\frac{2u_*}{\kappa}K_0\left(2\sqrt{\bar{\xi}}e^{\iota\frac{\pi}{4}}\right)$$

$$= \iota \frac{2u_*}{\kappa} \left\{ ker\left(2\sqrt{\bar\xi}\right) + \iota\, kei\left(2\sqrt{\bar\xi}\right) \right\} \tag{8.86}$$

(see ABRAMOWITZ and STEGUN (1965) [2]), which possesses the asymptotic representation

$$\mathsf{w} = \frac{u_*}{\kappa} \left\{ \frac{\pi}{2} + \bar\xi \ln \bar\xi + \iota(-2\gamma - \ln\gamma) \right\} \quad \text{as } \bar\xi \to 0, \tag{8.87}$$

in which $\gamma = 0.577\ldots$ is EULER's constant. Representation (8.86) agrees with ELLISON's (1956) [17] solution for the atmospheric boundary layer.

To examine the variation of the steady drift current with depth the solution given by (8.86) is plotted in **Fig. 8.14**. The velocity vector is indicated at increments of $\sqrt{\bar\xi} = 0.1$, with the surface current given by

$$\mathsf{w}_s = \frac{u_*}{\kappa} \left\{ \frac{\pi}{2} + \iota \left(-1.15 + \ln\left(30\frac{\kappa u_*}{k_s f}\right)\right) \right\} \tag{8.88}$$

from (8.87), and $k_s = 5$ cm as roughness length, to avoid the singularity at $\bar\xi = 0$. Note the extremely rapid decrease and rotation of the drift current with depth, a consequence of the logarithmic velocity deficit near the surface. Note, moreover, that according to (8.88), the deflection angle α_s between the surface shear stress and the steady surface drift current is given by

$$\tan\alpha_s = \frac{\pi/2}{-1.15 + \ln\left(30\dfrac{\kappa u_*}{k_s f}\right)}, \tag{8.89}$$
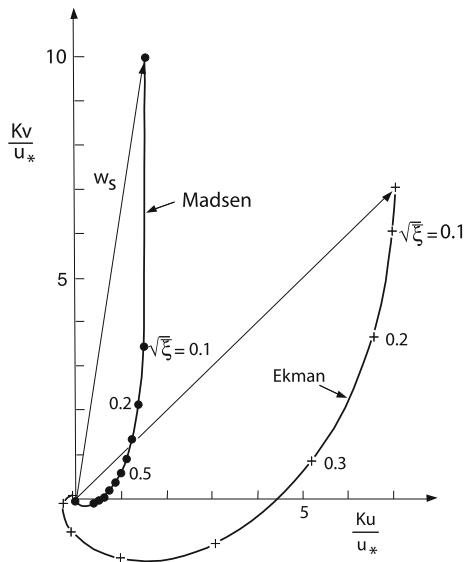
where the deflection is to the right in the Northern hemisphere. As can be inferred from this and Fig. 8.14, α_s is $\sim 10°$ and the velocity at $\sqrt{\bar\xi} = 0.1$ is approximately one-third of its value at the surface with a deflection angle of $\alpha = 25°$ as compared to $\alpha_s = 9°$. It is also evident from this figure that there is practically no motion at the depth corresponding to $\bar\xi = 1$; so,

$$z = \frac{\kappa u_*}{f} \tag{8.90}$$

can indeed be regarded as a measure of the extent of the frictional influence.

Interestingly, despite the considerable differences between the details of the velocity structure predicted by the EKMAN solution with constant vertical viscosity and this one, the two solutions share a common feature. The total mass transport predicted by (8.86) is found to be

Fig. 8.14 Vertical velocity
structure of a pure drift
current in an infinitely deep
homogeneous sea of finite
lateral extent, comparing the
spiral based on $\nu = \kappa u_* z$, ($\bullet$)
and the classical EKMAN
spiral, (+), from MADSEN
(1977) [34]. © American
Meteorological Society,
reprinted with permission

$$Q = Q_x + \iota Q_y = \frac{2u_*}{\kappa} \int\limits_0^\infty \left\{ -kei\left(2\sqrt{\bar{\xi}}\right) + \iota\, ker\left(2\sqrt{\bar{\xi}}\right) \right\} \mathrm{d}\bar{\xi}$$

$$= \frac{u_*^2}{f} \int\limits_0^\infty \{-\beta\, kei\,\beta + \iota\beta\, ker\,\beta\}\, \mathrm{d}\beta = \frac{u_*^2}{f}, \qquad (8.91)$$

which is identical to the result obtained from EKMAN's theory as it should be since
the result is independent of ν.

The above solution of the complex valued differential equation (8.79) exhibits a
logarithmic singularity at $z = 0$. To avoid it, a coordinate shift

$$\bar{z} = z + z_0, \qquad \text{where } z_0 > 0 \qquad (8.92)$$

is applied. The two-point boundary value problem now becomes

$$\left.\begin{array}{ll} \left((\bar{z} + z_0)\mathsf{w}'\right)' = \dfrac{\iota f}{\kappa u_*}\mathsf{w}, & 0 < \bar{z} < \infty, \\[2mm] \rho\kappa u_*\,(\bar{z} + z_0) = -\iota\tau_s, & \text{at } \bar{z} = 0, \\[2mm] \mathsf{w} = 0, & \text{at } \bar{z} \to \infty. \end{array}\right\} \qquad (8.93)$$

Now, the singularity is avoided since $\bar{z} = 0$ is never attained. $z_0 > 0$ is a *roughness
length* and of the order of millimeters, e.g. $z_0 = 1.5$ mm.

HEAPS (1984) [24] writes: 'The results obtained by O.S. MADSEN, compared with
those by EKMAN's theory show a more rapid decrease and rotation of the current
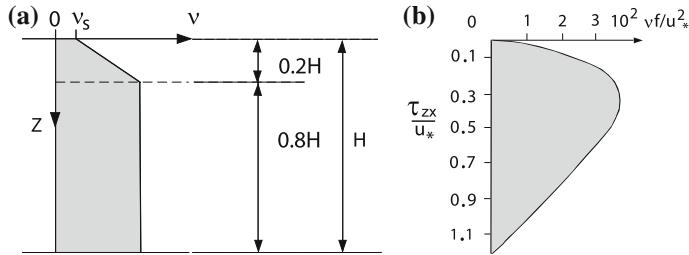
Fig. 8.15 a Eddy viscosity distribution with a surface wall layer. **b** Eddy viscosity distribution from SVENSSON's turbulence model, using $k - \varepsilon$ closure condition, adapted from HEAPS (1984) [24]. © Laboratory of Hydraulics, Hydrology and Glaciology at ETH Zurich

vector with depth, due to a steep logarithmic fall of the velocity component in the wind direction, near to the surface and downwards from it. For a range of wind speeds, MADSEN's model gives a deflection angle of the surface current to the right of the wind stress about 10° and a wind factor of approximately 0.03. These values agree with deductions made from surface drift experiments and observations of oil spill trajectories (B.R. PEARCE and C.K. COOPER (1981) [37], Figure 1 […]). MADSEN's model shows that the depth of the wind-induced motion (down to a level of practically no current) is approximately $0.41u_*/f$, a length which corresponds to D in the Ekman theory. Setting $D = 0.41u_*/f$ […] [and using the definition (8.58) of the frictional depth] yields an expression for the corresponding constant eddy viscosity in the EKMAN theory:

$$\nu = 0.008 \frac{u_*^2}{f}. \tag{8.94}$$

(from N.S. HEAPS (1984) [24])'.

A linear increase of the eddy viscosity with depth cannot be realistic, since turbulent intensity decreases with depth and may die out completely at large depth. N.S. HEAPS continues: 'URBAN SVENSSON (1979) [51] employed a turbulence model (using $k - \varepsilon$ closure condition[13]) to determine the vertical structure of current in the surface EKMAN layer. A vertical eddy viscosity distribution of the form shown in **Fig. 8.15**b was obtained, showing a linear increase in viscosity near the sea surface as in MADSEN's model, turning, however, into a decrease lower down. The depth

---

[13]In the $k - \varepsilon$-model the kinematic viscosity ν is parameterized according to

$$\nu = c_\mu \frac{k^2}{\varepsilon}$$

where $c_\mu = 0.09$ is a dimensionless constant, k is the specific turbulent kinetic energy with dimension $m^2 s^{-2}$ and ε the specific dissipation rate of turbulent kinetic energy with dimension $m^2 s^{-3}$. The model is complemented by postulating evolution equations for k and ε, so that the kinematic viscosity can vary with time and position. For the presentation of the $k - \varepsilon$ model, see Vol. 2, Chap. 15.

of penetration of the motion was found to be approximately $1.0u_*/f$. The use of a constant eddy viscosity

$$\nu = 0.026u_*^2 \tag{8.95}$$

was found to give velocity and shear-stress distributions in good agreement with those obtained from the turbulence model […]. An eddy viscosity decaying with depth reflects the expected condition of diminishing turbulence intensity as distance below the surface increases.' (HEAPS (1984) [24]). Theories prescribing different vertical variations of the eddy viscosity and treating the EKMAN problem in a homogeneous fluid of infinite or finite depth are summarized in **Table 8.2**. Accordingly, the eddy viscosity either increases or decreases as the free surface is approached from below. HEAPS (1984) [24] writes: 'While a decrease seems most likely on the weight of evidence so far available, there appears to be little or no observational evidence to confirm this for the full range of wind speeds. According to work performed by GABRIEL T. CSANADY between 1976 and 1982 (see Table 8.2) the surface EKMAN layer can be considered to consist of a relatively thin layer at the free surface through which the eddy viscosity varies linearly with depth from a small surface value ν_s and an outer layer through which the eddy viscosity remains constant. Thus,

$$\nu = \begin{cases} \kappa u_* z + \nu_s, \ 0 \leqslant z < \dfrac{h}{\kappa \mathbb{R}}, \\ \dfrac{u_* h}{\mathbb{R}} + \nu_s, \ \dfrac{h}{\kappa \mathbb{R}} \leqslant z \leqslant h, \end{cases} \tag{8.96}$$
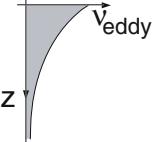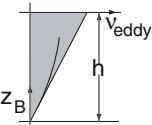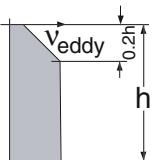
where h is the depth of the EKMAN layer and $\mathbb{R}$ a REYNOLDS number lying between 12 and 20', implying that $h/(\kappa \mathbb{R}) \in [0.125, 0.208]$. Then, with $h = 0.4u_*/f$ say, the eddy viscosity in the outer layer takes the value

$$\nu = (0.02 - 0.033)\frac{u_*^2}{f} + \nu_s. \tag{8.97}$$

According to HEAPS (1984) [24], 'PEARCE and COOPER (1981) [37] have used (8.96) for computations of wind induced flows in shallow water of depth h (Fig. 8.15a) employing a slip condition at the sea bed. BOWDEN et. al. (1959) [7] proposed a similar distribution of vertical eddy viscosity to account for the presence of the wall layer adjacent to the sea bed in tidal flow; the corresponding theory was worked out by HEAPS and JONES (1984) [25]. Generally, the profile of eddy viscosity is modified by a wall layer at the sea surface and a wall layer at the sea bed. These layers have distinct length and velocity scales when the corresponding EKMAN layers do not overlap. At the bottom, the stress, and hence u_*, depends on the motion of the water'.

Practically, the construction of the current is determined by a patching together of a near surface PRANDTL layer in which, because of its thinness, the CORIOLIS effects due to the rotation of the Earth are ignored, and an EKMAN solution below this viscous PRANDTL layer. The stress is assumed to remain constant through the

Table 8.2 Vertical distributions of eddy viscosity used by various authors for the solution of the EKMAN problem in an infinite homogeneous fluid layer

Exponential decay with depth ($h \to \infty$)	DOMBROKLONSKIY (1969) [13]
	LAI and RAO (1976) [31]
	WITTEN and THOMAS (1976) [60]
Proportional to the height z_B above the bottom surface	THOMAS (1975) [52]
Proportional to $z_B^{4/3}$ linearly distributed to a certain depth ($0.2h$) from the surface, then constant	FJELDSTAD (1930) [18]
	CSANADY (1976)–(1982) [8–12]
	PEARCE and COOPER (1981) [37]
	BOWDEN et al. (1959) [7]
	HEAPS and JONES (1984) [25]

PRANDTL layer, but the eddy viscosity is taken as linearly increasing through this layer. Consequently, if the uniform wind stress τ_s points in the positive y-direction, the momentum equations in this layer take the forms

$$
\begin{aligned}
-\rho(\kappa u_* z)\frac{\partial u}{\partial z} &= 0, \\
-\rho(\kappa u_* z)\frac{\partial v}{\partial z} &= \tau_s = \rho u_*^2,
\end{aligned}
\tag{8.98}
$$

whence

$$
\begin{aligned}
\frac{\partial u}{\partial z} &= 0 & \longrightarrow & \quad u = u_s, \\
\frac{\partial v}{\partial z} &= -\frac{u_*}{\kappa z} & \longrightarrow & \quad v = v_s - \frac{u_*}{\kappa}\ln\left(\frac{z}{z_0}\right).
\end{aligned}
\tag{8.99}
$$

Thus, the velocity profile through the PRANDTL layer is logarithmic and parallel to the wind shear stress; u_s and v_s denote the components of the current at the free surface (the top of the PRANDTL layer) taken at $z = z_0 > 0$ to avoid the logarithmic singularity. At the bottom of this PRANDTL layer, at $z = z_1$, the velocity components u_1 and v_1 are given by what is obtained as surface current of the EKMAN problem (of finite or infinite) depth, e.g. (8.63) for the infinite depth case. This is so, because the wind stress is transmitted through the PRANDTL layer without change. Therefore, from (8.99),

$$u_s = u_1, \qquad v_s = v_1 + \frac{u_*}{\kappa} \ln\left(\frac{z_1}{z_0}\right). \tag{8.100}$$

N.S. HEAPS remarks that 'this says that the surface current obtained with a PRANDTL layer may be obtained from the surface current derived from the pure EKMAN theory by adding a logarithmic contribution in the direction of the wind. Such an addition increases the magnitude of the surface current and reduces its deflection angle from the wind direction'.

CSANADY (1982) [12] proposed instead of (8.100)

$$u_s = u_1, \qquad v_s = v_1 + \frac{u_*}{\kappa} \ln\left(\frac{z_1}{z_0}\right) + 8.5u_*, \tag{8.101}$$

but gives no justification for the last term of (8.101).

(γ) *Further results*

The above EKMAN-type solutions of layer flows on the rotating Earth are all characterized by an infinite horizontal extent of the fluid basin. Such an idealization prevents formation of horizontal pressure gradients, because of the absence of boundaries. So-called *gradient currents* are established if the horizontal gradient does not vanish. Such analyses have been performed e.g. by LACOMB [29] and GEDNEY and LICK in 1972 [23] on the basis of GEDNEY's Ph.D. Dissertation [22]. The mathematical method goes back to WELANDER [57], and applications have been presented by BONHAM-CARTER and THOMAS [5] and WITTEN and THOMAS [60].

Yet a further extension of this layer method concerns the addition of time dependency and spatial finiteness of the domains of solutions. The principal handling and explicit construction of the associated initial boundary value problems has already been proposed by FJELDSTAD (1930) [18] and HIDAKA (1933) [26] and has been applied and perfected by FORISTALL [19, 20], FORISTALL et al. [21], and above all PLATZMAN[14] [38].

An exposition on these methods is given by HUTTER et al. in Chap. 9 [28].

---

[14]For a biography of PLATZMAN see **Fig. 8.16**.

Fig. 8.16 George W. Platzman (19. April 1920–2. Aug. 2008)

GEORGE W. PLATZMAN, meteorologist, who earned his bachelor's and master's degrees in mathematics and physics from the Universities Chicago and Arizona in 1940 and 1941, respectively, and a Ph.D. in meteorology from the University of Chicago in 1947, joined the faculty of the University's Meteorology Department in 1948. He remained there when he retired as Professor Emeritus. PLATZMAN, one of the founders of modern meteorology, transformed weather forecasting from qualitative guesswork to quantitative science. He specialized in dynamic meteorology and oceanography, including numerical weather prediction and storm surges, which are caused by wind and in the Great Lakes' area due to Hurricanes. He has pioneered weather forecast by computer, laid down the theory of storm surges and participated in the development of advanced computer software to model and forecast variations of surface elevation fields in the ocean and in lakes. He summarized his research in seminal papers, e.g. articles on the ocean tides and the storm surge theory and a comprehensive review of the ROSSBY wave. PLATZMAN's personal interests included collecting early printed editions of musical compositions by Fréderic CHOPIN. He established the Rose K. PLATZMAN Memorial Collection at the University of Chicago Library in honor of his mother.

The text is based on http://news.uchicago.edu/.

8.3 Simple Unsteady Flows
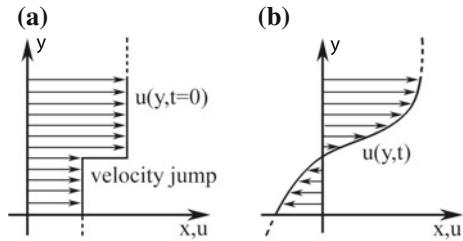
Consider a density-preserving NAVIER-STOKES fluid with vanishing body force subject to the velocity field with the Cartesian components

$$u = u(y, t), \qquad v = w \equiv 0. \tag{8.102}$$

Assume that the fluid motion is 'generated' either by a moving wall or a jump in the velocity field $u(y, t)$ as shown in **Fig. 8.17**. In this case the continuity equation (div $\boldsymbol{v} = 0$) is identically satisfied and the momentum equations take the forms

$$\frac{\partial u}{\partial t} = -\frac{1}{\rho}\frac{\partial p}{\partial x} + \nu\frac{\partial^2 u}{\partial y^2},$$
$$0 = -\frac{1}{\rho}\frac{\partial p}{\partial y}, \quad 0 = -\frac{1}{\rho}\frac{\partial p}{\partial z}. \tag{8.103}$$

Fig. 8.17 Plane layer flow of a viscous fluid induced either starting from a jump discontinuity of the initial velocity profile (**a**) or by a moving wall (**b**)

Equation $(8.103)_{2,3}$ imply that the pressure can only depend on x and t, and from $(8.103)_1$ one then deduces that the pressure gradient depends only on t, so that p is linear in x.

8.3.1 Oscillating Wall

Consider the half space $y > 0$ bounded at $y = 0$ by an oscillating wall, moving harmonically as

$$u_0 = U \, \exp(\iota\omega t), \quad y = 0 \tag{8.104}$$

with prescribed frequency ω and amplitude U. It is assumed that the fluid is at rest for $y \to \infty$ and with constant pressure, $p_\infty = $ constant. According to (8.103), p does not depend on y and is linear in x. It is further assumed that its x-gradient vanishes, i.e. there exists no driving pressure gradient, $\partial p / \partial x = 0$. As a consequence, (8.103) reduces to

$$
\begin{aligned}
\frac{\partial u}{\partial t} &= \nu \frac{\partial^2 u}{\partial y^2}, & 0 < y < \infty, \\
u &= 0, & y \to \infty, \\
u &= U \, \exp(\iota\omega t), & y = 0.
\end{aligned}
\tag{8.105}
$$

This diffusive boundary value problem is solved with the trial solution

$$u(y, t) = f(y) \, \exp(\iota\omega t), \tag{8.106}$$

which transforms $(8.105)_1$ into the ordinary differential equation

$$f'' - \frac{\iota\omega}{\nu} f = 0 \tag{8.107}$$

with the solution

$$f(y) = A \, \exp\left(\sqrt{\frac{\omega}{2\nu}}(1 + \iota)y\right) + B \, \exp\left(-\sqrt{\frac{\omega}{2\nu}}(1 + \iota)y\right). \tag{8.108}$$

Requesting regularity of $f(y)$ as $y \to \infty$, implies $A = 0$, and the boundary condition at $y = 0$ implies $B = U$. Thus,

$$u(y, t) = U \, \exp\left[\iota\omega t - (1 + \iota)\sqrt{\frac{\omega}{2\nu}}y \right], \tag{8.109}$$

or when restricted to its real part

$$u(y, t) = U \, \exp\left(-\sqrt{\frac{\omega}{2\nu}}y \right) \cos\left[\omega t - \sqrt{\frac{\omega}{2\nu}}y \right]. \tag{8.110}$$

This function represents a wave with frequency ω, wave number $k = \sqrt{\omega/(2\nu)}$ and phase speed $c = \sqrt{2\nu\omega}$, oscillating forth and back as shown in **Fig. 8.18**, with wave length λ and period T,

$$\lambda = \frac{2\pi}{k} = 2\pi\sqrt{\frac{2\nu}{\omega}} = 2\pi\delta, \quad \delta = \sqrt{\frac{2\nu}{\omega}},$$

$$T = \frac{2\pi}{\omega}. \tag{8.111}$$

The shear stress at the wall is given by

$$\begin{aligned}
\tau_{xy}|_{y=0} &= \eta\frac{\partial u}{\partial y}\Big|_{y=0} \\
&= U\eta\sqrt{\frac{\omega}{2\nu}}\{-\cos(\omega t) + \sin(\omega t)\} = -U\eta\sqrt{\frac{\omega}{\nu}}\cos\left(\omega t + \frac{\pi}{4}\right) \\
&= -U\sqrt{\omega\eta\rho}\cos\left(\omega t + \frac{\pi}{4}\right). \tag{8.112}
\end{aligned}$$
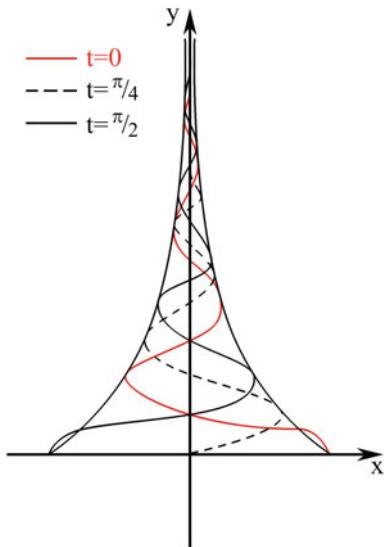
Compared with (8.110) the velocity u lags behind the shear traction by $45°$.

Finally, the mean power that must be brought by the tractions at the wall is given by

$$\begin{aligned}
\bar{L} &= -\frac{1}{T}\int_0^T \tau_{xy}(t)|_{y=0}u(t)|_{y=0}\, dt \quad \left(T = \frac{2\pi}{\omega} \right) \\
&= -\frac{1}{T}\int_0^T \left(-U^2\sqrt{\omega\eta\rho} \right)\cos(\omega t)\cos\left(\omega t + \frac{\pi}{4}\right) dt \\
&= \frac{U^2}{2}\sqrt{\frac{\omega\eta\rho}{2}}. \tag{8.113}
\end{aligned}$$

This is the problem, which originally has been solved by GEORGE GABRIEL STOKES in 1851 [50].

Fig. 8.18 Snapshots of the velocity u in (8.110) for the time slices $T = \{0, \frac{T}{4}, \frac{T}{2}\}$. *The amplitude of the velocity decays exponentially with the distance y from the wall.* $\delta = \lambda/(2\pi)$ *can be interpreted as a boundary layer thickness. Figure is only qualitative*

8.3.2   Adjustment of a Velocity Jump

Let's, as a start, assume the somewhat academic situation that at time t a velocity field $u_0(y)$, periodic in the y-direction, is at the disposal, which for $t > 0$, can freely evolve. The ensuing velocity distribution $u(y, t)$ is sought. If it is further assumed that the other two velocity components v, w vanish, then the NS-equations reduce to the initial value problem

$$\frac{\partial u}{\partial t} = \nu \frac{\partial^2 u}{\partial y^2}, \qquad -\infty < y < \infty, \quad t > 0$$
$$u(y, 0) = u_0(y), \qquad -\infty < y < \infty, \quad t = 0. \tag{8.114}$$

The trial separation of variables solution $u = \exp(\iota k y) f(t)$ leads to the ordinary differential equation

$$f' + \nu k^2 f = 0 \quad \text{with the solution} \quad f = U \exp(-\nu k^2 t),$$

so that

$$u = U \exp(\iota k y) \exp(-\nu k^2 t), \tag{8.115}$$

and when restricted to the real part

$$u = U \cos(ky) \exp(-\nu k^2 t). \tag{8.116}$$

The harmonic, spatial velocity differences are exponentially attenuated in time.

Consider next the slightly more general case, in which the initial velocity distribution $u_0(y)$ is arbitrary, but expressible by the following FOURIER integral

$$u_0(y) = \int_{-\infty}^{\infty} f(k) \, \exp(\iota ky) \, dk, \quad f(k) = \frac{1}{2\pi} \int_{-\infty}^{\infty} u_0(y) \, \exp(\iota ky) \, dy. \quad (8.117)$$

For this case, with the aid of (8.115), the general solution can be expressed as

$$u(y, t) = \int_{-\infty}^{\infty} f(k) \, \exp(\iota ky) \, \exp(-\nu k^2 t) dk, \quad (8.118)$$

in which $f(k)$ is given by $(8.117)_2$, implying[15]

$$u(y, t) = \frac{1}{2\pi} \int_{-\infty}^{\infty} u_0(\sigma) d\sigma \underbrace{\int_{-\infty}^{\infty} \exp\left[\iota k(y - \sigma) - \nu k^2 t\right] dk}_{I}$$

$$= \frac{1}{2\sqrt{\pi \nu t}} \int_{-\infty}^{\infty} u_0(\sigma) \, \exp\left[-\frac{(y - \sigma)^2}{4\nu t}\right] d\sigma. \quad (8.119)$$

As an example for the evaluation of (8.119), consider the initial value distribution as shown in **Fig. 8.19**

---
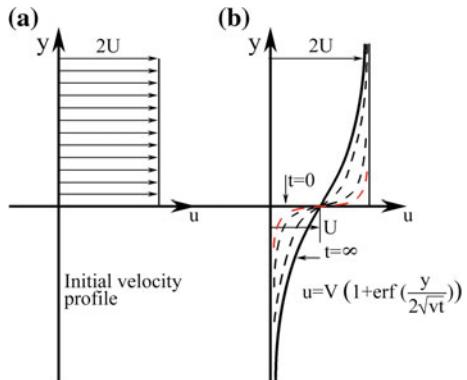
[15]To evaluate the integral I, let

$$\iota k(y - \sigma) - \nu k^2 t = -\left\{\sqrt{\nu t}\, k - \iota \frac{(y - \sigma)}{2\sqrt{\nu t}}\right\}^2 - \frac{(y - \sigma)^2}{4\nu t},$$

and $\sqrt{\nu t}\, k = z$, $dk = dz/\sqrt{\nu t}$. Then,

$$I = \frac{\exp\left(-\dfrac{(y - \sigma)^2}{4\nu t}\right)}{\sqrt{\nu t}} \int_{-\infty}^{\infty} \exp\left\{-\underbrace{\left(z - \frac{\iota(y - \sigma)}{2\sqrt{\nu t}}\right)^2}_{\zeta}\right\} dz$$

$$= \frac{\exp\left(-\dfrac{(y - \sigma)^2}{4\nu t}\right)}{\sqrt{\nu t}} \underbrace{\int_{-\infty}^{\infty} \exp\left(-\zeta^2\right) d\zeta}_{\sqrt{\pi}} = \sqrt{\pi}\, \frac{\exp\left(-\dfrac{(y - \sigma)^2}{4\nu t}\right)^2}{\sqrt{\nu t}}.$$

Fig. 8.19 Adjustment of a
velocity jump *Initial velocity
profile* (**a**)*, which transforms
to a smooth diffused profile
in panel* (**b**)

$$u_0(y) = \begin{cases} 2U, & y \geqslant 0, \\ 0, & y < 0. \end{cases} \tag{8.120}$$

Substituting (8.120) into (8.119) yields

$$u(y, t) = \frac{U}{\sqrt{\pi \nu t}} \int_0^\infty \exp\left(-\frac{(y - \sigma)^2}{4\nu t}\right) d\sigma. \tag{8.121}$$

With the variable transformation

$$\frac{y - \sigma}{2\sqrt{\nu t}} = \zeta \quad d\sigma = -2\sqrt{\nu t}\, d\zeta$$

Eq. (8.121) can be expressed as

$$u(y, t) = -\frac{2U}{\sqrt{\pi}} \int_{\frac{y}{2\sqrt{\nu t}}}^{-\infty} \exp\left(-\zeta^2\right) d\zeta = \frac{2U}{\sqrt{\pi}} \int_{-\infty}^{\frac{y}{2\sqrt{\nu t}}} \exp\left(-\zeta^2\right) d\zeta$$

$$= \frac{2U}{\sqrt{\pi}} \left\{ \int_{-\infty}^{0} \exp\left(-\zeta^2\right) d\zeta + \int_{0}^{\frac{y}{2\sqrt{\nu t}}} \exp\left(-\zeta^2\right) d\zeta \right\}$$

$$= U \left\{ 1 + \frac{2}{\sqrt{\pi}} \int_{0}^{\frac{y}{2\sqrt{\nu t}}} \exp\left(-\zeta^2\right) d\zeta \right\}$$

$$= U \left\{ 1 + \mathrm{erf}\left(\frac{y}{2\sqrt{\nu t}}\right) \right\}, \tag{8.122}$$

in which 'erf' is the error function. In particular, one has

$$u(0, t) = U, \quad u(\infty, t) = 2U, \quad u(-\infty, t) = 0, \tag{8.123}$$

which states that at all times the value of the velocity on the x-axis is the arithmetic mean of the velocities far away from this axis. The *boundary layer thickness* depends thereby on the time according to the square root rule

$$\delta = \sqrt{\nu t}. \tag{8.124}$$

As an *example* of application consider the half space $y > 0$, filled with a NAVIER-STOKES fluid. At $t = 0$ the wall at $y = 0$ will suddenly be set in motion with a velocity $2U\mathcal{H}(t)$, where $\mathcal{H}$ is the HEAVISIDE[16] function. The solution to this case can be constructed by composing the flow $2U$ in $y \geqslant 0$ with the negative of (8.122) as follows:

$$u = 2U - U \left(1 + \text{erf} \left(\frac{y}{2\sqrt{\nu t}} \right) \right) = U \left(1 - \text{erf} \left(\frac{y}{2\sqrt{\nu t}} \right) \right)$$
$$= U\text{erfc} \left(\frac{y}{2\sqrt{\nu t}} \right), \tag{8.125}$$

in which 'erfc' is the complementary error function. Indeed, at $t = 0^+$ (8.125) implies $u = 0$ with $u(\infty, t) = 0$. The layer thickness is given by $\delta = \sqrt{\nu t}$ as in (8.124), and the velocity is characteristically given as displayed in **Fig. 8.21**.

This problem has first been solved by RAYLEIGH in 1911 [42]. A problem closely related to it was attacked by L. HOWARTH in 1950 under the title 'RAYLEIGH's problem for a semi-infinite plate' [27]. He writes: 'With Cartesian axes (xyz) an infinitely thin semi-infinite plate coincident with the half plane $y = 0$, $x \geqslant 0$ is initially at rest surrounded by viscous fluid, also at rest; starting at $t = 0$, the plate is made to move uniformly with velocity W parallel to $0z$, and we require to determine the subsequent motion of the fluid'. In anticipation of the analysis, we are tempted to assume that this transverse motion is possible without motion of the fluid also parallel to the plane $0xy$.

The initial-boundary-value problem that must be solved for w is the differential equation
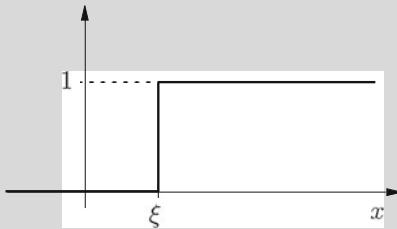
$$\frac{\partial w}{\partial t} = \nu \left(\frac{\partial^2 w}{\partial x^2} + \frac{\partial^2 w}{\partial y^2} \right) \tag{8.126}$$

---

[16]For a biography of OLIVER HEAVISIDE see **Fig. 8.20**.

Heaviside function

$$\mathcal{H}(x - \xi) = \begin{cases} 1, \, x > \xi \\ 0, \, x < \xi \end{cases}$$

Fig. 8.20 OLIVER HEAVISIDE (18. May 1850–3. Feb. 1925)

OLIVER HEAVISIDE grew up in London; he was short and red-headed, and suffered of scarlet fever when young, which left him with a hearing impairment. He went to grammar school, but his parents could not keep him at school after he was 16, so he continued studying for a year by himself and had no further formal education. He learned in 1868 the profession of telegraph operator in Denmark, receiving the support by his uncle CHARLES WEATSTONE (a physicist and original co-inventor of the first commercially successful telegraph in the mid 1830s). In the year 1870 he returned to England, was working in Newcastle at the *Great Northern Telegraph Company*, where he soon was chief telegraphist. Since 1872 he published articles on electricity, which caught the attentiveness of JAMES CLERK MAXWELL. He was fascinated by MAXWELL's work. 1874 he gave up his professional activity and moved to his parents to London to concentrate on the study of the theory of electricity. All his mathematical ability and knowledge was self-taught, and he needed years to absorb MAXWELL's work. He ultimately developed his own mathematical methods, which were much ahead of those at the time, and which simplified the electromagnetic theory and the mathematical treatment of electric circuits.
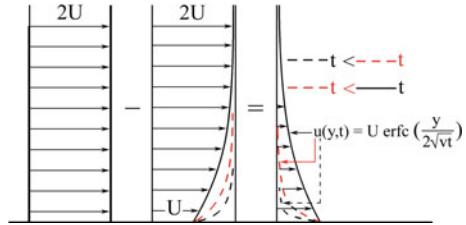
Starting in 1882 HEAVISIDE published regularly in *The Electrician*. He was recognized as a respected natural philosopher by LORD KELVIN, FRANCIS FITZGERALD, HEINRICH HERTZ and others. This brought him membership of the Royal Society, London (1891), American Academy of Arts and Sciences (1899) and an honorary doctorate from the University of Göttingen (1905), among others. 1912 he was nominated for the Nobel Prize.

HEAVISIDE's innovations and discoveries in mathematical physics are exceptional: (i) He was active in developing and advocating *vector methods* and the vector calculus and bringing the MAXWELL equations into a form comprising variables ($\boldsymbol{B}, \boldsymbol{E}, \boldsymbol{J}$ and ρ) [MAXWELL had 20 equations]. (ii) He invented the HEAVISIDE step function. (iii) He invented the *operator methods* for solving linear differential equations (recall LAPLACE transforms and inverse LAPLACE transforms). (iv) He postulated the existence of the ionosphere layer in the atmosphere which was experimentally corroborated by EDWARD VICTOR APPLETON who won the 1945 Physics Nobel Prize with it. (v) He developed the transmission line theory (telegrapher's equations). (vi) He independently discovered the pointing vector.

Today, our knowledge is almost exclusively reduced to the definition of his function $\mathcal{H}$; HEAVISIDE's tremendous achievements are taken simply for granted without being tied to the inventor.

The text is based on http://www.wikipedia.org

Fig. 8.21 Velocity profile of
a viscous half space due to a
sudden constant motion of
the bounding wall with
$u = 2U$ for $t \geqslant 0$

for the velocity component in the z-direction; ν is the kinematic viscosity, and (8.126)
is subject to the initial conditions

$$w = 0 \quad \text{for } t = 0, \tag{8.127}$$

and the boundary conditions

$$\left.\begin{array}{l} w = W \text{ when } y = 0, x \geqslant 0, \\ w \to 0 \text{ as } |y| \to 0, \text{ when } x > 0, \\ w \to 0 \text{ as } |x| \to 0 \text{ or } |y| \to 0, \text{ when } x < 0, \end{array}\right\} \quad t > 0. \tag{8.128}$$

It can readily be verified that with (8.126)–(8.128) the continuity equation and hori-
zontal momentum equations are satisfied with $u \equiv 0$ and $v \equiv 0$. L. HOWARTH [27]
constructs solutions in two forms: (i) A solution in series of the equations in polar
coordinates, and (ii) a solution by operational methods of the equations in parabolic
coordinates. Both methods express the velocity w in series of special functions; the
mathematical analysis as such is not difficult, even though it is complex.
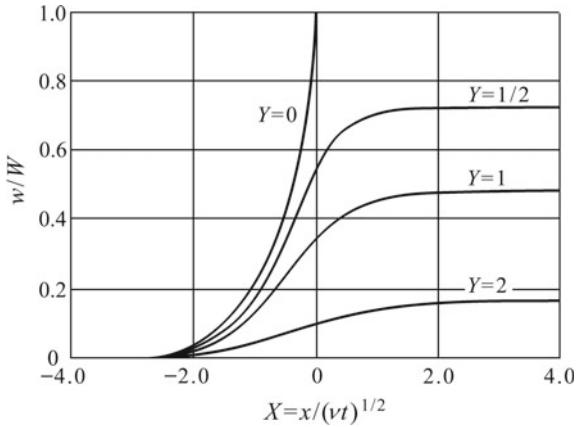
HOWARTH [27] also performed the necessary numerical computations and dis-
played the results graphically in **Fig. 8.22**, in which w/W is plotted against $X = x/\sqrt{\nu t}$ for various values of $Y = y/\sqrt{\nu t}$. It is seen that the non-dimensionalized
velocity w/W vanishes for all values of Y when $x \to -\infty$. Moreover, w/W has a
singularity as $y \to 0^-$, but for all values $Y \neq 0$ the values of w/W remain bounded
and grow monotonically as $Y \to 0$.

Finally, note that RAYLEIGH's problem determined a time dependent velocity
field due to *horizontal* oscillations of the wall, whilst HOWARTH's problem assumed
a *vertical* time dependent motion of a semi-infinite wall.

8.4   Stationary Axisymmetric Laminar Jet

We consider here an exact solution of the NS-equations in axisymmetric spherical
coordinates, r, θ, where r is the radial distance from the origin of the spherical
coordinates and θ is the angle between the symmetry axis and the radial distance in
any meridional plane. The NS-equations, formulated in these coordinates are given

Fig. 8.22 Transverse velocity distribution w/W for the semi-infinite RAYLEIGH problem *Plotted against* $X = x/\sqrt{\nu t}$ *for various values of* $Y = y/\sqrt{\nu t}$, *adapted from* [27]

in Vol. 2, Chap. 11, Eqs. (11.16) and (11.17)[17]; they read

$$\nu \mathcal{L}^4 \psi = \frac{1}{r^2 \sin \theta} \left\{ \frac{\partial \psi}{\partial \theta} \frac{\partial}{\partial r} - \frac{\partial \psi}{\partial r} \frac{\partial}{\partial \theta} + 2\cotan \frac{\partial \psi}{\partial r} - \frac{2}{r} \frac{\partial \psi}{\partial \theta} \right\} \mathcal{L}^2 \psi, \tag{8.129}$$
$$\mathcal{L}^2 \psi := \frac{\partial^2 \psi}{\partial r^2} + \frac{\sin \theta}{r^2} \frac{\partial}{\partial \theta} \left(\frac{1}{\sin \theta} \frac{\partial \psi}{\partial \theta} \right),$$

in which ψ is the stream function. The radial, v_r, and azimuthal, v_θ, velocity components are given by

$$v_r = \frac{1}{r^2 \sin \theta} \frac{\partial \psi}{\partial \theta}, \quad v_\theta = -\frac{1}{r \sin \theta} \frac{\partial \psi}{\partial r}. \tag{8.130}$$

With these assignments of the velocities the continuity equation is identically satisfied, see Chap. 11, Eqs. (11.19) and (11.20).

In this section we seek solutions of the separation of variables form as follows:

$$\psi(r, \theta) = \nu r \hat{f}(\theta) = \nu r f(\xi), \tag{8.131}$$

with

$$\xi = \cos \theta \quad \longrightarrow \quad \frac{\partial}{\partial \theta} = \frac{\partial}{\partial \xi} \frac{d\xi}{d\theta} = -\sin \theta \frac{\partial}{\partial \xi} = -\sqrt{1 - \xi^2} \frac{\partial}{\partial \xi}. \tag{8.132}$$

It is a straightforward exercise using the transformation (8.132) to evaluate $\mathcal{L}^2 \psi$ and the nonlinear operator on the right-hand side (RHS) of (8.129)$_1$ as referred to the coordinates r and ξ:

[17]The solutions presented in this section were constructed by LANDAU in 1944 [32] and SQUIRE in 1951 [47]. BATCHELOR [3] and SHERMAN [46] also present computational details.

$$\mathcal{L}^2\psi \quad = \frac{\partial^2\psi}{\partial r^2} + \frac{\sqrt{1-\xi^2}}{r^2}\left(-\sqrt{1-\xi^2}\frac{\partial}{\partial\xi}\left(-\frac{\sqrt{1-\xi^2}}{\sqrt{1-\xi^2}}\frac{\partial\psi}{\partial\xi}\right)\right)$$

$$= \frac{\partial^2\psi}{\partial r^2} + \frac{1-\xi^2}{r^2}\frac{\partial^2\psi}{\partial\xi^2},$$

$$\mathrm{RHS}[(8.129)_1] = \frac{1}{r^2\sqrt{1-\xi^2}}\left\{-\sqrt{1-\xi^2}\frac{\partial\psi}{\partial\xi}\frac{\partial}{\partial r} - \frac{\partial\psi}{\partial r}\left(-\sqrt{1-\xi^2}\frac{\partial}{\partial\xi}\right)\right.$$

$$\left. + \frac{2\xi}{\sqrt{1-\xi^2}}\frac{\partial\psi}{\partial r} + \frac{2}{r}\left(\sqrt{1-\xi^2}\frac{\partial\psi}{\partial\xi}\right)\right\}\mathcal{L}^2\psi. \tag{8.133}$$

When substituting (8.131) into (8.133), one can readily deduce the following expressions:

$$\mathcal{L}^2\psi \quad = \frac{\nu(1-\xi^2)}{r}f''(\xi),$$

$$\frac{\partial^2(\mathcal{L}^2\psi)}{\partial r^2} \quad = \frac{2\nu}{r^3}\left(1-\xi^2\right)f''(\xi),$$

$$\frac{\partial^2(\mathcal{L}^2\psi)}{\partial\xi^2} \quad = \frac{\nu}{r}\left[\left(1-\xi^2\right)f''(\xi)\right]'', \tag{8.134}$$

$$\nu\mathcal{L}^4\psi \quad = \frac{\nu^2}{r^3}(1-\xi^2)\left\{2f'' + \left[\left(1-\xi^2\right)f''\right]''\right\},$$

$$\mathrm{RHS}[(8.129)_1] \quad = \frac{\nu^2}{r^3}\left(1-\xi^2\right)\left(3f'f'' + ff'''\right).$$

If we now equate $(8.134)_3$ to $(8.134)_4$ the NS-equation, restricted to the stream function (8.131), is obtained as

$$2f'' + \left[\left(1-\xi^2\right)f''\right]'' = 3f'f'' + ff''', \tag{8.135}$$

an ordinary differential equation, which can easily be integrated. To this end, we multiply both sides of (8.135) with 2; this yields

$$4f'' + 2[(1-\xi^2)f'']'' = 6f'f'' + 2ff''' = (2ff')'',$$

from which we deduce

$$4f + 2(1-\xi^2)f'' = 2ff' + c_1\xi + c_2,$$

where c_1 and c_2 are constants of integration. Adding and subtracting on the left-hand side of this equation $4\xi f'$, one obtains

$$(4f + 4\xi f') - 4\xi f' + 2(1-\xi^2)f'' = (f^2)' + c_1\xi + c_2$$

or

$$4(\xi f)' + \left(2(1 - \xi^2)f'\right)' - \left(f^2\right)' = c_1\xi + c_2.$$

A further integration now yields

$$4\xi f + 2(1 - \xi^2)f' - f^2 = \tfrac{1}{2}c_1\xi^2 + c_2\xi + c_3. \tag{8.136}$$

In the subsequent analysis we focus only on solutions for which $c_1 = c_2 = c_3 = 0$. Equation (8.136) then reduces to

$$f^2 - 2(1 - \xi^2)f' - 4\xi f = 0. \tag{8.137}$$

With the transformation

$$f(\xi) = (1 - \xi^2)g(\xi) \tag{8.138}$$

Equation (8.137) reduces to

$$g'(\xi) - \tfrac{1}{2}g^2(\xi) = 0 \quad \longrightarrow \quad \int \frac{\mathrm{d}g}{g^2} = \int \frac{1}{2}\mathrm{d}\xi, \tag{8.139}$$

with the solution

$$g(\xi) = \frac{2}{1 + c - \xi}, \tag{8.140}$$

in which $1 + c$ is the constant of integration. Hence, from (8.138) and (8.131) we obtain

$$f(\xi) = \frac{2(1 - \xi^2)}{1 + c - \xi} \quad \longrightarrow \quad \psi = \frac{2\nu r(1 - \xi^2)}{1 + c - \xi}, \tag{8.141}$$

or upon returning to the original variable θ via (8.132)

$$\psi(r, \theta) = \frac{2\nu r \sin^2 \theta}{1 + c - \cos \theta}. \tag{8.142}$$

The streamlines in the meridian plane are now given by setting ψ equal to a constant. Thus, we now set $\psi/\nu = A = \text{constant}$ and then obtain from (8.142)

$$r = \frac{A}{2} \frac{1 + c - \cos \theta}{\sin^2 \theta}. \tag{8.143}$$
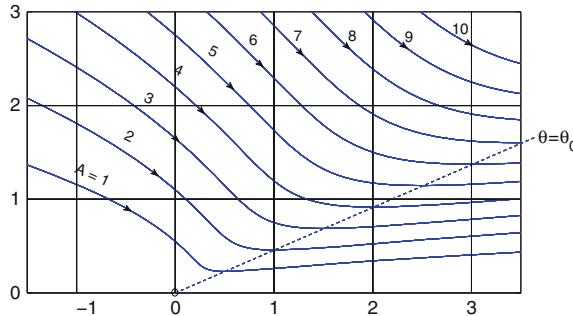
Fig. 8.23 Streamlines of an axisymmetric axial laminar jet in the meridian plane plotted for $c = 0.1$ ($\theta_0 = 24.5°$) and $A \in [1, 10]$. *The dashed straight line, given by $\theta = \theta_0$, is the location of the jet boundary, marking the minimum distance of the streamlines from the symmetry axis. The ring marks the origin of the coordinate system, adapted from* [3, 46]

For $c = 0.1$ and a number of different values of $A \in [1, 10]$ the streamlines are displayed in **Fig. 8.23**. The flow is reminiscent of a jet stream emanating from the origin, which drags fluid from the environment of the fluid region. The boundary of the jet can be defined by the angle $\theta = \theta_0$ for which the streamlines possess the minimum distance from the axis. This location can be determined from

$$y = r \sin \theta = \frac{A}{2} \frac{1 + c - \cos \theta}{\sin \theta} \quad \longrightarrow \quad \frac{dy}{d\theta} = \frac{A}{2} \frac{\sin^2 \theta - (1 + c - \cos \theta) \cos \theta}{\sin^2 \theta}$$

and setting $dy/d\theta = 0$, which yields
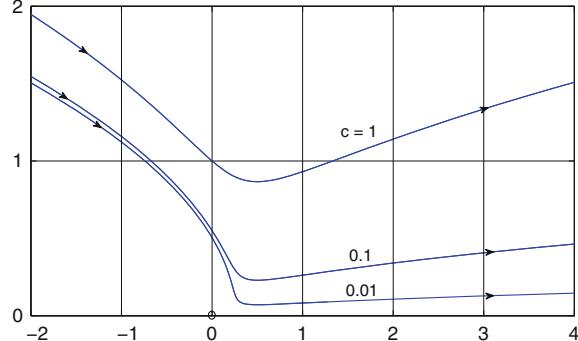
$$\cos \theta_0 = \frac{1}{1 + c} \quad (\sim 1 - c \text{ if } |c| \ll 1). \tag{8.144}$$

Evidently, θ_0 does not depend on position. The jet is bounded by a straight line. It is narrow and θ_0 is small for small positive values of c. **Figure 8.24** displays streamlines for $A = 1$ and a number of different c-values. The velocity remains bounded except in the origin $r = 0$. This singularity is idealized expression of the physical cause, which generates the jet. To expound this cause, consider the steady conservation law of momentum

$$\underbrace{\frac{d}{dt} \iiint_{\mathcal{V}} \rho \boldsymbol{v} dv}_{0} = \underbrace{\iint_{\mathcal{A}} \rho \boldsymbol{v}(\boldsymbol{v} \cdot \boldsymbol{n}) da}_{(i)} = \underbrace{- \iint_{\mathcal{A}} p \boldsymbol{n} da}_{(ii)} + \underbrace{\iint_{\mathcal{A}} t^R \boldsymbol{n} \, da}_{(iii)} + \boldsymbol{F}, \tag{8.145}$$

where $\boldsymbol{F}$ is the total force exerted by external forces on the fluid particles in the volume $\mathcal{V}$. When gravity is ignored the only contribution is at the origin, the singular point, at which momentum is provided from outside. Because of the rotational symmetry

Fig. 8.24 Same as Fig. 8.23, but for $A = 1$ and $c_1 = (0.01, 0.1, 1)$ corresponding to $\theta_0 = (8°, 24.5°, 60°)$. The *ring* marks the origin of the coordinate system, adapted from [3, 46]

the force can only point into the direction of the axis and is given by the terms (*i*), (*ii*) and (*iii*) in (8.145), which can now be written as

$$F = \int_0^\pi \{\rho v_r(v_r \cos\theta - v_\theta \sin\theta) + (p - \sigma_r)\cos\theta + \tau_{r\theta}\sin\theta\}\, 2\pi r^2 \sin\theta d\theta, \quad (8.146)$$

in which v_r and v_θ are to be substituted from (8.130) with ψ given by (8.142) and the stresses σ_r, $\tau_{r\theta}$, given by (11.30) in Chap. 11. The pressure can be assumed to have the form

$$p = \rho \frac{\nu^2}{r^2} h(\theta).$$

This expression is substituted into the NS-equations together with the simultaneous application of the solution (8.142). The result of the entire computation leads to the following final result:

$$\frac{F}{2\pi\rho\nu^2} = \underbrace{\frac{32}{3}\frac{1+c}{c(2+c)}}_{\text{Contribution from the momentum flux}}$$

$$+ \underbrace{4(1+c)^2 \log\frac{c}{2+c} + 8(1+c)}_{\text{Contribution from the stresses in (8.146)}}. \quad (8.147)$$

The computational details for (8.147) can be found in [3, 46]. We conclude that there is a unique connection between F and c. For small c, $0 < c \ll 1$ the second term on the right-hand side of (8.147) can be ignored in comparison to the first term, because it only has a logarithmic singularity. One may then approximately set

$$\frac{F}{2\pi\rho\nu^2} = \frac{32}{3}\frac{1}{2c},$$

and since

$$\cos \theta_0 \approx 1 - \frac{\theta_0^2}{2} \overset{(8.144)}{\sim} 1 - c \quad \longrightarrow \quad c \simeq \frac{1}{2}\theta_0^2. \tag{8.148}$$

Combining the last two results allows to express the force F in terms of the opening angle of the jet,

$$\frac{F}{2\pi \rho \nu^2} \approx \frac{32}{3\theta_0^2}. \tag{8.149}$$

The larger F is, the smaller will be the opening angle θ_0. The constant c can be related to a characteristic REYNOLDS number. To this end, we evaluate v_r as given in (8.130) with ψ given by (8.142). This yields

$$v_r = \frac{2\nu}{r} \frac{2\cos \theta (1 + c - \cos \theta) - \sin^2 \theta}{(1 + c - \cos \theta)^2}. \tag{8.150}$$

On the jet axis, $\theta = 0$, this gives

$$\underbrace{\frac{v_r r}{\nu}}_{\mathbb{R}_r} = \frac{4c}{c^2} = \frac{4}{c} \overset{(8.148)}{=} \frac{8}{\theta_0^2} \quad \longrightarrow \quad \theta_0 = \sqrt{\frac{8}{\mathbb{R}_r}}. \tag{8.151}$$

$\mathbb{R}_r$ is a radial (axial) REYNOLDS number. At sufficiently small $\mathbb{R}_r$ the jet covers only a very narrow region.

Remarks:

- For very large REYNOLDS numbers ($c \ll 1$) the expression for F has been obtained by ignoring the contribution of the stresses in comparison to that of the momentum flux. Such a jet can be realized by pressing fluid out of a nozzle of cross section $\tilde{A}$ with average velocity v. Then, one has $F = \rho \tilde{A} v^2$. However, the mass flux through the closed control area of the idealized above flow is zero. The realization of the jet will be closer to the above solution, the smaller the mass flux $\rho \tilde{A} v$ will be. We, thus, request the limit

$$\tilde{A}v \to 0, \quad v \to \infty \quad \text{at fixed } F.$$

- The expression for v_r, (8.150), can with (8.144) be written as

$$v_r = \frac{2\nu}{r} \frac{2\cos \theta \left(\dfrac{1}{\cos \theta_0} - \cos \theta\right) - \sin^2 \theta}{\left(\dfrac{1}{\cos \theta_0} - \cos \theta\right)^2}.$$

If both, θ and θ_0, are small, this can be approximated as

$$v_r = \frac{8\nu}{r\theta_0^2} \frac{1}{\left(1 + (\theta/\theta_0)^2\right)^2} \overset{(8.149)}{=} \frac{3F}{8\pi\rho\nu} \frac{1}{r} \frac{1}{\left(1 + (\theta/\theta_0)^2\right)^2}. \tag{8.152}$$

This formula can be used to verify the theory. The momentum flux F is prescribed and v_r can be measured as a function of the position $[r, (\theta/\theta_0)]$.

8.5 Viscous Flow in a Converging Two-Dimensional Channel
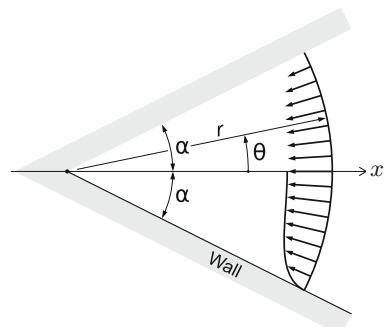
Consider a wedge of infinite extent and apex angle 2α, see **Fig. 8.25**. Let r, θ be polar coordinates with origin at the apex and θ measured from the symmetry line. Assume, moreover, purely radial motion with velocity $u(r, \theta)$, positive as motion away from the apex. Outward motion is referred to as diverging, inward motion as converging. With azimuthal velocities vanishing the steady NAVIER-STOKES (NS) equations take the form

$$u\frac{\partial u}{\partial r} = -\frac{1}{\rho}\frac{\partial p}{\partial r} + \nu\left\{\frac{1}{r}\frac{\partial}{\partial r}\left(r\frac{\partial u}{\partial r}\right) + \frac{1}{r^2}\frac{\partial^2 u}{\partial\theta^2} - \frac{u}{r^2}\right\},$$

$$0 = -\frac{1}{\rho}\frac{1}{r}\frac{\partial p}{\partial\theta} + \nu\frac{2}{r^2}\frac{\partial u}{\partial\theta}. \tag{8.153}$$

Here, ρ is the constant density, p the pressure and ν the kinematic viscosity.

Physically, one might expect that u is the larger the closer the flow is to the origin of the coordinates (at the apex). Moreover, if we envisage no-slip boundary conditions at the side walls $\theta = \pm\alpha$, u will also enjoy a symmetric θ-dependence. Thus, it is

Fig. 8.25 Plane diverging or converging flow in a two-dimensional cone. *The apex has opening angle 2α. The (x, y) coordinates divide the wedge in two symmetric halves with opening angle α, each; θ is measured from the x-axis*

tempting to try a solution in the form[18]

$$u = \frac{1}{r}F(\theta).$$ (8.154)

Substituting (8.154) into (8.153) yields

$$-\frac{1}{r^3}F^2 = -\frac{1}{\rho}\frac{\partial p}{\partial r} + \frac{\nu}{r^3}F'',$$

$$0 = -\frac{1}{\rho}\frac{\partial p}{\partial \theta} + \frac{2\nu}{r^2}F',$$ (8.155)

in which primes denote differentiation with respect to θ. After elimination of the pressure,

$$-2FF' = \nu F''' + 4\nu F'$$ (8.156)

is obtained. Boundary conditions will be imposed as follows:

$$
\begin{array}{lll}
F = 0, & \text{at } \theta = \alpha, & \text{(no-slip condition)}, \\
F = F_0, \quad F' = 0, & \text{at } \theta = 0, & (u \text{ is even in } \theta).
\end{array}
$$ (8.157)

With scalings and transformations, respectively, given by

$$\eta = \frac{\theta}{\alpha}, \quad \frac{d}{d\theta} = \frac{1}{\alpha}\frac{d}{d\eta}, \quad f = \frac{F}{F_0},$$ (8.158)

Eqs. (8.156) and (8.157) can be written as

$$
\begin{array}{ll}
2\alpha\mathbb{R}ff' + f''' + 4\alpha^2 f' = 0, & \text{where } \mathbb{R} := \frac{\alpha F_0}{\nu}, \\
f = 0, & \text{at } \eta = 1, \\
f = 1, \quad f' = 0, & \text{at } \eta = 0,
\end{array}
$$ (8.159)

in which $\mathbb{R}$ has the meaning of a REYNOLDS number.
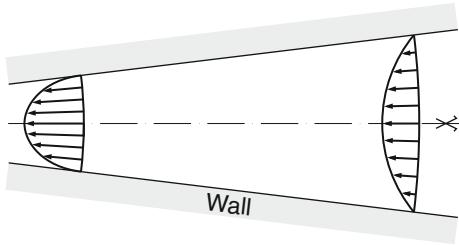
Consider a very special case and simplified situation for which

$$\alpha \ll 1 \quad \text{and} \quad |\alpha\mathbb{R}| \ll 1.$$

These are conditions of a narrow gap, for which (8.159)$_1$ reduces to $f''' = 0$ with the solution

---

[18]Note that $u = r^\gamma F(\theta)$ with constant exponent γ would be more general, but $\gamma = -1$ is seen to generate from (8.153)$_1$ an ordinary differential equation.

Fig. 8.26 Flow through a
narrow gap. *The velocity is
parabolically distributed
with increasing intensity as r
becomes smaller, such that
the area is preserved. As
r → 0 the velocity peak is
∞. Hence r = 0 is a
singularity (principal sketch)*

$$f = (1 - \eta^2),$$

which obeys the no-slip boundary condition at the side walls. The velocity profile is parabolic and the velocity amplitude is proportional to $1/r$, as is evident from (8.154) and **Fig. 8.26**.

Let us return now to the general case (8.159). This differential equation can be integrated twice as follows:

$$\left[\alpha\mathbb{R}f^2 + f'' + 4\alpha^2 f\right]' = 0,$$

$$\rightarrow \quad \alpha\mathbb{R}f^2 + f'' + 4\alpha^2 f = a, \quad (\times f'),$$

$$\longrightarrow \quad \alpha\mathbb{R}f^2 f' + f'' f' + 4\alpha^2 f' f = af',$$

$$\longrightarrow \quad \left[\frac{\alpha\mathbb{R}}{3}f^3 + \frac{1}{2}\left(f'\right)^2 + 2\alpha^2 f^2\right]' = af',$$

$$\longrightarrow \quad \frac{2}{3}\alpha\mathbb{R}f^3 + \left(f'\right)^2 + 4\alpha^2 f^2 = Af + B. \tag{8.160}$$

Here, A and B are two constants of integration. Using the boundary condition at $\eta = 0$ ($f' = 0, f = 1$) yields

$$A = \tfrac{2}{3}\alpha\mathbb{R} + 4\alpha^2 - B. \tag{8.161}$$

If this is substituted in (8.160) and the resulting equation is solved for $(f')^2$, then

$$(f')^2 = (1 - f)\left\{\tfrac{2}{3}\alpha\mathbb{R}(f^2 + f) + 4\alpha^2 f + B\right\} \tag{8.162}$$

is obtained or

$$\int_0^f \frac{\mathrm{d}\bar{f}}{\sqrt{(1 - \bar{f})\left\{\tfrac{2}{3}\alpha\mathbb{R}(\bar{f}^2 + \bar{f}) + 4\alpha^2\bar{f} + B\right\}}} = (1 - \eta), \tag{8.163}$$

in which the remaining boundary condition, $f = 0$ at $\eta = 1$, has been implemented. Equation (8.163) is the exact solution. The integral on the left-hand side can be expressed in terms of JACOBIan elliptic functions [2].

Let us investigate (8.163) for radial flow in a convergent/divergent channel.

(a) For a convergent channel.
The flow is toward the center, $u < 0$, implying that $F_0 < 0$ and $\mathbb{R} < 0$ (see (8.154), (8.157), and (8.159)$_1$). In this case, (8.163) can be written as

$$\frac{1}{\sqrt{-\frac{2}{3}\alpha\mathbb{R}}} \int_0^f \frac{\mathrm{d}\bar{f}}{\sqrt{(1-\bar{f})\left(-\bar{f}^2 - \bar{f} - \frac{6\alpha}{\mathbb{R}}\bar{f} - c\right)}} = (1-\eta), \qquad (8.164)$$

in which c is a new constant. It is determined with the aid of the boundary condition $\eta = 0, f = 1$ (the two other boundary conditions are then also satisfied). Thus,

$$\int_0^1 \frac{\mathrm{d}f}{\sqrt{(1-f)\left(-f^2 - f - \frac{6\alpha}{\mathbb{R}}f - c\right)}} = \sqrt{-\frac{2}{3}\alpha\mathbb{R}}. \qquad (8.165)$$

The determination of c from this formula is complicated by the fact that $\mathbb{R}$ arises both in the integrand function and on the right-hand side of the equation. An appropriate solution is at least possible for large $|\mathbb{R}|$, for which (8.165) reduces to

$$\int_0^1 \frac{\mathrm{d}f}{\sqrt{(1-f)(-f^2 - f - c)}} \to \infty. \qquad (8.166)$$

In words, by adequate choice of c one must see to it that the integral (8.166) diverges; this can be achieved at the upper limit of the integral, if

$$-f^2 - f - c = 0, \quad \text{for } f = 1 \implies c = -2. \qquad (8.167)$$

It is hoped that this value of c is also adequate for finite but very large values of the REYNOLDS number. Incidentally, since

$$2 - f - f^2 = (1-f)(2+f), \qquad (8.168)$$

the large $\mathbb{R}$-approximation of (8.163) can be written as

$$\int_0^f \frac{\mathrm{d}\bar{f}}{(1-\bar{f})\sqrt{2+\bar{f}}} = \sqrt{-\frac{2}{3}\alpha\mathbb{R}}(1-\eta). \qquad (8.169)$$

With the variable transformations

$$z = \sqrt{f+2}, \quad dz = \frac{1}{2\sqrt{f+2}}df, \quad \sigma = \frac{z}{\sqrt{3}},$$
$$z^2 = f+2, \quad 1-f = 3-z^2, \quad d\sigma = \frac{dz}{\sqrt{3}}, \tag{8.170}$$

Eq. (8.169) can be written as

$$\int_{\sqrt{2}}^{\sqrt{f+2}} \frac{2dz}{3-z^2} = \frac{2}{\sqrt{3}} \int_{\sqrt{2/3}}^{\sqrt{(f+2)/3}} \frac{d\sigma}{(1-\sigma^2)} = \sqrt{-\frac{2}{3}\alpha\mathbb{R}}\,(1-\eta). \tag{8.171}$$

Because[19]

$$\mathrm{atanh}(x) = \int \frac{dx}{1-x^2},$$

the integral equation (8.171) possesses the solution

$$\mathrm{atanh}\sqrt{\frac{f+2}{3}} = \sqrt{-\frac{\alpha\mathbb{R}}{2}(1-\eta)} + \mathrm{atanh}\sqrt{\frac{2}{3}},$$
$$\sqrt{\frac{f+2}{3}} = \tanh\left\{\sqrt{-\frac{\alpha\mathbb{R}}{2}(1-\eta)} + \mathrm{atanh}\sqrt{\frac{2}{3}}\right\}.$$

The ultimate result, thus, takes for this convergent flow the form

$$f = \frac{F}{F_0} = 3\tanh^2\left\{\sqrt{-\frac{\alpha\mathbb{R}}{2}(1-\eta)} + \mathrm{atanh}\sqrt{\frac{2}{3}}\right\} - 2. \tag{8.172}$$

The essential part of the $\tanh^2$-function in this formula is of the form $\tanh^2(\beta x)$ [$x := 1-\eta$, $\beta := \sqrt{-\alpha\mathbb{R}/2}$], of which the qualitative distribution is sketched in **Fig. 8.27**. The larger the REYNOLDS number is, the more conspicuous will be the boundary layer behaviour for f in the vicinity of $\eta = 1$. The thickness of this boundary layer can be expressed by the angle $\Delta\theta$, which is half of the opening angle of the wedge. Thus, setting $\eta \sim 1 - \Delta\theta/\alpha$, we obtain

$$\sqrt{-\frac{\alpha\mathbb{R}}{2}}\left(1-1+\frac{\Delta\theta}{\alpha}\right) = 1,$$

---

[19] atanh is the inverse function of tanh.
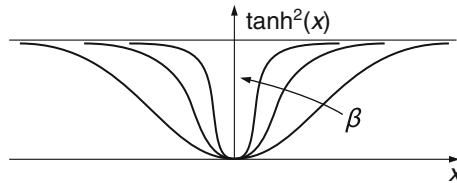
Fig. 8.27 Qualitative behaviour of the function $\tanh^2(\beta x)$. As the parameter β increases the function $\tanh^2(\beta x)$ develops a boundary layer in the vicinity of $x = 0$

and then get

$$\Delta\theta = \frac{\alpha}{\sqrt{-\dfrac{\alpha\mathbb{R}}{2}}} = \frac{1}{\sqrt{-\dfrac{\mathbb{R}}{2\alpha}}} \overset{(8.159)}{=} \frac{1}{\sqrt{-\dfrac{F_0}{2\nu}}} \overset{(8.154)}{=} \frac{1}{\sqrt{\dfrac{r|u_0|}{2\nu}}} \propto \frac{1}{\sqrt{\mathbb{R}_r}}. \tag{8.173}$$

$\Delta\theta$ is thus inversely proportional to the square root of the REYNOLDS number $\mathbb{R}_r$. This means that the boundary layer will be thin far away from the vertex of the wedge, but it will grow when this apex is approached and have a square root singularity there. This is in conformity with the sink that must exist at $x = 0$ to maintain the flow.

(b) For a divergent channel.
The flow is away from the wedge center, $u > 0$, implying that $F_0 > 0, \mathbb{R} > 0$, so that (8.164) now takes the form

$$\int_0^f \frac{\mathrm{d}\bar{f}}{\sqrt{(1-\bar{f})\left(\bar{f}^2 + \bar{f} + \dfrac{6\alpha}{\mathbb{R}}\bar{f} + c^*\right)}} = \sqrt{\frac{2}{3}\alpha\mathbb{R}}\,(1-\eta) \tag{8.174}$$

with positive constant c^*. Its value follows again by satisfying the boundary condition $f = 1, f' = 0$ at $\eta = 0$, implying

$$\int_0^1 \frac{\mathrm{d}f}{\sqrt{(1-f)\left(f^2 + f + \dfrac{6\alpha}{\mathbb{R}}f + c^*\right)}} = \sqrt{\frac{2}{3}\alpha\mathbb{R}}. \tag{8.175}$$

For divergent flow, $f \geqslant 0$, and since $0 \leqslant f < 1$, the square root expression in the integrand function of (8.175) is strictly positive. The boundary condition, however, cannot be fulfilled for arbitrary values of $\mathbb{R}$, but only for $\mathbb{R} < \mathbb{R}_{\text{limit}}$. Hence for fixed α this limit is reached for the minimum $c^* = 0$. For this case (8.175) reduces to

$$\int_0^1 \frac{\mathrm{d}f}{\sqrt{(1-f)\left(f^2+f+\dfrac{6\alpha}{\mathbb{R}_m}f\right)}} = \sqrt{\frac{2}{3}\alpha\mathbb{R}_m}, \tag{8.176}$$

in which $\mathbb{R}_m$ stands for the minimum REYNOLDS number. An approximate solution to (8.176) is again based on the assumption that $\mathbb{R}_m$ is large, so that $6\alpha f/\mathbb{R}_m$ can be ignored. This yields a first estimate for $\alpha\mathbb{R}_m$ via

$$\int_0^1 \frac{\mathrm{d}f}{\sqrt{f(1-f^2)}} \simeq \sqrt{\frac{2}{3}\alpha\mathbb{R}_m} \quad \text{or} \quad \alpha\mathbb{R}_m = \frac{3}{2}\left\{\int_0^1 \frac{\mathrm{d}f}{f(1-f^2)}\right\}^2 \approx 10.31. \tag{8.177}$$

We conclude: For given α a pure divergent flow is not possible for arbitrarily large REYNOLDS numbers. At large REYNOLDS numbers an inward flow is generated close to the wall.

8.6   Closing Remarks

The aim of this chapter has been to elaborate on the construction of exact solutions of initial boundary value problems in the theory of fluid flow of linearly viscous liquids. This has been and still is a popular topic of fluid mechanics treated in many textbooks in the theory of linearly viscous liquids. The focus was here on steady and some unsteady flows bounded by plane boundaries, such as HAGEN- POISEIULLE flow, two- and three-dimensional stagnation point flow, channel flow, swirling flow and, in particular, EKMAN flow and some of its generalizations. Steady laminar fluid motion through circular, elliptical, rectangular and triangular ducts was equally looked at. For these, stream function approximations were proposed, which satisfy the boundary conditions exactly but only approximate the describing differential equations. In these cases it became evident, how much more elaborate the construction of exact solutions to the initial boundary value problems were as compared to rather obvious choices of guessed stream functions. The selection of problems could easily be vastly extended. A useful collection has been presented—as already mentioned earlier—by DRAZIN and RILEY [14].

At these times, at which *numerical* solutions are favored and almost every problem, expressible in mathematical equations, are constructed, the reader may find it superfluous to present the somewhat complex analyses to exact solutions as done in this chapter. We disagree with such attitudes and need not to defend us; the beauty of rigor and the depth of insight into the physics of the particular problems stand sufficiently out in their own defense. Neither need it be mentioned how valuable such exact solutions are, when numerical software is to be tested for accuracy and convergence properties against trustworthy alternative results.

Appendix 8.A: Construction of the Solution (8.22) to the Boundary Value Problem (8.8)

Here, we wish to demonstrate how the solution (8.22) to the boundary value problem (8.8) is constructed for a rectangle as shown in **Fig. 8.28**.

VALENTIN BOUSSINESQ [6] chose a trial solution of the form

$$u(y, z) = -\frac{1}{2}\frac{p'h^2}{\eta}\left[\frac{y}{h} - \left(\frac{y}{h}\right)^2\right] + f(y, z). \tag{8.178}$$

The first term on the right of this equation satisfies the POISSON equation (8.8) exactly and the boundary conditions at $y = 0$ and $y = h$. Thus, the correcting function f satisfies the LAPLACE equation, zero boundary conditions at $y = 0$ and $y = h$ and $f(y, 0) = f(y, \ell) = \frac{1}{2}\frac{p'h^2}{\eta}\left(y/h - (y/h)^2\right)$. So, the boundary value problem for the function f is given by

$$
\begin{aligned}
\frac{\partial^2 f}{\partial y^2} + \frac{\partial^2 f}{\partial z^2} &= 0, && \text{in } \mathcal{D}, \\
f &= 0, && y = 0, \quad y = h, \\
f &= \frac{1}{2}\frac{p'h^2}{\eta}\left(\frac{y}{h} - \left(\frac{y}{h}\right)^2\right), && z = 0, \quad z = \ell.
\end{aligned}
\tag{8.179}
$$

Trying with the product ansatz $f(y, z) = f_1(y)f_2(z)$, the LAPLACE Eq. (8.179)$_1$ yields
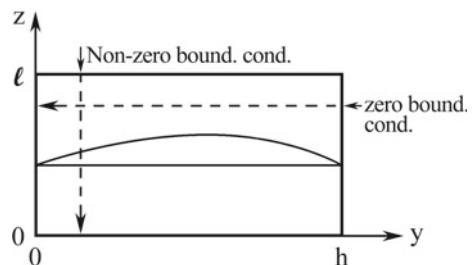
$$\frac{f_1''}{f_1} = -\frac{f_2''}{f_2} = -\lambda^2 \quad\Longrightarrow\quad \begin{cases} f_1'' + \lambda^2 f_1 = 0, \\ f_2'' - \lambda^2 f_2 = 0. \end{cases} \tag{8.180}$$

Of the trigonometric functions

$$f_1^{(m)} = \sin\left(\frac{m\pi}{h}y\right), \quad \cos\left(\frac{m\pi}{h}y\right)$$

the cosine function violates the boundary conditions at $y = 0$ and $y = h$. So, the correct solution will be a combination of the sine-functions for some $m =$

Fig. 8.28 Construction of the laminar velocity profile through a rectangular chute

1, 2, 3, ..., ∞. It is also obvious that $\lambda = m\pi/h$. With this value then follows that $(8.180)_2$ gives rise to the independent solution functions

$$\sinh\left(\frac{m\pi}{h}z\right), \qquad \sinh\left(\frac{m\pi}{h}(\ell - z)\right). \tag{8.181}$$

These are chosen in this form, since the function $f(y, z)$ must primarily be corrected where the trial solution (8.178) does not satisfy the boundary condition.

It follows that the linear combination

$$f = \sum_{m=1}^{\infty} \sin\left(\frac{m\pi}{h}y\right)\left\{A_m \sinh\left(\frac{m\pi}{h}z\right) + B_m \sinh\left(\frac{m\pi}{h}(\ell - z)\right)\right\}. \tag{8.182}$$

is in principle able to match the boundary conditions $(8.179)_3$; explicitly,

$$\sum_{m=1}^{\infty} \sin\left(\frac{m\pi}{h}y\right) B_m \sinh\left(\frac{m\pi\ell}{h}\right) = \frac{1}{2}\frac{p'h^2}{\eta}\left(\frac{y}{h} - \left(\frac{y}{h}\right)^2\right), \tag{8.183}$$

plus the same equation, in which B_m is replaced by A_m. Thus, $B_m = A_m$ and these coefficients can be determined by standard FOURIER series inversion. The result is given in (8.25).

References

1. Aczel, A.D.: Pendulum. Leon Foucault and the Triumph of Science. Washington Square Press, New York (2003)
2. Abramowitz, M., Stegun, I.A. (eds.): Handbook of Mathematical Functions. Dover Publications, New York (1965)
3. Batchelor, K.G.: An Introduction to Fluid Dynamics. Cambridge University Press, Cambridge (1967)
4. Berker, R.: Intégration des équations du mouvement d'un fluide visqueux incompressible. In: Flügge, S. (ed.) Ecyclopedia of Physics, vol. VIII/2, pp. 1–384. Springer, Berlin (1963)
5. Bonham-Carter, G., Thomas, J.H: Numerical calculation of steady wind-driven currents in Lake Ontario and the Rochester embayment. In: Proceedings of 16th Conference on Great Lakes Research, International Association Great Lakes Research, pp. 640–662 (1973)
6. Boussinesq, J.: Sur l' influence des frottements dans les mouvements reguliéres des fluides. J. Math. Pure Appl. **13**, 377–438 (1868)
7. Bowden, K.F., Fairbairn, L.A., Hughes, P.: The distribution of shearing stresses in a tidal current. Geophys. J. R. Astr. Soc. **2**, 288–305 (1959)
8. Csanady, G.T.: Mean circulation in shallow seas. J. Geophys. Res. **81**, 5389–5399 (1976)
9. Csanady, G.T.: Turbulent interface layers. J. Geophys. Res. **83**, 2329–2342 (1978)
10. Csanady, G.T.: A developing turbulent surface shear layer model. J. Geophys. Res. **84**, 4944–4948 (1979)
11. Csanady, G.T.: The evolution of a turbulent Ekman layer. J. Geophys. Res. **85**, 1537–1547 (1980)
12. Csanady, G.T.: Circulation in the Coastal Ocean, 245 pp. D. Reidel Publishing Company, Dordrecht, Netherlands (1982)

13. Dombroklonskiy, S.V.: Drift current in the sea with an exponentially decaying eddy viscosity coefficient. Oceanology **9**, 19–25 (1969)
14. Drazin, P.G., Riley, N.: The Navier-Stokes equations: a classification of flows and exact solutions, pp. 1–196. Cambridge University Press (2006)
15. Dryden, H.L., Munaghan, F.D., Bateman, H.: Hydrodynamics. Bulletin of the National Research Council, Washington, No. 84 (1932). (Reprinted in 1956 by Dover Publications, New York)
16. Ekman, V.W.: On the influence of the Earth's rotation on the ocean currents. Ark. Mat. Astr. Fys. **2**(11), 1–52 (1905)
17. Ellison, T.H.: Atmospheric turbulence. In: Batchelor, G.K., Davies, R.M. (eds.) Surveys in Mechanics, pp. 400–430. Cambridge University Press (1956)
18. Fjeldstad, J.D.: Ein Beitrag zur Theorie der winderzeugten Meeresströmungen. Gerlands Beitr. Geophys. **23**, 237–247 (1930)
19. Foristall, G.Z.: Three-dimensional structure of storm-generated currents. J. Geophys. Res. **79**, 2721–2729 (1974)
20. Foristall, G.Z.: A two-layer model for Hurricane-driven currents on an irregular grid. J. Phys. Oceanogr. **23**, 237–247 (1980)
21. Foristall, G.Z., Hamilton, R.C., Cordane, V.J.: Continental shelf currents in tropical storm Delia: observations and theory. J. Phys. Oceanogr. **9**, 1417–1438 (1938)
22. Gedney, R.T.: Numerical calculations of wind-driven currents in Lake Erie. Ph.D. Dissertation, Case Western Reserve University, Ckleveland, OH (1971)
23. Gedney, R.T., Lick, W.: Wind-driven currents in Lake Erie. J. Geophys. Res. **77**, 2714–2723 (1972)
24. Heaps, N.S.: Vertical structure of current in homogeneous and stratified waters. In: Hutter, K. (ed.) Hydrodynamics of Lakes. CISM Lectures No 286, pp. 152–207. Springer, Vienna-New York (1984)
25. Heaps, N.S., Jones, J.E.: Development of a three-layered spectral model for the motion of a stratified sea. II. Experiments with a rectangular basin representing the Celtic Sea. In: Johns, B. (ed.) Physical Oceanography of Coastal and Shelf Seas, pp. 401–465. Amsterdam, Elsevier (1984)
26. Hidaka, K.: Non-stationary ocean currents. Mem. Imp. Mar. Obs. Kobe, **5**, 141–266 (1933)
27. Howarth, L.: Rayleigh's problem for a semi-infinite plate. Proc. Camb. Philos. Soc. **46**, 127–140 (1950)
28. Hutter, K., Wang, Y., Chubarenko, I.: Physics of Lakes. Volume I: Foundation of the Mathematical and Physical Background, 470 pp. Springer, Berlin-Heidelberg-NewYork (2010). ISBN: 978-3-642-15177-4
29. Lacomb, H.: Cours d' Oceanography Physique. Gauthier-Villars, Paris (1965)
30. Lagerstrom, P. A.: Laminar Flow Theory. Princeton University Press (1996) (Originally published in Moore, F.K. (ed.) Theory of Laminar Flows. Princeton University Press, Princeton, NJ (1964))
31. Lai, R.Y.S., Rao, D.B.: Wind drift currents in deep sea with variable eddy viscosity. Arch. Met. Geophys. Bioklim **A25**, 131–140 (1976)
32. Landau, L.: A new exact solution of Navier-Stokes equations. Akademija Nauk SSSR (Moskwa) **43**, 286–288 (1944)
33. Laska, M.: Characteristics and modelling of physical limnology processes. Mitt. Versuchsanstalt für Wasserbau, Hydrologie und Glaziologie an der ETH Zürich, Nr. 54, 1–230 (1981)
34. Madsen, O.S.: A realistic model of the wind-induced Ekman boundary layer. J. Phys. Oceanogr. **7**, 248–255 (1977)
35. Navier, C.-L.-M.-H.: Mémoire sur les lois du movement des fluides. Mem. Acad. Sci. Inst. France **6**(2), 389–440 (1827)
36. Newton, I.: Philosophiae Naturalis Principia Mathematica. Royal Society (1687)
37. Pearce, B.R., Cooper, C.K.: Numerical circulation model for wind induced flow. J. Hydraul. Div. Am. Soc. Civ. Eng. **107**(HY3), 285–302 (1981)

38. Platzman, G.W.: The dynamic prediction of wind tides on Lake Erie. Meteorol. Monogr. Am. Meteorol. Soc. **4**(26), 44 pp. (1963)
39. Poisson, S.-D.: Oire sur les équations générales de l' équilibre et du mouvement des corps solides élastique et des fluides. J. Ec. Polytech. **13**, cahier 20, 1–174 (1831)
40. Prandtl, L.: Neuere Ergebnisse der Turbulenzforschung. Zeitschrift VDI **77**, 105–113 (1933)
41. Proudman, I.: Notes on the motion of viscous liquids in channels. Philos. Mag. **28**(5), 30–36 (1914)
42. Rayleigh, L., Strutt, J.W.: On the motion of of solid bodies through viscous liquids. Philos. Mag. **21**, 697–711 (1911)
43. Rowell, H.S., Finlayson, D.: Screw viscosity pumps. Eng. Lond. **126**, 249–250, 385–387 (1928) [see also Berker [4], p. 71]
44. Saint-Venant, B.: Mémoire sur la dynamique des fluides. C. R. Acad. Sci. Paris **17**, 1240–1242 (1843)
45. Schlichting, H.: Boundary Layer Theory, 7th edn. London Pergamon Press (1979). See also: Schlichting, H., Gersten, K.: Boundary Layer Theory. Springer (2000)
46. Sherman, F.S.: Viscous Flow. McGraw Hill Publishing Company, New York (1990)
47. Squire, H.B.: The round laminar Jet. Q. J. Mech. Appl. Math. **4**, 321–329 (1951)
48. Stokes, G.G.: On the theories of the internal friction of fluids in motion, and of the equilibrium and motion of elastic solids. Trans. Camb. Philos. Soc. **8**, 287–305. [Also Math. Phys. Papers **1**, 75–129 (1880)] (1845)
49. Stokes, G.G.: Report on recent researches on hydrodynamics. Rep. Br. Assoc. 1–20. [Also Math. Phys. Papers, **1**, 156–187 (1880)] (1846)
50. Stokes. G.G.: On the effect of the internal friction of fluids on the motion of pendulums. Trans. Camb. Phil. Soc. **9**, 8 (1851)
51. Svensson, U.: Ph.D. Thesis (1979), see in Heaps (1984)
52. Thomas, J.H.: A theory of steady wind-driven currents in shallow water with variable eddy viscosity. J. Phys. Oceanogr. **5**, 136–142 (1975)
53. Truesdell, C.A.: The Kinematics of Vorticity. Indiana University Press (1954)
54. Wang, C.Y.: Exact solutions of the Navier-Stokes equations. Appl. Mech. Rev. **42**, 269–282 (1989)
55. Wang. C.Y.: Shear flow over convection cells—an exact solution of the Navier-Stokes equations. Z. Angew. Math. Mech., **70**, 351–352 (1990)
56. Wang. C.Y.: Exact solutions of the steady-state Navier-Stokes equations. Annu. Rev. Fluid Mech. **23**, 157–177 (1991)
57. Welander, P.: Wind action on a shallow sea: some generalizations of Ekman's theory. Tellus **9**, 45–52 (1957)
58. Wheeler, L.: Flow rate estimates for rectilinear pipe flow. J. Appl. Mech. **41**, 903–906 (1974)
59. Whitham, G.B.: The Navier-Stokes equations of motion. In: Rosenhead, L. (ed.) Laminar Boundary Layers, pp. 114–162. Clarendon Press, Oxford (1963)
60. Witten, A.J., Thomas, J.H.: Steady wind driven currents in a large lake with depth-dependent eddy viscosity. J. Phys. Oceanogr. **6**, 85–92 (1976)

Chapter 9
Simple Solutions of Boundary Layer Equations

Abstract In this chapter two- and three-dimensional boundary layer flows in the vicinity of a stagnation point are studied as are flows around wedges and along wedge sidewalls. The flow, induced in the half plane above a rotating plane, is also analyzed. The technique of the boundary layer approach is commenced with the BLASIUS flow, but more importantly, the boundary layer solution technique for the NAVIER-STOKES equations is explained by use of the method of matched asymptotic expansions. Moreover, the global laws of the steady boundary layer theory are explained with the aid of the Holstein-Bohlen procedure. The chapter ends with a brief study of non-stationary boundary layers, in which e.g. an impulsive start from rest, flow in the vicinity of a pulsating body, oscillation induced drift current and non-stationary plate boundary layers are studied.

Keywords Stagnation point flow · Flows around wedges and along wedge side walls · Flow on top of a rotating plane · BLASIUS flows · Boundary layer solutions of the NAVIER-STOKES equations by matched asymptotic expansions · HOLSTEIN-BOHLEN procedure based on global laws · Nonsteady boundary layers

List of Symbols

Roman Symbols

$a = 0.47$	Parameter arising in the quadrature formula of WALZ
a, b, c, d	Coefficients in the boundary layer profile of the HOLSTEIN-BOHLEN procedure
$b = 6.0$	Parameter arising in the quadrature formula of WALZ
c_f	Drag coefficient of the wall shear stress of the BLASIUS boundary layer
F, f	Auxiliary functions in the construction of similarity solutions of viscous flows, Axial momentum flux of a round jet Damping force on a body
f^i, f^o	Inner and outer expansion of f in a matched asymptotic expansion

$f_1(\kappa), f_2(\kappa)$	Functions arising in the HOLSTEIN-BOHLEN integration
$\mathfrak{G}(m)$	Dimensionless coefficient of the displacement thickness for flow around a corner (see Eq. 9.58)
g, h	Auxiliary functions for the azimuthal and axial velocities in steady flow above a rotating disk
$\iota = \sqrt{-1}$	Imaginary unit
K	Kinetic energy
L, ℓ	length scales
$L, \bar{L}$	Power of working of all forces on a body, time average of L
m	Power exponent in similarity solution of boundary layer flow over a wedge
N_1, N_2	Sliding coefficients
Q	Volume flux of a round axial jet
$\mathbb{R}, \mathbb{R}_x, \mathbb{R}_\ell$	REYNOLDS numbers: $\mathbb{R}_x = \frac{Ux}{\nu}, \mathbb{R}_\ell = \frac{U\ell}{\nu}$
U	Constant velocity, generally representing parallel flow
U_2	Drift velocity at the outer edge of the boundary layer
$u_1, v_1; u_2, v_2$	First and second order perturbation velocities in the x- and y-directions
u, v, w	Velocity components in the x-, y- and z-directions
$\tilde{u}, \tilde{v}$	x-, y-components of a potential flow
v_r, v_θ, v_z	Velocity components in the radial, azimuthal and axial directions of a cylindrical coordinate system
x, y, z	Cartesian coordinates
x_0	Virtual position of the origin of a round jet
	Body displacement amplitude
$Z = \theta^2/\nu$	Variable arising in the HOLSTEIN-BOHLEN integration

Greek Symbols

α	Semi opening-angle of a two-dimensional wedge
$\beta = (m+1)/2$	Power exponent of similarity solutions of boundary layer flows past a wedge
$\gamma = (m-1)/2$	Power exponent of similarity solutions of boundary layer flows past a wedge
Δ	LAPLACE operator, $\Delta = \nabla^2$
Δp	Pressure change across boundary layer
$\delta(\eta)$	Asymptotic dimensionless displacement thickness function
δ	Boundary layer thickness
δ^*	Displacement thickness
$\delta u, \delta v$	Far from boundary layer, see (9.20): $\delta u = (u - \tilde{u}), \delta v = (v - \tilde{v})$
ε	Perturbation parameter
	Small positive parameter
	Parameter quantifying the ellipticity of a potential flow
η	Dimensionless transverse coordinates (perpendicular to the boundary layer flow)

θ	Azimuthal angle in rotating stagnation point flow
	Momentum thickness
	Azimuthal coordinate in a cylindrical coordinate system
κ	See (9.208) and (9.213)$_2$: $\kappa = \frac{\theta^2}{\nu}\frac{dU}{dx} = Z\frac{dU}{dx}$
$\Lambda = \frac{\delta^2}{\nu}\frac{dU}{dx}$	Form parameter in the HOLSTEIN-BOHLEN integration
ν	Kinematic viscosity
τ_0	Wall shear stress
ϕ	Velocity potential for a density preserving inviscid fluid
	Dimensionless auxiliary function in the construction of similarity solutions of viscous flows
	Dissipative power
ψ	Stream function
ω	Angular frequency

9.1   Preview

In this chapter the aim is the presentation of exact and approximate solutions for flow of linearly viscous bodies in simple geometries of mainly two-dimensions, either plane or axisymmetric flow. Most problems have been solved in the first half of the twentieth century, but research is still going on now in the twenty-first century. Particularly important were the boundary layer equations as presented by LUDWIG PRANDTL in 1904 [30]. These postulate that the flux terms of the momentum (or energy) equations close to the solid boundaries of the flow are only important perpendicular to the bounding walls, whereas those parallel to them can be dropped. Moreover, the pressure in the boundary layer is given by the pressure as evaluated with an ideal fluid. Later, in the second half of the twentieth century, when the methods of singular perturbations and methods of matched asymptotic expansions were developed to approximately solve initial-boundary-value problems, PRANDTLs boundary layer equations were recognized to be the lowest order equations of an entire hierarchy of approximations in solving the complete NAVIER-STOKES equations.

In what follows, simple steady flows of two-dimensional and three-dimensional motions in the vicinity of stagnation points around wedges and a rotating disk problem of infinite extent are looked at. These are then generalized to some unsteady flows of this sort. Steady flow of a viscous fluid past a flat semi-infinite plate—the so-called BLASIUS flow—and steady laminar flow of an axisymmetric jet then closes the first part of the contribution of exact solutions of the NAVIER-STOKES equations with boundary layer character.

Boundary layers are then looked at as successive approximations of the NAVIER-STOKES equations in the context of asymptotic expansions. The BLASIUS boundary layer problem is treated in this context, but not further developed. The reader must consult additional literature on this topic by KLAUS GERSTEN, HEINZ HERWIG,

WILHELM SCHNEIDER, PH. GITTLER and others (for references see e.g., HERRMANN SCHLICHTING and KLAUS GERSTEN [36]).

The third part of this chapter concentrates on the derivation and use of the approximate boundary layer equations, the introduction of the global forms of the balance laws of mass and momentum, leading to the definitions of the displacement and momentum thicknesses and their application in the HOLSTEIN-BOHLEN procedure. Unsteady boundary layers conclude this chapter by treating fluid flow induced by oscillating bodies, the analysis of oscillation-induced drift currents and unsteady plate boundary layers.

Turbulent boundary layers are not treated here.

9.2 Two-Dimensional Boundary Layer Flow in the Vicinity of a Stagnation Point

We commence this section by repeating the formulae representing inviscid stagnation point potential flow,[1]

$$
\phi = \frac{U}{2\ell}\left(x^2 - y^2\right) \quad \longrightarrow \quad \begin{cases} \tilde{u} = \dfrac{\partial \phi}{\partial x} = \dfrac{U}{\ell}x, \\ \tilde{v} = \dfrac{\partial \phi}{\partial y} = -\dfrac{U}{\ell}y, \end{cases}
\tag{9.1}
$$

where the tilde identifies variables of the inviscid fluid. Its pressure distribution can be obtained with the aid of the BERNOULLI equation,

$$
\tilde{p} + \frac{\rho}{2}\left(\tilde{u}^2 + \tilde{v}^2\right) = p_0,
$$

where p_0 is the stagnation pressure,

$$
p_0 - \tilde{p} = \frac{\rho}{2}\left(\tilde{u}^2 + \tilde{v}^2\right) = \frac{\rho U^2}{2\ell^2}\left(x^2 + y^2\right).
\tag{9.2}
$$
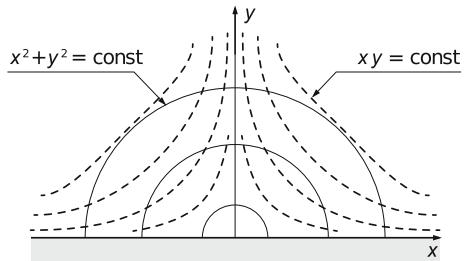
As evident from the above formulae, the equi-potential lines are hyperbolas with center at the stagnation point, and the isobars are circles with center at the stagnation point. Moreover, the streamlines are given by

$$
\frac{\mathrm{d}y}{\mathrm{d}x} = \frac{\tilde{v}}{\tilde{u}} = -\frac{y}{x} \quad \longrightarrow \quad \ln y = \ln \frac{C}{x} \quad \longrightarrow \quad xy = C
$$

and represent for each C hyperbolas. Both the x and y axes are streamlines, see **Fig. 9.1**.

---

[1] See e.g. Chap. 5, p. 257, Fig. 5.30 and Chap. 6, p. 282, Fig. 6.6.

Fig. 9.1 Streamlines (*dashed*) and isobars (*solid*) of a plane potential flow

$x^2 + y^2 = \text{const}$ $xy = \text{const}$

Even though the above solution also satisfies the plane NS-equations, it violates the boundary conditions at $y = 0$ ($u(x, 0) \neq 0$). To satisfy these boundary conditions we now start from the two-dimensional incompressible steady NS-equations

$$u \frac{\partial u}{\partial x} + v \frac{\partial u}{\partial y} = -\frac{1}{\rho} \frac{\partial p}{\partial x} + \nu \left(\frac{\partial^2 u}{\partial x^2} + \frac{\partial^2 u}{\partial y^2} \right), \tag{9.3}$$

$$u \frac{\partial v}{\partial x} + v \frac{\partial v}{\partial y} = -\frac{1}{\rho} \frac{\partial p}{\partial y} + \nu \left(\frac{\partial^2 v}{\partial x^2} + \frac{\partial^2 v}{\partial y^2} \right).$$

The trial solution

$$u = x f'(y), \quad v = -f(y), \quad p - p_0 = -\frac{\rho U^2}{2\ell^2} \left(x^2 + F(y) \right), \tag{9.4}$$

in which $f(y)$ and $F(y)$ are unknown functions and the prime denotes differentiation with respect to y, transforms (9.3) to

$$(f')^2 - f f'' = \frac{U^2}{\ell^2} + \nu f''', \tag{9.5}$$

$$f f' = \frac{U^2}{2\ell^2} F'(y) - \nu f''.$$

These equations show that the variable x drops out of the field equations, making them ordinary differential equations. Moreover, with u and v as given by (9.4)$_{1,2}$, the velocity field is automatically solenoidal. The equations must be subjected to the boundary conditions

$$u = v = 0, \quad \text{at } y = 0,$$
$$u = \frac{U}{\ell} x, \quad \text{as } y \to \infty. \tag{9.6}$$

In other words, for $y \to \infty$ the viscous flow goes over to the potential flow. Equations (9.5) require four boundary conditions, but (9.6) are only three; we, therefore, set arbitrarily

$$F(y) = 0, \quad \text{at } y = 0. \tag{9.7}$$

This means according to $(9.4)_3$ that the stagnation pressure is also here given by p_0.

In order to non-dimensionalize Eqs. (9.5), let

$$f(y) = A\phi(\eta), \quad \eta = \alpha y, \tag{9.8}$$

in which A and α are constants, which must be suitably estimated. Substitution of (9.8) into $(9.5)_1$ generates the differential equation

$$(\phi')^2 - \phi \phi'' = \underbrace{\frac{U^2}{(A\alpha\ell)^2}}_{=1} + \underbrace{\frac{\nu\alpha}{A}}_{=1} \phi''', \tag{9.9}$$

where $\phi' = \mathrm{d}\phi/\mathrm{d}\eta$. Setting the underbraced quantities equal to unity yields

$$A = \sqrt{\frac{\nu U}{\ell}}, \quad \alpha = \sqrt{\frac{U}{\ell\nu}}, \tag{9.10}$$

so that

$$f(y) = \sqrt{\frac{\nu U}{\ell}}\phi(\eta), \quad \eta = \sqrt{\frac{U}{\ell\nu}}y. \tag{9.11}$$

The boundary value problem for ϕ, thus, takes the form[2]

$$\begin{aligned}
(\phi')^2 - \phi \phi'' &= 1 + \phi''', & 0 < \eta < \infty, \\
\phi = \phi' &= 0, & \text{at } \eta = 0, \\
\phi' &\to 1, & \text{as } \eta \to \infty.
\end{aligned} \tag{9.12}$$

Once this nonlinear boundary value problem is solved, the velocities are recovered from

$$u = xf' = xA\alpha\phi' = \frac{U}{\ell}x\phi'(\eta), \tag{9.13}$$

$$v = -f = -A\phi = \sqrt{\frac{\nu U}{\ell}}\phi(\eta).$$

The boundary value problem (9.12) has been numerically integrated by KARL HIEMENZ[3] (1911) [15]. Some results are displayed in **Fig. 9.3**. Its interpretation is fascinated by writing

---

[2]The differential Eq. $(9.12)_1$ is a special case of the FALKNER-SKAN equation [10] and (9.12) is a two-point boundary value problem of an ordinary differential equation arising in viscous boundary layer flows past wedges.

[3]For a short biography of KARL HIEMENZ see **Fig. 9.2**.

$$\phi(\eta) = \int\limits_0^\eta \phi'(\overline{\eta})\mathrm{d}\overline{\eta} = \eta - \int\limits_0^\eta \left(1 - \phi'(\overline{\eta})\right)\mathrm{d}\overline{\eta} = \eta - \Delta(\eta). \qquad (9.14)$$
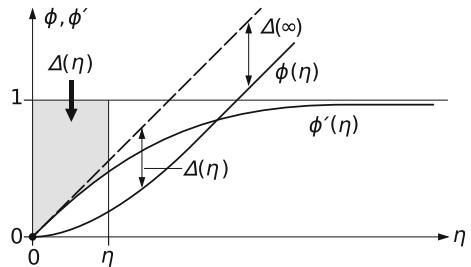
Fig. 9.2 KARL HIEMENZ (19. Jan. 1885–2. June 1973)

KARL HIEMENZ studied mathematics and physics, first in Darmstadt at the 'Technische Hochschule', then at the University in Göttingen, where he became an assistant to FELIX KLEIN. LUDWIG PRANDTL in 1907 assigned him as doctoral topic the study of the boundary layer flow of a viscous fluid past a circular cylinder; he received his degree in 1910 with the text [15], published later in 1911. Subsequently, he worked as an assistant of mechanics in the physics department of the 'Technische Hochschule Darmstadt', but moved in 1914 to the Hamburg Technical College, where he occupied a position of a teacher of mathematics and electro-technique from 1922 to 1950, when he retired.

Apart of the work described in this book, HIEMENZ made and described observations, which caught VON KÁRMÁN's attention and later became the VON KÁRMÁN vortex street. HIEMENZ preferred teaching to research, as did his colleague HEINRICH BLASIUS. As teachers of the same school they remained friends for their whole lives.

Figure and text from and based on: HAGER, W.H.: 'Karl Hiemenz. Hydraulicians in Europe 2': 1091. IAHR, Madrid (2009)

Fig. 9.3 Construction and
interpretation of $\phi'(\eta)$ and
$\phi(\eta)$ as described in the main
text

$\Delta(\eta)$ can be regarded as a dimensionless asymptotic displacement thickness. It
turns out that $\phi'(\eta)$ is monotonically increasing for growing η from $\phi'(0) = 0$
to $\lim_{\eta \to \infty} \phi'(\eta) = 1$ and is characteristically given as shown in Fig. 9.3. Once this
curve is determined, the function $\Delta(\eta)$ is obtained as the shaded area of Fig. 9.3.
The function $\phi(\eta)$ must for $\eta \to \infty$ be parallel to the $45°$-line (- - -) and start from
$\phi(0) = 0$. Its trace for large η is $\Delta(\eta)|_\infty = 0.65$ units below the $45°$-line. With
(9.13) the velocities for large values of η and large values of x are given by

$$
\begin{aligned}
u &\to \frac{U}{\ell}x, \\
v &\to \sqrt{\frac{\nu U}{\ell}} \left\{ \sqrt{\frac{U}{\nu \ell}} y - 0.65 \right\} = -\frac{U}{\ell}\left(y - \delta^*\right),
\end{aligned}
\tag{9.15}
$$

in which δ^* is the so-called **displacement thickness**, expressible as

$$
\delta^* = \frac{0.65\ell}{\sqrt{\mathbb{R}}}, \quad \mathbb{R} = \frac{U\ell}{\nu}.
\tag{9.16}
$$

The denotation 'displacement thickness' can be understood, if one compares (9.15)
with the velocities of the potential theory, (9.1). The asymptotic velocities are the
same, but v is so distributed as if the fluid mass would be lifted (or displaced) by
a mechanism by the amount δ^* from the wall. The expression of the displacement
thickness can be written as

$$
\delta^* = \int_0^\infty \left(1 - \frac{u}{u_\infty}\right) \sqrt{\frac{\nu \ell}{U}}\,\mathrm{d}\eta = \int_0^\infty \left(1 - \frac{u}{u_\infty}\right)\mathrm{d}y, \quad \text{where } \phi'(\eta) = \frac{u}{u_\infty}
$$
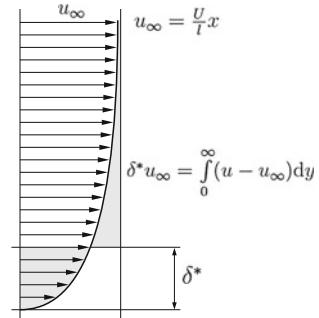
has been used. This formula is interpreted in **Fig. 9.4**. The value of the displacement
depth is at the position for which the two shaded regions have the same size.

The above discussion is based on the solution of equation (9.5), or (9.12). In the
above Eq. $(9.5)_2$ has not been touched. However, it can be written as

$$
F'(y) = \frac{2\ell^2}{U^2}\left(ff' + \nu f''\right) = \frac{\ell^2}{U^2}\left((f^2)' + 2\nu f''\right).
\tag{9.17}
$$

Fig. 9.4 Wall distance plotted against wall-parallel velocity. *The location of the displacement thickness is where*
$$\delta^* u_\infty = \int_0^\infty (u - u_\infty) \mathrm{d}y$$

Integrating this equation once and using (9.8) yields

$$F(y) = \frac{\ell^2}{U^2} \left(f^2 + 2\nu f' \right) \stackrel{(9.8)}{=} \frac{\ell^2}{U^2} \left(A^2 \phi^2 + 2A\nu\alpha\phi' \right)$$
$$\stackrel{(9.10)}{=} \frac{\ell\nu}{U} \left(\phi^2 + 2\phi' \right). \tag{9.18}$$

At the outer margin of the boundary layer $(\phi^2 + 2\phi')$ has a fixed value of order unity. One may, therefore, equally say that the pressure change at fixed x across the boundary layer is given by

$$\Delta p = \frac{\rho U^2}{2\ell^2} F(\delta) \propto \frac{\rho U^2}{2\ell^2} \frac{\ell\nu}{U} = \frac{\rho U^2}{2} \frac{1}{\mathbb{R}}, \quad \mathbb{R} = \frac{U\ell}{\nu}.$$

Since we have already found that $\delta \propto \ell/\sqrt{\mathbb{R}}$ (see (9.16)) there follows

$$\frac{\partial p}{\partial y}\bigg|_{\text{boundary layer}} \propto \frac{\Delta p}{\delta} \propto \frac{\rho U^2}{2} \frac{1}{\mathbb{R}} \frac{\sqrt{\mathbb{R}}}{\ell} = \frac{\rho U^2}{2\ell} \frac{1}{\sqrt{\mathbb{R}}}. \tag{9.19}$$

For $\mathbb{R} \to \infty$ this statement demonstrates that $\Delta p|_{\mathbb{R}\to\infty} \to 0$.

Let us next investigate the transition to the *limit of the inviscid flow*. This limit is achieved by considering the process $\mathbb{R} \to \infty$. As before, variables of the inviscid fluid will be identified with a tilde. In view of (9.1) and (9.13) we may write

$$\delta u := u - \tilde{u} = \frac{U}{\ell} x \left(\phi'(\eta) - 1 \right) = \tilde{u} \left(\phi'(\eta) - 1 \right), \tag{9.20}$$

$$\delta v := v - \tilde{v} = -\frac{U}{\ell}\left(\sqrt{\frac{\nu\ell}{U}}\phi(\eta) - y\right) = -\frac{U}{\ell}\left\{\sqrt{\frac{\nu\ell}{U}}\left(\eta - \Delta(\eta)\right) - y\right\}$$

$$= -\frac{U}{\ell}\left\{\sqrt{\frac{\nu\ell}{U}}\left(\sqrt{\frac{U}{\nu\ell}}y - \Delta(\eta)\right) - y\right\} = \frac{U}{\ell}\sqrt{\frac{\nu\ell}{U}}\Delta(\eta). \qquad (9.21)$$

We begin with δv and define

$$\Delta(\eta)_{\text{max}} := \max_{\eta \in [0,\infty)}\left(\Delta(\eta)\right) = 0.65.$$

Then we have

$$|\delta v| \leqslant \frac{U}{\sqrt{\mathbb{R}}}\Delta(\eta)_{\text{max}} \quad \longrightarrow \quad \lim_{\mathbb{R}\to\infty}|\delta v| \leqslant \lim_{\mathbb{R}\to\infty}\frac{U}{\sqrt{\mathbb{R}}}\Delta(\eta)_{\text{max}} = 0. \qquad (9.22)$$

This result holds for all $\eta \in [0, \infty)$, implying that $\lim_{\mathbb{R}\to\infty}\delta v = 0$. On the other hand, we obtain for δu

$$\delta u = \tilde{u}\left(\phi'\left(\frac{\sqrt{\mathbb{R}}}{\ell}y\right) - 1\right).$$

It is known that $\phi' \neq 0$ for all $y > 0$, and $\phi' = 1$ for $y \to \infty$. For fixed y the argument $(\sqrt{\mathbb{R}}/\ell)y$ of ϕ' tends to infinity if $\mathbb{R} \to \infty$. Therefore,

$$\lim_{\mathbb{R}\to\infty}\delta u = 0. \qquad (9.23)$$

We have, thus, proved that the *viscous velocity distribution approaches the inviscid limit when* $\mathbb{R} \to \infty$. On the other hand,

$$\lim_{y\to\infty,\ \mathbb{R}\text{ fix}}\delta u = 0, \quad \text{but} \quad \lim_{y\to\infty,\ \mathbb{R}\text{ fix}}\delta v = -\frac{U\delta^*}{\ell}, \qquad (9.24)$$

a result that is also logical when considering the physical interpretation of the displacement thickness.

9.3   Three-Dimensional Boundary Layer Flow in the Vicinity of a Stagnation Point

The two-dimensional potential flow that was introduced at the beginning of the last section and its alteration by viscous effects belongs to a class of potential flows with the velocity potential

$$\phi(x, y, z) = \frac{U}{2\ell} \left(\varepsilon x^2 + (1 - \varepsilon)y^2 - z^2\right). \tag{9.25}$$

The two-dimensional case of Sect. 9.2 corresponds to the parameter value $\varepsilon = 1$ (whereby also y is replaced by z). The velocity components belonging to (9.25) are

$$\tilde{u} = \frac{\partial \phi}{\partial x} = \varepsilon \frac{U}{\ell} x, \quad \tilde{v} = \frac{\partial \phi}{\partial y} = (1 - \varepsilon)\frac{U}{\ell} y, \quad \tilde{w} = \frac{\partial \phi}{\partial z} = -\frac{U}{\ell} z. \tag{9.26}$$

Tildes indicate the restriction to the potential flow. It is evident that the plane $z = 0$ is a stream surface ($\tilde{w} = 0$), which can be replaced by a fixed wall. In this way a three-dimensional stagnation point flow is obtained with stagnation point at $x = y = z = 0$, see **Fig. 9.5**. The pressure is again obtained with the aid of the BERNOULLI equation,

$$\tilde{p} - p_0 = \frac{\rho U^2}{2\ell^2} \left(\varepsilon^2 x^2 + (1 - \varepsilon)^2 y^2 + z^2\right). \tag{9.27}$$
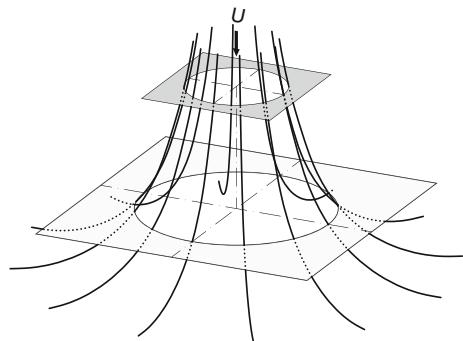
If p_0 is chosen as the stagnation pressure, then the difference pressure $p - p_0$ is, for fixed z, constant along horizontal ellipses given by (9.27) $= 0$. Along these ellipses also the modulus of the velocity is constant.

Consider especially rotation-symmetric stagnation point flow. In this case $\varepsilon = \frac{1}{2}$. The horizontal velocity field is now radially oriented, so that

$$\tilde{v}_r = \frac{U}{2\ell} r, \quad \tilde{v}_\theta = 0, \quad \tilde{v}_z = -\frac{U}{\ell} z. \tag{9.28}$$

In what follows we shall write $v_r =: u$, $v_z =: w$; with this notation the axisymmetric ($\partial/\partial\phi = 0$) NS-equations take the forms

Fig. 9.5 Three-dimensional elliptical stagnation point flow. *Streamlines and the asymptotic velocity U are shown (in perspective view). The ellipses trace the intersection of the streamlines with horizontal planes*

$$\frac{\partial u}{\partial r} + \frac{u}{r} + \frac{\partial w}{\partial z} = 0,$$

$$u\frac{\partial u}{\partial r} + w\frac{\partial u}{\partial z} = -\frac{1}{\rho}\frac{\partial p}{\partial r} + \nu\left\{\frac{\partial^2 u}{\partial r^2} + \frac{1}{r}\frac{\partial u}{\partial r} - \frac{u}{r^2} + \frac{\partial^2 u}{\partial z^2}\right\}, \qquad (9.29)$$

$$u\frac{\partial w}{\partial r} + w\frac{\partial w}{\partial z} = -\frac{1}{\rho}\frac{\partial p}{\partial z} + \nu\left\{\frac{\partial^2 w}{\partial r^2} + \frac{1}{r}\frac{\partial w}{\partial r} + \frac{\partial^2 w}{\partial z^2}\right\}.$$

As for the two-dimensional flow, see (9.4), a trial solution, which satisfies the continuity equation, is sought. Such an ansatz has the form

$$u = rf'(z), \quad w = -2f(z), \quad p - p_0 = -\frac{\rho}{2}\frac{U^2}{4\ell^2}\left(r^2 + F(z)\right). \qquad (9.30)$$

With it $(9.29)_2$ can be shown to reduce to

$$(f')^2 - 2ff'' = \frac{U^2}{4\ell^2} + \nu f''', \qquad (9.31)$$

subject to the boundary conditions

$$\begin{aligned} f = f' &= 0, \quad \text{at } z = 0, \\ f' &\to \frac{U}{2\ell}, \qquad \text{for } z \to \infty, \end{aligned} \qquad (9.32)$$

which require that $u(r, 0) = 0$, $w(r, 0) = 0$, $p(0, 0) = p_0$ and that $u(0, \infty)$ approaches the potential flow limit $(9.28)_1$. At last we now set

$$f := \sqrt{\frac{\nu U}{2\ell}}\phi(\eta), \quad \eta := \sqrt{\frac{U}{2\nu\ell}}y. \qquad (9.33)$$
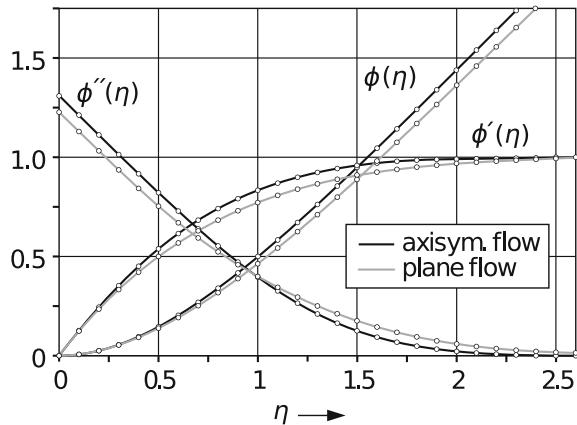
With this similarity-variables description, (9.31) and (9.32) define the boundary value problem

$$\begin{aligned} (\phi')^2 - 2\phi\,\phi'' &= 1 + \phi''', \quad 0 < \eta < \infty, \quad (\cdot)' = \tfrac{d(\cdot)}{d\eta}, \\ \phi = \phi' &= 0, \qquad\qquad \text{at } \eta = 0, \\ \phi' &\to 1, \qquad\qquad \text{for } \eta \to \infty, \end{aligned} \qquad (9.34)$$

which is analogous to (9.12) in the two-dimensional case. In fact, the two boundary value problems differ only by the pre-factor 1 (two-dimensional case) and 2 (axisymmetric three-dimensional case) of the term involving ϕ'' of the ordinary differential equation.

The boundary value problem (9.12) for plane stagnation flow was integrated by KARL HIEMENZ (1911) [15]. The corresponding three-dimensional axisymmetric boundary value problem (9.34) was solved more than 20 years later by F. HOMANN (1936) [16]. Both articles are essentially the doctoral dissertations done under the

Fig. 9.6 Plots of $\phi(\eta)$, $\phi'(\eta)$ and $\phi''(\eta)$. *They are obtained as solutions of (9.12) (plane case, obtained by* HIEMENZ*) and (9.34) (axisymmetric case, obtained by* HOMANN*). From F.* HOMANN *[16], © Z. angew. Math. Mech, WILEY-VCH Verlag GmbH & Co. KGaA, Weinheim*

supervision of LUDWIG PRANDTL. **Figure 9.6** displays the graphs for $\phi(\eta)$, $\phi'(\eta)$ and $\phi''(\eta)$ for the plane two-dimensional and axisymmetric three-dimensional plots for these functions. Details of the computations are given by F. HOMANN.

9.4   Boundary Layer Flows Around Wedges

9.4.1   Boundary Layer Equations

The boundary layer equations were presented in 1905 by LUDWIG PRANDTL [30][4] as approximations of the NS-equations. Basic idea is the recognition that for sufficiently large REYNOLDS numbers the viscous effects of the flow are essentially restricted to thin layers close to walls. Outside these layers the flow is dominated by inviscid behavior, see **Fig. 9.7**.

Consider a plane wall with the x-axis in the wall and the y-axis perpendicular to it. Denote by tilde variables of the flow of an inviscid fluid close to the wall:
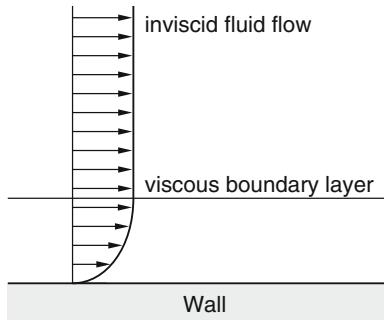
- $\tilde{u}_w = f(x)$ is the velocity of the flow of the inviscid fluid immediately at the wall;
- $\tilde{p}_w(x)$ is the pressure of the flow of the inviscid fluid immediately at the wall.

Introduce the following assumptions:

1. The pressure p within the boundary layer as it varies along the wall is essentially that of the inviscid fluid at the outer edge of the boundary layer.

---

[4]This is the formal paper, where the boundary layer theory is presented. PRANDTL, however, had a preliminary lecture titled 'Flüssigkeitsbewegung bei sehr kleiner Reibung' in 1904 to the 'Heidelberger Mathematiker Kongress' which contains all essential elements of the boundary layer theory. The essential part of PRANDTL's text in German alongside with K.H.'s translation into English is given in Appendix 16.A to Chap. 16, Vol. 2, or [19] pp. 467–469.

Fig. 9.7 Boundary layer
flow. *Close to the wall (inner
region) effects of viscous
behaviour are dominant;
distant from the wall (outer
region) the response is
essentially that of an inviscid
fluid*

2. The boundary layer is so thin that the variations of the viscous stresses within
   the layer perpendicular to the wall are much larger than the variations in the
   x-direction.

Based on these assumptions the following simplifications can be implemented in the
NS-equations:

- $\dfrac{\partial p}{\partial x}$ is replaced by $\dfrac{\partial \tilde{p}_w}{\partial x}$;

- $\left| \dfrac{\partial^2 u}{\partial x^2} \right| \ll \left| \dfrac{\partial^2 u}{\partial y^2} \right|$ is ignored;

- $\left| \dfrac{\partial^2 v}{\partial x^2} \right| \ll \left| \dfrac{\partial^2 v}{\partial y^2} \right|$ is ignored.

Consequently, the two-dimensional NS-equations are replaced by the two-
dimensional boundary layer equations[5]

$$
\begin{aligned}
&\frac{\partial u}{\partial x} + \frac{\partial v}{\partial y} = 0, \\
&\frac{\partial u}{\partial t} + u\frac{\partial u}{\partial x} + v\frac{\partial u}{\partial y} = -\frac{1}{\rho}\frac{\partial \tilde{p}_w}{\partial x} + \nu\frac{\partial^2 u}{\partial y^2}, \\
&\frac{\partial v}{\partial t} + u\frac{\partial v}{\partial x} + v\frac{\partial v}{\partial y} = -\frac{1}{\rho}\frac{\partial p}{\partial y} + \nu\frac{\partial^2 v}{\partial y^2}.
\end{aligned}
\tag{9.35}
$$

Note that $(9.35)_2$ involves the pressure $\tilde{p}_w$ of the inviscid fluid, whereas $(9.35)_3$ has
p of the viscous fluid, which is one of the unknowns. Equations $(9.35)_{1,2}$ are used
to determine the velocity field u, v. Once these components are known, $(9.35)_3$ is
used for the determination of the y-dependence of the pressure field p. As boundary
conditions one usually requests

---

[5]It is quite obvious, how these equations look like in the three-dimensional case.

1.

$$u = v = 0, \ \text{at } y = 0, \text{no-slip condition at the wall.} \qquad (9.36)$$

2. Far away from the wall the x-component of the velocity field, u, should merge into the u-component of the inviscid outer flow.

$$\lim_{y \to \infty} u(x, y) \to \tilde{u}_w(x). \qquad (9.37)$$

For v a corresponding boundary condition for large values of y cannot be requested.
3. As 'initial condition' for a position $x = x_0$ far upstream, one prescribes the x-velocity profile

$$u(x_0, y) = g(y). \qquad (9.38)$$

The problem for $u(x, y)$ is analogous to an initial value problem for the heat conduction equation. For an 'initial profile' $g(y)$ the velocity profile $u(x, y)$ can be continued into the downstream region. If the initial profile satisfies the outer boundary condition, then one may dispense with the prescription of outer boundary conditions.
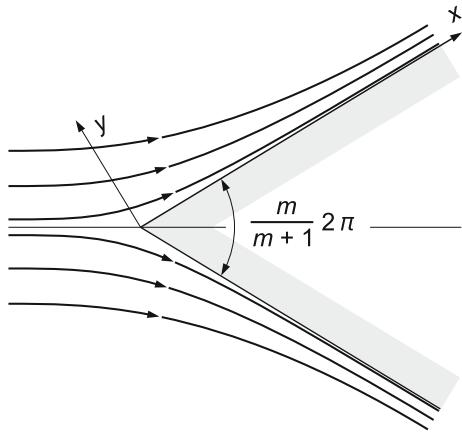
We close this brief introduction into the boundary layer equations by the following remarks.

- The boundary layer assumptions are *not* extended by corresponding approximations in the convective acceleration terms, e.g., $\partial u/\partial x$ versus $\partial u/\partial y$ or $\partial v/\partial y$, etc. For a density-preserving fluid balance of mass, $\partial u/\partial x + \partial v/\partial y = 0$, provides an argument, why such omissions would be wrong. Indeed $|\partial u/\partial x|$ and $|\partial v/\partial y|$ are equal to satisfy mass balance in this case.
- The boundary layer equations are in their mathematical structure much different from the NS-equations, also in steady state. By the omission of the term $\partial^2 u/\partial x^2$ the elliptic steady NS-equations become parabolic boundary layer equations. Physically, this means that the diffusion of the vorticity in the x-direction is ignored as compared to that in the y-direction.
- By the a posteriori evaluation of the pressure one may corroborate whether the assumption $p = \tilde{p}_w(x)$ is fulfilled with sufficient accuracy across the entire boundary layer.
- The boundary layer equations can also be motivated by the methods of matched asymptotic expansions (see Sect. 9.6).

9.4.2 Flow Along Sidewalls of Wedges

Starting point of the following considerations is the symmetric flow of an inviscid fluid past an infinitely long wedge with an opening angle of 2α, for which the velocity

Fig. 9.8 Viscous flow past
an infinite wedge. *The flow
close to the side flanks of the
wedge is interpreted as a
boundary layer flow of the
NS-equations*

distribution is given by[6]

$$\tilde{u}_w = U \left(\frac{x}{\ell}\right)^m = A x^m, \quad A = \frac{U}{\ell^m}, \quad 2\alpha = \frac{m}{m+1} 2\pi. \tag{9.39}$$

The aim is the determination of the boundary layer flow in the vicinity of the wedge.
To this end, the coordinate system of **Fig. 9.8** is used. For the derivation of the bound-
ary layer flow the pressure distribution of the outer flow is needed. This distribution
is obtained by the BERNOULLI equation

$$\tilde{p}_w + \frac{\rho}{2}\tilde{u}_w^2 = \text{const.} \quad \longrightarrow \quad \frac{\partial \tilde{p}_w}{\partial x} = -\rho \tilde{u}_w \frac{\mathrm{d}\tilde{u}_w}{\mathrm{d}x}, \tag{9.40}$$

or with (9.39)

$$-\frac{1}{\rho}\frac{\partial \tilde{p}_w}{\partial x} = \tilde{u}_w \frac{\partial \tilde{u}_w}{\partial x} = m A^2 x^{2m-1}. \tag{9.41}$$

This expression will be used in (9.35)$_2$ when solving the boundary layer equations.
Introducing the stream function ψ and requesting that

$$u = \frac{\partial \psi}{\partial y}, \quad v = -\frac{\partial \psi}{\partial x}, \tag{9.42}$$

the continuity Eq. (9.35)$_1$ is identically satisfied; the steady state x-momentum
Eq. (9.35)$_2$ then takes the form

---

[6]See also Chap. 6, Sect. 6.1.2, "Generalized stagnation point flow", p. 282–286.

$$\underbrace{\psi_y \psi_{xy}}_{(1)} - \underbrace{\psi_x \psi_{yy}}_{(2)} = \underbrace{m A^2 x^{2m-1}}_{(3)} + \underbrace{\nu \psi_{yyy}}_{(4)}, \tag{9.43}$$

in which the indices x, y denote differentiation with respect to these variables. In the two-dimensional stagnation point flow the corresponding partial differential equation was transformed to an ordinary differential equation by introducing a similarity representation for ψ, see (9.30)–(9.32). This will also be tried here by writing

$$\psi(x, y) = Bx^{\beta} \phi(\eta), \quad \eta = Cyx^{\gamma}, \tag{9.44}$$

in which B, C, β, γ are constants to be suitably chosen. With

$$\frac{\partial \eta}{\partial x} = \gamma \frac{\eta}{x}, \quad \frac{\partial \eta}{\partial y} = Cx^{\gamma}, \tag{9.45}$$

one easily deduces

$$\begin{aligned}
&\psi_y = CBx^{\beta+\gamma} \phi', && \psi_x = Bx^{\beta-1} \left(\beta\phi + \gamma\eta\phi' \right), \\
&\psi_{yy} = C^2 Bx^{\beta+2\gamma} \phi'', && \psi_{xy} = CBx^{\beta+\gamma-1} \left((\beta+\gamma)\phi' + \gamma\eta\phi'' \right). \\
&\psi_{yyy} = C^3 Bx^{\beta+3\gamma} \phi''',
\end{aligned} \tag{9.46}$$

Substituting these expressions into (9.43), the individual terms, indicated by the underbraced numerals, have the following dependences

$$\begin{aligned}
&(1): \ x^{2\beta+2\gamma-1}, && (3): \ x^{2m-1}, \\
&(2): \ x^{2\beta+2\gamma-1}, && (4): \ x^{\beta+3\gamma}.
\end{aligned} \tag{9.47}$$

For the x-dependence in (9.43) to drop out of the equation the exponents in (9.47) must all have the same value. This request implies

$$\left. \begin{aligned}
2\beta + 2\gamma - 1 &= 2m - 1, \\
\beta + 3\gamma &= 2m - 1,
\end{aligned} \right\} \quad \longrightarrow \quad \beta = \frac{m+1}{2}, \quad \gamma = \frac{m-1}{2}. \tag{9.48}$$

With this choice and (9.44), Eq. (9.43) takes the form

$$\phi''' + \frac{\beta B}{\nu C} \phi \phi'' + \left(\frac{m A^2}{\nu C^3 B} - \frac{(\beta+\gamma)B}{\nu C} \right) (\phi')^2 = 0. \tag{9.49}$$

This equation is further simplified by special choices for the parameters B and C. It is customary to choose

$$\frac{\beta B}{\nu C} = \frac{(m+1)B}{2\nu C} = 1 \quad \text{and} \quad \frac{m A^2}{\nu C^3 B} = \frac{(\beta+\gamma)B}{\nu C} = \frac{m B}{\nu C}. \tag{9.50}$$

The second of these implies $A^2 = B^2 C^2$; so, with $B = \alpha\sqrt{A}$ and $C = \frac{1}{\alpha}\sqrt{A}$ the first equation yields $\alpha^2 = 2\nu/(m + 1)$ and, consequently,

$$B = \sqrt{\frac{2\nu A}{m + 1}}, \quad C = \sqrt{\frac{(m + 1)A}{2\nu}}. \tag{9.51}$$

With these results (9.49) takes the form

$$\begin{aligned}
&\phi''' + \phi\,\phi'' + \frac{2m}{m + 1}\left(1 - (\phi')^2\right) = 0, \\
&\phi(0) = \phi'(0) = 0, \\
&\lim_{\eta \to \infty} \phi(\eta) = 1,
\end{aligned} \tag{9.52}$$

in which the boundary conditions have been added. They correspond to the conditions

$$\begin{aligned}
u = v = 0, &\quad \phi = \phi' = 0, &\quad \text{for } \eta = 0, \\
u = \tilde{u}_w, &\quad \phi' = 0, &\quad \text{for } \eta \to \infty.
\end{aligned}$$

Once this boundary value problem is solved, the stream function and the x-velocity take the forms

$$\begin{aligned}
\psi(x, y) &\stackrel{(9.44),(9.51)}{=} \sqrt{\frac{2\nu A}{m + 1}}\, x^{(m+1)/2}\phi(\eta) \stackrel{(9.39)}{=} \sqrt{\frac{2}{m + 1}}\sqrt{\nu x \tilde{u}_w}\,\phi(\eta), \\
\eta(x, y) &\stackrel{(9.44)}{=} \sqrt{\frac{(m + 1)A}{2\nu}}\, y x^{(m-1)/2} \stackrel{(9.39)}{=} \sqrt{\frac{m + 1}{2}}\sqrt{\frac{\tilde{u}_w}{\nu x}}\, y, \\
u(x, y) &= \psi_y = \tilde{u}_w \phi'(\eta), \\
v(x, y) &= -\psi_x = -\sqrt{\frac{2}{m + 1}}\sqrt{\frac{\nu}{x}\tilde{u}_w}\,\phi(\eta).
\end{aligned} \tag{9.53}$$

Remarks

- The differential equation $(9.52)_1$ is known as FALKNER-SKAN equation [10] for $\phi(\eta)$, and (9.52) may be called the FALKNER-SKAN boundary value problem. It was numerically solved by them in 1931 and by DOUGLAS HARTREE (1897–1958)[7] [14] in 1937.
- The boundary value problem (9.52) contains the following flows as special cases
  (i) $m = 1$: plane stagnation flow, see (9.12). As we have seen in the last section, this case is an *exact* solution of the full NS-equations, not just the boundary layer equations. The reason is that $\partial^2 u/\partial x^2 \equiv 0$ and $p = \tilde{p}_w$.
  (ii) $m = 0$: Flow over a plane, semi-infinite plate, so-called **Blasius flow**. This case will be dealt with in Sect. 9.5.

---

[7]DOUGLAS HARTREE (1897–1958) was an English mathematician, most famous for the development of numerical analysis and its application to the HARTREE-FOCK equations of atomic physics and the construction of a differential analyzer using MECCANO.

- The boundary value problem (9.34) for axi-symmetric three-dimensional stagnation flow can also be solved by using a FALKNER-SKAN equation. To see this, take $m = 1/3$; the FALKNER-SKAN equation (9.52) then has the form

$$\phi''' + \phi\,\phi'' + \tfrac{1}{2}\left(1 - (\phi')^2\right) = 0. \tag{9.54}$$

With the substitution

$$\tilde{\phi} = \frac{\phi}{\sqrt{2}}, \quad \tilde{\eta} = \frac{\eta}{\sqrt{2}} \quad \longrightarrow \quad \frac{\partial\phi}{\partial\eta} = \frac{\partial\tilde{\phi}}{\partial\tilde{\eta}} \tag{9.55}$$

the boundary value problem (9.54) for ϕ goes over into the boundary value problem (9.34) for $\tilde{\phi}$. So, we solve the FALKNER-SKAN boundary value problem for $\tilde{\phi}$ with $m = 1/3$ and then multiply the solution by $\sqrt{2}$ to obtain ϕ.
- The 'true' wedge solutions correspond to values $m > 0$, however, also negative values $m < 0$ are possible and meaningful. One then has

$$\tilde{u}_w = Ax^m = \frac{A}{x^{|m|}}. \tag{9.56}$$

For such outer flows the velocity at the outer edge of the boundary layer is decreased; the motion is slowed down. One example for negative values of m is the flow past corners, or **corner flows**, in which the motion behind the corner is slowed down (see **Fig. 9.9**).
- The first existence and uniqueness proof for the FALKNER-SKAN boundary value problem has been given by HERMANN WEYL (1885–1955) in 1942 [46]. This analytical problem was re-analysed by W.A. COPPEL in 1960 [9] and again for slightly more general boundary conditions—which, by the way, are difficult to interpret physically—by HUSSAINI and LAKIN in 1986 [18].

The numerical solution of the boundary value problem (9.52) delivers so-called FALKNERX-SKAN profiles [10] or HARTREE profiles [14]. It is customary to plot $\phi'(\eta)$ as a function of η, or η as a function of $\phi'(\eta)$; the stream function ψ can be deduced

Fig. 9.9 Flow of a viscous fluid around a corner
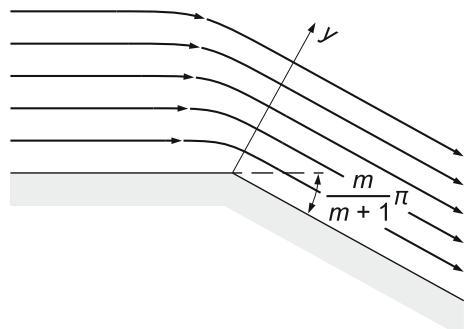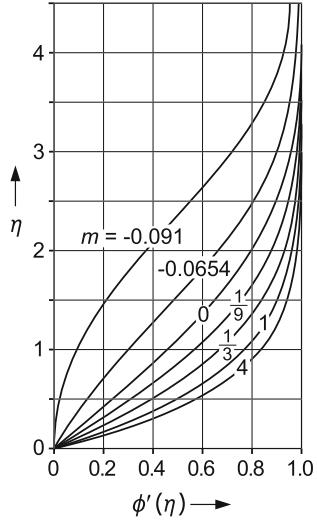
from (9.44). **Figure 9.10** displays the $\phi'(\eta)$ diagrams for the indicated selected values
of m. For $m > 0$ (accelerated motion) the $\phi'(\eta)$-curves show no inflection points.
As evident from $(9.53)_3$ the $\phi'(\eta)$-profiles are parallel to the u-velocity profiles.

Next, let us compute the **displacement thickness** δ^*. To this end the following
representations for η are needed:

$$
\eta \overset{(9.53)}{=} \sqrt{\frac{m+1}{2}}\sqrt{\frac{A}{\nu}}\, y x^{(m-1)/2} = \sqrt{\frac{m+1}{2}}\sqrt{\frac{A\ell^{m+1}}{\nu}}\frac{y}{\ell}\left(\frac{x}{\ell}\right)^{(m-1)/2},
$$

$$
= \sqrt{\frac{m+1}{2}}\sqrt{\mathbb{R}}\,\frac{y}{\ell}\left(\frac{x}{\ell}\right)^{(m-1)/2}, \qquad \mathbb{R} := \frac{A\ell^{m+1}}{\nu}, \tag{9.57}
$$

$$
\frac{\partial \eta}{\partial y} = \sqrt{\frac{m+1}{2}}\sqrt{\mathbb{R}}\,\frac{1}{\ell}\left(\frac{x}{\ell}\right)^{(m-1)/2}.
$$

Alternatively,

$$
\delta^* := \int_0^\infty \left(1 - \frac{u(x,y)}{\tilde{u}_w(x)}\right)\mathrm{d}y \overset{(9.57)}{=} \frac{\displaystyle\int_0^\infty \left(1 - \phi'(\eta)\right)\mathrm{d}\eta}{\sqrt{\dfrac{m+1}{2}}\sqrt{\mathbb{R}}\,\dfrac{1}{\ell}\left(\dfrac{x}{\ell}\right)^{(m-1)/2}}
$$

$$
= \frac{\ell}{\sqrt{\mathbb{R}}}\left(\frac{x}{\ell}\right)^{(1-m)/2}\mathfrak{G}(m), \tag{9.58}
$$

$$
\mathfrak{G}(m) = \sqrt{\frac{2}{m+1}}\int_0^\infty \left(1 - \phi'(\eta)\right)\mathrm{d}\eta.
$$
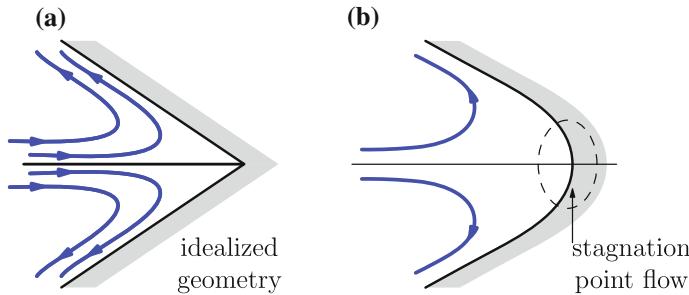
Fig. 9.11 Laminar flow inside a wedge. **a** *Sharp edge in an idealized pure wedge*. **b** *Smooth wedge with local stagnation point flow*

Figure 9.10 indicates that $\phi'(\eta)$ remains bounded. This is also true for $\mathfrak{G}(m)$; consequently, $\lim\limits_{\mathbb{R}\to\infty} \delta^* = 0$ as would be expected.

Remarks: Taking the displacement thickness δ^* as a measure for the boundary layer thickness, formula (9.58) suggests the following inferences:

- The boundary layer is the thinner the larger the REYNOLDS number is or the smaller the viscosity is.
- For $m < 1$, $\delta^*(x = 0) = 0$. The boundary layer starts with thickness zero and grows in the direction of the flow.
- For $m = 1$ the displacement thickness is independent of x. This is the case for plane stagnation flow.
- For $m > 1$ the displacement thickness decreases with growing x. This behaviour is observed with strongly accelerated flows. Note that (9.58) implies here that $\delta^*(x = 0) \to \infty$. In spite of this, such solutions demonstrate practical significance as boundary layers of flows into a corner.
  The idealized situation in this case is as shown in **Fig. 9.11**a. However, in reality the tip of the wedge is generally not sharp, but smoothed out as shown in panel (b). In the vicinity of such round edges the flow will therefore develop typically as a stagnation point flow.

The above results also allow qualitative inferences on general boundary layer flows. These inferences are better understood, if one recalls the parameterization of the viscous stress tensor of a NAVIER-STOKES fluid: $\tau_{xy} \propto \partial u/\partial y$, in two-dimensions. If within the boundary layer the flow varies along the y-axis, then $\partial \tau_{xy}/\partial y$ will be the dominant term in the x-momentum equation which grossly determines whether the flow is accelerated or decelerated in the x-direction. The HARTREE profiles, which are proportional to the wall-parallel velocity profiles, show that for $\phi'' > 0$ the flow is—according to this argument—accelerated when $m > 0$ and the boundary layer thickness is small. Alternatively, for $0 > m > -0.091$ the profiles exhibit a change in inclination; close to the wall $\phi'' < 0$ and the boundary

layer flow is decelerated. One can also see from these HARTREE profiles (with $m < 0$) that the boundary layer thickness grows rapidly.

This behavior can be typified under slightly more general situations as follows:

(i) Under accelerated motion the boundary layer thickness grows only weakly or it will even decrease. No point of inflection change in the velocity profile arises.

(ii) Under decelerated motion a rapid growth of the boundary layer thickness arises; with a possible returning separation flow develops, see **Fig. 9.12**a.

(iii) In a flow around a slender body (Fig. 9.12b) the part behind the frontal stagnation point is subjected to an accelerated flow and a pressure decrease, which merges into a decelerated flow regime in the downstream part. In that regime the flow can separate from the wall. In this situation the prerequisites of boundary layer behavior are summarized in **Fig. 9.13**.

Computation of the wall shear stress.
With the wall shear traction defined as

$$\tau_w = \nu \rho \frac{\partial u}{\partial y}\Big|_{y=0}, \tag{9.59}$$

one obtains in view of (9.53) and (9.57)

$$\tau_w = \nu \rho \tilde{u}_w \frac{\partial^2 \phi}{\partial \eta^2} \frac{\partial \eta}{\partial y}\Big|_0 = \nu \rho \tilde{u}_w \sqrt{\frac{m+1}{2}}\, \phi''(0)\sqrt{\mathbb{R}}\, \frac{1}{\ell}\left(\frac{x}{\ell}\right)^{(m-1)/2}. \tag{9.60}$$

If we introduce the short hand notation

$$T(m) := 2\sqrt{\frac{m+1}{2}}\phi''(0), \tag{9.61}$$

the drag coefficient can be computed as

$$c_f = \frac{\tau_w}{\frac{1}{2}\rho\tilde{u}_w^2} = \frac{T(m)}{\sqrt{\mathbb{R}}}\frac{1}{\left(\frac{x}{\ell}\right)^{(m+1)/2}}, \tag{9.62}$$

in which (9.39), $\tilde{u}_w = U(x/\ell)^m$, has also been used. It is evident that for $\mathbb{R} \to \infty$, $c_f \to 0$. Two special cases are:

• $m = 0$, which corresponds to the plate or BLASIUS **boundary layer**. In this case $T(0) = 0.664$ and

$$c_f = \frac{0.664}{\sqrt{\mathbb{R}_x}}, \quad \mathbb{R}_x := \frac{Ux}{\nu}. \tag{9.63}$$
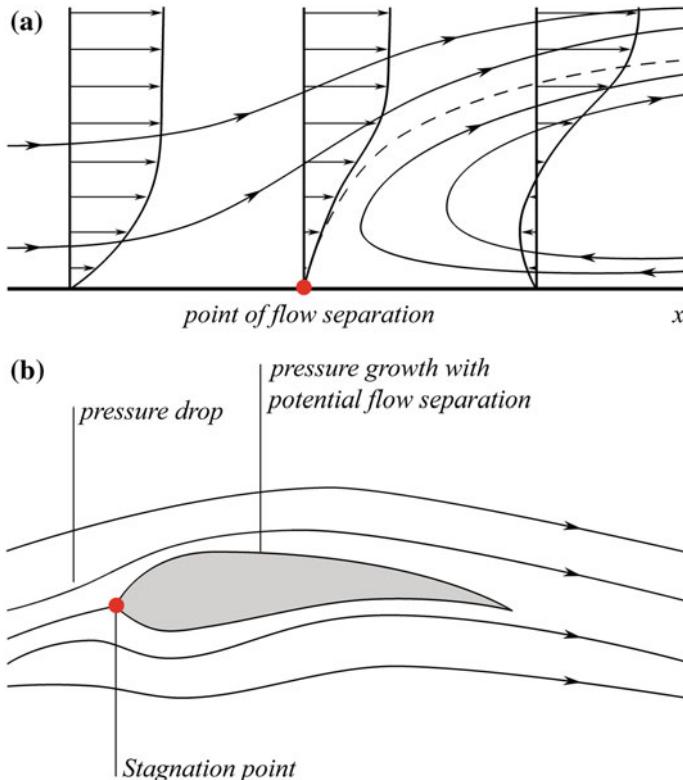
Fig. 9.12   Boundary layer flow along a flat wall and a slender body. **a** *Flow from a steady accelerated regime to a decelerated regime, where the inflection point of the velocity profile arises, the wall shear stress vanishes and flow separation is initiated (middle profile). When further deceleration occurs, return flow will arise (right profile).* **b** *Flow over a slender body with a regime of pressure loss just behind the stagnation point and a regime of pressure growth with a likelihood of flow separation*
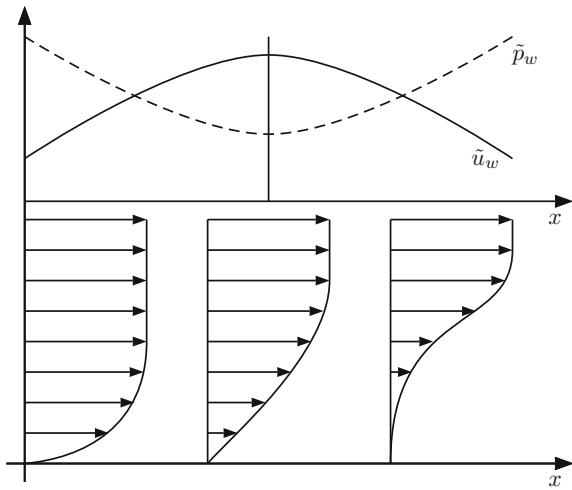
In other words, the drag coefficient at $x = 0$ has a square root singularity. This is integrable, i.e. the total force exerted on the plate is finite.

- For $m = -0.091$, $T(-0.091) \approx 0$, one obtains a drag resistance which is practically zero. This is the location, where the flow separates from the plate.

9.4.3   *Rotating Disk of Infinite Extent*

Consider a permanently rotating disk of infinite extent with constant angular velocity ω, rotating about a vertical axis. Let the two half spaces above and below the disk be filled with the same incompressible NEWTONian fluid. Let, moreover, r,
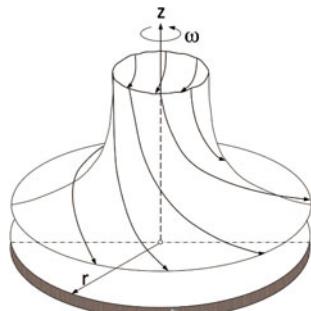
Fig. 9.13 Typical boundary
layer behavior along a flat or
slightly curved surface with
pressure $\tilde{p}_w$, and velocity,
$\tilde{u}_w$-profiles of the outer flow
inducing the velocity
boundary layer profiles
before separation

θ, z be cylindrical coordinates and u, v, w the corresponding velocity components
of a NEWTONian fluid that is driven by the disk. The flow induced by the disk is
reminiscent of a rotating stagnation point flow, see **Fig. 9.14**, in which the azimuthal
velocity, v, is non-zero, and all velocity components are independent of the azimuth
angle θ. With $\partial(\cdot)/\partial\theta = 0$ the steady state NS-equations then reduce to (**Fig. 9.15**)

$$
\begin{aligned}
&\frac{\partial u}{\partial r} + \frac{u}{r} + \frac{\partial w}{\partial z} = 0, \\
&u\frac{\partial u}{\partial r} - \frac{v^2}{r} + w\frac{\partial u}{\partial z} = -\frac{1}{\rho}\frac{\partial p}{\partial r} + \nu\left\{\frac{\partial^2 u}{\partial r^2} + \frac{1}{r}\frac{\partial u}{\partial r} - \frac{u}{r^2} + \frac{\partial^2 u}{\partial z^2}\right\}, \\
&u\frac{\partial v}{\partial r} + \frac{uv}{r} + w\frac{\partial v}{\partial z} = \nu\left\{\frac{\partial^2 v}{\partial r^2} + \frac{1}{r}\frac{\partial v}{\partial r} - \frac{v}{r^2} + \frac{\partial^2 v}{\partial z^2}\right\}, \\
&u\frac{\partial w}{\partial r} + w\frac{\partial w}{\partial z} = -\frac{1}{\rho}\frac{\partial p}{\partial z} + \nu\left\{\frac{\partial^2 w}{\partial r^2} + \frac{1}{r}\frac{\partial w}{\partial r} + \frac{\partial^2 w}{\partial z^2}\right\}.
\end{aligned}
\tag{9.64}
$$

Fig. 9.14 Sketch of a
viscous flow induced by a
rotating disk of finite extent

Finding an analytical or semi-analytical solution to the above equations seems to be very difficult; however, THEODORE VON KÁRMÁN (1881–1963)[8] [43] realized that these equations allow a solution, for which u/r, v/r and w only depend on z. For such a solution, Eq. (9.64)$_4$ implies

$$\frac{\partial}{\partial z}\left(\frac{w^2}{2}\right) = -\frac{1}{\rho}\frac{\partial p}{\partial z} + \nu\frac{\partial}{\partial z}\left(\frac{\partial w}{\partial z}\right),\tag{9.65}$$

or after an integration with respect to z

$$\frac{p}{\rho} = \nu\frac{\partial w}{\partial z} - \frac{w^2}{2} + F(r).\tag{9.66}$$

Very far from the disk, for $z \to \infty$, the velocity is parallel to the rotation axis, implying that the pressure there does not radially vary: So, we may set $F(r) = $ const. $= 0$ (in (9.66)). It follows, p/ρ is equally only a function of z. With the above VON KÁRMÁN assertion and this result, it is possible to prove that the remaining NS-equations (9.64)$_{1,2,3}$ reduce to

$$\frac{2u}{r} + \frac{dw}{dz} = 0,$$
$$\left(\frac{u}{r}\right)^2 + w\frac{d(u/r)}{dz} - \left(\frac{v}{r}\right)^2 = \nu\frac{d^2(u/r)}{dz^2},\tag{9.67}$$
$$\frac{2uv}{r^2} + w\frac{d(v/r)}{dz} = \nu\frac{d^2(v/r)}{dz^2},$$

or after elimination of u/r with the aid of the first equation

$$\frac{1}{4}\left(\frac{dw}{dz}\right)^2 - \frac{1}{2}w\frac{d^2w}{dz^2} - \left(\frac{v}{r}\right)^2 + \frac{1}{2}\nu\frac{d^2}{dz^2}\left(\frac{dw}{dz}\right) = 0,$$

$$\frac{v}{r}\frac{dw}{dz} - w\frac{d}{dz}\left(\frac{v}{r}\right) + \nu\frac{d^2}{dz^2}\left(\frac{v}{r}\right) = 0.\tag{9.68}$$

In these equations ∂ has been replaced by d, since u/r, v/r and w are only functions of z. Equations (9.67), (9.68) are subject to the boundary conditions

$$\begin{aligned} u = w = 0, \quad & v = \omega r, \quad \text{at } z = 0,\\ u = v = 0, \quad & \qquad\quad\ \text{for } z \to \infty.\end{aligned}\tag{9.69}$$

Based on dimensional arguments we seek a solution of the form

---

[8]For a biographical sketch of THEODORE VON KÁRMÁN (1881–1963), see Fig. 9.15.

$$\frac{v}{r} := \omega g(\zeta), \quad w := \sqrt{\omega \nu}\, h(\zeta), \quad \zeta := \sqrt{\omega/\nu}\, z \quad \longrightarrow \quad \frac{u}{r} := -\frac{1}{2}\omega h' \quad (9.70)$$

and obtain after substitution into (9.68) and (9.69) the following boundary value problem

$$\left.\begin{array}{l} \frac{1}{2}(h')^2 - hh'' - 2g^2 = -h''', \\ -gh' + g'h = g'', \end{array}\right\} \quad \text{in } 0 < \zeta < \infty,$$
$$\begin{array}{llll} h = h' = 0, & g = 1, & \text{at } \zeta = 0, \\ h' \to 0, & g \to 0 & \text{as } \zeta \to \infty. \end{array} \tag{9.71}$$
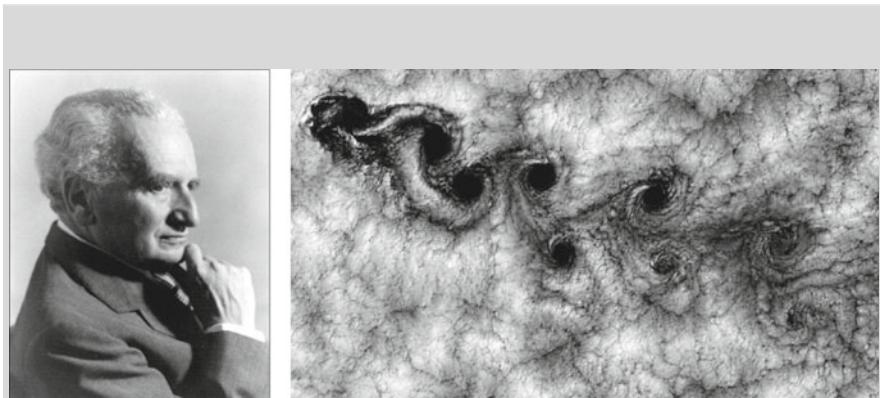
Fig. 9.15 THEODORE VON KÁRMÁN (11. May 1881–7. May 1963) (Right photo) This Landsat 7 image of clouds off the Chilean coast near the Juan Fernandez Islands (also known as the Robinson Crusoe Islands) on September 15, 1999, shows a 'von Kármán vortex street'. *Source* Landsat

THEODORE VON KÁRMÁN was a Hungarian-American applied mathematician, aerospace engineer and physicist, who was primarily active in the fields of aeronautics and astronautics, with key advances in aerodynamics, notably his work on supersonic and hypersonic air foil characterization. He is regarded as the outstanding aerodynamic theoretician of the 20th century.

THEODORE VON KÁRMÁN, born in Budapest, studied engineering at the city's Royal Joseph Technical University (now Budapest University of Technology and Economics). After graduation in 1902 he entered Göttingen University in Germany for his doctoral study with LUDWIG PRANDTL, which he completed in 1908. He subsequently taught in Göttingen for 4 years. During this period he published his famous paper on the THEODORE VON KÁRMÁN-vortex street and, together with MAX BORN, he wrote a paper on the specific heat of crystal lattices. In this same period fell also his work on the strength of ideal elasto-plastic materials in the encyclopedia of Mathematical Sciences (in parts with AUGUST FÖPPL and his invention of the triaxial apparatus. In 1912 he accepted the directorship of the Aeronautical Institute of RWTH Aachen. Here he became in 1913 professor of Mechanics and Flight-Aerodynamics.

During the years 1915–1918 he served in the Austro-Hungarian Army, where he designed helicopters. In 1922 VON KÁRMÁN was among the founders of IUTAM (International Union of Theoretical and Applied Mechanics) and co-organized in September 1922 its first conference in Innsbruck. He left RWTH Aachen in 1930 and accepted the directorship of the *Guggenheim Aeronautical Laboratory* at the *California Institute of Technology* (GALCIT). Here, he became an important leader of research of supersonic motion. He founded the *Aerojet* company to manufacture rocket motors, which became important during World War II to aid heavy loaded bombers during lift-off. In 1944 he and others affiliated with GALCIT founded the *Jet Propulsion Laboratory* (JPL) (now a federally funded research and development center).

THEODORE VON KÁRMÁN left CALTECH in 1944 for Washington DC to act as a long-range planning consultant to the military. At the age 81 VON KÁRMÁN was the recipient of the first National Medal of Science, bestowed in a White House ceremony by President John F. Kennedy. While on a trip to Aachen in 1963 VON KÁRMÁN died. He was buried in Pasadena, USA.

The text is based on http://www.wikipedia.org

This problem of steady momentum-integral solution was first posed by THEODORE VON KÁRMÁN in 1921 [43], but it contained errors, which were pointed out by W.G. COCHRAN (1934) in a paper suggested to him by SIDNEY GOLDSTEIN [7]. He solved the system (9.71) as a singular perturbation problem by matching series expansions centered at $\zeta = 0$ and $\zeta \to \infty$. E.R. BENTON (1966) [3], following an idea by COCHRAN, changed the independent variable ζ in (9.71) by the transformation

$$\lambda = \exp(-c\zeta), \quad \text{where} \quad c > 0 \tag{9.72}$$

and, thus, achieved thereby that the semi-infinite interval $\zeta \in [0, \infty)$ of integration becomes bounded as $\lambda \in [1, 0]$, making the new system for g and h better apt for numerical integration.

Plots for the functions $g(\zeta)$, $h'(\zeta)$ and $h(\zeta)$ are displayed in **Fig. 9.16**. Evidently, as seen in the graphs for g and h, defined by the variable ζ, the boundary layer thickness is given by

$$\delta \sim \sqrt{\nu/\omega}. \tag{9.73}$$
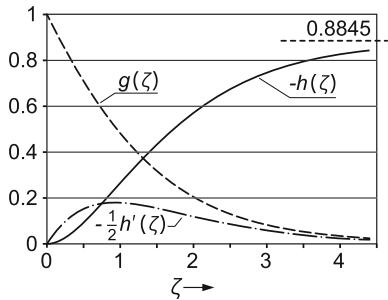
Outside this layer the functions g and h' drop quickly to zero, and h approaches a constant value

$$\lim_{\zeta \to \infty} w = -0.8845\sqrt{\omega\nu}. \tag{9.74}$$

Of importance are the values of the azimuthal shear stresses

$$\tau_{z\theta} = \eta \frac{\partial v}{\partial z}\Big|_{z=0} = \eta r\omega\sqrt{\frac{\omega}{\nu}}g'(0) = \rho\sqrt{\nu}\omega^{3/2}rg'(0). \tag{9.75}$$

Fig. 9.16 Distribution of g, h and $-h'/2$ plotted against ζ for the rotating disk problem based on a table by E.R. BENTON [3]

With these stresses the torque exerted by the fluid on a disk of radius a can be computed. This yields

$$M = 2 \int_0^a \tau_{z\theta} r \, 2\pi r \mathrm{d}r = 4\pi\rho\sqrt{\nu}\omega^{3/2} g'(0)\frac{a^4}{4}, \qquad (9.76)$$

provided the disk is wetted by the fluid from both sides (explaining the factor 2). With $g'(0) = -0.616$ from the numerical solution, this yields

$$M = -0.616\pi\rho\sqrt{\nu}\omega^{3/2}a^4. \qquad (9.77)$$

This problem of steady viscous flow due to a rotating disk has been generalized in several directions. E.R. BENTON (1966) [3] was looking at the impulsively started rotating disk from rest, reaching the asymptotic steady state at permanent rotation as $t \to \infty$. Following precursory articles by H.K. THIROT (1940) [41] and S.D. NIGAM (1951) [28], he expanded the velocity components u, v into powers of the angle of rotation of the disk

$$\varphi = \omega t$$
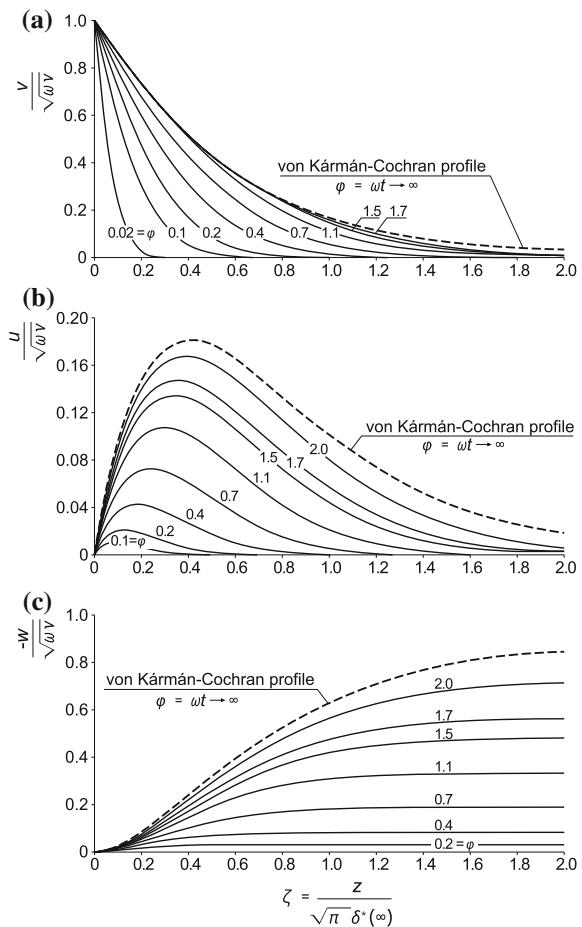
and expressed u and v as functions of ζ and t. **Figure 9.17** shows the growth in time of the three velocity profiles toward steady VON KÁRMÁN-COCHRAN profiles. In these figures, the abscissa variable is

$$\zeta = \frac{z}{\sqrt{\pi}\delta^*(\infty)}, \quad \text{where} \quad \delta^*(\infty) = 1.27\sqrt{\frac{\nu}{\omega}}. \qquad (9.78)$$

$\delta^*(\infty)$ is proportional to the steady state boundary layer thickness (9.73). The panels of Fig. 9.17 show a continuous but attenuated approach toward the VON KÁRMÁN steady profiles. For more details on the elegant integration technique, see [3].

Another extension of the flow of a viscous fluid due to a *rough* rotating disk has been presented by M. MICLAVCIC and C.Y. WANG (2004) [25]. They look at the steady rotation of the disk, but allow a *frictional sliding law* between fluid and

Fig. 9.17 Temporal growth, expressed by $\phi = \omega t$, towards the VON KÁRMÁN-COCHRAN steady state velocity profiles. **a** *Circumferential flow*, **b** *radial flow*, **c** *axial flow*. *From* [3] *with changes* © *J. Fluid Mech, Cambridge University Press, reproduced with changes*

disk and also consider *suction* of fluid through the disk. The differential equations $(9.71)_{1,2}$, and the boundary condition at $\zeta \to \infty$, $(9.71)_4$, remain the same, but the boundary conditions at $\zeta = 0$ change now. M. MICLAVCIC and C.Y. WANG employ a viscous sliding law, generally anisotropic, and relate the basal tangential velocity to the shear traction in the form

$$u|_{z=0} = N_1 \rho \nu \frac{\partial u}{\partial z}|_{z=0}, \quad v|_{z=0} - \omega r = N_2 \rho \nu \frac{\partial v}{\partial z}|_{z=0}, \tag{9.79}$$

in which N_1 and N_2 are sliding coefficients in the radial and azimuthal directions, respectively. For isotropic sliding we have $N_1 = N_2$. Let

$$\lambda_r = N_1 \rho \sqrt{\nu\omega}, \quad \lambda_\theta = N_2 \rho \sqrt{\nu\omega}. \tag{9.80}$$

Then, eliminating N_1, N_2 between (9.79) and (9.80) and using the definitions (9.70), one obtains

$$h'(0) = \lambda_r h''(0), \quad g(0) - 1 = \lambda_\theta g'(0). \tag{9.81}$$

If there is a uniform suction velocity W on the disk, then (9.70)$_2$ and $s = W/\sqrt{\nu\omega}$ imply the further condition

$$h(0) = s \quad \text{(suction condition)}. \tag{9.82}$$

So, (9.71) is now replaced by

$$\left.\begin{array}{l} (h')^2 - hh'' - 2g^2 + h''' = 0, \\ -gh' + g'h - g'' = 0 \end{array}\right\} \text{ in } 0 < \zeta < \infty,$$

$$\left.\begin{array}{l} h(0) = s, \\ h'(0) = \lambda_r h''(0), \\ g(0) - 1 = \lambda_\theta g'(0) \end{array}\right\} \text{ at } \zeta = 0,$$

for which the boundary conditions at $\zeta \to \infty$

$$h'(\infty) = 0, \quad g(\infty) = 0 \tag{9.84}$$

must also be satisfied. The boundary value problem (9.83) can be interpreted as an initial value problem with initial values selected as
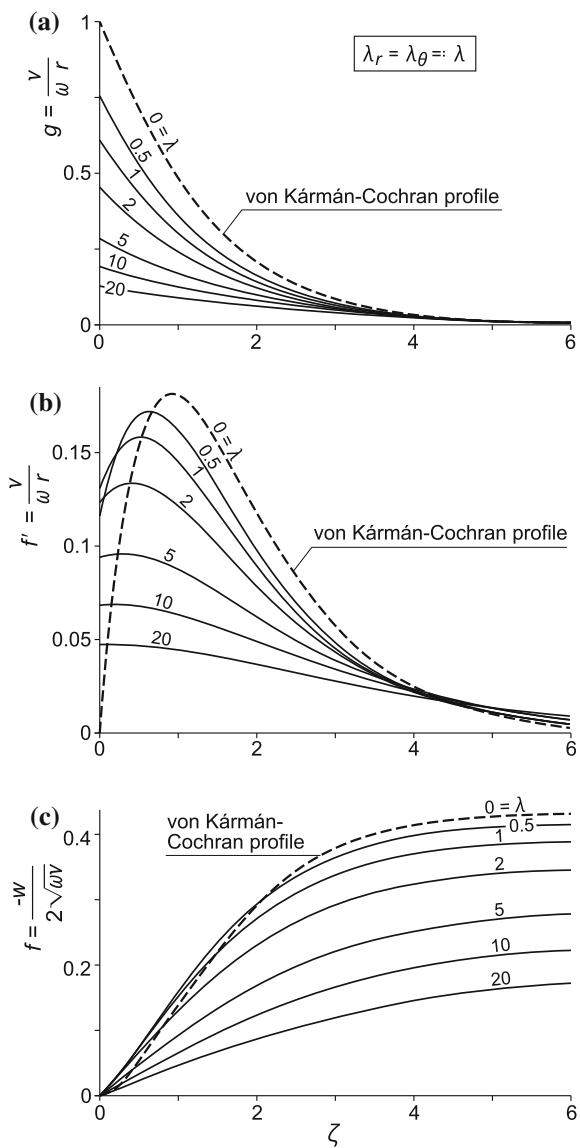
$$h(0) = s, \quad h'(0) = \lambda_r \alpha, \quad h''(0) = \alpha, \quad g(0) = 1 + \lambda_\theta \beta, \quad g'(0) = \beta \quad (9.85)$$

with unknowns α and β, which must be so determined that the conditions (9.84) are satisfied. The shooting method or minimization of a minimizing functional can be used to determine α and β, see [25].

Figure 9.18 shows for isotropic sliding, $\lambda_r = \lambda_\theta$, the azimuthal velocity profile (panel (a)), the radial velocity profile (panel (b)) and the vertical velocity profile (panel (c)).The value of the azimuthal velocity generally decreases as the slip resistance is increased, and its decay is exponential for large ζ. 'The induced radial velocity profile is caused by the centrifugal forces. For the no-slip condition between fluid and disk (THEODORE VON KÁRMÁN's original problem), the radial velocity starts from zero and reaches a maximum at $\zeta = 0.92$, beyond which it decays to zero. With slip the maximum velocity decreases and its location moves towards the disk. Notice the prominent crossover of the curves near $\zeta = 4$, showing that, although slip decreases the velocity near the disk, it increases the velocity far from the disk [...]' [25].

M. Miclavčič and C.Y. WANG present also an existence proof for the general anisotropic case. This proof is similar to that shown by J.B. MCLEOD and J. SERRIN [23, 24]. P.J. ZANDBERGEN and D. DIJKSTRA [48] give a general review of the subject (**Fig. 9.19**).

Fig. 9.18 Steady velocity profiles due to a rough rotating disk for isotropic basal friction ($\lambda_r = \lambda_\theta =: \lambda$) and vanishing suction. **a** *Azimuthal (circumferential) velocity profile* **b** *radial velocity profile*, **c** *axial (vertical) velocity profile. From* [25] *with changes.* © *Birkhäuser Verlag, reproduced with changes*
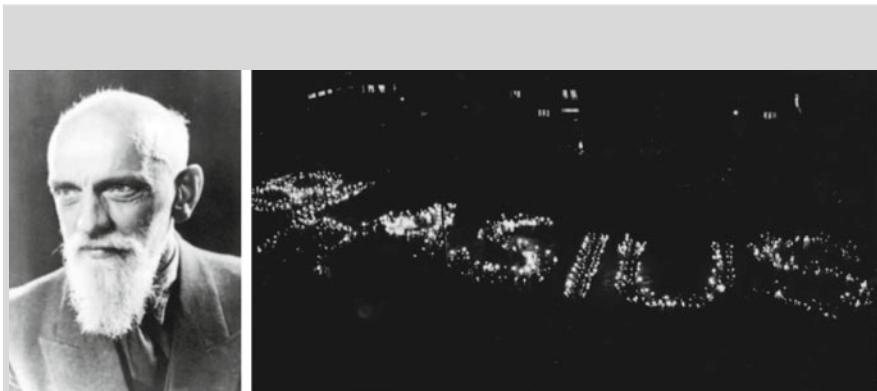
Fig. 9.19 PAUL RICHARD HEINRICH BLASIUS (9. Aug. 1883–24. April 1970)

PAUL RICHARD HEINRICH BLASIUS, born in Berlin, studied at the Universities of Marburg and Göttingen, 1902–1906. He was subsequently one of the first doctoral students of LUDWIG PRANDTL and, starting in 1908, an assistant in the Hydraulic Laboratory at the 'Technische Hochschule' (Technical University) in Berlin. From 1912 to 1962 BLASIUS was a regular teacher at the Hamburg Technical College (University of the Applied Sciences) for 50 years, and he continued teaching there beyond his retirement until his death in 1970.

HEINRICH BLASIUS loved teaching, but despite this devotion, he had performed research work as a theoretical fluid dynamicist in his younger years from 1907 to approximately 1913 and wrote educational technical books on elementary mechanics [4] and heat [6]. His scientific memoirs comprise his dissertation [4], complex analysis of two-dimensional potential flows [5], where the formula expressing the net force on a fixed submerged body in a two-dimensional steady potential flow is now known as the BLASIUS theorem. He is further known for designing potential flows around symmetric and non-symmetric airfoils using conformal mapping. W.H. HAGER gives the complete list of his entire work.

In April 1970, BLASIUS had taught 50 years long when he was 78 years old. On this occasion the students of the Engineering College organized a torch-light procession through Hamburg, with the torches forming the name BLASIUS.

The text is based on http://www.wikipedia.org and HAGER, W.H.: Blasius: A life in research and education. *Experiments in Fluids*, **34**, 566–571 (2003) [12]

9.5   The BLASIUS Boundary Layer

The flow of a viscous fluid past a plate of semi-infinite length is contained among the boundary layer flow solutions past a wedge of vanishing opening angle ($m = 0$), see **Fig. 9.20**. With $m = 0$, the essential formulae of the last subsection can be summarized as follows [see (9.39), (9.53), (9.58), (9.60)][9]:

---

[9]For a short biography of PAUL RICHARD HEINRICH BLASIUS see Fig. 9.19.

Blasius boundary layer at semi-inf. plate
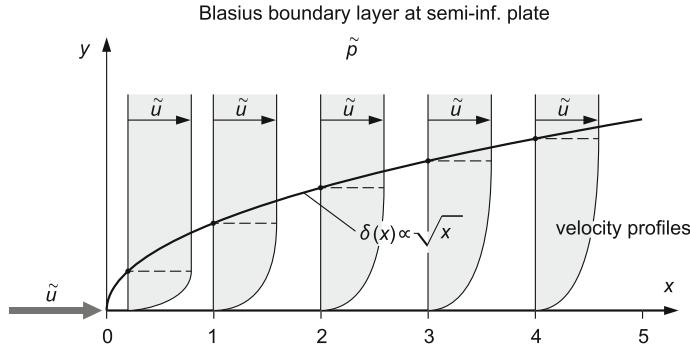
Fig. 9.20 Flow of a viscous fluid past a semi-infinite plate

$$\tilde{u}_w = U = \text{const.}, \quad \eta = \sqrt{\frac{U}{2\nu}} \frac{y}{\sqrt{x}},$$
$$\delta^* \sim \sqrt{x}, \qquad \tau_w \sim \frac{1}{\sqrt{x}}. \tag{9.86}$$

These express that the outer flow velocity is a constant everywhere, the boundary layer thickness varies as $\sqrt{x}$, thus has a square root growth with x, whilst the shear traction τ_w has a square root singularity $\sim 1/\sqrt{x}$ at the leading edge of the plate. The solution of the BLASIUS boundary value problem is given by the FALKNER-SKAN equation for $m = 0$, see (9.52). Its numerical solution need not be discussed here; it is given for the general FALKNER-SKAN equation.

We shall be concerned in this section rather with the analytical demonstration that the BLASIUS boundary value problem indeed possesses solutions which are unique. This means that the BLASIUS boundary value problem

$$\phi''' + \phi\,\phi'' = 0, \quad 0 < \eta < \infty,$$
$$\phi = \phi' = 0, \qquad \eta = 0, \qquad (\cdot)' = \frac{\mathrm{d}}{\mathrm{d}\eta}, \tag{9.87}$$
$$\phi' = 1, \qquad \eta \to \infty$$

is well posed.

Note that the BLASIUS differential equation $(9.87)_1$ can, alternatively, be written as $(\ln \phi'')' + \phi = 0$ and, thus, can be integrated once to yield

$$\phi'' = \phi''(0) \exp\left(-\int_0^\eta \phi(\bar{\eta})\mathrm{d}\bar{\eta}\right). \tag{9.88}$$

This equation is useful, because it allows to prove *uniqueness* and *existence* of the BLASIUS profiles. The proof is based on two auxiliary lemmas.

Lemma 9.1 $\phi''(0) > 0$, *i.e. the slope of the velocity profile at the wall is positive.*

Proof We integrate (9.88) and obtain

$$\phi'(\eta) - \underbrace{\phi'(0)}_{=0,\ \text{bound. cond.}} = \phi''(0) \int\limits_0^\eta \exp\left(-\int\limits_0^{\overline{\eta}} \phi(\tilde{\eta})\mathrm{d}\tilde{\eta}\right)\mathrm{d}\overline{\eta}.$$

This result implies

$$\lim_{\eta\to\infty} \phi'(\eta) = \phi''(0) \underbrace{\int\limits_0^\infty \exp\left(-\int\limits_0^{\overline{\eta}} \phi(\tilde{\eta})\mathrm{d}\tilde{\eta}\right)\mathrm{d}\overline{\eta}}_{>0\ \text{and bounded}} = 1. \qquad (9.89)$$

Since $\exp(a) > 0$ for any real a, the integrand function is positive as is the indefinite integral of it. The underbraced integral is bounded, because it is the exponential integral with negative exponent. With this recognition, (9.89) also allows the inference that $\phi''(0) > 0$. This proves Lemma 9.1. ∎

Lemma 9.2 *Let* $\phi_1(\eta)$ *be a solution of the* BLASIUS *boundary value problem. Then, also* $\phi_2(\eta) = \alpha\phi_1(\alpha\eta)$ *is solution of the* BLASIUS *boundary value problem.*

Proof This is obtained by straight-forward evaluation as follows:

$$\begin{aligned}
\phi_2(\eta) &= \alpha\phi_1(\alpha\eta), & \phi_2'(\eta) &= \alpha^2\phi_1'(\alpha\eta), \\
\phi_2''(\eta) &= \alpha^3\phi_1''(\alpha\eta), & \phi_2'''(\eta) &= \alpha^4\phi_1'''(\alpha\eta),
\end{aligned}$$

in which on the right-hand sides $\phi_1'(\alpha\eta) = \mathrm{d}\phi_1/\mathrm{d}\eta$. Thus,

$$\phi_2''' + \phi_2\phi_2'' = \alpha^4 \underbrace{\left(\phi_1''' + \phi_1\phi_1''\right)}_{=0} = 0. \qquad (9.90)$$

It is also easily seen that the boundary conditions for $\phi_2(\eta)$ are preserved. This proves Lemma 9.2. ∎

Based on these Lemmas, it can now be proved that *for the* BLASIUS *boundary value problem, if it indeed has a solution, this solution is unique.*

Proof Assume the contrary, i.e. that at least two different solutions $\phi_1(\eta)$ and $\phi_2(\eta)$ exist with

$$\phi_1''(0) = C, \quad \phi_2''(0) = K, \quad \text{where } C \neq K.$$

According to Lemma 9.2, $w(\eta) := \alpha\phi_2(\alpha\eta)$ is also a solution, if $\phi_2(\eta)$ is one, which satisfies the boundary conditions

$$w(0) = w'(0) = 0, \quad w''(0) = \alpha^3 \phi_2''(0) = \alpha^3 K.$$

Let $\alpha > 0$ be such that $\alpha^3 K = C$; since $K \neq C$, this implies $\alpha \neq 1$. Then, $w(\eta) = \phi_1(\eta)$ and, in particular,

$$\lim_{\eta \to \infty} w'(\eta) = \lim_{\eta \to \infty} \phi_1'(\eta) = 1, \quad \text{or} \quad \lim_{\eta \to \infty} \alpha^2 \phi_2'(\alpha \eta) = 1.$$

Now, since already $\lim_{\eta \to \infty} \phi_2'(\eta) = 1$, the boundary condition at $\eta \to \infty$ requires $\alpha = 1$; in other words, $w(\eta) = \phi_2(\eta) = \phi_1$, contrary to the assumption that $\phi_1 \neq \phi_2$. Thus, a second solution does not exist. ∎

To prove *existence* of the BLASIUS solution we shall proceed with the following three steps

(i) We first construct an iterative solution to the *initial* value problem with $\phi(0) = \phi'(0) = 0$ and $\phi''(0) = 1$.

(ii) Then, we show that for this solution one has $0 < \lim_{\eta \to \infty} \phi'(\eta) < \infty$, i.e. $\phi'(\infty)$ is positive, and

(iii) by choice of a positive $\alpha > 0$, one can achieve that $\alpha \phi(\alpha \eta)$ satisfies the boundary condition at $\eta \to \infty$.

Our starting point is (9.88), subject to the initial condition $\phi''(0) = 1$,

$$\phi''(\eta) = \exp \left\{ - \int_0^\eta \phi(\zeta) d\zeta \right\}. \tag{9.91}$$

Using integration by parts twice, it can be shown that with the above stated initial conditions the following identity holds:

$$\int_0^\eta \phi(\zeta) d\zeta = \int_0^\eta \phi''(\zeta) \frac{(\eta - \zeta)^2}{2} d\zeta. \tag{9.92}$$

Using, moreover, the shorthand notation

$$v(\eta) := \phi''(\eta), \tag{9.93}$$

combination of (9.91) and (9.92) yields the identity

$$v(\eta) = \exp \left\{ - \int_0^\eta v(\zeta) \frac{(\eta - \zeta)^2}{2} d\zeta \right\}. \tag{9.94}$$

This equation is now used to construct an iterative sequence to determine $v(\eta)$ and subsequently by integration $\phi(\eta)$.

The obvious iteration prescription is suggested by (9.94),

$$v_{n+1}(\eta) = \exp\left\{ -\int_0^\eta v_n(\zeta) \frac{(\eta - \zeta)^2}{2} d\zeta \right\}, \tag{9.95}$$

and the iterations, which follow from this, are given by

$$v_1 = 1,$$
$$v_2 = \exp\left(-\frac{\eta^3}{6}\right), \tag{9.96}$$
$$v_3 = \exp\left\{ -\int_0^\eta \exp\left(-\frac{\zeta^3}{6}\right) \frac{(\eta - \zeta)^2}{2} d\zeta \right\},$$
$$\vdots$$

Convergence of this sequence is proved, if one can show that for any η and any $\varepsilon > 0$

$$|v_{n+k} - v_n| < \varepsilon, \quad \text{provided that } n > N(\varepsilon).$$

Now, note that

$$|v_{n+1} - v_n| = \left| \exp\left\{ -\int_0^\eta v_n(\zeta) \frac{(\eta - \zeta)^2}{2} d\zeta \right\} \right.$$
$$\left. - \exp\left\{ -\int_0^\eta v_{n-1}(\zeta) \frac{(\eta - \zeta)^2}{2} d\zeta \right\} \right|, \tag{9.97}$$

and we conjecture that

$$|v_{n+1} - v_n| \leqslant \frac{\eta^{3n}}{(3n)!}. \tag{9.98}$$

This inequality is easily proved for $n = 1$ and v_1, v_2 given by (9.96)$_{1,2}$

$$|v_2 - v_1| = \left| \exp\left(-\frac{\eta^3}{6}\right) - 1 \right| \leqslant \frac{\eta^3}{6}, \quad \text{(which is correct).} \tag{9.99}$$

To prove convergence of the iteration procedure we must prove that (9.98) is correct for general n. To this end, we assume that (9.98) is correct for all indices smaller than n. We employ the estimate

$$\int_a^b \exp(-x)\mathrm{d}x = \exp(-a) - \exp(-b)$$

$$= (b - a)\exp(-c) \leqslant |b - a|, \qquad (9.100)$$

$$a \leqslant c \leqslant b, \quad \exp(-c) < 1 \text{ for } c > 0,$$

which follows from the mean value theorem of integral calculus or simply by inspection of the function $\exp(-x)$.

Applying inequality (9.100) on the right-hand side of (9.97) yields

$$|v_{n+1} - v_n| \leqslant \left| \int_0^\eta \frac{(\eta - \zeta)^2}{2}(v_n - v_{n-1})\mathrm{d}\zeta \right| \leqslant \int_0^\eta \frac{(\eta - \zeta)^2}{2}|v_n - v_{n-1}|\mathrm{d}\zeta$$

$$\overset{(9.98)}{\leqslant} \frac{1}{[3(n-1)]!} \underbrace{\int_0^\eta \frac{(\eta - \zeta)^2}{2}\zeta^{3(n-1)}\mathrm{d}\zeta}_{\frac{\eta^{3n}}{(3n-2)(3n-1)3n} \text{ (by evaluation)}}$$

$$= \frac{\eta^{3n}}{(3n)!} \underbrace{\frac{1}{(3n - 2)(3n - 1)}}_{<1 \text{ for } n \geqslant 1}$$

$$\leqslant \frac{\eta^{3n}}{(3n)!},$$

proving (9.98) for general n, in view of the induction initialization (9.99). Next, let us write

$$|v_{n+k} - v_n| \leqslant |v_{n+k} - v_{n+k-1}| + \cdots + |v_{n+1} - v_n|$$

$$\leqslant \frac{\eta^{(3n+k-1)}}{(3(n+k-1))!} + \cdots + \frac{\eta^{3n}}{(3n)!} < \varepsilon.$$

This inequality holds for sufficiently large n, since each term goes to zero individually as $n \to \infty$. This proves the statement (i) above.

Next, we wish to verify that ϕ' remains bounded for all $\eta \in [0, \infty)$. To this end we observe from (9.91) that $\phi''(\eta) > 0$ for all $\eta \in [0, \infty)$. This implies, by integration and initial conditions, that $\phi'(\eta) > 0$ and $\phi(\eta) > 0$ for $\eta > 0$. In other words, $\phi(\eta)$ is monotonically increasing. If we then write (9.91) as

$$\phi''(\eta) = \underbrace{\exp\left\{-\int_0^1 \phi(\zeta)d\zeta\right\}}_{=K} \exp\left\{-\int_1^\eta \phi(\zeta)d\zeta\right\}$$

$$= K \exp\left\{-\int_1^\eta \phi(\zeta)d\zeta\right\} \tag{9.101}$$

and because of the monotonicity of $\phi(\eta)$, we obtain the estimate

$$\int_1^\eta \phi(\zeta)d\zeta > (\eta - 1)\phi(1),$$

so that

$$\phi''(\eta) = K \exp\left\{-\int_1^\eta \phi(\zeta)d\zeta\right\} < K \exp\left\{-(\eta - 1)\phi(1)\right\}. \tag{9.102}$$

By integration and since $\phi'(0) = 0$, this yields the following estimate for $\phi'(\eta)$

$$\phi'(\eta) = \int_0^1 \phi''(\zeta)d\zeta + \int_1^\eta \phi''(\zeta)d\zeta$$

$$< \phi'(1) + K \int_1^\eta \exp\left(-(\zeta - 1)\phi(1)\right)d\zeta \quad \text{(where } \phi'(0) = 0 \text{ is used)}$$

$$= \phi'(1) + \frac{K}{\phi(1)}\left\{1 - \exp\left(-(\eta - 1)\phi(1)\right)\right\}. \tag{9.103}$$

Because $\phi(1)$ and $\phi'(1)$ are both bounded, this inequality implies that $\phi'(\eta)$ is bounded for all $\eta \in [0, \infty)$. This proves the above statement (ii).

There remains statement (iii) i.e. the construction of that $\phi(\eta)$-function which satisfies the boundary condition $\phi'(\infty) = 1$. The initial value problem with $\phi(0) = \phi'(0) = 0$ and $\phi''(0) = 1$ generates a BLASIUS profile for which

$$\lim_{\eta \to \infty} \phi'(\eta) = \gamma, \quad \text{where } \gamma > 0 \text{ is bounded.}$$

With this $\phi(\eta)$ also $\tilde{\phi}(\eta) = \alpha\phi(\alpha\eta)$ is solution of the BLASIUS differential equation for any bounded α (Lemma 9.2). Its slope is given by $\tilde{\phi}'(\eta) = \alpha^2\phi'(\alpha\eta)$. Thus, we choose $\lim_{\eta \to \infty} \tilde{\phi}' = 1 = \alpha^2\gamma$, from which we deduce

$$\alpha = \frac{1}{\sqrt{\gamma}}.$$

With this choice of $\alpha\tilde{\phi}(\alpha\eta)$ the BLASIUS solution with $\tilde{\phi}'(\infty) = 1$ is uniquely constructed and existence is proved. ∎

This rigorous proof of the existence and uniqueness of the BLASIUS problem (as well as the more general FALKNER-SKAN problem) is essentially due to HERMANN WEYL (1885–1955) in the year 1942 [46]. A further, different proof, applied to the BLASIUS equation subject to the boundary condition $f'(0) = -\lambda$, $\lambda > 0$, (instead of $\lambda = 0$) is given by HUSSAINI and LAKIN [18].

We close this discussion on the BLASIUS boundary layer by presenting an estimate for its conditions of validity. Necessary condition for this is certainly that[10]

$$\frac{d\delta^*}{dx} \ll 1, \quad \text{where } \delta^* = 1.73\sqrt{\frac{\nu}{U}}\sqrt{x}. \tag{9.104}$$

Therefore,

$$\frac{d\delta^*}{dx} = \frac{1.73}{2}\sqrt{\frac{\nu}{Ux}} = 0.865\frac{1}{\sqrt{\mathbb{R}_x}}, \quad \mathbb{R}_x := \frac{Ux}{\nu}, \tag{9.105}$$

and, consequently, $\mathbb{R}_x \gg 1$. With

$$u = U\phi'(\eta), \qquad \eta = \sqrt{\frac{U}{2\nu}}\frac{y}{\sqrt{x}}, \tag{9.106}$$

one may deduce

$$\frac{\partial^2 u}{\partial y^2} = \frac{U^2}{2\nu}\frac{\phi'''}{x}, \qquad \frac{\partial^2 u}{\partial x^2} = \frac{U}{2x^2}\left(\eta\phi'' + \frac{\eta}{2}\left(\eta\phi''\right)'\right).$$

The second boundary layer assumption $|u_{xx}| \ll |u_{yy}|$ is, therefore satisfied, provided $U/(2x^2) \ll U^2/(2\nu x)$, implying $Ux/\nu \gg 1$ or $\mathbb{R}_x \gg 1$, which is the same result.
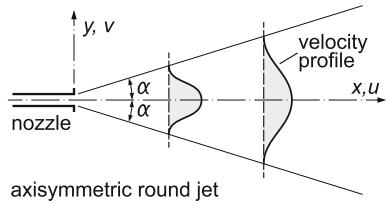
9.6 Round Laminar Jet—A Not So Simple Boundary Layer Problem

The axi-symmetric NS-equations are already given as Eq. (9.29) in Sect. 9.3; the radial and axial coordinates are denoted there by (r, z) and the corresponding velocity components by (u, w). In order to agree with the custom in the literature we change in this section the notation of the boundary layer theory as follows, see **Fig. 9.21**:

$$\begin{aligned}&\text{old notation (Sect. 9.3):} &(r, z) \quad (u, w),\\ &\text{new notation (this Section):} &(y, x) \quad (v, u).\end{aligned} \tag{9.107}$$

---

[10]The factor 1.73 is an approximation; the exact value is 1.729, see Sect. 9.8.

Fig. 9.21 Axisymmetric round jet shown in a meridian plane. *The cylindrical coordinates are: axial: x, radial: y and the corresponding velocity components are: axial, u; radial, v*

In this new notation the NS-equations (9.29) take the forms

$$
\frac{\partial u}{\partial x} + \frac{\partial v}{\partial y} + \frac{v}{y} = 0,
$$

$$
u\frac{\partial v}{\partial x} + v\frac{\partial v}{\partial y} = -\frac{1}{\rho}\frac{\partial p}{\partial y} + \nu\left\{\frac{\partial^2 v}{\partial y^2} + \frac{1}{y}\frac{\partial v}{\partial y} - \frac{v}{y^2} + \frac{\partial^2 v}{\partial x^2}\right\}, \qquad (9.108)
$$

$$
u\frac{\partial u}{\partial x} + v\frac{\partial u}{\partial y} = -\frac{1}{\rho}\frac{\partial p}{\partial x} + \nu\left\{\frac{\partial^2 u}{\partial y^2} + \frac{1}{y}\frac{\partial u}{\partial y} + \frac{\partial^2 u}{\partial x^2}\right\}.
$$

To identically satisfy the continuity equation $(9.108)_1$ the velocity components and the stream function ψ are related by

$$
u = \frac{1}{y}\frac{\partial \psi}{\partial y} \quad v = -\frac{1}{y}\frac{\partial \psi}{\partial x}. \qquad (9.109)
$$

The boundary layer assumptions can be stated as

- $\dfrac{\partial \tilde{p}}{\partial y} \approx 0 \quad \longrightarrow \quad \tilde{p} \approx \text{const.},$

  $\qquad\qquad\qquad\qquad\qquad\qquad\qquad\qquad\qquad\qquad (9.110)$

- $\dfrac{\partial^2 u}{\partial x^2} \ll \dfrac{\partial^2 u}{\partial y^2}.$

This makes $(9.108)_2$ superfluous, and $(9.108)_3$ takes the form

$$
u\frac{\partial u}{\partial x} + v\frac{\partial u}{\partial y} = \frac{\nu}{y}\frac{\partial}{\partial y}\left(y\frac{\partial u}{\partial y}\right). \qquad (9.111)
$$

Introducing the stream function ψ transforms it to

$$
\psi_y\psi_{xy} - \psi_x\psi_{yy} + \frac{1}{y}\psi_x\psi_y = \nu\left(\frac{\psi_y}{y} - \psi_{yy} + y\psi_{yyy}\right), \qquad (9.112)
$$

in which subscripts denote partial differentiations. This equation is now solved with the trial solution

$$\psi = \nu x^p f(\eta), \quad \eta = \frac{y}{x^q}, \tag{9.113}$$

where p and q are constants. Substituting (9.113) into (9.112) generates on the left-hand side the factor $x^{2p-1-2q}$ and on the right-hand side x^{p-2q}. An ordinary differential equation only ensues for $f(\eta)$ if

$$2p - 1 - 2q = p - 2q \quad \longrightarrow \quad p = 1, \quad q \text{ arbitrary.} \tag{9.114}$$

Therefore,

$$\frac{1}{\nu}\psi = xf(\eta), \quad \frac{1}{\nu}\psi_y = x^{1-q}f'(\eta), \quad \frac{1}{\nu}\psi_x = f - q\eta f' \tag{9.115}$$

or, owing to (9.109),

$$\frac{u}{\nu} = x^{1-2q}\frac{f'(\eta)}{\eta}, \quad \frac{v}{\nu} = -x^{-q}\left(\frac{f}{\eta} - qf'\right). \tag{9.116}$$

The exponent q is now determined by postulating a constant x-momentum flux,

$$\rho \int_0^\infty u^2 2\pi y\,\mathrm{d}y = 2\pi\nu^2\rho \underbrace{x^{2-4q}x^{2q}}_{x^{2-2q}=1} \int_0^\infty \frac{(f')^2}{\eta^2}\eta\,\mathrm{d}\eta = \text{const.} \quad \longrightarrow \quad q = 1.$$

Thus, we get from (9.115)$_1$, (9.116)

$$\psi = \nu xf\left(\frac{y}{x}\right) = \nu xf(\eta), \quad u = \frac{\nu}{x}\frac{f'(\eta)}{\eta}, \quad v = \frac{\nu}{x}\left(f' - \frac{f}{\eta}\right). \tag{9.117}$$

Substitution of (9.117)$_1$ into the boundary layer equation (9.112) generates

$$ff' - \eta(f')^2 - \eta ff'' = \eta^2 f''' + f' - \eta f'',$$

or

$$\underbrace{ff' - f' + \eta f''}_{w} = \underbrace{\eta\left((f')^2 + ff'' + \eta f'''\right)}_{\eta\frac{\mathrm{d}w}{\mathrm{d}\eta}}$$

$$\longrightarrow \quad \frac{\mathrm{d}\eta}{\eta} = \frac{\mathrm{d}w}{w}, \tag{9.118}$$

a differential equation, which, on the axis $y = 0$, must satisfy the conditions

$$f(0) = 0 \quad \text{(normalization)},$$
$$f'(0) = 0 \quad \left(v = 0 \;\; \rightarrow \;\; \frac{1}{y} \frac{\partial \psi}{\partial \eta} \frac{y}{x^2} = \frac{1}{x^2} \frac{\partial \psi}{\partial \eta} = 0 \right). \qquad (9.119)$$

Integrating (9.118) yields $w = C\eta$, where C is a constant of integration, which is determined by the condition that u and v should vanish as $\eta \to \infty$. Equations $(9.117)_{2,3}$ then suggest

$$f(\infty) = \text{bounded}, \quad f'(\infty) = 0, \quad f''(\infty) = 0. \qquad (9.120)$$

Substituting these values on the left-hand side of (9.118) yields $w(\infty) = 0$, implying that the constant of integration must vanish, $C = 0$; therefore, $w(\eta) = 0$ for all $\eta \in [0, \infty)$, or

$$ff' - f' + \eta f'' = 0 \quad \longrightarrow \quad \left(\tfrac{1}{2} f^2 - 2f + \eta f' \right)' = 0. \qquad (9.121)$$

The solution of this differential equation, subject to the boundary conditions (9.119), is given by

$$f(\eta) = \frac{\gamma^2 \eta^2}{1 + \dfrac{\gamma^2 \eta^2}{4}} = \tilde{f}(\mathfrak{x}) = \frac{\mathfrak{x}^2}{1 + \dfrac{\mathfrak{x}^2}{4}}, \quad \mathfrak{x} = \gamma \eta, \qquad (9.122)$$

$$\frac{1}{\gamma} f'(\eta) = \tilde{f}'(\mathfrak{x}) = \frac{2\mathfrak{x}}{\left(1 + \dfrac{\mathfrak{x}^2}{4} \right)^2},$$
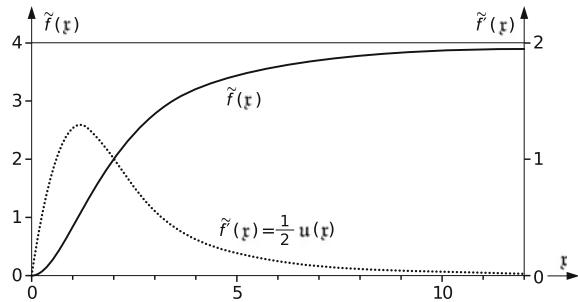
where γ is a constant.

The axial velocity is obtained from (9.117) as

$$u = \frac{\nu}{x} \frac{2\gamma^2}{\left(1 + \dfrac{\gamma^2 \eta^2}{4} \right)^2}$$

$$\longrightarrow \frac{u(\eta)}{\nu} \eta^2 x =: \mathfrak{u}(\mathfrak{x}) = \frac{2\mathfrak{x}^2}{\left(1 + \dfrac{\mathfrak{x}^2}{4} \right)^2} = \mathfrak{x} \tilde{f}'(\mathfrak{x}). \qquad (9.123)$$

Figure 9.22 displays the functions $\tilde{f}(\mathfrak{x})$, $\tilde{f}'(\mathfrak{x}) = \frac{1}{\mathfrak{x}} \mathfrak{u}(\mathfrak{x})$. This representation holds for any bounded value of $\gamma \neq 0$. This constant is determined by evaluating the axial momentum flux F, which is constant,

Fig. 9.22 'Universal' distribution of $\tilde{f}(\mathfrak{x})$ and $\tilde{f}'(\mathfrak{x})$, plotted against $\mathfrak{x}$ for an axissymmetric round jet. *The representations are 'universal', because the graph holds for all viscosities of* NEWTON*ian fluids and all opening angles* θ_0 *of the jet*

$$F = \rho \int_0^\infty 2\pi u^2 y \mathrm{d}y \overset{(9.123)}{=} 2\pi\rho\nu^2 \underbrace{\int_0^\infty \frac{4\gamma^4}{\left(1+\dfrac{\gamma^2\eta^2}{4}\right)^4} \eta \mathrm{d}\eta}_{(8/3)\gamma^2} = \frac{16}{3}\pi\rho\nu^2\gamma^2$$

or

$$\frac{F}{2\pi\rho\nu^2} = \frac{8}{3}\gamma^2 \overset{*}{=} \frac{32}{30\theta_0^2} \quad \longrightarrow \quad \gamma^2 = \frac{4}{\theta_0^2}. \tag{9.124}$$

Here, θ_0 can be interpreted as the opening angle of the jet, see the formula before (8.148). So,

$$u = \frac{\nu}{x}\frac{8}{\theta_0^2}\frac{1}{\left(1+\dfrac{\eta^2}{\theta_0^2}\right)^2}. \tag{9.125}$$

Next, let us compute the volume flux Q at a fixed position x:

$$Q = 2\pi \int_0^\infty u y \mathrm{d}y = 2\pi\frac{\nu}{x}\gamma^2 x^2 \int_0^\infty \frac{2\eta \mathrm{d}\eta}{\left(1+\dfrac{\gamma^2\eta^2}{4}\right)^2}$$

$$= 2\pi\nu x \underbrace{\int_0^\infty \frac{2\xi \mathrm{d}\xi}{\left(1+\dfrac{\xi^2}{4}\right)^2}}_{=4} = 8\pi\nu x. \tag{9.126}$$

This says that the volume flux grows linearly with x: The jet drags on fluid from the exterior region. This entrainment is constant per unit length, $\mathrm{d}Q/\mathrm{d}x = 8\pi\nu$.

Remarks

- If the above results are expressed in terms of the momentum flux F, then it is seen that

$$\theta_0 \sim \nu, \quad u \sim \frac{1}{\nu}, \quad Q \sim \nu, \quad \text{see } (9.124) - (9.126), \qquad (9.127)$$

In other words, with reduced viscosity the jet gets narrower, the axial velocity increases and the specific volume flux and the total flux decrease.

- In an exit flow from a circular nozzle the mean velocity u_0, the nozzle cross sectional area A and the volume flux Q are related by

$$Q = A u_0, \quad F = \rho A u_0^2 \quad \longrightarrow \quad Q = \sqrt{\frac{FA}{\rho}}. \qquad (9.128)$$

The virtual origin of the jet, thus, can be computed from

$$Q = A u_0 \overset{(9.126)}{=} 8\pi\nu x_0 \quad \longrightarrow \quad x_0 = \frac{A u_0}{8\pi\nu}. \qquad (9.129)$$

The virtual origin is behind the exit cross section by a distance, which grows with A and u_0 and decreases with viscosity, see **Fig. 9.23**.

- The above results can be applied to a laminar flame. The un-mixed and un-burned gas exits the nozzle with a volume flux $Q_0 = 8\pi\nu x_0$. If we assume that the gas and the air have the same viscosity, the air added to the jet at position x, is given by $Q_\ell = 8\pi\nu(x - x_0)$. The mixing ratio between air and gas is, thus given by
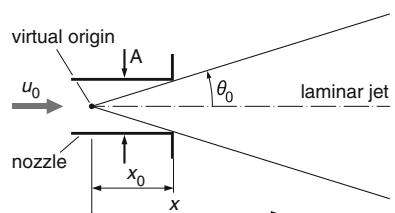
$$\frac{Q_\ell}{Q_0} = \lambda = \frac{8\pi\nu(x - x_0)}{8\pi\nu x_0} = \frac{x - x_0}{x_0}. \qquad (9.130)$$

The position, where combustion ends is given by a fixed constant value of λ. Consequently, the length ℓ of the flame is given by

$$\ell = \lambda x_0 = \lambda \frac{Q}{8\pi\nu} = \lambda \frac{A u_0}{8\pi\nu}. \qquad (9.131)$$

Fig. 9.23 Steady laminar axisymmetric jet. *Construction of the virtual origin position x_0 for given jet angle θ_0*

The length of the laminar flame is proportional to the volume flux (or exit velocity) and inversely proportional to the kinematic viscosity. (In turbulent jets the length of the flame is given only by the diameter of the nozzle).

9.7 Boundary Layers of the NAVIER-STOKES Equations Treated by Matched Asymptotic Expansions

In this section an introduction to the method of matched asymptotic expansions will be given. For the NS-equations this method is a systematic approach to PRANDTL's boundary layer equations; the method of matched asymptotic expansions provides equally a rational extension of the latter to higher accuracy of approximate solutions of the NS-equations.

Below we shall introduce the method of matched asymptotic expansions by means of a simple example of a two-point-boundary-value problem using a simple ordinary differential equation. As such, the method has developed itself into a formal branch of applied mathematics and systematic expositions are [20, 21, 26, 27, 42], to mention just a few.

9.7.1 A Simple Introductory Example

Let us start with a simple example, by which the mathematical method can be explained. Consider the two-point boundary value problem

$$\varepsilon f'' + f' = \tfrac{1}{2}, \quad 0 < x < 1, \tag{9.132}$$
$$f(0) = 0, \quad f(1) = 1$$

with constant ε; its exact solution is given by

$$f = \frac{\exp(-x/\varepsilon) - 1}{2(\exp(-1/\varepsilon) - 1)} + \frac{x}{2}. \tag{9.133}$$

For small values of $\varepsilon > 0$ this solution consists in nearly the entire interval $(0, 1]$ of the straight line $f = \tfrac{1}{2}(1+x)$. Only in a thin boundary layer near the wall, $x \in [0, \varepsilon)$ the solution drops to the boundary value $f(0) = 0$.

Let us now search for an approximate solution of (9.132) for the case that $\varepsilon \ll 1$. A naive regular perturbation attempt employs a power series expansion

$$f = \sum_{\varepsilon=0}^{\infty} \varepsilon^{\alpha} f_{\alpha} = f_0 + \varepsilon^1 f_1 + \varepsilon^2 f_2 + \cdots . \tag{9.134}$$

Substitution into $(9.132)_1$ generates the expression

$$\varepsilon f_0'' + \varepsilon^2 f_1'' + \cdots + f_0' + \varepsilon f_1' + \varepsilon^2 f_2' + \cdots = \tfrac{1}{2},$$

from which by equating members of equal power of ε one obtains

$$f_0' = \tfrac{1}{2}, \quad f_\alpha' = 0, \quad \alpha \geqslant 1.$$

Therefore, f_α is constant for all $\alpha \geqslant 1$ and $f_0 = \tfrac{1}{2}x + c$; if one requests that the boundary condition at the right boundary, $x = 1$ is satisfied we have

$$f(1) = 1 \quad \longrightarrow \quad f_0(1) = 1, \quad f_\alpha(1) = 0, \quad \forall \alpha \geqslant 1, \qquad (9.135)$$

that $c = \tfrac{1}{2}$ and $f_\alpha = 0$, for $\alpha \geqslant 1$. The solution is, consequently,

$$f^o(x) = \tfrac{1}{2}(1 + x). \qquad (9.136)$$

The superscript $(\ )^o$ stands for 'outer'. Solution (9.136) does not satisfy the boundary condition at the wall, $x = 0$, and only approximates the correct solution far away from the left boundary. For this reason it is called the outer solution. We remark that we could have also satisfied the boundary condition at the left end and would then have obtained $f = \tfrac{1}{2}x$. However, that this alternative is not a meaningful approximation cannot be cleared at this stage of the calculations.

Let us now observe the boundary layer region near $x = 0$ through a magnifying glass. Obviously, via a coordinate transformation we must see to it that in the transformed equation a naive perturbation expansion of f in ε preserves the second derivatives. With the so-called *stretching transformation*

$$f(x) = \phi\left(\frac{x}{\delta(\varepsilon)}\right) = \phi(\xi), \quad x = \delta(\varepsilon)\xi \qquad (9.137)$$

this goal can formally be reached. To this end we additionally assume that

$$\lim_{\varepsilon \to 0} \delta(\varepsilon) = 0 \qquad (9.138)$$

and wish to determine $\delta(\varepsilon)$ such that the second derivative of f in this stretching transformation is not lost. We have

$$f' = \frac{\phi'}{\delta}, \quad f'' = \frac{\phi''}{\delta^2}. \qquad (9.139)$$

Here and henceforth f' is the derivative of $f(x)$ with respect to x, whilst ϕ' denotes the derivative of $\phi(\xi)$ with respect to ξ. With these expressions $(9.132)_1$ can be written as
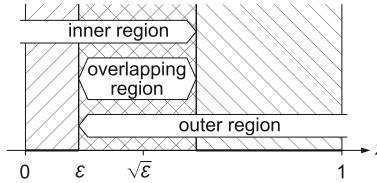
Fig. 9.24 Division of the interval $x \in [0, 1]$ into inner region (where the inner solution f^i is valid) and outer region (where the outer solution f^o is valid) and an overlapping region, (in which both are asymptotically equal)

$$\frac{\varepsilon}{\delta^2} \phi'' + \frac{1}{\delta} \phi' = \frac{1}{2}. \tag{9.140}$$

At this stage of the computations, two different 'balances' are possible

(i) $\delta = \varepsilon \quad \longrightarrow \quad \phi'' + \phi' = \frac{1}{2}\varepsilon \quad \longrightarrow \quad \phi'' + \phi' \to 0 \quad$ as $\varepsilon \to 0$.

(ii) $\delta = \sqrt{\varepsilon} \quad \longrightarrow \quad \phi' = \sqrt{\varepsilon}\left(\frac{1}{2} - \phi''\right) \quad \longrightarrow \quad \phi' \to 0 \quad$ as $\varepsilon \to 0$.

Of these, only the first one achieves the survival of ϕ'' when the limit $\varepsilon \to 0$ is approached. Thus, we now take

$$\phi'' + \phi' = \frac{\varepsilon}{2}$$

and obtain by regular perturbation expansion of ϕ in ε, $\phi(\xi) = \sum_{\alpha=0}^{\infty} \varepsilon^{\alpha} \phi_{\alpha}(\xi)$,

$$\phi_0'' + \phi_0' = 0, \quad \phi_1'' + \phi_1' = \frac{1}{2}, \quad \phi_{\alpha}'' + \phi_{\alpha}' = 0, \quad \alpha \geqslant 2, \tag{9.141}$$

all of which must obey the boundary conditions for $\xi = 0$

$$\phi_{\alpha}(0) = 0 \quad \text{for } \alpha \geqslant 0. \tag{9.142}$$

The solution of the above equations can readily be constructed and are given by

$$\begin{aligned} \phi_{\alpha} &= C_{\alpha}(1 - \exp(-\xi)) &\longrightarrow \quad f_{\alpha}^i &= C_{\alpha}(1 - \exp(-x/\varepsilon)) \quad \alpha \geqslant 0, \alpha \neq 1, \\ \phi_1 &= C_1(1 - \exp(-\xi)) + \frac{1}{2}\xi &\longrightarrow \quad f_1^i &= C_1(1 - \exp(-x/\varepsilon)) + \frac{1}{2}x, \end{aligned} \tag{9.143}$$

in which C_{α}, $\alpha \geqslant 1$ are still undetermined constants of integration and the super-script 'i' identifies the so-called *inner solutions*, 'inner' because they hold within the boundary layer near $\xi = 0$. The free constants of integration are so determined that the inner solutions are matched in an overlapping region with the outer solutions, see **Fig. 9.24**.[11]

---

[11] In such singular perturbation problems it is assumed that the regions of validity of the inner and outer solutions possess an overlapping region, in which inner and outer solutions are asymptotically equal to one another, so that by a common stretching transformation they 'agree' asymptotically to one another.

Let us try the transformation in the overlapping region as

$$\eta = x/\sqrt{\varepsilon}, \tag{9.144}$$

in which the outer, (9.136), and inner, (9.143), solutions take the forms

$$
\begin{aligned}
f^o &= \tfrac{1}{2}(1 + \sqrt{\varepsilon}\eta), \\
f^i &= C_0 \left(1 - \exp(-\eta/\sqrt{\varepsilon})\right) + \tfrac{1}{2}\eta\sqrt{\varepsilon} + \varepsilon C_1 \left(1 - \exp(-\eta/\sqrt{\varepsilon})\right) \\
&\quad + \varepsilon^2 C_2 \left(1 - \exp(-\eta/\sqrt{\varepsilon})\right) + \cdots .
\end{aligned}
\tag{9.145}
$$

These representations agree asymptotically with one another, provided that

$$\lim_{\varepsilon \to 0} \left(f^i(\eta) - f^o(\eta)\right) \to 0, \quad \forall \eta. \tag{9.146}$$

Substituting the expressions (9.145) into (9.146) and expressing the exponential functions in their MCLAURIN series, it is easily found that (9.146) can asymptotically be satisfied, if

$$C_0 = \tfrac{1}{2}, \qquad C_\alpha = 0, \quad \alpha \geqslant 1.$$

We remark that this asymptotic satisfaction of (9.146) provides the *a posteriori* proof that the choice of the transformation (9.144) was correct. The general solution is, therefore,

$$f^o(x) = \tfrac{1}{2}(1 + x), \quad f^i(x) = \tfrac{1}{2}(1 - \exp(-x/\varepsilon)) + \tfrac{1}{2}x. \tag{9.147}$$

Each of these solutions is only applicable in its own region of validity. A *composite (expansion) solution* is obtained by

$$f^c = f^o + (f^i)^o \ (= f^i + (f^o)^i)$$

in which $(f^i)^o$ is that part of f^i, which is not represented by the outer solution: $(f^i)^o = -\tfrac{1}{2}\exp(-x/\varepsilon)$. Thus,
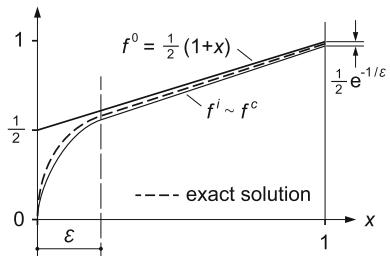
$$f^c \sim \tfrac{1}{2}(1 + x) - \tfrac{1}{2}\exp(-x/\varepsilon). \tag{9.148}$$

This result can also be obtained from the exact solution (9.133) by writing

$$f = \frac{1}{2}\left\{1 - \exp\left(-\frac{x}{\varepsilon}\right) + x\right\}\left\{1 + \exp\left(-\frac{1}{\varepsilon}\right)\right\} \sim \frac{1}{2}\left((1 + x) - \exp\left(-\frac{x}{\varepsilon}\right)\right)$$

with an error of order $\exp(-1/\varepsilon)$, see **Fig. 9.25**.

Fig. 9.25 Plots of the exact solution f (9.133) of (9.132) (*dashed*) and its outer, f^o (black) and inner f^i (*light black*) approximations

9.7.2 The Blasius Boundary Layer

Let us now apply this singular perturbation technique to the NS-equation of plane two-dimensional steady flows along a rough plate. With the stream function ψ, $u = \psi_y$, $v = -\psi_x$, the steady vorticity equation takes the form

$$\left(\psi_y \frac{\partial}{\partial x} - \psi_x \frac{\partial}{\partial y}\right) \Delta\psi = \nu \Delta\Delta\psi, \tag{9.149}$$

where Δ is the two-dimensional LAPLACE operator. Introducing the dimensionless variables $((x, y), (u, v)) = (L(\overline{x}, \overline{y}), U(\overline{u}, \overline{v}))$ its non-dimensional form is given by

$$\left(\psi_y \frac{\partial}{\partial x} - \psi_x \frac{\partial}{\partial y} - \frac{1}{\mathbb{R}}\Delta\right) \Delta\psi = 0, \quad \mathbb{R} = \frac{UL}{\nu}, \tag{9.150}$$

in which overbars have been dropped.

In the following we shall be content with the BLASIUS boundary layer, but many thoughts and arguments will have general character. The boundary conditions that must be observed for the BLASIUS solution are, see **Fig. 9.26a**,
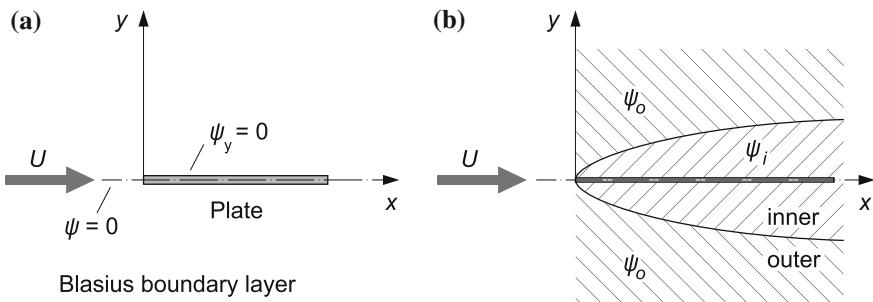
Fig. 9.26 Two dimensional flow past a semi-infinite plate. **a** *geometry and boundary conditions*, **b** *inner and outer regions*

$\psi(x, 0) = 0,$ (by choice, this is the stagnation point streamline),

$\psi_y(x, 0) = 0,$ for $x > 0$ (tangential velocity $= 0$),   (9.151)

$\psi_y(x, y) = 1,$ for $x \to -\infty$ or $|y| \to \infty$.

The boundary value problem (9.150), (9.151) is now solved for large REYNOLDS numbers: we set $1/\mathbb{R} = \varepsilon$ and seek perturbation solutions in series of powers of ε. Because ε is the coefficient of the term with the largest derivative, matched asymptotic expansions with inner and outer solutions are the proper approach to seek approximate solutions. The geometric situation is sketched in Fig. 9.26b.

For the *outer solution* we choose

$$\psi^o = \psi_0 + \theta_1(\varepsilon)\psi_1 + \theta_2(\varepsilon)\psi_2 + \dots \tag{9.152}$$

with $\lim_{\varepsilon \to 0}(\theta_n/\theta_{n-1}) = 0$. Substitution of (9.152) into (9.150) yields to lowest order

$$\left(\frac{\partial \psi_0}{\partial y}\frac{\partial}{\partial x} - \frac{\partial \psi_0}{\partial x}\frac{\partial}{\partial y}\right)\Delta\psi_0 = 0, \tag{9.153}$$

which is equivalent to $\mathrm{d}(\Delta\psi_0)/\mathrm{d}t = 0$ and states that $\Delta\psi_0$ is constant along streamlines. Now, as $y \to \infty$, $\Delta\psi_0 = 0$, since the flow there is a potential flow; consequently, because $\mathrm{d}(\Delta\psi_0)/\mathrm{d}t = 0$ in the entire plane $\mathcal{R}^2$, $\Delta\psi_0 = 0$ holds everywhere in $\mathcal{R}^2$. The ansatz

$$\psi_0 = y \tag{9.154}$$

satisfies (9.150) and all three boundary conditions (9.151), of which the second is irrelevant, because it belongs to the inner solution.

For the construction of the *inner solution* we choose the stretching transformation

$$\zeta = y/\delta(\varepsilon) \qquad \psi^i = \delta(\varepsilon)\phi(x, \zeta). \tag{9.155}$$

Note that ψ^i has been chosen to be of order $\delta(\varepsilon)$, to guarantee that $\psi_y^i = \mathcal{O}(\phi_\zeta)$. With the expansion

$$\phi = \phi_0 + \delta_1(\varepsilon)\phi_1 + \delta_2(\varepsilon)\phi_2 + \cdots, \quad \lim_{\varepsilon \to 0}\frac{\delta_n(\varepsilon)}{\delta_{n-1}(\varepsilon)} \to 0 \tag{9.156}$$

one obtains by re-substitution into (9.150) to lowest order the equation

$$(\phi_0)_\zeta(\phi_0)_{x\zeta\zeta} - (\phi_0)_x(\phi_0)_{\zeta\zeta\zeta} = \frac{\varepsilon}{\delta^2}(\phi_0)_{\zeta\zeta\zeta\zeta}. \tag{9.157}$$

Subscripts denote again differentiation. If the term with highest ζ-derivative in this equation is to be significant as $\varepsilon \to 0$, we must necessarily have

$$\varepsilon = \delta^2 \quad \longrightarrow \quad \delta = \sqrt{\varepsilon}. \tag{9.158}$$

With this choice (9.157) takes the form

$$\frac{\partial}{\partial \zeta} \left\{ (\phi_0)_{\zeta\zeta\zeta} + (\phi_0)_x (\phi_0)_{\zeta\zeta} - (\phi_0)_\zeta (\phi_0)_{x\zeta} \right\} = 0,$$

or after integration

$$(\phi_0)_{\zeta\zeta\zeta} + (\phi_0)_x (\phi_0)_{\zeta\zeta} - (\phi_0)_\zeta (\phi_0)_{x\zeta} = f^*(x), \tag{9.159}$$

where the function $f^*(x)$ remains presently undetermined and will later be determined in the matching procedure.

For the formulation of the overlapping condition, we introduce the stretching transformation

$$\eta = \frac{y}{\varepsilon^{1/4}}, \quad \longrightarrow \quad \zeta = \frac{\eta}{\varepsilon^{1/4}} = \frac{y}{\varepsilon^{1/2}}. \tag{9.160}$$

With this, and with (9.155) we obtain

$$\frac{\partial \psi^i}{\partial y} = \psi_y^i = \sqrt{\varepsilon} \frac{\partial \phi_0}{\partial \zeta} \frac{1}{\sqrt{\varepsilon}} = (\phi_0)_\zeta \left(x, \frac{\eta}{\varepsilon^{1/4}} \right). \tag{9.161}$$

Similarly, for the outer solution

$$\frac{\partial \psi^o}{\partial y} = \frac{\partial \psi^o}{\partial y} \left(x, \varepsilon^{1/4} \eta \right) \stackrel{(9.154)}{=} \frac{d}{dy} \left(\varepsilon^{1/4} \eta \right) = 1. \tag{9.162}$$

In the last two equations ψ_y^i and ψ_y^o have been expressed in the variable η of the overlapping region, and in (9.162) the BLASIUS solution $\psi^o = y = \varepsilon^{1/4} \eta$ has been used. In this region

$$\psi_y^i = \psi_y^o. \tag{9.163}$$

In other words, the y-derivatives of the inner and outer solutions must agree with one another. This condition expresses nothing else than the fact that

$$\lim_{y \to \infty} u(x, y) = \tilde{u}_w.$$

The function $f^*(x)$ in (9.159) is now determined by the condition that the limit of (9.159) as $\zeta \to \infty$ is considered,

$$
\begin{aligned}
\lim_{\zeta \to \infty} \{(9.159)\} &= \lim_{\zeta \to \infty} \left\{ (\phi_0)_{\zeta\zeta\zeta} + (\phi_0)_{x\zeta\zeta} - (\phi_0)_\zeta (\phi_0)_{x\zeta} \right\} \\
&\overset{(*)}{=} - \lim_{\zeta \to \infty} \left\{ (\phi_0)_\zeta (\phi_0)_{x\zeta} \right\} = f^*(x).
\end{aligned}
$$

Here, the step ($\overset{*}{=}$) is obtained, because higher ζ-derivatives of ϕ_0 are expected to be negligible in comparison to the lowest ζ-derivatives. Now, owing to the relation $\lim_{\zeta \to \infty} (\phi_0)_\zeta = \tilde{u}_w$, the last result implies

$$
f^*(x) = -\tilde{u}_w \frac{d\tilde{u}_w}{dx} \quad \left(\overset{\text{Blasius}}{=} 0 \right). \tag{9.164}
$$

Once $f^*(x)$ is determined, one still needs to implement the no-slip condition at the wall

$$
\phi_0(x, 0) = 0, \qquad (\phi_0)_\zeta(x, 0) = 0.
$$

So, one must solve the boundary value problem

$$
\begin{aligned}
&(\phi_0)_{\zeta\zeta\zeta} + (\phi_0)_x (\phi_0)_{\zeta\zeta} - (\phi_0)_\zeta (\phi_0)_{x\zeta} = -\tilde{u} \frac{d\tilde{u}_w}{dx}, \quad 0 < \zeta < \infty, \\
&\phi_0(x, 0) = 0 \quad (\phi_0)_\zeta(x, 0) = 0, \quad \zeta = 0, \\
&(\phi_0)_\zeta(x, \infty) = 1, \quad \zeta \to \infty.
\end{aligned} \tag{9.165}
$$

As a special case, in the example of the BLASIUS boundary layer we substitute $d\tilde{u}_w/dx = 0$ and choose

$$
\phi_0(x, \zeta) = \sqrt{2x}\phi(\hat{\eta}), \quad \hat{\eta} = \frac{\zeta}{\sqrt{2x}} \tag{9.166}
$$

and then obtain from (9.165) the BLASIUS boundary value problem for ϕ as already stated in (9.87). With the identification of (9.165) with (9.87) in this case the results have been reproduced that were already obtained by the classical boundary layer theory. This gives the boundary layer theory enhanced confidentiality.

Let us now determine the next higher approximation of the outer solution by not only matching ψ_y but also ψ itself. Physically, this means that not only the x-component, u, but also the y-component, v, is matched. We shall do this for the BLASIUS boundary layer and choose

$$
\begin{aligned}
\psi^o &= y + \theta_1(\varepsilon)\psi_1(x, y), \\
\psi^i &= \sqrt{\varepsilon}\sqrt{2x}\,\phi(\zeta/\sqrt{2x}), \quad \zeta = \frac{y}{\sqrt{\varepsilon}}.
\end{aligned} \tag{9.167}
$$

With the coordinate $\eta = y/\varepsilon^{1/4}$ of the overlapping region, Eq. (9.167) can be written as

$$\psi^o = \varepsilon^{1/4}\eta + \theta_1(\varepsilon)\psi_1(x, y), \tag{9.168}$$
$$\psi^i = \sqrt{\varepsilon}\sqrt{2x}\,\phi(\eta/(\varepsilon^{1/4}\sqrt{2x})).$$

In order to exploit these relations, solutions of the BLASIUS equation are needed for large arguments. It is easily seen that

$$\phi \sim \hat{\eta} - \beta \sim \frac{\zeta}{\sqrt{2x}} - \beta, \quad \beta = \text{const.} \tag{9.169}$$

is a solution of (9.87) that satisfies the boundary condition $d\phi/d\hat{\eta} = 1$ at infinity; so (9.169) is a valid large argument solution, which with (9.169) and (9.168) assumes the form

$$\psi^i = \sqrt{2x\varepsilon}\left\{\frac{\eta}{\varepsilon^{1/4}\sqrt{2x}} - \beta + \text{exponentially small terms}\right\}$$
$$\sim \varepsilon^{1/4}\eta - \sqrt{\varepsilon}\beta\sqrt{2x} + \text{exponentially small terms.} \tag{9.170}$$

We now match this inner solution with the outer solution (that is expressed in the same intermediate coordinates (9.168)). This yields, since the terms $\varepsilon^{1/4}\eta$ already match,

$$\theta_1(\varepsilon)\psi_1(x, 0) \sim -\sqrt{\varepsilon}\sqrt{2x}\beta + \text{asymp. small terms,}$$

or

$$\theta_1(\varepsilon) = \sqrt{\varepsilon}, \quad \psi_1(x, 0) = -\sqrt{2x}\beta. \tag{9.171}$$

This condition allows a transparent interpretation. To this end we ask for the geometric locus for which $\psi^o = 0$. With (9.167) and (9.171)$_1$ this yields

$$y = -\sqrt{\varepsilon}\psi_1(x, 0) \approx -\sqrt{\varepsilon}\left\{\psi(x, 0) + \sqrt{\varepsilon}\psi_y(x, 0) + \cdots\right\}$$
$$\approx -\sqrt{\varepsilon}\psi_1(x, 0) + \mathcal{O}(\varepsilon) \stackrel{(9.171)_2}{\sim} \sqrt{\varepsilon}\sqrt{2x}\,\beta + \mathcal{O}(\varepsilon). \tag{9.172}$$

This shows that the boundary of the BLASIUS boundary layer has an $\sqrt{x}$-dependence. For the determination of β, the BLASIUS solution is written as

$$\phi(\hat{\eta}) = \int_0^{\hat{\eta}} \phi'(\eta)\mathrm{d}\eta = \int_0^{\hat{\eta}} \left(1 + (\phi' - 1)\right)\mathrm{d}\eta = \hat{\eta} - \int_0^{\hat{\eta}} (1 - \phi')\mathrm{d}\eta$$

$$= \hat{\eta} - \underbrace{\int_0^{\infty} (1 - \phi')\mathrm{d}\eta}_{\beta} + \underbrace{\int_{\hat{\eta}}^{\infty} (1 - \phi')\mathrm{d}\eta}_{\text{negligible}}.$$

This agrees formally with (9.169). For β we get

$$\beta = \int_0^{\infty} \left(1 - \phi'\left(\frac{\zeta}{\sqrt{2x}}\right)\right) \frac{\mathrm{d}\zeta}{\sqrt{2x}} = \int_0^{\infty} \left(1 - \frac{u}{U}\right) \frac{\mathrm{d}\zeta}{\sqrt{2x}} \quad \text{or}$$

$$\sqrt{2x}\beta \overset{(9.167)_2}{=} \frac{1}{\sqrt{\varepsilon}} \int_0^{\infty} \left(1 - \frac{u}{U}\right)\mathrm{d}y = \frac{\delta^*}{\sqrt{\varepsilon}}. \tag{9.173}$$

In other words, the effective wall correction for the outer flow is in the second order approximation given by $y = \delta^*$.

Finally, we mention that, if

$$\psi^o = \psi_0 + \sqrt{\varepsilon}\psi_1$$

is substituted into the NS-equation (9.150), then

$$\left((\psi_0)_y \frac{\partial}{\partial x} - \underbrace{(\psi_0)_x}_{=0} \frac{\partial}{\partial y}\right)\Delta\psi_1 = 0$$

is obtained, which implies $\Delta\psi_1 = \text{const.} = 0$, where at $x = -\infty, \text{const.} = 0$ is obtained. So, *the outer flow remains to first order a potential flow*.
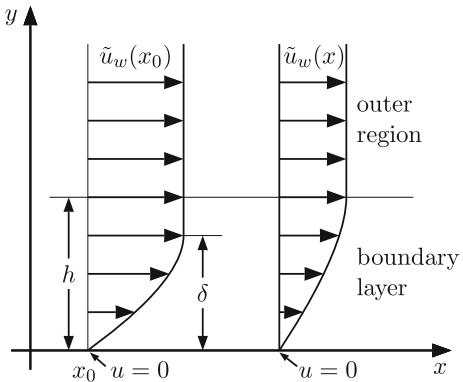
9.8 Global Laws of the Steady Boundary Layer Theory

9.8.1 Global Mass and Momentum Balances

Consider a plane steady boundary layer flow along a straight wall, **Fig. 9.27**. The boundary layer equations of mass and momentum are then[12]

---

[12]They are the steady forms of $(9.35)_{1,2}$ together with (9.40).

Fig. 9.27 Boundary layer flow along a flat plate. *The thickness h lies everywhere outside the boundary layer δ; it is constant along x, but the velocity may vary with x and y*

$$\frac{\partial u}{\partial x} + \frac{\partial v}{\partial y} = 0,$$

$$u\frac{\partial u}{\partial x} - \tilde{u}_w \frac{\mathrm{d}\tilde{u}_w}{\mathrm{d}x} + v\frac{\partial u}{\partial y} = \frac{\eta}{\rho}\frac{\partial^2 u}{\partial y^2}.$$

(9.174)

Integration of $(9.174)_2$ from $y = 0$ to $y = h$, (where the layer $y = h$ is everywhere outside the boundary layer and h is not a function of the x-coordinate), yields

$$\int_0^h \left\{ u\frac{\partial u}{\partial x} - \tilde{u}_w \frac{\mathrm{d}\tilde{u}_w}{\mathrm{d}x} + v\frac{\partial u}{\partial y} \right\} \mathrm{d}y = \frac{\eta}{\rho}\left\{ \frac{\partial u}{\partial y}\bigg|_h - \frac{\partial u}{\partial y}\bigg|_0 \right\}. \qquad (9.175)$$

In this equation the last, third term on the left-hand side can be transformed by application of integration by parts and use of the balance of mass, expl.,

$$\int_0^h v\frac{\partial u}{\partial y}\mathrm{d}y = vu|_0^h - \int_0^h u\frac{\partial v}{\partial y}\mathrm{d}y$$

$$= u(x, h)v(x, h) + \int_0^h u\frac{\partial u}{\partial x}\mathrm{d}y$$

$$= -u(x, h)\int_0^h \frac{\partial u}{\partial x}\mathrm{d}y + \int_0^h u\frac{\partial u}{\partial x}\mathrm{d}y.$$

Hence, Eq. (9.175) takes the form

$$\int_0^h \left\{ 2u \frac{\partial u}{\partial x} - \tilde{u}_w \frac{\mathrm{d}\tilde{u}_w}{\mathrm{d}x} - u(x,h) \frac{\partial u}{\partial x} \right\} \mathrm{d}y = \frac{\eta}{\rho} \left\{ \frac{\partial u}{\partial y} \Big|_h - \frac{\partial u}{\partial y} \Big|_0 \right\}.$$

The next imaginative step is to see that this equation can also be written as

$$\int_0^h \left\{ \frac{\partial}{\partial x} \left[u(u - \tilde{u}_w) \right] + \frac{\mathrm{d}\tilde{u}_w}{\mathrm{d}x} (u - \tilde{u}_w) + (\tilde{u}_w - u(x,h)) \frac{\partial u}{\partial x} \right\} \mathrm{d}y$$

$$= \frac{\eta}{\rho} \left\{ \frac{\partial u}{\partial y} \Big|_h - \frac{\partial u}{\partial y} \Big|_0 \right\}, \tag{9.176}$$

a step which can easily be corroborated. Because h does not depend on x, differentiation of the first term in the integral can be put in front of the integral. The same holds true for $\mathrm{d}\tilde{u}_w/\mathrm{d}x$ and $(\tilde{u}_w - u(x,h))$. Consequently,

$$\frac{\mathrm{d}}{\mathrm{d}x} \int_0^h u\,(u - \tilde{u}_w)\,\mathrm{d}y + \frac{\mathrm{d}\tilde{u}_w}{\mathrm{d}x} \int_0^h (u - \tilde{u}_w)\mathrm{d}y + (\tilde{u}_w - u(x,h)) \int_0^h \frac{\partial u}{\partial x}\mathrm{d}y$$

$$= \frac{\eta}{\rho} \left\{ \frac{\partial u}{\partial y} \Big|_h - \frac{\partial u}{\partial y} \Big|_0 \right\}, \tag{9.177}$$

$$\longrightarrow \quad \frac{\mathrm{d}}{\mathrm{d}x} \left\{ \tilde{u}_w^2 \int_0^h \frac{u}{\tilde{u}_w} \left(\frac{u}{\tilde{u}_w} - 1 \right) \mathrm{d}y \right\} + \tilde{u}_w \frac{\mathrm{d}\tilde{u}_w}{\mathrm{d}x} \int_0^h \left(\frac{u}{\tilde{u}_w} - 1 \right) \mathrm{d}y$$

$$+ (\tilde{u}_w - u(x,h)) \int_0^h \frac{\partial u}{\partial x}\mathrm{d}y = \frac{\eta}{\rho} \left\{ \frac{\partial u}{\partial y} \Big|_h - \frac{\partial u}{\partial y} \Big|_0 \right\}. \tag{9.178}$$

The last equation suggests the following definitions of boundary layer thicknesses:

Displacement thickness: $\qquad \delta^* = \lim_{h \to \infty} \int_0^h \left(1 - \frac{u}{\tilde{u}_w} \right) \mathrm{d}y,$

$$\tag{9.179}$$

Momentum thickness: $\qquad \theta = \lim_{h \to \infty} \int_0^h \frac{u}{\tilde{u}_w} \left(1 - \frac{u}{\tilde{u}_w} \right) \mathrm{d}y.$

It is assumed that both δ^* and θ are bounded away from ∞. In particular, this requires that

$$\int_0^\infty \left(1 - \frac{u}{\tilde{u}_w} \right) \mathrm{d}y < \infty, \quad \int_0^\infty (\tilde{u}_w - u)\,\mathrm{d}y < \infty, \tag{9.180}$$

which equally states that

$$\lim_{h \to \infty} (\tilde{u}_w - u(x, h)) = o\,(1/h)\,. \tag{9.181}$$

If these assumptions are expressed physically, (9.181) states that the boundary layer velocity at the outer edge and outside of the boundary layer agrees with the (constant) outer potential flow velocity, if merely the boundary layer thickness becomes sufficiently large.

Executing the limit operation, $\lim_{h \to \infty}(\cdot)$ in (9.178) shows that the third term on the left-hand side vanishes, whereas the first two terms survive, so that (9.178) reduces to

$$-\frac{\mathrm{d}}{\mathrm{d}x}\left(\tilde{u}_w^2\theta\right) - \tilde{u}_w\frac{\mathrm{d}\tilde{u}_w}{\mathrm{d}x}\delta^* = \frac{\eta}{\rho}\left\{\lim_{h \to \infty}\frac{\partial u}{\partial x} - \left.\frac{\partial u}{\partial y}\right|_0\right\} = -\frac{\tau_w}{\rho}, \quad \text{or}$$

$$\frac{\mathrm{d}}{\mathrm{d}x}\left(\tilde{u}_w^2\theta\right) + \delta^*\tilde{u}_w\frac{\mathrm{d}\tilde{u}_w}{\mathrm{d}x} = \frac{\tau_w}{\rho}, \tag{9.182}$$

in which τ_w is the wall shear stress.

Remarks

- The displacement and momentum thicknesses can geometrically-physically be interpreted:

  – Let us write $(9.179)_1$ in the form

$$\tilde{u}_w\left(\lim_{h \to \infty}\left(h - \delta^*\right)\right) = \lim_{h \to \infty}\int_0^h u(x, y)\mathrm{d}y. \tag{9.183}$$

  This equation states that δ^* is the distance, by which the surface would have to be moved in the direction perpendicular to the approaching velocity $\tilde{u}_w$ and away from the reference plane in an inviscid fluid stream of speed $\tilde{u}_w$ to give the same flow rate (volume flux) as does occur between the surface and the reference surface in a real fluid.
  – The difference of the momentum flux of both the outer (potential) flow and the corresponding viscous flow between $y = 0$ and $y = h$ is given by

$$\Delta(\text{momentum flow}) = \rho\int_0^h \left(u\tilde{u}_w - u^2\right)\mathrm{d}y$$

$$= \rho\tilde{u}_w^2\int_0^h \frac{u}{\tilde{u}_w}\left(1 - \frac{u}{\tilde{u}_w}\right)\mathrm{d}y$$

$$= \rho\tilde{u}_w^2\theta, \qquad \text{as } h \to \infty. \tag{9.184}$$

This result states that the modulus of the reduced momentum flux of the viscous flow compared with that of the inviscid flow at the mass flux of the viscous fluid corresponds for the former to a loss of momentum. This justifies the denotation *momentum 'loss' thickness* (Impuls*verlust*dicke) for θ, as it is denoted in German.

- An alternative form of the integrated momentum balance equation (9.182) can be written as follows:

$$U^2\theta' + 2UU'\theta + \delta^*UU' = \frac{\tau_w}{\rho}, \tag{9.185}$$

in which primes denote differentiation with respect to x and $\tilde{u}_w$ was replaced by U. If this equation is multiplied on both sides by $\theta/(\nu U)$, then

$$\frac{U\theta\theta'}{\nu} + \left(2 + \frac{\delta^*}{\theta}\right)\frac{U'\theta^2}{\nu} = \frac{\tau_w\theta}{\rho\nu U} \tag{9.186}$$

is obtained.

Application: Equation (9.182) can serve as basis for an approximate determination of the boundary layer thickness. This will now be demonstrated by use of the BLASIUS *boundary layer*. As above, we now select $\tilde{u}_w = U = $ const. so that (9.182) assumes the form

$$U^2\frac{\mathrm{d}\theta}{\mathrm{d}x} = \frac{\tau_w}{\rho}. \tag{9.187}$$

This equation would be an ordinary differential equation for θ if $\tau_w(\theta)$ would be known. To obtain such a relation for τ_w, a trial function for $u(x, y)$ is sought, e.g. here
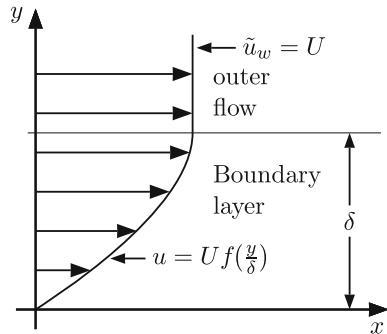
$$u(x, y) = \begin{cases} Uf\left(x, \dfrac{y}{\delta}\right), & y \leqslant \delta(x), \\ U, & y > \delta(x). \end{cases} \tag{9.188}$$

For the BLASIUS boundary layer f is independent of the x-coordinate: $f = f(y/\delta)$. The boundary conditions, which have to be posed for f, are easily 'guessed' with the aid of **Fig. 9.28**,

$$f(0) = 0, \quad f(1) = 1, \quad f'(1) = 0. \tag{9.189}$$

Further smoothness requirements at the outer edge of the boundary layer could also be required, e.g., $f''(1) = f'''(1) = \cdots = 0$. Moreover, f can be subjected to 'wall conditions', which can be derived from the boundary layer equations. For instance one has

Fig. 9.28 Boundary layer and constant outer flow for the steady BLASIUS layer

$$\nu \frac{\partial^2 u}{\partial y^2}\bigg|_{y=0} = -\tilde{u}_w \frac{\mathrm{d}\tilde{u}_w}{\mathrm{d}x},$$

which, for the BLASIUS boundary layer, reduces to $f''(0) = 0$ (since $\mathrm{d}\tilde{u}_w/\mathrm{d}x = 0$). A trial function, which satisfies (9.189), is given by

$$f(\eta) = 2\eta - \eta^2, \qquad \eta := \frac{y}{\delta}. \tag{9.190}$$

With this function, one obtains from the definition (9.179)$_2$

$$\theta = \delta \int_0^1 f(1-f)\mathrm{d}\eta$$

$$= \delta \int_0^1 (2\eta - \eta^2)(1 - 2\eta + \eta^2)\mathrm{d}\eta = \frac{2}{15}\delta. \tag{9.191}$$

Analogously,

$$\delta^* = \delta \int_0^1 (1 - f)\mathrm{d}\eta = \delta \int_0^1 (1 - 2\eta + \eta^2)\mathrm{d}\eta = \frac{1}{3}\delta. \tag{9.192}$$

The wall shear stress is now given by

$$\frac{\tau_w}{\rho} = \nu \frac{\partial u}{\partial y}\bigg|_0 = \frac{\nu U}{\delta} f'(0) \stackrel{(9.190)}{=} \frac{2\nu U}{\delta}. \tag{9.193}$$

With the relations (9.191)–(9.193) the boundary layer momentum balance (9.182) takes the form

Table 9.1 Functions $f(y/\delta) = f(\eta)$ with corresponding boundary values at $\eta = 0$ and $\eta = 1$ for the integrations (9.191)$_1$ and (9.192)$_1$

$f(\eta)$	Boundary values
η	$f(0) = 0, f(1) = 1$
$2\eta - \eta^2$	$f(0) = 0, f(1) = 1, f'(1) = 0$
$\frac{3}{2}\eta - \frac{1}{2}\eta^3$	$f(0) = f''(0) = 0$
	$f(1) = 1, f'(1) = 0$
$2\eta - 2\eta^3 + \eta^4$	$f(0) = f''(0) = 0$
	$f(1) = 1, f'(1) = f''(1) = 0$
$\sin\left(\dfrac{\pi\eta}{2}\right)$	$f(0) = f''(0) = 0$
	$f(1) = 1, f'(1) = 0$

$$\frac{2}{15}U^2\frac{\mathrm{d}\delta}{\mathrm{d}x} = \frac{2\nu U}{\delta} \quad \longrightarrow \quad \frac{\mathrm{d}\left(\delta^2\right)}{\mathrm{d}x} = \frac{30\nu}{U}. \tag{9.194}$$

This differential equation must be solved subject to the initial condition

$$\delta = 0, \quad \text{for} \quad x = 0. \tag{9.195}$$

It possesses the solution

$$\delta = \sqrt{30}\sqrt{\frac{\nu}{U}}\sqrt{x} = \sqrt{30}\frac{x}{\sqrt{\mathbb{R}_x}}, \quad \mathbb{R}_x = \frac{Ux}{\nu}. \tag{9.196}$$

Back substitution into the formula for the wall shear stress (9.193) yields for the drag coefficient c_f

$$c_f = \frac{\tau_w}{\frac{\rho}{2}U^2} = \frac{2\nu U}{\frac{1}{2}U^2\delta} = \frac{4\nu U}{U^2\sqrt{30}\sqrt{\nu/U}\sqrt{x}} = \frac{4}{\sqrt{30}}\frac{\nu}{U\ell}\sqrt{\frac{U\ell}{\nu}}\sqrt{\frac{\ell}{x}}$$

$$= 0.73\frac{(x/\ell)^{-1/2}}{\sqrt{\mathbb{R}_\ell}} = 0.73\frac{1}{\sqrt{\mathbb{R}_x}}, \quad \mathbb{R}_\ell = \frac{U\ell}{\nu}. \tag{9.197}$$

The exact value of the coefficient 0.73 is 0.664, see **Table 9.2**[13], below.

The above computations have been conducted for various trial functions and boundary conditions as shown in **Tables 9.1** and 9.2[13] (**Fig. 9.29**).

---

[13]K.H. found in 1988 these tables in handwritten pencil lecture notes of Prof. E. Becker (1929–1984), but was not able to identify the sources.

Table 9.2 Values of $\delta^*\sqrt{U/(\nu x)}$, $c_f\sqrt{\mathbb{R}_x}$ and δ^*/θ for different choices of $f(\eta)$

$f(\eta)$	$\delta^*\sqrt{\dfrac{U}{\nu x}}$	$c_f\sqrt{\mathbb{R}_x}$	δ^*/θ
η	1.732	0.578	3.00
$2\eta - \eta^2$	1.827	0.73	2.50
$\frac{3}{2}\eta - \frac{1}{2}\eta^3$	1.740	0.646	2.70
$2\eta - 2\eta^3 + \eta^4$	1.752	0.686	2.55
$\sin\left(\dfrac{\pi\eta}{2}\right)$	1.741	0.654	2.66
exact	1.729	0.664	2.61

9.8.2 Holstein-Bohlen Procedure

The above sketched computational procedure has been systematically improved. The idea goes back to THEODORE VON KÁRMÁN, and the details have been worked out by KARL POHLHAUSEN[14] [29]. Here, the procedure of H. HOLSTEIN and T. BOHLEN [17] is outlined. Let us start with the Eq. (9.185), here written in the form

$$U^2\frac{\mathrm{d}\theta}{\mathrm{d}x} + \left(2\theta + \delta^*\right)U\frac{\mathrm{d}U}{\mathrm{d}x} = \frac{\tau_w}{\rho}. \tag{9.198}$$

The velocity profile is assumed in the form

$$\frac{u}{U} =: f(\eta) = \begin{cases} a\eta + b\eta^2 + c\eta^3 + d\eta^4, & 0 \leqslant \eta \leqslant 1, \\ 1, & \eta > 1 \end{cases} \tag{9.199}$$

with yet undetermined coefficients a, b, c, d. These follow from the boundary conditions

$$\left.\begin{array}{l} y = 0, \qquad u = 0, \qquad\qquad\qquad \text{(already satisfied)} \\ \qquad\qquad \nu\dfrac{\partial^2 u}{\partial y^2} = -U\dfrac{\mathrm{d}U}{\mathrm{d}x}, \qquad \text{(condition at the wall)} \\ y = \delta, \qquad u = U, \quad \dfrac{\partial u}{\partial y} = 0, \quad \dfrac{\partial^2 u}{\partial y^2} = 0. \end{array}\right\} \tag{9.200}$$

If the conditions $(9.200)_{3,4,5}$ are substituted in (9.199), then the equations

$$\begin{aligned} a + b + c + d &= 1, \\ a + 2b + 3c + 4d &= 0, \\ 2b + 6c + 12d &= 0 \end{aligned} \tag{9.201}$$

---

[14]For a short biography of KARL POHLHAUSEN see Fig. 9.19.
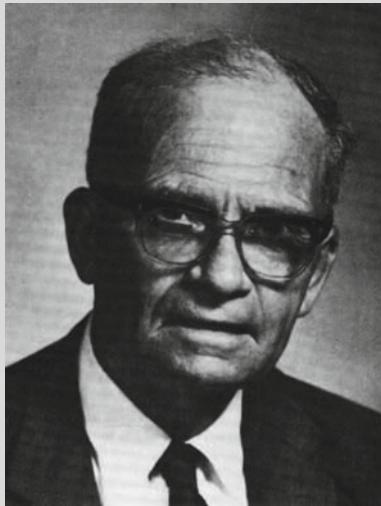
Fig. 9.29 KARL POHLHAUSEN (20. May 1890–18. Nov. 1980)

KARL POHLHAUSEN was an applied mathematician with education at the Universities of
Jena and Göttingen. The supervisor of his doctoral work was LUDWIG PRANDTL, to whom
he submitted a thesis on the experimental verification of the boundary layer theory with
graduation in 1919. He joined THEODORE VON KÁRMÁN who had just assumed the chair
of mechanics at the 'Technische Hochschule' in Aachen, where they published significant
work on the boundary layer theory. In 1922 POHLHAUSEN joined the company 'Siemens-
Schuckert' in Berlin where he was assigned work in electricity but left Germany in 1946
for the USA. During the following 20 years he was with the Office of Air Force, the Flight
Research Laboratory, and the Aeronautical Research Laboratory at Wright Field. He died
on 18 Nov. 1980.

According to [12] 'POHLHAUSEN's reputation as a legendary figure in fluid mechanics is
based on his 1921-article [29] in volume 1 of *Zeitschrift für Angewandte Mathematik und
Mechanik*, ZAMM. This paper includes the first proof that the PRANDTL boundary layer
equations are asymptotic forms of the NAVIER-STOKES equations for large REYNOLDS num-
bers; it demonstrates that the VON KÁRMÁN momentum equation can be derived from the
boundary layer equation by a simple integration; it introduces the smoothing conditions at
the outer edge of the boundary layers; and it points to the differences between the inner and
outer expansions.

Text and Photo from '*Hydraulicians in Europe 1800–2000*'. Vol. 2, IAHR, CRC Press,
Taylor and Francis (2009)' [13]
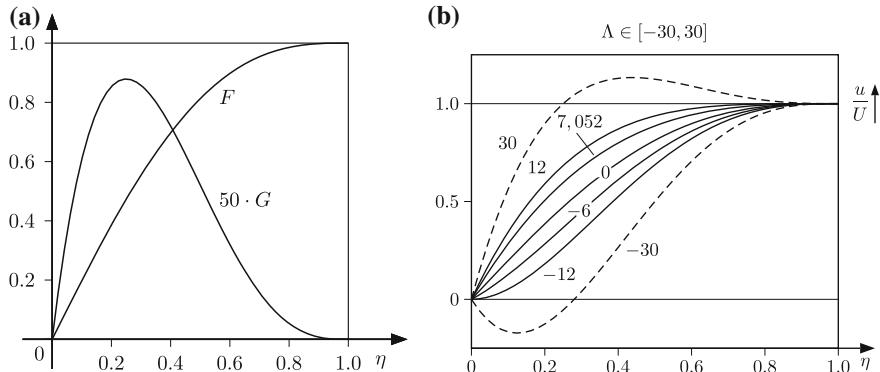
Fig. 9.30 Graphs for the functions $F(\eta)$, $G(\eta)$ (**a**) and $f(\eta)$ (**b**), with the functions defined in (9.205)

are obtained. From $(9.200)_2$ there follows

$$\frac{\nu U}{\delta^2} 2b = -U \frac{\mathrm{d}U}{\mathrm{d}x} \quad \longrightarrow \quad b = -\frac{1}{2} \frac{\delta^2}{\nu} \frac{\mathrm{d}U}{\mathrm{d}x} = -\frac{\Lambda}{2}, \tag{9.202}$$

with

$$\Lambda := \frac{\delta^2}{\nu} \frac{\mathrm{d}U}{\mathrm{d}x}, \tag{9.203}$$

known as '*form parameter*'. Solving (9.201)–(9.203) yields

$$a = 2 + \frac{\Lambda}{6}, \quad b = -\frac{\Lambda}{2}, \quad c = -2 + \frac{\Lambda}{2}, \quad d = 1 - \frac{\Lambda}{6}, \tag{9.204}$$

so that

$$\frac{u}{U} =: f(\eta) = \left(2\eta - 2\eta^3 + \eta^4\right) + \Lambda \frac{1}{6} \left(\eta - 3\eta^2 + 3\eta^3 - \eta^4\right),$$
$$= F(\eta) + \Lambda G(\eta), \quad 0 \leqslant \eta \leqslant 1. \tag{9.205}$$

Figure 9.30 shows $F(\eta)$ and $G(\eta)$ in the interval $0 \leqslant \eta \leqslant 1$. F is monotonically increasing from $\eta = 0$ to 1. By contrast, $G(0) = 0$, $G(1) = 0$ and $G(\eta) > 0$ for all $\eta \in (0, 1)$ with a maximum $50 \times G_{\max} \approx 0.8765$ at $x \approx 0.2661$. Panel (**b**) of Fig. 9.30 displays the distribution of $f(\eta)$ for the indicated values of Λ. The graph shows that

- for $\Lambda = -12$ the profile $f(\eta)$ shows a horizontal tangent at $\eta = 0$, a turning point!
- Values of $f(\eta)$ for $-12 < \Lambda < 12$ lie in the interval $0 < f(\eta) < 1$ for all $\eta \in (0, 1)$ (solid lines).

- Curves for $\Lambda < -12$ show negative values of u, and those for $\Lambda > 12$ display overshooting ($u > U$) (dashed in the panel for $\Lambda = +30$). For this case, these analytical solutions do not represent realistic flows, because such flows are likely unstable and unsteady.

The computations must, therefore, be restricted to values $-12 < \Lambda < +12$.

The next steps concern the evaluation of δ^*, θ, τ_w. These computations are elementary and listed in the literature, e.g., [36] and thus, only their results are stated:

$$\delta^* = \delta \int_0^1 (1 - F(\eta) - \Lambda G(\eta))\, d\eta = \delta \left(\frac{3}{10} - \frac{\Lambda}{120} \right),$$

$$\theta = \delta \int_0^1 (F(\eta) + \Lambda G(\eta))\, (1 - F(\eta) - \Lambda G(\eta))\, d\eta$$

$$= \delta \left(\frac{37}{315} - \frac{\Lambda}{945} - \frac{\Lambda^2}{9072} \right), \tag{9.206}$$

$$\frac{\tau_w}{\rho} = \nu \left. \frac{\partial u}{\partial y} \right|_{y=0} = \frac{\nu U}{\delta} f'(0) \quad \longrightarrow \quad \frac{\tau_w \delta}{\rho \nu U} = 2 + \frac{\Lambda}{6}.$$

Substitution of these expressions into the momentum balance (9.198) would yield a differential equation, which could be integrated. It is, however, easier to employ (9.198), which is now written as

$$\frac{U}{\nu} \theta \frac{d\theta}{dx} + \left(2 + \frac{\delta^*}{\theta} \right) \frac{1}{\nu} \frac{dU}{dx} \theta^2 = \frac{\tau_w \theta}{\nu \rho U}, \tag{9.207}$$

which can be interpreted as an equation for the determination of Λ. Indeed, if one sets

$$\kappa := \frac{\theta^2}{\nu} \frac{dU}{dx}, \tag{9.208}$$

one may derive, with the aid of (9.203) and (9.206), the relation

$$\frac{\kappa}{\Lambda} = \frac{\theta^2}{\delta^2} = \left\{ \frac{37}{315} - \frac{\Lambda}{945} - \frac{\Lambda^2}{9072} \right\}^2. \tag{9.209}$$

Moreover, with (9.206),

$$\frac{\delta^*}{\theta} = \frac{\dfrac{3}{10} - \dfrac{\Lambda}{120}}{\dfrac{37}{315} - \dfrac{\Lambda}{945} - \dfrac{\Lambda^2}{9072}} = f_1(\kappa), \tag{9.210}$$

$$\frac{\tau_w \theta}{\rho \nu U} = \left(2 + \frac{\Lambda}{6}\right)\frac{\theta}{\delta} = \left(2 + \frac{\Lambda}{6}\right)\left(\frac{37}{315} - \frac{\Lambda}{945} - \frac{\Lambda^2}{9072}\right) = f_2(\kappa).$$

Note that (9.209) implies that κ can be viewed as a function of Λ ($\kappa = \kappa(\Lambda)$) or vice versa ($\Lambda = \Lambda(\kappa)$). Therefore, also $f_{1,2}(\kappa)$ are such functions.

Substitution of (9.208)–(9.210) into (9.207) leads to the equation

$$\frac{U}{\nu}\theta\frac{\mathrm{d}\theta}{\mathrm{d}x} + (2 + f_1(\kappa))\,\kappa = f_2(\kappa). \tag{9.211}$$

Introducing the abbreviation

$$\frac{\theta^2}{\nu} =: Z \quad \longrightarrow \quad \frac{2\theta}{\nu}\frac{\mathrm{d}\theta}{\mathrm{d}x} = \frac{\mathrm{d}Z}{\mathrm{d}x}. \tag{9.212}$$

This, finally, transforms (9.211) into

$$\frac{\mathrm{d}Z}{\mathrm{d}x} = 2\frac{f_2(\kappa) - (2 + f_1(\kappa))\kappa}{U} = \frac{\mathbb{F}(\kappa)}{U}, \tag{9.213}$$

$$\kappa = Z\frac{\mathrm{d}U}{\mathrm{d}x},$$

in which the definition of κ, (9.208), has been added. Equations (9.213) are the two fundamental equations of the HOLSTEIN-BOHLEN integration procedure. Note that $f_1(\kappa)$, $f_2(\kappa)$ and $\mathbb{F}(\kappa)$ are 'universal' functions, i.e., they are independent of the velocity distribution $U(x)$. They are given in tabulated form e.g. by H. SCHLICHTING and K. GERSTEN [36].

In most situations the integration starts at the stagnation point of the circumflown body, where

$$U_0 = 0, \quad \left.\frac{\mathrm{d}U}{\mathrm{d}x}\right|_0 \neq 0,$$

in which the subscript '0' stands for values at the stagnation point. To avoid a singularity in (9.213)$_1$ this implies initially that $\mathbb{F}(\kappa)|_0 = 0$ or, with the aid of (9.209) and (9.210),

$$f_2(\kappa_0) - (2 + f_1(\kappa_0))\kappa_0 = 0$$

$$\longrightarrow \left(2 + \frac{\Lambda_0}{6}\right)\left(\frac{37}{315} - \frac{\Lambda_0}{945} - \frac{\Lambda_0^2}{9072}\right)$$

$$- \left(2 + \frac{\dfrac{3}{10} - \dfrac{\Lambda_0}{120}}{\dfrac{37}{315} - \dfrac{\Lambda_0}{945} - \dfrac{\Lambda_0^2}{9072}}\right)\left(\frac{37}{315} - \frac{\Lambda_0}{945} - \frac{\Lambda_0^2}{9072}\right)^2 \Lambda_0 = 0.$$

This is a polynomial equation for Λ with the real positive solution

$$\Lambda = \Lambda_0 = 7.052 \quad \text{implying via (9.206)} \quad \kappa = \kappa_0 = 0.077, \qquad (9.214)$$

and after back substitution into (9.212), (9.213)$_2$

$$Z_0 = \frac{\kappa_0}{(\mathrm{d}U/\mathrm{d}x)\,|_0} = \frac{0.077}{(\mathrm{d}U/\mathrm{d}x)\,|_0} \quad \text{and} \quad \theta_0^2 = \frac{0.077\nu}{(\mathrm{d}U/\mathrm{d}x)\,|_0}. \qquad (9.215)$$

This provides an initial value for Z in (9.213)$_2$, but integration is still complicated since $\mathbb{F}(\kappa_0)/U_0 = 0/0$. Application of the rule of BERNOULLI-HOSPITAL yields

$$\left.\frac{\mathbb{F}}{U}\right|_0 = \left.\frac{(\mathrm{d}\mathbb{F}/\mathrm{d}\kappa)(\mathrm{d}\kappa/\mathrm{d}x)}{(\mathrm{d}U/\mathrm{d}x)}\right|_0 \qquad \left(= \left.\frac{\mathrm{d}Z}{\mathrm{d}x}\right|_0\right).$$

Now, owing to (9.208),

$$\left.\frac{\mathrm{d}\kappa}{\mathrm{d}x}\right|_0 = \left.\left(\frac{2\theta}{\nu}\underbrace{\frac{\mathrm{d}\theta}{\mathrm{d}x}}_{=0}\frac{\mathrm{d}U}{\mathrm{d}x} + \frac{\theta^2}{\nu}\frac{\mathrm{d}^2U}{\mathrm{d}x^2}\right)\right|_0$$

<div align="center"><small>at stagnation point</small></div>

$$= \left.\frac{\theta^2}{\nu}\frac{\mathrm{d}^2U}{\mathrm{d}x^2}\right|_0 = \left.\kappa\,\frac{(\mathrm{d}^2U/\mathrm{d}x^2)}{(\mathrm{d}U/\mathrm{d}x)}\right|_0,$$

so that

$$\left.\frac{\mathrm{d}Z}{\mathrm{d}x}\right|_0 = \left.\frac{\mathbb{F}}{U}\right|_0 = \left.\frac{(\mathrm{d}\mathbb{F}/\mathrm{d}\kappa)\kappa(\mathrm{d}^2U/\mathrm{d}x^2)}{(\mathrm{d}U/\mathrm{d}x)^2}\right|_0 = \left.-0.0625\,\frac{(\mathrm{d}^2U/\mathrm{d}x^2)}{(\mathrm{d}U/\mathrm{d}x)^2}\right|_0. \quad (9.216)$$

With this value of $(\mathbb{F}/U)|_0$ the integration of (9.213) can be started. For some problems (e.g., the steady boundary layers for a wedge and the plate) the initial conditions are simply $Z = 0$ and $\kappa = 0$.

As an example, take the *plane plate* (the BLASIUS boundary layer), for which

$$U = \text{constant}, \quad \frac{\mathrm{d}U}{\mathrm{d}x} = 0, \quad \overset{(9.213)_2}{\longrightarrow} \quad \kappa = 0. \qquad (9.217)$$

Thus, $(9.213)_1$ is given by

$$Z' = \frac{\mathbb{F}(0)}{U} = 0.4698\frac{1}{U},$$

$$\longrightarrow Z = \frac{0.4698}{U}x,$$

$$\overset{(9.212)}{\longrightarrow} \theta = \sqrt{0.4698}\sqrt{\frac{\nu x}{U}} = \frac{0.686}{\sqrt{\mathbb{R}_x}}x \qquad (0.664 \text{ is exact}). \qquad (9.218)$$

The variables Z or θ can, approximately, also be determined by the following
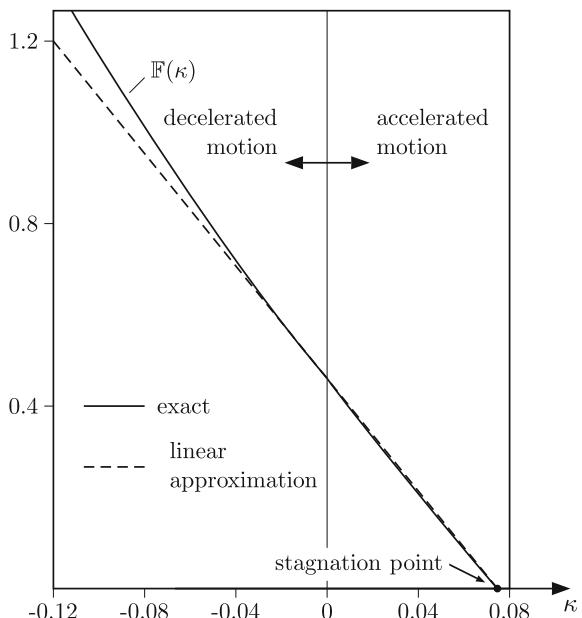
Quadrature formula of A. WALZ [44, 45]. This approximate formula is based on the fact that $\mathbb{F}(\kappa)$ as a function of κ can for small positive values of $\kappa > 0$ very well be approximated by the linear expression

$$\mathbb{F}(\kappa) \approx a - b\kappa, \qquad a = 0.47, \quad b = 6. \qquad (9.219)$$

For a corroboration of this fact, see **Fig. 9.31**. Therefore, according to $(9.213)_1$

$$U\frac{\mathrm{d}Z}{\mathrm{d}x} = a - b\kappa,$$

$$\rightarrow \frac{\mathrm{d}}{\mathrm{d}x}(UZ) - \frac{\mathrm{d}U}{\mathrm{d}x}Z \overset{(9.213)_2}{=} a - bZ\frac{\mathrm{d}U}{\mathrm{d}x},$$

$$\rightarrow \frac{\mathrm{d}}{\mathrm{d}x}(UZ) = a - (b-1)(UZ)\frac{\mathrm{d}U/\mathrm{d}x}{U}. \qquad (9.220)$$

Fig. 9.31 Plot of the function $\mathbb{F}(\kappa)$ for $-0.12 < \kappa < 0.08$. *The dashed straight line displays the function* $\mathbb{F}(\kappa) = 0.47 - 6\kappa$ *and agrees excellently with the graph of the exact function* $\mathbb{F}(x)$

This is a linear ordinary differential equation for UZ, whose solution can directly be constructed, if it is recognized that $U^{(b-1)}$ is an integrating factor; indeed, (9.220) is equivalent to

$$\frac{\mathrm{d}}{\mathrm{d}x}\left(U^{b-1}UZ\right) = U^{b-1}a, \tag{9.221}$$

with the solution

$$UZ = \frac{a}{U^{b-1}}\int\limits_0^x U^{b-1}\mathrm{d}x + \text{constant}. \tag{9.222}$$

The constant of integration is determined by the initial condition at $x = 0$, namely

$$
\begin{aligned}
Z &= 0, \ \ \text{when } U(0) \neq 0 \ \ \longrightarrow \ \ \text{const.} = 0, \\
U &\sim x, \ \ \text{when } U(0) = 0 \ \ \longrightarrow \ \ \text{const.} = 0,
\end{aligned}
\tag{9.223}
$$

as can easily be inferred from (9.222). With the definition (9.212) for Z, this yields the WALZ quadrature formula,

$$\frac{U\theta^2}{\nu} = \frac{0.47}{U^5}\int\limits_0^x U^5\mathrm{d}x. \tag{9.224}$$

Remark: A. WALZ's quadrature formula can, with appropriate assumptions, also be derived from the boundary layer momentum equation (9.186). Indeed, if one sets

$$\frac{\delta^*}{\theta} = H = \text{const.}, \quad \tau_w = \alpha\frac{\nu\rho U}{\theta}, \quad \alpha = \text{const.}, \tag{9.225}$$

then, (9.186) can be transformed to

$$\frac{1}{2}U\frac{\mathrm{d}Z}{\mathrm{d}x} + (2 + H)\frac{\mathrm{d}U}{\mathrm{d}x}Z = \alpha,$$

or

$$U\frac{\mathrm{d}Z}{\mathrm{d}x} + n\frac{\mathrm{d}U}{\mathrm{d}x}Z = 2\alpha, \quad n := 4 + 2H, \tag{9.226}$$

in which $Z = \theta^2/\nu$ has also been used. Equation (9.226) possesses the solution

$$Z := \frac{\theta^2}{\nu} = \frac{2\alpha}{U^n} \int\limits_0^x U^{n-1} dx. \qquad (9.227)$$

For $2\alpha = 0.47$ and $n = 6$ this agrees with (9.224).

9.9 Non-stationary Boundary Layers

In this section the assumption of stationarity of the flow processes is abandoned, and rather non-steady plane boundary layers are studied. Such motions are primarily either impulsive starts from a state of rest or else periodic. Experience in analyzing steady boundary layer problems has thought us that a characteristic length, ℓ, characteristic velocity, U, and the kinematic viscosity ν are the parameters, which influence the flow behavior of a density preserving linearly viscous fluid via the dimensionless REYNOLDS number $\mathbb{R} = U\ell/\nu$. Because non-stationary processes involve the time as an independent variable, the above ℓ, U, ν must be complemented by a characteristic time t_R. These four variables can be combined to two dimensionless characteristic numbers (also called Π-products in dimensional analysis, see Chap. 20),

$$\mathbb{R} = \frac{U\ell}{\nu}, \qquad \mathbb{T}_R = \frac{t_R U}{\ell}.$$

In general, unsteady flow of a viscous fluid will, therefore, be characterized by two (or more) characteristic parameters

H. SCHLICHTING and K. GERSTEN [36] point at the following complexity arising in unsteady flow: 'Start-up processes of bodies in a fluid at rest are carried out so that directly after the motion starts, irrotational potential flow is at hand in the entire field, apart from a thin layer at the body. The thickness of the boundary layer then increases with time'. This will eventually lead to separation, whose time needs to be determined. 'When separation starts, the outer flow is considerably changed by the separating boundary layer. A clear division between the irrotational outer flow and the rotational separated boundary layer is then in general no longer possible. In these cases boundary layer theory, which requires a clearly defined layered structure in the flow, can no longer be applied. This [...] is true for all boundary layers with distinct separation' [36]. An illustrative situation is parallel flow across a fixed rigid body (cylinder, sphere, ...) by the fluid or wind.

The flow in the upstream region of the obstacle is basically uniform and steady; when passing the submerged body, a viscous boundary layer develops, which then leads to a separation. Beyond the point of separation, an alternating arrangement of vortices with opposite orientation of rotation then develops which rhythmically leave the body and travel in the wake of the body. In atmospheric flows such a VON KÁRMÁN *vortex street* may be generated in the lee of an island (see **Fig. 9.32**).

Fig. 9.32 Vortex sheet. *Satellite picture taken on 11. July 2010. The vortices are seen in the lee of the island Tristan da Cunha (British island in the South Atlantic).* http://www.deutscher-wetterdienst.de/lexikon/index.htm?ID=K&DAT=Karman-Wirbelstrasse

Such situations of destruction of the layered structure of a laminar flow will not be studied in the subsequent analysis. Therefore, in what follows, we shall only consider unsteady boundary layers without, or prior to, separation. Summaries of this sort are e.g. given by KEITH STEWARDSON [39] and NORMAN RILEY [33], TELIONIS [40] and others, see [36].

In two-dimensional flow the boundary layer equations are described by Eq. (9.35)$_{1,2}$,

$$\frac{\partial u}{\partial x} + \frac{\partial v}{\partial y} = 0, \tag{9.228}$$

$$\frac{\partial u}{\partial t} + u \frac{\partial u}{\partial x} + v \frac{\partial u}{\partial y} = -\frac{1}{\rho} \frac{\partial \tilde{p}_w}{\partial x} + \nu \frac{\partial^2 u}{\partial y^2}.$$

9.9.1 Impulsive Start from Rest

Consider a rigid body, completely immersed in a density preserving fluid, which at $t = 0^+$ is suddenly set in motion to a speed U kept constant for $t > 0$. In the first instant, the motion will be potential flow with a boundary layer growing with time along the body's surface until steady state is reached. A coordinate system is chosen which is rigidly fixed to the moving body. The wall is assumed to be sufficiently flat, and the coordinates x and y are, respectively, measured along and perpendicular to the wall.

Because the potential flow is stationary, its momentum equation has the form

$$-\frac{1}{\rho} \frac{\partial \tilde{p}_w}{\partial x} = \tilde{u}_w \frac{\mathrm{d}\tilde{u}_w}{\mathrm{d}x}, \tag{9.229}$$

so that the x-component of the boundary layer momentum equation (9.228)$_2$ takes the form

$$\frac{\partial u}{\partial t} + u \frac{\partial u}{\partial x} + v \frac{\partial u}{\partial y} = \tilde{u}_w \frac{\mathrm{d}\tilde{u}_w}{\mathrm{d}x} + \nu \frac{\partial^2 u}{\partial y^2}, \tag{9.230}$$

in which the pressure gradient $\partial \tilde{p}_w / \partial x$ has now been eliminated. It is intuitively clear that for very small times $t > 0$ the thickness of the boundary layer must be small so that

$$\left| \nu \frac{\partial^2 u}{\partial y^2} \right| \gg \tilde{u}_w \frac{\mathrm{d}\tilde{u}_w}{\mathrm{d}x}.$$

Moreover, the convective terms on the left-hand side of (9.230) are likely also small and can to lowest order also be neglected. So, (9.230) reduces in first approximation to

$$\frac{\partial u}{\partial t} = \nu \frac{\partial^2 u}{\partial y^2}. \tag{9.231}$$

Incidentally, this limit equation can be justified by a scale analysis. Indeed, with the non-dimensionalizations $(u, v) = (Uu^*, (H/L)Uv^*)$, $(x, y) = (Lx^*, Hy^*)$ and $t = (H/U)t^*$ the dimensionless counterpart of (9.230) is given by

$$\frac{\partial u^*}{\partial t^*} - \frac{1}{\mathbb{R}} \frac{\partial^2 u^*}{\partial y^{*2}} = \varepsilon \left(\tilde{u}_w^* \frac{\mathrm{d}\tilde{u}_w^*}{\mathrm{d}x^*} - u^* \frac{\partial u^*}{\partial x^*} - v^* \frac{\partial u^*}{\partial y^*} \right), \tag{9.232}$$

where

$$\mathbb{R} := \frac{UH}{\nu}, \qquad \varepsilon = \frac{H}{L} \ll 1. \tag{9.233}$$

In the boundary layer, the velocity field must satisfy the following initial and boundary conditions:

$$u(x, y, 0) = \tilde{u}_w(x), \qquad \text{for } y > 0, \tag{9.234}$$

$$\left. \begin{array}{l} u(x, 0, t) = 0, \\ v(x, 0, t) = 0, \\ u(x, \infty, t) = \tilde{u}_w(x), \end{array} \right\} \qquad \text{for } t > 0.$$

The initial boundary value problem (9.231), (9.234) has been presented in Chap. 8 Sect. 8.3.2 and the result is as follows:

$$u = u_1 = \tilde{u}_w(x) \frac{2}{\sqrt{\pi}} \int_0^\eta \exp(-\overline{\eta}^2) \mathrm{d}\overline{\eta} = \tilde{u}_w(x)\mathrm{erf}(\eta), \qquad \eta = \frac{y}{2\sqrt{\nu t}}. \tag{9.235}$$

The corresponding transverse velocity component v_1 is obtained by use of the continuity equation,

$$\frac{\partial v_1}{\partial y} = -\frac{\partial u_1}{\partial x} = -\frac{d\tilde{u}_w}{dx}\,\mathrm{erf}(\eta),$$

and its integration with respect to y,

$$
\begin{aligned}
v_1 &= -2\sqrt{\nu t}\,\frac{d\tilde{u}_w}{dx}\int_0^\eta \mathrm{erf}(\bar{\eta})d\bar{\eta} \\
&\stackrel{*}{=} -2\sqrt{\nu t}\,\frac{d\tilde{u}_w}{dx}\left\{\eta\,\mathrm{erf}(\eta) - \frac{1}{\sqrt{\pi}}\left(1 - \exp(-\eta^2)\right)\right\},
\end{aligned}
\tag{9.236}
$$

where in the step '$\stackrel{*}{=}$' integration by parts has been used.

With growing time, the flow in the boundary layer deviates from the solution (9.235), (9.236). The next, improved, approximation is obtained by employing the full equation (9.230) and substituting the first order solution (9.235), (9.236) in the convective terms. With $u = u_1 + u_2$ this yields

$$\frac{\partial u_2}{\partial t} - \nu\frac{\partial^2 u_2}{\partial y^2} = \tilde{u}_w\frac{d\tilde{u}_w}{dx} - u_1\frac{\partial u_1}{\partial x} - v_1\frac{\partial u_1}{\partial y}.\tag{9.237}$$

[This corresponds to a second order regular perturbation expansion in solving (9.232)]. The velocity field u_2 must satisfy the initial and boundary conditions

$$
\begin{aligned}
u_2(x, y, 0) &= 0, \\
u_2(x, 0, t) &= 0, \\
u_2(x, \infty, t) &= 0.
\end{aligned}
\tag{9.238}
$$

Substitution of (9.235) and (9.236) into (9.237) yields the differential equation

$$\frac{\partial u_2}{\partial t} - \nu\frac{\partial^2 u_2}{\partial y^2} = \tilde{u}_w\frac{d\tilde{u}_w}{dx}\varphi(\eta),\tag{9.239}$$

$$\varphi(\eta) = 1 - (\mathrm{erf}(\eta))^2 + \frac{2}{\sqrt{\pi}}\exp\left(-\eta^2\right)\int_0^\eta \mathrm{erf}(\bar{\eta})d\bar{\eta}.$$

The solution of this inhomogeneous differential equation can successfully be obtained with the ansatz

$$u_2 = \tilde{u}_w\frac{d\tilde{u}_w}{dx}t f(\eta).\tag{9.240}$$

It leads to the following derivative expressions:

$$\frac{\partial u_2}{\partial t} = \tilde{u}_w \frac{d\tilde{u}_w}{dx} \left\{ f - \frac{1}{2}\eta f' \right\}, \tag{9.241}$$

$$\frac{\partial^2 u_2}{\partial y^2} = \tilde{u}_w \frac{d\tilde{u}_w}{dx} t \frac{f''}{4\nu t} = \tilde{u}_w \frac{d\tilde{u}_w}{dx} \frac{f''}{4\nu},$$

which, when substituted into (9.237) and (9.238), results in the following ordinary differential equation boundary value problem

$$f - \frac{\eta}{2} f' - \frac{1}{4} f'' = \varphi(\eta), \quad 0 < \eta < \infty, \tag{9.242}$$

$$f(0) = 0, \quad f(\infty) = 0.$$

Once this boundary value problem is solved, the component of the velocity to second order is given by

$$u = u_1 + u_2 = \tilde{u}_w \left(\operatorname{erf}(\eta) + t \frac{d\tilde{u}_w}{dx} f(\eta) \right). \tag{9.243}$$

The integration of (9.242) yields the graphs of $\operatorname{erf}(\eta)$ and $f(\eta)$ in **Fig. 9.33**. For $\eta > 0$ the functions $\operatorname{erf}(\eta)$ and $f(\eta)$ are positive, f' assumes its maximum at $\eta = 0$. This means that u in (9.243) changes its sign with the sign of $d\tilde{u}_w/dx$. Separation will therefore occur, if $d\tilde{u}_w/dx < 0$. Return flow is introduced at the wall, and the *critical region of separation* is given by

$$\left. \frac{\partial u}{\partial y} \right|_{y=0} = 0, \quad \xrightarrow{(9.243)} \quad \underbrace{(\operatorname{erf}(\eta))'\big|_{\eta=0}}_{2/\sqrt{\pi}} + t \frac{d\tilde{u}_w}{dx} f'(0) = 0, \tag{9.244}$$

Fig. 9.33 The functions $\operatorname{erf}(\eta)$ and $f(\eta)$ [which is the solution of (9.242)], plotted against η
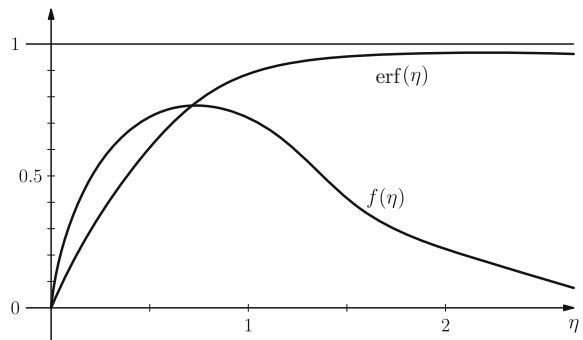
Fig. 9.34 The function $u/\tilde{u}_w(y)$ [see (9.242) and (9.243)] plotted for different times. The lowest curve has $(\mathrm{d}u/\mathrm{d}y)|_{y=0}$, thus a horizontal tangent at the wall
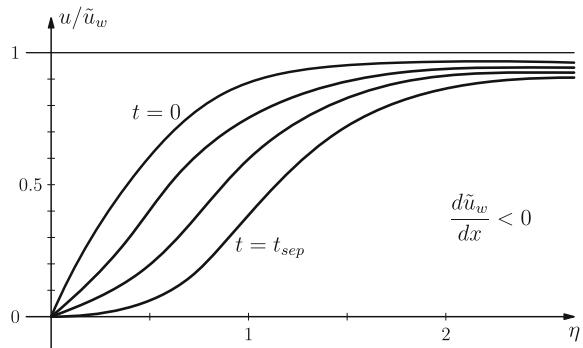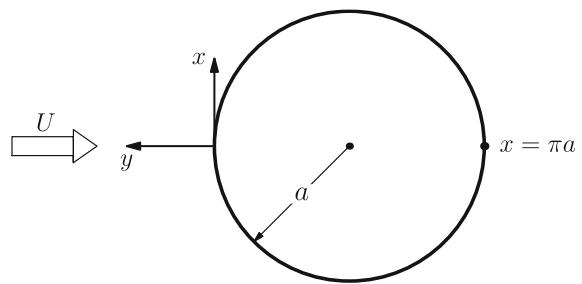
Fig. 9.35 Parallel flow around a circular cylinder. *The potential flow generates the boundary velocity gradient* $\mathrm{d}\tilde{u}_w/\mathrm{d}x = 2(U/a)\cos(x/a)$, *with minimum* (9.247)

which, when solved for t, gives the separation time,

$$t_{\text{sep.}} = -\frac{2}{\sqrt{\pi}}\frac{1}{f'(0)}\frac{1}{\mathrm{d}\tilde{u}_w/\mathrm{d}x} = -\frac{0.7}{\mathrm{d}\tilde{u}_w/\mathrm{d}x}. \tag{9.245}$$

The instant of the separation is indicated in **Fig. 9.34**.

As an example consider a circular cylinder of radius a in a parallel flow of speed U, **Fig. 9.35**, for which the wall-near flow velocity is given by

$$\tilde{u}_w = 2U\sin(x/a), \tag{9.246}$$

the gradient $|\mathrm{d}\tilde{u}_w/\mathrm{d}x|$ reaches its maximum at $x = \pi a$ so that

$$\left.\frac{\mathrm{d}\tilde{u}_w}{\mathrm{d}x}\right|_{x=\pi a} = -\frac{2U}{a}, \tag{9.247}$$

which yields, according to (9.245), $t_{\text{sep}} = 0.35(a/U)$.

The above solution construction has already been given by HEINRICH BLASIUS in 1908 [4]. The trial solution (9.240) has, according to NORMAN RILEY [33], been extended by a second, t^2-term by S. GOLDSTEIN and L. ROSENHEAD [11] and by the next five terms by W.M. COLINS and S.C.R. DENNIS in 1973 [8]. 'From these solutions it is possible to estimate the time and location at which it is possible to

estimate the time and location at which separation, characterized by the vanishing of the surface shear stress, takes place. For a circular cylinder of radius a, separation commences at the rear stagnation point at the estimated time $0.32(a/U)$, which is independent of ν [and close to the value $0.35(a/U)$, obtained by BLASIUS]'.

NORMAN RILEY further states that 'series of the type

$$u_N = \sum_{n=1}^{N} \tilde{u}_w \frac{\mathrm{d}\tilde{u}_w}{\mathrm{d}x} t^n f_n(\eta),$$
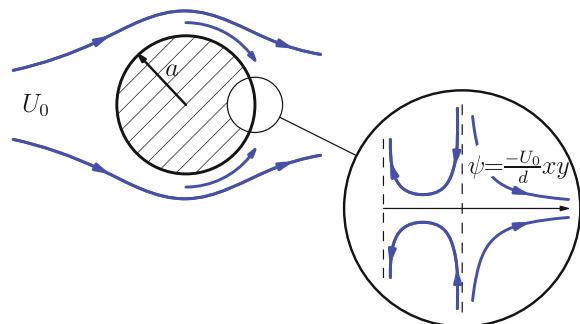
used in [4, 8, 11], can only be valid for a limited time'. Of equal, if not larger, importance is the behavior of the solution at the rear stagnation point for large times, i.e., the character of the boundary layer as it 'lifts-off' from the rear stagnation point and becomes wildly unsteady, such that the notion of a thin boundary layer embedded within an inviscid flow fails. However, NORMAN RILEY draws attention to 'a very important paper by PROUDMAN and JOHNSON [31] (the work later to be developed by ROBBIN and HOWARTH [34]), [who] demonstrate that this need not be the case. They argue that a reversal in sign of the shear stress at $y = 0$ does not signify a breakaway [of the fluid], and they envisage a situation including flow reversal, as shown in **Fig. 9.36**, in which there is a thin layer close to the boundary layer, embedded in the potential flow appropriate to a rear stagnation point, in which the boundary layer equations hold *for all finite times*', [33].

'The method of analyzing the flow in this layer is analogous to that for a forward stagnation point. The variables are made dimensionless by writing

$$\bar{x} = \frac{x}{d}, \quad \bar{y} = \sqrt{\frac{U}{\nu a}}y, \quad \bar{t} = \frac{Ut}{a}, \tag{9.248}$$
$$\psi = -2\sqrt{\nu a U}\,\bar{x}\,f(\bar{y}, t),$$

in which ψ is the stream function'. With this choice the continuity equation is identically satisfied and the two-dimensional NS-equations reduce to

Fig. 9.36 Unsteady flow in the neighborhood of a rear stagnation point. After NORMAN RILEY [33]

$$f_{\bar{y}\bar{t}} = f_{\bar{y}\bar{y}\bar{y}} - f\,f_{\bar{y}\bar{y}} - 1 + (f_{\bar{y}})^2 \tag{9.249}$$

subject to the boundary and initial conditions

$$\left.\begin{array}{ll} f = f_{\bar{y}} = 0 & \text{on } \bar{y} = 0 \;\; t \neq 0, \\ f_{\bar{y}} \to 1 & \text{as } \bar{y} \to \infty, \\ f_{\bar{y}} = 1 & \text{at } t = 0, \;\; \bar{y} > 0. \end{array}\right\} \tag{9.250}$$

'For small values of $\bar{t}$ the solution of this initial-boundary-value problem has orig-inally been developed by HEINRICH BLASIUS as discussed between (9.231) and (9.247). PROUDMAN and JOHNSON [31] and subsequently ROBINS and HOWARTH [34] developed asymptotic solutions of the equation for f for large $\bar{t}$, and also pur-sued the solution of that equation by numerical methods. PROUDMAN and JOHNSON argue that at large times, away from the immediate neighborhood of the wall, viscous forces will be unimportant in the rotational layer. They find a similarity solution for (9.249), (9.250) by writing

$$f = \exp(\bar{t})F(\eta), \qquad \eta = \bar{y}\,\exp(-\bar{t}) \tag{9.251}$$

which, upon substitution in (9.249), and on neglecting exponentially small terms as $\bar{t} \to \infty$, gives the equation for F,

$$(F - \eta)\,F'' + 1 - (F')^2 = 0, \tag{9.252}$$
$$F(0) = 0, \qquad F'(\infty) = 1.$$

In (9.252), since the viscous terms are of higher order than those retained, the no-slip condition has been ignored. The inviscid rotational *outer* solution is thus obtained as

$$F = \eta - \frac{2}{c}\,(1 - \exp(-c\eta)) \tag{9.253}$$

[the reader may easily verify this], where the unknown constant c corresponds to an uncertainty in the origin of time. As $\eta \to 0$, (9.253) shows [by Taylor series expansion] that $F \sim -\bar{y}$. Thus, [...] the no slip condition is not satisfied', [33].

NORMAN RILEY continues: 'ROBINS and HOWARTH complete the solution [of (9.249)] by writing

$$f = \phi(\bar{y}) + \mathcal{O}\left(\exp(-\bar{t})\right), \tag{9.254}$$

so that ϕ satisfies

$$\phi''' - \phi\,\phi'' - 1 + (\phi')^2 = 0, \tag{9.255}$$

with

$$\phi(0) = 0 = \phi'(0) = 0, \qquad \phi \sim -\bar{y} \;\text{ as } \bar{y} \to \infty, \text{ '} \tag{9.256}$$

and he states 'that this first term of the *inner* solution is simply the *forward* stagnation point solution of HIEMENZ [15]. ROBINS and HOWARTH also show how both, the outer (9.253) and inner (9.254) solutions may be continued in powers of $\exp(-\bar{t})$, [...]. Numerical solutions of (9.249) and (9.250) have also been carried out in [31, 34]. The results confirm the asymptotic results outlined above for large $\bar{t}$ and give a value $\bar{t} = 0.32$ at which reversed flow first takes place [...]' [33].

RILEY also considers in his review [33] the full numerical solutions of the unsteady boundary layer equations for the impulsive flow past a circular cylinder as presented by BELCHER et al. [2] and COLINS and DENNIS, [8]). To cut a long story short, this work seems to provide corroborative evidence for the validity of the asymptotic theory in [31].

9.9.2 Boundary Layer Formed at the Boundary of an Oscillating Body

Consider a cylindrical body, which oscillates orthogonally to its axis with circular frequency ω. Here, it is our intention to compute the flow in the boundary layer along the body's surface for sufficiently large frequency.

In the following the two-dimensional boundary layer equations will be referred to a coordinate system that is rigidly fixed to the moving body, as in Sect. 9.9.1. The wall is assumed to be sufficiently flat, so that, locally use of Cartesian coordinates is justified, and the coordinates x and y are, respectively, measured along and perpendicular to the wall, Fig. 9.35. The x-component of the boundary layer momentum equation is then given as

$$\frac{\partial u}{\partial t} + u\frac{\partial u}{\partial x} + v\frac{\partial u}{\partial y} = -\frac{1}{\rho}\frac{\partial \tilde{p}_w}{\partial x} + \nu\frac{\partial^2 u}{\partial y^2} + f_x, \tag{9.257}$$

where f_x is the x-component of the virtual-inertial force due to the non-inertial reference frame. At the outer boundary of the boundary layer the x-component of the potential flow momentum equation reads

$$\frac{\partial \tilde{u}_w}{\partial t} + \tilde{u}_w\frac{\partial \tilde{u}_w}{\partial x} = -\frac{1}{\rho}\frac{\partial \tilde{p}_w}{\partial x} + f_x. \tag{9.258}$$

Subtraction of the two last equations from one another eliminates $\tilde{p}_w$ and f_x from the emerging equation, which is given by

$$\frac{\partial u}{\partial t} + u\frac{\partial u}{\partial x} + v\frac{\partial u}{\partial y} = \frac{\partial \tilde{u}_w}{\partial t} + \tilde{u}_w\frac{\partial \tilde{u}_w}{\partial x} + \nu\frac{\partial^2 u}{\partial y^2}, \tag{9.259}$$

$$\frac{\partial u}{\partial x} + \frac{\partial v}{\partial y} = 0,$$

to which the continuity equation has also been added, in order to complete the system of partial differential equations for u and v. The boundary conditions, to which (9.259) must be subjected, are

$$u(0) = v(0) = 0, \quad \text{at the flat plate}, \tag{9.260}$$

$$\lim_{y \to \infty} u(x, y, t) = \tilde{u}_w(x, t).$$

(More will be said about $(9.260)_2$ below).

Let us now select an oscillating body, for which

$$\tilde{u}_w = U(x) \, \exp(\iota \omega t). \tag{9.261}$$

As already motivated and justified with the non-dimensionalized equation (9.232) the convective terms on the left-hand side of (9.259) can be neglected. In so doing it is assumed that e.g.

$$\left| \frac{\partial u}{\partial t} \right| \gg \left| u \frac{\partial u}{\partial x} \right|. \tag{9.262}$$

With the velocity scale U_0 and length scale L this assumption is equivalent to

$$U_0 \omega \gg \frac{U_0^2}{L} \implies \frac{\omega L}{U_0} \gg 1, \tag{9.263}$$

$$\text{or if } U_0 = x_0 \omega \implies \frac{x_0}{L} \ll 1,$$

where x_0 can be interpreted as a body displacement amplitude. Therefore, Eq. $(9.263)_2$ states that a typical body dimension in the x-direction must be much larger than the amplitude x_0 of the body displacement.

One expects a boundary layer thickness of the order $\delta = \sqrt{2\nu/\omega}$ (see (9.265)); this thickness must be small as compared to the body dimension, if a boundary layer model should be meaningful at all, i.e.,

$$\frac{\delta}{L} \ll 1 \implies \frac{\omega L^2}{\nu} \gg 1. \tag{9.264}$$

The quantity $\omega L^2/\nu$ can be interpreted as a REYNOLDS number, which must be larger than unity. Thus, if $\delta \ll L$, the outer flow is unaffected by the boundary layer (see, however the drift effects, discussed below in Sect. 9.9.3).

When the convective terms in (9.259) are ignored and (9.261) is substituted for $\tilde{u}_w(x, t)$, the differential equation

$$\frac{\partial u}{\partial t} = \frac{\partial}{\partial t} \{U(x) \exp(\iota \omega t)\} + \nu \frac{\partial^2 u}{\partial y^2}$$

is obtained, which is an inhomogeneous linear 'heat equation'. The homogeneous part can be solved with the trial solution $u_h = U \exp(\iota\omega t) f(y)$ and yields the differential equation

$$\frac{\iota\omega}{\nu} f + f'' = 0,$$

with the solution

$$f = \exp\left(-\sqrt{\frac{\iota\omega}{\nu}} y\right) = \exp\left(-(1+\iota)\frac{y}{\delta}\right), \qquad \delta = \sqrt{\frac{2\nu}{\omega}}. \qquad (9.265)$$
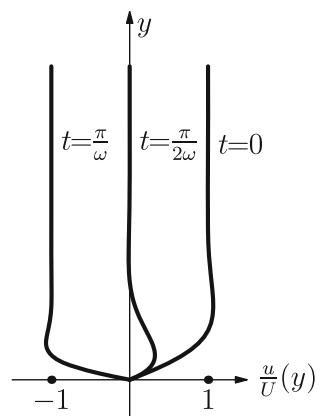
The second solution, $\exp(\sqrt{(\iota\omega)/\nu}\, y)$, does not stay finite as $y \to \infty$ and is, therefore, not applicable. The full solution is composed of the homogeneous solution plus the particular solution such that the boundary conditions at $y = 0$, $y \to \infty$ are satisfied:

$$u(x, y, t) = \mathrm{Re}\left\{U(x)\exp(\iota\omega t)\left[1 - \exp\left(-(1+\iota)\frac{y}{\delta}\right)\right]\right\} \qquad (9.266)$$

$$= \mathrm{Re}\Big\{U(x)\,(\cos(\omega t) + \iota\sin(\omega t))$$

$$\times\left[1 - \exp\left(-\frac{y}{\delta}\right)\left(\cos\left(\frac{y}{\delta}\right) - \iota\sin\left(\frac{y}{\delta}\right)\right)\right]\Big\}$$

$$= U(x)\left\{\cos(\omega t) - \exp\left(-\frac{y}{\delta}\right)\left[\cos\left(\frac{y}{\delta}\right)\cos(\omega t) + \sin\left(\frac{y}{\delta}\right)\sin(\omega t)\right]\right\}$$

$$= U(x)\left\{\cos(\omega t) - \exp\left(-\frac{y}{\delta}\right)\cos\left(\omega t - \frac{y}{\delta}\right)\right\}. \qquad (9.267)$$

The velocity profiles for a number of time slices are shown in **Fig. 9.37**. The velocity component perpendicular to the moving wall can be obtained from the continuity equation

Fig. 9.37 Distribution of the x-component of the velocity, (9.267), for $t = 0, \pi/(2\omega)$, $\pi/(\omega)$ as seen from the co-moving coordinate system

$$v = - \int_0^y \frac{\partial u}{\partial x}(x, y, t) \mathrm{d}y,$$

as follows

$$
\begin{aligned}
v &= -\mathrm{Re}\left\{ \frac{\mathrm{d}U}{\mathrm{d}x}\exp(\iota\omega t)\int_0^y \left[1 - \exp\left(-\frac{1+\iota}{\delta}\overline{y}\right)\right]\mathrm{d}\overline{y}\right\} \\
&= -\mathrm{Re}\left\{\frac{\mathrm{d}U}{\mathrm{d}x}\exp(\iota\omega t)\left[y - \frac{\delta}{1+\iota}\exp\left(-\frac{1+\iota}{\delta}y\right)\right]\right\} \\
&= -\frac{\mathrm{d}U}{\mathrm{d}x}\left\{\cos(\omega t)\left[y - \frac{\delta}{2}\exp\left(-\frac{y}{\delta}\right)\left(\cos\left(\frac{y}{\delta}\right) - \sin\left(\frac{y}{\delta}\right)\right)\right]\right. \\
&\qquad\left. + \sin(\omega t)\left[-\frac{\delta}{2}\exp\left(-\frac{y}{\delta}\right)\left(\cos\left(\frac{y}{\delta}\right) + \sin\left(\frac{y}{\delta}\right)\right)\right]\right\}. \quad (9.268)
\end{aligned}
$$

Physically obvious, the boundary layer induces a *dissipative force* acting on the body, which is consistently directed against the momentary velocity at the body. This force can most easily be computed by formulating the local *balance of kinetic energy*, which is obtained as the inner product of the local momentum balance with the velocity[15]:

$$
\begin{aligned}
\rho\dot{v}_i v_i &= -p_{,i}v_i + t_{ij,j}v_i + f_i v_i \\
\frac{\mathrm{d}}{\mathrm{d}t}\left(\rho\frac{|v|^2}{2}\right) &= -(pv_i)_{,i} + p\underbrace{v_{i,i}}_{0} + \left(t_{ij}v_i\right)_{,j} - t_{ij}v_{i,j} + f_i v_i \\
&= \underbrace{\left(-pv_i + t_{ij}v_i\right)_{,j}}_{(\mathrm{I})} + \underbrace{f_i v_i}_{(\mathrm{II})} - \underbrace{t_{ij}v_{i,j}}_{(\mathrm{III})}, \quad (9.269)
\end{aligned}
$$

in which the underbraced terms are

(I)   Power of surface forces,
(II)   Power of volume forces,
(III) Specific dissipation,

or in short

$$\dot{K} = L - \Phi \quad \Longrightarrow \quad L - \dot{K} = \Phi. \quad (9.270)$$

The difference of the powers of working of all the forces and the time rate of change of the specific kinetic energy equals the dissipative power. For two-dimensional flows

---

[15]This law is formulated relative to the frame at rest.

$$\Phi = \sigma_x \frac{\partial u}{\partial x} + \sigma_y \frac{\partial v}{\partial y} + \tau_{xy} \left(\frac{\partial u}{\partial y} + \frac{\partial v}{\partial x} \right),$$

which in the boundary layer approximation reduces to

$$\Phi \approx \eta \left(\frac{\partial u}{\partial y} \right)^2. \tag{9.271}$$

With the help of (9.266) we may deduce

$$\frac{\partial u}{\partial y} = U(x) \exp(\iota \omega t) \frac{1 + \iota}{\delta} \exp \left(-(1 + \iota) \frac{y}{\delta} \right)$$

$$= \frac{\sqrt{2} U(x)}{\delta} \exp \left(-\frac{y}{\delta} \right) \exp \left(\iota \left(\omega t - \frac{y}{\delta} + \frac{\pi}{4} \right) \right).$$

Forming the real part and squaring the emerging expression yields

$$\left(\frac{\partial u}{\partial y} \right)^2 = \frac{2 U^2(x)}{\delta^2} \exp \left(-2 \frac{y}{\delta} \right) \cos^2 \left(\omega t - \frac{y}{\delta} + \frac{\pi}{4} \right),$$

of which the time average over a cosine period becomes

$$\overline{\left(\frac{\partial u}{\partial y} \right)^2} = \frac{U^2}{\delta^2} \exp \left(-2 \frac{y}{\delta} \right). \tag{9.272}$$

The temporal mean value of the dissipated energy per unit area of the oscillating body is, thus, given by

$$\int_0^\infty \overline{\Phi(y)} \mathrm{d}y = \eta \frac{U^2(x)}{\delta^2} \underbrace{\int_0^\infty \exp \left(-2 \frac{y}{\delta} \right) \mathrm{d}y}_{=\delta/2} = \frac{U^2}{2\delta} \eta. \tag{9.273}$$

Consider next the damping force on the body. Its time dependence is in phase with the velocity of the oscillating body, so that

$$F = F_0 \cos(\omega t), \qquad U = U_0 \cos(\omega t). \tag{9.274}$$

The time average (over a cosine period) of its power of working is given by

$$\overline{L} = \frac{1}{2} F_0 U_0 = \frac{\eta}{2\delta} \int_{\text{body}} U^2(x) \mathrm{d}x, \tag{9.275}$$

and the value of $\overline{L}$ must agree with the time average of the power of working of the dissipation.

As an *example* consider a circular cylinder with radius a, for which

$$U(x) = 2U_0 \sin\left(\frac{x}{a}\right). \tag{9.276}$$

Here the distance is measured from the front stagnation point (see Fig. 9.35). Equation (9.276) implies

$$\frac{1}{2}F_0U_0 = \frac{\eta}{2\delta}4U_0^2\,2\underbrace{\int_0^{\pi a}\sin^2\left(\frac{x}{a}\right)\mathrm{d}x}_{(1/2)\pi a} = \frac{2\pi\eta aU_0^2}{\delta},$$

so that

$$F_0 = \frac{4\pi\eta aU_0}{\delta}, \tag{9.277}$$

or expressed by a dimensionless damping coefficient

$$c_\mathrm{d} := \frac{F_0}{\frac{\rho}{2}U_0^2 a} = \frac{8\pi\nu}{\delta U_0} = \frac{8\pi\nu}{U_0\sqrt{\frac{2\nu}{\omega}}} = \frac{8\pi\nu}{x_0\omega\sqrt{\frac{2\nu}{\omega}}} = \frac{4\sqrt{2}\pi}{\sqrt{\frac{U_0x_0}{\nu}}}, \tag{9.278}$$

a result, which matches experimental results as long as $x_0/a \leqslant 0.1$.

9.9.3   Oscillation-Induced Drift Current

We now continue the analysis of the last section dealing with the boundary layer flow close to the boundary of an oscillating body. In this regard, the reader may easily become convinced by inspection of (9.267) and (9.268) that

$$\overline{uv} \neq 0,$$

where the overbar is the averaging operator over the cosine-period $2\pi/\omega$. This implies that there exists a time-averaged momentum flux $\rho\overline{uv}$: it can only be generated by a stationary contribution to the current. To identify it, the second order velocity components are introduced according to

$$(u, v, \tilde{u}_w) = (u_1, v_1, \tilde{u}_{w_1}) + (u_2, v_2, \tilde{u}_{w_2}), \tag{9.279}$$

where the subscript $(\cdot)_1$ identifies the above first boundary layer approximation, corresponding to expressions (9.261), (9.267) and (9.268), and the index $(\cdot)_2$ denotes second order corrections. Note that also the potential flow 'component', $\tilde{u}_{w_2}$, receives such a correction. The boundary layer equation of the x-momemtum balance now reads (cf. (9.237))

$$\frac{\partial u_2}{\partial t} - \nu \frac{\partial^2 u_2}{\partial y^2} - \frac{\partial \tilde{u}_{w_2}}{\partial t} = \tilde{u}_{w_1} \frac{\partial \tilde{u}_{w_1}}{\partial x} - u_1 \frac{\partial u_1}{\partial x} - v_1 \frac{\partial u_1}{\partial y}, \qquad (9.280)$$

analogous to (9.259). Our immediate interest is here only in the time-averaged version of this equation:

$$- \nu \frac{\partial^2 \overline{u}_2}{\partial y^2} = \overline{\tilde{u}_{w_1} \frac{\partial \tilde{u}_{w_1}}{\partial x}} - \overline{u_1 \frac{\partial u_1}{\partial x}} - \overline{v_1 \frac{\partial u_1}{\partial y}}. \qquad (9.281)$$

The first and third terms on the left-hand side dropped out because of the time-periodicity of u_2 and $\tilde{u}_{w_2}$. The terms on the right-hand side of this equation can be computed and yield

$$(1) \left. \begin{array}{l} \tilde{u}_{w_1} = U(x)\cos(\omega t) \\ \dfrac{\partial \tilde{u}_{w_1}}{\partial x} = \dfrac{dU(x)}{dx}\cos(\omega t) \end{array} \right\} \longrightarrow \overline{\tilde{u}_{w_1}\dfrac{\partial \tilde{u}_{w_1}}{\partial x}} = \dfrac{1}{2}U(x)\dfrac{dU(x)}{dx} = \dfrac{1}{4}\dfrac{d}{dx}\left(U^2(x)\right),$$

$$(2) \quad \overline{u_1\frac{\partial u_1}{\partial x}} \quad \propto \quad \frac{1}{2}U(x)\frac{dU(x)}{dx} = \frac{1}{4}\frac{d}{dx}\left(U^2(x)\right),$$

$$(3) \quad \overline{v_1\frac{\partial u_1}{\partial y}} \quad \propto \quad \frac{1}{2}U(x)\frac{dU(x)}{dx} = \frac{1}{4}\frac{d}{dx}\left(U^2(x)\right).$$

It follows: in total the right-hand side of (9.281) is proportional to $\frac{1}{4}\frac{d}{dx}\left(U^2(x)\right)$ and is written as

$$\frac{1}{4}\frac{dU^2(x)}{dx}g(\eta), \qquad \eta = \frac{y}{\delta},$$

where the unknown 'coefficient of proportionality' is absorbed in g. Equation (9.281) now becomes

$$- \nu \frac{\partial \overline{u}_2}{\partial \eta^2} = \frac{\delta^2}{4}\frac{d(U^2(x))}{dx}g(\eta) \quad \overset{(9.265)_2}{\longrightarrow} \quad - \frac{\partial^2 \overline{u}_2}{\partial \eta^2} = \frac{1}{2\omega}\frac{d(U^2(x))}{dx}g(\eta). \quad (9.282)$$

The boundary conditions, which must be fulfilled by u_2, are

$$\overline{u}_2 = 0 \quad \eta = 0 \quad \text{and} \quad \lim_{\eta \to \infty} \overline{u}_2 < \infty. \qquad (9.283)$$

The solution of (9.282) by twofold integration is

$$\overline{u}_2 = \frac{1}{2\omega} \frac{\mathrm{d}\left(U^2(x)\right)}{\mathrm{d}x} \int\limits_0^\eta \left(\int\limits_\sigma^\infty g(\xi)\mathrm{d}\xi \right) \mathrm{d}\sigma. \tag{9.284}$$

The drift velocity at the outer edge of the boundary layer is given by

$$
\begin{aligned}
U_2 = \tilde{u}_{w_2} = \lim_{\eta \to \infty} \overline{u}_2 \; &= \frac{1}{2\omega} \frac{\mathrm{d}\left(U^2(x)\right)}{\mathrm{d}x} \int\limits_0^\infty \left(\int\limits_\sigma^\infty g(\xi)\mathrm{d}\xi \right) \mathrm{d}\sigma \\
&\overset{*}{=} \frac{1}{2\omega} \frac{\mathrm{d}\left(U^2(x)\right)}{\mathrm{d}x} \int\limits_0^\infty \xi g(\xi)\mathrm{d}\xi \\
&\overset{(+)}{=} -\frac{3}{8\omega} \frac{\mathrm{d}\left(U^2(x)\right)}{\mathrm{d}x},
\end{aligned}
\tag{9.285}
$$

in which at '$\overset{*}{=}$' integration by parts is used and '$\overset{\pm}{=}$' follows from $g(\xi) = \exp(-\frac{4}{3}\xi)$.
The drift velocity is evidently independent of the viscosity.

　　With this drift velocity the KNUDT's dust figures in steady vibrating tubes can be explained: the dust collects in those points of the particle laden fluid, where $\partial U/\partial x = 0$, because there, the drift velocity vanishes. Details can be found in http://en.wikipedia.org/ by selecting 'Knudt tube'.

9.9.4 Non-Stationary Plate Boundary Layer

Consider a half-infinite plate, which at $t = 0$ is instantaneously brought to its finite and then constant velocity U in the direction of the positive x-axis. It is expected that for $t \to \infty$ the transitory boundary layers will converge to the BLASIUS boundary layer of the semi-infinite flat plate. Our focus is the determination of the evolution of the unsteady boundary layer for $t \ll \infty$.

　　The initial boundary value problem (9.231), (9.234) can in this case equally be applied to determine a first approximation, given by (9.235), or

$$u = U\mathrm{erf}\left(\frac{y}{2\sqrt{\nu t}} \right), \quad v = 0, \tag{9.286}$$

where U is the constant approaching velocity. This is the famous RAYLEIGH solution [32] for the start-up of an infinite plate. Further approximations, however, cannot be computed with the aid of (9.286) in this case, because all convective terms in the boundary layer equation happen to vanish. The first approximation deviates more and more from the BLASIUS solution as the time grows larger. Moreover, it does not fulfill the condition of vanishing boundary layer thickness at the leading edge of the plate. We recall that the NS-equations involving $\partial u/\partial t$ and $\nu \partial^2 u/\partial x^2$ is a

parabolic partial differential equation (in these variables). By contrast the boundary layer equation, in which the diffusive term $\nu \partial^2 u / \partial x^2$ is omitted, is a *hyperbolic* equation. 'As a consequence, upon the initiation of the motion [for the NS-equation], *all points* on the plate are immediately aware of the presence of the leading edge due to lateral diffusion. In the boundary layer formulation [...] lateral diffusion is absent and diffusive effects act only in the direction normal to the plate as described by the term $\nu \partial^2 u / \partial y^2$. The disturbance caused by the presence of the leading edge propagates with the maximum local velocity, [say U_0]. Consequently, for $x > U_0 t$ the plate is unaware of the presence of the leading edge, the condition at [the leading edge] is not invoked, and the RAYLEIGH solution (9.286) is established as if the plate were infinite in extent, whereas for $x < U_0 t$ the flow very quickly settles down to the well-known BLASIUS flow', [33]. The situation is sketched in Fig. 9.40.

Two different ways of approach for the construction of an approximate solution will be demonstrated.

(α) **The momentum method**.

In this subsection, a generalization to non-steady flow of the momentum balance of the steady boundary layer formulation of Sect. 9.8.1 will be presented. The procedure is to integrate the momentum equation through the boundary layer. The near-wall boundary layer equation is as before, (9.259)$_1$,

$$\frac{\partial u}{\partial t} + u \frac{\partial u}{\partial x} + v \frac{\partial u}{\partial y} = \frac{\partial \tilde{u}_w}{\partial t} + \tilde{u}_w \frac{\partial \tilde{u}_w}{\partial x} + \nu \frac{\partial^2 u}{\partial y^2}, \qquad (9.287)$$

but now $\tilde{u}_w = \tilde{u}_w(x, t)$. This equation is integrated across the boundary layer as this was done with the aid of the continuity equation in Sect. 9.8.1. This process then leads to the equation (cf. (9.182))

$$\frac{\partial}{\partial t} \left(\tilde{u}_w \delta^* \right) + \frac{\partial}{\partial x} \left(\tilde{u}_w^2 \theta \right) + \delta^* \tilde{u}_w \frac{\partial \tilde{u}_w}{\partial x} = \frac{\tau_w}{\rho}, \qquad (9.288)$$

in which δ^* and θ are the displacement thickness and the momentum thickness, respectively.

For the plane half plate, dealt with here, we have

$$\tilde{u}_w = U = \text{constant}, \qquad (9.289)$$

so that (9.288) reduces to

$$U \frac{\partial \delta^*}{\partial t} + U^2 \frac{\partial \theta}{\partial x} = \frac{\tau_w}{\rho}. \qquad (9.290)$$

With the approximation of the boundary layer profiles as described in Sect. 9.8.1 one may choose the ansatz (see Table 9.1 or Eq. (9.190))

$$u = U\left(2\eta - \eta^2\right), \qquad \eta = \frac{y}{\delta} \tag{9.291}$$

and then obtains

$$
\left.\begin{array}{ll}
\delta^* = \dfrac{1}{3}\delta & \text{(see (9.192)} \\[2mm]
\theta = \dfrac{2}{15}\delta & \text{(see (9.191)} \\[2mm]
\dfrac{\tau_w}{\rho} = \dfrac{2\nu U}{\delta} & \text{(see (9.193))}
\end{array}\right\}
\longrightarrow
\begin{array}{l}
\delta^* = \dfrac{5}{2}\theta =: H\theta, \\[4mm]
\dfrac{\tau_w}{\rho} = \dfrac{4}{15}\dfrac{\nu U}{\theta}.
\end{array}
\tag{9.292}
$$

Substituting these expressions into the differential equation (9.290) yields, after some transformations

$$H\frac{\partial\theta^2}{\partial t} + U\frac{\partial\theta^2}{\partial x} = \frac{8}{15}\nu. \tag{9.293}$$

With the time scaling $Ut = s$ this equation can be transformed into

$$H\frac{\partial\theta^2}{\partial s} + \frac{\partial\theta^2}{\partial x} = \frac{8}{15}\frac{\nu}{U}. \tag{9.294}$$

The left-hand side of this equation defines a directional derivative of θ^2 in the (x, s)-plane: the set of parallel straight lines (**Fig. 9.38**). If α is the curve parameter (the distance along the lines), see Fig. 9.38, and if we set

$$\frac{\partial x}{\mathrm{d}\alpha} = 1 \quad \text{and} \quad \frac{\partial s}{\mathrm{d}\alpha} = H, \tag{9.295}$$

then (9.294) can, alternatively, be written as

$$\frac{\partial\theta^2}{\partial s}\frac{\partial s}{\partial\alpha} + \frac{\partial\theta^2}{\partial x}\frac{\partial x}{\partial\alpha} = \frac{\mathrm{d}}{\mathrm{d}\alpha}\left(\theta^2\right) = \frac{8}{15}\frac{\nu}{U}. \tag{9.296}$$
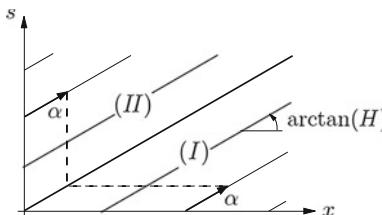
Fig. 9.38 Cartesian (x, s)-plane with the characteristic straight lines $s = Hx + \text{const.}$ inclined by the angle $\arctan(H)$. *The first quadrant is divided into two regions, (I) and (II) by the line $s = Hx$. Initial value $\alpha = 0$ for regions (I) and (II) are given by (9.297) and integrals of (9.296) are given by (9.299)*

This equation tells, how θ^2 varies along the α-lines; indeed this variation is governed by the term on the right-hand side, which is a positive constant. Thus in this case, the growth rate of θ^2 along the α-lines is constant.

Within the quadrant ($x \geqslant 0$, $s \geqslant 0$) the origin of the α-lines is chosen as

$$\alpha = 0, \quad \text{for} \quad \begin{cases} s = 0, & x \geqslant 0, \quad \text{(I)}, \\ x = 0, & s \geqslant 0, \quad \text{(II)}. \end{cases} \tag{9.297}$$

These conditions define in the (x, s)-plane two regions, which join along the straight line $s = Hx$, as shown in Fig. 9.38. Equation (9.297) implies

$$\begin{aligned} &\text{in region (I),} & s = H\alpha, \quad x \text{ arbitrary,} \\ &\text{in region (II),} & x = \alpha, \quad s \text{ arbitrary.} \end{aligned} \tag{9.298}$$

Integration can now be performed subject to the initial condition $\theta^2 = 0$ at $\alpha = 0$. This yields

$$\theta^2 = \frac{8}{15} \frac{\nu}{U} \alpha,$$

or when using (9.298)

$$\begin{aligned} &\text{in region (I):} & \theta^2 = \frac{8}{15} \frac{\nu}{U} \frac{s}{H} = \frac{8}{15H} \nu t, \quad \longrightarrow \quad \theta = \sqrt{\frac{8}{15H}} \sqrt{\nu t}, \\ &\text{in region (II):} & \theta^2 = \frac{8}{15} \frac{\nu}{U} x, \quad \longrightarrow \quad \theta = \sqrt{\frac{8}{15H}} \sqrt{\frac{\nu}{xU}}. \end{aligned} \tag{9.299}$$

The approximate solution (9.299) is in region (I) a boundary layer, independent of the position x and growing with time. In region (II)—the vicinity of the frontal edge of the plate—it is a time-independent (BLASIUS) boundary layer. The extent of this BLASIUS boundary layer grows with time and is given by the separating characteristic $s = Hx = Ut$, implying $x = Ut/H$, see **Fig. 9.39**.

(β) **The Rayleigh Method**.

In this method the spatially one-dimensional momentum equation,

$$\frac{\partial u}{\partial t} + u \frac{\partial u}{\partial x} = \nu \left(\frac{\partial^2 u}{\partial x^2} + \frac{\partial^2 u}{\partial y^2} \right) - \frac{\partial p}{\partial x},$$

is simplified by ignoring on the right-hand side $\partial^2 u/\partial x^2$ in comparison to $\partial^2 u/\partial y^2$ and replacing in the convective term of the left-hand side $u(\partial u/\partial x)$ by $U(\partial u/\partial x)$. The pressure gradient $\partial p/\partial x$ drops out, since p is constant. Thus, approximately,
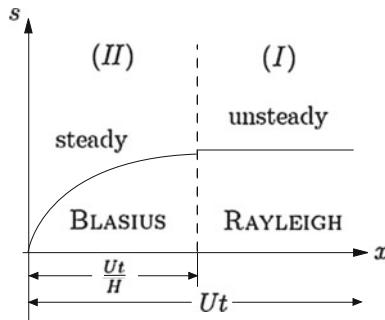
Fig. 9.39 Approximate unsteady boundary layer along a semi-infinite plate. *The boundary layer thickness farther away from the leading edge is independent of x and growing with time (region (I)). Close to the leading edge it is stationary and of* BLASIUS *type (region (II)). The two regions merge at* $x = Ut/H$

$$\frac{\partial u}{\partial t} + U\frac{\partial u}{\partial x} = \nu\frac{\partial^2 u}{\partial y^2}, \tag{9.300}$$
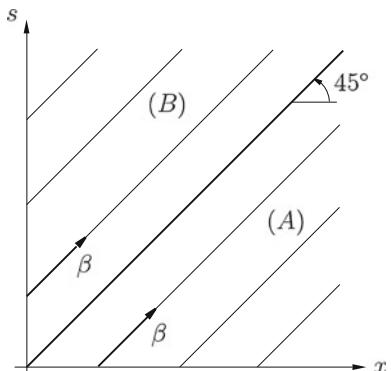
or with $Ut = s$, as before,

$$\frac{\partial u}{\partial s} + \frac{\partial u}{\partial x} = \frac{\nu}{U}\frac{\partial^2 u}{\partial y^2}. \tag{9.301}$$

Structurally this is of the same form as (9.294); on the left-hand side of (9.300) stands the derivative of u in a constant direction in the (x, s)-plane, see **Fig. 9.40**. So, defining the distance along this direction by β, we have

$$\frac{\partial s}{\partial \beta} = 1 \quad \text{and} \quad \frac{\partial x}{\partial \beta} = 1, \tag{9.302}$$

Fig. 9.40 (x, s)-plane analogous to Fig. 9.38. *Characteristics in the (x, s)-plane, $s = x$, with parameter β whose initial value $\beta = 0$ applies in regions (A) and (B) on the x-axis and s-axis, respectively. For details see main text*

with the aid of which (9.301) takes the form

$$\frac{\partial u}{\partial \beta} = \frac{\nu}{U}\frac{\partial^2 u}{\partial y^2} \quad \text{along the straight characteristics.} \tag{9.303}$$

Integration of (9.303) subject to the initial value $\beta = 0$ is performed

$$\begin{aligned}
\text{in region (A):} \quad &\beta = 0, \quad x \geqslant 0 \ \text{ at } s = 0 \ \longrightarrow \ s = \beta, &\tag{9.304}\\
\text{in region (B):} \quad &\beta = 0, \quad s \geqslant 0 \ \text{ at } x = 0 \ \longrightarrow \ x = \beta,
\end{aligned}$$

according to (9.302). The solution of (9.303), for which the boundary layer thickness vanishes for $x = 0$ or $t = 0$ and $u \to U$ for $y \to \infty$, is given by

$$u = U \operatorname{erf}\left(\frac{y}{2\sqrt{(\nu\beta/U)}}\right), \tag{9.305}$$

or owing to (9.302)

$$\begin{aligned}
\text{in region (A):} \quad &u = U \operatorname{erf}\left(\frac{y}{2\sqrt{\nu t}}\right), &\tag{9.306}\\
\text{in region (B):} \quad &u = U \operatorname{erf}\left(\frac{y}{2\sqrt{\nu x/U}}\right).
\end{aligned}$$

Qualitatively, thus, the same behavior is obtained as with the momentum method. In region (A) an instationary, spatially independent (RAYLEIGH) boundary layer is obtained, whereas in region (B) a stationary (BLASIUS) boundary layer is obtained. The solution in region (A) is exact (within the boundary layer theory); in region (B) it is closer to the BLASIUS boundary layer solution the closer one is to the leading edge, compare with Fig. 9.33.

References

1. Batchelor, G.K.: An Introduction to Fluid Dynamics. Cambridge University Press, Cambridge (1974)
2. Belcher, R.J., Burggraf, O.R., Stewartson, K.: On the generalized-vortex boundary layers. J. Fluid Mech. **52**, 753 (1972)
3. Benton, E.R.: Laminar boundary layer on an impulsively started rotating sphere. J. Fluid Mech. **23**, 781–800 (1966)
4. Blasius, H.: Grenzschichten in Flüssigkeiten mit kleiner Reibung. Ph.D. thesis, University Göttingen (1908)
5. Blasius, H.: Funktionstheoretische methoden in der hydromechanik. Z. Math. Phys. **58**, 90–110 (1910)
6. Blasius, H.: Wärmelehre—Physikalische Grundlagen vom technischen Standpunkt. Bosen and Maasch, Hamburg (1931). (3rd edn. 1949)
7. Cochran, W.G.: The flow due to a rotating disk. Proc. Camb. Phil. Soc. **30**, 365–375 (1934)

8. Colins, W.M., Dennis, S.C.R.: The initial flow past an impulsively started circular cylinder. Q. Math. Appl. Math. **26**, 53–75 (1973)
9. Coppel, W.A.: On a differential equation of boundary layer theory. Phil. Trans. Royal. Soc. London **A253**, 101–136 (1960)
10. Falkner, V.M., Skan, S. W.: Some approximate solutions of the boundary layer equations. Phil. Mag. Z. 865–896 (1931)
11. Goldstein, S., Rosenhead, L.: Boundary layer growth. Proc. Cambridge Philos. Soc. **32**, 394–401 (1936)
12. Hager, W.H.: Blasius: a life in research and education. Exp. Fluids **34**, 566–571 (2003)
13. Hager, W.H.: Karl Hiemenz, Hydraulicians in Europe 2: 1091. IAHR, Madrid (2009)
14. Hartree, D.R.: On an equation occurring in Falkner and Skan's approximate treatment of the equation of the boundary layer. Proc. Camb. Phil. Soc. **33**, 240–249 (1937)
15. Hiemenz, K.: Die Grenzschicht an einem in den gleichförmigen Flüssigkeitsstrom einge-tauchten geraden Kreiszylinder. Dinglers Polytech. J. **326**, 321–410 (1911)
16. Homann, F.: Der Einfluss grosser Zähigkeit bei der Strömung um Zylinder und Kugel. Zeitschr. Angew. Math. Mech. (ZAMM) **16**, 153–164 (1936)
17. Holstein, H., Bohlen, T.: Ein einfaches Verfahren zur Berechnung laminarer Reibungsschichten die dem Nährungsverfahren von K. Pohlhausen genügen. Lilienthal-Bericht **10**, 5–16 (1940)
18. Hussaini, M.Y., Lakin, W.D.: Existence and uniqueness of similarity solutions of a boundary layer problem. Q. J. Mech. Appl. Math. **39**(1), 15–23 (1986)
19. Hutter, K., Jöhnk, K.: Continuum Methods of Physical Modeling, p. 635. Springer, Berlin (2004)
20. Kevorkian, J., Cole, J.D.: Perturbation Methods in Applied Mathematics, p. 550. Springer, Berlin (1981)
21. Lagerstrom, P.A.: Asymptotic expansions—ideas and techniques. Applied Mathematical Sciences Nr 76. Springer, New York (1988)
22. Landau, L.: A new exact solution of Navier-Stokes equations. Akademija Nauk SSSR (Moskwa) **43**, 286–288 (1944)
23. McLeod, J.B.: von Kármán's swirling flow problem. Arch. Rational. Mech. Anal. **33**, 91–102 (1969)
24. McLeod, J.B., Serrin, J.: The existence of similarity solutions for some boundary layer problems. Arch. Rational. Mech. Anal. **3**, 288–303 (1968)
25. Miclavčič, M., Wang. C.Y.: The flow due to a rough rotating disk. Z. Angew. Math. Phys. **54**, 1–12 (2004)
26. Nayfeh, A.H.: Perturbation Methods. Wiley-VCH Verlag GmbH & Co.KGaA, Weinheim (2004)
27. Nayfeh, A.H.: Introduction to Perturbation Techniques. Wiley-VCH Verlag GmbH & Co.KGaA, Weinheim (2004)
28. Nigam, S.D.: Rotation of an infinite plane lamina: boundary layer growth. Motion started impulsively from rest. Quart. Appl. Math. **9**, 89–91 (1951)
29. Pohlhausen, K.: Zur näherungsweisen Integration der Differentialgleichung der laminaren Grenzschicht. ZAMM Z. Angew. Math. Mech. **1**, 252–268 (1921)
30. Prandtl, L.: Flüssigkeitsbewegung bei sehr kleiner Reibung. Krazer, A. (ed.) Verhandlungen des dritten internationalen Mathematiker Kongresses in Heidelberg 1904. Teubner Verlag, Leipzig (1905)
31. Proudman, I., Johnson, K.: Boundary layer growth near a stagnation point. J. Fluid Mech. **12**, 161–168 (1962)
32. Rayleigh, L.: On the motion of solid bodies through viscous liquids. Philos. Mag. **21**, 697–711 (1911)
33. Riley, N.: Unsteady laminar boundary layers. SIAM Rev. **17**, 274–297 (1975)
34. Robins, A.J., Howarth, J.A.: Boundary layer development at a two-dimensional rear stagnation point. J. Fluid Mech. **56**, 161–171 (1972)
35. Rogers, M.H., Lance, G.S.: The rotationally symmetric flow of a viscous fluid in the presence of an infinite rotating disk. J. Fluid Mech. **7**, 617–631 (1960)

36. Schlichting, H., Gersten, K.: Boundary Layer Theory, p. 799. Springer, Berlin (2000)
37. Sherman, F.S.: Viscous Flow. McGraw Hill Publ. Comp, New York (1990)
38. Squire, H.B.: The round laminar Jet. Quart. J. Mech. Appl. Math. **4**, 321–329 (1951)
39. Stewardson, K.: The theory of unsteady laminar boundary layers. Adv. Appl. Mech. **6**, 1–37 (1960)
40. Telionis, D.P.: Unsteady Viscous Flows. Springer, New York (1981)
41. Thirot, H.K.: Über die laminare Anlaufströmung einer Flüssigkeit mit einem rotierenden Boden bei plötzlicher Änderung des Drehungszustandes. Z. Angew. Math. Mech. (ZAMM) **20**, 1–13 (1940)
42. van Dyke, M.: Perturbation Methods in Fluid Dynamics—Annotated Edition. Parabolic Press, p. 284 (1975)
43. von Kármán, Th: Über laminare und turbulente Reibung. Z. Angew. Math. Mech. **1**(2), 233–252 (1921)
44. Walz, A.: Ein neuer Ansatz für das Geschwindigkeitsprofil der laminaren Reibungsschicht. Lilienthal Ber. **141**, 8–12 (1941)
45. Walz, A.: Strömungs- und Temperaturgrenzschichten. Braun-Verlag Karlsruhe (1966) English. Translation: boundary layers of flow and temperature. The M.I.T. Press, Cambridge, Mass (1969)
46. Weyl, H.: On the differential equations of the simplest boundary layer problems. Ann. Math. **43**, 381–407 (1942)
47. Zandbergen, P.J., Dijkstra, D.: Non-unique solutions of the Navier-Stokes equations for the Karman swirling flow. J. Eng. Math. **11**, 167–188 (1977)
48. Zandbergen, P.J., Dijkstra, D.: von Kármán swirling flows. Annu. Rev. Fluid Mech. **19**, 465–491 (1987)

Chapter 10
Pipe Flows

Abstract In this chapter pipe flows are studied for laminar HAGEN-POISEUILLE flows as well as turbulent flows; this situation culminates via a dimensional analysis in the well known MOODY diagram based on the pioneering work of JOHANN NIKURADSE's hydraulically smooth and rough pipes. Plane turbulent flow is mathematically modeled by PRANDTL and VON KÁRMÁN on the basis of PRANDTL's mixing length parameterization of the turbulent shear stress. Wall parallel flows can computationally be determined by two additional assumptions, (1) that the mixing length grows linearly with distance from the wall and (2) the shear stress velocity is constant across the turbulent boundary layer. The result is the well known logarithmic velocity profile. It culminates in PRANDTL's and VON KÁRMÁN's universal representation of the coefficient of resistance, λ. This universality property, assumed to hold since the 1930s, has been challenged by BARENBLATT and associates in the 1990s and later on. These authors negate the logarithmic law and show that the laminar sub-layer influences the outer turbulent boundary layer.

Keywords HAGEN-POISEUILLE flow · Laminar flow in cylindrical pipes of arbitrary cross section · Turbulent flows in pipes · MOODY diagram based on NIKURADSE's experiments · PRANTL-VON KÁRMÁN plane turbulent flows · Universal logarithmic turbulent boundary layer velocity profile · BARENBLATT et al.'s negation of the logarithmic velocity profile

List of Symbols

Roman Symbols

A	Area of the cross section of a vessel
a, b	Semi axes of an ellipse
d	Diameter of a circular cylinder
$D \in \mathcal{R}^n$	Domain in $\mathcal{R}^n$
$f(\mathbb{R}_\ell, \mathbb{R}^*)$	Dimensionless function characterizing boundary layer shearing
g	Gravity constant
h	Height/depth of the water in a vessel
h_a, h_e	Initial and end level of the water surface

k	Roughness scale parameter for pipe flow [a length]
k/d	Relative roughness
l	Length of a line segment, PRANDTL mixing length
l_e	Entrance length of a viscous flow into a pipe to reach a laminar parabolic velocity distribution
L, M	Dimensions for length, mass
p	Pressure
p_0	External (atmospheric) pressure
Q	Volume flow, volume transport
$\mathbb{R} = \frac{\bar{u}d}{\nu}$	REYNOLDS number based on $\bar{u}$ and the diameter of a pipe
$\mathbb{R}^* = \frac{v^*\delta}{\nu}$	Global REYNOLDS number
$\mathbb{R}_\ell = \frac{v^*y}{\nu}$	Local REYNOLDS number
$\mathbb{R}^*$	REYNOLDS number based on the shear velocity: $\mathbb{R}^* = \frac{Rv^*}{\nu} = \frac{\mathbb{R}}{2}\sqrt{\frac{\lambda}{\gamma}}$
$\mathcal{R}^n$	Real space of dimension n
r	Radial coordinate
r_0	Radius of a circular pipe
S	Prestress of a soap film or a membrane
T	Dimension of time
u	Axial velocity in a pipe flow
$\bar{u}$	Cross sectional mean of u
u', v'	Turbulent fluctuation velocity components
$v^* = \sqrt{\tau/\rho}$	Shear (stress) velocity
w	Displacement function of a soap film or membrane
x	Axial coordinate in a pipe flow
y	Boundary layer coordinate
x, y, z	Cartesian coordinates

Greek Symbols

$\beta = 5.5\kappa$	NIKURADSE constant for hydrodynamically smooth pipes
Δ	LAPLACE operator, $\Delta = \nabla^2$
Δp, $\Delta p'$	Pressure difference
Δt	Time difference
$\partial\mathcal{D}$	Boundary of $\mathcal{D}$
$\phi = \frac{\ell}{d}\lambda(\mathbb{R}, \kappa/d)$	Pipe pressure loss function
$\lambda(\mathbb{R}, k/d)$	Coefficient of resistance
$\lambda = 64/\mathbb{R}$	Coefficient of resistance for laminar HAGEN-POISEUILLE flow
$\kappa \approx 0.4$	VON KÁRMÁN turbulent constant
Π_1, Π_2, Π_3	Dimensionless Π-products (formulae (10.102))
τ	Shear stress

10.1 Introductory Remarks

The intention in this chapter is still the description of the motion of viscous liquids, but extended in the direction of *turbulent flow behavior*. In their experiments with flows of viscous fluids through pipes, OBORNE REYNOLDS (1842–1912) and MAURIEL COUETTE (1858–1943) realized that in fluid movements essentially two flow regimes exist. One of them is the **laminar flow regime**, in which the fluid particles move orderly in the axial direction of the pipe, see **Fig. 10.1** (left). The other, **turbulent flow**, is a much more complex flow configuration, in which the fluid particles swirl round vividly. The flow is still primarily directed axially, but in addition large transverse pulsating components are present, which contribute to a strong swirling motion of the fluid, which influences the axial current.

Laminar pipe flow, discovered by GOTTHILF HEINRICH LUDWIG HAGEN (1797–1884) in 1839 has been described and computationally modeled by JEAN LOUIS LÉONARD MARIE POISEUILLE (1797–1869) in 1840 and 1846. The decisive papers and the research efforts concerning turbulent flows emerged almost exclusively in the years 1910–1945, even though HENRI DARCY (1803–1858), HENRI BAZIN

Fig. 10.1 Laminar and turbulent flows. *Laminar and turbulent flows in a circular pipe. In order to make the flow visible, a fine jet of ink is added to a water filament in the middle of the pipe cross section at the upper end of the pipe. The capillary, from which the ink jet is added, is visible at the upper edge of the figure. In the panel on the right, axial velocities are larger than on the left. The streaklines entering from the capillary are now driven to the side and torn apart, so that eventually the entire cross section is filled with the dye added to the capillary fluid.* From P. FRAUENFELDER and P. HUBER, Einführung in die Physik, Ernst Reinhardt Verlag, Basel

(1829–1917), VALENTIN JOSEPH BOUSSINESQ (1842–1929) and ADHÉMAR JEAN CLAUDE BARRÉ DE SAINT-VENANT (1797–1886) and others already dealt deeply with the topic in the second half of the 19th century. We shall return to this topic later on.

Turbulence research has gained new impetus in the 1970's and is still one of the centers of research of fluid dynamics of the 21-st century. The core of this research is essentially the same as it already was at its inception and lies in the formulation of *phenomenological closure relations* as well as adequate *scaling rules* to understand the similarity properties and, thus to properly model the new turbulent correlation terms. As in the theory of laminar flows the original forms of these turbulent closure condition s consisted in the postulation of laws for the turbulent viscosity. Such a proposal goes back to VALENTIN JOSEPH BOUSSINESQ with his suggestion in the 1870s to model the turbulent viscous stresses with the aid of the concept of **eddy viscosity**. The simplest explicit suggestion is by LUDWIG PRANDTL (1875–1953) and his collaborators, who formulated algebraic expressions for the eddy viscosity in terms of the local stretching of the mean turbulent motion. This took place in the first half of the 20th century. Later, (i.e., in the seventies of the 20th century), differential equations for characteristic turbulent quantities of the mean motion (turbulent kinetic energy, turbulent dissipation, or turbulent mixing length, etc.) were proposed and related to the eddy viscosity. These concepts were later even further extended by directly postulating evolution equations (partial differential equations in time and space) for the REYNOLDS stresses (and other flux terms). In this chapter, we shall not address such higher order turbulent models, but shall come back to the topic in Vol. 2.
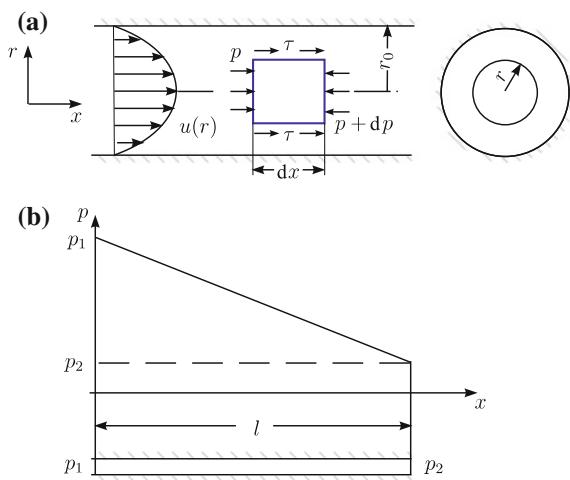
10.2   Laminar Pipe Flow

10.2.1   *The Law of Hagen-Poiseuille*

Consider a *steady laminar flow* through a circular pipe with radius r_0. Assume a flow state reminiscent of wall bounded shear flow, in which the axial velocity component is the only non-trivial velocity component, which may at most be a function of the radial coordinate, $u = u(r)$, see **Fig. 10.2**a. This assumption is approximately valid sufficiently distant from the entrance cross section. For the derivation of the equations of motion of the velocity field, consider a co-axial cylindrical element of length dx; at its mantle surface, the shear stresses τ apply, which, owing to ISAAC NEWTON's viscous law, can be expressed as

$$\tau(r) = \eta \frac{du(r)}{dr} \tag{10.1}$$

Fig. 10.2 Laminar viscous flow in circular pipes. **a** *Cylindrical circular fluid element with pressures and shear stresses indicated; in support of the derivation of* (10.2). **b** *The longitudinal pressure gradient is constant*

and equally also depend only upon the radial coordinate. The other horizontal forces acting on the cylindrical element are the pressures p and $p + \mathrm{d}p$ applied at the end surfaces. In analogy to the plane case, it may be assumed that the pressure is only a function of the axial (but not radial) coordinate, $p = p(x)$. [This property can be rigorously deduced from the NAVIER-STOKES equations as we shall see.] Because of the steadiness and axiality of the motion the acceleration vanishes everywhere, so that the momentum balance can be replaced by a force balance. If this is written in the horizontal direction for the cylindrical element of Fig. 10.2a, the equation

$$\{p - p - \mathrm{d}p\}r^2\pi + 2\pi r\tau(r)\mathrm{d}x = 0$$

is obtained or

$$\frac{\mathrm{d}p(x)}{\mathrm{d}x} = 2\frac{\tau(r)}{r}. \tag{10.2}$$

The expression on the left-hand side is only a function of x, whilst that on the right-hand side only depends on r. Equality can only prevail, if the expressions on both sides assume the same constant value. Therefore, we set

$$\frac{\mathrm{d}p}{\mathrm{d}x} = \frac{p_2 - p_1}{l} = \text{const.} \tag{10.3}$$

The pressures p_1 and p_2 can be identified with the pressures in the cross sections at the two ends of the pipe. As we shall soon see, a volume flow in the positive x-direction requires a negative pressure gradient $\mathrm{d}p/\mathrm{d}x$.

With (10.3) one obtains from (10.2) an expression for the shear stress and with (10.1) the following differential equation for the velocity field

$$\frac{du}{dr} = \frac{1}{2\eta} r \frac{p_2 - p_1}{l}. \tag{10.4}$$

Equations (10.3) and (10.4) are ordinary differential equations of the first order for the pressure and the velocity field. Subjected to the boundary conditions

$$u(r_0) = 0, \qquad p(x = 0) = p_1, \tag{10.5}$$

they can be integrated to

$$p(x) = -\frac{p_1 - p_2}{l} x + p_1, \tag{10.6}$$

$$u(r) = \frac{p_1 - p_2}{4\eta l} \left(r_0{}^2 - r^2 \right). \tag{10.7}$$

The velocity, thus, possesses the form of a rotational paraboloid, distributed symmetrically over the cross section and the pressure decreases linearly with x. The maximum value of the velocity arises at the middle axis of the pipe and is given by

$$u_{\max} = u(0) = \frac{p_1 - p_2}{4\eta l} r_0{}^2. \tag{10.8}$$

Finally, the *volume flow* or *volume transport* Q is given by

$$Q = 2\pi \int_0^{r_0} u(r) r \, dr = 2\pi \frac{p_1 - p_2}{4\eta l} \int_0^{r_0} \left(r_0{}^2 r - r^3 \right) dr,$$

or

$$Q = \pi \frac{p_1 - p_2}{8\eta l} r_0{}^4. \tag{10.9}$$

This result is known as **Hagen-Poiseuille formula**. According to it, the volume transport Q for given pipe length l and pressure difference $p_1 - p_2$ grows with the fourth power of the pipe radius r_0. If one defines the mean velocity $\bar{u}$ via $Q = \pi r_0^2 \bar{u}$ one obtains

$$\bar{u} = \frac{Q}{\pi r_0{}^2} = \frac{p_1 - p_2}{8\eta l} r_0{}^2 = \tfrac{1}{2} u_{\max}, \tag{10.10}$$

where (10.8) has also been used. For a circular pipe, the mean velocity $\bar{u}$ is exactly half as large as the maximum velocity $u_{\max}$.

10.2.2 *Laminar Flow in Cylindrical Pipes of Arbitrary Cross-Section*

Let us now generalize the HAGEN-POISEUILLE flow; more specifically, consider a steady laminar flow of a Newtonian fluid through a cylindrical pipe of arbitrary cross section, **Fig. 10.3**. Assuming again that the axial component is the only non-trivial velocity component, it is geometrically clear that this velocity component must now depend on both cross sectional coordinates, y and z, so that one may write

$$u = u(y, z), \qquad v = 0, \qquad w = 0. \tag{10.11}$$

With these representations one can easily show that the continuity equation (mass balance) is identically satisfied; moreover, $\dot{u} = \dot{v} = \dot{w} = 0$, so that the NAVIER-STOKES equations reduce to force balances, which take the forms
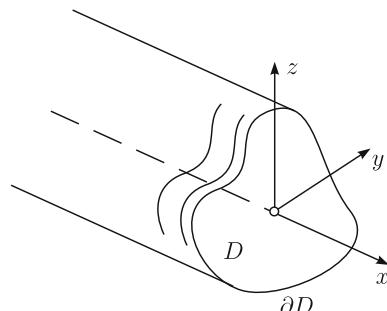
$$0 = -\frac{1}{\rho}\frac{\partial p}{\partial x} + \nu\left(\frac{\partial^2 u}{\partial y^2} + \frac{\partial^2 u}{\partial z^2}\right), \tag{10.12}$$

$$0 = -\frac{1}{\rho}\frac{\partial p}{\partial y}, \qquad 0 = -\frac{1}{\rho}\frac{\partial p}{\partial z},$$

where the specific body force has been ignored. The last two equations in (10.12) show that the pressure only depends on the x-coordinate; furthermore, the first equation of (10.12) implies $d^2 p/dx^2 = 0$, so that the pressure gradient dp/dx is constant and given by

$$\frac{dp}{dx} = \frac{p_2 - p_1}{l}, \tag{10.13}$$

in which p_1 and p_2 are again the pressures at the entrance and exit cross sections of the pipe, whilst l is the pipe length between the cross sections. If one requires the no-slip condition at the pipe wall, then (10.12) leads to the *boundary value problem* (BVP)

Fig. 10.3 Laminar flow in pipes with arbitrary cross section. *The only non-trivial velocity field is axial with dependences on the cross sectional coordinates y and z*

$$\triangle u = \frac{p_2 - p_1}{\eta l}, \quad \text{in } D,$$
$$u = 0, \qquad \text{on } \partial D,$$
(10.14)

in which D is the domain of the cross section, ∂D its boundary and $\triangle$ the two-dimensional **Laplace operator**. In Cartesian and polar coordinates, respectively, it is given by the formulae

$$\triangle u = \frac{\partial^2 u}{\partial y^2} + \frac{\partial^2 u}{\partial z^2} \qquad \text{(Cartesian coordinates)}, \qquad (10.15)$$

$$= \frac{\partial^2 u}{\partial r^2} + \frac{1}{r} \frac{\partial u}{\partial r} + \frac{1}{r^2} \frac{\partial^2 u}{\partial \varphi^2} \qquad \text{(Polar coordinates)}.$$

Because of the non-vanishing right-hand side of $(10.14)_1$ ($p_2 - p_1 \neq 0$) the differential equation (10.14) is called **Poisson equation**, else it is the **Laplace equation**. Solution of the BVP (10.14) delivers for a given cross section D the velocity distribution within D.

As a first example consider once more the HAGEN-POISEUILLE *flow*. We thus assume a circular cross section with a velocity distribution that is independent of the azimuth angle φ. Substituting $(10.15)_2$ into $(10.14)_1$ yields the ordinary differential equation

$$\frac{d^2 u}{dr^2} + \frac{1}{r} \frac{du}{dr} = \frac{1}{r} \frac{d}{dr} \left(r \frac{du}{dr} \right) = \frac{p_2 - p_1}{\eta l}, \qquad (10.16)$$

which can directly be integrated to

$$u(r) = \frac{p_2 - p_1}{4\eta l} \left(r^2 - r_0^2 \right), \qquad (10.17)$$

in which the boundary condition $u(r_0) = 0$ (no-slip) is already satisfied. Equation (10.17) agrees with (10.7) as expected.
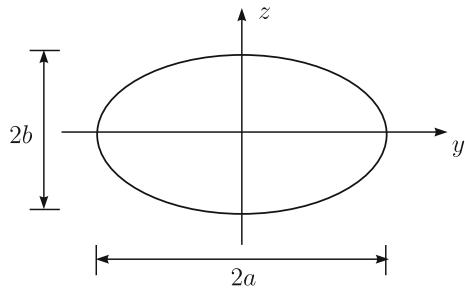
As a further example, consider a pipe of **elliptical cross section** of which the wall is given by the equation

$$\frac{y^2}{a^2} + \frac{z^2}{b^2} - 1 = 0, \qquad (10.18)$$

see **Fig. 10.4**. Inspired by this, one might be tempted to try a solution of the form

$$u = C \left(\frac{y^2}{a^2} + \frac{z^2}{b^2} - 1 \right), \qquad (10.19)$$

Fig. 10.4 Steady-state flow through a pipe with elliptical cross section. *Definition of the coordinates and the semi-axes of the ellipse*

where C is a constant. The trial solution (10.19) satisfies the no-slip condition, since (10.18) makes (10.19) to vanish at the boundary ∂D. That (10.19) also satisfies the differential equation (10.14) with Δ given by (10.15)$_1$ and C given by

$$C = \frac{1}{2\eta} \frac{p_2 - p_1}{l} \frac{a^2 b^2}{a^2 + b^2} \tag{10.20}$$

is a fortunate coincidence. The reader may verify this by substitution. For more general cross sections one must rely on more complex and analytical methods.

When estimating the velocity distributions for arbitrary cross sections, PRANDTL's **soap film** or **membrane analogy**[1] is helpful. According to this analogy there exists a unique identification between the velocity distribution of a linear viscous fluid in a cylindrical pipe of arbitrary cross section and the displacement distribution of a soap film that is spanned over a wire of the same form ∂D as the boundary of the cross section, see **Fig. 10.5**. Indeed, the displacement w and the load p within D of a membrane spanned along ∂D obey the boundary value problem

$$\begin{aligned}
\triangle w &= -\tfrac{p}{S}, & \text{in } D, \\
w &= 0, & \text{on } \partial D,
\end{aligned} \tag{10.21}$$

where S is the homogeneous prestress of the membrane. (We shall not present the derivation of this equation here). The BVPs (10.21) and (10.14) are formally identical; therefore, the two problems must equally correspond to each other. The value of the soap film analogy lies in the fact that displacements of soap films can more easily be visualized than velocity distributions in pipes. One may in this way be able to better estimate approximations.

---

[1] Actually, the soap film analogy was established by PRANDTL between membranes under transverse deflection and Saint Venant torsion of shafts. Correspondence between the BVPs of these two problems exists as well.
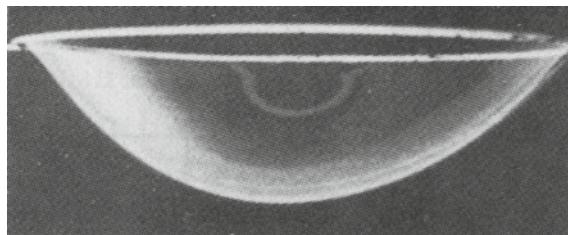
Fig. 10.5 PRANDTL's membrane analogy. *Displacement of a soap film loaded by a constant pressure and spanned by a wire ∂D corresponds to the steady velocity distribution of a linearly viscous fluid through a pipe of the same cross section D. Courtesy* C. ISENBERG: *The Science of soap films and soap bubbles*, Tieto, Ltd, England
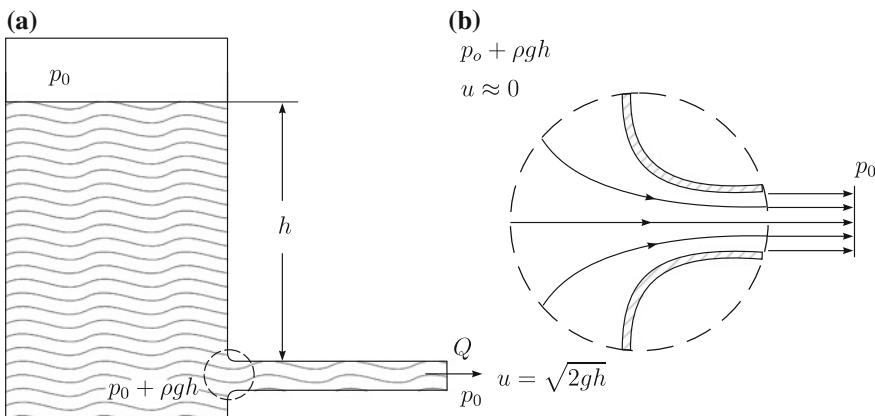
Fig. 10.6 Flow from a vessel through a pipe. **a** *View from the side.* **b** *Zoom of the transition from the vessel to the pipe*

10.2.3   Flow Out of a Vessel

Consider a viscous fluid in a vessel; see **Fig. 10.6**. At the level h below the free surface a thin horizontal circular pipe with radius r_0 and length l is sealed to the vessel allowing a through-flow Q. If one assumes that the flow through the pipe is laminar, the HAGEN-POISEUILLE law (10.9) applies, in which the pressure at the exit cross section, p_2, must be identified with the atmospheric pressure, p_0, and with the pressure immediately before the entrance cross section of the pipe, p_1. Apart from localized effects the velocity at depth h can be ignored, since the cross section of the vessel is assumed to be very large. The pressure p_1 is, therefore, practically hydrostatic and given by $p_1 = p_0 + \rho g h$. Thus, one obtains

$$p_1 - p_2 = p_0 + \rho g h - p_0 = \rho g h, \qquad (10.22)$$

and the through-flow Q in Eq. (10.9) can be given as

$$Q = \pi \frac{\rho g h}{8 \eta l} r_0{}^4. \tag{10.23}$$

This is the result which obtains if one starts with laminar flow of a NEWTONian fluid.

For a fluid with small viscosity, one may ignore the influence of the viscosity altogether and suppose the conditions of an inviscid fluid. Then, application of the BERNOULLI equation between a point at the free surface and exit cross section of the pipe leads to the **Torricelli formula**[2]

$$Q = \sqrt{2gh}\pi r_0{}^2. \tag{10.24}$$
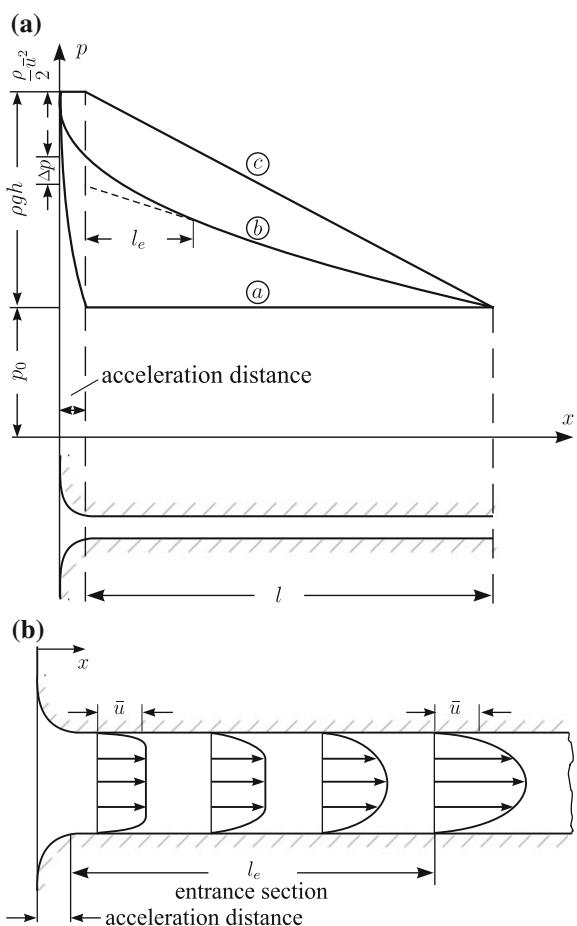
This formula is considerably distinct from (10.23). Indeed,

- The discharge Q (10.24) does not depend on the density of the liquid. So, discharges of water and mercury are the same if the remaining quantities are the same. Quite contrary, (10.23) shows a linear dependence on ρ.
- According to (10.23) Q grows with h and r_0^4 and decreases with l and η. For vanishing viscosity and pipe length, $\eta \to 0$ or $l \to 0$, we have $Q \to \infty$.
- According to (10.24) Q grows only with $\sqrt{h}$ and r_0^2, it does not depend on the pipe length and neither on the viscosity. Therefore, it remains for all conditions finite.

In order to clear, which of the two formulae ought to be applied in a concrete situation, consider pipe flow in the immediate vicinity of the entrance cross section. For the inviscid fluid the liquid is at rest at some distance before the entrance. There, the pressure is given by $p_0 + \rho g h$. Since the pipe does not exert a drag to the inviscid fluid, the pressure in the pipe is constant; in other words, immediately downstream of the entrance cross section of the pipe and throughout the total length of the pipe the pressure agrees with the atmospheric pressure p_0, and the velocity has risen to the value $u = \sqrt{2gh}$. The pressure distribution is indicated by ⓐ in **Fig. 10.7**a. *The pressure drop serves here completely to accelerate the fluid in the vicinity of the entrance.* For the viscous fluid the flow is equally accelerated in the vicinity of the entrance. Immediately behind the entrance cross section the mean velocity is $\bar{u} = Q/(\pi r_0^2)$; the corresponding pressure drop is given by $\bar{u}^2/2$. It reaches this value within a length, which is referred to as '*acceleration distance*'. It is followed by the 'entrance length' or 'entrance distance' l_e', within which the parabolic velocity profile is formed; this pressure drop is denoted by Δp, see Fig. 10.7b. Beyond this, there follows a linear pressure drop down to the atmospheric pressure at the end of the pipe. The pressure distribution corresponds to curve ⓑ in Fig. 10.7a. Finally, the pressure distribution following the HAGEN-POISEUILLE formula follows curve ⓒ in panel (a) of Fig. 10.7, in which the energy loss $\rho \bar{u}^2/2$ and the pressure loss Δp at

---

[2]After EVANGELISTA TORRICELLI (1608–1647), who published this formula in 1644. He was physicist and mathematician in Italy of GALILEI's time, whom he worked for and whose successor he became after GALILEI's death. His research on hydrodynamics was extremely well received in the 17th century of Europe. For a portrait and short biography, see Fig. 3.30.

(a)

(b)

the entrance, which both have the same order of magnitude, have been ignored. This
neglect is justified, provided that

$$\frac{\rho\bar{u}^2}{2} \ll \rho g h, \tag{10.25}$$

or with Eq. (10.10)

$$\rho\frac{\bar{u}}{2}\bar{u} = \rho\frac{\bar{u}}{2}\frac{\rho g h}{8\eta l}r_0^2 \ll \rho g h \quad \longrightarrow \quad \rho\bar{u}\frac{r_0}{\eta} \ll 16\frac{l}{r_0}. \tag{10.26}$$

If one introduces here the **kinematic viscosity** according to $\nu = \eta/\rho$ and the **Reynolds number**

$$\mathbb{R} = \frac{\bar{u}(2r_0)}{\nu} = \frac{\bar{u}d}{\nu}, \tag{10.27}$$

then necessary condition for the HAGEN-POISEUILLE formula to apply in applications takes the form

$$\mathbb{R} \ll 64\frac{l}{d}, \tag{10.28}$$

in which d is the interior diameter of the pipe. Thus, the HAGEN-POISEUILLE formula is only applicable if the REYNOLDS number is sufficiently small. Conversely, one may state that the TORRICELLI formula is applicable when (10.28) is violated. Finally, it may be mentioned that the inequality $l_e \ll l$ must hold. With the theory of cylindrically-symmetric **boundary layers** the entrance length, l_e, within which the parabolic velocity profile is established, is obtained as

$$l_e = 0.03\mathbb{R}d, \tag{10.29}$$

where the factor 0.03 is an estimate, obtained by experiment. With (10.28) there follows

$$l_e \ll 0.03 \times 64l \cong 2l. \tag{10.30}$$

Thus, if (10.28) is satisfied, so is (10.30).

10.2.4 Influence of the Wall Drag of a Pipe to the Exit Flow from a Vessel

Let us change the exit flow arrangement of Fig. 10.6 such that the exit pipe is now vertically connected to the vessel, see **Fig. 10.8**a. The flow is established in this case under simultaneous action of the pressure forces and the gravity force. With the aid of the NAVIER-STOKES equations one may easily show that for axis-parallel flow under steady conditions in the pipe, the pressure can only depend upon the x-coordinate, $p = p(x)$. If one then writes down the equilibrium conditions for the cylindrical fluid element, on which the x-parallel forces are drawn—they constitute of the shear stresses at the mantle surface, the pressure forces at the front and rear areas and the gravity force—the equation

$$-\frac{dp}{dx} + \frac{2}{r}\tau + \rho g = 0 \tag{10.31}$$
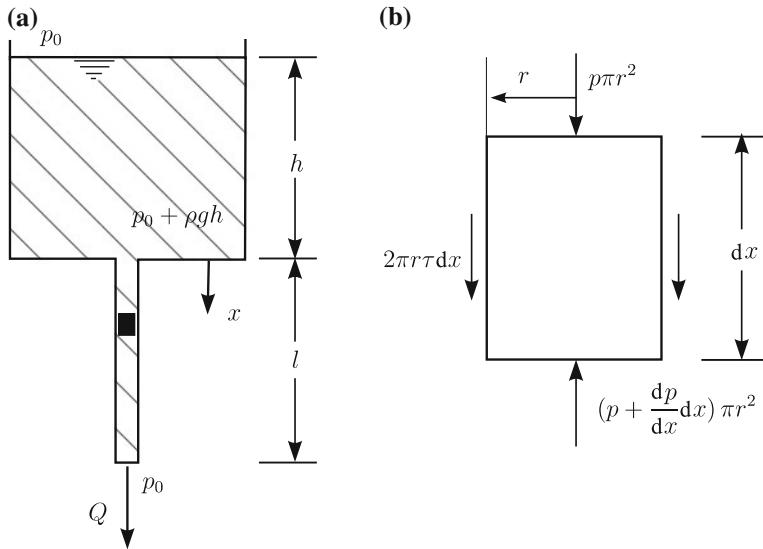
Fig. 10.8 Flow out of a vessel with vertical pipe. **a** *Geometry of vessel and pipe.* **b** *Cylindrical volume element with forces for the downward force balance*

is obtained, which, owing to (10.1), transforms to

$$\underbrace{\frac{\mathrm{d}u}{\mathrm{d}r}\frac{2\eta}{r}}_{f_1(r)} = \underbrace{\frac{\mathrm{d}p}{\mathrm{d}x} - \rho g}_{f_2(x)} . \tag{10.32}$$

The left and right-hand sides of this equation are functions of r and x, respectively; they must be equal to the same constant C. Hence the equation

$$\frac{\mathrm{d}p}{\mathrm{d}x} = C + \rho g = C_1 \quad \longrightarrow \quad p = C_1 x + C_2 \tag{10.33}$$

must hold, where the constants of integration follow from the boundary condition

$$p(0) = p_0 + \rho g h, \qquad p(l) = p_0 \tag{10.34}$$

at the entrance and exit cross sections of the pipe. The pressure distribution is now obtained as

$$p(x) = p_0 + \rho g h \left(1 - \frac{x}{l}\right). \tag{10.35}$$

Back-substitution of this result into (10.32) yields the differential equation

$$\frac{\mathrm{d}u}{\mathrm{d}r} = -\frac{r}{2\eta}\rho g \left(1 + \frac{h}{l}\right),$$

which, after integration and substitution of the boundary condition $u(r_0) = 0$, yields

$$u(r) = \frac{\rho g(h+l)}{4\eta l}\left(r_0{}^2 - r^2\right), \qquad Q = \pi\frac{\rho g(h+l)}{8\eta l}r_0{}^4 \tag{10.36}$$

for the velocity distribution and the volume flux. These are the formulae of HAGEN-POISEUILLE flow for a pressure difference

$$\triangle p = \rho g(h+l). \tag{10.37}$$

Finally, we wish to calculate the time interval which it takes for the vessel to be emptied from an initial position of the free surface at h_a to a final height h_e. If A denotes the constant cross section of this height, then mass (volume) balance implies

$$-A\frac{\mathrm{d}h}{\mathrm{d}t} = Q = \pi\frac{\rho g(h+l)}{8\eta l}r_0{}^4, \tag{10.38}$$

in which the negative sign on the left accounts for the fact that a positive $\mathrm{d}h/\mathrm{d}t$ corresponds to a negative volume flow. Equation (10.38) represents a separable differential equation, which can also be written as

$$\mathrm{d}t = -\frac{8\eta l A}{\pi\rho g r_0{}^4}\frac{\mathrm{d}h}{h+l} \tag{10.39}$$

and delivers through integration the result

$$\int_0^{\triangle t}\mathrm{d}t = -\frac{8\eta l A}{\pi\rho g r_0{}^4}\int_{h_a}^{h_e}\frac{\mathrm{d}h}{h+l}, \tag{10.40}$$

or

$$\triangle t = \frac{\eta}{\rho}\frac{8l A}{\pi g r_0{}^4}\ln\left(\frac{h_a+l}{h_e+l}\right). \tag{10.41}$$

This can readily be solved for the kinematic viscosity $\nu = \eta/\rho$ for the lowering of the free surface, which is needed. If for given h_a and h_e one measures the time Δt, which is needed for the lowering of the free surface from h_a to h_e, then with the aid of (10.41) the kinematic viscosity ν can be determined. This is done in the so-called **Engler viscometer**. However, one recognizes that NEWTONian material behavior was assumed to derive formula (10.41). With such an instrument, therefore, it cannot be tested, whether a fluid follows NEWTONian or non-NEWTONian material behavior.

10.3 Turbulent Flows in Pipes

The computations in Sect. 10.2 are based on the prerequisite of laminar flows, which are, as mentioned, only stable for sufficiently slow flows. In most practical cases turbulent flow prevails, for which computation of the pressure loss is rather more complicated. Historically, thus, the answer to the question of the pressure loss in turbulent pipe flow causes particularly severe difficulties. For, GASPARD CLAIR FRANÇOIS MARIE RICHE DE PRONY (1755–1839) and JOHANN ALBERT EYTEL-WEIN (1764–1848) concluded initially (incorrectly) on the basis of measurements by LOUIS-GABRIEL DU BUAT-NANÇAY (1732–1787) that the *frictional resistance was independent of the nature of the walls of the pipes*. Consequently, the opinion grew that processes, which take place in the vicinity of the walls of the pipes do not influence the volume flow closer to the center of the pipe, i.e., in its interior. HENRY PHILIBERT GASPARD DARCY (1803–1858),[3] and after him HENRI-ÉMILE BAZIN (1829–1917),[4] however, were among the first to prove that, contrary to the results of DE PRONY the frictional resistance depended upon the physical nature of the pipe walls. Only research in the first half of the 20th century by PAUL RICHARD HEINRICH BLASIUS (1883–1970), LUDWIG PRANDTL (1875–1953), THEODORE VON KÁRMÁN (1881–1963), JOHANN NIKURADSE (1894–1979) and others brought final clarity about the mechanism of the pressure loss in turbulent pipe flow.

10.3.1 Coefficient of Resistance

It has proved convenient for practical computations of the pressure drop in pipes to introduce the **coefficient of resistance**, λ. Let us motivate the functional connection for this coefficient with a simple dimensional analysis that can be made plausible, but can only be made rigorous with the formal theory of **dimensional analysis**, see Chap. 20.

---

[3]For a short biography of HENRY PHILIBERT GASPARD DARCY (1803–1858), see **Fig. 10.9**.
[4]For a short biography of HENRI-ÉMILE BAZIN (1829–1917), see **Fig. 10.10**.

For the motivation, consider once more HAGEN-POISEUILLE flow and look at formula (10.10), which shows that the pressure loss $p_1 - p_2 = \Delta p$ depends upon $\eta, \bar{u}, d, l$, where η is the shear viscosity, $\bar{u}$ the mean (cross sectional averaged) velocity, d the pipe diameter and l the pipe length, which corresponds to the pressure drop Δp. It is customary to weigh the pressure loss Δp by the stagnation pressure $\frac{1}{2}\rho\bar{u}^2$; so, the **normalized pressure loss** for laminar flow can be written as

$$\frac{\Delta p}{\frac{1}{2}\rho\bar{u}^2} = \Phi(\rho, \eta, \bar{u}, d, l), \qquad (10.42)$$

where Φ is an unknown function, which must somehow be determined. Generally, the functional relation (10.42) will not be motivated by starting with a known formula, but we will rather make up a list of possibly arising variables that are suggested by the physically stated problem. The two quantities ρ, η then represent the influence played by the material behavior, d and l those of the geometry and $\bar{u}$ that of the mean velocity. Now, the short historical note in the last section indicated that a parameter describing the nature of the wall should also arise as a variable of the function Φ. It is evident that this parameter represents the **roughness** of the wall, which can be characterized by the length k, see **Fig. 10.11**. The value of k is, therefore, a measure for the deviation of the actual pipe wall from an ideal smooth wall, so that (10.42) is to be replaced by

$$\frac{\Delta p}{\frac{1}{2}\rho\bar{u}^2} = \Phi(\rho, \eta, \bar{u}, d, l, k). \qquad (10.43)$$

Further dependences may be thought of, e.g. the wave length A of the roughness elements; one generally assumes, however, that a single quantity with the dimension of a length will suffice.

The number of independent variables in Eq. (10.43) is rather large, so that one intends to reduce these. This is indeed possible, and we shall now show that Φ, stated in (10.43), can only depend on two variables. To this end we employ the following principle: *The function Φ does not depend on the dimensional units of the independent variables and must be **dimensionally homogeneous***. The first of these requirements is obvious, the second says that in a formula, which relates physical quantities with one another, only quantities with the same dimension can be compared, added together or subtracted from one another. With reference to Eq. (10.43) this says the following: Because the left-hand side is dimensionless the right-hand side must equally be dimensionless, and, in particular, Φ must be a function of dimensionless combinations of six independent variables.

Darcy's experiment.
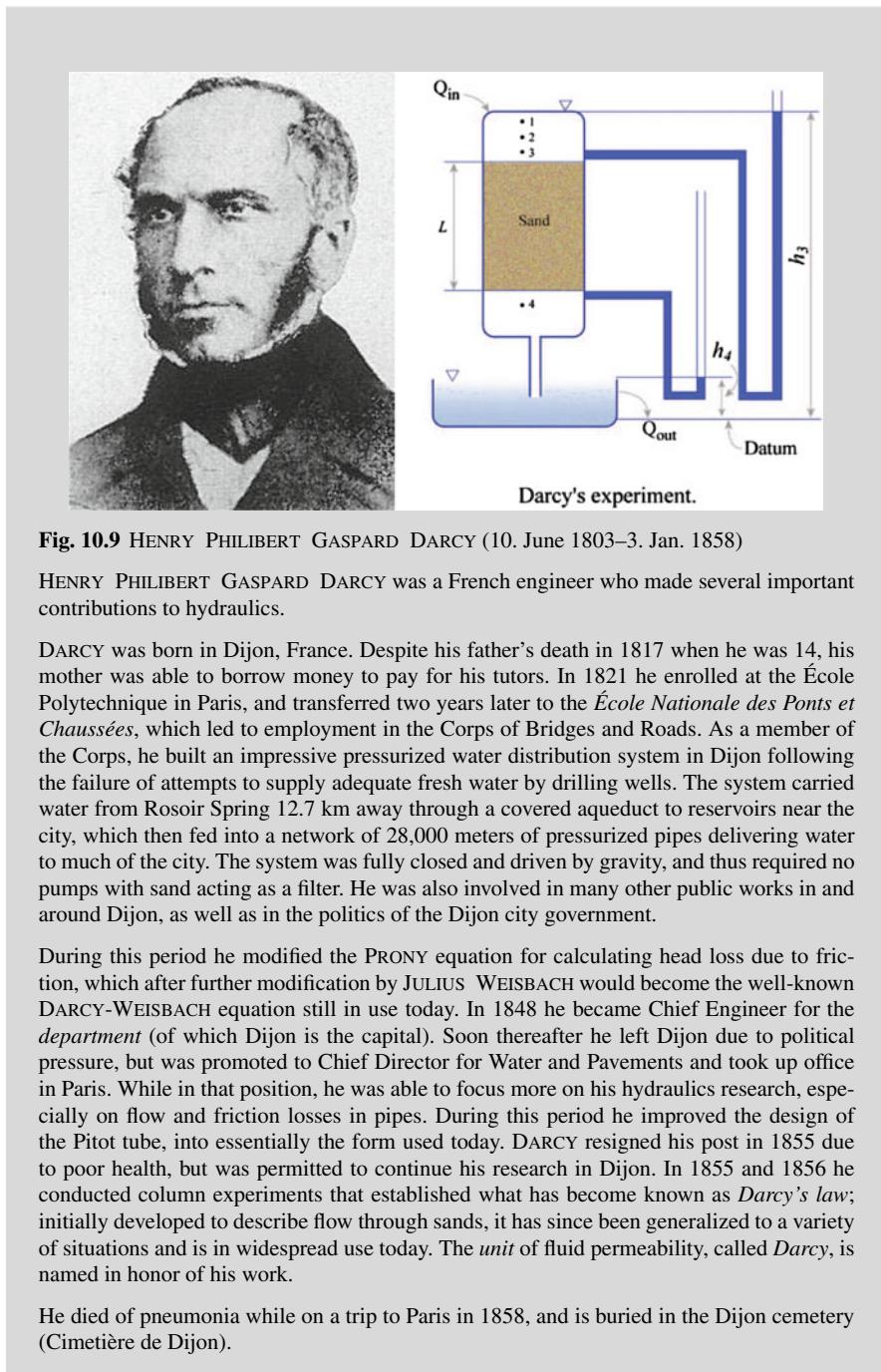
Fig. 10.9 HENRY PHILIBERT GASPARD DARCY (10. June 1803–3. Jan. 1858)

HENRY PHILIBERT GASPARD DARCY was a French engineer who made several important contributions to hydraulics.

DARCY was born in Dijon, France. Despite his father's death in 1817 when he was 14, his mother was able to borrow money to pay for his tutors. In 1821 he enrolled at the École Polytechnique in Paris, and transferred two years later to the *École Nationale des Ponts et Chaussées*, which led to employment in the Corps of Bridges and Roads. As a member of the Corps, he built an impressive pressurized water distribution system in Dijon following the failure of attempts to supply adequate fresh water by drilling wells. The system carried water from Rosoir Spring 12.7 km away through a covered aqueduct to reservoirs near the city, which then fed into a network of 28,000 meters of pressurized pipes delivering water to much of the city. The system was fully closed and driven by gravity, and thus required no pumps with sand acting as a filter. He was also involved in many other public works in and around Dijon, as well as in the politics of the Dijon city government.

During this period he modified the PRONY equation for calculating head loss due to friction, which after further modification by JULIUS WEISBACH would become the well-known DARCY-WEISBACH equation still in use today. In 1848 he became Chief Engineer for the *department* (of which Dijon is the capital). Soon thereafter he left Dijon due to political pressure, but was promoted to Chief Director for Water and Pavements and took up office in Paris. While in that position, he was able to focus more on his hydraulics research, especially on flow and friction losses in pipes. During this period he improved the design of the Pitot tube, into essentially the form used today. DARCY resigned his post in 1855 due to poor health, but was permitted to continue his research in Dijon. In 1855 and 1856 he conducted column experiments that established what has become known as *Darcy's law*; initially developed to describe flow through sands, it has since been generalized to a variety of situations and is in widespread use today. The *unit* of fluid permeability, called *Darcy*, is named in honor of his work.

He died of pneumonia while on a trip to Paris in 1858, and is buried in the Dijon cemetery (Cimetière de Dijon).

DARCY's law describes the water flow through an aquifer; it expresses the filter velocity $Q/A = v_f$ as

$$v_f = -\frac{\kappa}{\eta} \frac{p_4 - p_3}{L},$$

in which η is the dynamic viscosity of water, L is the specimen length and $(p_4 - p_3)/L$ is the pressure gradient through the sand specimen. Measuring $Q = v_f A$ and the pressures p_4 and p_3 allows experimental evaluation of κ.

The text is based on http://www.wikipedia.org

Fig. 10.10 HENRI-ÉMILE BAZIN (10. Jan. or 20. Oct. 1829 – 7. or 14. Feb. 1917)

HENRI-ÉMILE BAZIN was a French engineer and known for his research in Hydraulics. He was a student of *École Nationale des Ponts et Chaussées* and subsequently assistant to HENRY DARCY, whose work he continued. First he worked in Tonerre near Dijon, and, starting in 1854, he was assigned to the *Canal de Bourgogne*, which he enlarged for use by greater ships. 1875–1876 he became chief-engineer of the *Corps des Ponts et Chaussées* and in 1886 General Inspector. In 1900 he retired and, finally, in 1913, he became a member of the *French Academy of Sciences*.

BASIN's research was focused on water flow in open channels. He researched on the water distribution, free water surface and wave experiments. 1865 he published the report *Recherches Hydrauliques* in open channel flow; it was the basis of his fame. Beyond this, he developed his 'flow formula', which delivered the coefficient C, a parameter for the flow formula of CHÉZY

$$C = \frac{87}{1 + m/\sqrt{R}},$$

where m depends on the wall roughness and R is the hydraulic radius.

Text with support from http://www.wikipedia.org

After these introductory explanations we note with

$$[\rho] \quad = \frac{[\text{mass}]}{[\text{length}]^3},$$

$$[\eta] \quad = [\text{stress}] \times [\text{time}] = \frac{[\text{mass}]}{[\text{length}] \times [\text{time}]},$$

$$[\bar{u}] \quad = \frac{[\text{lengh}]}{[\text{time}]},$$

$$[d], [l], [k] = [\text{length}], \tag{10.44}$$

the physical dimensions of the independent variables of Φ. If m and m^* denote the mass of the body in two measuring systems, then the equation $m^* = \mu m$ connects the two units of measure of mass. μ is called the **scale** of the unit of mass. On the basis of the properties of the variables listed in (10.44) one obtains for the density and viscosity in the asterisks system

$$\rho^* = \mu\rho, \qquad \eta^* = \mu\eta,$$

whereas the other quantities remain unchanged. We, thus, have

$$\Phi^* = \Phi(\mu\rho, \mu\eta, \bar{u}, d, l, k). \tag{10.45}$$

Since Φ must be invariant under changes of scales, i.e., $\Phi^* = \Phi$, one necessarily has

$$\Phi = \Phi\left(\frac{\rho}{\eta}, \bar{u}, d, l, k\right) = \Phi(\nu, \bar{u}, d, l, k). \tag{10.46}$$
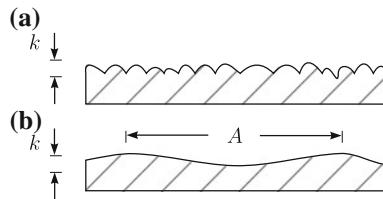
Fig. 10.11   Roughness of a wall. **a** *To describe the roughness of a wall one primarily uses a typical wall elevation k of its topography.* **b** *In a more detailed description of the wall, roughness is also characterized by the wavelength of the wall elevations*

If one changes next the scale for lengths and chooses

$$(d^*, l^*, k^*) = \lambda(d, l, k), \tag{10.47}$$

one obtains with (10.44)

$$\rho^* = \frac{\rho}{\lambda^3}, \qquad \bar{u}^* = \lambda\bar{u}, \qquad \eta^* = \frac{1}{\lambda}\eta, \tag{10.48}$$

and, therefore,

$$\Phi^* = \Phi\left(\frac{\rho}{\lambda^2\eta}, \lambda\bar{u}, \lambda d, \lambda l, \lambda k\right). \tag{10.49}$$

If one now requests invariance of Φ under changes of the units of lengths, $\Phi^* = \Phi$, we see that (10.45) must have the form

$$\Phi = \Phi\left(\frac{\rho d^2}{\eta}, \frac{\bar{u}}{d}, \frac{l}{d}, \frac{k}{d}\right), \tag{10.50}$$

in which the choice of the variables is not unique, but their numbers. One may, for instance, easily show that the choice

$$\Phi\left(\frac{\rho d^2}{\eta}, \frac{\bar{u}}{d}, \frac{l}{d}, \frac{k}{l}\right)$$

is equally invariant under changes of the units of length. Since $k/l = (k/d)(d/l)$, it is obvious that the representation (10.50) and the above representation are equivalent. Finally, if one also changes the unit of time, one obtains with

$$t^* = \tau t, \qquad \bar{u}^* = \frac{1}{\tau}\bar{u}, \qquad \eta^* = \frac{1}{\tau}\eta, \tag{10.51}$$

and, therefore,

$$\Phi^* = \Phi\left(\frac{\rho d^2}{\eta}\tau, \frac{\bar{u}}{d\tau}, \frac{l}{d}, \frac{k}{d}\right). \tag{10.52}$$

The request $\Phi^* = \Phi$ then yields

$$\Phi = \Phi\left(\frac{\bar{u}d}{\eta/\rho}, \frac{l}{d}, \frac{k}{d}\right). \tag{10.53}$$

Let us stop here to briefly weigh the result. In (10.43) the normalized pressure Φ was proposed as a function of six variables and the invariance request under changes of the scales of the physical units led in Eq. (10.53) to a dependence on merely three dimensionless variables. This is a drastic reduction of the dimensionality of the problem. One also recognizes in (10.53) the property of **dimensional homogeneity** for the functional relation of Φ for which the functional value and all independent variables are dimensionless.

This is as much as can be inferred by means of methods of dimensional analysis. Further reduction of Φ is based on assumptions, plausibility arguments or observations. For instance, it is certainly reasonable to suppose that $\Delta p = p_1 - p_2$ is proportional to the length of the pipe. This suggests to write (10.53) as

$$\Phi = \frac{l}{d}\lambda\left(\mathbb{R}, \frac{k}{d}\right), \tag{10.54}$$

in which $\mathbb{R} = \bar{u}d/\nu$ is the **Reynolds number** that is here formed with the mean velocity $\bar{u}$. The parameter $\lambda(\mathbb{R}, k/d)$ is called **coefficient of resistance**; it depends on the REYNOLDS number $\mathbb{R}$ and on the **relative roughness** k/d. With (10.54), (10.43) can now be written as

$$\frac{\Delta p}{\frac{\rho}{2}\bar{u}^2} = \frac{l}{d}\lambda\left(\mathbb{R}, \frac{k}{d}\right). \tag{10.55}$$

For the computation of the pressure drop in pipes it, therefore, suffices to know the coefficient of resistance as a function of the REYNOLDS number and the relative roughness.

As a single example, consider the laminar HAGEN-POISEUILLE flow, for which we had already stated that a dependence on the relative roughness is insignificant. With (10.55) and

$$\bar{u} = \frac{\Delta p}{8\eta l}\left(\frac{\mathrm{d}}{2}\right)^2$$

we deduce with the help of (10.10)

$$\lambda = \frac{\Delta p}{\frac{\rho}{2}\bar{u}^2}\frac{\mathrm{d}}{l} = \frac{2\Delta p}{\rho\bar{u}\bar{u}}\frac{\mathrm{d}}{l} = \frac{2\Delta p}{\rho\bar{u}}\frac{8\eta l}{\Delta p(d/2)^2}\frac{\mathrm{d}}{l} = \frac{64}{\underbrace{\frac{\bar{u}d}{\eta/\rho}}} = \frac{64}{\mathbb{R}}. \tag{10.56}$$

In turbulent pipe flow, there exists equally a regime for which the pressure loss is independent of the relative roughness. This obviously is the case when $k/d \to 0$, i. e., if the inner wall of the pipe has only very small roughness lengths k. Such pipes are called **hydraulically smooth** and were scrutinized in detail by T.E. STANTON and J.R. PANNEL [18], see **Fig. 10.12**. According to these results, there exists for both, laminar and turbulent flows a unique relation between λ and $\mathbb{R}$, which is only 'smeared' in the transition regime from laminar to turbulent flow and vice versa. In this regime λ depends also on unidentified perturbations, which may be due to peculiarities in the entrance and ahead of it. Depending on the form and size of these perturbations, this transition regime occurs for $1000 < \mathbb{R} < 2300$. The laminar regime is describable by formula (10.56). For the turbulent regime of hydraulically smooth pipes HEINRICH BLASIUS formulated the empirical law
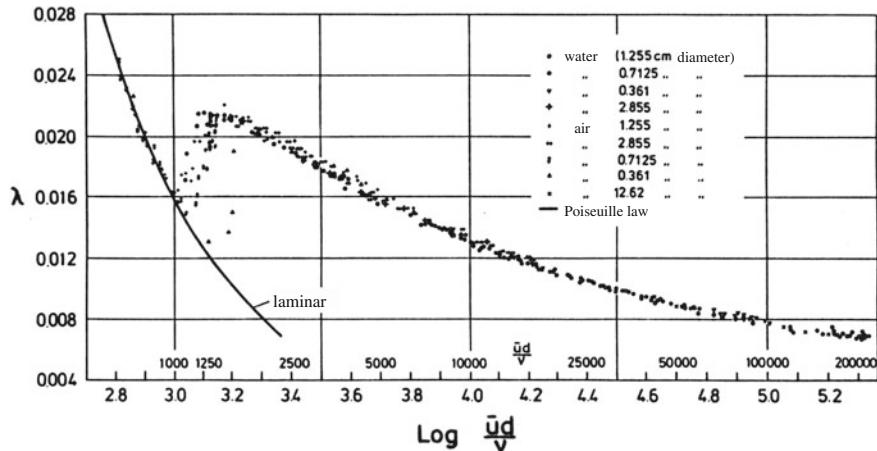
Fig. 10.12 Hydraulically smooth pipes. *Experiments, performed by* STANTON *and* PANNEL *[18] for the determination of the coefficient of resistance,* λ*, in hydraulically smooth pipes for air and water*

$$\lambda = 0.316\mathbb{R}^{-1/4}, \qquad 5 \times 10^3 \leqslant \mathbb{R} \leqslant 10^5, \tag{10.57}$$

which is only valid within the indicated interval of the REYNOLDS number.For the entire turbulent regime LUDWIG PRANDTL [14, 16, 17] proposed the theoretically motivated law.[5]

$$\frac{1}{\sqrt{\lambda}} = 2\log\left(\mathbb{R}\sqrt{\lambda}\right) - 0.8. \tag{10.58}$$

That was also experimentally verified by JOHANN NIKURADSE (1894–1979).[6] Its disadvantage is that λ appears implicitly as a function of $\mathbb{R}$.

More complicated is the determination of the coefficient of resistance, λ, when beyond the dependence on $\mathbb{R}$ also a dependence on the relative roughness arises. Two cases must be differentiated:

- If the wall roughness is of granular structure as in Fig. 10.11a, then the value of λ above a certain REYNOLDS number is independent of the REYNOLDS number, i.e., the pressure loss for $\lambda = $ const. is proportional to the square of the velocity. This limit is indicated in **Fig. 10.14** as the dashed line.
- If the wall is of wavy structure, see Fig. 10.11b, i. e., if the wall is wavy but essentially smooth, then λ decreases with growing REYNOLDS number. The λ-curve follows here approximately the curve of the smooth pipe (BLASIUS).

---

[5]log is the logarithm to the basis 10
[6]For a short biography of JOHANN NIKURADSE (1894–1979), see **Fig. 10.13**.
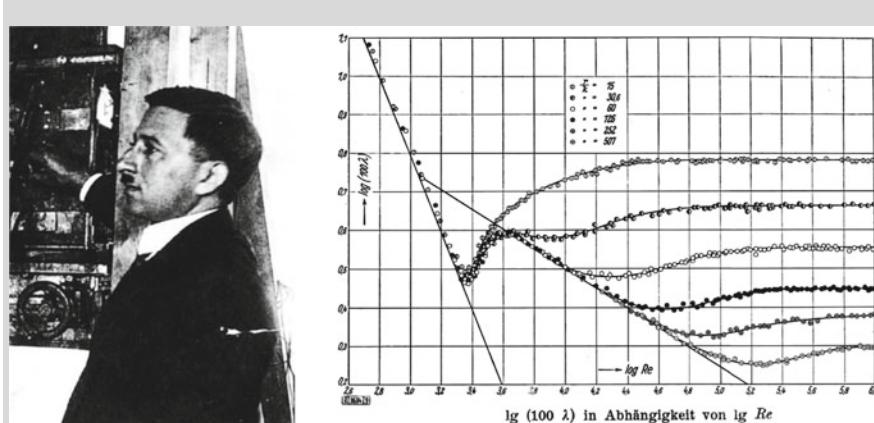
Fig. 10.13 Johann Nikuradse (20. Nov. 1894–18. July 1979)

The figure on the right shows Nikuradse's experimental points of $\log(100 \times \lambda)$ plotted against $\log(\mathbb{R})$ from his 1933-paper, [13].

Johann Nikuradse (in Georgian *Ivane Nikuradze*) was a Georgia-born German engineer and physicist. He is the brother of Alexander Nikuradse, also a Germany-based physicist and geopolitician, known for his role in saving many Georgians during World War II.

Johann Nikuradse was born in Samtredia, Georgia (then part of the Kutais Governorate, Imperial Russia) and studied at Kutaisi. In 1919, he went abroad for further studies to Germany. The 1921 Sovietization of Georgia precluded his return to homeland and Johann Nikuradse naturalized as a German citizen.

As PhD student of Ludwig Prandtl in 1920, he later worked as a researcher at the Kaiser Wilhelm Institute for Fluid Dynamics in Göttingen (now the Max Planck Institute for Dynamics and Self-Organization). He succeeded in putting himself in Prandtl's favour and thus advanced to the position of department head. In spite of his close ties with the Nazi Party, Nikuradse came, in the early 1930s, under fire of the Institute's National Socialist Factory Cell Organization whose members accused him of spying for the Soviet Union and of stealing books from the institute. Prandtl initially defended Nikuradse, but was eventually forced to dismiss him in 1934. He then served as a professor at the University of Breslau (1934–1945), and an honorary professor at the Aachen Technical University since 1945.

Johann Nikuradse lived mostly in Göttingen and engaged in hydrodynamics. His best known experiment was published in Germany in 1933. He carefully measured the friction which a turbulent fluid experiences as it flows down a rough pipe, He used grains of sand of different roughnesses and discovered that, the rougher the surface, the greater the friction, and hence pressure loss.

He discovered that: (i) In range I, for small Reynolds numbers the resistance factor is the same for rough as for smooth pipes. The causes of the roughening lie entirely within the laminar layer for this range. (ii) In range II (transition range), an increase in the resistance factor was observed for an increasing Reynolds number. The thickness of the laminar layer is here of the same order of magnitude as that of wall roughness in the boundary layer. (iii) In range III, the resistance factor is independent of the Reynolds number (quadratic law of resistance). Here all the sources of the roughening extend through the laminar layer, and the resistance factor λ is given by formula (10.59).

The text is based on http://www.wikipedia.org

JOHANN NIKURADSE glued sand grains in the diameter range $0.1 - 1.6$mm onto the
pipe wall to artificially control the wall roughness and, thus, determined the values of
the coefficient of resistance under controlled conditions. His results are summarized
in **Fig. 10.15**. This figure clearly shows in doubly logarithmic fashion the straight
lines, which draw the λ-dependences of the laminar pipe flow (POISEUILLE) and the
hydraulically smooth turbulent counterpart (BLASIUS). All $\lambda(\mathbb{R}, k/d)$-curves merge
for large REYNOLDS numbers into horizontal lines, each with its own value of k/d (in
the figure shown as k/r). A flow, represented by a point in this regime of the diagram
is referred to as a **fully developed rough turbulent flow**, for which THEODORE VON
KÁRMÁN [19] theoretically motivated, and NIKURADSE experimentally verified, the
formula

$$\lambda = \frac{1}{\left(2\log\left(\dfrac{d}{k}\right) + 1.74\right)^2}. \tag{10.59}$$

CYRIL FRANK COLEBROOK (1910–1997) [5, 6] unified the PRANDTL-formula
(10.58), which holds for hydraulically smooth turbulence, and the VON KÁRMÁN
formula (10.59) for fully developed rough turbulent flows into the single formula[7]

① Laminar $\lambda = 64/\mathbb{R}$
② Laminar-turbulent transition regime
③ Turbulent, hydraulically smooth pipe
④ Transition regime smooth-rough pipe
⑤ Fully developed rough flow regime
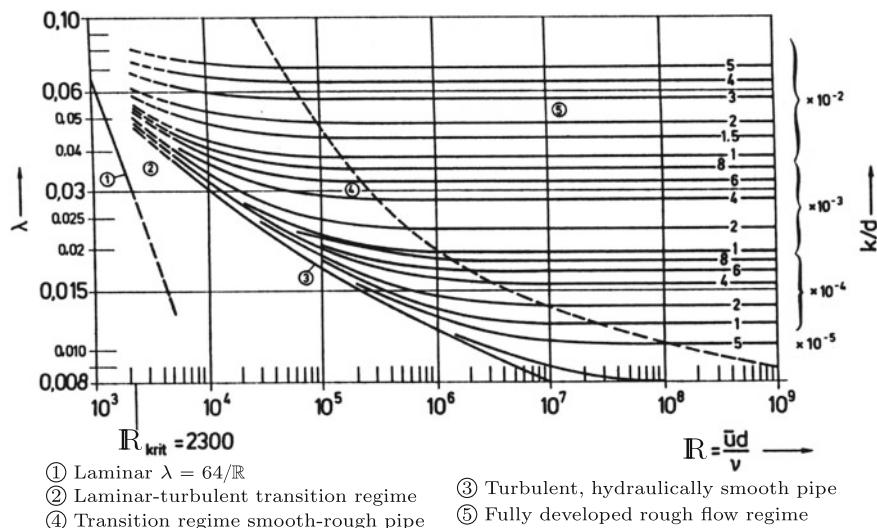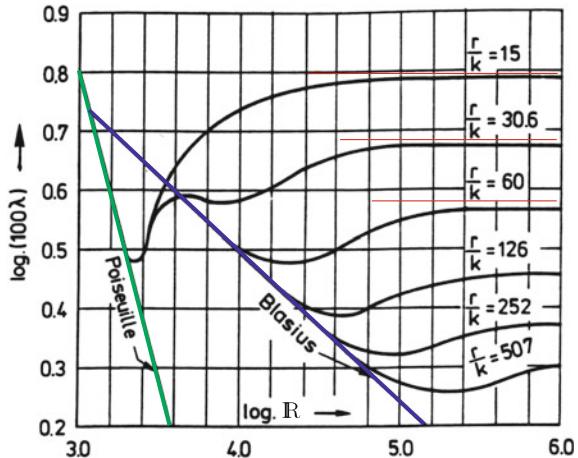
Fig. 10.14 MOODY diagram. *Coefficient of resistance, λ, as a function of the* REYNOLDS *number*
$\mathbb{R}$ *and the relative roughness k/d as proposed by* C.F. COLEBROOK [5, 6] *by formula* (10.60). *The*
dashed curve indicates the limit, beyond which the value of λ can be assumed to be independent of
the REYNOLDS *number*

---

[7]In the German hydrodynamic literature (10.60) is known as PRANDTL-COLEBROOK formula, in
the English literature it is often referred to as COLEBROOK-WHITE formula.

$$\frac{1}{\sqrt{\lambda}} = -2\log\left(\frac{2.51}{\mathbb{R}\sqrt{\lambda}} + 0.270\frac{k}{d}\right). \tag{10.60}$$

The curves in the MOODY-diagram [10], see Fig. 10.15, have been computed
with formula (10.60). For hydraulically smooth pipes the second number on the
right-hand side is absent and (10.60) reduces to (10.58). For fully turbulent-rough
flow, the first member on the right-hand side can be dropped and (10.59) emerges
(prove it!). In the flow regime of the laminar-turbulent transition, formula (10.60)
cannot, naturally exactly reproduce the correct behavior, because POISEUILLE flow
is not incorporated in (10.60). In spite of this (10.60) is used in many technical
computations also in the laminar-turbulent transition regime. Such ('virtual') pipes,
in which the λ-values are computed with (10.60) as coefficient of resistance are
called **technically rough**. **Table 10.1** lists some values of absolute roughnesses *k* of
technically relevant materials.

10.3.2 Plane Turbulent Flow According to Prandtl and von Kármán

The intention in this section is to demonstrate that turbulent flow parallel to walls
is susceptible to mathematical analysis, provided a few plausible assumptions are
made. A general description is not intended as we only present ideas here, which
were developed in the first half of the 20th century.

It is assumed that the plane velocity profile $u = u(y)$ of the turbulent flow is
pre-assigned; we wish to design a picture of the flow, see **Fig. 10.16**. To this end we
consider two neighboring small layers separated by a small distance l. The mean
velocities in these layers are $u(y)$ and, approximately $u(y) + l(\mathrm{d}u/\mathrm{d}y)$. They differ

Table 10.1 Some wall roughness lengths for technically important materials

Mean value for different materials	k [mm]
Cast iron (new)	0.5–1.0
Cast iron (slightly rusted)	1.0–1.5
Cast iron (rusted)	1.5–3.0
Cement (polished)	0.3–0.8
Cement (rough)	1.0–3.0
Wooden board (rough)	1.0–2.5
Raw stones	8.0–15.0

from one another by $l(\mathrm{d}u/\mathrm{d}y)$. A fluid element, which, owing to the turbulent motion, is exchanged from the upper to the lower layer, approaches a fluid particle in this lower layer with the relative velocity $u' = l(\mathrm{d}u/\mathrm{d}y)$. Consequently, due to reasons of continuity, a fluid particle from the lower layer must move upward with the velocity $v' = l(\mathrm{d}u/\mathrm{d}y)$.

This argument suggests that the mass $\rho l(\mathrm{d}u/\mathrm{d}y)$ will move through a horizontal surface element of unit area and unit time; this parcel will be subjected at the upper layer to a relative horizontal velocity increase of size $l(\mathrm{d}u/\mathrm{d}y)$. This corresponds to a momentum flux
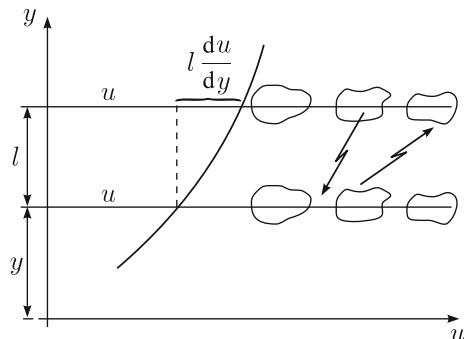
$$\rho u' v' = \rho \left(l\frac{\mathrm{d}u}{\mathrm{d}y} \right)^2, \tag{10.61}$$

which is to be set equal to the shear stress τ, which acts at the horizontal plane of the layer, viz.,

$$\tau = \rho \left(l\frac{\mathrm{d}u}{\mathrm{d}y} \right)^2 = \varepsilon \frac{\mathrm{d}u}{\mathrm{d}y}, \qquad \varepsilon = \rho l^2 \frac{\mathrm{d}u}{\mathrm{d}y}. \tag{10.62}$$

This is LUDWIG PRANDTL's formula for the turbulent shear stress in a shear flow; ε is a coefficient, which was already introduced in 1877 by JOSEPH BOUSSINESQ; it

Fig. 10.16 Turbulent shear flows. *Explaining the derivation of* PRANDTL's *formula for turbulent shear stress*

plays the same role as the shear viscosity in laminar flows of viscous fluids. For this reason ε is called **turbulent viscosity**; contrary to the shear viscosity of a NEWTONian fluid it is not a constant but depends upon the velocity gradient of the mean motion and contains a length l, the so-called **Prandtl mixing length**, for which additional closure assumptions must be postulated. A further difference of (10.62) from the corresponding laminar case is the fact that the turbulent viscosity is not a material constant, but rather a coefficient characterizing the turbulent motion.

The turbulent shear stress (10.62) is actually not a true frictional stress, but rather a **fictitious shear stress**, for it is formed because of its derivation, in which one refers the turbulent velocity fluctuations to the mean velocity field. These fluctuations give rise to the momentum exchange relative to the mean motion. For this reason one also speaks of **fictitious stresses**.

We shall now demonstrate how formula (10.58) for the turbulent coefficient of resistance of hydraulically smooth pipes can be motivated or derived with the aid of formula (10.62) for the turbulent shear stress plus two additional assumptions. The first assumption is a hypothesis about PRANDTL's mixing length l. If y is the distance from the wall, l can be assumed to be proportional to this distance, hence

$$ l = \kappa y, \qquad \kappa = \text{const.} \tag{10.63} $$

This assumption is plausible, because very close to the wall and for hydraulically smooth pipes laminar flow prevails, for which l must vanish, whereas it is reasonable to assume that it will grow with increasing distance from the wall. The simplest ansatz has the form (10.63). Substitution into (10.62) leads to

$$ \tau = \rho \left(\kappa y \frac{du}{dy} \right)^2, \qquad \frac{1}{\kappa} \sqrt{\frac{\tau}{\rho}} \frac{dy}{y} = du. \tag{10.64} $$

This equation, which, obviously, can only hold in the vicinity of the wall, could be integrated, if τ were known as function of the distance from the wall. This fact motivates the second assumption, namely to set τ equal to a constant.[8] One then writes

$$ v^* = \sqrt{\frac{\tau_0}{\rho}}, \tag{10.65} $$

and calls v^* the **shear stress velocity** of the wall or the **wall shear velocity**. Therefore, (10.64) can now be integrated to yield

$$ u = \frac{v^*}{\kappa} (\ln y - \ln y_0) = \frac{v^*}{\kappa} \ln \frac{y}{y_0}, \tag{10.66} $$

---

[8]This assumption is plausible, because very close to the wall du/dy is approximately constant, so that BOUSSINESQ's formula $\tau = \varepsilon du/dy$ also suggests $\tau = \text{constant}$

in which y_0 is a constant of integration. It determines the distance from the wall where u vanishes. With the wall-shear velocity v^* and the kinematic viscosity simple dimensional arguments suggest that

$$y_0 = \frac{\nu}{\beta v_*}, \qquad \beta = \text{const.}, \tag{10.67}$$

so that (10.66) may be written in the form

$$\frac{u}{v^*} = \frac{1}{\kappa} \left(\ln \frac{yv^*}{\nu} + \ln \beta \right). \tag{10.68}$$

This is the dimensionless *universal logarithmic velocity profile*. It says that the velocity, scaled with the wall shear velocity is merely a function of the REYNOLDS number

$$\mathbb{R}^* = \frac{yv^*}{\nu}. \tag{10.69}$$

The two empirical constants κ and β must be determined experimentally. κ is the VON KÁRMÁN constant; it is independent of the properties of the wall and has the value 0.4 (in certain sources 0.41). Quite contrary, β *does indeed depend* upon the properties of the wall. For *hydraulically smooth* pipes NIKURADSE found that $\beta = 5.5\kappa$. Therefore, (10.68) may with this value of β be written as

$$\frac{u}{v^*} = \left(2.5 \ln \frac{yv^*}{\nu} + 5.5 \right). \tag{10.70}$$

If one computes with this formula the maximum velocity on the pipe axis $y = R$, one obtains

$$\frac{u_{\max}}{v^*} = \left(2.5 \ln \frac{Rv^*}{\nu} + 5.5 \right), \tag{10.71}$$

and, therefore, for the difference $(u_{\max} - u)$

$$\frac{u_{\max} - u}{v^*} = 2.5 \ln \frac{R}{y}. \tag{10.72}$$

If one integrates this relation over the cross section of the pipe, one obtains for the mean velocity $\bar{u}$

$$\bar{u} = u_{\max} - 3.75 v^*,$$

or with (10.71)

$$\bar{u} = v^* \left(2.5 \ln \frac{Rv^*}{\nu} + 1.75 \right). \tag{10.73}$$

If one, finally, sets

$$\mathbb{R}^* = \frac{Rv^*}{\nu} = \frac{1}{2}\frac{\bar{u}d}{\nu}\frac{v^*}{\bar{u}} = \frac{\bar{u}d}{\nu}\frac{1}{2}\sqrt{\frac{\lambda}{8}} = \mathbb{R}\frac{1}{2}\sqrt{\frac{\lambda}{8}}, \qquad (10.74)$$

in which we set $v^*/\bar{u} = \sqrt{\lambda/8}$, one may easily show by substitution of (10.74) into (10.73) that

$$\frac{1}{\sqrt{\lambda}} = 2.035 \log\left(\mathbb{R}\sqrt{\lambda}\right) - 0.91. \qquad (10.75)$$

According to this law, the universal frictional law of hydraulically smooth pipes ought to form a straight line, if $1/\sqrt{\lambda}$ is plotted as a function of $\log(\mathbb{R}\sqrt{\lambda})$. This is indeed the case, as was demonstrated by NIKURADSE. The straight line through the experimental points, however, is somewhat different from the plot of the above relation and is given by

$$\frac{1}{\sqrt{\lambda}} = 2 \log\left(\mathbb{R}\sqrt{\lambda}\right) - 0.8 \qquad \text{(smooth pipes)}. \qquad (10.76)$$

This formula has already been given in (10.58).

Finally, let us state the universal roughness function for pipes as deduced by PRANDTL-NIKURADSE. To derive it, we start with Eq. (10.59) for rough pipes and write it in the form

$$\left(\frac{1}{\sqrt{\lambda}} - 2 \log\frac{d}{2k}\right) = 1.74. \qquad (10.77)$$

Alternatively, it follows from (10.76) that

$$\underbrace{\left(\frac{1}{\sqrt{\lambda}} - 2\log\frac{d}{2k}\right)}_{y} = 2\left[\log\left(\mathbb{R}\sqrt{\lambda}\right) - \log\left(\frac{d}{2k}\right)\right] - 0.8$$

$$= 2\left[\log\left(\mathbb{R}\sqrt{\lambda/8}\right) - \log\left(\frac{d}{k}\right)\right] - 0.8 + 2\log\sqrt{8} + 2\log 2$$

$$= 2\underbrace{\left[\log\left(\mathbb{R}\sqrt{\lambda/8}\right) - \log\left(\frac{d}{k}\right)\right]}_{x} + 0.705. \qquad (10.78)$$

For fully rough walls and pure turbulence without viscosity one may, thus, expect that according to (10.77) the variable $y = (1/\sqrt{\lambda} - 2\log(d/(2k)))$ is independent of the REYNOLDS number; on the other hand, the corresponding curve for hydraulically smooth pipes follows Eq. (10.78) and is linear in the variable $x = [\log(\mathbb{R}\sqrt{\lambda/8} - \log(d/k)]$. These two limiting curves have to be connected in the intermediate regime as beautifully shown by the experimental points of **Fig. 10.17**.
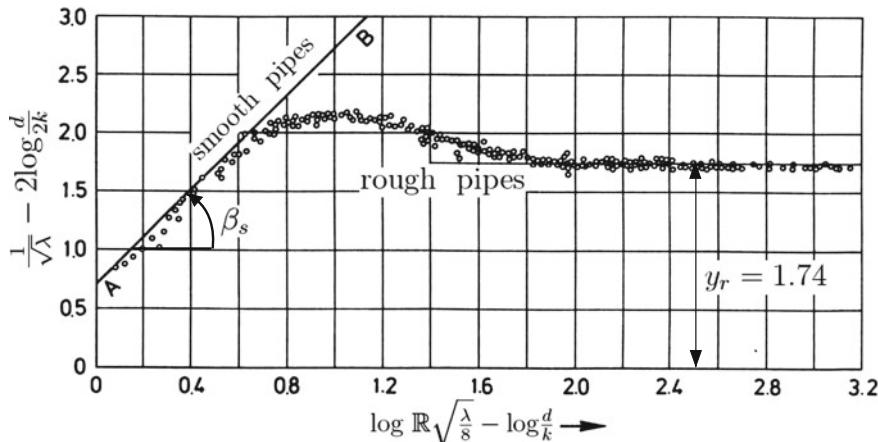
Fig. 10.17 Coefficient of resistance λ. *Universal plot of the coefficient of resistance λ. All experimental points fall in this representation on a single curve*

Critical in this representation is the fact that with the chosen variables x and y only a single curve emerges *for all* wall frictions. This is indeed so as shown in Fig. 10.17 for the experimental points of NIKURADSE. This graphical representation is due to PRANDTL. The entire range, which represents all conduits, can be represented by two straight lines and a transition curve connecting the two. We note that the behavior for the hydraulically smooth and rough pipes is very different from one another. This representation masterly combines measurement of λ as well as velocities. It can be said that it stays at the climax of the PRANDTL-VON KÁRMÁN turbulence theory of circular pipes.

It is evident from Fig. 10.17 that smooth and rough pipe behaviors are adequately reproduced by straight lines, when being compared with experimental results. However, the transition region, even though the experimental results mimic such universal behavior adequately, has not been represented by a formula. Such a formula can easily be proposed with the aid of a fit to data. If we denote the abscissa and ordinate of the coordinates of Fig. 10.17 by x and y, respectively, then

$$(y - y_r) = -\mathcal{A}(x - \alpha_\ell)(x - \alpha_r)^2 \left[1 - \mathcal{B} \exp\left(-\left(\frac{x - \alpha_\ell}{\sigma} \right)^2 \right) \right],$$

$$\alpha_\ell = 0.58, \qquad \alpha_r = 2.0 \qquad\qquad\qquad (10.79)$$

parameterizes the experimental points in Fig. 10.17 in the interval $0.58 \leq x \leq 2.0$. Formula (10.79) approximates the curve at $x = \alpha_\ell$ and $x = \alpha_r$ such that

$$(y - y_r)(\alpha_\ell) = 0, \ (y - y_r)'(\alpha_\ell) = \tan(\beta_s), \qquad\qquad (10.80)$$
$$(y - y_r)(\alpha_r) = 0, \ (y - y_r)'(\alpha_r) = 0,$$

where $\tan(\beta_s)$ is the slope of the smooth pipe segment $A - B$ in Fig. 10.17. The parameters $\mathcal{A}$, $\mathcal{B}$ and σ are so selected that

- $(y - y_r)'(\alpha_\ell) = \tan(\beta_s) = -\mathcal{A}(1.42)^2 \quad \longrightarrow \quad \mathcal{A} = -0.4960 \tan(\beta_s),$

- $\underbrace{(y - y_r)(1)}_{(y-y_r)_{\mathrm{opt}}=0.27} = -0.4960 \tan(\beta_s) \times 0.42 \times (1)^2 \left[1 - \mathcal{B} \exp\left(-\left(\frac{0.42}{\sigma}\right)^2\right)\right]$

$\longrightarrow \quad 0.2083 \tan(\beta_s) \left[1 - \mathcal{B} \exp\left(-\left(\frac{0.42}{\sigma}\right)^2\right)\right] = (y - y_r)_{\mathrm{opt}}$

$\longrightarrow \quad \mathcal{B} = \left\{1 - 4.8008 \frac{(y - y_r)_{\mathrm{opt}}}{\tan(\beta_s)}\right\} \exp\left(-\left(\frac{0.42}{\sigma}\right)^2\right).$

With $\tan(\beta_s) = 2.0$ and $(y - y_r)_{\mathrm{opt}} \approx 0.27$ (see Eq. (10.78) and Fig. 10.17), this yields

$$\mathcal{B} = \{1 - 4.8008 \times 0.135\} \exp\left(-\left(\frac{0.42}{\sigma}\right)^2\right) = 0.3519 \exp\left(-\left(\frac{0.42}{\sigma}\right)^2\right).$$

So, in summary we have

$$(y - y_r) = 0.0992(x - 0.58)(x - 2.0)^2$$
$$\times \left[1 - 0.3519 \exp\left(-\left(\frac{0.42}{\sigma}\right)^2\right) \exp\left(-\left(\frac{x - 0.58}{\sigma}\right)^2\right)\right].$$

There still remains a choice for a value of σ. This will be chosen as 0.42 so that the influence of the term involving $\mathcal{B}$ in (10.79) at $x = 1$ is moderate and at $x = 2$ is negligible. With this choice one gets

$$(y - y_r) = 0.0992(x - 0.58)(x - 2.0)^2 \times \left[1 - 0.1295 \exp\left(-\left(\frac{x - 0.58}{0.42}\right)^2\right)\right].$$

$$(10.81)$$

10.3.3 Calculation of Pressure Loss in Pipe Flows[9]

In Sect. 10.2.3 we treated the flow of a fluid from a vessel for two limiting cases: In one case we ignored the acceleration of the fluid, which follows from the BERNOULLI

---

[9]This subsection illustrates how pressure losses in a sequential arrangement of pipe segments are technically performed in the context of the PRANDTL-VON KÁRMÁN turbulence model. Conceptual thoughts on its theoretical limitation are given in the subsequent subsection.

equation as pressure loss but took into account the pressure loss of the laminar flow in the pipe; in the other case the pressure loss due to the fluid viscosity was ignored and only the pressure loss that needed to accelerate the fluid was accounted for. In turbulent pipe flows neither of the two limiting cases occurs with sufficient accuracy.

As already remarked in connection with the discussion of the pressure distribution in Fig. 10.7a the effective pressure difference, which is available for the transport of the fluid through the pipe is merely

$$\triangle p = \rho g h - \frac{\rho}{2}\bar{u}^2 - \triangle p'. \tag{10.82}$$

The first term, $\rho g h$ is the static pressure, which is established in the vessel at the level of the entrance cross section of the pipe; this value is reduced by the pressure $\rho \bar{u}^2/2$ that is necessary to accelerate the fluid to build the fully developed velocity profile. Because the fully developed velocity profile for the turbulent flow deviates much less from the uniform profile than for laminar flow, the pressure drop $\triangle p'$ is relatively small and can usually be ignored. If one substitutes the expression (10.82) so simplified into formula (10.55), the result can be written as

$$\rho g h - \frac{\rho}{2}\bar{u}^2 = \frac{\rho}{2}\bar{u}^2\lambda\frac{l}{d}, \tag{10.83}$$

which, after the addition of p_0 on both sides, can also be written as

$$p_0 + \rho g h = p_0 + \frac{\rho}{2}\bar{u}^2 + \xi_l\frac{\rho}{2}\bar{u}^2, \tag{10.84}$$
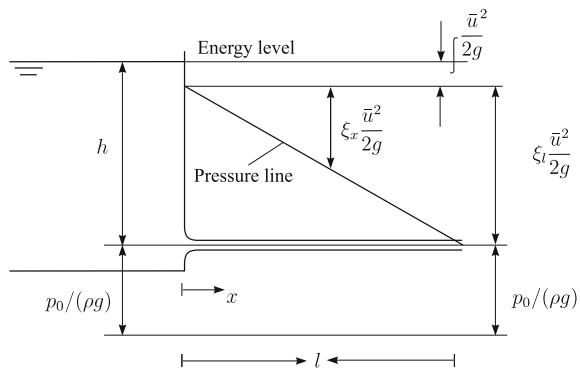
in which

$$\xi_l = \lambda\left(\mathbb{R}, \frac{k}{d}\right)\frac{l}{d} \tag{10.85}$$

is called **pressure loss coefficient**; p_0 is the atmospheric pressure. Equation (10.84) can be interpreted as an **extended Bernoulli equation** for a streamline connecting a point on the free surface in the vessel down to the end cross section of the exit pipe see **Fig. 10.18**. On the left-hand side of (10.84) one recognizes the sum of the atmospheric pressure and the hydrostatic pressure due to gravity relative to a horizon agreeing with the level of the pipe axis; on the right-hand side, apart from the atmospheric pressure, one has the stagnation pressure and the pressure loss due to the viscosity. If, therefore, the pressure losses in the BERNOULLI equation are added, then a balance equation is obtained as with the classical BERNOULLI equation. This property is perhaps even better recognized, if (10.84) is written as

$$\frac{p_0}{\rho g} + h = \frac{p_0}{\rho g} + \frac{1}{2g}\bar{u}^2 + \frac{\xi_l}{2g}\bar{u}^2 = C, \tag{10.86}$$

Fig. 10.18 BERNOULLI
equation. *Extending the*
BERNOULLI *equation by a*
pure pressure loss term

an equation, in which **pressure heights, geodetic heights, velocity heights** and
pressure loss heights are balanced. The height, corresponding to the value C is
called the **energy height** or **energy level**. The quantity

$$C - \frac{1}{2g}\bar{u}^2 - \frac{\xi_l}{2g}\bar{u}^2 \tag{10.87}$$

is called **pressure line**; it pictures the distribution of the pressure in the pipe.

Equations (10.84) and (10.86) can also be solved for the velocity, and then one
obtains
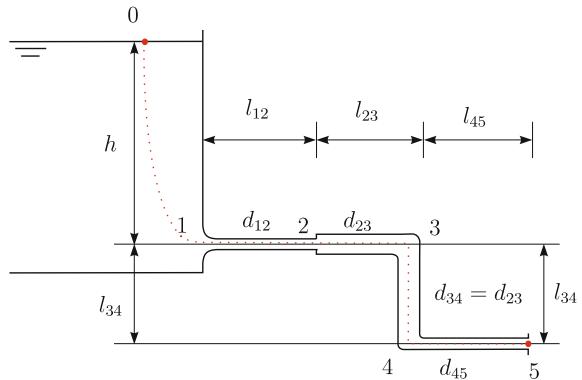
$$\bar{u} = \sqrt{\frac{2gh}{1 + \xi_l}}. \tag{10.88}$$

If the pipe length l and the pressure height in the vessel h are known, then Eq. (10.88)
allows computation of the mean velocity $\bar{u}$ in the pipe and, thus, also the volume
flow, provided the pressure loss coefficient ξ_l is also known. In general, however, the
latter is a function of the REYNOLDS number, see (10.85), which itself depends on $\bar{u}$.
In such cases, $\bar{u}$ can only iteratively be computed with (10.88). For fully developed
turbulence of rough pipes λ and, therefore, ξ_l are independent of the REYNOLDS
number, and $\bar{u}$ is, therefore, immediately determinable from (10.88).

This method of computation can be applied to a complete cord of a conduit. To
explain this, consider **Fig. 10.19**. We scale all velocities in the conduit net with the
velocity in the exit cross section and then may write, on using the continuity equation,

$$\bar{u}_{12} = \left(\frac{d_{45}}{d_{12}}\right)^2 \bar{u}_{45} = \left(\frac{d_{45}}{d_{12}}\right)^2 \bar{u}, \tag{10.89}$$

$$\bar{u}_{23} = \left(\frac{d_{45}}{d_{23}}\right)^2 \bar{u}, \quad \bar{u}_{34} = \left(\frac{d_{45}}{d_{23}}\right)^2 \bar{u}.$$

Fig. 10.19 Computation of the pressure loss in a conduit

If the extended BERNOULLI equation of this pipe system is written for a streamline between the point 0 and 5, then one obtains analogously to (10.83)

$$\rho g(h + l_{34}) = \frac{\rho}{2}\bar{u}_{12}^2 + \xi_{\text{tot}}\frac{\rho}{2}\bar{u}^2 = \frac{\rho}{2}\Big[\Big(\frac{d_{45}}{d_{12}}\Big)^4 + \xi_{\text{tot}}\Big]\bar{u}^2, \qquad (10.90)$$

or

$$\bar{u} = \sqrt{\frac{2g(h + l_{34})}{\Big(\dfrac{d_{45}}{d_{12}}\Big)^4 + \xi_{\text{tot}}}}, \qquad (10.91)$$

in which the **total pressure loss coefficient** ξ_{tot} is composed of all pressure loss coefficients in the conduit $1-5$. For their evaluation we first note that in Eq. (10.91) the 'entrance loss' due to the acceleration of the fluid is included. The remaining losses are composed as follows:

- Entrance loss in cross section 1, which is obtained by the fact that the entrance is edged and, thus, not optimally built. Consequently, a contraction of the fluid jet is formed; the fluid detaches from the wall and attaches to the wall only further downstream

$$\triangle p_E = \hat{\xi}_E \frac{\rho}{2}\bar{u}_{12}^2 = \hat{\xi}_E \Big(\frac{d_{45}}{d_{12}}\Big)^4 \frac{\rho}{2}\bar{u}^2 = \xi_E \frac{\rho}{2}\bar{u}^2,$$

$$\xi_E \qquad\qquad = \hat{\xi}_E \Big(\frac{d_{45}}{d_{12}}\Big)^4. \qquad (10.92)$$

- Pressure loss in element $1-2$:

$$\triangle p_{12} = \lambda_{12}\frac{l_{12}}{d_{12}}\frac{\rho}{2}\bar{u}_{12}^2 = \lambda_{12}\frac{l_{12}}{d_{12}}\left(\frac{d_{45}}{d_{12}}\right)^4\frac{\rho}{2}\bar{u}^2 = \xi_{12}\frac{\rho}{2}\bar{u}^2,$$

$$\xi_{12} \qquad\qquad = \lambda_{12}\frac{l_{12}}{d_{12}}\left(\frac{d_{45}}{d_{12}}\right)^4. \tag{10.93}$$

- CARNOT pressure loss at the sudden extension of the pipe from the element $1-2$ to element $2-3$:

$$\triangle p_C = \xi_C\frac{\rho}{2}\bar{u}_{12}^2 = \hat{\xi}_C\left(\frac{d_{45}}{d_{12}}\right)^4\frac{\rho}{2}\bar{u}^2,$$

in which Eq. (3.227) in Chap. 3

$$\hat{\xi}_C = \left(1 - \left(\frac{d_{12}}{d_{23}}\right)^2\right)^2$$

has been used. The pressure loss due to sudden cross section enlargement, thus, can be written as

$$\triangle p_C = \xi_C\frac{\rho}{2}\bar{u}^2 \tag{10.94}$$

with

$$\xi_C = \left[\left(1 - \left(\frac{d_{12}}{d_{23}}\right)^2\right)\left(\frac{d_{45}}{d_{12}}\right)^2\right]^2.$$

- Pressure loss due to friction in element $2-3$:

$$\triangle p_{23} = \lambda_{23}\frac{l_{23}}{d_{23}}\frac{\rho}{2}\bar{u}_{23}^2 = \lambda_{23}\frac{l_{23}}{d_{23}}\left(\frac{d_{45}}{d_{23}}\right)^4\frac{\rho}{2}\bar{u}^2 = \xi_{23}\frac{\rho}{2}\bar{u}^2,$$

$$\xi_{23} \qquad\qquad = \lambda_{23}\frac{l_{23}}{d_{23}}\left(\frac{d_{45}}{d_{23}}\right)^4. \tag{10.95}$$

- Curvature loss at 3:

$$\triangle p_K^3 = \hat{\xi}_K^3\frac{\rho}{2}\bar{u}_{23}^2 = \hat{\xi}_K^3\left(\frac{d_{45}}{d_{23}}\right)^4\frac{\rho}{2}\bar{u}^2 = \xi_K^3\frac{\rho}{2}\bar{u}^2,$$

$$\xi_K^3 \qquad\qquad = \hat{\xi}_K^3\left(\frac{d_{45}}{d_{23}}\right)^4. \tag{10.96}$$

Such losses depend chiefly on the angle of curvature and the ratio of the radius of curvature to the radius of the pipe.

- Pressure loss in element $3-4$:

$$\triangle p_{34} = \lambda_{34}\frac{l_{34}}{d_{23}}\frac{\rho}{2}\bar{u}_{34}^2 = \lambda_{34}\frac{l_{34}}{d_{23}}\left(\frac{d_{45}}{d_{23}}\right)^4\frac{\rho}{2}\bar{u}^2 = \xi_{34}\frac{\rho}{2}\bar{u}^2,$$

$$\xi_{34} \qquad\qquad = \lambda_{34}\frac{l_{34}}{d_{23}}\left(\frac{d_{45}}{d_{23}}\right)^4.$$

(10.97)

- Pressure loss due to the curvature at 4 with subsequent reduction of the cross section. Since we assume that the reduction of the cross section is smooth here, the loss reduces to a loss due to curvature alone.

$$\triangle p_K^4 = \hat{\xi}_K^4\frac{\rho}{2}\bar{u}_{34}^2 = \hat{\xi}_K^4\left(\frac{d_{45}}{d_{23}}\right)^4\frac{\rho}{2}\bar{u}^2 = \xi_K^4\frac{\rho}{2}\bar{u}^2,$$

$$\xi_K^4 \qquad\qquad = \hat{\xi}_K^4\left(\frac{d_{45}}{d_{23}}\right)^4.$$

(10.98)

- Pressure loss in element $4-5$ due to friction

$$\triangle p_{45} = \xi_{45}\frac{\rho}{2}\bar{u}^2.$$

(10.99)

The total pressure loss is obtained by summation of all contributions and obtains

$$\triangle p_{tot} = \triangle p_E + \triangle p_{12} + \triangle p_C + \triangle p_{23} + \triangle p_K^3 + \triangle p_{34} + \triangle p_K^4 + \triangle p_{45}$$

$$= (\xi_E + \xi_{12} + \xi_C + \xi_{23} + \xi_K^3 + \xi_{34} + \xi_K^4 + \xi_{45})\frac{\rho}{2}\bar{u}^2$$

$$= \xi_{tot}\frac{\rho}{2}\bar{u}^2,$$

(10.100)

a value which has been used already in (10.90) and led to (10.91). The actual computation of $\bar{u}$ (and consequently of the volume flow) obtains by an iterative procedure: One estimates a first value of $\bar{u}$ with the aid of (10.91) by setting inthere $\xi_{tot} = 0$ and application of a small reduction of $\bar{u}$. With this value of $\bar{u}$ and use of (10.89), estimates of $\bar{u}_{12}, \bar{u}_{23}, \bar{u}_{34}$ can be obtained, with the aid of which $\xi_E, \xi_{12}, \xi_{23}, \xi_{34}$, $\xi_{45},\xi_K^3, \xi_K^4$ can be computed, which then yield an improved value for $\bar{u}$. Often it is recommendable to start the iteration with estimates for ξ-values. Indeed, if one initially assumes conditions of hydraulically rough pipes and fully developed turbulence, the λ-values are independent of the velocity and an iterative value for ξ_{tot} can relatively accurately be determined. Since the λ-values vary only slightly within the turbulent flow regime, the back coupling of ξ_{tot} with $\bar{u}$ is modest. In other words, a rapid convergence of the iteration procedure can be expected.

10.3.4   Questioning the Prandtl-von Kármán Logarithmic Velocity Profile[10]

Let us return to formula (10.68) and its analogues in subsequent equations, valid for the hydraulically rough regime as exhibited by the horizontal line of Fig. 10.17. We restart the analysis leading to formula (10.68) once more and ask how the wall-parallel velocity changes in the direction perpendicular to the wall.

In the neighborhood of the wall, which is bounding the flow, it will be assumed that the shear stress parallel to the wall is constant, i.e., independent of (time and) the x-coordinate. It is then natural to assume that the transverse velocity gradient du/dy at a distance y depends on (1) the wall shear stress, τ, (2) the density of the fluid, ρ, (3) the kinematic viscosity of the fluid, ν, (4) the distance, y, from the wall, and (5) the boundary layer thickness, δ, of the near wall layer. The dimensional matrix of these variables is then given by

$$
\begin{array}{c|cccccc}
 & du/dy & y & \delta & \rho & \nu & \tau \\
\hline
M & 0 & 0 & 0 & 1 & 0 & 1 \\
L & 0 & 1 & 1 & -3 & 2 & -1 \\
T & -1 & 0 & 0 & 0 & -1 & -2
\end{array}
\tag{10.101}
$$

has rank 3 and thus gives rise to the following three independent Π-products[11]:

$$
\Pi_1 = \frac{y \dfrac{du}{dy}}{v^*}, \quad \Pi_2 = \mathbb{R}_\ell = \frac{v^* y}{\nu}, \quad \Pi_3 = \mathbb{R}^* = \frac{v^* \delta}{\nu},
\tag{10.102}
$$

in which the *shear stress velocity* is defined as

$$
v^* = \sqrt{\frac{\tau}{\rho}}
\tag{10.103}
$$

and $\mathbb{R}_\ell$ and $\mathbb{R}^*$ are local and global REYNOLDS numbers. These stand, respectively, for the flow conditions immediately outside the laminar sublayer and the outer boundary layer flow; both are relatively large and are in pipe and channel flows of the order of $\mathbb{R}_\ell \geqslant 10^2$ and $\mathbb{R}^* \geqslant 10^4$. BUCKINGHAMS's theorem then suggests the general equation

---

[10]We follow in this subsection closely Chap. 30 in *Physics of Lakes*, Vol. 3 [9].

[11]We have anticipated here consequences of the BUCKINGHAM theorem, in details explained in Chap. 20 of Volume 2.

$$\frac{y\dfrac{\mathrm{d}u}{\mathrm{d}y}}{v^*} = f(\mathbb{R}_\ell, \mathbb{R}^*). \tag{10.104}$$

A rather bold assumption is to conjecture that $f(\mathbb{R}_\ell, \mathbb{R}^*) \approx f(\infty, \infty) = \text{const}$. This assumption supposes that for large arguments the function f in (10.104) approaches a constant limit value. This was THEODORE VON KÁRMÁN's choice,

$$\kappa = \frac{1}{f(\infty, \infty)} \approx 0.4, \tag{10.105}$$

and with it, (10.104) can be integrated to yield

$$\frac{u(y)}{v^*} = \frac{1}{\kappa}\ln(y) + C_1 = \frac{1}{\kappa}\ln(\mathbb{R}_\ell) + C \tag{10.106}$$

with $C = C_1 - \ln(v^*/\nu)/\kappa$. Because $\mathbb{R}^*$ does not arise in this formula, one may say that outside the viscous sublayer the viscosity of the fluid is insignificant. The above *logarithmic law* for the distribution of the mean velocity, u, was proposed by VON KÁRMÁN in 1930 [19]. In the words of BARENBLATT et al. (2000) [4] "the constants κ (the VON KÁRMÁN constant) and C should be identical for all turbulent wall-bounded shear flows at high REYNOLDS numbers, and the law (10.106) should be valid in *intermediate regions* between ... the viscous sublayer and ... the external parts of the flows, e.g. the vicinity of the axis in pipe flow, or the vicinity of the external flow in the boundary layer. In 1932, PRANDTL [15] came to the law (10.106) using a different approach, but effectively with the same basic assumption. The law (10.106) is known as the VON KÁRMÁN-PRANDTL universal logarithmic law."

   According to the logarithmic law (10.106), all experimental points in the turbulent boundary layer region should collapse on a single universal straight line in the coordinates $(\mathbb{R}_\ell, u/v^*)$. BARENBLATT[12] et al. [4] state that experiments showed systematic deviations from the universal logarithmic law "even if one is willing to tolerate a variation in the constants κ and C (from less than 0.4 to 0.45 for κ and from less than 5.0 to 6.3 for C)". They showed that "the fundamental VON KÁRMÁN hypothesis on which the derivation of the universal law (10.106) was based, i.e., the assumption that the influence of viscosity disappears totally outside the viscous sublayer, is inadequate. In fact, this hypothesis should be replaced by the more complicated [postulate of] incomplete similarity, so that the influence of viscosity in the intermediate region remains, but the viscosity enters only in power combination with other factors. This means that the influence of the global REYNOLDS number, i.e., both of the viscosity and external length scale, ..., remains and should be taken into account in the intermediate region".

---

[12]For a short biography of GRIGORY ISAAKOVICH BARENBLATT see **Fig. 10.20**.

Thus, BARENBLATT et al. [4] negate complete similarity as expressed in (10.106) and postulate

$$f(\mathbb{R}_\ell, \mathbb{R}^*) = \tilde{f}(\mathbb{R}^*)(\mathbb{R}_\ell)^{\lambda(\mathbb{R}^*)}. \tag{10.107}$$

This product decomposition makes the transverse velocity profile a power law in y with the power exponent being a function of the global REYNOLDS number. With (10.104) and (10.102)$_2$ it yields

Fig. 10.20 GRIGORY ISAAKOVICH BARENBLATT (10. July 1927–)

GRIGORY ISAAKOVICH BARENBLATT is a Russian mathematician who graduated from Moscow State University, Department of Mechanics and Mathematics. He received his Ph.D in 1953 from Moscow State University under the supervision of A.N. KOLMOGOROV. He received his Habilitation degree (the Russian doctoral degree) from the Lomonossow University and was promoted to professor in 1962. G. BARENBLATT researched in the Petroleum Institute of the Soviet Academy of Sciences; since 1962 he was Head of the Section of Theory of Plasticity at the Institute of Mechanics of the Lomonossow University and from 1975 to 1992 the theoretical section of the Institute of Oceanography of the Soviet Academy of Sciences. Then he moved to the West and was from 1992 to 1994 G.I. TAYLOR professor of Fluid Mechanics at Cambridge University and is its Emeritus since then.

G. BARENBLATT traveled intensely after 1992 to universities and research centers in Europe and America. He is a member of the American Academy of Arts and Sciences, the National Academy of Engineering, the Academy of Science of Europe and the National Academy of Sciences of the USA. He is since the mid-90s of the last century Professor in residence at the Department of Mathematics at the University of California at Berkeley and a mathematician at the Lawrence Berkeley National Laboratory. His research specialties are fracture mechanics, fluid and gas flows in porous media, the mechanics of non-classical deformable solids, turbulence and self-similarity, asymptotics and dimensional analysis.

The text is based on http://www.wikipedia.org

$$\frac{\mathrm{d}u}{\mathrm{d}y} = \frac{v^{*\lambda+1}}{\nu^{\lambda}} \, \tilde{f}(\mathbb{R}^*) \, y^{\lambda-1}, \tag{10.108}$$

or after integration,

$$\frac{u(y)}{v^*} = \left(\frac{v^* y}{\nu}\right)^{\lambda(\mathbb{R}^*)} \underbrace{\frac{\tilde{f}(\mathbb{R}^*)}{\lambda(\mathbb{R}^*)}}_{:=\hat{f}(\mathbb{R}^*)} = \hat{f}(\mathbb{R}^*)(\mathbb{R}_\ell)^{\lambda(\mathbb{R}^*)}. \tag{10.109}$$

This is the velocity profile above the laminar sublayer as expressed for incomplete similarity. It is advantageous to write (10.109) as

$$\ln\left(\frac{u}{v^*}\right) = \underbrace{\ln\left(\frac{\tilde{f}(\mathbb{R}^*)}{\lambda(\mathbb{R}^*)}\right)}_{(1)} + \underbrace{\lambda(\mathbb{R}^*)\ln(\mathbb{R}_\ell)}_{(2)}. \tag{10.110}$$

For $\mathbb{R}^* \to \infty$, but finite $\mathbb{R}_\ell$ outside the viscous sublayer, complete similarity is expected, but with respect to $\mathbb{R}^*$ and not $\mathbb{R}_\ell$. This means that for $\mathbb{R}^* \to \infty$

$$\left.\begin{array}{l} \tilde{f}(\infty) = \text{constant}, \\ \lambda(\mathbb{R}^*) = \dfrac{c}{\ln(\mathbb{R}^*)}, \end{array}\right\} \longrightarrow \hat{f}(\mathbb{R}^*) \propto \ln(\mathbb{R}^*).$$

With this choice the term (2) in (10.110) tends to zero as $\mathbb{R}^* \to \infty$ for all finite $\mathbb{R}_\ell$ and the term (1) shows a double logarithmic behavior, which qualitatively corresponds to the VON KÁRMÁN logarithmic profile. Thus, we write

$$\phi = \frac{u(y)}{v^*} = \left\{C_0 \ln(\mathbb{R}^*) + C_1\right\} (\mathbb{R}_\ell)^{c/\ln(\mathbb{R}^*)}, \tag{10.111}$$

where C_0, C_1 and c are constants. This formula is equation (2) in BARENBLATT et al. [4], which these authors introduce with the statement "using some additional analytic and experimental arguments, the present authors came to the REYNOLDS-number dependent *scaling law* of the form (10.111)". Our above estimation shows, there is a clear rational argument behind (10.111).

The law (10.111) holds for any turbulent shear flow with constants C_0, C_1 and c which must be universal. BARENBLATT et al. [4] state that they have matched (10.111) with NIKURADSE's 1932 [12] data for pipe flow and obtained

$$c = \frac{3}{2}, \quad C_0 = \frac{1}{\sqrt{3}}, \quad C_1 = \frac{5}{2},$$

while $\mathbb{R}^* = \bar{u}\, d/\nu$ is based on the average velocity; $\bar{u}$ is the mean pipe velocity and d is the interior pipe diameter. Thus,

$$\phi = \frac{u(y)}{v^*} = \left(\frac{1}{\sqrt{3}}\ln(\mathbb{R}^*) + \frac{5}{2}\right)(\mathbb{R}_\ell)^\alpha = \left(\frac{\sqrt{3}+5\alpha}{2\,\alpha}\right)(\mathbb{R}_\ell)^\alpha, \qquad (10.112)$$

$$\alpha = \frac{3}{2\,\ln(\mathbb{R}^*)}.$$

This scaling law produces separate curves $\phi(\ln\mathbb{R}_\ell, \mathbb{R}^*)$ in the $(\ln\mathbb{R}_\ell, \phi)$-plane, one for each value of $\mathbb{R}^*$. BARENBLATT et al. [4] emphasize that this fact "is the principal difference between the law (10.112) and the universal logarithmic law (10.106)" They also say 'that the family (10.112) of the curves having $\mathbb{R}^*$ as parameter has an envelope, and that in the $(\ln\mathbb{R}_\ell, \phi)$-plane, this envelope is close to a straight line, analogous to (10.106) with the values $\kappa = 0.4$ and $C = 5.1$.'

BARENBLATT et al. [4] analyze a huge wealth of data and generally plot $\log\phi$ against $\log\mathbb{R}_\ell$ for different values of $\mathbb{R}^*$. In one group of experiments it is shown that the data outside the viscous sublayer ($\log\mathbb{R}_\ell > 1.5$) have the characteristic slope of a broken line, represented by (I) $\phi = A\mathbb{R}_\ell^\alpha$ and by (II) $\phi = B\mathbb{R}_\ell^\beta$, where A, α, B, β are constants, obtained by 'statistical processing', as they say. In the other experiments the straight lines of the data are not broken. The authors also check the *universality of the scaling law* by transforming (10.112) into

$$\psi = \frac{1}{\alpha}\ln\left(\frac{2\alpha\,\phi}{\sqrt{3}+5\alpha}\right) = \ln\mathbb{R}_\ell \qquad (10.113)$$

and plotting $(\ln\mathbb{R}_\ell, \psi)$-curves, in which $\ln\mathbb{R}_\ell$, obtained from the data is plotted against ψ, which is also obtained from the data, but is based on the above theory-based logarithmic function. All points cluster ideally very close to the 45°-line of the graphs, which corroborates the universality of the law (10.112).

10.4 Concluding Remarks

In this chapter linearly viscous fluid flow through the circular pipes was closely analyzed in the regimes from pure laminar behavior at low REYNOLDS numbers to fully turbulent behavior at moderate to large REYNOLDS numbers. We saw that the laminar flow was independently discovered by GOTTHILF HINRICH LUDWIG HAGEN and JEAN LOUIS LÉONARD MARIE POISEUILLE, a German, respectively, a French scientist, who derived the parabolic radial velocity distribution of laminar flow in the mid 19th century. Generalization of their work to linearly viscous flow through pipes of arbitrary cross sections showed that the axial velocity distribution within the cross section is governed by a boundary value problem involving the POISSON equation subject to DIRICHLET boundary conditions (zero longitudinal velocity component at

the pipe wall) with prescribed longitudinal pressure gradient. Gravity driven slow creeping flow from a vessel with free surface through a circular pipe was shown to be usable as a viscometric instrument (ENGLER viscometer) to determine numerical values for the fluid viscosity by measurement (provided the fluid was known to be linearly viscous (NEWTONian))

Research on turbulent pipe flow at moderate to large REYNOLDS numbers started in the 18th century by initially (incorrectly) concluding that the frictional resistance was independent of the nature of the walls of the pipes (GASPARD CLAIR FRANÇOIS MARIE RICHE DE PRONY (1755–1839), JOHANN ALBERT EYTELWEIN (1764–1849), PIERRE DU BUAT (1734–1809)[13]). It needed, beyond the certainly ingenious conjecture of existence of the turbulent (eddy) viscosity by BOUSSINESQ, in the 1870s, experimental and theoretical work by LUDWIG PRANDTL and THEODORE VON KÁRMÁN and their associates (HEINRICH BLASIUS, JOHANN NIKURADSE, ...) and many others to show that the pressure loss in circular pipes was expressible in the form (10.55), in which the coefficient of resistance, λ, was in general a function of the REYNOLDS number $\mathbb{R}$ and the relative wall roughness $k/d : \lambda = \lambda(\mathbb{R}, k/d)$. Three regimes of this functional relation have experimentally been detected and computationally been modeled. In the laminar regime, formula (10.56) shows that λ depends only on the REYNOLDS number. For turbulent flow, the function λ exhibits three different behaviors (see e.g. Figs. 10.14 or 10.17). Between the two dashed lines ① and ④ dependences on $\mathbb{R}$ and k/d are exhibited. Curve ① shows only an $\mathbb{R}$ dependence as does curve ③, which is an envelope for all k/d-value, the λ-curves are horizontal. This describes hydraulically smooth behavior. All other λ-curves between the dashed lines clearly show dependences on $\mathbb{R}$ *and* k/d. However, to the right of curve ④ the λ-curves are horizontal and, thus, independent of $\mathbb{R}$. This is the hydraulically rough flow regime.

All the preceding analyses are in more than a hidden form based on a logarithmic boundary layer velocity profile of the form (10.68) or (10.106). The result expressed by these formulae are the manifestation of the fact that the viscosity outside the viscous sublayer loses its influence on the turbulent flow. This is tantamount to negate complete similarity and postulate that a local and a global REYNOLDS number influence the turbulent velocity profile as shown in (10.107). J.J. ALLEN et al. [1] state this difference as follows: 'BARENBLATT et al. [3] and BARENBLATT & CHORIN [2], however, proposed that the velocity profile is not universal, but in fact a weakly varying power law with coefficients that vary with the REYNOLDS number. This suggestion has important implications for the prediction of high REYNOLDS number flows because the correct formulation of scaling laws enables us to make predictions beyond the range of REYNOLDS numbers achievable in the laboratory'. ALLEN et al. [1], however, are in the remainder of their experimental paper somewhat inconclusive whether incomplete similarity is exhibited in large REYNOLDS number pipe flows, and they state a number of references supporting this view.

Certainly, there is still more to come in the near future.

---

[13]For brief biographies of PRONY, EYTELWEIN and DU BUAT, see [7].

References

1. Allen, J.J., Shockling, M.A., Kunkel, G.J., Smits, A.J.: Turbulent flow in smooth and rough pipes. Phil.Trans. R. Soc, Lond, **A365**, 699–714 (2007)
2. Barenblatt, G.I., Chorin, A.J.: Scaling of the intermediate region of wall-bounded turbulence: the power law. Phys. Fluids **10**, 1043–1044 (1998)
3. Barenblatt, G.I., Chorin, A.J., Prostokishin, V.M.: scaling laws for fully developed turbulence in pipes. Appl. Mech. Rev. **50**, 413–429 (1997)
4. Barenblatt, G.I., Chorin, A.J., Prostokishin, V.M.: Self-similar intermediate structures in turbulent boundary layers at large Reynolds numbers. J. Fluid Mech. **410**, 263–283 (2000)
5. Colebrook, C.F.: Turbulent flow in pipes, with particular reference to the transition region between smooth and rough pipe laws. J. Inst. Civ. Eng. Lond. **11**, 133–156 (1939)
6. Colebrook, C.F., White, C.M.: Experiments with fluid friction in roughened pipes. Proc. R. Soc. Lond. **61**, 367–378 (1937)
7. Hager, W.H.: Hydraulicians in Europe 1800–2000. International Association, Hydraulic Engineering and Research (2003)
8. Hutter. K.: Fluid und Thermodynamik–Eine Einführung. Springer, Berlin, etc. 1. Auflage (1995); 2. Auflage (2003)
9. Hutter, K., Wang, Y., Chubarenko, I.: Physics of Lakes–Vol. III Methods of Understanding Lakes as Components of the Geophysical Environment. Springer, Berlin etc., pp. 605 (2014)
10. Moody, L.F.: Friction factors for pipe flow. Trans ASME **66**(8), 671–684 (1944)
11. Nikuradse, J.: Untersuchungen über die Geschwindigkeitsverteilung in turbulenten Strömungen, Dissertation, Göttingen (1926), VDI—Forschungsheft **281**, Berlin, 44p. (1926)
12. Nikuradse, J.: Gesetzmäßigkeiten der turbulenten Strömung in glatten Rohren. Forschungsarb. Ing-wesen **356**, 36p. (1932)
13. Nikuradse, J.: Strömungsgesetze in rauhen Rohren. Forschungsarb. Ing-wesen **361**, 22p. (1933)
14. Prandtl, L.: Bericht über Untersuchungen zur ausgebildeten Turbulenz. Zeitschrift für angewandte Mathematik und Mechanik (ZAMM) **5**(2), 136–139 (1925)
15. Prandtl. L.: Zur turbulenten Strömung in Rohren und längs Platten. Ergeb. Aerodyn. Versuch., Series 4, Goettingen, 18–29 (1932)
16. Prandtl, L.: Neuere Ergebnisse der Turbulenzforschung. Zeitschr. VDI **77**, 105–113 (1933)
17. Prandtl, L.: Über ein neues Formelsystem für die ausgebildete Turbulenz. Nachr. Akad. Wiss. Göttingen Math.-Phys. Klasse, 6–19 (1945)
18. Stanton, T.E., Pannel, J.R.: Similarity of motion in relation to the surface friction of fluids. Trans. R. Soc. Lond. A **214**, 199–224 (1914)
19. von Kármán, Th.: Mechanische Ähnlichkeit und Turbulenz. Nachr. Ges. Wiss. Göttingen, Weidmannsche Buchh., Berlin (1930)

List of Biographies

Name	Figure Nr.	Page Nr.
Theodore von Kármán	Fig. 9.15	509
Gustav Robert Kirchhoff	Fig. 3.42	124
Martin Wilhelm Kutta	Fig. 3.54	140
Josph-Louis Lagrange	Fig. 5.23	246
Pierre-Simon Laplace	Fig. 5.12	221
Gottfried Wilhelm Leibniz	Fig. 3.12	74
Louis Melville Milne-Thomson	Fig. 6.23	304
Richard von Mises	Fig. 3.43	125
Claude-Louis Navier	Fig. 7.3	357
Franz Ernst Neumann	Fig. 5.13	222
Carl Gottfried Neumann	Fig. 5.14	223
Isaac Newton	Fig. 3.17	84
Johann Nikuradse	Fig. 10.13	600
Blaise Pascal	Fig. 2.9	28
George W. Platzman	Fig. 8.16	459
Karl Pohlhausen	Fig. 9.29	545
Jean Léonard Poiseuille	Fig. 7.7	361
Siméon Denis Poisson	Fig. 8.6	435
Joseph Proudman	Fig. 4.13	187
Markus Reiner	Fig. 7.2	355
Georg Friedrich Bernhard Riemann	Fig. 5.27	252
Carl David Tolmé Runge	Fig. 3.55	141
Karl Hermann Amandus Schwarz	Fig. 6.34	316
George Gabriel Stokes	Fig. 7.4	358
Evangelista Torricelli	Fig. 3.30	107
Erich Immanuel Trefftz	Fig. 6.20	300

Name Index

623

Subject Index